Number 7 Volume 23 1959

P11

BULLETIN

of the

ACADEMY OF SCIENCES OF THE USSR

— PHYSICAL SERIES —

(Izvestiya Akademii Nauk SSSR)

(Seriya fizicheskaya)

Reproduction rights reserved
by
Columbia Technical Translations
5 Vermont Avenue
White Plains, New York

Single Issues
$20

Annual Subscription
$215

Lithoprinted in U.S.A.
EDWARDS BROTHERS, INC.
Ann Arbor, Michigan

Transactions

of the

Ninth All-Union Conference on Nuclear Spectroscopy

(Khar'kov, 26 January to 2 February 1959)

Continued from Vol. 23, No. 2; to be continued in Vol. 23, No. 12.

MAGNETIC ALPHA-SPECTROMETER

- B.S.Dzhelepov, R.B.Ivanov, V.G.Nedovesov and V.G.Chumin

The most accurate α-particle energy determinations are made by means of magnetic spectrometers, a number of which have been described in the literature.[1-6] All these spectrometers except that of Cotton[1] utilize an inhomogeneous magnetic field for improving the focusing and thick (nuclear) emulsions for detecting the α-particles. The spectrometers developed by different groups have different resolutions (line half-width $\Delta H\rho/H\rho$ from 0.05 to 0.08%), but as a rule a relatively low transmission factor (effective solid angle from 0.01 to 0.08% of 4π). Yet for a number of scientific problems it is important to have an α-spectrometer with as high a transmission as possible. For example, investigation of the fine structure of α-spectra, which yields important information on high-lying nuclear levels, requires investigation of low intensity components. The theory of $\pi\sqrt{2}$ focusing developed for β-spectrometers shows that the problem of increasing the transmission by an appreciable factor, while retaining a resolution of 0.1% (in momentum), can be solved.

The purpose of the present work was to develop an α-spectrometer which together with a resolution of ~0.10% would have a transmission factor of the order of 0.3% of 4π, i.e., at least an order of magnitude higher than most α-spectrometers.

Description of the instrument

The magnetic field of the developed α-spectrometer is produced by a cyclotron type magnet, the dimensions of which are: length - 3.5 meters, width - 1.4 meters, height - 2.3 meters. The weight of the magnet is 70 tons. The one meter diameter pole pieces are made of grade 15 steel. They are specifically shaped to produce an inhomogeneous field (Fig.1). The height of the working gap at the center of the magnet is 160 mm.

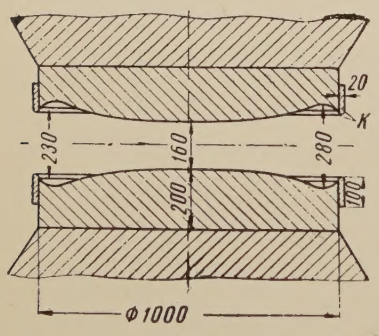

Fig.1. Magnet pole pieces.

For the purpose of reducing the fringe effect and correcting the field, the pole pieces are bound with steel rings (K in Fig.1). By shifting these rings up or down one can vary the field topography in the gap to 120 mm in from the edge of the pole pieces.

The magnet winding consists of 672 turns of copper bus having a cross section of 4.1 x 40 mm. The resistance of the winding is about 0.45 ohm. The magnet is air cooled.

The electromagnet is supplied with regulated dc current from a 230 v, 88 kw generator. At the maximum current of 400 amp, the field strength at the center of the magnet is 20 000 oersted. The supply current is regulated within 0.03% by a thyratron stabilizer.

The spectrometer chamber is cylindrical and is made of brass; the thickness of the side walls is 30 mm, the thickness of the bottom and cover - 19 mm. The inside diameter of the chamber is 1005 mm; the height - 120 mm. The weight of the chamber is about 500 kg. A diagram of the chamber (cover removed) is shown in Fig.2.

The chamber is evacuated through the fitting 1 by a VN-2 type forepump and a 500 liter oil diffusion pump. The working vacuum - 10^{-5} mm Hg - is attained some 30-40 minutes after starting the pumps. The vacuum is monitored by an ion meter. Upon attainment of the working vacuum, the forepump can be switched off: normal operation of the diffusion pump for 5-6 hours is assured by the ballast tank connected to the forepump.

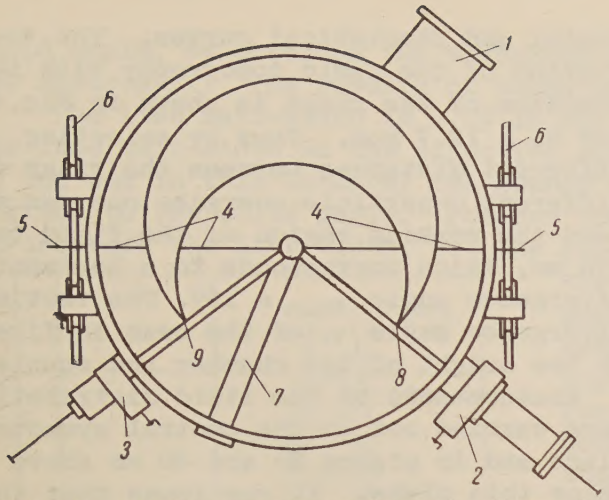

Fig.2. Alpha-spectrometer chamber: 1 - vacuum line coupling, 2 - vacuum lock for interchange of α-sources, 3 - vacuum lock for loading photographic plates, 4 - defining diaphragms, 5 - graduated rods, 6 - rails, 7 - tube for insertion of proton resonance probe, 8 - source, 9 - photographic plate.

The radioactive sources are installed and changed without disturbing the vacuum through the air lock 2. A similar air lock (3) is provided for the photographic plates.

The geometry of the α-particle beam is regulated by the defining diaphragms 4, by means of which one can vary both the horizontal and vertical divergence of the beam. The diaphragm positions can be adjusted without disturbing the vacuum by means of the graduated rods 5. In case of necessity the entire chamber can be withdrawn from the magnet gap, since it is suspended on two rails (6). The chamber is positioned (to within ±0.2 mm) in the magnetic fields by means of special bolts (not shown in the figure).

Tube 7 extending from the outside to the center of the chamber serves for insertion of a proton resonance probe.

Measurement of the magnetic field

For focusing the α-particles we chose an axially symmetric magnetic field, having the property of focusing the beam in two directions. The focusing angle is $\pi\sqrt{2}$. It has been shown by theoretical analyses[7-9] that spectrometers using a field of this type have an optimum resolution to transmission ratio. The axial component of such a field is described by

$$H_z(r) = H(r_0)\left[1 - \frac{1}{2}\frac{(r-r_0)}{r_0} + \beta\frac{(r-r_0)^2}{r_0^2} + \cdots\right].$$

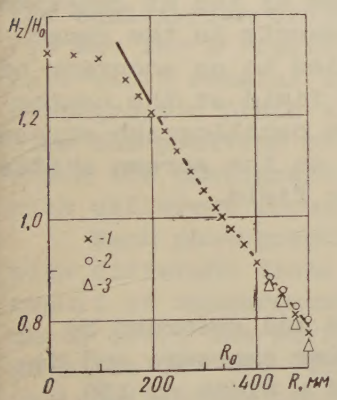

Fig.3. Field distribution in the magnet gap. Solid line - calculated curve for β = 1/8 and R_0 = 335 mm; experimental points: 1) H_z = 10.7 koe, 2) H_z = 12.7 koe, 3) H_z = 14 koe.

The focusing properties of the field depend on the constant β. In the expression for the width of the image, the terms depending on the horizontal divergence angle φ_r vanish for β = 1/8, while the terms depending on the vertical divergence angle φ_z vanish for β = 3/8. It follows, therefore, that for most accurate focusing in spectrometers with a large φ_r and a small φ_z, the constant β should be taken equal to 1/8. Inasmuch as the geometry of our chamber allows of making $\varphi_{r\max} = 20^\circ$ and $\varphi_{z\max} \sim 4^\circ$, β = 1/8 is the best choice under our conditions.

The topography of the magnetic field was surveyed by means of a flip coil. The coil was made of manganin (Mn-Ni-Cu alloy) and had 100 turns of 3 x 16 mm^2 area. The emf induced in the coil was measured by a ballistic galvanometer with an accuracy to 0.1-0.2%. The results of the field measurements are shown in Fig.3.

The measurements showed that the experimental points fit the theoretical curve for R_0 = 335 mm in the R range from 220 to 400 mm. As will be evident from Fig.3, the field topography at the edges depends on the absolute value of the field. By varying the distance between the pole piece rings, one can obtain the best agreement between the experi-

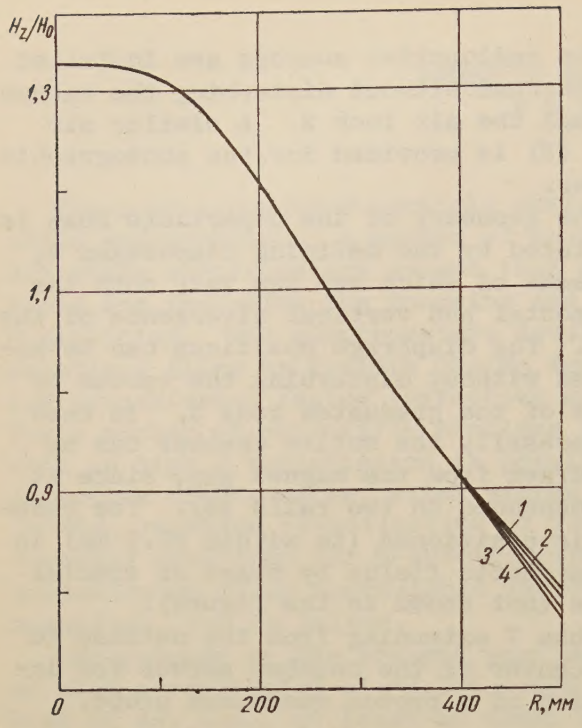

Fig.4. Variation of the magnetic field topography with the distance between the rings around the pole pieces (H_z = = 12.7 koe). Separation between rings: 1 - 182 mm, 2 - 188 mm, 3 - 200 mm, 4 - 208 mm.

mental and theoretical curves. The variation of the field topography with the position of the rings is shown in Fig.4 for H_z = 12.7 koe. Thus by selecting different distances between the rings for different α-particle energies one can extend the working region of the field to 470 mm, which corresponds to a horizontal divergence angle $\varphi_{r\max} = 15^\circ$. The vertical divergence angle φ_z of the beam is fixed by the height of the chamber and equals 4°.

Measurements of the field distribution were carried out in the central symmetry plane and in planes 20 and 40 mm above and below this plane. It was found that the field topography is the same in all five planes, except for the regions near the edge of the pole pieces. Plots of the axial symmetry of the field showed that the law characterizing the falling off of the field is the same in all directions from the center.

The magnetic field was maintained constant during the entire measurement period by the proton resonance technique. The proton resonance equipment consists of a high-frequency generator, an amplifier, an EO-7 oscillograph and a 528 type wavemeter. The high-frequency generator is connected by a 3 to 5 mm long RK-50 cable with the probe, which is a 10 turn coil wound on a plexiglass frame, inside which is a 1.5 cm^3 sample of $MnSO_4$ solution in water. The probe is inserted (through tube 7, Fig.2) and positioned at the center of the magnet, where the field is uniform. The frequency range of the hf generator extends from 10 to 80 Mc, which allows of making field measurements in the range from 2500 to 19 000 oersted. Our wavemeter measures frequencies to an accuracy of 0.05%; hence this is the accuracy of determining the magnetic field at the center of the magnet. The proton resonance signal is observed on the oscillograph screen. If the field deviates by 0.01% from the set value, the signal on the screen shifts, thereby providing continuous and close control of the magnetic field.

Detection and recording

In testing the spectrometer the α-particles were detected and recorded by means of NIKFI thick emulsion (50 μ) photographic plates. After exposure and development, the number of tracks in a strip of given length and a width of 150 μ were counted under a microscope. The variation in the number of tracks per strip as a function of the strip's position on the photographic plate is the α-spectrum.

Basic characteristics of the spectrometer

We investigated the characteristics of the spectrometer by means of a Po^{210} source prepared by electrochemical deposition of polonium on a silver base. In the test, source sections of different widths and heights were defined by the entry diaphragm. In most of the experiments the defined source area was 1 x 10 mm. Setting the diaphragms in different positions and thereby varying the effective

solid angle, we obtained the variation of the resolution with the transmission of the instrument. The results of these measurements are shown in Fig.5.

The line half-width is 0.1% in the Hρ scale (11 kev). There is no change in the line half-width as the effective solid angle is increased from 0.05 to 0.21% of 4π, and in this interval the number of tracks at the line peak increases in proportion to the solid angle. Further increase of the solid angle does not noticeably increase the line width, but the proportionality between the number of tracks at the line peak and the magnitude of the solid angle is disturbed, which indicates appreciable enhancement of the line "tail". Hence a solid angle of 0.28% was chosen as the optimal one. The fact that the resolution of the instrument does not vary with φ_z indicates that the actual topography of the magnetic field is in close agreement with the theoretical distribution for $\beta = 1/8$.

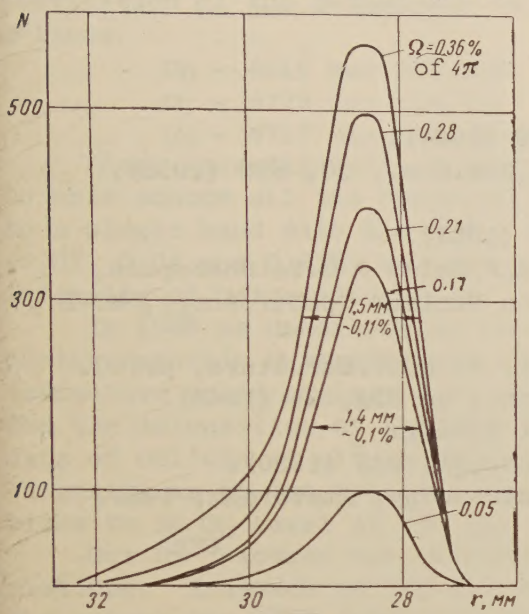

Fig.5. Variation of the resolution with the transmission of the spectrograph.

With the variation in the width and height of the source the experimental line half-width varies in accord with the theoretical formula (Ref.10). Thus, increase of the source height to 20 mm does not broaden the line. With a source width of 0.2 mm and height of 10 mm, the the line half-width equals 6 kv ($\Delta H\rho/H\rho = 0.05\%$) and the transmission factor is 0.2% of 4π.

In investigating α-spectra by means of this instrument it is important to know the law characterizing the variation of the line half-width and shape as a function of its position on the photographic plate. We investigated this dependence experimentally for different solid angles. The results obtained show that the section of the spectrum in which the line half-width is not increased more than 0.1% relative to the half-width of the equilibrium orbit line amounts to 130 kev for transmission of 0.17% of 4π and 115 kev for a transmission of 0.28% of 4π. The energy range in which the line half-width remains approximately constant can be increased by positioning the photographic plate along the focal plane of the instrument. In order to determine the position of the focal surface, we undertook a series of experiments in which the photographic plates were mounted along the radius of the instrument with different focusing angles.

Each photographic plate was exposed with one and the same Po^{210} source but with different field values, so that there was recorded a series of lines. As a result of measurements it was established that the focal surface of the instrument, i.e., the surface of best focusing of off-equilibrium-orbit lines, forms an angle of ~45% with the direction of the radius passing through the focus on the equilibrium orbit. In this case the energy range in which the line width is virtually constant amounts to ~300 kv.

As was noted above, most present magnetic α-spectrometers have a fairly high resolution (~7.5 kev), but a relatively low transmission (to $8\cdot10^{-4}$ of 4π). Under optimal operating conditions ($\varphi_r = 13^\circ$ and $\varphi_z = \pm 2^\circ 40'$) the transmission factor of our instrument is $3\cdot10^{-3}$ of 4π, i.e., substantially higher than that of other spectrometers with relatively little sacrifice of resolution. If we restrict the exposure time to 100 hours, the parameters of our instrument allow of working with α-sources having an activity of 10^{-5} μC referred to the investigated line.

B.P.Shishin participated in the adjustment and calibration of the spectrometer. We are deeply grateful to K.I.Yakovlev of our laboratory for preparation and

installation of the proton resonance equipment. We also desire to thank D.M.Ziv and V.V.Fedorov for preparing the test source and the personnel of the A.P.Zhdanov Laboratory for instruction on the use and processing of thick emulsion photographic plates.

"V.G.Khlopin" Radium Institute,
Academy of Sciences of the USSR

References

1. E.Cotton, Ann.Phys., 6, 481 (1951).
2. F.L.Reynolds, Rev.Scient.Instrum., 22, 749 (1951).
3. L.L.Gol'din & E.F.Tret'yakov, Izv.AN SSSR,Ser.fiz., 20, 859 (1956). (Trans. Bulletin 20, No.8, 1781.)
4. D.L.Judd & S.A.Bludman, Nucl.Instr. 1, 46 (1957).
5. S.A.Baranov, V.V.Beruchko, A.G.Zelenkov, A.F.Malov & G.Ya.Shchepkin, Abstracts presented at the 9th Annual Conference on Nuclear Spectroscopy, M.-L., 1959.
6. J.Perlman & F.Asoro, in Proc.Rehovoth Conf. on Nucl.Structure, p.100.
7. K.Siegbahn & N.Svartholm, Arkiv. Mat.Astron., ys.33A, 21 (1946).
8. F.B.Shull & D.Dennison, Phys.Rev., 71, 681 (1947).
9. E.Persico & C.Geoffrian, Rev.Scient.Instrum.,21, 945 (1950).
10. K.Siegbahn (ed.), Beta- and Gamma-Ray Spectroscopy, Amsterdam, 1955.

ALPHA-SPECTRUM OF U^{233}

- B.S.Dzhelepov, R.B.Ivanov, V.G.Nedovesov & B.P.Shishin

The α-spectrum of U^{233} was first investigated by Asaro[1] on a magnetic spectrometer of the sector type. Three α-groups were detected in this study.

Subsequently, Gol'din and his co-workers[2,3] carried out a more thorough investigation of the α-spectrum of U^{233}. They report observing the following α-lines:

α_0 - 4816 kev (83.5%),	α_3 - 4655 kev (0.07%),
α_1 - 4773 kev (14.9%),	α_4 - 4582 kev (0.04%),
α_2 - 4717 kev (1.6%),	α_5 - 4489 kev (0.03%).

These investigators proposed a decay scheme based on their data; according to this scheme all the observed excited states of Th^{229} are rotational and belong to a single band with K = 5/2. The relative intensities of the last three lines (0.07, 0.04 and 0.03%) are not consistent with the theoretical formulas for the intensity of α-transitions.

In 1958 we undertook an investigation of the U^{233} α-spectrum on a double-focusing magnetic α-spectrometer.[4] The enhanced transmission of our instrument (effective solid angle - 0.2% of 4π) enabled us to obtain more accurate values for the intensities of the weak α-transitions. In addition, on the basis of the data of Gol'din et al[3] regarding the very slow decrease in intensity of the α--transitions to the levels with 11/2, 13/2 and 15/2, we hoped to detect transitions to an α_6 level at 440 kev (17/2).

Our U^{233} source was prepared by electrochemical deposition of uranium on platinum. Inasmuch as our aim was to obtain data on the very weak α-transitions, the source was made rather thick (30 μg/cm^2). The source was in the form of a strip 2.5 mm wide and 20 mm high. The α-line half-width under our experimental conditions was 22 kev.

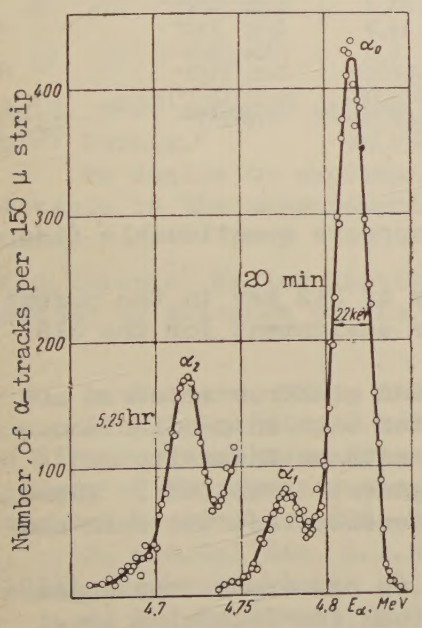

Fig.1. Alpha-spectrum of U^{233} (4.65 to 4.85 Mev region).

A-2 type thick (50 μ) emulsion photographic plates were used for recording the α-particles. The number of tracks was counted under a microscope in trips 150 μ wide and 20 μ long at 0.1-0.2 mm intervals over the width of the photographic plate. The α-spectrum was recorded in sections; three series of measurements with exposures of 50, 100 and 100 hours were made in the region of particular interest. The experimental curves are reproduced in Figs.1 and 2. Our data are compared with the data of Gol'din et al in Table 1.

As will be evident from the table there is good agreement between our data and those of Gol'din et al for the first four lines. The rise in the experimental points in the 230 kev region above the smooth curve for the neighboring sections of the spectrum can, apparently, be attributed to transitions to the 234 kev level. The intensity of the α_4 line, if it exists, is <0.007%. Measurement of the α_5 line energy indicate that the 333 kev value given by Gol'din et al is erroneous. According to our determination, this transition goes to a level at 316 kev, while its intensity agrees approximately with the data of Gol'din et al. We found no evidence of transitions to the hypothetical 440 kev level.

The fact that the intensity of the α_5 line is appreciably greater than the

intensity of the α_4 line gives reason to assert that the 316 kev level does not belong to the rotational band based on the Th^{229} ground state. It appears most probable that the 316 kev level is a single-particle level, inasmuch as vibrational levels in this nuclear region have a much higher excitation energy. Analysis of Nilsson's[5] level scheme for deformed odd nuclei shows that the assignment for a single-particle excited level for a nucleus with N = 139 (Th^{229}) may be 5/2-, 3/2+ or 1/2+. The value of F for the α-transition to the 316 kev level is 0.04; this means that there occurs a minor rearrangement of the nucleus incident to this transition, hence the 5/2- assignment for the 316 kev level appears questionable (the nuclear spin of U^{233} = 5/2+).

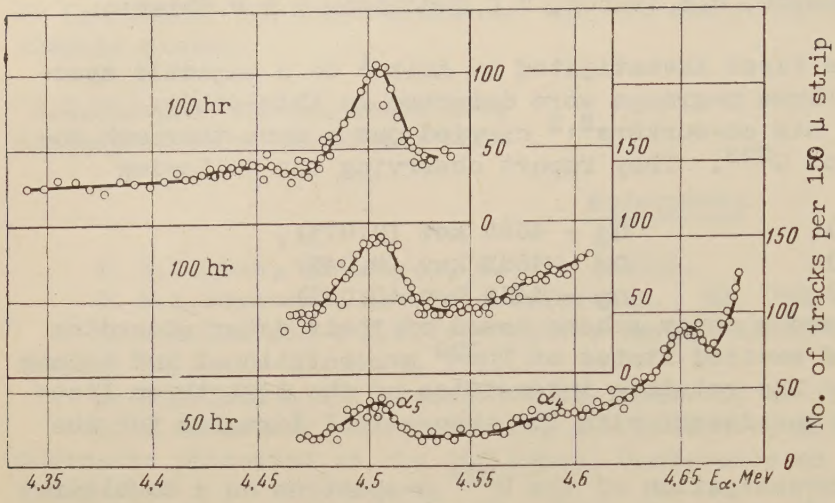

Fig.2. Alpha-spectrum of U^{233} (4.3 to 4.7 Mev region). The peak at the extreme right is formed by the α_3 group.

Table 1

Relative intensities of U^{233} α-groups

α-group	Gol'din et al[2,3]			Our data		
	Th^{229} level, kev	Intensity, %	Assignments, (K; I)	Th^{229} level, kev	Intensity, %	Assignments, (K; I)
α_0	0	83,5	5/2; 5/2+	0	83,4	5/2; 5/2+
α_1	43	14,9	5/2; 7/2+	43	14,9	5/2; 7/2+
α_2	100	1,6	5/2; 9/2+	100	1,6	5/2; 9/2+
α_3	164	0,07±0,04	5/2; 11/2+	166±3	0,060±0,015	5/2; 11/2+
α_4	237	0,04±0,02	5/2; 13/2+	(234±5)	<0,007	(5/2; 13/2+)
α_5	333	0,03±0,01	5/2; 15/2+	(316±3)	0,033±0,008	(3/2+)
α_6	—	—	—	(364±5)	<0,005	

The fact that there is a 3/2+ level with an energy of 312 kev in the parent nucleus U^{233} (Ref.6) in some measure justifies the 3/2+ assignment for the 316 kev level of Th^{229}.

Recently, Gol'din et al[7] investigated the conversion electron spectrum accompanying the decay of U^{233} on a toroidal β-spectrometer with an α-coincidence circuit. They report observing a 316 kev γ-transition with an intensity of 0.012% per disintegration. Their multipole order assignment is M1 (M2). These data are in good agreement with our results and the inference that the spin and parity of the 316 kev level are 3/2+.

Making the 3/2+ assignment for the 316 kev level, we can expect the appearance of a rotational band associated with this level; then the following level (spin & parity 5/2+) should have an energy of ~346 kev and the intensity of the U^{233} α-decay to it should be ~25% the intensity of the 316 kev transition (assuming equality of the moments of inertia for both rotational bands). Careful analysis of this section of the spectrum reveals a very weak peak which may be attributed to a transition to a level at 364 ± 5 kev. Its intensity is <15% the intensity of the 316 kev transition. Although in view of the appreciable statis-

Table 2

Comparison of the relative intensities of U^{233} α-transitions to levels of the main rotational band of Th^{229} with the theoretical data

α-group	Th^{229} level, kev	Relative α-group intensities: Experimental value	Calculated values: Geiger-Nettol formula[9]	Fröman formula[9]	Ter-Martirosyan formula[8]
α_0	0	1	1	1	1
α_1	43	0,178	0,513	0,132	0,177
α_2	100	0,0192	0,217	0,0181	0,0191
α_3	166	$0,72 \cdot 10^{-3}$	0,076	$1,21 \cdot 10^{-3}$	$1,36 \cdot 10^{-3}$
α_4	234	$<0,08 \cdot 10^{-3}$	0,0226	$9 \cdot 10^{-5}$	$8,9 \cdot 10^{-5}$

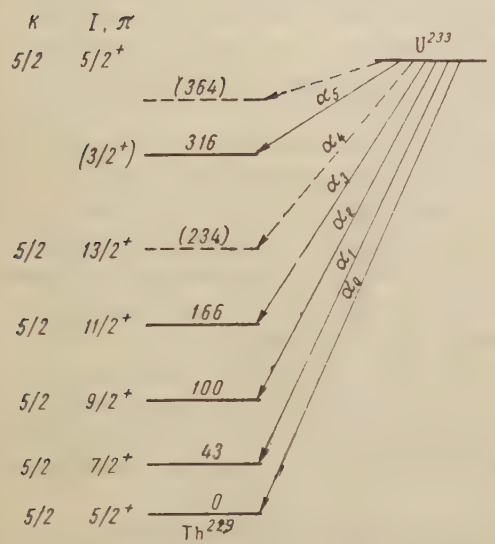

Fig.3. U^{233} α-decay scheme and Th^{229} levels.

tical uncertainty these data are not entirely reliable, it may safely be asserted that if this transition does exist, its energy and intensity differ appreciably from the expected values. This may be connected with change in the moment of inertia of the nucleus or may be due to the fact that the 3/2+ assignment for the 316 kev level is incorrect.

Accordingly, on the basis of our data we propose the decay sheme shown in Fig.3.

In conclusion, we want to note that the intensities of the U^{233} α-transitions to the rotational levels of Th^{229} (Fig.3) are in good agreement with the results of calculations by the formula of Ter-Martirosyan[8] and show an appreciable divergence from the results yielded by the formulas of Fröman[9] and Geiger-Nettol[9]. The experimental data are compared with the calculated values in Table 2.

We desire to express our gratitude to Yu.T.Puzynovich and V.N.Delaev for assistance in the measurements and to L.K.Peker for helpful discussion of the results.

"V.G.Khlopin" Radium Institute,
Academy of Sciences of the USSR

References

1. F.Asaro, UCRL, 2180 (1953).
2. L.L.Gol'din, E.F.Tret'yakov & G.I.Novikova, Sessiya Akademii nauk SSSR po mirnomu ispol'zovaniyu atomnoi energii. Zasedanie OFMN (Session of the USSR Academy of Sciences on the Peaceful Uses of Atomic Energy. Div. of Phys. & Math. Sciences Meeting), p.226, M.-L., 1955.
3. L.L.Gol'din, G.I.Novikova & E.F.Tret'yakov, Izv.AN SSSR,Ser.fiz.,20, 868 (1956). (Trans. Bulletin 20, No.9, 789.)
4. B.S.Dzhelepov, R.B.Ivanov, V.G.Nedovesov & V.G.Chumin, Present issue of the Bulletin, p.779.
5. S.G.Nilsson, Dan.Mat.fys.Medd., 29, No.16 (1955).
6. B.S.Dzhelepov & L.K.Peker, Skhemy raspada radioaktivnykh yader (Decay schemes of radioactive nuclei), M.-L., 1958.
7. L.L.Gol'din, G.I.Grishuk & E.F.Tret'yakov, Abstracts of reports presented at the Ninth Annual Conference on Nuclear Spectroscopy, M.-L., 1959.
8. L.L.Gol'din. L.K.Peker & G.I.Novikova, Usp.fiz.nauk, 59, 459 (1956).
9. A.Bohr, P.O.Fröman & B.R.Mottelson, Dan.Mat.fys.Medd., 29, No.10 (1955).

COLLECTIVE EXCITED STATES OF NUCLEI

- A.S.Davydov

1. Introduction

It is now established that for many nuclei one can distinguish two types of excited states, namely, single-particle excitations, in which a single nucleon changes its state, and collective excitations, which are associated with simultaneous changes in the motion of many nucleons. When one recalls that nuclear matter is highly incompressible, one can often further subdivide relatively low-energy collective motions into excitations having to do with surface oscillations about some equilibrium shape and excitations due to changes in the orientation of the nucleus, namely its rotation.

In a sense, the distinction between collective and single-particle levels is reminiscent of the distinction made for molecular excitations as being due to electron or nuclear motion. Many of the properties of nuclear collective motion were first made clear in the work of Bohr and Mottelson[1], who made use of this analogy.

Strictly speaking, collective and single-particle excitations are related, and one can clearly distinguish between them only in even-even nuclei, where the minimum energy of the single-particle levels is of the order of 1.5 or 2 Mev, while the energy of the collective levels is much lower. In this review, therefore, we shall restrict our discussion to collective motion in even-even nuclei.

In addition to their low energy, collective levels are characterized by a high probability for electric quadrupole transitions both by gamma emission and by Coulomb excitation. In most cases the probability for electric quadrupole transitions from collective levels is one or two orders of magnitude greater than the corresponding transition probability from single-particle levels. Such high transition probabilities are, naturally, connected with the collective motion of a large number of nucleons.

It was assumed for a long time that all nuclei are spherically symmetric. The existence of electric quadrupole moments and rotational excited states, however, shows that many nuclei are actually far from spherical.

The first theoretical explanation of nonspherical nuclear shapes was given by Rainwater.[2] He showed that the shape is determined by competition between the nucleons in the filled shells, which tend to give the nucleus a spherical shape, and those in the unfilled shells, which tend to polarize the nucleus and distort its shape.

Double-magic nuclei are very stably spherical. The frequencies associated with collective levels in such nuclei correspond to surface oscillations about the equilibrium spherical shape. The oscillation energy hardly differs from that of single-particle motion. When there is a certain number of nucleons in the unfilled shells, the collective motion frequencies are substantially reduced, the equilibrium shape becomes distorted, and one can make a valid distinction between collective and single-particle levels.

As already mentioned, collective motion in nonspherical nuclei can be divided into internal excitations, (i.e., surface oscillations) and rotational motion, involving essentially no change in the internal state of the nucleus. Low-energy rotational levels are characteristic of nonspherical nuclei.

Until recently, it was usually assumed that the only nuclei with rotational bands were those in the following three regions of the periodic table:

$$A \sim 24,\ 150 \leqslant A \leqslant 190 \text{ and } A > 220. \qquad (1.1)$$

It was asserted* that nuclei with other mass numbers were spherical. It will be shown below that there are more nuclei with rotational spectra than those given by (1.1). It would seem necessary to reject the assumption that nuclei other than those in the regions of (1.1) are necessarily spherical. This inference is substantiated by determinations of the electric quadrupole moments for many nuclei: for even nuclei from the data on the Coulomb excitation probability and for odd nuclei from the data on the Coulomb excitation probability and on the fine structure of the molecular, atomic and solid-state spectra. As an illustration of the possible nonsphericities, we list in Table 1 the first excited-state energies for some even-even nuclei together with the values of the parameter β, which characterizes the deviation of the nucleus from the spherical shape. The values of β were calculated on the basis of the experimental data reported by Stelson & McGowan[4] and Alder et al[5].

Table 1

Values of the first excited-state energy and the nonsphericity parameter β

Nucleus	A	E, kev	β	Nucleus	A	E, kev	β	Nucleus	A	E, kev	β
Se	74	635	0,21	Cd	112	610	0,19	Dy	162	82	0,36
Se	76	567	0,30	Cd	114	555	0,20	Dy	164	73	0,41
Se	78	615	0,27	Cd	116	517	0,20	Er	164	90	0,33
Se	80	654	0,21	Te	120	560	0,17	Yb	170	84	0,30
Se	82	880	0,11	Te	122	570	0,16	Hf	176	89	0,29
Mo	94	874	0,17	Te	124	608	0,14	Hf	178	91	0,31
Mo	96	775	0,18	Te	126	673	0,16	Hf	180	93	0,27
Mo	98	780	0,17	Te	128	750	0,14	W	182	100	0,26
Mo	100	530	0,25	Te	130	850	0,13	W	184	112	0,24
Ru	96	840	0,16	Nd	146	455	0,09	W	186	124	0,24
Ru	98	654	0,21	Nd	148	300	0,15	Os	186	137	0,20
Ru	100	540	0,23	Nd	150	130	0,25	Os	188	155	0,18
Ru	102	475	0,25	Sm	148	562	0,12	Os	190	188	0,14
Ru	104	358	0,28	Sm	150	337	0,16	Pt	194	330	0,15
Pd	104	555	0,21	Sm	152	122	0,28	Pt	196	358	0,13
Pd	106	513	0,23	Sm	154	83	0,33	Pt	198	403	0,13
Pd	108	433	0,24	Gd	154	123	0,30	Hg	198	411	0,11
Pd	110	374	0,26	Gd	156	89	0,41	Hg	200	370	0,09
Cd	106	630	0,19	Gd	158	79	0,46	Hg	202	439	0,08
Cd	108	630	0,19	Gd	160	76	0,47	Th	232	52	0,18
Cd	110	656	0,19	Dy	160	86	0,35	U	238	44	0,28

According to Table 1, many nuclei that are not near the double-magic ones are nonspherical. If we approximate the nucleus by an ellipsoid, then for a given volume, its shape is determined by the two parameters β and γ, which are related by the expressions

$$a_0 = \beta\cos\gamma,\ a_1 = a_{-1} = 0 \text{ and } a_2 = a_{-2} = \frac{1}{\sqrt{2}}\beta\sin\gamma \qquad (1.2)$$

to the parameters a_μ which determine the nuclear shape according to

$$R(\vartheta\varphi) = R_0\left[1 + \sum_{\mu=-2}^{2} a_\mu Y_{2\mu}(\vartheta\varphi)\right] \qquad (1.3)$$

in the coordinate system fixed along the principal axes of the nucleus.

It follows from (1.2) that

$$\beta = \sqrt{a_0^2 + a_2^2 + a_{-2}^2} \geqslant 0$$

determines the total deviation of the nucleus from spherical symmetry. For a given β, a change in γ from 0 to 60° corresponds to a change in the nuclear shape

---

*See, for example, Sliv's forward in Ref.3.

from a prolate to an oblate spheroid. When $\gamma = 30^\circ$, the nucleus is "intermediate" between a prolate and an oblate ellipsoid.

The rotational spectrum of even-even nuclei is particularly simple in the case of axial symmetry. The rotational energy is then given by the simple expression

$$E_J = AJ(J+1) \quad (J = 0, 2, 4, \ldots), \tag{1.4}$$

where A is a constant (in the adiabatic approximation) depending on the moment of inertia of the nucleus about an axis perpendicular to the symmetry axis.

According to (1.4), the energy ratios of the levels should be

$$E_2 : E_4 : E_6 : E_8 = 1 : 3.3 : 7 : 12. \tag{1.5}$$

A classical example of a nucleus with a clearly evinced rotational spectrum is Hf^{180}, whose level diagram is given in Fig.1,a.

As yet few nuclei are known in which excited levels with spins 2, 4, 6 and 8 have been observed. On the other hand, comparatively many nuclei are known in which the spin 2 and 4 levels have energies consistent with (1.5). The excited levels of such nuclei are assumed to be rotational states of the nucleus with no change in the internal energy. Moreover, it is widely believed that the true rotational levels of even-even nuclei all have spins in the sequence 0,2,4,..., all with the same parity, and that their energy ratios agree with (1.5), the expression obtained for axially symmetric nuclei. Approximate agreement with (1.5) is taken to be proof of the axial symmetry of the nucleus in question. Thus, it is asserted on p.525 of the review article of Alder et al[5] that "The principal empirical evidence for the axial symmetry is the observed J(J + 1) type of rotational spectra." Bohr and Mottelson[1] state that "The spin of 4 for the second rotational excitation and the $E_4:E_2$ ratios confirm the expected axial symmetry of the nuclear deformations. For a nucleus with an asymmetric equilibrium shape, the rotational spectrum would exhibit a sequence of J-values and energy ratios different from (1.5)."

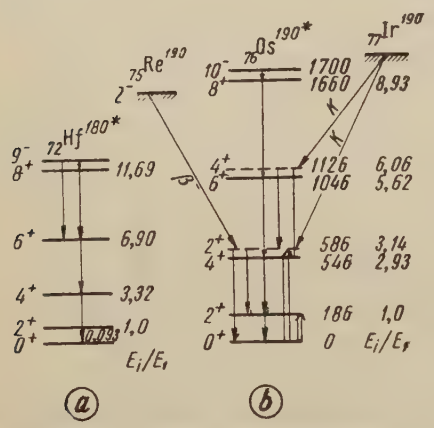

Fig.1. Level diagrams: a) Hf^{180} and b) Os^{190}.

These assertions seem to us to be without basis. Indeed, only those levels of nuclei are called rotational which satisfy (1.5), and then agreement with (1.5) is taken as proof of axial symmetry.

As will be shown below, the assumption that all nuclei are axially symmetric does not follow from the experimental data. Many phenomena involving low-energy excitation in even-even nuclei can be quite well explained by approximating the nucleus by an ellipsoid of three unequal axes.

Section 2 describes some of the basic results of investigations of rotational levels in even-even nonaxial nuclei (together with comparison with experiment) undertaken by the present author in collaboration with Filippov and Rostovskii[6,7]. Section 3 gives some further results of these investigations, concerning the probabilities for radiative transitions between rotational levels of nonaxial nuclei. Section 4 describes other work[8] concerning the probability for β-decay to such rotational levels. Section 5 presents some theoretical results of Gursky[9], Wilets & Jean[10], Geilikman[11], Zaikin[12], and Filippov and the writer[13], which show that the equilibrium shape of a nucleus may not have an axis of axial symmetry.

2. Rotational Energy Levels of Nonaxial Nuclei

The earliest attempt to study the rotational levels of nonaxial nuclei was that of Marty.[14] He treated the problem by perturbation theory and therefore omitted excited levels with odd total angular momentum; he made no attempt to compare his results with experiment. Filippov, Rostovskii and the writer[6,7] obtained exact solutions of the Schrödinger equation for the rotational levels of a nonaxial nucleus assuming no change in the internal energy. The energy levels were calculated for spins 2,3,4,5,6 and 8 for all possible values of the parameter γ which determines the extent to which the even-even nucleus is nonaxial.

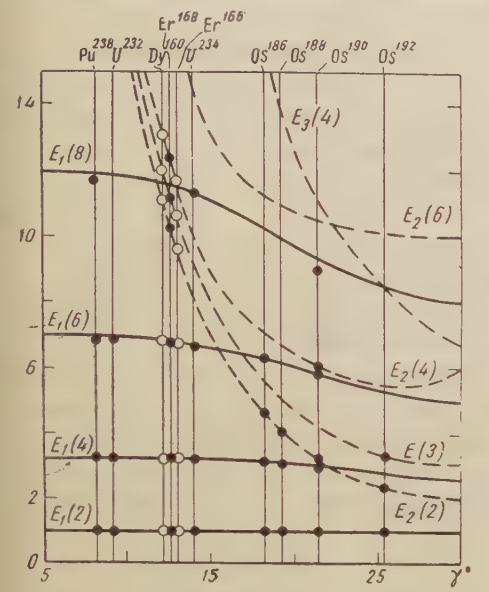

Fig.2. Variation of the ratio of the energy of rotational levels of even-even nuclei to the energy of the first excited (spin 2) level as a function of γ. The solid lines pertain to the normal (ground state) rotational band, while the dashed lines pertain to "anomalous" rotational states. The points on the vertical lines denote experimental values for the corresponding nuclei.

The ratios of the energy of levels with different J to the energy of the first excited spin 2 state are plotted in Fig.2 for values of γ from 0 to 30°. All energy levels of even-even nuclei are functions only of $\sin^2(3\gamma)$, so that by symmetrical extension of the plots with respect to the $\gamma = 30°$ ordinate we obtain the results for $\gamma = 30$ to 60°. As might be expected, the sequence of spins and the energy ratios are in agreement with the results for axial nuclei when γ is 0 or 60°.

Those levels which remain observable as $\gamma \to 0$ we will call levels of the normal (ground state) rotational band. We will denote their energies by $E_1(J)$, where J is the spin of the level. The rotational levels themselves will be designated as J1 (e.g., 21, 41, ...). When $\gamma \neq 0$, there exist in addition to these levels others with spin 2,3,4,5,6,... The energies of these levels increase without bound as $J \to 0$ or 60°. We shall call these "anomalous" rotational levels.

The set of rotational states of a nucleus comprises only two rotational levels with spin 2, one with spin 3, three with spin 4, two with spin 5, four with spin 6, etc. Of the two levels with spin 2, one belongs to the normal rotational band, and the other is anomalous. The ratio of the energies of these two levels is given by

$$\frac{E_2(2)}{E_1(2)} = \frac{1+\sqrt{1-{}^8/_9\sin^2(3\gamma)}}{1-\sqrt{1-{}^8/_9\sin^2(3\gamma)}}. \qquad (2.1)$$

As γ varies from 0 to 30°, this energy ratio decreases from ∞ to 2.

An experimental measurement of the energy ratio of the spin 2 rotational levels can be inserted into (2.1) to determine γ, and then Fig.2 can be used to find the energies and spins of all the other rotational levels, both anomalous and in the normal band.

It will be evident from Fig.2 that when the nucleus deviates from the axially symmetric shape, relation (1.5) is no longer satisfied by the levels of the normal rotational band. For small γ the energy ratios hardly differ from (1.5), but as γ increases, the deviation from the regularities of (1.5) grows, particularly for levels with high spin values. When $\gamma = 30°$, for instance, the energies of the normal band levels should be related as 1 : 2.67 : 5 : 8.

The solid and open circles in Fig.2 give experimental excited-state energy ratios for a number of nuclei, taken from the data of Refs.15-18. It will be evident that the theory reproduces rather accurately the spin sequences and experimental

energy ratios. Small deviations of the experimental points from theory can in part be reconciled by the correction term

$$-a\,J^2(J+1)^2, \tag{2.2}$$

which takes into account coupling between the rotation and internal excitation. Speaking roughly, (2.2) allows for the increase in moment of inertia owing to centrifugal forces. In fact the magnitude of the correction term necessary to bring about agreement with experiment may serve as criterion for the validity of the adiabatic approximation. It should be mentioned that when axial symmetry was assumed, in dealing with rotational spectra, any deviation of the experimentally observed level-spacings from relation (1.5) was explained entirely by the inapplicability of the adiabatic approximation. In this way the importance of the correction term accounting for deviations from adiabaticity was exaggerated. Actually, the deviation from (1.5) comes largely from the fact that the nucleus is not axially symmetric.

In this connection the experimental data on the spin 2,4,6 and 8 levels of Os^{190} are particularly interesting (see Fig.1,b & Fig.2). These energy levels were obtained[19,20] in investigating cascade γ-transitions in the decay of the 10 min isomer of Os^{190}, the assignment for which is 10-. As the authors referred to note, the experimentally observed spin sequence is in good agreement with that for the levels of Hf^{180} (see Fig.1), which has a clear-cut rotational level structure. The observed energy-level ratios, however, differ considerably from the theory for axially symmetric nuclei. The investigators also note that the experimental ratios 1 : 2.93 : 5.62 : 8.93 cannot be obtained by adjusting the two parameters in the expression

$$E_J = AJ(J+1) - aJ^2(J+1)^2.$$

As can be seen from Fig.2, if one assumes the Os^{190} nucleus to be nonaxial ($\gamma = 21.4^\circ$), one obtains energy ratios close to the experimental ones (even without introducing corrections for departure from the adiabatic approximation).

In addition to changing the level spacing in the normal rotational band, departure from axial symmetry introduces the new (anomalous) levels. Such are, for instance, the second spin 2 and 4 levels in Os^{190} (Fig.1,b). These levels are not evinced in the decay of the 10 min Os^{190} isomer, but they do appear in the K-capture decay of Ir^{190} (see Section 4). The second excited spin 2 level is also observed in Coulomb excitation and in β-decay of Re^{190}. These properties of Os^{190} are related to the large value of γ, namely, 21.4°, given by the experimental ratio $E_2(2)/E_1(2) = 3.15$.

We must classify as anomalous rotational levels the spin 3 levels of Dy^{160}, Er^{168}, and Pu^{238} (Fig.3) and many other nuclei.

It is interesting that according to the theory of nonaxial nuclei, the energy of the spin 3 level should equal the sum of the energies of the two spin 2 levels (regardless of the value of γ), i.e.,

$$E(3) = E_1(2) + E_2(2). \tag{2.3}$$

The accuracy with which this relation is fulfilled is independent of any specific choice of energy moments of the nucleus but depends only on the degree of applicability of the adiabatic approximation. Thus (2.3) may be used as an applicability criterion. It has been shown[6] that (2.3) is satisfied with good accuracy (to within 1%) for many nuclei in which the energies of the two spin 2 and one spin 3 levels are known.

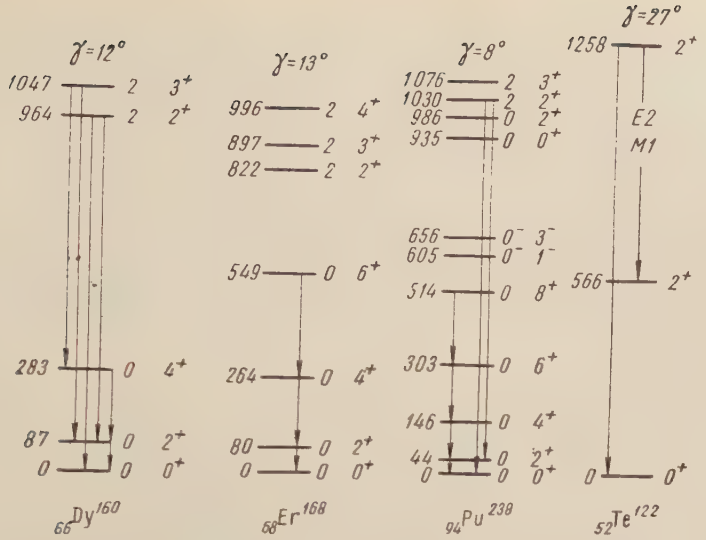

Fig.3. Level diagrams for several nuclei. The values of γ indicated above the diagrams are calculated from the experimental energy ratios of the spin 2 levels. The figures at the right of the levels are the values of K and J, respectively.

According to Fig.2, when $\gamma > 21^\circ$ the spin 4 level of the normal band lies above the second anomalous spin 2 level, while for $\gamma < 21.5^\circ$, on the contrary, it lies below. In any case, it is always above the first spin 2 level. The qualitative regularities must hold for the rotational levels of all even-even nuclei.

These collective excited states of even-even nuclei which have often been called γ-oscillations with quantum number K = 2 and have been arbitrarily attributed to an energy $\hbar\omega_\gamma$ are, according to our new interpretation, anomalous rotational levels of nonaxial nuclei. Such energy levels are possessed, for instance, by Dy^{160} (964 and 1047 kev), Er^{168} (822, 897 and 996 kev), Pu^{238} (1030 and 1076 kev) (see Fig.3), Er^{166} (787, 861 and 958 kev), and a number of other nuclei.

In nuclei which are close to axially symmetric ($\gamma < 15^\circ$) the anomalous rotational levels lie relatively high. As will be shown below (Section 3), such high-lying levels may be identified as levels with K = 2 (Fig.3).

The usual treatment mentioned of levels with K = 2 as γ-oscillations with an energy $\hbar\omega_\gamma$ requires the introduction of the empirical constant ω_γ. A consistent treatment of γ-oscillations, taking into account both the invariance of the wave functions under the replacements

$$\gamma' = \gamma + \frac{2\pi}{3} \quad \text{and} \quad \gamma' = -\gamma,$$

and the explicit form of the kinetic energy operator[1]

$$-\frac{\hbar^2}{2B\beta^2}\frac{1}{\sin(3\gamma)}\frac{\partial}{\partial\gamma}\left(\sin 3\gamma\frac{\partial}{\partial\gamma}\right)$$

of such oscillations, shows that in a certain sense these γ-oscillations are equivalent to rotations. Their energy can be written approximately as the sum of two terms[21] in the form

$$E_\gamma \approx \frac{9\hbar^2}{B\beta_0^2} + 0.1\left[\frac{\partial^2 V(\gamma)}{\partial\gamma^2}\right]_{\gamma=\gamma_0}, \qquad (2.4)$$

the first of which is nine times the energy of the first rotational level, and in the second of which $V(\gamma)$ is the potential energy of the nucleus as a function of the parameter γ. Order of magnitude calculations[21] show that (2.4) is about equal

to the energy of single-particle excitations, but that the probability for exciting γ-oscillation levels is several orders of magnitude lower than that for exciting rotational levels by quadrupole radiation. These results lend further support to the assertion that the above levels with K = 2 should be considered rotational levels of nonaxial nuclei. This inference becomes even more convincing when one notes the good agreement between the observed quadrupole transition probabilities and those predicted by the nonaxial theory (see Section 3).

For $\gamma > 20^\circ$ the anomalous rotational levels drop significantly in energy (see Fig.2). At $\gamma = 30^\circ$, the two anomalous levels with spins 2 and 3 together with the first excited (spin 2) level, form a sequence of three equidistant levels with the spin sequence 2, 2 and 3. When $\gamma = 27^\circ$, the value of $E_2(2)/E_1(2)$ is close to 2. Nuclear excitations in which this ratio is close to 2 have been explained as β-oscillations of the nuclear surface and have been called "nearly harmonic oscillations" as a harmonic oscillator would give such an energy ratio, and it was not known that rotational levels could do the same.

If the spin 2 and 3 excitations are regarded as β-oscillations, $E_2(2)$ and E(3) must be considered two- and three-phonon nuclear surface oscillations and should then be triply and quintuply degenerate states with spins 0, 2 and 4 for $E_2(2)$, and spins 0,2,3,4 and 6 for E(3). Attempts were made to explain the deviation of the experimental $E_2(2)/E_1(2)$ ratio from 2 by the presence of higher order (anharmonic) terms in the collective Hamiltonian. Such an interpretation required the introduction of new parameters to describe the influence of the anharmonic terms. While the observed energy ratio could be explained in this way for some nuclei, the problem of the remaining spin 3 and spin 4 anomalous collective levels remains. If, however, all of these levels are assumed to be rotational, the experimental value of the single ratio $E_2(2)/E_1(2)$ can be used to predict theoretically the energy positions of all the other rotational levels. At the same time this energy ratio, as will be shown in Section 3, unambiguously determines the relative probabilities for electromagnetic transitions between all the rotational levels without introducing any further hypotheses such as those needed when these levels are identified variously as γ-oscillations, β-oscillations, and normal rotational levels.

From the above one should not conclude that all collective excited states are to be regarded as rotational, for many cannot be. Among such states, for instance, are the odd parity levels (605 and 656 kev) of Pu^{238} (see Fig.3) and of some other even-even nuclei. At present these levels are considered to be octupole surface oscillations. In addition, there are the spin 0 and spin 2 excited states (935 and 286 kev) of Pu^{238} (see Fig.3), the spin 0 state (810 kev) of U^{234}, the spin 4,0 and 2 states (1286, 1308 and 1368 kev) of Cd^{114}, and some other excited states in even-even nuclei; these would seem to be β-oscillations of the nuclear surface. Finally, excited states of nearly spherical nuclei cannot in general be clearly divided into collective and single-particle states, so that in this case it is also impossible to identify rotational levels.

3. Electromagnetic Transitions Between Rotational States of Nonaxial Nuclei

In no rotational excited states of nonaxial nuclei (with the exception of spin 3 states) is K a good quantum number. Their wave functions can therefore be written in the form

$$\psi_{Ji} = \sum_K A_{Ki}\Phi_{JK}, \tag{3.1}$$

where the index i numbers the levels with given spin J; the normal rotational band corresponds to $i = 1$, and the anomalous levels, to higher values. The sum in (3.1) is taken over positive even K only:

$$\Phi_{JK} = \sqrt{\frac{2J+1}{16\pi^2(1+\delta_{K0})}}\{D^J_{mK} + (-1)^J D^J_{m,-K}\}, \qquad (3.2)$$

$$\delta_{iK} = \begin{cases} 1, & \text{when } i = K, \\ 0, & \text{when } i \neq K; \end{cases}$$

where the D^J_{mK} are generalized spherical functions which depend on the Euler angles defining the orientation of the nucleus.

The spin 3 wave function is given by the simple expression

$$\psi_3 = \Phi_{32} = \sqrt{\frac{7}{16\pi^2}}\,(D^3_{m2} - D^3_{m,-2})$$

The coefficients A_{Ki} for the other rotational levels in (3.1) have been calculated.[6,7] As an example we give the wave functions of the first rotational states of Os^{190} (with $\gamma = 21.4^\circ$):

$$\begin{aligned}
\psi_{21} &= 0.996\,\Phi_{20} + 0.087\,\Phi_{22}; \\
\psi_{41} &= 0.95\,\Phi_{40} + 0.3\,\Phi_{42} + 0.02\,\Phi_{44}; \\
\psi_{22} &= -0.087\,\Phi_{20} + 0.996\,\Phi_{22}; \\
\psi_3 &= \Phi_{32}; \\
\psi_{42} &= -0.3\,\Phi_{40} + 0.95\,\Phi_{42} + 0.02\,\Phi_{44}; \\
\psi_{61} &= 0.85\,\Phi_{60} + 0.52\,\Phi_{62} + 0.06\,\Phi_{64} + 0.002\,\Phi_{66}.
\end{aligned} \qquad (3.3)$$

It has been shown[6,7] that for nuclei with $E_2(2)/E_1(2) > 6.9$, which corresponds to $\gamma < 15^\circ$, the rotational-level wave functions can be approximated by expressions with only a single K. For instance, the wave functions for the spin 2 states may be approximated by the expressions (in order of increasing energy)

$$\psi_{21} = \Phi_{20} = \sqrt{\frac{5}{8\pi^2}}\,D^2_{m0}\,,$$

$$\psi_{22} = \Phi_{22} = \sqrt{\frac{5}{16\pi^2}}\,(D^2_{m2} + D^2_{m,-2}). \qquad (3.4)$$

The spin 4 wave functions can be approximated by

$$\begin{aligned}
\psi_{41} &= \sqrt{\frac{9}{8\pi^2}}\,D^4_{m0}, \\
\psi_{42} &= \sqrt{\frac{9}{16\pi^2}}\,(D^4_{m2} + D^4_{m,-2}) \\
\psi_{43} &= \sqrt{\frac{9}{16\pi^2}}\,(D^4_{m4} + D^4_{m,-4})\,, \text{ etc.}
\end{aligned} \qquad (3.5)$$

For such cases, then, the rotational excited states can be characterized by the two quantum numbers J and K. In this approximation the normal rotational levels have K = 0. The anomalous levels can be subdivided into those with different values of the projection of the total angular momentum on the nuclear symmetry, i.e., K = 2,4,6,.... Fig.3 shows the level structures of Dy^{160}, Er^{168} and Pu^{238}, together with the presently accepted values of K and J.

Since the wave functions of the rotational states can be uniquely determined if γ (or $E_2(2)/E_1(2)$) is known, it is possible to calculate the reduced probabilities for radiative transitions between these levels. For instance, the reduced probabilities for quadrupole transitions are easily calculated when one recalls that the quadrupole transition operator is

$$\hat{Q}_{2\mu} = eQ_0\left\{D^2_{\mu 0}\cos\gamma + \frac{1}{\sqrt{2}}\,(D^2_{\mu 2} + D^2_{\mu,-2})\sin\gamma\right\},$$

where Q_0 is the internal electric quadrupole moment of the nucleus.

The reduced electric quadrupole transition probabilities are given in units of $e^2Q_0^2/16\pi^2$ (the reduced electric quadrupole transition rate to the first level of an axially symmetric nucleus) in Table 2.

The reduced probabilities for transitions between rotational levels in even-even nuclei satisfy certain sum rules. For instance, the sum of the reduced probabilities for transitions from both levels with spin 2 to the ground state is equal (in $e^2Q_0^2/16\pi^2$ units) to unity; i.e.,

$$b(E2;\ 21\to 0) + b(E2;\ 22\to 0) = 1; \qquad (3.6)$$

further

$$b(E2;\ 3\to 22) + b(E2;\ 3\to 21) = {}^{25}/_{14}. \qquad (3.7)$$

Table 2

Reduced electric quadrupole transition probabilities

b	γ				
	0	10	20	25	30
$b(E2;\ 21\to 0)$	1,0	0,97	0,93	0,96	1,0
$b(E2;\ 22\to 0)$	0	0,028	0,067	0,042	0
$b(E2;\ 22\to 21)$	0	0,051	0,36	0,86	1,43
$b(E2;\ 3\to 21)$	0	0,05	0,12	0,079	0
$b(E2;\ 3\to 22)$	1,78	1,77	1,67	1,70	1,78
$b(E2;\ 3\to 41)$	0	0,034	0,41	0,82	1,0
$b(E2;\ 41\to 21)$	1,43	1,39	1,37	1,36	1,39
$b(F2;\ 41\to 22)$	0	0,002	0,03	0,04	0
$b(E2;\ 42\to 21)$	0,59	0,57	0,48	0,43	0,59
$b(E2;\ 42\to 3)$	1,33	1,28	0,98	0,45	0
$b(E2;\ 42\to 41)$	0	0,06	0,31	0,31	0,27
$b(E2;\ 61\to 41)$	1,57	1,55	1,62	1,70	1,73
$b(E2;\ 61\to 42)$	0	0,008	0,05	0,01	0

It follows from Table 2 that the electric quadrupole transitions between rotational levels of even-even nuclei can be divided into three types:

1. Transitions, the reduced probabilities for which are of the order of unity. Among these are cascade transitions between levels of the normal rotational band and transitions between anomalous levels with different spin, for example, 3→22, 42→3, 42→22 transitions.

2. Transitions between levels of the normal band and anomalous levels of different spin. For example, 3→21, 41→22, 42→21, 61→42 and similar transitions. The reduced transition probabilities for this group are zero for $\gamma = 0^\circ$ or 30° and small for other values of γ.

3. Transitions between levels with the same spin, for instance, 22→21, 42→41 and similar transitions. The reduced transition probabilities for this group are zero for $\gamma = 0^\circ$ and increase with γ, attaining a maximum (of the order of unity) at $\gamma = 30^\circ$. The 3→41 transition is also of this type.

When the rotational motion is such that K is approximately a good quantum number, as described above, the nonzero reduced quadrupole transition probabilities between levels with given J and K are given by the simple expressions

$$b(E2;\ JK\to J'K) = 5\,(2J\,0K\,|\,J'K)^2\cos^2\gamma;$$
$$b(E2;\ JK\to J'K+2) = {}^5/_2\,(1+\delta_{K0})\,(2J2K\,|\,J'K+2)^2\sin^2\gamma;$$
$$b(E2;JK\to J'K-2) = {}^5/_2\,(1+\delta_{K2})\,(2J2K\,|\,J'K-2)^2\sin^2\gamma,$$

where the $|(J_1J_2m_1m_2|Jm)$ are Clebsch-Gordan (or vector addition) coefficients. Thus when $\gamma < 15^\circ$, the most probable E2 transitions take place when

$$\Delta K = 0. \qquad (3.8)$$

Transitions in which the selection rule (3.8) is violated are usually called K-forbidden. When $\gamma > 15^\circ$, one must use the exact wave functions, since for such nuclei K is no longer a good quantum number. The explicit expressions for the reduced transition probabilities between the two spin 2 levels and the neighboring levels with spin 0 and 3 are then of the form

$$b(E2;\ 21\to 0) = \frac{1}{2}\left(1 + \frac{3-2\sin^2(3\gamma)}{\sqrt{9-8\sin^2(3\gamma)}}\right);$$

$$b(E2;\ 22\to 0) = \frac{1}{2}\left(1 - \frac{3-2\sin^2(3\gamma)}{\sqrt{9-8\sin^2(3\gamma)}}\right);$$

$$b(E2;\ 22\to 21) = \frac{10\sin^2(3\gamma)}{7(9-8\sin^2(3\gamma))};$$

$$b(E2;\ 3\to 22) = \frac{25}{28}\left(1 + \frac{3-2\sin^2(3\gamma)}{\sqrt{9-8\sin^2(3\gamma)}}\right);$$

$$b(E2;\ 3\to 21) = \frac{25}{28}\left(1 - \frac{3-2\sin^2(3\gamma)}{\sqrt{9-8\sin^2(3\gamma)}}\right).$$

Thus our theory[6,7] of rotational levels of nonaxial nuclei can be used to calculate the quadrupole transition probabilities between all rotational states of a nucleus. All of these rates are proportional to the square of the internal electric quadrupole moment of the nucleus. The ratios of the transition rates will therefore depend only on γ, or on the energy ratio for the two spin 2 levels.

Table 3

Ratios of reduced electric quadrupole transition probabilities

Nucleus	$\frac{E_2(2)}{E_1(2)}$	γ	$\frac{b(E2;\ 22\to 21)}{b(E2;\ 22\to 0)}$		$\frac{b(E2;\ 22\to 21)}{b(E2;\ 21\to 0)}$	
			theo.	exp.	theo.	exp.
Pu^{238}	23,4	8,1	1,2	1,3—1,5		
Th^{232}	15,4	10,3	1,7	1,8	0,052	0,014
W^{182}	12,1	11,6	1,7	1,6		
Dy^{160}	11,0	12,2	1,9	2,4		
Sm^{152}	8,9	13,5	1,9	1,7		
Gd^{154}	8,1	14,0	2,6	1,94		
W^{184}	8,0	14,1	3,0	2,4	0,18	0,12
Os^{188}	4,1	19,3	4,5	2,7	0,32	0,19
Os^{190}	3,0	21,4	7,1	9,7	0,50	0,52
Hg^{198}	2,7	23,2	13	25		
Os^{192}	2,4	25,4	21	9,1	0,90	0,68
Te^{122}	2,2	26,3	40	30	1,29	2,8
Cd^{144}	2,17	26,8	78	77,9		
Te^{126}	2,14	27,5	104	200		
Pt^{196}	1,97	30	∞	>2500		

Table 3 gives $E_2(2)/E_1(2)$, the corresponding values of γ, the experimental and theoretical ratios[6,7] of the reduced transition probabilities for the cascade and cross-over transitions from the second spin 2 level, and the values of the reduced probability ratio $\frac{b(E2;\ 22\to 21)}{b(E2;\ 21\to 0)}$. It will be evident that the theory satisfactorily predicts the experimental results. Thus, as γ varies from 8.1° to 27.5°, the theoretical value of $\frac{b(E2;\ 22\to 21)}{b(E2;\ 22\to 0)}$ changes by approximately two orders of magnitude, in agreement with experiment.

It is interesting to consider the ratio of the reduced probabilities for transitions from the ground state to the two spin 2 levels; this is,

$$\frac{b(E2;\ 0\to 22)}{b(E2;\ 0\to 21)} = \frac{\sqrt{9-8\sin^2(3\gamma)} - 3 + 2\sin^2(3\gamma)}{\sqrt{9-8\sin^2(3\gamma)} + 3 - 2\sin^2(3\gamma)}. \qquad (3.9)$$

It is important to know this ratio if one want to evaluate the possibility of exciting the 22 level by the Coulomb field of fast charged particles.

The ratio in (3.9) is greatest when $E_2(2)/E_1(2)$ lies between 2.4 and 6.28 ($25^\circ > \gamma > 15^\circ$) and becomes very small when $E_2(2)/E_1(2)$ is greater than 64 or less than 2.01. The theoretical and experimental values of this ratio are given in Table 4 (the experimental Coulomb excitation data were taken from the work of Jean & Touchard[22]).

Table 4

Ratios of the reduced probabilities for transitions to the spin 2 levels

Nucleus	$\frac{E_2(2)}{E_1(2)}$	γ	$\frac{b(E2;\ 0\to 22)}{b(E2;\ 0\to 21)}$ theo.	exp.	Nucleus	$\frac{E_2(2)}{E_1(2)}$	γ	$\frac{b(E2;\ 0\to 22)}{b(E2;\ 0\to 21)}$ theo.	exp.
Os^{190}	2,9	20	0,072	0,04	Ru^{102}	2,24	25,1	0,043	0,015
Ru^{100}	2,55	23,7	0,057	0,024	Pd^{106}	2,20	26,5	0,027	0,017
Ru^{104}	2,56	24	0,055	0,013	Pd^{108}	2,18	27	0,02	0,01
Gd^{116}	2,35	25	0,044	0,021	Cd^{114}	2,17	27	0,02	0,02

In order to avoid uncertainties associated with different populations of the various rotational levels, one should compare transitions from some one given initial state to different final ones. Unfortunately, there are, as yet, only scanty pertinent data available. Nathan and Waggoner[23] give experimental values for the intensity ratio of the E2 transitions 3→41 and 3→21 in Sm^{152}. This ratio leads to an experimental transition probability ratio of 1.88. From the energy ratio $E_2(2)/E_1(2) = 8.9$ it follows that $\gamma = 13.5^\circ$ for Sm^{152}; then the theoretical transition probability ratio is 1.37, which is in satisfactory agreement with the experimental value.

According to Waddell and Jensen[24], $\frac{b(E2;\ 3\to 21)}{b(E2;\ 3\to 22)} = 0.016$ in Kr^{82}. This gives a value of γ slightly larger than 29°. A γ value between 29° and 30° is in good agreement with the observed spin 2 energy ratio of 1.9, when one recalls that in this nucleus the adiabatic conditions are not very well satisfied.

In conclusion to this section we shall discuss the second excited level with spin 2 in tungsten isotopes. In a recent contribution by Alkhazov et al[25] it was asserted that the second spin 2 levels at 1222, 891 and 730 kev in W^{182}, W^{184} and W^{186} are γ-oscillation states. In their principal argument in favor of this view, Alkhazov et al make use of the experimental reduced probability ratio for electric quadrupole transitions to the ground and first excited states of these nuclei. In our notation, this ratio may be written as

$$\frac{B(E2;\ 22\to 0)}{B(E2;\ 22\to 21)} \qquad (3.10)$$

If one assumes that the assignments for the second excited state are J = 2 and K = 2 and that for the rotational levels K = 0, Alaga's theory[26] predicts that this ratio should be 0.7 for all the tungsten isotopes. Table 5 gives the experimental values of this ratio according to Alkhazov et al[25], the spin 2 level energy ratios, the values of γ corresponding to these ratios, and the value of (3.10) predicted by our[6,7] nonaxial theory.

Table 5

Ratios of reduced electric quadrupole transition probabilities

Nucleus	$\frac{E_2(2)}{E_1(2)}$	γ	$\frac{B(E_2;\ 22\to 0)}{B(E_2;\ 22\to 21)}$ theo.[26]	exp. [25]	theo.[6,7]	experimental [27, 28]	experimental [29]
W^{182}	12,1	11,6	0,7	1,2	0,59	0,62	—
W^{184}	8,0	14,1	0,7	0,69	0,42	—	0,55
W^{186}	6	15,2	0,7	0,53	0,37	—	0,42

Numbers in [ ] are Refs.

If we allow for the considerable uncertainty in the data of Alkhazov et al[25] for W^{182} (the authors mention that the results were obtained by averaging only four runs), it follows from Table 5 that our nonaxial theory reproduces rather well the reduced probability ratio values and the variation of the ratio in going from one isotope to another. The experimental data are not in agreement with Alaga's value of 0.7, and support our theoretical inference that K is not a good quantum number.

These levels of tungsten cannot be single-particle levels. If they were, the ratio of the competing magnetic dipole and electric quadrupole modes of the 22→21 transition would be greater than unity. Actually, the transition is almost entirely electric quadrupole, which tends to support the contention that these levels are essentially rotational (see also Davydov and Filippov[30]).

We hope that the accumulation of new experimental data on the transition probabilities in even-even nuclei will enable us to effect a fuller comparison with the predicitions of the theory of rotational states of nonaxial nuclei.

4. Intensity Rules for β-Transitions to Different Rotational States of Even-Even Daughter Nuclei

When one knows the wave functions of the rotational states of even-even nuclei, one can sometimes calculate the relative intensities of β-decay from a given initial state of the odd-odd parent nucleus to the different rotational levels of the daughter nucleus. These relative intensities obey rules analogous to the intensity rules for the fine and hyperfine structure of atomic spectra. Alaga and his co-workers[26] considered these rules for axially symmetric nuclei. In a recent contribution[31] the writer investigated the rules for the nonaxial case.

In the adiabatic approximation the wave function of the initial spin I state of the parent nucleus may be written

$$\varphi_{IM} = \varphi_I(r) \sum_K a_K D^I_{MK}. \tag{4.1}$$

If in the β-decay the electron and neutrino carry away angular momentum L, the ratios of the reduced probabilities for β-transitions from a given initial state to the different rotational levels corresponding to a single internal state of the daughter nucleus are given by

$$\frac{B(L; I \to J'i')}{B(L; I \to J''i'')} = \frac{\left| \sum_{KK'} a_K A^{J''}_{K''i''} (ILKK' - K \mid J'K') \right|^2}{\left| \sum_{KK''} a_K A^{J''}_{K''i''} (ILKK'' - K \mid J''K'') \right|^2}, \tag{4.2}$$

if

$$L < \begin{cases} \min(K + K'), & \text{for } K' \neq 0 \text{ and } K \neq 0, \\ \min(K + K''), & \text{for } K'' \neq 0 \text{ and } K \neq 0. \end{cases}$$

If the nucleus is axially symmetric and therefore K is a good quantum number, (4.2) goes over into the expression obtained by Alaga et al[26] for the rotational band of a daughter nucleus with a given (fixed) value of K', namely,

$$\frac{B(L; IK \to J'K')}{B(L; IK \to J''K')} = \frac{(ILKK' - K \mid J'K')^2}{(ILKK' - K \mid J''K')^2}.$$

For β-transitions allowed either by Fermi or Gamow-Teller selection rules, the reduced transition probability is inversely proportional to τf_0, where τ is the half-life and f_0 is the Fermi function, the integral of the electron energy distribution function.

In the general case there is no such relation for forbidden transitions, probably because such transitions involve a combination of different types of interaction, the relative contributions from which are difficult to evaluate. An exception is formed by the so-called "unique β-transitions" (see Section 38 of the author's book[32]).

In the case of unique n-fold forbidden transitions ($L = n + 1$, parity changes for odd n) the reduced transition probability is inversely proportional to τf_n, where f_n is the integral of the distribution function for the given type of decay. If one neglects the influence of the Coulomb field, Davidson[33] has shown that one may write approximately

$$f_n = \bar{c}_n f_0, \tag{4.3}$$

where $\bar{c}_n$ is a quantity depending on the transition energy (E_0) and given roughly by

$$\bar{c}_n \approx (E_0^2 - m^2c^4)^n. \tag{4.4}$$

Thus for Gamow-Teller allowed transitions ($n = 0$) and unique transitions, we have

$$\frac{\tau f_n (I \to J'i')}{\tau f_n (I \to J''i'')} = \frac{B(L; I \to L''i'')}{B(L; I \to J'i')}, \tag{4.5}$$

where $L = n + 1$ and the ratio of the relative probabilities is given by (4.2). In comparing (4.5) with experiment one must bear in mind that the experimental τf values usually given are τf_0, inasmuch as Fermi's formula for allowed transitions is commonly employed to evaluate f. For unique transitions, therefore, one must introduce a correction according to (4.3).

As an illustration of the above, let us calculate the ratios of the reduced probabilities for the decay of Re^{186} to the rotational spin 2 levels of Os^{186} with energies 764 and 137 kev. According to Guss, Killion & Porter[34], the ground state of Re^{186} has spin zero and odd parity. In the β-decay to the first excited level (end-point energy 934 kev; $\log \tau f_0 = 8.0$) $L = 2$ and the parity changes. Thus this transition is a once forbidden unique transition. This conclusion is supported by the large τf value and the shape of the β-decay spectrum, which, when the correction factor is taken into account (see Section 38 of Ref. 32), gives a rectilinear Kurie plot.

The ground state of Re^{186} has $J = K = 0$, and the wave functions of the two Os^{186} rotational levels ($\gamma = 18^\circ$ for $E_2(2)/E_1(2) = 5.56$) are of the form

$$\psi_{21} = 0.997\,\Phi_{20} + 0.065\,\Phi_{22},$$
$$\psi_{22} = -0.065\,\Phi_{20} + 0.997\,\Phi_{22},$$

where Φ_{20} and Φ_{22} are the wave functions for $K = 0$ and $K = 2$, respectively. Using these facts and (4.1), we find

$$\left\{\frac{B(2; 0 \to 21)}{B(2; 0 \to 22)}\right\}_{\text{theo.}} = 1.3.$$

Experiment gives the ratio $\dfrac{\tau f_0 (0 \to 22)}{\tau f_0 (0 \to 21)} = 7.94.$

The end-point energy in the β-decay to the second excited level is 307 kev. Using (4.3) and (4.4), we find

$$\frac{\tau f_1 (0 \to 22)}{\tau f_1 (0 \to 21)} = 1.47,$$

which agrees with the theoretical ratio.

Let us further consider the excitation of the rotational Os^{190} levels by β--decay of Re^{190} and K-capture in Ir^{190}. The relevant decay schemes are shown in Fig.1,b. In (3.3) we have given the wave functions of the Os^{190} rotational states. If one assumes that the ground states of Re^{190} and Ir^{190} are approximately characterized by the wave functions φD^2_{m2} and φD^3_{m3}, we can use (4.5) to calculate the ratio of the reduced β-decay (L = 1) and K-capture probabilities to the different rotational levels of Os^{190}. The results of such a calculation[8] are shown in Table 6, where the values are given in units of the reduced probability for decay to the second excited spin 2 level.

Table 6

Ratios of the reduced probabilities for K-capture of Ir^{190} and β-decay of Re^{190}

j	$\frac{B(1;2\to j)}{B(1;2\to 22)}$, $Re^{190}\to Os^{190}$	$\frac{B(1;3\to j)}{B(1;3\to 22)}$, $Ir^{190}\to Os^{190}$
41	0	$6\cdot10^{-4}$
21	$7.6\cdot10^{-3}$	$8\cdot10^{-4}$
61	0	0
42	0	$7.4\cdot10^{-2}$

Table 6 yields a qualitative explanation of the experimental observation that Re^{190} β-decays only to the 22 rotational level, and that K-capture in Ir^{190} excites only the 22 and 42 levels in Os^{190}.

Unfortunately, it is difficult to compare theory with experiment, since the a_K coefficients of (4.1) are not known for the odd-odd parent nuclei. If we had experimental τf_n values for unique β-transitions to the different rotational levels of the daughter nucleus, we could calculate the a_K from (4.5) and (4.2), and thus obtain the wave functions (4.1). This might be of help in understanding the properties of odd-odd nuclei.

5. On the Equilibrium Shape of Even-Even Nuclei

As has been pointed out above, many properties of the first excited states of even-even nuclei, such as the sequence of spins, the energies, and the probabilities of radiative transitions between them, can be understood if one assumes that the equilibrium shape of the nucleus is not axially symmetric. In fact, in view of the experimental data, it must be assumed that the "nonaxiality" parameter γ for some nuclei is ~30°.

The deviation of nuclear shape from axial symmetry requires explanation. In the literature one sometimes comes across insufficiently critical assertions such as "The preference for axial symmetry is also consistent with theoretical estimates of the equilibrium shape for the nuclear shell structure" (Alder et al[5], footnote on p.525). Whenever the theoretical energy minimum corresponds to an axially symmetric nuclear shape, many authors[1,2,35,36] introduce the assumption of axial symmetry into the premises from which they construct their theories. Formally this is equivalent to dropping those parts of the Hamiltonian which are not diagonal in the components of the nucleon angular moments along the nuclear symmetry (z) axis. Thus, in averaging the energy of interaction of the outer nucleons with deformations of the nuclear surface, only nucleon states in which this component of the angular momentum is a good quantum number were included. In other words it was assumed that

$$\sum_i j_{zi} = 0. \tag{5.1}$$

It is of course natural that when one restricts the consideration to the states of outer nucleons which satisfy (5.1) as a supplementary condition, one finds that the equilibrium shape of the nucleus is axially symmetric.

The first indications that nuclei may have nonaxial equilibrium shapes were given in some calculations by Gursky[9], the results of which are described by Wilets and Jean.[10] These calculations showed that the minimum energy of a system consisting of 55 protons and 91 neutrons moving in the field of an ellipsoid with

three unequal axes is obtained when $\beta = 0.04$ and $\gamma = 7.5^\circ$. Independently and in the same approximation, similar calculations were performed by Geilikman[11] for a three-dimensional oscillator potential, and by Zaikin[12] for a square well potential. From these works it became clear that in many cases minimizing the energy of a system of nucleons will lead to a nonaxial nucleus. In spite of the fact that they did not include the spin-orbit interaction and made rather special choices of the form of the potential, the qualitative results obtained by these authors would seem to be incontrovertible.

Filippov and the writer[13] studied the equilibrium nuclear shape using a model of a core formed of a number of nucleons with two additional equivalent nucleons in an outer shell of definite angular momentum j. The energy of the system was calculated as a function of the total angular momentum J of the outer pair and the parameter γ (β was held constant), with the operator giving the interaction of the core and the outer nucleons chosen as

$$H_{int} = \beta T \{\cos\gamma\,(3\hat{J}_z^2 - \hat{J}^2) + \sqrt{3}\sin\gamma\,(\hat{J}_x^2 - \hat{J}_y^2)\}, \tag{5.2}$$

where T is a parameter giving the strength of the interaction.

Our calculation was made for the case in which the outer pair was in the $j = 3/2$ or $5/2$ shell, while Wan Lin performed a similar calculation for $j = 7/2$ and $9/2$. The calculations showed that if the outer pair is in a shell with $j = 1/2$ or $3/2$, the nucleus has an axial equilibrium shape. For $j \geqslant 5/2$ this shape is no longer axial. Figure 4 shows curves of the γ-dependence of the ground-state energy (in units of the energy of the first rotational level) for several values of the dimensionless parameter

$$l = 4\beta T \Big/ \left(\frac{\hbar^2}{B\beta^2}\right), \tag{5.3}$$

which gives the strength of the coupling between the outer pair and the surface deformations.

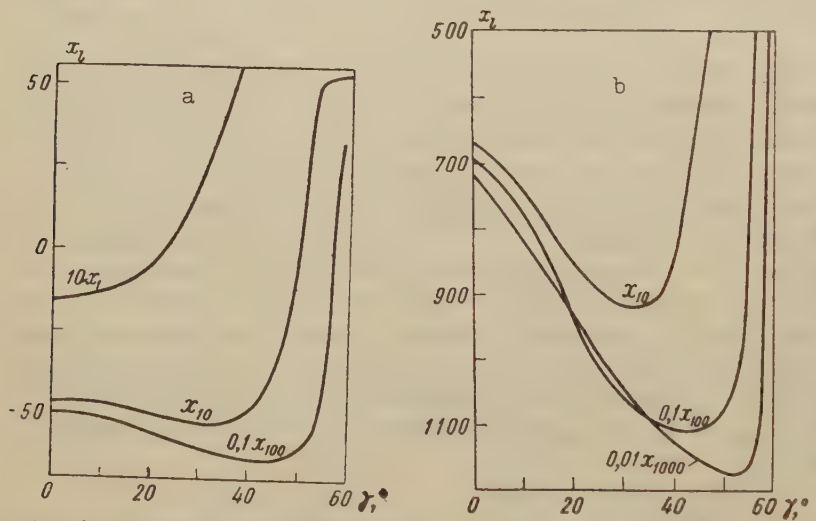

Fig.4. Ground-state energy of even-even nuclei as a function of γ_0 for several values of the strength (given by the parameter l - Eq.(5.3)) of the coupling between the outer nucleon pair and the nuclear surface deformation. The ordinates give the energy in the dimensionless units $x_l = \varepsilon \Big/ \left(\frac{\hbar^2}{B\beta^2}\right)$: a - nucleon pair in $j = 5/2$ shell; b - nucleon pair in $j = 9/2$ shell.

It will be seen from Fig.4 that for $j \geqslant 5/2$ and $l > 1$, the energy minimum gives a nonaxial nucleus. When $l \sim 10$, the energy minimum gives $\gamma_0 \approx 30^\circ$ (maximum nonaxial deformation). As l increases, the nucleus becomes more nearly axially symmetric, with $\gamma_0 \to 60^\circ$ as $l \to \infty$.

The dimensionless coupling constant (5.3) is proportional to the ratio of βT to the energy of the first rotational level of the nucleus. By setting $T \approx 40$ Mev and taking the experimental values for β and the energy of the first rotational level, one can evaluate l for different nuclei and make a qualitative comparison of the theoretical and experimental values of γ_0.

The experimental values of γ_0 are obtained (with an accuracy to the transformation $\gamma_0' \rightleftarrows 60 - \gamma_0$) by use of (2.1). It can be shown in this way that the most strongly deformed nuclei ($27^\circ < \gamma_0 < 33^\circ$) are Pd^{108}, Pd^{106}, Cd^{114}, Te^{122}, Te^{126}, Pt^{192}, Pt^{196} and some others in which the number of protons differs from the magic numbers 50 and 84 by two or four. One finds that with $T \approx 40$ Mev and with β as calculated from Coulomb excitation, the coupling constant l for these nuclei lies between 15 and 80.

For nuclei in which $E_2(2)/E_1(2)$ lies between 20 and 2.9, which corresponds to γ_0 between 10° and 20° or between 50° and 40°, the constant l takes on values from 300 to 600. Finally, for nearly axially symmetric nuclei with $E_2(2)/E_1(2) > 23$ (i.e., $\gamma_0 < 10^\circ$ or $\gamma_0 > 50^\circ$), we obtain $l > 1000$. These numbers show that the curves of Fig.4 explain qualitatively the observed shapes of even-even nuclei. A full quantitative comparison would involve taking into consideration several pairs of inequivalent nucleons outside the core. This we have done[13] only indirectly, through choice of the value of β. It would also be of interest to develop the theory of equilibrium shapes of odd nuclei.

Conclusions

Rotational levels of nonspherical nuclei are one of the most important forms of low-energy collective excitations. These excitations play a significant role in many phenomena, among which are γ-radiation, Coulomb excitation, α- and β-decay, etc. We have here reviewed the work which attempts to explain the properties of rotational levels in even-even nuclei by assuming that the nucleus may not be an ellipsoid of revolution.

The theory of rotational excitations is still in its initial stages of development. There is as yet no such theory for nonaxial odd nuclei. The limits of applicability to rotational states of the adiabatic approximation have not yet been subjected to theoretical analysis. The solution of these problems requires further development of the theory in addition to experimental studies of the intensity of radiative transitions between different excited states, of the probability for Coulomb excitation of rotational levels, of the probability for α- and β-decay to collective states, and determinations of the electric quadrupole moments of nuclei in the ground state and, particularly, in various excited states.

The problem of rotational excitations is closely related to the problem of the nuclear moment of inertia. An axially symmetric nucleus rotates only about an axis perpendicular to its axis of symmetry, so that one may speak of a single moment of inertia determined from the excitation energy of the first excited level. In order to characterize the rotational state of a nonaxial nucleus, one needs to know the position of the first rotational level as well as the energy ratio of the two spin 2 levels.

Very recently Kazarnovskii[37] put forward the interesting idea that the moment of inertia of a nonspherical nucleus, which is evinced in the occurrence of rotational states, is composed in the main of the moment of inertia of the nucleons in the unfilled shells, with a small correction due to the tidal wave induced in the core by these outer nucleons. Just one outer nucleon (or a vacancy in a filled shell) introduces a moment of inertia $M\langle r^2\rangle$, where M is the nucleon mass and $\langle r^2\rangle$ is the mean square distance from the outer nucleon to the axis of rotation. For more than one outer nucleon, $M\langle r^2\rangle$ is multiplied by some effective parameter which becomes unity for one nucleon (or one vacancy), and attains a maximum value when the shell is half filled. The moment of inertia of the core is calculated in the hydrodynamic approximation, in which nuclear matter is treated as an irrotational incompressible fluid.

This simple model seems to be capable of reproducing the basic regularities in the behavior of the moment of inertia as a function of A and Z.

Considerable success in explaining nuclear moments of inertia has also recently been attained as a result of the work of Migdal[38] who has used the methods of superconductivity theory to account in a consistent way for the residual nucleon interaction, which is not included in the usual shell model theory.

References

1. A.Bohr, Dansk.Mat.-Fys.Medd.,26, No.14 (1952); A.Bohr & B.Mottelson, Ibid., 27, No.16 (1953).
2. J.Rainwater, Phys.Rev., 79, 432 (1950).
3. L.Sliv (ed.), Deformatsiya atomnykh yader. (Deformation of atomic nuclei,- translated articles on), L., 1958.
4. P.Stelson & F.McGowan, Phys Rev., 110, 489 (1958).
5. K.Alder, A.Bohr, T.Huus, B.Mottelson & A.Winter, Rev.Mod.Phys., 28, 432 (1956).
6. A.S.Davydov & G.F.Filippov, Zhur.eksp.i teor.fiz., 35.440 (1958) (Trans.- Soviet Phys. - JETP); A.S.Davydov & G.F.Filippov, Nuclear Phys.,8, 237 (1958).
7. A.S.Davydov & V.S.Rostovskii, Zhur.eksp.i teor.fiz., 36, 1788 (1959) (Trans. Soviet Phys. - JETP.)
8. A.S.Davydov, Ibid., 37, 137 (1959) (Trans. JETP).
9. M.Gursky, Phys.Rev., 98, 1205 (1955).
10. L.Wilets & M.Jean, Ibid., 102, 788 (1956).
11. B.T.Geilikman, Zhur.eksp.i teor.fiz., 35, 989 (1958) (Trans. - JETP)
12. D.A.Zaikin, Ibid., 35, 529 (1958).
13. A.S.Davydov & G.F.Filippov, Ibid., 36, 1497 (1959).
14. C.Marty, Nuclear Phys., 1, 85 (1956); Ibid., 3,193 (1957).
15. B.S.Dzhelepov & L.K.Peker, Skhemy raspada radioaktivnykh yader (Decay schemes of radioactive nuclei)., M.-L., 1958.
16. D.Strominger, J.Hollander & G.Seaborg, Table of Isotopes, Revs.Mod.Phys., 30, 585 (1958).
17. R.Diamond & J.Hollander, Nuclear Phys., 8, 143 (1958).
18. K.Jacob, J.Mihelich, B.Harmatz & T.Handley, Bull.Amer.Phys.Soc., 3, 558 (1958).
19. G.Scharf-Goldhaber, D.Alburger, G.Harbottle & M.McKeown, Ibid.,2,25 (1957).
20. A.G.Aten, G.deFeyfer, M.Sterk & A.Wapstra, Physica, 21,740,990 (1955).
21. A.S.Davydov & D.A.Zaikin, Zhur.eksp.i teor.fiz., 36,233 (1958) (Trans.JETP)
22. M.Jean & J.Touchard, J.Phys.et radium, 19, 56 (1958).
23. O.Nathan & M.Waggoner, Nucl.Phys., 2, 548 (1956/57).
24. R.Waddell & E.Jensen, Phys.Rev., 102, 816 (1956).
25. D.G.Alkhazov, A.P.Grinberg, M.G.Gusinskii, K.I.Erokhina & I.Kh.Lemberg, Zhur.eksp.i teor.fiz., 35, 1325 (1958). (Trans. JETP)
26. G.Alaga, F.Boehm, P.Marmier & J.DuMond, Dansk.Mat.-Fys.Medd.,29,9 (1955).
27. F.Boehm, P.Marmier & P.DuMond, Phys.Rev., 95, 864 (1954).
28. J.Murray, F.Boehm, P.Marmier & J.DuMond, Ibid., 97, 1007 (1955).
29. F.McGowan, Report presented at the International Congress on Nuclear Physics, Paris, 1958.
30. A.S.Davydov & G.F.Filippov, Zhur.eksp.i teor.fiz., 35,703 (1958) (Trans. (JETP)
31. A.S.Davydov, Ibid., 37, 137 (1959).
32. A.S.Davydov, Teoriya atomnogo yadra (Theory of the atomic nucleus), 1958.
33. J.Davidson, Phys.Rev., 82, 48 (1951).
34. D.Guss, L.Killion & F.Porter, Ibid., 95, 627 (1954).
35. K.Ford, Ibid., 90, 29 (1953).
36. S.Nilsson, Dansk.Mat.-Fys.Medd., 29, No.16 (1955).
37. M.V.Kazarnovskii, Present issue of the Bulletin, p. 899.
38. A.B.Migdal, Zhur.eksp.i teor.fiz.,37, 245 (1959). (Trans. JETP)

CONVERSION ELECTRONS FROM Yb^{166} AND Tm^{166}

V.Barbets, K.Ya.Gromov, B.S.Dzhelepov, A.G.Dmitriev & V.A.Morozov

The spectrum of conversion electrons emitted in the decay series

$$Yb^{166} \xrightarrow[60\ hr]{EC} Tm^{166} \xrightarrow[7.7\ hr]{EC} Er^{166}\ (stable)$$

was investigated on a Ketron type (enhanced focusing, magnetic) β-spectrometer. The resolution of the instrument was ~0.5%; the transmission ~0.4% of 4π. The Yb^{166} and Tm^{166} were obtained by spallation of tantalum. To this end a tantalum target was bombarded with 660 Mev protons in the Joint Institute for Nuclear Research synchrocyclotron for 3-4 hours. The chemical operations, namely, extraction of the group of rare earths from the tantalum and chromatographic (ion exchange) separation of the rare earths, were carried out some 10-15 hours later in Leningrad.

1. Conversion electrons from Tm^{166}

In view of the fact that Tm^{166} is a daughter of Yb^{166}, it appeared not only in the thulium fraction of the rare earths but also sometime after the ion exchange separation in the ytterbium fraction. Thus we had available three types of sources for investigating the Tm^{166} conversion spectrum:

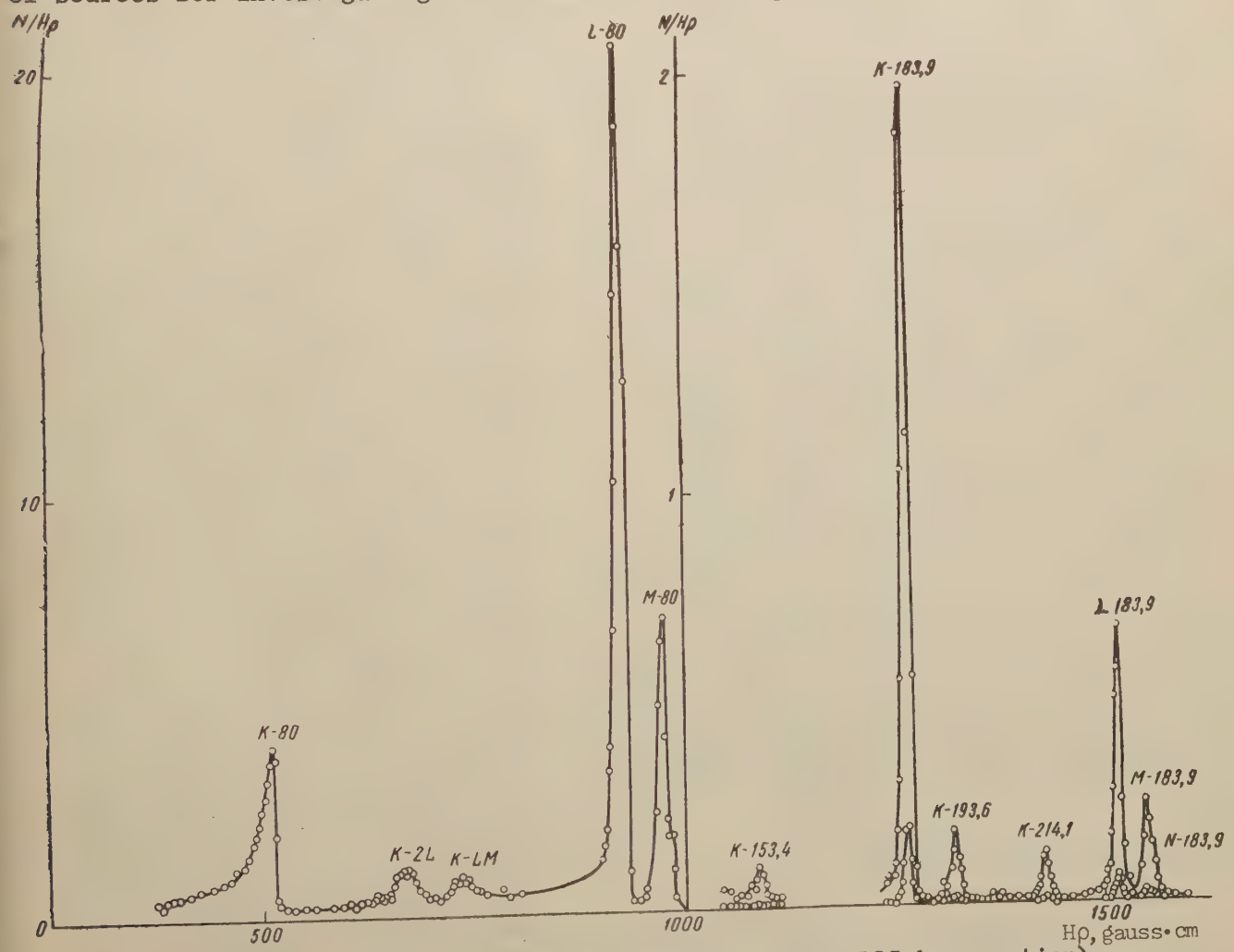

Fig.1. Tm^{166} conversion electron spectrum (10 to 185 kev section).

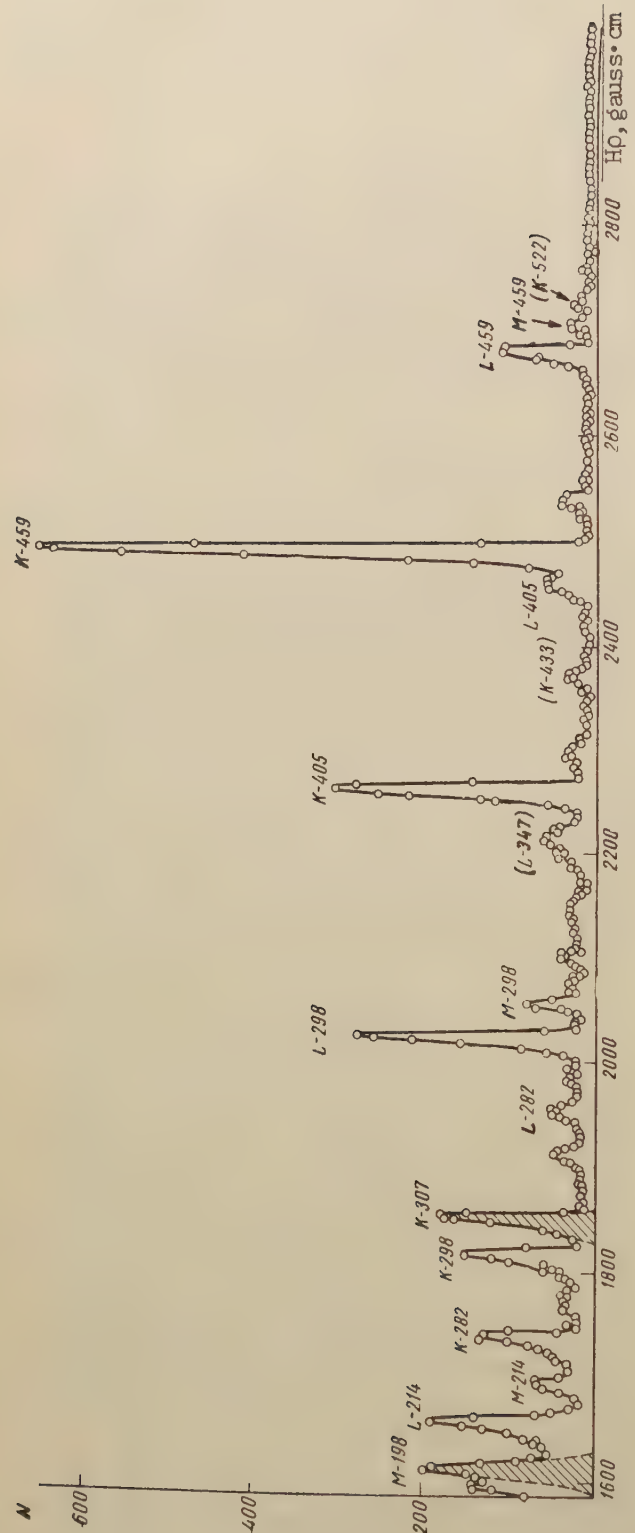

Fig.2. Tm^{166} conversion electron spectrum (200 to 500 kev section). The hatched lines pertain to Yb^{169}.

1. Thulium fraction - the thulium obtained by chromatographic separation of the rare earths extracted from the tantalum target. In this sample there were present all the isotopes of thulium forming in the reaction on tantalum: 7.7 hour Tm^{166}, 29 hour Tm^{165} and 9.6 day Tm^{167}. Tm^{168} with a period of 80 days is also formed in this reaction, but since the formation rate is low we did not observe electrons from Tm^{168} in the sources produced by 3-4 hour proton bombardment.

Off hand it would seem that in view of the short half-life of Tm^{166} there should be no difficulty in distinguishing its conversion electron lines from those of the other thulium isotopes; however, the problem is made somewhat more difficult than it would appear by the complexity of the conversion electron spectrum of Tm^{165}.

2. Ytterbium fraction - the ytterbium species obtained by chromatographic separation of the rare earth elements. In the electron spectrum of this material there were detected the conversion electron lines of two ytterbium isotopes: 60 hour Yb^{166} and 30.6 day Yb^{169}. The time to attainment of Yb^{166}—Tm^{166} equilibrium is about 20 hours. In investigating the ytterbium-thulium mixture, however, there is little difficulty in identifying and subtracting the Yb^{169} lines inasmuch as the conversion electron spectrum of Yb^{169} is well known, while the period of Yb^{166} differs appreciably from that of Yb^{169}, on the one hand, and the Tm^{166}, on the other.

3. Thulium activity - the material extracted from the ytterbium fraction approximately 20 hours after chromatographic separation, i.e., after attainment of equilibrium of the Yb^{166} + Tm^{166} mixture. This activity contains virtually pure Tm^{166}, since the decay product of Yb^{169} is stable Tm^{169}.

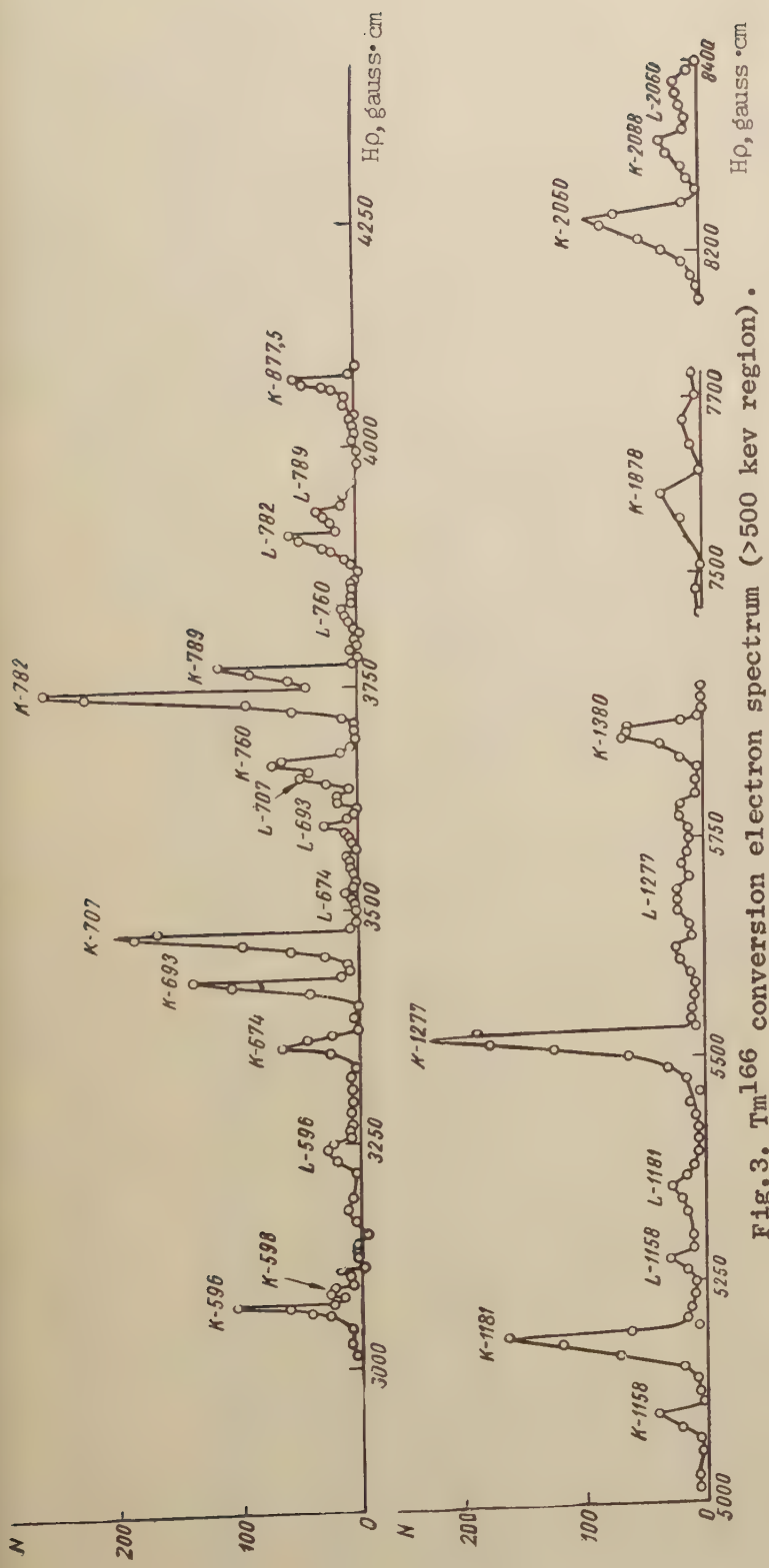

Fig.3. Tm^{166} conversion electron spectrum (>500 kev region).

The experimental results obtained for the conversion electron spectrum of Tm^{166} are summarized in Table 1. It will be evident from the table that the most complete spectrum was obtained in investigating the ytterbium fraction. This is due to the fact that the intensity of the Tm^{166} conversion lines falls off here with the period of the parent substance (60 hr) and hence this source is more convenient for studies of the present type. The conversion electrons detected in investigating the ytterbium fraction can belong to either Tm^{166} or Yb^{166}. One can attribute a given conversion line with certainty to Tm^{166} only if the same line is detected in investigating at least one of the other two sources; in case it is detected in the thulium fraction, it is also essential to know that it does not belong to Tm^{165}, i.e., that its period is 8 hours rather than 29 hours. There are other considerations which can be utilized for solving the assignment problem. For example, Gorodinskii et al[1] investigated the γ-spectrum of the ytterbium fraction immediately after separation of thulium from it and established that the ytterbium fraction does not have γ-rays with $E_\gamma > 300$ kev (the energy of the hardest Yb^{169} γ-rays is 308 kev). The value of these results, however, depends on quantitative evaluation of the intensity bounds for γ-rays with $E_\gamma > 300$ kev. Unfortunately, Gorodinskii et al made no such evaluation. In order to be safe in attributing conversion electrons in the 500 to 800 kev region to Tm^{166} one must be sure that the limiting intensity of the Yb^{166} γ-rays in this region does not exceed 0.005 of the Yb^{166} 81 kev γ-ray intensity (see below). One can arrive at

Table 1

Experimental data on the conversion electrons of Tm^{166}

No.	Tm fraction		Yb fraction		Pure Tm^{166}		Averages		Identification
	E_e, kev	Relat. intens.	E_e, kev	Relat. intens.	E_e, kev	Relat. intens.	E_e, kev	Relat. intens.	
1					22,5	16	22,5	16	*K*-80,0
2					36	2,2	36	2,2	*K*—2*L*
3					45	1,1	45	1,1	*K*—*LM*
4					70,4	36	70,4	36	*L*-80,0
5					77,6	9,9	77,6	9,9	*MM*-80
6					79,2		79,2		*N*-80
7			96,2	0,10	95,6	0,08	95,9	0,09	*K*-153,4
8	126,9	2,20	126,3	2,15	126,2	2,26	126,4	2,2	*K*-183,9
9					136,1	0,24	136,1	0,24	*K*-193,6
10			157,9	0,10	156,6	0,18	157,2	0,14	*K*-214,1
11			173,8	1,00	173,8	1,00	174,6	1,00	*L*-183,9
12			182,6	0,35	180,7	0,33	181,6	0,34	*M*-183,9
13					182,2		182,2		*N*-183,9
14			205,5	0,025			205,5	0,025	*L*-214
15			212,7	0,010			212,7	0,010	*M*-214
16			224,4	0,019			224,4	0,019	(*K*-282)
17			241,3	0,017			241,3	0,017	*K*-299
18			289,2	0,022			289,2	0,022	(*L*-299 *K*-347)
19			295,1	~0,006			295,1	~0,006	*M*-299
20			336	0,009			336	0,009	(*L*-347)
21			347,5	0,022			347,5	0,022	*K*-405
22			~375	~0,010			~375	~0,010	(*K*-433)
23			~394	~0,003			~394	~0,003	*L*-405
24	403,4		401,9	0,060	400,7	0,058	402,0	0,059	*K*-459,5
25			449,7	0,012			449,7	0,012	*L*-459,5
26			~458,1	~0,003			~458,1	~0,003	*M*-459
27			~464	~0,003			~464	~0,003	(*K*-522)
28	535,0		538,7	0,022			538,7	0,022	*K*-596
29	538,7		542,8	0,006			540,8	0,006	*K*-598
30			548,9	0,003			548,9	0,003	
31			585,9	0,008			585,9	0,008	*L*-596
32	617,5		616,2	0,017			616,8	0,017	*K*-674,3
33	635,7	0,040	635,7	0,032			635,7	0,032	*K*-693
34	650,5	0,052	649,4	0,053			649,9	0,053	*K*-707
35			662,9	0,001			662,9	0,001	*L*-674
36			683,3	0,006			683,3	0,006	*L*-693
37			691,4	0,004			691,4	0,004	(*K*-749)
38			698,1	0,009			698,1	0,009	*L*-707
39	705,2		702,7	0,017			702,7	0,017	(*K*-760)
40	725,6	0,079	723,4	0,059			724,5	0,059	*K*-782
41	731,6		731,4	0,026			731,5	0,026	*K*-789
42			750,0	0,004			750,0	0,004	*L*-760
43			771,9	0,015			771,6	0,015	*L*-782
44			779,6	0,006			779,6	0,006	*L*-789
45			820,4	0,012			820,4	0,012	*K*-877,5
46			1100,5	0,005			1100,5	0,005	(*K*-1158)
47	1121,2	0,027	1125,2	0,027			1124	0,027	*K*-1181
48			1150,9	0,003			1151	0,003	(*K*-1209)
49			1173,4	0,002			1173	0,002	*L*-1181
50	1218,0	0,036	1224	0,040			1220	0,038	*K*-1277
51			1252	—0,002			1252	0,002	(*K*-1309)
52			1272	0,002			1272	0,002	*L*-1277
53	1319,7	0,015	1323,6	0,012			1322	0,013	*K*-1380
54			1366	0,002			1366	0,002	(*K*-1423)
55			1820,6	0,008			1820,6	0,008	(*K*-1878)
56	2001,3	0,012	2004	0,017			2003	0,015	*K*-2060
57	2029	0,005	2031	0,006			2030	0,006	*K*-2088

analogous inferences utilizing the Yb^{166}-Tm^{166} mass differences following from Levy's empirical formulas[2] (436 kev) and Cameron's semi-empirical formula[3] (117 kev). The uncertainty in these formulas is very great (400 kev), nevertheless it may be assumed that no hard γ-rays are emitted in the decay of Yb^{166}. We therefore accept it as a fact that no γ-radiation except the 81 kev γ-rays are emitted in the $Yb^{166} \rightarrow Tm^{166}$ decay process.

Fig.1 shows the conversion electron spectrum of Tm^{166} in the region from 10 to 185 kev based on measurements of the thulium source extracted from the ytterbium fraction. The intensity of all the lines shown in Fig.1 fell off with a period of about 8 hours. Investigation of this section of the spectrum in the radiation from the thulium and ytterbium fractions was hampered by the presence of intense lines due to the other isotopes. Fig.2 shows the Tm^{166} spectrum in the region from 200 to 500 kev; Fig.3 - the conversion spectrum in the region above 500 kev. This section of the spectrum could be investigated properly only with the ytterbium fraction source.

Table 2

Comparison of the experimental K/L ratios with the theoretical ones for different multipole orders

E, kev	$K/L_{exp.}$	$K/L_{theo.}$						Multipole order assignments
		E1	*E2*	*E3*	*M1*	*M2*	*M3*	
80,0	0,45±0,05	7,0	0,42	0,27	7,2	3,8	0,66	*E2* *
153,4	>3	6,6	1,6	0,33	6,4	4,5	1,9	*E1*; (*M1*+*E2*); *M2*
183,9	2,2±0,2	6,7	2,0	0,53	6,6	4,4	2,4	*E2* *
214,1	6±0,1	6,5	2,4	0,7	7,1	4,4	2,8	*E1*; (*M1*+*E2*)
459,3	5±1	6,9	4,6	3,2	6,8	5,9	4,2	*E1*; (*M1*+*E2*) (*M2*+*E3*)

*Multipole orders unambiguously assigned in Table 3.

Table 3

Comparison of the relative K, $L_I + L_{II}$ and L_{III} conversion line intensities with the theoretical values for different multipole orders

$K:L_I+L_{II}:L_{III}$	80 kev	183.9 kev
Experimental		
Our data	87:(193)*	364 : (166) *
Ref.5	23 : 100 : 98	330 : 100 : 66
Ref.6	110 : 100 : 103	—
Ref.7	119 : 100 : 110	—
Calculated		
E1	890 : 100 : 27	780 : 100 : 16
E2	83 : 100 : 93	300 : 100 : 50
E3	5,3 : 100 : 99	84 : 100 : 58
M1	730 : 100 : 1,2	670 : 100 : 1,1
M2	500 : 100 : 2,8	490 : 100 : 10
M3	136 : 100 : 120	35 : 100 : 40

*Figures in ( ) are the integral $L_I + L_{II} + L_{III}$ intensities.

In working with the thulium sources we succeeded in detecting only the most intense conversion lines. Hence there can be no doubt that the most intense lines in this section belong to Tm^{166}. (In view of the reasons adduced above, we believe it highly probable that all the other lines in this region also belong to Tm^{166}.)

In view of the results of our measurements of the conversion electron spectrum of the equilibrium Yb^{166} + Tm^{166} mixture, it may be safely asserted that the intensity of any conversion lines in the 820 to 1100, 1350 to 1820 and 2100 to 3000 kev intervals does not exceed 0.002 (in the units of Table 1).

The experimental K/L conversion line ratios are compared with the theoretical ratios for different multipole orders in Table 2. The theoretical values were calculated from the tables of Sliv & Band[4]. It will be evident from Table 2 that the experimental K/L ratios for the 80.0 and 183.9 kev γ-transitions are close to the theoretical ratios for E2 transitions. A number of investigators[5-7] give reliable data on the relative intensities of the $(L_I + L_{II})$ and L_{III} conversion lines. Comparison of all the available experimental data with the theoretical conversion coefficients leads to the unambiguous multipole order assignments for these transitions listed in Table 3.

The most probable assignments for the other γ-transitions are shown in the last column of Table 2.

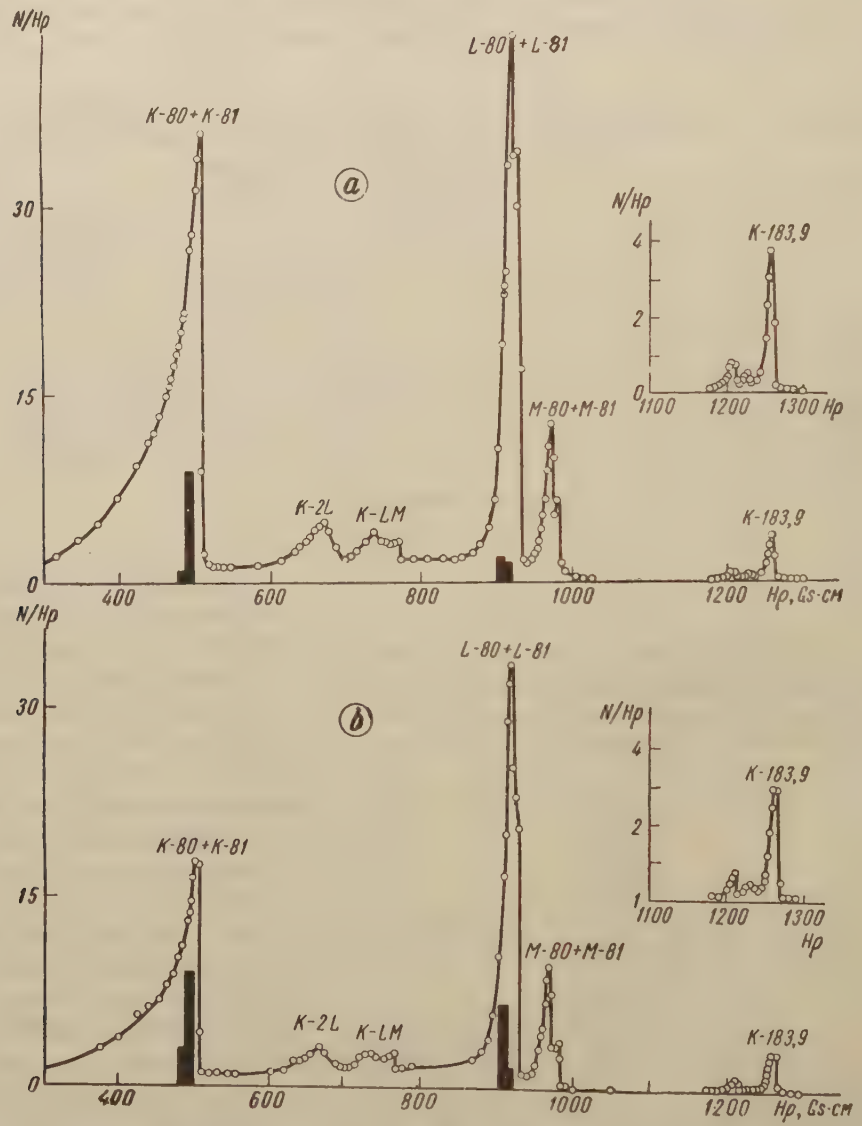

Fig.4. Conversion electron spectrum of Yb^{166}: a) 1 hour after extraction of Tm^{166} from the Yb^{166} sample; b) after attainment of Yb^{166}-Tm^{166} equilibrium (i.e., about 60 hours after chromatographic separation). The solid columns indicate the relative intensities of the conversion electron lines.

2. Conversion electrons from Yb^{166}

In investigating the conversion electron spectra of the ytterbium fraction and the pure Tm^{166} sample we discovered that the intensity ratio of the K and L conversion lines associated with the 80 kev γ-transition differed appreciably in the two cases. Baranovskii & Pokrovskii[8] investigated the γ-spectrum of the ytterbium fraction immediately after separation of thulium from it and established that γ-rays with an energy of about 80 kev are emitted in the decay of Yb^{166}.

Grigor'ev et al[6] investigated the conversinn lines associated with γ-transitions of about 80 kev energy appearing in the decay of Yb^{166} and Tm^{166}. They employed a double-focusing β-spectrometer with an instrument line half-width of 0.3%. The higher resolution of their instrument, as compared with ours, enabled Grigor'ev et al to resolve the structure of the integral L line associated with the ~80 kev γ-transitions in Yb^{166} and Tm^{166} and thus establish the precise energies of these γ-transitions. They found that the energy of the transition occurring in the $Yb^{166} \rightarrow Tm^{166}$ decay is 81.0 ± 0.2 kev; that of the transition in the $Tm^{166} \rightarrow Er^{166}$ is 79.4 ± 0.2 kev.

In order to determine the relative intensities of the K and L conversion lines of the 81.0 kev transition in Tm^{166}, we followed the variation in the intensity of the conversion lines in the spectrum of the ytterbium fraction in the interval from 10 to 150 kev, starting 1 hour after separation of the daughter thulium.

In all we carried out eight series of measurements over a period of approximately 60 hours. The spectra obtained in the first and last series are shown in Fig.4. It was established that the intensity of the K line associated with the 183.9 kev transition in Tm^{166} (see Table 1) increases in accord with the rate of build-up of Tm^{166} from Yb^{166}. In view of this it may be asserted that the K-183.9 kev line is due solely to Tm^{166}. Utilizing the intensity of this line and the data on the relative intensities of the Tm^{166} conversion electrons from Table 1, we could determine the relative intensities of the Yb^{166} lines at any instant. The mean value (average for the eight series of measurements) of the K/L ratio for the 81.0 kev γ-transition is 5.8 ± 0.5. The extreme values, obtained in the first and sixth series were 5.2 and 6.8, respectively.

Our K/L value is in good agreement with the data of Grigor'ev et al[6] (6.3 ± 2) and closest to the theoretical ratio for E1 and M1 type transitions. In the work of Grigor'ev et al the multipole order of this transition was established unambiguously as M1 from the $(L_I + L_{II})/L_{III}$ ratio.

The relative intensities of the conversion electrons associated with the 79.4 and 81.0 kev transitions in the equilibrium Yb^{166} + Tm^{166} mixture are the following (in units of Table 1):

Tm^{166}		Er^{166}	
K-81.0	49	K-80.0	16
K - 2L	2.7	K - 2L	2.2
L-81.0	8.3	L-80.0	36
		K-183.9	2.2

Nervik & Seaborg[9] measured the energies of th γ-rays accompanying $Yb^{166} \rightarrow Tm^{166} \rightarrow Er^{166}$. Gorodinskii et al[1] established that all these γ-rays, except the 110 and 140 kev γ-rays, follow the decay of Tm^{166}. We did not detect any conversion electrons associated with the 110 and 140 kev γ-transitions. The upper bound for the intensity of the L-110 line referred to the intensity of the K-80 line is 0.2%; the upper bound of the intensity of the L-140 line is 0.5%.

3. Intensity of the K - 2L Auger electrons

As will be evident from an examination of Figs.1 & 2 there are no conversion lines in the region of the K - 2L Auger peak in the conversion spectra of Tm^{166} and Yb^{166}. Hence one can evaluate the intensity of the K - 2L Auger electrons. The evaluation is hampered somewhat by the extended slope of the L lines associated with the 80 and 81 kev transitions, but the error in evaluating the K - 2L Auger intensity probably does not exceed 50%.

Comparison of these data with the x-ray intensity gives us the Auger yield. The yield of K - 2L Auger electrons is ~2.7 ± 1.4%. Bearing in mind that the K - 2L Auger yield accounts for about 60% of the total yield of K Auger electrons (Ref.10), we obtain a value of 4.5 ± 2.2% for the total K Auger effect yield. This value is consistent with the data on the Auger effect in this region (~6.5%) given in the literature[11,12].

"V.G.Khlopin" Radium Institute,
Academy of Sciences of the USSR

References

1. G.M.Gorodinskii, A.N.Murin, V.N.Pokrovskii & B.K.Preobrazhenskii, Izv.AN SSSR,Ser.fiz., 21, 1624 (1957).(Trans. Bulletin 21, No.10, 1611.)
2. Table of Levy's Empirical Atomic Masses, CRP-654, Chalk River, 1956.
3. A Revised Semi-Empirical Atomic Masses Formula, CRP-690, Chalk River,1957.
4. L.A.Sliv & I.M.Band, Tablitsy koeffitsientov vnutrennei konversii γ-luchei (Tables of internal conversion coefficients), Part I - K-shell; Part II - L-shell M.-L., 1957-58.
5. J.W.Mihelich & B.Harmatz, Phys.Rev.,106, 1232 (1957).
6. E.P.Grigor'ev, A.V.Zolotavin & B.S.Dzhelepov, Izv.AN SSSR,Ser.fiz., 23, 188 (1959).(Trans. Bulletin 23, No.2, 180.)
7. J.M.Cork, M.K.Brice, K.G.Helmer & R.M.Woods, Phys.Rev.,110,526 (1958).
8. V.I.Baranovskii & V.N.Pokrovskii, Present issue of the Bulletin, p.813.
9. W.Nervik & G.Seaborg, Phys.Rev., 97,1092 (1955).
10. B.S.Dzhelepov, B.K.Preobrazhenskii & V.L.Sergienko, Izv.AN SSSR,Ser.fiz., 22, 795 (1958).(Trans. Bulletin 22, No.7, 789.)
11. K.Siegbahn (ed.), Beta- and Gamma-Ray Spectroscopy, Amsterdam, 1955.
12. J.Laberrique-Frolow & P.Radvanyi, Phys.et radium, 17,944 (1956).

GAMMA-SPECTRUM OF Tm^{166} AND Yb^{166}

- V. I. Baranovskii & V. N. Pokrovskii

As part of our study of the rare earth products of spallation of tantalum under bombardment by 660 Mev protons, we investigated the genetic series $Yb^{166} \xrightarrow{EC} Tm^{166} \xrightarrow{EC} Er^{166}$. We employed the scintillation technique described in Ref.1.

Even in the first experiments[1] it became apparent that there is a great similarity between the spectra of the Yb^{166} + Tm^{166} mixture and pure Tm^{166}, separated by the ion exchange procedure from the Yb fraction. Measurements showed that these γ-spectra consist of lines with the following energies: 80, 153 (weak), 190 (group), 400-600 (series of weak lines), 690, 780, 1180, 1280, 1380, 1880 and 2060 kev. Inasmuch as the energies of these lines and their relative intensities in the >100 kev regions of the spectra of Yb^{166} + Tm^{166} and pure Tm^{166} virtually coincide, it may be inferred that Yb^{166} has no noticeable lines in this region, or if Yb^{166} does have such γ-lines, their energies are virtually identical with the energies of the Tm^{166} γ-rays and their intensity is at least 10-20 times lower than the intensity of the corresponding Tm^{166} γ-lines. The fact that Yb^{166} emits no γ-rays with $E_\gamma > 100$ kev is consistent with the Yb^{166}-Tm^{166} mass difference, which is estimated to be 436 ± 300 kev (Ref.2) or 117 ± 300 kev (Ref.3).

The relative intensity of the 80 kev γ-line in the spectrum of Yb^{166} + Tm^{166} proved to be higher than in the spectrum of pure Tm^{166}; hence it was natural to assume that Yb^{166} does have a γ-line of approximately this energy. To check this we carefully followed the variation in the intensity of the ~80 kev line and the 190 kev group in the spectrum of a Yb source purified of Tm prior to measurement. In processing the experimental results, we kept in mind that in addition to Yb^{166} a certain amount of Yb^{169} was present in the ytterbium fraction. Resolution of the intensity variation curves for the 80 and 190 kev γ-lines showed that the 190 kev γ-group is due exclusively to build up of Tm^{166} (not over 5% of the intensity of this line group can be attributed to Yb^{166}), whereas the 80 kev line is due to the activity of both Tm^{166} and Yb^{166}. The relative intensity of the 80 kev γ-transition in Yb^{166} is 1.5 ± 0.2 times higher than the intensity of the 80 kev transition in Tm^{166}.

We note that according to our experimental data the half-life of Yb^{166} is 56 ± 1 hour (Nervik & Seaborg[4] report 53.8 hours; Michel & Templeton[5] - 58 ± 1 hours). Our data on the γ-spectrum of Tm^{166} are in excellent agreement with the data on the conversion electron spectrum of this isotope reported by Brabets et al[6]. It should be noted that in the γ-spectrum of Tm^{166} there also appear diffuse lines with energies of ~1.0 and ~1.6 Mev. They presumably have a secondary origin and are due to pair production by the ~2060 kev gammas.

Using our data on the shape of the γ-lines and the efficiency of our crystal in detecting γ-rays of different energies, we carried out a resolution of the Tm^{166} γ-spectrum into individual components and calculated their relative intensities. In the process, however, a number of close line groups (for example, the 780 kev group consisting of lines at 760, 782 and 789 kev) were not resolved into individual components. The results are summarized in the table.

Energies and relative intensities of Tm^{166} γ-lines

E_γ, kev	48	80	153	184	194	215	450	524	596	690	780	1180	1280	1380	1880	2060
I_γ (x)	102	10	0.7*	13	~3	5	8	~5	11	30	40	17	27	12	8	40

*Upper bound

The resolution is hampered to some extent by the complexity of the γ-spectrum, so that the uncertainty in determining relative intensities varies from 10% (in the most favorable cases) to 20%. Owing to these difficulties we were unable to evaluate the intensities of the γ-lines in the region from 280 to 400 kev, although Brabets et al[6] list the energies of a number of lines in this region. Here we can only note that the intensities of these γ-transitions are at least one order of magnitude lower than the intensity of the 184 kev transition.

We acknowledge our gratitude to A.N.Murin for his interest in the work and valuable suggestions in discussing the results, and B.K.Preobrazhenskii and A.V. Kalyamin for carrying out the chromatographic separations.

"V.G.Khlopin" Radium Institute,
Academy of Sciences of the USSR &
Joint Institute for Nuclear Research

References

1. G.M.Gorodinskii, A.N.Murin, V.N.Pokrovskii & B.K.Preobrazhenskii, Izv.AN SSSR,Ser.fiz., 21, 1004 (1957).(Trans. Bulletin 21, No.7, 1005.)

2. J.Riddel, A Table of Levy's Empirical Atomic Masses, CRP-654, Chalk River, 1956.

3. A Revised Semi-Empirical Atomic Masses Formula, CRP-690, Chalk River, 1957.

4. W.Nervik & G.Seaborg, Phys.Rev., 97, 1092 (1955).

5. M.Michel & L.Templeton, Ibid., 93, 1422 (1954).

6. V.Brabets, E.Gromov, B.Dzhelepov, A.Dmitriev & V.Morozov, Present issue of the Bulletin, p.805.

ON THE DECAY SCHEME OF Tm^{166}

- K.Ya.Gromov, B.S.Dzhelepov & V.N.Pokrovskii

1. Multipolarities of the Transitions in Er^{166}

Experimental data on the radiations accompanying the decay of Tm^{166} will be found in Refs.1 & 2 (the preceding two articles). In column 1 of Table 1 herewith we list the energies of the γ-transitions identified in investigating the conversion electron spectrum. Where the identification is doubtful the energies are listed in parentheses. In column 2 we list the relative intensities of the K conversion electrons in the units of Ref.1, i.e., referred to $I_{L-183.9}$ taken as unity. In column 3 we list the γ-ray intensities in units chosen so that the K and L conversion coefficients of the 80 kev transition would correspond to the theoretical coefficients for an E2 type transition (this assignment is made unambiguously in Ref.1). From the data of Table 1 we can readily calculate the K conversion coefficients for a number of the transitions, and then comparing these experimental values with the theoretical ones, determine the multipole orders of these transitions.

The experimental value of α_K for the 183.9 kev transition agrees with the theoretical value for E2. This substantiates the assignment made in Ref.1 for this transition.

Table 1

Experimental data on the radiations accompanying the decay of Tm^{166}

E_γ, kev	Relative intensities experimental: K electrons (I_γ)	Relative intensities experimental: γ-rays (I_γ)	Relative transition intensities in our scheme	α_K, experimental	α_K, theoretical: E1	α_K, theoretical: E2	α_K, theoretical: M1	Multipole order assignment	Transition intensity in % per decay
x-rays	—	92	—	—	—	—	—	—	102
80,0	16	9	—	1,78	0,52	1,78	5,0	$E2$	78
153,4	0,09	<0,6	—	0,15	0,089	0,35	0,71	$M1+E2$, $M2$	—
183,9	2,2	11,5	—	0,19	0,054	0,199	0,43	$E2$	17
193,6	0,24	2,6	—	0,09	0,048	0,17	0,37	$E1$, $E2$	—
214,1	0,14	4,7	—	0,03	0,035	0,13	0,29	$E1$	5,5
282	0,019	—	0,3	—	0,018	0,061	0,12	—	0,33
299	0,017	—	—	—	0,016	0,052	0,12	—	—
347	—	—	—	—	0,011	0,033	0,079	—	—
405	0,022	—	—	—	0,0074	0,022	0,051	—	—
433	0,010	7,4	—	—	0,0065	0,019	0,043	—	8
459	0,059		—	—	0,0056	0,016	0,037	($E1$)	
522	0,003	—	0,2	—	0,0044	0,012	0,028	—	0,30
596	0,022	10	9,0	0,0024	0,0032	0,0083	0,019	($E1$)	10
598	0,006		0,7	—	0,0032	0,0083	0,019	—	0,8
674	0,017	27	12,5	0,0013	0,0025	0,0063	0,014	($E1$)	14
693	0,032		5,3	—	0,0023	0,0060	0,013	—	5,9
707	0,053		9,2	—	0,0022	0,0057	0,013	—	10,2
749	0,004	18	18	0,0012	0,0020	0,0050	0,011	($E1$)	20
760	0,017				0,0020	0,0049	0,010		
782	0,059	36	12,5	—	0,0019	0,0047	0,0095	—	14
789	0,026	—	5,7	—	0,0018	0,0046	0,0093	—	6,4
(807)	(0,003)	—	0,7	—	—	—	—	—	0,8
877	0,012	—	3,5	—	0,0015	0,0034	0,0071	—	3,9
(1158)	0,005	15	—	—	—	—	—	—	17
1181	0,027		—	0,002	0,00088	0,0021	0,0036	$E2$; $M1+E2$	
(1209)	0,003	—	—	—	—	—	—	—	
1277	0,038	24	—	0,0016	0,00076	0,0018	0,0030	$E2$; $M1+E2$	26
(1309)	~0,002	—	—	—	—	—	—	—	—
1380	0,013	11	—	0,0012	0,00067	0,0015	0,0025	$E2$; $M1+E2$	12
(1423)	~0,002	—	—	—	—	—	—	—	—
1878	0,008	8	—	0,0010	0,00040	0,00086	0,0012	$E2$; $M1+E2$	9
2060	0,015	36	—	—	0,00034	0,00071	0,00092	—	40
2088	0,006		—	—	0,00033	0,00070	0,00091	—	

Evaluation of the experimental value of α_K (>0.15) for the 153.4 kev transition indicates that the E1 possibility listed in Ref.1 can be excluded; we are therefore left with the alternatives (M1 + E2) and M2.

The multipole order of the 214.1 kev transition is undoubtedly E1. The 459 and 596 kev transitions are also probably E1.

The experimental conversion coefficients for the 1181, 1277,1380 and 1878 kev transitions are in good agreement with the theoretical values for E2 type transitions. Apparently, the multipole orders of these γ-transitions are either E2 or (M1 + E2).

Multipole order assignments for the other γ-transitions cannot be made in this way, inasmuch as the complexity of the Tm^{166} γ-spectrum precludes accurate determination of the intensity of all the γ-lines.

2. Absolute Gamma- and Conversion Line Intensities

On the basis of the x-ray intensity, taken from Ref.2 and listed in Table 1, we can calculate the total number of orbital electron captures in Tm^{166}. Taking into account the fluorescence yield in erbium (0.93) and the total intensity of all the conversion lines and assuming the L to K capture ratio to be 0.13 (allowed capture), we obtain a value of 90 ± 13 (in the units of Table 1) for the total intensity of orbital electron capture. Wilkinson & Hicks[3] established that the decay of Tm^{166} is accompanied by the emission of positrons. The end point of the β^+-spectrum is 2.1 Mev. According to these authors, the positron intensity is low, namely, 0.5% of the number of disintegrations. This value is substantially lower than the uncertainty in the deduced number of orbital electron captures. Hence we shall assume hereinafter that the figure 90 ± 13 characterizes the total disintegration intensity (in $I_{L-183.9} = 1$ units). Hence to obtain the numbers of electrons and photons per disintegration one must divide the values for I_K and I_γ listed in Table 1 by 90 ± 13.

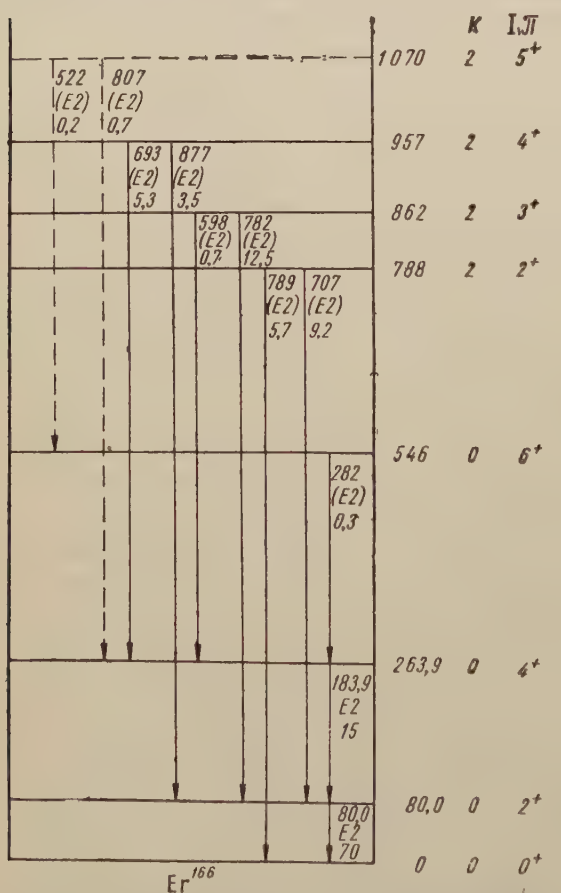

First and second rotational bands of Er^{166}

3. The Two Rotational Bands of Er^{166}

The first diagram of the levels in Er^{166} excited in the decay of Tm^{166} was published by Dzhelepov & Peker[4]. Jacob et al[5] reported that in the decay of Tm^{166} there are also populated levels comprising a second rotational band: 788(2+), 862(3+) and 957(4+) kev. The experimental data obtained in the present investigation allow of refining the decay scheme for Tm^{166}.

A. Levels of the ground state rotational band

It was established in investigating β^--decay of Tm^{166} that the 80.0 kev γ-transition determines the height of the first excited level in Er^{166}: 80.0 kev (2+). Obviously, this is the first level of the rotational band based on the ground state of Er^{166}. The height of the second level (4+) is determined by the 183.9 kev γ-transition. As was shown above, the 80.0 and 183.9 kev

transitions are E2. The energy of the second level is 263.9 kev. Knowing the energy of two excited levels in the ground state rotational band, we can calculate the parameters in the following formula for the energy of rotational band levels

$$E = E_0 + A[I(I+1) - K(K+1)] - B[I(I+1) - K(K+1)]^2. \quad (1)$$

Calculations yield A_1 = 13.37 kev and B_1 = 0.0082 kev. These values of the constants are close to the corresponding values for neighboring even-even nuclei.[6]

The energy of the 6+ level calculated by means of Eq.(1) using the above values for A_1 and B_1 comes out to be 547.5 kev. If we assume that the 282 kev transition listed in Table 1 is a transition from the 6+ level to the 4+ level, we obtain a value of 545.9 kev for the energy of the 6+ level. This value is in fair agreement with the energy calculated by Eq.(1). It must be noted, however, that there are no other arguments in favor of the inferred position for the 282 kev transition.

B. Levels of the second rotational band

The levels of the first and second bands in Er^{166} are diagramed in the accompanying figure. In Table 2 we list the values of the sums of the γ-transition energies determining the positions of the levels of the second rotation band, obtained in investigating the conversion electron spectrum of Tm^{166}.

Table 2

Sums of γ-transition energies

E, kev	Sums of γ-transition energies, kev	
788	789;	707+80,0=787;
862	782+80=862;	598+263,9=861,9;
957	877,5+80,0=957,5;	693+263,9=956,9;
1070	(522)+545,9=1067,9;	(807)+263,9=1070,9

As will be evident from Table 2, the various energy sums are in satisfactory agreement with each other. Calculations of the parameters A and B in Eq.(1) based on the first three levels of the second rotational band yield A_2 = 12.53 kev and B_2 = 0.0327 kev. Assuming these values to be correct, the energy of the 5+ level of the second rotational band should be 1070 kev. It may be hypothesized that the 522 kev γ-transition (Table 1) goes from the 5+ level to the 6+ level (546 kev). It is also possible that part of the intensity of the 750 kev conversion line (Ref. 1) is associated with conversion of the 807 kev γ-transition in the K shell. The spins and parities of the levels of the second rotational band have not been determined experimentally.

Table 3

Comparison of the rotational level energies calculated by means of Davydov's[7] formulas with the experimental values

Assignments		Level energy, kev	
I	K	calc.	exper.
2	0	*	80,0±0,5
4	0	264,8	263,9±0,5
6	0	546,8	546±1
2	2	*	788±2
3	2	867,9	862±2
4	2	978,1	957±2
5	2	1108	1070

*Experimental values taken for the energy ratio.

The theory of rotational states of nonaxial nuclei, developed by Davydov[7], enabled us to calculate the energies of the rotational levels in question, using only one parameter, namely, the ratio of the energies of the two rotational levels with spin 2. The results of such calculations are compared with the experimental data in Table 3.

C. Intensity of transitions in the band

According to our decay scheme, all the transitions must be E2 or E2 with an insignificant admixture of M1. Transitions from levels of the second rotational band (K = 2) to levels of the first

rotational band (K = 0) should be almost pure E2, inasmuch as M1 transitions in this case are forbidden by the K selection rule ($\Delta K = -2$), whereas E2 transitions are not forbidden. By virtue of this equality of the multipole orders, we can determine the intensities of the transitions from the intensities of the conversion lines. The intensity values listed in our diagram (in the units of Table 1) are deduced in this manner. Having the relative γ-transition intensities, we can compare the experimental ratios of the reduced intensities of the competing γ-transitions from levels of the second rotational band with the theoretical ratios calculated according to Alaga and Davydov (Table 4).

Table 4

Comparison of the experimental ratios of the reduced intensities of competing γ-transitions from levels of the second rotational band with the theoretical ratios for the reduced probabilities

γ	E_γ, kev	Initial		Final		$\left(\frac{I_{\gamma_1}}{I_{\gamma_2}}\right)_{exp.}$	Ratios of reduced probabilities		
		I	K	I	K		exper.	Alaga	Davydov
γ_1	789	2^+	2	0	0	0,62	0,35	0,7	0,52
γ_2	707	2	2	2	0				
γ_1	782	3	2	2	0	18	5	2,5	1,2
γ_2	598	3	2	4	0				
γ_1	877	4	2	2	0	0,66	0,2	0,34	0,10
γ_2	693	4	2	4	0				
γ_1	807	5	2	4	0	~3,5	0,33	1,75	—
γ_2	522	5	2	6	0				

Let us consider the 596 kev transition which competes with the 782 kev transition from the 862 kev (3+) level. In this case the experimental ratio $I_{\gamma 782}/I_{\gamma 596} = 4.8$ and the ratio of the reduced probabilities is 1.3. We note that for the first three transition pairs (Table 4) the experimental ratios of the reduced probabilities are closer to the theoretical ratios calculated according to Davydov. The fourth and last pair is as yet inadequately studied and hence the indicated experimental values may be doubtful.

We utilized the intensities of the γ-transitions included in our diagram for calculating the intensities of the 596, 674, 749 and 760 kev transitions. The results of these calculations are listed in column 1 of Table 1.

4. Concerning the Other Excited Levels of Er^{166}

Table 1 lists an appreciable number of other transitions that do not fit into the rotational bands pictured in the diagram. Apparently, there are many other levels in Er^{166}. Some of these, for example, the 1462 and 1610 kev levels, have been observed in investigating the decay of Ho^{166}. The existence of some of the other levels excited in the decay of Tm^{166} can be substantiated by the energy data.

Thus, for example, introducing the levels with energies of 2140 and 2168 kev, we can fit four additional transitions into the scheme in each case:

2060 + 80 = 2140 kev,
1878 + 264 = 2142 " ,
1277 + 862 = 2139 " ,
1181 + 957 = 2138 " ,

2088 + 80 = 2168 kev,
1380 + 788 = 2168 " ,
1309 + 862 = 2171 " ,
1208 + 957 = 2165 " .

To elucidate the sequence of the high-lying excited states of Er^{166} and their spins and parities one must carry out further, more accurate measurements of the conversion electron energies and appropriate coincidence experiments.

"V.G.Khlopin" Radium Institute,
Academy of Sciences of the USSR &
Joint Institute for Nuclear Research

References

1. V.Brabets, K.Gromov, B.Dzhelepov, A.Dmitriev & V.Morozov, Present issue of the Bulletin, p.805.

2. V.Baranovskii & V.Pokrovskii, Present issue of the Bulletin, p.813.

3. G.Wilkinson & H.G.Hicks, Phys.Rev., 75, 1687 (1949).

4. B.S.Dzhelepov & L.K.Peker, Skhemy raspada radioaktivnykh yader (Decay schemes of radioactive nuclei), M.-L., 1958.

5. K.P.Jacob, J.W.Mihelich, B.Harmutz & T.H.Handley, Bull.Amer.Phys.Soc., Ser.2, 3, 358 (1958).

6. B.S.Dzhelepov & L.K.Peker, Deformirovannye yadra v oblasti Nd-Os. (Deformed nuclei in the Nd-Os region), Report presented at the Conference on Radiochemistry and Nuclear Spectroscopy, Joint Inst. for Nuclear Research,p.247, Dubna, 1958.

7. A.S.Davydov & G.F.Filippov, Zhur.eksp.i teor.fiz., 35, 440 (1958); A.S. Davydov & V.S.Rostovskii, Ibid., 36, 1788 (1959).(Trans. Soviet Physics - JETP.)

GAMMA-RADIATION FROM Cs^{134}

- B.S.Dzhelepov, V.P.Prikhodtseva & Yu.V.Khol'nov

We investigated the γ-spectrum of Cs^{134} by means of magnetic spectrometers, utilizing Compton recoil electrons. The purpose of the measurements was a more accurate (than in earlier studies) determination of the relative γ-ray intensities. The source was cesium carbonate with an activity of ~1.5 Curie.

The spectrum of recoil electrons ejected from a 50 μ thick cellophane target, as recorded on the Ritron[1], is shown in the upper part of the accompanying figure (a). Under the experimental conditions, the line half-width in the 1 Mev region was 3.3%. Clearly apparent are peaks associated with 1368, 1168 and 1038 kev γ-lines. The peak corresponding to the two close 797 and 802 kev γ-lines is not resolved; the joint peak is located at 797 kev. This is understandable inasmuch as the intensity of the 802 kev γ-line, according to the data of several investigators[2-4], is approximately one tenth the intensity of the 797 kev line.

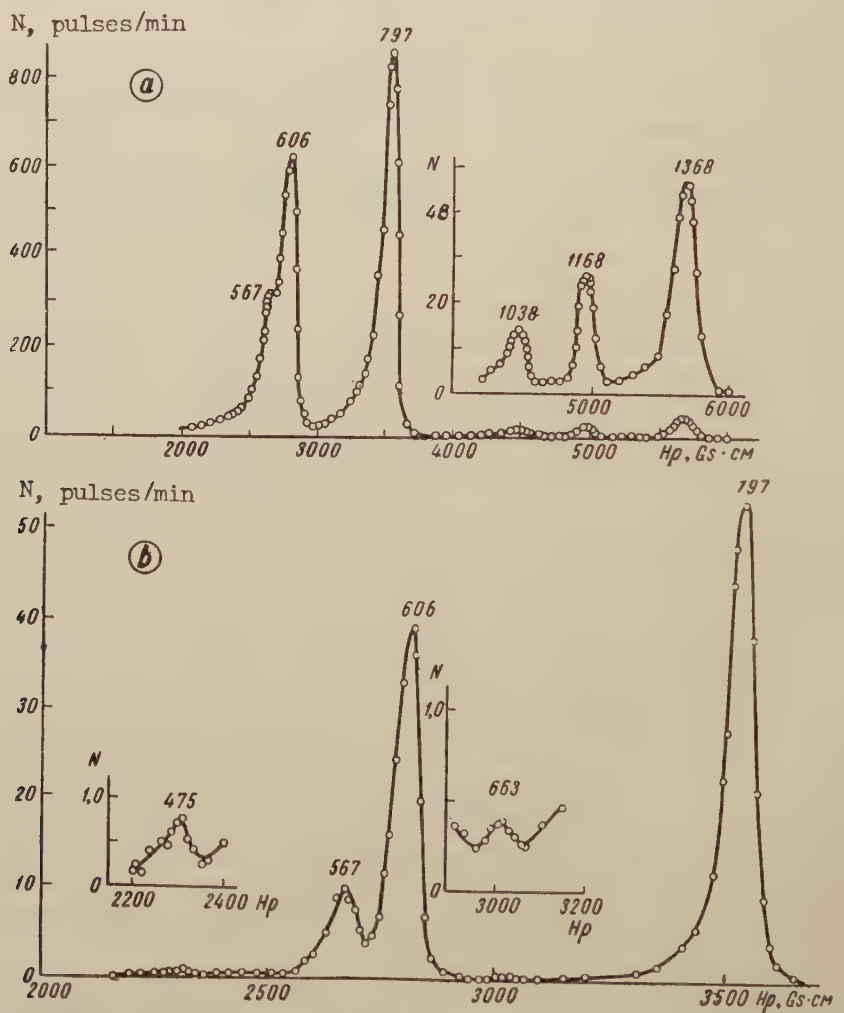

Spectra of recoil electrons from the γ-rays of Cs^{134}, recorded on a - the Ritron and b - the Elotron

In the soft region of the spectrum there appears a line at 606 kev and a poorly resolved line at 567 kev. The latter, according to the data of Verhaeghe & Demrynch[3], consists of two close γ-lines (565 and 571 kev) with comparable intensities. Further, it is reported in the literature that Cs^{134} has a very weak 475

γ-line (Refs.3-9) and a weak 663 kev γ-line (Refs.3-5). For better resolution of the lines in the low energy part of the spectrum and in order to bring out the above mentioned weak γ-lines, we investigated the γ-spectrum of Cs^{134} in the region to 820 kev by means of the Elotron[10]. In this case the recoils were ejected from a 17 μ thick cellophane target. Owing to better focusing of the recoil electrons, the relative line half-width in the 1 Mev region in this case was 1.6% with some sacrifice (approximately one order of magnitude) of transmission. The electron recoil spectrum obtained on the Elotron is shown in the lower part of the figure (b). It will be seen that the 696 and 567 kev lines are better resolved than with the Ritron. Furthermore, the Elotron brought out the recoil electron lines corresponding to the 475 and 663 kev γ-rays (see enlarged scale inserts).

The principal results of the investigation are summarized in the following table:

Energies and relative intensities of the γ-rays from Cs^{134}

E_γ,kev	475	567	606	663	797	1038	1168	1368
		$\begin{cases}565\\571\end{cases}$						
I_γ	2.5±0.5	28±3 $\begin{cases}10\pm3\\18\pm3\end{cases}$	100	0.5±0.3	101±4.3	1.16±0.04	2.26±0.08	3.79±0.15

The 567 kev line group was resolved into components assuming a standard line shape for the known (from other investigations) energies of these lines. The 797 kev line is the sum of two unresolved γ-lines: 797 and 802 kev. Firsov and Bashilov[11], using a scintillation spectrometer, detected three lines in the 1600 to 2100 kev region. The intensities of these lines are very low ($\sim 10^{-6}$ photons per decay). We investigated the Cs^{134} γ-spectrum in the range from 1400 to 2800 kev and failed to detect any γ-lines in excess of $0.5 \cdot 10^{-3}$ in the units of the table. This of course does not conflict with the results of Firsov & Bashilov, inasmuch as the sensitivity of our instrument was too low to detect such weak components.

Graduate students V.A.Eliseev and A.Ushakova participated in the measurements; we take this opportunity to thank them. We are grateful to N.N.Zhukovskii for allowing us to use the Elotron.

"V.G.Khlopin" Radium Institute,
Academy of Sciences of the USSR

References

1. B.S.Dzhelepov, N.N.Zhukovskii & Yu.V.Khol'nov, Izv.AN SSSR,Ser.fiz.,18, 599 (1954) (Trans.Bulletin, 18, No.5,285.); B.S.Dzhelepov, V.P.Prikhodtseva, A.I. Feoktistov & Yu.V.Khol'nov, Ibid.,(Bulletin 20, No.12a, 1245); I.B.Golovanov, B.S.Dzhelepov, L.S.Lebedev, V.P.Prikhodtseva & Yu.V.Khol'nov, Ibid.,21,958 (1957) (Bulletin 21, No.7, 987.)
2. A.Bashilov, N.Anton'eva, M.Blinov & B.Dzhelepov, Ibid.,18, 43 (1954).
3. J.Verhaeghe & J.Demrynch, Compt.Rend., 239, 1374 (1954).
4. H.Forster & J.Wiggins, Nuovo Cim., 2, 854 (1955).
5. J.Cork, J.LeBlanc, W.Nester, D.Martin,& M.Brice, Phys.Rev.,90,444 (1953); Ibid., 89, 907 (1953).
6. G.Keister, E.Lee & F.Schmidt, Ibid., 97, 451 (1955).
7. H.Forster & J.Wiggins, Ibid., 99, 660 (1955).
8. M.Joshi & B.Thosar, Ibid., 96, 1022 (1954).
9. K.Johansson, Arkiv Fys., 10, 247 (1956).
10. B.S.Dzhelepov, N.N.Zhukovskii, V.G.Nedovesov & G.E.Shchukin, Izv.AN SSSR, Ser.fiz., 21, 996 (1957).(Trans. Bulletin 21, No.7, 968.)
11. E.Firsov & A.Bashilov, Ibid., 21,1633 (1957).(Trans.Bulletin 21,No.12,1619)

Ta^{182} GAMMA-RADIATION IN THE 300 TO 1500 kev REGION

- N.A.Voinova, B.S.Dzhelepov & N.N.Zhukovskii

In the disintegration of 111-day Ta^{182} there are excited states of W^{182} with energies up to ~1600 kev. The even-even nucleus W^{182} has a clearly pronounced rotational level structure, characteristic of nuclei with stable deformation in the $155 < A < 185$ region. It has been established in numerous investigations that the ground state rotational band of W^{182} is represented by two levels with energies of 101 and 329 kev; other excited levels are located above 1222 kev. There are no indications in the literature regarding the existence of excited levels in the energy range from 329 to 1222 kev.

We investigated the γ-radiation of Ta^{182} on the Elotron for the purpose of obtaining more accurate γ-line intensity values and to search for lines in the 300 to 1500 kev interval. The source was a neutron activated tantalum foil weighing 1.8 g and having an activity of ~400 mC. The measurements were carried out under the standard Elotron conditions.[1] The experimental spectrum of recoil electrons from a polystyrene target is reproduced in Fig.1. It will be evident that in the $H\rho$ = 1500 to 3700 gauss·cm region ($h\nu$ = 300 to 850 kev) there are virtually no rises of the spectroscopic curve above the background; hence it may be asserted that in this region there are no γ-rays with an intensity exceeding 0.5% the intensity of the 1122 kev γ-radiation.

Energies and relative intensities of the γ-rays from Ta^{182}

No.	$h\nu$, kev	Relative intensities				
		Our data	Ref.2 (crystl. spectr.)	Ref.3 (crystl. spectr.)	Ref.4 (photo-electrons)	Ref.5 (scint. spectro.)
1	(893)	<1,4	—	—	—	—
2	927	3±2	—	—	—	—
3	960	2,5±1,5	—	—	—	—
4	1003	9±3	—	—	—	—
5	1122	100	100	100	100	100
6	1155	<4	6,5	9	—	—
7	1192	45±8	45	60	—	~21
8	1222	84±8	95	156	—	(75) 113
9	1231	35±10	50			(38)
10	1257	6±2	—	—	4	—
11	1275	3±2	—	—	3	—
12	1290	5±2	—	—	2	—
13	1331	<0,6	—	—	—	—
14	1375	<1,4	—	—	<0,3	—
15	1437	<0,5	—	—	<0,3	—

Fig.2 illustrates resolution of the 850 to 1350 kev section of the spectrum into individual components, taking into account the apparatus line shape. In this region our analysis brought out seven γ-rays with energies of 927, 960, 1003, 1122, 1192, 1222 and 1231 kev.

In addition there is observed an appreciable rise of the experimental points above the "background" in the region of the high energy side of the 1222-1231 kev γ-lines. According to other investigators, there is a series of lines of almost negligible intensity in this region. Analysis of the remainder obtained after subtraction of the high energy sides of the intense 1222 and 1231 kev lines gives reason to assert that in this energy region there actually do exist the γ-lines with energies of 1257, 1275 and 1290 kev, reported by other authors (for example, Bäckström[4]).

In the low energy range there is a noticeable rise of the experimental points above the background at about 893 kev.

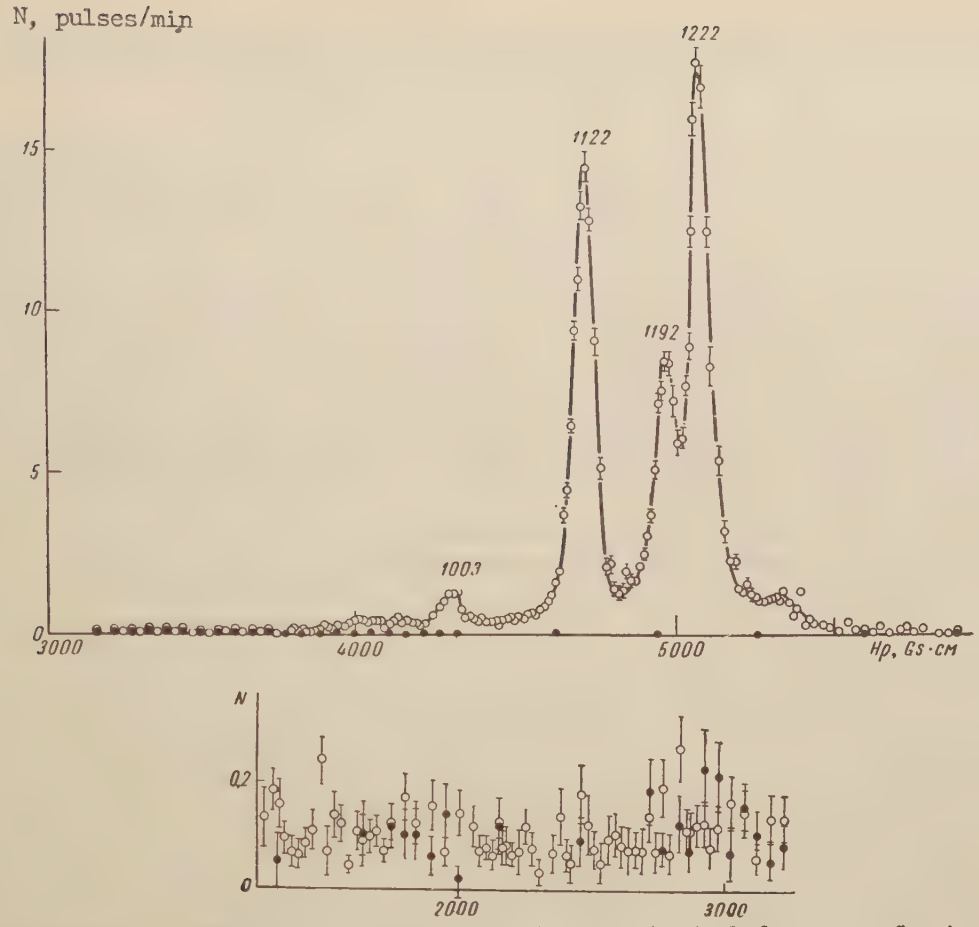

Fig.1. Experimental spectrum of recoil electrons ejected from a polystyrene target by Ta^{182} γ-rays. Solid points - instrument background.

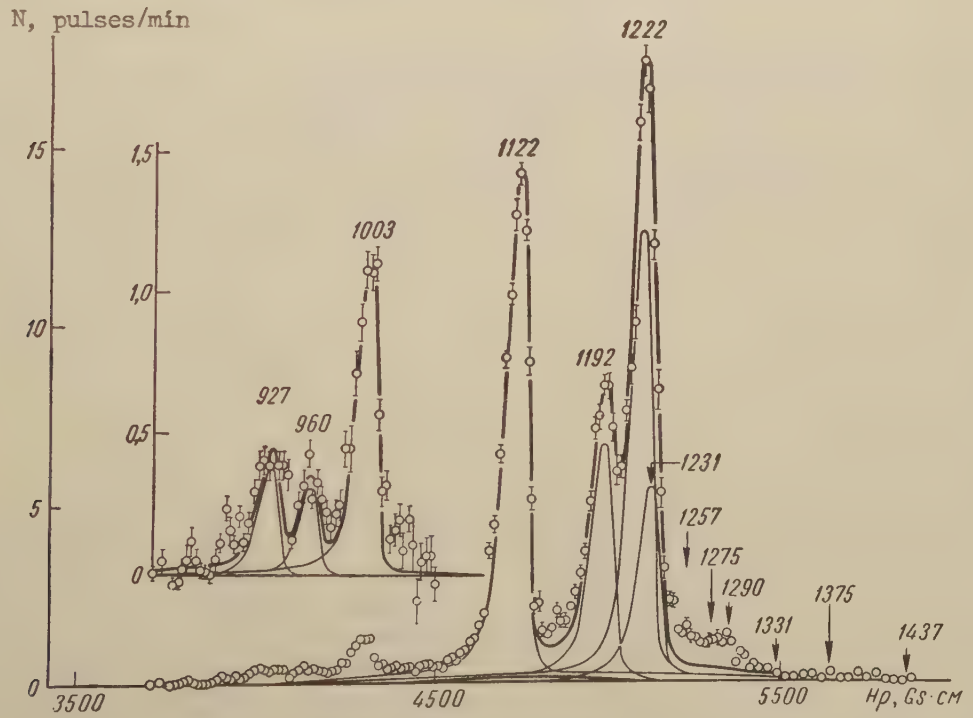

Fig.2. Resolution of the 3500 to 5500 gauss·cm (850 to 1350 kev) section of the Ta^{182} γ-spectrum into individual lines.

The data on the γ-rays observed in the present study are listed and compared with the results of other authors in the accompanying table.

"V.G.Khlopin" Radium Institute,
Academy of Sciences of the USSR

References

1. B.Dzhelepov, N.Zhukovskii, V.Nedovesov & G.Shchukin, Izv.AN SSSR, Ser.fiz.,21, 966 (1957).(Trans.Bulletin, 21,No.7, 968.)
2. J.Murray, F.Boehm, P.Marmier & J.DuMond, Phys.Rev.,97, 1007 (1955).
3. O.Sumbaev, Zhur.eksp.i teor.fiz.,32,247 (1957)(Trans. Soviet Physics - JETP.); Izv.AN SSSR,Ser.fiz.,21, 987 (1957).(Trans. Bulletin, 21, No.7, 989.)
4. G.Bäckström, Arkiv fys., 10, 387 (1956).
5. P.Fröman & H.Ryde, Ibid., 12, 399 (1957).

SPECTRA OF NEUTRON-DEFICIENT Hf ISOTOPES

- V.I.Baranovskii & A.V.Kalyamin

We employed the scintillation technique described in Ref.1 to investigate the Hf fraction separated from a tantalum target bombarded with 680 Mev protons in the Joint Institute for Nuclear Research synchrocyclotron. The active material was separated chemically with a Zr carrier by precipitation of $BaZrF_6$ with subsequent chromatographic purification (KU-2 cationite), which yielded chemically pure Hf.

We devoted primary attention to the low energy part of the spectrum (up to about 700 kev) inasmuch as the presence of a large number of poorly resolved high energy lines (to ~2.5 Mev) greatly hampers study of the hard region of the spectrum. In the low energy region we observed two groups of lines with half-lives of 23.5 and 13 hours.

We identified the hafnium isotope with a period of 2.3 hours as Hf^{173}*; in the literature its periods are reported variously as 23.6 hr (Wilkinson and Hicks[2]), 44 hr (Nervik and Seaborg[3]) and 28 hr (Wapstra and Jongejans[4]). According to our data, the γ-spectrum of Hf^{173} comprises a 125 kev line and a ~300 kev group with an intensity ratio of 100:60, which is in agreement with the data of Wapstra & Jongejans[4].

We attributed the 13 hour activity to Hf^{171}*; in the literature we find 16 hr (Wilkinson & Hicks[2]) and 12 hr (Nervik & Seaborg[3]). In the spectrum of Hf^{171}, in addition to the known 175 (180) kev line, we detected a group of lines in the 400 to 700 kev region. No intense lines belonging to other isotopes were observed in this energy range.

We resolved the spectrum of Hf^{171} into individual components; the evaluated relative intensities are:

E_γ, kev	480	530	580	620	680
Relative intensity	0.75	0.35	0.81	1	0.5

The 175 kev line decayed with a period of 16 hours, which may be explained by the presence in this energy region of the 162.3 kev line of Hf^{173} and the 180 kev line of Lu^{171}, which builds up from Hf^{171}.

We desire to express our sincere gratitude to the operating personnel of the Joint Institute for Nuclear Research synchrocyclotron for the proton bombardment and to A.N.Murin and G.M.Gorodinskii for their interest in the work and discussion of the results.

"V.G.Khlopin" Radium Institute
Academy of Sciences of the USSR.

References

1. G.M.Gorodinskii, A.N.Murin, V.N.Pokrovskii & B.K.Preobrazhenskii, Izv.AN SSSR,Ser.fiz.,21, 1004 (1957). (Trans.Bulletin,21, No.7,1005.)
2. G.Wilkinson & H.G.Hicks, Phys Rev., 81, 540 (1951).
3. W.E.Nervik & G.T.Seaborg, Ibid., 97, 1092 (1955).
4. A.H.Wapstra & C.Jongejans, Physica, 20, 36 (1954).
5. D.Strominger, J.M.Hollander & G.T.Seaborg, Table of Isotopes, Revs.Mod.Phys., 30, 585 (1958).

---

* In Seaborg's table[5] the mass number assignments for these isotopes are classified as "probable".

HIGH ENERGY PART OF THE GAMMA-SPECTRUM OF RADIUM IN EQUILIBRIUM WITH ITS DECAY PRODUCTS (3100-5600 kev)

- B.S.Dzhelepov, B.A.Emel'yanov, Yu.N.Podkopaev, V.N.Podymakhin, I.F.Uchevatkin & S.A.Shestopalova

Most of the high energy γ-rays emitted in the radium decay series are associated with the RaC→RaC' transition. The γ-spectrum of this transition extends to 3200 kev.[1,2]

It may be hypothesized, however, that harder γ-rays are emitted in the radium decay series: first, the RaC-RaC' mass difference is 3260 ± 30 kev (Fig.1) and, consequently, there may be γ-rays from RaC→RaC' with energies up to 3260 kev; second, the RaC''-RaD mass difference is even greater, namely, 5420 kev; consequently hard γ-rays may be emitted in the decay of RaC''. Emission of high energy γ-rays in α branches is doubtful, inasmuch as the probability of α-decay to high-lying excited levels is low, owing to the Coulomb barrier.

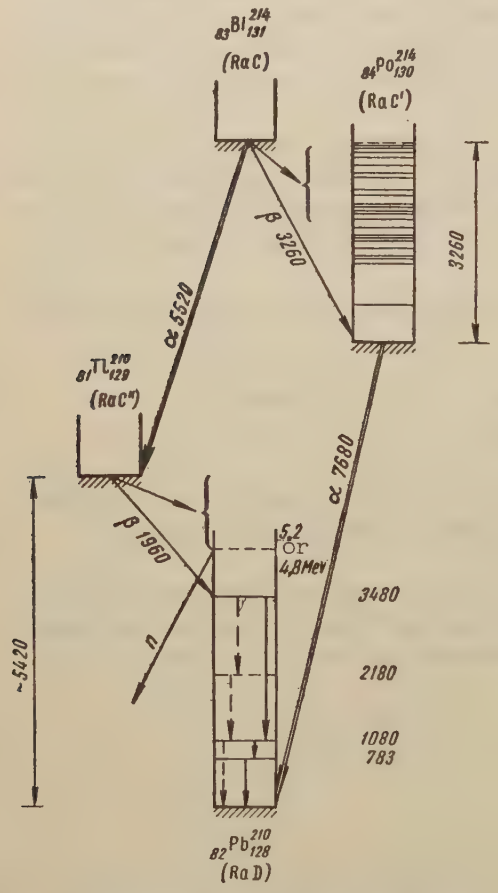

Fig.1. Branching in the radium decay series.[3]

There have been numerous attempts to detect hard γ-rays in the radium family. Thus, for example, Nishida[4] observed tracks of electrons with energies of 3100, 4000 and 4900 kev in a radium irradiated Wilson chamber. Devons & Neary[5] detected γ-rays of up to about 5000 kev energy by the absorption method. In 1950, Bishop, Wilson & Halban[6] searched for hard γ-rays by means of a deuterium filled ionization chamber but failed to detect any. For the RaC''→RaD transition (~4000 kev) these authors give only an upper bound of $< 2 \cdot 10^{-5}$ photons per disintegration. They assert that the intensity of any ~3000 kev γ-rays emitted in the RaC→RaC' decay cannot exceed 10^{-4} photons per disintegration. It is known, however, that such γ-rays are emitted in the amount of $2 \cdot 10^{-3}$ photons per disintegration.[1]

In a 1958 investigation[2] of the 2450 to 3400 kev region of the radium spectrum by means of an Elotron spectrometer there was found an excess of recoil electrons corresponding to γ-rays with an energy of 3120-3220 kev and an intensity of $(4 \pm 2) \cdot 10^{-5}$ photons per disintegration. A more detailed investigation of so small an excess was impossible on the Elotron.

In the present work we used an instrument with a higher transmission factor, namely, the Leningrad State University gamma-nodoscope[7,8]. The source was a 4 g sample of Ra.[9]

Two series of measurements were carried out. In the first series the strength of the magnetic field was chosen so that the region of detection extended from the high energy side of the last line identified in the work of Ref.2 (the 3070 kev line) all the way to 5600 kev. Lines softer than 3070 kev were virtually not detected. The results are given in Fig. 2 in the form of a histogram. The smooth curve corresponds to the experimental shape of the spectral line as determined by Chubinskii[8]. It will be evident from the figure that above the high energy side of the 3070 kev line there is an excess of recoil electrons extending all the way to 3800 kev.

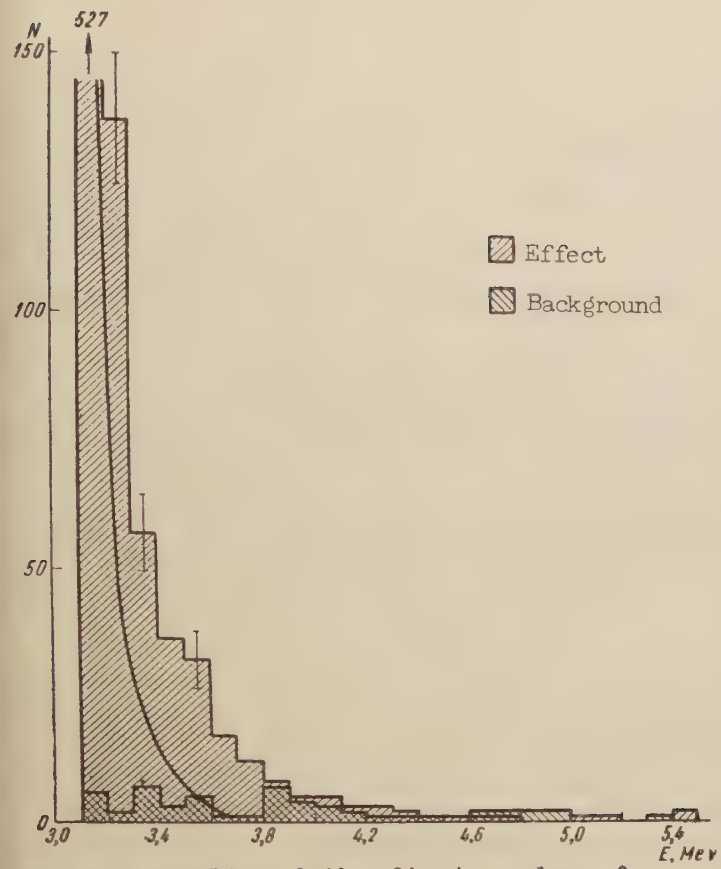

Fig.2. Results of the first series of measurements.

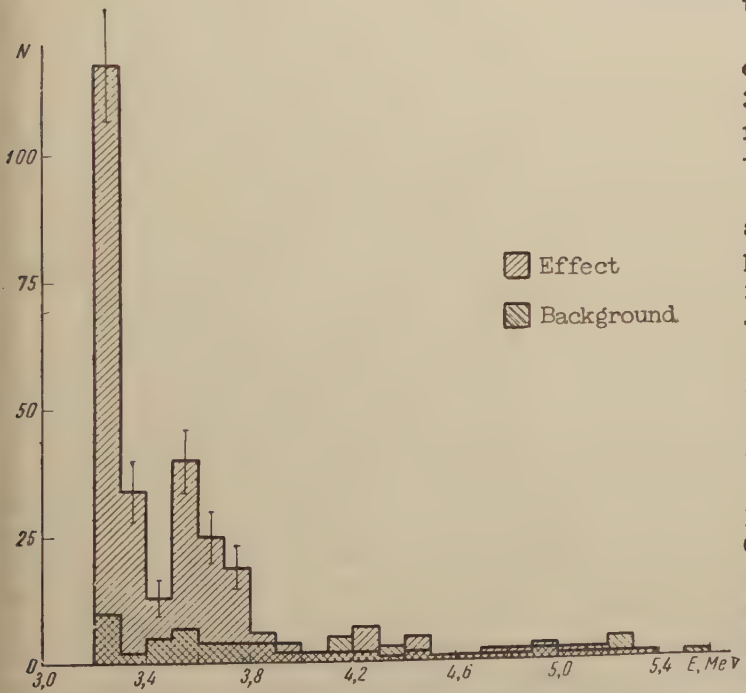

Fig.3.Results of second series of measurements.

In the second series of measurements the magnetic field was chosen so that the 3070 kev γ-rays would not be detected at all; the detecting region extended from just above 3200 kev (so that if there is a 3200 kev line[2] only its high energy side would be recorded) up to 5600 kev. The results obtained in this series of measurements are shown in Fig.3.

It will be evident from Figs. 2 & 3 that there undoubtedly exists a γ-line with an energy of 3100-3200 kev. An approximate evaluation of the intensity of these γ-rays yields a value of $2 \cdot 10^{-5}$ photons per disintegration, which is in good agreement with the results of the above mentioned study[2].

There is also clearly evident in Fig.3 an excess of recoil electrons in the 3500 to 3800 kev interval. The experimental number of "frames" in this region, normalized to one hour of measurement, is equivalent to 0.38 ± 0.16 coincidences per hour, which corresponds to an intensity of $(1^{+1}_{-0.5}) \cdot 10^{-6}$ photons per disintegration. From the experimental data on the line half-width in this region[8], it follows that this excess is probably due not to a single line but to at least two.

It is evident therefore that the excess of recoil electrons in the 3500 to 3800 kev region is due to γ-rays accompanying the RaC"→RaD transition.

One cannot make an unambiguous attribution of the ~3200 kev line at present: these γ-rays may be emitted in either the RaC"→RaC' or the RaC" →RaD transitions.

No γ-rays with energies above 3900 kev were detected. If they exist their intensity is less than $5 \cdot 10^{-8}$ photons per disintegration.

We take this opportunity to express our deep gratitude to O. V. Chubinskii for making available the experimental data on the spectral sensitivity and efficiency of the gamma-hodoscope, i.e., the data used in evaluating the line intensities.

"D. I. Mendeleev" All-Union Scientific Research
Institute of Metrology &
"A. A. Zhdanov" Leningrad State University

References

1. I.Uchvatkin & S.Shestopalova, Izv.AN SSSR,Ser.fiz., 21, 1002 (1957). (Trans. Bulletin 21, No.7, 1003.)
2. B.Dzhelepov, S.Shestopalova & I.Uchevatkin, Nucl.Phys.,5, 413 (1958).
3. B.Dzhelepov & L.Peker, Skhemy raspada radioaktivnykh yader (Decay schemes of radioactive nuclei), M-.L., 1958.
4. S.Nishida, Proc.Phys.-Math.Soc., Japan (3), 19, 809 (1937).
5. S.Devons & G.Neary, Proc. Camb. Phil. Soc., 33, 154 (1937).
6. G.Bishop, R.Wilson & H.Halban, Phys.Rev., 77, 416 (1950).
7. B.Dzhelepov, Izv.AN SSSR,Ser.fiz., 21, 1580 (1957). (Trans. Bulletin 21, No.12, 1569.)
8. O.Chubinskii, Ibid., 21, 1583 (1957). (Trans. Bulletin 21, No.12, 1572.)
9. B.Dzhelepov & S.Shestopalova, Ibid., 21, 990 (1957). (Trans. Bulletin 21, No.7, 992.)

INVESTIGATION OF THE LOW-LYING LEVELS OF Cl^{33} BY MEANS OF THE $S^{32}(p,\gamma)Cl^{33}$ REACTION

- A.K.Val'ter, V.Yu.Gonchar, A.N.L'vov & C.P.Tsytko

The low lying levels of Cl^{33} were investigated in the work of Middleton et al[1] by analysis of the angular distribution of neutron groups from the reaction S^{32}(d, n)Cl^{33}. In this study there were detected levels in Cl^{33} with energies of 0.76 ± ±0.07, (1.89), 2.84 ± 0.06 and 4.44 ± 0.08 Mev. According to Middleton et al the spin and parity assignments are 1/2+ for the 0.76 Mev level and 1/2- or 3/2- for the 2.84 and the 4.44 Mev levels.

Van der Leun & Endt[2] also investigated the low lying levels of Cl^{33}, utilizing the $S^{32}(p,\gamma)Cl^{33}$ reaction. Bombarding thin ZnS targets with a natural mixture of sulfur isotopes with protons of 0.2 to 0.8 Mev energy, they detected one resonance at E_p = 594 ± 5 kev, corresponding to an excited level in Cl^{33} at 2.86 Mev, and measured the γ-ray spectra and angular distributions corresponding to this resonance. Van der Leun & Endt give a diagram of the γ-transitions from the 2.86 Mev level of Cl^{33} and indicate that the assignment for this level is 3/2+.

Meyerhof & Lindstrom[3] on the basis of the log ft value for the positron branch of Cl^{33} decay to the 2.9 Mev state of S^{33} infer that the parity of this state is even. Hence the same parity assignment can be tentatively made for the corresponding level of the mirror nucleus Cl^{33}.

Thus there are conflicting data for the parity of the 2.9 Mev state of Cl^{33}. In view of the fact that its mirror nucleus S^{33} has three levels in this energy region, this conflict can be explained by the presence of very close lying levels in Cl^{33} near 2.9 Mev. To check this assumption we undertook an investigation of the $S^{32}(p,\gamma)Cl^{33}$ reaction in the 2.9 Mev excitation region of Cl^{33}.

The protons were supplied by the Physical-Technical Institute (Ukrainian SSR Ac. of Sci.) four Mev electrostatic generator, which is characterized by a high degree of stabilization of the accelerating potential and hence yields a highly monoenergetic proton beam.[4]

We used thin targets of separated S^{32} obtained by driving 20 kev S^{32} ions into a tantalum backing in the electromagnetic separator[5], and, also, thin targets with the natural mixture of sulfur isotopes, prepared by vacuum evaporation of ZnS onto a tantalum backing. The targets had a thickness of the order of 6 kev and withstood a current of 10-15 μa for many days.

For measuring the γ-ray yield we used a scintillation counter with a 3 cm diameter, 2 mm thick CsI(Tl) crystal and a discriminator with associated counting equipment. The discriminator threshold was set to detect all γ-rays with energies over 1.5 Mev. The γ-ray spectrum was measured by means of the scintillation spectrometer, also with a CsI(Tl) crystal, described in Refs.6 & 7. In addition, to bring out certain lines of the spectrum, we utilized NaI(Tl) and stilbene crystals.

The β-activity was measured using a special target chamber with a thin window for exit of the β-particles. After proton bombardment the target was rotated 180° and positioned in front of the window. The emerging particles were detected by a scintillation counter with a 3 cm diameter, 0.2 cm thick CsI(Tl) crystal, subtending a solid angle of about 1 steradian.

For investigating the γ-ray angular distribution we measured the spectra by means of a scintillation spectrometer with provision for rotation from 0 to 150° right and left with respect to the photon beam direction. For each given energy the γ-ray intensity was determined from the area under the peak corresponding to complete absorption of the given γ-rays in the spectrometer crystal. Inasmuch as the intensity of the investigated resonances was low, we also measured the background individually for each point in the angular distribution. By way of monitor we used a scintillation counter fixed at an angle of 90° to the direction of the incident proton beam as well as a current integrator.

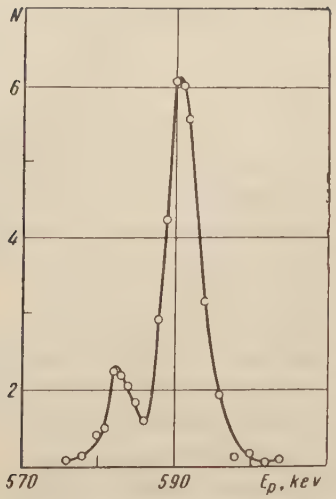

Fig.1.Resonances in the $S^{32}(p,\gamma)Cl^{33}$ reaction.

In investigating the γ-rays from the targets containing S^{32} we found two close resonances located at E_p = = 583 ± 0.7 and 590 ± 0.7 kev (Fig.1). Measurements of the decay period of the induced activity corresponding to both resonances yielded a value of 2.3 ± 0.3 sec, which is in good agreement with the half-life of Cl^{33} (2.53 ± 0.02 sec) reported by Muller et al[8]. In view of the good agreement it may safely be inferred that both these resonances belong to the $S^{32}(p,\gamma)Cl^{33}$ reaction.

On the basis of our comprehensive investigation of the γ-rays emitted at different angles we established the scheme of γ-transitions from the two detected Cl^{33} levels with energies of 2.850 and 2.857 Mev, and determined the relative transition intensities (Fig.2).

We measured the angular distributions for the most intense γ-transitions. Processing the experimental data by the method of least squares,we obtained the angular distribution functions (see table) for the cross-over transitions to the Cl^{33} ground state and also for the transition from the 2.857 Mev resonance level to the 0.81 Mev level. The measurement results are given in Figs.3 & 4.

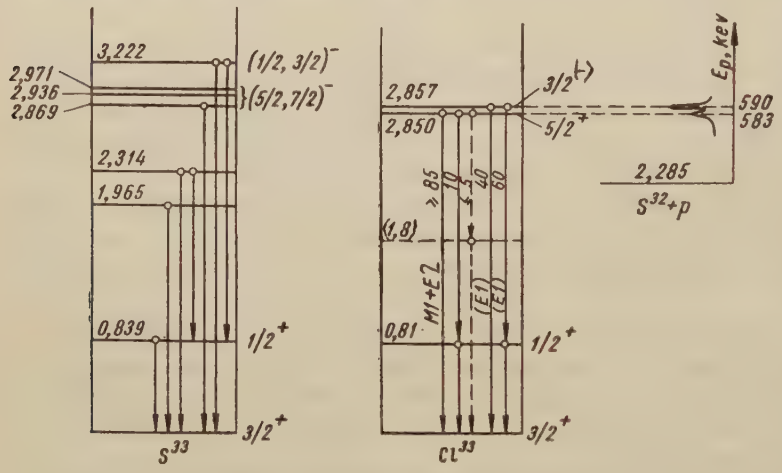

Fig.2. Level diagrams for the mirror nuclei S^{33} and Cl^{33}.

Comparison of the experimental angular distribution for the transition from the 2.850 Mev level to the ground state with the calculated distributions (for different tentative spin and multipole assignments) showed that the spin of the 2.850 Mev level is 5/2. The best agreement with experiment is obtained on the assumption that this is a dipole transition with a small admixture of quadrupole radiation, the E2 to M1 amplitude ratio being about 0.12. Hence from the character of the transition and the nature of the admixture we conclude that the spin and parity of the 2.850 Mev state are 5/2+.

Angular distribution of γ-rays from the $S^{32}(p,\gamma)Cl^{33}$ reaction

Transition	Multipole order	Angular distribution	Desig. in Fig.3	E_γ, kev	Experimental angular distribution
3/2→3/2	Dipole	$1+0.75\cos^2\theta$	a	2.857	$1+(0.78\pm0.03)\cos^2\theta$
	Quadrupole	Isotropic	b		
5/2→3/2	Dipole	$1-0.5\cos^2\theta$	c	2.85	$1-(0.74\pm0.05)\cos^2\theta$
	Quadrupole	$1-1.87\cos^2\theta+2.5\cos^4\theta$	d		
7/2→3/2	Quadrupole	$1+3.65\cos^2\theta-2.74\cos^4\theta$	e		
3/2→1/2	Dipole	$1-0.6\cos^2\theta$	Fig.4	2.05	$1-(0.62\pm0.10)\cos^2\theta$

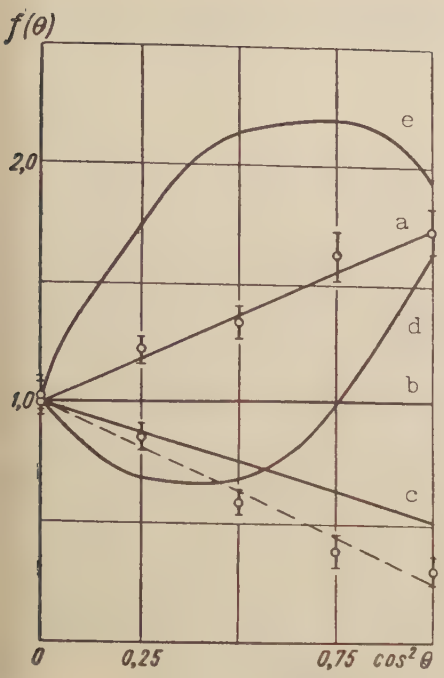

Fig.3. Angular resolution of the 2.850 and 2.857 γ-rays (see table).

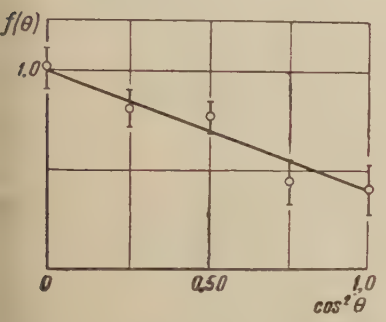

Fig.4. Angular resolution of the 2.04 γ-rays.

A similar comparison was carried out for the two other experimental angular distributions; as a result we arrived at a spin assignment of 3/2 for the 2.857 Mev level and substantiated the 1/2+ assignment for the 0.81 Mev level. In both cases the transitions involved are pure dipole ones.

Through comparison of the level diagrams for Cl^{33} and S^{33} shown in Fig.2, one can establish the correspondence between the levels in these mirror nuclei in the 2.9 Mev excitation region. Thus the S^{33} level to which Cl^{33} β-decays may have spin and parity 5/2+ and thus correspond to the 2.850 Mev (5/2+) level of Cl^{33}. The second level of S^{33} may be characterized by 3/2- and thus correspond to the 2.857 Mev level of Cl^{33} which has a spin of 3/2 and apparently also odd parity. The following evidence may be cited in favor of this assignment.

1. As determined in our measurements the intensity of the γ-rays from the 2.857 Mev level is five times the intensity of the radiation from the 2.850 Mev level. This fact can be explained by the different penetrability of the potential barrier owing to the difference between the orbital angular momenta l_p of the captured protons. The 5/2+ assignment for the 2.850 Mev level corresponds to $l_p = 2$. Inasmuch as proton capture to the 2.857 Mev level occurs with a higher probability, l_p must be smaller than 2, i.e., must equal 1. Consequently with a spin of 3/2 its parity must be odd.

2. We found that the γ-transitions from the 2.857 Mev level to the ground and first excited states of Cl^{33} are pure dipole transitions; this is consistent with there being E1 transitions inasmuch as M1 transitions usually have an admixture of E2.

3. It may be inferred that the even parity assignment made by Van der Leun & Endt[2] for the 2.86 Mev (3/2) level is erroneous, the mistake being due to distortion of the β-ray angular distribution owing to surposition of greatly different angular distributions from two unresolved resonances. Using the angular distributions obtained in our work one can show that under certain conditions of surposition of two resonances there may be obtained angular distributions similar to those observed in the work of Van der Leun & Endt.

The assumption that the third level of S^{33} in the above mentioned energy region has the assignment 5/2- or 7/2- and consequently $l = 3$, can explain the absence of a corresponding level in Cl^{33}, which has not been detected owing to the low probability of its excitation. β-decay of Cl^{33}, which has a ground state spin and parity of 3/2+, to this level as well as to the level with 3/2- must also be forbidden.

Thus we have suggested an explanation for the discrepancy in the work of different investigators[1-3] as regards the parity assignment for the 2.9 Mev level of Cl^{33} and have made an attempt to establish the correspondence between the levels of the mirror pair S^{33} and Cl^{33} in the 2.9 Mev excitation region.

We desire to express our sincere gratitude to M.I.Guseva for preparing the targets containing S^{32}, to E.V. Inopin for his interest in the work and valuable

discussions, to Yu.P.Antuf'ev and E.G.Kopants for their assistance in performing the measurements and to A.A.Tsygikalo, Yu.A.Kharchenko and their co-workers for skilled operation of the electrostatic generator.

Physical-Technical Institute,
Academy of Sciences of the Ukrainian SSR

References

1. R.Middleton, F.A.El-Bedewi & C.T.Tai, Proc.Phys.Soc. A,66, 95 (1953).
2. C.Van der Leun & P.M.Endt, Physica, 22, 1234 (1956).
3. W.E.Meyerhof & G.Lindstrom, Phys.Rev., 93, 949 (1954).
4. A.K.Val'ter & A.A.Tsygikalo, PTE (Instruments & Exp.Techniques), No.4, 3 (1957).
5. M.I.Guseva, Ibid., No.5, 112 (1957).
6. N.G.Afanas'ev & V.Yu.Gonchar, Atomnaya energiya, 4, No.3 289 (1958). (Trans. Soviet Journal of Atomic Energy.)
7. N.G.Afanas'ev & V.Yu.Gonchar, Materialy sesii AN USSR po ispol'zovaniyu atomnoi energii v mirnykh tselyakh (Transactions of the session of the Ukrainian SSR Academy of Sciences on the Use of Atomic Energy for Peaceful Purposes) Kiev, 1958.
8. T.Muller, E.S.Gelsema & P.M.Endt, Physica, 24, 577 (1958).
9. J.R.Holt & T.N.Marsham, Proc.Phys.Soc. A,66, 467 (1953).

Note added in proof: After submitting the present report to the editors we learned of the article by Van der Leun & Endt, published in Physica, 24, 1095 (1958), in which these authors confirm the existence of and the assignments for the two levels of Cl^{33} discovered and studied in the present investigation.

ELASTIC SCATTERING AND RADIATIVE CAPTURE OF PROTONS BY N^{14}

- A.K.Val'ter, A.S.Deineko, I.Ya.Malakhov, P.V.Sorokin & A.Ya.Taranov

Introduction

Investigation of elastic scattering of protons by N^{14} can yield information on the levels of O^{15}, lying above 7 Mev. Owing to the fact that the O^{15} nucleus differs by only one nucleon from the double magic nucleus O^{16}, its high-lying levels are rather widely spaced. This in a number of cases makes it feasible to use the isolated (single) level formulas in analyzing the resonances observed in measuring the elastic scattering cross section.

Elastic scattering of protons by N^{14} nuclei has been investigated by a number of authors[1-7]. In addition, Duncan & Perry[8] investigated the $N^{14}(p,\gamma)$ reaction. The results obtained in these studies are summarized in Table 1: in column 1 we give the resonance energies, in column 2 the width of the corresponding levels, and in column 3 the spin and parity assignments arrived at as a result of phase analysis.

Table 1

Characteristics of the excited levels of O^{15}
(The figures in brackets are Refs.)

E_R, keV	Γ, keV	Spin & parity
1060 [2, 4] 1050 [5], 1054±3 [6], 1064 [8]	3±1 [6], 4,8±1 [8]	$^1/_2^+$ [4], $3/2^+$ [6]
1550 [1, 2], 1530 [3], 1554 [4], 1540 [5], 1544±6 [6], 1557 [7], 1550±20 [8]	34±4 [2], 50±20 [8]	$^1/_2^+$ [3, 4, 6]
1740 [1, 4], 1720 [3], 1730 [5], 1737±4 [6], 1748±5 [8]	4±1 [6], 11±3 [8]	$3/2^-$ [3], $3/2^-$, $5/2^-$ [4], $\leqslant 5/2$ [6]
1805 [1], 1803 [4], 1799±5 [6], 1815±4 [8]	4±1 [6], 7±1,5 [8]	3,2^-, $5/2^-$ [4], $3/2^-$, $1/2^-$ [6]
2360 [1], 2320 [5], 2356±8 [8]	14±4 [8]	
2490 [1], 2450 [5], 2489±7 [8]	11±3 [8]	
3200 [1], 3130 [5]		
3400 [1], 3330 [5]		
2300 [7], 2600±50 [8]	500[7], 1270±50[8]	$^1/_2^+$ [7], $^1/_2^+$, $3/2^+$ [8]

It will be evident from the table that the elastic scattering cross section for <2 Mev protons has been investigated rather thoroughly. The resonance energies and the widths of the corresponding levels have been determined with fair accuracy. As regards the spins and parities, however, consistent results have been obtained only for the level corresponding to the resonance at 1.55 Mev.

In the proton energy range above 2 Mev only the resonance energies have been determined as a result of elastic scattering cross section measurements[1,7]. There is no information available regarding the widths of the levels and their spins and parities, except for the level corresponding to the broad resonance at 2.3 Mev.[7] The widths of the 2360 and 2490 kev resonances have been determined by means of the $N^{14}(p,\gamma)$ reaction.[1]

In the present work we investigated the p-N^{14} elastic scattering cross section in the energy range from 1.7 to 3.5 Mev.

Experimental Procedure

The experimental arrangement is diagramed in Fig.1. The proton beam, accelerated by the Physical-Technical Institute (Ukrainian SSR Acad. of Sci.) electrostatic generator was analyzed by a magnet with a 90° deflection angle and, after being defined by the 2 and 2.5 mm diameter, respectively, apertures A and B, entered the scattering chamber filled with nitrogen at a pressure of 5 mm Hg. The chamber was isolated from the accelerating tube by a mica foil 2 μ thick cemented over the 4 mm diameter aperture C. To protect the foil against proton damage, it was covered with a semitransparent layer of aluminum deposited by vacuum evaporation.

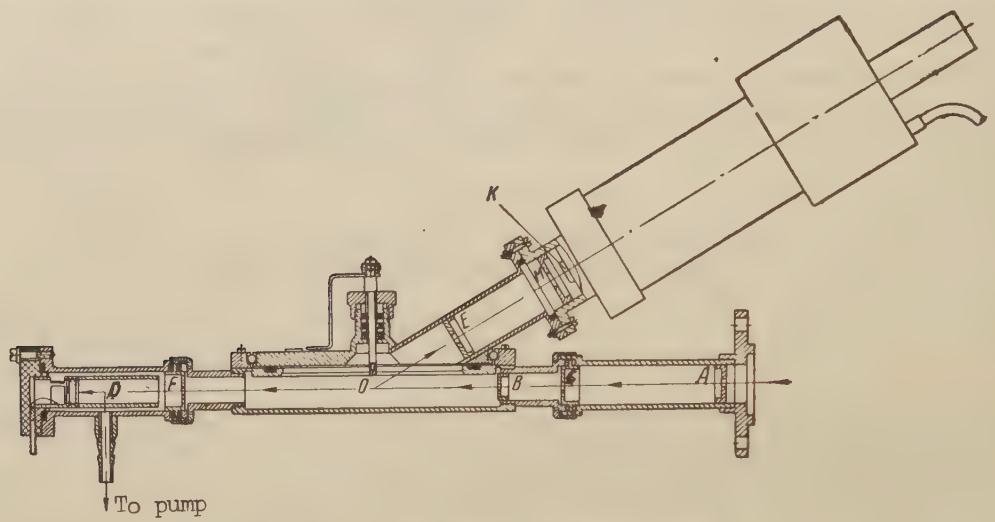

Fig.1. Diagram of apparatus.

The number of protons passing through the chamber was measured by means of the Faraday cup D and a current integrator. The Faraday cup chamber was separated from the scattering chamber by a 5 μ thick aluminum foil cemented over the 15 mm diameter aperture F. A vacuum of 10^{-6} mm Hg was maintained in the cup chamber by an oil diffusion pump.

To obviate possible contamination of the target, a continuous flow of nitrogen was maintained through the chamber during the experiment. This was realized by means of a capillary and an oil shutter designed so that with a gas flow of of 10 cm^3 per hour the chamber pressure would remain at 5 mm Hg.

The scattered protons, after passing through the 3 x 15 mm^2 slit E and the 4 mm diameter aperture M, were detected by the 0.5 mm thick CsI(Tl) crystal K coupled to an FEU-25 photomultiplier. To protect the photomultiplier from light due to ionization of the gas by the proton beam, the surface of the crystal was covered with a thin layer of aluminum applied by vacuum evaporation. The distance O to M was 120 mm; the aperture E was mounted half-way between O and M. With this geometry the solid angle was $8.6 \cdot 10^{-4}$ steradian. The effective target thickness

$$d = \frac{6}{\sin \theta} \text{ mm}$$

(θ is the scattering angle) did not exceed 12 mm. The chamber design allowed of varying the scattering angle from 30 to 150° in the laboratory system without disturbing the vacuum. A detailed description of the chamber design will be found in Ref.9.

Experimental Results and Discussion

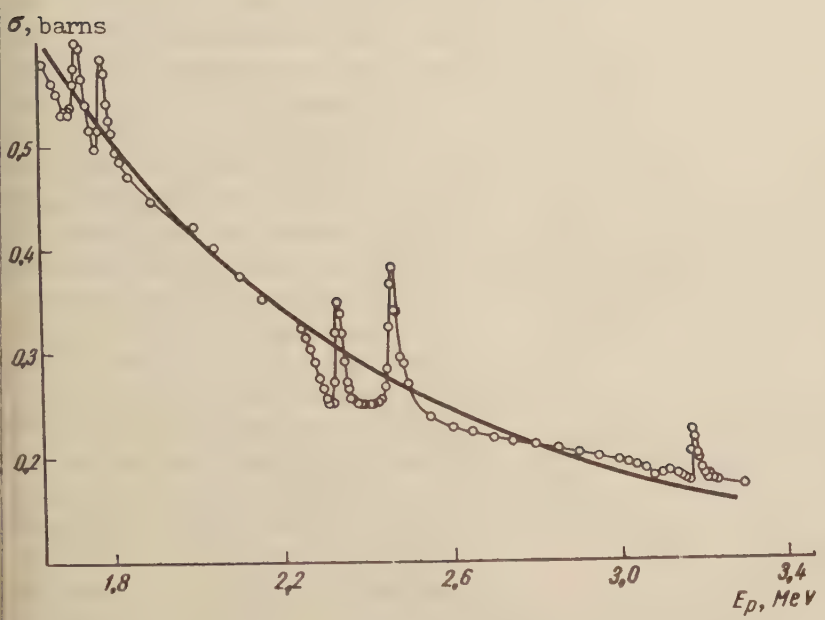

Fig.2. Cross section for elastic scattering of protons from N^{14} at $\theta_{c.m.} = 54^{\circ}$. The solid line gives the Rutherford scattering cross section.

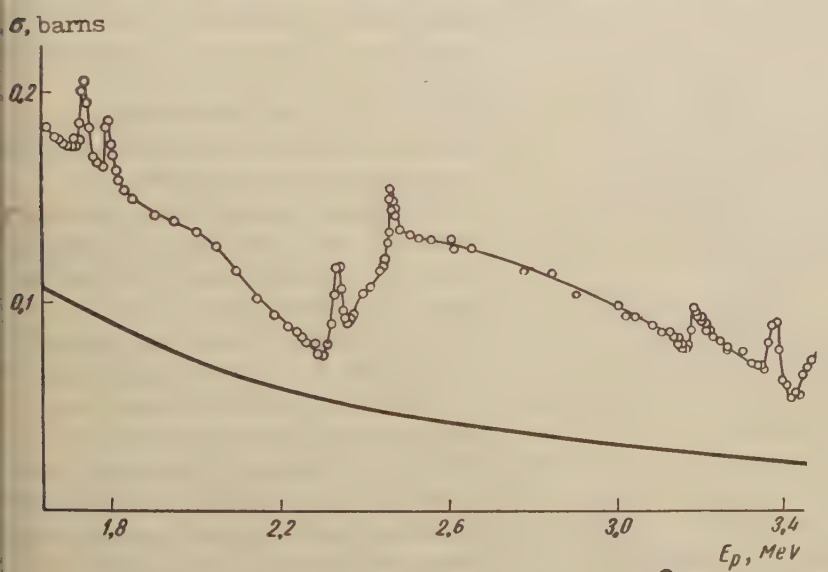

Fig.3. Same as Fig.2, but for $\theta_{c.m.} = 90^{\circ}$.

We measured the elastic scattering cross section for protons on N^{14} at angles of 54, 90, 125, 141 and 154° in the center-of-mass system in the energy range from 1.7 to 3.5 Mev. The choice of the first four angles was dictated by the consideration that for each of them one of the Legendre polynomials in the expression for the scattering cross section vanishes, which obviously facilitates phase analysis.

The measurement results are shown in Figs.2-6 by circles; the solid lines in the figures give the Rutherford (Coulomb) scattering cross section. In the vicinity of the resonances, the measurements were made at 4 kev steps. The statistical accuracy at each point was 2%. For determining the absolute scattering cross section values we compared our relative values with the results of measurements[6,7] of the cross section at an angle of 154° in the 1.6 to 1.7 Mev energy interval. Inasmuch as the statistical accuracy of our measurements did not exceed 2%, the uncertainty in the absolute values was determined by the accuracy of the utilized calibration data and is estimated to be 5-6%.

It will be evident from the figures that in the investigated energy range there are six narrow resonances and one broad ($\Gamma = 300$ kev) resonance at $E_p = 2.4$ Mev. It does not appear feasible to determine the width of the levels corresponding to the narrow resonances directly from the experimental data. Incident to passage of the proton beam through the entrance window and the gas layer between the window and the point of scattering, the energy homogeneity of the beam deteriorates appreciably owing to fluctuation in the energy loss. This leads to "blunting" and broadening of the narrow peaks.

In fact some difficulties are also encountered in phase analysis of the experimental data obtained under conditions when the level width is less than the energy spread ΔE in the incident proton beam, inasmuch as comparison of the experi-

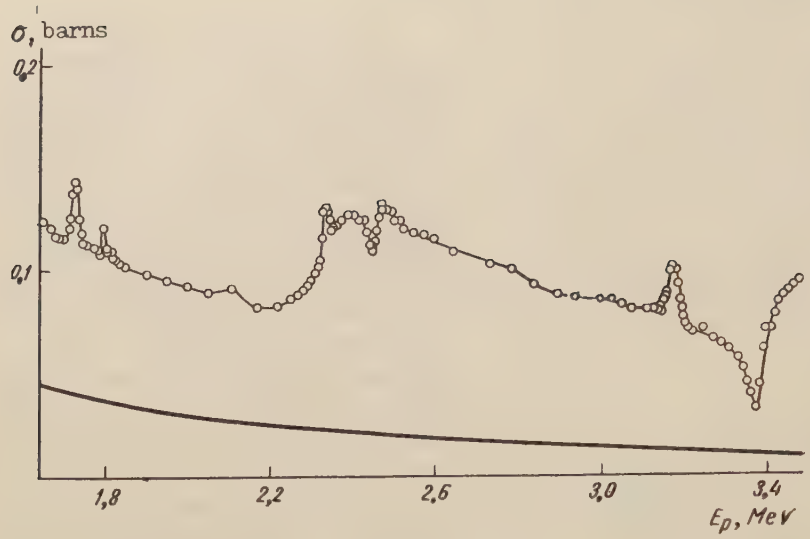

Fig.4. Same as Fig.2, but for $\theta_{c.m.} = 125^{\circ}$.

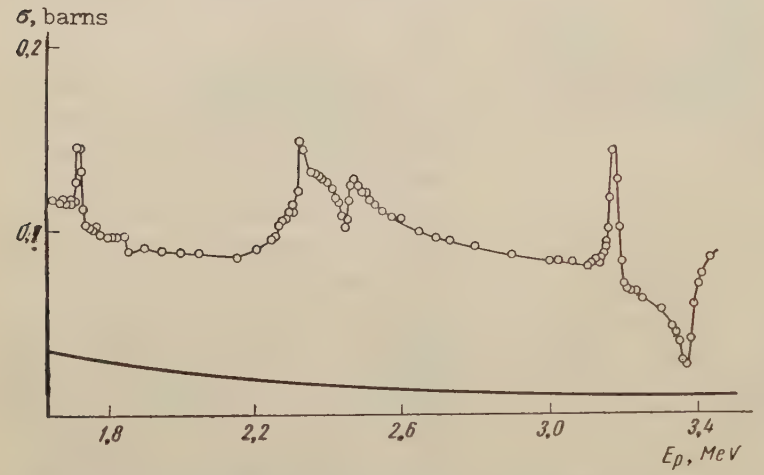

Fig.5. Same as Fig.2, but for $\theta_{c.m.} = 141^{\circ}$.

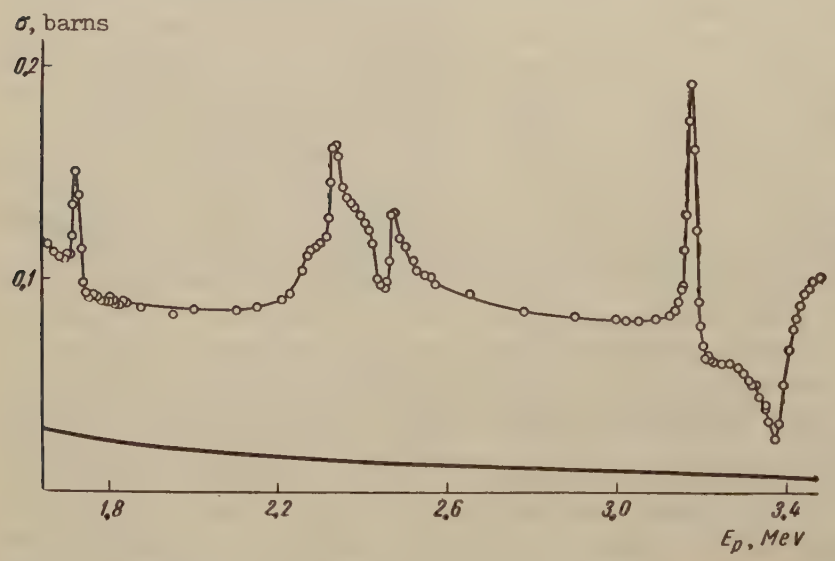

Fig.6. Same as Fig.2, but for $\theta_{c.m.} = 154^{\circ}$

mental data with the calculated requires averaging of the latter over the ΔE interval, the magnitude of which is unknown.

In order to determine the level widths, refine the resonance energy values and evaluate the actual energy spread of the proton beam in the scattering experiments, we investigated the $N^{14}(p,\gamma)$ reaction. The target for these experiments was prepared by knocking 20 kev N^{14} ions, discriminated by an electromagnetic separator, into a 0.5 mm thick tantalum backing. The γ-ray yield was measured by a 30 mm diameter, 20 mm thick CsI(Tl) crystal coupled to an FEU-19 photomultiplier. The amplifier discrimination threshold was set so that the equipment would record γ-rays with energies above 1.5 Mev.

The thickness of the target was determined through measurements of the (p,γ) resonance width at a proton energy of 1.054 Mev. According to the data of Hagedorn et al[6] and Duncan & Perry[8], the width of this resonance is 3.5 kev. The experimental resonance width in our measurements was found to be 7.5 ± 0.5 kev. Inasmuch as the energy spread in the incident proton beam was 0.05%, the observed broadening of the resonance was connected only with the thickness of the target. The experimental resonance width,

$$\Gamma_{exp} = \sqrt{d^2 + \Gamma^2};$$

whence we find that for $E_p = 1$ Mev, the target thickness $d = 6.6$ kev.

The relative γ-ray yield was measured with the same target in the regions of the

The relative γ-ray yield was measured with the same target in the regions of the 1.8, 2.35 and 2.48 Mev resonances observed in investigating the p-N^{14} elastic scattering cross section. The experimental results are given by the points in Figs.7 & 8. The solid lines in the figures are the curves calculated by the Breit-Wigner formula for the indicated resonance energies and widths. Using the determined target thickness for E_p = 1 Mev and assuming that the proton energy loss in the target varies as $1/E_p$, we find that the target thicknesses for E_p = 1.8 Mev and 2.4 Mev are 3.7 and 2.7 kev, respectively. Introducing the correction for target thickness leads to the following width values: 3.7 kev for the 1.806 resonance, 11 kev for the 2.350 Mev resonance and 9.3 kev for the 2.478 Mev resonance.

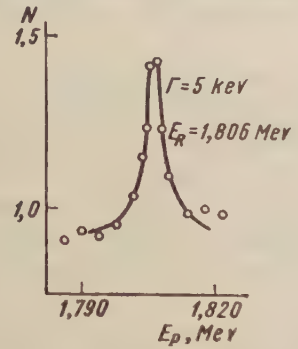

Fig. 7

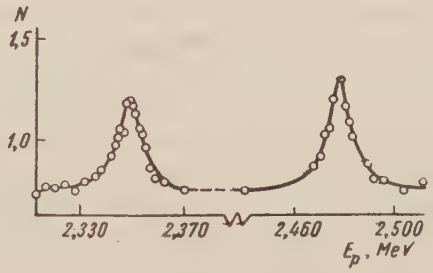

Fig. 8

Fig.7. $N^{14}(p,\gamma)$ resonance at E_p = 1.806 Mev (Γ = 5 kev). The solid line represents the curve calculated by means of the Breit-Wigner formula.

Fig.8. Same as Fig.7, but at E_p = 2.350 Mev (Γ = 11.3 kev) and E_p = = 2.478 Mev (Γ = 9.7 kev).

Because of the great increase in background, we did not investigate the $N^{14}(p,\gamma)$ reaction in the vicinity of the 3.2 and 3.4 Mev resonance energies.

If we now compare the measured widths with the corresponding values for the elastic scattering resonances, we can determine the energy spread ΔE in the incident proton beam. Comparison showed that ΔE is virtually independent of the proton energy and equals ±8 kev.

This information on the energy nonhomogeneity of the proton beam enabled us to determine the widths of the levels corresponding to the 3.2 and 3.4 Mev scattering resonances. The widths were found to be 17 ± 4 and 40 kev, respectively.

Comparing the energies of the protons at the output of the electrostatic generator, corresponding to anomalies in the elastic scattering cross section, with the corresponding quantities observed in investigating the $N^{14}(p,\gamma)$ reaction, we determined the energy loss incident to passage of the protons through the entrance window and the gas layer in the chamber. The energy loss was found to be 64 kev for E_p = 1.8 Mev and 52 kev for E_p = 2.5 Mev. These loss values proved to be some 12 kev lower than the values calculated by the familiar formulas for ionization loss. Thus comparison of the calculated and experimental energy loss values proved to be essential for determining the energies of the levels corresponding to the two last resonances.

Inasmuch as the energy loss in the gas did not exceed 5 kev, the proton energy loss observed in the scattering experiments and the energy spread ΔE associated therewith are due almost entirely to the entrance window.

Our final results for the levels of O^{15} are presented in Table 2. The first line lists the observed resonance energies; the second and third lines the widths and energies of the O^{15} levels.

Table 2

E_R, kev	1744±2	1806±2	2350±27	2400±50	2478±2	3200±10	3390±10
Γ, kev	⩽3,5	3,7±0,5	11,0±0,5	300±50	9,3±0,5	17±4	~40
E_r, Mev	8,975	9,033	9,540	9,59	9,660	10,33	10,51

It will be evident from a comparison of Tables 1 and 2 that our results as regards the resonance energies are in best agreement with the data of Bolmgren et al[1]. Our width values for the levels corresponding to the resonances at 1.744 and 1.806 Mev virtually coincide with the results of Hagedorn et al[6], while our widths for the levels corresponding to the resonances at 2.350 and 2.478 Mev are in good agreement with the data of Duncan & Perry[8].

Phase analysis of the broad resonance at 2.4 Mev, carried out by the method described by Christy[10], showed that it is predominantly due to S-wave formation. This analysis, however, did not provide an adequate basis for a definitive assignment for this level (the alternatives are 1/2+ or 3/2+). Analysis of this resonance is greatly hampered by the fact that it is overlapped by the resonances at 2.350 and 2.478 Mev and by the fact that at proton energies above 2 Mev nonresonant scattering with $l>0$ makes a substantial contribution to the scattering cross section.

The appreciable contribution of potential scattering with $l>0$ is, apparently, also the principal reason for failure of attempts to explain the off-resonance behavior of the scattering cross sections. This factor (nonresonant scattering) gives rise to great difficulties in phase analysis of narrow resonances. Thus, for example, arriving at unambiguous spin assignments under these conditions becomes extremely difficult.

We take this opportunity to thank M.I.Guseva for preparing the N^{14} target on the electromagnetic separator, and thank A.A.Tsygikalo, Yu.A.Kharchenko and the personnel servicing the electrostatic generator.

Physical-Technical Institute,
Academy of Sciences of the Ukrainian SSR

References

1. C.R.Bolmgren, G.D.Freier, J.G.Likely & K.F.Famularo, Phys.Rev., 105, 210 (1957).
2. T.S.Webb, C.W.Li & W.A.Fowler, Phys.Rev., 92, 1084 A (1953).
3. H.E.Gove, A.J.Ferguson & J.T.Sample, Phys.Rev., 93, 928 A, (1954).
4. G.W.Tautfest & S.Rubin, Phys.Rev., 103, 196 (1956).
5. S.Bashkin, Physica, 22, 1124 (1956).
6. F.Hagedorn, F.S.Mozer, T.S.Webb, N.A.Fowler & C.C.Laritsen, Phys.Rev., 105, 219 (1957).
7. A.J.Ferguson, Bull.Amer.Phys.Soc., 3, 1, 26 (1958).
8. D.B.Duncan & J.E.Perry, Phys.Rev., 53, 447 (1951).
9. A.K.Val'ter, P.V.Sorokin & A.Ya.Taranov, Trudy (Proceedings), Kharkov State University, 7, 98 (1958).
10. R.F.Christy, Physica, 22, 1009 (1956).

ELASTIC SCATTERING OF PROTONS BY A^{40}

- A.K.Val'ter, I.Ya.Malakhov, P.V.Sorokin & A.Ya.Taranov

Investigation of elastic scattering by A^{40} can yield information on the levels of K^{41} lying above 8 Mev, inasmuch as the proton binding energy in K^{41} is 7.84 Mev. There is reason to expect that at these excitation energies the level spacing will be of the order of 10 kev.[1] In view of this, investigation of the levels of K^{41} necessitates good energy resolution.

In contrast to proton scattering from light nuclei, a large contribution to the p-A^{40} scattering cross section is made by pure Coulomb scattering. This contribution, however, should not be so large as to mask completely the effects associated with the presence of excited levels. It can easily be shown that the Coulomb and nuclear scattering amplitudes at angles greater than 90° for proton energies above 2 Mev are approximately equal, which means that strong resonances may be observed in the p-A^{40} scattering cross section.

Freier et al[2] observed two strong resonances at 1.9 and 2.48 Mev in the p-A^{40} elastic scattering cross section vs energy curves measured at 155°. These investigators also measured the angular distributions for the p-A^{40} interaction at these resonance energies. Their results, however, were not adequate for definitive spin-parity assignments for the levels associated with the observed resonances. To make such assignments, one must measure the scattering cross section for several angles at different proton energies.

In the present work we measured the p-A^{40} elastic scattering cross section at scattering angles of 90, 125 and 150° in the center-of-mass system in the energy range from 1.7 to 2.7 Mev.

Procedure and results

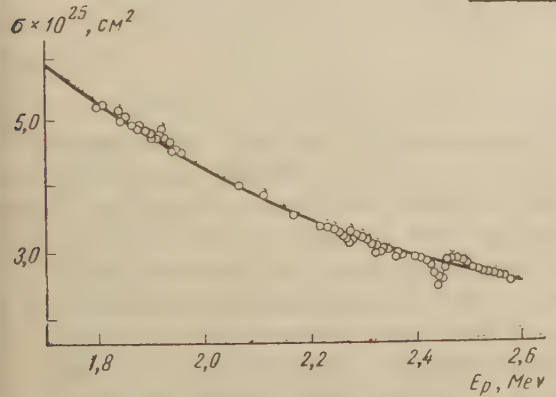

Fig.1. Cross sections for elastic scattering of protons by A^{40} at $\theta_{c.m.} = 90°$.

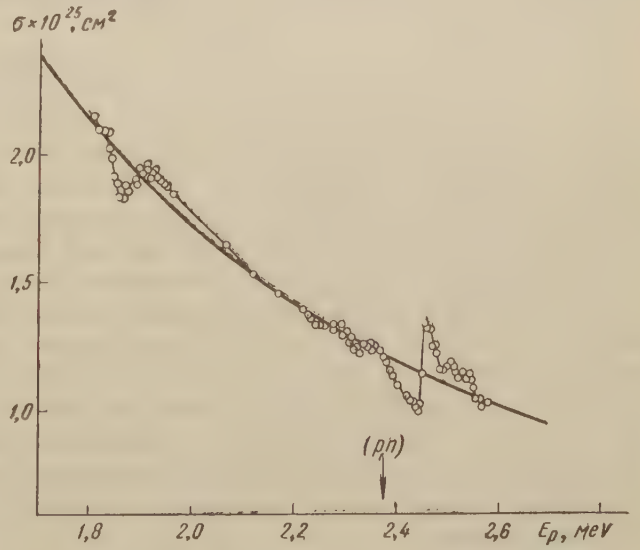

Fig.2. Same as Fig.1, but at $\theta_{c.m.} = 125°$.

The cross section measurements were carried out by means of the equipment described in Ref.3 (preceding article). By way of target we used gaseous argon having the natural isotopic composition (99.6% A^{40}). The pressure in the scattering chamber was maintained at 5 mm Hg. As was shown in Ref.3, the energy spread of the proton beam is connected with its passage through the entrance window and in the present experiments was about ±8 kev. This spread determined the energy resolution in our experiments.

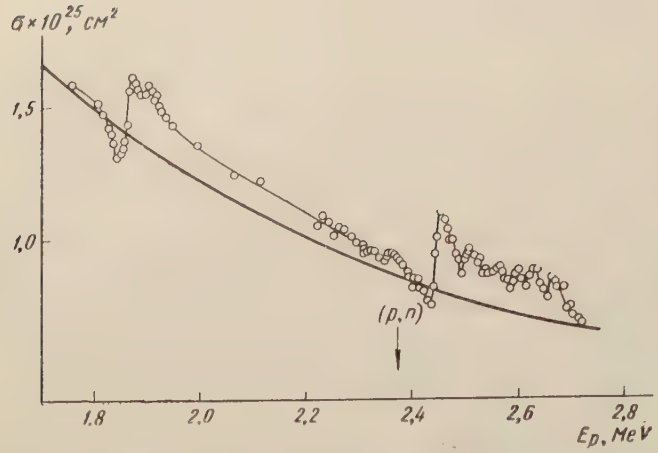

Fig.3. Same as Fig.1, but at $\theta_{c.m.} = 150^{\circ}$.

In the vicinity of the resonances the measurements were made in 4 kev steps; the statistical error in each cross section measurement did not exceed 1%. The cross section was also carefully investigated in the vicinity of the threshold (2.37 Mev[4]) of the A^{40}(p.n) reaction, where, according to Baz'[5], there may be observed an anomaly with a width of about 20 kev.

The absolute values of the cross section were determined from its ratio to the cross section at 60°, where the cross section is given by the Rutherford formula.

The experimental results are shown by the circles in Figs.1,2 & 3. The heavy lines in the figures represent the Rutherford scattering cross section. It will be evident from the figures that there are two strong resonances at 1.86 and 2.45 Mev and a number of resonances above 2.5 Mev. Off-resonance the cross section at angles of 90 and 125° virtually coincides with the Rutherford value; at 150° it is approximately 10 times higher than the Rutherford value.

No anomalies with a relative change in cross section exceeding 5% were observed in the vicinity of the threshold of the A^{40}(p,n) reaction. Inasmuch as the widths of the observed resonances are comparable with the experimental energy resolution, we could not reliably determine the level widths. Approximate evaluations showed, however, that they are less than 10 kev.

Discussion

It will be seen in Fig.3 that the 1.86 Mev resonance is split. This means that this peak is associated with at least two levels of K^{41}. Phase analysis of such resonances is extremely difficult. If it be assumed, however, that the shape of the observed resonance is determined primarily by the properties of one level, one can, utilizing the graphic method described by Laubenstein & Laubenstein[6], show that the shape of the resonance at 1.86 Mev is qualitatively reproduced for $l = 1$. The shape of the resonance at 2.45 Mev, on the same assumption, is similarly reproduced for $l = 0$. This means that the principal contribution to the resonance at 1.86 Mev is made by a level with spin 1/2- or 3/2-; that to the resonance at 2.45 Mev by a level with spin 1/2+. Quantitative comparison of the experimental curves with the calculated ones is not feasible. This is due to the fact that the level widths in this case remain unknown and to the fact that it is virtually impossible to evaluate the contribution from interference with neighboring resonances.

The absence of an anomaly in the p-A^{40} cross section that could be definitely associated with the threshold of the A^{40}(p,n) reaction can, presumably, be explained using the results of Baz', according to which the magnitude of the expected anomaly is proportional to the inelastic scattering cross section. For the A^{40}(p.n) case σ_{inel} near the threshold should be small. Thus, it follows from considerations of conservation of momentum and parity in the A^{40}(p,n)K^{40} reaction (K^{40} in the ground state) that this reaction can be realized only by protons with $l = 3$ and $l = 5$. Hence the neutron yield corresponding to the ground state of

K^{40} will be very small. This inference has been substantiated in the work of Holland et al[4] who observed only neutrons corresponding to transitions to the second and third excited states of K^{40} (i.e., no zero neutron group) in bombarding A^{40} with protons in a wide energy range.

In this case one should expect the appearance of an anomaly at an energy of 2.4 Mev, which corresponds to the threshold for formation of the first excited state of K^{41}. But, as will be evident from Figs.2 & 3, in the vicinity of the threshold energy the scattering cross section changes sharply owing to the presence of the resonance at 2.45 Mev. The influence of this resonance is apparently sufficiently great to conceal any anomaly associated with the reaction threshold.

We evaluated the level spacing in K^{41} at an excitation energy of 10 Mev on the basis of the observed resonances at energies above 2.4 Mev. If we assume that each resonance corresponds to one level, the average distance between levels proves to be about 20 kev. This value is in agreement with the results of Freier et al[2] and those of Preston et al[1] who arrived at a value of 16 kev for the mean spacing between the levels of Ca^{40} at an excitation energy of 12.37 Mev.

Physical-Technical Institute,
Academy of Sciences of the Ukrainian SSR

References

1. R.S.Preston, J.P.Schiffer, L.L.Lee & N.Rosenzweig, Bull.Amer.Phys.Soc., 3, 380 (1958).
2. G.D.Freier, K.F.Famularo, D.M.Zipoy & J.Leigh, Phys.Rev., 110, 446 (1958).
3. A.K.Val'ter, A.S.Deineko, I.Ya.Malakhov, P.V.Sorokin & A.Ya.Taranov, Present issue of the Bulletin, p.833.
4. R.E.Holland, F.J.Lynch & Kineo Tsukado, Bull.Amer.Phys.Soc., 3, 103 (1958).
5. A.I.Baz', Zhru.eksp.i teor.fiz., 33, 923 (1957). (Trans.Soviet Physics-JETP).
6. R.A.Laubenstein & M.J.W.Laubenstein, Phys.Rev., 84, 18 (1951).

EXCITED STATES OF Ga^{67} AND Ga^{68}

- A.K.Val'ter, I.I.Zalyubovskii, V.A.Klyukharev & V.A.Lutsik

Earlier[1] we reported on the preliminary findings of our investigation of the energy states of Ga^{67}. In the present article we give the results of a careful investigation of the γ-radiations from the $Zn^{66}(p,\gamma)Ga^{67}$, $Zn^{67}(p,n\gamma)Ga^{67}$ and $Zn^{67}(p,\gamma)Ga^{68}$ reactions. We also investigated the decay of Ga^{67}. The proton energy was varied from 1.6 to 3.4 Mev; the protons were accelerated by the Physical-Technical Institute (Ukrainian SSR Academy of Sciences) 4 Mev electrostatic generator.

Experimental results

The measured energies of the observed γ-lines are listed and compared with the results of other investigators in Table 1. The γ-spectra are reproduced in Figs.1,2 and 3. The isotopic compositions of our targets are given in Table 2.

Table 1

Energies (in kev) of γ-rays emitted from proton bombarded Zn^{66} and Zn^{67} targets

№	[3]		[4]		Our data			
	(p, n)				Zn^{67} target			Zn^{66}
	Ga^{67}	Ga^{68}	$Ge^{67}\rightarrow Ga^{67}$	$Ga^{67}\rightarrow Zn^{67}$	Zn^{67}	Ga^{68}	Ga^{67}	Ga^{67}
1				90—92	90—92			
2						(122±3)		
3		188±8	170	182	182	188±4	(172)	172±3
4				296	296			
5	357±12	342±10		388	(388)		359±3	359±3
6						510±10	510±10	510±10
7		574±13				580±15		
8	850±20					830±15	820±10	820±10
9				880	880		905±10	900±20
10							1205±15	1200±20
11	1540±20						1420±20	

Table 2

Isotopic composition of targets

	Zn^{64}	Zn^{66}	Zn^{67}	Zn^{68}	Zn^{70}
Zn^{66}	2,1	96,7	0,4	0,6	>0,1
Zn^{67}	3,5	15,5	71,4	8,8	0,8

In investigating the γ-spectrum from the Zn^{67} target in the 172-188 kev region, we found that the γ-peak shifts to the side of lower energies with increase of the proton energy from 1.8 to 2.5 Mev. The reason for this shift is the following: at proton energies under 1.96 Mev, when the 172 kev state of Ga^{67} is not yet excited, there is observed 188 kev γ-radiation from the $Zn^{67}(p,\gamma)Ga^{68}$ reaction and 182 kev radiation from the $Zn^{67}(p,p'\gamma)$ reaction. With increase of the proton energy there appear Ga^{67} 172 kev γ-rays. At proton energies above 2.1 Mev, there is evinced intense γ-radiation in the 120 to 240 kev region as a result of interaction of the neutrons from the $Zn^{67}(p,n)Ga^{67}$ reaction with the scintillator crystal. The γ-spectrum of this interaction is complex and can be allowed for by measuring the neutron flux from the Zn^{67} target and comparing it with the neutron flux at the same energy from a target for which there are no other lines in this energy region except those produced by neutrons in the scintillator.

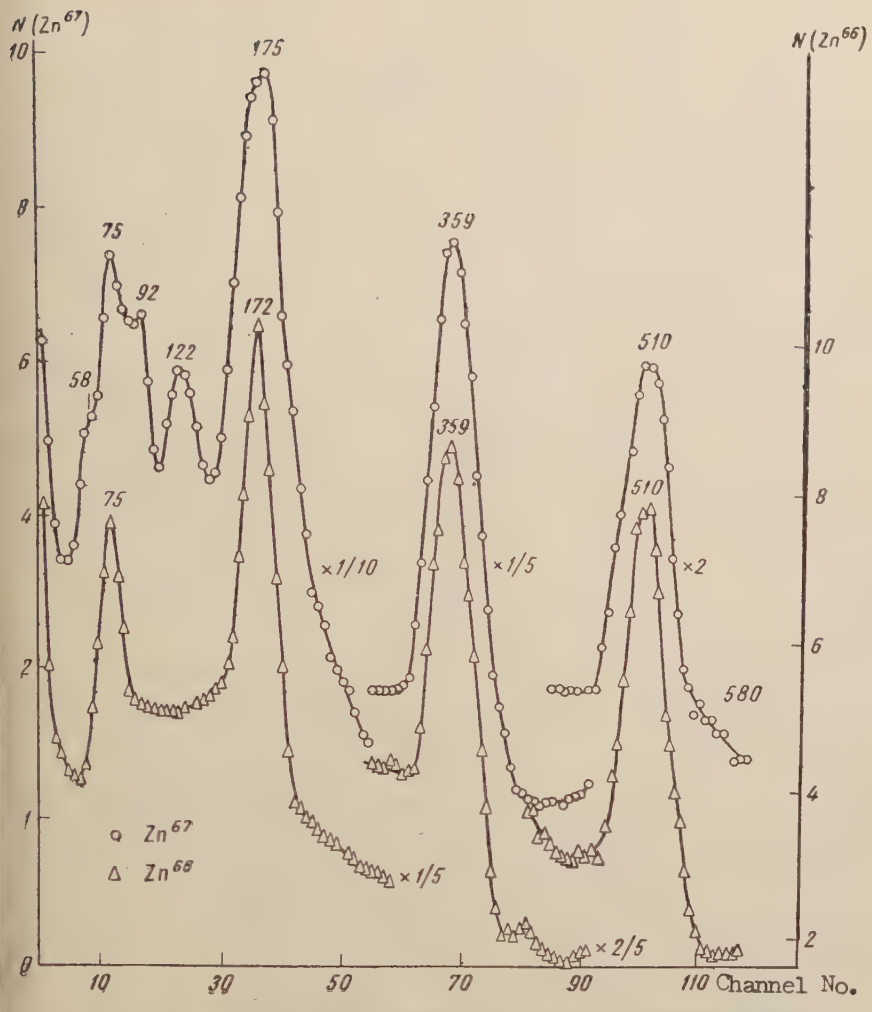

Fig.1. Low energy part of the γ-spectrum from the Zn^{66} and Zn^{67} targets bombarded with 2.5 Mev protons.

We used the $Co^{59}(p,n)Ni^{59}$ reaction, the threshold of which lies at 1.86 Mev. The γ-spectrum from the neutron interaction with the NaI(Tl) scintillator is shown in Fig.4. Inasmuch as the 58 kev γ-line is due to the $I^{127}(n,n'\gamma)$ reaction[2], it can serve as a measure of the neutron flux of the given energy. Comparing the intensities of this γ-line in the spectra of Zn^{67} and Co^{59} (Figs. 1 & 4), and taking into account the greater width of the 163 kev γ-line (Fig.4), we conclude that there should be no noticeable displacement of the peak in the case of Zn^{67}, although the intensity contribution from the neutron interaction is appreciable.

We did not undertake to subtract this background, inasmuch as in addition to it one should subtract the contributions from the $Zn^{67}(p,p\gamma)$ (E_γ = 182 kev), $Zn^{67}(p,\gamma)Ga^{68}$ (E_γ = 188 kev) and $Zn^{66}(p,\gamma)Ga^{67}$ (E_γ = = 172 kev) reactions (in order to plot the excitation function for 172 kev gammas from the $Zn^{67}(p,n\gamma)Ga^{67}$ reaction). We established that the contribution from the $Zn^{66}(p,\gamma)Ga^{67}$ reaction amounts to less than 5% of the total intensity of the γ-radiation (associated with the main isotope) in the 172-188 kev region. Hence the shift of the γ-peak with increase in proton energy can be explained only by the presence of γ-radiation of 172 kev energy, arising from the $Zn^{67}(p,n\gamma)Ga^{67}$ reaction.

In investigating the $Zn^{68}(p,n)Ga^{68}$ reaction, Chapman & Slattery[3] detected a neutron group corresponding to a 342 kev excited state of Ga^{68}. We failed to observe a γ-line of approximately this energy from the $Zn^{67}(p,\gamma)Ga^{68}$ reaction against the background of the 359 kev line from $Zn^{66}(p,\gamma)Ga^{67}$ and the 388 kev line from $Zn^{67}(p,p'\gamma)$. The existence of the 388 kev γ-rays from the last reaction is connected with the existence of 296 kev γ-rays, which we did observe and which are associated with a cascade transition from the 388 kev level through the 92 kev level in Zn^{67} (Fig.5 & Table 3).

In our previous contribution[1] we hypothesized the existence of an 850 kev level in Ga^{67}, which was assumed to de-excite by a cascade transition through the 359 kev level. There are indications in the literature[6] that such a level does exist. In the present study we did not succeed in detecting γ-radiation with an

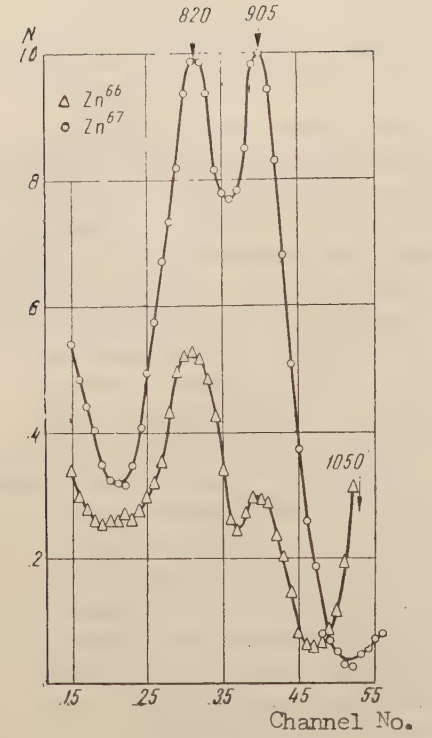

Fig. 2

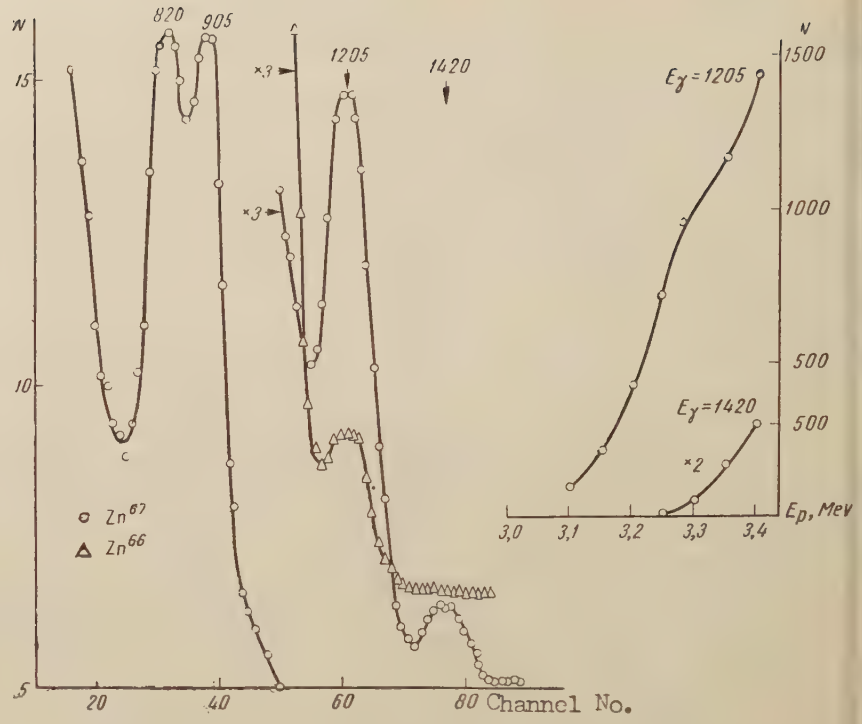

Fig. 3

Fig.2. Spectra of γ-rays from the Zn^{66} and Zn^{67} targets bombarded with 3.0 Mev protons.

Fig.3. High-energy part of the γ-ray spectrum from the Zn^{66} and Zn^{67} targets bombarded with 3.4 Mev protons. The insert at the right is the excitation function for the 1205 and 1420 kev γ-rays.

Table 3

Intensity ratios of γ-rays emitted in $Ga^{67} \rightarrow Zn^{67}$ decay

E_γ, kev	90	92	182	210	296	388	All other
Our data	—	100	40±3	—	24±3	9,5±1	—
Ref.5	7,0±0,5	93±0,5	44,1±3	3,0±0,8	27,5±1	9,7±1	1
Ref.6	6,8	93,2	75,6	1,9	50,4	12,1	2,5
Ref.7	—	100	34	3,2	19,4	4,8	—
Ref.8	5±1	95±1	53,5±5	5,5	49±6	15±3	1,6

energy of 500 kev and an intensity sufficient to distinguish it against the background from annihilation radiation appearing as a result of positron creation by the high energy γ-rays and in the decay of Ga^{68}.

In investigating the γ-spectra from the Zn^{66} and Zn^{67} targets, we established the existence of two close γ-lines, namely, 820 and 905 kev, in the radiation from both targets (Fig.2). In view of the exact coincidence of the energies in both spectra, one can attribute these γ-rays to Ga^{67}; moreover, the excitation threshold for E_γ = 820 and 905 kev in the $Zn^{67}(p,n\gamma)Ga^{67}$ reaction indicates that these departure levels are excited states of Ga^{67}.

Chapman & Slattery[3] probably could not resolve the corresponding neutron group owing to the great thickness of their target (100 kev); hence they give only an average energy value of 850 kev. Owing to inadequate separation of the

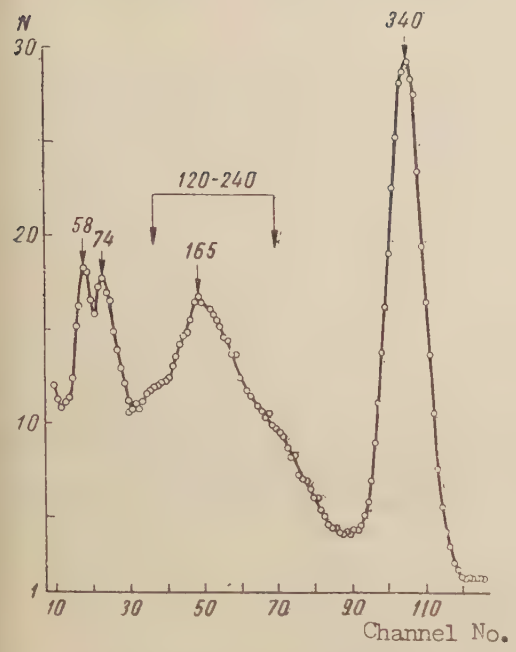

Fig.4. Low-energy section of the γ-spectrum due to interaction of neutrons with the scintillator (except the 74 and 340 kev γ-lines). Results obtained in bombardment of Co^{59} with 2.5 Mev protons.

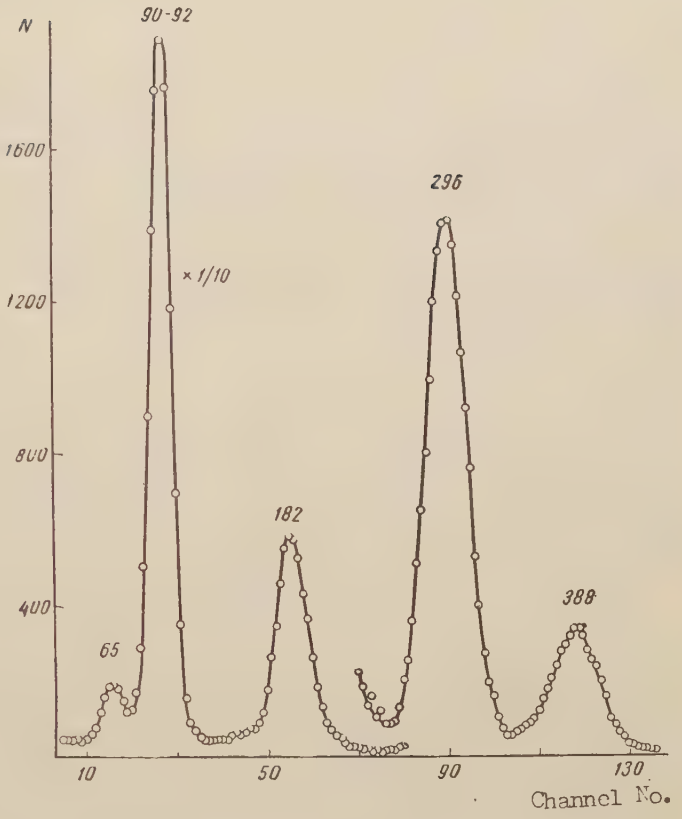

Fig.5. Spectrum of γ-rays emitted in $Ga^{67} \rightarrow Zn^{67}$ decay.

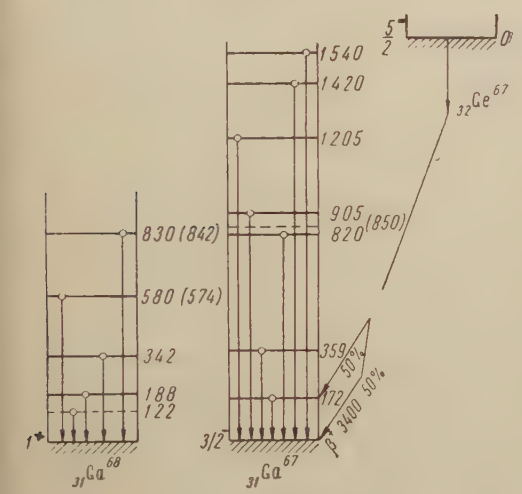

Fig.6. Levels of Ga^{67} and Ga^{68}.

820 and 905 kev lines and the presence of admixtures from other reactions, we did not measure the excitation function.

At proton energies below the excitation threshold for these levels in the $Zn^{67}(p,n)Ga^{67}$ reaction we observed 830 kev γ-rays, which we attributed to the $Zn^{67}(p,\gamma)Ga^{68}$ reaction, and weak 880 kev γ-radiation, which we associated with the $Zn^{67}(p,p'\gamma)Zn^{67}$ reaction.

We did determine the excitation functions for the 1205 and 1420 kev γ-lines (Fig.3). The excitation thresholds equal the calculated values, and both γ-lines correspond to excited states of Ga^{67}. There are no data regarding these excited states of Ga^{67} in the literature.

If we analyze the variation of the ratio of slow to fast neutrons with the proton energy given by Chapman & Slattery[3], we find that there is evidence in the experimental curve of a neutron group corresponding to these excited states, although Chapman & Slattery do not mention them.

We attributed the 122 ± 3 kev γ-line to Ga^{68}, although one cannot exclude the possibility that it appears from the $Zn^{70}(p,n\gamma)Ga^{70}$ reaction.

On the basis of our measurements we propose the level diagrams for Ga^{67} and Ga^{68} shown in Fig.6. The Ga^{67} level at 1540 kev was taken from the work of Chapmen & Slattery[3].

We also investigated the γ-radiation accompanying $Ga^{67} \rightarrow Zn^{67}$ decay (Fig.5). The peak at 65 ± 2 kev corresponds to absorption of 92 kev γ-rays (28 kev x-rays subtracted) by the iodine of the scintillator. The intensity ratios of the investigated γ-lines are listed in Table 3.

Physical-Technical Institute,
Academy of Sciences of the Ukrainian SSR &
"A.M.Gor'kii" Kharkov State University

References

1. A.K.Val'ter, I.I.Zalyubovskii, A.P.Klyucharev, G.E.Krivets & V.A.Lutsik, Izv.AN SSSR, Ser.fiz., 23, 225 (1959). (Trans.Bulletin 23, No.2, 217.)
2. B.S.Dzhelepov & L.K.Peker, Skhemy raspada radioaktivnykh izotopov (Decay schemes of radioactive isotopes), M.-L., 1958.
3. R.A.Chapman & J.S.Slattery, Phys.Rev., 105, 633 (1957).
4. A.H.W.Aten, T.de Vries-Hamerling & L.Lindner, Physica, 19, 1046 (1953).
5. W.Meyerhof, L.Mann & H.West, Phys.Rev., 92, 758 (1953).
6. B.Ketell, A.Brosi & E.Porter, Phys.Rev., 90, 567 (1953).
7. A.Mukerji & P.Preiswern, Helv.phys.acta, 25, 376 (1952).
8. L.H.Kietjens & H.S.Van der Bold, Physica, 21, 701 (1955).

FINE STRUCTURE OF THE ALPHA-SPECTRUM OF Th^{229}

- G.E.Kocharov, A.P.Komar, G.A.Korolev, I.N.Marov & Yu.A.Surkov

Radioactive Th^{229} is produced in α-decay of U^{233} with a period of $1.62 \cdot 10^5$ years. Inasmuch as the period of Th^{229} is 7000 years, its activity builds up very slowly. Consequently, a large amount of U^{233} is needed to obtain sufficient Th^{229} activity for measurement purposes. Thus, for example, a ten year old one gram sample of U^{233} contains only about 40 μg of Th^{229} (~8 μC). The difficulty of obtaining sufficient amounts of Th^{229} undoubtedly explains why there have been only a few studies of the α-decay of this isotope.

In their investigation of the 4n + 1 radioactive series, Hagemann et al[1] investigated the α-decay of Th^{229} in an ionization chamber. Owing to the low energy resolution of their equipment they were able to resolve reliably only the most intense α-particle group with an energy of 4850 kev. In addition, they identified two weaker groups with energies of 4940 and 5020 kev.

The present investigation was undertaken with a view to checking and refining the data of Hagemann et al, taking advantage of the high resolution of our ionization α-spectrometer[2,3].

Chemical separation of Th^{229}

As the initial step in the preparation of the source, U^{233} uranyl uranate was dissolved in concentrated nitric acid. The resultant uranyl nitrate solution was evaporated to minimal volume and then diluted with nitric acid to obtain a 2-3 N solution. The major portion of the uranium was separated by extraction of the uranyl nitrate from the solution with ethyl ether. The extraction operation was repeated 6-8 times. It is known that thorium is virtually not extracted by ethyl ether.

Further purification of the thorium was realized by the ion exchange technique. To this end a water solution of the uranyl nitrate and decay products, after extraction and precipitation of the ammonium diuranate, was dissolved in concentrated hydrochloric acid. According to the data of Kraus & Nelson[5], U(VI) is readily absorbed by anionites from concentrated hydrochloric acid solutions. On the other hand, thorium is not absorbed by anionites from HCl solutions at any concentrations.

The resultant solution of the chlorides of uranium and its decay products in an 8 N solution of HCl was passed through a 6 mm diameter, 40 cm long column filled with EDE-10n ion exchange resin, flushed beforehand with an 8 N solution of HCl. It must be noted that the thorium appears in the filtrate much later than might be expected on the basis of the data of Refs.5 & 6. As regards activity, the first 30-40 ml of the filtrate contained primarily the daughter products of thorium; after which thorium appeared. The process was monitored by observing the α-spectra in an ionization chamber.

The anionite was washed with 8 N solution of HCl until traces of uranium appeared in the filtrate (after the passage of 100-130 ml 8 N HCl solution). Final purification of the Th^{229} from uranium and the decay products was realized by passing a solution of the chlorides of these elements in 2 N HCl solution through a layer of KU-2 cationite. The thorium under these conditions is stably absorbed by the cationite.[4,6] After passage of the solution the cationite was washed with 30-40 ml 2 N HCl solution in order to expel the residues of uranium and decay products from the cationite. The thorium was extracted from the cationite by means of 30-50 ml 1 N solution of $H_2C_2O_4$. This purified thorium product was used for preparing the α-particle sources, including film sources for measurement of α-e_K coincidences.

α-Spectrum of Th^{229}

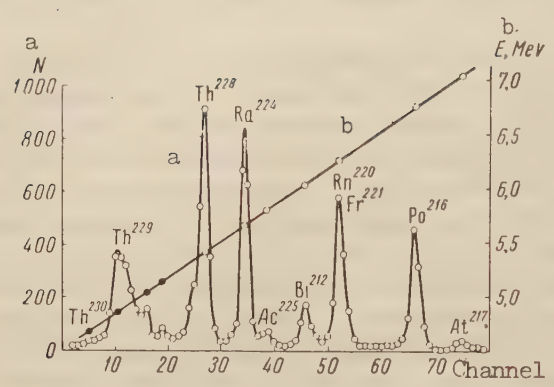

Fig.1

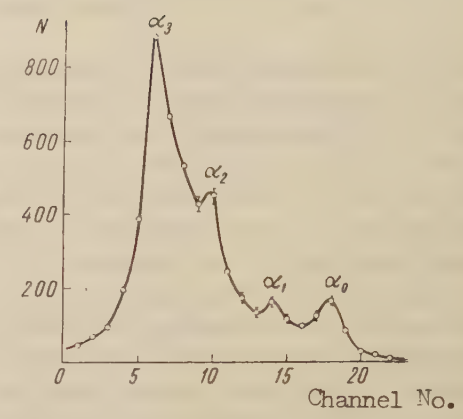

Fig.2

Fig.1. a - Spectrum recorded without collimation; b - calibration curve (scale at right). The solid points pertain to unknown lines; the open circles to known lines.

Fig.2. α-Spectrum of Th^{229} obtained with electric collimation. Channel width - 17 kev.

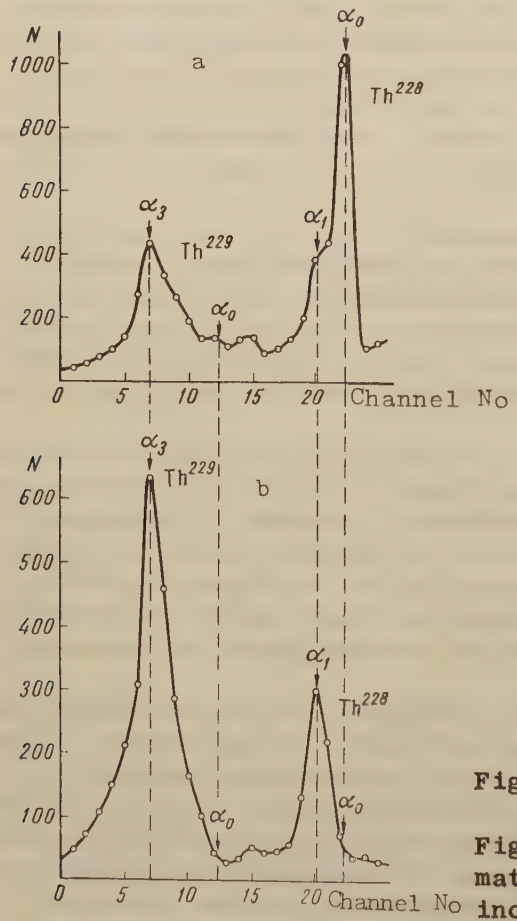

Fig.3

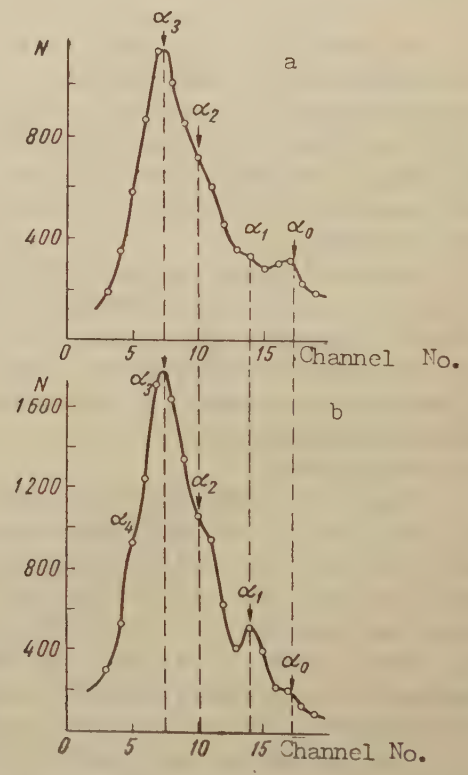

Fig.4

Fig.3. α-Spectrum of Th^{228} and Th^{229} recorded without coincidences, b - α-e_K coincidences.

Fig.4. α-Spectrum of Th^{229} recorded without collimation. Channel width - 21 kev; a - without coincidences, b - α-e_K coincidences. Note bulge due to the α_4 group evident in the latter spectrum.

As noted above, the energy spectrum of the α-particles from Th^{229} was investigated by means of an ionization α-spectrometer.

In our U^{233}, in addition to Th^{229}, there was present a certain amount of Th^{228}. The well known α-lines of Th^{228} and its daughters were utilized for determining the energy of the unknown α-lines. Thus the α-particles from Th^{229} and the reference lines were analyzed under the same conditions. One of the recorded calibration curves is shown in Fig.1. The reference lines utilized were the α-lines of Th^{229} (5421 kev), Ra^{224} (5681 kev), Rn^{220} (6282 kev) and Po^{216} (6775 kev). As was shown in the work of Harwey et al[7], imperfect screening of the grid, the thickness of the source and differences in pulse rise times all shift the peak of the α-particle pulse distribution to the side of lower energies. Inasmuch as the magnitude of the shift varies with the energy, the α-particle spectrum is distorted. Hence we introduce all necessary corrections. The energy of the principal α-particle group from Th^{229}, determined as a result of several series of measurements, proved to be 5040 ± 5 kev.

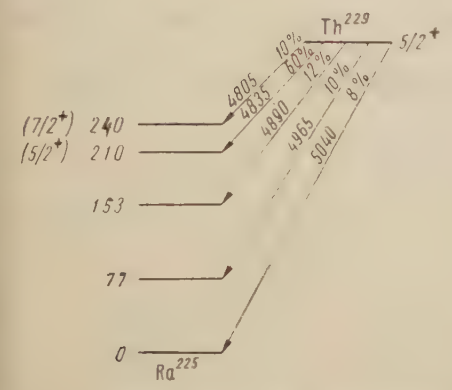

Fig.5. Decay Scheme of Th^{229}.

The energies of the other α-groups were determined from the spectrum recorded using electric collimation (Fig.2). In addition to the principal (α_0) line, there were clearly discernible three more fine structure lines.

The fact that the α_0 group is associated with transition to the ground state of the Ra^{229} daughter is substantiated by measurements of coincidences of the α-particles with conversion electrons. The conversion electrons were detected by a proportional counter located inside the ionization chamber.[8] The principal α-particle groups are absent from the α-spectra recorded in coincidence with conversion electrons. This is evident, for example, in the spectrum of Th^{228} shown in Fig.3.

It may also be noted (Fig.4) that the peak associated with the α_0 group is effaced from the Th^{229} spectrum recorded in coincidence with conversion electrons with a narrower channel width. In addition to the above mentioned Th^{229} groups, we found evidence of yet another group - α_4 - in the low energy region. The thorium α-line energies and relative intensities as determined from the experiments are listed in the following table:

Line	α_0	α_1	α_2	α_3	α_4
E_α, kev	5040±5	4965±10	4890±10	4835±5	4805±5
Relative intensity,%	8	10	12	60	10

On the basis of the experimental results we propose the decay scheme shown in Fig.5.

Inasmuch as the favored transition occurs without change of K (projection of the total angular momentum on the nuclear symmetry axis), the assignment for the 210 kev level should be 5/2+. Apparently, a rotational band with K = 5/2 is based on this level. The first level of this band is located at 240 kev and has spin 7/2.

We are now undertaking an investigation of the spectrum of conversion electrons accompanying the α-decay on a magnetic β-spectrometer for the purpose of determining the assignments for the other levels.

We desire to express our sincere gratitude to E.A.Damaskinskii, graduate student of Leningrad Polytechnic Institute, for assistance in the work.

Physical-Technical Institute,
Academy of Sciences of the USSR

References

1. F.Hagemann, L.I.Katzin, M.H.Studier, G.T.Seaborg & A.Ghiorso, Phys.Rev., 79, 3, 435 (1950).

2. B.A.Bochagov, G.E.Kocharov & G.F.Kirshin, PTE (Instruments & Experimental Techniques) No.6, 72 (1957).

3. B.A.Bochagov, A.P.Komar & G.E.Kocharov, Zhur.eksp.i teor.fiz., 32, 1257 (1957). (Trans.Soviet Physics - JETP.)

4. The Actinide Elements, Edited by G.T.Seaborg & J.J.Katz, N.Y., 1953. (Cited in Russian trans., 1955.)

5. K.A.Kraus & F.Nelson, Chemistry of Nuclear Fuels. Collected reports of foreign scientists at the International Conference on the Peaceful Uses of Atomic Energy, p.353, GITIKhL, M., 1956.

6. K.Heid, Ibid., p.393.

7. B.G.Harwey, H.G.Jackson, T.A.Estwood & G.C.Hanna, Canad.J.Phys., 35, 258 (1957).

8. A.P.Komar, G.A.Korolev & G.E.Kocharov, Izv.AN SSSR, Ser.fiz., 22, 824 (1958). (Trans.Bulletin, 22, No.7, 818.)

CONVERSION ELECTRON COINCIDENCES IN $Se^{75} \rightarrow As^{75}$ DECAY

- V.E.Bunakov, B.S.Dzhelepov, I.Zvol'skii & V.A.Sergienko

We investigated coincidences between the conversion electrons emitted in $Se^{75} \rightarrow As^{75}$ (T = 127 days) decay on the twin magnetic lens β-spectrometer described in Ref.1. The Se^{75} was prepared by neutron irradiation of selenium enriched in Se^{74}. The activity was deposited in the form of a selenide on a lightly aluminized mica film. The effective diameter of the source did not exceed 5 mm.

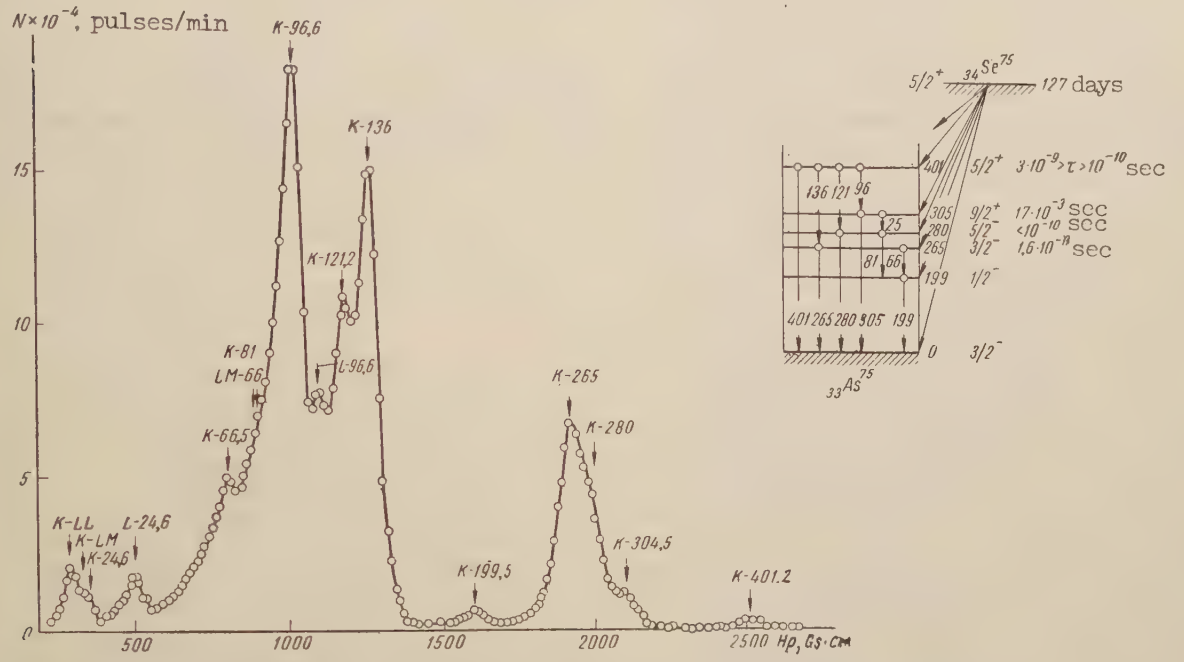

Fig.1. Singles $Se^{75} \rightarrow As^{75}$ conversion electron spectrum. At right - the section of the As^{75} level scheme corresponding to our results.

The decay of Se^{75} has been investigated by a number of authors. The latest results are given in the work of Grigor'ev et al[2]. Gamma-rays with energies of 25, 66, 77, 81, 96, 121, 136, 199, 265, 280, 305, (370), 401 (475) and 572 kev were recorded. Coincidences between γ-rays were investigated by Lu et al[3], Schardt et al[4] and Van den Bold et al[5] by means of scintillation spectrometers. Coincidences between the following γ-rays were observed: 66 & (121 + 136), 66 & 199, (121 + 136) & 199, and (121 + 136) & (265 - 280) kev.

The decay scheme based on the latest data is shown in Fig.1 (insert).[2,6]

The singles conversion electron spectrum of Se^{75} up to 400 kev, as recorded by the magnetic lens of our spectrometer viewing the activity side of the source, is shown in Fig.1. Inasmuch as the mica backing was very thin, the singles spectrum obtained on the other half of the spectrometer differed very little from that reproduced in Fig.1. The energies of the lines and their relative intensities agree with the data of Refs.2 & 4.

Coincidences between conversion electrons emitted in $Se^{75} \rightarrow As^{75}$ decay

In recording electrons with both halves of the twin spectrometer there were observed coincidences between the following conversion electrons: K-136 & K-66, K-136 & K-265, K-121 & K-280, K-199 & K-55, and K-199 & (K-66.5 + K-81). The coincidence rates at the line peaks and the numbers of chance and true coincidences

Line on 1st spect. (thru backing)	Counting rate at peak, 10^{-4} c/min	Line on 2nd spect	Counting rate at peak, 10^{-4} c/min	Coincidences per hour		
				Total	Chance	True
K- 66	10	K-136	29	755	463	292
K-136	29	K-265	18	1758	1162	596
K-121	21	K-280	13	604	274	330
K-199	1,2	K- 66	10,5	205	55	150

are listed in the accompanying table.

As will be evident from the table, the ratio of true to chance coincidences was small in all cases: from 0.5 to 3. This is explained by the low values of the internal conversion coefficients of the γ-transitions (light nucleus).

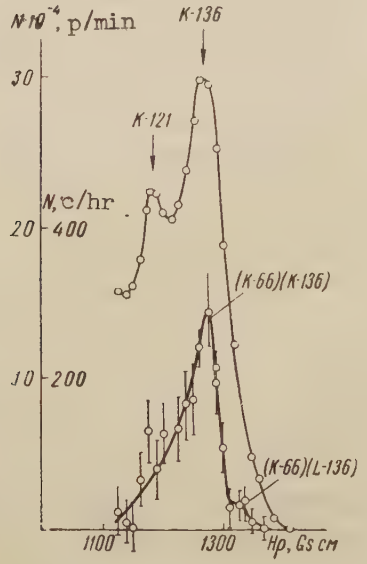

Fig.2. Heavy line - coincidences with the K-66 electrons; light line - K-121 and K-136 lines recorded on a single spectrometer.

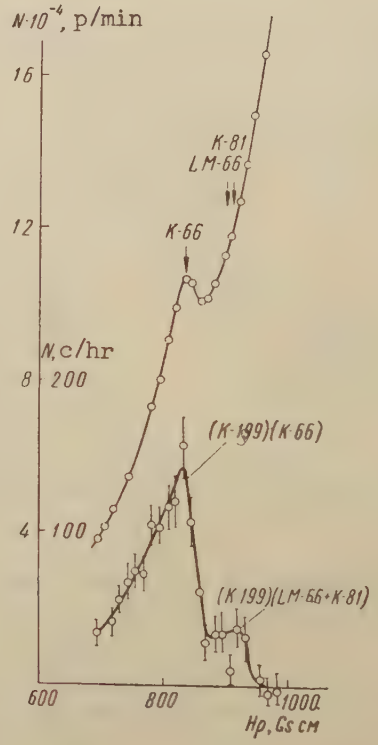

Fig.3. Heavy line - coincidences with K-199 electrons; light line - singles K-66 line.

The occurrence of coincidences between the 66 and 136 kev transitions is illustrated in Fig.2. Our data also indicate that these transitions are in cascade. According to the Se^{75} decay scheme (Fig.1), there should be observed coincidences between the electrons from the 121 and 66 kev transitions if there is a 15 kev transition between the 265 and 280 kev levels. We did not detect this transition: the number of (K-66)-(K-121) coincidences did not exceed the statistical fluctuations (Fig.2).

Fig.3 shows the results of investigating coincidences between the K-99 electrons and the K-66, LM-66 + K-81 and K-96 electrons. There is clearly evident a strong peak due to (K-199)-(K-66) coincidences in the region of the K-66 line. The M-66 and K-81 lines were not evinced in the singles spectrum; in the coincidence spectrum, however, one can discern a (K-199)-(LM-66 + K-81) peak. Accord-

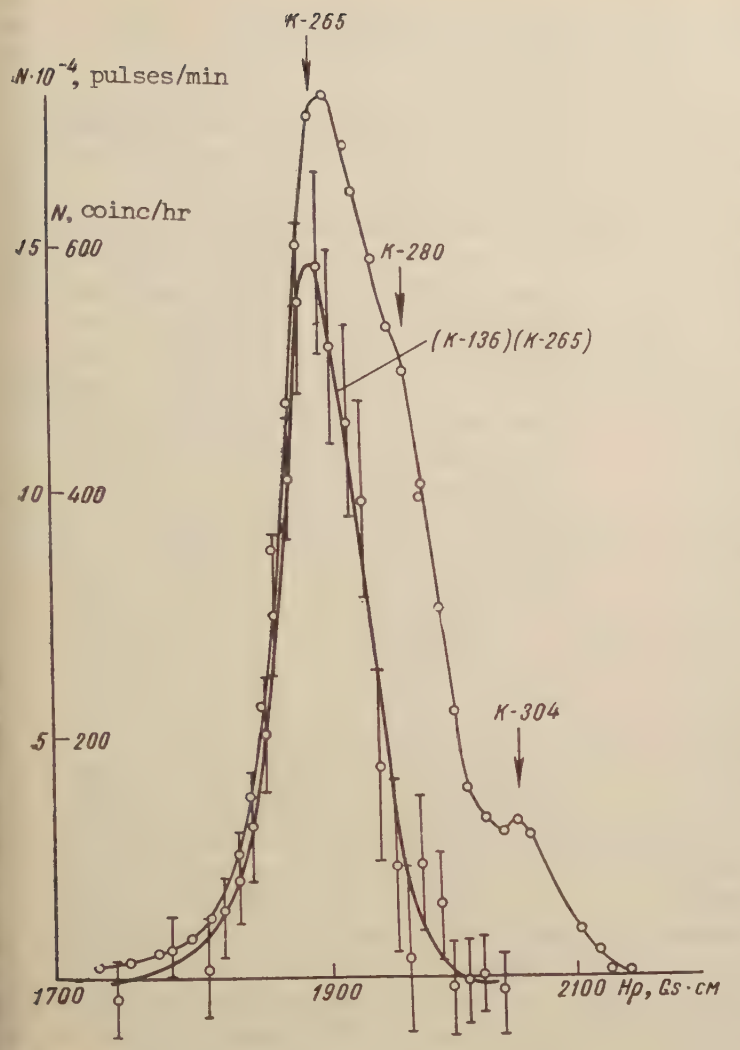

Fig.4. Heavy line - coincidences with K-136 electrons; light line - K-265, K-280 and K-305 lines recorded on single spectrometer.

ing to the decay scheme (Fig.1), in addition to (K-199)-(K-66) coincidences, there should also be observed coincidences between K-199 and K-81 electrons.

On the basis of the intensity balance data given by Grigor'ev et al[2] the ratio of the (K-199)-(LM-66) to (K-199)-(K-81) coincidence rates should be 32 to 1. In our experiments the coincidence counting rate at the peak of the coincidence curve in the region of LM-66 + K-81 was only 36 pulses per hour. The observed coincidences were apparently primarily coincidences between K-199 and LM-66 electrons. It will be evident from Fig.3 that there are no coincidences between the K-199 and K-96 conversion electrons, although the 199 and 96 kev transitions are shown in sequence in the decay scheme (transition series: 96→25→81→199 kev). The reason for the absence of these coincidences is that the 305 kev level, at which the 96 kev transition terminates, is an isomeric state (lifetime - $17 \cdot 10^{-3}$ sec).

The occurrence of coincidences between the 136 and 265 kev transitions is illustrated in Fig.4. The (K-136)-(K-265) coincidence curve has a half-width approximately equal to the half-width of a singles line. It may safely be asserted that there are (K-136)-(K-265) coincidences, but no noticeable (K-136)-(K-280) coincidences, in conformity with the decay scheme. Fig.1 shows that the K-136 line is appreciably more intense than the K-121 line; when the stationary channel of the spectrometer is set on the K-136 line it may also pick up a certain number of K-121 electrons, which could give coincidences with the K-280 electrons.

When the stationary channel of the spectrometer is set at the K-121 line (Fig.5), there is obtained a broad coincidence peak. It is, apparently, the result of surposition of two coincidence lines: the main (K-121)-(K-280) coincidence curve and the auxiliary (K-136)-(K-265) coincidence curve that appears owing to the fact that, in addition ot the weak K-121 line electrons, the spectrometer picks up the electrons of the strong neighboring K-136 line, which give rise to the (K-136)-(K-265) coincidences (see Fig.4). Thus the 136 & 265 kev and 121 & 280 kev transitions form twin cascades.

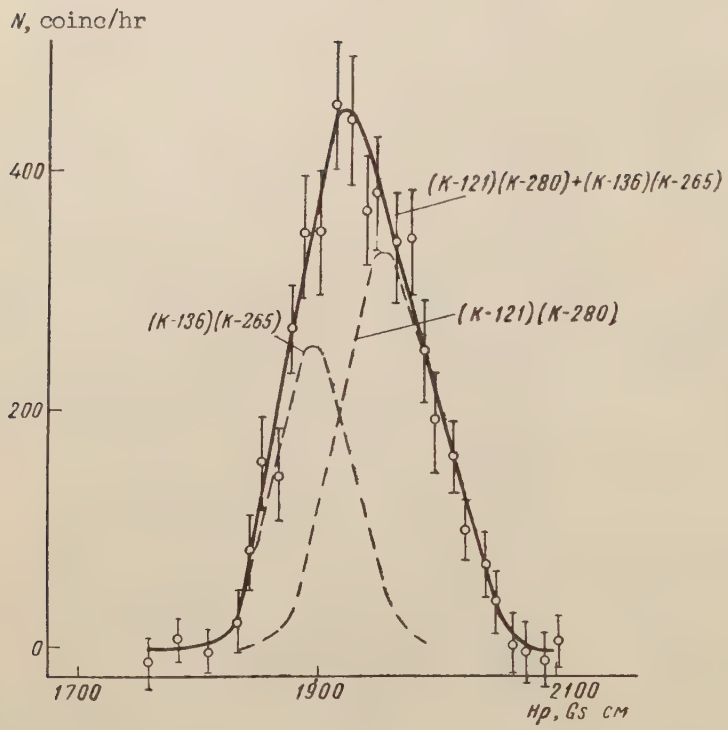

Fig.5. Coincidences with the K-121 line, which may include an admixture of K-136. The broad experimental peak can be resolved into two peaks: (K-121)-(K-280) and (K-136)--(K-265).

Thus our results amplify and refine the data of Refs.3-5 on the coincidences between γ-rays and generally substantiate the Se^{75} decay scheme shown in Fig.1.

We take this opportunity to thank A.V.Zolotavin for providing the Se^{75} activity, making available his experimental results prior to publication and valuable discussion. L.Gorzhak, student of Leningrad State University, participated in the measurements.

Scientific Research Physical Institute,
"A.A.Zhdanov" Leningrad State University

References

1. V.A.Sergienko, Izv.AN SSSR, Ser.fiz., 22, 198 (1958). (Trans.Bulletin 22, No.2, 195.)

2. E.Grigor'ev, A.Zolotavin, V.Klement'ev & R.Sinitsyn, Ibid. 23, 159 (1959). (Trans.Bulletin 23, No.2, 153.)

3. D.C.Lu, W.H.Kelly & M.L. Wiedenbeck, Phys.Rev., 97, 139 (1955).

4. A.W.Schardt & Joan Welker, Phys.Rev., 99, 810 (1955).

5. H.I.Van den Bold, I.Van de Gejn & P.M.Endt, Physica, 24, 1, 23 (1958).

6. B.S.Dzhelepov & L.K.Peker, Skhemy raspada radioaktivnykh yader (Decay schemes of radioactive nuclei), M., 1958.

REGARDING $Er^{160} \rightarrow Ho^{160}$ AND $Yb^{166} \rightarrow Tm^{166}$ TRANSITIONS

- E.P.Grigor'ev, B.S.Dzhelepov & A.V.Zolotavin

Recently there have been a number of investigations devoted to the decay series $Er^{160} \rightarrow Ho^{160}$ (Refs.1-5) and $Yb^{166} \rightarrow Tm^{166} \rightarrow Er^{166}$ (Refs.6-8).

In the present contribution we want to call attention to some distinctive features of the first transitions in these series (possible versions of the decay schemes are shown in Fig.1).

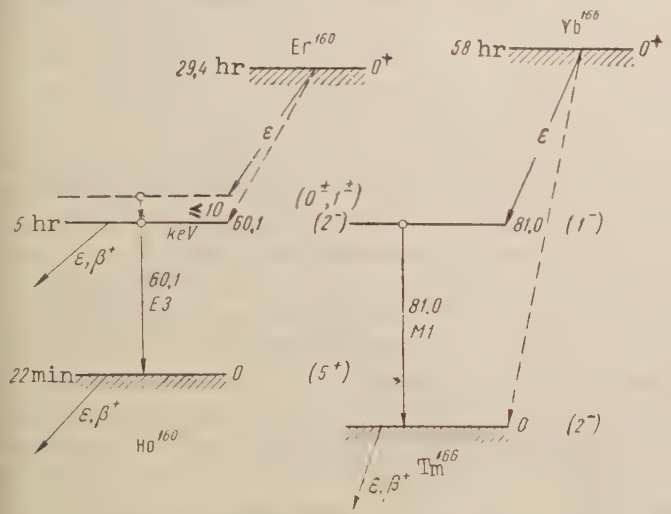

Fig.1. Tentative decay schemes for Er^{160} and Yb^{166}.

1. $Er^{160} \rightarrow Ho^{160}$

Ho^{160} is known to have two isomeric states with half-lives of 22 min[9,10] and ~5 hr (4.6 hr)[11]. The 5 hour isomer decays primarily by emission of conversion electrons corresponding to a 60 kev transition; comparison of the theoretical and experimental values of the ratio $(L_I + L_{II})/L_{III}$ and the period leads to the inference that this is an E3 transition[4].

At present the spins and parities are not known for any of the states of Ho^{160}. It has been suggested in the theoretical studies of Bohr & Mottelson[12] and Peker[13] that among the low-lying states of odd-odd nuclei there must be two levels with the same parity and spin $I = \Omega_p \pm \Omega_n$, where Ω_p and Ω_n are the nuclear spins associated with the odd proton and neutron, respectively. This rule holds well for the odd-odd nuclei neighboring with Ho^{160}. The values of Ω_p and Ω_n, according to Peker[13] are 7/2- and 3/2-. Hence one can expect states with 5+ and 2+ in Ho^{160}. One cannot, however, assert that these states are the two experimentally observed isomeric states (22 min & ~5 hour) inasmuch as the 5+→2+ transition must be of the M3 + E4 type, rather than E3. The ground state of Er^{160} (even Z and N) is 0+. Hence direct excitation of 5+ and 2+ states in Ho^{160} must be forbidden (at least twice) in the decay of Er^{160}.

We want to call attention to the fact that judging from the half-life and decay energy, there occurs an allowed or once forbidden transition in Er^{160}, and consequently, the decay must go to some other as yet unknown level of Ho^{160}. The energy of the $Er^{160} \rightarrow Ho^{160}$ transition apparently does not exceed 1 Mev. This may be inferred from the following facts.

1. No positron spectrum or annihilation radiation was observed from Er^{160} purified of Ho^{160} (Ref.4).

2. No γ-rays with energies above 60 kev (Ref.3) or conversion electrons with energies exceeding 10 kev (except those from the 60 kev transition) were observed in the decay of Er^{160} purified of Ho^{160} (Ref.2).

3. The Er^{160}-Ho^{160} mass difference calculated by the semi-empirical and empirical formulas of Cameron[14] and Levy[15] equals 526 and 623 kev, respectively.

Curve a in Fig.2 shows the variation of $\log f_x t$ with the decay energy for τ = = 29 hours. Under f_x we understand the sum of the functions f_β, f_K and f_{L_I}, pertaining to allowed β^+-decay, K and L_I capture[16]; $f_x t$ is equal in magnitude to the usual ft value. Allowed (not mirror) transitions have log ft values from 4.0 to

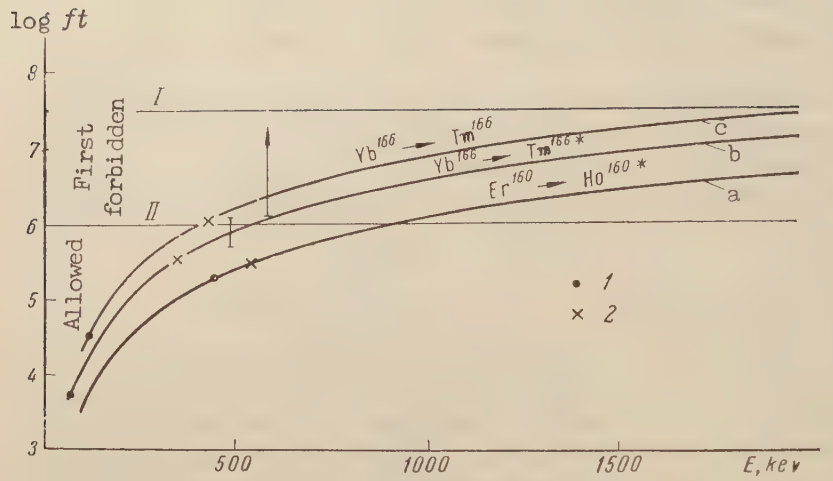

Fig.2. Variation of log ft with the energy for the decays: a) $Er^{160} \rightarrow Ho^{160*}$, b) $Yb^{166} \rightarrow Tm^{166}$ and c) $Yb^{166} \rightarrow Tm^{166}$. I - mean value of log ft for once forbidden transitions, II - lower bound of log ft. 1 - transition energy according to Cameron, 2 - transition energy according to Levy-Riddell. The uncertainties indicated by the vertical bars on curves b and c are connected with the fact that the precise fraction of decays to the excited state of Tm^{166} is not known. * = metastable.

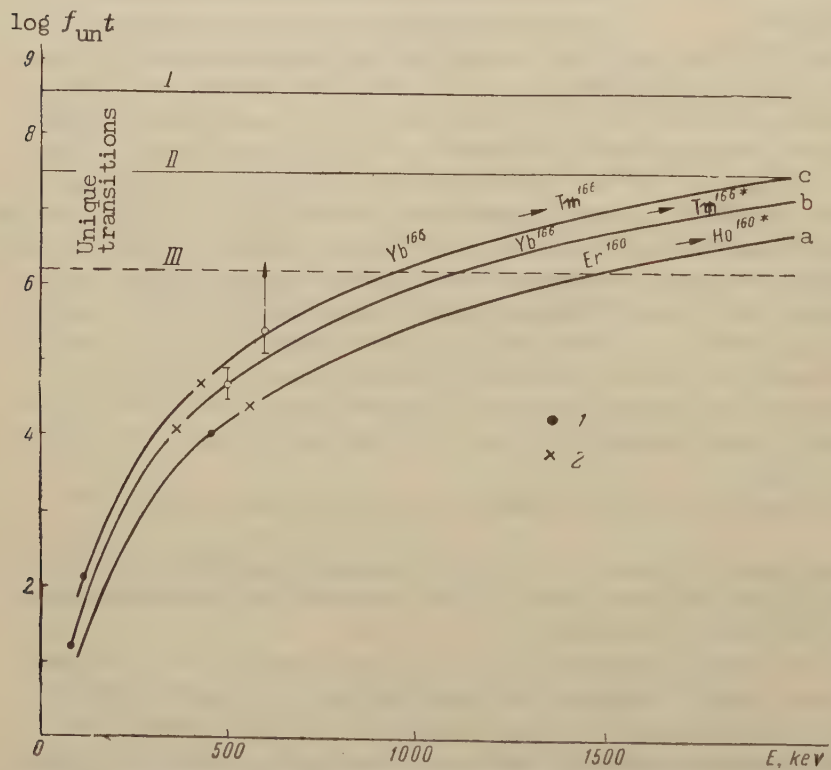

Fig.3. Variation of log $f_{un}t$ with energy for the decays: a) $Er^{160} \rightarrow Ho^{160*}$, b) $Yb^{166} \rightarrow Tm^{166}$ and c) $Yb^{166} \rightarrow Tm^{166}$. I - mean value of log $f_{un}t$, II - lower bound of log $f_{un}t$ for "true" unique transitions, III - lower bound of log $f_{un}t$ for all transitions now loosely classed as unique. 1 - transition energy according to Cameron, 2 - transition energy according to Levy-Riddell.

6.0 (with l inhibition to 9.0); once forbidden (not unique) transitions have log ft from 6.0 to 8.0, while unique transitions have log ft from 7.1 to 9.8. For twice forbidden transitions log ft is always > 12 (see the β-decay systematics of Mayer, Moszkowski & Nordheim[17,18]). Thus it may be inferred from Fig.2 that if the Er^{160} decay energy is less than 1 Mev, the decay is either allowed or once forbidden.

The function f for unique β-transitions can be calculated unambiguously: we write

$$f_{un} = f_{\beta}^{un} + f_{K}^{un} + fL_{I}^{un}$$

The products $f_{un}t$ form a more compact group than $(ft)_{un}$, and log $f_{un}t$ equals 6.2 to 8.5. Fig.3 (plotted in the same way as Fig.2) shows that if the Er^{160} decay energy is less than 1 Mev, this decay can be classed as a unique transition. It follows therefrom that the level to which the decay goes cannot have the spin and parity 2-. There remain for it only the assignments of 0± and 1±.

In earlier studies it was assumed that the assignment for the ground state of Ho^{160} is 5+, and that for the isomeric (~5 hour) state 2-. An indirect substantiation of the 5+ assignment for the Ho^{160} ground state is to be found in analysis of the β+-spec-

trum of Ho^{160} (5 hour) and the theoretical work of Gallagher & Moszkowski[19]. Later, on the basis of the multipole order of the transition the isomeric state was again attributed the spin and parity 2-. The theoretically predicted 2+ level has not been observed.

Our assertion is that the decay of Er^{160} passing through the ~5 hour isomer goes not to levels with 5+, 2- or 2+ but to some other higher lying level. This level, however, must be located not higher than 10 kev above the isomeric one, since otherwise the corresponding conversion electrons would have been detected in the experiments of Refs.2 & 4.

2. $Yb^{166} \rightarrow Tm^{166}$

Tm^{166} is an odd-odd nucleus with a half-life of 7.7 hours. It has an excited level at 81 kev; presumably most of the electron captures in Yb^{166} go to this level (according to the data of our experimental study[7] 75 ± 30% of the decays go to the excited state of Tm^{166}). The level is de-excited by an 81 kev M1 type transition. No other excited levels in Tm^{166} have been detected, nor is there any experimental evidence for a positron spectrum corresponding to $Yb^{166} \rightarrow Tm^{166}$. The Yb^{166}-Tm^{166} mass difference equals 117 kev according to Cameron's formula, or 436 kev according to Riddell's. Consequently, as in the case of Er^{160}, the Yb^{166} decay energy should not exceed 1 Mev. Curve b in Fig.2 shows that for this energy the transition to the excited level of Tm^{166} may be either allowed or once forbidden. It is apparent from Fig.3 that the transition to the excited level of Tm^{166} (curve b) cannot be a unique one; however, the transition to the ground state (curve c) can be unique.

According to the spin-parity rules for odd-odd deformed nuclei, the assignment for the ground state of Tm^{166} may be 2- or 3- according to Peker[13] or only 3- according to Gallagher & Moszkowski[19].

In view of the above said it may be concluded that either the Tm^{166} nucleus is an exception to the rule of Gallagher & Moszkowski[19] (Ho^{166} is also an exception) or in addition to the 81 kev level it still has another close (within 10 kev) excited level through which an appreciable fraction of the Yb^{166} decay branches.

We desire to thank L.N.Zyryanova for clarifying the systematics of β-decay and discussion of some of the results and L.K.Peker for discussion of the work as a whole.

Scientific Research Physical Institute
"A.A.Zhdanov" Leningrad State University

References

1. F.W.Mihelich, B.Harmatz, I.H.Handley & I.I.Pinajian, Bull.Amer.Phys.Soc., 1, 330 (1956).

2. B.S.Dzhelepov, B.K.Preobrazhenskii, I.M.Rogachev & P.A.Tishkin, Izv.AN SSSR, Ser.fiz., 21, 962 (1957). (Trans.Bulletin 21, No.7, 964.)

3. G.M.Gorodinskii, A.N.Murin, V.N.Pokrovskii & B.K.Preobrazhenskii, Ibid., 21, 1624 (1957). (Trans.Bulletin 21, No.12, 1611.)

4. E.P.Grigor'ev, B.S.Dzhelepov, A.V.Zolotavin, O.E.Kraft, B.Kratsik & L.K. Peker, Ibid., 22, 101 (1958). (Trans.Bulletin 22, No.2, 99.)

5. G.Bitterlikh, E.P.Grigor'ev, B.S.Dzhelepov, A.V.Zolotavin & B.Kratsik, Abstracts of Reports presented at the Ninth Annual Conference on Nuclear Spectroscopy in Khar'kov, M.-L., 1959.

6. K.Ya.Gromov, B.S.Dzhelepov, A.G.Dmitriev, V.A.Morozov & B.K.Preobrazhenski: Program and abstracts of the Eighth Annual Conference on Nuclear Spectroscopy, M.-L, 1958.

7. E.P.Grigor'ev, B.S.Dzhelepov & A.V.Zolotavin, Izv.AN SSSR, Ser.fiz., 23, 188 (1959). (Trans.Bulletin 23, No.2, 180.)

8. K.P.Jacob, F.W.Mihelich, B.Harmatz & T.H.Hanley, Bull.Amer.Phys.Soc., 3, 357 (1958).

9. G.Wilkinson & H.G.Hicks, Phys.Rev., 74, 1733 (1948); Phys.Rev., 79, 815 (1950).

10. T.H.Handley, Phys.Rev., 94, 945 (1954).

11. W.E.Nervik & G.I.Seaborg, Phys.Rev., 97, 1092 (1955).

12. A.Bohr & B.Mottelson, Kgl.danske Vid.Selskab Mat.-Fys.medd., 27, No.16 (1953).

13. L.K.Peker, Izv.AN SSSR, Ser.fiz., 21, 1029 (1957). (Trans.Bulletin 21, No.7, 1030.)

14. A.G.W.Cameron, A Revised Semi-Empirical Atomic Mass Formula. - Chalk River, Mar.1957.

15. F.Riddell, A Table of Levy's Empirical Atomic Masses. - Chalk River, July, 1956.

16. I.M.Band, L.N.Zyryanova & Yu.P.Suslov, Izv.AN SSSR, Ser.fiz., 22, 952 (1958). (Trans.Bulletin 22, No.8, 943.)

17. M.Mayer, S.Moszkowski & L.Nordheim, Revs.Mod.Phys., 23, 315 (1951).

18. L.Nordheim, Revs.Mod.Phys., 23, 322 (1951).

19. C.J.Gallagher & S.A.Moszkowski, Phys.Rev., 111, 1282 (1958).

Ho^{160} DECAY AND Dy^{160} LEVEL DIAGRAM

- E.P.Grigor'ev, B.S.Dzhelepov, A.V.Zolotavin, B.Kratsik & G.Bitterlikh

The level diagram of Dy^{160} arrived at on the basis of investigation of the decay of Tb^{160} and Ho^{160} (from Er^{160}) has been given in Ref.1. The energy of the highest-lying level shown in the diagram is 1718 kev. Analysis of all the available facts, however, led us to the conclusion that in the decay of Ho^{160} there must appear excited states of Dy^{160} with energies up to 2900 kev; this was, in fact, substantiated by subsequent experiments.

In the present report we give the results of investigation of the transitions from high-lying levels of Dy^{160} and cite some supplementary data that tend to substantiate the proposed scheme for the low-lying levels of Dy^{160}.

1. Experimental Conditions

We investigated the positron and conversion electron spectra by means of a β-spectrometer with a resolution of 0.4-0.5% under the same conditions as in the work of Refs.1 & 2. The erbium fraction source was obtained by chromatographic separation of the rare earths extracted chemically from a tantalum target bombarded with high energy protons.

The observed internal conversion lines were identified as belonging to Ho^{160} on the basis of the half-life of Er^{160} (29.2 hours). Careful observation of the radiations from the ytterbium fraction over a prolonged period showed that there were present in it minor admixtures of Tm, Yb and Lu. The conversion lines attributed to these species were excluded from further consideration.

Our source had a high activity. Owing to the presence in its spectrum of high energy γ-rays the background of the detecting system, which consisted of two counters operating in coincidence, increased from 5 to 20 counts per min. In addition, there was observed a continuous electron background that varied with change in the strength of the magnetic field. The magnitude of this background amounted to several hundred counts per minute in the low energy region of the spectrum and some tens of counts per minute in the 400 to 600 kev region at a counting rate of several tens of thousands of pulses per minute at the peaks of the strong conversion lines. Obviously, this background hindered observation of very weak conversion lines.

2. β^+-Spectrum

We studied the composition of the β^+-spectrum in the low energy region. In analyzing the experimental data, we assumed that the low intensity high energy component has the end-point energy and shape described in Ref.3. The other parts of the spectrum were analyzed by resolution into components of Fermi shape.

The Fermi-Kurie plot for the spectrum is shown in Fig.1; the quantitative data on the spectrum components are listed in Table 1. A certain excess of positrons was observed in the region below 160 kev. This excess may be associated with yet another component, but in view of the statistical accuracy of the measurements we cannot at present claim that the existence of this component is proved.

We found that $I_{\beta+}/I_{K\text{-}730} = 2.2 \pm 0.2$ (the intensities were measured with the same source). From the data on the conversion spectrum (Table 2) it follows that $I_{K\text{-}730}/I_{LMN\text{-}60} = 0.0025$.

The intensity balance for the transitions in Ho^{160} (Table 3) shows that the 60 kev transition occurs in 66% of the disintegrations. On the basis of all the data considered jointly, we infer that the total of all positrons per disintegration is 0.36%.

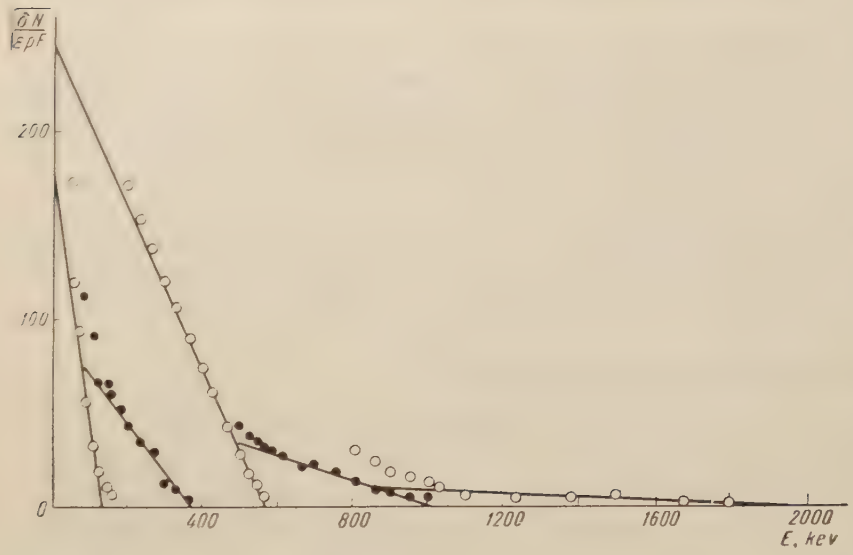

Fig.1. Kurie plot for the Ho^{160} β^+-spectrum.

Table 1

Composition of the β^+-spectrum of Ho^{160}

End-point energy, kev	Relative intensity	Branching, %	log *ft*	
			T=5 hr	T=22 min
120± 40*	1,6	0,006	5,1	4,0
310± 30	4,0	0,014	6,3	5,1
566± 20	66	0,240	5,9	4,8
1015± 30	22	0,079	7,5	6,4
1900±100 [3]	6,4	0,023	9,3	8,2

*The resolution of the component with end-point energy 120 ± 40 kev is tentative.

[3] = Ref.3

Inasmuch as it is not known whether the β^+-decay of Ho^{160} departs from the ground or isomeric level, we have listed the two alternative values of log *ft* for each component in Table 1.

3. Conversion Electron Spectrum

In the present experiments we found 55 new conversion lines, and, in a number of cases, also obtained more accurate values for the energies and relative intensities of the lines listed in Ref.1. The results of the present and previous investigations are summarized in Table 2.

The uncertainty in determining the conversion line energies ranges from 0.1 to 0.3%, depending on their intensity and the degree of overlapping. The energy difference between the K and L lines for all transitions (except for the 2675 kev transition) is close to the difference between the binding energies in the K and L shells of Dy^{160}.

The conversion lines observed only in one series of measurements, recorded with inadequate statistical accuracy or obtained as a result of resolution of several close lines have been classed as "doubtful" and the data for them are given in parentheses. Lines marked with an asterisk in Table 2 could not be satisfactorily fitted into the proposed Dy^{160} level diagram.

The experimental values of K/L were compared with the theoretical ratios for different multipole orders. In some cases a discrepancy between the experimental and theoretical values indicates that one or more K lines from other transitions are superimposed on the L line in question. Specifically, this is the evidence for the existence of the K-1419 and K-1476 lines.

Two sections of the Ho^{160} conversion electron spectrum are reproduced in Figs.2 and 3. The K-1264 and K-1273 lines have half-widths of 0.4%, whereas the half-width of the K-1285 line is 0.57% (Fig.2). This indicates that the observed line is a double one, i.e., the result of surposition of two close lines.

The half-width of the close L-1264 and L-1273 lines is 0.56%, which again is greater than the half-width of single lines (0.4%). The data[4] on the radiations from Tb^{160} indicate that there may be a 1314 kev transition in Ho^{160}. The K-1314 line should be located between the L-1264 and L-1273 lines. Assuming that the 1314 kev line is present in the spectrum of Ho^{160}, we carried out another version

Energies and intensities of conversion electrons emitted in $Ho^{160} \rightarrow Dy^{160}$ decay

Table 2

№	E_{e^-}, kev	Identification	$h\nu$, kev	Relative intensity	№	E_{e^-}, kev	Identification	$h\nu$, kev	Relative intensity
1	51,2	L_1+L_2	60,1	1150±120	59	909,6	K	963,4	2,1±0,3
2	52,05	L_3	60,1	1050±100	60	912,9	K	966,6	1,8±0,3
3	57,9	M	60	430±25	61	952,9	L	961,9	0,48±0,12
4	59,2	N	59,6	110±8	62	958,4	L	967,4	0,40±0,10
5	33,0	K	86,8	814±150	63		M	960,1	
6	34,3—40,3	$K-LL$		400±80	64	964,9	M	966,6	0,07±0,04
7	41,4—46,7	$L-LM$		180±40	65	994	K	1048	0,11±0,02
8	76,3	L_1+L_2	86,2	790±80	66	1040	L	1048	0,03±0,01
9	78,4	L_3	86,2	610±60	67	1015	K	1069	0,24±0,03
10	84,5	M	86,2	400±20	68	1061	L	1069	0,048±0,010
11	86,1	N	86,5	100±7	69	1079	K	1133	0,085±0,012
12	53,9	K	107,7	10±1	70	1124	L	1133	0,066±0,015
13	99,3	L	107,2	2,8±0,6	71	1126	K	1180	
14	142,2	K	196,2	100±5	72	1147	K	1201	0,070±0,015
15	189,7	L	197,0	37±3	73	1210	K	1264	0,11±0,03
16	195,6	M	197,3	8,4±0,8	74	1254	L	1263	0,034±0,012
17	196,5	N	196,9	2,8±0,6	75	1218	K	1272	0,11±0,03
18	161,0	K	214,8	0,3±0,05	76	1265	L	1274	0,036±0,013
19	243,4	K	297,2	3,0±0,2	77*	1231	K	1285	0,09±0,03
20	244,6	K	298,4		78	1275	L	1284	0,015±0,009
21	290,7	L	298,5	0,9±0,1	79	(1260	K	1314	0,028±0,010)
22	297,0	M	298,7	0,26±0,05	80	(1284	K	1338	0,02±0,01)
23	256	K	310	0,16±0,05	81*	1291	K	1345	0,025±0,015
24	301	K	363	0,22±0,05	82	(1296	K	1350	0,013±0,009)
25	339	K	393	0,09±0,04	83	1323	K	1375	0,080±0,012
26	353	K	407	0,40±0,06	84*	(1338	K	1392	0,012±0,008)
27	399	L	407	0,06±0,03	85*	(1347	K	1401	0,018±0,010)
28*	437,6	K	491,4	0,076±0,02	86	1356	K	1410	0,030±0,012
29	460,6	K	514,4	0,75±0,04	87*	1365	K	1419	0,036±0,013
30	506,1	L	514,8	0,08±0,02	88	1365	L	1374	
31	485	K	538,9	2,25±0,15	89	1379	K	1433	0,054±0,016
32	531,1	L	540,0	0,42±0,06	90	(1385	K	1439	0,019±0,011)
33	539,4	M	541,1	0,15±0,05	91	1422	K	1476	0,024±0,014
34	593,8	K	647,6	5,25±0,30	92	1422	L	1431	
35	638,4	L	647,1	0,85±0,10	93*	1465	K	1519	0,010±0,005
36	647,0	M	648,7	0,26±0,07	94	1617	K	1671	0,026±0,009
37	620,1	K	673,9	0,032±0,012	95	1665	K	1719	0,023±0,007
38	630,3	K	684,1	0,11±0,03	96	(1717	K	1771	0,010±0,006)
39	654,8	K	708,6	0,098±0,020	97	1730	K	1784	0,018±0,005
40	675,9	K	729,7	6,9±0,4	98*	(1739	K	1793	0,004±0,004)
41	720,5	L	729,6	1,1±0,1	99	1753	K	1807	0,015±0,006
42	729,4	$M+N$	731,1	0,32±0,08	100	(1766	K	1820	0,011±0,007
43	700,9	K	754,7	0,63±0,11	101	(1799	K	1853	0,003±0,003
44	745,4	L	754,5	0,10±0,03	102	(1810	K	1864	0,004±0,004
45	751,8	M	753,5	0,036±0,018	103	1818	K	1872	0,008±0,004
46	713	K	766,7	0,80±0,13	104	1873	K	1927	0,016±0,005
47	757,1	L	766,1	0,14±0,04	105	1905	K	1959	0,016±0,005
48	765,5	$M+N$	767,2	0,056±0,022	106*	1954	K	2008	0,015±0,004
49*	773,3	K	827,1	0,10±0,03	107*	2015	K	2069	0,006±0,003
50*	(783,8	K	837,6	0,05±0,03)	108*	(2035	K	2089	0,007±0,004
51*	(791,7	K	845,5	0,04±0,02)	109*	2136	K	2190	0,007±0,003
52	804,5	K	858,3	0,10±0,03	110	2496	K	2550	0,010±0,004
53	819,4	K	873,9	0,92±0,13	111	2565	K	2619	0,010±0,005
54	863,8	L	872,9	0,14±0,04	112	2584	K	2638	0,011±0,005
55	826,0	K	879,8	2,6±0,4	113*	(2596	K	2650	0,006±0,004)
56	871,0	L	880,0	0,40±0,08	114	2621	K	2675	0,016±0,005
57	879,6	$M+N$	880,3	0,15±0,06	115	(2661	L	2670	0,002±0,001)
58	(889,2	K	943,0	0,07±0,04)	116*	(2674	K	2728	0,002±0,002)
					117	2709	K	2763	0,003±0,002

*Presumably double lines. [Also see third paragraph under Section 3, page 860. Translation editor.]

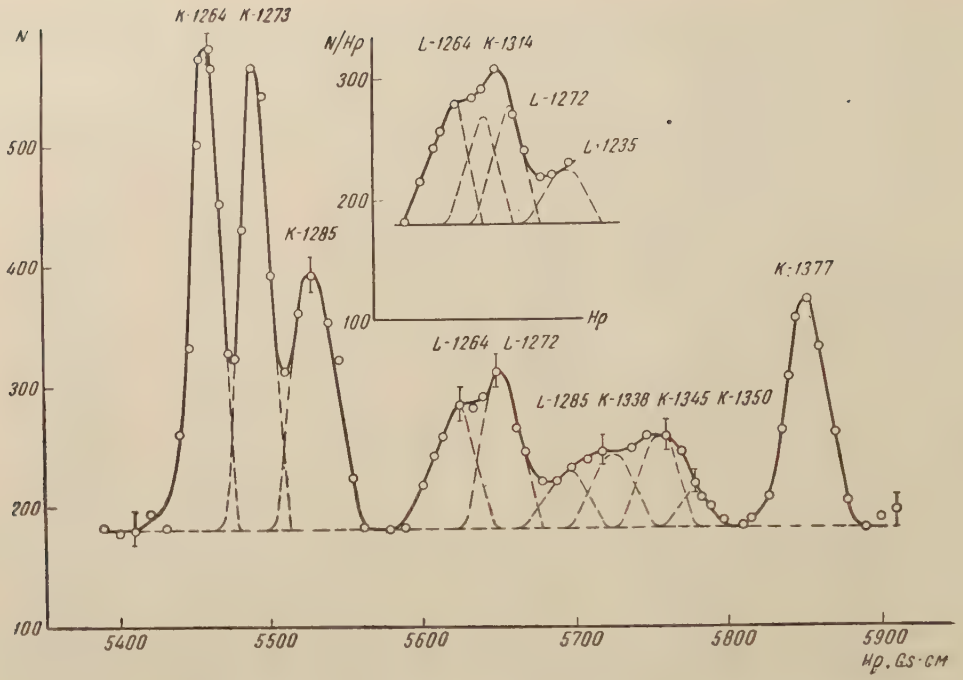

Fig.2. Section of the Ho^{160} conversion electron spectrum in the Hρ range from 5400 to 5900 gauss·cm. The dashes indicate the resolution of the lines. The width of the K-1285 line is greater than the apparatus width. Insert - second variant of resolution of the group of L-conversion lines bringing out the K-11314 line.

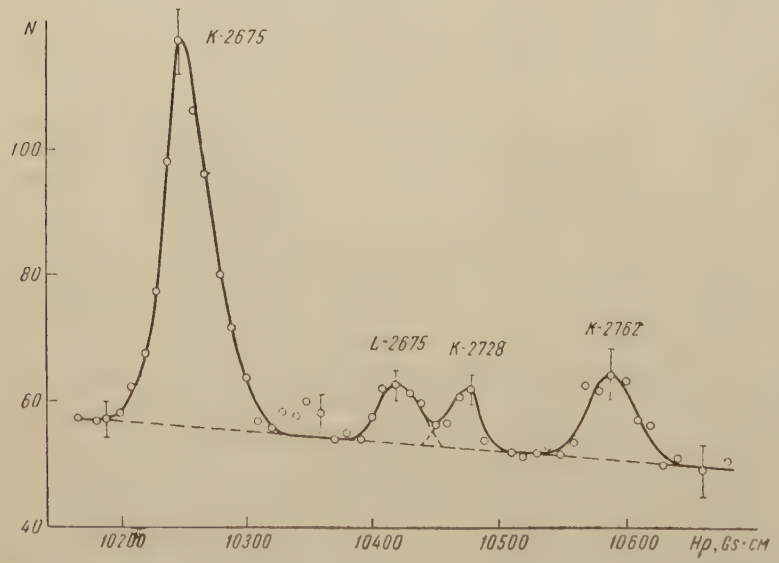

Fig.3. Internal conversion lines associated with the highest energy transitions in Ho^{160}.

of resolution of this section of the spectrum, assuming that the half-width of all the lines is 0.4% (insert in Fig.2). With this variant of the resolution, the K/L ratios for the 1264 and 1273 kev transitions are in better agreement with the theoretical values of K/L than with the first variant, but in this case the ratios are appreciably lower than the theoretical values for low multipole orders. This indicates that the experimental L-1264 and L-1273 lines may contain an admixture of yet other lines.

To the high energy side of the lines in Fig.2 there is a group of unresolved lines, identification of which is very difficult. By analytic resolution one can determine four lines, namely, L-1285 K-1338, K-1345 and K-1350. We classed the K-1338 and K-1350 lines among the doubtful ones, inasmuch as they are weak and it is difficult to resolve them unambiguously; moreover, the statistical uncertainty here is appreciable. If a 1314 kev

transition actually does occur in Ho^{160}, the L line associated with it should be in this group, close to the K-1350 line.

The highest energy section of the Ho^{160} conversion spectrum is shown in Fig. 3. The shape of the K-2675 line differs from the standard shape in that it is broadened to the high energy side, possibly due to a weak line in this region. The presence of such a line would lead to overestimates in determining the energy and intensity of the K-2675 line. This in fact may explain the difference in the energy values for this transition determined from conversion on the K and L shells.

We classed the K-2728 also among the doubtful ones owing to the paucity of the points for it in the first series of measurements (Fig.3) and the inadequate statistical accuracy in the second series.

The K-2762 line is the highest energy and at the same time the weakest line, the existence of which has been reliably established. It was recorded in three series of measurements. Although the statistical uncertainty is appreciable, there can be no doubt regarding the actual existence of this line.

4. Dy^{160} Level Diagram

As a result of the present measurements we were able to supplement and amplify the level diagram for Dy^{160} given in Ref.1 (Fig.4). In the present experiments we detected for the first time the following transitions between already known levels of Dy^{160};

684.1 kev:	966.5 kev	(2+)	→	283 kev	(4+)
1476 "	1565 "	(3,4)	→	86.5 "	(2+)
1410 "	1696 "	(4+)	→	283 "	(4+)
673.0 "	1721 "	(3)	→	1049 "	(3+)

In addition, we were also able to determine the energies of a number of the highest-lying levels of Dy^{160}.

A new level was introduced into the level diagram on the basis of energy considerations only when there were observed at least four transitions departing from it to lower-lying levels with close spins. Further, it was assumed that the error in determining the conversion line energies did not exceed 0.3%.

The following levels were found to satisfy the above conditions:

I. 1909 kev level

86.5	(2+)	+ 1820	= 1906.5	kev
966.5	(2+)	+ 943	= 1909.5	"
1049	(3+)	+ 858.3	= 1907.3	"
1156	(4+)	+ 754.7	= 1910.7	"
1200	(1-)	+ 708.6	= 1908.6	"
Average			1908.5	kev

Most probable assignments: 2- or 3-

II. 2637 kev level

Ground state	(0+)	+ 2638	= 2638	kev
86.5	(2+)	+ 2550	= 2636.5	"
966.5	(2+)	+ 1671	= 2637.5	"
1200	(1-)	+ 1433	= 2633	"
1264	(3-)	+ 1375	= 2639	"
Average			2637	kev

Most probable assignments: 1- or 2+

III. 2768 kev level

86.5	(2+)	+ 2675	= 2761.5	kev
966.5	(2+)	+ 1807	= 2773.5	"
1049	(3+)	+ 1719	= 2768	"
1721	(3)	+ 1048	= 2769	"
Average			2768	kev

Most probable assignments: 2- or 3-

IV. 2830 kev level

966.5	(2+)	+ 1864	= 2830.5	kev
1049	(3+)	+ 1784	= 2833	"
1565	(3-)	+ 1264	= 2829	"
1696	(4+)	+ 1133	= 2829	"
Average			2830	kev

Most probable assignment: 3-

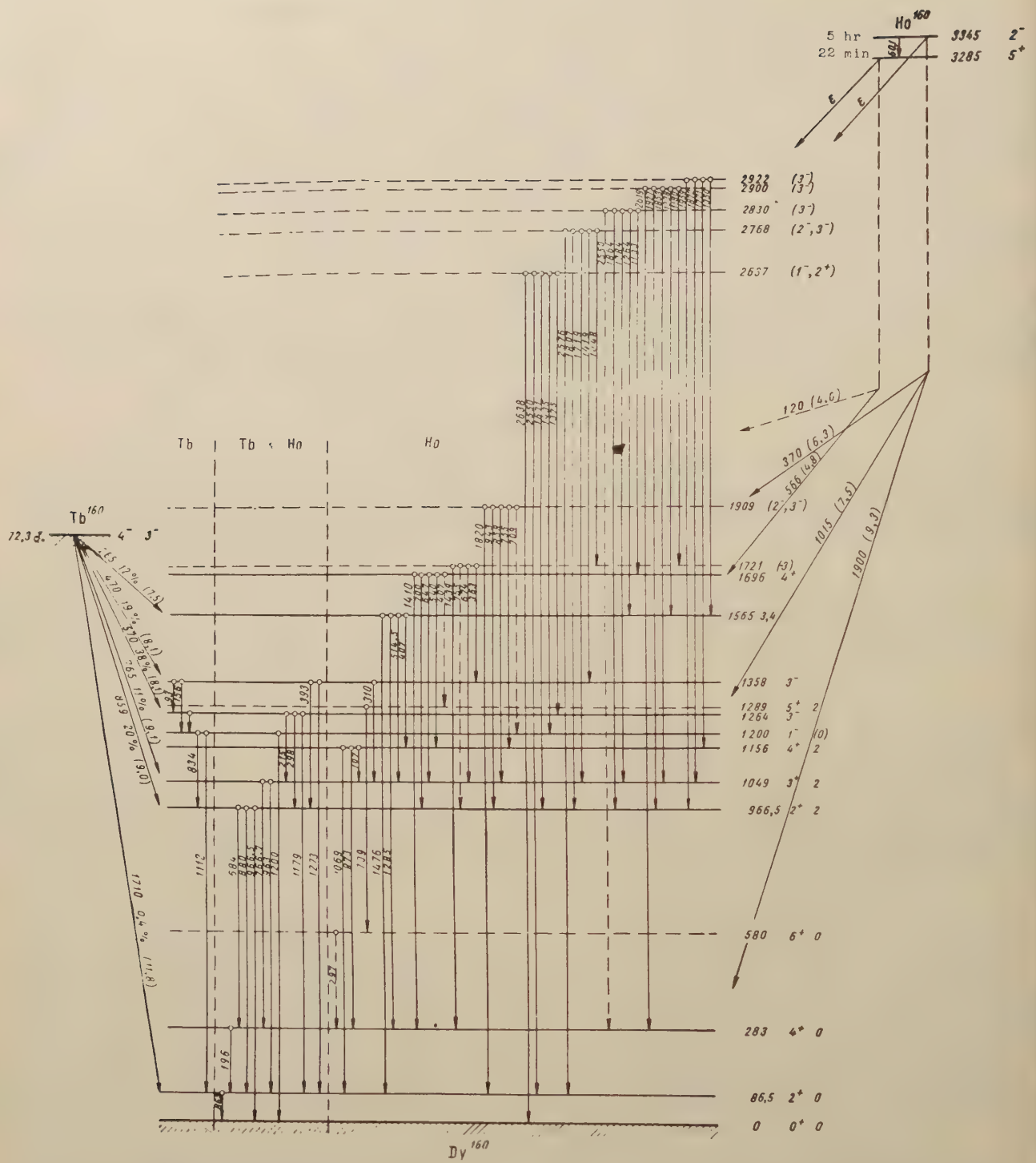

Fig.4. Decay scheme for Ho^{160} and Tb^{160} based on the data of the present investigation and Ref.4.

The observed 2550 kev transition could be interpreted as departing from a level at 2833 kev: 283 (4+) + 2550 = 2833 kev; however, this transition was located earlier between the 2637 and 86.5 kev levels.

V. 2900 kev level

283 (4+) + 2619 = 2902 kev
966.5 (2+) + 1927 = 2893.5 kev
1049 (3+) + 1853 = 2902 "
1565 (3-) + 1338 = 2903 "
Average 2900 kev
Most probable assignment: 3-

VI. 2922 kev level

966.5 (2+) + 1959 = 2925.5 kev
1049 (3+) + 1872 = 2921 "
1156 (4+) + 1771 = 2927 "
1565 (3.4) + 1350= 2915 "
Average 2922 kev
Most probable assignment: 3-

It is possible that the 2638 kev transition, which was inserted between the 2637 kev level and the ground state, actually occurs between the 2922 and 283 kev (4+) levels.

It is also not impossible that the 1719 kev transition may feed the 1200 kev level: 1200 (1-) + 1719 = 2919 kev. It is more probable, however, that the 1719 kev transition extends between the 2768 and 1049 kev levels as indicated in the diagram. Thus, of the 74 transitions observed in our experiments we have succeeded in ranging 57 in the proposed scheme; 17 transitions remain unallocated.

If levels are introduced on the basis of 2-3 transitions from them to lower lying levels, one can insert almost all the observed γ-transitions. Such an approach could yield reliable results only if the energies of the transitions were known to one more decimal place.

5. Tentative Intensity Balance in Ho^{160}

We drew up a balance of intensities for the transitions arriving at and departing from the various levels shown in the proposed Ho^{160} decay scheme (Fig.4) on the basis of the relative intensities of the conversion lines. In each case the total transition probability was determined taking into account the conversion coefficient for radiation of the multipole order that follows from the data on K/L from the decay scheme (Fig.4) or from the data on the decay of Tb^{160} (Ref.4).

Table 3

Tentative intensity balance in the decay of Ho^{160}

Level energy, kev	Arrival at level, %	Depart. from level, %	Bal. rem. for β^- decay & K capture
0 Ho^{160}	66±12	—	
0 Dy^{160}	100±12	—	
86,5	71,0±8,3	79,2±8,6	?
283	17,3±2,2	19,1±1,1	?
966,5	43,5±4,9	35,6±4,6	0
1049	22,1±2,4	17,8±2,5	0
1156	8,0±1,2	9,6±1,3	?
1200	2,4±0,8	2,2±0,4	0
1264	1,2±0,2	5,8±0,9	4,6±1,1
1358	1,9±0,7	4,5±1,3	2,6±2,0
1565	5,4±1,8	9,4±1,5	4,0±3,3
1696	2,4±0,4	51,0±2,8	48,6±3,2
1721	4,5±0,8	1,6±0,8	0
1909	—	6,0±1,3	6,0±1,3
2637	—	6,2±1,2	6,2±1,2
2768	—	8,1±1,8	8,1±1,8
2830	—	7,9±1,7	7,9±1,7
2900	—	5,2±2,0	5,2±2,0
2922	—	2,7±1,4	2,7±1,4
			96±19

For mixed M1 + E2 transitions we assumed that the fraction of each type of radiation was 0.5. We took the high energy transitions, the multipolarities of which had not been determined, to be E1. Further, we assumed that the 17 low intensity, high energy γ-transitions, which were not fitted into the decay scheme, occur between high-lying levels with spins 1-, 2- and 3- and levels of the first rotational band with 0+, 2+ and 4+. The probable contribution of these transitions to the intensity balance was taken into account in accord with their statistical weight as evaluated on the basis of the spin values. Taking the sum of the intensities of the transitions to the ground state of Dy^{160} as 100%, we arrived at the results listed in Table 3. Undoubtedly, the balance calculations involve a considerable uncertainty stemming, on the one hand, from experimental errors in determining the conversion line intensities, and, on the other hand, from possible mistakes in inserting a number of transitions into the diagram and some degree of arbitrariness in making the multipole order assignments. Despite this, as will be evident from Table 3, there are no glaring conflicts in the intensity balance.

We desire to express our sincere thanks to the personnel of the Joint Institute for Nuclear Research for bombarding the tantalum target, the staff of the "A.N.Murin" Laboratory headed by B.K.Preobrazhenskii for skillful preparation of the sources, and K.Ya.Gromov for assistance in organizing the work connected with preparation of the sources.

Scientific Research Physical Institute,
"A.A.Zhdanov" Leningrad State University

References

1. E.P.Grigor'ev, B.S.Dzhelepov, A.V.Zolotavin, O.E.Kraft, B.Kratsik & L.K. Peker, Izv.AN SSSR, Ser.fiz., 22, 101 (1958). (Trans.Bulletin 22, No.2, 99.)

2. E.P.Grigor'ev, B.S.Dzhelepov, A.V.Zolotavin, B.Kratsik, B.K.Preobrazhenskii & I.S.Yanchevskaya, Doklady AN SSSR, 117, 53 (1957). (Trans.Soviet Physics - Doklady.)

3. B.S.Dzhelepov, O.E.Kraft & B.K.Preobrazhenskii, Ibid., 116, 581 (1957). (Trans.Soviet Physics - Doklady.)

4. E.P.Grigor'ev, A.V.Zolotavin & B.Kratsik, Izv.AN SSSR, Ser.fiz., 23, 191 (1959). (Trans.Bulletin 23, No.2, 183.)

ON CALCULATION OF THE REDUCED LIFETIME OF NUCLEI FOR UNIQUE BETA-TRANSITIONS

- L.N. Zyryanova

The probability per unit time for β-decay of a nucleus in the usual notation of theory is given by the familiar expression

$$\lambda = \frac{g^2}{2\pi^3} \int_1^{E_0} F(E,Z)\, Ep\, (E_0 - E)^2\, C_n(E,E_0, Z)\, dE,$$

where C_n is the correction factor for an n times forbidden β-spectrum.

In the case of allowed β-transitions, knowing the Fermi integral

$$f_0 = \int_1^{E_0} F(E,Z)\, Ep\, (E_0 - E)^2\, dE$$

we can calculate the reduced lifetime $f_0 t$ of the nucleus, which yields information on the change in state of the nucleus incident to the β-transition.

In view of the ambiguity of the expression for C_n in the case of forbidden β-transitions (the ambiguity is connected with the fact that the precise value of the nuclear matrix elements is not known), in calculating the product ft for forbidden transitions, use is commonly made of the integral for allowed transitions, f_0, instead of

$$f_n = \int_1^{E_0} F(E,Z)\, Ep\, (E_0 - E)^2\, C_n\, dF$$

The case of unique β-transitions, which is distinguished by the fact that the theoretical expression is unambiguous, allows of including the energy dependence of the correction factor C_n in the expression for f_n^{un}. Here the values of $f_n^{un} t$ found for the β-transitions give more direct information on the nuclear matrix elements than the values of $f_0 t$.

In the present work we obtained numerical values of the Fermi integral f_n^{un} for first and second forbidden β-transitions.

The correction factor for first forbidden transitions with $\Delta I = 2$ is given by[1]

$$C_1 = \left(\frac{1}{12} K^2 L_0 + \frac{3}{4} L_1\right) \sum_{ij} |B_{ij}|^2,$$

where $K = E_0 - E$ is the neutrino energy and L_0 and L_1 are combinations of the β-particle wave functions.

For finding the numerical values of the integral

$$f_1^{un} = \int_1^{E_0} F(E; Z)\, Ep\, (E_0 - E)^2 \left(\frac{1}{12} K^2 L_0 + \frac{3}{4} L_1\right) dE$$

we used the values of the functions $F(E, Z)$, L_0 and L_1 (Ref.2), calculated taking into account the Coulomb field, screening and finite nuclear size.

The values of

$$\langle C_1 \rangle = f_1^{un} / f_0$$

for β^-- and β^+-spectra are listed in Tables 1 and 2. The numerical values of f_0 were taken from the Tables of Ref.2.

Having the precise values of $\langle C_1 \rangle$, we can evaluate the approximate expressions for this quantity given in the literature[3-5].

For example, the approximation

$$\langle C_1 \rangle \approx {}^1/_{24}\, (E_0^2 - 1)$$

given by Perlman et al[5] satisfactorily renders the character of the transition energy dependence of $\langle C_1 \rangle$ but yields numerical values which may differ from the

Table 1

Values of $\langle C_1\rangle = f_1^{un}/f_0$ for first forbidden electron emission

Z	E_0, kev					
	100	200	500	1000	2000	4000
10	0,0118	0,0289	0,1055	0,314	1,025	3,57
20	0,0129	0,0291	0,1045	0,302	1,005	3,55
30	0,0141	0,0294	0,1024	0,294	0,988	3,53
40	0,0152	0,0298	0,0983	0,288	0,971	3,51
50	0,0164	0,0302	0,0953	0,284	0,958	3,51
60	0,0176	0,0306	0,0940	0,280	0,949	3,50
70	0,0188	0,0312	0,0933	0,277	0,939	3,50
80	0,0199	0,0318	0,0931	0,274	0,933	3,51
90	0,0209	0,0325	0,0930	0,271	0,928	3,51
98	0,0216	0,0332	0,0931	0,268	0,923	3,51

Table 2

Values of $\langle C_1\rangle = f_1^{un}/f_0$ for first forbidden positron emission

Z	E_0, kev					
	100	200	500	1000	2000	4000
10	0,0147	0,0385	0,113	0,321	1,017	3,61
20	0,0169	0,0402	0,115	0,325	1,008	3,57
30	0,0194	0,0428	0,116	0,326	0,993	3,52
40	0,0224	0,0436	0,116	0,326	0,975	3,49
50	0,0262	0,0440	0,114	0,323	0,953	3,43
60	0,0298	0,0438	0,111	0,315	0,928	3,33
70	0,0319	0,0432	0,107	0,303	0,898	3,21
80	0,0327	0,0416	0,103	0,288	0,864	3,05
90	0,0315	0,0381	0,0945	0,264	0,817	2,86
98	0,0290	0,0325	0,0860	0,239	0,774	2,72

data of Tables 1 & 2 by up to 25% for large E_0 and up to 50% for low end-point energies.

The correction factor for second forbidden transitions with $\Delta I = 3$ is given by[1]

$$C_2 = \frac{1}{72}\left(\frac{1}{15}K^4L_0 + 2K^2L_1 + 15L_2\right)\sum_{ijk}|B_{ijk}|^2.$$

Numerical integration of the expression

$$f_2^{un} = \int_1^{E_0} F(E, Z)\, Ep\,(E_0 - E)^2 \cdot \frac{1}{72}\left(\frac{1}{15}K^4L_0 + 2K^2L_1 + 15L_2\right)dE$$

was carried out using the tabular values given in Ref.2.

Table 3

Values of $\langle C_2\rangle = f_2^{un}/f_0$ for second forbidden electron emission

Z	E_0, kev				
	100	500	1000	2000	4000
10	$2{,}64\cdot10^{-5}$	$1{,}93\cdot10^{-3}$	0,0166	0,182	2,08
20	$2{,}76\cdot10^{-5}$	$1{,}90\cdot10^{-3}$	0,0158	0,168	2,00
30	$2{,}92\cdot10^{-5}$	$1{,}87\cdot10^{-3}$	0,0152	0,160	1,95
40	$3{,}12\cdot10^{-5}$	$1{,}83\cdot10^{-3}$	0,0147	0,154	1,91
50	$3{,}36\cdot10^{-5}$	$1{,}79\cdot10^{-3}$	0,0142	0,150	1,91
60	$3{,}66\cdot10^{-5}$	$1{,}74\cdot10^{-3}$	0,0138	0,148	1,92
70	$4{,}06\cdot10^{-5}$	$1{,}70\cdot10^{-3}$	0,0134	0,146	1,94
80	$4{,}62\cdot10^{-5}$	$1{,}64\cdot10^{-3}$	0,0128	0,145	1,97
90	$5{,}60\cdot10^{-5}$	$1{,}59\cdot10^{-3}$	0,0123	0,144	2,03
98	$8{,}75\cdot10^{-5}$	$1{,}55\cdot10^{-3}$	0,0119	0,143	2,07

Table 4

Values of $\langle C_2 \rangle = f_2^{un}/f_0$ for second forbidden positron emission

Z	E_0, keV				
	100	500	1000	2000	4000
10	$3,83 \cdot 10^{-5}$	$2,11 \cdot 10^{-3}$	0,0170	0,172	2,09
20	$5,40 \cdot 10^{-5}$	$2,23 \cdot 10^{-3}$	0,0180	0,171	2,05
30	$6,21 \cdot 10^{-5}$	$2,30 \cdot 10^{-3}$	0,0181	0,169	2,00
40	$6,66 \cdot 10^{-5}$	$2,34 \cdot 10^{-3}$	0,0179	0,164	1,95
50	$7,01 \cdot 10^{-5}$	$2,33 \cdot 10^{-3}$	0,0174	0,155	1,87
60	$7,14 \cdot 10^{-5}$	$2,28 \cdot 10^{-3}$	0,0163	0,146	1,79
70	$7,23 \cdot 10^{-5}$	$2,20 \cdot 10^{-3}$	0,0151	0,134	1,70
80	$7,28 \cdot 10^{-5}$	$2,03 \cdot 10^{-3}$	0,0135	0,120	1,61
90	$7,30 \cdot 10^{-5}$	$1,84 \cdot 10^{-3}$	0,0120	0,104	1,51
98	$7,32 \cdot 10^{-5}$	$1,63 \cdot 10^{-3}$	0,0106	0,0898	1,42

The values of $\langle C_2 \rangle$ for β^-- and β^+-spectra are listed in Tables 3 & 4. This correction factor is characterized by an even stronger energy dependence than the factor in the case of first forbidden β-transitions.

The probability for decay of a nucleus by K electron capture may be represented by the same formulas as the probability for β-decay if for first forbidden captures we write

$$(f_K)_1^{un} = \frac{1}{12} q_K^2 (f_K)_0,$$

and for second forbidden

$$(f_K)_2^{un} = \frac{1}{1080} q_K^4 (f_K)_0;$$

here q_K is the energy of the neutrino emitted in K capture, and $(f_K)_0 = \frac{\pi}{2} q_K^2 G_K^2$ is the value of the function f_K for allowed capture (G_K is the K electron wave function). The numerical values of $(f_K)_0$ are listed in Ref.6.

The numerical values for the ratios $\frac{(f_K)_1^{un}}{(f_K)_0}$ and $\frac{(f_K)_2^{un}}{f_0}$ for a number of β-transitions are listed in Tables 5 & 6.

Table 5

Values of $(f_K)_1^{un}/(f_K)_0$ for first forbidden K capture

ΔM_a, $m_e c^2$	Z				
	20	40	60	80	98
0,02	$1,220 \cdot 10^{-5}$				
0,10	$7,078 \cdot 10^{-4}$	$3,497 \cdot 10^{-4}$	$1,808 \cdot 10^{-5}$		
0,30	$7,110 \cdot 10^{-3}$	$5,342 \cdot 10^{-3}$	$3,842 \cdot 10^{-3}$		
0,50	0,02018	0,01800	0,01433	$3,484 \cdot 10^{-3}$	$4,658 \cdot 10^{-3}$
1,00	0,08202	0,07757	0,06973	0,05843	0,04519
1,50	0,1855	0,1788	0,1668	0,1490	0,1274
2,00	0,3307	0,3217	0,3055	0,2813	0,2513
3,00	0,7461	0,7325	0,7080	0,6709	0,6240
5,00	2,077	2,054	2,013	1,950	1,869
8,00	5,323	5,286	5,220	5,119	4,988

The correction factors listed in Tables 1-6 should be used in calculating the product ft for unique transitions as follows

$$(f_n t)_{un} = (f_0 t)_{allowed} \cdot \langle C_n \rangle.$$

Table 6

Values of $(f_K)_2^{un}/(f_K)_0$ for second forbidden K capture

ΔM_a, $m_e c^2$	Z				
	20	40	60	80	98
0,02	$1,983 \cdot 10^{-11}$				
0,10	$6,661 \cdot 10^{-8}$	$1,630 \cdot 10^{-8}$	$4,360 \cdot 10^{-11}$		
0,30	$6,740 \cdot 10^{-6}$	$4,551 \cdot 10^{-6}$	$1,968 \cdot 10^{-6}$	$3,296 \cdot 10^{-7}$	$1,629 \cdot 10^{-9}$
0,50	$5,429 \cdot 10^{-5}$	$4,321 \cdot 10^{-5}$	$2,739 \cdot 10^{-5}$	$1,199 \cdot 10^{-5}$	$2,893 \cdot 10^{-6}$
1,00	$8,969 \cdot 10^{-4}$	$8,022 \cdot 10^{-4}$	$6,483 \cdot 10^{-4}$	$4,553 \cdot 10^{-4}$	$2,724 \cdot 10^{-4}$
1,50	$4,589 \cdot 10^{-3}$	$4,262 \cdot 10^{-3}$	$3,708 \cdot 10^{-3}$	$2,961 \cdot 10^{-3}$	$2,164 \cdot 10^{-3}$
2,00	0,01458	0,01380	0,01244	0,01055	$8,418 \cdot 10^{-3}$
3,00	0,07421	0,07154	0,06683	0,06001	0,05192
5,00	0,5750	0,5625	0,5403	0,5069	0,4660
8,00	3,778	3,725	3,633	3,493	3,317

It is evident from the systematics of β-transitions that taking the factor $\langle C_n \rangle$ into account appreciably reduces the scatter in the ft values for known unique transitions. The influence of the factor is particularly great in the case of transitions with very low or high end-point energy. Table 7 lists some examples of such transitions[7]. The log $f_0 t$ values for these transitions lie outside the 7.5 to 9.5 range characteristic of most unique transitions. As compared to log $f_0 t$, the log $f_1^{un} t$ values are much more closely grouped about the average value.

Table 7

Log $f_0 t$ and log $f_1^{un} t$ values for some unique β-transitions

Transitions	E_0, kev	lg $f_0 t$	lg $f_1^{un} t$	Transitions	E_0, kev	lg $f_0 t$	lg $f_1^{un} t$
N^{16} (β-) O^{16}	10400	6,3	7,7	Se^{79} (β-) Br^{79}	160	10,8	9,1
S^{37} (β-) Cl^{37}	4300	7,0	7,6	Zr^{93} (β-) Nb^{93}	34	10,7	8,8
Ca^{41} (ε) K^{41}	440	10,6	9,4	Tl^{204} (ε) Hg^{204}	376	10,1	8,5
				Tl^{204} (β-) Pb^{204}	765	9,7	9,0

I desire to express my sincere gratitude to B.S.Dzhelepov for his interest in the work and to F.I.Langelen for assistance in carrying out the calculations.

Scientific Research Physical Institute,
"A.A.Zhdanov" Leningrad State University

References

1. E.J.Konopinski & G.Uhlenbeck, Phys.Rev., 60, 308 (1941).

2. B.S.Dzhelepov & L.N.Zyryanova, Vliyanie elektricheskogo polya atoma na B-raspad (Influence of the electric field of the atom on β-decay), M.-L., 1956.

3. M.Taketani, S.Nakamura, M.Umezawa, K.Ono & Y.Yamaguchi, Phys.Rev., 82, 441 (1951).

4. J.P.Davidson, Phys.Rev., 82, 48 (1951).

5. M.L.Perlman, J.P.Welker & M.Wolfsberg, Phys.Rev., 110, 381 (1958).

6. I.M.Band, L.N.Zyryznova & Tsin Chei-Zhui, Izv.AN SSSR, Ser.fiz., 20, 1387 (1956). (Trans.Bulletin 20, No.12a, 1269.)

7. B.S.Dzhelepov & L.K.Peker, Skhemy raspada radioaktivnykh yader (Decay schemes of radioactive nuclei), M.-L., 1958.

CONTRIBUTION TO THE THEORY OF FOCUSING CRYSTAL SPECTROMETERS (CHOICE OF THE REFLECTING PLANES)

- O. I. Sumbaev

In selecting the system of reflecting planes of the crystal wafer utilized in a focusing crystal spectrometer, the designer is usually guided by the magnitude of the interplanar spacing d and the structure factor F. The interplanar spacing determines the dispersion of the instrument:

$$\frac{d\vartheta}{d\lambda} = \frac{1}{2d\cos\vartheta},$$

where ϑ is the Bragg angle, and λ is the wavelength of the investigated radiation. The reflection intensity (area under the line contour) depends on the integral reflection coefficient R_ϑ. For a perfect thick crystal R_ϑ is given by the familiar relation

$$R_{\vartheta I} \approx p r_0 d (F/V)\lambda, \qquad (1)$$

where p is a factor depending on the polarization (for small ϑ close to 1), V is the volume of a unit cell of the crystal, and

$$r_0 = \frac{e^2}{mc^2}.$$

Lind, West & DuMond[1] and later Sumbaev[2] investigated the λ-dependence of R_ϑ for a quartz crystal bent to a cylinder in a Cauchois type focusing spectrometer. This dependence proved to be quadratic and characteristic for a mosaic crystal with small primary extinction. For such a crystal the integral reflection coefficient is given by

$$R_{\vartheta II} \approx p^2 r_0^2 d \left(\frac{F}{V}\right)^2 \lambda^2 T, \qquad (2)$$

where T is the thickness of the crystal. An identical expression was obtained theoretically by Sumbaev[2] for a perfect thick crystal bent to a cylinder, taking into account distortion of the reflecting planes.

The expression for the surface of the bent reflecting planes which prior to bending were perpendicular to the axis of the wafer (Fig.1) can, with some approximation be written

$$z = fy^2, \qquad (3)$$

where

$$f = \frac{1}{2\rho} \frac{a_{34} - \frac{a_{35}}{a_{55}} a_{45}}{a_{33} - \frac{a_{35}^2}{a_{55}}},$$

and the a_{ij} are elastic coefficients.

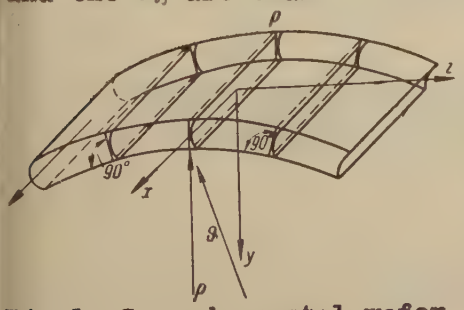

Fig.1. Curved crystal wafer. P - reflecting planes.

For an anisotropic wafer, in particular, for a wafer of α-quartz, the factor f is in general not zero. Its magnitude can be such that the thickness Δy of a coherently scattering lamina (the crystal wafer is subdivided into such laminae in thickness as a result of bending) proves to be smaller than the primary extinction distance t_x.[2] Under these conditions R_ϑ is given by relation (2).

The elastic constants depend on the orientation of the wafer relative to the crystallographic

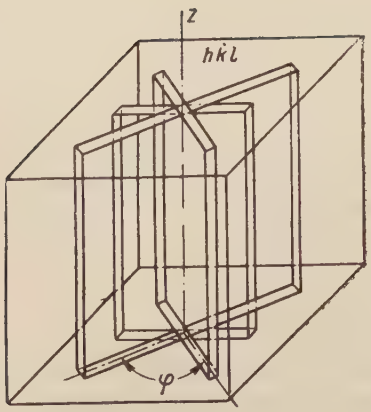

Fig.2. Family of plates with identical reflecting planes hkl but different values of the factor f characterizing their distortion.

axes. For some particular orientations f may be equal to or at any rate close to zero. In this case the normal cross sections remain planar and are only rotated to form a fan-like arrangement, while the coefficient R_ϑ obeys the relation (1).[1]

Let us consider a system of plates cut from a cube, the two opposite faces of which coincide with the hkl planes (Fig.2). All these plates have identically oriented reflecting planes (hkl). Consequently, the values of d and F will also be the same. Transforming the elastic constants in Eq.(3) according to the conventional rules for the transformation of the components of a tensor incident to rotation about one axis (z), we obtain the variation of the factor f with the angle of rotation φ:

$$f = \frac{1}{2\rho} \frac{(a_{34}a_{55} - a_{35}a_{45})\cos\varphi + (a_{45}a_{34} - a_{44}a_{35})\sin\varphi}{(a_{33}a_{44} - a_{34}^2)\sin^2\varphi + (a_{45}a_{33} - a_{34}a_{35})\sin 2\varphi + (a_{33}a_{55} - a_{35}^2)\cos^2\varphi}, \qquad (4)$$

where the a_{ij} are the elastic constants for the orientation of the plate taken as the initial position (i.e., that from which φ is reckoned). We find that f for given d and F is in general a variable quantity. The values of $f(\varphi)$ for some planes of α-quartz (the ones most convenient for use in x- and γ-ray spectrometers) are given in the accompanying table and Fig.3.

Parameters of the planes of α-quartz most convenient for use in spectrometers (for ρ = 200 cm)

Index	d, X	F	$f \cdot 10^4$, cm^{-1}	f_{tr} at 10^5, cm^{-1}
$10\bar{1}0$	4246,09	15,6	$f_0^*=0$; $f_{90}^{**}=8,3$	1,5
$11\bar{2}0$	2451,40	17,5	$R\equiv 0$	1,1
$13\bar{4}0$	1177,64	26,9	$f_0^*=1,8$; $f_{90}=-6,2$	1,2
$22\bar{4}3$	1012,75	15,6	$f_0^{***}=-12$; $f_{90}=6,4$	0,3
$50\bar{5}2$	810,00	21,7	$f_0^{****}=0$; $f_{90}=-12$	0,5

*Plates cut so that the optical axis of the crystal lies in the plane of the large face and parallel to the side edge. **The subscript to f indicates the angle of rotation from the initial position about the longitudinal axis of the plate. ***Plate prepared from a Y-cut crystal by 55°48' clockwise rotation about the Y axis. ****Plate prepared from an X-cut crystal by 72°30' counterclockwise rotation about the X axis.

Let us determine the values of f above which one should expect a quadratic λ-dependence of R_ϑ. We assume that $\Delta y = t_x$. Performing the substitutions

$$\Delta y = \sqrt{\frac{d}{2\pi f}} \qquad \text{(Ref.2)}$$

and

$$t_x = \left[2r_0\left(\frac{F}{V}\right)pd\,\tan\vartheta\right]^{-1} \approx \left[r_0\left(\frac{F}{V}\right)p\lambda\right]^{-1} \qquad \text{(Ref.3)}$$

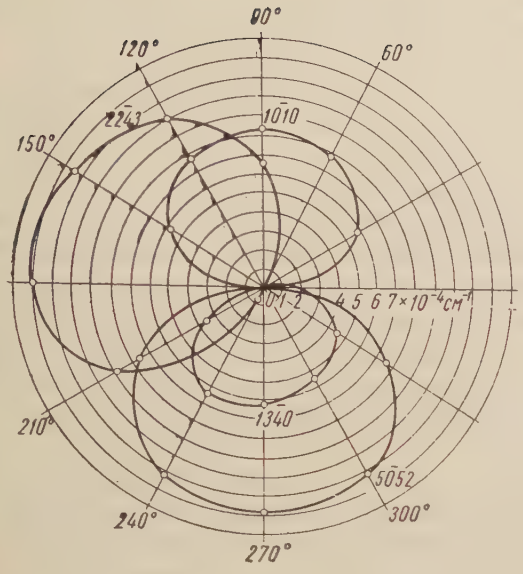

Fig.3. Variation of the factor f characterizing the distortion of the reflecting planes with the angle φ of rotation of the crystal plate about the z axis.

we obtain after suitable transformations

$$f_{tr} = \frac{1}{2\pi}\left(\frac{R_{\vartheta_{II}}}{T}\right).$$

The numerical values of f_{tr} (for E = 100 kev (λ = 120 mÅ) and ρ - 200 cm) are listed in the last column of the table. Comparing the values of f and f_{tr}, we see that in a large range of rotation angles φ (for E $\geq$ 100 kev) for all the plates in question (except the plate with $1\bar{1}20$ reflecting planes) one may expect quadratic variation of R_ϑ with λ. For all these plates, however, there is a range of φ in which $f < f_{tr}$ and the λ-dependence of R_ϑ becomes linear.

After publication of the work of Lind, West & DuMond[1] in which there was experimentally established the quadratic character of the λ-dependence of R_ϑ for bent quartz plates with perpendicularly oriented $13\bar{4}0$ planes, there was a tendency in evaluating the spectral sensitivity of γ-spectrometers to assume a quadratic dependence of R_ϑ on λ even for plates with other reflecting planes.[3] Yet it follows from the above that this assumption may be erroneous even for plates with the indicated reflecting planes normal to the wafer surface, if the rotations of the plates about the z axis (Fig.2) are different. Bending of the reflecting planes has a substantial effect on the other properties of the instrument as well, in particular, on the line shape and width.[4] Hence this dependence must be taken into account in considering all the parameters.

In conclusion, we must emphasize that the above analysis was carried out for plates perpendicular to the longitudinal axis of a plane-parallel wafer. Planes, the orientations of which deviate from the perpendicular to the longitudinal axis, will be somewhat bent owing to projection of the curvature of the plate, and this bending may play the same role as the above described effect connected with anisotropy[5]. For cross sections deviating from the perpendicular, the factor f may be written in the form $f = f_0 + \alpha/\rho$, where f_0 is the factor for normal planes as given by Eq.(3), while the term α/ρ takes into account the bending connected with deviation by the small angle α from the normal.

References

1. D.A.Lind, W.J.West & J.W.M.DuMond, Phys.Rev., 77, 475 (1950).
2. O.I.Sumbaev, Zhur.eksp.i teor.fiz., 32, 1276 (1957). (Trans.Soviet Physics - JETP).
3. O.Beckman, Nuclear Instruments, 3, 27 (1958).
4. O.I.Sumbaev, PTE, 3, 27 (1958). (Trans.Instruments & Exp.Techniques.)
5. D.W.Berreman, Phys.Rev., 110, 992 (1958).

ANGULAR CORRELATION OF THE GAMMA-RAYS FROM Ne^{21}

- A.G.Khabakhpashev & E.M.Tsenter

We investigated the γ-γ angular correlation in neon-21 using a Po-O neutron source. The source was a solution of Po^{210} nitrate in water enriched to 24% in O^{18}. The $O^{18}(\alpha,n)Ne^{21}$ reaction in such a source is accompanied by the emission of γ-rays with energies 0.35 and 1.38 Mev. The 0.35 Mev γ-rays are associated with the first excited level of Ne^{21} and their intensity with respect to the neutron yield is 45%. The 1.38 Mev γ-rays are associated with the transition from the second excited level to the first; their intensity is 10%. The upper bound of the intensity of the cross-over transition from the second excited level to the ground level is 1%. The upper bound of the transitions departing from the third level at 2.84 Mev is 4%. These data on the γ-radiation from a Po-O source were obtained by means of a scintillation spectrometer and a n-γ coincidence circuit.

For measuring the angular correlation we used a fast-slow coincidence circuit (see accompanying figure) incorporating scintillation counters with 40 x 40 NaI crystals. The pulse selector in the second channel was set on the photopeak of the 1.38 Mev line. The first channel was adjusted to detect 0.35 Mev γ-rays. The number of coincidences for different angles between the source-to-counter directions was determined from the area of the 0.35 Mev line peak, which was measured by means of a 50 channel pulse analyzer.

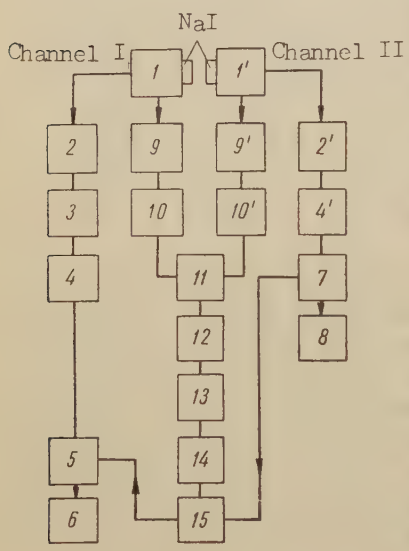

Block diagram of the equipment for measuring angular correlation: 1 & 1') FEU-IV photomultipliers, 2 & 2') preamplifiers, 3) delay line, 4 & 4') linear amplifiers, 5) gating circuit, 6) 50 channel pulse analyzer, 7) selector, 8) PS-10 000, 9 & 9') 200 Mc amplifier, 10 & 10') pulse shapers, 11) coincidence circuit ($\tau = 10^{-8}$ sec), 12) amplifier, 13) discriminator, 14) delay stage, 15) coincidence circuit ($\tau = 10^{-6}$ sec).

This experimental arrangement with a lead shield about the stationary counter virtually excluded detection by one crystal of photons scattered in the other. Moreover, the fast-slow coincidence circuit reduced the relative number of chance coincidences to 0.3%. Possible counting instability in the second channel was excluded by normalizing the coincidence counting rate with respect to the counting rate at the selector output. Instability in the operation of the first channel could lead only to displacement of the 0.35 Mev line peak but not to change in the area under the peak and, consequently, could have no effect on the measurement results.

The source, which had an intensity of 10^5 neutrons per sec, was mounted on the axis of rotation of the second counter at a distance of 62 mm from each crystal. Measurements were carried out at angles of 90, 120, 150 and 180°. The experimental results were processed by the method of least squares. Appropriate corrections were made for finite angular resolution, scattering in the source and the finite dimensions of the source.

Finite angular resolution of the detectors, like scattering in the source, leads to "smearing out" of the angular correlation; it is convenient to calculate the corrections for these two effects together. If scintillation counters with good energy resolution are employed and there are detected only the pulses corresponding to complete absorption of the γ-rays in the crystal, scattered photons

will be detected only when the scattering angle is less than ψ. The magnitude of ψ depends on the width of the analyzer gate and the energy of the γ-rays.

Let the correlation be described by

$$W = 1 + \sum_{1}^{k_m} A_{2k} P_{2k} (\cos \vartheta).$$

We shall use n_1 to denote the ratio of the number of gammas with energy E_1 emerging from the source without scattering to the total number of gammas that can be detected by the first counter. Then the fraction of gammas emerging from the source and scattered through angles smaller than ψ_1 will be $1 - n_1$. We shall use the same notation with the subscript 2 for the gammas with energy E_2. Then for the experimental correlation function we can write

$$\begin{aligned} \overline{W}(\vartheta) = {} & n_1 n_2 \int W(\vartheta')\, d\Omega_1 d\Omega_2 \varepsilon_1(\alpha_1)\, \varepsilon_2(\alpha_2) + \\ & + n_2 (1 - n_1) \int W_1'(\vartheta')\, d\Omega_1 d\Omega_2 p_1(\alpha_1 \psi_1)\, \varepsilon_1^s \varepsilon_2(\alpha_2) + \\ & + n_1 (1 - n_2) \int W(\vartheta')\, d\Omega_1 d\Omega_2 \varepsilon_1(\alpha_1)\, p_2(\alpha_2 \psi_2)\, \varepsilon_2^s + \\ & + (1 - n_1)(1 - n_2) \int W(\vartheta')\, d\Omega_1 d\Omega_2 p_1(\alpha_1 \psi_1)\, \varepsilon_1^s p_2(\alpha_2 \psi_2)\, \varepsilon_2^s, \end{aligned} \tag{1}$$

where ϑ is the angle between the axes of the cylindrical crystals, ϑ' is the angle between the directions of the gammas, $d\Omega_1$ is the solid angle element for the first gamma, $\varepsilon_1(\alpha_1)$ is the efficiency of the first counter for detecting the first gamma, α_1 is the angle between the axis of the crystal and the direction of motion of the first gamma, $p_1(\alpha_1 \psi_1)$ is the probability that the first gamma emerging at the angle α_1 will, after scattering through an angle $< \psi_1$, enter the first counter, and ε_1^s is the mean efficiency for detecting the scattered gamma by the first counter. The corresponding symbols with the subscript 2 pertain to the second gamma.

The first term in Eq. (1) represents the unscattered part of the radiation and takes into account the finite angular resolution of the detectors. The second term represents the part of the radiation in which the first gammas are scattered through angles smaller than ψ_1; the third term corresponds to the same scattering of the second gammas, and the fourth term to scattering of both the first and second gammas simultaneously. Inasmuch as the terms describing the scattering are small compared with the first term, and the angles ψ_1 and ψ_2 are not large, for calculating these terms we can assume that for $\alpha_i > \psi_i$, the probability $p_i = 0$, while for $\alpha_i \leqslant \psi_i$,

$$p_i = \int_0^{\gamma_i'} d\Omega_i \Big/ \int_0^{\psi_i} d\Omega_i,$$

where $\gamma_i' = \operatorname{arc\,tan} \frac{r_i}{R_i + h_i/2}$, r_i is the radius of the crystal, R_i is the distance from the source to the crystal, and h_i is the height (thickness) of the crystal. Further, we assume that the efficiency for detecting scattered gammas does not depend on the angles α and ψ. Under these assumptions, Eq. (1) can readily be reduced to[1]

$$\overline{W}(\vartheta)\, \text{const} = 1 + \sum_{1}^{k_m} (B_{2k} / B_0) A_{2k} P_{2k} (\cos \vartheta). \tag{2}$$

Here we have employed the following notation:

$$\begin{aligned} B_{2k} = {} & n_1 n_2 I_{2k}^1 I_{2k}^2 + n_2 (1 - n_1) I_{2k}^{1s} I_{2k}^2 + n_1 (1 - n_2) I_{2k}^1 I_{2k}^{2s} + \\ & + (1 - n_1)(1 - n_2) I_{2k}^{1s} I_{2k}^{2s} \qquad (k = 0,\ 1 \ldots k_m); \end{aligned} \tag{3}$$

$$I_{2k}^i = 2\pi \int_0^{\gamma_i} P_{2k} (\cos \alpha)\, \varepsilon_i(\alpha) \sin \alpha\, d\alpha \quad (i = 1, 2); \tag{4}$$

$$I_{2k}^{is} = 2\pi p \varepsilon_i^s \int_0^{\psi_i} P_{2k}(\cos\alpha)\sin\alpha\, d\alpha; \qquad (5)$$

$$\gamma_i = \arctan r_i / R_i. \qquad (6)$$

The value of the integral (4) must be determined numerically. For separate determination of the influence of scattering on the weakening of the measured anisotropy one must compare the total attenuation coefficient B_{2k}/B_0 with the attenuation produced by the angular resolution of the detectors:

$$I_{2k}^1 I_{2k}^2 / I_0^1 I_0^2.$$

We calculated the corrections for angular resolution and scattering by means of Eq.(3). For a function of the form $1 + a_2\cos^2\vartheta$, the correction for angular resolution amounts to 11%, while the correction for scattering in the source equals 3%. The calculations were carried out for a source with a volume of 2.3 cm^3, enclosed in a steel container with 3 mm thick walls.

The correction for finite size of the source was determined by Walter's formula given in Ref.2. This formula allows of taking into account only the linear dimensions of the source in the direction of the axis of rotation of the second counter. For a source having a "length" of 20 mm the correction equals 1%. With these corrections taken into account, the correlation function has the form

$$W = 1 + (0{,}20 \pm 0{,}02)\cos^2\vartheta. \qquad (7)$$

This result is in agreement with the theoretical correlation function for a dipole-dipole transitions of the 3/2→5/2→3/2 type. For such a transition $a_2 = 0.226$.

It is known from the work of Koch & Rasmussen[3] and Hubbs & Grosof[4] that the nuclear spin of Ne^{21} is 3/2. Middleton & Tai[5], on the basis of investigation of the angular distribution of protons from the $Ne^{20}(d,p)Ne^{21}$ reaction and comparison of the cross sections for the formation of Ne^{21} in the ground and first excited states came to the conclusion that the spins of these states are 3/2 and 5/2, respectively. These data are in agreement with the results of our measurements. For the second excited level, Middleton & Tai give alternate assignments of 1/2 or 3/2.

If we accept that one of the transitions in the cascade is a mixture of M1 + + E2, it follows from the results of angular correlation measurements that for the 1/2→5/2→3/2 transition the admixture of E2 should be 9%, for the 5/2→5/2→ →3/2 transition - 11% and for the 7/2→5/2→3/2 transition - 2%.

To determine the possible influence of interaction of the magnetic moment of the nucleus in the compound state with the electron shell of the atom and with other atoms on the results of the angular correlation measurements, we carried out a determination of the lifetime of the first excited level of Ne^{21}, and obtained $\tau = (1.0 \pm 1.1)\cdot 10^{-10}$ sec. Here the uncertainty is the root mean square deviation obtained in processing nine series of measurements.

Moscow Engineering-Physical Institute

References

1. M.E.Rose, Phys.Rev., 91, 610 (1953).
2. H.Frauenfelder, Annual Rev.Nucl.Sci., 2, 129 (1953).
3. J.Koch & E.Rasmussen, Phys.Rev., 76, 1417 (1949).
4. J.C.Hubbs & G.M.Grosof, Phys.Rev., 104, 715 (1956).
5. R.Middleton & C.T.Tai, Proc.Phys.Soc., 65 (A), 752 (1952).

SPECIFIC STOPPING LOSSES IN HEAVY IONS IN DIFFERENT SUBSTANCES

- A.P.Grinberg & I.Kh.Lemberg

Through investigation of Coulomb excitation one can, in a number of cases, (particularly, for even-even nuclei) reliably determine the lifetime τ of excited nuclear levels in the range from 10^{-12} sec down. In experiments with protons and α-particles in the case of higher excitation energies ($\Delta E \approx 1$ Mev), owing to an interfering γ-background from nuclear reactions, one can in practice investigate only nuclei with $A > 50$. The use of heavier particles, namely, ions, allows of extending the lifetime measurements into the range of nuclei with $A < 50$.[1]

As a rule thick targets are used in Coulomb excitation experiments. Hence for calculating the values of τ one must have available precise data on the specific energy loss, $\varepsilon = dE/dR$, involved in the slowing down of C, N and other suitable ions in different substances as a function of the ion energy. The available experimental material on energy losses is extremely scanty; moreover, some of the reported data are of doubtful accuracy. The paucity of data is particularly acute for the ion energy range of interest to us, namely, 10 to 36 Mev, and for cases of absorption in materials other than nuclear emulsions and gaseous media. In fact one can name only two investigations in which the range-energy relation for heavy ions in metals was measured: Reynolds, Scott & Zucker[2] measured the range of N^{14} ions in nickel; Webb, Reynolds & Zucker[3] determined the range of nickel ions in aluminum. The maximum ion energy in the work referred to was 28 Mev.

In investigations of Coulomb excitation of nuclei by heavy ions carried out in the cyclotron laboratory of the Physical-Technical Institute, by way of targets we used a large number of different metals and other solids, by way of bombarding particles not only N^{14} ions with energies to ~36 Mev, but also C^{12}, O^{16}, Ne^{20} and Ne^{22} ions. Hence it was necessary to choose some consistent theoretical or semi-empirical method of calculating ε. Below we list three known methods for such calculation and briefly describe their distinctive features.

1. Longchamp's method. Using the results of a number of theoretical investigations, in which the average charge of the ion as a function of its velocity was calculated by means of the statistical Thomas-Fermi atomic model, Longchamp[4] calculated the ratio $k = R/R_\alpha$ for Li^7, Be^9, B^{10}, C^{12}, N^{14} and O^{16} ions as a function of their velocity v_i (here R is the range of the given ion having the initial velocity v_i, and R_α is the range of an α-particle with the same initial velocity in the same substance). It is assumed that k for a given ion is the same for slowing down in different solid media.

Thus the data on $k(v_i)$ (which for practical calculations it is convenient to represent in the form of a smooth curve) given by Longchamp allow of plotting a range-energy curve for any of the enumerated ions in any solid medium if one knows the range-energy curve for α-particles in this medium.*

Then from the R(E) curve one can find $\Delta E/\Delta R = f(E)$ and from these data plot the curve for $f(E)$.

2. Proton method. This method is based on the familiar Bethe-Bloch equation

$$\varepsilon = \frac{dE}{dR} = aZ_1^2 \frac{N}{v^2} B(v, Z_1, Z_2), \qquad (1)$$

where a is a numerical constant, Z_1 and Z_2 are the charges of the slowed down particle and of the nucleus of the absorber atoms (expressed in elementary charges), v is the velocity of the particle at the point of its range under consideration, N is the number of atoms per cm^3 of the absorber, and B is the "atomic stopping power" of the material.**

---

*Detail data on the ranges of α-particles in different substances are given by Waling.[5]

**(See bottom of next page.)

In the case of singly charge particles (protons or deutrons) with an energy $\geqslant$1 Mev, one can assume that virtually over the entire range of the particle in the absorber its charge remains the same (i.e., unity) and that the value of B for a given medium and a given velocity will be the same for protons and deuterons.

In the case of slowing down of multiply charged ions, the charge Z_1 of each ion changes discretely owing to loss or capture of orbital electrons in collisions with the atoms of the medium. For each velocity v there will be a certain mean charge $\bar{Z}$, i.e., the average value for a multitude of particles. This mean ionic charge gradually decreases with decrease in the velocity of the ion as it moves through the medium. Obviously, also in the case of slowing down of multiply charged ions, Z_1 will depend not only on the ion velocity in the medium but also on the nuclear charge (Z_{1n}) of the given ion.

One can attempt to apply Eq.(1) to the case of slowing down of multiply charged ions making the following assumptions: a) that instead of Z_1 one can to the first approximation use the mean value $\bar{Z}$ and, b) that the magnitude of $\bar{Z}$ for an ion of a given kind depends only on the velocity of the ion at the given point in its range and does not depend on the medium in which it is stopped. We are speaking here only of different solid media; in this case numerous measurements of $\bar{Z} = f(v)$ substantiate the validity of assumption b.[6,7]

Under the above assumptions, considering the slowing down of a multiply charged ion in two different media I and II and the slowing down of a proton with the same initial velocity in the same two media, one can on the basis of Eq.(1) deduce the following relationships

$$\frac{\varepsilon_{\bar{i}}^{I}}{\varepsilon_{\bar{i}}^{II}} = \frac{\varepsilon_{\bar{p}}^{I}}{\varepsilon_{\bar{p}}^{II}} = \varkappa_{I,II}(v). \tag{2}$$

Thus we obtain

$$\varepsilon_{\bar{i}}^{I} = \varepsilon_{\bar{i}}^{II}\varkappa_{I,II}. \tag{3}$$

Equation (3) is the working formula of the "proton method" for calculating the specific energy loss of multiply charged ions. For practical evaluation purposes one should plot the $\varkappa_{I,II}(E)$ curve in the particle velocity range of interest; data on $\varepsilon_{\bar{p}}(E_{\bar{p}})$ for a large number of metals and other substances can be found in the literature, for example, in Waling's survey.[5]

As will be evident from (3), the "proton method" allows of calculating the specific energy loss $\varepsilon(E)$ for a given multiply charged ion in medium II if one knows the specific energy loss for the same ion in medium I as a function of its energy.

3. Average ion charge method. If we assume that for multiply charged ions B in Eq.(1) is only weakly dependent on Z_1, then in the first approximation we can neglect this dependence. In this case and, in addition, retaining assumption "a" above, from the Bethe-Bloch formula (1) we obtain

$$\frac{\varepsilon_{i\bar{1}}}{\varepsilon_{i\bar{2}}} = \left(\frac{\bar{Z}_{i\bar{1}}}{\bar{Z}_{i\bar{2}}}\right)^2. \tag{4}$$

This relation pertains to stopping in the same medium of two different multiply charged ions (i1 and i2) having the same velocity. From Eq.(4) we obtain the "working formula" of the average ion charge method, namely,

---

**(from preceding page) We shall not dwell here on the restrictions that may limit the applicability of the Bethe-Bloch equation or on the questionable nature of some of the assumptions made in its derivation.

$$\varepsilon_{i1} = \varepsilon_{i2}\left(\frac{\bar{Z}_{i1}}{\bar{Z}_{i2}}\right)^2. \qquad (5)$$

Thus to find unknown values of $\varepsilon_{i1}(E)$ on the basis of the known values of $\varepsilon_{i2}(E)$, we must have data on the average charge of each of the two types of ions in the given medium (or in practice, taking into account the above mentioned results of measurements of $\bar{Z}(v)$ in any solid medium) as a function of their velocities.

By way of the "i2" particles, one can, in particular, consider protons or α-particles. For ~0.5 Mev protons one can take $\bar{Z} = 1$; for α-particles $\bar{Z} = 2$ for $v > 12 \cdot 10^8$ cm/sec ($E_\alpha > 3$ Mev), while for lower velocities the variation of $\bar{Z}$ as a function of velocity is given by Allison[8]. However, data on the values of $\varepsilon_\alpha(v)$ for different stopping media are far more scanty and less reliable than data on the values for $\varepsilon_p(v)$.

If by way of the "i2" particles we consider protons, then for calculating ε_{i1} by means of Eq.(5) we need only have experimental data on the variation of $\bar{Z}_{i2}$ as a function of v. So far, however, such data are not available as a rule. According to the suggestion of Papineau[9] this difficulty can be overcome as follows. From analysis of the experimental data it follows that the curve characterizing $\bar{Z}/Z_{1n} = f(v/Z_{1n}^{3/2})$ and plotted on the basis of the experimental data on $\bar{Z}(v)$ for N^{14} ions in nickel[2] is universal in the sense that to within a certain accuracy it is applicable to any stopping medium and to any multiply charged ion (with $Z_{1n} < 10$). Measurements of $\bar{Z}(v)$ in the work of Reynolds et al[2] were carried out only in the ion energy range to 28 Mev. At 28 Mev the value of $\bar{Z}/Z_{1n}$ does not yet attain unity. Hence one must extrapolate the "universal curve" into the $\bar{Z}/Z_{1n} \simeq$ $\simeq 0.9$-1 region. Papineau[9] gives such an extrapolated curve in his published report. Later he made the upper part of the curve steeper in order to obtain more satisfactory agreement between the experimentally measured ranges of different ions in different media and the ranges calculated by means of the "universal curve" (this later variant of the curve has not been published but Papineau sent copies of it to a number of laboratories including ours).

As will be evident from the above, it may be assumed that the third calculating method, in contrast to the second, allows of obtaining only rough evaluations of $\varepsilon(E)$, inasmuch as Eq.(5) is based on the assumption that B is independent of Z_1, which is not borne out by experiment, and since one must use a curve the "universality" of which is only approximate.

Naturally, it is of interest to know the limits of error with which one can calculate the values of $\varepsilon(E)$ for different multiply charged ions. The best way of evaluating this error would be direct comparison with reliable experimental data. Unfortunately, even reasonably accurate experimental data are lacking and we must restrict ourselves to comparison of calculated values obtained in different ways; in addition, we can make some comparisons with the most nearly suitable experimental results. We carried out numerous cross checks of this type; some of our results are given below.

Fig.1 shows the R(E) curve for N^{14} ions in nickel calculated by Longchamp's method together with the experimental curve based on the data of Reynolds et al[2]. It will be seen that in this case the computational method gives satisfactory results in the 10 to 26 Mev ion energy range.

As noted above, we are interested primarily in data on $\varepsilon(E)$. These can be obtained by taking the values of $\Delta E/\Delta R$ from the range-energy curve. The results of such calculations are shown in Fig.2 (a smooth curve was drawn through the points). Unfortunately, the experimental curve breaks off at a relatively low ion energy (~26 Mev). In the same figure we also show the $\varepsilon_{N^{14}}^{Ni}$ vs energy curve calculated by the third method on the basis of data on the values of ε_p^{Ni}.

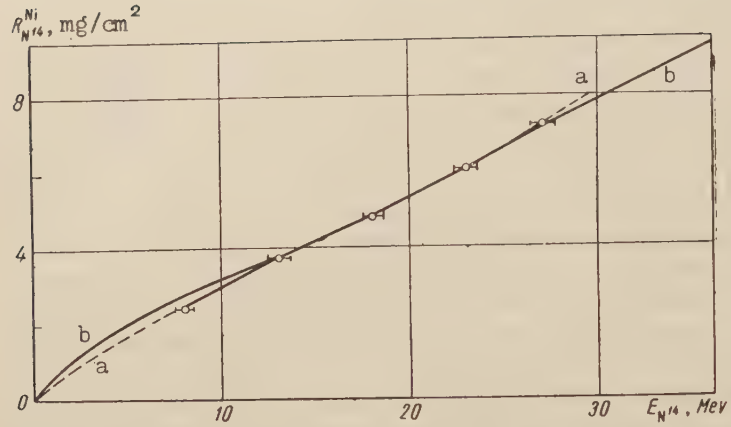

Fig.1. Range-energy curves for N^{14} ions in nickel: a) experimental curve given by Reynolds et al[2], b) curve calculated by Longchamp's method.

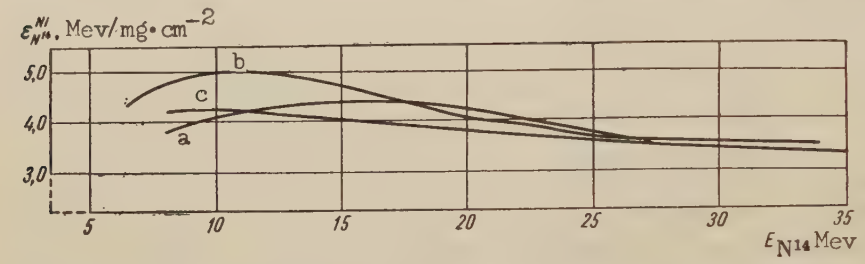

Fig.2. Specific energy losses of N^{14} ions in nickel: a) according to the experimental range-energy curves, b) according to the range-energy curve calculated by Longchamp's method, c) according to the ε^{Ni}_{p} curve (recalculated by the third method).

In the <15 Mev region the divergence of curve b from the experimental curve is rather large, while for E $\geqslant$ 15 Mev the divergence of both calculated curves from the experimental does not exceed 10%. Inasmuch as in the region above 25 Mev, where there are no experimental data, the two calculated curves are close (divergence 3%) it may be hopefully assumed that the values of $\varepsilon^{Ni}_{N^{14}}$ given by these curves in the high energy region differ little from the true ones. In this case for the stopping of N^{14} ions in nickel we can plot a partially experimental, partially calculated curve for the energy variation of ε in the 8 to 35 Mev region. Then using this curve as the initial curve for the second computational method, we can calculate $\varepsilon(E)$ for N^{14} ions in any solid. If we restrict our consideration to a relatively narrow energy region, for example, from 15 to to 25 Mev, then for this region we can average $\varepsilon(E)$ and calculate a mean value $\bar{\varepsilon}_{N^{14}}$ for each of the stopping media of interest. The results of such calculations are shown in Fig.3. We calculated the values of $\varepsilon_{N^{14}}$ for stopping in Li, Be, Al, Ni, Ag and Au (in the cases of Al and Ni the calculations were based directly on the experimental data) and drew a smooth curve through the resultant points; this curve represents $\bar{\varepsilon} = f(Z_2)$ for N^{14} ions.

We carried out a number of check calculations for the purpose of comparing the results of the different computational methods. For example, using Longchamp's

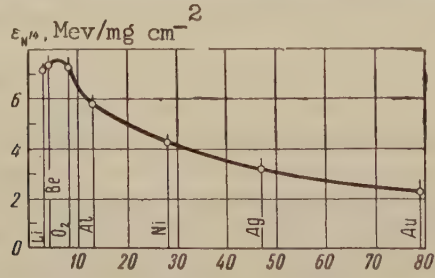

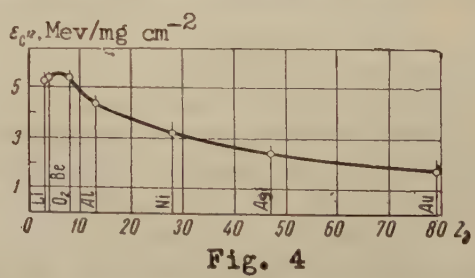

Fig. 4

Fig.3. Average values of the specific energy loss of N^{14} ions in the 15 to 25 Mev energy range as a function of the atomic number of the stopping medium.

Fig.4. Average values of the specific energy loss of C^{12} ions in the 15 to 25 Mev energy range as a function of the atomic number of the stopping medium.

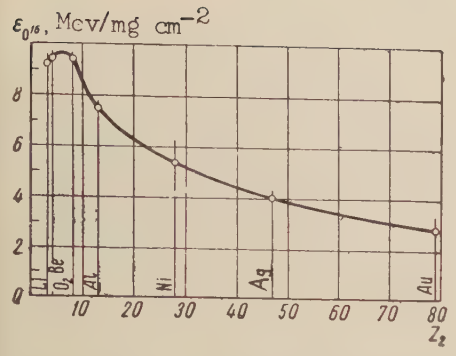

Fig.5. Average values of the specific energy loss of O^{16} ions in the 15 to 25 Mev energy range as a function of the atomic number of the stopping medium.

method, we plotted the R(E) curve for N^{14} ions in silver and from it calculated the mean value of $\bar{\varepsilon}^{Ag}_{N^{14}}$.

It proved to be 3.24 Mev/mg·cm^{-2} in the 15 to 31 Mev region. On the other hand, the method of calculation described above yields $\bar{\varepsilon}^{Ag}_{N^{14}}$ = 3.12 Mev/mg·cm^{-2} in the 15 to 25 Mev region (Fig.3). The disagreement amounts to ~4%.

If we plot the $\varepsilon^{Al}_{N^{14}} = f(E)$ curve for E = 8 to 24 Mev on the basis of the experimental data[3] on the range of N^{14} ions in aluminum, and compare it with the curve calculated by means of the "proton method" on the basis of the $\varepsilon^{Ni}_{N^{14}}$ curve (curve a in Fig.2), we find that the values of ε given by the calculated curve differ from the experimental values by not over ±12%.

Summarizing this part of the calculations, one can say that where stopping of N^{14} ions with energies up to 35 Mev in different solid media is concerned, we have satisfactory data on the specific energy loss as a function of the ion energy and of Z_2.

In analogous fashion we obtained the values of $\varepsilon(E)$ for C^{12} and O^{16} ions. For each of these ions we plotted the R(E) curve for stopping in nickel on the basis of Longchamp's method and then calculated the mean values of ε in the 15 to 25 Mev region. Then by the "proton method" we calculated the values of ε for a number of stopping media. The results of these calculations are shown in Figs. 4 & 5. Unfortunately, there are as yet no experimental data on the ranges of C^{12} and O^{16} ions with energies of interest to us in even a single solid medium. Hence at present we cannot reliably evaluate the accuracy of the calculated values of ε.

One can, however, make certain indirect checks. For example, we found $\varepsilon_{C^{12}}$ for stopping in aluminum directly from the range-energy curve calculated by Longchamp's method and compared this value with that shown in Fig.4. The difference amounts to ~4%.

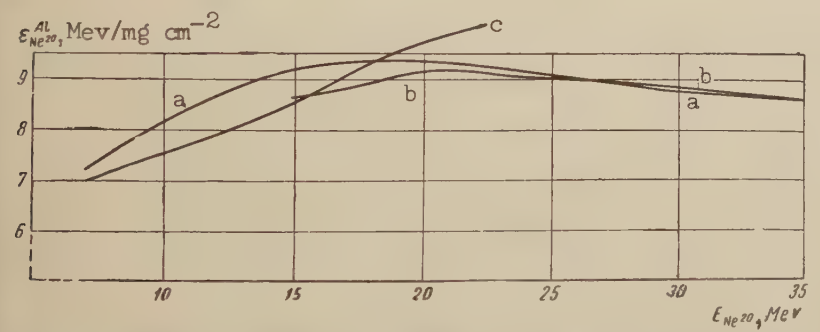

Fig.6. Specific energy losses of Ne^{20} ions stopped in aluminum. Curves calculated on the basis of the particle energy dependences of a) ε^{Al}_{p}, b) $\varepsilon^{Al}_{\alpha}$ and c) $\varepsilon^{Al}_{N^{14}}$.

Longchamp[4] gives no data on the values of $k(v)$ for neon ions. Hence we calculated $\varepsilon^{Al}_{Ne^{20}}$ by the third computational method. Actually we carried out three separate calculations: in the first variant as the initial curve we took the $\varepsilon^{Al}_{p} = f(E_p)$ curve, for the second the $\varepsilon^{Al}_{\alpha} = f(E_\alpha)$ curve and for the third the $\varepsilon^{Al}_{N^{14}} = f(E)$ curve calculated from the experimental data of Webb et al[3]. The results are shown in Fig.6. It will be evident that the first two variants yield values of $\varepsilon^{Al}_{Ne^{20}}$ in satisfactory agreement with each other, whereas the results of the third computational variant depart substantially from the results given by the first two.

Calculations of the $\varepsilon^{Al}_{Ne^{20}} = f(E)$ curve on the basis of ε^{Al}_{p} (first variant) showed that the values of $\varepsilon^{Al}_{Ne^{20}}$ and $\varepsilon^{Al}_{Ne^{22}}$ taken for the same Ne^{20} and Ne^{22} ion energy differ by less than 3% in the 8 to 35 Mev energy region.

In view of the scarcity of experimental data on the specific energy losses of different ions in different media, we feel that our calculated curves (Figs. 3-5) can serve as useful reference material. On the basis of the cited checks and comparisons it may be asserted that the values of $\varepsilon = f(E)$ calculated by means of the described methods differ from the true values by not more than 10-12%. Further evidence in support of this assertion is furnished by the results of calculations of the lifetime τ of nuclear levels excited by the Coulomb field of multiply charged ions. On the basis of analysis and review of the experimental data obtained in our laboratory as a result of investigation of Coulomb excitation of different nuclei by α-particles and heavy ions of different energies, it may safely be assumed that the values of $\varepsilon(E)$ used by us in calculating τ are reasonably accurate. Using the above described methods, it should be feasible in the future to obtain much more accurate data on the specific energy losses of heavy ions when there become available experimental values of ε for C^{12}, O^{16} and N^{20} in at least one solid medium (for example, in nickel or aluminum) in a sufficiently wide ion energy range.

Physical-Technical Institute,
Academy of Sciences of the USSR

References

1. D.G.Alkhazov, A.P.Grinberg, G.M.Gusinskii, K.I.Erokhina & I.Kh.Lemberg, Zhur.eksp.i teor.fiz., 35, 1056 (1958). (Trans.Soviet Physics - JETP)
2. H.L.Reynolds, D.W.Scott & A.Zucker, Phys.Rev., 95, 671 (1954).
3. W.H.Webb, H.L.Reynolds & A.Zucker, Phys.Rev., 102, 749 (1956).
4. J.P.Longchamp, phys.et radium, 14, 89 (1953).
5. W.Walling, Handbuch der Physik, 34, 193 (1958).
6. K.G.Stephens & D.Walker, Proc.Roy.Soc.A, 229, 376 (1955).
7. V.S.Nikolaev, L.N.Fateeva, I.S.Dmitriev & Ya.A.Teplova, Zhur.eksp.i teor. fiz., 32, 965 (1957). (Trans.Soviet Physics - JETP)
8. S.K.Allison, Revs.Mod.Phys.,30,1137 (1958).
9. A.Papineau, Compt.rend, 242, 2933 (1956).

RANGE AND SPECIFIC IONIZATION OF MULTICHARGED IONS

- Ya.A.Teplova, V.S.Nikolaev, I.S.Dmitriev & L.N.Fateeva

In view of the relative scarcity of experimental data on the stopping of multicharged ions in matter we continued our measurements[1] of the range, specific ionization and equilibrium ion charge distribution in a wider range of nuclear charges. In the present measurements, in addition to ions with $Z \leqslant 10$, we worked with Na^{23}, Mg^{25}, Al^{27}, P^{31}, Cl^{37}, A^{40}, K^{39}, Br^{81} and Kr^{84} ions. Some of the experimental results are given below.

Measurements procedure

The ion source was a 72-cm cyclotron capable of yielding ions with velocities from 2.5 to $12 \cdot 10^8$ cm/sec, which corresponds to energies from 25 to 600 kev per nucleon. The focused ion beam, after passing through a ~40 $\mu g/cm^2$ thick celluloid window, entered the "stopping" chamber which was filled with air to the desired pressure. The particles were detected by two proportional counters: the entire beam traversed the first (monitor) counter; the second counter could be moved along the beam path in the chamber and thus allowed of measuring the number of particles at different distances from the entry window. By way of illustration, typical experimental curves are reproduced in Fig.1. From such curves we determined the mean and extrapolated ranges. The difference between the two ranges corresponds to the range straggling. The uncertainty in the range measurements at ion velocities of $(4.0\text{-}12) \cdot 10^8$ cm/sec varied from 2 to 3%. The range straggling varied for different ions from 3 to 9%.

The pulse heights in the second proportional counter gave the specific ionization (in relative units). As in the work of Ref.1, we evaluated the ion range from the point of intersection of the specific ionization curve with the horizontal axis. We term the range determined in this manner the maximum range; the maximum ranges proved to be 3-5% higher than the extrapolated ranges.

In order to investigate the slowing down of ions in solids, films of known thickness without backing were mounted in the path of the beam. Specifically, we

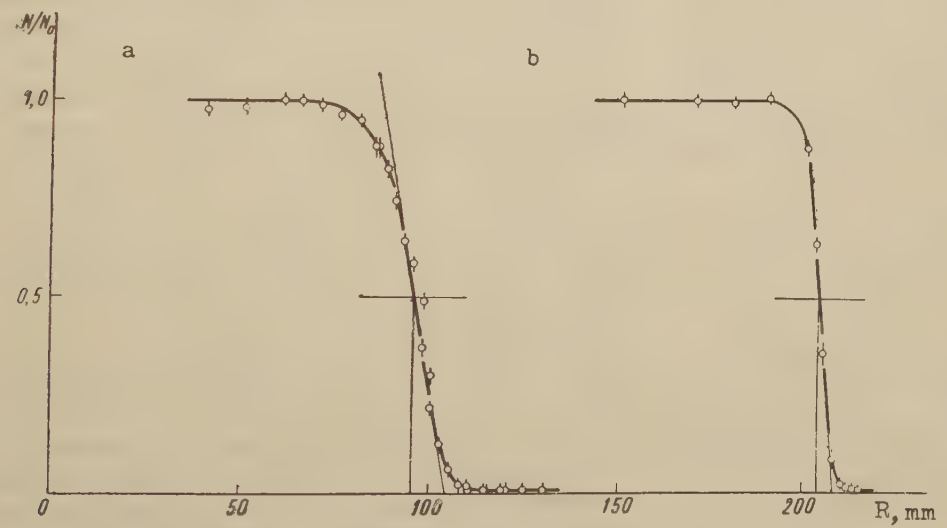

Fig.1. Variation in the relative number N/N_0 of particles as a function of the distance from the entrance window of the "stopping" chamber: a) for P^{31} ions (air pressure 26.8 mm Hg, t = 19°), b) for He ions (p = 141 mm Hg, t = 19°).

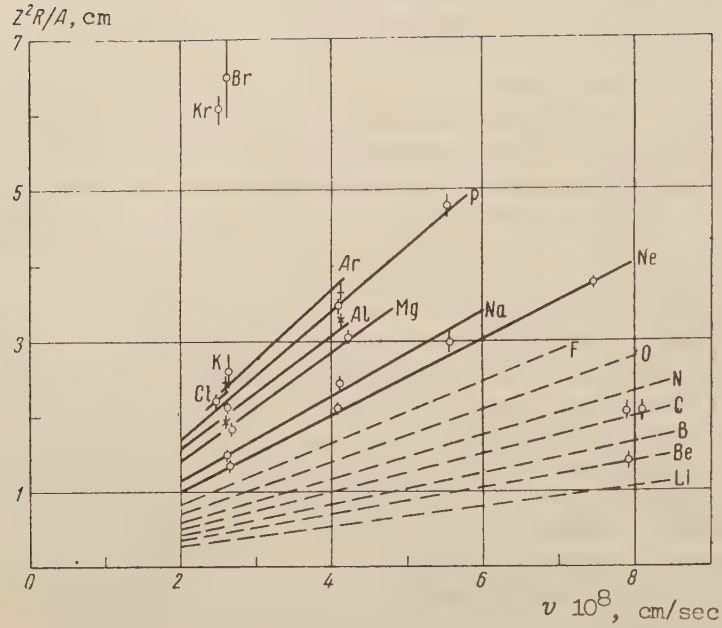

Fig.2. Variation of ion range in air with the velocity at p = 760 mm Hg, t = 19°. The dashed lines represent the results of Ref.1.

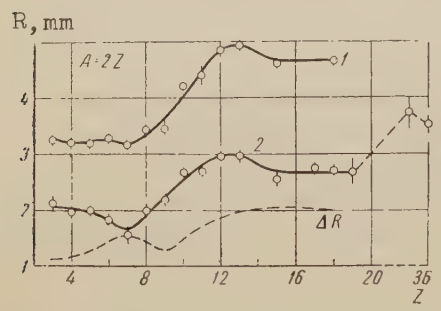

Fig.3. Variation of the ion range in air with Z at 760 mm Hg & t = 19°: 1) v = = $4.1 \cdot 10^8$ cm/sec, 2) $2.6 \cdot 10^8$ cm/sec.

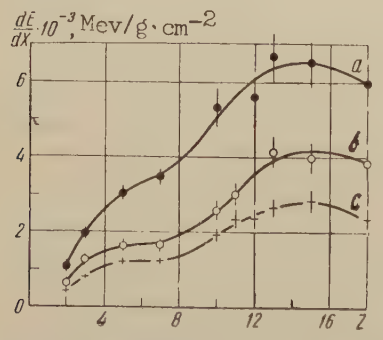

Fig.4. Variation of the specific energy loss dE/dx with Z in a) celluloid, b) Al and c) Ag for $v = 3.5 \cdot 10^8$ cm/sec.

used films of celluloid, aluminum and silver ranging from 50 to 300 μg/cm^2 in thickness. From the range difference with and without the films we determined the air equivalent of the films for the given ion velocity. The ratios of air equivalents for different ions were determined with an accuracy from 7 to 10%; the absolute equivalents with an accuracy of 10-15%.

The equilibrium ion charge distribution and the mean charge were measured by the procedure described earlier[2,3]. The ion velocities were determined on the basis of the focusing magnet field strength to within 1-2%.[1]

Discussion

The measurements showed that for ions with $Z > 10$, having velocities less than $5 \cdot 10^8$ cm/sec, the specific ionization in air is approximately (within ±10%) proportional to the residual range. This was to be expected inasmuch as according to the results of Ref.1, the maximum of the specific ionization for lighter ions (Li^7, B^{11} & N^{14}) is attained at velocities of $(6-8) \cdot 10^8$ cm/sec. Accordingly, the range of ions with velocities $\leqslant 6 \cdot 10^8$ cm/sec should be approximately proportional to the velocity. The results of measurement of the maximum ion range in air are shown in Fig.2. It will be seen that the experimental points deviate from straight lines drawn through the origin by not over 5%.

It is of interest to examine the Z-dependence of the ranges of different ions with equal initial velocities (Fig.3). The measurements show that the range R changes relatively little with increase of Z from 3 to 36: for example for $v = 2.6 \cdot 10^8$ cm/sec the range of Kr^{84} ions is approximately twice the range of N^{14} ions. However, the Z-dependence of R is not monotonic but is characterized by appreciable fluctuations (~30%). This is also true of the Z-dependence of the range difference ΔR for the given velocity difference (dashed lines in Fig.3). Inasmuch as this quantity is inversely proportional to the specific energy loss, the Z-dependence of $\frac{dE}{dx}$ should also be characterized by similar fluctuations. Unfortunately, the accuracy of measuring

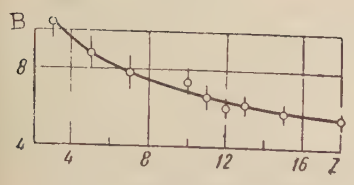

Fig.5. Z-dependence of the stopping power B of air for $v = 3.5 \cdot 10^8$ cm/sec.

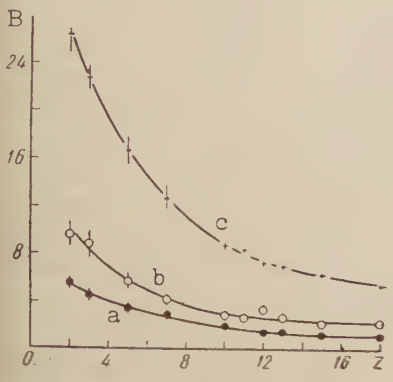

Fig.6. Variation of B with Z in a) celluloid, b) Al, and c) Ag for $v = 3.5 \cdot 10^8$ cm/sec.

ΔR was not high, hence the observed regularities can be regarded as only approximate.

On the basis of the experimental data of the air equivalents of the solid films, we calculated the specific energy losses in these solids. As will be evident from Fig.4, in general the specific energy loss increases with increase of Z, although the variation is not uniform over the entire range of values.

A similar Z-dependence is observed for the experimental values of the mean square ion charge for the same velocities and is explained by the characteristics of the electron structure of the ions. Hence the product $\frac{1}{\bar{i}^2} \cdot \frac{dE}{dx}$ is a monotonic function of Z. From the experimental values of $\frac{dE}{dx}$ and $\bar{i}^2$, we calculated the stopping power of the film materials as

$$B = \frac{dE}{dx} \Big/ \frac{4\pi e^4 \bar{i}^2}{mv^2} N,$$

where v is the ion velocity, e is the charge and m is the mass of an electron, and N is the number of atoms per cm^3 of the material. The results are shown in Figs.5 & 6.

The experimental values of the stopping power of air for ions with Z from 3 to 18 substantiate the Z-dependence of B observed earlier for ions with $Z \leqslant 10$. The decrease of B with increase of Z, as was pointed out in Ref.1, is consistent with the Bloch formula for specific energy loss.

Inasmuch as the difference between the mean ion charge in gases and solids increases rapidly with increase of Z, the Z-dependence of B in solids is much stronger than in air. The stopping power of air for A^{40} ions with $v = 3.5 \cdot 10^8$ cm/sec is about half that for Li^7 ions, whereas the stopping powers of solids for the same ions differ by a factor of 4-5.

Some authors[4-6] neglect the Z-dependence of the stopping power in calculating the specific energy loss of multicharged ions. It will be evident from the above cited data that such disregard of the Z-dependence of the stopping power can lead to appreciable errors.

Scientific Research Institute for Nuclear Physics,
Moscow State University

References

1. Ya.A.Teplova, V.S.Nikolaev, I.S.Dmitriev & L.N.Fateeva, Zhur.eksp.i teor. fiz., 34, 559 (1958). (Trans.Soviet Physics - JETP.)

2. V.S.Nikolaev, L.N.Fateeva, I.S.Dmitriev & Ya.A.Teplova, Ibid., 32, 965 (1957). (Trans.Ibid.)

3. V.S.Nikolaev, I.S.Dmitriev, L.N.Fateeva & Ya.A.Teplova, Ibid., 33, 1325 (1957). (Trans.Ibid.)

4. J.P.Longchamp, J.phys.et radium, 14, 89 (1953).

5. D.L.Livesey, Can.J.Phys., 34, 203 (1956).

6. I.S.Dmitriev, Zhur.eksp.i teor.fiz., 32, 570 (1957). (Trans.Soviet Phys. JETP.)

CASCADE GAMMA-TRANSITIONS IN Cl^{36} AND S^{33}, ACCOMPANYING THERMAL NEUTRON CAPTURE

- V.R.Burmistrov

1. Experimental procedure

We investigated the two-stage transitions in Cl^{36} and S^{33}, accompanying thermal neutron capture, by the "addition upon coincidence" method described by Hoogenboom[1]. In the case of S^{33} we also carried out measurements by the conventional γ-γ coincidence method with energy analysis of the coinciding radiations.

The experimental arrangement is diagramed in Fig.1.

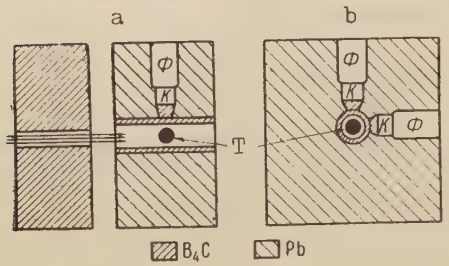

Fig.1. Experimental arrangement: a) vertical section in line with neutron beam; b) vertical section perpendicular to neutron beam. K - crystals, ϕ - photomultipliers, T - target.

The neutron beam from the pile of the first atomic power station[2], after collimation, irradiated the target T (Fig.1), mounted between the two scintillation counters. The neutrons scattered in the target were absorbed by a layer of B_4C. The counters were lead shielded and mounted at right angles to each other in order to minimize the number of spurious coincidences owing to detection by one crystal of γ-rays scattered in the other. Such spurious cross detection was not fully suppressed, however, for energies exceeding 0.51 Mev, which led to the appearance in the coincidence spectra of apparatus peaks associated with pair formation in the crystals.

The scintillation spectrometer was equipped with 40 x 40 mm NaI(Tl) crystals and had a resolution of 12% at a γ-ray energy of ~1 Mev. We employed a fast-slow coincidence system with a resolving time of $8 \cdot 10^{-8}$ sec. The uncertainty in determining energy was estimated to be 3%. The background of chance coincidences when using the "addition upon coincidence" technique did not exceed 5%, and hence was disregarded. The contribution from epicadmium neutrons did not exceed 10% and was also not taken into account.

A more detailed description of the equipment and experimental technique will be found in Refs.3 & 4.

2. Measurement results

Chlorine

The coincidence spectrum associated with Cl^{36} neutron capture γ-radiation has been investigated previously by Recksiedler & Hammermesh[5] and Trumpy[6], who obtained preliminary evidence for the existence of 7.78-0.79, 7.42-1.16, 6.98-1.60 and 6.62-1.95 Mev cascades; Recksiedler & Hamermesh also detected the new line of 0.735 Mev energy.

In our experiments the sample consisted of chemically pure $PbCl_2$ contained in a paper cup 5 mm in diameter and 5 mm high. The gate of the controlling channel was set at the neutron binding energy in Cl^{36}(8.58 Mev). The contribution from neutron capture in Cl^{37} was completely excluded by this setting of the control channel, inasmuch as the neutron binding energy in Cl^{38} is 6.1 Mev.

The capture γ-ray spectrum recorded by the coincidence method is shown in Fig.2. The spectrum was recorded in two stages with different amplification factors in the analyzed channel. The vertical scale is laid off in terms of the number of pulses in a 20 kev wide channel normalized to a constant integral number of pulses in the control channel. The two sections are joined in the 1.5-2.0

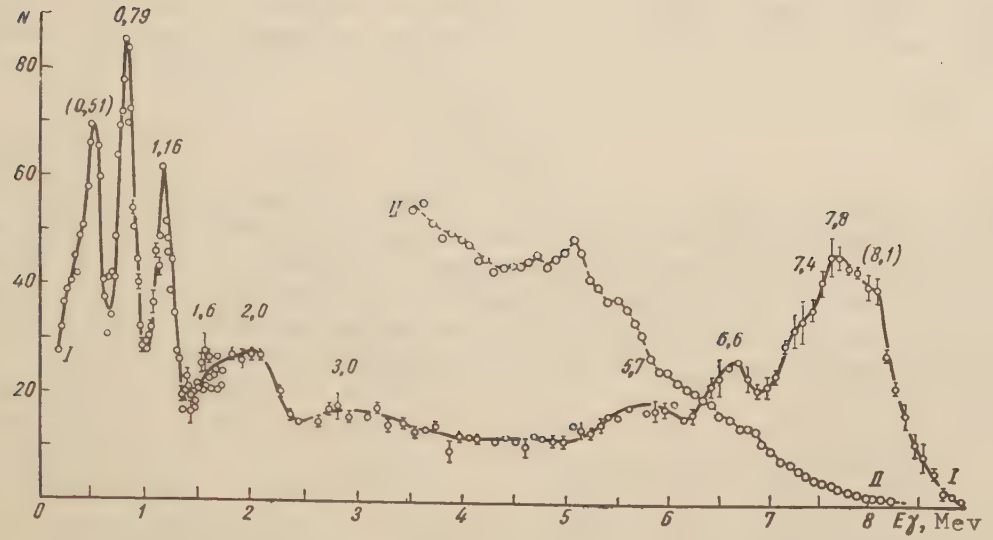

Fig.2. Chlorine capture γ-ray spectrum recorded by the method of addition upon coincidence (I) and without coincidences (II).

Mev region. The uncertainties indicated at some of the points are root mean square errors. The final identification of the peaks as regards energy was carried out by comparison of our data with the results of Groshev et al[7]. The dashed line (II) in Fig.2 is the thermal neutron capture spectrum of Cl obtained with a single spectrometer (without coincidences) plotted to an arbitrary scale.

The extreme peaks at 8.1 and 0.51 Mev are apparatus peaks associated with pair formation in the spectrometer crystals by the ~8.6 Mev γ-radiation. They appear when one of the annihilation quanta leaves the crystal in which the pair is formed and is detected by the other crystal.

The peaks at 7.8 and 0.79 Mev correspond to a 7.8-0.79 Mev cascade transition through the 0.79 Mev level.

The 7.41 and 1.16 Mev peaks correspond to a cascade through the 1.16 Mev level.

The indistinctly evinced peak at 1.6 Mev should be complemented by a peak at ~7.0 Mev; the latter, however, is not resolved from the neighboring γ-rays.

The comparatively sharp peaks at 6.6 ± 0.1 and 2.0 ± 0.05 Mev form a pair corresponding to a 6.6-0.95 Mev cascade through the 1.95 Mev level.

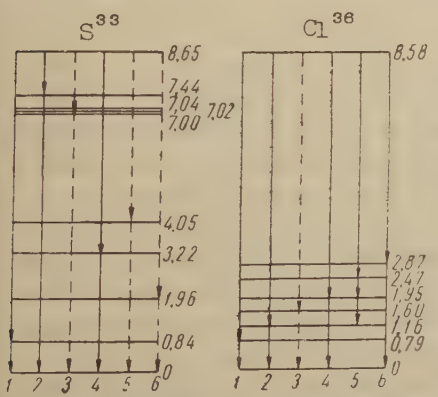

Fig.3. Diagram of two-stage transitions in S^{33} and Cl^{36}.

The peak at 5.7 ± 0.1 Mev corresponds to a 5.7 Mev γ-ray; the peak at 3.0 ± 0.1 Mev to one of three γ-rays: 3.08, 3.02 or 2.88 Mev. In view of the fairly high certainty in identifying the first peak, the energy of the second peak may be assumed to be 2.88 Mev. This pair of peaks corresponds to a 5.72-2.88 Mev cascade through the 2.87 Mev level.

The level scheme for Cl^{36}, following from the coincidence measurements, is given at the right in Fig.3. By the method of "addition upon coincidence" we identified the following cascades: 1) 7.79-0.79, 2) 7.42-1.16, 3) 6.97-1.60, 4) 6.64-1.95, and 6) 5.72-2.88 Mev. All these cascades were also detected by the conventional coincidence technique[3]; in addition, there was found the cascade 5) 6.11-0.51--0.79 Mev (the cascade numbers above correspond to

the numbers given in the diagram). In both cases the 6.97-1.60 Mev cascade was not clearly evinced, which is presumably due to its low intensity. The deduced decay scheme substantiates the transition scheme proposed for the above mentioned cascades by Groshev et al[7].

Sulfur

The sample was a cylinder of chemically pure, fused sulfur weighing 0.8 g, contained in a paper cup (without top or bottom). In the measurements by the "addition upon coincidence" method the control channel was set at 8.65 Mev (the neutron binding energy in S^{33}). The contribution from neutron capture in S^{34} was excluded inasmuch as the neutron binding energy in S^{35} is 6.99 Mev. The contribution from neutron absorption in S^{33} is negligibly small.

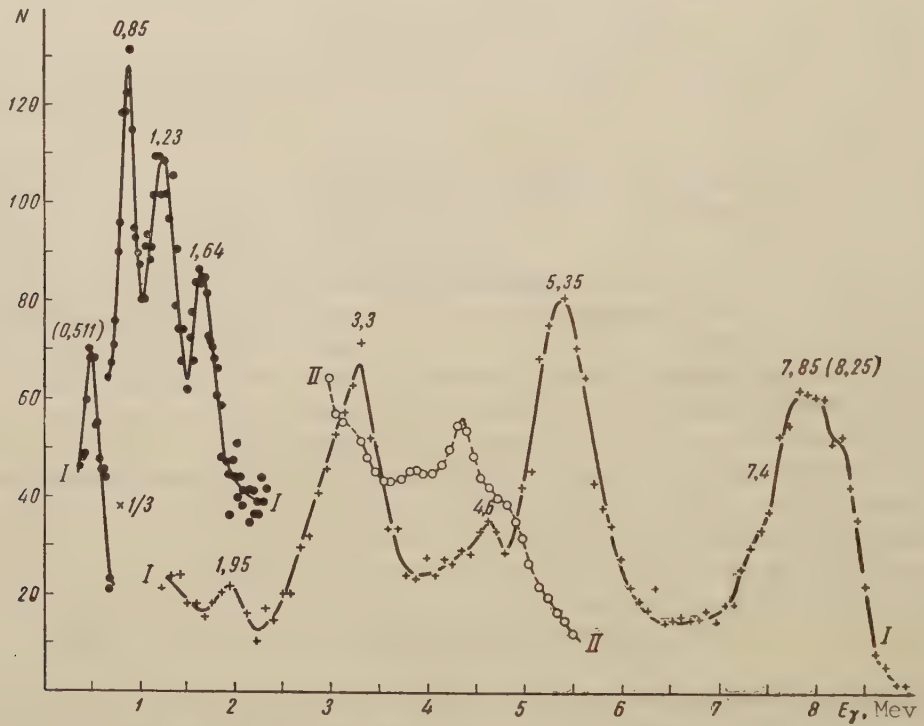

Fig.4. Sulfur capture γ-ray spectrum obtained by the method of addition upon coincidence (I) and without coincidences (II).

The experimental spectrum is shown in Fig.4. The spectrum was again recorded in two stages: the soft section from 0.4 to 2.0 Mev was recorded with a control gate width $\Delta = 6.1\%$; the hard section from ~1.6 to 9.0 Mev with $\Delta = 3.0\%$. The measurement results are normalized to a 20 kev channel width and the same integral number of pulses in the control channel. Owing to the use of different control gate widths (because of different coincidence counting rates) the two sections do not join in the intensity scale. This is immaterial where the immediate results are concerned inasmuch as we are not drawing any inferences here regarding the relative intensities of the transition cascades. The singles spectrum plotted to an arbitrary scale is shown by the dashed line (II).

The extreme peaks at 8.2 and 0.51 Mev are apparatus peaks.

The peaks at 7.85 ± 0.2 and 0.85 ± 0.02 Mev correspond to a 7.80-0.84 Mev cascade transition through the 0.841 Mev level.

The peak at 1.23 ± 0.05 Mev and the step in the 7.40 ± 0.1 Mev region correspond to a 1.21-7.42 Mev cascade through the 7.44 Mev level. A transition from this level to the ground state was hypothesized earlier by Groshev et al[7], but no 1.23 Mev line was detected. The clear manifestation of the 1.23 Mev peak and the undoubted existence of 7.4 γ-rays in the coincidence spectrum are strong evidence in favor of this cascade.

The peak at 1.64 ± 0.05 Mev should be complemented by a peak with energy 8.65 - (1.64 ± 0.05) = 7.01 ± 0.05 Mev. However, the latter peak is not evinced in the spectrum, possibly due to the inadequate resolving power of the equipment and the low intensity of the corresponding γ-rays. It must be noted that no line of this energy was observed in measurements with magnetic spectrometers. But in view of the specific characteristics of the given measurement procedure (single peaks cannot be evinced in the coincidence spectrum), its presence in the γ-spectrum is nevertheless possible. The 1.64 ± 0.05 Mev γ-rays should be regarded as part of a two-stage transition going through one of the following S^{33} levels: 7.04, 7.02 or 7.00 Mev (these level energies are taken from the work of Groshev et al[7].)

The next peak, i.e., the peak at 1.95 ± 0.05 Mev, is visible only in the lower curve and is not evinced in the upper curve owing to inadequate statistical accuracy of the corresponding measurements. This peak should be complemented by a peak at ~6.6 Mev, but the latter was not observed. Hence we classify the corresponding cascade as uncertain.

The clear peaks at 3.3 ± 0.1 and 5.25 ± 0.15 Mev correspond to the most intense 5.44-3.22 Mev cascade which goes through the 3.22 Mev level.

There should be a peak at 4.05 Mev complementing the 4.6 ± 0.1 Mev peak, but it is apparently masked by the 3.25 Mev peak.

Groshev et al[7] inferred the existence of a 4.58-3.21-0.841 Mev cascade. It follows from our measurements that there is a 4.58-4.05 Mev cascade passing through the known 4.049 Mev level. The existence of this cascade, however, is not reliably proved. Measurements by the conventional coincidence technique bring out only two cascades clearly, namely, 7.8-0.84 and 1.21-7.42 Mev. The intensity ratio of these cascades is consistent with the intensities proposed by Groshev et al.

The transition diagram for S^{33} is shown on the left in Fig.3. The certain cascades 1) 7.8-0.84, 2) (1.20)-7.42, 3) (1.64)-(7.02), and 4) 5.44-3.21 Mev (the γ-rays given in parentheses above were not observed in the magnetic spectrometer measurements of Groshev et al) are indicated by solid line arrows; the somewhat doubtful cascades 5) 4.58-4.05 and 6) 6.62-2.00 Mev are indicated by dash line arrows. In the main the given decay scheme agrees with that proposed in the work of Groshev et al[7].

I take this opportunity to thank A.K.Krasin for his interest in the work and V.P.Radchenko for assistance in carrying out the measurements.

References

1. A.M.Hoogenboom, Nucl.Instr., 3, 57 (1958).
2. D.I.Blokhintsev, N.A.Dollezhal' & A.K.Krasin, Atomnaya energiya No.1, 10 (1956). (Trans.Journal of Atomic Energy).
3. V.R.Burmistrov, Ibid., No.9 (1959).
4. V.R.Burmistrov, Present issue of the Bulletin, p.890.
5. A.L.Recksiedler & B.Hamermesh, Phys.Rev., 96, 109 (1954).
6. G.Trumpy, On the Determination of Nuclear Spins by the Study of Neutron Capture Gamma Rays, Oslo, 1957.
7. L.V.Groshev, A.M.Demidov, V.N.Lutsenko & V.I.Pelekhov, Atlas spektrov γ-luchei radiatsionnogo zakhvata teplovykh neitronov (Atlas of γ-ray spectra emitted in radiative thermal neutron capture), M., 1958.

CASCADE GAMMA-TRANSITIONS IN Nd^{144}

- V.R.Burmistrov

The γ-transitions in Nd^{144}, daughter of Pr^{144}, have been the subject of many investigations[1-3], which led to a rather simple level scheme with two excited states. Firsov & Bashilov[4] recently introduced two additional levels at 2.8 and 1.7 Mev.

In the present work we carried out a further investigation of the decay scheme of Nd^{144} by the method of γ-γ coincidences.

1. Equipment and Procedure

For investigating the γ-transitions in Nd^{144} we used the conventional γ-γ coincidence procedure and the "addition upon coincidence" method[5], using two scintillation counters.

In the "addition upon coincidence" method the pulses in the two counters are fed simultaneously into a coincidence circuit and into a linear pulse adding circuit. If the pulses coincide in time and the sum of their energies equals the set value, i.e., corresponds to the energy of the nuclear level from which the transition cascade under investigation departs, the pulses from one of the counters are passed for analysis. This method allows of determining two-step transitions from the investigated nuclear level, inasmuch as for each given two-step transition there appear in the coincidence spectrum only two photopeaks without Compton or pair peaks, which obviously facilitates interpretation of the spectra.

A block diagram of the experimental arrangement is shown in Fig.1,a. The pulses are fed to the fast coincidence circuit through a 10 Mc passband amplifier. The gate of the differential discriminator is set on the pulse amplitude corresponding to the energy of the investigated nuclear level, and upon the arrival of a pulse from the fast coincidence circuit (the discriminator incorporates a slow coincidence circuit), the discriminator pulse opens the analyzer gate for analysis of the pulses from one of the counters.

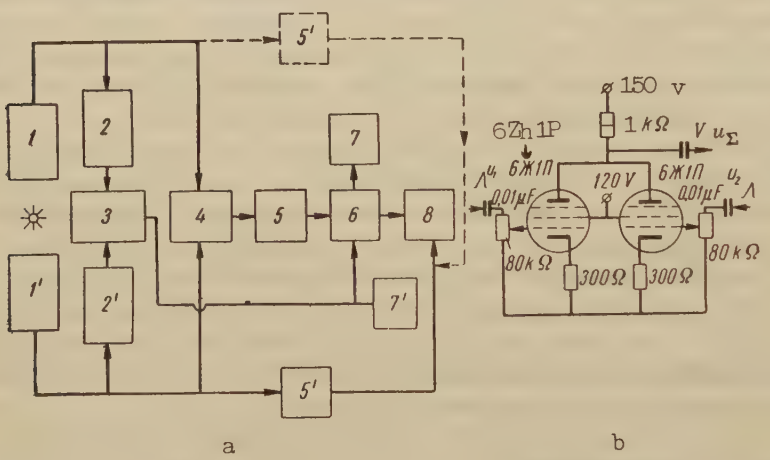

Fig.1. a - Block diagram of the experimental arrangement: 1 & 1') scintillation counters (NaI(Tl) photomultiplier and cathode follower), 2 & 2') wide band USh-10 amplifiers, 3) fast coincidence circuit, 4) pulse addition circuit, 5 & 5') linear amplifiers, 6) differential discriminator, 7 & 7') scalers, 8) pulse analyzer; b - pulse adding circuit.

The pulses from either of the two counters can be taken for analysis (another possible way of connecting the components is indicated by the dashed line in Fig. 1,a). Fig.1,b shows a diagram of our pulse adding circuit; it differs from the circuit described by Hoogenboom[5] in that it can handle higher pulse loads. Potentiometers in the grid circuits of the 6Zh1P (6Ж1П) tubes serve for fine adjustment of the energy calibration of both counters (the rough adjustment of the calibration is realized by varying the voltage on the photomultipliers).

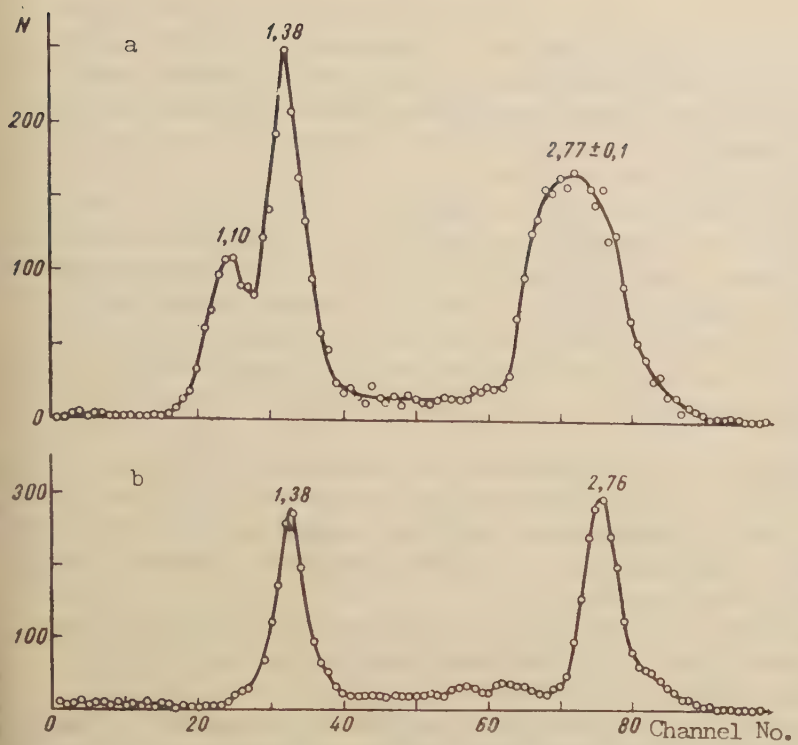

Fig.2. Effect of inaccurate setting of the differential discriminator gate. Source - Na^{24}. a - case of inaccurate gate setting, b - correct gate setting. The energy calibrations in the two cases are somewhat different.

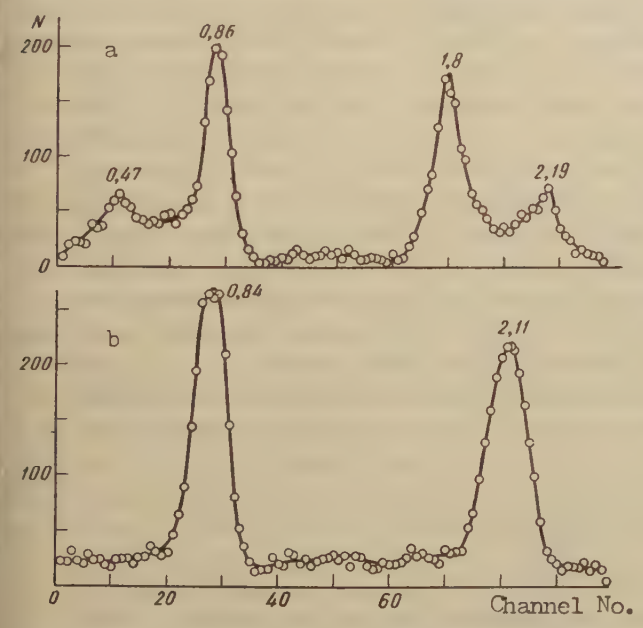

Fig.3. Influence of a higher lying level on the coincidence spectrum recorded by the method of "addition upon coincidence". Source - Mn^{56}.

The principle of the "addition upon coincidence" method has been fully described by Hoogenboom[5] and will not be detailed here. We must, however, say a few words regarding the accuracy of setting the discriminator gate on the investigated energy level, or what is practically the same thing, on the influence of higher lying energy levels. Inaccuracy of setting the gate of the analyzer of the summing channel of the discriminator on the investigated energy level leads to displacement of the coincidence spectrum peaks, i.e., to distortion of the spectrum.

Such inaccuracy in setting the gate leads either to the appearance of spurious peaks (if the center of the gate E_c is set so that $E_c < E_o$, where E_o is the energy of the investigated level) or simply to loss of coincidence counts (with $E_c > E_o$).

In our work no displacement of the peaks was observed within the limits of the accuracy of energy determination.

Fig.2,b shows the coincidence spectrum obtained with an Na^{24} source. It is known that Na^{24} has a 2.76-1.38 Mev cascade departing from the 4.12 Mev level.[1] In this case the center of the control gate was set at 4.12 Mev. In this figure (and in those below) N is the number of pulses recorded during the measurement period.

In the case of simultaneous detection of a 1.38 Mev quantum by, for example, the lower counter (Fig.1) and a 2.76 Mev quantum by the upper counter, the coincidence circuit is triggered. A pulse appears at the discriminator output only if the sum of the pulses from both counters equals E_c and this is possible only on condition of complete absorption of both the quanta in the respective crystals. In this case the analyzer receives a pulse corresponding to the 1.38 Mev photopeak. On the other

hand, if the lower counter receives and detects a 2.76 Mev quantum and the upper a 1.38 Mev quantum, the analyzer will be fed a pulse corresponding to the 2.76 Mev peak. Under the given conditions there can be no other combinations (provided, naturally, that there is no scattered γ-radiation from one crystal to the other). Thus, in the given case there will appear two photopeaks in the coincidence spectrum: one at 1.38 and the other at 2.76 Mev.

The spectrum in Fig.2,a illustrates the case of incorrect setting of the control gate, i.e., the case of setting the control gate at E_c = 3.9 Mev or somewhat below the energy of the 4.12 Mev level. As will be evident from the figure, the coincidence spectrum comprises the 1.38 and 2.76 Mev peaks (corresponding to the γ-rays that are actually in cascade) and in addition and next to these, peaks at 2.6 and 1.1 Mev, (in Fig.2,a the 2.6 and 2.76 Mev peaks are not resolved); it will be noted that the sums of the peak energies, i.e., 1.38 + 2.6 Mev and 7.6 + 1.1 Mev are equal to E_c.

The 1.38 and 2.6 Mev peaks appear in the spectrum in the case of complete absorption of the 1.38 Mev photon in one crystal and Compton scattering of the 2.76 Mev photon in the other, the scattering being such that the energy of the Compton electron $E_{re} = E_c$ - 1.38 Mev, i.e., the difference between the gate setting energy and energy of the completely absorbed photon.

Analogously, the peaks at 1.1 and 2.76 Mev are associated with complete absorption of a 2.76 Mev photon in one crystal and Compton scattering of a 1.38 Mev photon in the other so that $E_{re} = E_c$ - 2.76 Mev.

Fig.3 shows the coincidence spectra obtained with an Mn^{56} source and illustrates the influence of a higher lying level from which cascade transitions may occur. The lower curve represents the spectrum obtained when the gate of the control channel is set on the 3.02 Mev level[1]. In this case there are evident in the coincidence spectrum clear peaks at 2.11 and 0.84 Mev, corresponding to the two-step 2.13-0.845 Mev transition. These peaks are comprised in the continuous pulse distribution due to weak cascade transitions from higher lying levels.

The upper curve gives the coincidence spectrum with the control gate set at 2.60 Mev, the energy of the level from which the intense 1.81-0.845 Mev cascade departs. In this case there are clearly evident in the spectrum peaks at 1.80 ± ± 0.04 and 0.86 ± 0.02 Mev, corresponding to this cascade. In addition, there is evident in the spectrum a pair of peaks at 2.19 ± 0.04 and 0.47 ± 0.02 Mev, associated with a 2.13-0.84 Mev cascade from the 3.02 Mev level. For this level the E_c = 2.60 Mev setting is inaccurate ($E_c < 3.02$ Mev), and we have a case similar to that characterized by the curve of Fig.2,a, i.e., two pairs of peaks: 2.19 Mev (photopeak) - 0.47 (Compton) and 0.86 (photopeak - 1.79 (Compton), the sum of the corresponding peak pairs being equal to E_c. The pair of peaks associated with the 2.13-0.845 Mev cascade from the 3.02 Mev level is masked by the peaks corresponding to the 1.81-0.845 Mev cascade from the 2.6 Mev level.

In general, however, the origin of spurious peaks can easily be clarified by observing the changes in energies and intensities of the peaks with variation of the gate setting.

2. Experimental Results

The sample for investigating the levels of Nd^{144} was a Ce^{144}-Pr^{144}-Nd^{144} mixture stored for two years after separation of the U fission products. The source, having a superficial density of 0.5 g/cm^2, was enclosed in a steel container with a wall thickness of 0.2 mm. To prevent the appearance of bremsstrahlung due to penetration of the hard β-radiation into the lead shielding, the container was surrounded with a 10 mm thick layer of plastic.

The radiation was detected by 40 x 40 mm NaI(Tl) crystals in lead shielding, oriented at right angles to each other.

The spectra obtained by the method of addition upon coincidences are shown in Fig.4. Fig.4,b is the spectrum obtained with the 200 kev wide gate of the differential discriminator set on 2.87 Mev. In this spectrum there are clearly evident peaks at 0.70 ± 0.01 and 2.19 ± 0.01 Mev; these correspond to a 0.69--2.18 Mev cascade from the 2.87 Mev level.

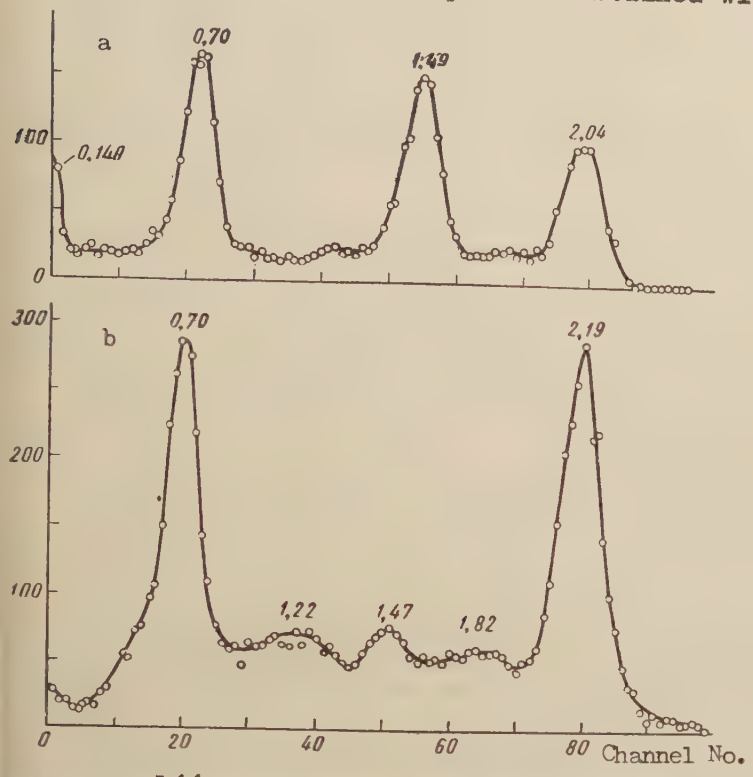

Fig.4. Nd^{144} coincidence spectra obtained by the addition upon coincidence method: a) cascades from the 2.18 Mev level, b) from the 2.87 Mev level.

At the center of the spectrum there is a peak at 1.47 ± ± 0.03 Mev. Actually, the average energy value of this peak, on the basis of five series of measurements, is 1.44 ± 0.02 Mev. In view of the fact that a single peak cannot appear in the coincidence spectrum, it must be assumed that this peak corresponds to a (1.44 ± 0.02)-(1.44 ± 0.02) Mev cascade.

To the right and left of the central peaks are diffuse peaks with energies 1.22 ± 0.05 and 1.82 ± 0.05 Mev. The average values based on four runs are (1.18 ± 0.02) and (1.79 ± 0.03) Mev; these peaks correspond to a cascade of γ-transitions with these energies. The order of emission of these γ-rays will be considered below.

There is no difficulty about determining the area under the clear 0.70 and 2.19 Mev peaks; the matter is somewhat more difficult when it comes to the lower peaks. These intermediate peaks sit on a plateau. In the spectrum of Fig.2,b the area of the plateau between the extreme peaks amounts to 17% of the total area. In the spectrum of Fig.3,b (assuming that the plateau to the sides of the peaks represent the contribution from higher lying levels), the plateau area amounts to ~5%. The last case is most similar as regards energy to that under consideration, hence we assumed that the area of the plateau between the peaks, due to contributions from the 0.70 and 2.19 Mev peaks, equals 5%. Further, using the efficiency formula deduced by Hoogenboom[5] and the experimentally determined photocontribution, we found the intensity ratio of the cascades. The evaluated relative intensities of the cascades and the areas under the peaks corresponding to them (Fig.4,b) are listed in the table.

Cascade	Area under peak pair, %	Cascade intensity
0.69 ± 2.18	67	1
1.44 ± 1.44	8	0.4
1.2 ± 1.8	25	0.98

Fig.4,a shows the spectrum obtained with the control channel gate set on the 2.18 Mev level, the gate width being 96 kev. The two clear peaks at 1.49 ± 0.01 and 0.70 ± 0.01 Mev correspond to the well known 1.48-0.69 Mev cascade.

The clear 2.04 ± 0.02 Mev peak and the

complementary 0.140 Mev peak (only the right-hand part of which appears in the figure) are due to the 2.18-0.69 Mev cascade from the higher lying 2.87 Mev level. This case differs somewhat from that illustrated in Fig.3,a, inasmuch as in this case the energy of one of the γ-rays of the cascade, namely, the 2.18 Mev γ-ray, is equal to the setting of the control channel gate. Hence the spurious peaks associated with the cascades from the higher lying level are evinced here in the following, somewhat different manner.

The 2.18-0.69 Mev cascade yields the peaks: 2.04 (Compton peak from the 2.18 Mev gammas) - 0.14 (Compton peak from 0.69 Mev) and 0.69 (photopeak) - 1.48 (Compton peak from 2.18 Mev); the last pair of peaks is superposed on the principal peaks.

The 1.44-1.44 Mev cascade yields peaks which are superposed on the peaks of the effect.

The 1.2-1.8 Mev cascade yields the following peaks: 1.8 (photopeak from 1.8 Mev) - 0.38 (Compton from 1.2 Mev) and 1.2 (photopeak from 1.2 Mev) - 1.0 (Compton peak from 1.8 Mev). The 1.8 Mev peak is evinced as a slight rise between the 1.49 and 2.04 Mev peaks, while the 1.2 and 1.0 Mev peaks are manifested by the slight rise between the 0.69 and 1.49 Mev peaks.

Fig.5 shows the results of measurements by the conventional coincidence method. The reproduced curve is the spectrum of coincidences with the 0.690 Mev γ-rays. The background of chance coincidences (equal to 30% of the true coincidences at ~2.18 Mev, 4% at 1.48 Mev and 20% at 0.69 Mev) and the contribution from the Compton distribution on which the 0.690 Mev photopeak sits have been subtracted. Of the entire area defined by the control channel the Compton pedestal accounted for ~20%, while the spectrum coinciding only with the γ-rays that form this pedestal was determined by measurement of the coincidences when the control channel was set on a region where there is no contribution from the 0.690 Mev γ-rays.

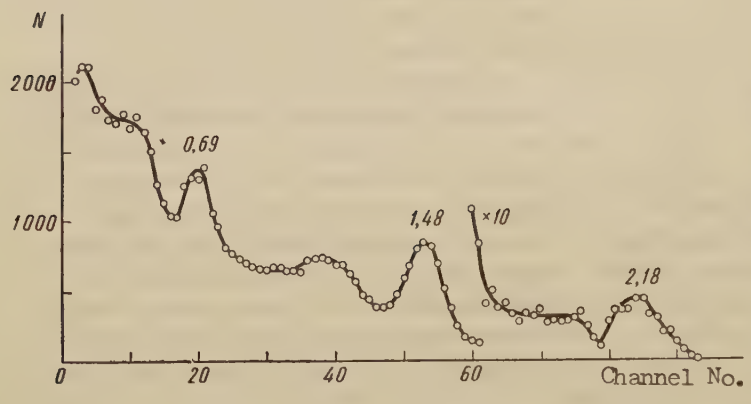

Fig.5. Spectrum of coincidences with the 0.69 Mev γ-rays of Nd^{144} recorded by the conventional coincidence method.

As will be evident from Fig.5, γ-rays with energies 1.48, 2.18 and 0.69 Mev yield coincidences with the 0.690 Mev γ-rays. Coincidences of the last two γ-rays with the 0.690 Mev γ-rays have not been reported hitherto. From the areas under the photopeaks (taking into account the photocontribution), we found that the relative intensities of the coincidences of the 0.69, 1.48 and 2.18 Mev γ-rays with the 0.690 Mev rays are 1.2 ± 0.2, 17.2 ± 2.5, and 1, respectively. We note that the determination of the photocontributions and the relative γ-line intensities were based on the average ratios of the 0.690, 1.48 and 2.18 Mev γ-line intensities equal to $1:(0.18 \pm 0.01):(0.494 \pm 0.002)$, respectively. The relative intensities of these γ-lines were taken from Refs.3 and 6.

It follows from the results obtained by the addition upon coincidence method that there must obtain coincidences between γ-rays having the following energies: 1.2 & 1.8 Mev and 1.4 & 1.4 Mev. However, no clear indication of these cascades was obtained in investigating coincidences with γ-rays in the energy region from 0.8 to 2.4 Mev. Firsov & Bashilov[4], using a single crystal spectrometer, detected a 2.87 Mev γ-line; our equipment did not resolve this peak. We

evaluated the intensity of this line as $\leqslant 0.001$ the intensity of the 2.18 Mev γ-line.

3. Level and Transition Scheme

The level and transition scheme most consistent with the experimental results is shown in Fig.6. No account was taken of possible β-transitions in constructing this scheme.

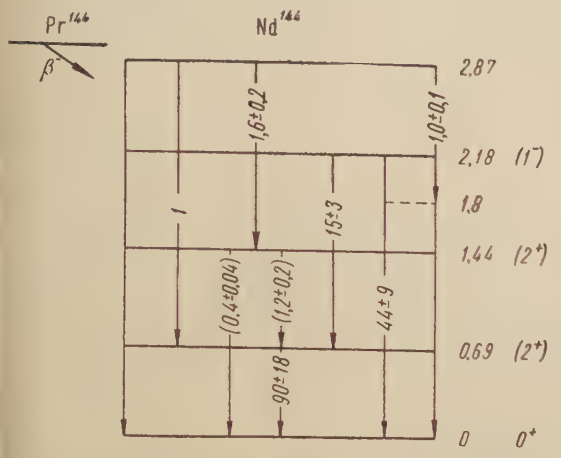

Fig.6. Proposed level and transition scheme for Nd^{144}.

The 2.87 Mev level was first introduced by Firsov & Bashilov as a result of observation of 2.87 Mev γ-rays and a 1.1-1.7 Mev cascade. It will be apparent from the spectrum of Fig.4,b that a 1.2-1.8 Mev cascade actually does exist; but, in addition, deexcitation of the 2.87 Mev level also proceeds by means of two other cascades, namely, 1.44-1.44 Mev and 2.18-0.69 Mev, which were detected for the first time in the present investigation.

The 1.44-1.44 Mev cascade indicates the existence of a level at 1.44 ± 0.02 Mev. As regards energy, this level is consistent with two-phonon nuclear excitation[7]. It is also consistent with the intensity ratio of the transitions from this level to the first excited level and to the ground state of the nucleus. If we accept that the 1.44 Mev level is the second level and is due to quadrupole vibrations relative to the equilibrium spherical shape, the possible assignments for it are 0, 2 or 4+. The 0+ assignment is excluded by the fact that if this assignment obtained, γ-transitions from this level to the ground state would be forbidden. Of the other two possibilities, one must give preference to 2+ by analogy with other even-even nuclei with an octupole vibrational spectrum.

We interpret the 2.18-0.69 Mev cascade as a two-step transition through the 0.69 Mev level. An inverse order cascade through the 2.18 Mev level or the occurrence of both cascades would be in conflict with the intensity ratio for the 1.48 and 2.18 Mev γ-rays obtained by Graham et al[3] and Kreger & Cook[6].

In principle, the 1.2-1.8 Mev cascade could go either through a 1.8 Mev or a 1.2 Mev level. Firsov & Bashilov gave preference to the 1.8 Mev (more accurately 1.74 Mev) level, since earlier[8] there was detected a β-transition with an endpoint energy of 1.3 Mev. We note that this transition was not identified with certainty, hence the inferences of Cheng, John & Kurbatov[8] are open to question. In view of its doubtful character, we have indicated this level by a dashed line in Fig.6.

We have taken the energy of the highest lying level as 2.87 Mev inasmuch as there have been observed γ-rays of this energy[4] presumably associated with a cross-over transition to the ground state. Furthermore, the clearly evinced 2.18-0.69 Mev cascade indicates an energy value of 2.87 ± 0.02 Mev for this level.

The spectrum shown in Fig.4,a substantiates the existence of a level at 2.18 Mev and of the well known 1.48-0.69 Mev cascade.

In the vertical transition lines we have indicated the relative intensities of the respective γ-transitions. We have enclosed in parentheses the intensity values that would increase (uniformly) if there is a β-transition to the 1.44 Mev level.

The spin and parity of the 1.44 Mev level are assumed to be 2+. The spins of the 2.18 and 0.69 Mev levels were determined from the angular correlation of the 1.46 and 0.69 Mev γ-rays in a number of investigations[1,3], but in none of these was the influence of the 2.18 Mev γ-rays taken into account. If we accept the proposed level and transition scheme, we note that the new cascades introduce a considerable contribution (not less than 16%) which must be taken into account in investigating the angular correlation of the 1.48 and 0.69 Mev γ-rays from the 2.18 Mev level. This admixture of new cascades may significantly alter the assignments for the 2.18 and 0.69 Mev levels. For this reason we have given the spins for these levels in parentheses, indicating that they are in need of further verification. The assignment for the 1.44 Mev level is also given in parentheses inasmuch as it still requires experimental determination.

References

1. B.S.Dzhelepov & L.K.Peker, Skhemy raspada radioaktivnykh yader (Decay schemes of radioactive nuclei), M.-L., 1958.

2. R.Hickok, W.A.McKinley & S.C.Fultz, Phys.Rev., 109, 113 (1958).

3. R.L.Graham, J.S.Geiger & T.A.Eastwood, Canad.J.Phys., 36, 1084 (1958).

4. E.I.Firsov & A.A.Bashilov, Izv.AN SSSR, Ser.fiz., 21, 1633 (1957). (Trans.Bulletin 21, No.12, 1619.)

5. A.M.Hoogenboom, Nucl.Instr., 3, 57 (1958).

6. W.Kreger & C.Cook, Phys.Rev., 96, 855, 1276 (1954).

7. G.Scharff-Goldhaber, Phys.Rev., 90, 587 (1953); G.Scharff-Goldhaber & J.Weneser, Phys.Rev., 98, 212 (1955).

8. L.Cheng, G.John & J.Kurbatov, Phys.Rev., 85, 487 (1952).

CONTRIBUTION TO THE THEORY OF SUPERFLUIDITY OF NUCLEON GAS

- Yu.V.Tsekhmistrenko

We consider a system of interacting neutrons and protons. We assume that the forces acting between the nucleons are central and that the number of protons differs from the number of neutrons. Under these assumptions the system is described by the Hamiltonian[1]:

$$H = \sum_{ks}\left[E(k) - \lambda_+\left(\frac{1}{2}+\tau\right) - \lambda_-\left(\frac{1}{2}-\tau\right)\right]\overset{+}{a}_{ks}a_{ks} - \frac{1}{2V}\sum_{kk's_2s_1s_2's_1'} I_{s_2s_1|s_2's_1'}(k,\ k')\,\overset{+}{a}_{ks_1}\overset{+}{a}_{-ks_2}a_{-k's_2'}a_{k's_1'}, \quad (1)$$

where

$$\lambda_+ - \lambda_- \neq 0. \quad (2)$$

Here $s = (\sigma,\ \tau)$; $\sigma = \pm\frac{1}{2}$ describes the z-component of the ordinary spin and $\tau = \pm\frac{1}{2}$ the z-component of the isotopic spin. In the usual case of central forces, we can write $I_{s_1s_2|s_2's_1'}(k,\ k') = I^{*}_{s_1s_2|s_2's_1'}(k,\ k')$ in the form

$$I_{s_1s_2|s_2's_1'}(k,\ k') = j_{s_1s_2}(k,\ k')\,\delta_{s_1s_1'}\delta_{s_2s_2'} + j_{s_1s_2|s_2's_1'}(k,k')\,\delta_{s_1+s_2,\,0}\delta_{s_1'+s_2',\,0}; \quad (3)$$

$$j_{s_1s_2} = j_{s_2s_1};\ j_{s_1s_2|s_2's_1'} = j_{s_2's_1'|s_2s_1} = j_{s_2s_1|s_1's_2'};\ j_{s_1s_2|s_2's_1'} = j_{s_1s_2|s_2s_1'} = 0.$$

We choose Bogolyubov's well-known canonical transformation in such a way as to leave the total momentum operator diagonal:

$$a_{ks} = \sum_{s'}(u_{kss'}\alpha_{ks'} + v_{kss'}\overset{+}{\alpha}_{-ks'});$$

$$u_{kss'} = \overset{*}{u}_{kss'};\quad v_{kss'} = \overset{*}{v}_{kss'}. \quad (4)$$

The unitarity of the transformation is assured by the conditions

$$\sum_{s'}(u_{kss'}u_{ks_1s'} + v_{kss'}v_{ks_1s'}) = \delta_{ss_1};$$

$$\sum_{s'}(u_{kss'}v_{ks_1s'} + u_{ks_1s'}v_{kss'}) = 0. \quad (5)$$

We introduce the "distribution functions"

$$F_{kss_1} = \sum_{s'} v_{kss'}v_{ks_1s'}$$

and

$$\Phi_{kss_1} = \sum_{s'} u_{kss'}v_{ks_1s'} = -\Phi_{ks_1s}, \quad (6)$$

which, as Bogolyubov has shown, must satisfy conditions equivalent to (5):

$$F_{kss'} - \sum_{s''}(\Phi_{ks''s}\Phi_{ks''s'} + F_{kss''}F_{ks''s'}) = 0$$

and

$$\sum_{s''}(F_{kss''}\Phi_{ks''s'} + F_{ks's''}\Phi_{ks''s}) = 0. \quad (7)$$

We thereby reducel the problem of finding the ground-state energy of (1) to the problem of minimizing the functional

$$\overline{H} = \langle C^* H C \rangle; \quad \langle C^* C \rangle = 1; \quad \alpha_{ks} C = 0 \tag{8}$$

under the supplementary conditions (7). Taking (7) into account, by means of appropriate Lagrange multipliers, we solve the variational problem in the variables F and Φ. By purely algebraic transformations we find, in consequence of (2), that if τ and τ' are different, then

$$\Phi_{kss'} = F_{kss'} = 0. \tag{9}$$

It will readily be seen that this result implies ineffectiveness of the interaction between the neutrons and protons. The solution actually corresponds to minimum $\overline{H}$ (as was shown by a separate investigation) since the second variation of $\overline{H}$ for this solution is a positive definite quadratic form.

Thus, despite the presence of neutron-proton interaction in the Hamiltonian (1) the nucleons behave as regards superfluidity like two entirely independent Fermi systems. The assumption of different chemical potentials for the protons and neutrons (2), which leads to this situation, is fully justified, since in all nuclear systems known to us the neutron density differs from the proton density. Special analysis of the $\lambda_+ - \lambda_- = 0$ case shows that the expression for the ground-state energy in this case remains the same, but the functions F and Φ are no longer uniquely determined simply by the variational equations and the supplementary conditions. Mathematically, this arises from the fact that for $\lambda_+ - \lambda_- = 0$ the Hamiltonian (1) possesses higher symmetry in isotopic-spin space.

This work was done at the suggestion of N.N.Bogolyubov, to whom the author expresses sincere thanks.

Reference

1. N.N.Bogolyubov, Doklady AN SSSR, 119, 52 (1958). (Trans.Soviet Physics - Doklady.)

MOMENTS OF INERTIA OF NUCLEI

- M.Kazarnovskii

It is not impossible that the nucleus can be treated as a system consisting of a number of weakly interacting particles (for example, several shells or an outer unfilled shell and a core). Then, if the lifetime of the nucleus in the rotational state is short compared with the time necessary for transfer of angular momentum from one particle of the nucleus to another, the rotational states of nuclei can be realized in different ways. The wave functions of such states are not the eigenfunctions of the nuclear Hamiltonian even if one neglects the interaction of the nucleons with the electromagnetic field. Possibly an analogous situation obtains also in the case of other types of collective motion in nuclei (for example, oscillations of the nuclear surface).

It is logical to assume that most readily excited are rotations of the surface parts of the nucleus, which, in the case of nonspherical nuclei, then partially draw the internal parts (core) into rotation. Hence the expectation value of I is comprised of the moment of inertia I_1 of the outer (unfilled) shells and the moment of inertia I_0 of the core. The last may obviously be regarded as "hydrodynamic". For the moment of inertia of the outer shells we can write

$$I_1 = n_{\text{eff}} M\overline{R^2},$$

where n_{eff} is the effective number of nucleons in the unfilled shells, participating in the rotation, M is the mass of a nucleon, and $\overline{R^2}$ is the mean square of the distance from the axis of rotation to the said shells. Inasmuch as the angular momenta of the outer nucleons are on the average rather large, it may be assumed that these nucleons are located primarily on the surface of the nucleus, i.e.,

$$I_1 \approx \frac{5}{3}\frac{n_{\text{eff}}}{A} I_{\text{sb}},$$

where I_{sb} is the "solid body" moment of inertia of the nucleus, and A is the mass number (the factor 5/3 is equal to the ratio of the moments of inertia of a hollow sphere and a solid ball with equal masses). If the number n_n of nucleons in the unfilled shells is small and the nucleus is greatly elongated, the coupling of these nucleons with the axis of axial symmetry of the nucleus will be greater than the coupling with each other and they will all participate in the rotation, i.e., $n_{\text{eff}} = n_n$; analogously, if these shells are almost filled, then $n_{\text{eff}} = n_h$ the number of "holes" in them. Hence for sufficiently elongated nuclei we can approximately set

$$n_{\text{eff}} = \min(n_n, n_h)_P + \min(n_n, n_h)_N, \qquad (1)$$

where the indices P and N pertain to proton and neutron shells respectively. Further, inasmuch as

$$I_{\text{sb}} = \frac{2}{5} M r_n^2 A^{5/3}(1 + 0.31\beta + 0.44\beta^2 + \cdots);$$

$$I_0 = 0.358 M r_n^2 A^{5/3}\beta^2\left(1 - \frac{n_{\text{eff}}}{A}\right)(1 - 0(\beta^2)),$$

where $r_n A^{1/3}$ is the nuclear radius, and β is the deformation parameter related to the interval quadrupole moment Q_0 by the formula

$$Q_0 = \frac{3}{\sqrt{5\pi}} Z r_e^2 A^{2/3}\beta(1 + 0.16\beta + \cdots)$$

($r_e A^{1/3}$ is the radius of charge distribution in the nucleus), we have

$$I = \frac{2}{3} M r_n^2 A^{5/3} [n_{eff}(1 + 0.31\beta - 0.10\beta^2 + \ldots) + 0.537 A\beta^2 + \ldots]. \quad (2)$$

The value of the energy of the first excited rotational level $(E_{2+})_{theo} = 3\hbar^2/I$, calculated by means of (2) (for $r_n = 1.35 \cdot 10^{-3}$ cm and $r_e = 1.2 \cdot 10^{-13}$ cm) for even-even nuclei* with a clearly pronounced rotational spectrum are listed in the accompanying table. The values of Q_0 are taken from Townes' Handbook[1]. Comparison with the experimental energy values $(E_{2+})_{exp}$, taken from Seaborg's table[2], shows satisfactory agreement despite the approximate nature of the initial assumptions.

Comparison of the experimental and theoretical values of the moments of inertia (first rotational level energies) of even-even nuclei

Nucleus	$Q_0 \cdot 10^{24}$, cm²	β	n_{eff}	$(E_{2+})_{theo}$ kev	$(E_{2+})_{exp}$ kev	Nucleus	$Q_0 \cdot 10^{24}$, cm²	β	n_{eff}	$(E_{2+})_{theo}$ kev	$(E_{2+})_{exp}$ kev
$_{12}Mg^{24}$			8	1540× ×(1− −0,31β)	1368	$_{70}Yb^{170}$	7,4	0,30	30	83	84
						Yb^{172}	7,0	0,28	32	80	79
						Yb^{174}	7,0	0,28	34	75	76,5
$_{60}Nd^{150}$	4,7	0,25	18	150	131	Yb^{176}	7,0	0,28	32	78	82
$_{62}Sm^{152}$	5,5	0,27	20	132	122	$_{72}Hf^{176}$	6,9	0,27	32	80	88
Sm^{154}	6,0	0,30	22	115	82	Hf^{178}	7,5	0,29	30	81	93
$_{64}Gd^{154}$	5,3	0,25	22	125	123	Hf^{180}	7,0	0,27	28	87	93
Gd^{156}	7,9	0,37	24	94	89	$_{74}W^{182}$	7,1	0,26	26	93	100
Gd^{158}	8,2	0,38	26	86	79,5	W^{184}	6,5	0,24	24	102	111
$_{66}Dy^{160}$	6,7	0,30	28	92	84	W^{186}	6,4	0,23	22	110	123
Dy^{162}	8,0	0,35	30	80	81	$_{76}Os^{186}$	5,5	0,20	22	116	137
Dy^{164}	9,0	0,39	32	71	73	Os^{188}	5,1	0,18	20	129	155
$_{68}Er^{164}$	6,9	0,30	28	90	91	$_{90}Th^{232}$	7,0	0,18	24	93	50
Er^{166}	7,5	0,32	30	82	80,6	$_{92}U^{238}$	10,3	0,26	30	66	45
Er^{168}	7,5	0,32	32	77	80						
Er^{170}	7,5	0,31	34	74	79						

The appreciable deviation between the experimental and theoretical values of E_{2+} in the case of the heaviest nuclei (U and Th) can apparently be explained by the fact that in these nuclei the nucleons of the core become involved in the rotation to a greater extent. Somewhat strange is the relatively great divergence between the experimental and theoretical values of E_{2+} for Sm^{154}.

It must be noted that the given nuclear model does not explain the fact that the moments of inertia of odd nuclei are approximately 20% higher than those of even-even nuclei. According to the present model, there may in principle exist rotational states differing from the rotation of the surface nucleons considered here (for example, as was shown by Khokhlov[3] there can apparently exist rotational states with $I \geqslant I_{sb}/14$ even in the case of spherical nuclei). It is, however, difficult to detect such rotation in closed shells inasmuch as it can be excited only either in direct encounters with fast particles or in reactions accompanied by a substantial change in the nuclear structure, and in such cases it is difficult to distinguish the rotational states against the background of other forms of nuclear excitation.

In conclusion I desire to express my deep gratitude to A.S.Davydov, D.A.Zaikin, I.M.Frank, Yu.K.Khokhlov and F.L.Shapiro for valuable discussions.

References

1. C.H.Townes, Handbuch der PHysik.XXXVIII, 1, 377 (1958).
2. D.S.Strominger, J.M.Hollander & G.T.Seaborg, Revs.Mod.Phys., 30,585 (1958).
3. Yu.K.Khokhlov, Zhur.eksp.i teor.fiz., 35, 240 (1958). (Trans.Soviet Phys. - JETP.)

*It is assumed that the shells close for the magic numbers of nucleons: 8, 20, 50, 82 and 126.

CONTRIBUTION TO THE THEORY OF SUPERFLUIDITY OF NUCLEAR MATTER

- B.B.Dotsenko

Recently the concept of nuclear matter has been employed fairly widely in the theoretical investigation of the fundamental properties of nuclei.[1,2] By nuclear matter we understand an aggregate of nucleons occupying an infinite volume, wherein the nucleon density corresponds to that within heavy nuclei. It is assumed that the properties of nuclear substance in small volumes deep inside heavy nuclei (where it is possible to neglect the influence of the nuclear surface) are fairly well approximated by the properties of equally small amounts of nuclear matter.

It has been shown[1,2,3] that, in spite of the strong two-body interaction between nucleons, the model of a gas of weakly interacting fermions can be applied to nuclear matter. The effective mass of these fermions is assumed to be approximately half that of free nucleons (a self-consistent field is introduced).

However, it has also been shown[4,5] that a system of fermions with weak two-body attraction may form a kind of condensate of pairs of particles with equal and oppositely directed momenta and spins and of the similar pairs of holes, at temperatures close to absolute zero. As regards properties, this condensate is to some extent reminiscent of superfluid liquid He^4.

In connection with this there is a sound basis for the hypothesis of N.N. Bogolyubov that nuclear matter constitutes a concrete example in investigating the superfluidity attributes of fermion systems by the new theoretical superconductivity method proposed by this author (see Ref.4, p.30).

In order to apply this method, we consider the following model Hamiltonian for a system of fermions having spin σ and isotopic spin τ*:

$$H = \sum_{k,\sigma,\tau} \{E(k) - \lambda\} a^{+}_{k,\sigma,\tau} a_{k,\sigma,\tau} - \frac{1}{2V} \sum_{(k,k';\sigma,\sigma';\tau,\tau')} I(k,k') a^{+}_{k,\sigma_1,\tau_1} a^{+}_{-k,\sigma_2,\tau_2} a_{-k',\sigma'_2,\tau'_2} a_{k',\sigma'_1,\tau'_1}, \quad (1)$$

where $E(k)$ is the energy of a particle with momentum $k\,(\hbar = 1)$, λ is a parameter having the significance of the chemical potential of the system and in the normal state equal to the Fermi energy, and $I(k,k') = I(k,-k;\,k',-k'\,|\,\sigma_1,\sigma_2;\,\sigma'_1,\sigma'_2\,|\,\tau_1,\tau_2;\,\tau'_1,\,\tau'_2)$ is the essential part of the interaction between the particles, which leads to the formation of the superfluid condensate of nucleon (and hole) pairs with opposite momenta and spins or isotopic spins.

In straightforward application of perturbation theory, divergent terms will appear in the resulting series, connected with the production of the above-mentioned pairs of particles and holes. Therefore we must go over from the creation and annihilation amplitudes $a^{+}_{k,\sigma,\tau}$ and $a_{k,\sigma,\tau}$ for real particles to the amplitudes for the new quasiparticles, having the significance of elementary energy excitations: $\alpha^{+}_{k,\sigma,\tau}$ and $\alpha_{k,\sigma,\tau}$ This is accomplished by the canonical transformation:

$$a_{4\sigma\tau k,\sigma,\tau} = u_k \alpha_{k,-\sigma,-\tau} + 2\sigma v_k \alpha^{+}_{k,\sigma,-\tau} + 2\tau \varphi^{*}_k \alpha^{+}_{k,-\sigma,\tau} + 4\sigma\tau\chi^{*}_k \alpha_{k,\sigma,\tau}, \quad (2)$$

satisfying the conditions of orthonormality and single-valuedness (see Appendix 1 in Ref.4). In this new formulation we are no longer restricted by the requirement that the number of particles remain constant.

---

*For a small volume of nuclear matter one can disregard the Coulomb forces between nucleons and take account of the nucleon charges by using the isotopic spin formalism. The present work differs from that of Solov'ev[6] and of Belyaev[7] in explicitly taking into account the isotopic spin.

Inserting (2) into (1), we obtain a new expression of 272 terms for the Hamiltonian. After application of perturbation theory to this Hamiltonian, there appear in the resulting series divergent terms, corresponding to the creation of pairs of quasiparticles with the same momenta. To eliminate them, it is necessary to select the coefficients of the canonical transformation so that the total contribution of these terms vanishes to the appropriate order (in our case, the first). This is the essence of Bogolyubov's compensation principle. Proceeding according to this principle, we obtain two basic equations for the coefficients u_k, v_k, φ_k, and χ_k:

$$2\{E(k)-\lambda\}(u_k^* \pm \chi_k)(v_k \mp \varphi_k^*) - \frac{1}{V}\sum_{k'} I(k, k')\,[(u_k^* \pm \chi_k)^2 (u_{k'}^* \pm \chi_{k'})(v_{k'} \mp \varphi_{k'}^*) -$$

$$-(v_k \mp \varphi_k^*)^2 (u_{k'}^* \pm \chi_{k'})(v_{k'}^* \mp \varphi_{k'})] = 0. \qquad (3)$$

In deriving these equations, we use the charge independence hypothesis:

$$I(\vec{n}\sim\overleftarrow{n}) = I(\vec{p}\sim\overleftarrow{p}) = I(\vec{n}\sim\vec{p}) = I(k, k'); \qquad (4)$$

here $I(\vec{n}\sim\overleftarrow{n})$ is the interaction between two neutrons with opposite spins (spin singlet), $I(\vec{p}\sim\overleftarrow{p})$ is the same for proton pairs, and $I(\vec{n}\sim\vec{p})$ is the interaction of a neutron and proton with parallel spins (spin triplet).

We seek a solution of Eqs. (3) in real functions.* Writing

$$u_k + \chi_k = x_k; \quad v_k - \varphi_k = y_k; \quad v_k + \varphi_k = z_k; \quad u_k - \chi_k = w_k,$$

we obtain

$$2\xi(k)\,x_k y_k - \frac{1}{V}\sum_{k'} I(k, k')(x_k^2 - y_k^2)\,x_{k'} y_{k'} = 0, \qquad (5)$$

$$\xi(k) = E(k) - \lambda.$$

From the conditions of orthonormality and single-valuedness we have

$$x_k^2 + y_k^2 = 1. \qquad (6)$$

Analogous relations are obtained for z_k and w_k. We solve equations (5) following Bogolyubov[4] and obtain the "trivial" solution

$$x_k = \begin{cases} 0, & E(k) < \lambda \\ 1, & E(k) > \lambda \end{cases}, \quad y_k = \begin{cases} 1, & E(k) < \lambda \\ 0, & E(k) > \lambda \end{cases} \qquad (7)$$

and the nontrivial solution

$$x_k = \pm\sqrt{\frac{\widetilde{\varepsilon}(k) + \xi(k)}{2\widetilde{\varepsilon}(k)}}, \quad y_k = \pm\sqrt{\frac{\widetilde{\varepsilon}(k) - \xi(k)}{2\widetilde{\varepsilon}(k)}}, \qquad (8)$$

where

---

*A solution also exists, when u_k and χ_k are real, and v_k and φ_k are imaginary (and vice versa); but since these cases lead to the same results, we shall not consider them. The case when u_k, v_k, φ_k and χ_k have both real and imaginary parts simultaneously different from zero will be considered separately.

$$\tilde{\varepsilon}(k) = \sqrt{C^2(k) + \xi^2(k)};$$

$$C(k) = \omega\,[K(k, k_F)/K(k_F, k_F)]\exp(-1/\rho);$$

$$\rho = \frac{k_F^2}{(2\pi)^2}\frac{K(k_F, k_F)}{E'(k_F)}; \quad K(k, k') = \frac{1}{(2\pi)^2}\int_{-1}^{+1} I(k, k')\,dt;$$

$$t = \cos(\widehat{\vec{k}, \vec{k}'}) \tag{9}$$

$$\ln\omega = -\frac{1}{2}\int_0^\infty \frac{d}{dk'}\left[\left(\frac{K(k_F, k')}{K(k_F, k_F)}\right)^2 \frac{k'^2}{k_F^2}\frac{(k'-k_F)E'(k_F)}{|E(k')-E(k_F)|}\right]\ln 2E'(k_F)\,|k'-k_F|\,dk';$$

$$E'(k_F) = (dE/dk)_{k=k_F}.$$

Further,

$$w_k = \pm x_k; \quad z_k = \pm y_k.$$

Then

$$u_k = \begin{cases} x_k; \\ 0 \end{cases} \quad \chi_k = \begin{cases} 0, & w_k = +x_k \\ x_k, & w_k = -x_k \end{cases}, \quad v_k = \begin{cases} y_k; \\ 0 \end{cases} \quad \varphi_k = \begin{cases} 0, & y_k = +z_k \\ -x_k, & y_k = -z_k \end{cases}. \tag{10}$$

We now find the energy of the ground state of our system; we have

$$E_0 \equiv \langle C_v^* H C_v\rangle = 4\sum\{E(k) - \lambda\}(v_k^* v_k + \varphi_k^*\varphi_k) -$$

$$-\frac{4}{V}\sum_{k,\,k'} I(k, k')\,[(u_{k'}\varphi_{k'}^* - v_{k'}\chi_{k'}^*)(u_k^*\varphi_k - v_k^*\chi_k) + (u_{k'}v_{k'} - \varphi_{k'}^*\chi_{k'}^*)(u_k^* v_k^* - \varphi_k\chi_k)]; \tag{11}$$

whence, taking into account (7), (8) and (10), we find that the difference between the energies of the normal and the superfluid ground states

$$E_0^{(n)} - E_0^{(s)} = 2\sum_k \{\tilde{\varepsilon}(k) - E(k) + E_F\} \tag{12}$$

is always positive, i.e., the superfluid state is more stable than the normal and is therefore realized (E_F is the Fermi energy and C_v is the "vacuum" wave function: $\alpha_{k\sigma\tau}C_v = 0$).

Analogously we find that the energy of a one-fermion elementary excitation is

$$E_e = \langle C_v^* \alpha_{k++} H \overset{+}{\alpha}_{k++} C_v\rangle = \tilde{\varepsilon}(k). \tag{13}$$

For the superfluid state, we have

$$E_e^{(s)} = \tilde{\varepsilon}^{(s)}(k) = \sqrt{C^2(k) + \{E(k) - E_F\}^2} = \sqrt{C^2(k) + (E_e^{(n)})^2}, \tag{14}$$

i.e., the energy of the one-fermion excitation is separated from the superfluid ground state by a gap given by the nontrivial $C(k)$.

Further, in considering the case corresponding to very heavy nuclei, when the chemical potential λ_p of the proton subsystem differs substantially from the chemical potential λ_n of the neutron subsystem, it turns out that when one imposes a definite relationship (taking into account the inequality $\lambda_n \neq \lambda_p$) on the amplitudes a_p and a_n, the factors multiplying $I(n \sim p)$ in all corresponding terms vanish. From this it follows that for the case of different proton and neutron densities, when $\overline{(\partial H/\partial\lambda_p)} = Z \neq \overline{(\partial H/\partial\lambda_n)} = N$, the superfluid state is apparently realized separately for the proton and neutron subsystems (also see Ref.8). However, strictly speaking, this case is not an equilibrium one and should be regarded merely as a quasistationary approximation.

I desire to express my sincere gratitude to N.N.Bogolyubov for suggesting the subject and for his interest in the work and valuable comments. I am also

grateful to A.M.Korolev, A.F.Lubchenko and other colleagues for support and useful discussions.

Physical Institute,
Academy of Sciences of the Ukrainian SSR

References

1. K.A.Brueckner, Phys.Rev., 97, 1353 (1955).
2. L.C.Gomes, J.D.Walecka & V.F.Weisskopf, Ann.Phys., 3, 241 (1958).
3. E.Clementel & C.Villi, Nuovo Cimento, 9, 950 (1958).
4. N.N.Bogolyubov, V.V.Tolmachev & D.V.Shirkov, Novyi metod v teorii sverkhprovodimosti (New method in the theory of superconductivity), M. 1958.
5. J.Bardeen, L.N.Cooper & I.R.Schrieffer, Phys.Rev., 106, 162 (1957); Ibid., 108, 1175 (1957); L.N.Cooper, Phys.Rev., 104, 1189 (1956).
6. V.G.Solov'ev, Priprinty Ob"eden. inst. yadrenykh issledovanii (Preprints of the Joint Inst. for Nuclear Research), P-217 & P-219 (1958); Doklady AN SSSR, 124, 625 (1958). (Trans.Soviet Phys. - JETP.)
7. S.T.Belyaev, Preprinty raboty v Institute teor.fiz. (Preprints of work in the Institute of Theoretical Physics), Effect of pairing correlations on the nuclear properties. Copenhagen 1958.
8. Yu.V.Tsekhmistrenko, Ukr.fiz.zhur. (Ukrainian Jour. of Physics), No.1, 37 (1959).

STATISTICAL THEORY OF THE NUCLEAR POTENTIAL IN THE "EFFECTIVE MASS" APPROXIMATION

- L.Rapoport and S.Kadmenskii

It has been shown in a series of theoretical papers[1-5] that if we neglect the Coulomb repulsion, an arbitrarily large number of nucleons form a stable system with an equilibrium density $\rho = 1.72 \times 10^{38}$ cm^{-3} and a binding energy of 15 Mev per particle. Such a system has been given the name "nuclear matter". In nuclear matter the nucleons move as independent particles, that is, the potential energy of a nucleon does not depend on its position but does depend on its velocity. This velocity dependence is most frequently expressed in terms of the "effective" mass of the nucleon. One of the principal differences in treating the properties of nuclear matter as against those of an actual nucleus is that for the former the effect of finite size is neglected. In the present paper we shall discuss the depth and form of the potential acting on a nucleon within a nucleus, and also the magnitude of its effective mass and the dependence of this mass on the distance of the nucleon from the center of the nucleus; the finite dimensions of the nucleus and the Coulomb forces between the protons are included in this calculation based on the statistical theory of the nucleus. It is found that the protons are included in this calculation based on the statistical theory of the nucleus. It is found that the "self-consistent" potentials have the usual form, i.e., the form employed for instance, in the nuclear shell model. The magnitude of the effective mass obtained is approximately the same as for nuclear matter. The general form of the potential, which depends on position and momentum, can be expressed as a generalized non-local potential, representing the action of the entire nucleus on the nucleon.

1. Derivation of the velocity-dependent potential from the statistical theory of the nucleus

Consider the general statistical theory of the nucleus. If the n-p, n-n and p-p interactions, respectively, are expressed in the form

$$v_{np} = -I(r_{np})\,\hat{p}\,(\mathbf{r}_n, \mathbf{r}_p), \tag{1}$$

$$v_{nn'} = -\frac{1}{3} I(r_{nn'})\,(\vec{\sigma}\vec{\sigma}'), \tag{2}$$

$$v_{pp'} = -\frac{1}{3} I(r_{pp'})\,(\vec{\sigma}\vec{\sigma}'), \tag{3}$$

where

$$I(r_{ik}) = \frac{\gamma}{|\mathbf{r}_i - \mathbf{r}_k|} \exp\left(-\frac{|\mathbf{r}_i - \mathbf{r}_k|}{r_0}\right),$$

and $\hat{p}$ is the operator which transposes the coordinates, $r_0 = \frac{h}{m_\pi c}$, and γ is the constant of the force law, then in a calculation of the interaction energy between identical particles only the exchange part remains. With this the binding energy comes out correctly.[6]

Under the usual assumptions[6] for a statistical calculation, the exchange potential V_{np} of one neutron with all the nuclear protons has the form

$$V_{np} = -\frac{4\gamma}{h}\left[\frac{1}{4p}(p_{\mu p}^2 - p^2 + p_0^2)\ln\frac{(p_{\mu p}+p)^2 + p_0^2}{(p_{\mu p}-p)^2 + p_0^2} + p_{\mu p} - p_0 \operatorname{arctg}\frac{p_{\mu p}+p}{p_0} - p_0 \operatorname{arctg}\frac{p_{\mu p}-p}{p_0}\right], \tag{4}$$

where $p_{\mu p}$ is the maximum momentum and $p_0 = \frac{h}{2\pi r_0}$.

The interaction potential (4) depends on the coordinates (thru $p_{\mu p}$) and the momentum p of the neutron. In the final analysis, the dependence on the distance from the center of the nucleus is expressed by the proton density distribution $\rho_p(r)$, which is related to $p_{\mu p}$ by

$$p_{\mu p} = (3\pi^2)^{1/3}\frac{h}{2\pi}\rho_p^{1/3}. \tag{5}$$

Below, in place of $p_{\mu p}$ we introduce the dimensionless function

$$\omega_p = \frac{p_{\mu p}}{p_0}. \tag{6}$$

For small momenta, we can represent the potential (4) as a series in the parameter $\frac{p}{p_{\mu p}} = \frac{p}{\omega_p p_0} \ll 1$ and separate the spatial dependence from the momentum dependence. We limit the expansion to the second power of the parameter, and find

$$V_{np}(r, p) = -\frac{8\gamma p_0}{h}\left[\omega_p - \operatorname{arctg}\omega_p - \frac{\omega_p^3 p^2}{3p_0^2[1+\omega_p^2]^2}\right]. \tag{7}$$

In an analogous fashion we obtain the exchange potentials of one neutron with all the neutrons $V_{nn}(r, p)$ and of one proton with all the protons $V_{pp}(r, p)$*:

$$V_{nn}(r, p) = -\frac{2\gamma p_0}{h}\left[\omega_n - \operatorname{arctg}\omega_n - \frac{\omega_n^3 p^2}{3p_0^2[1+\omega_n^2]^2}\right], \tag{8}$$

$$V_{pp}(r, p) = -\frac{2\gamma p_0}{h}\left[\omega_p - \operatorname{arctg}\omega_p - \frac{\omega_p^3 p^2}{3p_0^2[1+\omega_p^2]^2}\right]. \tag{9}$$

Using (7), (8) and (9), we can get the general potential acting on a neutron in the nucleus. Here the spatial and momentum dependencies are separate from one another. Keeping in mind that we will later substitute this potential in the Schrödinger equation, we write $V_n(r, p)$ in the form

$$V_n(r, p) = V_n(r) - \frac{\varphi_n(r)}{4}p^2 - p\frac{\varphi_n(r)}{2}p - p^2\frac{\varphi_n(r)}{4}, \tag{10}$$

where

$$V_n(r) = -\frac{8\gamma p_0}{h}\left\{\omega_p + \frac{\omega_n}{4} - \operatorname{arctg}\omega_p - \frac{1}{4}\operatorname{arctg}\omega_n\right\} \tag{11}$$

and

$$\varphi_n(r) = -\frac{1}{3p_0^2}\left\{\frac{\omega_p^3}{[1+\omega_p^2]^2} + \frac{\omega_n^3}{4[1+\omega_n^2]^2}\right\}\frac{8\gamma p_0}{h}. \tag{12}$$

We get an analogous formula for $V_p(r, p)$:

$$V_p(r, p) = V_p(r) - \frac{\varphi_p(r)}{4}p^2 - p\frac{\varphi_p(r)}{2}p - p^2\frac{\varphi_p(r)}{4}, \tag{13}$$

The expressions for $V_p(r)$ and $\varphi_p(r)$ differ from (11) and (12) by the interchange of ω_p and ω_n.

At present the functions $\omega_n(r)$ and $\omega_p(r)$ in Eqs. (10) and (13) remain arbitrary. The choice of these is defined by the requirement that the correct binding energy per nucleon result, i.e., by the "self-consistency" requirement. Accordingly, we write an expression for the total energy of the nucleus as a function of $\omega(r)$:

$$E = E_k + E_j + E_A + E_c + E_R, \tag{14}$$

*The Coulomb interaction will be taken into account below.

where E_k is the Fermi kinetic energy of the nucleons, E_j is the Weizsäcker energy, which takes into account the finite size of the nucleus, E_A is the total nucleon interaction exchange energy, E_c is the repulsive Coulomb energy of the protons, and E_R is the Coulomb exchange energy of the protons. Following Gombash[6], we choose ω_n and ω_p in the form

$$\omega_p = \omega_{p_0} \exp\left(-\frac{a^2 r^2}{3r_0^2}\right), \tag{15}$$

where ω_{p_0} is determined by the normalization condition for the total number of protons (Z):

$$\omega_{p_0} = (9\pi)^{1/6} Z^{1/3} a \tag{16}$$

and

$$\omega_n = \omega_{n_0} \exp\left(-\frac{a^2 r^2}{3r_0^2}\right), \tag{17}$$

where

$$\omega_{n_0} = (9\pi)^{1/6} N^{1/3} a \tag{18}$$

(N is the total number of neutrons).

Minimization of the total energy gives the value of the variational parameter a; calculation of the binding energy per nucleon and comparison with experiment allows of determining the constant γ of the force law[3]:

$$\gamma = \lambda \varepsilon_0 r_0, \tag{19}$$

where

$$\lambda = 4{,}14; \quad \varepsilon_0 = 17{,}01 \ \text{Mev}.$$

Besides the purely nuclear potential affecting a proton, there is still the Coulomb potential due to all the other protons. If we neglect the exchange part of the Coulomb interaction, then the remaining "ordinary" potential will not depend on the momentum and can be calculated in the following manner

$$v_c(r) = \frac{e^2}{2} \int \frac{\rho_p(\mathbf{r}')}{|\mathbf{r} - \mathbf{r}'|} d\mathbf{r}'. \tag{20}$$

Invoking (5) and (6) to introduce ω_p in place of $\rho_p(r)$ and then choosing ω_p of the form (15), we find

$$v_c(r) = \frac{2e^2 \omega_{p_0}^3}{3\pi a^3} \frac{1}{r} \Phi\left(\frac{ra}{r_0}\right), \tag{21}$$

where $\Phi(x) = \int_0^x e^{-u^2} du$ is a Gaussian transcendental function. Here

$$v_c(0) = \frac{2e^2 \omega_{p_0}^3}{3\pi a^2 r_0}. \tag{22}$$

The total potential acting on a proton in the nucleus is now given by the sum

$V_p(r, p)$ from (13) plus $v_c(r)$ from (21) and (22).

2. The effective mass approximation

With the help of formulas (15) and (17) the explicit form of the potentials acting on the neutrons and protons in the nucleus is fully determined. In the present approximation the momentum dependence turns out to be quadratic. Therefore we can introduce the approximation of the radial "effective" mass of a nucleon, reflecting the interaction of the given nucleon with all remaining nucleons.

By considering the relation

$$\frac{1}{8}\left(\hat{p}^2\frac{1}{M}+\frac{1}{M}\hat{p}^2+\hat{p}\frac{2}{M}\hat{p}\right)+V(r,\ \hat{p})=\frac{1}{8}\left(\frac{1}{M^*}\hat{p}^2+\hat{p}\frac{2}{M^*}\hat{p}+\hat{p}^2\frac{1}{M^*}\right)+V(r),$$

we find the following expression for the ratio of the effective mass M^* to the actual mass M

$$\gamma=\frac{M^*}{M}=\{1-2M\varphi(r)\}^{-1}. \tag{23}$$

Invoking (11) and (12), we find for the neutron

$$\gamma_n=\left\{1+\frac{16M_n\gamma}{3hp_0}\left[\frac{\omega_p^3}{[1+\omega_p^2]^2}+\frac{\omega_n^3}{4\,[1+\omega_n^2]^2}\right]\right\}^{-1}. \tag{24}$$

For the proton γ_p has an analogous form, with ω_n and ω_p interchanged.

Fig.1 shows the variation of the ratio M/M^* with the distance of the nucleon from the center of the nucleus for a nucleus with A = 126. As will be evident from the figure, the effective masses of the neutron (curve I) and the proton (curve II) virtually coincide. The strongest momentum dependence of the potential $V(r, p)$ occurs for the medium distances of the nucleon from the center of the nucleus.

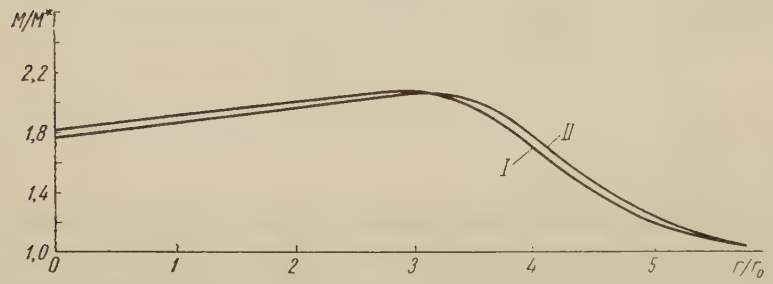

Fig.1. Variation of the ratio of the actual mass M of a neutron (curve I) and a proton (curve II) to the "effective" mass M* for a "standard" nucleus with A = 126 as a function of the distance from the center of the nucleus.

For comparison with the results of earlier studies, we calculated the average value of the effective mass for a standard nucleus with A = 126. By averaging the expression in the brackets in Eq.(24) over the nuclear volume according to the formula

$$\frac{1}{\Omega}\int_{\Omega}\left[\frac{\omega_p^3}{(1+\omega_p^2)^2}+\frac{\omega_n^3}{4\,(1+\omega_n^2)^2}\right]d\Omega$$

and by choosing the parameter a = 0.509, corresponding to A = 126, we obtain

$$\gamma = 0.57.$$

This value of γ is close to the corresponding value deduced in Refs.3,4 and 7 for "nuclear matter".

Plots of the variation of the potentials $V_n(r)$ and $V_p(r)$ with the distance from the center of the nucleus are given in Fig.2, from which it will be clear that the potential acting on a neutron (curve I) has the form usually assumed in the nuclear shell model. The potential acting on a proton (curve II) differs from that acting on a neutron in that it is higher at the center of the nucleus and has a Coulomb barrier at the nuclear surface. The figure also shows the form of the nuclear exchange potential (13) for a proton (curve III) and the Coulomb potential (21) for a proton (curve IV).

For heavy nuclei the choice of a single-parameter dependence for $\omega_n(r)$ proves to be rather crude. As was shown in our previous paper[8], a significantly better result is obtained with the following form for the density distribution, which now depends on two parameters, namely, ρ_0 and R_0/R:

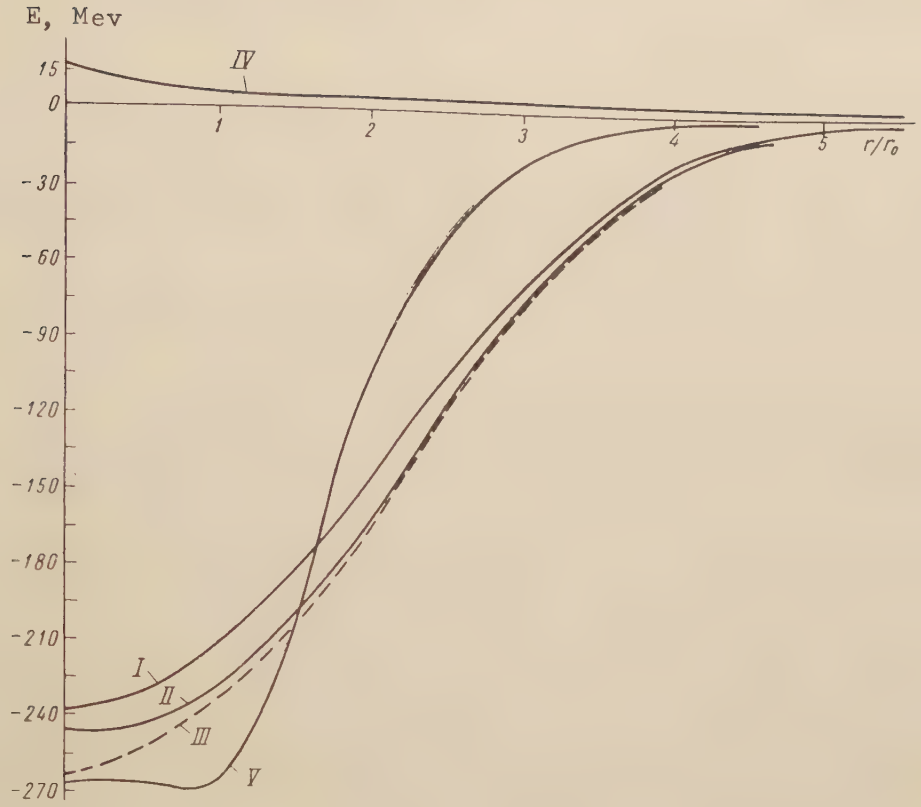

Fig.2. Variation of the nucleon potential energy with the distance from the center in a standard nucleus with A = 126: I - neutron; II - proton; III - proton exchange energy; IV - proton Coulomb energy (all the above were calculated for the density distribution given by Eq.(15); V - neutron potential (calculation based on the density distribution given by Eq.(25)).

$$\rho = \begin{cases} \rho_0 \text{ for } r \leqslant R_0 \\ \rho_0 \exp\left[-\left(\frac{r-R_0}{R}\right)^2\right] \text{ for } R_0 < r. \end{cases} \tag{25}$$

The potential calculations in this case were made by means of the same formulas as before, but now, owing to the presence of a plateau of constant density, the general form of the potential is significantly closer to actuality. A graph of $V_n(r)$ (curve V) for a "standard" nucleus with A = 126 is given in Fig.2 (the necessary parameters were taken from Ref.8). It will be seen that this potential best approaches the potential usually postulated, namely, a well with eroded edges. An estimate of the average effective mass in this case leads to $\gamma = 0.77$ for A = = 126.

The distance-from-center dependence of the nucleon mass in the statistical model indicates that here the nucleons are "quasinucleons". The maximum Fermi energy for such "quasiparticles" near the nuclear surface (Figure 1) ought to be approximately twice as large as that usually assumed in such calculations. It is possible that this effect may account for the high-energy nucleons, that are invoked to explain such reactions (occurring at the nuclear surface) as, for instance, "pick up". If this is so, it is not necessary to postulate a strong two-body interaction within the nucleus, as was done, for example by Brueckner,

Eden and Francis[9].

Voronezh State University

References

1. K.Brueckner, G.Levinson & H.Mahmud, Phys.Rev., 95, 17 (1954).
2. K.Brueckner, Phys.Rev., 96, 508 (1954).
3. K.Brueckner, Phys.Rev., 97, 1353 (1955).
4. K.Brueckner & C.Levinson, Phys.Rev., 97, 1344 (1955).
5. L.C.Gomes, J.D.Walecka & V.F.Weisskopf, In Problemy sovr.fiz., 5, 56 (1958). (Prob. trans. of Ann.Physik., 3, 241 (1958).
6. P.Gombash, Uspekhi fiz.nauk, 49, 385 (1953).
7. E.Clementel & C.Villy, Nuovo cimento, 9, 950 (1958).
8. L.Rapoport & V.Filimonov, Zhur.eksp.i teor.fiz., 27, 243 (1954).
9. K.Brueckner, R.Eden & N.Francis, Phys.Rev., 98, 1445 (1955).

ON BETA-DECAY OF NEUTRONS WITH ORIENTED SPIN

- B.K.Kerimov

In this study we use the theory of Dirac particles with oriented spin to calculate the angular asymmetry and the degree of longitudinal polarization of the electrons formed in β-decay of free polarized neutrons $(n \to p + e^- + \bar{\nu})$. The wave functions in the interaction Hamiltonian representing the free Fermi particles are given by the solution of the simultaneous equations

$$\left(-\frac{1}{ic}\cdot\frac{\partial}{\partial t} - \frac{1}{i}(\vec{\alpha}\vec{\nabla}) - \rho_3 k_0\right)\psi = 0 \qquad \left(\frac{\vec{\sigma}\vec{\nabla}}{ik} - s\right)\psi = 0, \tag{1}$$

where $\vec{\alpha} = \rho_1\vec{\sigma}$, ρ_3 are the well-known Dirac matrices, s is the eigenvalue of the operator $\frac{\vec{\sigma p}}{|p|}$, which characterizes the longitudinal polarization of the spin $(s = \pm 1)$, and $p = \hbar k$ is the momentum of the particle.

In such treatment of β-decay[1], in distinction to the consideration in the works of other authors[2-4], the interaction Hamiltonian is written as a sum of only the S, V, T, A and P interaction terms with coupling constants C_i; it does not explicitly contain terms with the pseudoscalar factor γ_5 and the corresponding coupling constants C_i. The formula $w(\theta, s_e, s_{\bar{\nu}})$ for the angular distribution of the decay electrons contains, in addition to the usual terms, terms proportional to s_e and $s_{\bar{\nu}}$, which characterize the longitudinal polarizations of the electron and antineutrino spins. We shall show that V ∓ A forms of coupling allow of the decay of a polarized neutron with emission of an antineutrino with spin parallel to its momentum, $s_{\bar{\nu}} = 1$ (the antineutrino with positive helicity considered by Sokolov[1,5] and Feynman & Gell-Mann[6]), while S ∓ T type coupling leads to the antineutrino having its spin antiparallel to its momentum, $s_{\bar{\nu}} = -1$ (the antineutrino with negative helicity of the two-component theory). It would appear, therefore, that V - A interaction is consistent with the latest experimental data on the decay of polarized neutrons.

The interaction Hamiltonian, leading to the β-decay of a free neutron,

$$n \to p + e^- + \bar{\nu} \tag{2}$$

may be written as

$$H_{\text{int}} = \sum_j C_j (\psi_p^+ O_j \psi_n)(\psi_e^+ O_j \psi_\nu), \cdot \tag{3}$$

where j equals V, A or S, T;

$$O_V = \alpha_\mu = (i\vec{\alpha},\ I);\ O_A = \sigma_\mu = (\vec{\sigma},\ i\rho_1);\cdot$$

$$O_S = \rho_3;\ O_T = \frac{1}{\sqrt{2}}\alpha_{\mu\nu} = \frac{1}{\sqrt{2}}(\rho_3\vec{\sigma},\ i\rho_2\vec{\sigma});\quad \vec{\alpha} = \rho_1\vec{\sigma}.$$

The coefficient $C(t)$, characterizing the probability for the transition (2), is defined by the formula

$$C_p(t) = -\frac{i}{\hbar}\sum_j \int_0^t dt \int C_j (\psi_p^+ O_j \psi_n)(\psi_e^+ O_j \psi_\nu)(d\vec{r}). \tag{4}$$

We choose the wave functions of the free neutron (ψ_n), the proton (ψ_p), the electron (ψ_e^+) and the antineutrino (ψ_ν) in the form of plane waves. The neutron decay probability per unit time is then given by the expression

$$W\,dK_e\,d\Omega_e\,d\Omega_\nu = \frac{\partial}{\partial t} C_f^+(t)\,C_f(t) = \frac{1}{(2\pi\hbar)^5}\,k_e K_\nu\,(\Delta K_{en} - K_\nu)^2\,|R_{fn}|^2\,dK_e\,d\Omega_e\,d\Omega_\nu. \tag{5}$$

where

$$|R_{fn}|^2 = \sum_{i,j} C_i C_j' (b_n^+ O_i^+ O_j' b_p b_e^+ O_i b_n)^* (b_n^+ O_i^+ O_j' b_p b_e^+ O_i b_n). \tag{6}$$

$$i, j = V, A \text{ or } S, T.$$

Here $b_n \equiv b_n(\mathbf{k}_n, s_n, \varepsilon_n)$, $b_p \equiv b_p(\mathbf{k}_p, s_p, \varepsilon_p)$, $b_e \equiv b_e(\mathbf{k}_e, s_e, \varepsilon_e)$ and $b_\nu \equiv b_\nu(\mathbf{k}_\nu, s_\nu, \varepsilon_\nu)$ are Dirac spinor amplitudes for the neutron, proton, electron, and antineutrino, respectively. The quantities ε_n, ε_p, and ε_e determine the sign of the energy for the corresponding state. In the case of neutron decay $\varepsilon_n = \varepsilon_p = \varepsilon_e = 1$, and $\varepsilon_\nu = -1$. The wave vector of the antineutrino is $\mathbf{k}_\nu = -\mathbf{k}_\nu$, $k_\nu = k_\nu$; the wave vectors of the neutron, proton and electron are equal to $\mathbf{k}_n$, $\mathbf{k}_p$ and $\mathbf{k}_e$, respectively. The quantity $s_\xi = \pm 1$ ($\xi = n, p, e$ or ν) characterizes the component of double the spin moment $\vec{s}$ parallel and antiparallel to the direction of the particle of momentum; for $s_\xi = 1$ the spin is parallel, while for $s_\xi = -1$ it is antiparallel to the particle motion. Further, $\Delta K_{en} = K_n - K_p - K_e$, $K_e = \sqrt{k_e^2 + k_{0e}^2}$, $k_{0e} = \frac{m_{0e}c}{\hbar}$ is the proton rest mass; $K_e = \sqrt{k_e^2 + k_{0e}^2}$, $k_{0e} = \frac{m_{0e}c}{\hbar}$ is the electron rest mass; $k_\nu = \Delta K_{en} - K_e$. Here and below we assume that the neutrino rest mass is zero, i.e., that $K_\nu = k_\nu$. We will consider the neutron to be at rest: $\mathbf{k}_n = 0$, $K_n = k_{0n} = \frac{m_{0n}c}{\hbar}$.

According to Sokolov[1], the matrix elements for the decay process, taking into account the longitudinal polarization of the particles, are calculated by the following formula[1,7]:

$$\langle \gamma_{\mu'\nu'}, \gamma_{\mu\nu} \rangle \equiv b^+(\mathbf{k}, s, \varepsilon)\,\gamma_{\mu'\nu'}\,b(\mathbf{k}', s', \varepsilon')\,b^+(\mathbf{k}', s', \varepsilon')\,\gamma_{\mu\nu}\,b(\mathbf{k}, s, \varepsilon) = \frac{1}{4}\,\rho_{\mu'\mu}\,\sigma_{\nu'\nu}, \tag{7}$$

where

$$\rho_{\mu'\mu} = \frac{1}{4}\,Sp\,\rho_{\mu'}\left(1 + \rho_1 s' s' \frac{k'}{K'} + \rho_3 s' \frac{k_0'}{K'}\right)\rho_\mu\left(1 + \rho_1 s s \frac{k}{K} + \rho_3 s \frac{k_0}{K}\right);$$

$$\sigma_{\nu'\nu} = \frac{1}{4}\,Sp\,\sigma_{\nu'}\left(1 + s'\frac{\vec{\sigma}\mathbf{k}}{k}\right)\sigma_\nu\left(1 + s\frac{\vec{\sigma}\mathbf{k}}{k}\right);$$

$\gamma_{\mu\nu} = \rho_\mu \sigma_\nu = \sigma_\nu \rho_\mu$ ($\mu, \nu = 1, 2, 3, 4$) are Dirac matrices; $\sigma_4 = \rho_4 = 1$; $\sigma_k = \vec{\sigma}\mathbf{n}$; $\mathbf{n}$ is an arbitrary unit vector. In Eq.(7) all primed quantities refer to Fermi particles with rest mass $k_0' = \frac{m_0'c}{\hbar}$, and unprimed quantities to Fermi particles with rest mass $k_0 = \frac{m_0 c}{\hbar}$.

We make a non-relativistic approximation for the nucleons. Then for the V + A and S + T forms of interaction, we find, from (6) and (7), the following expression for $|R_{fn}|^2$ (with fixed orientation of the electron and antineutrino spins):

$$\begin{aligned}
\sum_{s_p=\pm 1} |R_{fn}|^2 = {} & \frac{1}{4}\left(1 \mp s_\nu s_e \frac{k_e}{K_e}\right)\cdot\{|C_{V,S}|^2\cdot(1 - s_n s_e (\mathbf{k}_e^0 \mathbf{k}_\nu^0)) + \\
& + |C_{A,T}|^2\cdot(3 + s_n s_e (\mathbf{k}_e^0 \mathbf{k}_\nu^0) + 2 s_n s_e (\mathbf{k}_n^0 \mathbf{k}_e^0) + 2 s_n s_\nu (\mathbf{k}_n^0 \mathbf{k}_\nu^0)) + \\
& + (C_{V,S}^+ C_{A,T} + C_{V,S}\cdot C_{A,T}^+)(s_n s_\nu (\mathbf{k}_n^0 \mathbf{k}_\nu^0) - s_n s_e (\mathbf{k}_n^0 \mathbf{k}_e^0)) - \\
& - i\,(C_{V,S}^+ C_{A,T} - C_{V,S} C_{A,T}^+)\,s_n s_\nu s_e (\mathbf{k}_n^0 \mathbf{j})\,(\mathbf{j}[\mathbf{k}_e^0 \mathbf{k}_\nu^0])\}.
\end{aligned} \tag{8}$$

Here $s_n = s_n \mathbf{k}_n^0$ is the neutron spin vector, which we take along the z-axis ($s_n = 1$); $\mathbf{j}$ is a unit vector; $\mathbf{k}_q^0 = \frac{\mathbf{k}_q}{k_q}$ with $q = e, \bar{\nu}, n$ represents a unit vector along the momentum of the particle. In the factor $\left(1 \mp s_e s_{\bar{\nu}} \frac{k_e}{K_e}\right)$, the upper sign refers to V + A interaction, the lower to S + T interaction.

The last term in Eq. (8), describing the correlation of the three vectors s_n, $\mathbf{k}_{\bar{\nu}}$ and $\mathbf{k}_e$ (or s_n, $s_{\bar{\nu}}$ and s_e),

$$O_- = D_0 (s_n [\mathbf{s}_{\bar{\nu}} \mathbf{s}_e]) \mp D_0 \frac{(s_n [\mathbf{k}_{\bar{\nu}} \mathbf{k}_e])}{k_{\bar{\nu}} K_e}, \tag{9}$$

where $\mathbf{s}_{\bar{\nu}} = s_{\bar{\nu}} \mathbf{k}_{\bar{\nu}}^0$, $\mathbf{s}_e = s_e \mathbf{k}_e^0$, and

$$D_0 = -i (C_{V,S}^{+} C_{A,T} - C_{V,S} C_{A,T}^{+}), \tag{10}$$

will be non-vanishing if the coupling constants C_i are complex quantities. The presence of the term (9), as was shown by Lee[3] and Jackson et al[4], would mean the breakdown of time reversal invariance for the β-decay Hamiltonian. Recent experiments[8] on the β-decay of free polarized neutrons give a value of -0.04 ± 0.07 for the coefficient D_0 in the second term of (9). Integrating (8) over the antineutrino angular variables, we obtain the following equation for the angular distribution of the electrons from the decay of free polarized neutrons at rest:

$$w(\theta, s_e, s_{\bar{\nu}}) = \int \sum_{s_p = \pm 1} |R_{ev}|^2 \, d\Omega_\nu = \pi \eta_{VA,ST} \left\{ 1 \mp \eta_2^{VA,ST} \cdot s_{\bar{\nu}} \frac{v_e}{c} \cos\theta + s_e \left(\eta_2^{VA,ST} \cos\theta \mp s_{\bar{\nu}} \frac{v_e}{c} \right) \right\}. \tag{11}$$

Here θ is the angle between the neutron spin and the electron momentum:

$$\cos\theta = s_n (\mathbf{k}_n^0 \mathbf{k}_e^0) = (s_n \mathbf{k}_e^0);$$

$$\eta_{VA,ST} = |C_{V,S}|^2 + 3|C_{A,T}|^2;$$

$$\eta_2^{VA,ST} = \frac{1}{\eta_{VA,ST}} (2|C_{A,T}|^2 + C_{V,S} C_{A,T}^{+} + C_{V,S}^{+} \cdot C_{A,T}). \tag{12}$$

For the degree of longitudinal polarization of an electron emitted at an angle θ to the neutron spin, we find from (11)

$$P(\theta) = \frac{[w(\theta, s_e, s_{\bar{\nu}})]_{s_e=1} - [w(\theta, s_e, s_{\bar{\nu}})]_{s_e=-1}}{[w(\theta, s_e, s_{\bar{\nu}})]_{s_e=1} + [w(\theta, s_e, s_{\bar{\nu}})]_{s_e=-1}} = \frac{\eta_2^{VA,ST} \cos\theta \mp s_{\bar{\nu}} \frac{v_e}{c}}{1 \mp \eta_2^{VA,ST} \cdot s_{\bar{\nu}} \frac{v_e}{c} \cos\theta}. \tag{13}$$

Summing (11) over the electron spin states (s_e), we arrive at the electron angular distribution

$$w(\theta) = \sum_{s_e = \pm 1} w(\theta, s_e, s_{\bar{\nu}}) = 2\pi \eta_{VA,ST} \left(1 \mp \eta_2^{VA,ST} \cdot s_{\bar{\nu}} \frac{v_e}{c} \cos\theta \right). \tag{14}$$

In Eqs. (11), (13) and (14), the upper sign pertains to V + A coupling, the lower to S + T. An antineutrino with positive helicity is described by $s_{\bar{\nu}} = 1$; one with negative helicity by $s_\nu = -1$.

Present-day data on the decay of polarized neutrons give an electron angular distribution[9] of the form

$$w_{\exp}(\theta) = 1 + a \frac{v_e}{c} \cos\theta, \tag{15}$$

where $a = -0.11 \pm 0.02$ (Ref.8). For the correlation between the antineutrino momentum and the neutron spin the data give

$$w = 1 + b(s_n k_\nu^0), \quad b = +0.88.$$

Taking into account that $\frac{C_{A,T}}{C_{V,S}} = -\lambda$, where $\lambda > 0$ for V - A and S - T coupling and $|\lambda| = 1.2$ (Ref.9), we can conclude from (14) the following:

1) In the case of V + A interaction and an antineutrino with right-handed polarization $(s_{\bar\nu} = 1)$, the coefficient a of the angular correlation between the electron momentum and the neutron spin is

$$a = -\eta_2^{VA} \cdot s_{\bar\nu} = -1;$$

while for an antineutrino with left-handed polarization $(s_{\bar\nu} = -1)$,

$$a = +1.$$

2) In the case of V - A interaction $\left(\frac{C_A}{C_V} = -1.2\right)$ and an antineutrino with $s_{\bar\nu} = 1$, the coefficient $a = -\eta_2^{VA} \cdot s_{\bar\nu} = -0.09$; in the case of an antineutrino with with $s_{\bar\nu} = -1$,

$$a = +0.09.$$

3) For S + T coupling $a = \eta_2^{ST} \cdot s_{\bar\nu} = +1$ for $s_{\bar\nu} = 1$, and $a = -1$ for $s_\nu = -1$.

4) For S - T coupling $a = \eta_2^{ST} \cdot s_{\bar\nu} = 0.09$ for $s_{\bar\nu} = 1$, and $a = -0,09$ for $s_{\bar\nu} = -1$.

From this it is clear that V - A coupling with a positive helicity antineutrino $(s_{\bar\nu} = +1)$ is consistent with the experimental results for the decay of polarized neutrons.

I wish to thank Prof. A.A.Sokolov for helpful discussions.

Moscow State University

References

1. A.Sokolow & B.Kerimow, Ann.Phys., 7, 46 (1958).
2. T.D.Lee & C.N.Yang, Phys.Rev., 104, 254 (1956).
3. T.D.Lee, in Problemy sovr.fiz., No. 1 (1958).
4. J.D.Jackson, S.B.Treiman & H.W.Wyld, Phys.Rev., 106, 517 (1957).
5. A.Sokolov, Atomnaya energiya, 4, 385 (1958). (Trans.Jour. of Atomic Energy); Nucl.Phys., No.9, 420 (1959).
6. R.Feynman & M.Gell-Mann, Phys.Rev., 109, 193 (1958).
7. A.Sokolov, Vvedenie v kvantovuyu elektrodinamiku (Introduction to quantum electrodynamics). M. 1958.
8. M.T.Burgy, V.E.Krohn, T.B.Novey, G.R.Ringo & V.L.Telegdi, Phys.Rev.Letters, 1, 324 (1958).
9. M.T.Burgy, V.E.Krohn, T.B.Novey, G.R.Ringo & V.L.Telegdi, Phys.Rev., 110, 1214 (1958).

PRODUCTION OF ELECTRON-POSITRON PAIRS IN THE COLLISION OF TWO POLARIZED GAMMA-RAYS

- F.S.Sadikhov & B.K.Kerimov

As is known, experiments on nonconservation of parity in weak interactions have demonstrated the occurence of longitudinally (circularly) polarized electrons, positrons and γ-rays in β-decay of nuclei. Longitudinally polarized γ-rays (spin of the γ-ray directed either parallel or antiparallel to its momentum) occur also in the bremsstrahlung of high-energy longitudinally polarized electrons.[1-6] Moreover, there have been obtained from a 1.5 Bev electron synchrotron beams of high energy bremsstrahlung γ-rays ($E\gamma$ = 0.5 to 1 Bev). Thus there is definite interest in the question of electron-positron pair production by the collision both of polarized and of non-polarized γ-rays.

In the present work we use the theory of Dirac particles with oriented spin to calculate the cross section for electron-positron pair production by the collision of two longitudinally polarized γ-rays. We take into account the longitudinal polarization of the resulting electron-positron pair.

The cross section (see Eq.(9)) consists of two parts; the first (σ_0) represents the cross section without the polarization effects; the second (σ_1), the cross section associated with the longitudinal polarization of the γ-rays ($l, l' = \pm 1$), the electron ($s_- = \pm 1$), and the positron ($s_+ = \pm 1$). Equation (9) for σ, with fixed orientation of the γ-ray spins, enables us to consider the dependence of the pair production cross section on the state of longitudinal polarization of the electron and positron.

The Dirac equation, describing the process

$$\gamma + \gamma' \to e_- + e_+, \tag{1}$$

may be written in the form

$$D\psi_2 = \{U(\varkappa) D^{-1} U(\varkappa') + U(\varkappa') D^{-1} U(\varkappa)\}\psi_0, \tag{2}$$

where

$$D = -\frac{\hbar}{i}\cdot\frac{\partial}{\partial t} - \frac{\hbar c}{i}\rho_1(\sigma\vec{\nabla}) - \rho_3 m_0 c^2,$$

and $U(\varkappa)$ and $U(\varkappa')$ are the operators for the interaction of the electrons with γ-rays having momenta $\hbar\vec{\varkappa}$ and $\hbar\vec{\varkappa}'$. The operators are given by the expressions

$$U(\varkappa) = eL^{-3/2}\sqrt{\frac{2\pi c\hbar}{\varkappa}}\rho_1(\vec{\sigma}\,\mathbf{a}_l)\,g_l e^{-ic\varkappa t + i\vec{\varkappa}\vec{r}}$$

and

$$U(\varkappa') = eL^{-3/2}\cdot\sqrt{\frac{2\pi c\hbar}{\varkappa'}}\rho_1(\vec{\sigma}\,\mathbf{a}'_{l'})\,g'_{l'} e^{-ic\varkappa' t + i\vec{\varkappa}'\vec{r}}, \tag{3}$$

where ρ_3, ρ_1, $\vec{\sigma}$ are Dirac matrices; $\mathbf{a}_l \equiv \mathbf{a}_l(\vec{\varkappa})$ and $\mathbf{a}'_{l'} \equiv \mathbf{a}_{l'}(\vec{\varkappa}')$, respectively, are vectors describing the polarization of the γ-rays:

$$\mathbf{a}_l = \frac{1}{\sqrt{2}}\left(\vec{\beta} + il\left[\vec{\varkappa}^0\vec{\beta}\right]\right); \qquad \mathbf{a}'_{l'} = \frac{1}{\sqrt{2}}\left(\vec{\beta} + il'\left[\vec{\varkappa}'^0\vec{\beta}\right]\right); \tag{4}$$
$$l = \pm 1; \qquad l' = \pm 1;$$

$\vec{\beta}$ is a unit vector perpendicular to the momenta of the γ-rays; $\vec{\varkappa}^0 = \frac{\vec{\varkappa}}{\varkappa}$ and $\vec{\varkappa}'^0 = \frac{\vec{\varkappa}'}{\varkappa'}$ are unit vectors along the momenta of the first and second γ-rays, respectively. In the case $l = l' = 1$, we have right-hand polarized γ-rays (spins

parallel to the momenta), and in the case $l = l' = -1$, left-hand polarized (spins antiparallel to the momenta).

The amplitudes $g_l \equiv g_l(\vec{\varkappa})$ and $g'_{l'} \equiv g_{l'}(\vec{\varkappa}')$, connected with the number of γ-rays, satisfy the relations

$$g^+_{l_1} g_l = \delta_{l_1 l}, \qquad g'^+_{l'_1} g'_{l'} = \delta_{l'_1 l'}. \tag{5}$$

The function ψ_0 describes the initial state in which there are no electrons and positrons, and the function ψ_2, the final state in which there is an electron-positron pair. These functions are chosen to have the following form

$$\psi_0 = L^{-3/2} \sum_{\vec{k}} b(\mathbf{k}, s, -1)\, e^{icKt - i\mathbf{kr}};$$
$$\psi_2 = L^{-3/2} \sum_{\vec{k}'} C(\mathbf{k}', s', 1, t)\, b(\mathbf{k}', s', 1)\, e^{-icK't + i\mathbf{kr}}; \tag{6}$$

here $\mathbf{p} = \hbar\mathbf{k}$ and $\mathbf{p}' = \hbar\mathbf{k}'$ are the momenta of the electrons with negative and positive energy respectively, $K = \sqrt{k^2 + k_0^2}$, $K' = \sqrt{k'^2 + k_0^2}$, $k_0 = \frac{m_0 c}{\hbar}$; $b(\mathbf{k}, s, -1)$ and $b(\mathbf{k}', s', 1)$ are Dirac spinor amplitudes for the electrons with negative energy and with positive energy. The quantities $s = \pm 1$ and $s' = \pm 1$ characterize the polarization (spin parallel or antiparallel to the momentum) for the electron with negative energy $(\varepsilon = -1)$ and with positive $(\varepsilon' = 1)$ energy.

By using Eqs.(2)-(6) and by applying the method of separation[9] on the operator we find the following expression for the coefficient $C(\mathbf{k}', s', 1, t)$, which determines the probability for pair formation;

$$C(\mathbf{k}', s', 1, t) = -\frac{2\pi i e^2}{\hbar L^3} \cdot \frac{1}{\varkappa} b^+(\mathbf{k}', s', 1)\, R\, b(\mathbf{k}, s, -1)\, g_l g'_{l'} \cdot \int_0^t e^{-2ic(\varkappa - K)t}\, dt \tag{7}$$

where

$$R = \rho_1(\vec{\sigma}\,\vec{\mathbf{a}}'_{l'}) \frac{\rho_1 \vec{\sigma}(\vec{\varkappa} - \mathbf{k}) + \rho_3 k_0}{-2(K^2 - \mathbf{k}\vec{\varkappa})} \rho_1(\vec{\sigma}\,\vec{\mathbf{a}}_l) + \rho_1(\vec{\sigma}\,\vec{\mathbf{a}}_l) \frac{-\rho_1 \vec{\sigma}(\vec{\varkappa} + \mathbf{k}) + \rho_3 k_0}{-2(K^2 + \mathbf{k}\vec{\varkappa})} \rho_1(\vec{\sigma}\,\vec{\mathbf{a}}'_{l'}).$$

We have used the conservation laws in the center of mass system, namely

$$\vec{\varkappa} + \vec{\varkappa}' = 0; \qquad \varkappa = \varkappa'$$
$$\mathbf{k} + \mathbf{k}' = 0; \quad k = k'; \quad K = K'. \tag{8}$$

We calculate the matrix elements R^+R with the help of Eqs.(21) and (15) of Ref.9, and then set

$$\mathbf{k} = \varepsilon \mathbf{k}_+, \quad \mathbf{k}' = \varepsilon' \mathbf{k}_-, \quad \varepsilon = -\varepsilon' = -1,$$
$$k_+ = k_- = k, \quad s = s_+, \quad s' = s_-.$$

Thus we find the total cross section for the production of a polarized electron-positron pair by the collision of two polarized γ-rays:

$$\sigma = \frac{1}{2N} \cdot \frac{\partial}{\partial t} \sum_{\mathbf{k}'} C^+(\mathbf{k}', s_-, 1, t)\, C(\mathbf{k}', s_-, 1, t) = \sigma_0 + \sigma_1(l, l', s_-, s_+), \tag{9}$$

where

$$\sigma_0 = \frac{\pi}{8}\left(\frac{e^2}{\hbar c}\right)^2 \cdot (F_1 + F_2 - F_3)$$
$$\sigma_1(l, l', s_-, s_+) = \frac{\pi}{8}\left(\frac{e^2}{\hbar c}\right)^2 [ll'(F_1 - F_2) + s_- s_+ \cdot (F_1 - F_2 - F_3 + F_4) +$$
$$+ ll' s_- s_+ (F_1 + F_2 - F_4) + (l + l')(s_- + s_+) F_5].$$

Here $N = \frac{c}{L^3} + \frac{c}{L^3} = \frac{2c}{L^3}$ is the γ-ray flux and

$$F_1 = \frac{2k}{K^3} + \frac{1}{2}\left(\frac{k^2}{K^4} - \frac{1}{K^2}\right)q; \quad F_2 = -\frac{k}{K^3} + \frac{1}{2}\left(\frac{1}{K^2} + \frac{k^2}{K^4}\right)q;$$
$$F_3 = \frac{k(3k_0^2 + 2k^2)}{K^5} + \left(\frac{k^4}{2K^6} + \frac{k^2}{K^4} - \frac{3}{2K^2}\right)q;$$
$$F_4 = \frac{3k_0^2 + 2k^2}{kK^3} + \left(\frac{k^2}{2K^4} + \frac{1}{K^2} - \frac{3}{2k^2}\right)q; \tag{10}$$
$$F_5 = \frac{k^2}{K^4} + \frac{kk_0^2}{2K^5}q; \quad q = \ln\frac{K+k}{K-k}.$$

Here $p_- = p_+ = \hbar k$ is the momentum of the electron (positron). For $s_- = 1$ $(s_+ = 1)$ we have an electron (positron) with right-handed polarization, and for $s_- = -1$ $(s_+ = -1)$, left-handed polarization.

From (9) it follows that the collision of two γ-rays with right $(l = l' = 1)$ or left $(l = l' = -1)$ longitudinal polarization may produce an electron-positron pair with either right-handed $(s_- = s_+ = 1)$ or left-handed $(s_- = s_+ = -1)$ polarization, although with different probabilities. Such collisions, however, are not able to produce an electron with right-handed $(s_- = 1)$ polarization and a positron with left-handed $(s_+ = -1)$ polarization, and conversely $(s_- = -1,\ s_+ = +1)$, since for these events the cross section goes to zero. As follows from Eq.(9), we have the following relations among the pair production cross sections

$$\sigma_{l=l'=1}^{s_-=s_+=1} = \sigma_{l=l'=-1}^{s_-=s_+=-1} = \frac{\pi}{4}\left(\frac{e^2}{\hbar c}\right)^2 \cdot (2F_1 - F_3 + 2F_5);$$
$$\sigma_{l=l'=1}^{s_-=s_+=-1} = \sigma_{l=l'=-1}^{s_-=s_+=1} = \frac{\pi}{4}\left(\frac{e^2}{\hbar c}\right)^2 \cdot (2F_1 - F_3 - 2F_5); \tag{11}$$

$$\sigma_{l=l'=1}^{s_-=-s_+=\pm 1} = \sigma_{l=l'=-1}^{s_-=-s_+=\pm 1} = 0. \tag{12}$$

In the ultra-relativistic case, that is, when $\varkappa \gg k_0, k \gg k_0$, Eq.(9) gives the cross section

$$G_{\text{u-rel}} = \frac{\pi}{4}\left(\frac{e}{\hbar c}\right)^2 \cdot \frac{1}{k^2}\left\{(1 + s_- s_+)\,ll' + \right.$$
$$\left. + (1 - ll')\left[s_- s_+ - (1 - s_- s_+)\cdot\left(\frac{1}{2} - \ln\frac{2k}{k_0}\right)\right] + \frac{1}{2}(s_- + s_+)(l + l')\right\}. \tag{13}$$

This gives the high-energy selection rule, namely, that the collision of two right-longitudinally polarized γ-rays can produce only an electron-positron pair with right-handed polarization, and analogously left-longitudinally polarized γ-rays can only produce a pair with left-handed polarization.

By averaging (9) over the γ-ray spin states and summing over the electron and positron spin states, we find the pair production cross section for the collision of two non-polarized γ-rays:

$$\frac{1}{4}\sum_{l,l',s_-,s_+}\sigma = 4\sigma_0. \tag{14}$$

We wish to thank A.A.Sokolov for his constant interest in the work.

Moscow State University

References

1. M.Goldhaber, L.Grodzins & A.W.Sunyar, Phys.Rev., 109, 1015 (1958).
2. S.Galster & H.Schopper, Phys.Rev.Letters, 1, 330 (1958).
3. A.Bisi & L.Lappa, Phys.Rev.Letters, 1, 332 (1958).
4. B.K.Kerimov & I.M.Nadzhafov, Izv.AN SSSR, Ser.fiz., 22, 886 (1958). (Trans.Bulletin, 22, No.7, 879.)

5. B.K.Kerimov & I.M.Nadzhafov, Nauch.dokl.Vysshei shkoly Ser.fiz.-mat. (College Scientific Reports, Phys -Math Series), 1, 95 (1958).
6. K.W.McVoy, Phys.Rev., 106, 828 (1957).
7. J.DeWire, H.Jackson & R.Littauer, Phys.Rev., 110, 1208 (1958).
8. P.Stein & K.Rogers, Phys.Rev., 110, 1209 (1958).
9. A.Sokolov, Vvedenie v kvantovuyu elektrodinamiku (Introduction to quantum electrodynamics), M. 1958.

Bulletin of the Academy of Sciences of the USSR - Physical Series
Vol. 23, No. 7 - July 1959

Transactions of the Ninth All-Union Conference on Nuclear Spectroscopy
(Continued from Vol.23, No.2; to be continued in Vol.23, No.12)

TABLE OF CONTENTS

	Page Orig.	Trans.
Magnetic alpha-spectrometer - B.S.Dzhelepov, R.B.Ivanov, V.G. Nedovesov & V.G.Chumin	782	780
Alpha-spectrum of U^{233} - B.S.Dzhelepov, R.B.Ivanov, V.G.Nedovesov & B.P.Shishin	788	785
Collective excited states of nuclei - A.S.Davydov	792	788
Conversion electrons from Yb^{166} and Tm^{166} - V.Brabets, K.Ia.Gromov, B.S.Dzhelepov, A.G.Dmitriev & V.A.Morozov	812	805
Gamma-spectrum of Tm^{166} and Yb^{166} - V.I.Baranovskii & V.N.Pokrovskii	819	813
On the decay scheme of Tm^{166} - K.Ia.Gromov, B.S.Dzhelepov & V.N. Pokrovskii	821	815
Gamma-radiation from Cs^{134} - B.S.Dzhelepov, V.P.Prikhodtseva & Iu.V.Khol'nov	826	820
Ta^{182} gamma-radiation in the 300 to 1500 kev region - N.A.Voinova, B.S.Dzhelepov & N.N.Zhukovskii	828	822
Spectra of neutron-deficient Hf isotopes - V.I.Baranovskii & A.V.Kaliamin	831	825
High-energy part of the gamma-spectrum of radium in equilibrium with its decay products (3100-5600 kev) - B.S.Dzhelepov, B.A.Emel'ianov, Iu.N.Podkopaev, V.N.Podymakhin, I.F.Uchevatkin & S.A.Shestopalova	832	826
Investigation of the low-lying levels of Cl^{33} by means of the $S^{32}(p,\gamma)Cl^{33}$ reaction - A.K.Val'ter, V.Iu.Gonchar, A.N.L'vov & S.P.Tsytko	835	829
Elastic scattering and radiative capture of protons by N^{14} - A.K.Val'ter, A.S.Deineko, I.Ia.Malakhov, P.V.Sorokin & A.Ia.Taranov	839	833
Elastic scattering of protons by A^{40} - A.K.Val'ter, I.Ia.Malakhov, P.V.Sorokin & A.Ia.Taranov	846	839
Excited states of Ga^{67} and Ga^{68} - A.K.Val'ter, I.I.Zaliubovskii, V.A.Kliucharev & V.A.Lutsik	849	842
Fine structure of the alpha-spectrum of Th^{229} - G.E.Kocharov, A.P.Komar, G.A.Korolev, I.N.Marov & Iu.A.Surkov	855	847
Conversion electron coincidences in $Se^{75} \rightarrow As^{75}$ decay - V.E.Bunakov, B.S.Dzhelepov, I.Zvol'skii & V.A.Sergienko	859	851
Regarding $Er^{160} \rightarrow Ho^{160}$ and $Yb^{166} \rightarrow Tm^{166}$ transitions - E.P.Grigor'ev, B.S.Dzhelepov & A.V.Solotavin	864	855
Ho^{160} decay and Dy^{160} level diagram - E.P.Grigor'ev, B.S.Dzhelepov, A.V.Zolotavin, B.Kratsik & G.Bitterlikh	868	859
On calculation of the reduced lifetime of nuclei for unique β-transitions - L.N.Zyrianova	875	867
Contribution to the theory of focusing crystal spectrometers (Choice of the reflecting planes) - O.I.Sumbaev	880	871
Angular correlation of the gamma-rays from Ne^{21} - A.G.Khabakhpashev & E.M.Tsenter	883	874
Specific stopping losses in heavy nuclei in different substances - A.P.Grinberg & I.Kh.Lemberg	887	877

Range and specific ionization of multicharged ions - Ia.A.Teplova, V.S.Nikolaev, I.S.Dmitriev & L.N.Fateeva	894	883
Cascade gamma-transitions in Cl^{36} and S^{33}, accompanying thermal neutron capture - V.R.Burmistrov	898	886
Cascade gamma-transitions in Nd^{144} - V.R.Burmistrov	902	890
Contribution to the theory of superfluidity of nucleon gas - Iu.V.Tsekhmistrenko	910	897
Moments of inertia of nuclei - M.Kazarnovskii	912	899
Contribution to the theory of superfluidity of nuclear matter - B.B.Dotsenko	914	901
Statistical theory of the nuclear potential in the "effective mass" approximation - L.Rapoport & S.Kadmenskii	918	905
On beta-decay of neutrons with oriented spin - B.K.Kerimov	924	911
Production of electron-positron pairs in the collision of two polarized gamma-rays - F.S.Sadykhov & B.K.Kerimov	929	915

Translated in 1960 by
Columbia Technical Translations
5 Vermont Avenue, White Plains, N.Y.

Number 8 Volume 23 1959

BULLETIN

of the

ACADEMY OF SCIENCES OF THE USSR

— PHYSICAL SERIES —

(Izvestiya Akademii Nauk SSSR)
(Seriya fizicheskaya)

Reproduction rights reserved
by
Columbia Technical Translations
5 Vermont Avenue
White Plains, New York

Single Issues
$20

Annual Subscription
$215

Transactions

of the

Second All-Union Conference on Gaseous Electronics

(Moscow, October 2-26, 1958)

FORMATION OF A HIGH-FREQUENCY DISCHARGE AT LOW PRESSURES

- G.N.Zastenker & G.S.Solntsev

In most investigations of electric discharges the fundamental characteristic of initiation of the discharge (breakdown) is assumed to be the ignition voltage. From the standpoint of elucidating the elementary processes involved in the development of discharges knowledge of this parameter alone is insufficient. This explains a number of attempts to measure another parameter characterizing the onset of discharges, namely, the discharge formation time. Investigation of the discharge formation time involves observation of the time variation of the various parameters characterizing the state of the discharge gap.

The purpose of the present work was to investigate the formation of high-frequency (3.3 Mc) discharges in argon at pressures from 0.4 to 15 mm Hg.

Apparatus and Procedure

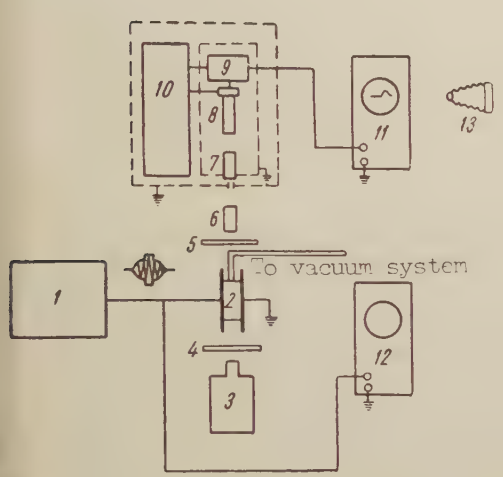

Fig.1. Diagram of the experimental arrangement: 1) hf pulse generator, 2) discharge tube, 3) mercury tube, 4 & 5) light filters, 6 & 7) lenses, 8) photomultiplier, 9) cathode follower, 10) power supply, 11 & 12) oscillographs, 13) camera.

The experimental procedure consisted of applying a high-frequency (hf) voltage of constant amplitude to the discharge gap and observing the ensuing condition of the gas, i.e., recording the integral luminous output by means of an FEU-19 photomultiplier coupled to an oscillograph. The advantage of this procedure is that by means of it one can detect very weak light fluxes, that is, radiation at very early stages in the development of the discharge.

The experimental set-up is diagramed in Fig.1. The discharges were initiated in the cylindrical glass tube 2 mounted between two metallic plates and connected to the vacuum system. The diameter of the tube was 45 mm, its length 22 mm; the electrodes measured 70 mm. The tube was filled with spectroscopically pure argon at different pressures.

The hf pulse generator supplied pedestal type pulses with a rise time of the second step appreciably shorter than the duration of the investigated processes. The amplitude of the preliminary voltage was always lower than that of the ignition voltage under continuous generation conditions. Prior to each series of measurements, we carried out control experiments which showed that the discharge formation time did not depend on the preliminary voltage.

The shape and amplitude of the hf pulses were monitored by means of the I0-4 oscillograph (12), the accuracy of voltage amplitude measurement being 1-3%. The discharge gap was imaged by the lenses 6 & 7 on the cathode of the photomultiplier. The resultant photocurrent pulses displayed on the screen of the I0-4 oscillograph (11) were photographed. The time was measured with reference to the time markers to within 2-5%.

In order to reduce the statistical delay time we used the technique of illuminating the discharge gap by a mercury tube. Tests showed that this illumination had no effect on the magnitude of the ignition voltage and the discharge formation time. The photomultiplier was shielded from the radiation of the mercury tube by appropriate light filters.

A number of measurements were made with simultaneous recording of the discharge current. To this end we used the compensation circuit proposed by Francis[1], which allows of excluding the current due to interelectrode capacitance. The results obtained by both procedures agreed.

The procedure of oscillographic recording of the voltage in the discharge gap, which has been used by most investigators, has the shortcoming that the voltage variation in the discharge gap is a reaction of the generator to changes in load, i.e., depends on the output resistance of the generator at any given instant. In addition, measurement of the voltage across the discharge gap hampers interpretation of the experimental results inasmuch as the development of the discharge occurs under conditions of a varying external field. In the present experiments the variation of the voltage in the process of development of the discharge did not exceed 1-2%.

Initially we used the familiar method based on investigating the dependence of the ignition voltage on the duration of the hf pulse. The instant of initiation of the discharge was determined visually, i.e., from the light output. By this procedure one can roughly evaluate the formation time, but one cannot investigate the development of the discharge and the later stages in which the luminous output is still appreciable.

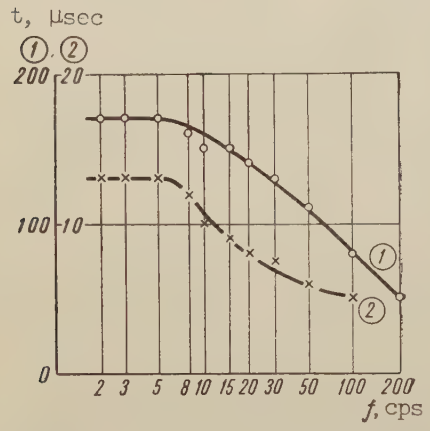

Fig.2. Variation of the discharge formation time with the pulse repetition rate

In carrying out experiments with repeating pulses one must make sure that the development of each successive discharge is not influenced by the preceding discharge, i.e., one must insure that the ionization of the discharge gap between pulses decays to a level no higher than that due to external ionizing factors. In this case each discharge will be a single discharge in contrast to the self-sustaining discharge obtaining at a high pulse repetition rate.

The boundary between these forms of discharge, i.e., the critical repetition rate at which the transition from single to self-sustaining discharges occurs, can be determined experimentally by measuring the formation time as a function of the pulse repetition rate. The formation time at a pressure of 12.3 mm Hg decreases with increasing repetition rate above 6 pps (Fig.2) which indicates that at rates above 6 pps the development of each succeeding discharge is influenced by the preceding one. At lower repetition rates, we have true single discharges. We determined the critical repetition rate at each pressure in a similar manner. The appreciable duration of the discharge gap de-ionization time is apparently explained by processes occurring on the surface of the glass.

Results

Typical discharge luminance oscillograms are shown in Fig.3. The discharge formation time may be divided into three stages: a weak current stage (AB in Fig.3,a) during which the light intensity lies below the photomultiplier response threshold, a strong current stage (BC) during which the instruments record rapid build up of the light output and discharge current, and a luminance decay stage (CD) which precedes the steady-state discharge.

At low pressures there is a monotonic increase of the luminous output up to a certain constant level corresponding to a steady-state discharge. At high pressures the decrease in luminance is the more pronounced, the higher the gas pressure.

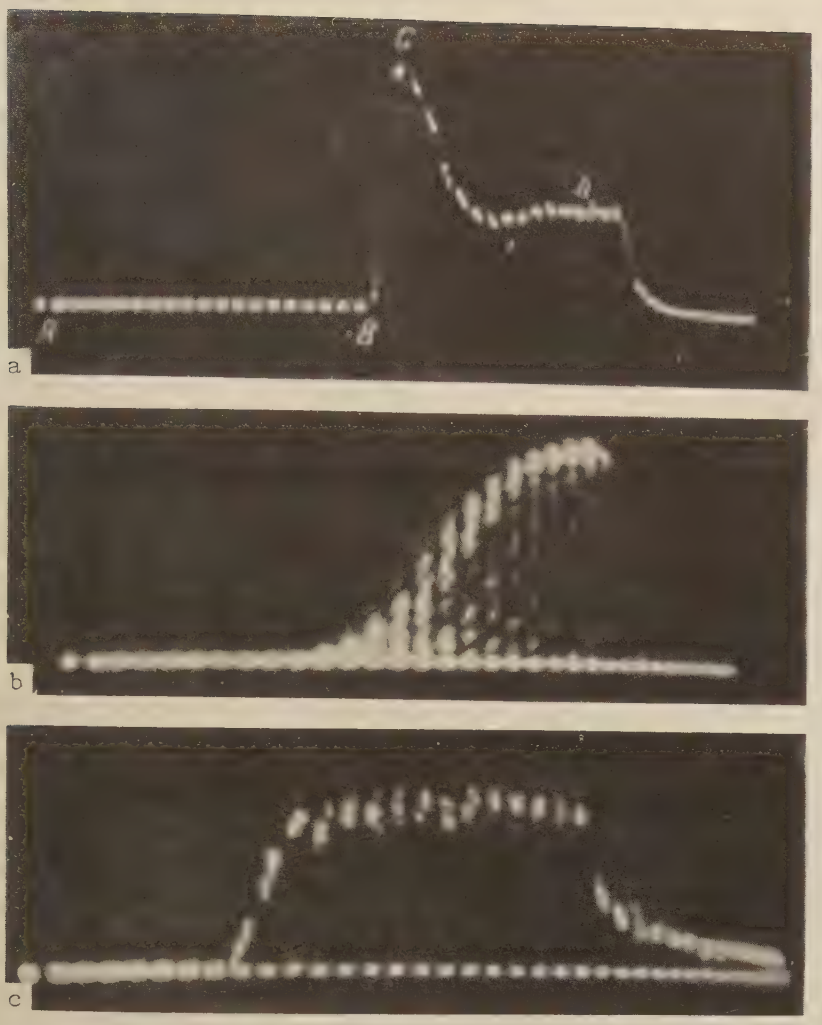

Fig.3. Oscillograms of discharge luminance output: a) single pulse, p = 9.6 mm Hg, overvoltage W = 39.5%, time markers - 10 μsec; b) 100 light pulses; same conditions as in a but time markers - 1 μsec; c) single pulse, p = 2.6 mm Hg, W = 5%, time markers - 10 μsec.

In investigating the development of discharges an important problem is distinguishing between the statistical delay time and the formation time (i.e., the time from appearance of a free electron to attainment of the steady-state discharge). The experimental difficulty here lies in the fact that the initial discharge formation stages cannot be recorded by the measuring equipment and hence observations yield an apparent increase of the statistical delay time (i.e., an underestimate of the discharge formation time). To get around this difficulty we photographed on a single frame a sufficiently high number (100 voltage pulses) of oscillograms of the radiation build up in the discharge (Fig.3,b). The time interval from the beginning of the sweep to appreciable deviation of the trace corresponds to development of the discharge with very small statistical delays, i.e., is the formation time (weak current stage).

As in other types of electric discharges, the formation time of an hf discharge at low pressures depends on the overvoltage. It will be seen from Fig.4 that the luminance build-up time, i.e., the time from beginning of development of the discharge to the instant of attainment of maximum luminous output, decreases with increase of the voltage above the ignition level under continuous generation conditions. The decrease is greatest for the duration of the weak current stage. The duration of the luminance decay stage, on the other hand, does not depend on the amplitude of the voltage applied to the discharge gap. The results show that the duration of the weak current stage is determined primarily by the external field applied to the discharge gap, i.e., that space charges play no significant role in the development of the discharge during this initial stage. The fact that the duration of the luminance decay stage is independent of the overvoltage together with the absence of this stage in the case of low pressures are evidence that this stage is connected with rearrangement of the space (and, possibly, surface) charges.

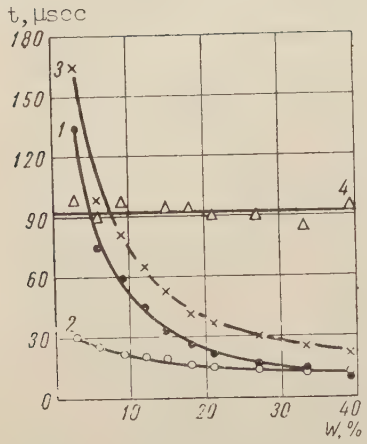

Fig.4

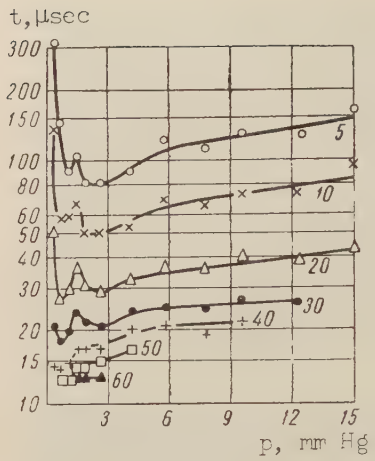

Fig.5

Fig.4. Different stages of discharge formation depending on the overvoltage, p = 9.6 mm Hg: 1) weak current stage, 2) strong current stage, 3) build up of luminous output to a maximum, 4) decay of luminous output.

Fig.5. Variation of luminance build-up time with the pressure at different overvoltages (as indicated in percent at the curves).

The results of measurements at different pressures and with different overvoltages are shown in Fig.5. The pressure dependence of the formation time proved to be similar to the pressure dependence of the ignition voltage. The right hand (high pressure) minimum in the curve occurs at the same pressure as the minimum in the Paschen curve. In addition, there is a second minimum (at lower pressures), the depth of which increases with increase of the overvoltage. This minimum is apparently due to the same factors as the second minimum in the Paschen curve for hydrogen, i.e., can be explained by increase in the relative contribution of electron drift as compared with diffusion[2,3].

Discussion

For the purpose of interpreting the experimental results we carried out approximate calculations of the formation time. The variation in electron concentration in an hf discharge at low pressure is given by the equation[4,5]

$$\frac{\partial n}{\partial t} = (\nu_i - \nu_{rem}) \cdot n \qquad (1)$$

where n is the electron concentration, ν_i is the mean ionization frequency, and ν_{rem} is the mean frequency of removal or elimination of electrons from the discharge region. If, following Golant[5] and Madan et al[6], we assume that ν_i and ν_{rem} do not depend on n and the coordinates in the discharge region and that further they do not vary with time, we can write

$$n = n_0 \exp[(\nu_i - \nu_{rem})\, t]. \qquad (2)$$

The assumption that ν_i and ν_{rem} do not vary with time is supported by the experimental fact that under our conditions the light flux does not fluctuate at the frequency 2ω.

In argon for $\omega \ll \nu_c$ one can use the "constant current analogy" method[4]. In this case the mean ionization frequency is found as

$$\nu_i = \alpha v_d, \qquad (3)$$

where α is the first Townsend coefficient and v_d is the electron drift velocity. Instead of the field strength used in the dc case, one can introduce an effective field $E_{eff} = E_o/\sqrt{2}$, where E_o is the crest value of the hf field.

Under our conditions $\nu_c = 10^{10}$ sec^{-1} and $\omega = 2 \cdot 10^7$ sec^{-1}; hence, using Eq. (3), we can calculate the mean ionization frequency from the data for α (Ref.7) and for a directional electron speed in argon (Ref.8).

The mean electron removal frequency can be found from experimental data on the pressure dependence of the discharge ignition voltage under continuous generation conditions. At the breakdown voltage

$$\frac{\partial n}{\partial t} = (\nu_i - \nu_{rem})\, n = 0. \tag{4}$$

If the electron removal mechanism includes diffusion as well as departure of electrons due to drift, which is taken into account by choice of the diffusion length in the discharge gap[2,3], then for a given E/p, we can write

$$\nu_{rem} \cdot p = \text{const}. \tag{5}$$

From (4) and (5), we obtain

$$\nu_i - \nu_{rem} = \nu_i \left(1 - \frac{p_2^2}{p_1^2}\right), \tag{6}$$

here p_1 is the pressure for which ν_{rem} is determined and p_2 is the pressure at which $\nu_i = \nu_{rem}$ for the given E/p.

From (2) and (5), we find that the time required for attaining a given concentration n_k is given by

$$t = \frac{\ln \frac{n_k}{n_0}}{\nu_i \left(1 - \frac{p_2^2}{p_1^2}\right)}. \tag{7}$$

It follows from the experimental data that for pressures in the region of the right branch of the Paschen curve the growth in luminous output is exponential. Deviation from the exponential law to the side of slower growth begins to be evident upon approach to the maximum. From the oscillograms one can determine the interval from the instant of beginning of discharge formation to the instant of deviation of the luminance build-up from the exponential law (i.e., the exponential growth time) and then compare it with the time to attainment of a given concentration calculated by means of Eq. (7).

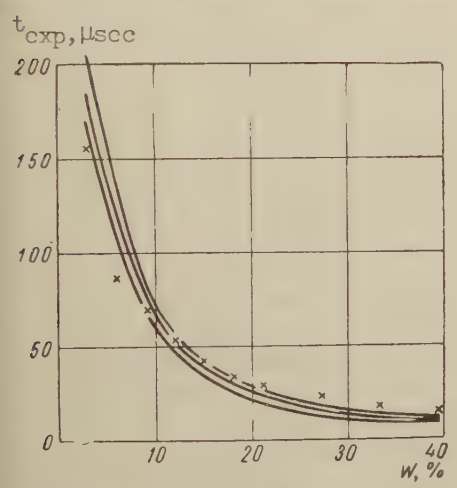

Fig.6. Duration of exponential growth of luminous intensity: p = 9.6 mm Hg. Calculated curves: upper - $n_k/n_0 = 10^{10}$, middle - $n_k/n_0 = 10^9$, lower - $n_k/n_0 = 10^8$; crosses experimental data.

The experimental and calculated data for a pressure of 9.6 mm Hg are compared in Fig.6. The simple theory correctly predicts the variation of the exponential growth time with the overvoltage. The calculated luminance built-up times differ little with variation of n_k/n_0 in the range from 10^8 to 10^{10}. A similar comparison carried out for a pressure of 15.1 mm Hg also showed satisfactory agreement between the calculated and experimental data. Unfortunately, there are no data on the directional velocity of electrons in argon at lower pressures. Moreover, near the minimum in the Paschen curve and in the region of its left branch, the electron oscillation amplitude becomes large and hence the equation based on diffusional removal becomes inapplicable.

It must be noted that the assumption that ν_i and ν_{rem} do not vary with time is not valid at high concentrations in the later stages of development of the discharge. First, space charges and charges on the tube walls build up, which leads to transition from free electron diffusion to ambipolar diffusion. Second, there occurs a redistribution of the field in the discharge gap so that the field in the central part decreases and, consequently, so does the effective ionization coefficient.

However, variations of ν_i and ν_{rem} with increase of n have opposite effects on the build up time. Moreover, a substantial change in these coefficients is evinced only for $n \approx 10^8$-10^9 cm^{-3}, i.e., only at the end of the formation time. Consequently, the exponential luminance build-up time does not change greatly compared with that calculated by the simple law, which explains the fairly good agreement of theory with experiment (Fig.6).

Conclusions

1. The developed experimental procedure is suitable for investigating the time variation of different parameters of a high-frequency discharge (the voltage on the gap, the discharge current and the luminous output of the gas) in the process of its formation.

2. The formation time of an hf discharge at low pressure (in the range of our experimental conditions) varies from 300 to 10 microsec with variation of the overvoltage from 5 to 60%.

3. The pressure dependence of the discharge formation time is similar to the pressure dependence of the ignition (breakdown) voltage.

4. Theoretical calculation of the duration of the initial stage of discharge development, during which the role of space charge is minimal, yields satisfactory agreement with the experimental data for pressures exceeding 9 mm Hg.

Physics Faculty,
Moscow State University

References

1. G.Francis, Proc.Phys.Soc.B., 68, 137 (1955).
2. T.Kihara, Revs.Mod.Phys., 24, 45 (1952).
3. S.M.Levitskii, Zhur.tekh.fiz., 27, 970 (1957). (Trans.Soviet Phys. - Tech.Phys.)
4. V.E.Golant, Usp.fiz.nauk, 65, 39 (1958).
5. V.E.Golant, Zhur.tekh.fiz., 27, 756 (1957). (Trans.Soviet Physics - Tech.Phys.)
6. M.P.Madan, E.I.Gordon, S.J.Buchsbaum & S.C.Brown, Phys.Rev., 106, 839 (1957).
7. A.A.Kruithoff & E.Penning, Physica, 4, 430 (1937).
8. J.S.Townsend & V.A.Baily, Phil.Mag, 44, 1033 (1922).

INVESTIGATION OF A SELF-SUSTAINING SUPER-HIGH FREQUENCY PULSE DISCHARGE IN AIR AND ITS INITIATION PROCESS

- P.S.Bulkin, G.S.Solntsev & V.N.Ponomarev

Introduction

There are two types of super-high frequency (shf) discharge: 1) single pulse discharges, all the processes in which are characterized by parameters having values within the pulse duration, i.e., in the range from 0 to τ_{sec}, and 2) self-sustaining discharges, which are commonly understood to be "steady", periodically repeating discharges in which all the processes within each pulse repeat.

In investigating the formation of shf pulse discharges one must distinguish between the process of formation of the discharge during the pulse under steady conditions and establishment of these conditions, i.e., attainment of the self-sustaining discharge state.

Most investigations[1-8] in the field have had as their purpose measurement of the breakdown field strength (or power) and the discharge lag time. In the present work our aim was to develop a procedure for investigating the processes involved in the formation of a shf pulse discharge in air at a frequency of 9400 Mc in the pressure range from 0.1 to 40 mm Hg.

1. Formation of a self-sustaining discharge during the pulse

Our experimental arrangement enabled us to 1) determine the variation in amplitude of the reflected wave in the waveguide (the discharge acts as an abrupt termination), 2) investigate the time variation of the linear dimensions of the discharge by means of an image converter (IC), and 3) investigate the light emission from any part of the discharge by means of a photomultiplier (PM).

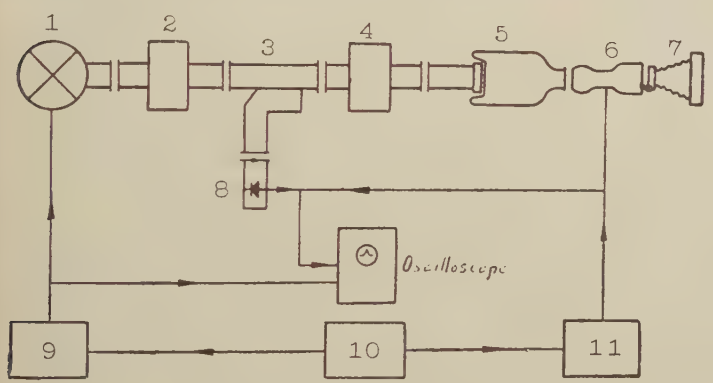

Fig.1. Block diagram of experimental set-up: 1) magnetron, 2) power divider, 3) directional coupler, 4) matcher, 5) discharge tube, 6) image converter tube, 7) camera, 8) detector head, 9) 26-I trigger generator, 10) GIS-1 sync pulse generator, 11) high-voltage pulse generator.

The discharges occured on the flat bottom of a glass discharge tube held in intimate contact with a flange of the waveguide. This arrangement provided for better observation of the development of the discharge as compared with sparking in the waveguide. The discharge could be observed from three mutually perpendicular directions through two windows in the walls of the tube. These windows also admitted the radiation of a PRK-4 mercury tube which served to reduce the statistical delays.

A block diagram of the experimental arrangement is shown in Fig.1. The operation of the unit was synchronized by pulses from the GIS-1 generator (10 in Fig.1). This supplied pulses to the 26-I generator driving the magnetron and pulses with a variable delay for triggering the high-voltage square pulses (0.3 to 1 μsec duration) for controlling the IC.

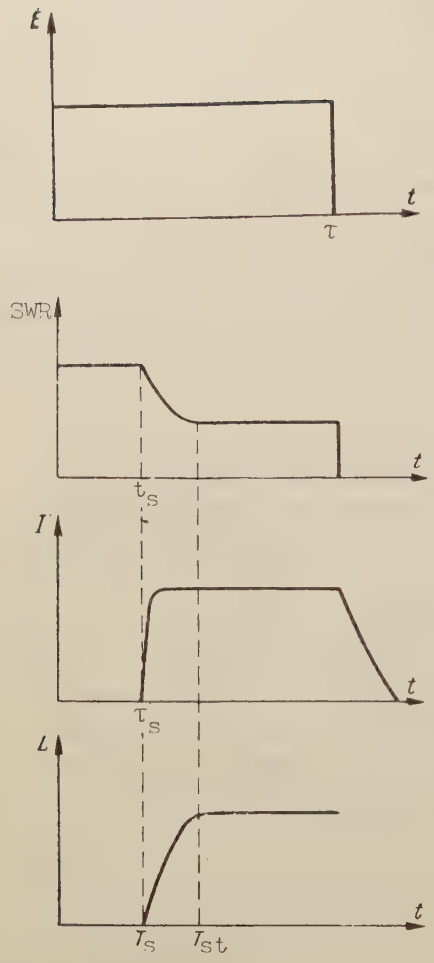

Fig.2. Time variation of the pulse field strength E, standing-wave ratio SWR, luminous intensity I at the center of the discharge and the linear dimensions L of the discharge.

A similar set-up was used in investigating the luminous emission of the discharge, except that the emitted light was recorded by means of an FEU--19 photomultiplier with a cathode follower. In this case the region of the discharge (cross section area ~5 mm^2) characterized by the maximum field strength was focused on the photocathode.

The appearance of the luminance oscillograms depends on the frequency of the shf pulses. At low repetition frequencies a statistical delay is observed within the pulse. At high frequencies there are virtually no delays. Our measurements were carried out at frequencies for which no delays were discernible. Upon the application of an shf pulse, there is at first an interval with no detectable light emission. There then follows a sharp growth in luminous output (Fig.2). The instant of sharp increase in luminosity coincides with the instant t_s of beginning of shorting of the waveguide as indicated by a sharp change in the standing-wave ratio. The local light intensity, after build up to a certain level, remains virtually constant to the end of the pulse.

At the instant t_s there appears on the IC screen a small spot at the point in the image corresponding to the maximum strength of the shf field (Fig.3,a). The dimensions of the luminous spot increase with time. The discharge expands in the plane normal to the waveguide axis. The linear growth of the discharge may either cease within the pulse or may continue to the very end of the pulse (Fig.3,b).

On the basis of measurements of photographs of the IC screen we plotted the time variation of the linear dimensions of the discharge in two mutually perpendicular directions; the resultant curves are shown in Fig.4. At low pressures the discharge dimensions quickly attain a maximum value and thereafter remain constant (Fig.4,a); at high pressures, after the instant t_s and initial rapid increase in the dimensions, there follows a period of slower growth which continues to the end of the pulse (Fig.4,b).

2. Establishment of a self-sustaining discharge

In studying the establishment of a self-sustaining discharge, we used a circuit by means of which we could repeatedly reproduce the process of transition to the steady state. Basically the set-up was similar to that described above. The principal difference was that in this case the driving generator produced groups of pulses, i.e., pulse packets. The packet repetition rate was 50 pps. The interval between pulses within a packet could be varied from 0.1 to 70 μsec. The number of pulses per packet could be varied but was usually 5. As before, the pulse packets triggered the magnetron through the 26-I generator.

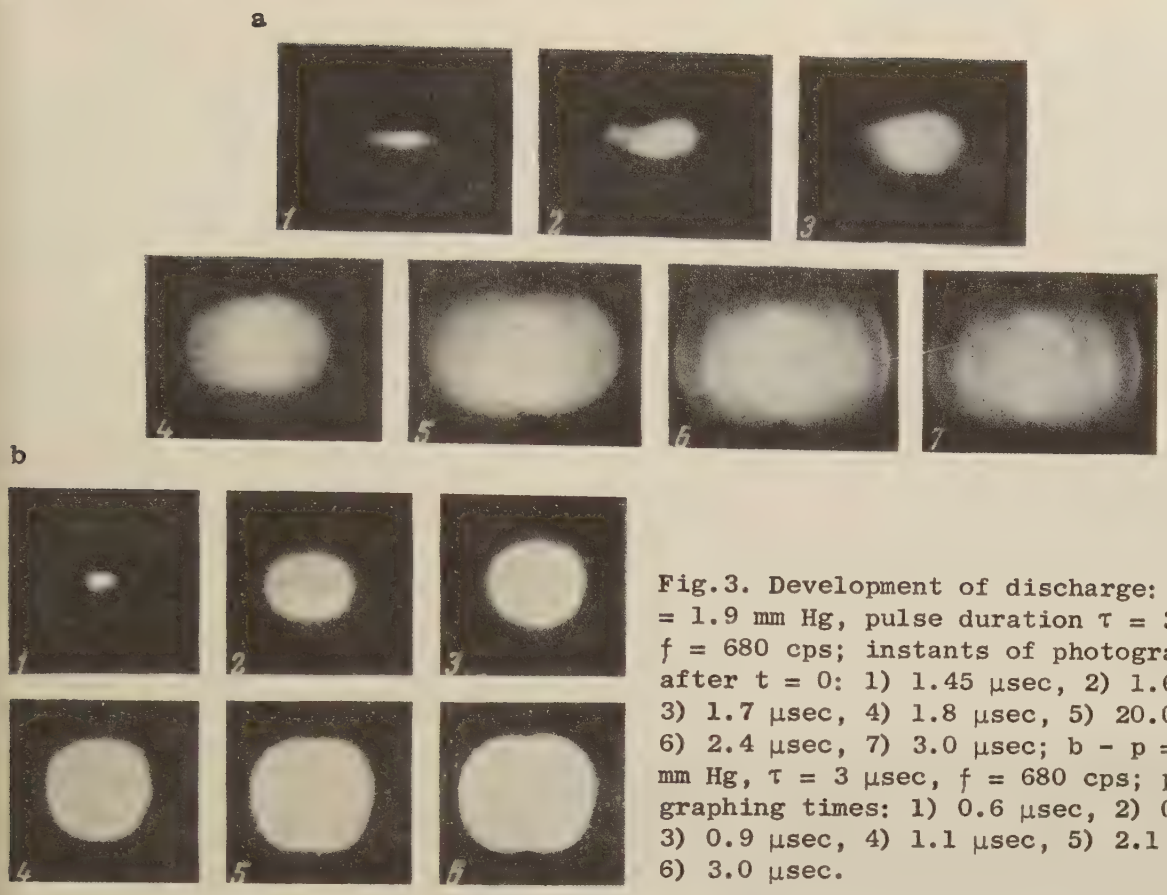

Fig.3. Development of discharge: a - p = = 1.9 mm Hg, pulse duration τ = 3 μsec, f = 680 cps; instants of photographing after t = 0: 1) 1.45 μsec, 2) 1.6 μsec, 3) 1.7 μsec, 4) 1.8 μsec, 5) 20.0 μsec, 6) 2.4 μsec, 7) 3.0 μsec; b - p = 25.4 mm Hg, τ = 3 μsec, f = 680 cps; photographing times: 1) 0.6 μsec, 2) 0.7 μsec, 3) 0.9 μsec, 4) 1.1 μsec, 5) 2.1 μsec, 6) 3.0 μsec.

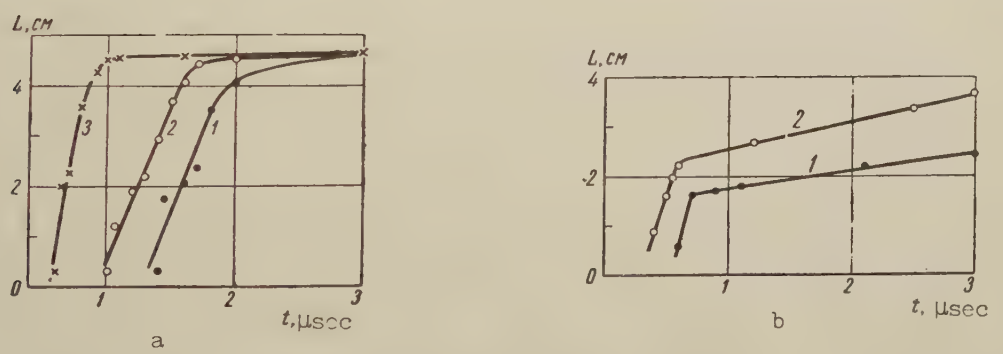

Fig.4. Time variation of the linear dimensions of discharges at different overvoltages K: a - p = 1.9 mm Hg: 1) K = 106%, 2) 111%, 3) 120%; b - 25.4 mm Hg: 1) K = 112%, 2) 147%.

The luminous output of the discharge was recorded oscillographically. Specifically, we observed the integral variation in luminous intensity owing to variation of local brightness and in the dimensions of the discharge. Since there is statistical variation in the light intensity corresponding to each pulse, in the experiments we recorded the maximum luminance.

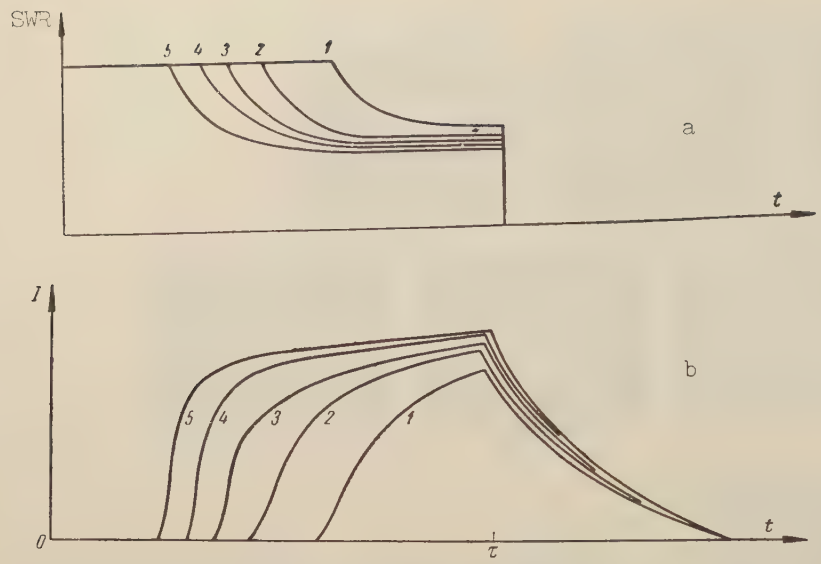

Fig.5. Variation of the standing-wave ratio and luminous intensity with time during five successive pulses of a packet.

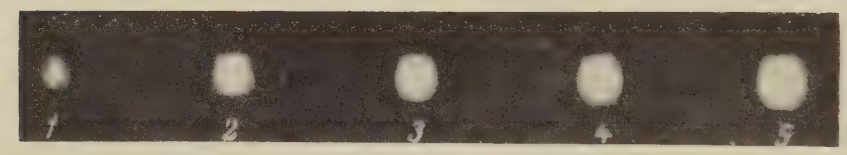

Fig.6. Photographs of a discharge during successive pulses of a five-pulse packet.

We also observed the variation in the amplitude of the reflected wave. Further, the increase in the dimensions of the discharge from pulse to pulse was also recorded by motion picture photography (SKS-1 camera with continuous film motion).

The experiments showed that a self-sustaining discharge is not always established within a single pulse. Actually, the transient period may extend over an appreciable number of pulses. The luminous output oscillograms for five successive pulses are superimposed in Fig.5,b. It will be evident that in each succeeding pulse the luminous output increases without repeating the initial growth exhibited in the preceding pulse.

It will also be evident from similar oscillograms (Fig.5,a), characterizing the amplitude of the reflected wave, that the time to beginning of shorting of the waveguide decreases from pulse to pulse. This means that the "shorting" electron concentration is attained more rapidly in each succeeding pulse.

High speed photography showed that the dimensions of the discharge increase with each succeeding pulse of a packet (Fig.6).

We also investigated the variation in the growth of the luminous amplitudes as a function of the pressure, overvoltage and pulse repetition rate or interval between pulses in a packet. Fig.7 shows the light output amplitude in each of five pulses of a packet for different pressures and intervals between pulses. In these measurements the amplitude of the shf field was maintained constant for each given pressure.

With decrease of the pulse separation, the luminance of succeeding pulses increases more rapidly and the number of pulses to establishment of a self-sustaining discharge is reduced. The time to establishment of a self-sustaining discharge also decreases with decreasing pressure. Obviously, the amplitude of the first light flash at any given pressure does not depend on the interval between the shf pulses.

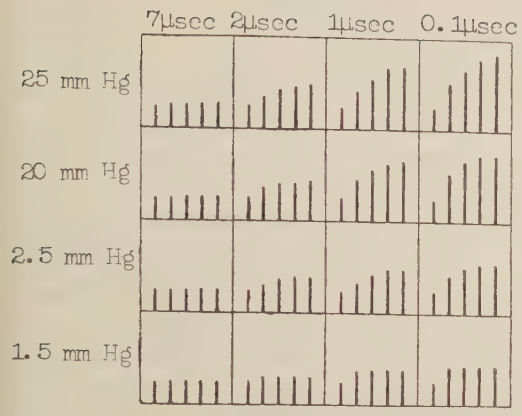

Fig.7. Variation of the luminous amplitude in each pulse of a packet as a function of the pressure and interval between succeeding pulses.

3. Discussion

In the case of discharges with dc voltage or CW high-frequency oscillations, the discharge formation time is generally understood to be the time from the instant of application of the voltage to attainment of a steady discharge (excluding statistical delays). In the case of a pulsed field, however, the discharge may not attain a steady condition during the period of the first pulse. Hence one cannot speak of the formation time in the same sense as in the case of CW generation.

By detecting the reflected wave one can determine the instant t_s of beginning of noticeable short-circuiting of the waveguide. The measured time will naturally depend on the sensitivity of the reflected wave detector, but t_s is not explicitly correlated with the variation in the dimensions of the discharge. A noticeable change in the standing-wave ratio depends not only on the electron concentration as such but also on the size of the region in which this concentration is sufficiently high to cause reflection.

By detecting the local light output at the point of the maximum shf field one can measure the time τ_s to the beginning of detectable light emission (see Fig.2). Obviously, the results will depend on the sensitivity of the photomultiplier and the size of the region focused on the PM cathode.

In observing the dimensions of the discharge by means of an IC, the instant T_s of appearance of luminous emission is determined from the intersection of the discharge growth curve with the time axis. From the same plot one can determine the instant T_{st} of an abrupt change in the rate of growth of the discharge (see Fig.2).

The measured values of t_s, τ_s and T_s proved to be equal within the limits of the experimental error. In view of this it may be asserted that the process of development of a discharge within a pulse can be characterized by two parameters: a) the time from the beginning of the pulse to the instant $t_s = \tau_s = T_s$, as determined by any one of the procedures described above; in the physical sense this interval corresponds to the time of attainment of a local steady state: actually, formation of a "plasma plug" which prevents further development of the discharge in the direction of propagation of the electromagnetic wave; b) the time from the beginning of the pulse to the instant T_{st} corresponding to attainment of a steady state in the entire region occupied by the discharge; this time can be measured by means of an IC or a reflected wave detector. These two times are the basic characteristics of the development of the discharge; one can take either one or the other as the discharge formation time, depending on the preferred definition and the practical purposes involved.

The development of a discharge during a pulse may be said to consist of three stages.

The first stage consists in growth of the electron concentration at the point of maximum strength of the shf field, from zero concentration to 10^9-10^{10} cm^{-3}.[7] The duration of this stage can be determined by any of the three procedures outlined above (within the investigated pressure range).

The second stage is marked by a rapid increase in the dimensions of the discharge, which can be observed by means of an IC. The rate of growth of the linear dimensions of the discharge in the plane perpendicular to the waveguide axis is $\sim 10^7$ cm/sec. This stage is associated with distortion of the shf field by the "plasma plug". The fact that the rate of discharge growth varies little with changes in pressure can be understood only if one takes into account both the behavior of the ionization coefficient and the distortion of the shf field.

The third stage is characterized by a slower rate of growth of the dimensions of the discharge. At low pressures (1-5 mm Hg), this growth is virtually nil. At pressures from 20 to 40 mm Hg, the rate of growth may attain 10^5-10^6 cm/sec. The fact that such growth is observed only at higher pressures gives reason to infer that it is connected with increase in the temperature of the neutral gas in the discharge region. This inference is substantiated by the intense heating of the surfaces in contact with the discharge at high pressures.

In the case of a series of shf pulses, the first pulse, obviously, acts as an independent single pulse. The formation of the discharge in the first pulse begins under conditions that are independent of the pulse repetition frequency. Consequently, all processes during the first pulse must occur in the same way as in the formation of a single pulse discharge.

The development of the discharge under the influence of succeeding pulses, in addition to the factors influencing the formation of a single pulse discharge, will be affected by processes occurring during the interval between pulses, primarily by the residual electron concentration. The entire sequence terminates in the establishment of a self-sustaining pulse discharge. Consequently, the establishment process may be regarded as a transition from a single pulse discharge to a self-sustaining discharge. The influence of the preceding pulse on the succeeding pulse consists in modification of the "initial" conditions for the given succeeding pulse, i.e., increasing the initial electron concentration and altering its spatial distribution. This obviously influences the rate of formation of the discharge.

The higher the initial concentration, the more quickly is the instant of beginning of short-circuiting of the waveguide attained. Obviously, at the same time the intervals between the beginning of the pulse and the appearance of a detectable light output and between the beginning of the pulse and noticeable distortion of the field, i.e., to the second and third discharge stages, are reduced. Consequently, the size of the discharge increases with each succeeding pulse up to the steady state.

With increase of the intervals between pulses the residual electron concentration increases and the transition to a self-sustaining discharge occurs earlier. Increase of the overvoltage has a similar boosting effect on the residual concentration.

Inasmuch as the residual electron concentration is connected with the "de-electronization" coefficient, i.e., the rate of disappearance of electrons, the duration of the transition period must obviously depend on the pressure. The rate of "de-electronization" increases with increasing pressure. Hence other conditions (overvoltage, repetition frequency, etc.) being equal, the time to establishment of a self-sustaining discharge decreases with increasing pressure.

Conclusions

1. We developed a procedure for comprehensive investigation of the formation of super-high frequency pulse discharges by recording the variation of the standing-wave ratio, the local luminous output and the dimensions of the discharge. The three experimental procedures yield consistent results.

2. We established the existence of three stages in the development of a self-sustaining super-high frequency discharge in air at pressures from 1 to 40 mm Hg.

3. Through experiments with pulse packets, we found that the build-up to the steady self-sustaining discharge state may extend over several pulses, the number depending on the pressure, overvoltage and pulse repetition rate.

Physics Faculty
Moscow State University

References

1. D.Q.Posin, Phys.Rev., 73, 496 (1948).
2. R.Cooper, Proc.IEE, 94, III, 315 (1947).
3. V.E.Mitsuk, G.S.Solntsev, M.Z.Khokhlov, P.S.Bulkin & G.N.Zastenker, Radiotekhnika i elektronika, 3, 698 (1958). (Trans.Radio Eng. & Electronics.)
4. M.Z.Khokhlov, P.S.Bulkin, V.E.Mitsuk & T.F.Taskaeva, Ibid., 3, 304 (1958).
5. P.S.Bulkin & M.Z.Khokhlov, Ibid., 3, 806 (1958).
6. G.S.Solntsev & G.N.Zastenker, Ibid., 3, 811 (1958).
7. L.W.Roberts & L.Gould, J.Appl.Phys., 27, 1164 (1956).
8. V.E.Golant, Usp.fiz.nauk, 65, 39 (1958).
9. W.A.Prouse, Proc.IEE, 99, IV, 194 (1952).

MEASUREMENT OF THE CHARGE CONCENTRATION IN PLASMA BY MEANS OF SUPER-HIGH FREQUENCY PROBES

- S.M.Levitskii & I.P.Shashurin

Within the last decade significant advances have been made in the investigation of gas discharges, owing to the introduction of a new microwave method, namely, the resonant cavity method.[1] Without detracting from the recognized merits of this method, we want to mention some of its disadvantages.

1. To employ the resonant cavity method, the design of the discharge tube must be adapted to the design of the cavity, which may not always be possible or convenient.

2. In its simplest variant the method allows only of measuring relatively low electron concentrations ($\sim 10^9$ cm^{-3}).[2] The method yields only the average charge concentration for the volume in which the plasma interacts with the microwave field.

3. Use of the interferometric method[3] which is based on free transmission of radiowaves through the plasma, largely eliminates the first two shortcomings, but in this case, too, the electron concentration obtained is an average value.

For local measurement of plasma parameters one can hardly propose any method not based on the introduction of some type of probe into the plasma. In order to retain the advantages of the microwave methods and at the same time obtain local values of charge concentration, the introduced probe must be an shf oscillating system with a locally concentrated electric field penetrating to a limited extent into the surrounding plasma. By immersing such a system into the discharge and observing its behavior one can judge of the charge concentration in its vicinity.

By way of shf probes one can use such oscillating systems as various types of symmetrical and asymmetrical dipoles, a two-conductor (twin) line, etc. One should, naturally, give preference to systems in which the electric field is more concentrated and which are characterized by low emission.

In our work we used an asymmetrical dipole and a twin line.

1. Asymmetrical dipole

In the asymmetrical dipole arrangement (Fig.1,a) the oscillating system was a section of conductor 1 having a length of 27 mm and a diameter of 0.8 mm. It was mounted normal to the metallic disk 2 of comparatively large diameter. This disk also served as the anode of the discharge tube. The tube was filled with saturated mercury vapor. When a discharge was realized between the disk anode and the heavy oxide coated cathode 3, the dipole was surrounded by plasma.

The dipole was excited through the coaxial feeder 4, which in turn was coupled with the waveguide 5 and excited by the mode propagated in the waveguide. Matching of the feeder and waveguide was accomplished by adjusting the two pistons 6. The waveguide was coupled to a generator through a measuring line, which was decoupled from the generator by a 20 db attenuator.

The measurements were carried out in the range from 8 to 13 cm, the wavelength being measured by a wavemeter. The temperature of the tube walls was maintained at 50-60°. The electron concentration in the discharge was measured by the cylindrical probe[7].

With the system matched, the standing-wave pattern in the waveguide was strongly dependent on the operation of the dipole. Any change in the charge concentration in the plasma surrounding the dipole led to a significant change of both the standing-wave ratio and the position of the nodes in the measuring line.

Thus our problem reduced to measurement of the input impedance of the dipole. If we think of our asymmetrical dipole as a uniform line immersed in a medium

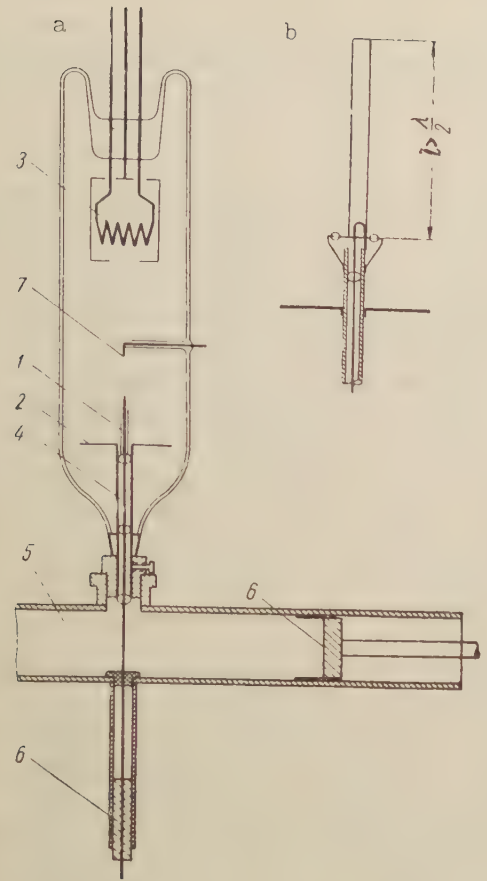

Fig.1. a) Design of experimental tube, shf asymmetrical dipole probe and associated excitation system; b) design of shf probe in the form of a section of two-conductor line.

with a dielectric constant ε, its input reactance, i.e., its input impedance neglecting resistive loss, will be given by[4]

$$X_{in} = -\frac{W_1}{\sqrt{\varepsilon}} \operatorname{ctg} \alpha_1 l \sqrt{\varepsilon}, \qquad (1)$$

where l is the length of the dipole, W_1 is the characteristic impedance of the line and α_1 is the propagation constant with $\varepsilon = 1$.

Having determined ε from Eq.(1), we can find the charge concentration in the plasma by means of the familiar expression

$$\varepsilon = 1 - \frac{4\pi e^2 n_e}{m\omega^2} \qquad (2)$$

(under the conditions of our experiment $\nu^2 \ll \omega^2$).

The measuring line yielded the values of the impedance only for the cross section at its output flange. Hence we had to represent the section of the system from the line flange to the feeder output as a two-terminal pair network, determine the parameters of this network and then convert the impedance values accordingly.[5]

The measurement results for a wavelength of 10 cm are shown in Fig.2, together with the curves calculated by means of Eqs.(1) and (2). The discontinuity of the function occurs at $\varepsilon = 0$. As will be seen from the figure, in the experiment this point is obtained at higher discharge intensities than follows from calculation.

Simultaneously with measurement of the input impedance of the dipole, we investigated its emissivity. To this end a receiving antenna was mounted at some distance from the tube and the power intercepted by it measured.

When the dielectric constant of the plasma in the vicinity of the dipole drops to zero, the effective electrical length of the dipole should also become zero and its emission should cease. This effect was observed experimentally, but complete cessation of detectable emission occurred, as a rule, at electron concentrations somewhat higher than indicated by Eq.(2).

In analyzing the operation of the vertical dipole as a microwave probe it must be noted that it does not fully satisfy the requirements set for such a system. The dimensions of the region occupied by the electric field of the dipole are of the order of magnitude of the length of the dipole which amounts to approximately 1/3 the tube diameter. Hence in the given case one can speak of local measurements only in an approximate sense.

2. Twin line

The arrangement in which the shf oscillating system was a section of two-conductor line (Fig.1,b) proved to be more convenient from the practical standpoint. The diameter of the conductors was 0.8 mm, the separation between their center lines 3.5 mm. Both ends of the line section were shorted. The geometric

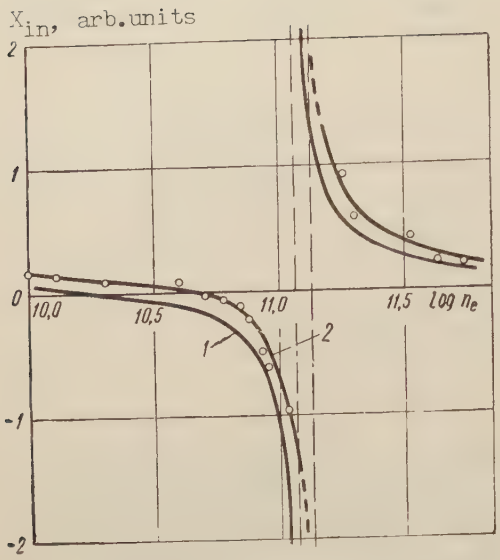

Fig.2. Variation of the input impedance of the asymmetrical dipole with the electron concentration in the plasma. λ = 10 cm. 1 - calculated curve; 2 - experimental curve.

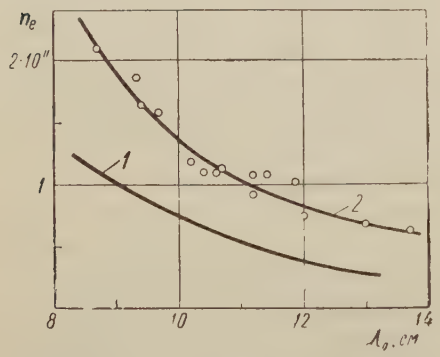

Fig.3. Variation of the electron concentration with the wavelength at which resonance of the twin line probe was observed: 1) calculated curve, 2) electron concentration measured by means of a Langmuir cylindrical probe.

length of the section was greater than the half-wavelength of the exciting mode.

The line was excited inductively from a small loop terminating the coaxial feeder. In other respects the arrangement (tube and shf circuit) was identical with that described above. The twin line was insulated from the anode and feeder by two glass beads and in the plasma acquired the corresponding wall potential.

With increase of the electron density in the plasma surrounding the probe the electrical length of the line, $l_{el} = l\sqrt{\varepsilon}$, decreased and at some value of the electron concentration became equal to the half-wavelength. At this point resonance occurred; this was enhanced by marked absorption of rf energy from the waveguide and a radical change in the standing-wave pattern. The instant of resonance could readily be detected by the sharp swing of the instrument connected to the line.

The results of measurement are shown in Fig.3. The lower curve corresponds to values of the electron concentration determined by observation of resonance; the upper curve to values obtained by means of conventional cylindrical probe. It will be evident that the shf probe technique yields consistently lower charge concentration values. Similar results were obtained in tests with 3 cm waves. The divergence can be explained by assuming that, owing to the presence of wall potential, a space charge layer forms about the line conductors.

Further, according to current concepts, under the space charge layer there should be a so-called transition layer with a lower electron concentration.[6] The thickness of this layer is unknown, but it is probably greater than the thickness of the space charge layer proper. In any case the plasma in the vicinity of the twin line is impoverished in electrons as compared with the undisturbed plasma. Presumably this is the reason for our low concentration values.

Summarizing the results of the experiments, it may be concluded that the attempt to measure the local concentration of electrons by the introduction of an shf oscillating system into the plasma is justified in principle. So far the measurement results are distorted by ionic layers forming on the surface of the probe. If these distorting effects can be minimized or taken into account by means of an appropriate correction, we will have a new microwave technique for investigating plasmas, a technique which has virtually all the advantages of the resonant cavity method, is no more complicated than this method and at the same time is free of the shortcomings listed at the beginning of this report.

We desire to express our sincere gratitude to Prof.N.D.Morgulis for his interest in the work and for discussion of the results.

Electronics Faculty
Kiev State University

References

1. M.D.Raizer & I.S.Shpigel', Usp.fiz.nauk, 64, 641 (1958).
2. S.J.Buchsbaum & S.C.Brown, Phys.Rev., 106, 196 (1957).
3. R.F.Whitmer, Phys.Rev., 104, 572 (1956).
4. B.P.Aseev, Osnovy radiotekhniki (Basic Radio Engineering), p.243, M., 1947.
5. Spravochnik po volnovodam (Waveguide Handbook), p.135, M., 1952.
6. A.Guthrie & R.Wakerling, Characteristics of Electrical Discharges in Magnetic Fields, N.Y., 1949.

INITIATION OF SUPER-HIGH FREQUENCY PULSE DISCHARGES IN INERT GASES

- V.E.Golant

It has been shown[1-4] that the condition for microwave gas discharge breakdown is usually attainment of a certain critical value of the mean ionization frequency:

$$\nu_i = \nu_{i.cr}. \tag{1}$$

This critical ionization frequency depends on the pulse duration τ and the initial electron concentration. For initiation of a self-sustaining discharge under the influence of periodically repeating microwave pulses

$$\nu_{i.cr} = \nu_r' \frac{T}{\tau}, \tag{2}$$

where ν_r' is the mean frequency of loss or removal of electrons during the period T between pulses (it is assumed that this frequency remains constant over the entire interval T).*

If the variation of ν_i with the field amplitude is known, one can calculate the critical field E_{cr} for shf pulse discharge breakdown by means of Eq.(1).

The writer has previously carried out such calculations for argon[3,4] and neon[5] wherein the E dependence of ν_i was determined by means of the electron energy distribution function. In the case of helium one can utilize the E dependence of ν_i found by Reder & Brown.[6] In the present report we give the results of calculation of ν_i for two other inert gases, namely, krypton and xenon. On the basis of these results we evaluate E_{cr} for shf pulse discharges in inert gases and compare the deduced values with experimental data.

Calculation of the mean ionization frequency for krypton and xenon

In order to calculate the electron velocity distribution function one must first deduce the analytic expression for the energy dependence of the electron-atom collision cross section. We shall use the following approximations for the momentum transfer cross section s^* in krypton and xenon:

$$\left.\begin{array}{ll} \text{for } x > 1 & s^* = \dfrac{s_0}{\sqrt{x}}; \\ \text{for } 1 > x > x_0 & s^* = s_0 x; \\ \text{for } x < x_0 & s^* = a - b\sqrt{x}. \end{array}\right\} \tag{3}$$

Here $x = U/U_0$, eU is the electron energy, U_0 is the lowest atomic level excitation potential ($U_{0\,Kr}$ = 9.9 v and $U_{0\,Xe}$ = 8.3 v), N is the atomic concentration and p is the gas pressure.

As will be evident from Fig.1, the assumed approximation is consistent with the experimental dependences for electron energies under 20-30 ev. For example,

for Kr: $\frac{Ns_0}{p}$ = 90 (cm·mm Hg)$^{-1}$, x_0 = 0.05, $\frac{Na}{p}$ = 10, and $\frac{Nb}{p}$ = 24.5 (cm·mm Hg)$^{-1}$;

---

*More accurately, the condition for hf pulse discharge breakdown is described by $\nu_i - \nu_r = \nu_{i.cr}$ (here ν_r is the mean electron removal frequency). However, in the case of pulses of short duration $\nu_r \ll \nu_i$ and hence electron removal processes can be neglected.

for Xe: $\frac{Ns_0}{p} = 125$ (cm·mm Hg)$^{-1}$, $x_0 = 0.08$, $\frac{Na}{p} = 45$, $\frac{Nb}{p} = 123$ (cm·mm Hg)$^{-1}$.

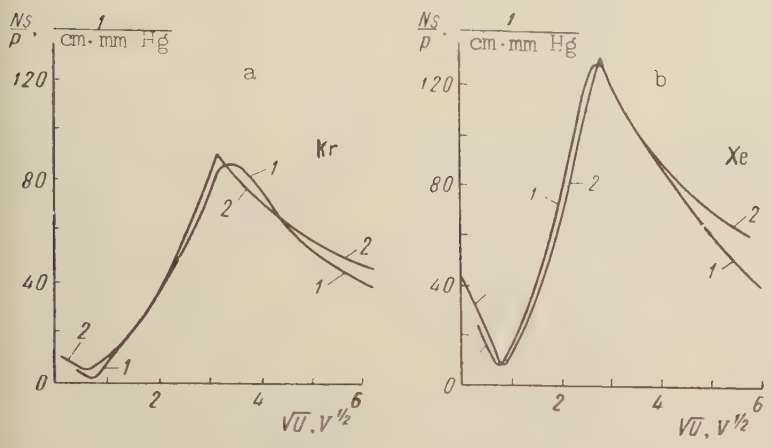

Fig.1. 1) Curve obtained from the results of measurement of the total cross section and angular distribution of scattered electrons[7], 2) approximating curve.

Unfortunately, we do not have experimental data on the total inelastic collision cross section (s_{in}) and the ionization cross section (s_i) in krypton and xenon. In view of the fact that the energy dependences of these cross sections near the excitation and ionization potentials appear to be nearly the same for different gases, below we shall use the same approximations for these dependences as were chosen earlier for argon[3], namely,

$$s_{in} = s_{0\,in} x^{1/2}(x-1); \qquad (4)$$

$$s_i = s_{0i}\left(\frac{U}{U_i} - 1\right), \qquad (5)$$

where U_i is the ionization potential (14.0 v for Kr and 12.1 v for Xe). The parameters $s_{0\,in}$ and s_{0i} in (4) and (5) are not known so far. By means of Eqs.(3)-(5) one can, however, construct and integrate the kinetic equation for the electron velocity distribution function.

Proceeding as we did earlier for argon[3] and making similar assumptions, we obtain the following expressions for the isotropic component of the electron distribution function $f_0(x)$:

$$\left.\begin{aligned}
&\text{for } x > 1 \qquad f_0(x) = Ax^{-3/4}(x-1)^{1/2}K_{1/3}\left[\frac{2}{3}\sqrt{\beta}\,(x-1)^{3/2}\right];\\
&\text{for } 1 > x > x_0 \quad f_0(x) = Bx - \frac{1}{2}\frac{B\xi}{x^2} + C;\\
&\text{for } x < x_0 \qquad f_0(x) = D(a\ln x - 2b\sqrt{x}) - D\xi\left(\frac{1}{ax} + \frac{2b}{a^2x^{1/2}} - \right.\\
&\qquad\qquad \left. - \frac{2b^2}{a^3}\ln\frac{\sqrt{x}}{a - b\sqrt{x}}\right) + G.
\end{aligned}\right\} \qquad (6)$$

Here

$$\beta = \frac{3}{2}\frac{U_0^2}{\left(\frac{E}{p}\right)^2}\left(\frac{Ns_0}{p}\right)\left(\frac{Ns_{0\,in}}{p}\right)(1+\xi);\ \xi = \frac{\left(\frac{\omega}{p}\right)^2}{v_0\left(\frac{Ns_0}{p}\right)}, \qquad (7)$$

$\omega = 2\pi\nu$ is the radian frequency, $v_0 = \left(\frac{2eU_0}{m}\right)^{1/2}$; A, B, C, D and G are constant coefficients which are determined by equating $f_0(x)$ and $f_0'(x)$ for $x = 1$ and $x = x_0$.

The mean ionization frequency is then calculated in the usual manner:

$$\frac{\nu_i}{p} = \frac{Ns_{0i}}{p}v_0\frac{\int_{x_0}^{\infty}\left(x\frac{U_0}{U_i} - 1\right)xf_0(x)\,dx}{\int_0^{\infty}x^{1/2}f_0(x)\,dx} \cdot \left(x_i = \frac{U_i}{U_0}\right). \qquad (8)$$

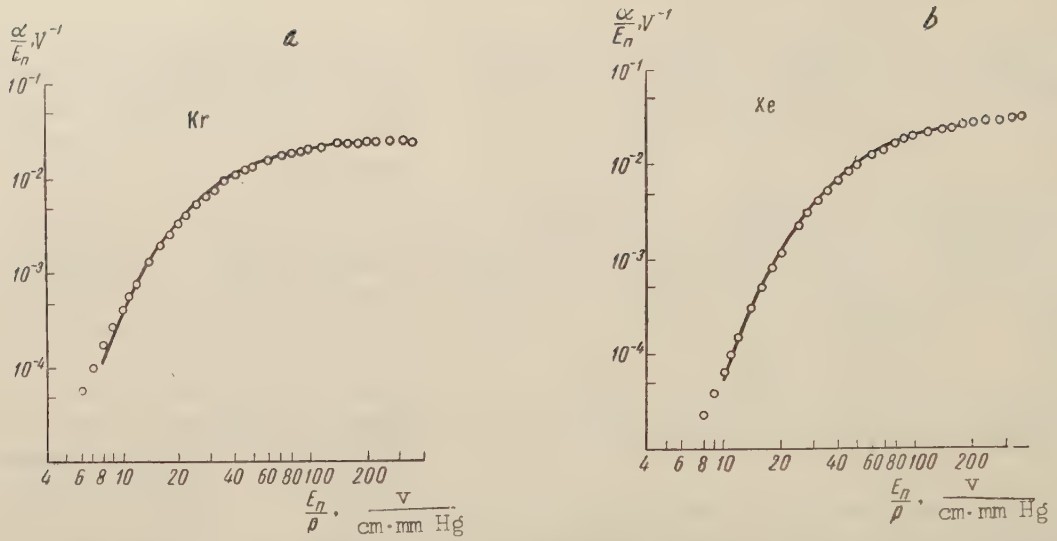

Fig.2. Comparison of the calculated curve and the experimental points from Ref.8.

Eq.(8) contains the two still undetermined parameters $s_{0\,in}$ and $s_{0\,i}$. Let us evaluate these parameters on the basis of Kruithof's experimental data[8] on the ionization coefficient α (first Townsend coefficient) for krypton and xenon atoms in a dc field.

From the deduced expressions for the isotropic component of the electron distribution in an shf field, one can readily determine the distribution function in a dc field.[1] To this end we need only set $\omega = 0$, i.e., $\xi = 0$ in Eqs.(6) and (7) and replace the microwave field by an equivalent effective dc field $E_e = E/\sqrt{2}$. Then by means of Eq.(8) we can find ν_i/p in a dc field and then determine the ionization coefficient

$$\frac{\alpha}{E_e} = \frac{\nu_i}{\mu E_e^2}. \tag{9}$$

Here μ is the mobility, which can be determined by means of the distribution function

$$\mu p = \frac{2}{3}\frac{e}{mv_0}\frac{\int_0^\infty f_0(x)\frac{d}{dx}\left(x \Big/ \frac{Ns^*}{p}\right)dx}{\int_0^\infty x^{1/2} f_0(x)\,dx}. \tag{10}$$

Recalling (7), we find from (9) the variation of α as a function of $s_{0\,in}$ and s_{0i} :

$$\frac{\alpha}{E_e} = \frac{s_{0i}}{s_{0\,in}}\varphi(\beta) = \frac{s_{0i}}{s_{0\,in}}\varphi\left[k\frac{Ns_{0\,in}}{p}\Big/\left(\frac{E_e}{p}\right)^2\right]; \tag{11}$$

$\varphi(\beta)$ is a now known function, and k is independent of E_e/p, $s_{0\,in}$ and s_{0i}.

Plotting the α/E_e vs E_e/p curve in logarithmic coordinates and fitting it to the experimental curve by appropriate choice of the origin, we can readily find the scale factors in (11) and hence $\frac{Ns_{0\,in}}{p}$ and $\frac{s_{0i}}{s_{0\,in}}$. Proceeding in this manner, we obtain the following values for the parameters:

for Kr $\frac{Ns_{0\,in}}{p} = 2.0 \pm 0.2$; $\frac{Ns_{0\,i}}{p} = 2.8 \pm 0.3$ $\frac{1}{cm \cdot mm\ Hg}$;

for Xe $\frac{Ns_{0\,in}}{p} = 3.0 \pm 0.3$; $\frac{Ns_{0\,i}}{p} = 3.6 \pm 0.4$ $\frac{1}{cm \cdot mm\ Hg}$.

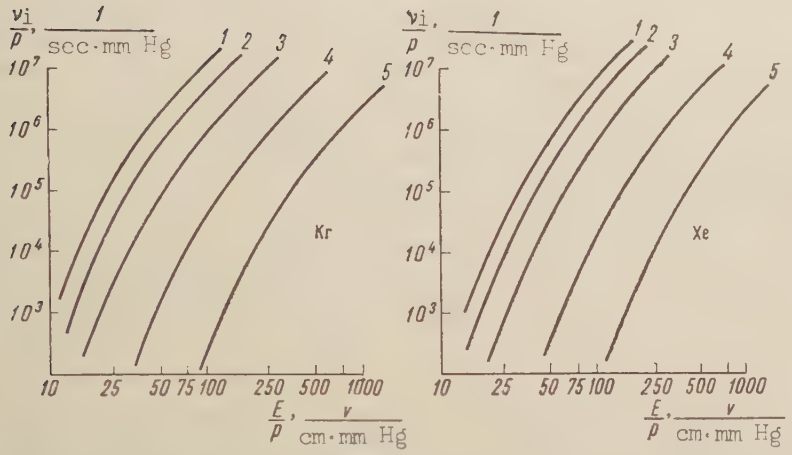

Fig.3. Kr: 1 — $\frac{\nu}{p} = 0$, 2 — $\frac{\nu}{p} = 1 \cdot 10^9$, 3 — $\frac{\nu}{p} = 2.5 \cdot 10^9$, 4 — $\frac{\nu}{p} = 7 \cdot 10^9$, 5 — $\frac{\nu}{p} = 2 \cdot 10^{10}$; Xe: 1 — $\frac{\nu}{p} = 0$, 2 — $\frac{\nu}{p} = 1.25 \cdot 10^9$, 3 — $\frac{\nu}{p} = 3.12 \cdot 10^9$, 4 — $\frac{\nu}{p} = 8.85 \cdot 10^9$, 5 — $\frac{\nu}{p} = 2.5 \cdot 10^{10}$

The calculated and experimental curves for α/E_e vs E_e/p are shown in Fig.2. It will be noted that the character of the curves does not depend on the values of the parameters. Hence the good agreement of the curves substantiates our calculations.

Having determined $s_{0\,i}$ and $s_{0\,in}$, we can return to Eqs.(6)-(8) and calculate the mean ionization frequency in a microwave field. The results of such calculations for several values of ν/p are shown in Fig.3.

Critical field strength for shf pulse discharge breakdown

As was noted above, the critical field strength is calculated from Eq.(1) in which the value of ν_i is determined by means of the electron energy distribution function. The results of such calculations for helium, neon, argon, krypton and xenon are shown in Fig.4 in the form of E_{cr}/ν vs p/ν curves for several values of $\nu_{i.cr}/\nu$.

For comparison, we also show in Fig.4 the experimental points based on the data obtained by Abramova and the writer[9]. These data (•1) pertain to initiation of a self-sustaining pulse discharge in the absence of a stable source of initial electrons. The discharges were realized in a glass tube with an inside diameter of ~4 mm and a discharge gap of 10 mm. The measurements were carried out at a frequency of 9400 Mc; the pulse duration was 10^{-6} sec, the pulse repetition rate 400 pps. The experimental conditions and procedure were similar to those described in Ref.4.

In addition, we also show the data obtained for neon and argon in earlier measurements at a frequency of 2800 Mc.[4,5] Comparison shows a systematic divergence between the calculated and experimental curves, indicating a consistent increase of $\nu_{i.cr}$ with decrease of p/ν. The divergence is particularly great for xenon and helium.

According to Eq.(2), variation of $\nu_{i.cr}$ should be connected with variation of the electron removal frequency ν_r'. If diffusion plays a significant role in the elimination of electrons during the interval between pulses, increase of ν_r' with decreasing pressure may be expected.

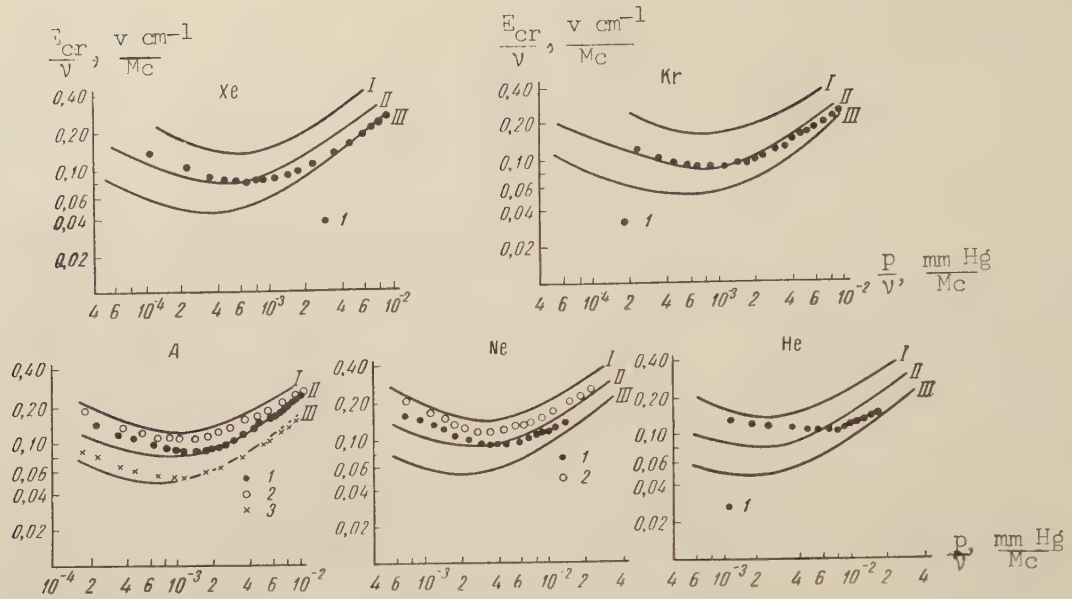

Fig.4. Calculated curves: I - $\frac{\nu_{i.cr}}{\nu} = 9.6 \cdot 10^{-3}$, II - $2.4 \cdot 10^{3}$, III - $5.4 \cdot 10^{-4}$.

Experimental points: 1 - ν = 9400 Mc, τ = 1 μsec, 1/T = 400 cps (based on data of Ref.9); 2 - ν = 2800 Mc, τ = 1 μsec, 1/T = 400 cps (Refs.4 & 5); 3 - ν = 9400 Mc, τ = 1.1 μsec (Ref.9; in the presence of a stable source of initial electron).

The divergence between the experimental and calculated curves may also be partially due to other factors, namely, the influence of diffusion in the process of discharge formation during pulses* (see Ref.9), inaccuracies in the assumed cross section approximations and the errors involved in the approximations made in integrating the kinetic equation.[1,3]

For resolving the question of the conditions determining shf pulse discharge breakdown in different cases, it would be desirable to carry out an experimental investigation in which the electron concentration would be measured in the process of discharge formation both during the pulses and in the intervals between pulses. The most suitable procedure for measurement of electron concentrations would appear to be the microwave cavity method employed by Madan et al[10].

"M. I. Kalinin" Leningrad Polytechnic Institute

References

1. V.E.Golant, Usp.fiz.nauk, 65, 39 (1958).
2. L.Gould & L.W.Roberts, J.Appl.Phys., 27, 1162 (1956).
3. V.E.Golant, Zhur.tekh.fiz.,27,756 (1957). (Trans.Soviet Phys.-Tech.Physics).
4. V.E.Golant, Ibid., 27, 771 (1957).
5. V.E.Golant, Ibid., 27, 1482 (1957).
6. F.H.Reder & S.C.Brown, Phys.Rev., 95, 885 (1954).
7. H.S.W.Massey & E.H.S.Burhop, Electronic and Ionic Impact Phenomena, Oxford, 1952. (Cited in Russian trans.)
8. A.A.Kruithof, Physica, 7, 519 (1940).
9. T.S.Abramova & V.E.Golant, Zhur.tekh.fiz.,28,1096(1958).(Trans.Soviet Phys. - Tech.Physics.)
10. M.P.Madan, E.I.Gordon, S.J.Buchsbaum & S.C.Brown,Phys.Rev.,106,839(1957).

*The influence of electron loss by diffusion during the pulse was not taken into account in our calculations.

CORRELATION BETWEEN THE CHARACTERISTICS OF SUPER-HIGH FREQUENCY AND DIRECT CURRENTS IN GASES

- V.E.Golant

A number of authors[1-4] have noted that under certain conditions one can establish a correlation between the characteristics of super-high frequency (shf) and direct currents in gases. This correlation has been utilized[5-8] for analysis of electric breakdown in shf fields. In an earlier contribution[4] the writer called this method of treating high frequency (hf) current in gases the "dc analogy" method. In the present paper we formulate the conditions under which one can establish a correlation between the characteristics of direct and shf currents in a gas and give examples of how this correlation can be utilized.

1. The electron velocity distribution function in an shf field can be written as the sum of the isotropic and directed components.[3] The isotropic component does not vary significantly with time within an interval comparable with the field period, provided the radian frequency ω is much greater than the "energy variation frequency":

$$\omega \gg \frac{m}{M}\nu_c \qquad (1)$$

here m and M are the masses of an electron and atom, and ν_c is the electron-atom collision frequency.

If this condition is satisfied, the kinetic equation for the isotropic component of the electron velocity distribution function $f_0(v)$ may be written in the form[3]

$$\frac{\partial (nf_0)}{dt} - \frac{v^2}{3\nu_c^*}\nabla^2(nf_0) - \frac{1}{3v^2}\frac{\partial}{\partial v}\left\{\left[\frac{a^2}{2\left[1+\left(\frac{\omega}{\nu_c^*}\right)^2\right]} + a_{sc}^2\right]\frac{v^2}{\nu_c^*}\frac{\partial (nf_0)}{\partial v}\right\} - \frac{v}{3\nu_c^*}\frac{\partial (nf_0)}{\partial v}\nabla \mathbf{a}_{sc} - \mathbf{a}_{sc}\nabla\left[\frac{v}{3\nu_c^*}\frac{\partial (nf_0)}{\partial v} + \frac{1}{3v^2}\frac{\partial}{\partial v}\left(\frac{v^3}{\nu_c^*}nf_0\right)\right] = \frac{\delta (nf_0)}{\delta t}. \qquad (2)$$

(the influence of the space charge field on the electron distribution function is taken into account in the above equation).

In Eq.(2) n is the electron concentration, $\nu_c^* = vNs^*$, N is the atomic concentration, s^* is the stopping collision cross section, $\mathbf{a} = \frac{e\mathbf{E}}{m}$; $\mathbf{a}_{sc} = \frac{e\mathbf{E}_{sc}}{m}$; $\mathbf{E}$ is the hf field amplitude, $\mathbf{E}_{sc}$ is the space charge field and $\frac{\delta (nf_0)}{\delta t}$ is the rate of change of nf_0 owing to electron collisions.

In a dc field the isotropic component of the distribution function is given by[3]

$$\frac{\partial (nf_0)}{dt} - \frac{v^2}{3\nu_c^*}\nabla^2(nf_0) - \frac{1}{3v^2}(\mathbf{a}_n + \mathbf{a}_{sc})^2\frac{\partial}{\partial v}\left[\frac{v^2}{\nu_c^*}\frac{\partial (nf_0)}{\partial v}\right] - \frac{v}{3\nu_c^*}\frac{\partial (nf_0)}{\partial v}\nabla \mathbf{a}_{sc} - (\mathbf{a}_{sc}+\mathbf{a}_n)\nabla\left[\frac{v}{3\nu_c^*}\frac{\partial (nf_0)}{\partial v} + \frac{1}{3v^2}\frac{\partial}{\partial v}\left(\frac{v^3}{\nu_c^*}nf_0\right)\right] = \frac{\delta (nf_0)}{\delta t}, \qquad (3)$$

wherein $\mathbf{a}_n = \frac{e\mathbf{E}_n}{m}$; $\mathbf{E}_n$ being the external electric field.

By comparing (2) and (3) we can determine the conditions under which the isotropic components of the electron velocity distribution functions in dc and hf fields coincide (the frequency of the hf field is assumed to be limited by condition (1). These conditions can be written as follows:

1) $\mathbf{E}_{\text{п}}\nabla(nf_0) = 0$; (4)

2) $\mathbf{E}_{\text{п}} \cdot \mathbf{E}_{\text{sc}} = 0$; (5)

3) $E_{\text{п}}^2 = \frac{1}{2}\frac{E^2}{1+\left(\frac{\omega}{\nu_c^*}\right)^2} = E_{\text{eff}}^2$; (6)

4) the shape of the current region and the boundary conditions in both cases must be the same.

The first condition means that electron diffusion in the direction of the dc field is negligible, or, at any rate, does not significantly affect the distribution function. In cases when the space charge is due solely to diffusion, the first and second conditions become identical (inasmuch as $\mathbf{E}_{\text{sc}} \parallel \nabla(nf_0)$).

The third condition must be fulfilled regardless of the electron velocity and coordinates. Hence coincidence of the distribution functions is possible only for gases in which ν_c^* is virtually independent of the electron velocity or under conditions when $\nu_c^{*2} \gg \omega^2$.

When the conditions formulated above are fulfilled, we can introduce, in accord with (6), an effective hf field $\mathbf{E}_{\text{eff}}$ characterized by an electron energy distribution equivalent to that obtaining in a dc field.

2. Conditions for identity of the isotropic components of the distribution function in dc and hf fields can also be obtained for the current in the presence of a constant magnetic field. Comparison of the corresponding equations for (these equations taking into account a magnetic field can be deduced following Allis[3]) leads to the following conditions for identity of the electron energy distribution functions in dc and hf fields:*

$$\mathbf{E}_{\text{п}\parallel}\nabla(nf_0) = 0;\ \mathbf{E}_{\text{п}\perp}\nabla(nf_0) = 0;\ [\mathbf{E}_{\text{п}\perp} \times \nabla_\perp(nf_0)]_\parallel = 0; \tag{7}$$

$$\mathbf{E}_{\text{п}\parallel} \cdot \mathbf{E}_{\text{sc}\parallel} = 0;\ \mathbf{E}_{\text{п}\perp} \cdot \mathbf{E}_{\text{sc}\perp} = 0; \tag{8}$$

$$\nabla\mathbf{E}_{\text{п}\parallel} = 0;\ \nabla\mathbf{E}_{\text{п}\perp} = 0; \tag{9}$$

$$E_{\text{п}\parallel}^2 + \frac{E_{\text{п}\perp}^2}{1+\left(\frac{\omega_H}{\nu_c^*}\right)^2} = \frac{1}{2}\frac{E_\parallel^2}{1+\left(\frac{\omega}{\nu_c^*}\right)^2} + \frac{1}{4}\frac{E_\perp^2}{1+\left(\frac{\omega-\omega_H}{\nu_c^*}\right)^2} + \frac{1}{4}\frac{E_\perp^2}{1+\left(\frac{\omega+\omega_H}{\nu_c^*}\right)^2}. \tag{10}$$

here $\omega_H = \frac{eH}{mc}$; H is the magnetic field strength and c is the velocity of light; the indices $\parallel$ and $\perp$ denote vector components parallel and perpendicular to the magnetic field, respectively.

Equality (10), as before, must obtain regardless of the electron velocity and coordinates. We note that the more complicated character of conditions (7)-(10), as compared with (4)-(6) is due to the anisotropy of the electronic conductivity and diffusion of electrons in the presence of a magnetic field.

Conditions (7)-(9) for $\mathbf{E}_{\text{п}} \parallel \mathbf{H}$ reduce to the requirements $\nabla(nf_0) \perp \mathbf{H}$ and $\mathbf{E}_{\text{sc}} \perp \mathbf{H}$ (i.e., diffusion may occur only in the direction perpendicular to the magnetic field); with $\mathbf{E}_{\text{п}} \perp \mathbf{H}$ these conditions require that $\nabla(nf_0) \parallel \mathbf{E}_{\text{sc}} \parallel \mathbf{H}$ (diffusion may occur only parallel to the magnetic field). In case there are magnetic field components parallel and perpendicular to $\mathbf{E}_{\text{п}}$ conditions (7)-(9) can be satisfied only if $\nabla(nf_0) = 0$ and $\mathbf{E}_{\text{sc}} = 0$, i.e., in the absence of electron diffusion.

3. Where the above conditions are fulfilled, it is feasible to utilize the results of investigation of dc current in a gas to obtain information on shf current. By way of illustration, let us make use of the "dc analogy" to calculate

---

*Obviously, the requirement as regards identity of boundary conditions still applies.

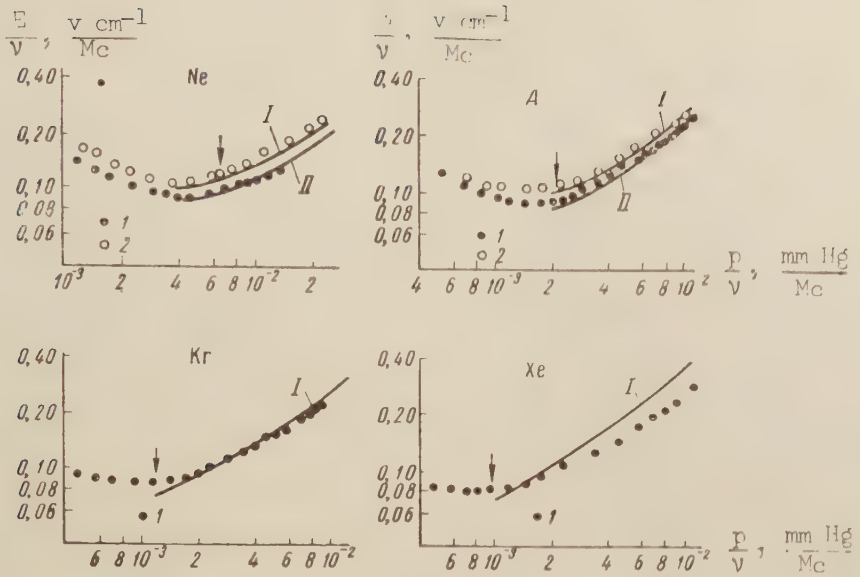

Curves calculated by the "dc analogy" method: I - $\nu_{i.cr}/\nu = 3.6\cdot10^{-3}$, II - $\nu_{i.cr}/\nu = 2\cdot10^{-3}$. Experimental points: 1 - ν = 9400 Mc, τ = 1 μsec, F = 400 cps[11]; 2 - ν = 2800 Mc, τ = 1 μsec, F = 400 cps[10]. Arrows identify the points corresponding to $(\bar{\omega}/\nu_c)^2 = 0.2$.

the critical field amplitude E_{cr} for hf pulse discharge breakdown in inert gases.

As was pointed out in Ref.4 the value of E_{cr} in many cases can be obtained from the condition

$$\nu_i = \nu_{i.cr}, \tag{11}$$

where ν_i is the mean ionization frequency. Hence to evaluate E_{cr}, we need only determine the electric field dependence of ν_i. For calculating ν_i we used the results of Kruithof's measurements of the ionization coefficient α in a dc field (the first Townsend coefficient). The relation between ν_i and α is given by

$$\nu_i = \alpha\mu E_n, \tag{12}$$

where μ is the electron mobility.

Since there are no experimental data on the variation of μ with E_n in the field range of interest, for determining ν_i from (12), we carried out an approximate evaluation of μ by averaging $\mu = \frac{e}{m\nu_c^*}$ over energies in the range from 1-2 to 15-20 ev. Such rough evaluation of μ apparently does not significantly affect the results of calculation of E_{cr} from (11) inasmuch as the variation of ν_i with E_n is determined primarily by the magnitude of αE_n.

Thus, E_{cr} can be calculated by means of Eqs.(11) and (12) on the basis of the "dc analogy". For the heavy inert gases ν_c^* is strongly dependent on the energy. Hence the "dc analogy" can be utilized only when $\nu_c^{*2} \gg \omega^2$. Accordingly, we carried out calculations for neon, argon, krypton and xenon in the range of pressures for which $\overline{\nu_c^{*2}} > 5\omega^2$. The results are shown in the accompanying figure.

It will be evident that the calculated curves are in satisfactory agreement with the experimental curves obtained by Abramova and the writer (for details concerning these measurements see Refs.10 & 11).

4. Until now, the "dc analogy" method has been used for analysis of hf discharge breakdown. It may be of interest to use this method for investigating breakdown in steady shf discharges. The validity of this approach stems from the possibility of making use of optical and microwave probe techniques for experimental investigation of the "dc model" of shf discharges. Direct use of these methods for studying discharges at super-high frequencies is generally hampered by the presence of metallic boundaries enclosing the discharge volume.

Under certain conditions it may also prove expedient to consider the inverse problem, i.e., to extend the results of investigation of hf current in a gas to direct current. Thus, for example, measurement of the mean ionization frequency by observing the increase in electron concentration under the influence of a pulsed shf discharge may in a number of cases prove to be simpler than determination of the ionization coefficient in a dc field. In such shf measurements the requirements as regards the purity of the gas may be less exacting because in pulse discharges (with sufficiently short pulses) electron removal processes associated with excitation of metastable levels are less likely and hence should not distort the experimental results.

"M.I.Kalinin" Leningrad Polytechnic Institute

References

1. T.Holstein, Phys.Rev., 70, 367 (1946).
2. H.Margenau, Phys.Rev., 73, 297 (1948).
3. W.P.Allis, Handbuch der Physik, 21, 383 (1956).
4. V.E.Golant, Usp.fiz.nauk, 65, 39 (1958).
5. S.Krasik, D.Alpert & A.McCoubrey, Phys.Rev., 76, 722 (1948).
6. L.Gould & L.W.Roberts, J.Appl.Phys., 27, 1162 (1956).
7. S.C.Brown, Handbuch der Physik, 22, 531 (1956).
8. D.I.Rose & S.C.Brown, J.Appl.Phys., 28, 561 (1958).
9. A.A.Kruithof, Physica, 7, 519 (1940).
10. V.E.Golant, Zhur.tekh.fiz., 27, 771, 1482 (1957). (Trans.Soviet Physics - Tech.Physics.)
11. V.E.Golant, Present issue of the Bulletin.

OBTAINING HIGH TEMPERATURES BY MEANS OF A SPARK DISCHARGE

- M.P.Vanyukov & A.A.Mak

In connection with the general problem of developing light sources of high intensity, it is of interest to determine what are the highest temperatures obtainable in the channel of a spark discharge and how the temperature distribution varies over the cross section of the channel.

The temperature of weak spark discharges, in which there is virtually no reabsorption, is generally determined from the intensity ratio of two appropriate lines (Ornstein method). In heavy discharges, however, there is usually appreciable reabsorption in the current carrying channel, hence preference must be given to temperature determination from the absolute intensity of the emitted radiation. Usually one measures the spectral radiant intensity (density of radiant energy) of the continuous radiation, from which one can calculate the brightness temperature. To find the true temperature one must, in addition to the brightness temperature, know the absorption power of the plasma. If the plasma itself radiates like a black body, which is the case, for example, for saturation of the channel luminance, the absorption power is equal to unity and the brightness temperature equals the true temperature.[1]

In this paper we give the results of an investigation of the temperature of the channel of a spark discharge by measurement of the spectral radiant intensity at the centroids of the greatly broadened ionized-atom lines under discharge conditions at which the continuous radiation brightness has not yet attained saturation.

Measurement of the absolute radiant intensity in the lines has a certain advantage over measurement of the continuous background inasmuch as the absorption of the plasma in the lines is higher than in the continuous spectrum owing to the fact that its radiation in the lines is appreciably more "black", consequently, the brightness temperature determined from the lines will correspond to the true temperature even for the discharge conditions under which the plasma in the region of the continuous background is largely transparent.

In the present work we used the measurement procedure described in Ref.1. The measurements were carried out with a monochromator slit width of 1.8 to 2.7 Å. The time resolution of the apparatus was $5 \cdot 10^{-8}$ sec. The sensitivity of the setup was calibrated with reference to a ribbon filament lamp with a quartz window.

The line radiation was studied in argon at wavelengths of 4806, 4348 and 3588 Å, in xenon at 2900 and 2600 Å, and in nitrogen at 5045, 5011 and 4097 Å. The discharges in the inert gases were realized with C = 0.05 μf, V = 12 kv and values of L varying from 0.086 to 1.28 μh; the discharges in nitrogen were realized with C = 0.05 μf, V = 15 kv, and L = 0.086 to 0.79 μh. The pressures were argon - 4 atm, xenon - 5 atm and nitrogen - 2 atm.

The results of measurement of the spectral density of radiant energy b_λ of the discharge channel in argon for wavelengths corresponding to the centroids of the enumerated lines and the continuum at different values of the spark circuit inductance, which characterizes the rate of energy input into the channel, are shown in Fig.1. As will be evident from the figure, in the investigated range of variation of the circuit inductance, the line radiation virtually attained saturation, whereas the continuous spectrum in the range $\lambda < 4000$ Å is still far from saturation. Similar results were obtained for the other two investigated gases[2].

We used Planck's radiation formula to evaluate the temperatures corresponding to b_λ for the wavelengths of the line and continuous spectra for which saturation of luminance was observed. The results are shown in Fig.2. It will be seen that the temperature values determined in different regions of the spectrum

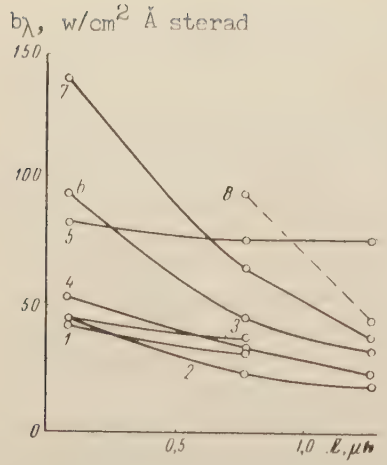

Fig.1. Variation of the maximum spectral radiant intensity of the spark channel in argon with the inductance of the discharge circuit for continuous radiation: λ = = 2600 (8), 2900 (7), 3400 (6), 3990 (4) and 4680 Å (2) and for individual lines: λ = 3588 (5), 4348 (3) and 4806 Å (1).

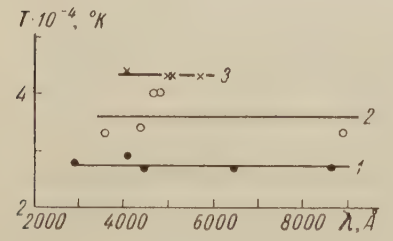

Fig.2. Values of the temperature calculated from the maximum values of b_λ measured in different regions of the spectrum with reference to the continuous and line radiations: 1) in Xe (5 atm), 2) in A (4 atm), 3) in N (2 atm).

from the line and continuous radiations are in close agreement. These results give reason to assert that the temperature of the spark channel remains virtually constant in a rather wide range of variation of the rate of energy input into the channel and attains a limit value under discharge conditions at which saturation of the brightness of the continuum is not yet reached.

The fact that no self-reversal of the ionized-atom lines was observed under any of the discharge conditions gives reason to assume that there are no steep temperature gradients over the cross section of the discharge channel. As is known, arc lines may be strongly self-reversed in a discharge,[3] but this characterizes the sheath or surrounding cloud rather than the current-conducting channel itself.

Thus, concurrent investigation of the intensity of the continuous and line radiations gives reason to assume that saturation of the luminous intensity of the spark discharge channel is due to saturation of its temperature rather than to screening of the high temperature radiation by the cooler surface layers of the plasma as it is sometimes inferred. Evidence in favor of this assumption is also furnished by the results of measurements of the brightness of a capillary discharge. These measurements showed that the luminous intensity observed from the end of the capillary channel for a discharge in air agrees in the entire investigated spectral range with the intensity measured in the direction perpendicular to the discharge axis[4]; the temperature of such a discharge is 60 000°K, whereas the maximum temperature obtained for an unconfined discharge in nitrogen was only 43 000°K. If screening played a significant role, the luminous intensity found in the end measurements should be less than with observation from the side.

It should be noted that the absence of steep temperature gradients in the current-carrying channel of a spark discharge was established earlier in the work of Dolgov & Mandel'shtam[5], who investigated a transparent plasma.

At present one can list the probable factors limiting the possibility of increasing the discharge channel temperature; for quantitative evaluation one must determine the temperature dependences of the energy losses due to ionization and radiation, heat conduction and electric conductivity, the rate of expansion of the discharge channel and a number of other factors.[6]

References

1. M.P.Vanyukov, A.A.Mak & N.V.Parazinskaya, Optika i spektroskopiya, 1, 642 (1956).

2. M.P.Vanyukov & A.A.Mak, Doklady AN SSSR, 123, 1022 (1958). (Trans.Soviet Physics - Doklady).

3. M.P.Vanyukov & L.D.Khazov, Doklady AN SSSR, 92, 523 (1953).

4. A.A.Mak, Ibid., 123, 671 (1958). (Trans.Soviet Phys. - Doklady.)

5. P.G.Dolgov & S.L.Mandel'shtam, Zhur.eksp.i teor.fiz., 24, 691 (1953).

6. M.P.Vanyukov & A.A.Mak, Usp.fiz.nauk, 66, 301 (1958). (Trans.Soviet Phys. - Uspekhi.)

SOME RESULTS OF INVESTIGATION OF THE EXCITATION FUNCTIONS OF THE N_2^+ NEGATIVE SYSTEM BANDS

- I.P.Zapesochnyi & S.M.Kishko

Knowledge of atomic and molecular excitation functions is important for the solution of many scientific and practical problems. So far the excitation functions of some of the spectral lines and bands of only a few atoms and molecules have been determined experimentally. In the case of diatomic molecules, excitation functions have been investigated only in the case of nitrogen and carbon monoxide.[1-4] The techniques available at the time these studies were carried out were far from perfect so that the results obtained are doubtful and qualitatively discordant.

We undertook to obtain reliable data on the excitation functions of different bands of ionized N_2. So far we have carried out careful measurements of the excitation functions of the bands of the negative system corresponding to the $B^2\Sigma \rightarrow X^2\Sigma$ transition (the wavelength of the investigated bands are 4278 and 3914 A).

Earlier experimental investigations of the excitation functions of both atoms and molecules were based on use of the photographic method of recording spectra, which is inferior to the photoelectric technique as regards both sensitivity and accuracy. Use of the photoelectric procedure for investigating excitation functions[5] allows of obtaining the optical excitation function under more favorable conditions (low gas pressure and small current density of the exciting electrons). Use of the photoelectric procedure in conjunction with a nearly monoenergetic (0.5-1 ev spread) electron beam made it possible for the first time to detect the fine structure of the excitation function of some lines of mercury.[6] The experimental procedure consisted in determining the intensity of the above mentioned bands of N_2^+ excited by electron impact in the gas at low pressure (below 10^{-3} mm Hg) at different electron energies. The discharge tube used in our experiments yielded a satisfactorily monoenergetic electron beam. The electron source was an oxide-coated equipotential cathode. The other electrodes (two anodes, electron collector and shielding cylinder) were made of thin nickel sheet.[7] The radiation was analyzed by an ISP-51 three-prism glass spectrograph and an FEU-17 photomultiplier coupled to a dc amplifier. The spectroscopically pure nitrogen was prepared by heating pure sodium azide (the purity of both the reagent and the nitrogen was checked spectroscopically). The nitrogen was introduced into the discharge tube through a metering system and the pressure determined by an LT-4 pressure gage. The tube supply voltage was closely regulated; the current and voltage were measured by precision instruments.

It has been reported[8] that nitrogen poisons oxide-coated cathodes, i.e., has a negative influence on the emission characteristics; however, precise data on the matter are lacking. Accordingly, we undertook a number of special experiments[9] which showed that up to 10^{-2} mm Hg the emission of an oxide-coated cathode in nitrogen is virtually the same as in vacuum.

To determine the conditions necessary for obtaining undistorted optical excitation functions of N_2^+, we carried out control experiments to determine the specific influence of nitrogen pressure, the current density and other factors on the state of the experimental curves.

Having determined the conditions under which the effects of nitrogen pressure and electron current density on the shape of the excitation function are negligible, we carried out our measurements for the above mentioned bands. The experimental curves are reproduced in Fig.1, from which it will be apparent that each excitation function has several clearly pronounced peaks, appearing at electron energies of 49, 56 and 67 ev. Beyond these peaks there is a broad maximum in the

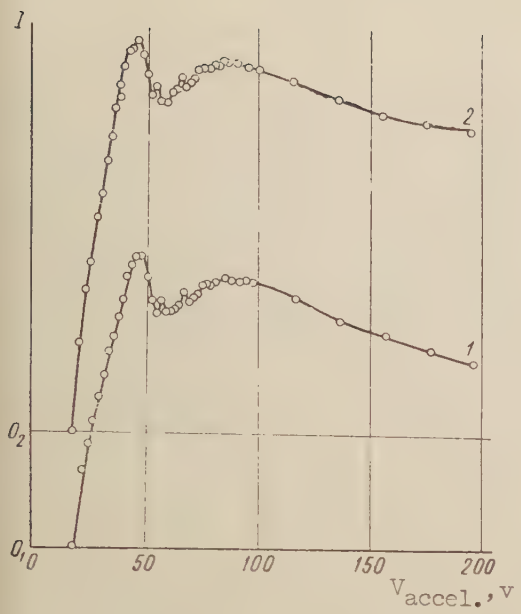

Fig.1. Excitation functions for λ = 4278 Å (1) and 3914 Å (2).

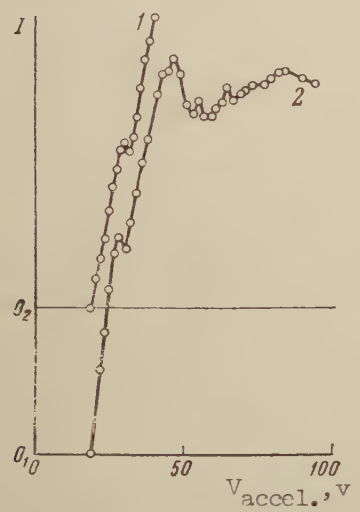

Fig.2. Excitation function of the 0→1 band (λ = 4278 Å) with experimental points recorded at close intervals: 1) initial section, 2) section from the excitation potential to 100 v.

85 to 95 ev region. The beginning of the excitation function of these bands lies at about 19 ev, which is in agreement with the excitation potential of the $B^2\Sigma$ level (18.7 v).

The curves of Fig.1 were obtained with an electron energy spread of about 1.3 ev the points being taken at 3 v intervals. For a relatively narrow range of accelerating potential (50-100 v), it proved feasible to obtain the experimental points at closer intervals (1.5-2 v). Fig.2 shows two curves for the initial section of the excitation function of the 0→1 band; here the experimental points were obtained at intervals of 1.5-2 v and the electron beam was more monoenergetic (spread $<$1 ev). This brought out an additional sharp narrow maximum located on the rise of the excitation function curve at 29 v. Thus we found that the excitation functions exhibit five peaks, located at 29, 49, 56, 67 and 85-90 ev.

All the noted maxima were observed in numerous measurements at exactly the same energies in different tubes. Hence there can be no doubt regarding their existence.

With gradual increase of the gas pressure (and the accompanying impairment of the monoenergetic characteristics of the beam) the peaks in the curves are smoothed out and the shape of the curves becomes similar to that obtained by Bandy[3] and Stewart[4].

The appearance of several maxima in the excitation function of the investigated bands cannot be explained as being due to transitions from higher lying electron levels to the $B^2\Sigma$ level (as in the case of the mercury lines[6,7]) inasmuch as, so far as we know, the corresponding systems are not observed.

The presence of some of the peaks can be explained by comparing the potentials to which the maxima in the excitation function correspond with the electron energies at which there occur the elementary processes of dissociation and ionization of nitrogen molecules to neutral atoms and ions. The population of the excited $B^2\Sigma$ state increases owing to the reverse processes, which in turn leads to increased intensity of the given band.

We desire to express our sincere gratitude to S.E.Frish for his support in the work and valuable advice.

Uzhgorod State University

References

1. A.E.Lindh, Z.Phys., 67, 67 (1931).
2. O.Thieme, Z.Phys., 78, 412 (1932).
3. F.P.Bandy, Phys.Rev., 52, 698 (1937).
4. D.T.Stewart, Proc.Phys.Soc.A, 69, 437 (1956).
5. I.P.Zapesochnyi, Nauchn.zap. (Scientific notes), Uzhgorod Univ., 18, 147 (1957).
6. S.E.Frish & I.P.Zapesochnyi, Doklady AN SSSR, 55, 917 (1954).
7. I.P.Zapesochnyi, Vestnik, Leningrad State University, No.11, 67 (1954).
8. Yu.A.Katsman, Raschet radiolamp (Vacuum tube design), M.-L., 1953.
9. S.M.Kishko & I.P.Zapesochnyi, Radiotekhnika i elektronika, 3, 433 (1958). (Trans.Radio Engineering and Electronics.)

EXCITATION CROSS SECTIONS FOR SOME SPECTRUM LINES OF POTASSIUM AND ARGON

- L.M.Volkova

In the present work we determined the variation of the excitation cross sections for some spectrum lines of potassium and argon as a function of the bombarding electrons. The energy spread in the exciting electron beam was about 0.9 ev. In the case of potassium vapor, the measurements were carried out at a pressure of $1.3 \cdot 10^{-4}$ mm Hg, the pressure being calculated by the formula given in Ref.1. In the work with argon the pressure was $1 \cdot 10^{-3}$ mm Hg.

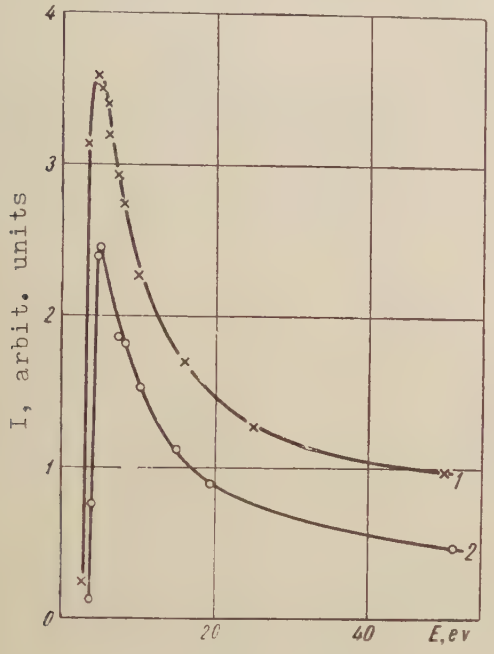

Fig. 1

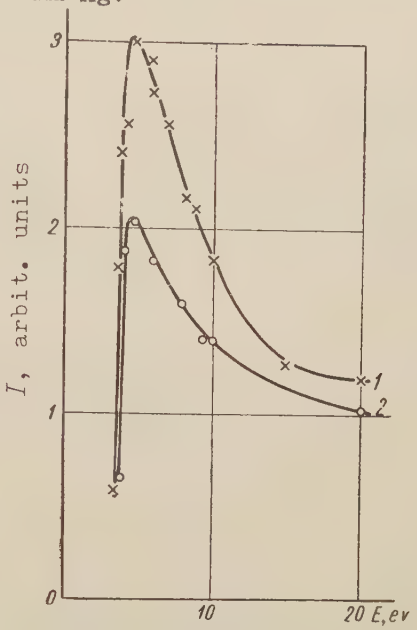

Fig. 2

Fig.1. Excitation function curves: 1) λ = 5359.52 Å $(4^2P_{3/2} - 8^2D_{5/2,3/2})$, 2) λ = 5112.2 Å $(4^2P_{3/2} - 9^2D_{5/2,3/2})$

Fig.2. Excitation function curves: 1) λ = 5782.77 Å $(4^2P_{1/2} - 7^2S_{1/2})$, 2) λ = 5832.31 Å $(4^2P_{3/2} - 7^2D_{5/2,3/2})$

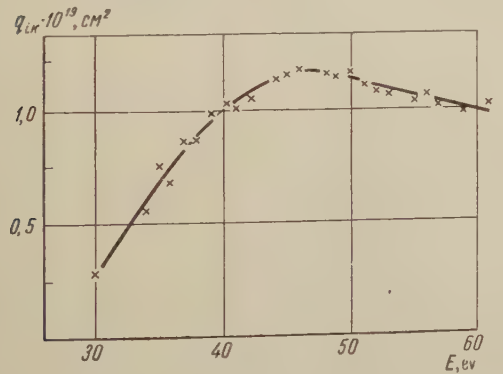

Fig. 3

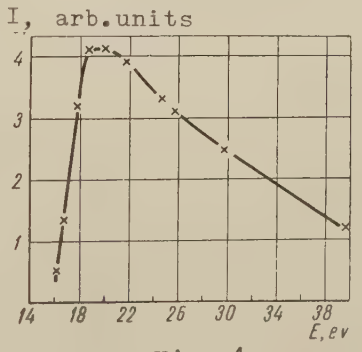

Fig. 4

Fig.3. Variation of the excitation cross section with the bombarding electron energy for the 4222.98 Å spark line of potassium: $3p^5\,(^2P^0_{1/2})\,4p - 3p^5\,(^2P^0_{1/2})\,4s$, $J=1$ $J=1$

Fig.4. Variation of the excitation function for the 8115.31 Å arc line of argon: $3p^5\,(^2P^0_{1^1/_2})\,4p - 3p^5\,(^2P^0_{1^1/_2})\,4s$, $J=3$ $J=2$

The variation of the excitation functions of the spectrum lines of potassium was measured by two procedures: photographic photometry using an ISP-51 spectrograph with an f = 270 mm camera and photoelectrically using the same spectrograph with a PS-381 attachment.

In the case of argon the measurements were made only by the photographic procedure.

Inasmuch as the wavelengths of the investigated lines lie in the range extending from 4000 to 8500 Å, it was necessary to choose specially sensitized fast films for different intervals of the spectrum.* In all we measured the variation of the excitation functions of four arc and three spark lines of potassium and six arc lines of argon.

The potassium arc line excitation functions (Figs.1 & 2) begin at the excitation potential of the given line, rise rapidly to a peak (~5 ev) and then fall off more slowly. The difference between V_{max}, the potential of the line peak, and the excitation potential is about 2 v.

Fig.3 shows the variation of the excitation cross section with the electron energy for the spark line of potassium:

$$\lambda = 4222{,}98 \text{ Å}: \underset{J=1}{3p^5(^2P^0_{1/2})4p} - \underset{J=1}{3p^5(^2P^0_{1/2})4s}.$$

Similar dependences were obtained for the spark lines:

$$\lambda = 4134{,}72 \text{ Å}: \underset{J=2}{3p^5(^2P^0_{1^1/_2})4p} - \underset{J=2}{3p^5(^2P^0_{1^1/_2})4s}$$

and

$$\lambda = 4149{,}17 \text{ Å}: \underset{J=1}{3p^5(^2P^0_{1/2})4p} - \underset{J=1}{3p^5(^2P^0_{1/2})4s}.$$

Fig.4 shows the energy variation of the excitation function for the arc line of argon:

$$\lambda = 8115{,}31 \text{ Å}: \underset{J=3}{3p^5(^2P^0_{1^1/_2})4p} - \underset{J=2}{3p^5(^2P^0_{1^1/_2})4s}.$$

This curve is characterized by a rapid rise to the maximum and a subsequent only slightly less rapid fall. Similar curves were obtained for the other five arc lines of argon:

$$\lambda = 8424{,}65 \text{ Å}: \underset{J=2}{3p^5(^2P^0_{1^1/_2})4p} - \underset{J=2}{3p^5(^2P^0_{1^1/_2})4s};$$

$$\lambda = 8408{,}21 \text{ Å}: \underset{J=2}{3p^5(^2P^0_{1/2})4p} - \underset{J=1}{3p^5(^2P^0_{1/2})4s};$$

$$\lambda = 8264{,}52 \text{ Å}: \underset{J=1}{3p^5(^2P^0_{1/2})4p} - \underset{J=1}{3p^5(^2P^0_{1/2})4s};$$

$$\lambda = 8014{,}79 \text{ Å}: \underset{J=2}{3p^5(2P^0_{1^1/_2})4p} - \underset{J=2}{3p^5(^2P^0_{1^1/_2})4s};$$

$$\lambda = 7948{,}18 \text{ Å}: \underset{J=1}{3p^5(^2P^0_{1/2})4p} - \underset{J=0}{3p^5(^2P^0_{1/2})4s}.$$

The data on the electronic configurations of the atoms before and after the transitions were taken from the tables in Refs.2,3 & 4. In determining the ex-

---

*The personnel of the NIKFI were of great assistance in selection of the photographic materials; particular thanks are due to Engineer N.M.Parfenova.

citation cross sections for the spectrum lines of potassium, we employed the procedure described in the work of Fischer[5] and Frish[6].

I take this opportunity to thank N.A.Kaptsov for his constant interest in the work.

Physics Faculty,
Moscow State University

References

1. Smithsonian Physical Table, 1954.
2. T.L.DeBruin, Z.Phys., 38, 94 (1926).
3. C.Moore, Atomic Energy Levels, 1949.
4. R.F.Bacher, Atomic Energy States, 1932.
5. O.Fischer, Z.Phys., 86, 646 (1933).
6. S.E.Frish, Usp.fiz.nauk, 43, 512 (1951).

EFFECT OF DISAPPEARANCE OF NEGATIVE IONS ON THEIR CONCENTRATION IN THE DISCHARGE COLUMN

- M.V.Konyukov

1. The negative component of the plasma in the positive column of a discharge in electronegative gases (or in media with an appreciable admixture of such gases) consists of electrons and negative ions. The latter are apparently responsible for some of the distinctive characteristics of such discharges (anomalous gradients, the formation and subsequent behavior of striations, facilitated contraction of the column, etc.), and hence it may be of interest to calculate their concentration. The purpose of the present work was to evaluate the influence of the decay of negative ions on their concentration.*

2. To investigate the positive column with negative ions under diffusion conditions (λ_e, λ_p, $\lambda_n \ll R$), we make use of the following charged particle balance equations

$$\begin{aligned} \frac{1}{r}\frac{\partial}{\partial r}\left\{rD_e\frac{\partial Ne}{\partial r}+rb_eN_eE_r\right\}+ZN_e+\gamma N_n-\beta N_e=0,\\ \frac{1}{r}\frac{\partial}{\partial r}\left\{rD_n\frac{\partial N_n}{\partial r}+rb_nN_nE_r\right\}+\beta N_e-\gamma N_n-\alpha N_pN_n=0,\\ \frac{1}{r}\frac{\partial}{\partial r}\left\{rD_p\frac{\partial N_p}{\partial r}-rb_pN_pE_r\right\}+ZN_e-\alpha N_pN_n=0, \end{aligned} \qquad (1)$$

where α is the volume recombination coefficient for negative ions (we neglect recombination of electrons and positive ions), β is the electron sticking frequency and γ is the dissociation frequency for negative ions; the other designations are in the usual notation.**

In view of the fact that the set of equations (1) is nonlinear, it is difficult to solve for the relative concentration $\varkappa = N_n/N_e$ in the general case; consequently, we will restrict our consideration to a number of particular cases involving quasi-neutral ambipolar diffusion.

a) Case $\alpha = \gamma = 0$.

Here we can assume $\varkappa = \text{const}$ (in general, $\varkappa$ is a function of the radius, but with reasonable approximation we may assume that it is constant over the entire cross section). Then, providing $(D_e/D_p)(Z-\beta)(Z+\beta)^{-2}\beta \ll 1$, we obtain[4]:

$$\varkappa = \frac{De}{2D_p}\frac{Z+\beta}{Z-\beta}. \qquad (2)$$

The negative ion concentration in a column with no loss proves to be two orders of magnitude higher than the electron concentration inasmuch as only on this condition is the diffusion flow to the wall greater than the flow to the axis owing to the radial electric field.***

---

*The theory of a positive column with negative ions has been considered by Holm,[1] Seeliger[2,3] and others. In most of these studies, however, the concentration was regarded as a variable parameter rather than the quantity sought.

**In the presence of several kinds of ions the descriptive equations will be similar but the magnitudes of α, β and γ will depend on the concentrations of the different kinds of ions.

*** $\varkappa = (D_e/2D_p) - 1$ is the limiting value of the concentration at which the flow of negative ions to the wall owing to diffusion and the reverse flow due to the radial electric field are equal in magnitude.

b) Case $\alpha = 0$, but $\gamma \neq 0$.

We can again assume that $\varkappa = \text{const}$ over the entire cross section. Then the equation* characterizing $\varkappa$ assumes the form

$$\frac{2\varkappa(1+\varkappa)(D_p/D_e)-\varkappa}{1+2\varkappa} = \frac{\beta-\gamma\varkappa}{Z-(\beta-\gamma\varkappa)}. \tag{3}$$

Graphic solution of Eq.(3) for $D_e/D_p \approx 10^2$ and $Z/\beta \approx 2$ yields the following values of $\varkappa$ as a function of the chosen parameter γ/Z:

γ/Z	0	0.01	0.1	0.2	0.3	0.5	0.7	0.9
$\varkappa$	150	50	10.5	5.7	3.5	2.2	1.55	1

These data indicate a considerable decrease of the negative ion concentration, owing to the effect of volume losses. With increase in the concentration (or, what is equivalent, with decrease of the rate of dissociation of the negative ions) the character of the carrier motion changes. It is convenient to investigate this change by analyzing the $\varkappa$ dependence of the diffusion lifetimes.

Electrons

Introducing the electron diffusion lifetime under conditions of ambipolar diffusion in the absence of negative ions,

$$\tau_{ea} = \frac{1}{\mu^2 D_a}, \tag{4}$$

we obtain the following expression for the dimensionless lifetime of electrons** in a column with negative ions

$$\tau_e = \frac{\tau^e_{\text{dif}}}{\tau_{ea}} = \frac{1+2\varkappa(b_p/b_e)}{1+2\varkappa}. \tag{5}$$

Eq.(5) gives a monotonic decrease of the electron diffusion lifetime with increasing concentration. At $\varkappa = 0$, the diffusion lifetime equals τ_{ea}; with increasing concentration, τ^e_{dif} asymptotically approaches the diffusion lifetime corresponding to electron diffusion $(D_e\mu^2)^{-1}$. The reason for this is decrease of the transverse electric fields retarding the electrons.***

Positive Ions

The expression for the dimensionless diffusion lifetime of positive ions is

$$\tau_p = \frac{\tau^p_{\text{dif}}}{\tau_{ea}} = \frac{1+2(b_p/b_e)\varkappa}{1+2(D_p/D_e)\varkappa}. \tag{6}$$

Eq.(6) indicates a monotonic increase of the diffusion lifetime from τ_{ea} to the value corresponding to free diffusion of ions. It is interesting that at concentrations $\varkappa(b_p/b_e) \ll 1$, there is a difference between the movement of positive ions and electrons with $\varkappa \approx 1$.

---

*In carrying out the necessary simplifications we assumed that $D_e \gg D_p$, $D_p \approx D_n$, $b_e \gg b_p$ and $b_p \approx b_n$.

**In the presence of negative ions each of the carriers is characterized by its own diffusion time.

***The strength of the transverse electric field, $E_z = -\left[\frac{D_e}{(b_e+2\varkappa b_p)}\right]\frac{\partial N_e}{\partial z}$ monotonically falls off from the value corresponding to ordinary ambipolar diffusion to zero.

Negative Ions

The behavior and motion of negative ions differ from those of electrons and positive ions. For negative ions the diffusion lifetime is given by

$$\tau_n = \frac{\tau_{dif}^n}{\tau_{ea}} = \frac{1 + 2\varkappa(b_p/b_e)}{2\varkappa(D_n/D_e) - 1}. \tag{7}$$

At concentrations in the range $(D_e/2D_p) - 1 < \varkappa < \infty$ the lifetime τ_{dif}^n is positive* and decreases from ∞ to $1/\mu^2 D_n$, i.e., the lifetime for free ion diffusion. Here the diffusion flow to the wall is greater than the opposite flux due to the field. That is, the wall serves as a sink for negative ions with a capacity per unit column length characterized by

$$q = 2\pi \int_0^R (\beta - \gamma\varkappa) N_e r dr. \tag{8}$$

For concentrations in the range $0 < \varkappa < (D_e/2D_p) - 1$, the diffusion lifetime becomes negative and with increase in concentration decreases from τ_{ea} to $-\infty$. In this case the wall is a source of negative ions** with the linear capacity

$$q = 2\pi \int_0^R (\gamma\varkappa - \beta) N_e r dr. \tag{9}$$

For $\varkappa = (D_e/2D_p) - 1$, the diffusion lifetime becomes infinite. In this case the wall plays no part in maintaining the steady state, and the kinetics of the discharge is determined exclusively by volume processes.[6]

c) Case α and $\gamma \neq 0$.

In this case we cannot assume a constant concentration over the entire cross section; however, with some sacrifice in accuracy, we can select a small region close to the axis of the discharge in which we can assume $\varkappa = \text{const}$. The equation characterizing the concentration can be deduced in the same way as Eq.(6a) in Ref.4 and has the form

$$\frac{\varkappa - 2\varkappa(1+\varkappa)(D_p/D_e)}{1+2\varkappa} \frac{Z-\beta}{\beta} + 1 = \frac{\gamma}{\beta}\varkappa + \frac{\alpha N_e^0}{\beta}\varkappa(1+\varkappa). \tag{10}$$

This equation can be solved by similar methods. It must be noted that volume recombination leads to the presence of spatial sources. At sufficiently low negative ion concentrations we can distinguish two regions: an outer region near the wall in which creation of negative ions predominates over their disappearance, and an outer region in which disappearance predominates over creation.

3. The negative ion concentration can be evaluated from measurements of the time constant of the process of decrease in electron concentration incident to deionization. Following the method developed by Granovskii[7], we obtain the following expression for the time constant for the beginning of deionization:

$$\tau_e = \frac{1}{\mu^2 D_{ae} + \beta - \gamma\varkappa} \tag{11}$$

---

*A positive diffusion lifetime corresponds to migration of particles created in the discharge space to the wall; a negative diffusion lifetime corresponds to migration of particles appearing at the wall into the discharge volume.

**Günterschulze[5] introduced the concept of an ionic layer located near the wall and acting as a surface source of negative ions.

wherein

$$D_{ae} = D_a \frac{1 + 2\varkappa}{1 + 2\varkappa(b_p/b_e)}.$$

To make use of Eq.(11) we must know the rate of formation and decay of negative ions.

More convenient for purposes of evaluation is the time constant for the decrease* in concentration of positive ions, which is given by

$$\tau_p = \frac{b_e}{\mu^2 D_e b_p} \frac{1 + 2\varkappa(b_p/b_e)}{1 + \varkappa(D_r/D_e)}. \qquad (12)$$

I desire to express my gratitude to A.A.Zaitsev for valuable discussions.

Tula Pedagogical Institute

References

1. R.Holm, Z.Phys., 75, 171 (1932).
2. R.Seelinger & R.Kruschke, Phys.Z., 34, 833 (1933).
3. R.Seelinger, Ann.Phys., 6, 93 (1949).
4. M.V.Konyukov, Zhur.eksp.i teor.fiz., 34, 908 (1958). (Trans.Soviet Physics - JETP, 7, 629 (1958).)
5. A.Günterschulze, Z.Phys., 91, 724 (1934).
6. M.V.Konyukov, Zhur.eksp.i teor.fiz., 34, 1634 (1958). (Trans.Soviet Physics - JETP, 7, 1122 (1958).)
7. V.L.Granovskii, Elektronnye i ionnye pribory (Electronic and ionic instruments), p.98, M.-L., 1940.

---

*In contrast to the column in electropositive gases each carrier here is characterized by its own time constant.

NEW RESULTS OF INVESTIGATIONS OF A LONG SPARK

- I.S.Stekol'nikov

The growth and development of spark discharges in different types of gaps (rod-rod, rod-plane, etc.) ranging in length from 1 to 5 meters were investigated in our laboratory by means of oscillographs, multiple cell shutters, image converter tubes and probes designed and constructed in the laboratory. The sparks were realized with pulse, alternating (50 cps) and dc voltages.

Below we give some of the results obtained by E.N.Brago, A.Ya.Inkov, I.G. Pulavskaya, G.I.Smirnov and the writer.

1. Pulse corona

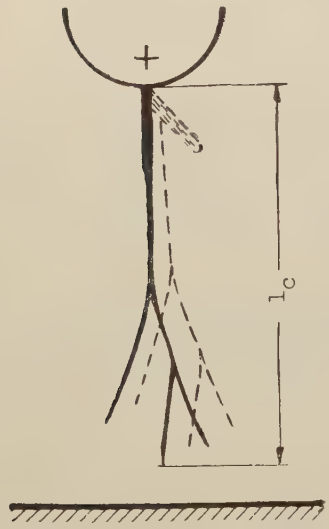

Fig.1

With a view to amplification of the published data on pulse discharge coronas, we studied the development of coronas in a sphere-plane gap with simultaneous optical and electric recording. The results for gaps of up to 265 cm are in agreement with the data obtained earlier for narrower gaps.[1] The corona consists of discrete elements, each of which is sharply divided into two parts: a bright rectilinear stalk developing directly from the surface of the sphere and a group of weakly glowing, long filaments exhibiting a dendritic structure. The structure of the stalk is not uniform; it is divided into two parts by a bunch of brightly glowing filaments branching off at an angle of 90°; these filaments have almost the same luminous intensity as the stalk and a similar structure. The corona current is observed in the form of a single pulse with a leading edge of $\sim 10^{-8}$ sec and a magnitude measuring in the tens of amperes.

Fig.1 shows a schematic sketch of a corona element and its development in time. According to time resolution data, the rate of advance of the stalk is $\sim 10^8$ cm/sec; the average rate of the branches is $\sim 10^9$ cm/sec. Curves characterizing the length of the corona element as a function of the voltage on the discharge gap are shown in Fig.2. Our measurements showed that for different diameters of the sphere electrode the variation of the initial corona ignition voltage V_{ic} as a function of the gap length S_o is linear; the slope of the plots increases with increasing electrode diameter.

At a voltage amplitude equal to V_{ic}, the instant of ignition of a pulse corona, which is identical with the beginning of steep rise of the discharge current, is shifted behind the leading edge of the voltage pulse; the precorona time, i.e., the time from t_{max}, when the voltage on the electrode attains the value $V_{max} = V_{ic}$ to the instant t_c of ignition of the corona becomes indefinite, i.e., depends

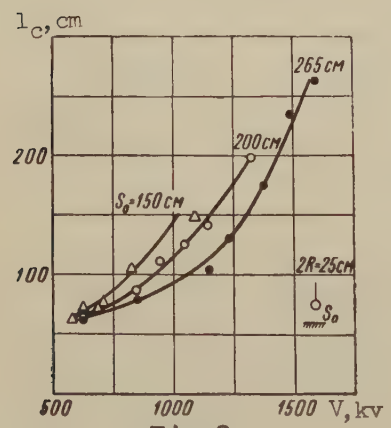

Fig.2

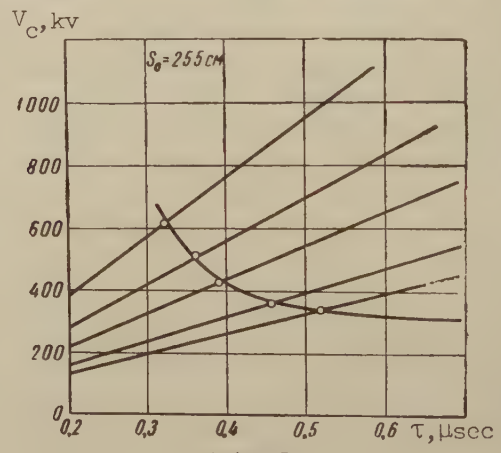

Fig.3

on chance factors. If the amplitude of the applied voltage pulse is increased, the ignition of the corona occurs during the rise of the voltage wave; V_c is increased, while the fluctuation in time decreases. Consequently, each value of V_c is characterized by its own voltage-time characteristics similar to the characteristics observed for breakdown voltages. A typical characteristic for oblique voltage pulses of different steepness is shown in Fig.3.

Other conditions being equal, V_c determines the current pulse of the corona. If one changes the ignition potential of a pulse corona (by varying the steepness of the applied voltage pulse), there will be a corresponding change in the amplitude of the corona current. Measurements show that the corona current does not depend on the maximum value of the voltage pulse.

A correlation was established experimentally between the shape of the current pulse and the spatial structure of the corona stalk. If the stalk has no nodes, the current is recorded in the form of a single pulse with a single maximum; on the other hand, if the stalk is split into two parts at a node, the current is recorded in the form of a pulse with two peaks. In the latter case, the current pulse may be regarded as a surposition of two single pulses from each part of the twin corona stalk.

The described type of corona differs from the familiar form observed for points and thin conductors with dc and 50 cycle ac voltages, commonly defined as "a corona continuous in space and time" (more correctly, it should be termed the "avalanche" form of corona). In view of its specific characteristics, the above described form of discharge has been termed a "pulse" corona.

For the purpose of elucidating the form of corona forming at an electrode of small curvature with 50 cycle ac voltages, there were carried out experiments with a sphere-plane gap (sphere diameter 12.5 cm) having a length S_o = 125 cm. Fig.4 shows a schematic sketch based on photographs of the effects observed with smooth and gradual increase of the ac voltage to the critical value V_{ic}. At V_{ic} = = 254 kv there suddenly (i.e., without preliminary audible or visible warning) forms during the positive half-period a corona element, the appearance of which is identical with that observed with a pulse voltage (Fig.1); the length of its stalk (2-3 cm) and branches (13-20 cm) are approximately equal to the corresponding features of a pulse corona obtained in discharges in the same gap. This gives reason to infer that the mechanism of corona formation is the same with both types of voltage. Inasmuch as in the given case we are considering the appearance of a corona during the first half-wave, an important feature of the experiments is the substantial decrease in the steepness of the applied 50 cycle ac wave. During the subsequent 10-15 sec interval of application of the ac voltage, there are recorded only elements of a negative corona during negative half-waves, which have the appearance of straight unbranched stalks some 3-4 cm in length. Increase of the ac voltage to V_{max} = 264 kv leads to more frequent formation of corona elements with a somewhat more extensively developed system of branches and more intense luminous emission and then to formation of corona elements from the stalk of which there originate retarded leaders,

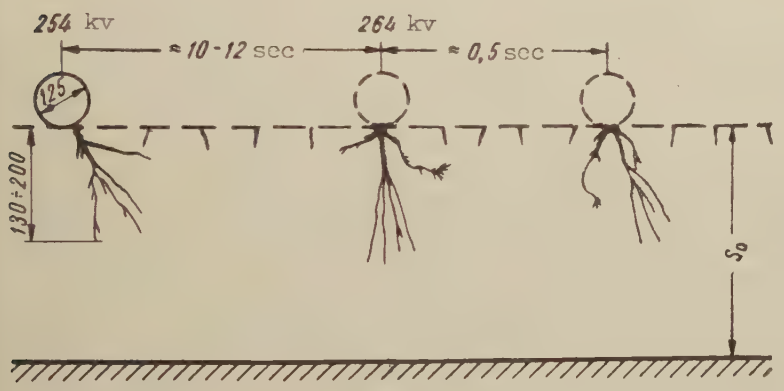

Fig.4.

much as was observed for pulse voltages.

Subsequent development of the corona elements is influenced by space charge, which inhibits repeat formation of the elements from the same point on the electrode with the result that successive stalks depart from different points on the surface of the electrode. Photographs obtained with a still camera show bunches consisting of a succession of superimposed brush-like branches similar to those obtained for a succession of voltage pulses. The formation of such bunches has frequently been observed in the case of conductors 1-2 cm or more in diameter.

In evaluations of corona energy losses in the case of electric transmission lines the width of the high-field zone, i.e., the zone wherein there occurs intense ionization of the air adjacent to the surface of the electrode, is assumed to be very small: from a few millimeters to 1 cm for wires used in practice. Sometimes the width of the ionization zone is assumed to be zero, and the role of the zone is expressed by assuming a constant gradient at the conductor surface. These concepts are valid only for avalanche coronas.

The conditions for formation and persistence of a self-sustaining discharge are determined by reproduction of photoelectrons capable of initiating new avalanches. The criterion for photoelectron reproduction has been given by Loeb and his school and developed further in the work of Aleksandrov[2] and other authors. Due attention should be given to further and more detailed investigation and analysis of the enumerated forms of coronas.

With increase of V, following the pulse corona on the electrode surface, there begins development of retarded leaders, which appear with increasing frequency. Finally, at $V = V_b$ the leader reaches the plane electrode and is followed by the formation of the principal discharge channel. The described discharge mechanism as regards the development of the leader and principal channel stages has also been observed in our laboratory in the case of dc voltage.

2. Leader stage

In recent experimental work there have been established a number of significant details as regards the structure of the leader and the influence of the test circuit parameters on the development of the leader process.

Comparison of the optical pictures and the quantitative characteristics (variation of i, V and l as a function of time[3]) for two gaps of different configuration (rod-plane and ring-plane) with different retarding resistances R_o and front capacitances C_f led to the deduction that in principle it is feasible to realize "ideal" test circuits, i.e., circuits with parameters such that they will not influence the course of the leader process and will in effect represent a source of "infinite" power for the process. The appropriate values of $R_o = R_{op}$ are determined by the maximum value of the leader current in the given gap with a source of infinite power ("power capacity" of the gap) or, in specific terms, by the gap geometry and the voltage on it. Increase of R_o above R_{op} leads to increase of iR_o and decrease of V. Owing to decrease of V, the current and rate of development of the leader decrease. When R_o is only slightly larger than R_{op}, the changes in V, i and v occur only at the end of the leader process, where the current is greatest. In this case, $i = f(t)$ changes and the shape of the voltage pulse is distorted, but the total time of the leader process changes little. In cases when R_o is much greater than R_{op}, changes in i, V and v occur during the entire leader process, the shape of the voltage pulse is distorted little, but the absolute values of i, V and v are appreciably decreased, which leads to substantial increase of the leader development time. The fact that the influence of R_o is strongest towards the end of the leader process makes the development of the leader with increase of R_o more uniform.

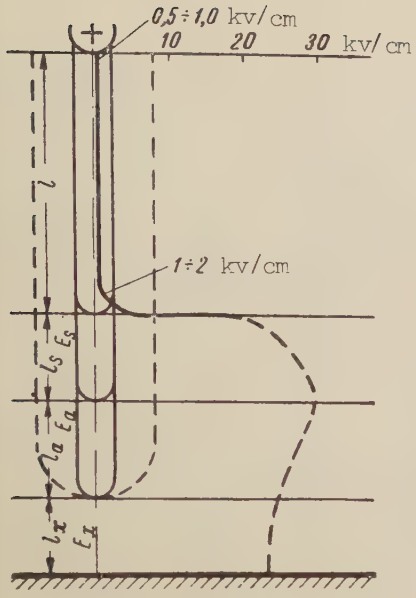

Fig.5.

The presence of C_f allows of increasing R_{op}, since it provides an additional source of supply for the leader at the end of its development.

The influence of R_o and C_f on the development of the leader process leads to disagreement between the voltage-time characteristics obtained under different conditions and in different laboratories. This disagreement is the greater, the greater the "energy capacity" of the gap. Moreover, analysis of lightning strokes shows[4] that in this case there acts on the gap a source of infinite power. Possibly, this is also true of the operation of insulation under high voltages. Consequently, it is desirable to record voltage-time (and other) characteristics under the conditions of an "ideal" circuit.

The following recommendations were made on the basis of the experimental work:

1) The parameters of "ideal" circuits in the case of "low energy capacity" gaps should be $C_o \geqslant 15\,000$ pf, $R_o \leqslant 150$ ohm and $C_f \geqslant 2000$-4000 pf,

2) For elaborating new insulation standards and specifications:

a) C_o should be such that at the specified energy drain the voltage drop on the capacitors does not exceed 5%;

b) the value of R_o should be between 50 and 150 ohm;

c) the inductance of the discharge circuit should be minimal.

The longitudinal potential gradient E in the leader channel in the vicinity of the electrode was measured by a specially developed probe technique. The experiments[5] showed that the value of E varies between 0.3 and 0.5 kv/cm.

The experimentally determined variation of the channel conductivity as a function of the overvoltage of the gap made it possible to plot, on the basis of certain assumptions, the variation of E along the entire length l of the leader channel. In Fig.5 the dashed line shows the evaluated values of the gradient in the streamer (section l_s) and the avalanche (l_a) parts of the leader and in the air gap (l_x). The excess positive charge of the leader is contained not only in its channel but also in the cylindrical space indicated by the U-shaped dashed line in Fig.5.

High Voltage Gas Discharge Laboratory,
Power Institute, Academy of Sciences of the USSR

References

1. H.Norinder & O.Salka, Arkiv.Fis., 3, No.4-5, 347 (1952).

2. G.N.Aleksandrov, Zhur.tekh.fiz., 26, 1769 (1956). (Trans.Soviet Physics - Tech.Physics.)

3. I.G.Pulavskaya & I.S.Stekol'nikov, Izv.AN SSSR, Otd.tekhn nauk, (Bulletin, USSR Ac.of Sci., Tech.Sciences Section), No.10, 64 (1956).

4. I.S.Stekol'nikov, Ibid., No.1, 37 (1957).

5. A.Ya.Inkov, Issledovaniya predrazryadnoi stadii dlinnykh iskr. Peredovoi nauchno-tekhnicheskii i proizvodstvennyi opyt. Tema 26 Vses.n.-l.in-t tekhn.inf. AN SSSR (Investigation of the pre-discharge stage of long sparks. Leading scientific-technical and industrial experiments. Report 26, All Union Scientific Research Institute of Technical Inf., USSR Ac.of Sci.), E-57-39/9, M., 1957.

PROBE INVESTIGATIONS OF THE FIELD OF AN AC CORONA

- V. I. Levitov, A. G. Lyapin & V. I. Popkov

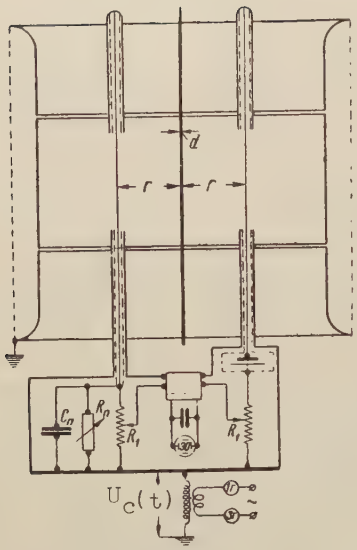

Fig.1. Diagram of experimental arrangement.

The principles underlying the theory of probe measurements in the field of an ac corona have been set forth in Ref.1. Essentially, they reduce to certain requirements regarding the relation between the cross sectional dimensions of the probe and the period of the investigated process. On the basis of the probe measurements one can plot for each instant of time the current-voltage characteristics of the probe, similar to the characteristics for a dc corona.

To plot such current-voltage characteristics one must have the variation of only the convection current. The probe current, however, generally contains, in addition to the convection current component, a displacement current component due to variation with time of the probe charge. In practice it is difficult to insure a constant probe charge, i.e., zero displacement current. Hence the displacement current must be excluded from the results in a different way. The problem is solved by using a probe with a grid or a differential (double) probe.

A differential probe consists of two identical cylindrical probes located symmetrically to the corona electrode in the investigated field. Owing to the symmetry, the probe currents and their components (the convection current and the displacement current) are equal, i.e., the current difference is zero. When a source of dc (bias) voltage is connected to one of the probes, the balance is disturbed and a difference current appears. To clarify the influence of the dc voltage on the components of the probe current, let us examine the following equations characterizing the probe potentials

$$\left.\begin{aligned} U_{\sim}+U_{=} &= \alpha_{1-1}q_1+\alpha_{1-2}q_2+\alpha_{1-w}\,q_w+U_1(q_s)\\ U_{\sim}+0 &= \alpha_{2-1}q_1+\alpha_{2-2}q_2+\alpha_{2-w}\,q_w+U_2(q_s)\end{aligned}\right\}, \qquad (1)$$

where $U_{\sim}$ is the alternating component of the potential, which is the same for both probes, $U_{=}$ is the dc component of the potential on the first probe, $U_1(q_s)$ and $U_2(q_s)$ are the fractions of the potentials on the first and second probes due to space charge, and q_1, q_2 and q_w are the charges on the probes and the conductor (wire). Inasmuch as $\alpha_{1-2}=\alpha_{2-1}$, $\alpha_{1-1}=\alpha_{2-2}$ and $\alpha_{1-w}=\alpha_{2-w}$, we have

$$q_1-q_2=\frac{U_{=}}{\alpha_{1-1}-\alpha_{1-2}}-\frac{U_1(q_s)-U_2(q_s)}{\alpha_{1-1}-\alpha_{1-2}}.$$

From this the difference between the convection current components is

$$i_{1c}-i_{2c}=\frac{p(t)\cdot k}{\alpha_{1-1}-\alpha_{1-2}}\{U_{=}-[U_1(q_s)-U_2(q_s)]\}$$

and the difference between the displacement currents is

$$i_{1e}-i_{2e}=\frac{1}{\alpha_{1-1}-\alpha_{1-2}}\cdot\frac{d}{dt}[U_1(q_s)-U_2(q_s)].$$

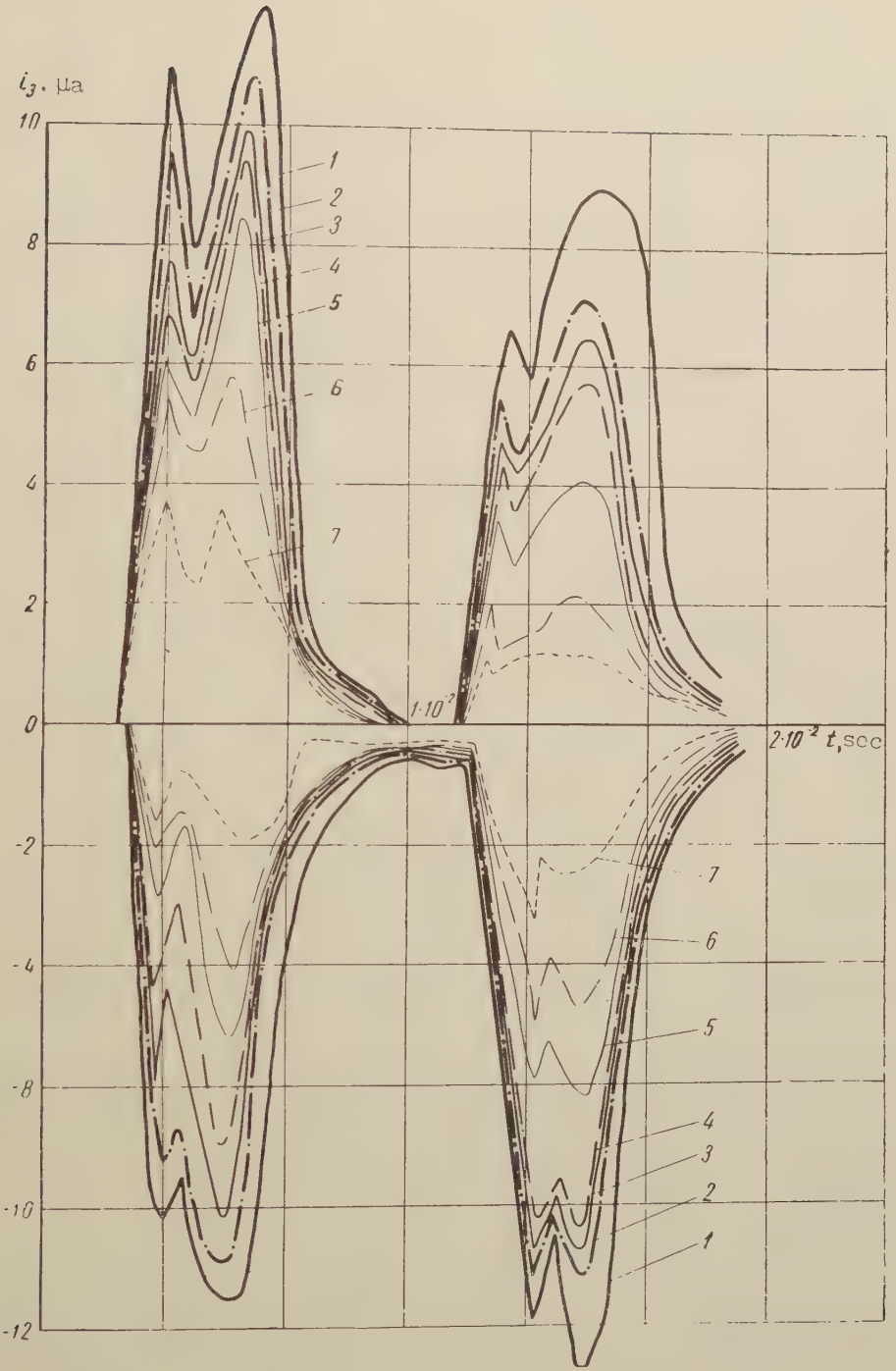

Fig.2. Time variation of the unbalance current for r = 17.5 cm and different values of the dc bias voltage U_n: 1) 2365, 2) 1950, 3) 1760, 4) 1380, 5) 1045, 6) 820 and 7) 625 v.

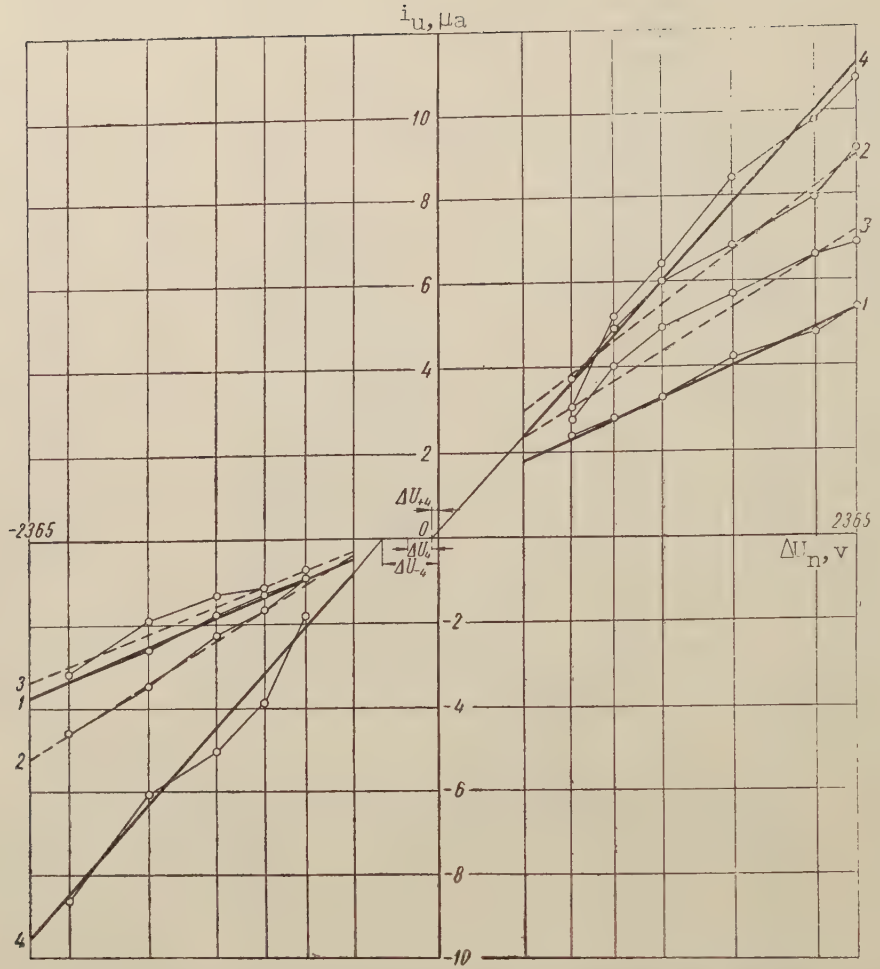

Fig.3. Current voltage characteristics of the differential probe (d_{wire} = 3.09 mm, m = 2, r = 17.5 cm) for ωt: 1) 36°, 2) 45°, 3) 51° and 4) 62°.

In the absence of influence of the probes on the main discharge, which is obviously one of the fundamental conditions for meaningful probe measurements, the difference $U_1(q_s) - U_2(q_s)$ is zero. Consequently, the difference between the capacitative currents is also zero, i.e., for the case of a differential probe we have automatic compensation of the capacitive currents. This is what makes it feasible to plot current-voltage characteristics similar to the charac teristics for the steady-state case on the basis of probe measurements.

The influence of the probes on the main discharge is negligible because the alternating voltage (applied to the probes from a special source) is at every instant close in value to the space potential that would obtain at the locations of the probes if these were not present. In our experiments the requisite amplitude and phase of the alternating voltage were set on the basis of the compensation criterion which in the case of use of a differential probe is the condition for coincidence of the current-voltage characteristics of the investigated discharge before and after introduction of the probe. In practice this was realized by adjusting the ac circuit so that the current-voltage characteristic on the oscillograph screen with the probes in place would coincide with the characteristic, traced in India ink on the oscillograph screen, at the same voltage on the corona electrode in the absence of the probes.

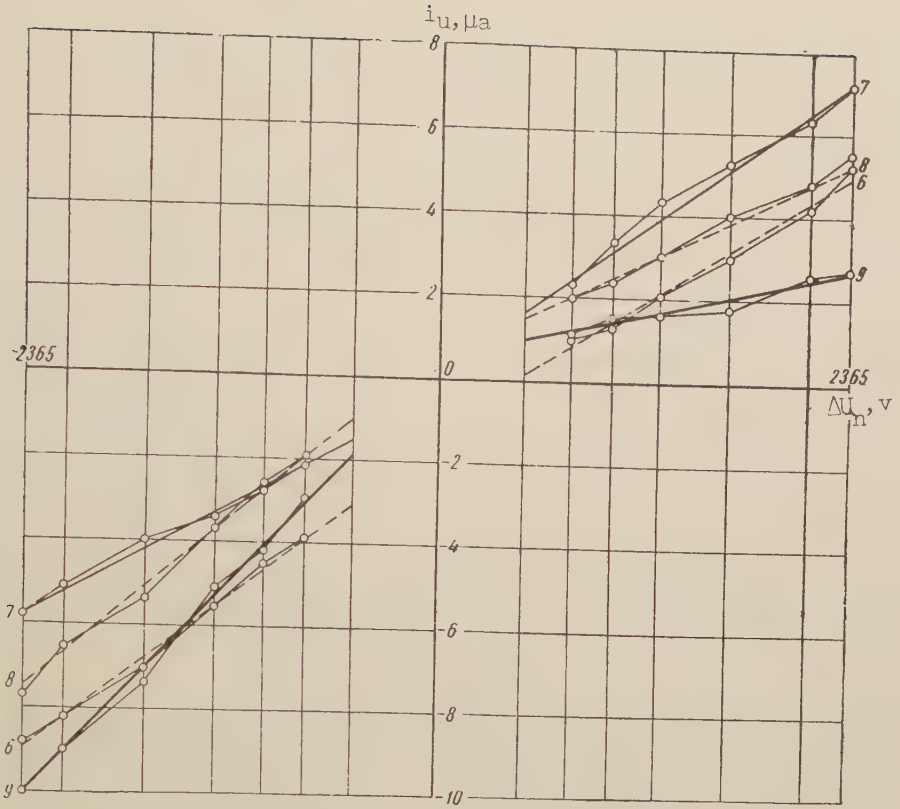

Fig.4. Current voltage characteristics of the differential probe (d_{wire} = 3.09 mm, m = 2, r = 17.5 cm for ωt: 6) 214°, 7) 264°, 8) 276° and 9) 288°.

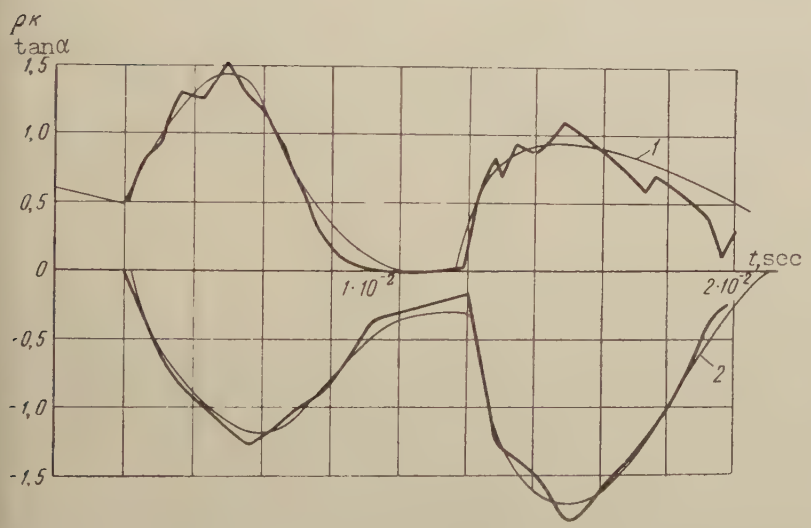

Fig.5. Variation of ρk with time for r = 17.5 cm: 1 - $\rho k = f(t)$ for positive ions and 2 - $\rho k = f(t)$ for negative ions.

After satisfactory compensation-adjustment of the ac circuit, the chosen dc bias voltage was applied to one of the electrodes and the oscillogram of the probe current difference was recorded. These oscillograms were essentially the primary experimental data which were then subjected to the interpretation and processing described below.

The differential probe measurements were carried out in the experimental set-up diagramed in Fig.1. The apparatus and circuit are described in detail in Ref.2, which also gives the results of investigations by means of a grid probe.

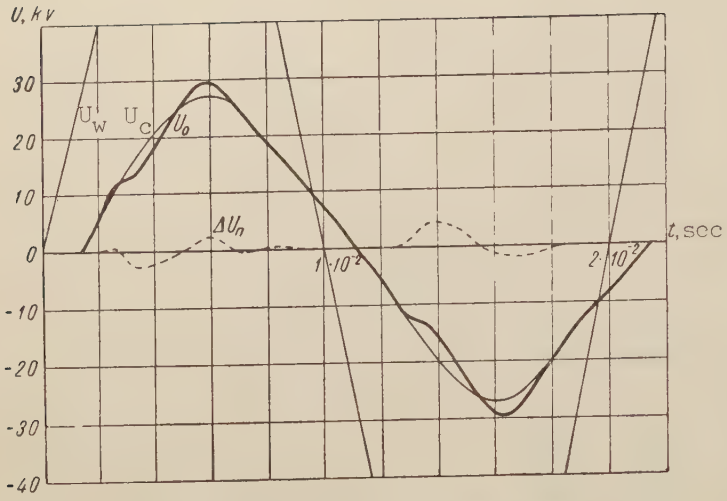

Fig.6. Space potential vs time curve for r = = 17.5 cm.

The differential probe measurements were carried out in the field of a 3.09 mm diameter corona electrode mounted in a 2 meter diameter cylinder with a relative overvoltage $U_m/U_0 = 2$.

Curves giving the variation of the unbalance current (the difference between the probe currents) as a function of the dc bias voltage for a probe to conductor distance r = 17.5 cm are shown in Fig.2. The corresponding curves for a number of other distances are similar. It will be evident from an examination of these curves that increase of the dc voltage (of either polarity) is accompanied by a virtually proportional increase in the amplitude and instantaneous values of the current, which is due, as has already been noted, to increase of the ionic component of the current through one of the probes.

On the basis of the unbalance current curves, we plotted the variation of the instantaneous current values (at different instants) with the dc bias voltage, i.e., the current-voltage characteristics of the differential probe. A series of such characteristics, corresponding to the curves of Fig.2, is shown in Figs.3 & 4. It will be seen that the plotted current-voltage characteristics are broken rather than straight lines. The experimental points deviate not to one side (which would indicate either a systematic error or mistakes in the theoretical inferences) but to both sides of the "average" straight line. This indicates the presence of experimental errors due to chance factors. Among such factors may be fluctuation of the supply voltage, zero creep of the dc amplifiers and uncertainties in scaling the values off the oscillograms, which were greatly enlarged.

The slope of the average current-voltage characteristics[1] gives the product of the space charge ρ times the ion mobility at the given point in the field and the given instant, i.e.,

$$\tan \alpha_i = \rho(t_i)\, k \frac{C}{\varepsilon_0},$$

where

$$C = (\alpha_{1-1} - \alpha_{1-2})^{-1}.$$

The ρk vs time curves for positive and negative ions obtained in this manner for the r = 17.5 cm case are given in Fig.5. These curves, like the unbalance current curves, have the shape of two successive "pulses". The amplitude of the first pulse corresponding to "forward" motion of the ions is appreciably higher than the amplitude of the second pulse corresponding to "reverse" motion.

In addition to ρk, one can also determine the space potential from the current-voltage characteristics. This is done by prolonging the characteristics to intersection with the voltage axis. The intercepts between the points of intersection and the origin give the difference ΔU between the instantaneous value of the compensating alternating voltage U_C on the probe and the instantaneous value of the space potential U_O at the investigated point.

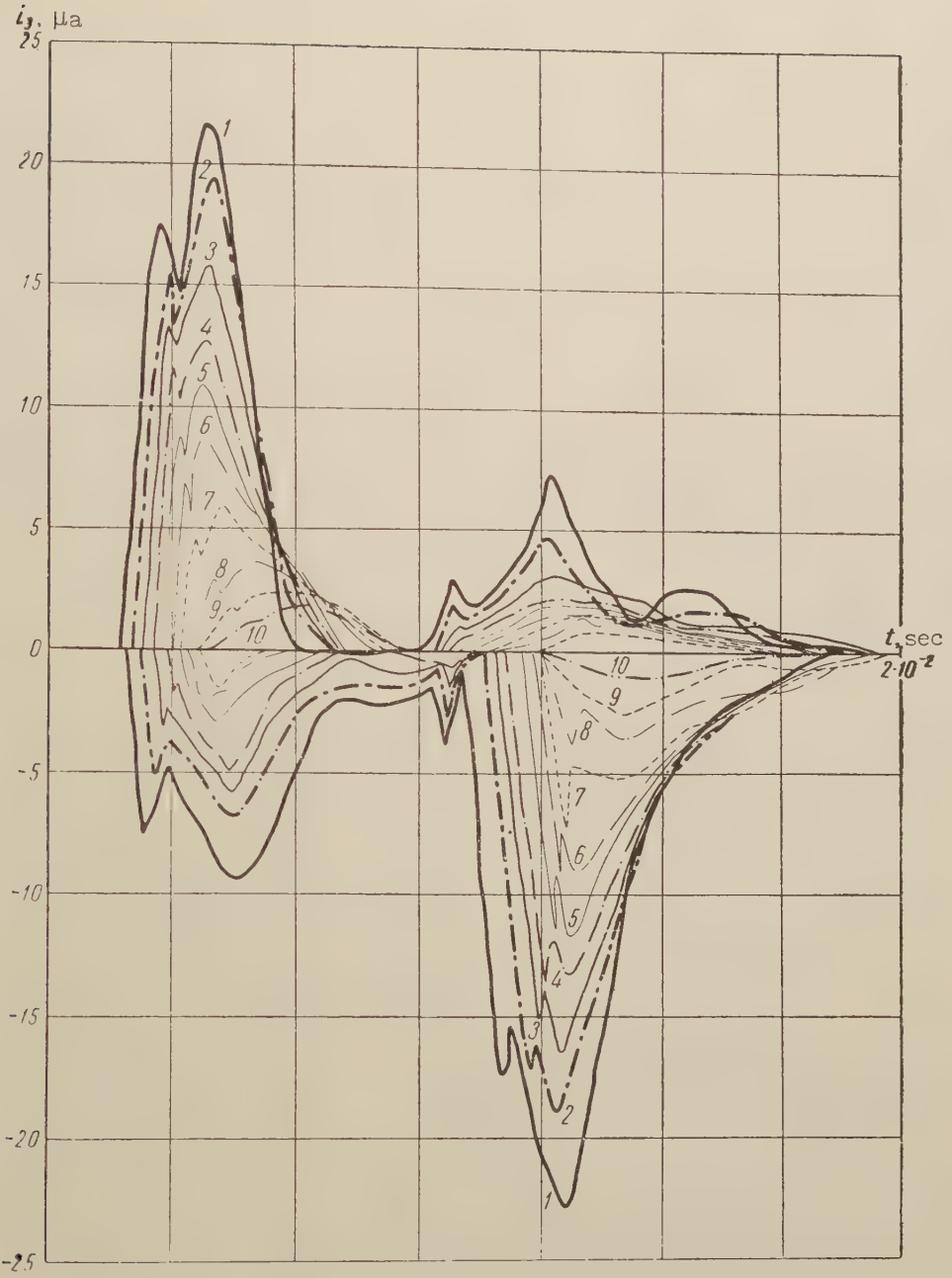

Fig.7. Variation of the unbalance current for different field cross sections (probe to electrode distances r) for d_{wire} = 3.09 mm, m = 2 with U_n = 2365 v: 1) r = 15 cm, 2) 17.5 cm, 3) 20 cm, 4) 22.5 cm, 5) 25 cm, 6) 27.5 cm, 7) 30 cm, 8) 32.5 cm, 9) 35 cm, 10) 37.5 cm.

In the absence of measurement and data processing errors, the current-voltage characteristics of the positive and negative charges plotted for the same instants should intersect the axis at the same point. Owing to unavoidable uncertainties, however, the positive and negative characteristics for the same instants intersect the axis at different, although close, points. Hence for determining ΔU we used the average value

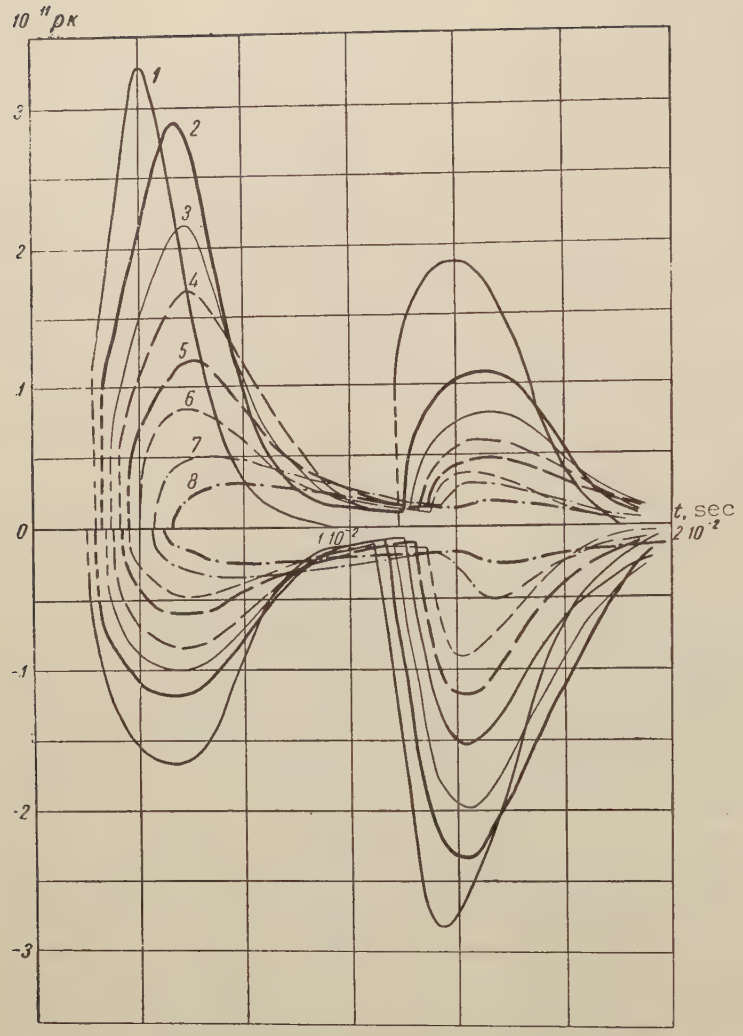

Fig.8. Variation of ρk for different r: 1) r = 15 cm, 2) 17.5 cm, 3) 20 cm, 4) 22.5 cm, 5) 25 cm, 6) 27.5 cm, 7) 35 cm, 8) 37.5 cm.

$$\Delta U_{av} = \frac{\Delta U_+ + \Delta U_-}{2}.$$

The variation of ΔU_{av} with time for r = 17.5 cm is shown in Fig.6, together with the curve for the compensating voltage $U_c = f(t)$ and the curve for the space potential $U_o = f(t)$. This curve is the sum of the other two curves, i.e.,

$$U_0(t_i) = U_c(t_i) + \Delta U_{av}(t_i).$$

Similar measurements and calculations were carried out for probe to conductor distances in the range from 12.5 to 42.5 cm. The unbalance current curves for a number of probe-to-conductor distances (r) obtained with a dc bias voltage U_n = 2365 v are shown in Fig.7. It will be evident that the points corresponding to the beginning of the forward current pulses, i.e., to the arrival of the space charge wave at the given point in space, shift to longer times with increase of r.

The $\rho k = f(t)$ curves for a number of distances are given in Fig.8. A notable feature of these curves is the diminution of the difference between the amplitudes of the forward and reverse pulses with increase of the probe to conductor distance; at the same time both amplitudes decrease. For distances r greater than 30 cm the difference becomes so small that one can justifiably speak of the virtual time invariance and spatial uniformity of the space charge density at these points.[3]

On the basis of the maximum values of ρk and the known mobility values for normal ions (k_+ = 1.4 cm^2 v^{-1} sec^{-1} and k_- = 1.8 cm^2 v^{-1} sec^{-1}) we obtained the variations of the maximum space charge density as a function of r shown in Fig.9.

In addition to the data on ρk, we obtained the space potential vs time curves (Fig.10) for different r from the experimental current-voltage characteristics. These curves for relatively small probe-to-conductor distances are distinctly distorted, the influence of third and fifth harmonics being particularly evident. With increase of r, the distortion of the space potential curves decreases and the shape of the curves approaches the shape of the total charge curve of the investigated corona gap.

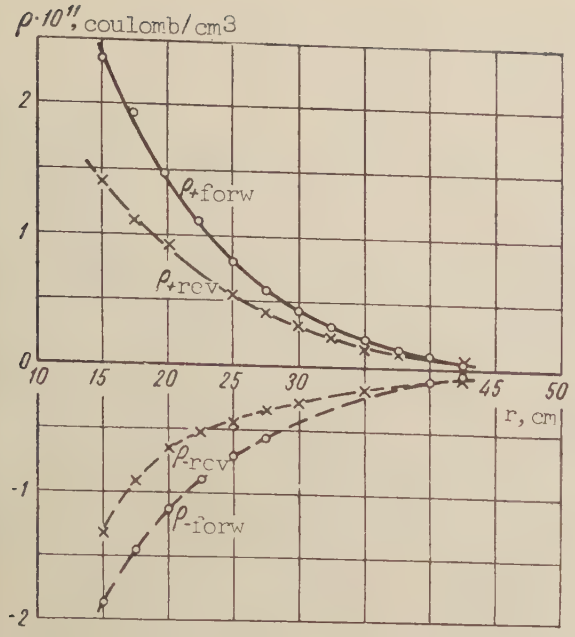

We shall not analyze the experimental results in greater detail here, inasmuch as the primary purpose of the present work was to develop a probe procedure for investigation of ac corona fields.

In conclusion, it may be noted that our experimental results show that it is feasible to realize probe measurements in an ac field; they also substantiate the validity of the theoretical concepts upon which the experimental procedure is based.

←Fig.9. Variation of the maximum space charge density as a function of the field cross section (probe to electrode distance r).

Fig.10. Space potential vs time curves for different r: 1) 12.5 cm, 2) 15 cm, 3) 17.5 cm, 4) 20 cm, 5) 25 cm, 6) 30 cm.

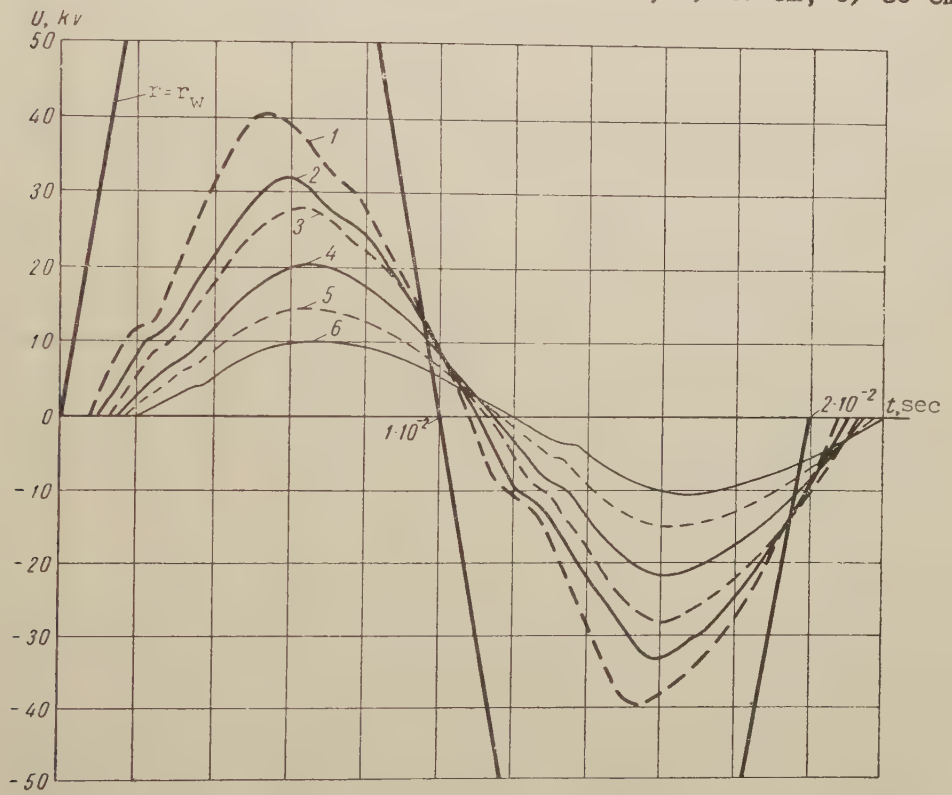

References

1. V.D.Kravchenko & V.I.Levitov, Izv.AN SSSR, Otd.tekh.nauk., (Bulletin, USSR Ac.of Sci., Div.Tech.Sciences) No.10, 6 (1955).
2. V.I.Levitov, A.G.Lyapin & V.I.Popkov, Ibid., No.1, 14 (1957).
3. V.I.Popkov, Ibid., No.7, 58 (1954).

ELEMENTARY PROCESSES IN THE IONIZATION ZONE OF CORONA DISCHARGES AT ATMOSPHERIC PRESSURE

- G.N. Aleksandrov

An understanding of the elementary processes occurring in the ionization zone of corona gaps is essential to determination of the field intensity on the surface of corona electrodes.

Corona discharges occur in highly inhomogeneous fields and are characterized by the presence of two regions in the discharge gap. The inner region comprises the ionization zone and has a very high field intensity. In the outer (dark) region the ions formed by the discharge move in a relatively weak field.

The current of a positive corona at low corona voltages is not continuous: it consists of an irregular sequence of avalanche pulses alternating with streamers. The rise pulses, i.e., surges of corona current, is connected with the existence of local conditions for self-maintenance of the discharge for brief intervals. During such intervals the current through the corona gap increases by 2-3 orders of magnitude. When the voltage is increased above the starting value, the current fluctuations rapidly die down and there is established a steady-state positive corona. The current fluctuations in a positive corona are determined by the conditions of the formation of the outer region of the corona gap and do not depend on any processes in the ionization zone. The transition from a fluctuating to a steady state in the case of a positive corona is not marked by any changes in the character of the corona current vs voltage curve. Hence in the present report we shall not discuss the conditions for a steady-state positive corona.

The natural source of secondary electrons in a unipolar positive corona is photoionization in the ambient gas. The condition for the appearance of a positive corona are usually formulated as the condition for production of individual avalanches. Loeb and his co-workers[1] have shown, however, that absorption by the gas of the radiation of an individual avalanche can lead to the appearance of several photoelectrons, each of which in turn can initiate a more or less powerful electron avalanche. All these avalanches participate in the development (or maintenance) of the discharge. Analysis of the conditions for formation of a positive unipolar corona taking into account all the avalanches occurring in the ionization zone led to a new formulation of the condition for the appearance of a corona as the condition for production of the full number of photons in the ionization zone, generated (by excitation of the gas molecules) by the initial and subsequent avalanches:[3]

$$0.5\, k\eta_1\mu \int_0^{\infty} k_{\text{eff}} [\exp (\int_{r_0}^{r_0+\rho} \alpha dr - \mu\rho)] d\rho = 1, \qquad (1)$$

where $k = \theta^0/\alpha$ (α is the first Townsend ionization coefficient), θ is the number of photons produced by an electron avalanche per 1 cm path, η_1 is the quantum yield of photoelectrons, μ is the radiation absorption coefficient of the gas, r_0 is the radius of the conductor, ρ is the distance from the point on the surface of the conductor, that may be regarded as the point of emergence of all the photons produced by the initial avalanche*, to an arbitrary point in the gas volume, and k_{eff} is the photoelectron efficiency coefficient which takes into account differences in the power of the avalanches initiated by absorption of photons and propagating in different directions with ρ = const. Eq. (1), which does not contain the number of photons of the initial avalanche and which was deduced from the condi-

---

*The assumption that all the photons emerge from one point is justifiable at gas pressures close to atmospheric or higher.

tion of production of the total number of photons in the ionization zone, is the condition for the generation of an individual photon in the ionization zone.

The value of $k\eta_1$ calculated[3,4] from the results of measurements of the initial potential of a positive corona with a conductor 1.4 cm in diameter (E_i^+ = = 41.5 kv/cm) for $\mu = 6$ cm^{-1} proved to be $1.74 \cdot 10^{-3}$, which is a plausible value. This figure is almost three times smaller than the value of $k\eta_1$ ($4.7 \cdot 10^{-3}$) obtained from the same data on the assumption of an individual avalanche production mechanism.[5] Inasmuch as it would appear therefore that the mechanism of generation of the total number of photons in the ionization zone is energetically more advantageous than the mechanism of production of an individual avalanche, it follows that the former mechanism responsible for the appearance of positive coronas.

Negative coronas do not have a steady state. The positive and negative space charges formed by the corona accumulate close to the corona "spot" at different distances from the electrode surface. This leads to a sharp increase in the intensity of the discharge. However, owing to differences in the rates of removal of positive and negative ions from the corona gap, the discharge from a given "spot" soon ceases.[6] The current of a negative corona therefore consists of a series of regular pulses (Trichel pulses) of 10^{-7} to 10^{-6} sec duration and with a current rise time of the order of 10^{-7} sec. A discharge of this character can be assured only by photoelectric processes, namely, photoionization in the volume of the gas and a photoeffect on the electrode surface. Calculations (carried out for conductor diameters of up to 1.5 cm) showed that the contribution of the first process to the production of secondary electrons in a negative corona is small compared to the contribution of the latter process.[3] The condition for the appearance of a negative corona may therefore be approximately formulated as the condition for production of an individual avalanche propagating from the surface of the conductor; mathematically it is described by the relation[3]

$$k\eta_2 \int_{r_0}^{r_i} g_\mu \alpha \left[\exp\left(\int_{r_0}^{r_0+\rho} \alpha dr - \mu\rho\right)\right] dr = 1, \qquad (2)$$

where η_2 is the quantum yield of electrons from the conductor surface, r_i is the radius of the outer boundary of the ionization zone and g_μ is a geometric factor taking into account different photon losses due to absorption in the gas and inhomogeneities of the electric field.

Calculations showed that condition (2) is in agreement with the experimental dependence of the initial voltage of a negative corona on the radius of the conductor in a wide range of conductor radii for $\mu = 6$ cm^{-1} and a constant value of the quantum yield of electrons ($k\eta_2 = 0.68 \cdot 10^{-2}$). At the same time, the experimental dependence of the initial corona voltage on the radius of the conductor satisfies the condition for self-maintenance of the discharge in the form

$$\gamma\left[\exp\left(\int_{r_0}^{r_i} \alpha\, dr\right) - 1\right] = 1, \qquad (3)$$

which assumes emergence of electrons from the surface of the conductor because of bombardment by positive ions, only if one assumes a substantial variation of γ with the conductor radius. Thus, according to the data of Tikhodeev[7] for thin conductors, γ must be of the order of 10^{-3}, whereas for thick conductors (radius over 1 cm) it should be of the order of 10^{-4}. So appreciable a variation of γ cannot be theoretically justified.

Bipolar corona discharges may occur in the case of dc voltages with two oppositely charged conductors or in the case of ac voltages with all possible corona systems (gap configurations) assuring retention of ions in the gap. Such

bipolar corona discharges are characterized by the intrusion into the positive or negative ionization zone at each conductor of ions of opposite charge formed in the ionization zone of the other conductor in the case of dc voltage or during the preceding half-cycle in the zone of the same conductor in the case of ac voltage.[8] It will be apparent that bipolar coronas actually obtain in virtually all corona systems of interest from the practical standpoint.

The intrusion of positive ions into the ionization zone of a negative corona cannot have a significant effect on the condition for self-maintenance of the discharge because, as was noted above, the specific interrupted character of negative coronas can be assured only by photoelectric processes. Hence condition (2) is also entirely valid for negative coronas in bipolar discharges.

When negative ions invade the ionization zone of a positive corona, they may decay with the formation of free electrons. The decay of negative ions has been investigated repeatedly. According to the data collected in Loeb's book,[9] the highest probability is for decay in a second order collision with an excited atom or molecule ($M^- + N' \rightarrow M + N + e$), particularly if the excitation energy of the molecule is close to the energy necessary for detaching an electron from the ion. From the data cited by Loeb, it may be inferred that the excitation energy of the first vibrational levels of O_2 and N_2 molecules is close to the energy for detachment of an electron from O_2^-. Inasmuch as in the ionization zone of a positive corona electron avalanches excite a far greater number of molecules than are ionized, the probability of decay of negative ions within the ionization zone must be fairly high. Thus a continuous inflow of negative ions may serve as an addition source of initiating electrons in the ionization zone of a positive corona; this, however, can have an appreciable influence on the condition for self-maintenance of the discharge only if it is steady (not intermittent). Since, as noted above, intermittent effects close to the voltage of initiation of a unipolar positive corona are determined only by the conditions of formation of the outer region of the corona discharge and are not connected with any specific processes, we can consider the conditions for self-maintenance of a continuous positive corona in the presence of a continuous flux of negative ions, treating the space charge of negative ions as a sort of stabilizer of the positive corona under bipolar discharge conditions. In this case the condition for the appearance of a positive corona under bipolar conditions may be written in the form[3,5]:

$$0.5\, k\eta_1\mu \int_0^{\infty} k_{\text{eff}} [\exp\left(\int_{r_0}^{r_0+\rho} \alpha\, dr - \mu\rho\right)]\, d\rho = 1 - \xi\phi\, n^-/n^+ [\exp\left(\int_{r_0}^{ri} \alpha dr\right) - 1], \qquad (4)$$

where ϕ is the probability for disintegration of ions within the ionization zone, ξ is the efficiency coefficient of the forming electrons and n^+ and n^- are the concentrations of the positive and negative ions, respectively, at the boundary of the ionization zone of the positive corona.

The critical positive corona voltage defined by Eq. (4) is lower than the starting voltage for a positive corona characterized by Eq. (1) as a function of the concentration ratio of positive and negative ions at the boundary of the ionization zone. The highest n^-/n^+ ratio will obtain close to the voltage of the initiation of the corona, when virtually all the ions formed in the ionization zone of the negative corona approach the ionization zone of the positive corona, inasmuch as at the prevailing low ion concentrations under these conditions ion recombination is not intense. With increase of the voltage above the corona initiating value, the concentrations of ions of both polarities increase. At the same time recombination becomes more intense. Moreover, in the case of an ac voltage[8] part of the space charge formed in the preceding voltage half-cycle does

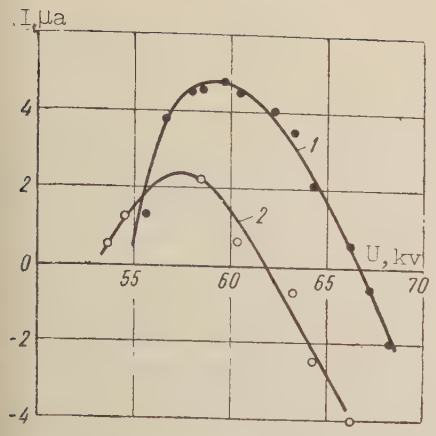

Fig.1. Variation of the dc component of the corona current (0.588 cm diameter conductor in a 30 cm diameter cylinder) with the amplitude of the 50 cps voltage: 1) clean electrode surface, 2) soap film on electrode surface.

not return to the electrode in the succeeding half-cycle, but continues to drift in the corona gap. With a 1.5-2-fold overvoltage (relative to the initial corona voltage) the ratio n^-/n^+ both with dc voltage (bipolar corona)[10] and with ac voltage[8] does not exceed 0.1-0.2. Consequently, a bipolar corona discharge starts at the lowest possible critical voltage E_c of the positive corona given by Eq.(4) for $n^-/n^+ \approx 1$. With increase of the voltage above the initial (starting) one, the critical voltage of a positive corona increases with decrease of n^-/n^+ in accord with (4).

In accord with the above, the process of initiation of a bipolar corona with either dc or ac voltage may be described as follows. With gradual smooth increase of the voltage on the gap, first, upon attainment of a voltage E_i^- on the surface of the negatively charged conductor, there appears a negative corona (in the range of variation of conductor radii of practical interest, $E_i^- < E_i^+$). The negative ions forming in the ionization zone of the negative corona after a certain period invade the region of the strong field of the positively charged conductor (self-sustaining discharge region). A chance electron avalanche leads to the formation of a brief spark which is rapidly extinguished in the absence of an additional source of secondary electrons (photons). The negative ions, decaying upon collision with gas molecules, excited by such a series of avalanches, play the role of such an auxiliary source of electrons. A chance avalanche, which in the absence of an external source of electrons, could not lead to the onset of a self-sustaining discharge, in the presence of negative ions initiates the process of self-maintaining ionization.

If $E_c^+ < E_i^-$, the bipolar corona current is maintained at a voltage lower than the voltage for initiation of an ordinary negative corona. Actually, if the amplitude of the ac voltage across the corona system is gradually increased, the corona current (the compensated current through the gap) is established suddenly at a voltage corresponding to E_i^- (for both polarities of the voltage). With gradual decrease of the voltage amplitude, the corona current does not cut off at the initiation voltage but continues to decrease down to a certain voltage somewhat below this, at which point it ceases.[5] This effect can be observed only when $E_c^+ < E_i^-$, inasmuch as the initial voltages of the negative coronas in unipolar and bipolar discharges are equal. Thus near the initial voltage a bipolar corona is maintained with different charges on the conductors:

$$q_0^+ = 2\pi r_0 E_c^+ < q_0^- = 2\pi r_0 E_i^-$$

This inequality is compensated by an excess of positive space charge. Thus, in the case of dc voltage, the zero potential line is shifted toward the negative conductor.[11] In the case of ac voltage, one can observe a positive dc component of the corona current near the initial voltage (Fig.1) although the mobility of positive ions is less than that of negative ions. It is interesting to note that with increase of the voltage the positive dc component gives way to a negative one (see Fig.1), which indicates a change in the ratio between E_c^+ and E_i^-.

Further confirmation of the picture of this effect is furnished by the following experiment. After recording the current-voltage characteristic of the dc component of the corona current as shown by curve 1 in Fig.1, a soap film was

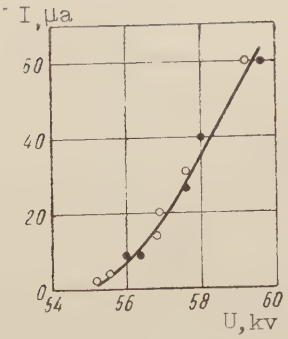

Fig.2. Current-voltage characteristic of a unipolar positive corona (0.588 cm diameter conductor in a 30 cm diameter cylinder) on the basis of measurements with a clean surface conductor and with a soap film on the conductor surface: ● - clean surface; o - with soap film.

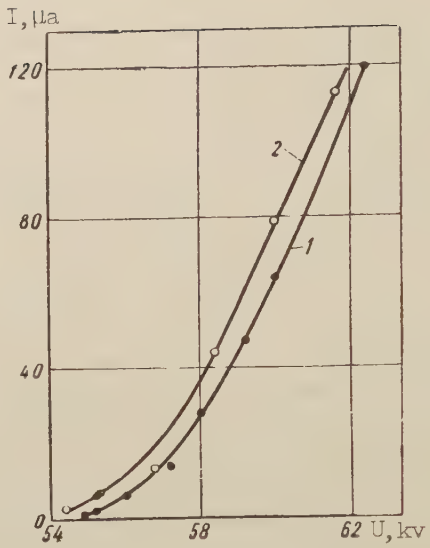

Fig.3. Current-voltage characteristics of negative corona (0.588 cm conductor in 30 cm diameter cylinder): 1) clean conductor surface, 2) soap film on conductor.

applied to the electrode. That the current-voltage characteristic of a unipolar positive corona is not altered by the application of such soap film is indicated by absence of distortion of the field near the conductor (see Fig.2). On the other hand, as will be evident from Fig. 3, the initial (starting) voltage of the negative corona was reduced as a result of application of the soap film. As will be evident from curve 2 in Fig.1, the current-voltage characteristic of the dc component of the corona current with ac voltage was greatly altered by the soap film. The maximum of the curve went down and the zero current point shifted to the side of lower voltages. This occurred because in the presence of the soap film the difference between E_c^+ and E_i^- was appreciably reduced, owing to the fact that E_i^- decreased substantially, whereas E_c^+ remained virtually constant.

In view of the noted distortion of the field in the discharge gap by the ionic space charge (predominance of positive space charge over negative), one can define the equivalent critical corona voltage in a bipolar discharge by the relation:

$$E_{cb} = (E_c^+ + E_i^-)/2; \qquad (5)$$

by means of this relation one can readily obtain the critical voltage for a positive corona from the measured values of E_{cb} and E_i^- (E_{cb} is the voltage at which the discharge ceases as the amplitude of the ac voltage is gradually decreased). For example, the following data were obtained in measurements[5] of the initial corona voltages with a conductor 1.4 cm in diameter in a 30 cm diameter, 2 m long cylinder:

$$E_i^+ = 41.5 \text{ kv/cm}, \quad E_i^- = 40.6 \text{ kv/cm} \quad \text{and} \quad E_{cb} = 40.1 \text{ kv/cm}.$$

From this we obtain

$$E_c^+ = 2 \times 40.1 - 40.6 = 39.6 \text{ kv/cm} \quad \text{and} \quad \frac{E_i^+ - E_c^+}{E_i^+} = 4.6\%.$$

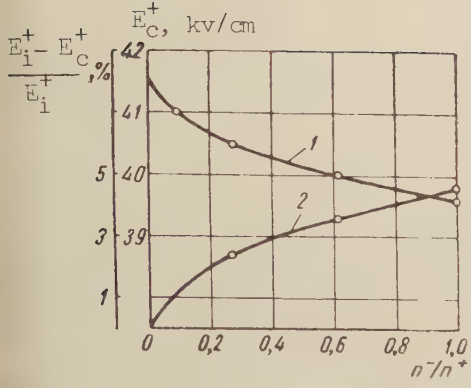

Fig.4. Variation of the critical voltage of a positive corona of a 1.4 cm diameter conductor (1) and deviation of this critical voltage from the initial voltage for a positive corona (2) as functions of the ratio n^-/n^+, obtained from Eq. (4). The value of $0.65 \cdot 10^{-3}$ for $\xi\psi$ was obtained on the assumption that at the critical voltage of an ac corona $n^-/n^+ = 1$.

The variation of the critical voltage of a positive corona as a function of n^-/n^+ and calculated by means of (4) is shown in Fig.4. It will be evident that under conditions of practical interest ($n^-/n^+ = 0.1$-0.2) the critical voltage of a positive corona is approximately equal to the initial voltage of a negative corona, i.e., $E_c^+ \approx E_i^-$.

In view of the above there can be no doubt that there exists a critical positive corona regime that arises in the presence of a counterflow of negative ions. In view of the premises upon which the derivation of (4) was based, it may be inferred that a positive corona discharge in a bipolar (critical) regime is continuous from the instant of its initiation (in contrast to a unipolar positive corona). Naturally, this inference is still in need of experimental verification.

References

1. L.Loeb & R.Wijsman, J.Appl.Phys., 19, 797 (1948).

2. L.Loeb & C.Miller, J.Appl.Phys., 22, 494 (1951).

3. G.N.Aleksandrov, Zhur.tekh.fiz., 26, 2640 (1956). (Trans.Soviet Physics - Tech.Physics).

4. C.Duchene, J.phys.et radium, 7, 533 (1936).

5. G.N.Aleksandrov, Zhur.tekh.fiz., 26, 1769 (1956). (Trans.Soviet Physics - Tech.Physics.)

6. G.N.Aleksandrov, Ibid., 26, 2634 (1956).

7. N.N.Tikhodeev, Dissertation, Leningrad Polytechnic Inst., 1955.

8. G.N.Aleksandrov, Zhur.tekh.fiz., 25, 1905 (1955); Ibid., 27, 784 (1957). (Trans.Soviet Physics - Tech.Physics).

9. L.B.Loeb, Fundamental Processes of Electrical Discharges in Gases, N.Y., 1939. (Cited in Russian trans.)

10. L.E.Tsyrlin, Dissertation, Leningrad Polytechnic Inst., 1958.

11. V.I.Popkov, Izv.AN SSSR, Otd., tekhn.nauk., (Bulletin, USSR Ac. of Sci., Div. Tech.Sciences), No.4, 433 (1948).

CHARGE DENSITY OSCILLATION WAVES IN A CYLINDRICAL PLASMA

- M.Ya.Vasil'eva, A.A.Zaitsev & E.D.Zndryukhina

In an ionized gas there may appear acoustical modes associated with electrostatic oscillations of the positive ions. The ion oscillation frequency is

$$f_i = \left(\frac{ne^2}{\pi m_i + \frac{ne^2 m_i \lambda}{kT_e}} \right)^{1/2}, \tag{1}$$

where m_i is the ion mass, T_e is the absolute temperature of the electron gas, and λ is the wavelength of the plane waves (for nonsinusoidal perturbations, λ is approximately equal to the displacement of the ions). At values of λ that are large compared to the Debye length, the oscillation frequency f_i equals $\left(\frac{kT}{m_i}\right)^{1/2} \Big/ \lambda$; in this case the group and phase velocities attain a value of

$$v_{g,p} = \left(\frac{kT_e}{m_i} \right)^{1/2}. \tag{2}$$

Electroacoustic waves have been treated theoretically by Langmuir[1], Spitzer[2] and a number of other authors. So far, however, they have not been observed experimentally.

The results of the present work show that at low gas pressures there are observed in the plasma of the positive column wave-like processes that move from the cathode to the anode with a velocity that is nearly independent of the frequency. The measured values of the velocity are close to the values calculated by means of Eq.(1).

Noise in a wide band of frequencies (from kilocycles to megocycles) and oscillations with discrete frequencies are often generated in gas discharges. Under ordinary conditions the oscillations, which may have an amplitude of 10 v or more, are, as a rule, produced either by instability of the anode fall of potential or by the presence of moving striations in the positive column. In practice, one can expect to detect ionic oscillations only under conditions when anode oscillations and moving striations are absent. The conditions determining the appearance of anode oscillations depend on the size and shape of the anode surface; through appropriate choice of the anode geometry one can assure a fully stable anode potential fall. The mechanism responsible for the striations and the reasons for their presence or absence must be sought in the specific attributes of the positive column plasma.

Earlier one of us[3] described experiments in which moving striations were produced artificially. When the positive column shows a tendency to striate under the influence of periodic oscillations applied to the discharge from an external source, one can artificially produce and maintain striations traveling from the anode to the cathode (hereinafter "anode striations"). Depending on the character of the external perturbing source and the condition of the discharge itself, the striations appear either over the entire length of the positive column or only in a part of it (generally in the part between the anode and the point where the disturbing oscillations are injected).

The anode striations may also form in the transient state following a one-time disturbance of the discharge. In this case, however, the striations soon disappear and the positive column returns to its initial condition. This effect can obviously be utilized for investigating the formation of anode striations.

The present work is a continuation of the research described in Ref.3. Here we give the results of an experimental investigation of the wave-like processes induced in the positive column by artificial periodic disturbance of the discharge

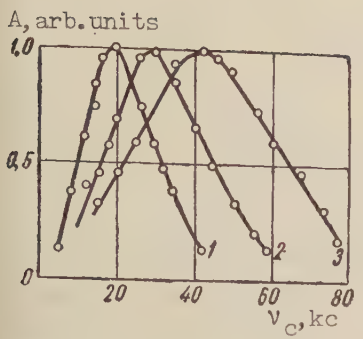

Variation of the amplitude of the luminous intensity oscillations of the column associated with artificial anode striations as a function of the frequency (i = = 0.1 amp): 1) p = 0.8 mm Hg, 2) 0.5 mm Hg, 3) 0.2 mm Hg.

and consider the following questions.

1. Is there a lower bound of the pressure at which the anode striations disappear (as the pressure in the discharge tube is gradually reduced)?

2. Aside from anode striations, can there exist other wave-like effects in the discharge column and, if so, what are their characteristics?

In the present experiments we used discharge tubes 2.2, 3 or 3.6 cm in diameter, 42 cm in length and filled with argon, helium or xenon. In each case the cathode was an oxidized spiral; the anodes were made in the form of a hollow cone, inasmuch as this anode design assures a small and stable anode potential fall. The anode current values ranged up to 300 ma. To disturb the discharge we used the ac voltage from an oscillator, which was applied between the cathode and an auxiliary electrode, i.e., a wire located 2-3 mm in front of the cathode. The appearance of the wave-like effect in the positive column and the direction of its motion were detected and observed by means of a photomultiplier (or two probes) and a cathode-ray oscillograph. Specifically, we measured the frequency ν_c and the length l_c (thickness along the tube) of the mobile striations (the period of the wave-like process). For measuring l_c the oscillograph sweep was synchornized with the frequency of the oscillator. With displacement of the photomultiplier a distance equal to the thickness of a striation the trace on the screen shifted one period.

In helium filled tubes no natural (spontaneous) anode striations were observed at a pressure of 0.9 mm Hg and currents weaker than 60-130 ma. At lower pressures, natural striations do not form even with stronger currents. There is, however, generated noise with an amplitude at least an order magnitude lower than that of the oscillations associated with the moving striations. Under these conditions application of the external periodic perturbing agency (i.e., an oscillating voltage) leads to the formation of artificial striations at pressures ranging down to a few hundredths of a millimeter Hg. The number of artificial striations passing per second is equal to the frequency of the external oscillator.

The variation of the amplitude of oscillation of the luminous intensity of the positive column as a function of the frequency is shown in the accompanying figure. A noteworthy feature of the curves is the presence of a "resonance frequency", i.e., a frequency characterized by a pronounced maximum amplitude. At this frequency, the artificial striations are sharpest. The frequency dependence of the striations was noted earlier in Ref.4. With decreasing pressure the entire picture is shifted to the side of higher frequencies, and moreover, the frequency band of the artificial striations is broadened. For natural striations, the frequency ν_c is proportional to the pressure p, i.e, is a function of the product of the tube radius r by the pressure. The values of the resonance frequency to pressure ratio for artificial layers fit the prolongation of the $\nu_c/p = f(rp)$ curve for natural striations.

The values of the length and frequency of the striations and of the velocity of the anode to cathode travel of the striations in helium at different pressures and two tube radii are listed in Table 1. In all cases the discharge current was 100 ma.

Some authors have discussed the formation mechanism of the moving striations from the standpoint of the theory of electro-acoustic waves in plasma.[5,6] However, moving striations, in contrast to acoustic waves, are characterized by a

higher dispersion. This effect was first observed in the work of Ref.3. In the present investigation we studied this effect in greater detail.

Table 1

r = 1.5 cm	$p = 0,7$ mm Hg	ν_c, kc	10	15	20	25	30	35
		l_c, cm	8	8,3	8,5	8,8	8,9	9,0
		v, m/sec	$8 \cdot 10^2$	$12,4 \cdot 10^2$	$17 \cdot 10^2$	$22 \cdot 10^2$	$26,7 \cdot 10^2$	$31,5 \cdot 10^2$
	$p = 0,4$ mm Hg	ν_c, kc	15	20	30	40	50	70
		l_c, cm	8,1	8,2	8,5	8,8	9,0	9,3
		v, m/sec	$12,1 \cdot 10^2$	$16,4 \cdot 10^2$	$25,5 \cdot 10^2$	$35,2 \cdot 10^2$	$45 \cdot 10^2$	$65,1 \cdot 10^2$
	$p = 0,07$ mm Hg	ν_c, kc	30	40	60	70	80	95
		l_c, cm	8,2	8,4	9,0	9,2	9,5	9,8
		v, m/sec	$24,6 \cdot 10^2$	$33,6 \cdot 10^2$	$54 \cdot 10^2$	$64,4 \cdot 10^2$	$75 \cdot 10^2$	$93,1 \cdot 10^2$
r = 1.1 cm	$p = 0,8$ mm Hg	ν_c, kc	14	18	20	25	27	30
		l_c, cm	5,5	6,3	6,6	7,2	7,5	7,7
		v, m/sec	$7,7 \cdot 10^2$	$11,3 \cdot 10^2$	$13,2 \cdot 10^2$	$18 \cdot 10^2$	$20,2 \cdot 10^2$	$23,1 \cdot 10^2$

At a pressure of 0.01 mm Hg new effects appear in helium. First, there is a noticeable change in the character of the cathode glow as a result of application of an external disturbing influence. Whereas in an undisturbed discharge there is a dark space with definite boundaries separating the positive column from the cathode glow, upon application of the disturbing oscillations the dark region disappears and the positive column luminosity fills the entire tube. Under these conditions there appears in the column a wave-like process that travels from the cathode to the anode ("cathode striations"). The cathode striations appear only within a certain range of variation of the external oscillation frequency. Propagation of the wave-like process is accompanied by periodic alterations in the luminous intensity of the gas over the length of the column. By moving the photomultiplier (or probes) along the length of the discharge tube, one can observe that the phase of the luminous oscillations varies continuously. The results of measurements for a helium filled tube of 1.5 cm radius with i = 30 ma are shown in Table 2.

Table 2

$p = 0,01$ mm Hg	ν_c, kc	250	350	400
	l_c, cm	13,1	9,9	8,7
	v, m/sec	$32,6 \cdot 10^3$	$34,7 \cdot 10^3$	$34,8 \cdot 10^3$
$p = 0,009$ mm Hg	ν_c, kc	250	300	500
	l_c, cm	13,6	11,6	7,8
	v, m/sec	$34 \cdot 10^3$	$34,8 \cdot 10^3$	$39 \cdot 10^3$
$p = 0,007$ mm Hg	ν_c, kc	300	400	500
	l_c, cm	12	9,3	7,6
	v, m/sec	$36 \cdot 10^3$	$37,2 \cdot 10^3$	$38 \cdot 10^3$

It will be evident from the tabular data that with increasing frequency the thickness of the cathode striations decreases, while their rate of travel changes little. We can take advantage of this data to compare the behavior of the cathode striations with that of

the electro-acoustic waves. According to Eq.(2), the velocity of electro-acoustic waves is determined by the electron temperature and the ion mass. The electron temperature in helium at a pressure of 0.01 mm and i = 30 ma, as determined by a Langmuir probe, proved to be $205 \cdot 10^3$°K. Substitution of this value of T_e in the theoretical formula leads to $20.5 \cdot 10^3$ m/sec for the electro-acoustic wave velocity; this is about 30% lower than the velocity of the cathode striations measured under the same conditions. In a tube of 1.8 cm radius ($p = 6.5 \cdot 10^{-3}$ mm Hg, i = 70 ma, $\nu_c = 250$ kc) the striation travel velocity was $31 \cdot 10^3$ m/sec. We made an attempt to observe cathode striations in tubes of smaller radius (0.7 and 1 cm), but found that in narrower tubes the discharge dies out at a pressure of about 0.01 mm Hg.

Propagation of the wave-like process (cathode striations) from the cathode to the anode was also observed in argon and xenon. In these gases, the anode striations disappear at lower pressures ($3\text{-}4 \cdot 10^{-3}$ mm Hg). Accordingly, the minimum pressure at which cathode striations appear in these gases is also reduced. In the heavier gases, the cathode striations are quickly attenuated in moving down the positive column. Thus in a tube of 1.8 cm radius filled with argon at $3 \cdot 10^{-3}$ mm Hg cathode striations having a length of 4.5 cm are observed at distances up to 7-9 cm from the cathode. The velocity of the striations at a frequency of 110 kc is $4.95 \cdot 10^3$ m/sec. Probe measurements under these conditions yield an electron temperature of $84 \cdot 10^3$°K. According to Eq.(2), the electro-acoustic wave velocity at this temperature should be $4.2 \cdot 10^3$ m/sec.

It must be noted, however, that the theory of electro-acoustic waves is based on a homogeneous infinite plasma. Actually, in the plasma of a gas discharge in a cylindrical tube the density of the charged particles over the cross section is not uniform. Hence one must be cautious in comparing theory with experiment. Nevertheless, some of the attributes of cathode striations are qualitatively described by the theory of electro-acoustic waves.

Physics Faculty,
Moscow State University

References

1. I.Langmuir & L.Tonks, Phys.Rev., 33, 195 (1929).
2. L.Spitzer, Physics of Fully Ionized Gases, N.Y., 1956.
3. A.A.Zaitsev, Vestnik, Moscow State University, No.10, 41 (1951).
4. A.A.Zaitsev, Doklady AN SSSR, 84, 41 (1952).
5. T.C.Chow, Phys.Rev., 37, 574 (1931).
6. N.Labrum & E.Bigg, Proc.Phys.Soc.B, 65, 356 (1952).

POSITIVE DISCHARGE COLUMN UNDER DIFFUSION CONDITIONS

- V.M.Zakharova, Yu.M.Kagan & V.I.Perel'

Whereas the theory of the positive column in low pressure discharges, developed by Schottky[1] and Langmuir & Tonks[2], has been subjected to careful and systematic comparison with experiment in the work of B.N.Klyarfel'd, the processes occurring in the column under conditions where diffusion is significant have scarcely been studied. At present such investigation has become possible owing to the appearance of reliable data on the cross section for charge exchange of ions with the atoms of the parent gas and on the mobility of atoms in the parent gas.

It was assumed by Schottky[1] and Tonks & Langmuir[2] that the ion drift velocity in the radial direction is proportional to the field strength. Experimental results[5] show that this is true only in weak fields when $eE/pq \ll 1$, where E is the field strength, p is the gas pressure and q is the cross section for ion-atom collisions. In the positive column the radial field strength is a function of the distance from the axis of the discharge, and the above inequality is fulfilled only for the region in the vicinity of the axis. This was pointed out by Frost[4], who using the balance equation for electrons and ions in the plasma (on the assumption of quasi-neutrality and a Boltzmann distribution of electrons over the cross section),

$$\frac{1}{r}\frac{d}{dr}[r\bar{v}e^{-\eta}] = Ze^{-\eta}, \tag{1}$$

where $\eta = -\frac{eV(r)}{kT_e}$ and v is the ion drift velocity, investigated the influence of variable ionic mobility on the distribution of potential $V(r)$ and concentration $n(r)$ over the radius and on the relation between the number Z of ionizations per electron per unit time and the electron gas temperature

In the present work, making use of Frost's theory, we derived a number of relationships convenient for comparison with experiment and carried out a comparison for the positive column in discharges in Hg, A and K. We also consider the question of the boundary of the plasma and the region of the wall layer (sheath).

1. In view of the fact that in Frost's work the results for variation of the field and concentration, which were obtained by numerical integration of the balance equation, are given in the form of curves only for one value of the parameter, it proved necessary to carry out similar calculations for a number of other values of the parameter for the purpose of obtaining interpolation formulas. We determined the coefficients μ_0 and a in the approximate expression for the drift velocity proposed by Frost,

$$\bar{v} = \frac{\mu_0 E}{(1+aE/p)^{1/2}}, \tag{2}$$

from the following expressions for the ion drift velocity:[5]

$$\mu_0 = 0.24\sqrt{\frac{2kT}{M}}\,\frac{e}{pq} \quad \text{and} \quad a = 0.05\pi\,\frac{e}{q}, \tag{3}$$

where T is the temperature of the gas and e and M are the ion charge and mass.

These relationships make it possible to make use of Frost's approximation even in cases when the experimental dependence of $\bar{v}$ on E/p is not clearly known (mercury and alkali metals). The calculated distributions of potential and concentration for $\eta \leqslant 1$ are closely approximated by the formulas

$$\eta = -K \ln J_0\left(2.4 \frac{s}{s_\infty}\right) \quad \text{and} \quad n = n_0 \left[J_0\left(2.4 \frac{t}{s_\infty}\right)\right]^K, \tag{4}$$

where $K = \left(\frac{s_\infty}{2.4}\right)^{5/3} < 1$; the factor 2.4 is the first root of the Bessel function F_0; $s = \alpha r$;

$$\alpha = \left(\frac{Ze}{\mu_0 k T_e}\right)^{1/2}; \tag{5}$$

s_∞ is the value of s at which the field strength becomes infinite. The interpolation formula for s_∞ is

$$s_\infty = 2.4 - 0.71 \log (1.57\,\delta + 1), \tag{6}$$

where $\delta = 1.8 \frac{T_e}{T} \frac{\lambda}{R}$; λ is the ion free path, and R is the radius of the discharge tube. In the Schottky case (ion mobility constant) $\delta \ll 1$. Obviously, this criterion does not agree with the criterion for diffusion conditions ($\lambda/R \ll 1$), owing to the large value of the factor T_e/T. Thus the influence of variable ionic mobility must become significant in the pressure range where

$$\frac{T}{2T_e} < \frac{\lambda}{R} \ll 1. \tag{7}$$

As will be shown below, in the case of interest to us the boundary of the quasi-neutral plasma is close to s_∞ and the wall layer may be regarded as thin. Then, $\frac{s}{s_\infty} = \frac{r}{R}$ and by means of Eq. (5) we obtain the following balance equation

$$Z = 0.133 \sqrt{\frac{2kT}{M}} \frac{1}{R} \delta s_\infty^2. \tag{8}$$

The number N of ions per unit column length and the density ρ_p of the ion current to the wall on the basis of calculations may be approximated by the formulas

$$N = \frac{n_0 \pi R^2}{s_\infty} \quad \text{and} \quad \rho_p = 0.07 \sqrt{\frac{2kT}{M}} \quad n_0 e \delta \cdot s_\infty, \tag{9}$$

where n_0 is the electron concentration at the discharge axis.

2. Following Tonks & Langmuir[2], we define the boundary of the plasma as the line beyond which the degree of deviation from quasi-neutrality (determined by the relation $\frac{n_p - n_e}{n_p} = \varepsilon$, where n_p and n_e are the ion and electron concentrations, respectively) is no longer small. Poisson's equation can be written in the form

$$\varepsilon = \alpha^2 \frac{n_0}{n_p} h^2 \Delta_s \eta, \tag{10}$$

where $h = \left(\frac{kTe}{4\pi n_0 e^2}\right)^{1/2}$ is the Debye radius, and the derivatives in the Laplacian are taken with respect to s. It follows from Eq. (1) that at the plasma boundary

$$\frac{d\eta}{ds} = \frac{1}{2} \frac{1}{s_\infty - s}, \qquad \frac{n_p}{n_0} = 0.16 \sqrt{2\delta \cdot s_\infty (s_\infty - s)}, \quad \text{and} \quad \varepsilon = 2.2 \left(\frac{h}{R}\right)^2 \left[\frac{s_\infty^3}{\delta (s_\infty - s)^5}\right]^{1/2}. \tag{11}$$

Let us set $\varepsilon = 0.1$. Then for a discharge in mercury vapor at a pressure of 10^{-1} mm Hg in a tube of radius R = 1.5 cm, we have

$$T_e = 1.2 \cdot 10^4 \ ^\circ\text{K}, \ \delta = 1.7 \text{ and } s_\infty = 2.$$

With a current of 400 ma, $n_0 = 2\cdot10^{11}$ and $s_\infty - s = 2\cdot10^{-2}$.

With a current of 1.5 amp, $n_0 = 10^{12}$ and $s_\infty - s = 1.2\cdot10^{-2}$.

These examples show that the boundary of the region of quasi-neutrality is very close to the value of s_∞. For these cases $aE/p \sim 10 \gg 1$, and, consequently, the assumption made by Schottky and Tonks & Langmuir that the ion mobility is constant is inadmissible near the plasma boundary. For the drift velocity and ion concentration near the plasma boundary we obtain

$$\bar{v} = 0.25 \sqrt{\frac{2kT}{M}}\, \delta^{3/5} s_\infty^{1/5} \left(\frac{R}{h}\right)^{2/5} \varepsilon^{1/5}, \qquad \frac{n_p}{n_0} = 0.3 \left[\frac{\delta^2 s_\infty^4 h^2}{R^2 \varepsilon}\right]^{1/5}. \tag{12}$$

Making use of Eq.(12) and the relation $\eta = \ln n_0/n_e$, we can find the potential near the plasma boundary. For the above illustrated cases we obtain 0.06 and 0.05, respectively, for n_p/n_0, and 2.8 and 3.0 for η.

Turning to the question of the space charge layer near the walls, we note that in the pressure range of interest to us, it is expedient to examine the case when the layer thickness $d \lesssim \lambda$, where λ is the ion free path. Here we make a number of simplifying assumptions. First, ignoring the distribution of ions in velocity, we will consider a flux of ions having equal velocities.

We assume a Boltzmann distribution for the electrons in the layer. Then, taking into account the draining off of electrons by the wall leads to the expression

$$n_e = \frac{1}{2} n_0 e^{-\eta} [1 + \Phi(\sqrt{\eta_2 - \eta})],$$

where Φ is the probability integral and η_2 is the wall potential. This expression differs from the Boltzmann one only near the wall, where the influence of electrons can be neglected in general.

We determined the boundary between the plasma and the wall layer from the condition that the mean ion velocity in it is equal to

$$\bar{v}_1 = \sqrt{\frac{kT_e}{M}}. \tag{13}$$

As has been repeatedly noted in the literature[7], this condition insures continuity of the derivative of the charge density at the plasma-wall layer boundary.

At high electron concentrations, quasi-neutrality may extend beyond the boundary determined by condition (13) into the region of the wall layer; however, as will be evident from what follows, this boundary lies very close to the boundary of the region of quasi-neutrality. Invoking Eqs.(12) and (13), we find that for the plasma boundary

$$\varepsilon_1 = \frac{34}{s_\infty}\left(\frac{T_e}{T}\right)^{-1/5}\left(\frac{h}{R}\right)^2\left(\frac{R}{\lambda}\right)^3, \qquad s_\infty - s = 0.3 \cdot s_\infty \frac{\lambda}{R},$$
$$\left(\frac{d\eta}{ds}\right)_1 = \frac{1{,}7}{s_\infty}\frac{R}{\lambda}, \qquad e^{-\eta_1} = \left(\frac{n_p}{n_0}\right)_1 = 0.17 \cdot s_\infty \frac{\lambda}{R}\left(\frac{T_e}{T}\right)^{1/5}. \tag{14}$$

Eq.(13) is applicable for determining the plasma boundary only for $\varepsilon_1 \ll 1$. Violation of this condition means that quasi-neutrality is disturbed before the ion velocity attains the value $\bar{v}_1$. Eq.(14) shows that the concentration of charged particles at the boundary is already small and that ionization in the layer can be neglected. Inasmuch as we are restricting our consideration to the case when $d \lesssim \lambda$, the layer may be regarded as plane. Poisson's equation for the

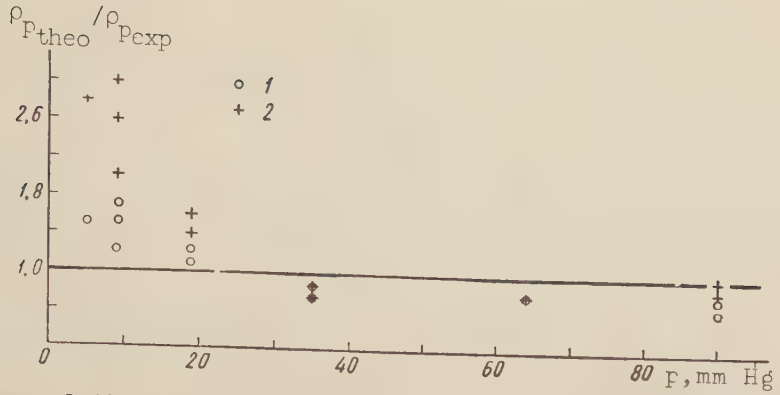

Fig.1. Variation of the ratio of the theoretical to experimental value of ρ_p with the pressure in mercury vapor: 1 - according to Eq.(18), 2 - according to Schottky's theory.

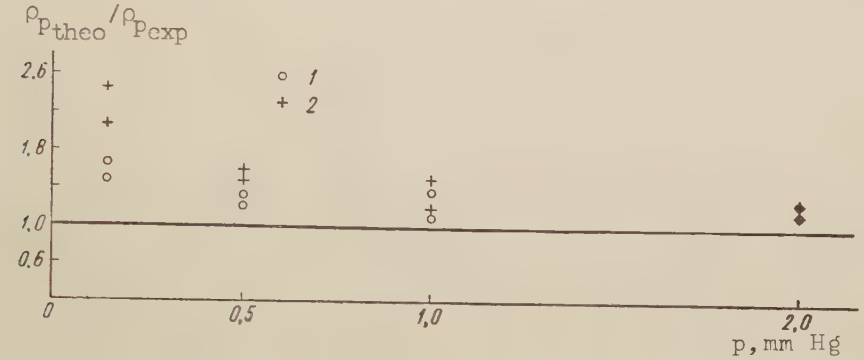

Fig.2. Same as Fig.1, but for argon (R = 1 cm; I = 50 to 500 ma).

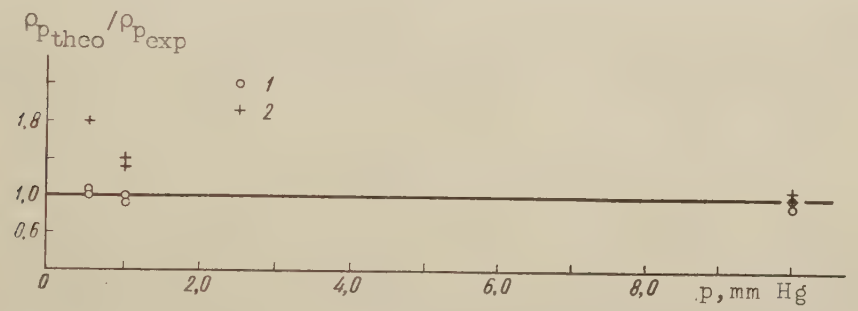

Fig.3. Same as Fig. 1, but for potassium (R = 1 cm; R = 100 and 300 ma).

layer under the given assumptions is of the form

$$\frac{\varepsilon_1}{2\left(\frac{d\eta}{ds}\right)_1^2}\frac{d^2u}{dx^2}=\frac{1}{\sqrt{2u+1}}-e^{-u}, \qquad (15)$$

where $x=s-s_1$ and $u=\eta-\eta_1$, for the boundary conditions $u=0$ and $\frac{du}{dx}=\left(\frac{d\eta}{ds}\right)_1$, when $x = 0$. Equation (15) was integrated numerically for values of ε_1 ranging from 10^{-1} to $5\cdot10^{-4}$. The potential fall in the layer was determined from the condition of zero current to the wall (7). From this equation it follows that

$$\rho_p = e\sqrt{\frac{kT_e}{2\pi m}}\, n_0 e^{-(\eta_2-\eta_1)},$$

where m is the electron mass; on the other hand,

$$\rho_p = en_0\sqrt{\frac{kT_e}{M}},$$

and for the potential fall in the layer we obtain

$$\eta_2 - \eta_1 = \ln\sqrt{M/2\pi m}.$$

Calculations show that the layer thickness d for the case of mercury ($\eta_2 - \eta_1 = 5.5$) can be approximated by the formula

$$d = 2.2 \cdot \lambda \cdot \varepsilon_1^{0.35} \tag{16}$$

Invoking (14), we obtain the following expression for the potential difference between the wall and the tube axis:

$$\eta_2 = \ln\left[\frac{15}{2\sqrt{\pi}}\sqrt{\frac{M}{m}\frac{T_e}{T}}\frac{1}{\delta \cdot s_\infty}\right]. \tag{17}$$

Eq.(16) shows that the condition $d < \lambda$ is fulfilled if $\varepsilon_1 \ll 1$.

3. We carried out comparisons with experiment for discharges in mercury, argon and potassium. Specifically, we compared the values of the current density to the wall calculated by means of Eq.(9) with the values of ρ_p obtained by means of plane wall probes. We used the following values for the charge exchange cross section: $q = 10^{-14}$ cm^2 for mercury (deduced from the data of Kungdon & Lawton[8] on the mobility of mercury ions in the parent gas in strong fields); $q = 7.5\cdot10^{-15}$ cm^2 for argon[9]; $q = 3.5\cdot10^{-14}$ cm^2 for potassium[10].

The electron gas temperature was determined by the conventional probe procedure; it was found to be the same at the axis and at the wall. The electron concentration in the mercury and the potassium vapors was determined from the electronic and in argon from the ionic part of the characteristic by means of the formula:[11,12]

$$I_p = 0.4 \cdot n_0\sqrt{\frac{2kT_e}{M}}\, s_1, \tag{18}$$

where I_p is the ionic current and s_1 is the area of the space charge layer. The numerical coefficient in (18) was taken from Guthrie & Wakerling[11] as the most reliable value available.

The data for discharges in mercury are shown in Fig.1. In addition to our own experimental values for a tube of radius R = 1.5 cm, in the current range from 0.1 to 1.5 amp we used the results of Granovskii[13] obtained for tubes with R = 3.25 and 5.25 cm. The data for argon are shown in Fig.2; those for potassium in Fig.3. In all cases for purposes of comparison we also calculated the values according to Schottky's theory ($s_\infty = 2.41$).

It will be evident from the figures that the agreement of theory with experiment is satisfactory in all cases when diffusion may be considered significant. In the pressure range in which condition (7) is fulfilled, Schottky's theory yields poorer agreement with experiment.

References

1. W.Schottky, Phys. Z., 25, 342 (1924).
2. L.Tonks & I.Langmuir, Phys.Rev., 34, 876 (1929).
3. J.Hornbeck, Phys.Rev., 84, 615 (1951); R.Varney, Phys.Rev., 88, 362 (1952).
4. L.Frost, Phys.Rev., 105, 354 (1957).
5. Yu.M.Kagan & V.I.Perel', Doklady AN SSSR, 98, 675 (1954).
6. G.Schulz & S.Brown, Phys.Rev., 98, 1642 (1955).
7. V.L.Granovskii, Elektricheskii tok v gazakh (Electric current in gases), 1952.
8. K.Kungdon & E.Lawton, Phys.Rev., 56, 215 (1939).
9. Yu.M.Kagan & B.I.Perel', Zhur.eksp.i teor.fiz., 29, 884 (1955). (Trans. Soviet Physics - JETP.)
10. R.M.Kushnir, B.M.Palyukh & L.A.Sena, Transactions, Second All-Union Conference on Gaseous Electronics, 1958.
11. A.Guthrie & R.Wakerling (eds.), Characteristics of Electrical Discharges in Magnetic Fields, N.Y., 1949.
12. Yu.M.Kagan, V.I.Perel' & P.O.Ripatti, Vestnik, Leningrad State University, No.8, 129 (1955).
13. V.L.Granovskii, Trudy (Proceedings), All-Union Power Institute, 41, 98 (1940).

INVESTIGATION OF THE INITIAL STAGES OF A HIGH-FREQUENCY DISCHARGE FROM A POINT IN AIR AT ATMOSPHERIC PRESSURE

- A.M.Prokof'ev, O.F.Kabardin & K.F.Kuddu

Introduction

The initial stages of a high-frequency (hf) discharge from a point have been studied little, inasmuch as direct investigation of such discharges during discrete half-periods of the hf voltage is a complicated problem. The initial stages of a dc corona from a point, on the other hand, have been studied fairly thoroughly, particularly by Loeb[1] and his co-workers. We felt that the initial stages of an hf discharge from a point could be correlated with the effects observed in a dc corona. This inference has been substantiated by a number of experiments.

Before describing these experiments, let us recall the distinctive features of the initial stages of dc corona discharges from a point. The initial stages of a positive corona from a point are characterized by the appearance of "pulses" of two types: flickering or flash pulses and preliminary or pilot-streamer pulses. The former are discharge pulses propagating over the surface of the point; the latter are due to development of the discharge into the depth of the discharge gap through the operation of the streamer mechanism.

The initiation of a negative corona from a point is characterized by the appearance of periodic pulses of constant amplitude, called Trichel pulses. The periodic suppression of the negative corona current is attributed to the effect of the space charge of negative ions at the point.[1] A high-frequency discharge from a point may be observed in the form of a high-frequency corona or a jet discharge, depending on the frequency.[2]

Apparatus

Our experiments were carried out on a set-up consisting of an hf generator, a high voltage rectifier and a discharge gap. The discharge gap was inductively coupled to the generator, which made it possible to apply both an hf and a dc voltage to the discharge gap simultaneously. The discharge gap consisted of a point and a plane electrode, the point to plane separation being 4 cm. The point electrodes were platinum rods; four of them terminated in hemispheres with diameters of 1.25, 1.0, 0.5 and 0.2 mm; the fifth electrode, which was 5 mm in diameter, had a conical tip.

Experimental Results

To bring out the possible correlation between the initial stages of an hf discharge from a point and the behavior of a dc corona, we first carried out measurements of the initial voltages for the beginning of positive and negative corona pulses from a point (i.e., with dc voltage only) and the initial voltages for initiation of an hf discharge from a point (in the frequency range from $1.25 \cdot 10^6$ to $4 \cdot 10^7$ cps). The hf discharge initiation voltages proved to be consistently lower than the initial voltages for the appearance of both positive and negative dc corona pulses (here and below in referring to the hf voltage we mean the crest voltage).

The decrease of the hf discharge initiation voltage (compared to the initial dc corona voltage) is only weakly dependent on the shape and dimensions of the point and the configuration of the discharge gap, but is strongly dependent on the frequency. To eliminate the possible influence of chance factors, all measure-

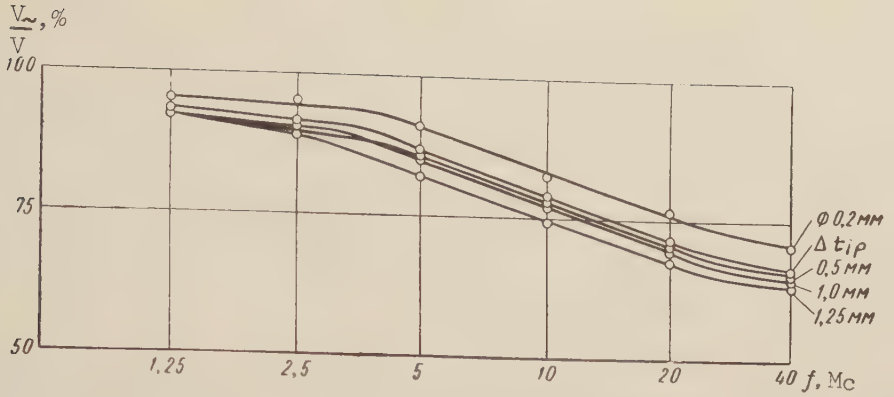

Fig.1. Ratios of the hf discharge initiation voltage to the initial voltage for the appearance of Trichel negative corona pulses for different electrode configurations (points) and frequencies.

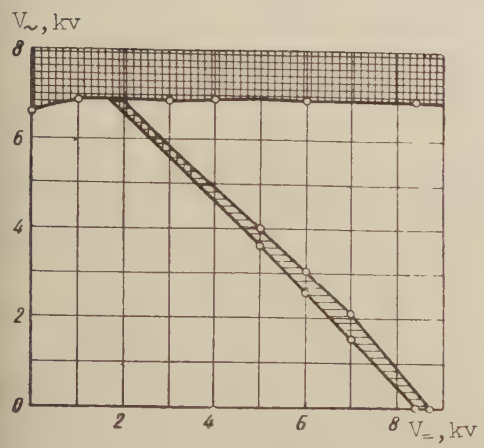

Fig.2. Voltage regions in which there appear preliminary streamer pulses of a positive corona and pseudo-hf and hf discharges at f = 10 Mc.

ments were repeated 10 times; the averaged results for five different points are plotted in Fig.1. The maximum deviation of individual measurement results from the average values did not exceed 3%.

Next we measured the discharge initiation and extinction voltages with simultaneous application of dc and hf voltages in different proportions. As the proportion of hf is increased one can readily observe the transition from preliminary dc streamers to preliminary streamers with two (dc & hf) voltages, then the transition to a discharge similar to a high-frequency one (hereinafter pseudo-hf discharge) and finally to a true hf discharge.

By way of illustration, the results of measurements at a frequency of 10 Mc with the 1.25 mm diameter point are shown in Fig.2. The voltage region in which we observed the appearance of preliminary streamers of a positive corona is hatched horizontally (☰); the region of minimum voltages at which we observed formation of pseudo-hf discharges is indicated by double hatching (⊞). We also noted that flashes similar to hf ones in the case of two voltages again appear in the region of appreciable overvoltages; in Fig.2 this region near the top of the figure is also double hatched. However, we shall not discuss the characteristics of discharges at appreciable overvoltages here.

Similar measurements were carried out at frequencies of 1.25, 2.5, 5, 10, 20 and 40 Mc with different points, different configurations of the discharge gap and different intensities of the initial ionization in the discharge gap. It was found that the contours of the region characterizing the minimum voltages for formation of a pseudo-hf discharge and for formation of positive corona preliminary streamers strongly depend on the dimensions and shape of the point, the frequency of the hf voltage and the intensity of initial ionization. In all cases, however, one regularity is observed, namely, the region of pseudo-hf discharge initiation voltages is always a natural extension of the region of the initial

voltages associated with the appearance of the preliminary streamer pulses of a positive corona (doubly and singly hatched band in Fig.2). This indicates that in the case of simultaneous application to a point-plane gap of a dc voltage and an hf voltage, a pseudo-hf discharge can develop from a preliminary streamer pulse forming during one of the positive half-periods of the hf voltage.

We carried out analogous measurements with a negative dc voltage on the point. These measurements showed that in the case of simultaneous application of an hf voltage and a dc voltage with the point negative, a pseudo-hf discharge from the point can develop from a Trichel negative corona pulse, forming during one of the negative half-periods of the hf voltage.

Conclusions

At minimal voltages, a discharge similar to a high-frequency discharge from a point, i.e., a pseudo-hf discharge, can form in air at atmospheric pressure in the frequency range from 1.25 to 40 Mc either from the preliminary streamer of a positive corona or from the Trichel pulse of a negative corona.

The reason for decrease of the initiation (breakdown) voltage for a pure hf discharge from a point (as compared with the initiating voltage when a dc voltage is present) is, apparently, build-up of an ionic space charge in the vicinity of the point.

References

1. L.B.Loeb, Basic Processes of Gaseous Electronics, U.of Calif.Press, 1955.
2. N.A.Kaptsov, Elektronika (Electronics), M., 1956.

INVESTIGATION OF RESONANCE CHARGE EXCHANGE IN MONATOMIC GASES AND METAL VAPORS

- R.M.Kushnir, B.M.Palyukh & L.A.Sena

Resonance charge exchange is one of the most important processes in the interaction of ions with atoms and is the determining factor where ion motion in the parent gas is concerned. Knowledge of the resonance charge exchange cross section and the variation of this cross section with the ion velocity is highly important in the physics of electric discharges in gases.

A number of authors have attempted to evaluate the resonance charge exchange cross section theoretically. The first calculations, which, it is true, pertained only to helium ions and atoms, were carried out by Massey & Smith[1] and Dallaporta and his co-workers.[2] Some time ago Sena[3] gave an approximate evaluation of the resonance charge exchange cross section in the general case on the basis of a number of simplifying assumptions. This evaluation leads to a monotonic decrease of the cross section with increase of the ion velocity and gives a limit formula which is applicable in the case of not excessively high ion velocities (when adiabatic treatment is still admissible). According to the limit formula[3], the charge exchange cross section is inversely proportional to the square of the ionization potential of the gas. Demkov[4] on the basis of quantum mechanical calculations deduced a more rigorous formula which is suitable for atomic hydrogen and helium; this was subsequently generalized[4] to other monatomic gases and metal vapors. According to Demkov's formula, the charge exchange cross section is inversely proportional to the ionization potential. Demkov's formula also gives the variation of the cross section with the ionic mass and energy. For the case of slow ions and atoms, for which the S state is normal, Firsov[5] gives a formula which contains the charge exchange cross section in implicit form and from which one can deduce the variation of the cross section with the ion velocity.

Sena's formula[3] gives particularly high values of the charge exchange cross section for ions and atoms of alkali metals, the atoms of which have the lowest ionization potentials. The formulas of Demkov[4] and Firsov[5] give substantially lower cross section values for this case. In view of the fact that at present there is no sufficiently general, rigorous and consistent theory of resonance charge exchange, experimental investigation of this process is particularly important.

Over the past few years we have carried out measurements of the resonance charge exchange cross sections of argon, krypton, xenon, potassium and cesium in the laboratory of the "I.Franko" L'vov State University. This work is a continuation of the mercury vapor studies started earlier in the Leningrad Scientific Research Institute for Direct Current. In the present report we summarize the results of these investigations and compare them with the deductions from extant theories.

The experimental procedure used for the measurements differs little from that described earlier[6] for measurements in mercury vapor. The incorporation of a large number of electrodes in the measuring apparatus made it possible to obtain lower energy ion beams and to carry out a series of special measurements for the purpose of taking into account the effect of secondary electron emission from the electrode.

The measurements were based on the retarding field method. In addition to using the retarding field procedure in its pristine form, we carried out some measurements using a modification of this technique, namely, the method of a constant collector potential[6], for inert gases. For the alkali metals, we also used the method of extraction of slow ions.[7,8] For determining the charge exchange cross section we used the exponential formula for attenuation of the beam, which gives a linear relation between log (I_0/I) and p_0 with l = const and between

log (I_0/I) and l with p_0 = const. Here I_0 is the ion current penetrating into the collision chamber, I is the current of ions not undergoing charge exchange over the path l in the collision chamber, and p_0 is the gas pressure reduced to 0°.

Special experiments were carried out for the purpose of evaluating the influence of secondary emission processes; these experiments showed that secondary electron emission under the influence of fast ions and atoms could have an appreciable influence on the measurement results. The secondary emission current in some cases was taken into account (specifically, in the measurements for argon, krypton and xenon) and in other cases (alkali metal vapors) was suppressed by means of a weak (~30 oersted) magnetic field directed perpendicular to the ion beam. The results of measurements by the different procedures were in agreement within the limits of the experimental error.

The principal source of error in the case of determining the charge exchange cross section in alkali metal vapors is inaccuracy in determining . The temperature of the liquid phase was determined to within 0.2°; however the tabular data on the vapor pressure given by different authors differ by 8-10% for potassium in the temperature interval of interest (135 to 160°) and by 15% or more for cesium (78 to 105°). The vapor pressure was determined by means of the equation given in Dushman's book.[9] The total error in the determined charge exchange cross section values connected with uncertainties in measuring I_0, I and l did not exceed 10%.

Experimental Results

The measurements for argon, krypton and xenon were carried out in the energy interval from 10 to 990 ev and for potassium and cesium in the range from 6 to 656 ev with scattering gaps ranging from 2 to 4.5 cm and different gas and vapor pressures. Graphs of log (I_0/I) vs p_0 for a given l and of log (I_0/I) vs l for a given p_0 were plotted for each of the chosen ion energies. According to the formula for attenuation of the primary ion beam in a gas, this dependence should be linear. This was actually the case in our experiments. In almost all cases the rectilinear plots pass through the origin, which indicates that the contribution from surface (skin) effects is negligible.

Reflection of ions from the collector could have some influence on the measurement results in the case of the alkali metals. However, since the charge exchange cross section in our experiments was determined from the slope of the

$$\frac{\log \frac{I_0}{I}}{p_0} = \frac{1}{2{,}3} Ql,$$

plots, the error introduced by these surface effects is presumably small.

The measurements of the charge exchange cross section for argon were carried out primarily for the purpose of comparing the results obtained by our procedure with the experimental results of other authors. Our curve occupies an intermediate position and lies close to the curve given by Hasted[10]. If our curve is prolonged into the region of higher velocities, we obtain a smooth transition to the experimental points obtained by Fedorenko[11].

Comparison of our results for krypton, xenon and mercury with the results of Dillon et al[12] shows that the cross section values obtained by Dillon et al for krypton and xenon are only slightly smaller than ours, but that for mercury they are smaller by more than a factor of 2.

The average values of the charge exchange cross section obtained as a result of numerous measurements at different pressures and with different scattering gaps are listed in the accompanying table.

Average values of the charge exchange cross section Q (in cm^2/cm^3 mm Hg)

Ion energy, ev	Q						Ion energy, ev	Q					
	Ar	Kr	Xe	Hg	R	Cs		Ar	Kr	Xe	Hg	K	Cs
6					1475	1540	105					950	
9					1250		110						1100
10			298				140	104					
12						1410	165				316		
17		218					210	99	150	204			
28					1145		280	97					
36						1310	335					700	800
53	122	190	239		1080		425		138	190	286		
70		180					656					550	670
75				351			990	80	118	173	258		

Comparison with Theory

Our experimental results are compared with the deductions from the different extant theories in Figs.1 and 2. The solid lines in Fig.1 give the experimental curves for argon, krypton and xenon. The dashed curves are based on Demkov's theoretical formula.[4] The horizontal dashed lines represent the data calculated by means of Sena's limit formula.[3] The solid curves in Fig.2 give the experimental results for cesium, potassium and mercury. The dashed curves are the corresponding theoretical curves according to Firsov.[5] The dash-dot curves are the theoretical curves representing Demkov's formula.[4] The horizontal straight lines give the data calculated by means of Sena's limit formula.[3]

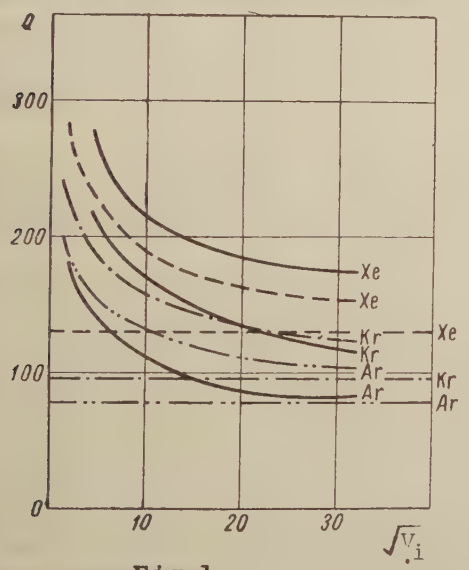

Fig.1

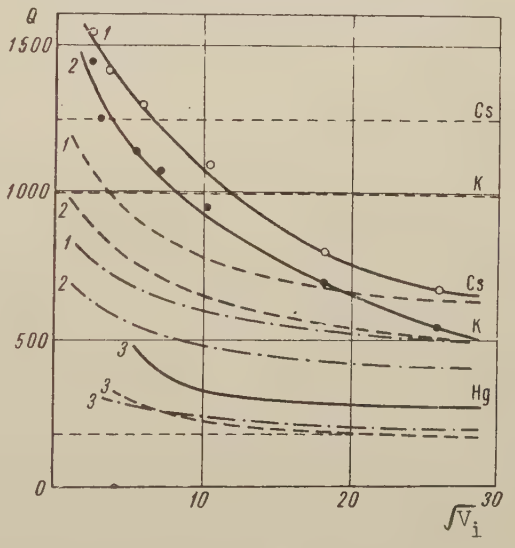

Fig.2

Fig.1. Variation of the charge exchange cross section with the ion velocity ($\sqrt{V_i}$) in inert gases. Solid curves - experimental; dashed curves - Demkov's theory[4]; horizontal straight lines - Sena's limit formula[3].

Fig.2. Variation of the charge exchange cross section with the ion velocity ($\sqrt{V_i}$) in metal vapors. Solid curves - experimental; dashed curves - Firsov's theory[5]; dash-dot curves - Demkov's theory[4]; horizontal straight lines - Sena's limit formula[3].

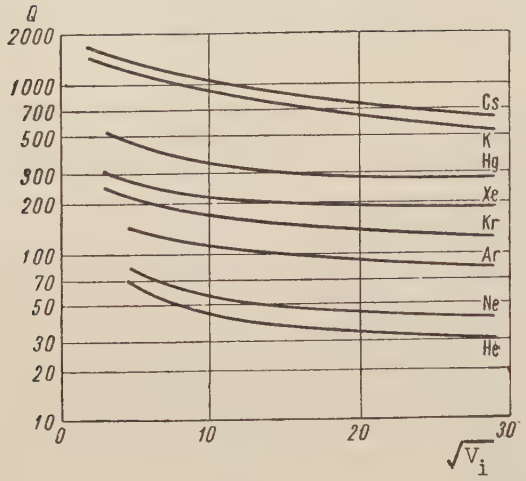

Fig.3

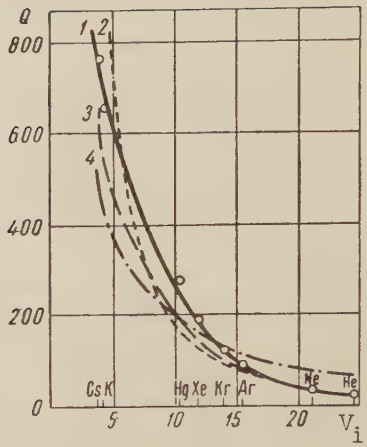

Fig.4

Fig.3. Variation of the charge exchange cross section with the ion velocity plotted to a semilogarithmic scale. The curves for neon and helium are based on the data of Rostani[3].

Fig.4. Variation of the charge exchange cross section with the atomic ionization potential (in ev) for ions with an initial energy of 400 ev: 1) experimental data, 2) curve based on the limit formula[3], 3) curve based on Firsov's formula[5], 4) curve based on Demkov's formula[4].

Comparison of the experimental results with the theoretical curves shows that the experimental results are in best agreement with the theoretical data of Firsov[5]. True, the experimental curves for the charge exchange cross section Q vs the ion velocity rise more steeply in the range of low velocities than the theoretical curves. Unfortunately, Firsov's calculations are not applicable to argon, krypton and xenon.

In Fig.3 we have plotted our results in semilogarithmic coordinates in the form of curves giving the variation of Q with the ion velocity for argon, krypton, xenon, mercury, potassium and cesium. In the same figure we show the curves for neon and helium based on the data of Rostani.[3]

Summarizing the results of our work we note that, in agreement with the deductions from theory, the resonance charge exchange cross section decreases monotonically with increase of ion velocity and exhibits a consistent dependence on the ionization potential of the gas: the cross section decreases with increase of the ionization potential. This fact is illustrated in Fig.4 in which the variation of the charge exchange cross section is plotted against the ionization potential for ions having an initial energy of 400 ev. In the region of high ionization potentials, all the theoretical evaluations lead to results that are close to the experimental data. In the case of atoms with a low ionization potential, however, there is a noticeable divergence: the Sena formula[3] yields higher values in this region, while the Demkov[4] and Firsov[5] formulas lead to underestimates. The divergence of the Demkov and Firsov formulas from experiment is particularly noticeable in the region of low velocities, while the divergence between experiment and the Sena formula is more appreciable in the region of higher velocities.

"I.Franko" L'vov State University

References

1. Massey & Smith, Proc.Roy.Soc., 142, 142 (1933).
2. Dallaporta, Atti Acad.Sci.Torino, 75, 101 (1939); Dallaporta & Bonfiglioli, Comm.Pontif.Acad.Sci., 7, 141 (1943).
3. L.A.Sena, Zhur.eksp.i teor.fiz., 9, 1320 (1939); L.A.Sena, Stolknoveniya elektronov i ionov s atomami gaza (Collisions of electrons and ions with gas atoms) M.-L., 1948.
4. Yu.N.Demkov, Uch.zap. (Scientific Notes), Leningrad State University, 146, No.8, 74 (1952).
5. O.B.Firsov, Zhur.eksp.i teor.fiz., 21, 1001 (1951).
6. B.M.Palyukh & L.A.Sena, Ibid., 20, 481 (1950).
7. R.M.Kushnir, Ukr.fiz.zhur. (Ukrainian Phys.Journal), 3, 343 (1958).
8. R.M.Kushnir, Ibid., 3, 788 (1958).
9. S.Dushman, Scientific Foundations of Vacuum Technique, N.Y., 1949 (Cited in Russian trans.)
10. J.B.Hasted, Proc.Roy.Soc., A205, 421 (1951).
11. N.V.Fedorenko, Zhur.tekhn.fiz., 24, 2113 (1954).
12. J.A.Dillon, W.F.Shendon, H.D.Edwards & G.H.Ghosh, J.Chem.Phys., 22, 974 (1954).

INVESTIGATION OF ANODIC OSCILLATIONS IN A LOW-PRESSURE DISCHARGE

- A. A. Zaitsev & K. I. Efendiev

The anodic region of a gas discharge may be characterized by appreciable instability. Sonic and ultrasonic oscillations observed in discharge circuits are often associated with instability of the anode fall of potential. We investigated these oscillations in arc discharges in mercury vapor with a liquid cathode and in discharges with an oxide-coated cathode in inert gases. These investigations were motivated by the following considerations: 1) anodic oscillations may be a source of interference in the operation of ionic devices and in experimental studies of gas discharge plasma, and 2) investigation of anodic oscillations can further our understanding of the processes occurring in the region of the anode (at present our knowledge of these processes is based primarily on experiments with a steady anode potential fall).

The oscillations were detected and studied by means of an oscillograph by observing either the variation of the overall discharge voltage or the variation of the voltage between the anode and a movable probe inserted into the positive column. The probe procedure allows of measuring both the maximum and minimum value of the anode fall and the mean value of the anode fall under identical conditions.

Audio-frequency oscillations in a low pressure mercury arc were studied earlier by Granovskii & Bykhovskaya.[1] They showed that the point of origin of these oscillations is the anode region. It is a familiar fact that the properties of the anode region are determined by the magnitude of the ratio of the density of the chaotic electronic current in the plasma to the density of the directed current to the anode and by the factors controlling the ionization of the gas in the region of the anode; of particular significance here are the shape and dimensions of the anode surface.[2,3]

In our work with discharges in mercury vapor we paid particular attention to elucidating the influence of the anode geometry on the anodic oscillations. By way of anodes we used a number of electrodes differing as regards size and design, namely, 1) a divided electrode consisting of three insulated flat sections with equal surfaces, 2) pin electrodes and 3) hollow cylinders. The discharge current was varied from 0.1 to 7 amp. The mercury vapor pressure was regulated by means of a water bath.

The following results were obtained. The oscillation mechanism, which also includes the anode glow effect, is favored by small size of the anode. An anode glow appears when the dimensions of the anode are small compared with the cross section of the positive column. When the glow is restricted to a part of the anode surface (a bright band standing out on the anode surface), more or less ordered oscillations are observed in the discharge circuit. Sometimes several such bands appear simultaneously; in this case the oscillations are more complicated. The mean anode fall of potential in the case of regular oscillations is always higher than the excitation potential of mercury atoms. Ordered oscillations occur both with a stationary and with a wandering cathode spot. The motion of the cathode spot, without disturbing the form and stability of the anodic oscillations, gives rise to irregular oscillations, which are superimposed on the basic anodic oscillations. This means that small chaotic current oscillations induced by the motion of the cathode spot have no noticeable effect on the state of the anode region. The variation of the oscillation amplitude as a function of the discharge current and gas pressure is similar to the variation of the anode potential fall. With decrease of the mercury vapor pressure and increase of the discharge current, both the oscillation amplitude and the mean anode fall increase.

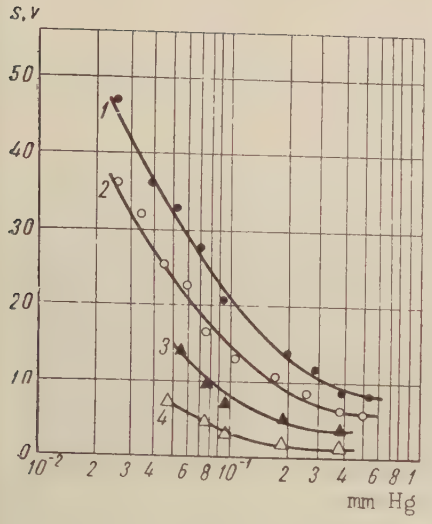

Fig.1. Variation of the anodic oscillation amplitude with pressure: 1 & 2) neon, 3 & 4) krypton; 1 & 3) i = = 100 ma, 2 & 4) i = 30 ma.

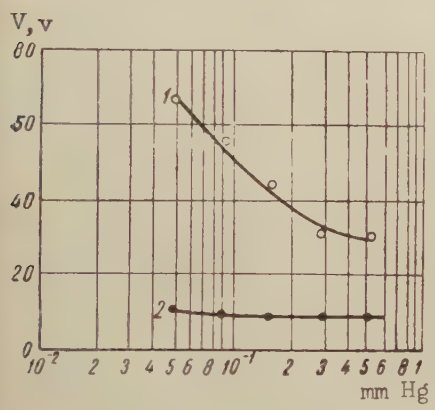

Fig.2. Variation of the maximum (1) and minimum (2) values of the anode potential fall with the pressure in neon; i = 75 ma; anode - 2 mm diameter wire.

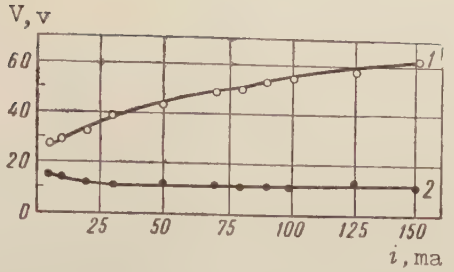

Fig.3. Variation of the maximum (1) and minimum (2) values of the anode potential fall in neon with the current strength; p = $1.4 \cdot 10^{-1}$ mm Hg.

In the absence of anode glow, a condition which obtains in the case of anodes with a large collecting surface, there are observed chaotic oscillations of small amplitude. Under our conditions we did not observe passage of the oscillation amplitude through a maximum or regular establishment of ordered oscillations; nor did we have occasion to observe transitions from ordered oscillations to chaotic and vice versa. When the anode is a pin, the oscillations under all conditions are ordered. The oscillation frequency lies in the range from 10^4 to 10^5 cps. Within this range it increases with increase of the mean discharge current.

The anodic oscillations in inert gases (He, Ne, A and Kr) were investigated at pressures from 10^{-3} to 1 mm Hg and with discharge currents from a few to 300 ma. In these experiments the anodes were made of molybdenum wire of different diameters and were shielded on the sides by glass insulation so that only the end surface served as the collecting surface ("point" anode). In general, anodic oscillations in inert gases are more stable as regards phase and frequency than in mercury vapor. We were able to measure the oscillation frequency in inert gases by comparison with the frequency of a standard signal generator. The variation of the oscillation amplitude with the pressure in neon and krypton for two values of the discharge current is shown in Fig.1. The variation of the oscillation amplitude is associated primarily with variation of the maximum value of the alternating anode fall of the potential. This will be clearly evident from an examination of the experimental results shown in Figs.2 & 3. It is significant that at low pressures and with heavy currents the maximum value of the anode fall greatly exceeds the ionization potential of the gas; at the same time, the minimum value of the anode fall is substantially lower than the excitation potential of the gas.

Both the amplitude s and the frequency ν of the oscillations tend to increase with decrease of the anode diameter. The pertinent data for discharges in neon are listed in Table 1.

Anodic oscillations may also be observed when there is no positive column and the anode borders on the Faraday dark space or the negative glow.[4] Measurements showed that there is a positive anode potential fall in the vicinity of a "point" anode in the Faraday dark space. The following results were obtained for

discharges in neon (i = 30 ma, cathode-anode distance 3 cm, anode wire diameter 2 mm):

p, mm Hg	$7 \cdot 10^{-1}$	$5.2 \cdot 10^{-1}$	$4.1 \cdot 10^{-1}$	$3 \cdot 10^{-1}$	$2.2 \cdot 10^{-1}$	$9 \cdot 10^{-2}$	$4 \cdot 10^{-2}$
Anode fall, v	15.5	15.5	17.0	18.0	21*	27*	42*

Table 1

Anode dia. mm	$i = 20$ ma		$i = 30$ ma		$i = 40$ ma	
	s, v	ν, kc	s, v	ν, kc	s, v	ν, kc
2	4,5	345	6,0	378	7,85	413
1,2	5,6	513	6,3	525	8,4	536
0,8	5,9	592	6,7	625	9,8	657
0,5	6,15	673	8,7	712	10,6	741

At pressures above $3 \cdot 10^{-1}$ mm Hg, the anode fall was stable, while at lower pressures the potential fall fluctuated (the figures identified by asterisks in the table above denote average values of the varying anode fall). The anode region becomes unstable when the anode fall of potential approaches the value of the ionization potential of the gas. The presence of positive column plasma in front of the anode has an indirect influence on the oscillation excitation conditions. When the anode is contiguous to the positive column, the anode fall has a somewhat higher value than when the anode is in or adjacent to the Faraday space. Hence in the presence of positive glow, anodic oscillations may develop even under conditions not conducive to their appearance in the absence of a positive column.

In the case of continuous increase of the distance between the anode and cathode the characteristics of the anode oscillations are affected by the longitudinal inhomogeneities in the distribution of the electric parameters in the beginning of the positive column: the curves characterizing the variation of the amplitude and frequency of the oscillations vs the interelectrode distance have a wave-like appearance (Fig.4). The curves are gradually smoothed out as the interelectrode distance is increased and the positive column attains a homogeneous state.

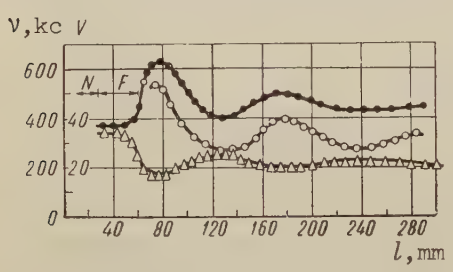

Fig.4. Variation of the frequency (1 & 2) and amplitude (3) of the oscillations in neon with the anode to cathode distance: 1 & 3) p = $= 6.3 \cdot 10^{-2}$ mm Hg, 2) p = $= 3.5 \cdot 10^{-1}$ mm Hg. N - negative glow region, F - Faraday dark space; i = 50 ma.

In a striated discharge with very sharp striations the electric conditions in the gas vary greatly along the length of the discharge tube. In this case, as the anode is moved further away from the cathode, anodic oscillations appear and disappear with a regularity corresponding to the alteration of light and dark regions in the column.[4] A similar behavior of the oscillations is also observed in the presence of moving striations in the positive column. The initiation of moving striations is evinced in the discharge circuit by the appearance of oscillations with a frequency characteristic of the striations and differing from the frequency of the anodic oscillations. The movement of the striations from the anode to the cathode gives rise to a periodic variation of the conditions obtaining near the anode. As a result the anodic oscillations are modulated as regards both frequency and amplitude (Fig.5). If the moving striations are sufficiently sharp, the anodic oscillations may be interrupted (suppressed) during some part of the period of the oscillations associated with the moving striations. In other words, similar variations occur in the character of the anodic oscillations in the case of a positive column with stationary striations as the interelectrode distance is gradually increased and in the case of moving striations as these travel from the anode to the cathode.

The influence of the type of gas on the frequency of the anodic oscillations may be seen from the following data ($p = 3 \cdot 10^{-1}$ mm Hg, i = 70 ma, diameter of anode wire - 2 mm):

Gas	He	Ne	A	Kr	Hg
Frequency, kc	1550	550	290	180	75

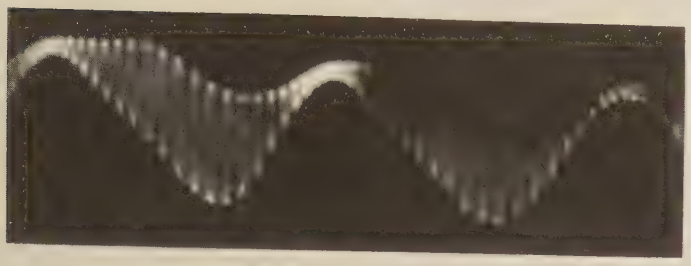

Fig.5. Oscillogram showing simultaneously occurring anodic oscillations and oscillations associated with moving striations.

It will be evident that the frequency decreases with increasing atomic weight of the gas.

The results of our experiments clearly show that the characteristics of anodic oscillations depend on the type of gas, the pressure, current density and shape and size of the anode. In the work of Ref.5 anodic oscillations were investigated in a glow discharge with a cold cathode. It was found that the conditions for onset of anodic oscillations and their character as regards amplitude and frequency do not depend on the design of the cathode.

Langmuir[2] indicated that two different forms of the anode region may exist in the case of a positive anode fall of potential. If the area of the anode is small compared with the cross section of the column, the chaotic current arriving from the plasma to the cathode does not assure maintenance of the current in the discharge circuit; then in the zone adjacent to the cathode there forms a space charge of electrons which in turn is responsible for the appearance of the positive anode potential fall (negative charge condition). With growth of the voltage, the ionization increases, and there may be circumstances under which the ratio of the number of ions forming in the anode layer to the number of primary electrons arriving in the layer will be greater than $\sqrt{m_e / m_i}$, where m_e and m_i are the masses of an electron and an ion, respectively. Then the electron space charge is neutralized and the anode fall abruptly decreases. A new plasma develops inside the positive column plasma; at its boundary with the main plasma there forms a double layer of electric charges (plasma condition). With the formation of the second plasma the conductivity of the anode region increases abruptly. According to Langmuir, the anode plasma is a stable formation.

The results of the present investigation show that the anode region in the case of anodes of small size is as a rule unstable. The anode potential fall undergoes periodic fluctuations. These fluctuations are essentially a form of relaxation oscillations and reduce to periodic variations in the conductivity of the gas near the anode. The tendency of the anode region to oscillate should be attributed to the fact that the second plasma is a dynamic formation similar to mobile striations. However, the anode plasma cloud is dissipated at a small distance from the anode. Thus the oscillations are not accompanied by a wave-like process propagating through the entire positive column. The motion of the anode plasma and its dissipation create conditions for repeated accumulation of electron space charge near the anode. In consequence, breakdown of the electron layer and transition of the state of the anode region from the negative space charge condition to the second plasma condition and back acquire the character of a periodically repeating process. The cyclic variation of the anode potential fall,

associated with the formation and dissipation of the plasma cloud near the electrode, corresponds to the period of the observed oscillations. Observations of the behavior of the glow at the anode by means of a rotating shutter with a slit furnish further confirmation of this view: under oscillation conditions the anode glow periodically assumes the form of either a thin film or a concentrated luminous cloud (second plasma).

The maximum value of the anode potential fall corresponds to the breakdown voltage of the electron layer at the anode. It is obvious 1) that breakdown of the anode layer will occur more readily at higher pressures, inasmuch as most of the electrons will then undergo collisions with gas molecules in passing through the layer and 2) that with increase in the density of the anode current the thickness of the electron layer decreases with the result that the number of collisions within the layer is reduced; hence the rate of ionization in the layer necessary for breakdown is attained at higher values of the anode potential fall. If we bear in mind that the potential drop in the double layer at the boundary of the second plasma is of the order of magnitude of the ionization potential of the gas and, in any case, is not lower than the excitation potential[2], we conclude that the observed values of the minimal anode potential fall indicate that in the phase of maximum ion density the field at the anode has the opposite direction. The other regularities observed for the anodic oscillations are also susceptible of qualitative interpretation.

Physics Faculty,
Moscow State University

References

1. V.L.Granovskii & L.B.Bykhovskaya, Zhur.tekh.fiz., 16, 823 (1946).
2. I.Langmuir & Mott-Smith, Gen.Electr.Rev., 27, 762 (1924); I.Langmuir, Z.Phys., 33, 954 (1929).
3. A.von Engel & M.Steenbeck, Elektrische Gasentladungen, ihre Physik und Technik, Berlin, 1932-4 (Cited in Russian translation).
4. A.A.Zaithes, Vestnik, Moscow State University, No.9, 55 (1950).
5. A.A.Zaitsev & Yu.L.Klimantovich, Ibid., No.12 (1951).

BROADENING AND SHIFT OF SPECTRAL LINES IN GAS DISCHARGE PLASMA

- S.L.Mandel'shtam & M.A.Mazing

Measurement of the spectral line widths is one of the fundamental methods of determining the concentration of charged particles in plasma. Investigation of line broadening is also of independent physical interest inasmuch as in a plasma the radiating atoms are subjected to external influences that cannot be duplicated under other conditions: the atoms are under the influence of strong, inhomogeneous, rapidly varying fields. Theoretical analysis of the interaction of a radiating atom with the ambient fields leads to certain relationships between the line width γ and the charged particle concentration N, i.e., the relationships that must be used in experimental determination of N.

In the present work, we carried out an experimental investigation of broadening under the influence of charged particles of lines exhibiting a quadratic Stark effect.

The usual Weisskopf-Lindholm theory of impact broadening, i.e., for the condition when a number of individual collisions are observed, leads to the following inferences. The broadened line should have the classical dispersion shape, and the broadening is accompanied by a shift of the entire line contour. The line width γ and the shift Δ of the line peak from the unperturbed position are given by the expressions

$$\gamma = 11.4 C_4^{2/5} v^{3/5} N; \quad \gamma/\Delta = 1.16 \text{ and } \Delta = 9.8 C_4^{2/5} v^{3/5} N; \tag{1}$$

here C_4 is the quadratic Stark effect constant, v is the relative velocity of the atom and the perturbing particle and N is the density of the perturbing particles.

For purposes of comparing experiment with theory one need only investigate two regularities: first, one can check the variation of the width and shift with the quadratic Stark effect constant, choosing lines with substantially different C_4; second, one can measure the width to shift ratio which, according to the Weisskopf-Lindholm theory, should be of the order of unity for all lines.

For the purposes of our study we chose the channel of a spark discharge, wherein, by virtue of the high degree of ionization, one may assume that the line broadening is due wholly to the influence of electrons and ions. The spark discharge was excited in an atmosphere of argon at normal pressure. The power source was an IG-2 (spectroscopic spark) generator; the circuit parameters were V = 14 kv, C = 0.02 μf and L = 10 μh. We observed the lines of ionized argon excited in the channel of the spark discharge. Experimental data are available on the Stark effect for a number of A II lines; all the lines are characterized by a quadratic Stark effect with values of C_4 differing by 1-2 orders of magnitude.

In all we measured the width and shift of about 40 A II lines by means of a DFS-3 diffraction grating spectrograph with a reciprocal dispersion of 2 Å/mm. The line width was measured by the conventional procedure, the estimated accuracy being 5-10%. The line shift in the spark spectrum was determined with reference to the same lines in the spectrum of a hollow cathode, wherein no significant line shift occurs; the estimated measurement accuracy was 0.02-0.05 Å.

Most of our measurement data pertain to the mean (averaged over time) radiation of the discharge. Actually, in an oscillating discharge the electron concentration may vary over the period of the discharge. Hence, at our request, V.G.Koloshnikov carried out control measurements of the line width and shift with the light beam being modulated by a Kerr cell gating 1.5 microsec pulses (the period of the discharge was 7-8 microsec). These measurements yielded virtually the same results; hence, hereinafter, we shall discuss only the data obtained for the averaged over time radiation.

Table 1

C_4, cm^4/sec	γ, Å	Δ, Å
$\leqslant 5\cdot10^{-15}$	0,3÷0,5	0,1
$5\cdot10^{-14}$	1,0	0,3÷0,4
$5\cdot10^{-13}$	1,5	0,7

The experimental results are in qualitative disagreement with the deductions from the Weisskopf-Lindholm theory.

The averaged data characterizing the variation of the line width and shift with C_4 are shown in Table 1. It will be seen that with a two orders of magnitude change of C_4 the line width changes not by a factor of 20 but only by a factor of 3. The line shift is somewhat more strongly dependent on C_4, but still is appreciably less than C_4 to the 2/3 power.

The width to shift ratio is not equal to 1.16 and is not the same for all lines. The data for a number of the narrowest and at the same time least displaced lines are shown in Table 2. Here the value of γ/Δ is of the order of 5, but in some cases rises as high as 10. The data for the wider and more strongly displaced lines are listed in Table 3. Here the width to shift ratio for most lines is of the order of 2. Data on the Stark effect is available for the lines listed in the left part of the table; we shall discuss the results for these lines in greater detail. Unfortunately, at present we have no Stark effect data for the other lines.

Table 2

λ, Å	Multiplet No.	γ, Å	Δ, Å	γ/Δ	λ, Å	Multiplet No.	γ, Å	Δ, Å	γ/Δ
4352,2	1	0,44	—0,07	~6	4726,9	14	0,57	—0,10	~6
4420,9	1	0,41	—0,07		4879,9	14	0,62	—0,10	
4847,9	6	0,57	—0,10	5,5	4764,9	15	0,60	—0,07	8,5
5062,1	6	0,56	—0,11		4589,9	31	0,46	—0,04	>10
4266,5	7	0,35	—0,06	5,5	4183,0	36	0,37	—0,10	3,7
4282,9	7	0,33	—0,06		2942,9	—	0,45	0,10	4,5
3928,6	10	0,32	—0,04	8÷10					
3729,3	10	0,29	—0,03						

Table 3

λ, Å	Multiplet No.	γ, Å	Δ, Å	γ/Δ	λ, Å	Multiplet No.	γ, Å	Δ, Å	γ/Δ
4131,7	32	1,32	0,65	2,0	3780,8	54	0,63	0,37	1,7
4474,8	38	1,57	0,82	1,9	3576,6	56	0,74	0,35	2,1
4502,9	—	3,0	0,35	8,5	4218,7	64	1,20	0,65	1,8
4277,5	32	0,98	0,22	4,5	3559,5	70	0,85	0,38	2,2
4732,1	38	0,91	0,40	2,3	4222,7	77	1,35	0,60	2,25
4598,8	38	0,94	0,30	3,1	3868,5	90	0,88	0,43	2,0
4367,9	98	0,95	—0,06	>10	3561,0	106	0,81	0,34	2,4
4385,0	98	1,45	0,13	~10	3083,0	120	0,38	0,17	2,2
					3139,0	47	0,65	0,29	2,25

The great qualitative divergence between the experimental data and the Weisskopf-Lindholm theory prompted a re-analysis of the premises upon which this theory is based. This analysis led to the development of a non-steady state broadening theory.[1] Fundamental to this theory is consideration of two effects. In the case of rapid passage of an electron near an atom, the electron shell of the atom does not have time to be polarized, as is assumed to be the case with slow variation of the field in the steady-state theory of Weisskopf & Lindholm. This leads to a reduction of the efficiency (as regards line broadening) of the electron-atom encounters. In addition, one must take into account the role of inelastic collisions, which significantly increase the line width but have no

effect on the line shift. In the non-steady state theory, the line width and shift are determined by a dimensionless parameter β, characterizing the term under consideration,

$$\beta = \frac{Z^2(2\pi c)^{3/2}(\Delta E_q)^{3/2}C_4^{1/2}}{v^2}; \qquad (2)$$

here Z is the ionic charge, ΔE_q is the distance (in cm^{-1}) from the term under consideration to the nearest perturbing term, i.e., the term with which dipole interaction is possible.

For $\beta \gtrsim 1$ the premises of the steady state theory are valid; for $\beta < 1$ deviation from this theory begins, and for $\beta \ll 1$ the deviation is already considerablt. It follows from (2) that for ions, owing to their low velocity, the steady-state theory should hold in a wide range. Actually, it turns out that under our conditions (T = 30 000°K) β is always much larger than unity for ions, whereas for electrons β is generally smaller than unity and is much smaller for a number of lines.

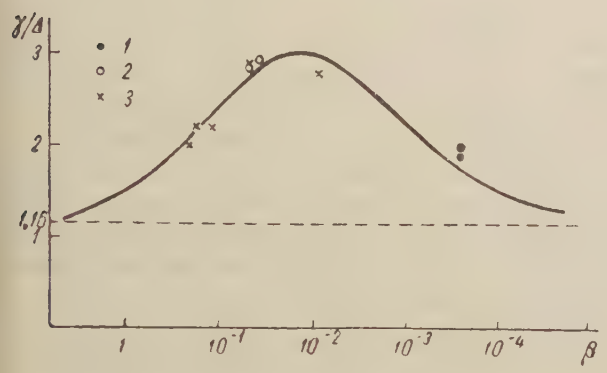

Theoretical variation of γ/Δ with β (solid curve); 1) our data for A II, 2) our data for He I, 3) the data of Wulff[2] for He I.

From the standpoint of the non-steady state theory, we obtain the following picture for line broadening by charged particles: for $\beta \approx 1$ Eqs.(1) for the width and shift hold; the principal contribution to the width and shift is made by electron collisions; for $\beta < 1$ the efficiency of the Weisskopf broadening mechanism decreases, while the contribution from inelastic collisions increases. Here the line width is determined in equal measure by the influence of electrons and ions. Inasmuch as inelastic collisions do not contribute to the line shift, the principal contribution to the line shift with $\beta < 1$ is made by ions.

In the non-steady state theory, the width to shift ratio is not constant, but also depends on β. The accompanying figure shows the theoretical variation of the width to shift ratio as a function of β together with some experimental data, namely, our data for a number of A II lines (for which the values of C_4 are known) and two He I lines, as well as the recently published data of Wulff[2] on some He I lines. The experimental points are at least consistent with the theoretical curve.

The values of the electron concentration N calculated by means of the expressions for the line width and shift given by the steady-state and non-steady state theories are listed in Table 4. Obviously, we could only make the calculations for lines with known C_4.

A comparison of columns 6 and 8 shows that calculations by menas of the non-steady state formula give a very small scatter of N (except for one line), whereas the differences obtained in calculations by the steady-state theory formula give a one to five spread. Moreover, the values of N calculated from γ and Δ according to the non-steady state theory are always closer than the corresponding values calculated by the formulas of the steady-state theory, even for the lines for which the measured width to shift ratio differs substantially from that calculated by means of the non-steady state theory.

It is interesting to note that despite the great spread in values of N obtained for individual lines in calculations by the steady-state and non-steady state formulas, the average figures prove to be rather close. This explains why

Table 4

λ, Å	C_4, cm4/sec	β	γ/Δ_{theo}	γ/Δ_{exp}	$N \cdot 10^{-17}$, cm^{-3}			
					non-steady state theor.		steady state theory	
					from γ	from Δ	from γ	from Δ
1	2	3	4	5	6	7	8	9
4460,6	$\leqslant 5 \cdot 10^{-15}$	0,35	1,85	5	1,6	0,5	1,9	0,5
4589,9	$\leqslant 5 \cdot 10^{-15}$	0,5	1,78	~ 10	1,5	0,4	1,8	0,4
4367,9	$3,5 \cdot 10^{-14}$	$5,5 \cdot 10^{-3}$	2,78	> 10	2,2	0,4	1,3	0,1
4385,1	$1,2 \cdot 10^{-14}$	$8,3 \cdot 10^{-3}$	2,90	~ 10	5,9	1,6	4,1	0,5
4277,5	$7,8 \cdot 10^{-14}$	$2,6 \cdot 10^{-3}$	2,53	4,5	1,7	1,0	0,8	0,2
4598,8	$7,8 \cdot 10^{-14}$	$2,6 \cdot 10^{-3}$	2,53	3,1	1,4	1,1	0,7	0,2
4732,1	$4,3 \cdot 10^{-14}$	$1,9 \cdot 10^{-3}$	2,44	2,3	2,1	2,2	0,9	0,5
4131,7	$5,5 \cdot 10^{-13}$	$2,6 \cdot 10^{-4}$	1,68	2,0	1,2	1,0	0,3	0,2
4474,8	$5,5 \cdot 10^{-13}$	$2,6 \cdot 10^{-4}$	1,68	1,9	1,2	1,1	0,3	0,2
4502,9	$5,5 \cdot 10^{-13}$	$2,6 \cdot 10^{-4}$	1,68	8,5	2,3	0,5	0,6	0,08
			Averages:		2,0	1,0	1,3	0,3

reasonable electron density values were obtained generally in all previously investigations based on the steady-state equations.

It will be evident that the experimental data so far available are in good agreement with the deductions from the non-steady state theory. Inasmuch as in theoretical calculations of the line width, it is essential to know the inelastic collision cross section, whereas this parameter does not enter into the non--steady state theory calculations for the line shift, it would appear preferable to use measured values of the line shifts for determining electron concentrations in plasma.

"P.N.Lebedev" Physical Institute,
Academy of Sciences of the USSR

References

1. I.I.Sobel'man & L.A.Vainshtein, Optika i spektroskopiya, 6, 440 (1959). (Trans. Optics and spectroscopy.)
2. H.Wulff, Z.Phys., 150, 614 (1958).

SEPARATION OF BINARY MIXTURES OF INERT GASES IN A DC DISCHARGE

- N.A.Matveeva

The passage of a direct current through a mixture of gases results in separation of the components. There is an increase in the concentration of the gas with the lower ionization potential and, as a rule, the greater atomic weight at the cathode, while the less readily ionized and lighter gas concentrates at the anode. There are two viewpoints regarding this separation mechanism: according to one, the separation is the result of transport of positive ions in the discharge in the direction of the cathode, i.e., the separation is due to the difference between the ionization potentials of the component gases;[1] according to the other view, the separation may be due to motion of neutral atoms under the influence of electron impact so that in this case the determining attribute involved is the difference in atomic weights.[2]

Finally, some investigators suggest that both transport mechanisms may operate simultaneously.[3,4]

The existence of directional migration or transport of ions in a discharge was demonstrated in the experiments of Frish & Kagan[5] involving observation of the Doppler shift of ion lines. Thus the transport of ions must play some role in the separation of the mixture. The available experimental data are as yet not sufficient for definitive elucidation of the separation mechanism.

Investigation of the separation of gases in a discharge is of interest not only because it can lead to a better understanding of the properties of electric discharges in gaseous mixtures, but also from the point of view of practical application, for it can be utilized for the separation of gases and isotopes[6], for the purification of gases[7] and for enhancing the sensitivity of analytic determination of minor impurities in gaseous mixtures[8]. Hence we undertook a systematic investigation of the separation in a discharge in a mixture of inert gases.

The principal shortcoming of most earlier experimental investigations[1-4,7] of gas separation was that the experimenters judged of the change in composition in the discharge from the variation in the spectral emission of the mixture along the length of the discharge column. This procedure cannot, however, yield quantitative information on the variation in concentration inasmuch as the intensity of spectrum lines depends not only on the concentration of the given gas but also on the conditions of excitation which, particularly in the presence of separation, are different in different parts of the positive column. In our work we drew samples of the gases from the regions in the vicinity of the two electrodes and then subjected these to quantitative spectrum analysis.

The discharge tube used in the experiments (Fig.1) had two end bulbs, having volumes of 400 and 1600 cm^3 and containing the nickel electrodes, connected by a 1 cm diameter tube. The length of this tube varied from 24 to 150 cm in different experiments. Branch tubes for the withdrawal of samples were located near each of the electrodes. The connecting tube contained a number of probes for measuring the electric characteristics of the discharge. The discharge was realized at a dc voltage of 1.5 kv. The direction of the discharge current was chosen so that the concentration of the minor component in the mixture would be enhanced in the smaller bulb. All the experiments were carried out with binary mixtures of helium, neon and argon.

The degree of separation was characterized by the ratio of the concentration of the impurity gas in the enriched sample to its concentration in the initial mixture: C_k/C. The experimental uncertainty consisted of the errors of spectrum analysis and the errors connected with the process of separation itself. The average scatter of relative changes in impurity concentration amounted to 5-10% referred to the measured quantity.

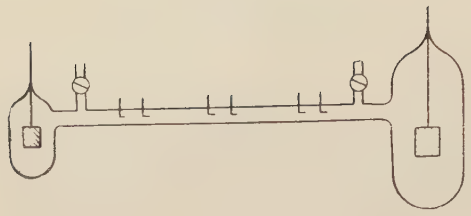

Fig.1. Discharge tube.

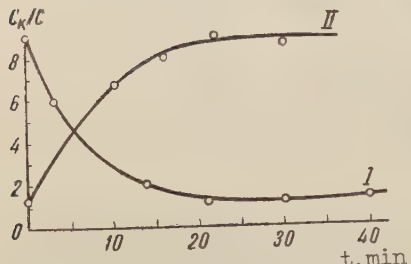

Fig.2

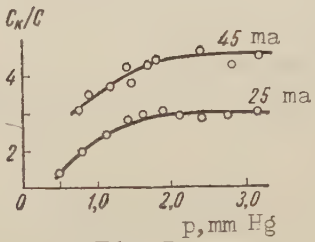

Fig.3

Fig.2. Variation in the concentration of the readily ionized impurity (9% A in He) at the anode: I) after initiation of the discharge, II) after cessation of the discharge (p = 1.6 mm Hg, i = = 50 ma, tube length - 150 cm).

Fig.3. Variation of the degree of separation as a function of the mixture pressure (0.7% A in He; tube length - 50 cm).

The results given below pertain to experiments with mixtures in which the impurity was gas with the lower ionization potential. In this case the impurity concentration increased in the vicinity of the cathode.

Measurements during the period of the discharge showed that upon initiation of the discharge at first there occurs a rapid change in the composition of the mixture along the length of the column and then, after a few minutes, a steady state is reached (Fig.2, curve I). This steady concentration condition is apparently attained when the number of particles transported per unit time under the influence of the electric forces is equal to the number of particles diffusing in the opposite direction owing to the concentration gradient. The time to the steady state increases linearly with increase in the concentration and depends little or not at all on the strength of the discharge current and the composition of the mixture. The separation time increases with increase in the length of the discharge tube.

In addition to the separation time, i.e., the time to attainment of the steady state in the discharge, we also measured the remixing time, i.e., the time to return to the initial gaseous mixture after cessation of the discharge (Fig. 2, curve II). It was found that the time characteristics of the two processes are analogous and that the mixing time is approximately equal to the separation time. This, we believe, indicates that diffusion is involved in the processes leading to establishment of the steady state in the separation of the gases.

In all subsequent measurements the samples were taken for analysis after attainment of the stationary state.

Measurements of the degree of separation carried out for mixtures of different composition and in a wide range of discharge currents (25 to 400 ma) showed that in the range of low pressures (0.4 to 1.5 mm Hg) there is a noticeable increase in the degree of separation with increasing pressure; at high pressures (1.5 to 4 mm Hg) the degree of separation varies little with the pressure. The probe measurements indicated a similar pressure dependence of the longitudinal potential gradient in the positive column of the discharge.

The degree of separation increases with increasing strength of the discharge current (Fig.4). At first there is a nearly linear increase, then, upon attainment of a high degree of separation, the growth slows down and the curves tend to a saturation value corresponding to complete separation of the mixture. At a sufficiently high current strength a small admixture of an easily ionized gas can be virtually completely eliminated from the base gas. Thus, in a 50 cm tube containing a mixture of argon and helium, the argon concentration decreased from 3% in the initial mixture to 10^{-3}% in the case of a 500 ma discharge current.

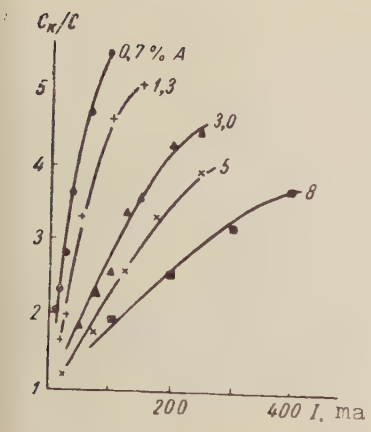

Fig.4

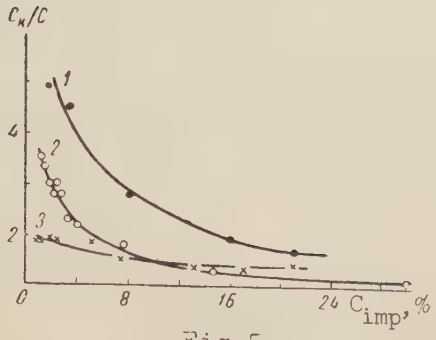

Fig.5

Fig.4. Variation of the degree of separation of a mixture of A and He with the discharge current (p = = 1.5 mm Hg; tube length - 50 cm).

Fig.5. Variation of the degree of separation with the concentration of the easily ionized gas (p = 1.5 mm Hg, i = 250 ma, tube length - 50 cm): 1) A + He, 2) A + Ne, 3) Ne + He.

With increase in the concentration in the easily ionized component, the dependence of the degree of separation on the pressure and current strength becomes weaker. The degree of separation with increasing concentration of the low ionization potential component falls off rapidly for mixtures of argon + helium and argon + neon and somewhat more slowly for a mixture of neon + helium (Fig.5). In the range of high concentration (>20%) of the easily ionized gas, the relative increase in its concentration at the cathode is small even with a discharge current of 1 amp.

In mixtures in which the main component is the easily ionized gas and the gas with the high ionization potential is the impurity there is virtually no separation. Thus, whereas in the case of a mixture of 3% argon in helium there was almost complete separation of the mixture at a discharge current strength of 500 ma, in a mixture of 3% helium in argon we observed no noticeable increase in helium concentration at either electrode even when the discharge current was increased to 1 amp. The separation becomes noticeable only at initial concentrations of the high ionization potential gas of the order of 15-20% and then increases with further increase of the concentration.

The steepness of the longitudinal potential gradient in the positive column of the discharge decreases with increasing concentration of the easily ionized impurity. The concentration dependence of the longitudinal potential gradient is roughly similar to the concentration dependence of the degree of separation.

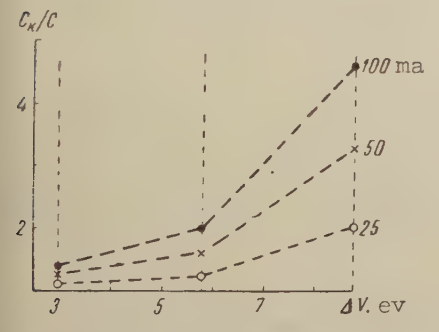

Fig.6. Variation of the degree of separation with increasing difference between the ionization potentials of the components: 1.4% of the easily ionized impurity in mixtures of A + He, A + Ne and Ne + He (p = 1.5 mm Hg, tube length - 50 cm).

The influence of composition on the steepness of the longitudinal potential gradient is also evinced in the fact that in the course of separation the potential gradient does not remain constant over the length of the positive column but decreases from the anode to the cathode, i.e., in the direction of increasing concentration of the easily ionized component.

One cannot unambiguously determine to what extent the degree of separation depends on the ionization potentials of the mixture components as against their atomic weights, inasmuch as when one gas is replaced by another both these parameters change. In the range of relatively low (<10%) concentrations of the easily ionized impurity, however, the degree of separation for all the investigated binary mixtures was the higher, the greater the difference between the ionization potentials of the components (Fig.6). At higher concentrations

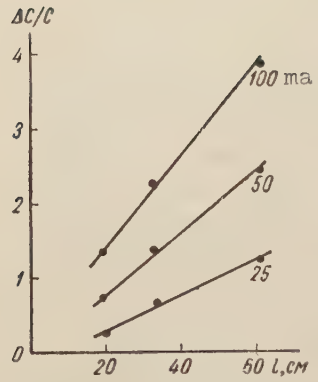

Fig.7. Variation of the difference between the concentrations of the impurity at the ends of the tube with the length of the tube and the discharge current (1.3% A in He; p = 1.5 mm Hg).

(> 20%) of the low ionization potential gas the degree of separation was the higher, the greater the potential gradient in the positive column.

For investigating the influence of tube length in the separation we used three different tubes in which the distances between the sampling branches were 19, 34 and 61 cm. These measurements were made with mixtures of argon + helium containing 1.3 and 6% argon at different pressures (0.5 to 2.5 mm Hg) and different values of the discharge current (25 to 200 ma). It was found that the relative concentration difference of the impurity at the ends of the tube increases in proportion to the tube length (Fig.7).

The experimental results can qualitatively be explained on the assumption that the principal process responsible for the separation is transport of ions. As is known, the addition of even a small amount of an easily ionized component to a gas leads to a reduction of the electron temperature in the discharge, which, in turn, leads to reduction of the degree of ionization of the base (high ionization potential) component. Hence in the ion current moving towards the cathode there will predominate ions of the easily ionized gas. Upon being neutralized at the cathode, they give rise to an increase in the concentration of this gas in the vicinity of the cathode. This explains the substantial separation observed at low concentrations of the low ionization potential component. The fact that there is virtually no separation in the case of low concentrations of the high ionization potential component indicates that the effect of separation due to difference in the atomic weights of the components is much weaker than the separation associated with ion transport.

The increase in the degree of separation with increasing difference between the ionization potentials of the components is due to the fact that with increase of the ionization potential difference, the role of the high ionization potential gas ions in the current flow is reduced. At high concentrations of the easily ionized gas, the electron temperature in the column is so low that virtually all the ions in the discharge column are those of the easily ionized gas. In this case the degree of separation is determined primarily by the ion transport rate. Thus we find that the degree of separation is higher in mixtures characterized by a steeper gradient of the longitudinal electric field.

The fact that the pressure and concentration dependences of the degree of separation and of the steepness of the potential gradient are similar shows that here the variation in the degree of separation is determined by variation in the ion transport velocity. The density of the ion current increases with the strength of the discharge current, which leads to the observed increase in the degree of separation.

The above description of the separation process is, naturally, a very rough one. To construct a quantitative separation theory, one must know the velocity of the ions and the relative degree of ionization of the components, as well as the variation of these parameters with the discharge conditions and the composition of the mixture.

It may be concluded from our experimental data, however, that separation of gases in a dc discharge can be utilized for purifying gases and for enhancing the sensitivity of analysis for minor impurities, but only in cases when the impurity

is a gas with an appreciably lower ionization potential than the main gas. To illustrate the use of this method of separation of mixtures for enhancing the sensitivity of analysis we plotted a working curve for determining argon in mixtures of argon with helium for argon concentrations in range from 10^{-5} to 10^{-4}% (without such enrichment the limiting sensitivity of analysis is of the order of 10^{-4}% A).[8]

In conclusion I desire to express my deep gratitude to S.E.Frish for suggesting the subject and guidance in the work.

Scientific Research Physical Institute,
Leningrad State University

References

1. M.J.Druyvesteyn, Physica, 2, 255 (1935).
2. F.Skaupy, J.Phys., 2, 213 (1920).
3. Ya.S.Vygodskii & B.N.Klyarfel'd, Zhur.tekh.fiz., 3, 610 (1933).
4. G.M.Malyshev & B.V.Pavlov, Vestnik, Leningrad State University, No.16, 32 (1957).
5. S.E.Frish & Yu.M.Kahan, Zhur.eksp.i teor.fiz., 17, 576 (1947); Ibid., 18, 519 (1948).
6. H.D.Beckey, W.E.Groth & K.H.Welge, Z.Naturforsch, 8a, 556 (1953).
7. R.Ries & G.H.Dieke, J.Appl.Phys., 25, 196 (1954).
8. N.A.Matveeva, Zavodsk.labor., No.6 (1958). (Trans.Industrial Laboratory.)

MEASUREMENTS OF ELECTRIC FIELDS IN A HIGH-FREQUENCY LOW PRESSURE DISCHARGE BY MEANS OF AN ELECTRON BEAM

- G.S.Solntsev, A.G.Porokhin & N.M.Chistyakova

The techniques of measuring electric fields in discharges by observing the deflection of an electron beam passing through the discharge has been used in a number of investigations of dc glow discharges at low pressures.[1,2] In a low pressure high-frequency (hf) discharge the electric field at each point may be represented in the form of a superposition of two fields: the hf field $E_{\sim}$, produced by the hf oscillator supplying the discharge, and a dc field $E_{=}$ due to distribution of space charges in the discharge gap.[3,4] By shooting an electron beam through the hf discharge one can simultaneously determine $E_{\sim}$ and $E_{=}$ and investigate the distribution of the two fields along the discharge axis.

Experimental Procedure

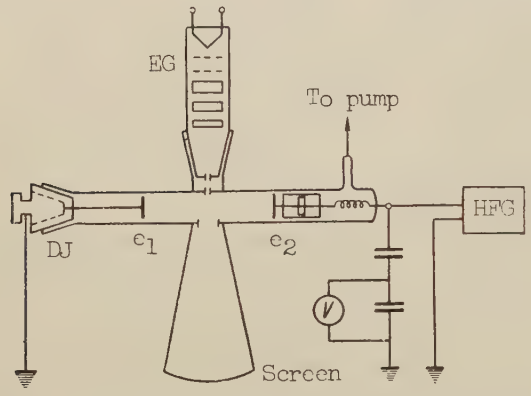

Fig.1. Discharge tube and electron beam probe: EG - electron gun, e_1 & e_2 - electrodes, DJ - double joint, HFG - hf generator.

The experimental arrangement is shown in Fig.1. To insure a long service life, the electron gun had a tungsten cathode and was operated at potentials of 5 to 10 kv; the gun current was 10^{-7} to 10^{-8} amp. After traversing the discharge tube at the chosen diameter, the electron beam passed through a slit in the tube wall and impinged on the fluorescent screen. To permit investigation of the field distribution along the length of the discharge, the discharge as a whole could be displaced (left or right in the figure) relative to the electron beam. The e_2 electrode was moved by means of a permanent magnet outside the tube; the other electrode e_1 by means of the special double joint at the end of the tube. Thus by simultaneous displacement of the two electrodes the electrode gap could be kept constant. The electrodes were brass disks 4 cm in diameter with rounded edges; the e_1 electrode was grounded. The electron spot on the beam was photographed, the deflection being determined with reference to a suitable grid on the screen.

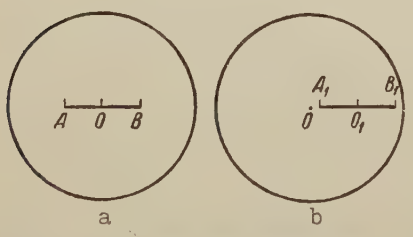

Fig.2. Picture observed on the fluorescent screen; a) with an hg voltage on the discharge tube electrodes but no discharge, and b) with a discharge.

In setting the accelerating potential, we were guided by the following factors: 1) obtaining a sufficient sensitivity for measurement of $E_{\sim}$ and $E_{=}$, 2) obviating electric breakdown between the gun electrodes, 3) obtaining adequate brightness of the spot and proper focusing, and 4) scattering of the beam by the gas atoms.

Fig.2 will serve to explain how $E_{\sim}$ and $E_{=}$ can be determined from the beam trace on the screen. Point O corresponds to the beam spot in the absence of a field. When an hf voltage is applied to the electrode but there is no discharge in the tube, the point becomes a line AB, the length of which is proportional to $E_{\sim}$ at the given cross section of the discharge gap.

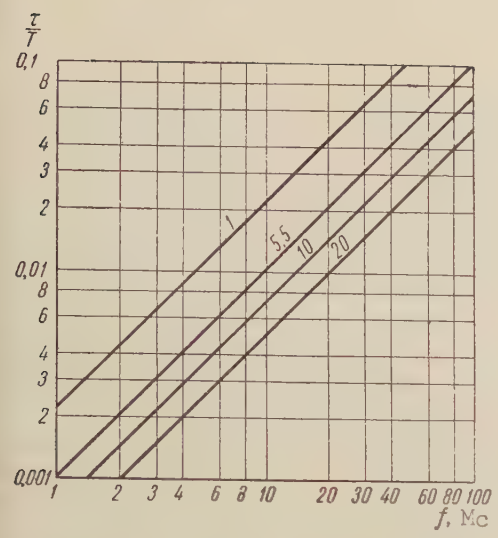

Fig.3. Variation of τ/T with the frequency for a 4 cm diameter tube and different accelerating potentials (indicated in kv at the plots).

When a discharge is ignited between the electrodes, instead of the line AB on the screen, we will have the line A_1B_1, the midpoint of which, O_1, will be displaced relative to O. Again the distance A_1B_1 gives the amplitude of the hf field $E_\sim$, while the distance OO_1 is associated with the strength of the dc field $E_=$ due to the space charge. Thus, one can separately determine the ac and dc components of the electric field in the discharge.

A necessary condition for effective application of the electron beam probe procedure for investigating hf discharges is that the electron transit time τ through the discharge must be shorter than the period T of the field. Fig.3 shows the variation of τ/T with the field frequency for a 4 cm diameter tube and different accelerating potentials. It will be evident that for a frequency of 3.3 Mc and V_a = 5-10 kv, the ratio τ/T = $= (3.3\text{-}2.3)\cdot 10^{-3}$.

In investigating discharges in cylindrical tubes, it is commonly assumed that the longitudinal component of the hf field in a given cross section does not depend on the distance from the tube axis. In other words, it is assumed that the skin effect due to the rapidly alternating field in the discharge is insignificant in the case of discharge currents in the range from a few to some tens of milliamps. In the case of heavier currents (10^2-10^3 amp), however, the skin effect should probably be taken into account.[5]

Inasmuch as in traversing the discharge the electron beam is deflected under the influence of the longitudinal field in the direction of the discharge axis, in the presence of an inhomogeneous field the deflection of the spot on the screen corresponds to an averaged value of the field; owing to superposition of the hf and dc fields the "averaging region" increases as compared with that obtaining in measuring $E_=$ in a dc discharge.

In utilizing the electron beam probe technique for investigating hf discharges, it must be borne in mind that it can be used only for determining the field in E-discharges, wherein all the processes are determined by electric fields rather than by rapidly varying magnetic fields, i.e., measurements can be made only in discharges in which eddy current fields are negligible.

The sensitivity of the equipment, which we arbitrarily define as the field strength producing a 1 mm deflection of the spot on the screen, may be determined in two ways. The first procedure consists of setting the electrodes fairly close to each other and applying a known hf potential; then the field strength is calculated and the beam deflection measured. The second method is based on equating the voltage applied to the electrode to the graphically obtained integral of the curve characterizing the distribution of the hf field in the discharge gap.

Actually, the difference between the values of $E_\sim$ obtained by the first and second procedures did not exceed 20 v/cm and is explained by the "barrel-shaped" configuration of the electric field between the discharge electrodes.

An obvious requirement where the electron beam probe procedure is concerned is that the disturbing effect of the electron beam on the investigated region of the discharge be small. Control experiments and theoretical evaluations taking into account both elastic and inelastic collisions of the beam electrons with the

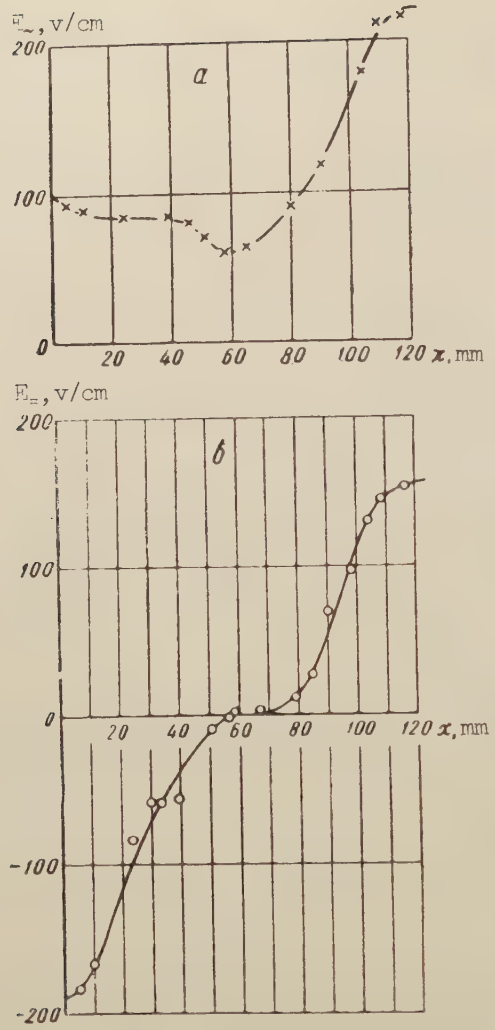

←Fig.4. Distribution of the hf field $E_{\sim}$ (a) and the space charge field $E_{=}$ (b) in a discharge in argon at $p = 10^{-2}$ mm Hg and f = = 3.3 Mc.

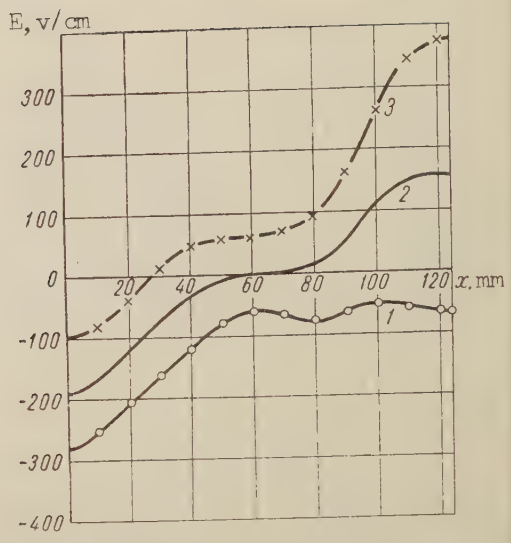

Fig.5. Instantaneous distribution of the sum field $E = E_{\sim} \cos \omega t + E_{=}$ at different times during the cycle: 1) $\omega t = 0$, 2) $\omega t = \pi/2$ and 3) $\omega t = \pi$.

gas atoms and the interaction of the electrons with the plasma showed that in our experiments this condition was satisfied.

Results

After preliminary tests, we carried out measurements of the electric field in argon at a pressure of 10^{-2} mm Hg at a field frequency of 3.3 Mc. The distributions of the hf field $E_{\sim}$ and the space charge field $E_{=}$ in the discharge with an electrode separation of 12.4 cm are shown in Fig.4. The asymmetric character of the curves near the electrodes is explained by the fact that the hf voltage was applied to the right electrode (Fig.1), while the left electrode was grounded. Hence the discharge was asymmetrical. Using the data of Fig.4 one can plot the instantaneous distribution of the sum fields $E = E_{\sim} \cos \omega t + E_{=}$ at different times during the cycle; this has been done in Fig.5.

Further, making use of the expression for the field in terms of the scalar potential (which is valid for E-discharges), we obtain the instantaneous distribution of the potential along the discharge gap for different instants during the cycle (Fig.6).

The space charge distribution at different instants can be calculated by means of Poisson's equation; this distribution is plotted in Fig.7. There is a positive space charge near each of the electrodes. The magnitude of the space charge near the hf electrode varies with time; it is greatest during the negative

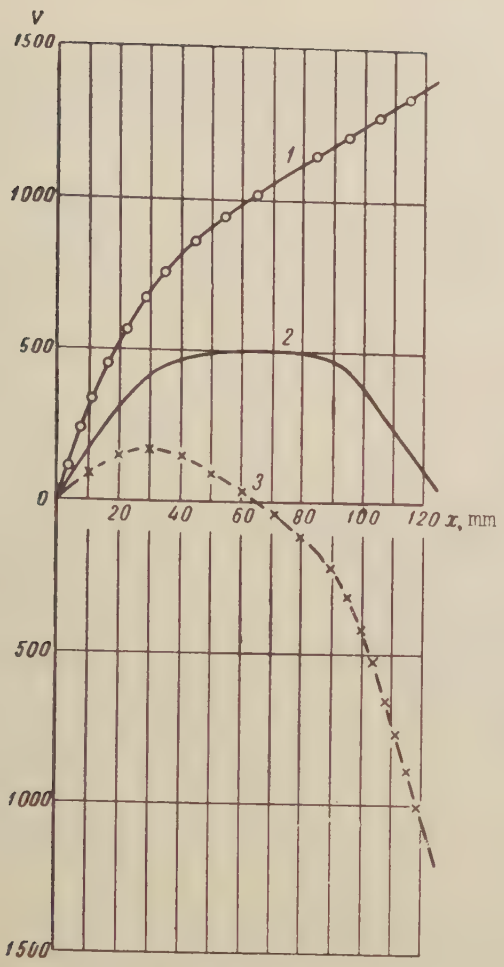

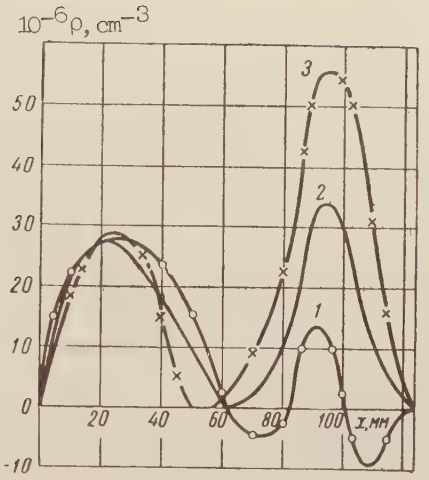

Fig.7. Distribution of space charge at different instants of the hf field cycle: 1) $\omega t = 0$, 2) $\omega t = \pi/2$ and 3) $\omega t = \pi$.

←Fig.6. Instantaneous distribution of the potential along the discharge gap: 1) $\omega t = 0$, 2) $\omega t = \pi/2$ and 3) $\omega t = \pi$.

half-cycle and minimal during the positive half-cycle. In contrast, near the grounded electrode the magnitude of the space charge is virtually independent of the field period. In the middle of the discharge gap the excess space charge is zero.

Interpretation of the results is hampered by the fact that the usual diffusion relationships for electron motion do not apply under our experimental conditions. On the basis of the behavior of the space charge near the electrodes and the data on the field distribution, it may be hypothesized that intense ionization of the gas occurs in the middle part of the discharge gap. The electrons are rapidly accelerated under the influence of the field and move towards the electrodes. The positive ions also move from the central region of intense ionization towards the electrodes, but their velocity is lower than that of the electrons so that positive space charges build up in the sections of the gap near the electrodes. In the high field region near the right electrode, the positive ions acquire a high energy which leads to active disintegration of the electrode surface and, possibly, to electron emission (γ-processes).

For a more complete interpretation of the results obtained for hf discharges at low pressure by means of the electron beam probe it is essential to extend the investigation to higher frequencies and to carry out measurements at different gas pressures and with electrodes of different materials. In addition, it would be desirable at this stage to use the electron beam probe procedure in conjunction with other methods of investigation (conventional probe, optical, etc.) in order to obtain comparable results and thus check the reliability of this procedure.

Conclusions

1. The electron beam procedure, which we employed for investigating a high-frequency, low pressure E-discharge, allows of simultaneous measurement of the hf field and the space charge field at different points in the discharge gap. The procedure has certain limitations and to obtain meaningful results for hf discharges certain specific requirements must be met.

2. In the present work there have been obtained for the first time data on the distribution of the electric field, potential and space charge in a high-frequency discharge in argon at a pressure of 10^{-2} mm Hg for different instants during the hf voltage cycle.

Physical Faculty,
Moscow State University

References

1. R.W.Warren, Rev.Sci.Instr., 26, 765 (1955). Phys.Rev., 98, 1650 (1955).
2. R.S.Stein, Phys.Rev., 89, 134 (1953).
3. S.M.Levitskii, Zhur.tekh.fiz., 27, 1001 (1957). (Trans.Soviet Physics - Tech.Physics.)
4. Kh.A.Dzherpetov & G.M.Pateyuk, Zhur.eksp.i teor.fiz., 28, 343 (1955). (Trans.Soviet Physics - JETP.)
5. R.Carruthers, App.Sci.Res., 135 (1955).

MEASUREMENT OF THE ELECTRIC FIELD IN A SUPER-HIGH FREQUENCY PLASMA

- V.E.Mitsuk, M.D.Koz'minykh & I.V.Talalaeva

The linear Stark effect has been successfully utilized for investigating the electric fields in the cathode region of dc glow discharges. However, it has proved impossible to extend the measurements to the positive column because fields of the order of 10^3 v/cm or higher are required to obtain a noticeable Stark effect.

In contrast to dc plasma, in microwave plasma very appreciable electric fields may obtain. As follows from even the simple one-electron model of a microwave discharge, when the frequency of the field is greater than or comparable to the collision frequency ($\omega \geqslant \nu_c$), an electron velocity amplitude sufficient for ionization at a frequency of about 10^{10} cps is attained with an electric field of the order of 10^4 v/cm. On the other hand, some of the specific characteristics of microwave plasma, in particular, the relatively low gas temperature, the absence of excess charge and the fact that Holtzmark type effects at pressures under 10 mm Hg are weak, give reason to assume that the principal effect in determining the Balmer line contours is the Stark effect.

A quantum mechanical theory of the Stark effect in an alternating field was proposed for the hydrogen atom by Blokhintsev[1]. He showed that the Stark contour for the case of an alternating field differs substantially from the static Stark contour. Earlier, one of us[2] carried out a comparison of the parameters of the H_β line Stark contour as calculated according to Blokhintsev's theory with the experimental results obtained at a frequency of 9400 Mc for hydrogen at pressures of the order of 1 mm Hg. It was shown that the Stark effect at super-high frequencies can be utilized for the measurement of electric fields in microwave plasma.

Below we give some results of further experimental work with the same equipment.

1. Stark contour in an alternating field

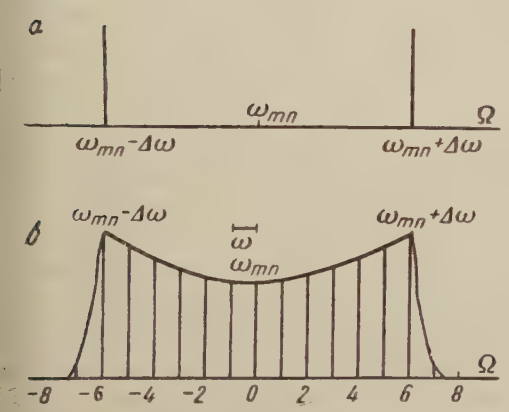

Fig.1. Line splitting: a) in a static field, b) in an alternating field.

Two cases are distinguished in analysis of the matrix element of the dipole moment of the atom in an external field of the form $E = E_0 \cos \omega t$ and having a linear Stark effect in a static field: case 1 obtains when the time τ of observation of the spectrum is much shorter than the period T of the external field ($\tau \ll T = 2\pi/\omega$), and case 2 when $\tau \gg T$.

In the first case the intensity maximum in the spectrum occurs at the frequency corresponding to the static field splitting components of the line ω_{mn}. In the limit ($\omega \to 0$), we obtain precisely the familiar static effect. If for the sake of simplicity we assume that in a static field the line ω_{mn} is split in two, we will have the situation pictured in Fig.1,a. The magnitude of the splitting $\Delta\omega$ is proportional to the field strength and can be calculated by the Epstein-Schwartzschild formula:

$$\Delta\omega = \frac{3h}{4\pi me} E_0. \qquad (1)$$

In the second case, which is the one of interest from the experimental standpoint, a different picture is obtained. Superficially, the spectrum is reminiscent of the spectrum of a frequency modulated signal. In addition to the fundamental atomic frequency ω_{mn}, there appear the combination frequencies

$$\omega_{mn} \pm p\omega, \tag{2}$$

where ω is the frequency of the external field and $p = 1,2,3....$

The qualitative aspect of the spectrum is shown in Fig.1,b for the case when $\Delta\omega/\omega \gg 1$. The envelope of the combination frequency intensities is arranged symmetrically relative to the unshifted (field-free) line; it has maxima near the frequencies $(\omega_{mn} \pm \Delta\omega)$ corresponding to the components of the static effect and falls off rapidly (exponentially) to zero outside the spectral region bounded by these frequencies. For the Balmer series, the static Stark structures will obviously have more than two components, but inasmuch as they are symmetrical with respect to the unshifted line the procedure for constructing the atomic spectrum in an alternating field reduces to superposition of the combination frequency intensities plotted independently for each pair of symmetrical static components.

By way of illustration the contour of the H_β line for ω = 9400 Mc and E_0 = $= 5 \cdot 10^3$ v/cm is shown in Fig.2. The contour as a whole may be characterized quantitatively by a suitable parameter, namely, the half-width δ, which, as has been shown in Ref. 2, is virtually a linear function of the electric field amplitude in the range from $2 \cdot 10^3$ to $20 \cdot 10^3$ v/cm. Thus the experimentally observed half-width of the Stark line contour gives us a measure of the amplitude of the external electric field in microwave plasma.

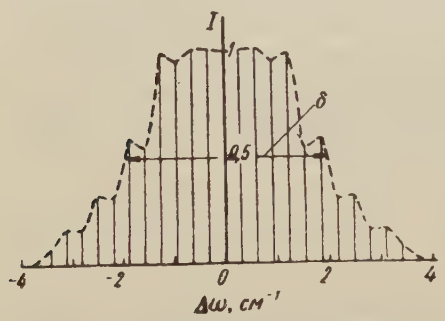

Fig.2. Calculated (theoretical) line structure in an alternating field (neglecting the fine structure of hydrogen).

2. Measurement of the field amplitude

A somewhat simplified version of the experimental set-up described in Ref.3 was utilized for checking the photographic recording procedure and comparing the results obtained by it with those obtained by it with those obtained by means of a photomultiplier.

The discharge tube, which was a hydrogen filled 1 mm diameter glass capillary with very thin walls, was mounted in the symmetry plane of a 23 x 10 mm waveguide. The discharge radiation passed through a window in the narrow wall of the waveguide and fell on the slit of a DFS-2 spectrograph. The capillary to slit distance was chosen so as to fill the spectrograph aperture with light. The pulsed microwave power (λ = 3.2 cm), fed into the waveguide from a magnetron, passed through the section containing the capillary with no substantial reflection or absorption. The field amplitude E_0 at the capillary axis was found from the average power P_{av} (measured by a thermistor instrument) by means of the familiar expression

$$P_{av}/\tau F = E_0^2 h Y_0/2 \tag{3}$$

where Y_0 is the characteristics admittance $\left(Y_0 = \frac{1}{2}\frac{a}{h}\sqrt{\frac{\varepsilon}{\mu}}\sqrt{1-\left(\frac{\lambda}{2a}\right)^2}\right.$, a is the width and h is the height of the waveguide, λ is the wavelength in free space, ε is the permittivity and μ is the permeability of the material filling the waveguide, τ is the pulse duration and F is the pulse repetition frequency (in our experiments τ = 1-2 μsec and F = 300-600 pps).

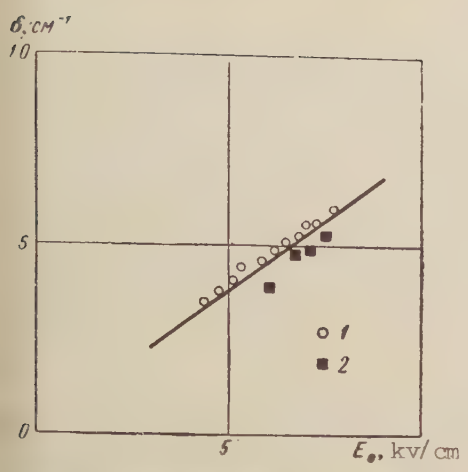

Fig.3. Variation of δ with E_0: 1) recorded by means of a photomultiplier, 2) recorded photographically.

The experimental results are shown in Fig.3, where δ is the half-width of the Stark contour obtained from the spectrograms* and E_0 is the electric field amplitude calculated by means of Eq.(3). For comparison we also give the results of experiments with photoelectric recording of the spectrum. It will be seen from the figure that the experimental points obtained by photographic recording lie below the theoretical curve, while the results obtained with PM recording lie consistently above the theoretical plot.

3. E = f(t) in a pulse shf discharge

For obvious reasons, it is desirable to know the field strength in the discharge at any given instant. In particular, knowledge of the field strength at different instants during the discharge should be of help in understanding the process of formation of an shf discharge.

The photographic method of recording can only give the value of the field strength averaged over the entire pulse. One can discriminate the requisite short intervals only by the photoelectric procedure, using time selection of the pulse from the photomultiplier (the photomultiplier output pulse should have the same shape as the light pulse). In principle, the problem can be easily solved: one need only provide for blocking and unblocking of the PM pulse circuit at the requisite instants. The selecting pulse must have a duration much shorter than the duration of the investigated pulse and there must be provision for shifting the narrow gate in sufficient small steps. Each instant will be characterized by its own particular line contour (I vs ν); then, as noted above, from the line contour we can uniquely determine the field strength. If the selection (gate) steps are sufficiently small, we can determine the variation of E with t over the entire shf pulse and even during a certain interval after cessation of the pulse (the limit is determined by the rate of decay of the discharge glow and the noise level of the photomultiplier circuit). A block diagram of the experimental set-up is shown in Fig.4.

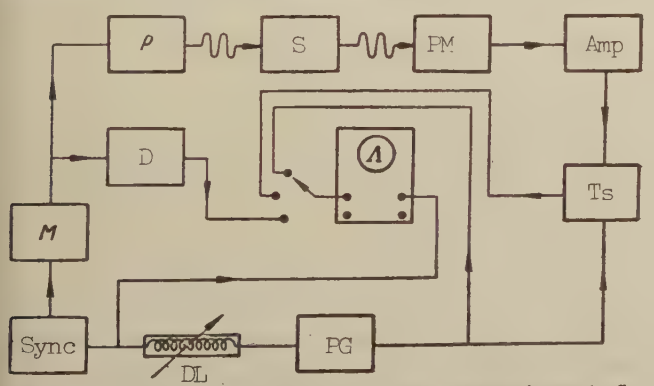

Fig.4. Block diagram of the experimental arrangement: P - discharge tube, S - spectrograph, PM - photomultiplier with cathode follower, Amp - wide band amplifier, M - magnetron, D - detector, Ts - time selector, Sync - synchronizing unit, DL - delay line, PG - pulse generator.

Analyzing the experimental requirements, we note that it is not necessary to record the full line contour by automatic scanning of the slit. Since essentially we are interested only in one parameter, namely, the half-width δ (the width at half-height), actually we need only measure δ. In practice, determination of the line half-width encounters certain difficulties connected with the necessity of taking into account the nonlinearity of all the electronic circuits from the photomultiplier to the recording instrument. The time selector in

---

*Some of the measurements were made by L.I.Prokoshina.

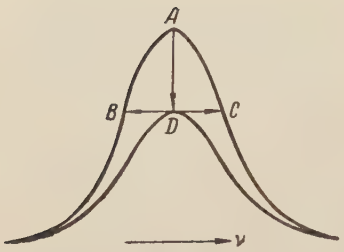

Fig.5.

particular may have a distinctly nonlinear amplitude characteristic.

The experimental procedure described below circumvents this difficulty. The measurement scheme is explained in Fig.5. First we move the photomultiplier back and forth in the focal (spectrum) plane to obtain the maximum signal (point A). This means that the PM is positioned at the peak of the line. Then we close down the slit in front of the PM cathode to half its initial width and note the signal level (point D). Next we reopen the slit to its initial width and move the PM first to one side and then to the other to where the signal is equal to the point D level (points B and C). The distance between the two PM positions (B and C) is, obviously, the line half-width.

This procedure is justified only if the slit in front of the photocathode is sufficiently narrow for the entering light flux to be proportional to the slit width throughout the range of slit width variation. Theoretically, the error due to finite size of the slit will not exceed 1-2% provided the slit width is not greater than 1/5 of the half-width of the spectrum line (in the plane viewed by the PM). Actually, however, the error in determining the half-width by this procedure is appreciably larger (up to 10%) owing to sugjective factors (in our work we carried out at least 10 measurements for each discharge instant). The experimental accuracy could be increased by one order of magnitude if the signal to noise ratio were substantially increased. In our experiments the signal to noise ratio was about 1-1.5.

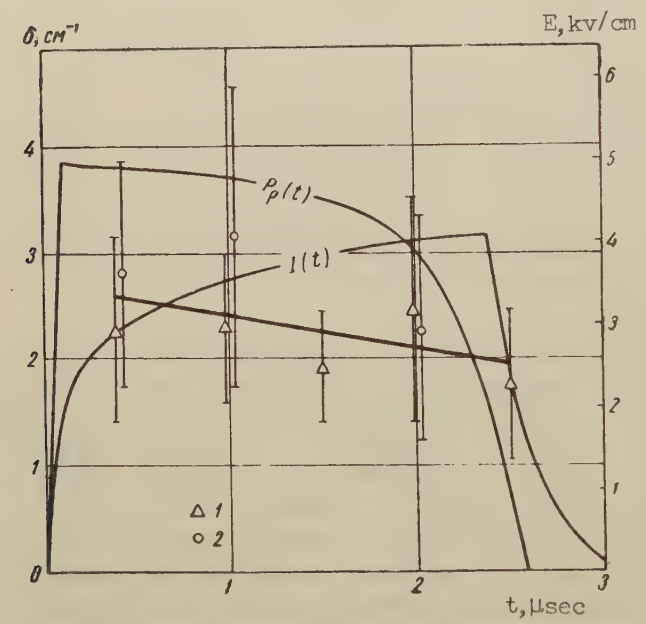

Fig.6. Variation of the shf pulse power p_p and the luminous intensity I of the discharge as functions of the time t: 1) p = 4.3 mm Hg, and 2) p = 23 mm Hg.

According to our evaluation, the error due to the finite width of the spectrograph engrance slit is not large. The ratio of the entrance slit width to the half-width of the line did not exceed 0.25, which results in an additional broadening[3] of the order of $\frac{1}{2}\left(\frac{d}{\delta}\right)^2$, i.e., 3%, inasmuch as $\frac{\delta'}{\delta} = \sqrt{1+\frac{d^2}{\delta^2}}$, where δ' is the half-width of the line broadened due to the finite width of the slit.

Fig.6 shows the results of experimental determination of E = f(t) in an shf pulse discharge in deuterium with τ = 2 microsec, p_p = 50 kv, τ_{sel} = 0.1 microsec and $\Delta\tau_{sel}$ = 0.1 microsec (δ is the line half-width at the given instant). Since the linearity of E = f(δ) is an experimentally established fact, we can safely infer that the plot in Fig.6 represents E = f(t).

We reckoned the time from the beginning of the leading edge of the shf power pulse. In order to correlate this time reckoning with the selection pulses (delay line steps), shf pulses from the magnetron and selection pulses, delayed a known interval by the delay line, were applied atlernately to the vertical input of the oscillograph. A rectangular grid

on the oscillograph screen served as an auxiliary reference system. As the zero value of δ we took the half-width of the contour for t = 3.0 microsec, when a faint afterglow is still observed. It may safely be assumed that the discharge field at this instant is nearly zero inasmuch as the shf power pulse terminated prior to t = 2.6 microsec. Hence we took the half-width determined for t = 3.0 microsec as the apparatus function. The apparatus function, in turn, determines the position of the horizontal axis, i.e., the δ or E zero.

In concluding, it must be noted that unfortunately the initial part of the luminous output pulse (specifically, the interval corresponding to the rise of the shf power pulse) was not encompassed in the measurements owing to the low luminous intensity (Fig.6).

References

1. D.I.Blokhintsev, Phys.Z.Sov.Union, 4, 501 (1933).
2. V.E.Mitsuk, Zhur.tekh.fiz., 28, 1316 (1958). (Trans.Soviet Physics - Tech.Physics.)
3. O.D.Dmitrievskii, B.S.Neporent & V.A.Nikitin, Usp.fiz.nauk, 64, 447 (1958).

INFLUENCE OF THE TEMPERATURE OF AN AUXILIARY ELECTRODE ON THE IGNITION OF A HIGH FREQUENCY DISCHARGE IN HELIUM

- Kh.A.Dzherpetov

In the work of Brown[1] and Kihara[2] the breakdown voltage of a high frequency discharge is assumed to correspond to the voltage of an infinite increase in the electron concentration. From the standpoint of this definition of breakdown, the theoretical breakdown voltage is independent of the initial ionization. It is, however, logical to assume that under any given conditions the instant of breakdown corresponds to increase of the charged particles to a certain final, critical concentration. This definition of breakdown allows of evaluating the influence of initial ionization on the magnitude of the breakdown voltage. Hence we felt it would be of interest to carry out an experimental study of the influence of the initial electron concentration on the breakdown voltage. To this end we designed a discharge tube with an auxiliary heated electrode: by regulating the heating current we could vary the initial electron concentration in the discharge gap at will.

The breakdown (ignition) voltages were measured both with internal and with external electrodes. The experiments showed that the ignition voltage beginning with a certain temperature of the auxiliary electrode falls off sharply and then remains virtually constant with further increase of the auxiliary electrode temperature.

The experimental ignition temperature vs auxiliary electrode temperature (heating current) curves obtained for the case of internal electrodes with a separation of 2 cm are shown in Fig.1. It will be evident from the curves that with increase of the heating current (temperature) the ignition voltage at first re-

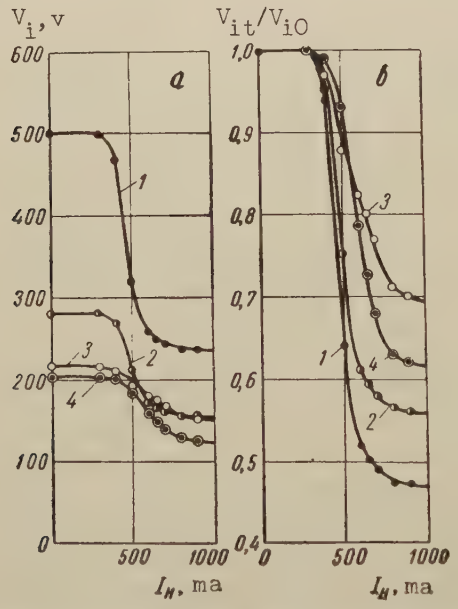

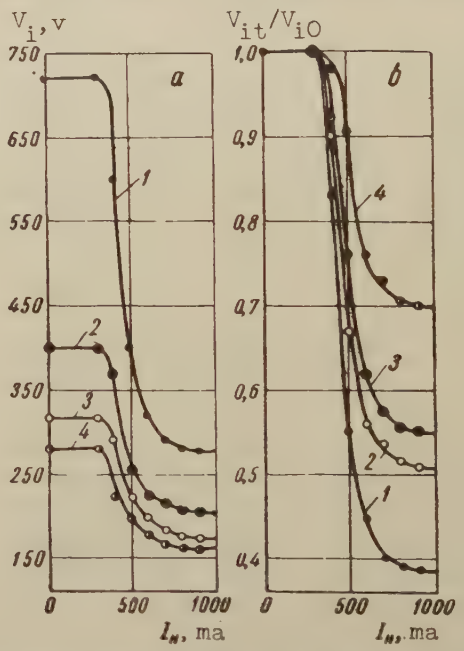

Fig.1. Variation of the ignition voltage (a) and ratio V_{it}/V_{iO} (b) as a function of the auxiliary electrode heating current for discharges in He between internal electrodes: 1) p = 0.8 mm Hg, 2) 1.4 mm Hg, 3) 5.2 mm Hg, 4) 7.3 mm Hg.

Fig.2. Same as Fig.1 but for external electrodes. Distance between external electrodes d = 1 cm; distance between internal electrodes L = 3 cm; 1) p = 0.55 mm Hg, 2) 0.8 mm Hg, 3) 1.1 mm Hg, 4) 2 mm Hg.

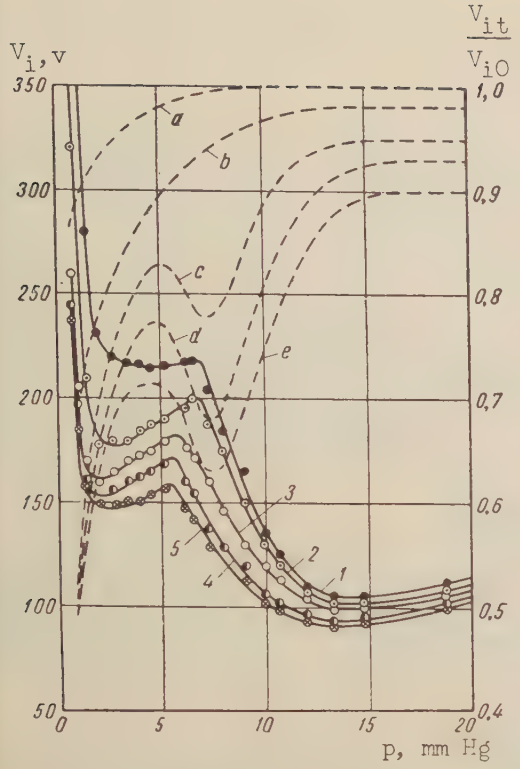

Fig.3. Variation of the ignition voltage (solid curves) and the ratio V_{it}/V_{i0} (dashed curves) with the He pressure at different values of the auxiliary electrode heating current: 1) $I_H = 0$, a) 400 ma, 2 & b) 500 ma, 3 & c) 600 ma, 4 & d) 700 ma, 5 & e) 800 ma.

mains the same, then falls off rapidly and finally levels off again.

Similar curves were obtained in the case of application of a high-frequency voltage to the external electrodes; in this case the position of the plates, formerly serving as internal electrodes, determined the linear dimensions of the discharge volume. The results of these measurements are shown in Fig.2. Here again, the ignition voltage remains constant, then in the heater current range from 400 to 700 ma (for all the listed pressures) decreases sharply, and finally levels off at a value dependent on the pressure.

To determine the pressure dependence of the V_{it}/V_{i0} ratio (ratio of the ignition voltage with the auxiliary electrode heated to the temperature T to ignition voltage with no heating of the auxiliary electrode) vs auxiliary electrode temperature curves, we carried out measurements in a wide range of pressures with a fixed interelectrode distance. Curves characterizing the variation of the ignition voltage and V_{it}/V_{i0} as a function of the pressure at different values of the auxiliary electrode heating current are shown in Fig.3. The hf discharges were realized at a frequency of 2 Mc with an electrode separation of 2 cm.

It will be seen from the figure that the ignition voltage vs pressure curves have two minima. With increase of the auxiliary electrode temperature above a certain value, the region of maximum values of V_{it} between the two minima is gradually shifted to the side of lower pressures. With increase of the heater current the region of the first ignition voltage minimum narrows. As a result of these two effects, the pressure dependence of V_{it}/V_{i0} has a minimum in a certain temperature region (1500 to 2000°). This is evinced by the dashed curves c,d & e, whereas curves a & b obtained with heating currents of 400 and 500 ma, i.e., at electrode temperatures under 1500, exhibit no minimum.

According to Brown[1], Kihara[2] and other authors the balance equation for electrons in the discharge gap at the instant of breakdown is

$$n\nu + q + \nabla^2 (Dn) = 0,$$

where n is the number of electrons per unit volume, ν is the number of ionizations per unit time by one electron, D is the diffusion coefficient, q is the number of electrons produced per sec in a unit volume under the influence of the external ionizer. In contrast to Brown and Kihara, we assume that the electron concentration at the electrodes prior to breakdown is not zero and depends on the initial ionization. Under this assumption the solution of this equation for the case of a discharge gap between two infinite plane electrodes gives the following expression for the electron density in the middle of the discharge gap:

$$n = \frac{n_0}{\cos\sqrt{\frac{\nu}{D}}\frac{L}{2}} + \frac{q}{\nu}\left\{\frac{1}{\cos\sqrt{\frac{\nu}{D}}\frac{L}{2}} - 1\right\},$$

where n_0 is the electron concentration at the electrodes and L is the interelectrode distance. In view of the fact that the first term in the above equation is much larger than the second one, we can disregard the latter and write

$$n = \frac{n_0}{\cos\sqrt{\frac{\nu}{D}}\frac{L}{2}}.$$

Let us assume that at the instant of breakdown the concentration of charged particles under the given conditions attains a certain critical value n_{cr} and that this critical concentration remains constant under the given conditions for other values of the initial ionization. Then for two different initial ionizations we can write

$$n_{cr} = \frac{n_{01}}{\cos\sqrt{\frac{\nu_1}{D_1}}\frac{L}{2}} = \frac{n_{02}}{\cos\sqrt{\frac{\nu_2}{D_2}}\frac{L}{2}}.$$

Making use of the functional dependence of ν on the ignition voltage U given by Kihara[2], we can rewrite the above equation in the form

$$\frac{n_{02}}{n_{01}} = \frac{\cos\sqrt{A\left(\frac{pL}{2}\right)^2 e^{-\frac{BpL}{U_2}}}}{\cos\sqrt{A\left(\frac{pL}{2}\right)^2 e^{-\frac{BpL}{U}}}}.$$

Here A and B are constants, equal to 4 and 50, respectively for He, p is the pressure in mm Hg and L is the interelectrode distance in cm. This equation shows that the ignition voltage should decrease with increase of the initial ionization (n_0). The introduction of an auxiliary electrode capable of injecting free electrons into the discharge region leads to an appreciable decrease of the hf discharge ignition voltage, inasmuch as the introduction of additional electrons into the discharge gap results in an increase of the initial ionization.

The displacement of the region of maximum values of V_{it} (between the two minima) in the ignition voltage vs pressure curves to the side of lower pressures with increase in the temperature of the auxiliary electrode (Fig.3) can be explained as follows. As was shown in earlier contributions[3,4], the electron oscillation amplitude in the region of the first minimum is greater than the distance between electrodes. As the region of maximum values of V_{it} is approached, the oscillation amplitude becomes equal to the interelectrode distance. In the region of the second minimum, the amplitude becomes smaller than the interelectrode distance. Increase of the auxiliary electrode temperature leads to reduction of the ignition voltage. In view of the fact that the electron oscillation amplitude is determined by the product $\lambda_e \cdot V_{it}$ (λ_e is the electron free path), decrease of the ignition voltage should be accompanied by displacement of the region of maximum values of V_{it} (region between the two minima) to the side of higher λ_e, i.e., to the side of lower pressures, which is what we observed in the described experiments.

I desire to thank Prof.N.A.Kaptsov for suggesting the subject and constant interest in the work.

References

1. S.Brown, Proc.IRE, 39, 1493 (1951).
2. Taro Kihara, Revs.Mod.Phys., 24, 45 (1952).
3. A.A.Zaitsev & Kh.A.Dzherpetov, Zhur.eksp.i teor.fiz., 24, No.5 (1953).
4. Kh.A.Dzherpetov, Vestnik, Moscow State University, No.5, 111 (1957).

CONDUCTIVITY OF WEAKLY IONIZED AIR AT HIGH FREQUENCIES

- H.Margenau, E.Desloge & D.Stillinger

Increasing preoccupation with the properties of the upper layers of the atmosphere from the standpoint of transmission of high-frequency electromagnetic waves through the ionosphere and similar disturbed media has stimulated interest in the conductivity of ionized air. In the present article we shall consider some special aspects of the problem of conductivity, in particular, the divergence between the theoretical formulas based on different approximations and the available experimental data. For consistency, in the first part of the article we will give the known results; in the second part we will present a new derivation of the fundamental conductivity formula, and in the third part will analyze the diverse approximations.

1. Review of Known Results

If an electromagnetic wave with an electric vector $Ee^{i\omega t}$ passes through a medium containing free charges, producing a displacement $D = Ee^{i\omega t}\varepsilon_0$, the current density $j = \sigma Ee^{i\omega t}$ and the relation between the permittivity and the imaginary part of the complex conductivity $\sigma = \sigma_r - i\sigma_i$ is given by

$$\varepsilon = \varepsilon_0 - \frac{4\pi\sigma_i}{\omega}. \tag{1}$$

The complex refractive index N is defined by the relation

$$\mathscr{E} = Ee^{-iN\frac{\omega}{c}x}, \tag{2}$$

while the Maxwell equations relate (1) and (2) by the formula

$$N^2 = E - \frac{4\pi i\sigma_r}{\omega} = E_0 - \frac{4\pi i}{\omega}\sigma. \tag{3}$$

If N is resolved into a real part n, corresponding to the usual index of refraction, and an imaginary part ik, which, according to (2) determines the absorption, Eq.(3) reduces to

$$n^2 - k^2 = \varepsilon; \quad nk = \frac{2\pi\sigma_r}{\omega}, \tag{4}$$

where

$$n^2 = \frac{\varepsilon}{2}\left\{1 \pm \sqrt{1 + \left(\frac{4\pi\sigma_r}{\varepsilon\omega}\right)^2}\right\},$$
$$k^2 = \frac{\varepsilon}{2}\left\{-1 \pm \sqrt{1 + \left(\frac{4\pi\sigma_r}{\sigma\omega}\right)^2}\right\}. \tag{5}$$

In these formulas the sign is chosen so that n^2 and k^2 will be positive.

It follows from the last formula that for large $\sigma_r/\varepsilon\omega$ the quantity $k^2 \to \frac{2\pi\sigma_r}{\omega}$.

Consequently, the condition $k > 1$, i.e., the condition of appreciable absorption per one wavelength path, is realized provided $\sigma_r/\varepsilon\omega \gg 1$. On the other hand, it follows from Eq.(1) that ε becomes negative with increase of σ_i/ω. Consequently, the real part of the conductivity determines the absorption, while the imaginary part determines the refractive index. Thus the conductivity σ is fundamental to our discussion. Let us calculate it.

To facilitate reference, let us write out the familiar expression for the reflection factor:

$$R = \frac{(n-1)^2 + k^2}{(n-1)^2 + k^2}. \tag{6}$$

Obviously, with increase of absorption, R approaches unity.

2. Derivation of the Expression for the Complex Conductivity

Earlier one of us deduced an equation for calculating the complex conductivity of an ionized gas in which the effect of electron relaxation is due to collisions between electrons and neutral molecules. This equation is applicable in cases when the distribution in energy is arbitrary and the electron collision cross section can be any function of their velocity. In this section we will deduce the same formula in a more direct manner, obtaining in the process of calculation a different expression which is applicable under certain conditions when the original formula becomes invalid owing to neglect of terms of higher order in the utilized expansion.

Let us consider a plasma in an alternating electric field $E\cos\omega t$. If we choose the x axis in the direction of the field, the Boltzmann transfer equation can be written in the form

$$\gamma\cos\omega t\,\frac{\partial\varphi(v_x, v_y, v_z, t)}{\partial v_x} + \frac{\partial\varphi(v_x, v_y, v_z, t)}{\partial t} = \frac{\partial\varphi(v_x, v_y, v_z, t)}{\partial t}, \tag{7}$$

where $\varphi(v_x, v_y, v_z, t)$ is the electron distribution function, which we normalize to unity, $\frac{d\varphi}{dt}$ is the rate of change of φ as a result of the influence of all agencies, except the electric field, and $\gamma = \frac{eE}{m}$.

Let

$$\frac{d\varphi}{dt} = \frac{d_c\varphi}{dt} + \frac{d_a\varphi}{dt}, \tag{8}$$

where $\frac{d_c\varphi}{dt}$ is the variation of φ resulting from collisions, and $\frac{d_a\varphi}{dt}$ is the variation of φ due to all other agencies (except the electronic field). Let us now assume that $\frac{d_a\varphi}{dt}$ is a function of the absolute magnitude of the velocity but not of its direction:

$$\frac{d_a\varphi}{dt} = G(v). \tag{9}$$

Let $W(v, v')\,d\tilde{v}'dt$ be the probability of an electron with velocity v undergoing a collision during interval dt and acquiring a final velocity in the interval from $\tilde{v}'$ to $\tilde{v}' + d\tilde{v}'$. We then obtain the following expression for the rate of change of φ as a result of collisions:

$$\frac{d_c\varphi}{dt} = \int[\varphi(\tilde{v}', t)\,W(\tilde{v}', \tilde{v})\,d\tilde{v}' - \varphi(\tilde{v}', t)\int W(\tilde{v}, \tilde{v}')\,d\tilde{v}'. \tag{10}$$

If the first term on the right in Eq. (10) is multiplied by $nd\tilde{v}$, where n is the electron concentration, it will represent the initial velocity from which, by virtue of collisions, the electron enters the velocity interval $\tilde{v}$ to $\tilde{v} + d\tilde{v}$. In order to calculate the mean electron velocity directly after collision, we must multiply this expression by $\tilde{v}$ integrate over all velocity space and divide

Note: $\tilde{v}$, $\tilde{v}'$, etc, denote vector quantities.

by the mean collision frequency. We assume that this expression is an even function* with respect to v_x, i.e.,

$$\int \varphi(\tilde{v}',\ t)\, W(\tilde{v}',\ \tilde{v})\, d\tilde{v}' = H(v_x,\ v_y,\ v_z,\ t) = H(-v_x,\ v_y,\ v_z,\ t). \tag{11}$$

If (11) is valid, the mean velocity component of the electron immediately after collision equals zero. The inverse is not true. The integral of the second term on the right in (10) is the collision frequency $\nu(\tilde{v})$. We assume that this expression is a function only of velocity, but not of direction. Then for this term we will have

$$\varphi(\tilde{v},\ t) \int W(\tilde{v},\ \tilde{v}')\, d\tilde{v}' = \varphi(\tilde{v},\ t)\, \nu(v). \tag{12}$$

Combining Eqs. (7)-(12), we obtain the following expression for the Boltzmann transfer equation

$$\gamma \cos \omega t \frac{\partial \varphi}{\partial v_x} + \frac{d_a \varphi}{dt} = k(v_x,\ v_y,\ v_z,\ t) - \varphi \nu(\tilde{v}), \tag{13}$$

where $k(v_x,\ v_y,\ v_z,\ t)$ is some unknown function that is even with respect to v_x.

Let us now introduce the two functions

$$\varphi_+ = {}^1/_2 [\varphi(v_x) + \varphi(-v_x)] \tag{14}$$

and

$$\varphi_- = {}^1/_2 [\varphi(v_x) - \varphi(-v_x)]. \tag{15}$$

After insertion of (14) and (15) in (13), we obtain

$$\gamma \cos \omega t \frac{\partial}{\partial v_x} [\varphi_+ + \varphi_-] + \frac{d_a}{dt} [\varphi_+ + \varphi_-] = k(v_x, v_y, v_z, t) - \nu(v) [\varphi_+ + \varphi_-]. \tag{16}$$

Replacing v_x by $-v_x$ and subtracting the resultant equation from (16), we obtain

$$\gamma \cos \omega t \frac{d\varphi_+}{dv_x} + \frac{d\varphi_-}{dt} = -\nu(v) \varphi_-; \tag{17}$$

at this point we make the following assumption: for arbitrary a and b

$$\int_a^b \varphi(v_x,\ v_y,\ v_z,\ t)\, dv_x = \int_{a-g(a, v_y, v_z, t)}^{b-g(b, v_y, v_z, t)} \varphi_0(v_x,\ v_y,\ v_z)\, dv_x, \tag{18}$$

here $\varphi_0(v_x,\ v_y,\ x_z,\ t) = \varphi_0(v)$ is the equilibrium distribution function** and $g = g(v,\ t)$. This is equivalent to the assertion that all the electrons, which in the equilibrium distribution are in a given velocity interval, are displaced by the electric field into a new interval in which the x component of the velocity differs from the initial x component by an amount g, while the y and z velocity components remain the same. This assumption means that the field acting on the electrons in the direction of v_x and the collisions add a velocity component g in the direction of v_x. The magnitude of this component in the absence of collisions would be a function of the time only. However, collisions also change

---

*If it is not assumed to be even, then for elastic collisions we can readily show that no matter what the collision frequency, it can be replaced by the collision frequency at the instant of transfer.[1] This however will only influence the qualitative results.

**We could make the more general assumption that $\varphi_0(v)$ is any function of v The form of this function may then be determined from an equation corresponding to (17).

g and since the collision frequency is a function of v alone, we may assume that $g = g(v, t)$.

Eq. (18) can be rewritten

$$\varphi(v_x, v_y, v_z, t) + \varphi_0(v_x - g_1, v_y, v_z)\left[1 - \frac{\partial g}{\partial v_x}\right]. \tag{19}$$

The same result can be obtained by replacing v_x by $v_x' - g(v_x')$ in the right part of (17). The presence of the factor $1 - \frac{\partial g}{\partial v_x}$ in (19) is explained by the fact that, although electrons in the given interval in equilibrium distribution are shifted to a new interval, the magnitudes of these two intervals in general are not equal and, consequently, the plane in velocity space represented by the distribution function is changed incident to the displacement.

If $\left|\frac{\partial g}{\partial v_x}\right| \ll 1$, Eq. (19) can be rewritten in the form

$$\varphi(v_x, v_y, v_z, t) = \varphi_0(v_x - g, v_y, v_z); \tag{20}$$

in this approximation Eqs. (14) and (15) become

$$\varphi_+ = {}^1/_2[\varphi_0(v_x - g) + \varphi_0(v_x + g)]; \tag{21}$$
$$\varphi_- = {}^1/_2[\varphi_0(v_x - g) - \varphi_0(v_x + g)]. \tag{22}$$

If we expand φ_+ and φ_- into series in powers of g and assume rapid convergence of these series, then

$$\varphi_+ \approx \varphi_0; \tag{23}$$
$$\varphi_- \approx -\frac{\partial \varphi_0}{\partial v_x} g. \tag{24}$$

Inserting (23) and (24) into (17) and solving the resultant differential equation for g, we find

$$g = \frac{\gamma\nu}{\omega^2 + \nu^2}\cos\omega t + \frac{\gamma\omega}{\omega^2 + \nu^2}\sin\omega t. \tag{25}$$

The current density is given by the relation

$$j = ne\int_{-\infty}^{\infty}\int\int\int v_x \varphi(v_x, v_y, v_z, t)\, dv_x dv_y dv_z. \tag{26}$$

There are a number of expressions that can be used to characterize the distribution function φ. If we set

$$\varphi = \varphi_+ + \varphi_- \approx \varphi_0 - \frac{\partial \varphi_0}{\partial v_x} g, \tag{27}$$

we obtain our earlier formula[2]:

$$j = \frac{ne}{3}\int g\frac{\partial \varphi_0}{\partial v} v d\tilde{v} = -\frac{4\pi Me}{3}\int g v^3 \frac{\partial \varphi_0}{\partial v} dv. \tag{28}$$

If we insert (20) in (26), then on the assumption that $g(v_x) \approx g(v_x - g)$, we obtain

$$j = 4\pi n \cdot \int\left[g + \frac{v}{3}\frac{\partial g}{\partial v}\right] v^2 \varphi_0 dv \tag{29}$$

Actually, Eqs. (28) and (29) are identical inasmuch as (29) can be obtained from (28) by integrating by parts.

If, however, instead of inserting (20) in (26), we use (19), then, transforming the axes we obtain (for the same assumptions):

$$j = 4\pi ne \int g v^2 \varphi_0 dv. \tag{30}$$

Expressions (23) and (24) show how important accuracy is for determining g but not for $\frac{dg}{dv_x}$. Actually, it would be surprising if this method gave a good value for $\frac{dg}{dv_x}$ inasmuch as approximations (23) and (24) are obtained as a result of disregarding terms in $\frac{dg}{dv_x}$. The accuracy of (30) depends only on the accuracy of g whereas the accuracy of (29) depends on both g and $\frac{dg}{dv_x}$. Consequently, we may expect (30) to give a more realistic value of the current than (29), provided, of course, that for the assumed form of the distribution function, (19) is physically a more reasonable approximation than (20).

It is interesting to note that (30) could be obtained on simple physical grounds from the Lorentz equation. According to Lorentz, the drift velocity for electrons with a collision frequency ν is obtained from the differential equation

$$m\ddot{x} + \nu m\dot{x} = eE\cos\omega t. \tag{31}$$

Solving for the drift velocity $\dot{x}$ and equating it with g we also obtain (25). Multiplying by e, we obtain the current produced by a single electron with a collision frequency ν. Summing over all electrons and bearing in mind their distribution in velocity, we obtain (30). If $\left|\frac{v}{3}\frac{dg}{dv}\right| \ll g$, the right parts of (29) and (30) are approximately equal. This is the case when ν is constant.

The character of the approximations used in deriving (29) and (30) hampers evaluation of the validity of these expressions on a purely mathematical basis. We carried out a comparison for a special form of the functions φ_0 and $\nu(v)$.

Negative conductivity, which is sometimes obtained in using (29), arises owing to the inaccuracy of this formula. This occurs, for example, if we used the experimental value for the electron collision frequency in air and assume that

$$\varphi_0 = (4\pi v'^2)\,\delta\,(v - v').$$

Equation (30) yields positive conductivity values for all v and differs from (29) by 50% even for velocities when both expressions are positive. This is undoubtedly an exceptional example, which is only of academic interest, particularly since use of the δ function in Eq.(24) is not absolutely necessary for a good approximation to (22) (the δ function can be replaced by a Gaussian function). On the other hand, if we use the same collision frequencies together with a Maxwellian distribution, then (29) and (30) prove to be in good agreement within the limits of the error in evaluating the integrals by the saddle-point method.[2]

Before turning to an analysis of the diverse approximations, we recall that (28) and (30) are the fundamental formulas for calculating the complex conductivity. For the case of constant ν they lead to the Lorentz formula:

$$j = \frac{ne^2E}{m}\,\frac{\nu\cos\omega t + \omega\sin\omega t}{\omega^2 + \nu^2}. \tag{32}$$

These formulas differ greatly, however, when either ν or φ varies rapidly with v. In this case Eq.(28), in contradistinction to (30), leads to negative conductivities. In practice, the difference between these two formulas is unimportant and in our work we used formula (28) as was done in his work by Brode[3]. Thus, we can write

$$\sigma_{ri} = \frac{ne^2}{m} I_{1,2}; \tag{33}$$

$$I_1 = \frac{4\pi}{3}\int \varphi_0 \frac{d}{dv}\left(\frac{\nu v^3}{\omega^2+\nu^2}\right)dv; \tag{34}$$

$$I_2 = \frac{4\pi}{3}\int \varphi_0 \frac{d}{dv}\left(\frac{\omega v^3}{\omega^2+\nu^2}\right)dv. \tag{35}$$

In these expressions, φ_0 and ν are functions of v. If ν is constant, the form of the function φ_0 is insignificant; on the other hand, σ_r does depend on the form of φ_0. In what follows we assume the distribution function to be Maxwellian.

3. Application to the Atmosphere

We make three approximations concerning ν. The first two represent an idealization frequently encountered in the literature, but still not fully utilized in practice. The third assumption is more substantial inasmuch as it is based on the experimental velocity dependence of ν. From our point of view, it is of particular interest to carry out a comparison of the quantitative results for these three cases. The quantities most convenient for our purpose are ωI_1 and ωI_2. These were calculated as functions of the radian frequency ω and have a parametric dependence on T_e, the electron temperature, (which is related with φ_0) and p/T_A, the ratio of the atmospheric pressure p to the atmospheric temperature T_A. This ratio was, of course, determined by the altitude at which the conductivity was studied.

1. The Lorentz case

In the Lorentz case (designated by the superscript L), we have

$$\omega I_1^L = \frac{\omega\nu}{\omega^2+\nu^2} \quad \text{and} \quad \omega I_2^L = \frac{\omega^2}{\omega^2+\nu^2}. \tag{36}$$

This is a good approximation which is used even when ν is not quite constant. In this case $\nu(v)$ is usually replaced by $\nu(\bar{v})$, where $\bar{v}$ is the root mean square velocity for the Maxwellian distribution:

$$\bar{v} = \left(\frac{3kT}{m}\right)^{1/2}. \tag{37}$$

Clearly, ωI_1^L has a maximum value of 1/2 at $\omega = \nu$. The plot of ωI_1^L as a function of ω/ν constructed in semilogarithmic coordinates, $\omega/\nu = e^x$, is symmetrical relative to the maximum and has a half-width equal to $x_{1/2} = 1.32$, where $x_{1/2}$ is the solution of the equation $\cosh x_{1/2} = 2$. Hence we can conveniently compare plots of other forms of ωI_1^L with a universal Lorentz curve whose maximum occurs at the point $\nu = \nu(\bar{v})$. On the other hand, ωI_2^L is a monotonically increasing function of ω growing from 0 to 1 and also having the value 1/2 at $\omega = \nu$.

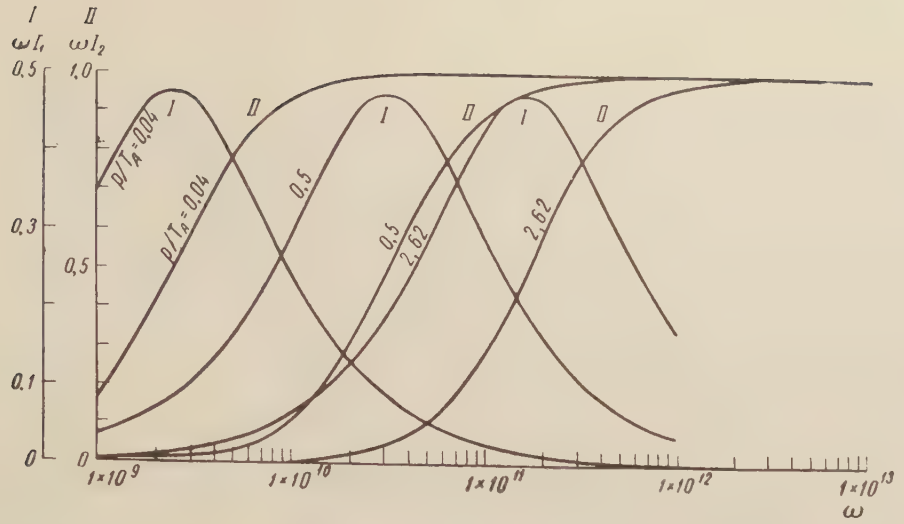

Fig.1. Variation of ωI_1 (I) and ωI_2 (II) with the microwave frequency for $\sqrt{T_e} = 10$.

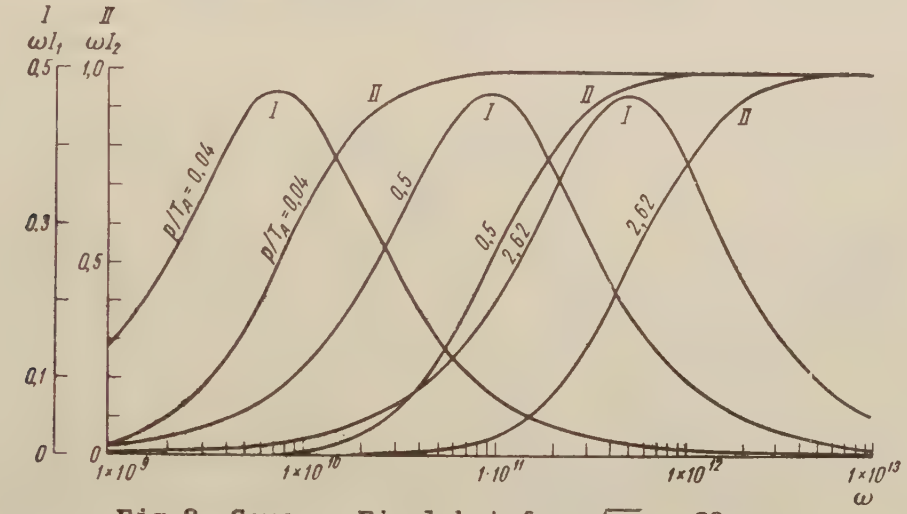

Fig.2. Same as Fig.1 but for $\sqrt{T_e} = 30$.

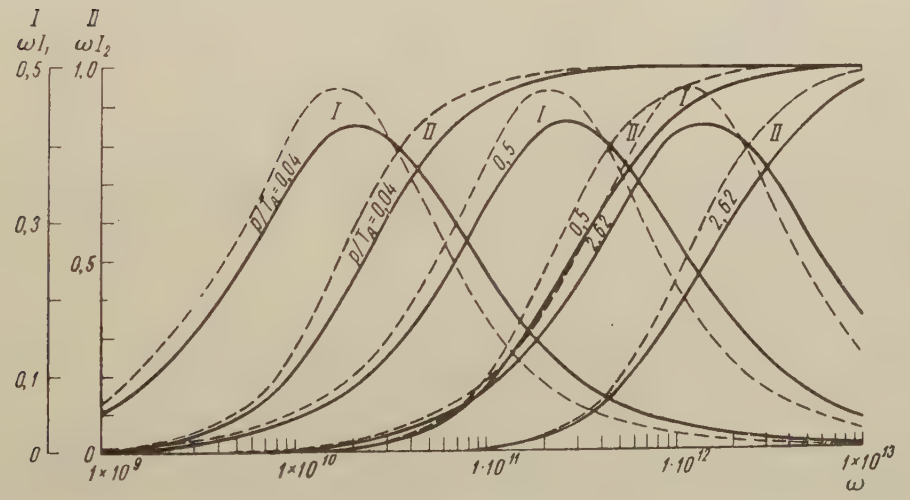

Fig.3. Comparison of the ωI_k^c & ωI_1^R (I) and ωI_2^c & ωI_2^R (II) vs ω curves for $\sqrt{T_e} = 70$.

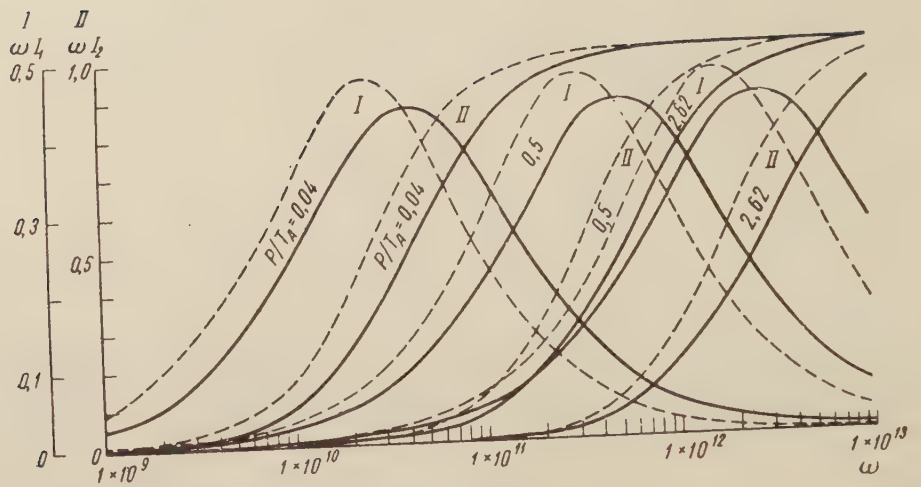

Fig.4. Same as Fig.3 but for $\sqrt{T_e}$ = 100.

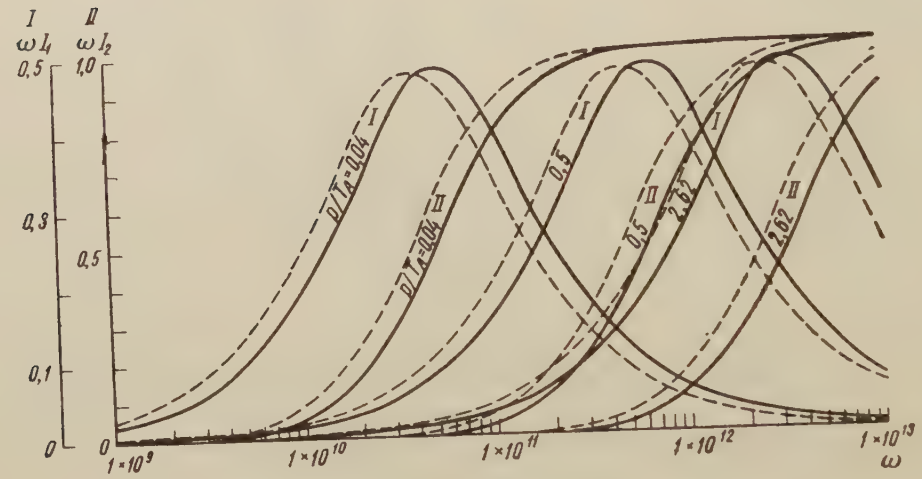

Fig.5. Same as Fig.3 but for $\sqrt{T_e}$ = 150.

2. Constant mean free path

Since the mean free path is v/ν, the present simplification implies direct proportionality between ν and v. This case has been treated previously[2] and leads to the results

$$\omega I_1^c = \frac{4}{3\sqrt{\pi}}\, r\,[1 - r^2 - \Omega^4 e r^4 E_i(-r^2)]\,; \tag{38}$$

and

$$\omega I_2^c = \frac{4}{3}\, r\,[1/2 - r^2 + \sqrt{\pi}\; r^3 e r^2 \{1 - \Phi(r)\}]\,, \tag{39}$$

where

$$r = \left(\frac{m}{2kT_e}\right)^{1/2} \frac{\omega}{\nu/v}\,, \tag{40}$$

and E_i and Φ are defined as in Jahnke & Emde (pp.1 & 24).

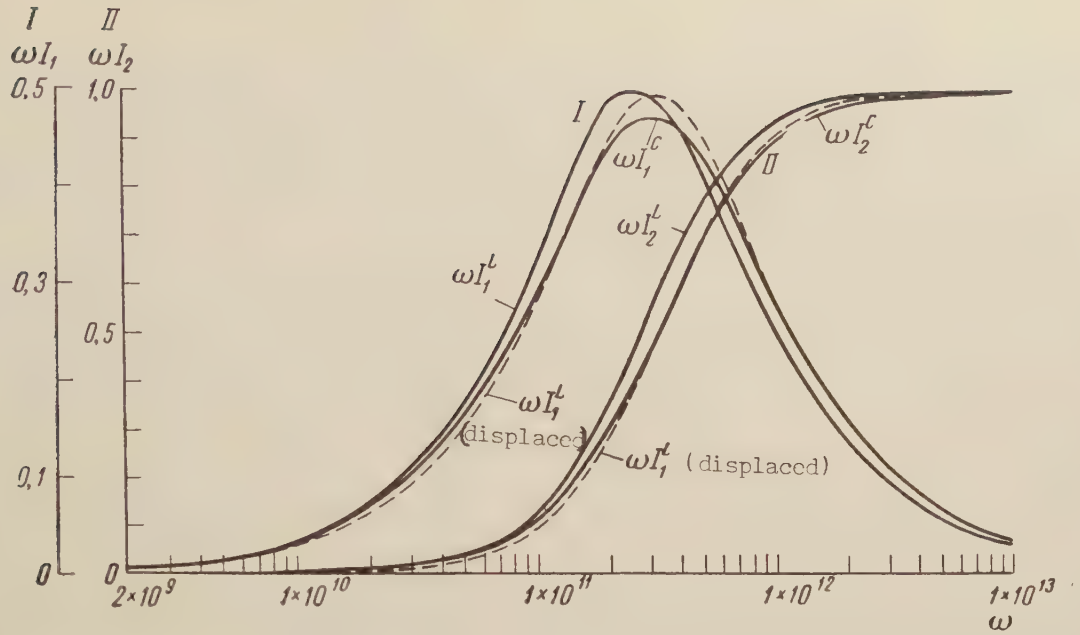

Fig.6. Comparison of the ωI_1^c & ωI_1^L (I) and ωI_2^c & ωI_2^L (II) vs ω curves for $\sqrt{T_e} = 100$ and $p/T_A = 0.5$.

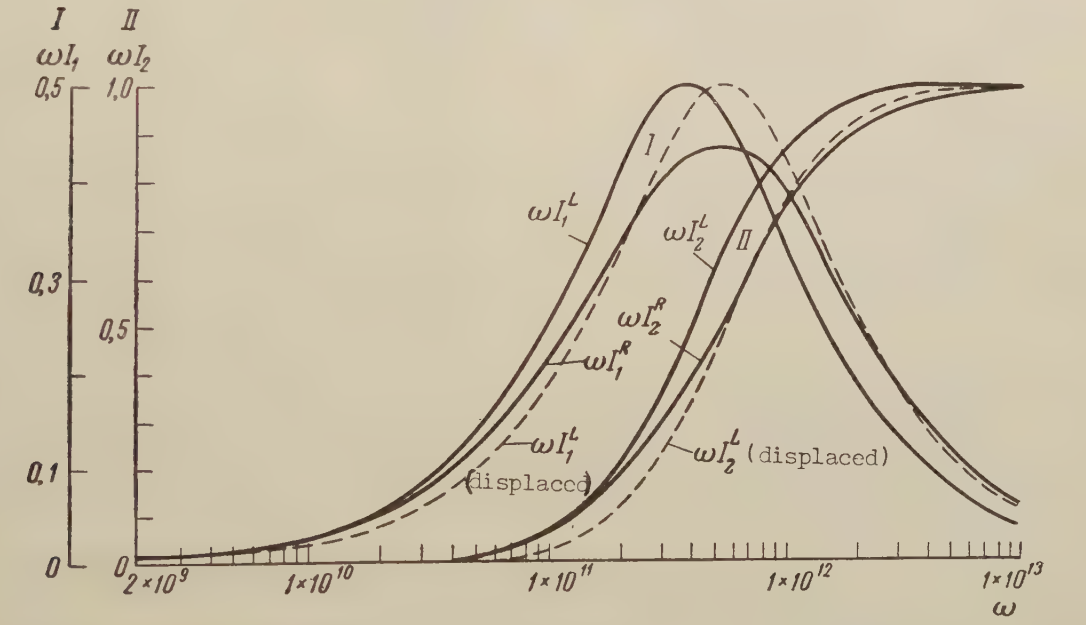

Fig.7. Comparison of the ωI_1^R & ωI_1^L (I) and ωI_2^R & ωI_2^L (II) curves for the same conditions.

3. "Realistic" collision frequency

Assumptions 1 and 2 are not fulfilled for air at normal pressure; actually $\nu(v)$ is very imperfectly known for small v. Graphs of ν for oxygen and nitrogen, based on the data of Brode[3], are given by Brown & Allis[1]. For oxygen, ν is consistent with the constant free mean path hypothesis, but for nitrogen the ν curve has a strong peak at an electron energy of 2.25 ev, i.e., at $v = 9 \cdot 10^7$ cm/sec. The approximate values of ν are given by the empirical expression

$$\nu_{air} = \left\{8000 + 13000 \exp\left[-\left(\frac{v - 9\cdot10^7}{2\cdot10^7}\right)^2\right]\right\} \frac{p}{T_A} v, \qquad (41)$$

where v is in cm/sec, p is in mm Hg and T_A in °K. The difference between cases 2 and 3 becomes most marked when T_e is such that many electrons have velocities corresponding to the maximum of Eq.(41). For smaller and larger values of T_e the results given by cases 2 and 3 should be close. To make these two cases comparable, the value of ν/v in Eq.(40) is chosen equal to 8000 p/T_A in accordance with Eq.(41) (outside the region of the peak).

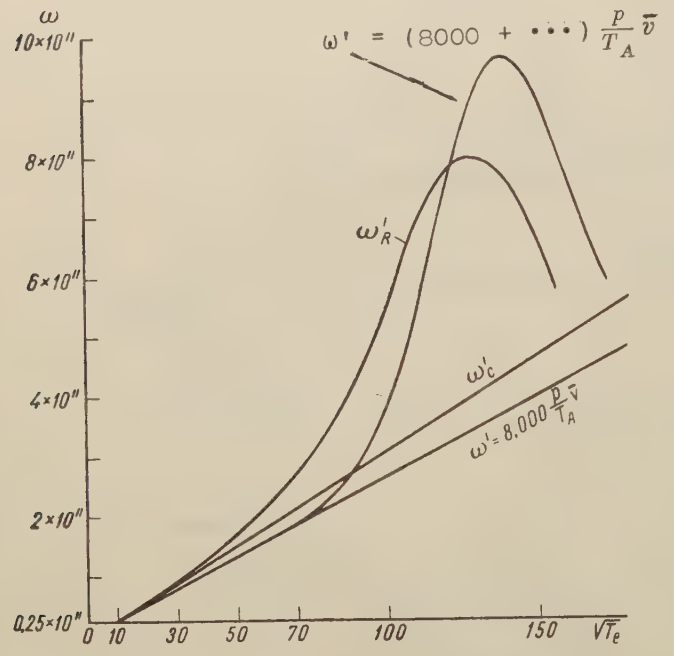

Fig.8. Comparison of the variations of ω' with $\sqrt{T_e}$ for different instances; p/T_A = 0.5.

Computations for the "realistic" collision frequency case were, of course, carried out numerically. The results are shown in the accompanying figures. Figs.1-5 serve to compare ωI_1^c with ωI_1^R and ωI_2^c with ωI_2^R. Only the ωI^R curves have been plotted for T_e = 100 and 900°K inasmuch as at these temperatures these curves are virtually identical for those for ωI^c. Comparison with the Lorentz results is made in Figs.6 & 7, where the ωI^L curves are plotted on the basis of Eq.(36). Two values for ν were used: $\nu = \nu(\bar{v})$, where $\bar{v}$ is calculated from (37), and $\nu = \omega'$, where ω' corresponds to the maximum of ωI_1^R or ωI_1^c. In the first instance we took two different values of $\nu(\bar{v})$: for comparison with ωI_1^c we took $\nu(\bar{v}) = 8000\ p/T_A \cdot \bar{v}$, while for comparison with ωI_1^R the value of $\nu(\bar{v})$ was computed from Eq.(41). An appreciable divergence between the curves appears at the maxima of ωI_1^c and ωI_1^R. The discrepancy decreases when the maximum of ωI_1^L is deliberately shifted (as indicated by the notation "displaced" in the figures) to coincide with the maximum of ωI_1^R or ωI_1^c. This was done to show how well the structure of the ωI_1^L curve near its maximum agrees with the structure of the less ideal curves. As will be evident from Figs.6 & 7, the Lorentz curve, even when appropriately shifted, may differ appreciably from the approximating functions.

The curves of Fig.8 show the behavior of ω' (the value corresponding to the maximum in the ωI_1 curves) varies as a function of $\sqrt{T_e}$ in different cases.

Laboratory of Marine Physics,
Yale University, New Haven, Conn.

References

1. S.C.Brown & W.P.Allis, Basic Data of Elec.Discharges,MIT Tech.Rept.,1,283(1957).
2. H.Margenau, Phys.Rev., 109, 6 (1958).
3. R.B.Brode, Revs.Mod.Phys., 5, 257 (1933).

We are grateful to Dr.Margenau and his co-authors for permission to publish this translation of their report. We also thank the Journal of Applied Physics for authorization to reproduce the sections based on the paper by Dr. H.Margenau & Dorothea Stillinger which appeared in the Vol.30, No.9 (p.1385) issue of the Journal.

Translation Editor

LOW-FREQUENCY WAVE-LIKE EFFECTS IN GLOW-DISCHARGE PLASMA

- L.Pekarek

In earlier studies[1] we used the method of artificially induced transient processes with small perturbation for investigating low frequency oscillations associated with the movement of striations (layers) in a discharge. The results of these investigations showed that the existence of such oscillations and their principal parameter, the frequency, are associated primarily with the properties of the positive column plasma. Local pulse perturbation of a homogeneous plasma leads to gradual appearance of a striated structure. The striations appear progressively from the cathode to the anode, but move (in a discharge in inert gases) in the opposite direction. We called this unique effect striation waves. Observations indicate that the movement of the layers is connected with the properties of the plasma itself. The striation motion in the end regions of the discharge gives rise to electric oscillations with a frequency $f = v/\lambda$ in the external circuit. The velocity v of the layers and their spacing λ in the case of a striation wave are determined exclusively by the properties of the positive column plasma. On the other hand, in the case of "self-oscillation", when there is strong interaction of the individual repeating striation waves, the oscillation frequency may differ appreciably from the frequency characteristic of free motion of the striations.[1] This difference is due to change in velocity of the layers owing to interaction of the striations.

Thus the problem of determining the microphysical causes of this type of oscillations reduces to the problem of elucidating the factors responsible for the appearance and motion of the striations in a discharge.

From this point of view it is, of course, of interest to carry out experimental investigation of transient processes with small perturbation in discharges wherein there are observed moving striations in some cases and stationary striations in others. Klyarfel'd[2] showed that in some cases one can stop the motion of moving layers or, on the contrary, set stationary layers in motion, by means of an external agency (for example a localized magnetic field). These experiments, however, do not yield an answer to the question of whether plasma is inherently characterized by stationary or moving layers. To resolve this question we carried out the following experiment.

We selected discharge conditions (discharge in low pressure hydrogen) such that there would be no moving striations and the stationary striations were attenuated to the vanishing point in approaching the anode. We mounted a metal ring outside the discharge tube at a point sufficiently far from the cathode, where the positive column was completely uniform. As a result there appeared a new series of stationary striations between the ring and the anode (Fig.1). This is similar to the effect described by Klyarfel'd[2] except that in his work the stationary layers appeared after an obstacle (probe or aperture) inside the tube.

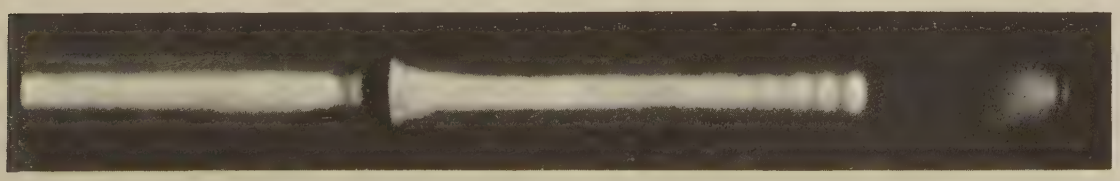

Fig.1. Photograph of discharge in hydrogen. Cathode at right; R - location of metal ring outside discharge tube with stationary striations to the left. Tube diameter - 2.2 cm; p = 2 mm Hg.

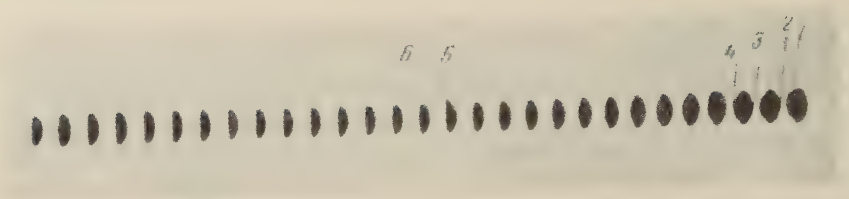

Fig.2. Stationary striations in a discharge in hydrogen. Cathode at the right. Discharge current, 4.3 ma, d = 2.2 cm, p = 2 mm Hg.

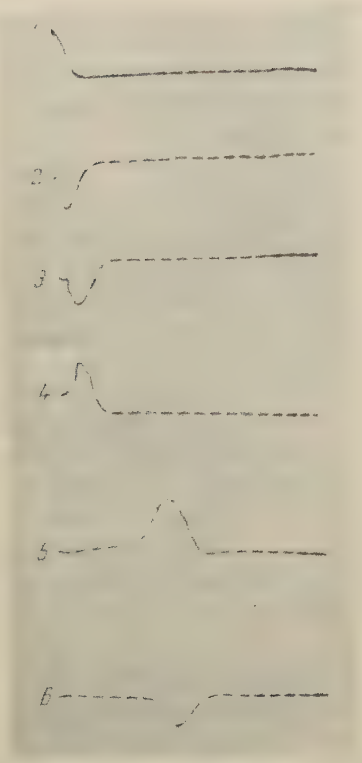

Fig.3. Oscillograms of the variation of luminous intensity at different points in the discharge shown in Fig. 2. Time markers = 20 microsec.

Maintaining the same discharge conditions, we then applied single electric pulses to the ring instead of the steady hf voltage. We found that such pulses result in gradual appearance of striations with delay to the side of the anode, i.e., to a striation wave. The striations did not remain stationary, however, but moved from the cathode to the anode. Consequently, local pulse perturbation produced moving rather than stationary striations. In other words, stationary striations are obtained only in the case of steady perturbation (steady hf voltage on the ring).

From these experiments it may be concluded that inherently the plasma is characterized by translational motion of the striations. The immobility of the layers in the case of a steady hf voltage on the ring is due to the steady character of the perturbation acting constantly at the same point in the discharge.

With a somewhat stronger discharge current (4.3 ma) there spontaneously appeared in the discharge stationary striations, which were sharp and distinct over the full length of the positive column. In order to compare the properties of the stationary striated structure with the properties of moving striations obtained with pulse excitation, we perturbed the cathode region of the discharge with electric pulses and followed the propagation of the disturbance by means of a photomultiplier, which could be displaced along the length of the discharge tube.

A photograph of a discharge in hydrogen with stationary sharp striations is reproduced in Fig.2. Oscillograms of the variations in luminous intensity at the different points in the discharge (indicated by the corresponding numerals in Fig.2) are shown in Fig.3. The beginning of the oscillogram corresponds to the initial moment of application of the perturbing pulse. It will be seen that the disturbance is propagated in the form of a short-term variation in luminous intensity in the dark and light regions of the individual striations down the full length of the discharge tube. As indicated, the first two oscillograms correspond to the first and second layers nearest the cathode. The different "polarities" of the light pulses

are due to the fact that the luminous intensity decreases in the light regions of the striations and increases in the dark regions. Thus the pulse is transmitted with alternating sign from one region to another in complete agreement with the concepts of the phenomenological theory of striations proposed by the writer[3].

In the present case the propagation velocity of the pulse is 1400 m/sec. The relaxation time, calculated according to the theory[3], equals 5 microsec.

References

1. L.Pekarek, Vestnik, Moscow State University, 73 (1954); Chekhosl.fiz. zhur. (Czech.Phys.Journal), 4, 221 (1954).
2. B.N.Klyarfel'd, Zhur.eksp.i teor.fiz., 66 (1951).
3. L.Pekarek, Chekhosl.fiz.zhur., 7, 533 (1957).

Bulletin of the Academy of Sciences of the USSR - Physical Series
Vol.23, No.8 - August 1959

Transactions of the Second All-Union Conference on Gaseous Electronics

TABLE OF CONTENTS

	Page Orig.	Trans.
Formation of a high-frequency discharge at low pressures - G.N.Zastenker & G.S.Solntsev	934	925
Investigation of a self-sustaining super-high frequency pulse discharge in air and its initiation process - P.S.Bulkin, G.S.Solntsev & V.N.Ponomarev	941	931
Measurement of the charge concentration in plasma by means of super-high frequency probes - S.M.Levitskii & I.P.Shashurin	948	938
Initiation of super-high frequency pulse discharges in inert gases - V.E.Golant	952	942
Correlation between the characteristics of super-high frequency and direct currents in gases - V.E.Golant	958	947
Obtaining high temperatures by means of a spark discharge - M.P.Vaniukov & A.A.Mak	962	951
Some results of investigation of the excitation functions of the N_2^+ negative system bands - I.P.Zapesochnyi & S.M.Kishko	965	954
Excitation cross sections for some spectrum lines of potassium and argon - L.M.Volkova	968	957
Effect of disappearance of negative ions on their concentration in the discharge column - M.V.Koniukov	971	960
New results of investigations of a long spark - I.S.Stekol'nikov	975	964
Probe investigations of the field of an ac corona - V.I.Levitov, A.G.Liapin & V.I.Popkov	980	968
Elementary processes in the ionization zone of corona discharges at atmospheric pressure - G.N.Aleksandrov	989	976
Charge density oscillation waves in a cylindrical plasma - M.Ia.Vasil'eva, A.A.Zaitsev & E.D.Andriukhina	995	982
Positive discharge column under diffusion conditions - V.M.Zakharova, Iu.M.Kagan & V.I.Perel'	999	986
Investigation of the initial stages of a high-frequency discharge from a point in air at atmospheric pressure - A.M.Prokof'ev, O.F.Kabardin & K.F.Kuddu	1004	992
Investigation of resonance charge exchange in monatomic gases and metal vapors - R.M.Kushnir, B.M.Paliukh & L.A.Sena	1007	995
Investigation of anodic oscillations in a low-pressure discharge - A.A.Zaitsev & K.I.Efendiev	1012	1000
Broadening and shift of spectral lines in gas discharge plasma - S.L.Mandel'shtam & M.A.Mazing	1017	1005
Separation of binary mixtures of inert gases in a dc discharge - N.A.Matveeva	1021	1009
Measurement of electric fields in a high-frequency low-pressure discharge by means of an electron beam - G.S.Solntsev, A.G. Porokhin & N.M.Chistyakova	1026	1014
Measurement of the electric field in a super-high frequency plasma - V.E.Mitsuk, M.D.Koz'minykh & I.V.Talalaeva	1031	1019

Influence of the temperature of an auxiliary electrode on the ignition of a high-frequency discharge in helium - Kh.A. Dzherpetov 1036 1024

Conductivity of weakly ionized air at high frequencies - H.Margenau, E.Desloge & D.Stillinger 1040 1027

Low-frequency wave-like effects in glow-discharge plasma - L.Pekarek 1050 1037

Translated in 1960 by
Columbia Technical Translations
5 Vermont Ave., White Plains, N.Y.

Transactions

of the

Twelfth All-Union Conference on Spectroscopy

(Moscow, November 19-26, 1958)

The present issue of the Bulletin contains part of the conference reports on atomic emission spectrum analysis. In issue No.10 there will be published the reports on molecular spectrum analysis, together with a listing of the reports scheduled for publication in other journals.

Editorial Board

OPENING ADDRESS

- S.L.Mandel'shtam

Comrades, annual conferences on spectroscopy have become a tradition with us; we all anxiously await the opportunity to meet and exchange information on our research.

At the preceding conference - the Twelfth Conference - held a year ago, we were concerned with problems of theoretical spectroscopy; the present conference is devoted to applied spectroscopy: atomic and molecular spectrum analysis in the widest sense of the work.

In the field of atomic spectrochemical analysis one of the most important problems posed by modern technology is the determination of small amounts of impurities. In earlier years there were developed adequate procedures for determining impurity concentrations of the order of 10^{-4}-10^{-6}%, the level required in the atomic and certain other branches of industry. Now we are faced with the problem of determining concentrations of the order of 10^{-7}-10^{-9}%, the degree of accuracy required, for example, in semiconductor technology. This involves the search for new approaches and techniques. We shall hear a special review by L.V.Lipis on this important problem.

We can note with satisfaction that in recent years there have been significant advances in research on the determination of gases in metals and alloys - a field in which Soviet spectroscopists have pioneered. Eight reports on this subject are included in the conference program. We are, however, still far from a fully satisfactory technical solution of this important practical problem.

Our industry has started to put out photoelectric equipment for spectrum analysis, in the production of which we have long lagged behind other countries. The importance of photoelectric techniques is a matter of common knowledge. These techniques and procedures speed up analysis, enhance its accuracy, make the analytic procedure automatic, and open the possibility of eventually incorporating the operation into automated production. We note, for example, that in 1956, about 12 million analyses were carried out in the plants of an American aluminum producer: of these 92% were made by photoelectric techniques, 5% by conventional photographic spectroscopy and only 3% by chemical methods. Fourteen reports on photoelectric methods of analysis will be presented at our conference. However, we still have many serious problems to solve in this field, both as regards design of equipment and development of analytic techniques. In connection with the use of the new photoelectric instruments, we must take steps to automate the operation of preparing the samples, making readings, preparing and checking working curves, and so on, making the widest possible use of the potentialities of electronics to this end.

We lag at present in the development of photoelectric x-ray spectroscopic methods of analysis; yet there can be no doubt that they are very important for the determination of very high concentrations. Unfortunately, we could include in the program only one survey lecture (by I.B.Borovskii) on the topic.

A large number of reports to be presented at the conference is devoted to further development of tried and proved methods of analysis, namely, analysis of powder samples, rare and dispersed elements, etc.

Lastly, we have a large group of reports devoted to the physical bases of spectrum analysis. We can safely assert that this field of scientific research is developing satisfactorily.

We can by now speak with legitimate pride of atomic spectrum analysis as a fully mature, independent scientific discipline that is firmly based on extensively developed theory, has at its disposal diverse experimental techniques and is regularly and consistently employed in practice.

The situation is different when it comes to molecular spectrum analysis. Our program includes many reports devoted to the theory of molecular spectrum analysis and the use of vibrational - infrared and Raman - spectra as well as of electronic spectra for analytic purposes. Some interesting and important problems have been solved, but actually serious work in this direction is only beginning.

Whereas in the field of atomic spectrum analysis we have what may be termed a continuous research front, that is, we have techniques and procedures that allow of solving almost all important practical problems, in the field of molecular spectrum analysis we possess so far solutions for only a few particular problems. In view of the fact that the scope of molecular spectroscopy is immeasurably greater than the scope of atomic spectroscopy, we must now turn our most serious attention to the development of molecular spectroscopy methods. The problems facing us here are serious and urgent. For example, the chemical industry, which is about to undergo great expansion, must be provided with spectroscopic methods of inspection and production control.

From the standpoint of techniques, the problems facing us are for the most part not easy; to characterize them we have included in the conference program three large surveys by V.M.Chulanovskii, P.A.Bazhulina & M.M.Sushchinskii and B.S.Neporent.

Molecular spectroscopy, in addition to continuing with the "classical methods" referred to above, is now turning to new procedures. In the last few years there have been extensive developments in the USSR in the fields of electronic nuclear and paramagnetic resonance; some of the results already obtained appear to be highly promising and may prove useful for purely analytic purposes. We shall hear ten reports devoted to problems in this field.

Very sensitive are the methods of luminescence analysis, which also hold great promise. These methods are being developed by F.D.Klement, E.V.Shpol'skii, A.F.Prikhot'ko and their co-workers. This observation also applies to spectral-polarization methods, which will be described in a report by P.P.Feofilov. Interesting prospects for spectroscopists are being opened in the fields of biochemistry and biology and, I fear that the report of L.A.Tumerman on these questions may turn us from our "righteous" physical path to this new and intriguing road.

For a long time a serious obstacle to the development of molecular spectroscopy was the lack of suitable equipment. The situation has now changed: our industry has developed very good new instruments for molecular analysis, namely, the IKS-4, SF-1 and DFS-12, and I trust that this field of spectroscopy will now move forward at a rapid rate.

Since the last conference, our contacts with spectroscopists abroad have expanded and improved. The achievements of Soviet spectroscopy were presented at the International Fair at Brussels. Soviet spectroscopists participated in international and national meetings in the Chinese Peoples Republic, the German Democratic Republic and the United States, familiarized themselves with the work of spectroscopic laboratories in a number of countries and became members of different international commissions. Soviet spectroscopists had the honor of receiving the Joint Commission on Spectroscopy and many foreign scientists. I am pleased to note that guests from a number of socialist countries are participating in our work and I take this opportunity to welcome them.

In the year that has passed since our last conference we have suffered a number of grievous losses: death has claimed S.A.Borovik, member of the Commission on Spectroscopy from the day of its founding and faithful participant in our conferences, I.A.Shoshin, member of our commission, who contributed so much to the development of spectroscopic instrument building, and recently, V.S.

Miliyanchuk, who so hospitably welcomed the participants of the Tenth Conference on Spectroscopy in L'vov.

We shall long honor the memory of G.S.Landsberg, who initiated our conferences and contributed greatly to their success. I request all present to stand in honor of our late colleagues.

* * *

I hereby declare the Twelfth Conference on Spectroscopy open and wish all participants success in their work.

DETERMINATION OF ATOMIC CONCENTRATIONS IN ARC DISCHARGE PLASMA FROM THE LINE WIDTHS AND CORRELATION BETWEEN CONCENTRATIONS IN THE SOLID AND GASEOUS PHASES

- I.M.Nagibina

One of the principal problems in the theory of quantitative spectrum analysis is that of the relation between the concentration of the determined element in the sample and the concentration of atoms or ions in the gas cloud of the discharge. The direct and natural approach to this problem consists in measuring the particle concentration in the discharge cloud.

Measurements of the atomic concentration in an arc discharge between carbon electrodes were recently made by Mel'chenko[1] by the procedure proposed sometime ago by Prilezhaeva & Goryachev[2]. In these measurements, however, the arc discharge was assumed to be a uniformly excited light source.

In the present report we give the results of measurements of some average atomic-ionic concentrations in the cloud of an ac arc taking into account the degree of inhomogeneity of the source, i.e., the nonuniformity in the distribution of excited and unexcited atoms over the discharge cross section. (The method of determining the degree of homogeneity is described in Refs.3 & 4.)

The method of determining the concentration of atoms or ions that was utilized in the present work is based essentially on the effect of absorption in the arc discharge model proposed by Cowan & Dieke[5]. According to this model, the fundamental parameter determining the concentration at a known degree of homogeneity of the source[6] is the ratio u/δ, where u is the line width in the presence of absorption, and δ is the line width for an infinitely thin layer.

At a sufficiently high particle density, self-reversal is observed in a nonuniformly excited light source. In this case the concentration can be determined from the value of

$$\log \frac{I_{max}}{I_o}$$

where I_{max} is the intensity at the maximum of the self-reversed contour, and I_o is the intensity at the center.

The theoretical dependences of u/δ and $\log (I_{max}/I_o)$ on the self-absorption parameter p can be calculated. In turn, the parameter p is related to the concentration of unexcited atoms:

$$fN = \frac{2mc\delta}{le^2} p, \qquad (1)$$

where f is the oscillator strength, N is the mean atomic concentration (per cm^3), m, c and e are known constants, and l is the length (thickness) of the source.

Thus the experimental problem consists in measuring either u/δ or $\log (I_{max}/I_o)$ and then determining p from the theoretical dependences. Then by means of (1) we can calculate N and juxtapose the resultant values with the concentration C of the element in the sample.*

In our study, using a Fabry-Perot etalon crossed with an ISP-22 spectrograph, we measured the width of the investigated lines in the discharge for different concentrations of the element in the sample. The measurement procedure is described in Ref.6. First, with successive decrease of the initial concentrations in the sample, we determined δ, and then with increasing concentrations at the electrode measured the line width u. The samples were water solutions of metallic salts. The solutions were applied to the flat end face of a carbon electrode, treated beforehand with a solution of polystyrene in benzene, and dried. Speci-

---

*The described method was utilized by Dvornikova[7] for plotting "growth curves".

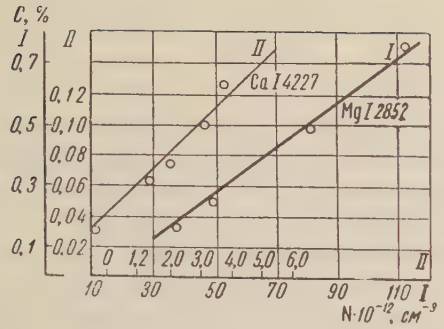

Fig.1. Correlation between the concentrations of manganese (I) and calcium (II) atoms in the sample and in the discharge cloud.

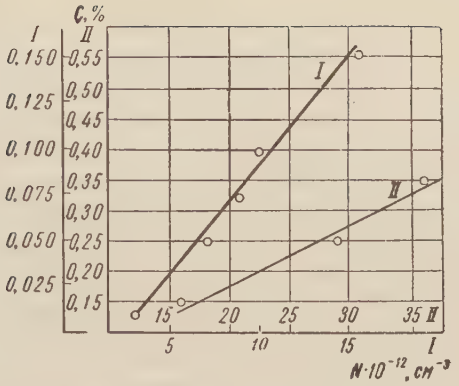

Fig.2. Correlation between the concentrations of manganese atoms in the sample and in the discharge cloud: I - calculated on the basis of u/δ; II - calculated from log (I_{max}/I_o).

fically, we investigated the lines of manganese, calcium and magnesium atoms and calcium ions.

The measurements yielded a direct proportionality (for the investigated lines) between the concentrations of the atoms and ions in the discharge cloud and in the investigated solution (Figs.1 & 2). This linear dependence characterizes the entry of the material into the discharge with the given method of introducing the sample solution.

The plots show that the utilized procedure is suitable for the determination of relatively low concentrations (10^{-12} cm^{-3}) and at the same time allows of carrying out measurements in a wide concentration interval (the concentration measurements for Mn I 2798 Å (Fig.1) were made successively with reference to absorption and to the self-reversed contours).

In the second part of the study we measured the entry of two different elements into the discharge cloud. To this end we used solutions of the salts of Mg and Ca, elements which are similar as regards both chemical properties and degree of ionization. The ratio of the numbers of atoms of the two elements was rigorously checked. We prepared water solutions with different concentrations of Mg and Ca, but with the same atomic ratios. The C_{Mg}/C_{Ca} ratio equalled 1.70. The difficulty of the experiment lay in the necessity of selecting such a concentration of Mg and Ca atoms in the discharge that the contours of the investigated Mg I 2852 Å and Ca I 4227 Å lines would be simultaneously deformed owing to absorption. Clearly, it was also necessary to determine δ for both lines. Then, as follows from Eq.(1)

$$\frac{N_{Mg}}{N_{Ca}} = \frac{p_{Mg}\delta_{Mg} f_{Ca} \lambda^2_{Ca}}{p_{Ca}\delta_{Ca} f_{Mg} \lambda^2_{Mg}}. \qquad (2)$$

In these experiments we used two alternate methods of introducing the solution:

1) application of a drop of the solution to the flat tip of the electrode (i.e., as described above), and

2) spreading of a thin layer of the solution over the surface of a metal plate (with subsequent drying).

The copper plate served as the lower electrode and was moved continuously relative to the stationary copper electrode during the discharge.

Table 1 presents the results of measurement of the atomic concentrations of Mg and Ca and their ratio in the discharge cloud in the case of copper plate electrodes. The measurement results in the case of carbon electrodes are shown in

Table 1*

λ, Å	δ, Å	$\frac{u}{\delta}$	$\overline{\left(\frac{u}{\delta}\right)}$	p	N, см$^{-3}$
MgI 2852	0,044	1,45 1,36 1,45 1,33	1,40	0,66	$3,5 \cdot 10^{12}$
CaI 4227	0,043	1,54 1,79 1,54	1,62	0,98	$2,2 \cdot 10^{12}$

* $C_{an} = 2,5\%$; $C_{Mg}/C_{Ca} = 1,7$; $N_{Mg}/N_{Ca} = 1,6$.

Table 2. In both cases the measurements were carried out with a concentration C = 2.5% in the solution (a number of measurements were also made with C = 5% in the case of the carbon electrodes). As will be evident from the listed data, the amount of material entering the discharge differs substantially with the two different introduction procedures. At equal concentrations (2.5%) in the solution a larger number of atoms enters the discharge in the case of carbon electrodes. The coefficient of "utilization" of the sample is also higher in the case of carbon electrodes, and consequently, the sensitivity of determination in this case must also be higher. It will be evident from the tabulated data that there obtain in the discharge cloud the same quantitative relations of the atoms as in the sample (within 10-15%). It would appear, however, that the entry of the material into the discharge in the case of copper plates occurs more uniformly than in the case of carbon electrodes.

Table 2*

λ, Å	δ, Å	C_{an}, %	$\lg\frac{I_{max}}{I_0}$	$\lg\frac{\bar{I}_{max}}{I_0}$	p	N, см$^{-3}$	$\frac{N_{Mg}}{N_{Ca}}$
MgI 2852	0,044	2,5	0,04 0,04	0,04	2,5	$13,1 \cdot 10^{12}$	1,4
		5	0,09 0,18 0,12 0,17	0,14	4,4	$22,9 \cdot 10^{12}$	1,9
CaI 4227	0,043	2,5	0,07 0,10 0,18 0,15	0,12	4,2	$9,5 \cdot 10^{12}$	—
		5	0,24 0,24 0,16 0,13	0,19	5,5	$12,4 \cdot 10^{12}$	—

* $C_{Mg}/C_{Ca} = 1,70$.

I desire to thank V.K.Prokof'ev for guidance in the work. Student G.A. Petrova participated in the measurements.

Leningrad Institute of Precision Mechanics and Optics

References

1. V.S.Mel'chenko, Optika i spektroskopiya, 1, 321 (1956).
2. N.A.Prilezhaeva & V.N.Goryachev, Izv.AN SSSR, Ser.fiz., 14, 732 (1950).
3. I.V.Dvornikova, G.P.Startsev & M.N.Golovanova, Transactions of the Tenth All-Union Conference on Spectroscopy, Vol.2, p.61, L'vov, 1958.
4. I.V.Dvornikova & I.M.Nagibina, Opt.i spektr., 4, 421 (1958).
5. K.D.Cowan & G.H.Dieke, Revs.Mod.Phys., 20, 418 (1948).
6. I.M.Nagibina, Opt.i spektr., 4, 430 (1958).
7. I.V.Dvornikova, Thesis, State Optical Institute, L., 1959.

DISTINCTIVE CHARACTERISTICS OF ARC DISCHARGES IN DIFFERENT GASES

- V.L.Marzuvanov

Table 1

Arc parameters in different atmospheres

Gas	Power W	Anode temperature* °C	Time of evaporation of 20 mg SiO_2, sec
Air	470	1940	110
Argon	160	1140	900
Helium	320	1480	--
Chlorine	190	1220	900
Carbon dioxide	430	1700	130

*The anode temperature was measured by means of an optical pyrometer at a distance of 2 mm from the electrode tip.

Although it is a familiar fact that changes in the composition of the gas in which an arc discharge takes place lead to appreciable changes in its energy and spectral properties of the discharge[1-4], these properties have not been adequately studied where a number of gases are concerned.

In the present work we investigated the characteristics (power, radiation spectrum, electrode temperature, rate of evaporation of elements from the electrodes, etc.) of arc discharges in helium, argon, air, nitrogen, chlorine and carbon dioxide.

We employed the discharge tube assembly described in Ref.5. The spectra were photographed on ISP-28 and ISP-51 spectrographs with an UF-84 camera. With a view to investigating radiation from different parts of the discharge, enlarged images of sections of the arc (in both the horizontal and vertical position) were focused on the spectrograph slit. The arc power was measured by means of a precision wattmeter. The current in all cases was 9 amp; the arc gap 4 mm.

Discharges in argon and helium* are distinguished by appreciably lower power of the arc between carbon electrodes as compared with discharges in air (Table 1). The arc power in going from air to argon is reduced by a factor of almost 3, which leads to lowering of the electrode temperature and decrease in the rate of evaporation of material from the crater. The power consumption is higher in helium than in argon, presumably due to the higher heat conductivity of helium.

The emission spectrum of a carbon arc (solid electrodes) in argon or helium consists of the lines of the given gas and the lines of carbon. The most characteristic lines are listed in Table 2. The spark lines of helium were not observed in the wavelength range from 2500 to 7000 Å. The arc lines of argon are emitted from all parts of the discharge, while the He I, A II, C II and C III lines are emitted primarily from the region at the cathode.

Photographs of parts of the arc spectra in argon and helium are reproduced in the accompanying figure. These photographs illustrate the distribution of radiation both along the arc column and across the section of the arc close to the cathode.

Table 2

Spectrum lines excited in argon and helium

Wavelength, Å	Excitation potential, ev	Remarks
A I 8115.31	13.07	Intense line, emitted from all parts of the discharge
A II 4348.11	19.49	Excited at the cathode
A II 4277.55	21.35	
He I 5875.62	23.06	Intense line near the cathode
He I 4921.93	23.72	Very weak line excited at the cathode
C II 6578.03	16.33	In argon only at the cathode; in helium over the full length of the arc but with a great increase in intensity at the cathode
C II 4267.27	20.94	
C II 2746.5	20.75	
C III 2296.89	18.01	

*Our helium contained 1% hydrogen.

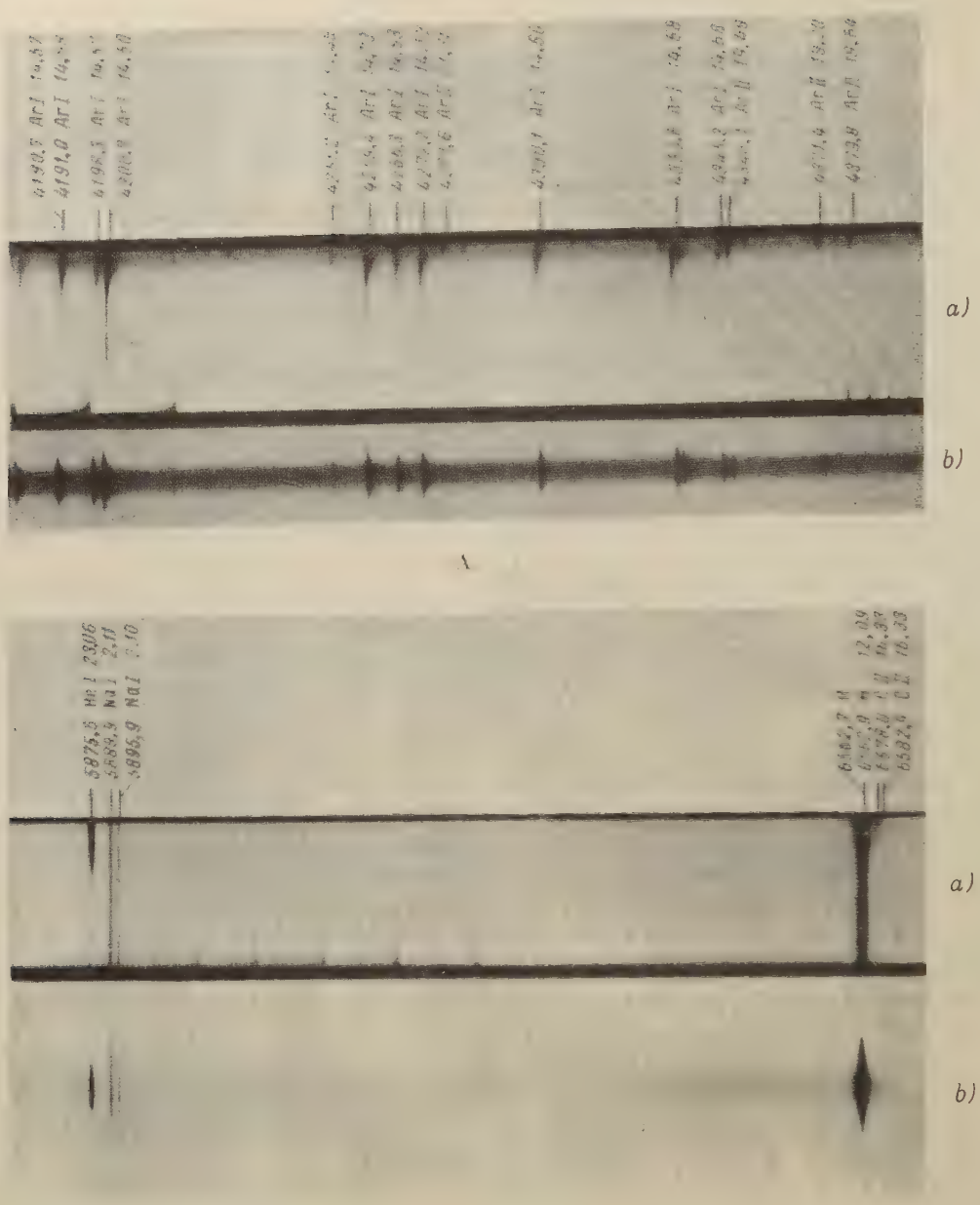

He

Intensity distribution of spectrum lines with a) arc parallel to slit and b) arc perpendicular to slit (section of arc at cathode projected on the slit).

The power of the arc in chlorine is appreciably lower than in air (Table 1). The electrode temperature is also lower, but owing to formation of volatile chlorides, there occurs intense evaporation of most elements including comparatively nonvolatile ones.[6] The spectrum contains the arc and spark lines of chlorine and the elements composing the electrode. As in inert gases, the lines of chlorine, iodine and carbon ions are emitted only from the region at the cathode. A distinctive feature of arc discharges in chlorine is the weak dependence of the relative intensity of spark and arc lines of elements (V, Ti, Ca, Ba and others) evaporated from the electrode on the composition of the sample. Thus, for example, in the case of introduction of KCl into an arc between pure carbon electrodes

$\log \frac{I_{V\ II2677,8}}{I_{V\ 12661,4}}$ changes by 1.74 in air, while in Cl_2 the change is only 0.18. The temperature in the central portion of the arc column evaluated from observation of Cu lines proved to be virtually constant. Thus use of a chlorine atmosphere minimizes the influence of the composition of the sample and thus makes it possible to enhance the accuracy of determination.

The characteristics of arc discharges in N_2 and CO_2 are similar to those of arcs in air. The spectra consists primarily of the lines of the elements evaporated from the electrode. The lines of the gases themselves are not observed in the spectrum, except for the most intense lines of oxygen with excitation potentials to 10.98 ev. The lines of ionized carbon also do not appear. This indicates that the temperature in the region at the cathode is substantially lower than in arc discharges in other gases.

The different characteristics (power, temperature distribution over the cross section and so on) of arc discharges in different gases may be explained by differences in the mechanism and intensity of heat exchange between the arc column and the surrounding medium. The arc power in inert gases increases in going from heavier to lighter gases. In polyatomic gases dissociation of the molecules plays a significant role in the removal of energy. This is the reason for the high power of arcs in nitrogen, carbon dioxide and air. In hydrogen, which combines a high heat conductivity with molecular dissociation, there is particularly intense energy transport, so that in hydrogen stable burning is attained only at high values of the current.

At the same time the atoms of the gaseous medium participate in the process of current flow through the arc gap, as is evinced by the spectral composition of the radiation: excitation of the lines of neutral atoms of the gas with excitation energies close to their ionization potential and the appearance of intense spark lines in the spectrum. The contribution of the gas to the arc conductance increases with decrease of its ionization potential.

Thus, the atmosphere in which the discharge takes place affects the characteristics of the discharge both directly by participating in the current flow and through its influence on the energy transport processes.

Knowing the characteristics of arc discharges in different gases, one can make a suitable choice of medium for the purposes of spectroscopic analysis and realize discharges with desired properties. Specifically, for example, by using a carbon dioxide atmosphere one can suppress the lines of cyanogen, which interfere with determination of a number of elements and, at the same time, retain the advantages of arc discharges in air.[5] By using an atmosphere of chlorine, one can minimize the influence of the composition of the sample on the relative intensity of the spectrum lines and thus enhance the analytic accuracy. An argon atmosphere makes it possible to increase the sensitivity in spectroscopic determination of volatile elements that are difficult to excite.

Of great potential interest and value is the use of mixtures of gases by means of which it should be feasible to realize different conditions of evaporation and excitation appropriate to the specific analytic problem.

References

1. K.N.Mochalov & E.L.Raff, Zhur.tekh.fiz., 26, 505 (1956). (Trans.Soviet Physics - Technical Physics.)
2. R.E.Thiers, Appl.Spectroscopy, 7, 157 (1953).
3. V.N.Kolesnikov & V.V.Bogdanova, Optika i spektroskopiya,1,846 (1956).
4. R.E.Thiers & B.L.Vallee, Spectrochim.acta,Colloquium Spectroscopicum Internationale VI (Amsterdam, 1956), 179, 1957.
5. S.K.Kalinin, V.L.Marzuvanov & É.E.Fain, Vestnik, AN Kazakh SSR,12,61 (1957).
6. S.K.Kalinin & V.L.Marzuvanov, Ibid., 9, 73 (1958).

ATLAS OF SPECTRUM LINES FOR HIGH-DISPERSION GRATING SPECTROGRAPHS
- S.K.Kalinin, V.L.Marzuvanov, E.E.Fain, G.M.Zamyatina, V.N.Perevertun & S.L.Terekhovich
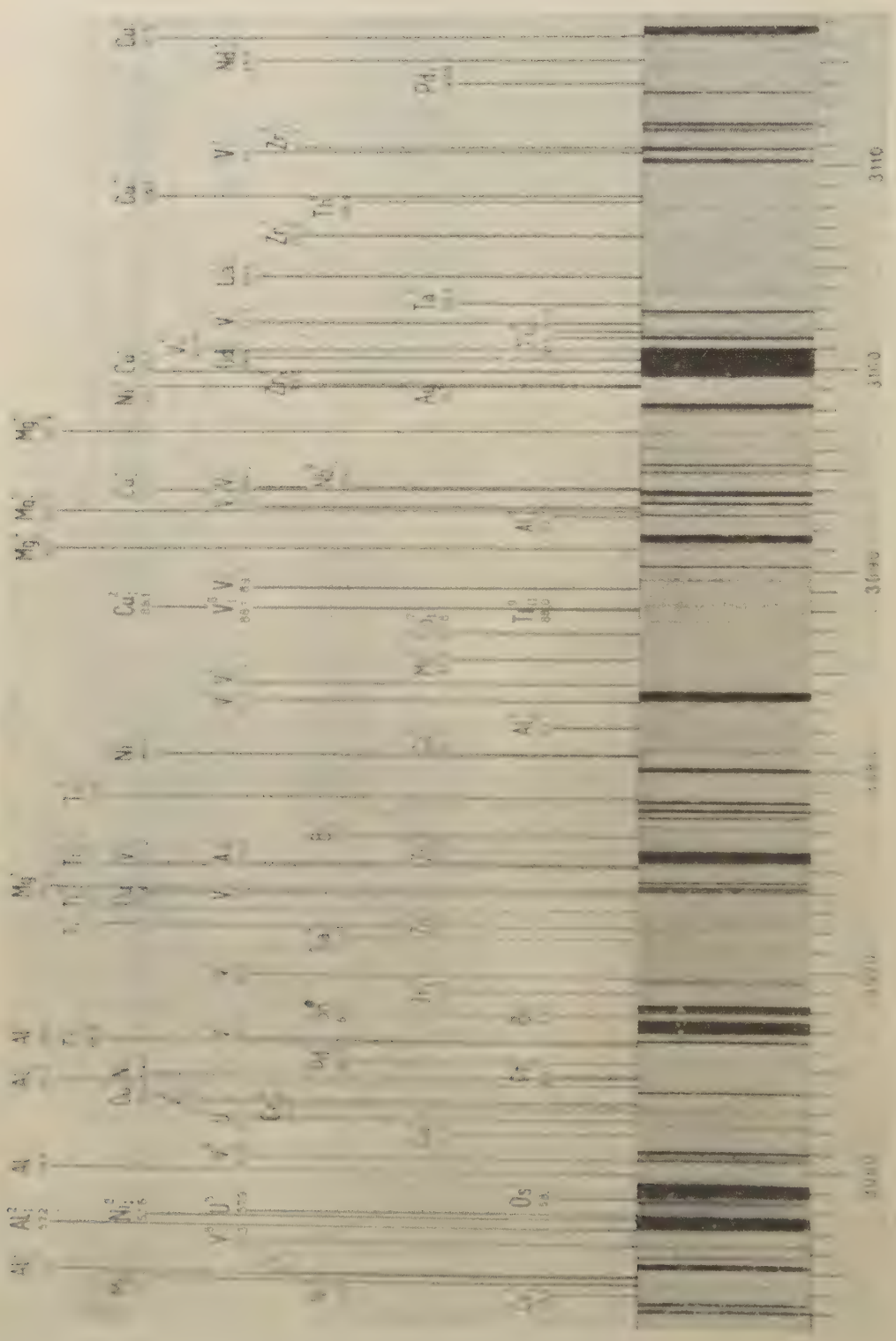
Plate from the atlas for high-dispersion spectrographs (reduced 2.3 X).

At present our instrument industry has started batch production of high-dispersion diffraction grating spectrographs. The introduction of these instruments opens the way to different spectroscopic investigations including spectrochemical analysis of ores, minerals, alloys, etc. The possibilities offered by the new instruments are not fully exploited, however, owing to the lack of tables, atlases and handbooks adopted to work with these instruments.

Earlier atlases[1-3] compiled for prism spectrographs cannot satisfy the requirements of specialists working with the new diffraction spectrograph. In view of this, this year we began work on an atlas intended for use in conjunction with instruments of this type. The atlas consists of plates, tables and text. Each plate represents a 66 Å section of the iron spectrum over a wavelength scale graduated in 1 Å divisions. Above the iron spectrum there are indicated the positions of characteristic lines; at each line, in addition to the element symbol, there is given the wavelength, the intensity in arbitrary units and the usual indication as to whether it belongs to the spectrum of neutral or ionized atoms.

The iron spectrum was photographed on a DFS-3 spectrograph with a 600 lines/mm grating (dispersion 4 Å/mm). The photographs were enlarged 20 X in accord with the standard magnification of spectrum projectors. The chosen 4 Å/mm dispersion meets the usual requirements of analytic practice. The atlas can easily be adopted to work with diffraction instruments having other plate factors.

In view of the large volume of the atlas the length of the plates has been increased to 370 mm. Plates of this size fit the standard projector table. The total length of the iron spectrum in the reproduced form equals approximately 25 meters.

All told, the atlas shows approximately 7000 lines of 85 elements. Most of the arc lines of the rock forming elements, Si, Ca, Mg, Al, K & Na, the principal elements forming nonferrous alloys (Cu, Pb, Sn & Zn), and the elements with comparatively few lines in their spectra are included in the atlas. For the other elements there are given only some of the more intense lines, useful for analysis. The plates also show the most intense lines of N, O, H, S, F, Cl, Br, I, He, Ne, A, Kr and Xe excited in a carbon arc. In addition there are indicated the edges of the characteristic bands of CN, CaF, CaO, AlO, IO and LaO.

The line intensities were evaluated in a 12-point scale. The spectrum lines appearing at concentrations of the element equal to ~10% or more are identified by the figure 1; those appearing at concentrations under 0.0001% by the figure 12. In the 1 to 9 interval this scale agrees with the conventional 10-point scale[1-3] and, at the same time, makes it possible to evaluate the intensity of the lines appearing at very low concentrations (<0.001%). These changes from the usual practice were deemed desirable in view of the higher analytic sensitivity attainable with the DFS-3.

The text, in addition to tables listing the important characteristics of the spectrum lines, includes practical recommendations for spectrochemical analysis.

Institute of Nuclear Physics,
Academy of Sciences of the Kazakh SSR

References

1. S.K.Kalinin, A.A.Yavnel', A.I.Alekseeva & L.E.Naimarkh, Atlas spektral'nykh linii dlya kvartsevogo spektrografa (Atlas of spectrum lines for a quartz spectrograph), M.-L., 1952.

2. S.K.Kalinin, L.E.Naimark, V.L.Marzuvanov & K.I.Ismagulova, Atlas spektral'nykh linii dlya steklyannogo spektrografa (Atlas of spectrum lines for a glass spectrograph), 1956.

3. A.K.Rusanov, Spektral'nykh analiz rud i mineralov (Spectrum analysis of ores and minerals), 1948.

ENTRY OF MATTER INTO ARC PLASMA. CASE OF BINARY Na + Li MIXTURES

- V.P.Zakharov & A.A.Shishlovskii

The most straight-forward method of determining the concentration of atoms in arc plasma is that of Rozhdestvenskii's "hooks".[1,2] We used this method for determining the concentration of atoms in an ac arc burning at atmospheric pressure, one of the most common spectroscopic sources (DG-1 source unit). We also used this procedure for investigating the influence of the composition of the sample on the rate of entry of the material into the plasma of a dc arc.

The experimental set-up consisted of a Rozhdestvenskii IT-23 interferometer crossed with an ISP-67 spectrograph. The investigated elements - Na and Li - were introduced in the form of mixtures of NaCl, Na_2CO_3, and Li_2CO_3 with carbon packed into the hollow of one of the carbon electrodes. This electrode served as the anode in the dc arc. The measurements were carried out with reference to the yellow Na doublet and the red Li 6708 Å line. Typical photographs of the "hooks" obtained with a 1500 mm focal length camera are reproduced in Fig.1.

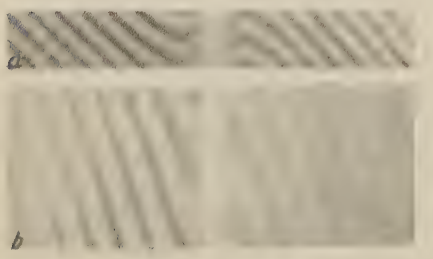

Fig.1. Photographs of "hooks": a) yellow Na doublet, b) Li 6708 A line.

The data on the entry of material into an ac arc were compared with the data for a dc arc under the same experimental conditions (content of the given element in the sample, current strength and interelectrode gap). The entry of Na atoms proved to be 1.33 and of Li atoms, 1.41 times greater into a dc arc as compared with an ac arc. This is connected with the power dissipated in the arcs. For equal values of the power (current strength) the rates of entry in both cases proved to be identical.

For the purpose of elucidating the mutual influence of the two elements, we measured the entry of Na and Li atoms into a dc arc with variation in the concentration of one component in the sample and with variation of the relative content of both components. In the first case (Fig.2), the number of Na atoms in the discharge gap is virtually independent of the Li content in the sample (the concentration of Li atoms in the discharge gap increases in proportion to the content of the Li salt in the sample).

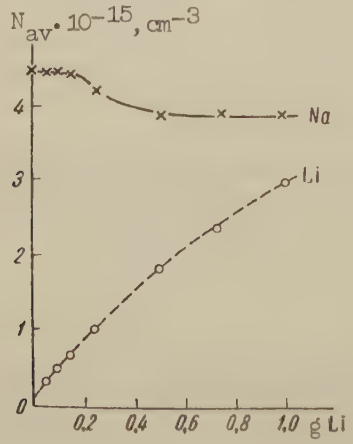

Fig.2

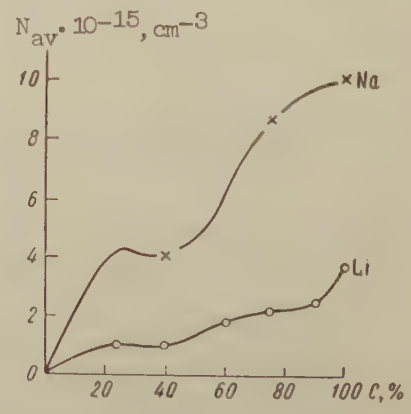

Fig.3

Fig.2. Variation of entry of Na and Li atoms into a dc arc with the content of the Li salt in the sample.

Fig.3. Variation of the entry of Na and Li atoms with the relative content of the Na and Li salts in the sample.

In the second case (Fig.3), the concentration of the given element in the discharge gap increases monotonically with increase in the relative content of this element in the sample, except for the 25 to 40% Na atom concentration range, where the dependence appears to be anomalous.

In both cases the concentration of Na atoms in the discharge gap is higher than the concentration of Li atoms for equal concentrations of the respective salts in the sample. The ratio of the number of Na atoms in the arc when the sample contains only Na salt to the number of Li atoms in the arc when the sample contains only Li salt is 2.5; the Na to Li ratio is 3-4 for samples containing large amounts of both salts. This disparity can be explained by the difference between the diffusion coefficients of Na and Li and also by the dependence of the rate of entry of a given element on the melting point of the salt packed into the electrode (we used carbonates).

Further, we investigated the entry of Na and Li atoms introduced in the form of the respective carbonates as a function of the melting point of the second, diluting component - Li, Na and K carbonates. If we use a certain average value $\bar{t}$ for the melting point of the mixture, we find that the entry of both Na and Li decreases with increase of $\bar{t}$.

When we used the carbonate of the bivalent element Ca (instead of monovalent Li) as the substituent (diluting) component, the entry of Na into the discharge gap was reduced by half (as compared with the binary Li-Na system), although the melting point of $CaCO_3$ is close to the melting point of Li_2CO_3. Apparently, the valence of the metal involved influences the processes occurring in the arc and, specifically, the entry of the electrode matter into the discharge gap.

At present we are unable to explain the anomalous character of the curves in Fig.3.

It must be emphasized that in work of this kind one must be very careful in analyzing the photographs inasmuch as there occurs the very interesting effect of pronounced asymmetry in the position of the "hooks": the "hook" at the weak line of the Na doublet is located further from the line than the "hook" at the strong line. This is particularly noticeable in investigating the peripheral part of the discharge zone. We are now investigating the nature of this effect.

References

1. E.I.Nikonova & V.K.Prokof'ev, Optika i spektroskopiya, 1, 298 (1956).

2. E.I.Nikonova, V.K.Prokov'ev & V.P.Zakharov, Materialy X Vsesoyuznogo soveshchaniya po spektroskopii (Transactions of the Tenth All-Union Conference on Spectroscopy), Vol.2, p.64, L'vov, 1958.

ENTRY OF SILICON BRASS INTO AN AC ARC

- N.K.Rudnevskii, G.I.Golitsyn & V.P.Rybochkin

It is a familiar fact[1-3] that in analysis of silicon brass in an ac arc the silicon exerts a strong influence on the relative intensity of the Zn and Pb lines. Diverse measures have been proposed[2-6] to allow for or suppress this influence. Actually, however, the nature of the influence of Si on the intensity of Zn spectrum lines in analysis of brasses has not been adequately studied. Until now there have been no data on the entry of the alloy materials into the arc cloud. Such data are essential for clarifying the mechanism of the influence of "third" elements[7].

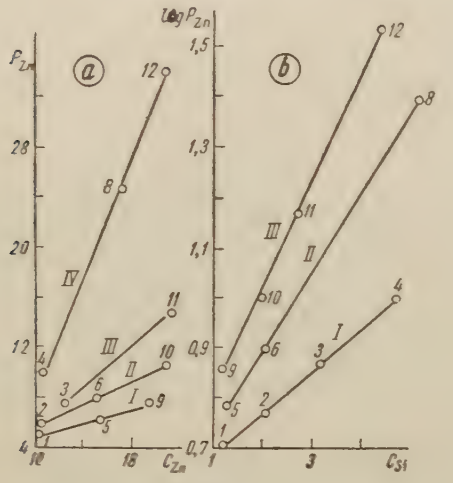

Fig.1.

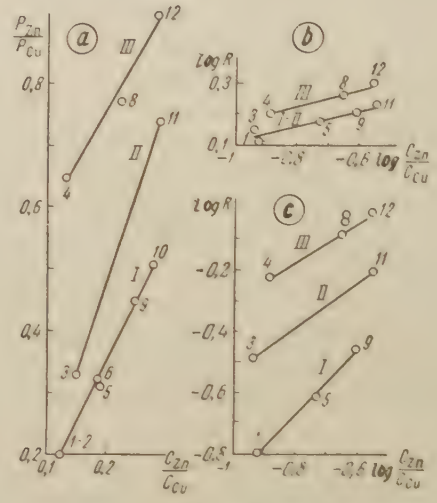

Fig.2.

Fig.1. a) Variation of P_{Zn} with the Zn concentration in the alloy: I - alloys with 1.2-1.3% Si, II - alloys with 2-2.1% Si, III - alloys with 2.6-3.1% Si, IV - alloys with 4.3-5.1% Si; b) variation of log P_{Zn} with the silicon concentration in the alloy: I - alloys with 10-12% Zn, II - alloys with 15-17% Zn, III - alloys with 19-21% Zn.

Fig.2. a) Variation of P_{Zn}/P_{Cu} with C_{Zn}/C_{Cu}; b) variation of log R for the Zn 3075.9 - Cu 2492.15 Å line pair with the reduced zinc concentration, i.e., with log (C_{Zn}/C_{Cu}); c) same but for the Zn 3072.0 - Cu 3146.8 Å line pair.

In the present work we investigated the entry of Zn and Cu into the cloud of the discharge. The results are compared with the spectroscopic data. Alloys Nos.4, 8 and 12 contained 10.7 to 20.5% Zn and 4.7 to 5.1% Si; alloys Nos.3 & 11 contained 12.5 to 21.1% Zn and 2.7 to 3.1% Si; Nos.2,6 & 10 contained 10.5 to 20.7% Zn and 2.0% Si, Nos.1,5 & 9 contained 10.3 to 19.3% Zn and 1.2-1.3% Si. (The points in the figures are numbered in accord with the alloy Nos.) In addition, all the alloys contained from 0.3 to 0.9% Pb. The arc discharge was excited by means of a PS-39 arc unit (I = 6 amp, d = 2 mm). The electrodes were in the form of 9 mm diameter, 12 cm long rods terminating in a truncated cone with a 2 mm diameter flat.

The entry of Zn and Cu into the gas cloud of the arc was investigated earlier by the procedure described in Refs.8 & 9. The vapor products were collected over a period of 20 sec, then transferred into solution, which was then analyzed by electrolysis for the Zn and Cu content.

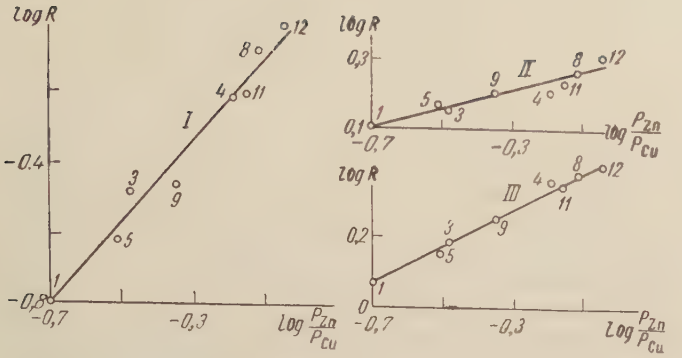

Fig.3. Variation of log R with log (P_{Zn}/P_{Cu}): I - for the Zn 3072.0 - Cu 3146.8 Å line pair, II - for the Zn 3075.9 - Cu 2492.15 Å line pair, III - for the Zn 3075.9 - Cu 3093.99 Å line pair.

The value of P_{Zn}, which characterizes the entry of zinc into the arc, depends in a complex manner on C_{Zn} and C_{Si} (the zinc and silicon concentrations in the samples) (Fig.1).

Further, we determined the values of P_{Zn}/P_{Cu}, which characterized the ratio of the numbers of Zn and Cu atoms in the arc cloud. The variation of P_{Zn}/P_{Cu} as a function of the reduced zinc concentration C_{Zn}/C_{Cu} in the alloy is shown in Fig.2,a, from which it will be evident that the Zn concentration in the gas cloud is greater than the Zn concentration in the corresponding alloys. Introduction of silicon into Cu-Zn alloys leads to enrichment of the arc cloud in zinc; this is the principal factor responsible for the shift of the log R vs log C curves for determination of Zn in silicon brass.

We also detected a certain degree of irregularity in the entry of the alloy material; this is particularly noticeable for alloys containing 15 to 20% Zn. The rate of entry of the material of these alloys into the arc cloud increases appreciably with increasing Si concentration. In the case of nonuniform entry, one may expect the shift of the curves plotted in the usual coordinates to depend also on the degree of reabsorption of the analytic Zn and Cu lines. The role of the last factor was checked by determining the displacements of curves plotted in terms of log R vs log (C_{Zn}/C_{Cu}) for a number of line pairs characterizing different degrees of reabsorption (Fig.2,b & c). As will be evident from the figure, the shifts and slopes of these curves are different. One cannot wholly eliminate displacement of the curves by selection of the line pairs. However, if we express the variation of log R for the investigated line pairs as a function of log (P_{Zn}/P_{Cu}), the curves for each line pair tend to merge into a single straight line (Fig.3).

The linear variation of log R with log (P_{Zn}/P_{Cu}) shows that the values of P_{Zn}/P_{Cu}, determined by the procedure outlined in Ref.9, can serve to characterize the relative concentrations of Zn and Cu atoms in the arc cloud.

Scientific Research Institute of Chemistry at
Gorki State University

References

1. V.K.Prokof'ev, Izv.AN SSSR, Ser.fiz., 9, 6 (1945).

2. Ya.P.Bel'kevich, Opyt spektral'nogo analiza splavov na mednoi osnove (The practice of spectrum analysis of copper alloys), 1955.

3. A.M.Borbat, Ivform.-tekhn. listok (Tech. information bulletin), Leningrad, DNTP, 105, 793 (1955).

4. E.I.Vorontsov, Zavodsk. laboratoriya (Industrial laboratory) 10, 1180 (1953).

5. A.I.Kislevskii, Inzh.-fiz.zh (Eng.-Phys.Journal), 6, 101 (1958).

6. V.S.Burakov, Ibid., 8, 46 (1958).

7. N.K.Rudnevskii, Tr. po khimii i khim.tekhnologii (Research reports on chemistry and chemical engineering) No.1, 84, Gorki, 1958.

8. N.K.Rudnevskii, A.I.Matyunin & E.S.Obukhova, Izv.AN SSSR, Ser.fiz., 19, 125 (1955). (Trans.Bulletin 19, No.1, 119.)
9. N.K.Rudnevskii & E.S.Obukhova, Tr.po khimii i khim.tekhnologii (see 7), No.2, 330, Gorki, 1958.

* * * * * * *

ENTRY OF LEAD BRASS INTO AN AC ARC

- N.K.Rudnevskii & E.S.Obukhova

It is known that zinc exerts a substantial influence on the intensity of the Pb lines in analysis of lead brasses in an ac arc. Earlier[1] it was shown that change in the concentration of "third" elements may lead to uneven entry of the sample material into the arc cloud, i.e., to an appreciable change in the relative concentration of the determined element in the gas cloud and some change in the cloud temperature. For the purpose of clarifying the influence of the first two factors in spectrum analysis of lead brasses, we undertook an investigation of the entry of the sample components into the arc cloud, using the procedure described earlier[3].

We investigated alloys containing from 9 to 40% zinc and from 0.4 to 2.2% lead. The ac arc was supplied by a DG-1 arc unit; current - 4 amp; gap - 1.9 mm; electrodes - carbon with truncated cone tips. Vapor samples were drawn from the arc cloud for a period of 35 sec without preliminary arcing of the electrodes. The vapor sampling operation was repeated 20 to 50 times. The collected vapor products were dissolved in dilute nitric acid and then the Cu, Zn and Pb contents in the solution were determined by electrolysis.

The experimental results show that the rate of entry of lead brass into the arc cloud depends on the amounts of Zn and Pb in the alloy. Thus with increase of the Zn concentration from 9 to 40% (Pb concentration constant at 1.7%), the rate of entry of the alloy material into the cloud increases by a factor of four. For the same change in the concentration of Zn in simple Cu-Zn brasses, the rate of entry of the material increases by only a factor of two. Change in the Pb concentration from 0.4 to 2.2% at a constant Zn concentration of 40% leads to an increase in the rate of entry by a factor of two. The magnitude of the parameter P, characterizing the rate of entry of lead into the arc cloud depends not only on the concentration of Pb in the alloy but also on the Zn concentration. This dependence, as will be evident from Fig.1, is described by the relation

$$P = \alpha C_{Pb} + bC_{Zn}.$$

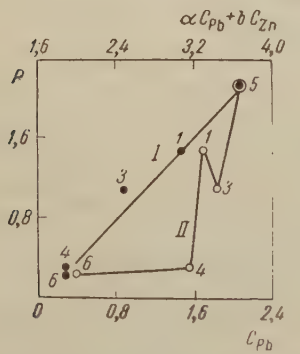

Fig.1. Variation of P with the Pb and Zn concentration in lead brass: I) $P = f(\alpha C_{Pb} + bC_{Zn})$, II) $P = f(C_{Pb})$.

The factor α can be determined from the slope of the $P = f(C_{Pb})$ curve plotted for alloys with a constant Zn content. The factor b can be found from the slope of the $P = f(C_{Zn})$ curve plotted for alloys with a constant Pb content.

Analysis of the vapor samples indicates that the arc cloud is enriched in Zn and Pb, i.e., that the concentrations of these elements in the cloud are higher than their concentrations in the alloys. The introduction of Pb into the brass tends to lower the Zn concentration in the arc cloud.

Thus variation in the Zn and Pb concentration in the brass is accompanied by uneven entry of the sample

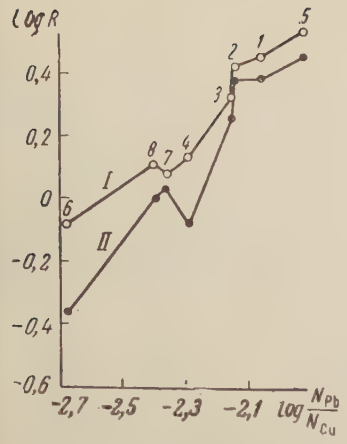

Fig.2. Variation of the relative intensity of Pb lines (log R) with the atomic concentration of Pb in lead brasses (log (N_{Pb}/N_{Cu})): I) Pb I 2873.32 - Cu I 3093.99 Å; II) Pb I 2873.32 - Cu I 2492.15 Å.

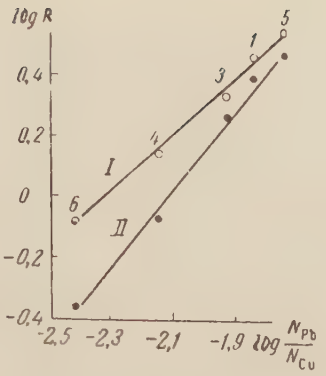

Fig.3. Variation of log R with log (N_{Pb}/N_{Cu}) characterizing the ratio of Pb to Cu atoms in the arc cloud: I) Pb I 2873.32 - Cu I 3093.99 Å; II) Pb I 2873.32 - Cu I 2492.15 Å.

material into the arc. At the same time there occurs an appreciable change in the concentration of the alloy components in the cloud. As a result, the experimental points for Pb do not fall on a straight line plotted in log R vs log (N_{Pb}/N_{Cu}) coordinates, where N_{Pb}/N_{Cu} is the ratio of Pb to Cu atoms in the sample (Fig.2). It must be noted that use of the Pb 2873.32 - Cu 3093.99 Å line pair results in a smaller scatter of the experimental points (curve I) than use of the Pb 2873.32 - Cu 2492.15 Å pair (curve II), which can be explained[1] by the different degrees of reabsorption of the Cu 3093.99 Å and Cu 2492.15 Å lines.

When, however, the experimental points are plotted in the form of log R vs log (N_{Pb}/N_{Cu}), where N_{Pb}/N_{Cu} is the ratio of the numbers Pb and Cu atoms in the arc cloud, they do fall on a straight line (Fig.3).

References

1. N.K.Rudnevskii, Tr. po khimii i khim. tekhnologii (Research reports on chemistry and chemical engineering), No.1, 84 Gorki, 1958.

2. N.K.Rudnevskii & E.S.Obukhova, Ibid., No.2, 330 Gorki, 1958.

CORRELATION BETWEEN THE COMPOSITIONS OF THE SOLID AND VAPOR PHASES IN SPECTROSCOPIC ANALYSIS OF IRON ALLOYS

- O. I. Nikitina, M.G. Sklyar, A.E. Gorevaya & N.K. Ivanova

In the present work we investigated the relation between the composition of the solid sample and the chemical composition of the vapor in the discharge cloud.

Samples of the binary alloys Fe-Cr, Fe-Mn, Fe-Si, Fe-W and Fe-C and of the ternary alloy Fe-Cr-C were prepared by adding ferroalloys of the enumerated elements to commercially pure iron. The electrodes were two 15 mm diameter rods of the test alloy, checked beforehand for uniform distribution of the elements. The analyses were carried out under the conventional arc and spark conditions as provided by the DG-1 and IG-2 arc and spark units.

The spectra were photographed on an ISP-22 spectrograph; at the same time the vapor products were collected in a glass vessel which communicated with the atmosphere, except in the case of the Fe-C alloys, when the collecting chamber was isolated from the atmosphere and filled with oxygen. Before recording the arc spectra the electrodes were sparked outside the collecting chamber for an appropriate period. The exposure time for the arc and spark spectra was the same.

To provide for an accumulation of vaporization products in an amount sufficient for analysis the spark spectra were recorded ten times. The electrodes were re-pointed before each recording. Three complete series of arc and spark vaporization tests were run for each alloy. The weight of the evaporation products deposited on the walls of the collecting vessel was determined to within 0.0001 g by weighing on an analytic balance. The concentration of elements in the deposits were determined by photocalorimetric and volumetric procedures.

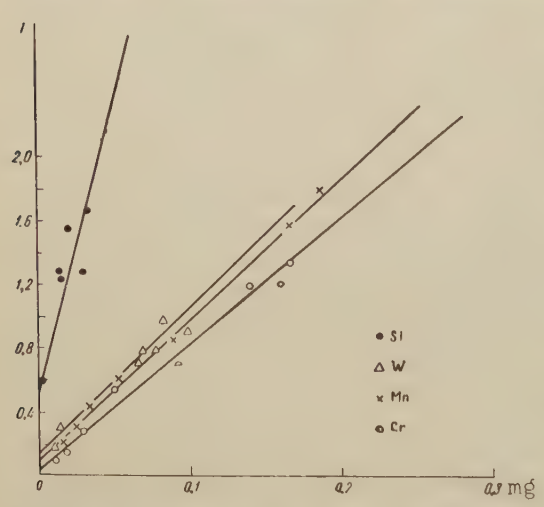

Fig.1. Variation of the line intensity of the alloying elements with the quantity (by weight) present in the deposit. IG-2 source spark.

For all the investigated alloys there were obtained rectilinear working curves over the entire chosen range of concentrations for both the spark and arc analyses. The only exception was the arc curve for determining Mn; this working curve has a bend at 12% Mn (the concentration sensitivity increases).

On the basis of the spark spectra of the binary alloys we plotted the variation of the absolute line intensity of the alloying elements with the amount of material going into the vapor phase (Fig.1). For all the investigated elements the spark line intensity increases in direct proportion to the increase in the amount of the given element in the vapor phase. The amount of material evaporated in an arc is approximately one order of magnitude greater than in the spark.

We investigated the dependence of the rate of evaporation of the elements on their concentration in the solid phase (we analyzed the condensates on the walls of the collecting vessel). It was found that the regularities characterizing the evaporation in a spark discharge are qualitatively the same for the Fe-Mn, Fe-W, Fe-Cr, Fe-Cr-C and Fe-Si systems.

As a rule, in the range of low concentrations of the alloying elements the weight of iron evaporated from the sample per unit time increases rapidly; then at a certain concentration of the alloying element in each system the rate of

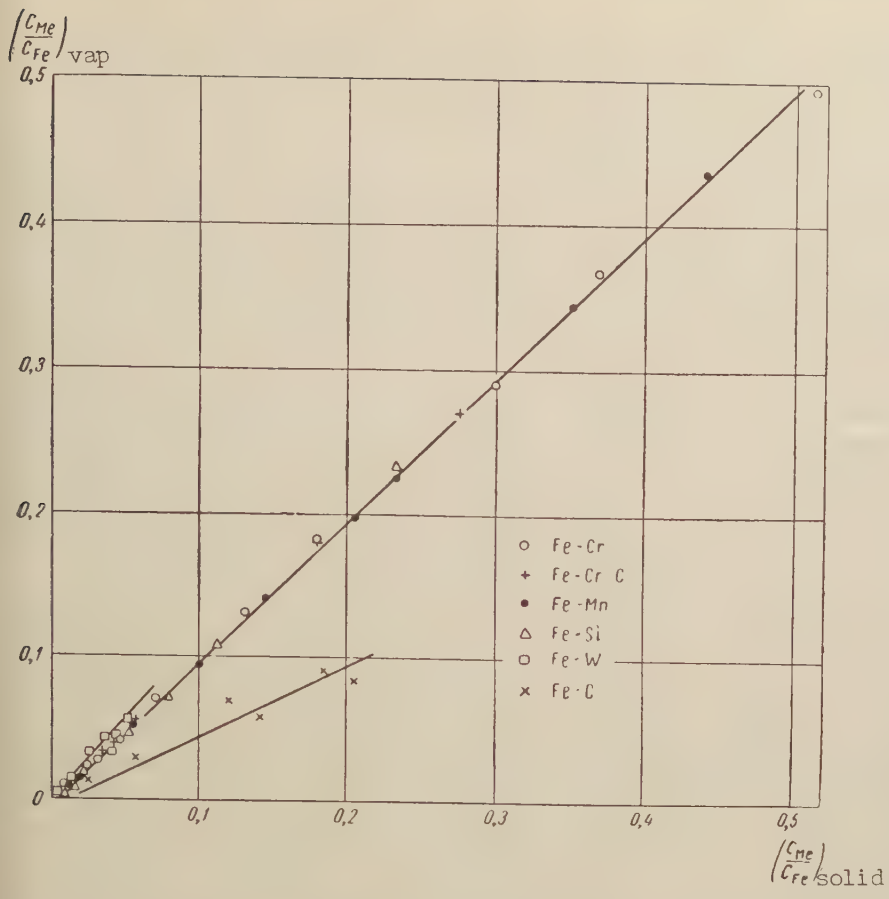

Fig.2. Correlation between the content of alloying elements in the solid and vapor phases for different alloys. IG-2 spark source.

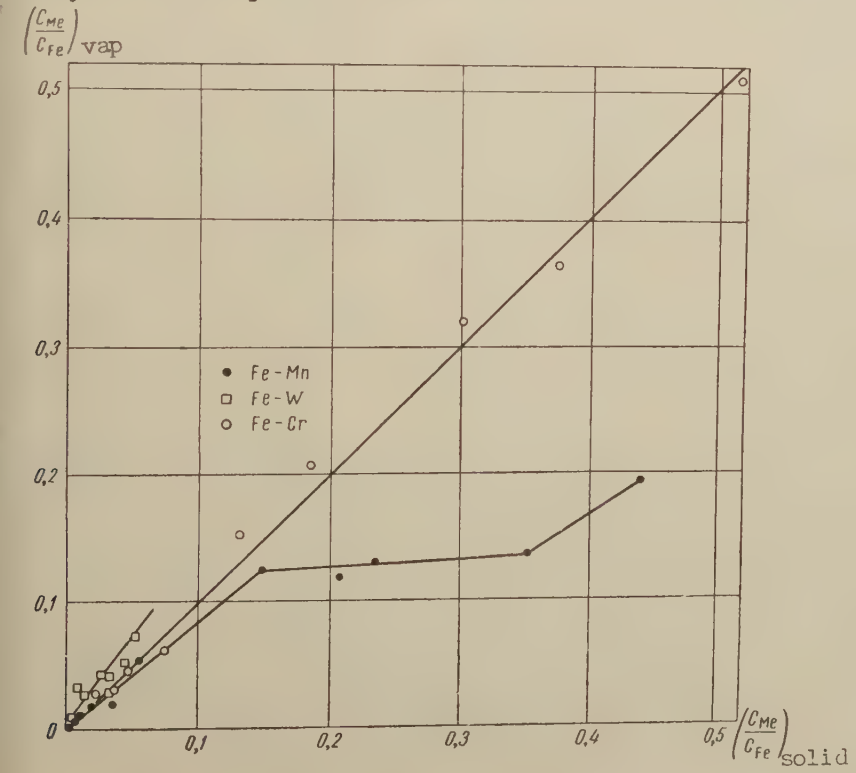

evaporation of the iron passes through a maximum and thereafter decreases.

Figs.2 & 3 show the variation in the concentration of the alloying elements in the condensates with the concentration of the respective elements in the solid alloys.

The plots are straight lines with a slope of 45° for the Fe--Cr, Fe-Cr-C, Fe-Mn and Fe-Si systems in the case of spark excitation and for the Fe-Cr system in the case of arc excitation; in other words, the relative atomic concentrations in the vapor and solid phases are equal. The equality of concentrations does not hold for the Fe-W and Fe--C alloys, but the relation between the concentrations remains linear, i.e., we obtain straight line plots but with a different slope; to some extent this deviation may be explained by the lower accuracy of the procedures employed in determining W and C. For the Fe-Mn system, in the case of arc vaporization the linear dependence persists up to 12% Mn content; above this concentration the slope of the plot changes twice. The dependence for the Fe-W system is linear over the entire investigated concentration range.

←Fig.3. Correlation between the content of alloying elements in the solid and vapor phases for different alloys. DG-1 arc source.

Juxtaposition of Figs.2 & 3 with the curves for spark vaporization leads to the inference that for most alloys the relative atomic concentrations of the elements in the solid and vapor phases remain equal, although the rate of vaporization of the sample depends on its chemical composition. The different rates of vaporization of alloys can be related with some of their physical properties.

In plots of the heat conductivity and electric resistivity vs the alloying element content the maximum of the conductivity curve and the minimum of the resistivity curve coincide with the maximum for the rate of vaporization of the material from the solid alloys. Increase in the resistivity and decrease of the heat conductivity lead to increase of the heat energy in the analyzed volume where the discharge acts on the electrodes.

The fact that the vaporization curves for different iron alloys have essentially the same character indicates that the same constant factors determine the vaporization conditions. These factors may be the temperature of the gas discharge and the thermal properties of the alloys. Up to a certain concentration of the alloying elements their rate of entry into the discharge cloud is proportional to their content in the alloy. With the passage of time, however, the accumulation of vapor in the discharge cloud leads to reduction of the discharge temperature and as a result the rate of vaporization of the elements is reduced.

Through comparison of the total weight of the condensates with the proportions by weight of the elements in the condensates, we established that the deposits consist of stable oxides (Fe_2O_3, Cr_2O_3, SiO_2, MnO_2, WO_3 and CO_2) forming as a result of direct reaction of the elements with oxygen at high temperatures.

We desire to thank V.K.Prokof'ev for his interest in the work and a number of valuable suggestions.

INFLUENCE OF DISCHARGE TIME ON THE RATE OF EVAPORATION OF PARTICLES FROM THE SURFACE OF METALLIC ARC ELECTRODES

- G.E. Zolotukhin & H.M. Zykova

Work with different light sources in analysis of complex substances and alloys has shown that the influence of individual components of the alloy on the entry of material into the gas cloud diminishes with reduction of the discharge time. Thus, for example, decrease of the discharge duration from 5 to 1.5 millisec in analysis of steels and aluminum alloys has the effect of reducing the probable analytic error by almost 50%.[1]

In the present work we investigated the influence of the discharge time on the evaporation from the surface of metallic electrodes in an ac arc and the subsequent excitation of the vapor. The rate of evaporation was compared with the discharge energy and the amount of heat taken up by the electrode surface per unit time. The discharge duration and energy were determined from oscillograms; the amount of heat was measured by the procedure described earlier.[2]

Specifically, we investigated samples of bronze, brass and copper containing small amounts of magnesium and iron. The samples were in the form of 18 mm long, 10 mm diameter rods. The base face of the rods was ground flat, polished and pressed into firm contact with the surface of a caisson cooled with flowing water. The electrode temperatures were measured by means of chromel-alumel thermocouples inserted into holes drilled near the cooled and heated ends of the electrodes. The thermocouples were connected to mirror galvanometers and the temperature variations were recorded photographically. The water circulation was measured by a flow meter with a 2 mm diameter diaphragm and a mercury monometer. The arc ignition phase was varied by adjustment of the power supply unit (generator equipped with electronic ignition control). The initial phase setting at which there was stable burning of the arc was 38°; the final phase was 118°. The effective current was maintained constant and equal to 6 amp in all the experiments. The rate of evaporation of particles from the electrodes was found from the loss in weight.

The heat balance at the electrodes as a function of their polarity and the discharge time is shown in Table 1.

Table 1

Thermal balance at the electrodes

Ignition phase, angle°	Discharge duration, millisec	Thermal flux in electrodes, Kcal/sec		Ratio of anode to cathode fluxes
		anode	cathode	
38	6,7	9,7	7,4	57 : 43
66	5,5	8,6	6,6	57 : 43
95	4,0	7,5	5,5	58 : 42
118	2,7	6,4	4,9	57 : 43

The amount of energy evolved at both the cathode and anode decreases with decreasing discharge time. Less energy is released at the cathode than at the anode. The ratio of the thermal fluxes in the cathode and anode is independent of the discharge time and equals about 43:57, which is in good agreement with the results obtained by Reider[3] and Germer[4] in measurements with a dc arc. Data on the rate of evaporation of particles from the surface of the anode as a function of the heat conductivity of the material and the discharge duration are given in Table 2; the corresponding data for the anode are listed in Table 3.

It will be evident from Table 2 that the rate of evaporation from the anode decreases with reduction of the discharge time. For the same discharge time, the rate of evaporation depends on the heat conductivity of the material: materials with a lower heat conductivity evaporate more rapidly.

The rate of evaporation of the cathode is 5-10 times higher than that of the anode and is only weakly dependent on the heat conductivity of the electrode material and the discharge time.

Table 2

Rate of evaporation of the anode (mg/cal)

Discharge duration, millisec	Copper ($\varkappa = 0.9 \frac{\text{cal}}{\text{cm sec deg}}$)	Bronze ($\varkappa = 0.18$)	Brass ($\varkappa = 0.13$)
6,7	$(0,28\pm0,03)\cdot10^2$	$(0,83\pm0,02)\cdot10^2$	$(1,2\pm0,1)\cdot10^2$
5,5	$(0,19\pm0,02)\cdot10^2$	$(0,75\pm0,02)\cdot10^2$	$(1,0\pm0,1)\cdot10^2$
4,0	$(0,14\pm0,02)\cdot10^2$	$(0,69\pm0,02)\cdot10^2$	$(0,8\pm0,1)\cdot10^2$
2,7	$(0,14\pm0,02)\cdot10^2$	$(0,55\pm0,02)\cdot10^2$	$(0,7\pm0,1)\cdot10^2$

Table 3

Rate of evaporation of the cathode (mg/cal)

Discharge duration, millisec	Copper	Bronze	Brass
6,7	$(2,5\pm0,2)\cdot10^2$	$(3,3\pm0,2)\cdot10^2$	$(3,3\pm0,2)\cdot10^2$
5,5	$(2,4\pm0,2)\cdot10^2$	$(3,5\pm0,3)\cdot10^2$	$(2,8\pm0,2)\cdot10^2$
4,0	$(2,1\pm0,2)\cdot10^2$	$(3,3\pm0,2)\cdot10^2$	$(2,5\pm0,2)\cdot10^2$
2,7	$(2,1\pm0,2)\cdot10^2$	$(2,1\pm0,2)\cdot10^2$	$(2,2\pm0,2)\cdot10^2$

Table 4

Reduced rate of evaporation of the electrodes (mg/cal)

Discharge dur. msec	Copper		Bronze		Brass	
	anode	cathode	anode	cathode	anode	cathode
6,7	0,029	0,34	0,085	0,45	0,12	0,45
5,5	0,022	0,36	0,087	0,53	0,12	0,42
4,0	0,019	0,38	0,092	0,06	0,11	0,45
2,7	0,022	0,43	0,086	0,43	0,11	0,45

Table 5

Influence of discharge time on the intensity of the Mg 2852 Å line and the temperature of the gas cloud

Discharge duration, millisec	Energy of each discharge, cal	Power of individual discharge cal/sec	Log relative line intensity		Arc temperature, °K
			anode	cathode	
6,7	0,48	720	1,30	1,55	5800
5,5	0,40	730	1,35	1,71	6000
4,0	0,36	900	1,38	1,85	6400
2,7	0,34	1260	1,45	1,90	6800

Table 4 lists the reduced rates of evaporation (i.e., rates normalized to a unit discharge energy) as function of the heat conductivity of the material and discharge time. It will be evident that the reduced evaporation rate is not the same for different materials and electrode polarities, but that approximately the same value of the reduced rate is obtained for a given material and electrode polarity regardless of the discharge duration (within the investigated range).

The influence of discharge duration on the relative intensity of the Mg 2852 Å line and the temperature of the gas cloud is illustrated by the data of Table 5. The temperature was determined from the Cu I 3319 and Cu I 3208 Å lines lines recorded on an ISP-28 spectrograph. In these measurements the upper electrode was a copper rod; the lower electrode the investigated alloy (brass) containing small amounts of magnesium. The experiments showed that with reduction of the discharge time the intensity of the Mg 2852 Å line increases more with evaporation of the cathode than with evaporation of the anode. Increase in intensity of copper lines with decrease of the discharge time has been reported in the work of V.P.Borzov.[1]

On the basis of the experimental results, for enhancement of the sensitivity of analysis of copper based alloys we recommend the use of a rectified ac arc with short pulses and connection of the sample as the cathode.

References

1. V.P.Borzov, Zhur.tekh.fiz., 26,9 (1956) (Trans.Soviet Physics - Technical Physics); Zavodsk. laboratoriya, No.6, 756 (1958) (Trans.Industrial Laboratory).

2. G.E.Zolotukhin, Fiz.metallov i metallovedenie (Physics of metals and metallography), 3, 508 (1956).

3. W.Rieder, Z.Phys., 146, 629 (1956).

4. L.Germer, Bell System Tech.Jour., 30, 939 (1951).

EFFECT OF SAMPLE POLARITY IN THE EXCITATION OF RECTIFIED ARC SPECTRA*

- E.A.Silin'sh & L.F.Taure

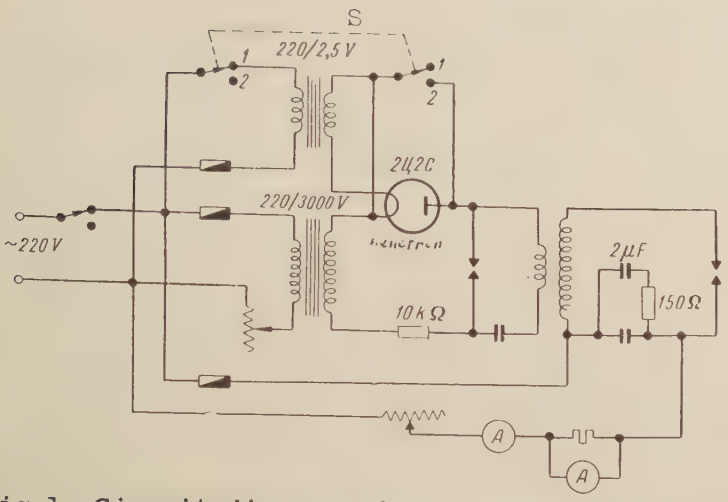

Fig.1. Circuit diagram of ac arc and unipolar arc power unit.

In the present report we give some of the results of our investigation of the influence of the polarity of the sample when this is used as one of the electrodes in a unipolar (rectified) ac arc.

The circuit diagram of the source-generator is shown in Fig.1. This source unit can provide a conventional ac arc with a frequency of 100 cps (switch S in position 2) or a unipolar arc with a flash frequency of 50 cps. With switch S in position 1 the 2Ts2S (2Ц2С) kenotron is connected to the output of the high voltage transformer and serves to block out alternate half-cycles. Hence the arc is excited every half-cycle with the same polarity, although the electrodes are constantly supplied with alternating voltage (220 v, 50 cps). A similar circuit was proposed by Borvik[1] for rectification of heavy alternating currents. This circuit is also suitable for supplying analytic light sources inasmuch as it is simple and more reliable than most other circuits for obtaining a unipolar arc (see, for example, Ref.2).

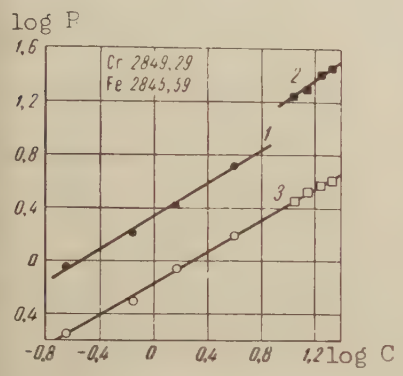

Fig.2. Effect of sample polarity on the position of the calibration curves: 1 - curve for determination of Cr in alloy steel with the sample as the anode, 2 - same for stainless steel, sample as the anode, 3 - curve for medium-alloy and stainless steels with the sample as the cathode.

We investigated the role of electrode polarity in spectrum analysis of carbon, medium-alloy and stainless steels and brass. We studied the calibration (working) curves, the burning time curves, the intensity distribution of the spectrum lines and the influence of the arc current strength on the line intensities as functions of the sample polarity. We observed the following regularities.

The absolute intensity of the spectrum lines with negative polarity of the sample is higher than with positive polarity by a factor of 1.5-2 for steel and 5-8 for brass. The ratio of the line intensities of all the alloying elements to the intensity of the matrix lines is higher with the sample connected as the anode; the ratio is particularly high in the case of Cr and Ni. The only exception to this is Zn in brass.

With the sample as the anode there is an appreciable shift of the calibration curve with increase in the number and concentration of "third" components (curves 1 & 2 in Fig.2); the shift is particularly great in the case of curves for determination of Cr, Ni and Si and is comparatively small

---

*L.Khomskaya, student at the Latvian State University, participated in the experiments.

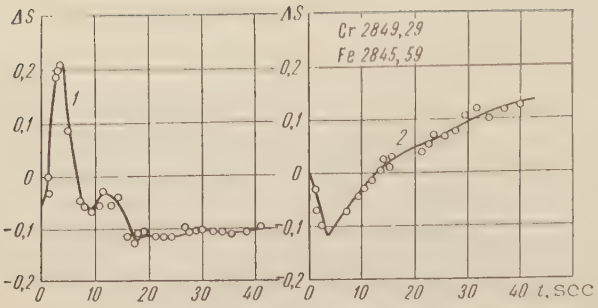

Fig.3. Burning time curves for Cr in a unipolar arc: 1) sample-cathode, 2) sample-anode.

in the case of curves for Mn. In contrast, with the sample negative, there is little or no shift of the calibration curves: the influence of "third" components decreases (curve 3 in Fig.2). Generally, the slope of the calibration curves with the sample as the cathode is less steep than with the sample as the anode.

The calibration curves obtained for an ordinary ac arc usually lie between the sample-anode and sample-cathode curves. It may be assumed that the ac arc curves represent a superposition of the anode and cathode effects. Presumably the shift reported[3] for ac working curves is due primarily to displacement of the sample-anode curve.

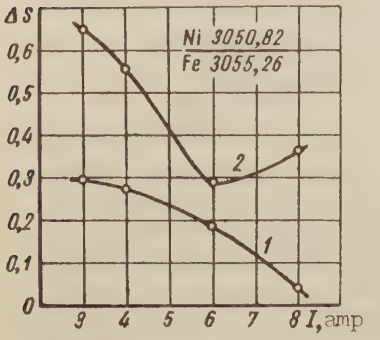

Fig.4. $\Delta S = \log (I_{Ni}/I_{Fe})$ vs arc current curves: 1) sample-cathode, 2) sample-anode.

The analytic error in using the sample as the cathode is the same order of magnitude as the analytic error with an ordinary ac arc. The reproducibility is impaired with the sample positive. For example, the probable error of an individual measurement in determining Mn in steel is 3.4% with an ac arc, 3.5% with the sample connected as the cathode and 5.6% with the sample as the anode.

With the sample connected as the cathode, the burning time curves are consistent with the regularities of Filimonov[4]: in the case of Mn, Cr and Si a maximum appears in the ΔS vs time curve; in the case of Ni - a minimum. With the sample positive the burning time curves for a number of elements, particularly Cr, Ni and Si, depart from the Filimonov regularities (Fig.3).

The topographic (spatial) distribution of the arc and spark line radiations through the discharge plasma also depends on the sample polarity.

The curves characterizing the relative intensity of the spectrum lines as a function of the arc current differ with the sample polarity (Fig.4). The intensity of oxidation and the composition of the products of electro-erosional transport (particularly in the case of alloy steel and brass) also depend on the sample polarity.

It may be assumed that, in addition to thermal and oxidation-reduction processes, an important role is played by electric processes in the evaporation of elements from the sample. These electric processes, which naturally depend on the electric parameters of the arc, include electric erosion[5], thermionic emission at the anode, the effect of electronic emission on evaporation from the cathode, the influence of electrodes potential on oxidation reactions, etc.

The observed decrease in the influence of "third" components with the sample as the cathode opens new possibilities for the application of unipolar arcs in spectroscopic analysis.

Physical Laboratory of the Riga Electric Machine Building Plant &
Spectroscopic Laboratory of the Riga "Avtoelektropribor" Plant

References

1. I.I.Borvik, Doklady AN SSSR, 42, 178 (1944).
2. A.I.Akimov, Optika i spektroskopiya, 3, 76 (1957).
3. A.G.Komarovskii, Inform.-tekhn.listok Leningr. (Tech.Info.Bulletin, Leningrad), DNTP, No.71, 412 (1952); No.36, 724 (1955).
4. L.N.Filimonov, Zavodsk. laboratoriya (Industrial laboratory) 15, No.8 (1949); 15, No.10 (1949).
5. K.I.Taganov, Priroda (Nature), 3, 3 (1948); N.S.Sventitskii & K.I.Taganov, Izv.AN SSSR, Ser.fiz., 12, 396 (1948).

* * * * * * *

INFLUENCE OF THE COMPOSITION OF POWDERED SUBSTANCES ON THE RELATIVE INTENSITY OF SPECTRUM LINES

- A.M.Shavrin & M.A.Zotin

In this paper we present some data on the influence of the composition of powder samples on the relative line intensity in the spectra of systems consisting of silica and the carbonates of alkaline earth metals when the sample is vaporized from a cup in a copper electrode.

For the purpose of investigating the intensity ratios of the Cd 3261.057 Å line to the Zn 3282.333, 3302.588/941 and 3345.02/572 Å lines we prepared a series of mixtures in which the SiO_2 content varied from 0 to 98.5% and that of the alkaline earth carbonate from 98.5 to 0%; the 1.5% remainder was $CdCO_3$. After preparation of the mixture, ZnO was introduced in the amount of 1.5% of the total.

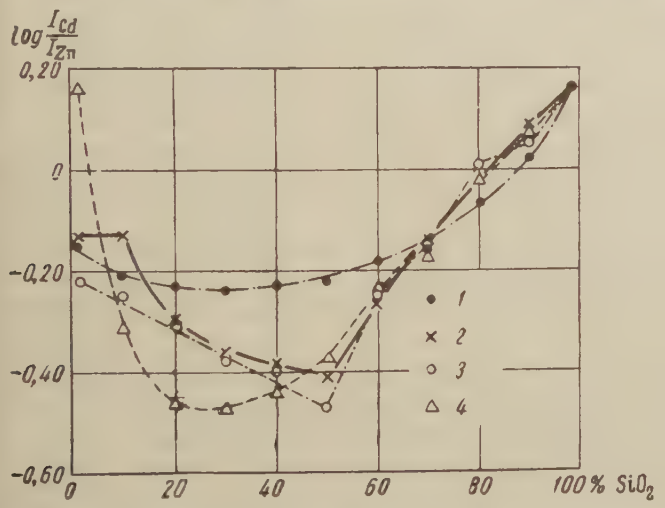

Fig.1. Variation of the relative intensity of the Cd 3261.057 Å and Zn 3302.588/941 Å lines with the composition of the mixture in the systems: 1) SiO_2-$MgCO_3$, 2) SiO_2-$CaCO_3$, 3) SiO_2-$SrCO_3$ and 4) SiO_2-$BaCO_3$.

The spectra were photographed on an ISP-22 spectrograph with a slit width of 0.025 mm. The source was an ac arc (supplied from a Sventitskii type circuit) between copper electrodes; the current strength was 5 amp; the gap 3 mm. The exposure time was 15 sec. The mixture was placed in a cup-like recess (7 mm diameter, 1.5 mm deep) in the lower electrode. The mean values of log (I_{Cd}/I_{Zn}) based on 26 spectra as a function of the composition of the mixture in the SiO_2-$MgCO_3$, SiO_2-$CaCO_3$, SiO_2-$SrCO_3$ and SiO_2-$BaCO_3$ systems are shown in Fig.1.

The complex composition dependence of the relative intensity is a result of the different variations of the absolute intensities of the Cd and Zn lines. By way of illustration we give the variation of the blackening of these lines in the SiO_2-$CaCO_3$ system in Fig.2. The greater increase in the intensity of the Zn lines as compared with the intensity of the Cd lines with increase in the $CaCO_3$ content from 0 to 55% is apparently due to the formation of cadmium, zinc and

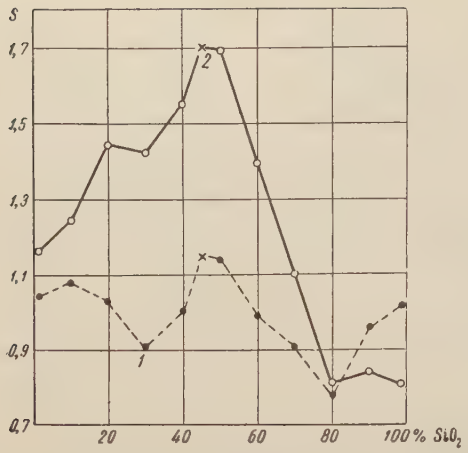

Fig.2. Variation in the degree of blackening of the Cd 3261.057 Å (1) and Zn 3302.588/ /941 Å (2) lines with the composition of the mixture in the SiO_2-$CaCO_3$ system.

calcium silicates; particularly the presence of calcium silicate favors transition of the mixture to the liquid state and, consequently, increases the rate of chemical reaction of the components.

There is good reason to assume that the silicates forming in the sample are responsible for the change in the rate of entry of the analytic elements into the arc. This assumption is substantiated by comparison of our experimental data with the melting and boiling points of the products of reaction of the sample components with SiO_2. In addition, with a view to checking the assumption further, we investigated the remains of the beads left after recording the spectra. The samples not containing alkaline earth carbonates virtually do not fuse; the elements enter the arc primarily from the initial compound. On the other hand, in the presence of alkaline earth carbonates in the mixture, the mixture fuses and beads remain on the electrode. Highly uniform and transparent beads are formed in the case of the mixture corresponding to the minimum relative intensity, i.e., log $(I_{Cd}/I_{Zn})_{min}$. In the SiO_2-$CaCO_3$ system, transparent beads are formed from the mixture with equimolecular proportions of the components. In systems containing strontium and barium, a transparent bead is obtained with the mixtures containing ~66 mole percent SiO_2 and ~33 mole percent of the alkaline earth carbonate. On the basis of these component proportions we calculated the formulas of the probable silicates of calcium, strontium and barium. The calculations showed that in the SiO_2-$CaCO_3$ system the primary bead component is calcium metasilicate (wollastonite); in the systems with strontium and barium carbonates, the respective metadisilicates are formed (investigation of the beads by means of a polarizing microscope substantiated the presence of the enumerated silicates).

We note that the proportion of silicon dioxide to calcium carbonate for which there are obtained uniform beads was established by geometric analysis of the variation of the relative intensity as a function of the composition of the SiO_2-$CaCO_3$ system.

We further checked the above inferences by analysis of mixtures prepared with natural wollastonite. Adding $CdCO_3$ and ZnO in the same amounts to the natural wollastonite and recording the spectra under the same conditions, we obtained the same relative intensity value, i.e., that corresponding to the minimum in the curve for the SiO_2-$CaCO_3$ system.

This result clearly indicates that there does occur a reaction between the silicon dioxide and the calcium carbonate leading to the formation of artificial wollastonite; moreover, this result points to the substantial role that may be played by the matrix components in analysis.

The absence of a clear minimum in the relative intensity curve for the SiO_2-$MgCO_3$ system may be explained by incomplete conversion of the mixture components to silicates since in this case the mixture is only partially fused during the exposure. Moreover, the basic properties of magnesium are more weakly evinced than those of calcium, strontium and, particularly, barium.

We also investigated the behavior of log (I_{Cd}/I_{Zn}) with variation of the composition in the $CaCO_3$-$SrCO_3$ system. In this case the relative intensity remains virtually constant. Thus in the absence of the chemically active component,

SiO_2, the entry of cadmium and zinc into the discharge is determined by the physical-chemical properties of the initial compound and does not depend on the proportion of the matrix component.

On the basis of the available experimental data it may be inferred that other elements belonging to the same group of the periodic table or their analogous compounds will in the presence of silicon dioxide have a similar influence on the relative intensities of the spectrum lines.

Hence in working with an activated arc between copper electrodes one can, making use of the periodic law, take appropriate practical measures to eliminate or minimize the influence of the mixture composition on the relative intensity of the analytic lines.

"A.M.Gorkii" Perm State University

* * * * * * *

INFLUENCE OF "THIRD" ELEMENTS IN SPARK ANALYSIS OF SOLUTIONS*

- A.K.Rusanov & L.I.Sosnovskaya

We investigated the dependence of spectrum line intensities on the properties of the analyzed solutions and the effect of different elements on each other. The experiments were performed under conditions minimizing the influence of processes occurring on the electrode and also under conditions when the influence of these processes is most clearly evinced.

The solutions were introduced into the discharge zone by means of rotating metallic or graphite disks mounted opposite each other. In the case of graphite disks the spark discharge forms between two films of the solution; the film thickness could be varied from 0.003 to 0.06 mm. In other experiments the solutions were introduced into the discharge by means of a capillary graphite electrode immersed in the solution; the stationary graphite counter electrode was mounted above the capillary electrode. The excitation source was an IG-2 spark generator employing the Raiskii (condensed spark) circuit. We devoted particular attention to determining the variation of the absolute and relative line intensities with the rate of rotation of the electrodes, the thickness of the solution film, the ability of the spark to break through this film, the amount of solution consumed in the discharge and also with the ionization potential and atomic concentration of extraneous elements in the solution.

It was found that the absolute line intensity decreases with increasing film thickness and, consequently, with increasing solution consumption. Variation in the film thickness has no effect on the line intensity in cases when the film is not punctured by the spark. The effect of film thickness on the line intensity is closely correlated with increase of the solution utilization factor in working with thin films.

In evaluating element concentrations from the absolute spectrum line intensities in the case of both rotating and capillary electrodes one must take into account the electric conductivity of the solution, the thickness of the solution film and the rate of its renewal (rate of rotation of the disks or diameter of the electrode capillary, the material and state of the surface of the electrodes, variations in the solution viscosity with temperature and changes in the chemical composition of the solution).

---

*Abstract. Complete report to be published in "Analiticheskaya khimiya" (Analytic Chemistry).

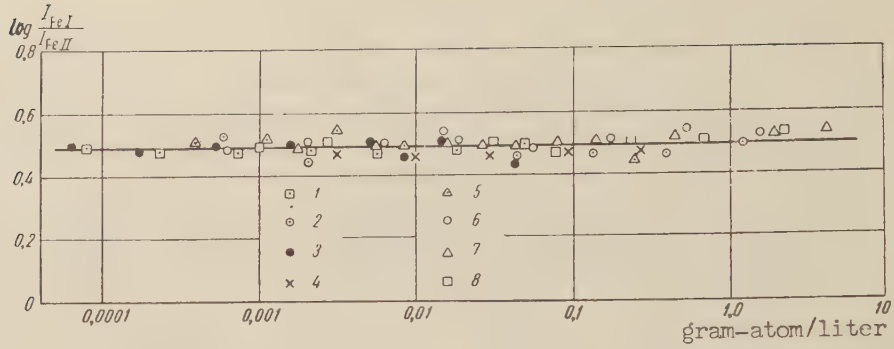

Fig.1. Variation of the relative intensity of the Fe I 3047.6 and Fe II 2739.6 Å lines with the atomic concentration of elements having different ionization potentials. Rotating graphite electrodes: 1) Cs (3.9 ev), 2) K (4.3 ev), 3) Ca (6.1 ev), 4) Cu (7.7 ev), 5) Zn (9.4 ev), 6) S (10.6 ev), 7) Cl (12.9 ev), 8) N (14.5 ev).

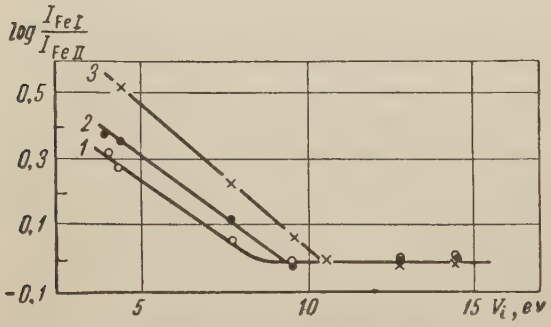

Fig.2. Variation of the relative intensity of the Fe I 3047.6 and Fe II 2739.6 Å lines with the ionization potential of the elements with introduction of the solution through a capillary graphite electrode: 1) element concentration 0.1 gram-atom/liter, 2) 0.25 gram-atom/liter, 3) 1 gram-atom/liter.

The effect of "third" elements on the absolute and relative spectrum line intensities depends on the ionization potential and the atomic concentration of the elements in question. The relative importance of these two factors differs, depending on the method of introduction of the solution into the spark discharge. Thus, for example, the influence of "third" elements is minimal when the discharge takes place between solution films not disrupted by the spark; the influence is greatly enhanced when the method of introduction favors development of processes occurring on the electrodes.

If a spark discharge occurs between two thick solution films coating rapidly rotating disk electrodes, the relative intensity of the arc and spark lines, which characterizes the variation in conditions of excitation, virtually does not depend on the ionization potential and atomic concentration of the extraneous elements in the solution (Fig.1).

The relative intensity of the arc and spark lines rapidly increases with decrease of the ionization potential and with increase of the atomic concentration of the elements when the solution is introduced into the discharge by means of a capillary graphite electrode (Fig.2). The enhanced influence of extraneous elements on the excitation conditions in going from rotating to capillary electrodes is apparently due to the fact that in the latter case the current-carrying spark channel is displaced to a greater extent relative to the center of the radiating gas cloud.

INFLUENCE OF "THIRD" ELEMENTS IN USING UNDISPERSED LIGHT AS THE INTERNAL STANDARD

- I.S.Abramson, S.N.Murzin & V.A.Slavnyi

When undispersed light is used as the internal standard, the reproducibility of photometric measurements generally proves to be no worse, and in many cases appreciably better, than when a spectrum line of the matrix is employed for this purpose. This is substantiated by laboratory investigations with photoelectric instruments[1,2], practical work with a photoelectric FES-1 Steelometer[3,4] and by a number of other studies[5-7]. However, good reproducibility in itself does not necessarily mean high accuracy of measurement in view of the more or less systematic influence of different factors, in particular, "third" elements. Hence we felt it would be of interest to determine how these factors are evinced when undispersed light is used as the internal standard.

Even our preliminary measurements showed that the absolute intensity of the spectrum lines of the matrix and the element being determined varied with changes in composition of the sample in a no less complex manner than the absolute intensity of the undispersed light, and consequently, the magnitude of these variations, which are connected with the total amount of material entering into the discharge gap, cannot serve as a criterion for evaluating the merits of different internal standards. Hence in our work the magnitude of the influences in using a matrix line and in using undispersed light was evaluated directly from relative measurements.

Specifically, the measurements were carried out for the case of determination of chromium and manganese in steels with the different arc discharges provided by the GEU-1 source unit. The investigated specimens were chosen so that the magnitude of the influences would be sufficiently large. The chromium determinations were carried out on LSO* standard samples Set No.6 in conjunction with binary alloys of the FE-Cr system. For the determination of manganese, we used samples from LSO Sets Nos.6 and 28 in conjunction with binary alloys of the Fe-Mn system. As a measure of the magnitude of the influence we used an arbitrary quantity, a factor characterizing the systematic deviation of the experimental points from the calibration curve and equal numerically to the difference between the logarithms of the concentrations. In the determinations we used the Cr 5345 & Fe 4957 Å and Mn 4823 & Fe 4859 Å line pairs. The experimental results are summarized in the accompanying table which gives the values of the "influence factor" calculated from measurements with reference to undispersed light (I), with reference to the matrix line (II) and, finally, with reference to the same matrix line, but with the curve plotted taking into account the dilution of the matrix (III) under the different experimental conditions. The accidental error in the tabular values lies between 0.005 and 0.010.

It will be evident from the table that in all cases the magnitude of the influence substantially exceeds the accidental measurement error. Hence we were unable to find excitation conditions under which the influence is wholly eliminated. We can only note that the influence is greatest for the case when the sample serves as the cathode and smallest when a full-wave arc is employed. This result is not general but pertains only to the investigated samples; thus, for example, within the range of one particular set of standards, the minimal influence obtained in a case when the sample served as the anode. There is no clear-cut correlation between the influence factor and the current strength. Finally, it follows from the table that when undispersed light is used, the magnitude of the influence is no greater and in some cases 1.5-2 times smaller than when a matrix line is employed as the internal standard. It must be noted that in case of comparison with other iron lines, the magnitude of the influence factor changes somewhat but qualita-

---

*LSO (ЛСО) - Laboratory of Standard Samples.

	Chromium									Manganese		
	4 a*			10 a			45 a**		70A**	10 a		
	±***	+	−	±	+	−	+	−	−	±	+	−
I	0,03	0,04	0,07	0,03	0,04	0,09	0,03	0,07	0,03	0,03	0,05	0,08
II	0,04	0,04	0,09	0,04	0,05	0,17	0,05	0,13	0,05	0,06	0,07	0,10
III	0,03	0,04	0,09	0,03	0,05	0,17	0,07	0,12	0,03	0,04	0,06	0,08

---

*All current values are crest values. **With 1 to 8 repetition rate scaling. ***The indicated polarities are for the sample.

tively the same results are obtained.

Further, we made attempts to suppress the influence of "third" elements by means of special devices. In particular, we tested the rotating electrode technique. In this procedure a new section of the sample is acted on by each subsequent discharge pulse. Hence it might be assumed that oxidation and diffusion processes on the electrodes, which might be the cause of the influences, will be evinced to a lesser degree than with a stationary electrode. Measurements under conditions I, II and III showed, however, that instead of decreasing, the magnitude of the influences actually increased somewhat. This is probably connected with structural effects which in this case should be manifested appreciably more strongly owing to less intense local heating of the sample. Moreover, this technique did not eliminate the influences connected with variation in the discharge temperature.

We also tested powerful pulse discharges[8]. The measurements were carried out at C = 30,000 μf and L = 0.33 mh. The counterelectrode was of carbon. For the purpose of localizing the discharge, the surface of the sample was coated with a thin layer of machine oil. The experiments showed that localization of the discharge reduces the magnitude of the influences but does not wholly suppress them; the influence factor, evaluated by the above mentioned procedure, proved to be 0.05 without localization of the discharge and 0.03 with localization, i.e., of the same order of magnitude as with an ordinary source. Moreover, it must be noted that with localization of the discharge, the slope of the calibration curve is rather flat (0.3-0.4) owing to the strong background, which is particularly undesirable in photoelectric measurements, when the measured quantity is the integral light flux passing through the exit slit. The reproducibility of the relative intensity values was within 3-4%; however, in view of the flat slope of the calibration curve, in the case of localization the error in determining the concentration was very large (of the order of 8-10% in individual measurements).

The results of work with undispersed light as the internal standard give reason to infer that this procedure, which has undoubted advantages as regards reproducibility, from the standpoint of influence where metallic samples are concerned, does not yield to the conventional technique of comparison with a spectrum line of the base material. In fact, in using undispersed light one can count on a certain diminution of the influences regardless of the method of excitation of the spectrum.

In conclusion, we believe that the solution of the problem of eliminating influences should be sought not in seeking or choosing between different internal standards, analytic lines, discharge conditions, electrode shapes and so on, but along the line of developing essentially new light sources.

Laboratory of the Commission on Spectroscopy,
Academy of Sciences of the USSR

References

1. I.S.Abramson, Zavodsk. laborat. (Industrial Laboratory), 20, 168 (1954).
2. L.P.Malyavkin & I.S.Abramson, Izv.AN SSSR, Ser.fiz., 19, 40 (1955). (Trans. Bulletin 19, No.1, 38.)
3. I.S.Abramson, L.P.Malyavkin, A.N.Mogilevskii & V.A.Slavnyi, Zavodsk. laboratoriya, 24, 695 (1958). (Trans.Industrial Laboratory).
4. N.V.Buyanov, S.L.Zubkovskii, T.V.Kovalenko, V.F.Korotkov & V.R.Lindstrem, Ibid., 24, 702 (1958). (Trans.Industrial Laboratory).
5. A.Hannick, A.Haus & M.Lacomble, Microchimica acta, 2-3, 637 (1955).
6. H.Krempl & G.Scheibe, Arch.Eisenhüttenwesen, 28, 135 (1957).
7. M.F.Hasler, Proceedings of the Colloquium Spectroscopicum, Internationale, VI, 76, Pergamon, 1957.
8. A.S.Aleksandrova, E.I.Vorontsov & S.S.Rimlyand, Transactions of the Tenth All-Union Conference on spectroscopy, Vol.2, p.231, L'vov, 1958.

* * * * * * *

EFFECT OF THE CHEMICAL COMPOSITION OF THE SAMPLE ON THE INTENSITY OF THE MATRIX SPECTRUM AND THE ANALYTIC RESULTS

- N.V.Buyanov

It is known that in analysis of simple and medium alloy steels the intensity of the matrix lines (internal standard) is virtually independent of the concentration of minor constituents (the elements being determined). In the analysis of complex alloys, however, when the concentration of all the alloying elements amounts to 20% or more, one may expect a decrease in the intensity of the matrix spectrum.[1-4]

We investigated the contribution of different alloying elements to this effect by means of a set of standards of binary alloys of Ni, Mn, Si, Cr, Ti, W, Al, V and C with Fe. Within each set the concentration of one alloying element varied over a wide range; the other elements had the same concentration. Spark and arc spectra of all the samples were photographed under identical conditions. The averaged results were then used to plot

$$\log I_{an} = f(\log C_{al}) \qquad (1)$$

and

$$\log \frac{I_{an}}{I_{Fe}} = f(\log C_{al}), \qquad (2)$$

where I_{an} is the intensity of the determined element line, I_{Fe} is the intensity of the comparison iron line and C_{al} is the concentration of the alloying element.

The principal results of the investigation are the following.

1. The diluting effect of the alloying element depends substantially on the light source used (see table). For example, the presence of more than 5% Mn or more than 0.4% Al in the sample leads to appreciable weakening of the matrix spectrum in the case of a spark source; with an arc source noticeable weakening of the matrix spectrum is observed only at 25% Mn and 13% Al.

2. The effect depends to some extent on the material of the counterelectrode, particularly when the sample contains Cr or C.

Maximum concentrations (in %) of alloying elements that do not weaken the iron spectrum

Source	Counter-electrode	Mn	Si	Cr	Ni	Ti	W	Al	V	C
Spark	Carbon	5,0	2,0	5,0	25,0	2,0	20,0	0,4	5,0	4,0
Arc	Carbon	25,0	23,0	5,0	25,0	18,0	20,0	13,0	24,0	4,0
	Copper	25,0	23,0	25,0	25,0	18,0	—	—	24,0	4,0

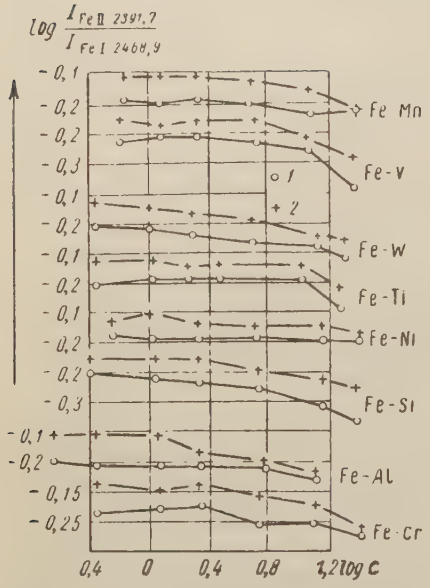

Fig.1. Relative intensity of the indicated iron line pair (proportional to the temperature as a function of the concentration of different "third" elements. Source - arc: 1) upper electrode carbon, 2) upper electrode copper.

3. A number of elements (Al, Ti, S & C) exert a substantial influence on the intensity of the matrix spectrum even at relatively low concentrations (0.4-4%).

4. Some alloying elements also influence the analytic results. Thus, for example, the results of determination of Mn in steel depend on the Si, Ni and C content; the results of determination of Mn, Ni and Si depend on the W content; the results of determination of Cr on the V content, etc. In most of these cases, the alloying elements do not noticeably weaken the matrix spectrum.

5. At the same time, some alloying elements weaken the matrix spectrum without affecting the analytic results as regards determination of other elements. This occurs when the intensity of the spectrum of the determined element varies with the concentration of the alloying element in the same way as does the intensity of the matrix spectrum. Such cases were observed in determination of Cr, Ni, Se and Mn in the Fe-Ti system, of Cr and Ni in the Fe-Si system, of Mn and Ni in the Fe-V system, of Ni and Si in the Fe-Al system, etc.

6. It follows from our data that almost all the investigated alloying elements have a specific individual effect on the stability of the matrix spectrum. This effect is not the result of dilution per se. We believe the effect is due primarily to the influence of the different elements on the structure of the alloy, leading to variations in the entry of the material into the discharge plasma.

The curves of Fig.1 show the variation of the arc discharge temperature (as indicated by the intensity ratio of the Fe II 2391.7 and Fe I 2468.9 lines) as a function of the concentration of different alloying elements. Generally, the arc temperature decreases with increase in concentration of the alloying elements; the decrease is particularly appreciable for the Fe-Si and Fe-W systems. For all systems, the arc with a copper electrode had a higher temperature than with a carbon electrode.

The variation of the absolute and relative line intensities of a number of alloying elements with the content of C and Si in the respective binary systems is shown in Figs.2 & 3.

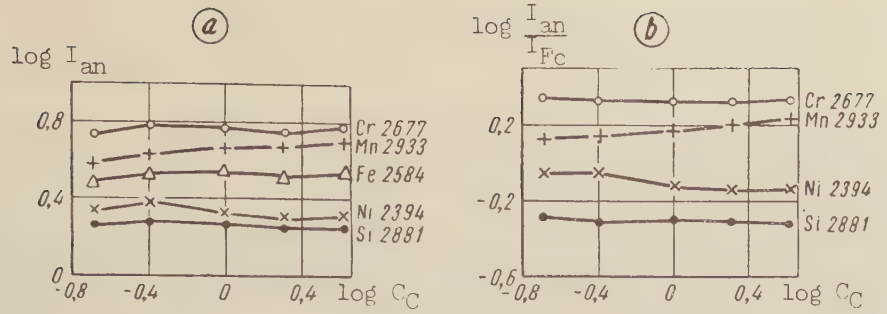

Fig.2. Variation of the absolute (a) and relative (b) line intensities of a number of alloying elements with the carbon content in the Fe-C binary system. Source - spark. Upper electrode - carbon. Reference line - Fe 2584 Å.

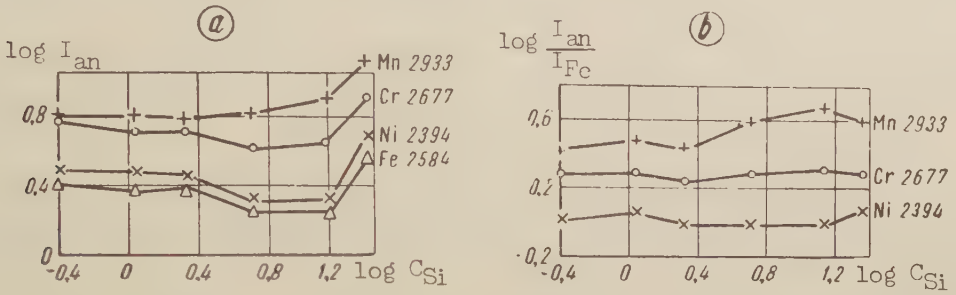

Fig.3. Variation of the absolute (a) and relative (b) line intensity of a number of alloying elements with the silicon content in the Fe-Si system. Source - spark. Upper electrode - carbon. Reference line - Fe 2584 Å.

References

1. A.N.Filippov, Spektral'nyi analiz i ego primenenie (Spectroscopic analysis and its applications), p.295, M., 1937.

2. S.L.Mandel'shtam et al, Zavodsk. laboratoriya, No.4, 447 (1936).

3. N.N.Sorokina, Izv.AN SSSR, Ser.fiz., 18, 2, 277 (1954).

4. D.Monterfield, F.J.Sykes & W.S.Sykes, J.Iron and Steel Inst., 1, 105 (1957).

RELATION BETWEEN THE DILUENT EFFECT OF "THIRD" COMPONENTS AND THE TRANSPORT OF MATERIAL IN LIGHT SOURCES FOR SPECTROSCOPY

- A.M.Borbat & A.A.Shishlovskii

The influence of "third" components in spectrum analysis is, in general, complex and many sided. In the present work, however, we shall consider it only from the standpoint of the diluent effect.

The concentration of a given element in a sample is frequently inferred from the relative intensity of the spectrum line of this element and a suitable line of the matrix; hence the analytic results must depend in general on the amount of the matrix element in the alloy. The last depends in turn both on the amount of the determined element present and on the amounts of third components[1]. It follows, first, that in the case of the diluent effect of "third" components only, the absolute intensity of the matrix line changes, while the intensity element line remains constant, and, second, that in carrying out analyses without taking this diluent effect into account (as is usually the case in industrial practice) the quantity of the matrix constituent in the standards must be constant, i.e., the total content of all other constituents except the "matrix" element must be constant or must vary within sufficiently narrow limits. The allowable limits of variation are considered in the present study.

For the purposes of the present investigation we chose aluminum and iron base alloys. First, we investigated the variation of the absolute intensity of the matrix line in a condensed spark spectrum with the content of the base constituent (matrix element).

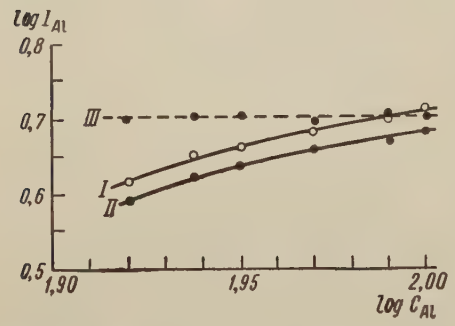

Variation in the intensity of the 2652.5 Å line of aluminum with its concentration in the sample: I - for a pair of self-electrodes, II - for a pure aluminum counterelectrode, III- for an aluminum counterelectrode in the case of absence of transport of its material.

The accompanying figure shows the variation in the intensity of the Al 2652.5 Å spectrum line with the aluminum concentration in the sample. The experiments showed that for a pair of self-electrodes, as might be expected, the line intensity varies in a consistent manner with the Al concentration (curve I). Somewhat unexpected, however, was the fact that in the case of a pure aluminum counterelectrode almost the same concentration dependence is obtained (curve II). At first glance it would seem that in this case the diluent effect of "third" components should be very weak. This "unexpected" result can be explained if we take into account the effect of material transfer in light sources. Pure metals, as is known, have a very high erosion resistance. Hence transport of material during sparking occurs primarily from the sample to the counterelectrode, and towards the end of the sparking period, the latter as regards composition of its surface layer becomes virtually identical with the sample, i.e., we have a case equivalent to that of a pair of self-electrodes.

To substantiate this inference we carried out experiments in which transport of material was artificially precluded, i.e., we reduced the exposure, eliminated presparking, increased the analytic gap and sharpened the counterelectrode to a point. It was found that in this case with a pure aluminum counterelectrode, the diluent effect of "third" constituents is absent (curve III). In the case of a graphite counterelectrode, however, the diluent effect was as strong as in the preceding cases.

Standard No.	Si	Cu	Mg	Mn	Fe	Zn	Al (base)
11	6,50	0,75	1,05	0,17	0,27	0,05	91,26
12	4,50	2,95	0,30	0,55	1,07	0,10	90,53
13	5,50	2,24	0,78	0,45	0,78	0,20	90,25
14	4,90	1,27	0,48	0,25	0,47	0,30	92,68
15	5,45	2,20	0,49	1,03	1,81	0,50	91,02

Similar experiments were carried out with iron base alloys. It was found that regardless of the kind of insert electrode - copper, aluminum, graphite or iron - the character of the diluent effect of "third" constituents in the presence of material transport was virtually the same. In cases when transport was suppressed, the diluent influence remained the same for copper, graphite and aluminum counterelectrodes, while in the case of an iron counterelectrode, it was absent.

Under the usual conditions of analysis there is always some transport of material and hence some diluent effect due to "third" constituents; consequently, the diluent effect must in general be taken into account. Actually, however, the concentration of the matrix element is usually high, while the concentration sensitivity of its spectrum lines, as a rule, is low. Hence one should attempt to choose a set of standards such that the error introduced by variation in the amount of the matrix element should not exceed three times the standard error of analysis[2].*

Such a set of standards can be used without taking into account the diluent infulence of "third" constituents. Thus we obtained a criterion for evaluating the allowable variation in the content of the matrix element in the standard and in the analyzed samples.

By way of concrete illustration let us consider the set of standards commonly employed for the aluminum alloy Al5. The chemical composition of standards Nos.11 through 15 is listed in the accompanying table. As we see, the variation in the amount of the matrix element, i.e., Al, relative to the mean content is 1.44%, which corresponds to a variation in the blackening of the Al line of ±2.1% and, according to Borzov and Sventipkii[3], is equivalent to an analytic error of ±4.5%.

Thus if the required analytic accuracy does not exceed ±4.5%, this set of standards can be used without taking into account the diluent effect of "third" constituents.

The above also allows of explaining the absence of a significant diluent effect of "third" constituents in the case of joint photographing of the spectra of the fifth and sixth UIM standards sets in a high-frequency spark with an iron counterelectrode[4]: our investigations showed that in a high-frequency spark from an induction type circuit there is virtually no transport of material to the opposite electrode; on the other hand, with a copper counterelectrode, the diluent effect of "third" constituents under the same conditions remains the same as before.

"T.G.Shevchenko" Kiev State University

References

1. N.N.Sorokina, Inform.-tekhn.listok (Tech. information bulletin), Leningrad, DNTP, No.6 (1956).

2. A.B.Shaevich, Zovodsk. laboratoriya (Industrial laboratory) 21, 3 (1955).

3. V.P.Borzov & N.S.Sventipkii, Inform.-tekhn. listok (Tech.information bulletin) DNTP, No.66 (1957).

4. K.S.Kudelya, Kievskoe gorodskoe soveshchanie po voprosam spektral'nogo analize (Kiev City Conference on the Problems of Spectrum Analysis), NTO, Priborprom (1956).

---

*Editor's note: It was established in Ref.2 that the systematic error in analysis should not exceed 1/3 σ.

VARIATION OF THE TOTAL INTENSITY OF SPECTRUM LINES WITH THE ATOMIC CONCENTRATION IN A PULSE DISCHARGE

- E. I. Vorontsov

1. Procedure and experimental conditions

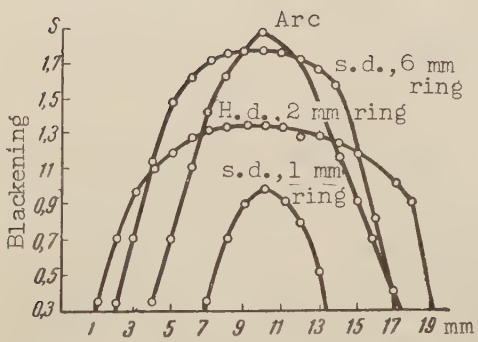

Fig.1. Variations in blackening over the length of the Si 2516 Å line in the spectrum of silumin for different pulse discharge conditions and for an ac arc.

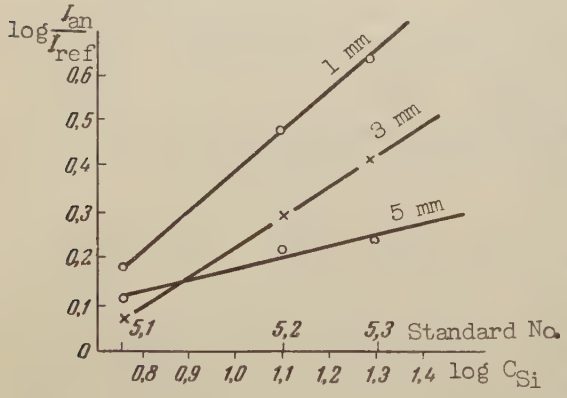

Fig.2. Working curves for determination of Si with different degrees of localization of the pulse discharge. The figures at the curve indicate the inside diameter of the localizing ring.

The present investigation of the relation between the spectrum line intensity and the atomic concentration in the discharge was based on the method of forced introduction of the electrode material into the spark gap by means of a pulse discharge localized on the surface of the sample by means of a restricting ring. As was shown in Ref.1, such localization limits the size of the discharge pits on the electrode, eliminates selectivity in entry of the material into the spark gap and suppresses the influence of "third" components. Forced introduction of a certain definite amount of sample material into the discharge, regardless of the gross composition of the electrodes, is a necessary condition for the investigation of the relation between the total spectrum line intensity and the atomic concentration. This follows directly from the results of investigation of deformation of the plasma depending on the character of the entry of the electrode material into the spark gap.

The pulse discharges were focused on the spectrograph slit with the electrodes horizontal. The results of measurement of the blackening along the Si 2516 Å line in the spectrum of silumin (Si-Al alloy) under different pulse discharge conditions and also for an ac arc are shown in Fig.1. The points were obtained at intervals of 1 mm along the line. For a "soft" pulse discharge localized by a flat ring with a 1 mm diameter opening and for the ac arc there is evident an abrupt decrease in blackening immediately to both sides of the central region of the radiating plasma. In the case of "hard" and "soft" discharges localized by a ring with an inside diameter of 6 mm, there is a central section with a relatively uniform emission. In this case self-reversal is clearly evident and is particularly strong near the ends of the spectrum line. This indicates considerable variation in the emission and absorption of the plasma.

Fig.2 shows the influence of the inside diameter of the localizing ring, deforming the discharge plasma under "soft" discharge conditions, on the slope of the working curves. These curves were plotted on the basis of the reduced concentration, i.e., the concentration referred to the actual content of the base element. It will be evident that the variations in slope are appreciable.

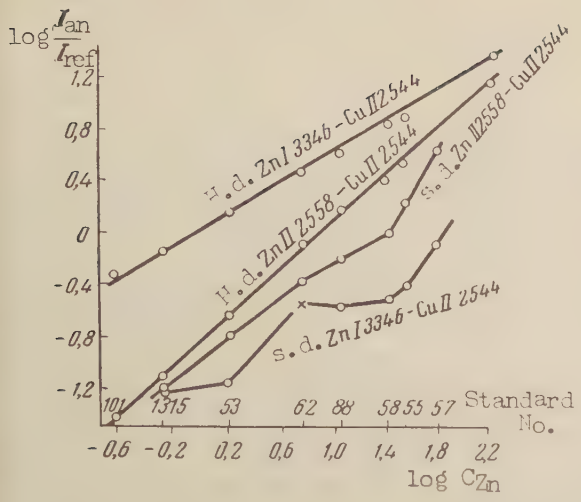

Fig.3. Working curves for determination of Zn in "soft" (S.d.) and "hard" (H.d.) localized pulse discharges.

Fig.3 gives the working curves for determination of zinc under "soft" and "hard" pulse discharge conditions. The analytic line pairs are Zn I 3346 & Cu I 2544 Å and Zn II 2558 & Cu II 2544 Å; the circuit capacitance in "soft" discharge operation was 48,000 μf, the inductance 0.55 mh; in "hard" discharge operation - 48,000 μf and 0.01 mh.

The experimental points for the arc line of zinc and "soft" discharge conditions do not fit a single straight line. Somewhat better results are obtained if the spark line of Zn is used. On the other hand, with "hard" discharge operation all the points for both spectrum lines fall on straight line plots.

The measurement of the size of the discharge pits on the electrode surfaces substantiated our inference regarding variation in the amount of material taken into the discharge depending on the composition of the samples. For example, the point identified by a cross on the lowest curve in Fig.3 pertains to a sample on which the discharge pit was exceptionally large. This shows that under "soft" discharge conditions one cannot fully stabilize the amount and rate of entry of the electrode material by localization of the discharge for any gross composition of the electrodes. Hence investigation of the variation of the spectrum line intensity with the concentration of the radiating atoms must always be carried out under "hard" discharge conditions. In this case the emitting atoms are distributed fairly uniformly in the discharge zone and the lines not subject to self-reversal should be more or less correctly described by homogeneous plasma theory.

2. Variation of the total intensity spectrum lines with the atomic concentration under "hard" pulse discharge conditions

Fig.4,a shows the working curves (2,3 & 4) for determination of Zn in brass and bronze in the range of concentrations from 0.39 to 62%. The element lines were the non-self-reversing spark lines Zn I 3346 Å and Zn II 2558 Å and the self-reversing arc line Zn I 3302.9 Å. The reference line in all cases was the spark line Cu II 2544 Å.

In addition, in Fig.4,a we give the curve (4) for determination of chromium in binary Cr-Ni alloys in the concentration range from 2 to 87%. This plot is based on the non-self-reversing Cr II 2855.7 Å line; the reference line was the spark line Ni II 2545.8 Å.

The curves in Fig.4,b show the variation of the total absorption as a function of the number Rl of absorbing oscillators in a column of 1 cm^2 cross section for different values of $d = \Delta\omega_L/\Delta\omega_D$, where $\Delta\omega_L$ is the Lorentz and $\Delta\omega_D$ is the Doppler line broadening.

It will be seen from Fig.4,a that a working curve with a slope of 45° was obtained for the Zn II 2558 Å spark line. The curve for the Cr II 2855.7 Å spark line has an initial slope of 45°, but the plot flattens out at a chromium concentration of about 20%. These plots are similar to the lower sections of the theoretical curves for $d>1$. The plot for the Zn I 3346 Å line is reminiscent of the upper part of the theoretical curves for $d>1$.

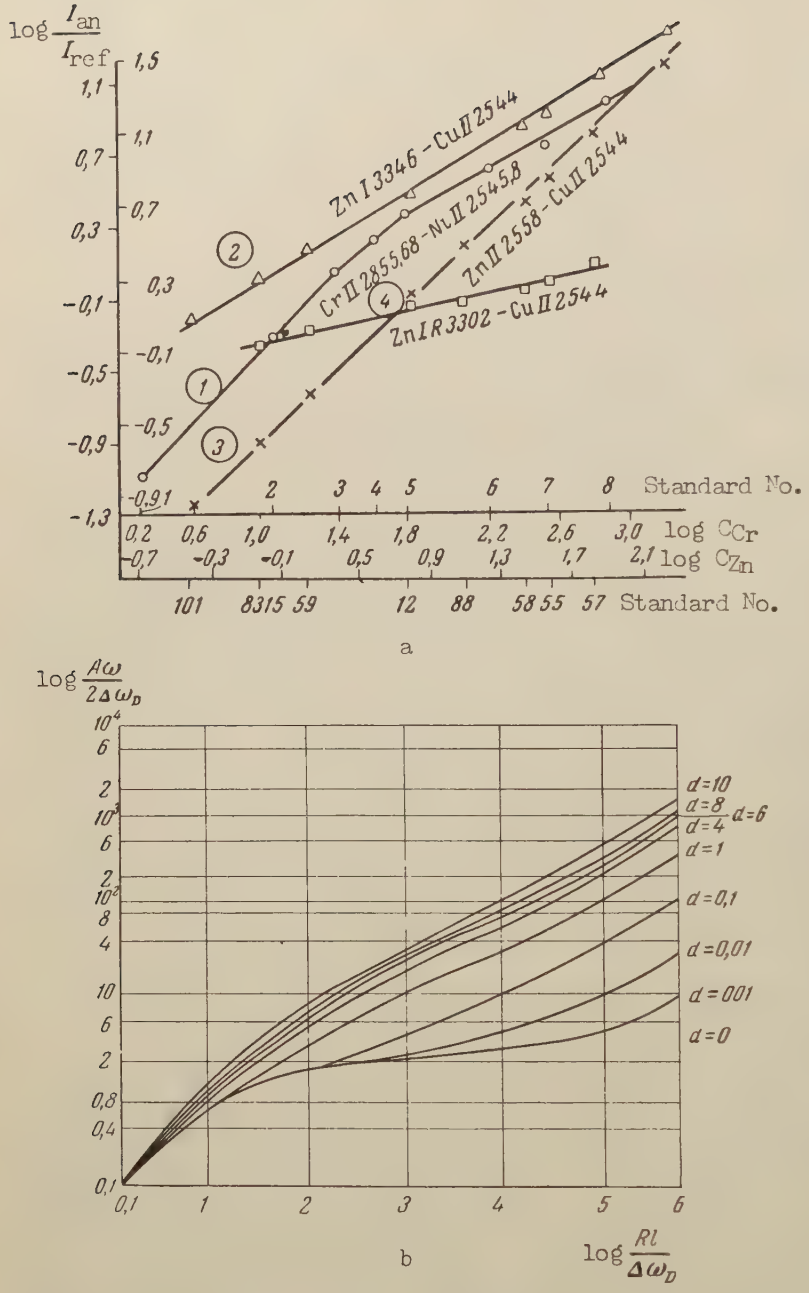

Fig.4. Comparison of the experimental working curves (a) for determination of Zn in brass and bronze and Cr in Cr-Ni alloys with the theoretical curves (b) characterizing total absorption.

Reference

1. E.I.Vorontsov, Zavodsk.laboratoriya (Industrial Laboratory), 10, 1180 (1953).

Apparently, the concentration of emitting atoms corresponds to the conditions for which only the upper part of the theoretical curves is applicable. The plot for the self-reversing Zn I 3302.9 Å arc line is flatter than the theoretical curves. Apparently, in this case absorption occurs in the central and cold outer layers of the plasma.

The practical interest of the present work stems from the theoretical possibility of obtaining working curves with a slope of 45° for spark lines up through relatively high concentrations of the determined element. This is substantiated by the plotted curves for analysis of steel, silumin and brass.

By way of illustration, in Fig.5 we show the curves obtained for determination of magnesium in silumin by means of the Mg II 2790.79 Å spark line and Mg I 2779.83 Å and Mg I 2852.12 Å arc lines. These curves illustrate the influence of the spectral origin of the lines on the slope of the working curves.

The use of spark spectrum lines also allows of enhancing the accuracy of analysis. These lines are relatively insensitive to variations in the geometric shape of the plasma.

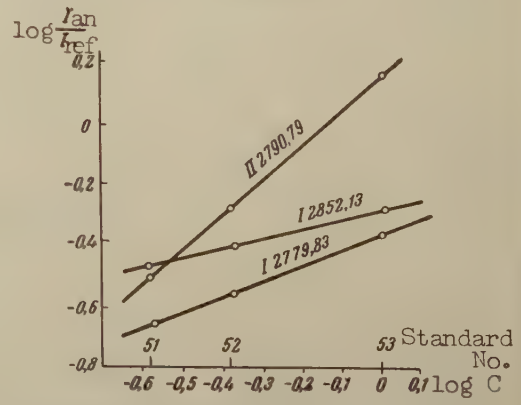

Fig.5. Working curves for determining Mg in silumin based on spark and arc lines.

INVESTIGATION OF THE CAUSES OF SELECTIVE DISINTEGRATION OF ALLOYS BY A SPARK DISCHARGE

- I.A.Grikit

It was established in earlier studies[1-4] that the action of a spark discharge results in selective disintegration of the sample surface, that is, there occurs preferential evaporation of the material from the weakest points: the grain boundaries and interdendritic spaces. It was suggested that the reason for this preferential disintegration of the grain boundaries is more frequent contact of the spark channel with individual carbides and intermetallides located on the crystallite boundaries.

However, the hypothesis regarding preferential contacts between the spark channel and the network of cast ledeburite [ledeburite = eutectic cementite-austenite mixture] carbides is invalidated, at least in the case of R18 steel, by our experimental data on forged samples in which fine carbides are rather uniformly distributed and the ledeburite eutectic network is thoroughly broken up. These experiments showed that in this case also there occurs selective destruction of the alloy surface with preferential entry of material from the grain boundaries. Selective disintegration of the sample surface is also observed for pure metals in which there are, of course, no carbides and intermetallide segregations.[4]

To check for the absence of selectivity in spark contacts with different materials, we carried out experiments involving sparking of joined (welded) plates of pure metals (armco, nickel) and metal-ceramic alloys consisting mainly of tungsten and titanium carbides.* The spark pit or spot after both short-term and prolonged sparking was located symmetrically to either side of the weld line; that is, there was no preferential contact of the spark channel with the carbide plate.

We carried out similar experiments with samples of armco iron, nickel and copper into which we pressed small pieces (0.3-0.5 mm^2 in cross section) of tungsten carbide. After grinding and polishing, these artificial "heterogeneous" alloys were subjected to sparking for 10 min. It was found that both the metallic "matrix" and the pressed in carbides were eaten away by the spark to the same extent.

An entirely different picture was observed, however, when the same carbides were pressed into lower melting point metals: Al, Zn, Mg or Sn. In this case, the metal surrounding the carbide plug was fused and evaporated by the action of the spark so that after the treatment the carbide plug projected above the disintegrated metal surface.

Some carbides have a melting or decomposition point close to the melting point of the parent alloy. Thus, for example, the melting point of $Cr_{23}C_6$ is 1550° (Ref.5), while the melting point of LK-4 alloy of which this carbide is a constituent is 1500°. The carbide Cr_3C_2 melts as it disintegrates.[6] Hence in the case of LK-4 alloy we do observe characteristic preferential removal of carbide particles at the grain boundaries and from the interdendritic spaces[1,2,4], inasmuch as the carbide in this case is more readily disintegrated than the alloy itself.

To obtain quantitative results, we measured separately the current flowing through a carbide and a metallic plate in a spark discharge. To this end we used electrodes consisting of plates of a pure metal (armco iron, nickel or copper) and a metal-ceramic hard alloy (VK-2) separated by a 0.3-0.5 mm thick mica insulator (see figure). The electrodes were connected to an IG-2 spark source. The current strength was measured by means of thermoelectric ammeters.

---

*VK-2 = 98% W carbide, 2% Co; T5K10 = 85% W carbide, 6% Ti carbide, 9% Co; T60K6 - 34% W carbide, 60% Ti carbide, 6% Co.

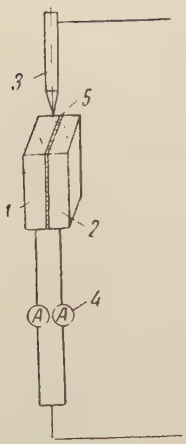

Arrangement for determining the current flowing as a result of contact of the spark channel with a carbide and a metal: 1 - pure metal, 2 - carbide, 3 - electrode, 4 - thermoelectric ammeters, 5 - mica.

It was found that the current in both circuits was virtually identical. Consequently, the spark channel makes equally frequent contact with the metal and the carbide. Hence the preferential destruction of crystallite boundaries in spark discharges is due to the lower melting point of the boundary material and perhaps to the higher mobility of atoms at interfaces.

References

1. I.A.Grikit, Spektral'nyi analiz metallov i splavov (Spectrum analysis of metals and alloys), M.-L., 1957.

2. I.A.Grikit, Transactions of the Tenth Conference on Spectroscopy, Vol.2, L'vov, 1958.

3. I.A.Grikit, Zavodsk. laboratoriya (Industrial laboratory), 23, 11, 1341 (1957).

4. I.A.Grikit, Dissertation, VIAM, 1957.

5. N.T.Gudtsov, Metallovedenie i termicheskaya obrabotka stali i chuguna (Handbook: Metallurgy and heat treatment of steel and cast iron), p.346, M.-L., 1956.

6. Tekhnicheskaya entsiklopediya (Technical encyclopedia) Vol.9, M., 1929.

INFLUENCE OF "THIRD" ELEMENTS IN SPARK SPECTROSCOPIC ANALYSIS OF MOLTEN ALLOYS

- L.E.Vvedenskii & V.I.Shekhobalova

Spectroscopic analysis of solid samples with spark excitation has a number of shortcomings which tend to reduce the reproducibility and accuracy. These shortcomings include the effect of sparking (temporal intensity variation), the influence of structure on the analytic results, the influence of "third" elements, and the influence of liquation.

Two ways of eliminating these deleterious influences are known: transfer of the sample into solution and analysis of the metal in the molten state. The former, naturally, greatly increases the total time required for analysis.

The molten metal procedure, proposed in 1941 by one of the authors[1], is promising but requires further research and development before it can be used for industrial purposes.

Solution of the problem of analysis of melts by the use of a stream of the molten metal[2] eliminates the influence of selective oxidation, segregation in the liquid phase and similar effects, but requires rigorous stabilization of the velocity of the stream, which so far has proved difficult to achieve in practice. Hence in the present work we used the procedure of a spark discharge between the stationary surface of the molten metal and a fixed carbon electrode.

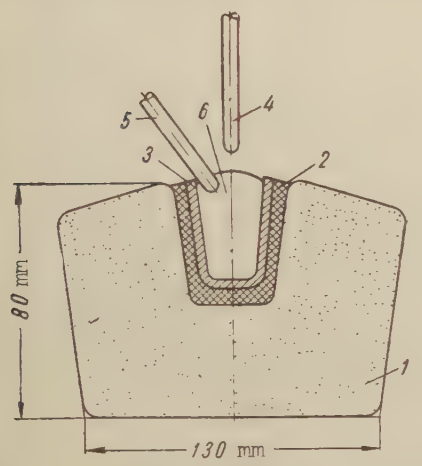

Fig.1. Double crucible for analysis of molten metals: 1) porpous ceramic, 2) asbestos, 3) graphite crucible, 4) fixed carbon electrode, 5) contact carbon electrode, 6) molten sample.

Apparatus and Procedure

The equipment consisted of an ISP-22 spectrograph, an IG-2 spark unit and a double crucible (Fig.1). After melting of the sample, the crucible was transferred from the furnace to the lower electrode holder of the ISP-22. The spark source was connected to the upper carbon electrode and through a contact carbon electrode to the molten sample.

The emulsion gamma was determined for each plate by photographing the spectrum with a 12-step weakener. The spectrograms were scanned on an MF-2 microphotometer.

For the purpose of the experiments we prepared five series of standards: 1) standards of duraluminum, 2) standards of aluminum-copper alloy (3 to 15% Cu), binary and doped with 6% Si, and 3) standards of aluminum-magnesium alloy (2 to 8% Mg), binary and doped with 5% Zn.

Investigation of the Reproducibility of Analysis of Duraluminum

The duraluminum spectra were excited using the following parameters in the Raiskii induction circuit (in the IG-2 source): C = 0.02 μf and L = 0.05 mh; the spark gap was 3.0 mm. The presparking time was 20 sec; the exposure time 30 sec.

The reproducibility δ evaluated on the basis of 50 spectrograms and expressed in percent of the given element is shown in the accompanying table (two-stage recording; second line of the pair in all cases: Al 2652 Å). As will be evident from the tabulated data, the reproducibility is approximately the same as in analysis of solid samples.

Reproducibility of analysis of molten duraluminum with spark excitation

Element	Line, Å	δ, %
Copper	3274	±4,8
Silicon	2516	±2,8
Magnesium	2779	±5,6
Iron	2599	±3,0
Manganese	2593	±2,3

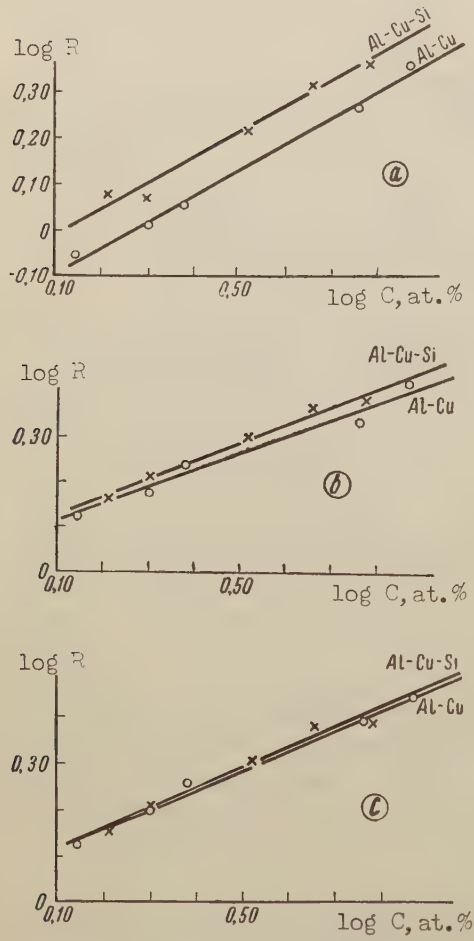

Fig.2. Influence of silicon on determination of Cu in Al-Cu alloys for solid samples (a) and molten samples at 660° (b) and 805° (c). Line pair: Cu 2246 - Al 2321 Å.

Effect of Sparking

The sparking curves for molten duraluminum showed that the sparking effect disappears completely for Cu, Fe and Si and is greatly reduced for Mg and Mn.[3] Apparently, by the time of ignition of the spark discharge selective oxidation has gone to completion and the effect of the spark does not substantially alter the composition of the oxide film.

In the case of a stream of molten metal, on the contrary, oxide films do not have time to form and the effect of sparking, also, is absent.

Diffusive effects in the case of molten samples play an insignificant role inasmuch as the rates of diffusion of the different elements in the melt are equalized.[4]

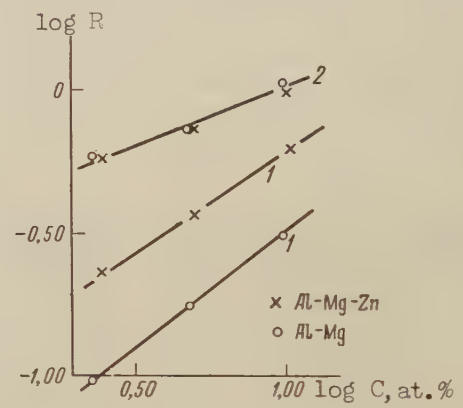

Fig.3. Influence of zinc on determination of Mg in Al-Mg alloys for solid samples (1) and molten samples at 770° (2). Line pair: Mg 2915 - Al 3050 Å.

Influence of "Third" Elements

In the experiments to determine the influence of "third" elements the Raiskii circuit parameters in the IG-2 source unit were C = 0.005 μf, L = 0.05 mh and gap = 3.0 mm. The presparking time for pairs of solid electrodes, cast in the form of rod ingots, was 1 min; that for molten samples with a fixed carbon electrode, 20 sec. The results for the Al-Cu alloy are shown in Fig.2; those for Al-Mg alloy in Fig.3. The spectrum of each standard was photographed four to six times.

Examination of the graphs shows that the influence of silicon on determination of copper in Al-Cu alloys virtually disappears at a melt temperature of 805°. Analogously the influence of zinc in analysis for Mg in Al-Mg alloys disappears at 770°.

Conclusions

1. Spectrum analysis of molten duraluminum samples with spark excitation can be realized with the same accuracy as analysis of solid samples.

2. The influence of "third" elements in spectrum analysis of molten aluminum alloys with reference to arc lines in a spark source disappears, which indicates that the influence of "third" constituents in a spark is connected with changes in the structure of the crystal lattice of the solid sample as the result of introduction of the "third" element into the binary alloy. Complete breakdown of the long range order in the metal by heating to 150-250° above the melting point eliminates the influence of the "third" elements.

3. Spectrum analysis of molten metals with spark excitation owing to the absence of the effect of sparking, the influence of structure and liquation, in cases when the influence of "third" elements is absent or negligible, is free of the systematic errors generally associated with analysis of solid samples.

4. It would be desirable to test the feasibility of analysis of molten metals by the photoelectric procedure. There is reason to expect increased accuracy of the photoelectric technique as a result of elimination of the errors and uncertainties connected with the state of the sample.

Moscow Aviation Technological Institute

References

1. L.E.Vvedenskii, Inventor's certificate No.74452 of 31 Jan.1949 - "Procedure and equipment for spectrum analysis of molten metals".

2. L.E.Vvedenskii, Izv.AN SSSR, Ser.fiz., 11, 281 (1947).

3. L.E.Vvedenskii & V.I.Shekhobalova, Trudy (Proceedings), Moscow Aviation Technological Institute, 1959.

4. V.V.Nalimov, Thesis, VNIIMS, Leningrad, 1956.

SPECTROSCOPIC INVESTIGATION OF ELECTROEROSION OF OXYGEN-CONTAINING TITANIUM

- N. S. Sventitskii & K. I. Taganov

Investigation of electroerosional disintegration of metals and alloys can be realized either by direct spectroscopic observation of the discharge producing the erosion or by obtaining the spectra of the transport products deposited on the counterelectrode. We investigated samples of titanium containing from 0.12 to 2.32% oxygen. All the samples had the same matrix and differed only as regards oxygen content and, consequently, hardness.

We were not able to detect in the spectra of the erosion producing discharge any indications that would allow of correlating the erosion stability of the titanium with the oxygen content. In the spectra of the transport products, however, the correlation could be established. In both cases the erosion of the samples was evaluated from the intensity of the titanium lines; the experiments were carried out with electric discharges in air.

In the absence of contacts between the electrodes in a spark or ac arc discharge there is observed a decrease of transport with increase in the oxygen concentration in the titanium (i.e., with increase in its hardness). This effect is evinced more stably if the samples are subjected to prearcing or sparking.

The differences in erosion stability stand out particularly clearly, however, in the case of contact-spark discharges. In this case the inverse dependence is observed: the transport of material increases with increasing oxygen concentration.

Calibration curves plotted in terms of "titanium line intensity vs oxygen concentration in percent" exhibit a relatively low concentration sensitivity and can serve only for evaluating the oxygen content. Observation of the regularities involved is of interest, however, since in this case we find the analytic criterion not in the oxygen spectrum but in the spectrum of the matrix (titanium). This makes feasible spectroscopic investigation of the physical-chemical properties of titanium on the basis of its electroerosional characteristics.

We carried out experiments on evaluation of the effect of polarity in contact-spark transport of titanium to copper counterelectrodes in air and in carbon tetrachloride. The effect was evaluated from the ratio of the intensity of the Ti 2531.25 Å line in burning in an arc of the transport product from the cathode to the intensity of the same line in burning the transport product from the anode (I_-/I_+).

It was found that in erosional discharges in air this ratio was 0.8 for a sample containing 0.12% oxygen and 0.5 for one containing 2.32% oxygen. In case of transport in carbon tetrachloride the respective ratios are 2.0 and 1.6. Thus the polarity effect is clearly evident: in air the anode is subject to the greatest disintegration; in carbon tetrachloride - the cathode.

It was noted that the presence of calcium in the titanium samples noticeably affects the excitation of the spectrum of the oxygen present. Evaluation of the effect of polarity in contact-spark transport showed that in this case the opposite regularity obtains: in air the cathode is subject to the most rapid disintegration; in carbon tetrachloride - the anode (the calcium content in the samples varied from 0.3 to 0.9%, the oxygen content from 0.3 to 0.8%.)

Hence we felt it would be of interest to determine the thermoelectric properties of titanium samples with different percentages of oxygen and different calcium contents. We found that there is a nearly linear relation between the oxygen content and the strength of the thermal current developed in the contacting copper-titanium couple. The results obtained for a titanium sample without calcium and with a minimal amount of oxygen fit the calibration curve plotted in "thermal current" vs "oxygen concentration" coordinates for the samples containing differ-

ent amounts of calcium; the other calcium free titanium samples (those containing more than the minimal amount of oxygen) yield individual curves deviating from the above.

Thus, in addition to showing the possibility of evaluating the oxygen content in titanium on the basis of its electroerosional properties by spectroscopic observation, we have established the possibility of checking the oxygen content of titanium samples on the basis of their thermoelectric properties.

* * * * * * * * *

SPECTROSCOPIC INVESTIGATIONS OF THE EFFECT OF POLARITY IN ELECTRIC EROSION OF METALS

- K. I. Taganov

The effect of polarity in electric erosion of metals is evinced in the different rate of disintegration of the electrodes of different polarity. With changes in the different discharge parameters, there may occur inversion of the electric erosion, i.e., reversal of the sign of the polarity effect.

Earlier we showed that such inversion may occur in an arc discharge as a result of change in the size of the interelectrode gap.[1] Thus in the case of a copper counterelectrode, iron as the cathode was eroded to a greater degree than iron as the anode with gaps up to 1.5 mm. When the interelectrode distance exceeded this value, the sign of the polarity effect was reversed. Later we observed variations in the effect of polarity of erosion also in contact-spark discharges with changes in composition of the counterelectrode or the magnitude of the inductance in the spark circuit.[2]

In the present work we investigated some new factors influencing the polarity effect. The experiments were carried out by the counterelectrode procedure.[1]

The effect of polarity was evaluated quantitatively on the basis of the ratio I_-/I_+), where I_- is the intensity of a chosen line in the spectrum of the products transported from the cathode and I_+ is the intensity of the same line in burning the products transported from the anode. The transport was realized to copper counterelectrodes from the same samples.

We investigated the transport of zinc, iron and molybdenum, i.e., metals differing substantially as regards their resistance to electric erosion, in a low voltage pulse discharge. The experiments showed substantial quantitative differences in transport from the cathode and from the anode with changes in the discharge parameters.

Increase of the interelectrode gap (at a voltage of 260 v and a discharge circuit capacitance equal to 1000 μf) leads in all cases to decrease of the material transport, particularly from the anode. For zinc in the same range of variation of the interelectrode gap (from 0.3 to 1.5 mm), the transport from the cathode remained virtually constant. This indicates predominance of the jet mechanism in the entry and transport of the material from the cathode in this type of discharge.

Of considerable interest is variation in the character of the transport as a function of the polarity in the case of a pulse discharge localized on the surface of the investigated metal. For localizing the discharges we used insulating bushings 1 mm thick with a central 1-2 mm diameter opening.

For all the investigated metals, the transport increased with localization of the discharge, which is undoubtedly connected with concentration of the discharge energy on a limited section of the metal surface. With localization there

was also observed a substantial difference in transport from the cathode as against the anode.

Localization of the discharge has a greater effect on increase of transport from the anode; in this case there is sometimes even observed inversion of the polarity effect. Thus, whereas the relative intensities of a number of spectrum lines of molybdenum, iron and zinc are concerned, the values of I_-/I_+ without localization of the discharge were equal to 8.1, 1.2 and 1.6, respectively, with localization the ratios were 0.4, 0.85 and 0.4 (voltage 260 v, capacitance of the discharge circuit 270 μf).

All these factors and effects should be borne in mind in choosing the optimum conditions for the use of low voltage pulse discharges as a light source for spectrum analysis.

Of independent interest are spectroscopic investigations of the effect of polarity in contact-spark transport. This is important both for selection of conditions for the burning of samples in spectrum analysis and for choice of the optimum parameters in electric discharge machining. Our experiments showed that a significant role in the polarity effect in contact-spark erosion of metals is played by processes occurring in the contact zone of two different metals. By way of illustration, one can cite the case of contact-spark transport in air from a bismuth electrode and an electrode of bismuth alloy with 5% tin onto a copper counterelectrode. Bismuth and the bismuth-tin alloy in contact with copper at the given polarity have opposite signs of the Peltier effect.

As evaluated from the I_-/I_+ ratio (Bi 3067.7 Å line), it was found that in the copper-bismuth case the transport from the anode exceeds the transport from the cathode by a factor of 2.5, while in the second case (copper-bismuth alloy with tin) the transport from the anode exceeds the transport from the cathode by 6.3. Consequently, the disintegration of the anode increases sharply with the addition of 5% tin.

In interpreting the observed regularities we recall that in an electric discharge preferential evolution of heat occurs at the anode. If the transport is realized from the anode and Peltier heat is evolved in the discharge, the amount of transported material increases as a result of volatilization by this additional heat. If the Peltier heat under these conditions is of opposite sign, i.e., if there is Peltier cooling, the transport of material is reduced. The given phenomenon will act in the opposite sense in the case of transport from the cathode, thereby further enhancing the effect of polarity.

We investigated the correlation between the spectroscopic evaluation of the magnitude of contact-spark erosion and the thermoelectric characteristics of the contacting metals. We measured the thermal current passing through a contact of the metal electrode with the investigated metal heated to 150°. In a number of cases we were able to establish a direct correlation between the magnitude of the thermal current and the concentration of a particular element. Moreover, the direction of the thermal current or the character of its variation in magnitude was found to be uniquely related with the experimentally observed change in the effect of polarity in electric erosion.

In conclusion, we note that checking of the composition of alloys by measuring the thermal current may serve as a useful auxiliary procedure in spectroanalytic classification or sorting of alloys. Measurement of the thermal current may also serve as a means for checking and taking into account the influence of the Peltier effect on the results of spectroscopic analysis where the sampling is realized by the contact-spark procedure.

References

1. K.I.Taganov, Izv.AN SSSR, Ser.fiz., 14, 634 (1950).
2. M.G.Mal'tsev, E.A.Ptitsyna & K.I.Taganov, Materialy X Vses. soveshchaniya po spektroskopii (Transactions of the Tenth All-Union Conference on Spectroscopy Vol.II, p.252, L'vov, 1958.

* * * * * * * * *

USE OF THE CONTACT-SPARK SAMPLING TECHNIQUE IN SPECTROANALYTIC STUDIES

- V.S.Burakov & A.A.Yankovskii

In the present work we used the contact-spark sample dosage technique[1] for investigating the variation of the spectrum line intensity with the amount of sample material burned in the spark or arc and the electric parameters of the light source.

The magnesium, zinc, iron and aluminum samples were picked-off and transferred to a copper electrode with capacitances of 20, 40, 80 and 160 μf in the contact-spark sampling circuit. The conditions of sample pick-off, burning the sample and photographing the spectra have been described earlier[2]. The amount of sample material taken up and transported to the copper electrode was determined by dissolving it in acids and subsequent spectrum analysis of the solutions.

It was established that with increase of the capacitance in the above mentioned range the amount of transported material increases most for magnesium and least for aluminum. Specifically, with C = 80 μf there were transported 0.14 mg magnesium, 0.10 mg zinc, 0.035 mg iron and 0.025 mg aluminum during the same sparking period. Tests showed that the amount of material picked-off can be controlled by varying the other electric parameters (V and L) of the contact-spark circuit.

The samples were burned in spark and arc sources; the line intensity was compared with the amount of transported material. For a low voltage condensed spark the relation between the spectrum line intensity and the amount of material burned in the source is more nearly linear, as a rule, than for an arc and a low voltage spark; this is probably due to the stronger reabsorption in the latter sources. Hence in using the contact-spark sampling technique[1] it is probably expedient to perform the subsequent analysis with excitation by a low voltage spark.

Naturally, the electric regime of the source has a significant influence on the intensity of the spectrum lines. Thus an increase in the current strength from 1 to 10 amp results in an increase in the intensity of the lines of Mg, Zn and Fe by a factor of 2 to 5. A similar increase in the line intensity of these elements in a low voltage spark occurs with increase of the circuit capacitance from 12 to 72 μf and in a high voltage condensed spark with an increase of C from 0.005 to 0.02 μf. Our tests showed that when bulk samples are used the dependence of the line intensity on the electric regime of the source is much stronger. This is presumably connected with change in the amount of material taken up into the discharge.

The observed increase in line intensity in burning dosed samples can be related with variation in the temperature conditions in the discharge. For two close electric regimes of the source, the ratio of intensities of the spectrum lines is described by

$$\log \frac{I_1}{I_2} = C(N,T) + 0.43 \frac{T_1 - T_2}{kT_1T_2} E_i, \quad (1)$$

where I_1 and I_2 are the intensities of the chosen spectrum lines in the compared regimes, C(N,T) is a function of the concentration of the material and the temperature in the discharge for the compared regimes, and E_i is the excitation energy of the upper level.

From the observed increase in the slope of the log (I_1/I_2) vs E_i plots it follows that the temperature of the discharge increases with increase of the arc current. In view of this the intensity of the Mg, Zn and Fe lines increases.

The variation in the line intensity in spark sources is also apparently associated with variation in the temperature conditions of the discharge. In practice, application of Eq.(1) is greatly hampered by the variation of temperature both in time and in different sections of the luminous discharge cloud.[3]

In a low voltage spark there are realized more favorable conditions for the excitation of arc and, particularly, spark lines. For example, in the case of burning of the same amount of magnesium, the intensity of the Mg II 2929 Å line in the low voltage spark is approximately 10 times higher than in an arc and 4 times higher than in a high voltage spark.

Thus investigation of the burning of dosed amounts of material picked-off in contact-spark sampling shows that by appropriate variation of the electric parameters of the light source one can substantially enhance the sensitivity of analysis. Moreover, in the case of copper base alloys the dosed spark sampling procedure virtually eliminates the influence of the "third" elements.[1-4]

References

1. K.I.Taganov, Sb.dokl. I n.-t.konf. po spektr.analizu (Collected reports of the First Scientific-Technical Conference on Spectrum Analysis), Minsk, 1956.
2. V.S.Burakov & A.A.Yankovskii, Doklady AN Belorussian SSR, 2, 156 (1958).
3. L.Huldt, Spec.Acta, 7, 264 (1955).
4. V.S.Burakov, Inzh.-fiz.zhur. (Engin.-Phys. Journal), 1, No.8, 46 (1958).

ANALYSIS OF AN OPTICAL SYSTEM FOR A MIRROR SPECTROGRAPH WITH LARGE PLATE LENGTH

- S.A.Khrshanovskii

Use of plane diffraction gratings[1] in conjunction with mirror optics makes it possible to design high quality spectrographs covering a wide range of the spectrum and at the same time possessing appreciable angular and linear dispersion[2-4]. The length of a flat plate in such instruments, however, usually does not exceed 200-220 mm, which in some cases is insufficient for certain spectroscopic purposes, for example, for investigating particularly complex spectra, etc.

In view of this we undertook a theoretical and experimental investigation of different plane grating spectrographic systems for the purpose of clarifying the possibility of designing spectrographs with a large plate length without sacrifice in the quality of the spectrum line image. In the initial stage of the study we turned to an investigation of the properties of the most commonly employed mount, which, according to the accepted system of classification[5], is called the vertically symmetric design (Fig.1).

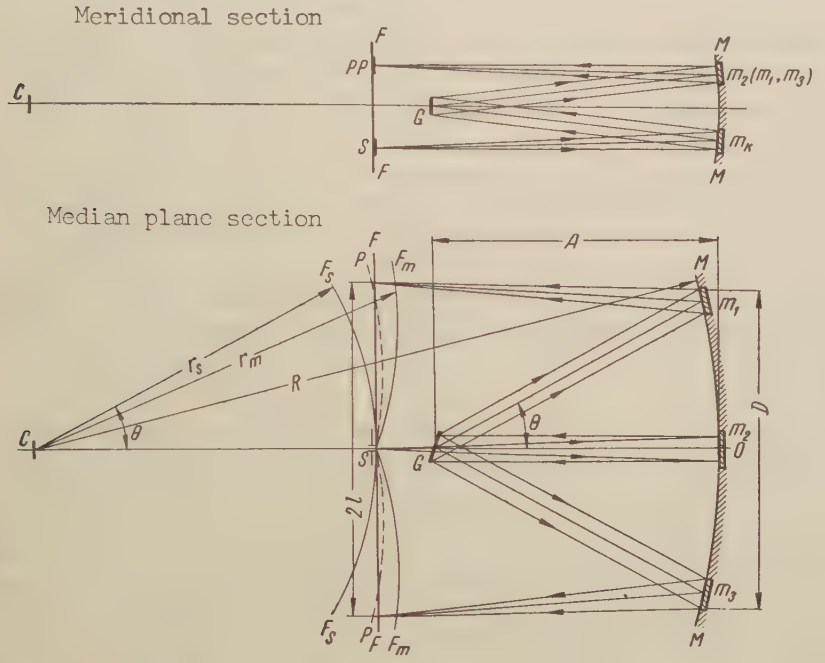

Fig.1. Vertically symmetric spectrograph design[5,6]: C - center of curvature of the mirror sphere (objective) M-M with radius R, S - entrance slit, G - dispersing element, located at a distance A from the center O of the spherical mirror, F-F - gaussian plane of the optical system, F_m-F_m & F_s-F_s - theoretical astigmatic focal surfaces (the formulas for their radii vectors are given in the footnote), P-P - surface of best focusing, $2l$ - length of photographic plate, θ - angle of deflection of the dispersed beam, m_k - collimating mirror, m_1, m_2 & m_3 - camera mirrors (see Fig.2), which are sections of one large spherical mirror surface M-M with a total working length D.

Design analysis of the theoretical focal curve* carried out for different versions of the system showed that the shape of the F_m-F_m, F_s-F_s and P-P curves (see Fig.1) and the degree of their deviation from the gaussian plane F-F depends greatly on the position of the dispersing element, i.e., on the distance A. A great advantage of the system under consideration is that for given values of the radius R and plate length $2l$ one can obtain a practically acceptable distance A for which a spectrum of reasonably good quality is focused on one long flat photographic plate (or a number of flat plates set side by side). If one

---

*For convenience we give the formulas for these focal curves, which we deduced earlier[6]:

$$r_m = \frac{R}{2}\sqrt{1+3c^2\sin^2\theta}; \qquad c = \frac{R-A}{R};$$

$$r_s = \frac{R}{2}\,\frac{1}{\sqrt{1-c^2\sin^2\theta}}; \qquad \theta = \alpha - \beta;$$

here α is the angle of incidence on the grating and β is the angle of diffraction.

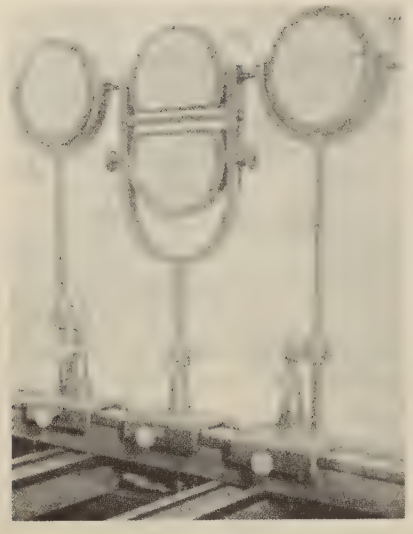

Fig.2. Mirror assembly of the experimental photographic set-up.[5]

accepts a noticeable curvature of the focal surface, then one can obtain an extremely long plate length with a high quality image. This is realized by increasing the distance A, the upper bound for which, however, in going over to values of A > R/2 is soon imposed by practical design factors[8].

The quality of the line image in spectrographic systems with an enhanced plate length was investigated on a special experimental set-up[5]. The essential part of this set-up is the mirror assembly (see Fig.2) comprised of spherical mirrors, one collimating mirror m_k and three camera mirrors, m_1, m_2 and m_3 (see Fig.1). All these mirrors have the same radius of curvature and are adjusted so that their reflecting surfaces lie on a single common sphere. The side camera mirrors m_1 and m_3 can be displaced sidewise to a distance of at least 0.5 meters from the central mirror m_2, which allows of obtaining photographs of narrow sections of the spectrum corresponding to the edges of one meter-long photograph. In the accompanying table we give some of the results obtained on the set-up; these characterize the quality of the image attainable in an optical system with the following parameters: $f'_{camera} = f'_{coll.}$ = 3000 mm; relative aperture 1:40; State Optical Institute 600 lines/mm plane grating; reciprocal linear dispersion in the first order 5.6 Å/mm; slit height 10-15 mm. From the data in the table one can evaluate the quality of the image obtained with different values of the parameters A and l.

Distance mm		Resolved iron lines	Separation between lines		Quality of image (sharpness of lines)
A	l		$\Delta\lambda$, Å	Δl, mm	
2800	0	3025,638—3025,842Å	0,20	0,035	Good
2800	260		0,20	0,035	Somewhat impaired
2800	0	3041,639/3041,738—3042,022Å	0,33	0,060	Good
2800	260		0,33	0,060	
2800	500		0,33	0,060	Slightly impaired but acceptable
1500	0		0,33	0,060	
1500	0	3099,971—3100,666—3100,304Å (triplet)	0,35—0,43	0,065—0,075	Approximately as above
1500	260		0,35—0,43	0,065—0,075	Noticeably impaired
1500	500		0,35—0,43	0,065—0,075	Strong diffusion

Our study shows that vertically symmetric mirror systems have an appreciable reserve of "quality", which makes it feasible in principle to utilize systems of this type for the design of spectroscopic instruments (spectrographs, polychromators and the like) with a great length of the simultaneously recorded plane spectrum.

References

1. F.M.Gerasimov, Izv. AN SSSR, Ser.fiz., 18, 662 (1954) (Trans.Bulletin 18, No.6, 345.); Optika i spektroskopiya, 4, 779 (1958).
2. S.A.Khrshanovskii, Tezisy IX nauchnoi konferentsee Leningradskogo instituta tochnoi mekhaniki i optiki (Program of the Ninth Scientific Conference at the Leningrad Institute of Precision Mechanics and Optics), p.10, L., 1954.
3. V.K.Prokof'ev, Izv.AN SSSR, Ser.fiz., 18, 643 (1954) (Trans.Bulletin 18, No.6, 330); Ibid., 22, 737 (1958) (Trans.Bulletin 22, No.6, 732.)
4. R.F.Jarrell, JOSA, 45, 259 (1955).
5. S.A.Khrshanovskii, Trudy (Proceedings), Leningrad Institute of Precision Mechanics and Optics), No.27, p.94 (1958).
6. S.A.Khrshanovskii, Ibid., No.19, 97 (1956).
7. S.A.Khrshanovskii, Izv.vysshikh uchebnykh zavedenii MVO SSSR; Priborostroenie (Bulletin, Higher Institutions of Learning, Ministry of Higher Education; Instrument Building), No.5, 141 (1958).
8. S.A.Khrshanovskii, Ibid., No.6, 72 (1958).

* * * * * * * * *

PHOTOELECTRIC EQUIPMENT FOR THE ISP-22 SPECTROGRAPH. A NEW METHOD OF AUTOMATIC SPECTROSCOPIC ANALYSIS OF ELECTROLYTES

- Yu.A.Yakobi & S.I.Maksimov

The photoelectric accessory for the ISP-22 spectrograph consists of a photoelectric attachment and two separate recording units of different types. The attachment contains one entrance slit which can be moved along the spectrograph guide rail to discriminate any desired spectrum line. Precise setting is made by means of a micrometer screw; play is eliminated by a spring assembly. The light beam entering the accessory slit is detected by an FEU-18 photomultiplier, which is rigidly mounted in the slit housing. A spectrogram photographed on the same spectrograph and mounted on the outside of the attachment serves as the setting guide. The slit housing also carried a wavelength indicator and magnifier. Precise setting of the slit is made with reference to an optical indicator tube (6E5), the control grid of which is coupled with the photomultiplier output. The initial wavelength setting of the entrance slit is realized either visually in the visible part of the spectrum or by means of a mercury tube and the indicator in the ultraviolet. Light scattered in the spectrograph is used as the reference signal.

The use of a photomultiplier to detect the radiation made it possible to utilize relatively simple recording circuits. The first version of the recording unit operates on the principle described in Ref.1. The circuit incorporates a dc amplifier with feedback, which is cut off during the measurement. The unit is characterized by a high degree of stability (instrument error - 0.3%) and maintains a constant reading value with variation of the absolute signal intensity in a 1 to 50 range. To stabilize the photomultiplier sensitivity between readings it is illuminated by a small glow lamp mounted in the spectrometer housing.

The second recording unit operates on the principle utilized in the work of Hasler et al[2], but differs from the unit described by Hasler in that it has only one scaling channel, an analytic one. The advantage of this variant is its simplicity. It consists essentially of a small attachment to a standard scaling unit. The instrument error of this recorder is 0.8%.

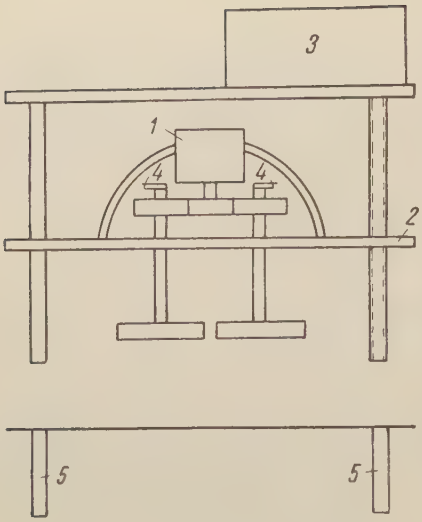

Diagram of electrolyte sampler unit.

The photoelectric accessory as a whole was tested for stability by discriminating the Cu I 2618.4 Å line excited in a 0.4 amp arc. The error of the first recorder was 0.5%; that of the second 1%. The equipment was then used for determining copper in lead in the concentration range from 0.0025 to 0.16%.

The potentialities of photoelectric spectroscopic equipment can be utilized to the full only in conjunction with automation of the entire process of taking and preparing the samples. We undertook an attempt to realize an automatic unit for analysis of electrolytes. We tested different ways of obtaining a discharge directly on the surface of the electrolyte. We demonstrated the possibility of realizing a discharge between two streams of the electrolyte; however, the brightness of the discharge in this case is very low because the major part of the voltage drop occurs in the electrolyte and also because of the negligibly low thermionic emission from the surface of the solution.

We developed a method based on the use of an auxiliary insert electrode; the metal is deposited electrolytically on this electrode and then the same electrode serves for excitation of the spectrum. After the analysis, the insert electrode is electrolytically cleaned to remove the coating and is thus made ready for the next analysis.

The use of this method enhances the sensitivity of analysis. As a result it becomes possible to reduce the discharge current and hence the erosion of the electrodes. The electrolytic cleansing procedure provides for complete removal of the preceding sample without recourse to mechanical abrasion or chemical reagents. In view of the fact that the discharge is realized on the electrolytic coating and the current is very weak, the insert electrode is well protected against the disintegrating action of the discharge, particularly with a sufficiently thick coating. For this reason possible contamination of the insert electrode plays no significant role.

A diagram of the sampler is shown in the accompanying figure; the sampling section consists of two graphite disk electrodes rotating in the horizontal plane. Rotation of the electrodes minimizes erosion and gives rise to favorable conditions for obtaining a compact coating at high current densities. Graphite disks are highly resistant to chemical and electrochemical action of the zinc electrolyte. The graphite disks are rotated by the motor 1 at the rate of 60 rpm. The motor is mounted in shelf 2, which can be raised and lowered by the reversing motor 3. The electrolysis and discharge voltages are brought in to the terminals 4. Auxiliary graphite electrodes (5) are mounted in the electrolytic bath to both sides of the sampler. Complete automation of the unit can be realized by appropriate electro-mechanical programing of the equipment.

The apparatus was used under laboratory conditions for determination of cadmium in a zinc electrolyte. The volume of the bath was 3 liters (flow through electrolyte). The density of the electrolysis current was 4200 amp/m^2. The arc current - 0.5 amp. The measurement error was ±5%.

References

1. R.Carpenter, E.DuBois & J.Sterner, JOSA, 37, 707 (1947).
2. M.F.Hasler, R.W.Lindhurst & T.W.Kemp, JOSA, 38, 789 (1948).

NEW PHOTOELECTRIC SPECTROGRAPHIC EQUIPMENT

- M.M.Averbukh, N.V.Artsishevskaya, N.V.Belyaev, I.I.Erina, D.I.Pen'kov & I.G.Strel'tsov

As part of a continuing program of research and development[1] there were recently designed two new four-channel instruments, the FESA-4 and FESA-4M. The recording arrangement in the new equipment differs from that used in earlier equipment in that battery supply of the amplifier is replaced by a regulated rectifier.

FESA-4 Instrument

Fig.1. FESA-4 installation.

The equipment consists of two units comprising a DG-2 arc power supply, a three-lens condenser system, the optical part of an ISP-52 spectrograph with a UF-84 camera and UF-61 collimator, a system with four entrance slits for disciminating the selected spectrum lines, and four StsV-4 photocells coupled to storing systems. The indicating instrument is an M-91 microammeter. The equipment is automated in the sense that the entire operation of the arc (ignition, preburning, exposure and switching off) is realized by a system of relays. The general appearance of the installation is shown in Fig.1.

Tests showed that the relative instrument error of the equipment does not exceed 0.5%. The results of test analyses of ferrous metals are shown in Table 1. The relative error indicated in the last column pertains to samples containing medium concentrations of the determined element.

Table 1

Results of tests of the FESA-4

Analyzed material	Determined element	Interval of determinable concentrations, %	Relative error,%
Malleable cast iron	Chromium	0.036-0.11	6.0
ShKh steel	"	1.02-1.70	2.3
High speed steel	"	3.52-7.50	2.5
Special grade case iron	"	2.0	2.6
Malleable cast iron	Manganese	0.23-0.49	5.1
ShKh steel	"	0.58-1.28	2.6
G-13 steel	"	8.86-14.0	1.4
Special grade cast iron	"	0.8	4.0
High speed steel	Tungsten	4.48-18.46	3.0
	Vanadium	0.82-3.12	3.6
Special grade cast iron	Nickel	16.50	1.8

The exposure time can be varied from 45 to 90 sec. The total time required for analysis of three elements from the time of delivery of the sample to the laboratory is ~5 min.

FESA-4M Instrument

This equipment consists of four separate assemblies and differs from the FESA-4 as regards the optical system and design and arrangement of the individual units (see Fig.2). The spectroscopic section is based on the optics of the SL-3 Steeloscope. The instrument has provision for regulating the spectrum line intensity by means of a system of step weakeners. The equipment is appreciably simpler than the FESA-4 as regards fabrication, operation and adjustment.

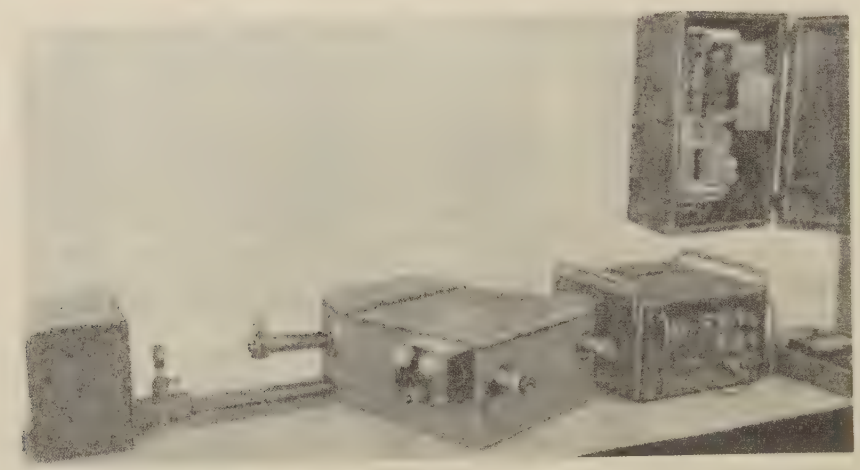

Fig.2. FESA-4M equipment.

Table 2

Results of tests of the FESA-4M

Analyzed material	Determined element	Interval of determinable concentrations,%	Relative error,%
Malleable cast iron	Chromium	0.036-0.20	5.5
Grey iron	"	0.19-0.68	4.3
Structural steel	"	0.7-1.88	4.3
Malleable cast iron	Manganese	0.23-0.70	5.0
Grey iron	"	0.45-1.23	4.0
High speed steel	Tungsten	4.10-11.57	3.3
	Vanadium	0.82-3.10	5.6
	Zinc	3.46-8.80	4.0
OTsS 5-5-3 bronze	Tin	2.07-4.73	6.7
	Lead	2.65-6.67	3.6

The results of tests of the FESA-4M for routine analyses of ferrous and nonferrous metals are shown in Table 2. The exposure time can be varied from 25 to 60 sec. The total time required for determination of three elements from the time of delivery of the sample to the laboratory is ~4 min.

Scientific Research Institute of Automobile Industry Technology

References

1. M.M.Averbukh, L.M.Ivantsov & A.V.Kandinov, Zavodsk. laboratoriya (Industrial Laboratory), No.1, 57 (1954); M.M.Averbukh, N.V.Artsishevskaya, N.V.Belyaev, A.V.Butuzov, A.S.Davydov, S.V.Kutovoi & I.G.Strel'tsev, Ibid., No.1, 62 (1954).

ANALYSIS OF HEAT RESISTANT AND LIGHT ALLOYS AND STEELS BY THE PHOTOELECTRIC PROCEDURE

- K.A.Sukhenko, K.A.Moiseeva, L.D.Metalina, I.G.Tishin, N.V.Penkina & D.G.Bakanov

In view of the fact that spectroscopic analysis of certain alloys was inadequate to meet the industrial requirements, we developed analytic procedures based on the use of a photoelectric steelometer bearing in mind that with the steelometer one can determine the various elements only in sequence[1].

Analysis of nickel alloys

Table 1

Alloy	Current, amp	Arc gap, mm	Counterelectrode material (8mm dia)	Slit width, mm	
				entrance	exit
Nickel	3	1.5	Copper	0.025	0.07
Aluminum	3	1.5	"00" aluminum	0.03	0.08
Magnesium	2	1.5	Pure magnesium	0.03	0.08
Steels	3	1.5	Copper	0.025- -0.03	0.08- -0.115

In analysis of nickel base alloys, the aluminum was determined on the basis of the Al 3961.52 Å line and the titanium with reference to the Ti 4681.9 Å line. The most accurate results were obtained with a copper permanent electrode with a hemispherical tip. We also tested nickel and carbon electrodes. The analytic conditions are listed in Table 1.

The spectra were excited by a GEU-1 source unit connected to produce an arc; ignition phase - 90°, voltage - 220 v, arcing time - 10 sec.

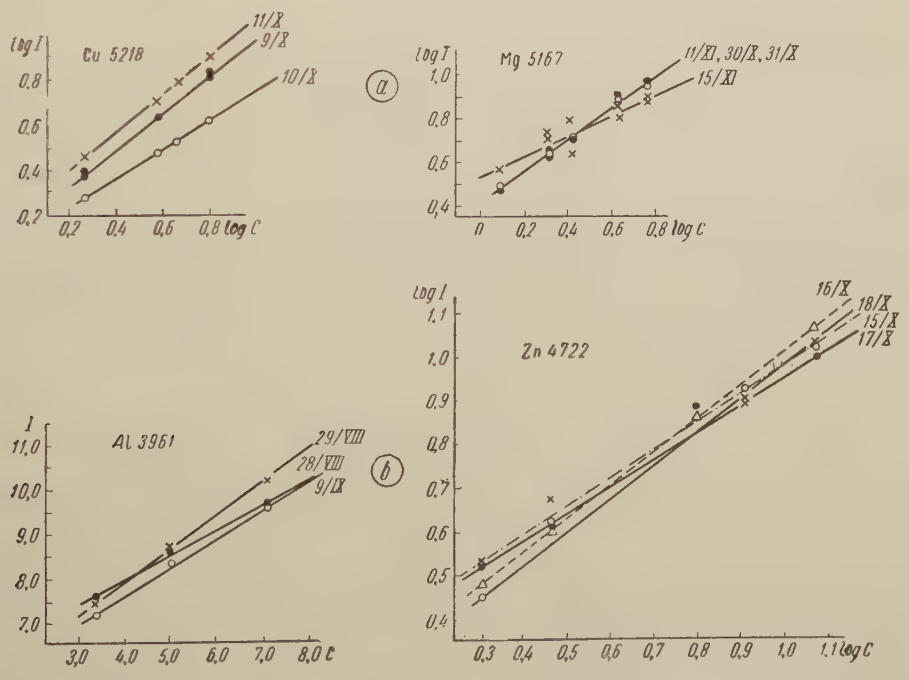

Fig.1. Shift of working curves with time for aluminum (a) and nickel (b) base alloys.

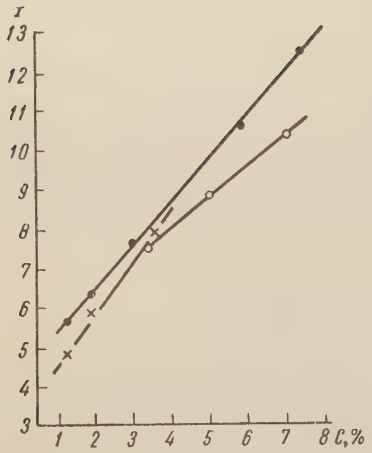

Fig.2. Working curves for determination of Al in three different nickel alloys.

For different series of measurements there was observed a parallel shift of the working curves, also a minor change in their slope (Fig.1). The reason for the shift of the curves was not determined. Temperature fluctuations in the laboratory did not exceed ±1%. The working curves were plotted daily and checked at least two times per working shift. The accuracy in determining aluminum was ±1.2%; titanium ±4.0%.

A large number of nickel alloy samples was analyzed by the developed procedure. The influence of "third" elements was brought out by comparison of the working curves for samples of different composition (Fig.2).

Analysis of aluminum and magnesium alloys

The analytic lines with reference to which one can obtain the best results in determining Mg, Zn, Si and Cu in aluminum alloys and Al in magnesium alloys are listed in Table 1 together with the determinable concentration ranges and the relative analytic errors (based on 60 determinations).

The curves for determination of Si in aluminum alloys Al-9 and Al-5 and in duraluminum exhibit a small parallel shift. To obtain a higher accuracy it is necessary to use standards of the same alloy as the sample.

Table 2

Determined	Analytic line, Å	Range of determinable concentrations, %	Relative analytic error, %
Copper	Cu I 5218.202	1.0-8.0	±3.2
Magnesium	Mg I 5172.699	0.1-2.0	±3.0
Magnesium	Mg I 5528.461	1.0-8.5	±3.0
Zinc	Zn I 4722.150	2.0-11.5	±4.0
Silicon	Si I 3905.52	0.2-12.0	±3.5
Aluminum	Al 3961.52	3.0-11.0	±2.5

Analysis of steels

The chosen analytic lines, the ranges of determinable concentrations and the accuracy of analysis of steels for tungsten, chromium, manganese, and silicon are given in Table 3.

Table 3

Determined elements	Analytic line, A	Slit width, mm		Range of determinable concentration %	Relative error, %
		entrance	exit		
Tungsten	W 4659,86	0,025	0,08	2,0—18,0	±1,0
Chromium	CrI 5206,04	0,03	0,105	0,2—4,0	±1,1
	CrI 5208,43				
	CrI 5345,80	0,025	0,115	8,0—27,0	±2,3
	CrI 5348,31				
Manganese	Mn 4783,42	0,03	0,105	0,2—2,0	±1,0
Silicon	Si 3905,52	0,03	0,08	0,1—3,5	±4,5

We note that in our experience determination of two or three elements in low alloy steels and also in nickel and aluminum alloys without refacing the samples after determination of each element substantially reduces the total analysis time per sample, although it does introduce a small additional error.

Use of the photoelectric attachment to the ISP-22 spectrograph for analysis of aluminum and magnesium alloys

We are now able to give the results of tests of the photoelectric attachment to the ISP-22 quartz spectrograph[2,3]. The light detectors in this attachment are special Geiger-Muller type counters which allow of recording radiation in the wavelength range from 2000 to 2900 Å.

Table 4

Source parameters	Aluminum alloys (elements determined and analytic pairs)					Magnesium alloys (elements determined and analytic pairs*)			
	Mg2790,8 Al2378,4	Fe2599,6 Al2321,6	Ni2310,9 Al2575,1	Mn2593,7 Al2321,6	Cr2677,1 Al2321,6	Al2631,5	Zn2502	Cu2136,99	Si2516,1
IG-2 spark unit, V = 200 v, C = 0.005 μf									
Inductance, mh	0	0,05		0,05		0	0,05	0,05	0,15
Current, amp	1	2		2		1	1	1	1
Standard error, %	5,0	5,0		5,0		5,0	3,5	6,0	5,0
Arc with electronic ignition control									
Current, amp	4,5	4,5	4,5	9	4,5				
Standard error, %	6,0	3,0	5,0	4,0	4,5				

*The Mg alloys were analyzed on the basis of the absolute line intensities.

The instrument error amounts to 2.5-3.0%. We used three different types of source units, namely, a DG-1 arc generator, an IG-2 spark unit and an arc generator with electronic control of the ignition, constructed in collaboration with the "P.M.Lebedev" Physical Institute of the USSR Academy of Sciences. The highest analytic accuracy was obtained with the last two sources. The attachment was not insulated against temperature fluctuations, hence we used wide entrance slits (0.2 mm).

The results of analysis of aluminum and magnesium alloys obtained with the IG-2 spark source and the electronically controlled arc generator are shown in Table 4.

References

1. I.S.Abramsov, Zavodsk. laboratoriya, 2, 168 (1954); A.Ya.Khashafyan, Ibid., 7, 875 (1958). (Trans.Industrial laboratory.)

2. K.A.Moiseeva, N.V.Penkina & I.P.Tindo, Ibid., 5, 625 (1957).

3. N.V.Penkina, Spektral'nyi analiz metallov i splavov (Materialy konferentsii predpriyatii aviatsionnoi promyshlennosti)(Spectroscopic analysis of metals and alloys (Transactions of the conference of aviation industry enterprises)), p.46, Oborongiz, 1958.

PHOTOELECTRIC STEELOMETER WITH VISUAL MONITORING OF THE POSITION OF INVISIBLE SPECTRUM LINES

- M.M.Butslov, A.K.Vinogradova, L.M.Ivantsov, G.N.Kutuzova & S.L.Mandel'shtam

The usefulness of the photoelectric FES-1 steelometer can be greatly extended by replacing the glass dispersing optics by quartz optics or a diffraction grating. Until recently, the obstacle to such modernization of the FES-1 steelometer was the lack of a reliable method of monitoring the position of invisible spectrum lines relative to the exit slit. This problem can now be solved by means of modern image converter tubes.

We developed and tested two operating versions or models based on the FES instrument, in which the position of the spectrum is monitored by means of an image converter with a cesium-antimony cathode and a uviol window. The converter provides for visual observation of the spectrum in the wavelength range from 2400 to 6000 Å. The two versions are diagrammed in Figs.1 & 2.

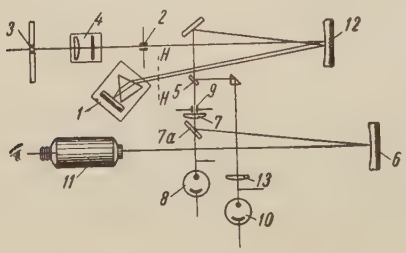

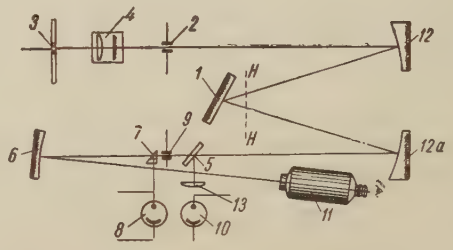

Fig.1. Optical system of model No.1: 1 - dispersing system, 2 - entrance slit, 3 - source, 4 - condenser, 5 - quartz plate, 6 - concave mirror, 7 - lens, 7a - plane mirror, 8 - photocell, 9 - exit slit, 10 - photocell, 11 - image converter, 12 - concave mirror, 13 - cylindrical lens.

Fig.2. Optical system of model No.2; component designations same as in Fig.1 except 7 - prism-lens.

Essentially, the instruments are constant deviation monochromators. Displacement of the spectrum relative to the exit slit is realized by rotation of the dispersing system 1. The entrance slit 2 is illuminated by the source 3 through the condenser 4 with cylindrical optics.

The intensity of the analytic lines is compared with the intensity of a 200-300 Å section of the spectrum discriminated by the quartz plate 5. The wavelength of the analytic line is always close to the median wavelength of the comparison section.

The cathodes of the photocells are illuminated by an image of a cross section of the light beam in plane HH, where the light intensity distribution varies very little with minor displacements of the source relative to the optical axis.

The observer checks the setting by observing the image (on the converter screen) of the spectrum lines visible through the rectangular opening (area 2 mm^2) framed in the exit slit 9. The analytic line is assumed to be in the working position if its image on the converter screen is located symmetrically relative to the slit edges. The image of the exit slit and spectrum is focused in the plane of the photocathode of the converter 11 by means of the concave mirror 6. The working light signal is directed onto the photocell 8 by the prism-lens assembly 7 from sections of the slit lying outside the "picture" observed through the converter. Thus the position of the spectrum lines can be monitored both before and during the process of measurement.

The principal characteristics of the two versions are the following.

Model 1. Mirror objective of collimator & tube: 40 mm diameter, f = 600 mm; quartz prism: refracting angle 60°, principal face 47 x 30 mm; effective height of entrance and exit slits 6 mm. The values of the reciprocal dispersion are 3.18, 5, 8.5, 21.4, 55.5, and 130 Å/mm for wavelengths of 2013, 2230, 2540, 3080, 4075 and 5880 Å, respectively.

Model 2. Mirror objective of collimator & tube: 120 x 120 mm, f = 750 mm; 60 x 50 mm grating with 600 lines per mm; effective height of entrance and exit slits 40 mm; concave spherical mirror, 50 mm dia., f' = 200 mm. The values of the reciprocal dispersion are 21.96, 21.85, 21.175, 21.57 and 21.4 Å/mm for wavelengths of 2000, 3000, 4000, 5000 and 6000 Å, respectively.

The image converter allows of observing fine details in the structure of complex spectra, in particular, the spectrum of iron. Thus, for example, the 4872.1 Å and 4871 Å lines of iron are readily resolved on the screen of the converter in model 2. With an entrance slit width of 0.02 mm the brightness of the iron spectrum on the converter screen in the 3000 to 4200 Å wavelength range is excessively high; in the other regions of the spectrum, the brightness is ample for visual work.

In our opinion image converters of the type used in our model instruments are devices with a great future. Through their use one can greatly simplify alignment and adjustment of optical and spectroscopic instruments for the ultraviolet. Image converters should prove particularly useful in visual monochromatic and heterochromatic photometry of ultraviolet radiation. Ultraviolet converters will undoubtedly find many other applications in optics and spectroscopy.

We tested both versions of our instrument under laboratory conditions. The spectrum was excited by means of a DG-1 arc source with a current strength of 4 amp. The tips of the steel rod electrodes were milled to hemispheric shape and mounted at a distance of 3 mm from the flat surface of the samples.

As a result of thermostatic temperature control of the model assemblies as a whole, the temperature shift of the spectrum lines with time was reduced to 2 μ. With an exposure time of 30 sec, the electric signal due to the dark current and scattered light amounted to 0.002-0.003 v. The signal associated with a line of average intensity falls off from 7 to 0.3 v as one progresses into the ultraviolet region. This falling off in the signal strength is due to selective losses at the mirror surfaces and decrease of the photocathode sensitivity.

The cited data may serve as a basis for evaluation of the spectral sensitivity of model instruments in determining small concentrations of impurities. Special control experiments showed that the chosen procedure for monitoring the position of the spectrum insures fully satisfactory reproducibility of photometric measurements.

ON STABILIZATION OF THE POSITION OF THE SPECTRUM BY THERMOSTATIC EQUIPMENT FOR SPECTROSCOPIC INSTRUMENTS

- A.P.Atamanov, V.N.Balandin & L.M.Ivantsov

Shifting of the spectrum relative to the exit slit due to temperature variations in the spectrometer room seriously impairs the accuracy of photoelectric spectrographic equipment.

We studied the feasibility of stabilizing the position of the spectrum by enclosing the equipment in a thermostatic chamber. The air space between the instrument and the thermostat was automatically maintained at a constant temperature by an electric heater controlled by a thermometric switch. After a certain time the spectrometric equipment came to the temperature to which the thermometric switch was set. The thermal "inertia" of the air layer is very small compared with that of the instrument. Hence the automatic heater control is very sensitive to variations in room temperature. The temperature sensitivity of the thermostatic installation increases with decrease of the air space inside it. Given the dimensions and shape of the thermostatic chamber and the spectrograph, one can easily calculate the characteristics and operating periods of the heater for the case when the instrument has already reached the temperature of the air layer, while the room temperature remains constant. If the thermometric switch is located much closer to the heater than the spectrometric instrument, such calculations give fully satisfactory results, even if made on the basis of the rough assumptions that 1) the heat from the heater is transferred only owing to the thermal conductivity of the air and 2) the thermostatic chamber is filled only with air.

The calculated and measured heater operation periods for the first installation were 5 and 5 minutes; for the second - 10 and 8 minutes, for the third - 12 and 12 minutes; the intervals between heating periods were 85 & 120 min, 200 & 150 min and 150 & 120 min.

We designed and constructed thermostatic chambers for 6 different spectrographs. Three of these weighed 400 to 450 kg and had a volume of 0.25 cubic meters each. The weights of the fourth, fifth and sixth instruments were 100, 60 and 30 kg; the volumes, 0.08 and 0.05 cubic meters. Thus the protected equipment differed substantially as regards both mass and dimensions. The installations were tested both in the Institute and under plant laboratory conditions with temperature differentials of up to 20°.

Thermostatic chambers Nos.1,2,3,4 & 6 were made in the form of wooden boxes lined on the inside with layers of asbestos, sheet iron and felt. The thermostatic chamber of installation No.5 was a casing made of thin dural lined on the inside with 3-4 mm thick asbestos sheets. All the thermostatic chambers had windows 30-50 mm in diameter for admitting the radiation. The heater coils were mounted on the walls of the chamber. For the tests, a thermometer was mounted on the frame of the spectrograph.

Curves a and b in the accompanying figure characterize the temperature variation and shift of the Hg 2573 Å line in the initial process of heating of installation No.1 and subsequent operation. Forty hours after the beginning of the test, the room temperature was reduced from 23 to 7° and maintained at this low level for over 2 hours.

Despite this, the temperature fluctuations after the initial period did not exceed 0.1°, while the mean shift of the mercury line was only 2.5 μ. A comparison of curves b and c shows that variations of 5-10 mm Hg in air pressure do not result in any noticeable shift of the spectrum lines. Comparative series of tests involving stirring of air in the chamber by means of a fan and relying exclusively on natural heat exchange by convection gave virtually identical results.

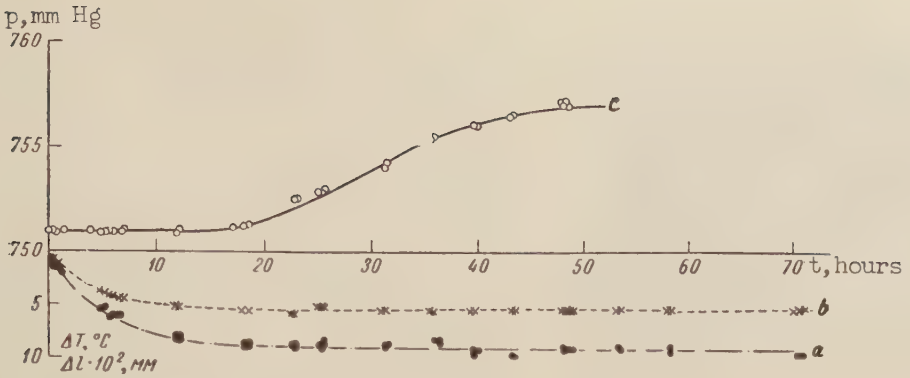

Performance of installation No.1: a - stabilization of temperature with time; b - stabilization of spectrum position with time, c - variation in atmospheric pressure with time.

Prolonged testing of the other five installations yielded results differing little from those for installation No.1, except, of course, that the time to attain the set temperature varied in accordance with the mass of the spectrometer. The respective times to constant temperature were 20 hours for No.1, 18 for No. 2, 22 for No.3, 31 for Nos.4 & 5 and 24 for No.6.

The results of our tests give reason to hope that it may prove feasible and technically worthwhile to provide similar thermostatic installations for large spectrographs such as the DFS-10 which, as is known, has a weight of 1.5-2 tons and a volume of about 1 cubic meter.

* * * * * * * * *

PHOTOELECTRIC ATTACHMENT FOR ISP-22 TYPE MEDIUM SPECTROGRAPHS

- L.M. Ivantsov & A.I.Sherudilo

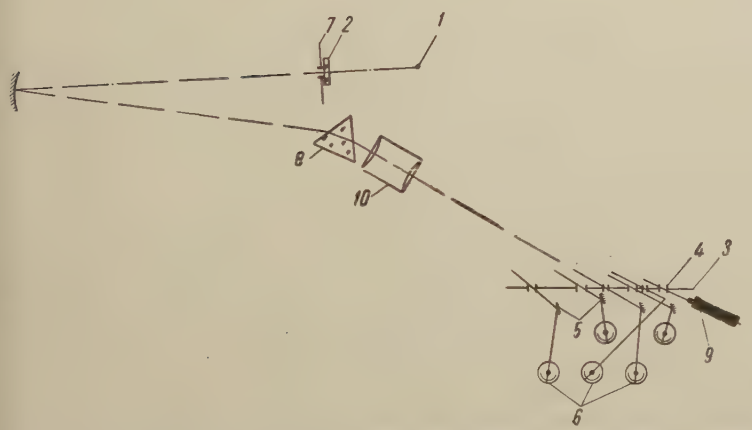

Fig.1. Optical system of the photoelectric attachment for the ISP-22 spectrograph: 1) source, 2) antivignetting lens, 3) interchangeable plane-parallel quartz plate, 4) exit slits cut in opaque aluminum coating on plate 3, 5) plane mirrors, 6) photocells, 7) entrance slit, 8) dispersing prism, 9) monitoring microscope, 10) camera lens.

The photoelectric attachment for medium spectrographs of the ISP-22 type developed and tested by us differs substantially as regards both design and operating characteristics from similar attachments of foreign manufacture[1].

The optical system of the attachment is diagrammed in Fig.1. The arc discharge 1 illuminates the spectrograph slit through the antivignetting lens 2. The quartz plate 3 is mounted in the focal plane of the spectrograph; the plate is coated with an opaque layer of aluminum in which there are cut the

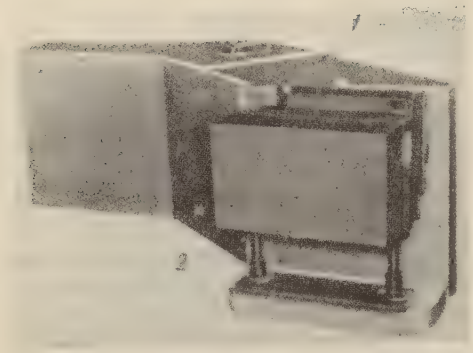

Fig.2. ISP-22 spectrograph in thermostatic chamber with photoelectric attachment installed.

exit slits 4. For work with close spectrum lines, slits of half the normal height can be provided. The mirrors 5 reflect the light passing through the slits in the direction of the corresponding STsV-6 phototubes 6 connected with storage capacitors. Automatic temperature stabilization of the spectrograph serves to suppress thermal shift of the spectrum lines. The thermostatic chamber has appropriate windows for passage of the light beam and access hatches. It was established by photographic tests that changes in the width of the entrance slit, removal and re-installation of the prism table and jarring of the spectrograph housing do not result in any displacement of the spectrum lines. The spectrograph is loaded with a metallic plate which carries guide rails for attaching the interchangeable slit plate. None of the other components of the attachment are in direct contact with the spectrograph. The design of the attachment provides for accurate and reproducable positioning of each slit plate and rapid interchange of the plates intended for analysis of different alloys. Thus in converting from analysis of one alloy to analysis of another involves no time consuming fine adjustment for discrimination of the chosen lines. Preliminary adjustment, i.e., positioning of the spectrum relative to the slits, is realized with reference to a visible line by means of the monitoring microscope; the final fine adjustment is made with reference to the photoelectric indications.

Fig.2 shows the photoelectric attachment mounted on an ISP-22 spectrograph.

We also developed and tested special equipment for cutting the exit slits according to a given spectrogram. The spectrogram and the aluminized quartz plate are mounted on the table of a microphotometer. The slits are cut by a tool clamped in a braced support mounted on the microphotometer bed. The cut is made when the selected analytic line in the spectrogram is photoelectrically disciminated. The requisite curvature of the slit is insured by a special templet. About 50 slits 18 mm in length and with a minimal width of 0.01 mm can be cut without resharpening the tool. The minimum separation between slits for which there is no noticeable deviation from parallelism with a magnification of 25 X is 0.01 mm. The displacement of the center of the slits relative to the center of the corresponding line on the spectrogram did not exceed 1-2 μ. No noticeable difference in the widths of 0.03 mm wide slits from one end to the other was detected visually at 25 X magnification or by means of a comparator.

The photoelectric attachment has successfully undergone laboratory tests. After temperature stabilization of the spectrograph, the relative line intensity in different channels does not vary with time within the limits of the reading error. The signal value in different channels with an exposure of 60 sec and storage capacitors with a capacitance from 300 to 1000 pf was 0.5 to 2.5 v. The signal level due to scattered light, dark current and leakage does not exceed 0.005-0.007 v. Five successive measurements with the slit plate removed and reinstalled between each measurement gave readings of 2.91, 2.91, 2.91, 2.87 and 2.91 v, respectively.

The reproducibility of the intensity ratio for a number of iron lines evaluated from the results of a large series of measurements was found to be 0.5-0.7%. The intensity ratio of one of the line pairs measured on successive days fluctuated within the following ranges: 3.40 ± 0.02, 3.37 ± 0.02, 3.37 ± 0.02 and 3.44 ± 0.023.

References

1. Hilger, ? , 11, No.2, 19 (1955).
2. A.P.Atamanov, V.I.Balandin & L.M.Ivantsov, Present issue of the Bulletin, p.1104.

* * * * * * * * *

SPECTROSCOPIC DETERMINATION OF OXYGEN IN COMMERCIAL GRADE TITANIUM

- K.A.Sukhenko, V.S.Grigorova, I.S.Lindstrom, N.S.Sventitskii & P.P.Galonov

In recent years there have been published a number of reports on spectroscopic determination of gases occluded in metals[1-6] and, in particular, of determination of oxygen in titanium. Of particular interest is the report of Fassel & Gordon[7] in which the authors describe an emission spectrometric method for determining oxygen in titanium and its alloys, based on excitation of the spectrum by a dc arc burning between carbon electrodes, a hollow in one of which contains the titanium sample in a platinum cup. The intensity ratio of the O I 7771.9 - A I 7891.1 Å lines is correlated with the oxygen content in the Ti sample. The range of determinable concentrations extends from 0.035 to 0.56%. The fact that the points for samples of different composition fit a single callibration curve led the authors[7] to infer that the influence of "third" elements is negligible. The oxygen content was determined with an accuracy comparable with the accuracy of the vacuum melting and bromine reduction procedures but required much less time. Unfortunately, this spectrometric method involved the use of very complex equipment, which virtually precludes its employment under industrial conditions.

For the purpose of determining oxygen in titanium we prepared a series of samples of commercial grade titanium with oxygen contents ranging from 0.01 to 2.0%. The preparation procedure was the following. The titanium sponge was mixed with TiO_2 in proportions corresponding to the desired oxygen concentration and the mixture was compacted cold. The electrodes obtained in this manner were remelted twice: first in an atmosphere of helium (160 mm Hg) and then in vacuum ($\sim 10^{-2}$ mm Hg), for the purpose of insuring uniform distribution of the oxygen. The resultant bars were then forged into rods of the requisite diameter.

We then used these standards:

1) To investigate the influence of "preliminary treatment" of the sample surface by the discharge.

2) To investigate the influence of vacuum heating on the concentration sensitivity of the oxygen lines.

3) To select the optimum excitation conditions for the oxygen lines.

In selecting the optimum conditions, we paid particular attention to determining the type of discharge with which one can obtain the best concentration sensitivity of the oxygen lines. Most of the experiments were carried out with a low voltage pulse generator since a pulsed source gives a favorable combination of sufficiently intense disintegration of the sample and a very short discharge time.

The electrodes were mounted in a special bulb which was evacuated to 10^{-2} mm Hg. The sample was connected as the cathode; the anode was a carbon rod with a truncated cone tip. The experiments showed that the use of a pulse discharge in itself does not insure obtaining an adequate concentration sensitivity. Only when the pulse discharge was used in conjunction with preliminary treatment of the sample was there obtained a noticeable concentration dependence both as re-

gards the O I 7771.9 Å line (proposed by N.G. Isaev) and as regards the O II 4705.3 Å line. The preliminary treatment consisted of cleaning the sample surface by pulse discharges at low pressure under conditions of continuous pumping of the bulb followed by sparking of the sample surface (spark from an IG-2 spark source) in an atmosphere of helium at approximately atmospheric pressure. Even in this case, however, the slope of the working curve is very flat and essentially inadequate for quantitative analysis.

We then undertook investigation of the influence of heat treatment designed to favor the entry of oxygen into the discharge through modification of the titanium. In this treatment the samples were heated in vacuum at 930° for 6 and 88 hours. Figs.1 & 2 show micrographs of the structure of samples with the highest and lowest oxygen concentrations before and after heat treatment. Tests of heat treated samples carried out under the conditions described above showed that this type of heat treatment has no significant effect.

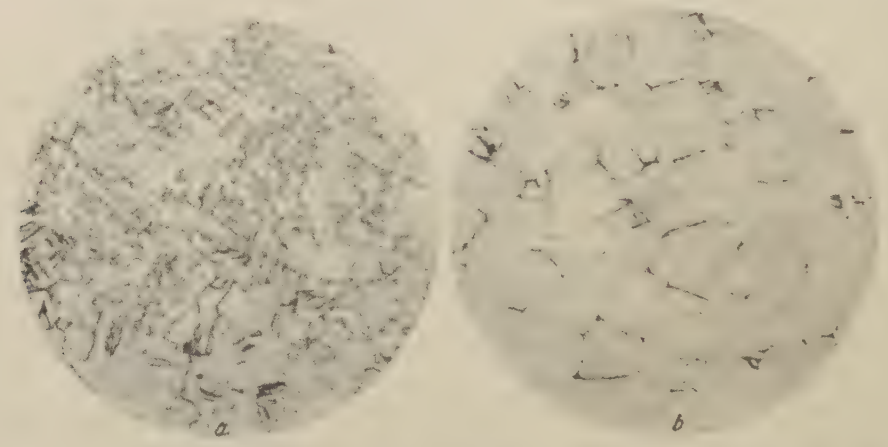

Fig.1. Structure of sample No.580 (0.1% oxygen): a) before and b) after heating.

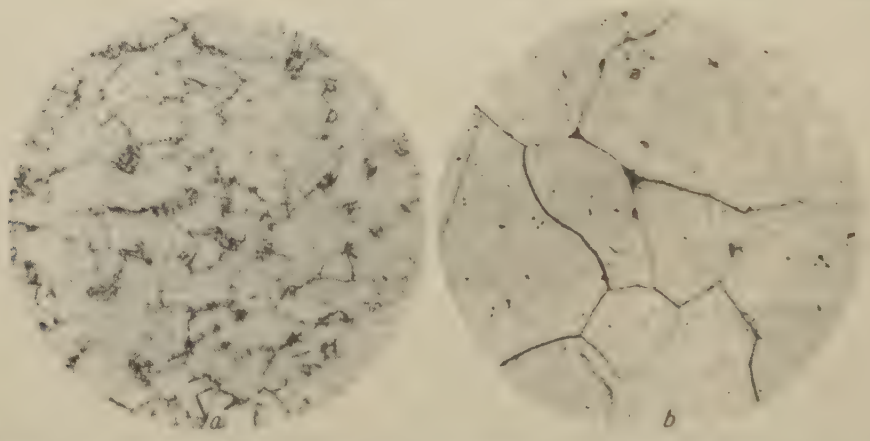

Fig.2. Structure of sample No.584 (2% oxygen): a) before and b) after heating.

The next step in the research was selection of light sources insuring optimum excitation conditions. Experiments showed that it is expedient to use a source the acts for a prolonged period on the sample, specifically, a low voltage spark.

The use of a low voltage spark generator[6] enabled us to obtain a concentration dependence of the line intensity for oxygen in the concentration range from 0.1 to 1.0%. A working curve based on several spectrograms is shown in Fig.3.

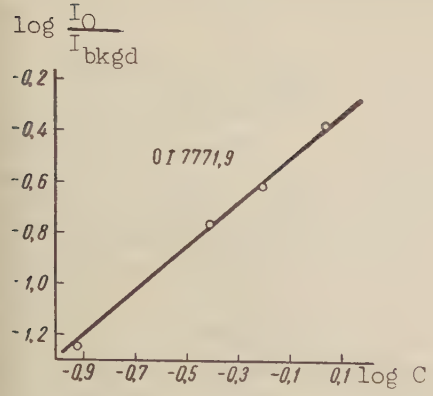

Fig.3. Averaged working curve for determination of oxygen in commercial grade titanium: O I 7771.9 Å line/background.

This curve was obtained under the following conditions: excitation source - low voltage spark, C = = 150 μf; ignition adjusted for two discharges per half cycle. The exposure time was 0.6 sec (controlled by a time relay in conjunction with a magnetic starter). The spectra were recorded on an ISP-51 spectrograph with a f = 270 mm camera. Slit width - 0.05 mm; counterelectrode - carbon rod with truncated cone tip; gap - 1 mm. The discharge bulb was first evacuated to 10^{-2} mm Hg and the discharge then realized in an atmosphere of helium at 700 mm Hg. The standards were samples of commercial grade titanium with different percentages of oxygen established by the vacuum melting procedure. The analytic line was the O I 7771.9 Å line. The continuum background was utilized as the internal standard.

Tests with different low voltage spark sources showed that the DG-1 arc generator connected for low voltage spark operation is suitable for excitation of the oxygen lines.

Although our preliminary results are positive and promising we feel they require further checking. There is not sufficient basis yet to regard the low voltage spark excitation variant as the best; we are carrying out further research on sources. It is also necessary to evaluate the influence of a number of factors, to minimize the deleterious contamination of the carbon electrode, and to enhance the concentration sensitivity in the range of oxygen concentrations under 0.2%.

References

1. Transactions of the Conference on Titanium. USA, October, 1955. (The Russian reference is to Tematicheskii sbornik referatov) (Abstracts journal) No.8/36, p.9, Oborongiz, 1956.
2. B.Rosen, Rev.univers. mines, 9, 445 (1953).
3. V.A.Fassel & R.W.Tabeling, Spectrochim. acta, 8, 201 (1956).
4. V.Gazzi, Metallurgia ital., 48, Suppl., 1, 3 (1957).
5. Symposium on Titanium, J.Metals, 9, 173 (1957).
6. N.S.Sventitskii, K.A.Sukhenko, P.P.Galonov, O.B.Fal'kova, M.S.Alpatov & K.I.Taganov, Zavodsk. laboratoriya (Industrial laboratory) 22, 668 (1956).
7. V.A.Fassel & W.A.Gordon, Analyt. Chem., 30, 179 (1958).

CONCERNING SPECTROSCOPIC DETERMINATION OF OXYGEN IN TITANIUM

- N.S.Sventitskii, K.I.Taganov & Z.I.Shlepkova

Spectroscopic determination of oxygen bound in titanium is seriously hindered by the low concentration sensitivity of the oxygen lines. The slope of the working curve for oxygen in titanium is only about 0.35 (Ref.1), whereas the plot for determination of oxygen in steel has a slope of 0.8 (Ref.2).

A somewhat better concentration dependence is obtained in the case of preliminary extraction of the oxygen with subsequent excitation of the gas mixture.[3,4] The preliminary extraction procedure is, however, complicated and requires the use of a special platinum bath, so that it is highly desirable to develop an analytic procedure combining extraction of the gas with excitation of the spectrum.

It was suggested that the reason for the low concentration sensitivity is the stability of the titanium oxide (either present in the metal or forming under the influence of the electric discharge). To check the validity of this suggestion and determine the most favorable conditions for obtaining spectra we observed the relative intensities of the Ti II 4571.9 and Cu II 4555.9 Å lines in the spectra of compacted briquettes of copper powder with 0.5 to 5% titanium dioxide. Since the copper powder was free of titanium, it was assumed that titanium could enter the light source only from its oxide. In view of this the given experiments could be carried out in air.

The results obtained indicate that the lines of titanium appear in different light sources but that they are most intense in a pulse discharge:

Light source	$\log \frac{I_{TiII4571.9}}{I_{CuII4555.9}}$
Dc arc; 120 v, 2 amp	-0.18
Arc from DG-1 arc unit; 220 v, 2 amp	-0.15
Spark from IG-2 spark unit, 0.02 μf, 0.05 mh	+0.37
High frequency spark; 220 v, 0.02 μf	-0.09
Pulse discharge, 270 v, 1000 μf	+0.47

Similar results were obtained for the Zr II 4156.2 and Cu II 4909.0 Å lines in the spectra of pellets containing ZrO_2.

Thus the experiments showed that the metal from stable titanium and zirconium oxide does enter the discharge in appreciable amounts in the case of pulse and spark excitation. Consequently, the bound oxygen must also enter the discharge cloud.

In the case of excitation of the spectra of the same pellets by a pulse discharge in an atmosphere of hydrogen, the O II 4596.13 Å line was very weak (unfortunately, the more intense O II 4705.3 Å line coincides with a copper line). The oxygen is evinced more strongly by the O I 7771.9 and O I 8446.4 Å lines[5] in the case of excitation by a high voltage spark.

If it is assumed that the pellets employed are equivalent to alloys, the concentration sensitivity for oxygen is evaluated to be 0.34. With excitation of the spectra by a pulse discharge with C = 1000 μf there was obtained a working curve with almost the same slope, namely, 0.39.

Flat working curves (slope ~0.3) are also obtained for both the arc and spark lines of oxygen in the spectra of samples of metallic titanium containing 0.33 to 0.80% oxygen with excitation by a pulse discharge and a high frequency spark. The last experiment was repeated with two series of commercial grade titanium samples containing from 0.12 to 2% oxygen. There was observed an appreciable decrease in the oxygen line intensity and virtually a complete loss of concentration dependence (the slope of the working curve was only about 0.14). Comparative analysis

of the samples showed that the first set differed from the second by the presence of calcium, the concentration of which varied from 0.30 to 0.48% in parallel with the variation of oxygen.

The experiments were repeated with more careful preparation of the electrodes and the medium. The discharge tube was evacuated to 10^{-4} mm Hg, the carbon electrodes were heated in vacuum, and the exposed surfaces of the samples were cleaned with a glow discharge in low pressure hydrogen. Specifically, we investigated the intensity of the O I 7772 line obtained in the spectra of discharges between electrode pairs of different materials.

Counterelectrode material	$\log \frac{I_{O\,I\,7772}}{I_{bkgd}}$
Spectroscopic carbon	-0.46
Tungsten	+0.02
Pure aluminum	+0.19
Iodide titanium	+0.23

These experiments again showed that it is expedient to use carbon electrodes. As before, however, the samples without calcium showed a very weak concentration dependence.

In the course of the experiments it was found that after four minute exposure to a high frequency spark in hydrogen at normal pressure the intensity of the oxygen line in pulse discharge (C = 400-500 μf) spectra increases noticeably and the concentration sensitivity rises to 0.32 (instead of 0.14 without preliminary sparking). In contrast, samples containing calcium yield a working curve with a slope of 1.3 after the same spark treatment.

The experiments on the whole show that the spectrum of oxygen from TiO_2 is satisfactorily excited in both pulse discharges and other light sources. The oxygen from metallic titanium, however, is evinced with a very low concentration dependence of its lines although this concentration dependence does increase somewhat with decrease in the energy of the exciting pulses and as a result of preliminary sparking with a high voltage spark.

It may be hypothesized that only a small fraction of the oxygen extracted from metallic titanium by a pulse discharge directly enters the discharge cloud. Most of the released oxygen forms oxides on the surface of the electrode and these become the primary source of oxygen in the subsequent excitation.

The role of calcium in the process is interesting but still far from clear; it appears to act as a "carrier" in the excitation of the oxygen spectrum.

References

1. N.S.Sventitskii, K.A.Sukhenko, P.P.Galonov, O.B.Fal'kova, M.S.Alpatov & K.I.Taganov, Zavodsk.laboratoriya (Industrial lab.), 22, 668 (1956).
2. O.B.Fal'kova, Ibid., 21, 1083 (1955).
3. V.A.Fassel & R.W.Tabeling, Spectrochim. acta, 8, 201 (1956).
4. V.A.Fassel & W.A.Gordon, Analyt.Chem., 30, 179 (1958).
5. V.Gazzi, Metallurgia ital., 48, Suppl. 1, 3 (1956).

ON THE USE OF THE SPECTRA-ISOTOPIC PROCEDURE FOR DETERMINING HYDROGEN

- T.F. Ivanova, M.E. Trentovius & V.V. Fedorov

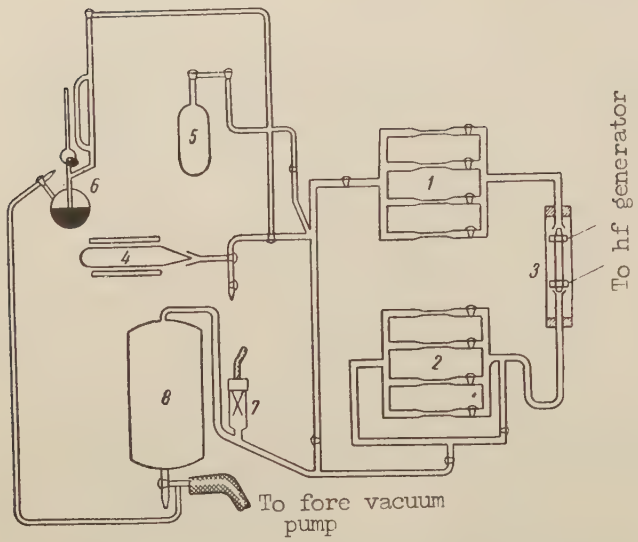

Fig.1. Vacuum system of the spectro-isotopic equipment: 1 & 2) capillary comb assemblies, 3) discharge tube, 4) exchanger, 5) deuterium tank, 6) pressure gage, 7) vacuum meter tube, 8) ballast tank.

In the present research we used a modification of the spectro-isotopic apparatus described by Zaidel' and his co-workers[1-4]. The apparatus consists of a DS-1 diffraction spectrograph, a photoelectric detecting-recording unit and a vacuum system (see Fig.1). In contrast to the system employed by Zaidel', this system operates at a pressure of $5 \cdot 10^{-3}$ mm Hg instead of 10^{-5} mm Hg; hence it is simpler and more reliable in operation (only a forepump is employed).

Table 1 lists the values of the corrections required (based on the data of "dry runs") as a function of the vacuum in the system together with the values obtained for the set-up of Zaidel' et al[1-4]. It will be seen that the absolute value of the correction in working only with a fore vacuum pump is higher (than in the case of the high vacuum used by Zaidel'). This increase may be partially connected with the quality of the exchanger material.

The magnitude of the correction increases with increase of the pressure in the system, but the scatter of correction values, which is the primary factor in determining the uncertainty of the method, remains virtually constant.

In case of gradual increase of the pressure in the system owing to impaired

Table 1

Corrections (in cm^3) required at different pressures in the vacuum system

"Dry run" experiment No.	Refs. 1-4	Our data		
		$2 \cdot 10^{-3}$ mm Hg	$6 \cdot 10^{-3}$ mm Hg	$9 \cdot 10^{-3}$ mm Hg
1	0,036	0,083	0,147	0,145
2	0,063	0,118	0,132	0,132
3	0,071	0,071	0,115	0,128
4	0,037	0,086	0,111	0,141
5	0,066	0,075	0,097	0,143
6	0,038	0,095		0,126
7	0,044	0,079		0,153
8	0,065	0,067		0,116
9	0,059	0,058		0,145
10	0,047	0,093		—
Average	0,053	0,083	0,121	0,136
Arithmetic mean deviation	±0,013	±0,012	±0,013	±0,010

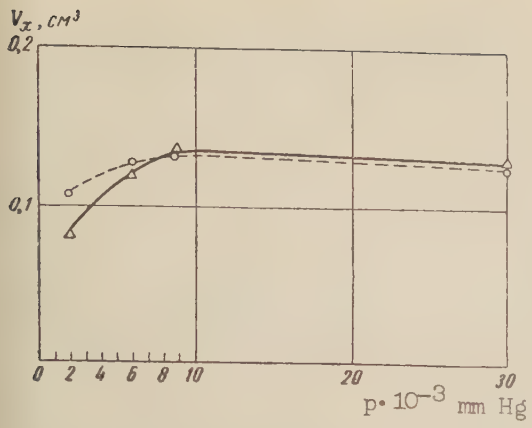

←Fig.2. Curve for correcting the "dry run experiment" correction as a function of the pressure in the system. Solid curve - data of Refs.1-4; dashed curve - our data.

operation of the forepump, the absolute magnitude of the "dry run experiment" correction can be corrected by means of the curve shown in Fig.2.

The procedure was also applied for investigating the distribution of hydrogen over the cross section of a forging of degassed Cr-Ni-Mo steel. The hydrogen content was determined at different points from the periphery to the center over the cross section of a 1000 mm diameter forged "washer" with a 100 mm diameter central opening.

We made an attempt to compare the results of the hydrogen determinations with the data on the plastic properties of the metal. The results of this study are shown in Fig.3. The horizontal scales are laid off in terms of the distance of the analyzed regions from the surface of the forging. The vertical scale in Fig.3,a gives the hydrogen content; the vertical scale in Fig.3,b gives the corresponding values of the relative constriction coefficient.

It will be evident from the general character of the curves that the hydrogen content increases from the periphery to the center of the forging; the opposite is true of the plastic properties.

More extensive use of the spectral-isotopic procedure for determining hydrogen in industrial laboratories is hampered by the fact that the requisite equipment is not standard but must be prepared on special order at considerable expense. We made an attempt to utilize standard components. We found that it is feasible to replace the nonstandard DS-1 diffraction spectrograph with a standard UF-85 camera (now being

Table 2

Results of determination of hydrogen in different types of steel

Analysis No.	Hydrogen content, $cm^3/100$ g		
	Kh18N9T	St50	U10
1	6,65	0,71	0,75
2	6,85	0,87	0,64
3	7,45	0,87	0,76
4	7,24	0,62	0,73
5	6,90	0,50	0,85
6	6,55	0,69	0,60
7	7,10	0,55	
8	6,58	0,68	
9	7,10	0,71	
10	7,05		
11	6,65		
12	6,75		
13	6,35		
14	6,72		
15	6,55		
16	6,60		
17	7,25		
18	6,85		
19	6,90		
20	7,25		
Average	6,87±0,24	0,69±0,12	0,72±0,09
Rms error of individual analyses	±3,5%	±17%	±13%

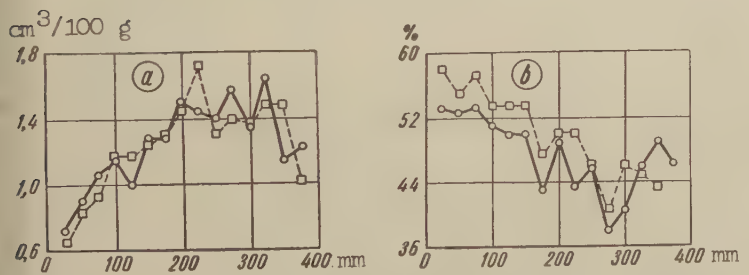

Fig.3. a) Variation of the hydrogen content in from the surface of a steel forging; b) variation of the coefficient of relative constriction. The solid and dashed curves are for two symmetrical cross sections.

produced by the GOMZ plant) in conjunction with a suitable diffraction grating or replica. The grating must have 600 lines/mm and should concentrate most of the light in the third order in the 6500 Å region, inasmuch as analysis in this case is made with reference to the H_α and D_α lines, the radiation being detected by a FEU-22 photomultiplier.

References

1. A.N.Zaidel' & A.A.Petrov, Zhur.tekh.fiz., 25, 14, 2571 (1955).
2. A.N.Zaidel' & K.I.Petrov, Zavodsk. laboratoriya, 8, 929 (1956).
3. A.N.Zaidel' & A.A.Petrov, Vestnik, Leningrad State University, 10, 40 (1957).
4. A.N.Zaidel', A.A.Petrov & G.V.Veinberg, Spektral'no-ezotopnyi metod opredeleniya vodoroda v stalyakh (Spectro-isotopic method of determining hydrogen in steels), Izvestiya (Bulletin), Leningrad University, 1957.

* * * * * * * * *

DETERMINATION OF NITROGEN IN DIFFERENT STEELS

- K.A.Sukhenko, P.P.Galonov & T.V.Barasheva

The purpose of the present work was to improve the extant procedure for determining nitrogen in steel, prepare a pilot lot of standards and develop a multiple purpose source unit for determination of gases.

In general the preparation of standards comprises the following four steps: 1) selection of the material, 2) founding, 3) determination of the precise chemical composition and 4) checking for homogeneity.

As the base material for the standards we chose stainless steel. The nitrogen was introduced in the form of nitrided ferrochromium. In all, we cast five melts of approximately 25 kg each. According to the proportioning of the batches the nitrogen content in the melts varied from 0.02 to 0.2%.

No nitrogen compound was added to the first melt. In order to obtain a matrix with a minimum nitrogen content, the steel was melted in a vacuum furnace at 10^{-1} mm Hg. The other four melts were made in the usual manner.

The nitrogen content in the standards was determined by chemical analysis in our Institute, in the Central Scientific Research Institute of Ferrous Metallurgy and in the Institute of Metallurgy of the USSR Academy of Sciences. The calculated nitrogen percentages and the analytic results are listed in Table 1. It will be seen that the agreement is good. The nitrogen content in standard

Table 1

Nitrogen content in standards (%)

Melt & Standard Nos.	Calculated amount N	Determined chemically			Established nitrogen content
		Lab.1	Lab.2	Lab.3	
M.1 - St.26	Traces	0,047	0,039	0,057	0,02
M.2 - St.36	0,05	0,052	0,041	0,052	0,05
M.3 - St.37	0,10	0,106	0,100	0,112	0,10
M.4 - St.14	0,15	0,154	0,15	0,116	0,15
M.5 - St.15	0,20	0,189	0,175	0,17	0,19

Table 2

Chemical composition of standards (%)

Melt & Standard Nos.	N	C	Si	Mn	S	P	Cr	Ni
M.1 – St.26	0,023	0,06	0,10	0,20	—	—	16,76	8,62
M.2 – St.36	0,05	0,08	—	—	0,020	0,020	18,26	9,40
M.3 – St.37	0,10	0,08	—	—	0,020	0,009	17,52	8,90
M.4 – St.14	0,15	0,125	—	—	—	0,0078	17,6	8,0
M.5 – St.15	0,189	0,11	—	—	—	0,009	18,4	8,40

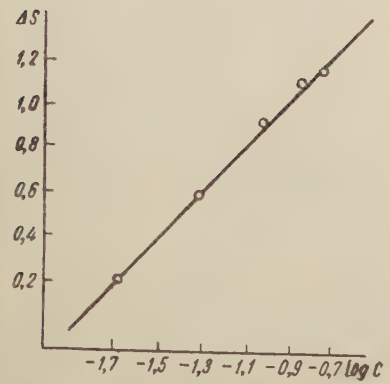

Fig.1. Calibration curve for determining nitrogen in steel; ΔS - difference between blackening of the N 3994.995 Å line and the background near the line.

No.26 was checked by spectroscopic analysis and taken equal to 0.02%. The standards were also analyzed for other elements; the results are shown in Table 2.

The homogeneity of the standards was checked spectroscopically and found to be satisfactory. We chose the following conditions for the determination of nitrogen in steel: light source - low voltage spark with C = 300 μf; two high frequency discharges per half-cycle of the line voltage; exposure - 1 sec (controlled by a time relay); analytic gap - 0.03 mm; counterelectrode - tungsten with hemispherical tip; photographic plates - type 3 spectroscopic, speed 16 GOST units.

Helium was employed as the neutral medium in the discharge chamber, which was first evacuated to $5 \cdot 10^{-2}$ mm Hg, then filled with helium to a pressure of 700 mm Hg.

The working curve is shown in Fig.1. The results of analyses of commercial steel samples are given in Table 3.

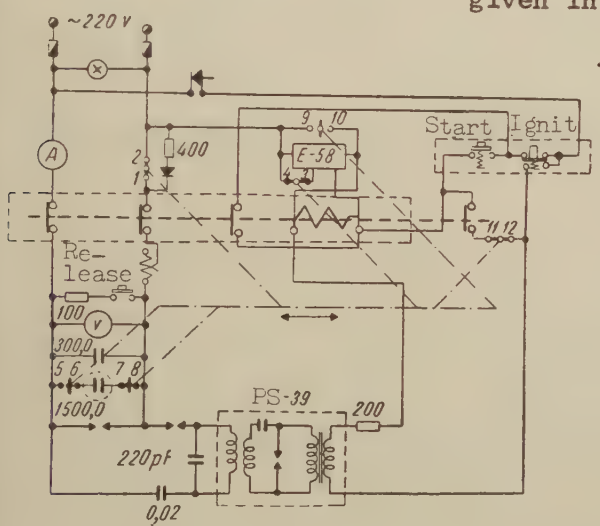

←Fig.2. Multiple purpose source unit. The contacts of the six-pole two-position switch are numbered 1 through 12. In the low voltage spark setting the contacts 1-2, 4-3 and 11-12 are closed. The contacts 1-2 shunt the rectifier (DGTs-24 semiconductor type), contacts 4-3 connect in the E-58 time relay, contacts 11-12 connect the line to the PS-39 transformer unit. In the second, pulse operation, setting contacts 1-2, 4-3, and 11-12 are open, while contacts 5-6, 7-8 and 9-10 are closed. The figure illustrates the "spark operation" setting.

Two types of source are utilized for determining gas in metals and alloys, namely, a low voltage spark and a pulse discharge. With a view to simplifying the installation we developed the multiple purpose unit diagramed in Fig.2. The circuit employs miniature electrolytic capacitors of the EF-800/300 V type and miniature paper capacitors of the MBGO-30/ /300 V type.

Table 3

Results of chemical and spectroscopic determination of nitrogen in commercial steel samples (%)

Sample Nos.	Chemical analysis		Spectrum analysis		Sample Nos.	Chemical analysis		Spectrum analysis	
	Lab. 1	Lab. 2				Lab. 1	Lab. 2		
48	0,014	0,014	0,025	0,027	A-1	0,020	0,033	0,023	0,046
			0,025	0,024				0,02	0,046
			0,017	0,023	A-3	0,024	0,011	0,03	0,03
			0,018	0,024				0,032	0,023
V	0,039	0,030	0,038	0,034				0,021	0,022
			0,048	0,035	1	0,022		0,035	
			0,032	0,033	2	0,048		0,042	
IO	0,056	0,02	0,028	0,024	3	0,031		0,037	
			0,030	0,028	4	0,195		0,2	
			0,024	0,025					

Table 4

Results of analysis by the control standard procedure (%)

Sample No.	Chemical analysis		Control standard procedure			Sample No.	Chemical analysis		Control standard procedure		
	Lab. 1	Lab. 2					Lab. 1	Lab. 2			
Я	0,014	0,015	0,0112	0,0145		27	0,043	0,06	0,051	0,044	0,052
			0,0117	0,0145					0,058	0,049	0,048
86	0,029		0,036	0,03	0,031	31	0,032	0,25	0,023	0,027	
			0,027	0,028					0,022	0,032	

Analysis of steels of different composition for nitrogen brought out the influence of "third" elements. Analyses, using our standards, of steel samples containing approximately 1% aluminum yield excessively high values for the N content. Curves plotted on the basis of samples with a higher content of chromium and a lower content of nickel have a steeper slope than the curves plotted on the basis of samples with a lower chromium content.

For analysis of samples differing in composition from the standards, we recommend using the "control standard" procedure which we checked on a number of commercial samples (Table 4).

INFLUENCE OF THE CHEMICAL COMPOSITION AND HEAT TREATMENT OF STEEL SAMPLES ON THE RESULTS OF SPECTROSCOPIC DETERMINATION OF NITROGEN

- N.V.Buyanov, L.M.Fedorova & V.F.Korotkov

The production of metals and alloys with a minimal content of gases is predicated on the development of reliable procedures for monitoring the gas content in metals. The recently proposed spectroscopic procedure for direct determination of gases in metals satisfies the requirements as regards simplicity and rapidity of analysis; practical experience has, however, brought up a number of new problems.

We investigated the influence of "third" elements and heat treatment of the samples on the results of determination of N in different types of steel.

The research was carried out on industrial samples analyzed three times in the chemical laboratory. The spectra were photographed in a vacuum chamber designed and constructed in our Institute. The chamber is designed to hold six samples and 12 auxiliary electrodes simultaneously. The electrodes are mounted vertically. The discharge gap is set with an accuracy of ±0.01 mm by the contact (backing off) technique by means of a micrometric screw. We chose the following conditions for excitation of the N spectrum; these are the conditions under which the working curve has the steepest slope and satisfactory reproducibility of the analytic results is assured.

The discharge chamber was evacuated to 10^{-1} mm Hg and then filled with helium to a pressure of 350 mm Hg; the auxiliary electrodes were of tungsten; the discharge gap - 0.35 mm; the exposure - 0.2 sec (realized by means of a time relay); light source sharply focused on the spectrograph slit (analytic line - N 3999.5 Å). The light spark was a low voltage spark with one discharge per half-cycle of the line voltage; circuit capacitance C = 400 μf; I = 16 amp. The analyses were carried out by the method of three standards with the working curves plotted in S_N (blackening) vs log C_N coordinates.

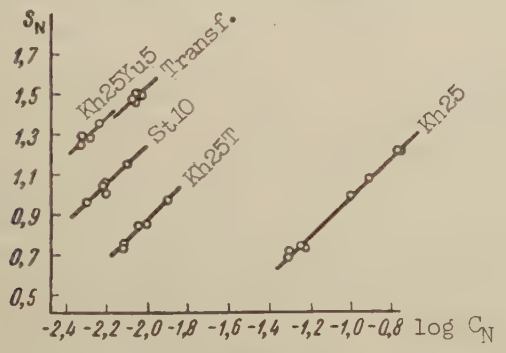

Fig.1.

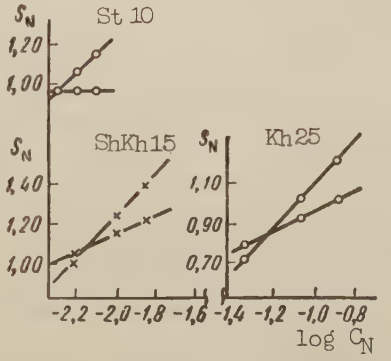

Fig.2.

Fig.1. Working curves for determination of nitrogen plotted on the basis of samples of different grades of steel.

Fig.2. Influence of heat treatment of sample on the slope of the working curves for different grades of steel. The plots with the flattest slopes pertain to quenched samples.

The influence of "third" elements, specifically, chromium, aluminum, titanium and silicon, was investigated for St10, Kh25, Kh25T, Kh25Yu10 and transformer steels.*

---

*St10 = Ст10, Kh25 = Х25, Kh25T = Х25Т, Kh25Yu5 = Х25Ю5, ShKh15 = ШХ15 .

The experimental results are shown in Fig.1. The working curve plotted for Kh25 steel (23-27% Cr) samples lies below the curve for St10 steel ($\leq$ 0.15% Cr), the separation ΔS being ~0.50. The plot for St10 steel (0.10-0.37% Si) lies below ($\Delta S \approx 0.30$) the plot for transformer steel (3% Si). Upon the addition of 1% titanium to Kh25 steel (i.e., on going to Kh25T steel) the blackening of the nitrogen line increases by 0.80. The addition of 5% aluminum to Kh25 steel (i.e., going to Kh25-Yu5 steel) greatly increases the intensity of the N line ($\Delta S \approx 1.50$). (The spectra of St10 steel and transformer steel samples were photographed on Panchrome film - speed 90 GOST units; those of the Kh25, Kh25T and Kh25Yu5 samples on ES type 1 emulsion 983 film.) It will be evident that additions of titanium, aluminum, chromium and silicon can seriously distort the results of nitrogen determination.

The effect of heat treatment was investigated on samples of St10, ShKh15 and Kh25 steels. The slope of the working curves changed greatly after quenching of the cast samples: from 46 to 26° for Kh2 steel and from 42 to 24° for ShKh15 steel. Quenching of samples of St10 steel leads to complete loss of concentration sensitivity, i.e., the working curve becomes horizontal (Fig.2). If, for example, we attempt to determine the nitrogen concentration in a quenched sample of Kh25 steel from the curve plotted for cast standards, we obtain C_N = = 0.13% instead of C_N = 0.18%. In a control experiment quenched samples of Kh25 steel were annealed and for them there was obtained a working curve similar to that for cast samples.

Consequently, the analytic results are influenced by the structure of the material. Annealing of cast samples improves the reproducibility; quenching has an adverse effect. For example, the analytic error for annealed Kh25 steel samples with a nitrogen concentration of 0.14% is ±9.2%, for a cast sample, ±10.4% and for a quenched sample ±27.6%.

Through appropriate variation of the current strength and the capacitance of the spark circuit one can reduce or virtually eliminate the separation between the working curves for cast and quenched Kh25 steel samples; the resultant common curve, however, has a much flatter slope than the curves obtained under conditions specifically selected for cast samples.

We note that the intensity of the N lines also depends on the purity of the helium in the discharge chamber. When the initial helium tank was replaced by a new tank we noted an appreciable change of the intensity of the analytic N line. Mass spectrometric determination showed that in the new tank the nitrogen content was 2.85% (as against 0.77% in the initial tank), the hydrogen content 2%, instead of 1%; the oxygen content 0.008% instead of 0.052%. With the shift to the new helium tank both the intensity of the continuum background and the number of spectrum lines increased. At the same time the slope of the working curves was reduced somewhat and for attaining the original slope it was necessary to increase the current strength in the spark circuit. All these effects are indicative of the influence of physical-chemical processes. The observed alterations of the spectrum cannot be attributed solely to the superposition of the spectrum of the nitrogen contained in the sample and the helium.

Our results show that in determination of nitrogen in different grades of steel one must take into account the chemical composition of the sample and its thermal history, and take care to insure adequate purity of the helium used in the discharge chamber.

DETERMINATION OF NITROGEN IN CHROMIUM AND TITANIUM*

- S. A. Skotnikov

Entry of the gas into the discharge gap and excitation of its spectrum are fundamental in spectroscopic determination of gases in general and nitrogen in particular in metals and alloys. These two factors determine the sensitivity of the analytic procedure.

It has been suggested that the chemical stability of metal nitrides must be an important consideration where choice of the optimum parameters of the spark source circuit are concerned. To check this we carried out an investigation of the conditions of determination of nitrogen in chromium and titanium, the stability of whose nitrides is very different: whereas for CrN the temperature corresponding to 1 mm Hg partial pressure is 719°, for TiN the corresponding temperature is 2912°.[1] Moreover, titanium is a getter; chromium is not. Our experiments showed, however, that the character of the dependence of log (I_l/I_b)** on the sparking conditions, which dependence may be taken as a measure of the sensitivity, is similar for the two metals.

The analytic line chosen was N II 3995 Å. The discharge was realized in an atmosphere of CO_2. For producing the sparks we used the electronic low voltage spark generator described by Borovskii & Skotnikov[2]; except as noted below, the unit was operated at a frequency of one ignition per half-cycle of the 220 v, 50 cycle supply voltage.

Variation of the circuit capacitance with constant inductance (L = 10 μh) yields first a rapid and then a slower increase of log (I_l/I_b). An adequate sensitivity is attained at C = 350-400 μf for both metals. The variations of log (I_l/I_b) with the inductance (C = 340 μf = const.) are also similar. At low values of L ($\leqslant$ 5 μh) the value of log (I_l/I_b) is unstable; above 5 μh, however, it becomes almost constant up to L = 25 μh. The instability at low inductance values is connected with increase in the diameter of the spark pit and increase in the depth of the spark penetration. It is, apparently, expedient to use an inductance of about 10 μf for both metals.

The variation of log (I_l/I_b) with the width of the electrode gap is shown in Table 1. The highest sensitivity for both metals is obtained with a gap of about 0.5 mm.

Table 1

Electrode gap, mm	$\log \frac{I_{Cr}}{I_b}$	Electrode gap, mm	$\log \frac{I_{Ti}}{I_b}$
0,3	—0,76	0,3	0,47
0,5	—0,68	0,6	0,49
1,0	—0,83	0,9	0,29
2,0	—0,91	1,2	0,18

With decrease of the CO_2 pressure from atmospheric, there is observed a decrease in intensity of the background and an increase of log (I_l/I_b); for very low pressures, however, the growth of log (I_l/I_b) ceases and the stability of the discharge is impaired. The optimum pressure appears to be 200-300 mm Hg for both chronium and titanium.

Mandel'shtam & Fal'kova[3] recommend approximately the same low voltage spark source parameters for determination of nitrogen in steel. Experiments on determination of nitrogen in steels under the conditions found optimal for titanium and chromium substantiated the suitability of these conditions for determination of nitrogen in steel as well. Thus it would appear that the same spark conditions (circuit parameters) are satisfactory for determination of nitrogen in different metals, having nitrides characterized by different stabilities and different melting points.

---

*Yu. A. Chumakov participated in the part of the work pertaining to titanium.

**I_b = the intensity of the background (continuum) in the vicinity of the analytic line.

Table 2

Spark rate per ½ cycle	1:1	1:2	1:4
$\log(I_{Cr}/I_b)$	−0,68	−0,49	−0,39
$\log(I_{Ti}/I_b)$	−0,18	+0,26	+0,38

In addition to the above enumerated conditions, mention should be made of the sparking frequency, i.e., number of discharges per alteration. For both titanium and chromium reducing the number of ignitions per half-cycle leads to an increase of the absolute sensitivity (Table 2).

The same holds true for steel. However, for steel and chromium for which the working curves have a slope of about 45° with sparking every half-cycle, the slope of the working curve falls to about 20° as the ignition frequency is reduced, i.e., the increase in absolute sensitivity is attained at the expense of reduction of the concentration sensitivity. Hence the expedient of reducing the sparking frequency per half-cycle may be regarded as useful primarily for analysis in the case of low N concentrations, i.e., concentrations at the lower bound of the sensitivity for one ignition each half-cycle.

An entirely different picture is observed in determining nitrogen in titanium. Experiments show that ignition each half-cycle in this case does not give an adequate concentration dependence, which is in agreement with the data of Kagan & Filimonov[4]. It is interesting that the spark traces on the sample surface in this case are oxidized. Possibly this oxidation of the titanium in the case of ignition every half-cycle was the interfering factor as regards determination of nitrogen.

When the sparking frequency is reduced to one ignition every fourth half-cycle, a noticeable concentration dependence appears and one obtains a working curve with a slope of about 40°; the analytic sensitivity is then about 0.05% by weight, and the spark traces are not oxidized. It must be emphasized that when the discharge frequency is thus reduced, the discharges become unipolar, and the sample should be connected as the cathode. The optimum circuit parameters determined for one spark per half-cycle were still the best for the spark every fourth half-cycle conditions.

By way of standards we used remelted titanium samples analyzed in the analytic laboratory of the IMET (Institute of Metallurgy). The proposed procedure was checked on two sets of Ts NIIChM (Central Scientific Research Institute of Ferrous Metallurgy) standards. Tests with the first set in which the standards differed only as regards nitrogen content substantiated the observed concentration and absolute sensitivities: the points all fell on a straight line. The standards of the second set differed not only as regards nitrogen content but also as regards the percentage of calcium. In working with this set we were unable to obtain a satisfactory working curve: the scatter of the points was too great.

Thus we recommend the following analytic conditions for determination of nitrogen in steels, chromium and titanium: light source - low voltage spark with C = 400 μf and L = 10 μh, discharge in CO_2 at 200-300 mm Hg; electrode gap - 0.5 mm; counterelectrode - copper, presparked. Ignition of the spark once every half-cycle (50 cps supply) for steels and chromium and once every fourth half-cycle for titanium assures a good concentration sensitivity. The absolute sensitivity under these conditions is 0.01% for chromium and 0.05% for titanium.

Institute of Metallurgy
Academy of Sciences of the USSR

References

1. Yu.A.Klyachko, A.G.Atlasov & M.M.Shapiro, Analiz gazov i vklyuchenii v stali (Analysis of gases and inclusions in steel), p.167, Metallurgizdat, 1953.

2. I.B.Borovskii & S.A.Skotnikov, Apparatura dlya spektral'nogo opredeleniya gazov v metallakh (Equipment for spectroscopic determination of gases in metals), VINITI, 1958.

3. S.L.Mandel'shtam & O.B.Fal'kova, Zavodsk. lab. (Indust. lab.), No.4, 430 (1950).

4. H.M.Kagan & L.N.Filimonov, Ibid., No.2, 185 (1957).

* * * * * * * * *

ANALYSIS OF HIGH CONCENTRATIONS ALLOWING FOR THE INFLUENCE OF "THIRD" COMPONENTS

- L. I. Topalov

The slopes of the working curves for alloys with high and variable concentrations of several components are determined primarily by the reciprocal influence of the components, and the steepest slopes are obtained by selection of excitation conditions favoring strongest manifestation of this influence. Steep slopes are also obtained by using analytic pairs consisting of lines with the greatest concentration sensitivity.[1] Through proper combination of these factors one can obtain working curves with a slope (tangent) of 4 to 6. The variation of ΔS with log c in such cases is nonlinear. Let us assume that the function

$$\frac{I_n}{I_m} = \varphi(c_n, c_m, c_r, \ldots, c_i) \tag{1}$$

is of the form

$$\frac{I_n}{I_m} = \frac{a_n}{a_m} \frac{c_n^{b_n} c_m^{b_m^n} c_r^{b_r^n} \ldots c_i^{b_i^n}}{c_n^{b_n^m} c_m^{b_m} c_r^{b_r^m} \ldots c_i^{b_i^m}}, \tag{2}$$

where b_r^n and b_i^m are coefficients characterizing the influence of components r and i on the line intensities of the components n and m and, consequently:

$$\gamma(b_n - b_n^m)\lg c_n + \gamma(b_m^n - b_m)\lg c_m + \gamma(b_r^n - b_r^m)\lg c_r + \ldots + \\ + \gamma(b_i^n - b_i^m)\lg c_i + \gamma \lg \frac{a_n}{a_m} = \Delta S_{n-m}. \tag{3}$$

The coefficients $(b_n - b_n^m)$, etc., in general, depend on the concentrations c_n, c_m, etc. Let us assume that in a certain limited concentration range they vary little and that within the limits determined by the reproducibility of ΔS can be regarded as constant. Then from Eq.(3) we can with the aid of a sufficient number of standards obtain the values of these coefficients and log (a_n/a_m) from which we can calculate ΔS for another group of standards and compare this with ΔS obtained from experiment. Divergences not exceeding 2-3 $\sigma(\Delta S)$ indicate that both assumptions are allowable.

Further, invoking the fact that

$$c_n + c_m + c_r + \ldots + c_i = \text{const},$$

by the method of successive approximations we can calculate the concentrations c_n, c_m, etc. in the sample. One can then go over to a constant graph (or table) constructed by means of the coefficients characterizing the relative intensities by the use of a curve plotted in terms of $\Delta S_{\text{main pl.}}$ vs $\Delta S_{\text{tech.pl.}}$ (see Ref.2).

The relative error is calculated by means of the formula

$$\sigma_{\varepsilon_n} = \pm \sqrt{\left[\frac{\sigma\Delta S_{n-m}\Delta \lg \frac{c_n}{c_m}\cdot 100}{0{,}43\delta\Delta S_{n-m}\left(1+\frac{c_n}{c_m}\right)}\right]^2 + \left[\frac{\sigma\Delta S_{n-r}\Delta \lg \frac{c_n}{c_r}\,100}{0{,}43\delta\Delta S_{n-r}\left(1+\frac{c_n}{c_r}\right)}\right]^2 + \ldots + \left[\frac{\sigma\Delta S_{n-i}\Delta \lg \frac{c_n}{c_i}\cdot 100}{0{,}43\delta\Delta S_{n-i}\left(1+\frac{c_n}{c_i}\right)}\right]^2}, \quad (4)$$

where $\Delta \log (c_n/c_m)$ is the difference between the logarithms of the ratios of c_n and c_m for two standards, and $\delta\Delta S_{n-m}$ is the difference between the corresponding values of ΔS_{n-m}. It will be evident from the formula that this approach insures decrease of the relative error with increasing concentration of the determined component.

Knowledge of the coefficients characterizing the relative intensities also allows of obtaining another solution (within the concentration ranges wherein these coefficients are known to be constant):

$$\Delta S_{n-m} = \gamma(b_n - b_n^m)\lg c_n + \gamma(b_m^n - b_m)\lg c_m + \gamma(b_r^n - b_r^m)\lg c_r + \gamma \lg \frac{a_n}{a_m}; \quad (5)$$

$$\Delta S_{m-r} = \gamma(b_m - b_m^r)\lg c_m + \gamma(b_r^m - b_r)\lg c_r + \gamma(b_n^m - b_n^r)\lg c_n + \gamma \lg \frac{a_m}{a_r}; \quad (6)$$

$$\Delta S_{r-n} = \gamma(b_r - b_r^n)\lg c_r + \gamma(b_n^r - b_n)\lg c_n + \gamma(b_m^r - b_m^n)\lg c_m + \gamma \lg \frac{a_r}{a_n}. \quad (7)$$

Then, from (5) and (6) or other combinations, we can obtain

$$\Delta S_{m-r} - \frac{\gamma(b_n^m - b_n^r)}{\gamma(b_n - b_n^m)}\Delta S_{n-m} = \left[\gamma(b_m - b_m^r) - \frac{\gamma(b_n^m - b_n^r)\gamma(b_m^n - b_m)}{\gamma(b_n - b_n^m)}\right]\times$$

$$\times \lg c_m + \left[\gamma(b_r^m - b_r) - \frac{\gamma(b_n^m - b_n^r)\gamma(b_r^n - b_r^m)}{\gamma(b_n - b_n^m)}\right]\lg c_r + \gamma \lg \frac{a_m}{a_r} - \frac{\gamma(b_n^m - b_n^r)}{\gamma(b_n - b_n^m)}\gamma \lg \frac{a_n}{a_m}. \quad (8)$$

From (5) and (7) or other combinations

$$\Delta S_{r-n} - \frac{\gamma(b_m^r - b_m^n)}{\gamma(b_m^n - b_m)}\Delta S_{n-m} = \left[\gamma(b_n^r - b_n) - \frac{\gamma(b_m^r - b_m^n)\gamma(b_n - b_n^m)}{\gamma(b_m^n - b_m)}\right]\times$$

$$\times \lg c_n + \left[\gamma(b_r - b_r^n) - \frac{\gamma(b_m^r - b_m^n)\gamma(b_r^n - b_r^m)}{\gamma(b_m^n - b_m)}\right]\lg c_r + \gamma \lg \frac{a_r}{a_n} - \frac{\gamma(b_m^r - b_m^n)}{\gamma(b_m^n - b_m)}\gamma \lg \frac{a_n}{a_m}. \quad (9)$$

Equations (8) and (9) give straight line plots for the variation of $\log c_m$ and $\log c_n$ with the directly measured quantities for $\log c_r = \text{const}$. The shift of both plots occurring with changes in $\log c_r$, calculated in units of $\log c_m$ and $\log c_n$ per unit of $\log c_r$, are also constant and independent of the properties of the photographic emulsion, and for $c_n + c_m + c_r = \text{const}$. are linearly related with each other. Hence, in addition to curves plotted for certain arbitrarily assumed value of $\log c_r$, we can readily calculate a table by means of which one can obtain the concentrations c_n, c_m and c_r on the basis of the values of $\log c_n$ and $\log c_m$ taken off the curves. To such curves one can apply the postulates of the control standard, conversion factor and other methods.

In the presence of a component with a constant concentration, we can take into account the influence of "third" components in a similar manner but without utilizing the condition $c_n + c_m + c_r + \ldots + c_i = \text{const}$. Without this condition one can also make out in the case of narrow ranges of variation of the concentration of all components, when the function (1) can be written in the form

$$\frac{I_n}{I_m} = (c_n c_m)^{k_n - k_m} c_r^{b_r^n - b_r^m}\frac{a_n}{a_m}, \quad (10)$$

where c_n, c_m and c_r are the major components.

Taking the respective logarithms and converting (10) to blackenings, also bearing in mind that

$$\Delta S_{n-m} = \Delta S_{r-m} - \Delta S_{r-n},$$

and solving the set of equations by means of standards separately for ΔS_{r-n} and ΔS_{r-m}, we can obtain

$$\Delta S_{nr-} = \gamma (k_n - k_m)' \lg (c_n c_m) + \gamma (b_r^n - b_r^m)' \lg c_r + \gamma \lg \left(\frac{a_n}{a_m} \right)', \quad (11)$$

$$\Delta S_{r-m} = (k_n - k_m)'' \lg (c_n c_m) + \gamma (b_r^n - b_r^m)'' \lg c_r + \gamma \lg \left(\frac{a_n}{a_m} \right)'', \quad (12)$$

whence

$$\Delta S_{r-n} - \frac{\gamma (k_n - k_m)'}{\gamma (k_n - k_m)''} \Delta S_{r-m} = \left[\gamma (b_r^n - b_r^m)' - \right.$$
$$\left. - \frac{\gamma (k_n - k_m)' \gamma (b_r^n - b_r^m)''}{\gamma (k_n - k_m)''} \right] \lg c_r + \gamma \lg \left(\frac{a_n}{a_m} \right)' - \frac{\gamma (k_n - k_m)'}{\gamma (k_n - k_m)''} \gamma \lg \left(\frac{a_n}{a_m} \right)'', \quad (13)$$

i.e., we can obtain a rectilinear plot. For further work we need only know the numerical value of

$$\frac{\gamma (k_n - k_m)'}{\gamma (k_n - k_m)''}.$$

The admissibility of the form of function (10) and a sufficiently small error arising as a result of separate solution of the set of equations for ΔS_{r-n} and ΔS_{r-m} can be checked with respect to a second group of standards and then controlled each time by obtaining a rectilinear plot in $\left(\Delta S_{r-n} - \frac{k'}{k''} \Delta S_{r-m} \right)$ vs $\log c_r$ coordinates from measurements with the standards.

For each specific analytic case one can select the most convenient of the described procedures and an optimal combination of the values of ΔS so that the relative error of determination of the components with a high concentration will not exceed ±1.2%.

The above exposition is fully substantiated by experimental data.

Zaporozhii Ferroalloy Plant

References

1. L. I. Topalov, in Sb. Sovremennye metody analiza v metallurgii (Collected articles on modern methods of analysis in metallurgy), p.64, Metallurgizdat, 1955.

2. L. I. Topalov, Zavodsk. laboratoriya (Industrial lab.), No.5, 549 (1957).

SPECTROSCOPIC DETERMINATION OF THE MAJOR COMPONENTS OF NOBLE METAL ALLOYS

- N.I.Varlamova & N.S.Sventitskii

Spectroscopic methods of checking noble metals for purity are now in fairly extensive use.[1-3] These methods, however, are still far from perfect, particularly where determination of the major components is concerned.

The two principal problems in analysis of noble metal alloys are determination of high concentrations with adequate reproducibility and meeting the requirement of minimal sample consumption, preferably with the possibility of analyzing finished products.

One of the conditions for successful solution of these problems is correct choice of the light source. Probably the best source is a high frequency spark. So far the specific potentialities of high frequency spark sources have been used primarily for investigation of biological specimens[4], for analysis of minute samples[5], for determination of carbon[6], and for analysis of welds[7,8]. Our experiments showed that the high frequency spark is a rather flexible light source. By varying the capacitance and inductance of the discharge circuit and replacing the conventional transformer by an autotransformer, one can obtain different excitation regimes. If the regime is characterized by the intensity ratio of the Cu II 2498.6 and Cu I 2492.1 Å lines, the range of feasible variation lies between the limits of -0.88 and +0.90. The reproducibility of conditional analysis with reference to these lines is 2-2.5%. The reproducibility of analysis with reference to the Cu I 5105.5 and Cu I 5153.2 Å lines is 1.2%.

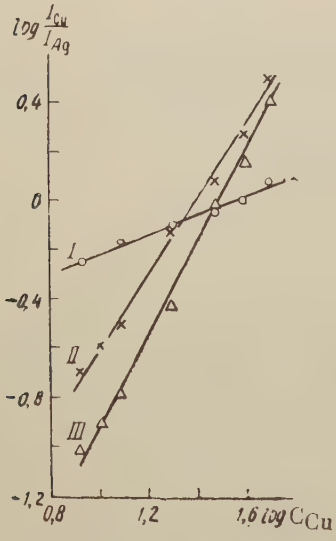

Variation of the relative intensities of analytic lines with the Cu content in binary Ag-Cu alloys: I) Cu I 3247.5 - Ag I 3382.9 Å (ISP-28 spectrograph), II) Cu I 5218.2 - Ag I 5209.1 Å (ISP-28 spectrograph), III) Cu I 5218.2 - Ag I 5209.0 Å (ST-7 steelometer).

We investigated binary alloys of silver with copper to evaluate the possibility of developing an analytic procedure for alloys of this type. Using a high frequency spark (0.5 amp, 220 ± 2 v) for analysis of alloys containing from 8 to 50% copper, it proved feasible to obtain a concentration dependence even for the resonance lines Cu I 3247.54 and Ag I 3382.89 Å and, although the slope of the working curve was not great (~0.4) the results of determination of copper (for the alloy with 40% Cu) reproduced with a probable single determination error of ±2.8%.

The spectrum of such a "soft" spark, however, proved sensitive to the physical condition of the samples. Thus analyses of forged samples yielded underestimates of the Cu concentration when the determinations were made on the basis of the curve plotted for cast samples.

Increase in the power of the discharge led to self-reversal of the above mentioned spectrum lines and loss of the concentration sensitivity. Better results were obtained with the green lines Ag 5209.1 and Cu 5218.2 Å (ISP-28 or ISP-22 spectrograph). The concentration sensitivity was much higher than for Ag I 3382.89 and Cu I 3247.54 Å lines (curves I and II in the accompanying figure). The intensity of both the silver and copper lines changed; the slope of the working curve increased to 1.4. Under the altered discharge conditions, the results of analysis for cast and forged samples fitted the same working curve. The reproducibility, however, did not improve and amounted

to ±3.0%; it was determined primarily by the inadequate quality of the "Izoorto" plates (speed 45 GOST units) and the small distance of the analytic lines from the edge of the plate. Visual determination by means of an ST-7 steelometer (curve III) was realized with a reproducibility of ±1.6%. Approximately the same deviations were obtained in analysis with the photoelectric FES-1 steelometer; in the last case the error could be reduced by comparing the intensity of the silver lines not with the integral radiation but with a neighboring copper line.

Similar results were obtained in determining copper in ternary Cu-Ag alloys with nickel and gold.

The experimental results obtained may serve as a basis for development of specific methods of analysis of noble metal alloys with excitation by high frequency sparks. The consumption of sample material is negligible. The reproducibility is generally satisfactory in analysis of components with high concentrations.

Low energy spark spectra can, apparently, serve as a useful means for investigating variations in the metallo-physical state of alloys.

References

1. A.L.Kheifits & S.M.Katchenkov, Izv.AN SSSR, Ser.fiz., 9, 301 (1947).
2. A.L.Kheifits & A.N.Cherezova, Ibid., 12, 462 (1948).
3. W.Koeher, Metall., 7, 422 (1953).
4. V.V.Gerlyakh, Spektrokhimicheskii emissionyi analiz (Spectrochemical emission analysis), ONTI, Khimteoreg, L., 1036.
5. A.N.Prokop'eva & K.I.Taganov, Zavodsk.labor. (Indust.lab.) 15, 299 (1949).
6. A.P.Oleinikov & K.I.Taganov, Ibid., 15, 59 (1949).
7. E.S.Kudelya, Ibid., 17, 1064 (1951).
8. E.S.Kudelya, Avtomat.svarka (Automatic welding), No.4, 54 (1952).

SPECTROSCOPIC DETERMINATION OF HIGH CONCENTRATION COMPONENTS IN STEELS AND OTHER ALLOYS

- A.G.Komarovskii

Spectroscopic determination of high concentrations of alloying elements - Mn, Si, Cr, Ni, Mo, W, Ti, V, Co, Nb and Al - encounters a number of difficulties, that become particularly serious in analysis of complex alloys in which the influence of "third" components is strongly evinced. This influence leads primarily to parallel displacement of the working curves in going from one system of steels or alloys to another. In some cases there is also observed a small change in the slope of the working curves.

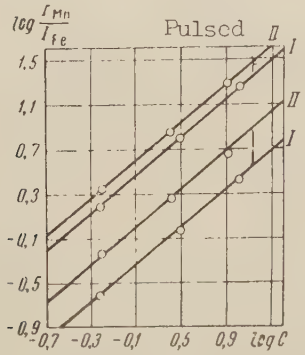

Fig.1

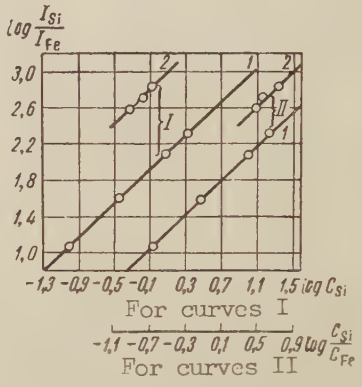

Fig.2

Fig.1. Working curves for determining Mn in simple (I) and high alloy (II) steels in a low voltage pulsed spark (upper curves) and in a condensed spark from an IG-s spark unit (lower curves). Analytic pair: Mn 3482.90 - Fe 3465.80 Å.

Fig.2. Working curves for determination of Si in simple (1) and more complex (2) alloys plotted in log (I_{Si}/C_{Fe}) vs log C coordinates (curves I) and in log (I_{Si}/I_{Fe}) vs log (C_{Si}/C_{Fe}) coordinates (curves II). Analytic pair: Si 2506.90 - Fe 2498.89 Å. Source - IG-3 spark unit.

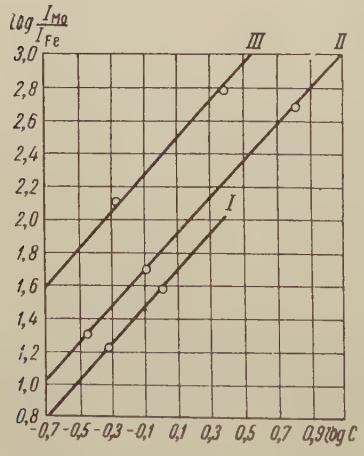

Fig.3

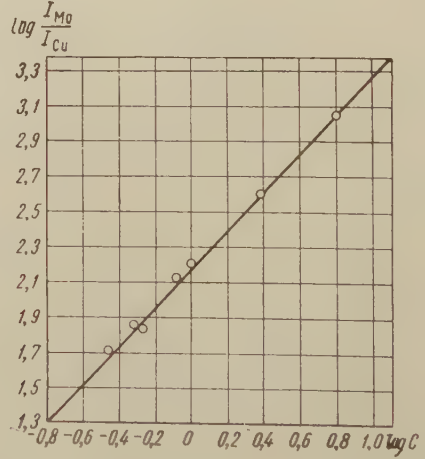

Fig.4

Fig.3. Working curves for determination of Mo in three types of steels and alloys with reference to the Mo 2816.15 - Fe 2823.28 Å line pair. Source - IG-3 spark unit.

Fig.4. Working curve for determination of Mo in different steels and alloys (same as those characterized by curves in Fig.3). Source - IG-3 spark unit. Counterelectrode - copper; analytic pair: Mo 2816.15 - Cu 2824.37 Å.

The present research was concerned with determining the causes of the influence of "third" elements and finding means of reducing or eliminating this effect. As a result of our experiments we established the following.

1. The use of a localized high-power low voltage spark discharge for analysis of steels and alloys leads to an appreciable reduction of the parallel shift of the working curve (plotted on the basis of samples of simple and high-alloy steels) as compared with the shift observed when an ordinary condensed spark such as that supplied by the IG-3 spark unit is employed. It must be noted, however, that the shift is not wholly eliminated (Fig.1).

2. Plotting the working curves in terms of log (I_{an}/I_{ref}) vs log (C_{an}/C_{ref}) instead of log (I_{an}/I_{ref}) vs log C also leads to a decrease of the parallel shift of the working curves (Fig.2).

3. The material of the upper counterelectrode has an appreciable influence on the intensity of the sample spectrum and on the accuracy of analysis. In a number of cases, when a spectrum line of the counterelectrode is used as the reference, the influence of the "third" elements is either reduced or completely eliminated (Figs.3 & 4).

Hence, our study showed that it is feasible to select excitation conditions under which the influence of "third" elements is minimized or completely suppressed.

Central Scientific Research Institute of Technology and Machine Building

STATISTICAL INVESTIGATION OF ANALYTIC RESULTS

- V.V.Nalimov

One of the problems of mathematical statistics consists of "convolution" (condensation) of information and presentation of it in compact form convenient for communication, storage and further processing. This problem has become particularly acute now in view of the accelerated increase in the amount of experimental material.

The results of each and every experiment comprise a certain degree of uncertainty, while every study as a whole contains an element of doubt; these are connected with experimental errors, the specific conditions of the experiment, the limitations of the experimental facilities, etc. Earlier when the number of published reports was small, the reader could form an idea of this element of uncertainty by careful reading of the description of the experimental conditions and the processing of the experimental data as described by the author. At present, when there may be tens or even hundreds of studies devoted to a specific topic or narrow field of specialization, comparison of the qualifying data when presented in the form of nonstandard extensive descriptions becomes impossible. Moreover, it must be borne in mind that owing to the large volume of reports presented, many scientific journals are forced to reduce the scope of individual articles, and in such condensation or abstracting much subsidiary information is necessarily eliminated.

Information on the accuracy and reliability of analyses given in different official instructions and in the analytic GOST's (All-Union State Standards), the data characterizing standard samples and the results of routine analysis, if they give the effective ranges or bounds, may also be regarded as "convolution" of information, i.e., condensation of the information contained in the extensive experimental research involved in the preparation of these instructions, standards, etc. It may be asserted that convolution of information must be an integral and essential part of each and every analytic operation.

At present it is feasible to give a classification of methodical errors with a view to facilitating application of statistical methods to planning experiments and processing their results and to indicate the conditions under which one can expect a normal distribution, a Poisson distribution or a binomial distribution in analytic work. In view of this one can now outline the general theory of the analytic process that can be constructed on the basis of the theory of probability, much as in its time there was constructed the general theory of measurement - metrology. The problem of constructing such a theory reduces essentially to expressing all the characteristics and features of a given analytic method and all the difficulties associated with it in a compact fashion in the language of statistics.

In order to be able to evaluate objectively the accuracy of any given analytic method (spectroscopic, chemical or other) one must determine and define the following quantities: 1) the error in intralaboratory measurements, characterizing the scatter of analytic results relative to an average value obtained within the laboratory, using one particular set of equipment and within a given short period of time; 2) the error due to factors varying slowly with time and characterizing the spread in the analytic results relative to an average value obtained within the same laboratory but over a prolonged period; 3) the interlaboratory error of reproducibility, characterized by the scattering of the analytic results relative to the average value obtained in different laboratories.

In evaluating the reliability of analysis, the results of determination carried out on a given series of samples by one method are commonly compared with the corresponding data obtained by a different method. In this case it is important to determine not only the magnitude of the deviation between the results of

analyses but also to evaluate the effect of interaction characterizing the dependence of the deviation of the analytic results from the actual composition of the sample. If the effect of interaction is statistically insignificant, then thereafter in routine work we can limit the consideration to comparison of two analytic methods as applied to one specific standard sample. Both these problems are solved by means of analysis of variance.

Spectroscopic emission analysis is based on plotting and subsequent use of working curves. Hence here it is essential to present in compact fashion all the information connected with solving the problem of "calibration". Specifically, it is necessary 1) to check the linearity hypothesis, i.e., to determine whether the scatter of the experimental points relative to the working curve is due solely to reproducibility errors, 2) to investigate the character of the time-fluctuation of the working curve parameters, and 3) to determine whether the working curves plotted on the basis of the primary standards agree with the working curves based on secondary standards. In principle, these problems of experiment planning and compact presentation of the results can be solved by means of regression analysis, which is a further generalization of variance analysis.

If for each analytic method and procedure there are indicated all the characteristics enumerated above, it will be easy to compare and evaluate them.

In giving out or publishing the results of routine analyses it is not sufficient to indicate only the reproducibility error. If the working curves are based on m standards, then using the methods of mathematical statistics one can determine the region of possible values for an (m + 1) standard which, in general, proves to be an area limited by two branches of a hyperbola. The interval of possible values for the results of a given determination will depend on the number of standards used for constructing the working curve, on the "position" of the standards relative to the center of the curve and on the standard error characterizing the scattering of the points relative to the working curve.

Design of the experiment, processing of the experimental results and final presentation of the analytic data must be carried out in a strictly uniform and standard manner. We note that foreign journals have long called on laboratory workers to renounce the use of the arithmetic mean error as a measure of the scatter of measurement results. The probable error is also no longer used in analytic work abroad. The properties of these two characteristics are such that they cannot be recommended for presenting the results of statistical analysis. We believe it desirable that our scientific workers, too, in presenting the results of statistical evaluations should only use the standard (root mean square) deviation as the uniform measure of scattering.

In so brief a report we can only formulate in the terms of mathematical statistics the problems that must be faced by scientific workers in developing new methods of analysis. The mathematical formalism for solution of the problems can be found in mathematical references and handbooks.

STANDARDS FOR DETERMINATION OF IMPURITIES IN PULVERIZED COMPLEX FERROALLOYS

- A.B.Shaevich

The preparation of ferroalloy standards is hampered by their high melting point, the complexity of controlling and determining the chemical composition, and the appreciable influence of "third" elements and the structure of the alloy on the spectroscopic results. Each of these difficulties taken separately can be overcome by appropriate measures, but unfortunately often when applied together these measures counteract and defeat each other. In this case it is not expedient to use synthetic working standards inasmuch as disparity between the standards and the samples would involve complicating the analytic procedure (for example, converting the metallic samples to oxides) and increase the time required for analysis. The use of primary synthetic standards for establishing the composition of the working standards by spectrum analysis[1] is also very inconvenient inasmuch as determination of impurities present in concentrations of 5 to 10% with the requisite accuracy requires a great deal of time. Analysis of such alloys in many cases, however, is facilitated by pulverizing the standards and samples.

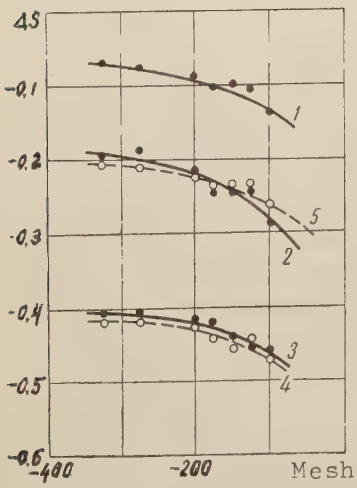

Influence of fining of the analyzed sample on the difference in blackening ΔS of the analytic line pair for determination of aluminum (1), silicon (2) and copper (3) in ferrotitanium, and aluminum (4) and titanium (5) in ferroniobium. Each point represents the average for 24 measurements. Line pairs: Al 2652.49 - Fe 2647.56 Å, Si 2435.16 - Fe 2443.91 Å, Cu 2824.37 - Fe 2828.81 Å (for determination of the impurities in ferrotitanium); Al 2660.39 - Fe 2635.81 Å, Ti 3072.97 - Fe 3068.18 Å (for determination of impurities in ferroniobium).

We came to the conclusion that the most effective method of preparing standards of such alloys consists in successive dilution of one "head" standard with a typical composition[2-4].* The possibility of restricting the number of standards to one typical standard is particularly valuable in the case of analysis of ferroalloys inasmuch as this eliminates one of the principal sources of disparity between the standards and the sample. The method of successive dilution was checked in practice in preparing standards for the determination of impurities in ferrotitanium, ferroniobium and ferromolybdenum.** Among other matters, we investigated the chance errors connected with unavoidable variation in the operation of diluting and mixing the components, the influence of the granulometric composition of the mixture on the intensity of the spectrum lines, and the residual influence of "third" elements and structure.

The "head" (diluted) standards were standard samples of the respective ferroalloys; the diluent was iron oxide (analytic reagent grade). The light source was an ac arc (the analytic procedure is described in detail in Refs.6 & 7). Evaluation of the magnitude of the different component errors, carried

---

*This dilution should not be confused with the dilution procedure proposed by Shavrin, the purpose of which is to make more uniform the composition of diverse initial samples by adding a common component.

**V.V.Bugrina, Ya.M.Kalinskii, N.I.Chabanenko, M.A.Perepelkina and A.G.Korovina participated in the experimental part of the work.

out by the variance method, showed that the deviations connected with unavoidable variations in the preparation of the mixture, amounts to approximately 0.4 of the total chance error σ, i.e., is close to the value corresponding to the criterion for insignificant errors ($\leqslant 0.3\ \sigma$).[8] We established the variation in the intensity of the lines of the determined elements and the diluent as a function of the powder particle size (see accompanying figure). The observed variation is consistent with the current concepts regarding the influence of the degree of development of the surface on the rate of evaporation. To eliminate this effect the sample should be ground to at least 200 mesh.

Introduction of graphite powder does not always radically reduce the influence of "third" elements and the structure of the sample. Quantitative evaluation carried out taking into account the requisite analytic accuracy showed that it is essential to use a "head" standard having the composition and structure characteristic of the analyzed samples.

Use of the described procedure for preparation of standards serving for analysis of complex ferroalloys made it possible to dispense with melting, casting and chemical analysis of series of standards, and to replace each series by one standard sample. This method can also be recommended for preparation of standards for analysis of other pulverizable complex alloys.

Ural Institute of Ferrous Metals

References

1. A.B.Shaevich, Zavodsk. laboratoriya (Indust. laboratory) 21, 332 (1955).
2. G.Sheive, Khimicheskii spektral'nyi analiz (Chem.spect.analysis), ONTI, 1938.
3. S.M.Katchenkov, Spektral'nyi analiz gornykh porod (Spectrum analysis of rocks), p.44, Gostoptekhizdat, 1957.
4. O.B.Fal'kova, Doklady AN SSSR, 48, 189 (1945).
5. A.M.Shavrin, Zavodsk.laboratoriya, 15, 66 (1949).
6. A.B.Shaevich, Ya.M.Kalinskii, N.I.Chabanenko & M.A.Perepelkina, Ibid., 24, No.12 (1958). (Trans.Industrial Laboratory.)
7. Ya.M.Kalinskii, A.B.Shaevich, V.V.Bugrina, N.I.Chabanenko & M.A.Perepelkina, Materialy II Ural'skogo soveshchaniya po spektroskopii (Transactions of the Second Ural Conference on Spectroscopy), Sverdlovsk, 1959.
8. M.F.Malikov, Osnovy metrologii (Fundamentals of metrology), Part 1, p.184, Committee on Weights and Measuring Instruments, M., 1949.

PREPARATION OF STANDARDS FOR SPECTROSCOPIC ANALYSIS OF NOBLE METALS

- A. A. Kuranov

In view of the expanding use of noble metals in industry and the ever more exacting requirements as regards their purity, it is essential to improve extant methods of analysis and to develop new ones. In recent years spectroscopic methods have been coming into increasing use.[1] Developments in this field, however, encounter the difficulty of preparing suitable standards; hence this problem merits particular attention.

There are three principal types of standards - cast, synthetic (powder) and solutions; we shall take these up in turn.

Cast standards

In preparing standards[2] for analysis of refined silver for Pt, Pd, Au, Cu, Pb, Bi, Sb and Fe in the concentration range from 10^{-5} to 10^{-2}%, the solubility of these elements is first evaluated on the basis of solubility diagrams[3]. All the enumerated elements except iron exhibit either limited or unlimited solubility in silver. Investigation[4] of Fe in silver showed that in some cases this element, which is normally insoluble in silver, can diffuse through it, particularly if there is present a so-called horophilic (segregating) element which combines with the Fe to yield a continuous series of solid solutions. Thus presumably the solubility of Fe in silver can be enhanced if palladium is added to the silver or if the iron is introduced into the silver in the form of Fe-Pd alloy.

In order to realize this and bring the melting point of the introduced metals close to the melting point of silver, we prepared a series of binary solutions having the following compositions:

Alloys and metals introduced into the silver melt

Metal	Melting point, °C
Silver	960
80% Palladium + 20% Iron	1390
Gold	1063
50% Lead + 50% Platinum	800
50% Bismuth + 50% Copper	910
50% Iron + 50% Antimony	1000

The standards were melted in graphite crucibles under a carbon shield in a high-frequency induction furnace which assured intense mixing of the melt. The impurities were introduced into the silver melt wrapped in silver foil. Spectroscopic studies showed that the impurities were uniformly distributed through the volume of the castings.

In this manner we prepared standards with large amounts of the chosen impurities; these standards were then used to prepare the other standards by dilution with the pure base (silver). The composition of the standards was monitored by chemical analysis; at the same time we checked for contamination by the method of "additions"[5]. This is feasible because the losses in melting are negligible.

Standards for analysis of high purity gold, platinum and numerous alloys of silver, gold and platinum were prepared by the same procedure.

Synthetic standards prepared of metal powders

In many cases owing to the high melting point of the metal and inadequacy of the control procedures, it is impossible to prepare standards by casting. In view of this, in recent years we have had increasing recourse to the procedure

of preparing standards of powdered metals. The metal powders are carefully mixed in the requisite proportions; then the mixture is compressed into briquettes which are annealed at a temperature close to the melting point of the base. As a result there are obtained homogeneous standards with impurity concentrations ranging from a few hundredths to some ten-thousandths of a percent. Uniformity of distribution of the impurity is checked spectroscopically and by means of radioactive tracers. In this fashion we prepared standards for analysis of silver[6] and subsequently for analysis of platinum-rhodium alloys for Pd, Ir, Ru, Au, Fe, Al, Cu, Ag, Pb, P, Bi, Zn, Sn, Ni and Si and of platinum-palladium alloys for Ir, Ru, Au, Rh, Fe, Al, Cu, Ag, P, Pb, Bi, Zn, Sn, Ni, Si and Sb.

The powder technique is applicable not only for metal standards but also for mixtures of metals with carbon powder. Present methods of analysis of rhodium and iridium[7-9] provide for the determination of only a small number of impurities owing to the complexity of preparing suitable standards. Actually, however, it is essential to determine Pt, Pd, Au, Ru, Ir, Si, Fe, Cu, Al, Pb, Ba and Ni in rhodium and Pt, Pd, Au, Ru, Rh, Si, Fe, Cu, Al and Pb in iridium. Experience shows that one cannot prepare standards for the determination of all these impurities by the melting technique. In such cases one can have recourse either to solutions[9] or to metal powder standards.

In preparation for tests of the solution technique, we prepared a series of titrated solutions of Al, Fe, Pb, Ni, Cu, Pt, Pd, Au and Ba by conventional procedures. The silicon was put into solution by baking with soda and subsequent leaching with water. Ir, Rh and Ru are virtually insoluble in acids. The method of dissolving in a glass test tube[9] leads to appreciable contamination of the solutions with silicon. Hence we used the alternating current technique for dissolving noble metals: two plates of the metal to be dissolved are immersed in a 20% solution of HCl; the metal is satisfactorily transferred into solution at a current density from 0.5 to 5 amp/cm^2. The standards are then prepared by mixing the resultant solutions and evaporating these to dryness. The dried salts are carefully ground and heated in a tubular furnace at 900° in a stream of hydrogen. The resultant metal sponge is mixed in the proportions of 2 to 1 with carbon for

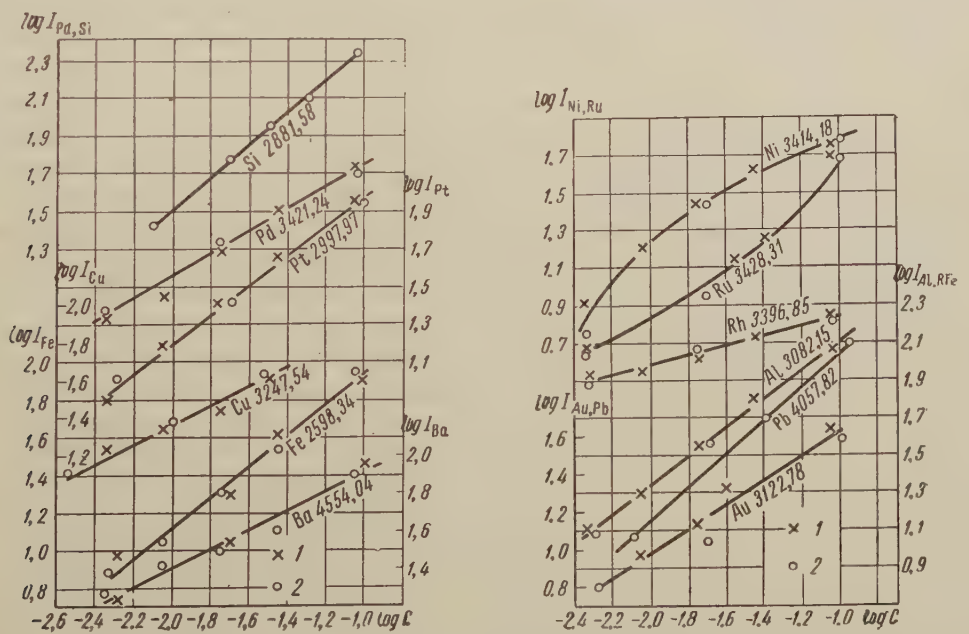

Comparison of the working curves based on solutions (1) and synthetic (powder) standards (2) for analysis of iridium.

a period of 12 hours and the final mixture is compressed into 0.15 g pellets.

A second series of standards was prepared by mixing metal powders using the base metal from the same lot. A 20 g batch consisting of a mixture of the metal, the impurity and carbon powder was thoroughly mixed for 14-18 hours and then compressed in a steel die 20 mm in diameter at a pressure of about 1600 kg/cm^2. The briquettes were subjected to homogenizing (diffusion) anneal for 5-6 hours at 1000° in a stream of hydrogen. After annealing the briquettes are ground in a mortar and 0.15 g portions of the mixture are taken for analysis. Comparison of the working curves plotted on the basis of the two series of standards (see fig.) show complete agreement.

Solution standards

Solution standards are used in our laboratory only for checking cast and synthetic standards and in cases when it is necessary to carry out an individual analysis of some new alloy. In such cases a series of titrated solutions of the elements in question is prepared; the requisite standards are prepared by mixing the appropriate solutions. Drops of the solution are applied by means of a pipette to carbon electrodes preheated to 60-80°. The electrodes have a neck-in some 10 mm from the tip to prevent the solution from penetrating too deep into the electrode. The electrodes are dried in a sand bath and then are ready for analysis.

References

1. W.Kochlor, Metall., 7, 422 (1955).

2. A.A.Kuranov & M.M.Sviridova, Materialy I Ural'sokogo soveshchaniya po spektroskopii (Transactions of the 1st Ural Conference on Spectroscopy), Sverdlovsk, 1958.

3. M.Hansen & K.Andreko, Constitution of Binary Alloys (Cited in Russ. trans.).

4. V.I.Arkharov & B.A.Yunikov, Trudy in-ta fiz.metallov (Proceedings of the Institute of Metal Physics) Ural Branch, USSR Ac. of Sci., No.16, 62 (1955).

5. V.K.Prokof'ev, Fotograficheskie metody kolichestvennogo spektral'nogo analiza metallov i splavov (Methods of quantitative spectrum analysis of metals and alloys), Vol.1, p.198, Gostekhizdat, 1951.

6. A.A.Kuranov & M.M.Sviridova, Sinteticheskie etalony dlya spektral'nogo analiza serbra. Zavods.laboratoriya (v pechati) (Synthetic standards for spectrum analysis of silver) (in print). (Trans.Industrial Laboratory).

7. A.V.Babaeva, V.I.Belova & L.A.Nazarova, Izv.sektora platiny (Bulletin of the platinum sector) IONKh AN SSSR, No.20, 172 (1947).

8. A.V.Babaeva & E.S.Lapir, Ibid., No.22, 145 (1948).

9. C.L.Lewis, W.Z.Ott & J.E.Hawley, Canad.Min. & Met.Bulletin, 48, 208 (1955).

METHODS OF CALIBRATION IN ANALYSIS OF ALLOYS

- E.S.Kudelya & A.S.Dem'yanchuk

In analyzing diverse industrial alloys we have made extensive use of two calibration methods based on the use of a single standard. Our experience shows that the resultant accuracy is no lower than that obtained by the method of three standards.

The first method, which we call the method of "fractional exposure", may be briefly described as follows. Usually exposure of alloy spectra is begun after a period of presparking of the electrode, when the intensity of the spectrum lines is stabilized. If the density values of the lines do not fall outside the rectilinear section of the characteristic curve of the emulsion, the increments in density of each spectrum line for equal exposure time increases will be virtually equal. If under these conditions we photograph on the same plate two spectrograms of the standard, one with an exposure time t equal to that used for analysis and a second with an exposure time t/2, the densities or blackenings of the impurity lines in the first spectrogram will correspond to the actual concentrations of the impurity in the standard and in the second spectrogram to half the concentration values. To equalize the blackenings of the lines of the matrix elements in the sample on both spectrograms one should without displacing the cassette after the second photograph, additionally photograph the spectrum of the matrix component, for example, in the case of steels and cast irons, the spectrum of iron. The auxiliary sample or standard should be presparked for the same period as in photographing the standard itself and the exposure time should be selected so that the total duration of exposure of the second spectrogram would be equal to the exposure used for analysis. Specifically, in using this single standard procedure we recommend obtaining four points for constructing the working curve. We photograph the spectrum of the standard with exposures of t, 2/3 t, 1/2 t and 1/3 t and then superpose on the last three spectrograms the spectra of the matrix element with exposures of 1/3 t, 1/2 t and 2/3 t, respectively. This procedure is repeated three times. The spectrograms are then processed in the same way as in employing the three standards procedure. In the absence of standards of the pure metal for the supplementary photographing, one must take into account the contents of the determined impurity in the alloy used for the supplementary spectra.

Fig.1 shows the working curve for determination of Si in steels obtained by this procedure using UIM (Ural Scientific Research Institute of Ferrous Metallurgy) standard No.57. The fractional indices following the standard number indicate the exposure time in fractions of t. To check the curve, we photographed the spectra of standards Nos.55, 56, 124 and 125 on the same plate.

The second procedure, which we call the method of "dosed exposure", consists of obtaining a series of spectra for the same standard with the duration of exposure for some of the spectrograms being a known fraction of the main exposure t and the duration of the exposure for the other spectra being multiples of t. The concentrations corresponding to all the spectrograms except the principal one (exposure t) are found by calculation. Then these calculated concentrations are used for plotting the working curve.

For analysis of low and medium alloy steels we chose UIM standard No.51 which contains almost all the alloying elements encountered in steels. Under our conditions, we took t = 20 sec and the dosed exposures equal to 10, 30, 40, 50 and 60 sec.

By way of illustration, in Fig.2 we show the working curve for determination of Ni in steel: curve 1 is plotted on the basis of standards set V, while curve 2 is plotted on the basis of standard No.51 for which the equivalent nickel

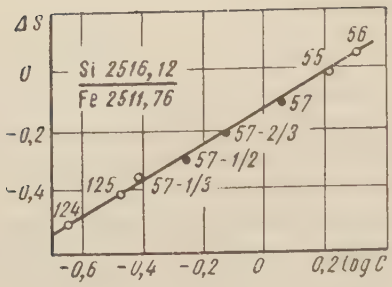

Fig.1

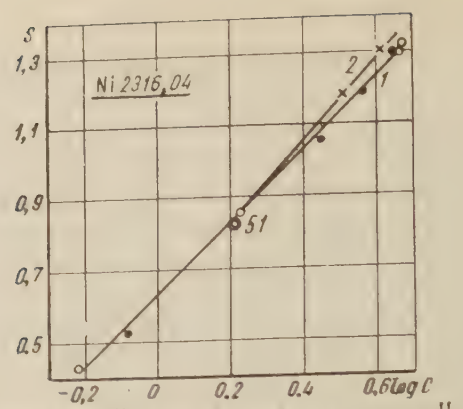

Fig.2

Fig.1. Working curve for determination of Si in steels ("fractional exposure" method).

Fig.2. Working curve for determining Ni in steels ("dosed exposure" method). Curve 1 is plotted on the basis of the standards of set V; curve 2 on the basis of UIM standard No.51 using Eq.(1); the auxiliary points on curve 1 were obtained by means of Eq.(2).

"contents" were calculated for the different exposures according to the formula

$$C_{t_n}\% = \frac{C_t t_n}{t}, \qquad (1)$$

where C_t is the actual concentration of the determined elements (Ni in this case) in the standard, t is the main exposure, i.e., the exposure used in photographing the spectrum of the analyzed sample, t_n is the value of the other exposure times in photographing the standard spectra, and C_{t_n} is the calculated impurity concentration.

As will be evident from Fig.2 this formula is valid only for concentrations lower than C_t: curves 1 and 2 coincide completely in this low concentration region. Agreement of the curves in the section for higher values of C_t requires fulfilment of following empirical regularity

$$C_{t_n} = \frac{C_t (t_n + r)}{t}, \qquad (2)$$

where r is the common difference of the arithmetic progression, which is found from experiment.

Both methods can be recommended for determining concentrations from 0.05% up (for phosphor from 0.01% up). Extensive use of both procedures in practice shows that they are applicable for quantitative spectrochemical analysis of metals for various alloying elements and impurities, including carbon and phosphorus.

"E.O.Paton" Institute of Electric Welding,
Academy of Sciences of the Ukrainian SSR

USE OF THE "FRACTIONAL EXPOSURE" PROCEDURE FOR ANALYSIS OF SOME ALLOYS

- E.P.Barankina

The method of "fractional exposure" proposed by Kudelya & Dem'yanchuk[1] (see preceding article) was tested by us for determination of a number of elements. The work was carried out on an ISP-22 spectrograph with excitation by means of the IG-2 spark source.

1. Determination of Si in steel

The standard was a commercial sample of steel containing 4.54% Si. The excitation circuit parameters were C = 0.01 μf, L = 0.05 mh, and I = 1.4 amp; the spectrograph slit width was 0.025 mm; the counterelectrode was a 6 mm diameter carbon electrode tapered at the tip to a cone with a 1.5 mm^2 flat. For dilution we used Armco iron containing 0.19% Si. The presparking time was 60 sec; the total exposure t_e = 24 sec. The analytic line pair was Si 2881.6 - Fe 2880.7 Å.

Table 1

Exposure times and calculated Si concentrations

Electrode	Si content, %	Reduced Si content, %	
		3/4 t_e = = 18 sec	2/3 t_e = = 16 sec
Standard	4,54	3,405	3,020
Armco iron	0,19	0,047	0,063
Calculated concentration		3,45	3,08

Table 2

Exposure times and calculated Al, Zn & Mn concentrations

Element	Calculated content in standards	
	3/4 t_e = 9 sec	1/2 t_e = 6 sec
Al	3,63	2,42
Zn	1,18	0,79
Mn	0,62	0,41

The exposure times in photographing the standard spectrum and the calculated concentrations of the determined elements are listed in Table 1. The deviation between the results of spectroscopic and chemical analyses is ±2.5% on the average.

2. Determination of Al, Zn and Mn in magnesium alloy

In this case the working curves for determination of Al and Zn were plotted by means of one standard containing 4.85% Al and 1.58% Zn. A second standard containing 0.82% Mn served for plotting the curve for determining Mn. In the future, with a view to reducing the photographing time, we hope to find among the production samples a single universal standard.

Spark circuit parameters: C = 0.005 μf, L = 0, I = 1.1 amp; slit = 0.025 mm; permanent electrode - magnesium with hemispherical tip; presparking time = 60 sec; full exposure time t_e = 12 sec.

The standards were diluted with pure magnesium to the calculated concentrations listed in Table 2.

We used the analytic lines: Al 3082.2, Zn 3345.0 and Mn 2949.2 Å. The reference was the Mg 3074.0 Å line. The deviations between the results of spectroscopic and chemical analyses amounted on the average to ±3% for determining aluminum, ±5% for zinc and ±5% for manganese. The calibration curve for determining Al is reproduced in Fig.1.

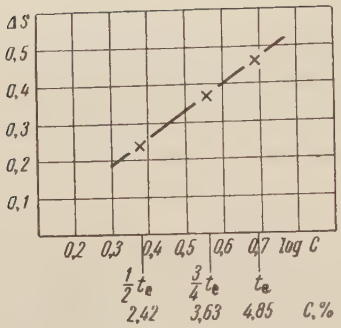

Fig.1. Working curve for determination of Al in magnesium alloy.

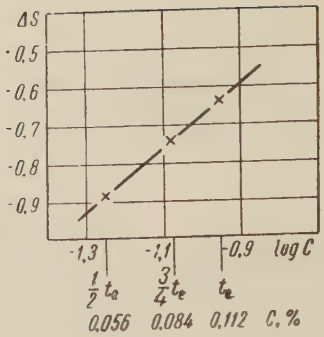

Fig.2. Working curve for determination of Ti in aluminum alloy.

3. Determination of Ti in aluminum alloy

The standard in this case was a commercial sample containing 0.112% Ti. Spark circuit parameters: C = 0.005 μf, L = 0.1 mh, I = 1.2 amp; spectrograph slit - 0.025 mm; permanent electrode - aluminum with hemispherical tip; prespark-ing time - 90 sec; total exposure time t_e = 36 sec.

The standards were diluted with pure aluminum to the calculated concentrations listed in Table 3.

Table 3

Exposure times and calculated Ti concentrations

Calculated Ti conc., %	
3/4 t_e = = 27 sec	1/2 t_e = 18 sec
0,084	0,056

Table 4

Exposure times and calculated Be concentrations

Standard No.	Calculated Be conc., %		
	1/2 t_e = = 6 sec	1/4 t_e = = 3 sec	1/6 t_e = = 2 sec
4	0,0010	0,0005	—
7	0,0006	0,0003	0,0002

The analytic pair was Ti 3349.4 - Al 3066.2 Å. The deviation between the results of spectroscopic and chemical analyses amounted to ±6% on the average. The working curve is shown in Fig.2.

4. Determination of Be in magnesium alloy

Beryllium concentrations in the range from 0.0002 to 0.0020% were determined with reference to spectrograms which also served for the determination of other elements, the concentrations of which varied from tenths to several percent. Hence the spectrum was photographed under the usual conditions for analysis of the magnesium alloy. The analytic Be 3130.4 Å line was very weak and the working curve was not a straight line. The relative intensity was gaged with reference to the continuum to the right of the Be line.

Spark circuit parameters: C = 0.005 μf, L = 0, I = 1.1 amp; permanent electrode - magnesium with hemispherical tip; presparking time - 60 sec, total exposure t_e = 12 sec. The standards available to us contained 0.0012% beryllium and higher. To enhance the accuracy in plotting the working curve we "diluted"

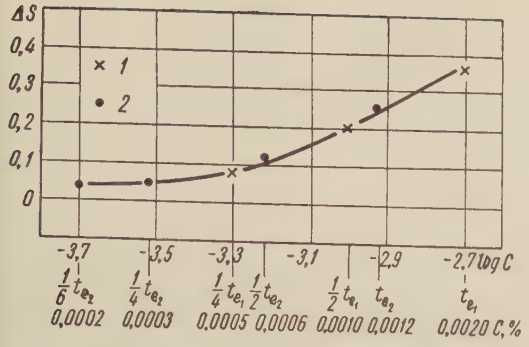

Fig.3. Working curve for determination of Be in magnesium alloy: 1) data for standard No.4; 2) data for standard No.7.

two standards with beryllium concentrations of 0.0020 and 0.0012%. The standards were diluted with pure magnesium to the concentrations indicated in Table 4.

No chemical analyses of the samples with low beryllium concentrations were made. According to calculations based on proportioning of the melts, the beryllium content in the samples amounted to 0.0002-0.0005%. The results of spectroscopic analysis substantiate this evaluation. The working curve is shown in Fig.3.

Thus we have shown that it is feasible to use the "fractional exposure" method of spectroscopic analysis. This procedure is now being employed where lack of suitable standards prevents the use of other methods.

References

1. E.S.Kudelya & A.S.Dem'yanchuk, Present issue of the Bulletin, p.1135.

* * * * * * * * *

PREPARATION OF STANDARDS OF DIFFERENT ALLOYS AND INVESTIGATION OF THE INFLUENCE OF "THIRD" ELEMENTS IN THEM

- K.A.Sukhenko, O.I.Mladentseva & A.V.Aksenova

To meet the different demands of industry we have developed, investigated and are now producing standards for analysis of aluminum, nickel and titanium alloys and heat-resistant steels. Many of these alloys are very complex as regards composition and in addition to a high concentration (20-30%) of some elements contain various impurities in concentrations from 0.01 to 0.0005%.

The technology of casting aluminum alloy standards is well developed and provides for obtaining a large number of standards of good quality. Thus, for example, standards of different types of aluminum and silicon alloys can now readily be prepared by the continuous casting method in the form of wire, which makes it possible to produce large sets of standards for analysis of these alloys and fully satisfy the requirements of industry.

Titanium alloy standards are prepared by the method of arc melting with two-fold remelting. The ingots obtained after the second remelting are forged into 12 mm diameter rods, cut into 110 mm lengths and finally machined on lathes.

The optimal conditions selected and specified by us for analysis of titanium alloys are the following: source unit - IG-2 spark generator (settings: C = = 0.01 μf, L = 0.01 mh), counterelectrode - carbon. For the VT-2, the spark gap should be 2 mm, sparking time - 1 min 30 sec; for the VT-3-4-5, 2.5 mm and 40 sec, respectively, and for the VT-6, 2.5 mm and 1 min 40 sec, respectively. The attainable accuracy is listed in the accompanying table.*

One of the fundamental problems in preparing standards is evaluation of the influence of "third" elements on the results of spectrochemical analysis. Re-

---

*K.A.Moiseev participated in this part of the work.

No.	VT-2		VT-3-4-5		VT-6	
	Analytic pair	Arith. mean dev.%	Analytic pair	Arith. mean dev.%	Analytic pair	Arith. mean dev.%
1	Al 3961 Ti 3989	±4,4	Al 3092 Ti 3038	±5,8	Al 2816 Ti 2820	±5,0
2	Al 3092 Ti 3048	±5,2	Mo 2848 Ti 3038	±7,3	V 2882 Ti 2820	±4,2
3	Cr 3040,8 Ti 3048,7	±5,0	Cr 2843 Ti 2841	±5,6	V 3093 Ti 2820	±5,2
4	Cr 2766,5 Ti 2841,9	±6,0	Mn 2605 Ti 2556	±10,0	Si 2881 Ti 2820	±9,0
5	Cr 2843 Ti 2841	±5,0	Si 2514 Ti 2520	±4,3	Fe 2599 Ti 2535	±11,3
6	—		—	—	Fe 2599 Ti 2520	±11,0

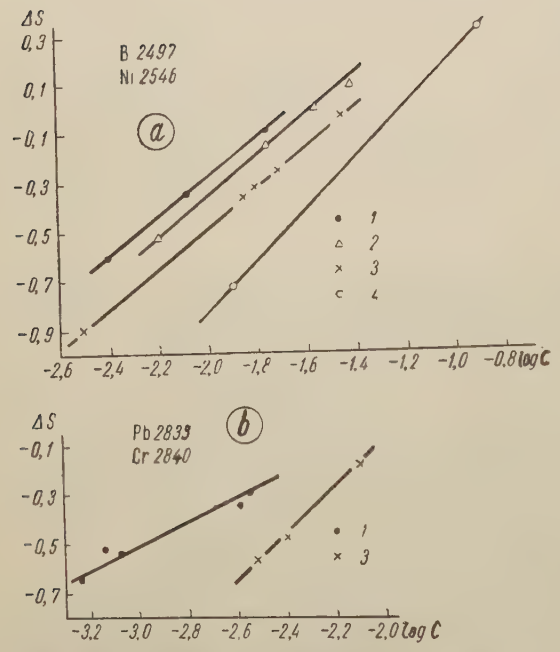

Working curves for determination of boron (a) and lead (b) in nickel alloys. Source - DG-1 arc unit, I = = 1-9 amp. The numbers identifying the points correspond to the standard Nos.

search in this field showed that this influence in some cases is negligible, and that one can therefore use a single set of standards for the analysis of several specific alloys. For example, it was established that one can use one set of standards for analysis of nickel alloys EI437 and EI435, duraluminum alloys D1, D16, D3P, D6 and certain others, aluminum alloy Al-7 and duraluminum, aluminum alloys Al-4 and Al-5, and magnesium alloys MA-4 and MA-5.

At the same time there are many cases when the introduction of a new element into the alloy produces a substantial change in the properties and structure of the alloy and leads to shift of the working curves. Thus, for example, the introduction of more than 0.5% Zn into most aluminum alloys has a strong effect on the determination of magnesium. Again, whereas nickel alloys EI437 and EI617 differ relatively little as regards composition, the working curves for determining Pb, B, Cr, Al and Ti in them are well separated.

A certain influence of "third" elements in analysis of complex nickel alloys is observed in the case of elements present in both low and high concentrations. By way of illustration we show in the accompanying figure the working curves for determination of B and Pb in nickel alloys of different composition.

With a view to minimizing the influence of "third" elements in determination of boron in nickel alloys with excitation of the spectrum by a DG-1 arc source, we carried out a series of experiments in which we varied the current strength, the material and shape of the permanent electrode and a number of other factors; no significant diminution of the influence was observed under any conditions. For other components, however, it was established that the influence of "third"

elements on the analytic results can be reduced by suitable choice of the light source and also by increasing the discharge power with any given source.

It has recently been reported by Vorontsov[1] and Shtutman and his co-workers[2] that the influence of "third" components in analysis of alloys can be minimized by using pulsed sources. We are undertaking a study of this technique in collaboration with the plant laboratories.

References

1. E.I.Vorontsov, Present issue of the Bulletin, p.1080.
2. N.N.Shtutman, V.P.Avdeenko, E.V.Zvereva, V.N.Shteinberg & T.A.Eremeeva, Materialy II Ural'sokogo soveshcheniya po spektroskopii (Transactions of the Second Ural Conference on Spectroscopy), Sverdlovsk, 1958.

* * * * * * * * *

RAPID SPECTROSCOPIC ANALYSIS OF METALLOMETRIC SPECIMENS FOR RARE ALKALI METALS, BORON, FLUORINE AND OTHER ELEMENTS

- P.A.Stepanov, E.A.Sergeev, M.V.Belobragina & M.S.Leshchinskaya

In routine spectrochemical analysis of metallometric specimens the elements Li, Rb, Cs, B, F and Be are not determined with the requisite sensitivity and hence are often reported simply as "traces".[1-3]

Adequately sensitive analysis of assay samples for Li, Rb and Cs can be realized under certain conditions by the familiar procedure of vaporizing the powdered sample from a hollow carbon electrode in an arc. The temperature of the discharge plasma is stabilized by the introduction of potassium (in the form of à 20% solution of KCl) into the sample after packing it into the electrode. The excess potassium serves to enhance the analytic sensitivity and suppresses the influence of variable concentration of the other alkali metals in natural samples on the analytic results.

In our work we carried out the analyses with reference to the strongest lines located in the infrared region of the spectrum, namely, Li 6707.8 and 8126.5, Rb 7947.6 or 7800.2 and Cs 8521.1 Å. The use of infrared "Infra-840" plates provides for simultaneous determination of Li, Rb and Cs with a sensitivity of 0.0002%. The concentrations of these elements were determined from the absolute line blackenings as measured by means of a microphotometer. The quality of the spectrograms was monitored with respect to the blackening of the potassium lines and the background (it was required that these intensities be constant). Evaluation of concentrations in the 0.0005 to 0.05% range was carried out on the basis of working curves plotted in terms of S vs log C for which purpose we recorded 10 standards spectra on each 9 x 12 cm plate (in addition to about 200 sample spectra).

A typical set of working curves is reproduced in the accompanying figure. The data of semiqualitative analyses, as is the practice in metallometric work, are expressed in terms of a one digit number. The specified burning conditions (current strength - 20 amp, exposure - 40 sec) insure virtually complete vaporization of the alkali metals in most mineral compounds. Thus differences in mineralogical composition have no significant influence on the analytic results. The reproducibility is approximately that usual for semiqualitative spectrum analysis: for Li and Cs the results of repeated analysis in 85% of the cases differ by less than a factor of two; for Rb by not more than a factor of 3. The

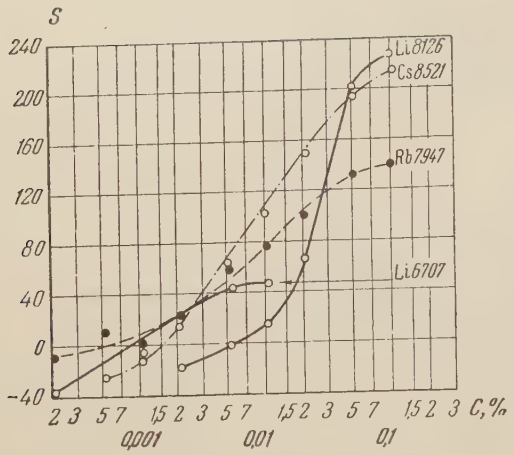

Working curves for determination of Li, Rb and Cs.

productivity of a working crew of four is 200 or more analyses per shift.

Most convenient for analysis is the ISP-51 spectrograph with an UF-84 camera. With some slight sacrifice of sensitivity, however, the procedure can be carried out on the ISP-51 with an f = 270 mm camera or on the ISP-28 or ISP-22 spectrographs, commonly employed in field laboratories. In the case of the ISP-28 the cassette should be shifted 15 mm to the right from the usual position; in the case of the ISP-22, on the contrary, the spectrum should be shifted to the left.

In 1957-58 tens of thousands of analyses of metallometric samples for Li, Rb and Cs were carried out by the described procedure. At a number of geological sites there were brought out anomalies in the concentrations of rare alkali elements, which clearly outlined the location of the rare-metal pegmatite body.

The sensitivity in determining Li, Rb and Cs attained with this procedure fully satisfies with requirements of metallometric work. The analytic procedure is described in Ref.4.

Analysis of metallometric specimens for B, Fl, Li and Be, together with determination of a number of other elements, can be carried out by the familiar procedure of sifting a fine powder through an arc between copper electrodes. In this case Fl is determined with reference to the molecular band with its edge at 5291 Å, boron with reference to the B 2497.5 and 2496.7 Å lines, lithium with reference to the Li 6707.8 Å line, and beryllium with reference to the Be 2348.6, 3131.0 and 2650.6 Å lines. The spectrum in the 2300 to 7000 Å range is photographed at the same time on two plates - positive and panchromatic. The excess calcium in the discharge zone necessary for formation of the CaF molecular bands is provided by the addition of $CaCO_3$ to the sample in the proportion of 3 to 1 by volume. At the same time, the addition of the calcium carbonate reduces the influence of the matrix on the results of determination of Be, B and Li.

The dusting is carried out by means of an AVR-2 shaker stand with the usual funnel replaced by a vibrating pan (after V.V.Nedler). Arc current - 20 amp, exposure - 15 sec, batch - 200 mg. The blackening of the lines is evaluated by the step-weakener method. The sensitivity of analysis is $2 \cdot 10^{-4}$% for Be and B, $5 \cdot 10^{-4}$% for Li, and $5 \cdot 10^{-2}$% for Fl. The procedure is rapid and efficient, and assures the reproducibility common to semiqualitative analyses: in 85% of the cases results of repeated analyses deviate by a factor of not more than 2-3.

At the same time a number of other elements is determined with reference to the corresponding line with the usual sensitivity.

References

1. T.F.Borovik-Romanova, Spektral'no-analiticheskoe opredelenie shchelochnykh elementov (Spectroanalytic determination of alkali metals), Pub., AN SSSR, 1956.

2. A.K.Rusanov & V.G.Khitrov, Zavodsk.labor. (Indust.lab.) 23, No.12, 175 (1957).

3. I.I.Smolyak, Izv.AN SSSR, Ser.fiz., 19, 217 (1955). (Trans.Bulletin 19, No.2, 199.)

4. Seriya "Obmen opytom" ("Exchange of experience" Series), All Union Institute of Prospecting Methods and Techniques, No.10 (1958).

QUANTITATIVE SPECTROSCOPIC DETERMINATION OF THE PRINCIPAL COMPONENTS OF INTRUSIVE ROCKS

- T.S.Reshetina

The analytic procedure proposed herein is based on the method of a common standard[1] in which some element present in all the tested samples is chosen as the common internal standard. In our case we chose Al as the internal standard; this is particularly convenient in view of the fact that its concentration is nearly constant (15 to 18% Al_2O_3) in normal calcareous alkali-metal rocks and minerals.

Let us use the chemical formulas for the respective compounds to denote the relative concentrations of the elements in the sample. Our procedure is predicated on calculations which are based on the fact that the total content of all oxides may be taken as 100%, i.e.,

$$SiO_2 + Al_2O_3 + MnO + MgO + Fe_{tot} \text{ in } Fe_2O_3 \text{ equivalent} + \\ + TiO_2 + CaO + K_2O + Na_2O + CO_2 + H_2O + \ldots = 100,$$

whence

$$Al_2O_3 = \frac{100}{1 + \frac{SiO_2}{Al_2O_3} + \frac{MnO}{Al_2O_3} + \frac{MgO}{Al_2O_3} + \frac{TiO_2}{Al_2O_3} + \frac{Fe_{tot} \text{ in } Fe_2O_3 \text{ equivalent}}{Al_2O_3} + \ldots}. \quad (1)$$

Analysis is carried out simultaneously for all the principal components. The constituents that are not determined by the spectroscopic procedure (CO_2, H_2O^+, H_2O^-, organic substances, etc.) are determined beforehand by chemical analysis, while K_2O and Na_2O are determined beforehand by flame photometry. The ratios SiO_2/Al_2O_3, MnO/Al_2O_3 and so on are found from calibration curves constructed on the basis of three standards (suitable samples of granite, gabbrodiorite and diabase repeatedly analyzed by chemical procedures) in terms of the difference in the degree of blackening of the line of the analyzed element and the reference element (Al) vs the logarithm of the ratio of the concentration of the element oxides to the concentration of Al_2O_3. The values of SiO_2/Al_2O_3, MnO/Al_2O_3, and so on taken off the curves are then substituted in Eq.(1). Finally, multiplying the values of SiO_2/Al_2O_3, MnO/Al_2O_3, etc., by the Al_2O_3 content we find the sought values of SiO_2, MnO, MgO, CaO, TiO_2 and Fe_{tot} (in Fe_2O_3 equivalent).

The actual measurement procedure we employed is the following.

The samples and standards are ground to a grain size of 0.05 mm and mixed in the proportion of 1 to 2 with spectroscopically pure carbon powder. The spectra are photographed on an ISP-22 spectrograph, using a dc arc source (10 amp, 220 v). The spectra of the samples and standards are photographed three times on each plate (Type 2 Spectroscopic, speed 12 GOST units).

We used the following analytic lines: Si 2568.6 and 2577.1 Å, Mn 2801.1 and 2949.2 Å, Mg 2779.8 and 2776.7 Å, Fe 2912.2 Å, Ti 2956.1 and 2933.6 Å, Ca 3181.3 and 3179.8 Å. The reference lines were Al 3064.3 and 2562.4 Å.

The described procedure was employed for analysis of 60 samples of diverse intrusive rocks. The results of spectroscopic analysis were compared with the results of chemical analysis. Some of the results of chemical and spectroscopic analyses for acid, neutral and basic rocks are juxtaposed in Table 1.

For a more dependable evaluation of the two methods of analysis, we also determined the reproducibility of the results (Table 2). The reproducibility of the spectrographic method was calculated for 10 samples on the basis of three spectrograms with three-time photography of each sample on a separate plate. The reproducibility of the chemical method was calculated for five samples, each being analyzed four times.

Table 1

Comparison of the results of spectroscopic analysis with the data of chemical analysis

Oxide	Acid rocks (10 samples)		Neutral rocks (10 samples)		Basic rocks (10 samples)	
	Rel. error, %	Conc. range, %	Rel. error, %	Conc. range, %	Rel. error, %	Conc. range, %
SiO_2	2,34	60÷80	2,87	45÷60	3,6	40÷50
Al_2O_3	7,00	10÷17	3,09	13÷19	3,38	12÷19
MnO	—	0,01÷0,1	17	0,1÷0,15	30	0,1÷0,15
MgO	—	0,01÷2	8,3	1÷10	7,4	2÷9
Fe_{tot} in Fe_2O_3 equivalent	15,2	0,5÷6	9,03	5÷15	7,9	8÷15
TiO_2	15,4	0,01÷1	17,6	0,4÷2,5	—	0,8÷5
CaO	16,0	0,05÷4	6,6	2÷12	6,9	3÷10

Table 2

Reproducibility of spectroscopic and chemical analyses

Oxide	Reproducibility	
	Spectrum	Chemical
SiO_2	2,19	0,24
Al_2O_3	3,13	5,60
MnO	6,56	13,3
MgO	7,8	6,19
Fe_2O_3	4,97	6,78
TiO_2	6,56	10,9
CaO	6,19	8,08

It will be evident from an examination of Table 2 that the reproducibility of the two methods differs for different components: as regards SiO_2 the reproducibility is better for the chemical method, whereas for Al_2O_3, MnO, Fe_2O_3, TiO_2 and CaO, on the contrary, the reproducibility of the spectrographic method is superior; for MgO the reproducibilities are nearly equal. Thus the reproducibility of spectrographic analysis in most cases is at least as good as that of chemical analysis and in individual cases distinctly superior.

Institute of the Geology of Ore Deposits,
Petrography, Mineralogy and Geochemistry,
Academy of Sciences of the USSR

References

1. W.H.Dennen & W.C.Fowler, Bull.Geol.Soc.Amer., 66, No.6 (1955).

* * * * *

CHEMICO-SPECTROSCOPIC DETERMINATION OF MOLYBDENUM AND TUNGSTEN IN IGNEOUS ROCK

- L. I. Pavlenko

The lack of sensitive, rapid and precise methods of determining W and Mo in concentrations of 10^{-3} to 10^{-6}% in rocks has until now hindered extensive geochemical studies and is the reason for the paucity of data on the content of W and its proportion to Mo in different geological formations.

The technique developed in our laboratory for determining small amounts of Mo and W in rocks has made it possible to elucidate the variation in the content of these elements in rocks of different alkalinity.[1]

In cases when the concentration of the elements exceeded 10^{-4}%, the most effective method for determining Mo proved to be that of direct spectroscopic analysis of the rocks[2], the mean error of which amounts to ~10%.

Analysis for W was carried out by the method of direct spectroscopic determination with the addition of silver chloride to the sample to enhance the sensitivity. The sensitivity of such determinations of W is $\sim 2 \cdot 10^{-4}$%; the mean error ±10%.

In most cases, however, spectroscopic determination must be preceded by chemical enrichment. To this end a 1 g sample of the rock is fused with sodium carbonate, the melt is treated with water (~150 ml), filtered, and washed with a 1% solution of Na_2CO_3. The filtrate is acidified with HCl to 0.18 to 0.2 N. Then a 2% solution of tannin and methyl violet is added to the filtrate; these precipitate the W and Mo. The precipitate is filtered, washed, dried, reduced to ash and then subjected to spectroscopic analysis.

Radioactive isotopes were used to determine the optimum conditions of analysis and degree of concentration of the determined elements. Obozhin[3] established that in contrast to many other precipitating agents, the mixture of methyl violet and tannin is capable of precipitating W and Mo in concentrations to $\sim 5 \cdot 10^{10}$ g-atom/liter. At a tungsten concentration of $\sim 4 \cdot 10^{-5}$%, the described enrichment procedure assures a virtually total concentration of the elements into the precipitate. A small decrease in the precipitation of W is observed only for tannin to methyl violet proportions appreciably exceeding 2 to 1.

The spectroscopic determination of molybdenum was carried out with dc arc excitation spectrograph with a three-lens condenser. We used carbon electrodes with a 3.5 mm diameter, 2.5 mm deep hollow for the sample. Spectrograph slit - 0.02 mm, arc current - 10 amp, exposure - 2.5 min, weight of sample - 10 mg (2 mg of the precipitate obtained after enrichment of the rock plus 8 mg of a silicate matrix). The spectrum was photographed on spectroscopic type II plates. The analytic line was Mo 3170.35 Å.

The tungsten content was determined on an ISP-51 spectrograph with a UF-85 camera. Under these conditions one can use the W 4294.6 Å line inasmuch as this is not overlapped by the lines of any other element present in the rocks. Otherwise the analytic conditions were the same as for determination of Mo.

The standards for plotting the working curves were prepared with the same matrix as used in diluting the samples for analysis. The investigated elements were introduced into the matrix in the form of MoO_3 and WO_3. The working curves were plotted by the method of three standards in terms of log R vs log C, where log R is the intensity of the line referred to the adjacent background.

The sensitivity of the described chemico-spectroscopic procedure is $2 \cdot 10^{-6}$% for determining Mo and $5 \cdot 10^{-5}$% for determining W. The systematic error involved in the procedure was checked by control experiments and by comparing the data obtained with the results of polarographic analysis. It was established that the arithmetic mean deviation in the chemico-spectroscopic determination does not exceed 12-15%.

"V.I.Vernadskii" Institute of Geochemistry & Analytic Chemistry
Academy of Sciences of the USSR

References

1. A.P.Vinogradov, E.E.Vainshtein & L.I.Pavlenko, Geokhimiya, No.5 (1958). (Trans.Geochemistry.)

2. É.E.Vainshtein & L.I.Pavlenko, Zhur.analit.khimii, 11, No.4 (1956). (Trans.J.Analytical Chemistry.)

3. V.N.Obozhin, Thesis, GEOKhI AN SSSR, 1956.

SPECTROSCOPIC ANALYSIS OF LUMINESCENCE-PURE ZINC SULFIDE AND SULFATE WITH THE AID OF CHEMICAL ENRICHMENT

- V.N.Vasil'eva, L.A.Dvorzhetskaya, L.Ya.Markovskii and L.Ya.Khlebnikova

The high requirements as regards purity set for zinc sulfide intended for synthesis of crystal phosphors make it imperative to develop reliable analytic procedures for determining minute amounts of the heavy metals Cu, Fe, Ni and Co. Calorimetric procedures for determination of the enumerated elements were developed in the IREA (Institute of Chemical Reagents).[1] The complexity of these procedures and the time required for an individual analysis, particularly, in determining Ni and Co, make it desirable to develop simpler and more rapid analytic methods.

According to the pertinent technical specifications, the maximum allowable amounts of the above mentioned metals in luminescence grade zinc sulfide are Cu - $5 \cdot 10^{-6}$%, Fe - $5 \cdot 10^{-5}$%, and Ni and Co - $1 \cdot 10^{-5}$%. The direct spectrum analysis technique for luminescence grade ZnS (see Ref.2) assures the requisite sensitivity of analysis only for Cu. In the case of Fe, the allowable percentage lies at the sensitivity threshold of the procedure. As for Ni and Co, the sensitivity of the analytic procedure for these elements is obviously inadequate; according to our data, the sensitivity is approximately 1.5 orders of magnitude lower than that required.

In view of the above we made an attempt to develop a spectroscopic method for determining Fe, Ni and Co in ZnS based on the use of chemical enrichment.

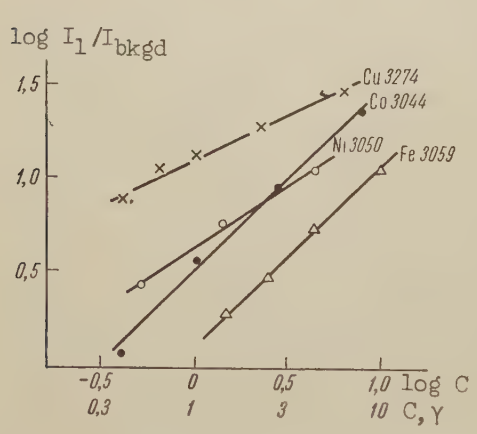

Working curves for determination of microimpurities in $ZnSO_4$ & ZnS.

According to the data in the literature[3-8], chemical extractive enrichment as a preliminary to spectrum analysis has been used for the determination of a number of substances with a sensitivity of up to ~10^{-5}%. In the present research we made the first experimental attempt at such enrichment for ZnS and $ZnSO_4$ (the latter is an intermediate product in the production of ZnS). In view of the fact that in the enrichment process, simultaneously with Fe, Ni and Co, copper is also separated out, we evaluated the possibility of determining this element as well.

The essential steps of the procedure are the following. A 10 g sample of ZnS is dissolved in HCl and converted to $ZnSO_4$.* The enrichment is realized with precipitation of the Fe, Ni, Co and Cu microimpurities by solutions of α--nitroso-β-naphthol, cupferron and dimethylglyoxime, and extraction of the resultant organo-metallic compounds with isoamyl alcohol and chloroform. After extraction the organic substances are eliminated by evaporation and subsequent heating.

In the case of analysis of $ZnSO_4$, the enrichment (50 ml 10% solution) is carried out in the same manner, using the same reagents but at a different pH. The degree of enrichment (referred to the Zn) equals ~100 in the case of ZnS and ~50 in the case of $ZnSO_4$.

---

*Enrichment in $ZnSO_4$ solutions proceeds better than in $ZnCl_2$ solutions.

The sample for spectroscopic analysis is taken in the form of a weakly acid water solution (0.6 ml) of the chlorides of zinc and the microimpurities. The spectroscopic source is an 8 amp dc arc between ordinary spectroscopic grade carbon electrodes. The lower electrode is first burned in and soaked with a solution of polystyrene in benzene. Then three drops of the investigated concentrate are applied to the tip of the electrode, and the electrode is dried by slow heating. It is then connected, while still hot, as the anode. The analysis is carried out on an ISP-28 spectrograph with three-lens illumination of the slit; the exposure is 30 sec. The spectrum is photographed on "spectroscopic" type 2 plates with a sensitivity of 16 GOST units. The blackening is measured on an MF-2 microdensometer. The analytic lines are Fe 3059 Å, Ni 3050 Å, Co 3044 Å, and Cu 3274 Å. The determination is made with reference to working curves plotted on the basis of standard $ZnSO_4$ solutions enriched according to the procedure developed for $ZnSO_4$.* The same working curves serve for determination of impurities in both $ZnSO_4$ and ZnS (see accompanying figure).

The data on the analytic sensitivity (in percent) are listed below. For Fe and Cu the sensitivity was determined by diluting the enriched concentrate.

	Ni	Co	Fe	Cu
ZnS	$2 \cdot 10^{-6}$	$4 \cdot 10^{-6}$	$\sim 10^{-6}$	$\sim 10^{-8}$
$ZnSO_4$	$4 \cdot 10^{-6}$	$7 \cdot 10^{-6}$		

The mean arithmetic error of analysis was evaluated to be 15% for Co and 25% for Ni and Fe. As regards Cu, the analytic results cannot be regarded as satisfactory: the error may attain 60%. It must be noted that owing to the unavailability of sufficiently pure ZnS samples, we were unable to check the determination of Fe in material containing less than $5 \cdot 10^{-5}$% Fe.

The present investigation showed that the method of chemical extractive enrichment allows of increasing the sensitivity of spectroscopic determination of Fe, Ni, Co and Cu impurities in ZnS and $ZnSO_4$ by two orders of magnitude. The results of test quantitative analyses for Fe, Ni and Co were satisfactory, all three elements being determined simultaneously. Nevertheless, we feel that the developed analytic procedure requires further improvement and amelioration.

State Institute of Applied Chemistry

References

1. I.G.Shafran, Izv.AN SSSR,Ser.fiz., 21, 661 (1957). (Trans. Bulletin 21, No.5, 660.)
2. G.I.Kibisov, M.I.Rezvova & E.N.Vinnichenko, Transactions of the Tenth All-Union Conference on Spectroscopy, Vol.2, L'vov, 1958.
3. F.Pohl, Z.anal.Chem., 141, No.1-6, 81 (1954).
4. F.Pohl, Ibid., 139, No.1-6, 241, 423 (1954).
5. H.Specker & H.Z.Hartkamp, Erzbergbau und Metallhüttenwesen, 10,117 (1957).
6. Stetter, Exler, Naturwissenschaften, 42, 2, 45 (1955).
7. Kaarina Lounamaa, Suomen Kem., 30, 12, B 232 (1957).
8. V.I.Kuznetsov, Usp.khim., 23, 654 (1954).

---

*Chemical analyses of the samples and initial solutions for the standards were carried out by the IREA procedures.[1] In carrying out the analysis it is essential to take into account the content of the various microimpurities in the reagents employed.

SPECTROSCOPIC DETERMINATION OF URANIUM BY THE METHOD OF ISOTOPIC DOPING

- N.P. Ivanov

It has been reported[1-3] that the accuracy and general applicability of spectroscopic procedures for the determination of uranium can be enhanced by the introduction of known quantities of its light isotopes, U^{235} and U^{238}, into the analyzed sample. In this article we give the principal results of further development of this procedure, which has been called the method of isotopic doping.

It is known that the spectrum background hampers evaluation of the relative intensities of the spectrum lines. These difficulties, which are particularly serious in the case of photographic recording, limited the accuracy of the original versions of the isotopic procedure in which the amounts of light isotopes added were of the order of 3-5%. We found it possible to increase the accuracy of analysis in two ways. In carrying out the analysis by the method of "equal blackenings" different amounts of the same light isotope are added to equal batches of the sample. The photometric data are then used for plotting the difference between the blackenings of the isotopic component lines, $\Delta S = S_{U238} - S_{U235}$, against the concentration of the light element, C_{U235}. The point of intersection of this plot with the concentration axis gives the concentration C°_{U235} at which the intensities of the lines of both components are equal (Fig.1). The sought concentration C_x is then calculated by means of the simple formula

$$C_x = C^{\circ}_{U235} \cdot D,$$

where D is a coefficient which is constant for all measurements carried out with the given specimen of the light isotope and is defined by the expression

$$D = [m_8/m_5 - 1/n] / [1 - k(1 - m_8/m_5)],$$

where m_8/m_5 is the ratio of the mass numbers of U^{238} and U^{235}, n is the isotopic ratio of the light isotope specimen used for doping, and k is a coefficient which takes into account the content of the light isotope in natural uranium and is numerically equal to 0.007. In view of the fact that in this case there is no need to take into account the background or convert from blackenings to intensities, the accuracy of analysis is enhanced. In tests of the equal blackenings procedure on samples containing high concentrations (1-10%) of uranium there was obtained an average reproducibility of ±1.2%. The deviation between the results of spectroscopic and chemical analyses was ±2.2%; the deviation between two consecutive determinations was 1.2% for the spectroscopic procedure, and 1.7% for the chemical procedure. In the case of low uranium concentrations (0.01-1%) the reproducibility was ±1.3%; the deviation between the results of spectroscopic and chemical analyses ±1.6%.

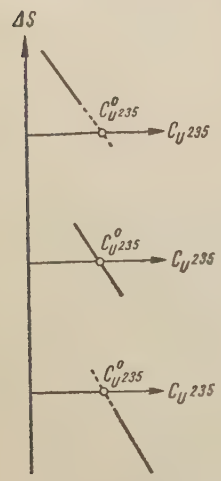

Fig.1. Three cases of location of the experimental curve (solid line); the upper and lower curves are extended to obtain the value of C°_{U235} at the point of intersection with the concentration axis (dashed line).

The method of "two isotopes" consists in the introduction simultaneously of two light isotopes. The sought concentration is found graphically from the two points corresponding to the known concentrations of U^{235} and U^{233} (Fig.2). The "two isotopes" procedure also dispenses with taking into account the background

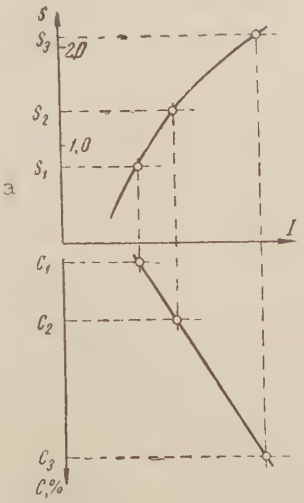

a

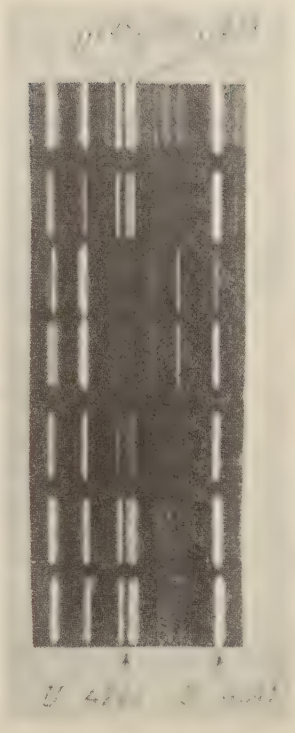

b

Fig.2. a - above characteristic curve of the photographic emulsion; below - working curve: C_1) U^{235} concentration, C_2) U^{238} concentration, C_3) U^{233} concentration. The sought concentration C_x is obtained by subtracting the amount of U^{238} introduced into the sample together with the light isotope from the value of C_2. b - expanded spectrum of sample containing light uranium isotopes; this illustrates the possibility of separating the isotopic components of the U 4244 Å analytic line from the neighboring lines of the other elements (ISP-51 spectrograph with UF-85 camera).

which makes it feasible to obtain results with an accuracy of the order of ±1-2%. The procedure is exceptionally simple and requires only one batch of the sample material for analysis. This makes it possible to employ preliminary chemical concentration, which, in view of identity of the chemical properties of isotopes, can be reduced to the simplest type. The method of "two isotopes" provides for the determination of uranium in very low concentrations (10^{-6}-10^{-7}%) with a very high accuracy for such low concentrations and also for determination of uranium in samples with a high content of elements close to uranium as regards chemical properties (thorium and the rare earths).

For certain technological and production control purposes what is important is not so much high accuracy of analysis as rapidity. To this end we developed a number of special procedures, one of which consists of the following.

Let C_o be the critical concentration, i.e., the concentration below which the given material is dumped and above which it goes for further processing. There is added to the sample a certain amount of the light isotope, C_U 235, calculated by means of the formula $C_o = C_{U235} \cdot D$. The spectrum is photographed or observed visually for the purpose of determining the ratio of intensities of the isotopic component lines. If the intensity of the U^{238} lines is higher than that of the U^{235} lines, the uranium concentration is higher than C_o and the material goes for further processing; with the inverse intensity ratio the material is dumped. This analytic procedure requires only a few minutes.

"V.I.Vernadskii" Institute of Geochemistry and Analytic Chemistry,
Academy of Sciences of the USSR

References

1. A.P.Vinogradov, Fiziko-khimicheskie metody kontrolya proizvodstva urana. (Physical-chemical control methods in uranium production). Reports of the Soviet Delegation at the Internation Conference on the Peaceful Uses of Atomic Energy. Geneva, 1955.

2. N.P.Ivanov, Transactions of the Tenth All-Union Conference on Spectroscopy, Vol.2, p.109, L'vov, 1958.

3. P.N.Palei, Zhur.analit.khimii, 12, No.5, 647 (1957). (Trans.J.Analyt.Chem.)

SPECTROSCOPIC DETERMINATION OF THE RELATIVE Sr AND Ca CONCENTRATIONS IN BIOLOGICAL SPECIMENS

- G.D.Litovchenko & S.A.Shipitsyn

The rare-earth elements Sr and, particularly, Ca, are widely distributed in nature both in inorganic and in organic substances. As a rule, Sr accompanies Ca and its concentration frequently varies with that of Ca.[1] The reasons for this are, first, that these elements have close ionic radii and hence their ions can replace each other in crystal lattices, and, second, that their chemical properties although not identical, are rather similar. As a result of some physical and chemical differences, however, the relative concentration of Sr usually decreases relative to that of Ca in going up the "biological scale", i.e., in going from the soil to plants and from plants to animals.

It is assumed that one can calculate the Sr concentration in animal organs if one knows its concentration in the soil of the neighborhood and has the values of the correlation factors or so-called protective coefficients characterizing the variation of the ratio of Sr to Ca: K_1 - the coefficient in going from soil to plants, K_2 - from plants to food, K_3 - from food to blood, and K_4 - from blood to bones. In addition, one must of course also know the Ca content in the organs. These same coefficients can be used for determining the content of radioactive Sr^{90} in bones if one knows its concentration in the soil.[2]

Our purpose was to apply spectroscopic analysis for the determination of the Sr to Ca concentration ratio. We analyzed samples of different bio- and geochemical origins: soil, plant ashes and animal husbandry products as well as dry residues of water samples.

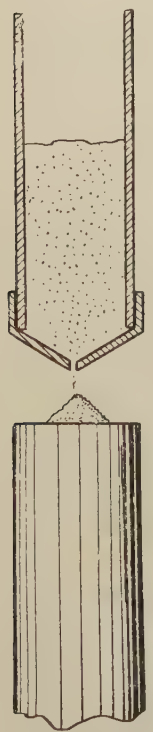

Electrode assembly for exciting the spark spectra of powdered samples.

With a view to reducing the influence of the principal components of the samples and increasing the reproducibility of the analyses, we employed a new variant of spark excitation of powder samples in which the upper electrode (see figure) is an aluminum or brass tube. The lower end of this tube is closed with a copper cap (a cartridge cap) pressed out to a cone, at the apex of which is a 0.8 mm diameter opening. The lower electrode is copper and has a flat face. The finely ground and thoroughly dried sample in the amount of 50-100 mg is loaded into the upper electrode. Approximately 5-7 mg of the sample are expended in obtaining each spectrogram (in the case of Ca concentrations above 10% the sample is diluted with NaCl). The operating conditions of the spark source are selected so that the explosive wave of each discharge train will agitate the powder in the tube and assure uniform discharge of the sample through the 0.8 mm diameter opening. Extremely "hard" discharge conditions may lead to partial ejection of the powder through the top of the tube particularly when there is little material left in the tube. In addition, there may appear interference lines with high excitation energies. On the other hand, a high inductance in the spark circuit, i.e., a condition under which the discharge approaches an arc, favors caking of the sample material and even clogging of the opening due to fusion.

In using the IG-2 spark source, the most suitable circuit parameters are L = 0.15 mh, C = 0.01 μf, auxiliary gap 3 mm, discharge gap 1.8 mm, one discharge train per half-cycle.

It must be noted that in the process of prolonged (repeat) recording of the spectra of some samples, the opening in the upper electrode does become partially caked and the rate of flow of the sample material is reduced. Hence for more effective utilization of the light flux with the three-lens condenser illuminating

system we reduced the exposure to 25-30 sec. The spectra of all samples were photographed 2-3 times. Between each run, the opening was cleared to size with a special needle.

In our work we used an ISP-22 spectrograph, recording the spectrograms through a two- or three-step weakener on type II spectrographic plates (speed 16 GOST units). The weakeners yielded convenient density steps and at the same time served for plotting the characteristic curve of the emulsion.

The first part of the work consisted in determining the absolute concentrations of Sr and Ca in the investigated materials. We used the following analytic lines: 4215.52 and 4077.71 Å for Sr, and 4226.72 Å for Ca in the range of low concentrations and 4318.65 Å for Ca concentrations above 0.3%. The last line cannot be used in the case of appreciable concentrations of Ti. The reference line was Cr 4254.35 Å. The standards were prepared with NaCl as the base and encompassed Sr concentrations from 0.01 to 1.0% and Ca concentrations from 0.1 to 10.0%. The reference element, Cr, was introduced in the form of $K_2Cr_2O_7$ into NaCl in a concentration of 1.0%. Both the standards and samples were mixed with this working mixture in the proportions of 2 to 1.

The working curves were plotted in terms of log (I/I_o) vs log C; from these we first determined the concentrations of Sr and Ca and then calculated their ratio. The concentration sensitivity of the method proved to be high; the standard error of an individual determination was evaluated to be 7.1% for Sr and somewhat higher for Ca.

The second part of the work consisted in finding the variation of log (I_{Sr}/I_{Ca}) with log (C_{Sr}/C_{Ca}). For this purpose we prepared standards with values of C_{Sr}/C_{Ca} in the range from 0.001 to 0.06. The curve plotted on the basis of photometric measurements of the spectrogram proved to be linear over almost the entire range of concentrations, but showed some tendence to saturation in the region of the highest concentrations. Using this curve we could, from the spectra of the samples without the reference element, find C_{Sr}/C_{Ca} from the relative intensities of the spectrum lines and hence calculate the protective coefficients. For example, for different soils and plants growing therein, we obtained values of K_1 ranging from 0.35 to 0.95. Thus it would appear that the protective coefficient for this step in the biological series is not constant but depends on the absolute concentrations of Sr and Ca and possibly a number of other factors.

Spectroscopic Laboratory,
"A. A. Zhdanov" Irkutsk State University

References

1. A. O. Voinar & L. N. Lazovskaya, Byul. eksperim. biol. i med. (Bulletin of experimental biology and medicine), 15, No. 1-2, 64 (1943).

2. O. I. Leipunskii, Atomnaya energiya 4, 63 (1958). (Trans. J. Atomic Energy.)

SPECTROSCOPIC DETERMINATION OF MICROELEMENTS IN TISSUE PROTEINS

- S.G.Bogomolov, F.D.Drobiz & A.G.Morozov

Spectroscopic procedures are now coming into extensive use for the determination of microelements.[1-2]

The present work was devoted to determination of Co, Ni and Cu in the concentration range from 0.1 to 0.001% in animal proteins. The proteins were extracted from different organs of white rats by precipitation with trichloroacetic acid, followed by washing with alcohol, acetone and ether. The extracted samples were dried at 105° to constant weight and then reduced to ash in a crucible furnace for 2 hours. This treatment led to 20-fold enrichment of the samples as regards the microelements. The analyses were carried out by the method of three standards on an ISP-28 spectrograph. The spectra were excited by an ac arc (8 amp) between spectroscopically pure carbon electrodes. The samples (25 mg) were packed into the hollow lower electrode.

The working curves were plotted in terms of ΔS vs log C. Each spectrum was photographed three times. The relative error is estimated to be ±15%.

For the purpose of plotting the working curves we prepared synthetic standards simulating the mineral composition of the protein ashes as regards the six principal elements: Fe - 0.025%, Na - 0.015%, P - 0.49%, Mg - 0.002% and K - 0.60%. This composition was established by comparing the line blackenings of a number of artificial mixtures and the protein ashes. The Ca concentration was not determined. Our data differ somewhat from those in the literature as regards the element concentrations in proteins.[4]

For preparing the principal standards we used the following salts: $Fe(OH)_3$, $MgSO_4 \cdot 7H_2O$, $Na_2HPO_4 \cdot 12H_2O$ and KH_2PO_4. The purity of the reagents was checked spectroscopically. The salts were mixed with graphite powder in appropriate proportions. To the matrix mixtures prepared in this manner there were added compounds of the investigated microelements in the form of $NiSO_4$, $CuCl_2 \cdot 2H_2O$ and $Co(CH_3COO)_2 \cdot 4H_2O$.

First we made the standards with the highest concentrations of the analytic elements; the other standards were then prepared by the method of successive dilution. In this manner we obtained standards with Co, Ni and Cu concentrations of 0.030, 0.01, 0.003 and 0.001%. We took special pains to insure homogeneity of the standards; this was achieved by careful and thorough grinding of the mixtures in an agate mortar followed by mixing in sealed tubes for several hours.

The reproducibility of analysis based on repeated determination of the same element is characterized by ±5% (arithmetic mean deviation).

By way of reference element we chose vanadium because its volatility is closest to that of the determined elements. It was introduced in the form of V_2O_5 in the amount of 0.1% both into the samples and the standards. We used the following analytic lines: Cu 3273.96 Å, Ni 3414.77 Å, and Co 3412.63 Å. The reference line in all cases was V 3185.40Å.

In all we analyzed the tissue proteins from 28 animals. Sixteen of these were injected with solutions of the salts of these elements; 12 were control animals. The analytic results (see table) showed that the developed procedure assures reliable determination of the microelements Co, Ni and Cu in the proteins of different tissues.

Our experimental data lead us to infer the following:

1. In the case of subcutaneous hypodermic administration of the chlorides of some microelements the concentration of these elements in the proteins extracted from some organs increases over the concentration in control animals.

2. The administered Co, Ni and Cu salts are selectively accumulated in the proteins of certain organs.

Concentrations of Cu, Ni and Co in ashed proteins from different tissues (in mg %) (average data for two animals)

Organs	Cu				Ni					Co			
	Control		Inj.		Control		Injected			Contr.	Injected		
Blood	4	3	12	12	Trace	Trace	3	3	5	None	Trace	Trace	Trace
Muscle	--	2	6	3	»	»	4	2	2	»	»	»	1
Lung	2	4	10	21	2	7	4	16	2	»	»	»	Trace
Liver	3	3	66	80	2	Trace	7	2	2	»	2	3	2
Heart	8	12	11	24	2	»	2	2	2	»	Trace	Trace	Trace
Spleen	5	5	6	9	Trace	»	4	4	4	»	»	1	»
Kidney	5	8	31	57	2	»	6	29	4	»	2	2	1
Skin	2	1	3	6	5	2	7	—	21	»	Trace	Trace	Trace
Brain	4	6	9	10	2	Trace	4	2	2	»	»	»	»

Note: Trace = <1 mg %.

3. This build up in the microelement concentration occurs in parallel with the increase of SH-group proteins, which substantiates the hypothesis of Drobiz[5] that the SH-group binds excess microelements.

Sverdlovsk Medical Institute

References

1. A.O.Voinar, Biokhimiya (Biochemistry), 11, 19 (1946); 18, 29 (1953).
2. A.O.Voinar & A.K.Rusanov, Ibid., 14, 102 (1949).
3. S.A.Shipitsyn, Izv.AN SSSR, Ser.fiz., 14, 677 (1950).
4. V.S.Asatiani, Biokhimicheskii analiz (Biochemical analysis), Part III, Tbilisi, 1953.
5. F.D.Drobiz, Trudy (Proceedings), Sverdlovsk Med. Inst., Sverdlovsk, 1956-7.

DEVELOPMENT OF METHODS OF SPECTROSCOPIC ANALYSIS OF BLAST FURNACE SLAG AND FLUXED SINTER

- O. I. Nikitina

The work was carried out by the following under the supervision of the author: L. I. Gudyrina, L. P. Berdnikova, N. K. Ivanova (Ukrainian Institute of Metals); A. I. Masurova, V. M. Dashchenko, N. N. Tsvetkova, E. I. Panasenko ("Petrovskii" Plant); I. K. Maiboroda ("Zaporozhstal'" Plant); M. N. Shtutman, E. V. Zvereva, Milyavskaya, Agafonova (Magnitogorskii Metallurgical Combine); A. V. Lukanin, A. I. Butova, K. T. Vil'skaya ("Kirov" Plant); Z. I. Brailovskaya ("Voroshilov" Plant); L. I. Topalov (Zaporozhskii Ferroalloy Plant); A. P. Atamanov, L. I. Kocherygova, A. S. Vitis, E. I. Bykova ("Azovstal'" Plant).

Previously, the Ukrainian Scientific Research Institute of Metals in collaboration with a number of metallurgical plants, carried out a research project on analysis of open-hearth slag[1]; as a result there was compiled an instruction bulletin giving recommended analytic procedures.

The present work was a continuation of the above research. Its purpose was to develop spectroanalytic procedures for blast furnace slag and fluxed sinter yielding an accuracy adequate for the purposes of technological control. There were investigated in detail methods of analysis of solutions, briquettes and powders. The two primary aims in the study were 1) determination of conditions for weakening the reciprocal influence of the components and reabsorption in analysis of diluted solutions and powders, and 2) choice of conditions favoring manifestation of the mutual influence of the components for the purpose of taking this influence into account in analysis by the method of nominal curves[2] or by the method of relative concentrations[3] in analysis of powder samples with little or no dilution.

The subjects of investigation were 35 samples of blast furnace slag and 25 samples of sinter analyzed by the chemical laboratories of the supplying plants and combines and again analyzed in the chemical laboratory of our Institute. Despite the fact that all chemical analyses were made with great care, comparison of the results obtained in different laboratories indicates that the accuracy of chemical analysis is rather low, particularly as regards the determination of Al_2O_3, MgO and MnO both in slag and in sinter.

The spectroanalytic investigations were carried out using the same samples. Investigation of the homologeneity of the 22 analytic line pairs (internal standards: Cr, Mo and V) with reference to the variation of ΔS with change in the inductance of the spark circuit and the length of the analytic gap led to identification of adequately homologous pairs for analysis for Ca, Mg and Mn and less homologous but still acceptable pairs for the determination of Si and Al (see Table 1).

On the basis of investigation of the spark source parameters there were established the following optimal operating conditions for the IG-2 spark generator: C = 0.01 μf, L = 0.05 or 0.15 mh, d = 2.0 mm, current strength - high enough to provide one discharge train per half-cycle. Counter electrode - 6 mm diameter carbon with truncated cone tip. By way of the lower electrode in analysis of solutions there was used a carbon rod 6 mm in diameter and 10 mm long, heated for 3 min at 900° beforehand. The electrode was mounted in the fulgurator holder with its tip 1 mm above the surface of the solution.

Solubility studies showed that some slag samples and all sinter samples do not dissolve fully in hydrochloric acid. It was established that preliminary roasting for 2 min of a small batch of slag or sinter powder mixed with flux

Table 1

Analytic lines, Å

Source	Determined element	Ref.element in slag		Ref.element in sinter		
		Cr	Mo	Cr	Mo	Fe
Spark	Ca 3158,86	3147,23	3152,81	3147,22	3152,81	3227,74
	Ca 3179,33				3152,81	
	Si 2516,12	2571,74		2571,74		2522,84
	Si 2881,57				2879,05	
					2872,88	
	Al 3092,71	3053,88	3077,66	3077,83	3116,09	3059,08
		3077,83				
	Al 3082,15		3077,66			
	Mg 2790,79	2789,40	2779,23	2789,30		2783,69
	Mg 2790,79		2863,8			
	Mg 2852,1		2779,23			
	Mg 2802,69				2784,99	
	Mn 2933,06		2934,29			
	Mn 2939,30	2941,88				
	Mn 2949,20		2807,75			
	Mn 2605,69	2608,16		2602,79		2607,08
	Mn 2576,10				2602,79	
Arc	Ca 3158,86	3197,07		3197,07		
	Si 2881,57	2928,14		3197,07		

Table 2

Variation of the reproducibility (δ/C) of spectroscopic analysis and agreement (ΔC/C) between spectroscopic and chemical analyses of blast furnace slag and fluxed sinter with the method of introducing the solution

Procedure	Accuracy parameter, %	CaO		SiO		Al_2O_3	MgO	MnO
		slag	sinter	slag	sinter	slag		
Fulgurator with carbon electrode	$\frac{\delta}{C}$	±1,89	±2,29	±1,79	±1,60	±3,28	±4,10	±2,13
	$\frac{\Delta C}{C}$	±1,22	±4,15	±1,49	±2,06	±3,66	±8,49	±5,17
Rotating disk Cu electrode	$\frac{\delta}{C}$	±2,33	±3,18	±2,00	±3,14	±3,07	±3,9	± 3,9
	$\frac{\Delta C}{C}$	±1,14	±5,30	±2,44	±3,93	±3,86	±8,77	±10,07

Note" δ/c was determined from one spectrogram on the basis of 81 measurements for slag and 51 measurements for sinter; ΔC/C was determined from 3 spectrograms on the basis of analysis of 27 slag samples and 17 sinter samples.

(consisting of two parts soda and three parts borax) in the proportions of 1 to 5 at a temperature of 1000° or roasting of the sinter mixed with sodium peroxide at 800-900° assures complete subsequent solution of the products in hydrochloric acid.

Comparison of the methods of introducing the slag and sinter solutions into the spark discharge (IG-2 spark source, C = 0.01 μf and L = 0.55 mh) by means of a fulgurator with a carbon electrode or by means of a rotating disk copper elec trode showed that the more satisfactory results are obtained with the fulgurator

Reproducibility of spectroscopic analysis of slag and sinter in solution and agreement between the results of spectroscopic and chemical analyses

Source	Laboratory	Parameter, %	Slag					Fluxed sinter				
			CaO	SiO_2	Al_2O_3	MgO	MnO	CaO	SiO_2	Al_2O_3	MgO	MnO
Spark	Inst. of Metals	$\frac{\delta}{C}$	±2,0	±2,6	± 5,2	± 3,4	± 4,3	± 2,5	± 4,2	± 2,5	± 2,8	± 2,9
		$\frac{\Delta C}{C}$	±2,62	±3,02	± 4,3	± 6,45	± 4,2	± 3,67	± 3,89	±14,4	±16,7	± 8,64
	Zaporozhstal'	$\frac{\delta}{C}$	±1,46	±0,94	± 3,50	± 2,26	± 7,0	± 1,07	± 1,67	—	—	—
		$\frac{\Delta C}{C}$	±3,15	±2,67	± 4,00	±15,08	± 4,57	—	—	—	—	—
	"Petrovskii" Plant	$\frac{\delta}{C}$	±2,66	±2,52	± 4,62	± 5,78	± 3,00	± 3,23	± 2,25	—	—	—
		$\frac{\Delta C}{C}$	±0,97	±0,91	± 3,81	± 3,98	± 2,82	± 3,40	± 5,29	—	—	—
	"Voroshilov" Plant	$\frac{\delta}{C}$	±1,90	±1,42	± 4,5	± 3,7	± 2,4	—	—	—	—	—
		$\frac{\Delta C}{C}$	±1,90	±3,39	± 8,39	±13,22	±17,42	—	—	—	—	—
	"Kirov" Plant	$\frac{\delta}{C}$	—	—	—	—	—	± 4,06	± 4,12	—	± 3,24	± 2,15
		$\frac{\Delta C}{C}$	—	—	—	—	—	± 2,08	± 5,81	—	±22,81	±17,22
Arc	Magnitogorsk Metallurg. Combine	$\frac{\delta}{C}$	±4,02	±3,42	—	—	—	—	—	—	—	—
		$\frac{\Delta C}{C}$	±2,44	±2,15	±13,29	±21,11	± 8,24	±10,06	± 4,96	±10,76	—	±21,79

Note: δ/c was determined from one spectrogram on the basis of 20-72 measurements; $\Delta C/C$ from three spectrograms on the basis of analyses of 20 samples.

(see Table 2). Comparison of results of analysis of slag solutions in a spark (IG-2 spark unit, C = 0.01 μf, L = 0.05 and 0.55 mh) and in an arc (DG-1 arc unit; I = 5 amp) with the solution fed into the discharge by the fulgurator showed that the reproducibility in the spark is appreciably higher than in the arc (see Table 3). The agreement between the results of spectroscopic analysis and chemical analysis of slag as regards the CaO and SiO_2 concentrations is virtually the same for arc and spark excitation; in the case of determination of Al_2O_3, MgO and MnO the reproducibility is better for spark than for arc excitation.

The reproducibility of spark excitation analysis of sinter from solutions by means of the fulgurator is approximately the same as in analysis of slag. The agreement between spectroscopic and chemical analyses in the case of sinter is poorer than for slag. It was also established that the greater the divergence between the results of chemical analyses, the greater the disagreement between the results of spectroscopic and chemical analyses.

Analysis of slags by the method of nominal curves[2] taking into account the mutual influence of the various components has not led to satisfactory results so far and requires further development.

Spectroscopic analysis of slag in the form of powder (packed into the hollow of the lower electrode) with spark excitation and using an internal standard resulted in separate curves for the slags from different iron mills. In the case of analysis of sinter this method resulted in a great scatter of the points.

Spark spectroscopic analysis of slag in the form of briquettes compacted with a copper or graphite base both by the method of relative concentrations and by the method of nominal curves (with reference to nomograms) yielded results for CaO and SiO_2 characterized by approximately the same reproducibility and agreement with the results of chemical analyses as analysis via solutions.

The developed methods of spectroscopic analysis of solutions are suitable for the determination of the principal components of blast furnace slag and fluxed sinter from different iron works with reference to a single common working curve for each component. The reproducibility of individual determinations of CaO and SiO_2 is ±2-3%; that for Al_2O_3, MgO and MnO is ±3-5%.

On the basis of the described research work we were able to compile a set of instructions for analysis of blast furnace slag and fluxed sinter for the five principal components.[4,5]

References

1. O.I.Nikitina, Transactions of the Tenth Conference on Spectroscopy, Part II, L'vov, 1958.

2. L.I.Topalov, Zavodsk.laboratoriya (Indus.laboratory), No.5, 549 (1957).

3. R.Kastro & R.Lud, Spectrochim.acta, 4, No.6, 496 (1952).

4. Metody spektral'nogo analiza oflyusovannogo aglomerata i domennogo shlaka (Methods of spectroscopic analysis of fluxed sinter and blast furnace slag), Urkainian Institute of Metals, Khar'kov, 1958.

5. O.I.Nikitina, Byul.n.-tekhn.inform. (Scientific-technical information bulletin), Ukrainian Scientific Research Institute of Metals, No.9, 79 (1959).

ON MINIMIZING THE INFLUENCE OF THE MINERALOGICAL COMPOSITION ON THE RESULTS OF SPECTROSCOPIC ANALYSIS OF FLUXED SINTER

- I.K.Maiboroda

The present work was carried out on samples of ferrocalcium fluxed sinter from different iron works. Investigation of their structure showed a clear correlation between the chemical and mineralogical compositions, on the one hand, and the mechanical strength on the other.[1] The sinter samples were taken in the form of powder ground to 150-200 mesh. The samples were loosely packed (by shaking only) into a 2 mm diameter, 3 mm deep hollow in the lower carbon electrode. The counterelectrode was also carbon, terminating in a truncated cone with a 2 mm diameter flat. The spark excitation was produced by an IG-2 spark source; C = = 0.01 μf, L = 0.01 mh and t_e = 10 sec. In determining CaO and SiO_2 we obtained good reproducibility (±0.02-0.03) of $\Delta S = S_{an} - S_{Fe}$.

The iron content in the sinter was approximately 50% with a variation of ±5% from sample to sample. However, the variation of ΔS with log C is not linear. It was noted that if the samples from the same batch are subjected to grinding under the same conditions but for different periods, the reproducibility of ΔS does not change but the value of ΔS continues to decrease to a certain limit. It was also established that the value of ΔS for a given fineness of the powder depends on the mechanical strength of the sinter, which is a complex function of the chemical composition, the sintering conditions and the conditions of cooling of the sinter.[2-4]

Petrographic analysis (carried out by T.I.Litvinova) showed that values of ΔS appreciably exceeding the limit value are obtained for sinter with a fairly nonuniform grain size: the large grains contain ferruginous material (magnetite); they are the strongest and their composition includes a certain amount of siliceous materials (olivine and calcium silicates).

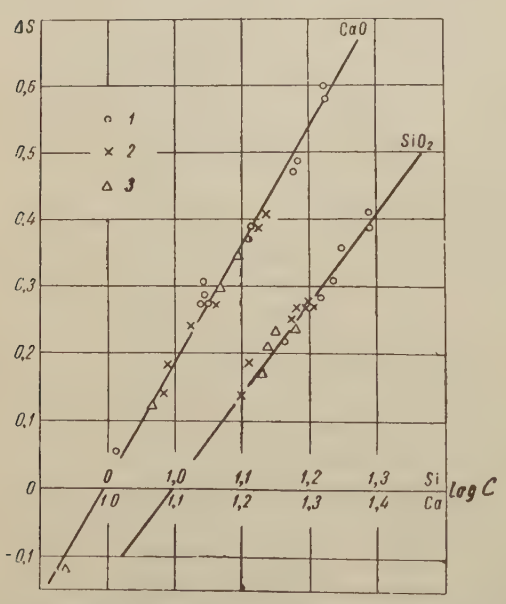

Working curves for determination of CaO and SiO_2 in fluxed sinter. Line pairs: Ca 3181.275 - Fe 3151.351 Å and Si 2881.578 - Fe 2876.802 Å. Samples from the 1) "Zaporozhstal'", 2) "Kirov" and 3) "Azovstal'" Plants.

Values of ΔS approaching the limit one correspond to even more nonuniform grinding. The strongest part of the sinter, containing magnetite, is present here in the form of large (rounded) grains, while the part containing olivine, glass and calcium silicates is more finely fragmented. There is a very appreciable discontinuity as regards grain size between the ferruginous and siliceous components of the sinter. In the case of prolonged grinding the malleable component is subjected to hardening and agglomeration as a result of rolling, while the siliceous minerals are separated and reduced to a very finely powdered fraction.

For degrees of pulverization corresponding to the limit value of ΔS, the variation of this parameter is satisfactorily described by an equation of the form $\Delta S = \gamma \log a + \gamma b \log C$ (see figure). It follows that sufficiently fine grinding of the samples insures obtaining reliable values of ΔS, characterizing the actual concentrations of CaO and SiO_2.

Adherence to the outlined procedure and conditions insures accuracy of analysis to within 4%. When a vibrational mechanical grinder driven by a 2500 rpm electric motor is used for pulverizing the specimens, the total time required for an analysis is 30 min.

"Zaporozhstal'" Plant

References

1. T.I.Litvinova, Domennoi proizvodstvo (Blast furnace operation) p.36, Metallurgizdat, 1957.

2. A.M.Bannykh, Dostizheniya domenshchikov Magnitogorskogo metallurgicheskogo kombinata (Achievements of blast furnace operators of the Magnitogorsk Metallurgical Combine), Metallurgizdat, 1957.

3. A.A.Soldatkin, Byul. (Bulletin), Ukrainian Inst. of Metals, No.7, 3 (1958).

4. V.P.Pevtsev. Thesis, Dnepropetrovsk Metallurgical Institute, 1958.

* * * * * * * * *

PNEUMATIC TECHNIQUE FOR INTRODUCING POWDER SPECIMENS INTO AN ARC

- R.S.Rubinovich & A.S.Pershin

Wider use of the method of introducing powders into the spectroscopic arc by means of an air stream[1,2] is blocked by certain shortcomings of the technique which lead to 1) incomplete vaporization of the powder particles and 2) variation in the rate of entry of the powder depending on its physical-chemical properties and other factors.

To insure complete vaporization of the particles in the arc it is essential that they enter the interelectrode gap well separated from each other, in a uniform stream and at a rate low enough to allow of complete evaporation at the given arc power. We attempted to satisfy these requirements by means of a pneumatic powder feed device[3].

The pneumatic device designed and constructed by us is shown in the photograph of Fig.1. Air at a pressure of 10 to 100 mm Hg is supplied to the atomizer bulb 2 through the tube 1 terminating in a capillary orifice. The powder is discharged into the arc through the vertical tube 3. A dimensional diagram of the atomizer bulb is shown in Fig.2. The bulb with a 0.05 to 0.2 g load of powder is mounted on the vibrator shelf 4 (Fig.1) and clamped in position by the spring fork 5. Spiral spring 6 provides for the return motion of the bulb. The bottom of the bulb rests on an opening in the vibrator stage and bears against the free end of a flat steel spring which is attached to the undersurface of the stage. When the cam on the motor shaft rotates, the oscillation of the spring is transmitted to the bulb. The distance between the tip of the discharge tube and the center line of the horizontal arc is 10 mm. In operation, the arc flame is deflected upwards a certain steady distance (if the air pressure is not excessive).

The device provides a steady supply of well separated powder particles in the form of a uniform stream 2 mm in diameter exactly into the center of the arc. Measurements give the following values for the amount of powder discharge per 25 sec as a function of the air pressure with a supply tube capillary diameter of 0.1 mm:

Pressure, mm Hg	10	20	30	40	50	80	100
Weight of powder per 25 sec, mg	2.8	5.2	9.0	16.0	21.5	34.5	51.1

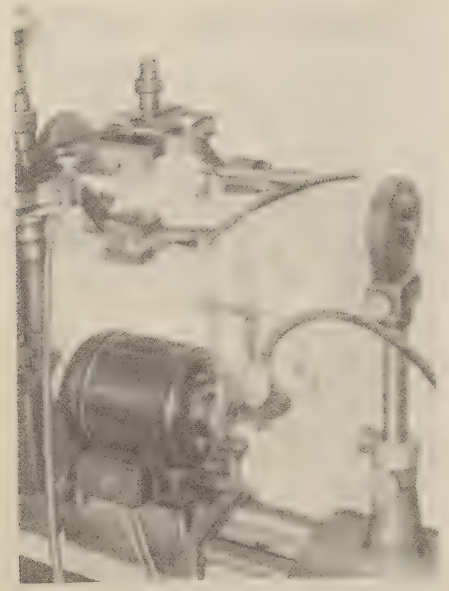

Fig.1. General view of the pneumatic feed device.

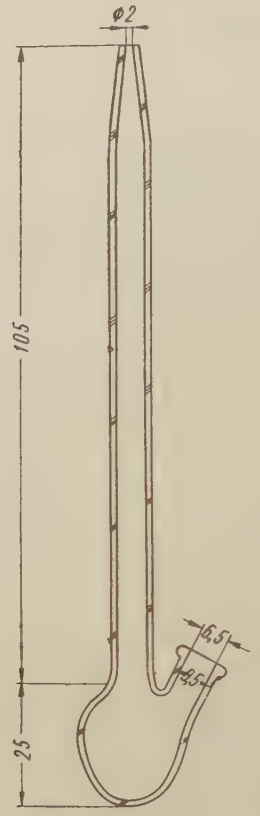

Fig.2. Diagram of atomizer bulb.

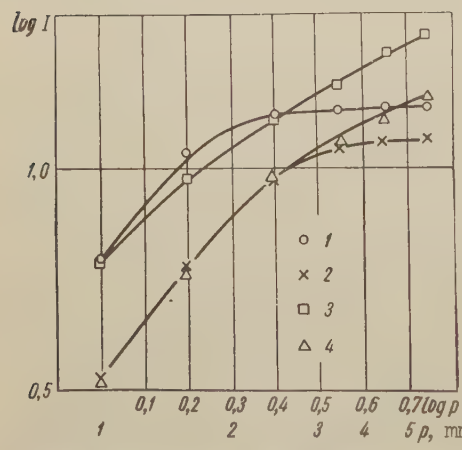

Fig.3. Variation of line intensity with pressure: La 3245.1 Å, 2) Nb 2950.9 Å, 3) Pb 2833.0 Å, 4) Hg 2536.5 Å.

At excessively high air pressures, the arc discharge becomes unstable; part of the powder is blown through the arc flame without being vaporized. For any given substance, however, one can usually find operating parameters (arc powder, air pressure, capillary diameter and discharge orifice) such that the vaporization will be complete.

With a view to determining the optimum pressure from the standpoint of sensitivity in analyzing for different elements, we investigated the variation in the spectrum line intensity with the air pressure. To this end we prepared standards with a silica powder base. The spectra were photographed on an ISP-28 spectrograph; arc current, 16 amp, interelectrode gap - 4 mm. Even at a relatively low pressure of 5-10 mm Hg, when only about 1-2 mg powder was discharged into the arc during the exposure time of 20-30 sec, spectra of normal intensity were obtained.

Fig.3 illustrates the pressure dependence for the following lines: Nb 2950.9 Å (Nb concentration 0.002%), La 3245.1 Å (0.01%), Hg 2536.5 Å (0.005%) and Pb 2833.0 Å (0.01%).

It is evident from the figure that with increase in air pressure the intensity of all the lines at first increases rapidly and then either ceases (for the lines of low volatility elements) or tends to increase more slowly (for the lines of high volatility elements). At a powder discharge rate of 30 mg/min (p = 30 mm Hg) there is obtained for all the elements in the beginning and middle of Rusanov's volatility series a sensitivity appreciably higher than with the conventional method of vaporization from a hollow electrode, but somewhat lower than was attained by Rusanov[2]. For low volatility elements the sensitivity appears to be 2-3 times higher than reported by Rusanov[2]. Thus, for example, the La 3245.1 Å line is clearly discernible down to an La concentration of $2 \cdot 10^{-3}$%, the Ta 2695.1 Å line down to a concentration of $4 \cdot 10^{-3}$%, the Nb 3163.4 down to $4 \cdot 10^{-4}$%, Y 3327.9 down to $5 \cdot 10^{-4}$%, Ce 3201.7 down to $4 \cdot 10^{-3}$% and Zr 3392.0 down to $3 \cdot 10^{04}$%.

Increase in the powder feed rate above 30 mg/min (p > 30 mm Hg) leads to incomplete vaporization of the particles in the arc. In connection with this, the intensity of the La and Nb lines levels off (see Fig.3), while the intensity of the background increases, which naturally results in reduction of the analytic sensitivity for these and other low volatility elements. On the other hand, the intensity of the lines of highly volatile elements continues to increase even at pressure above 30 mm Hg with the result that the analytic sensitivity for these elements continues to increase despite incomplete vaporization of the particles in the arc[2].

It must be borne in mind, of course, that the described procedure has certain shortcomings and limitations: the rate of discharge of the powder from the bulb does depend on the grinding procedure employed and on the hydroscopicity and other physical properties of the sample. A serious shortcoming of the pneumatic technique is fractioning of the powder particles according to size. Preferential discharge of the finer particles may give rise to appreciable analytic errors: up to 50% in particularly unfavorable cases. On the other hand, for uniform particle powders one can obtain an accuracy of 3-5%.

We desire to thank M.M.Kler, in whose laboratory in the Chemistry Department of Leningrad State University the present work was initiated, for his constant interest.

Scientific Research Institute for Geology of the Arctic

References

1. A.K.Rusanov & G.I.Tarasova, Zhur.analit.khimii, 10, 267 (1955). (Trans. J.Analytical Chemistry.)

2. A.K.Rusanov & V.G.Khitrov, Zavodsk.labor. (Industrial lab.) 2, 175 (1957).

3. N.N.Semenov, Ibid., 22, 457 (1956).

4. V.B.Nedler, Ibid., 5, 1469 (1936).

5. A.K.Rusanov, Spektral'nyi analiz rud i mineralov (Spectrum analysis of ores and minerals), Gosgeolizdat, 1948.

IMPROVED AVR-2 POWDER-FEEDING DEVICE

- I. I. Smolyak

More than two years work with the AVR-2 devices produced by the "Burovaya Tekhnika" ("Drilling Technology") Plant showed that this device, which is intended for analysis of powder samples by the method of blow-through, has a number of shortcomings. The most important of these is loss and scattering of a large amount of powder, which tends to contaminate the associated equipment, including the electrodes, and is dissipated into the air, giving rise to harmful conditions for the operating personnel.

We introduced a number of modifications to the AVR-2 with a view to eliminating this shortcoming.

1. The dust appearing during analysis, in the process of removing remains of samples and in cleaning the funnel by blowing, is caught and carried through four "wells" into the upper compartment of the combined box (Fig.1). The sample is put into the apparatus from a scoop through the hatch 5 (Fig.1). The conical valve 2 consists of two cones fitted base to base; when the valve is open there is formed an annular aperture. When the funnel is blown through for cleaning, the lower cone throws the dust onto the walls of the dust catcher. The dust that settles in the tube falls along the upper cone without entering the funnel. The draft is regulated by vertical displacement of the conical valve, which varies the effective cross section of the annular aperture. A new direct blowing tube has been introduced through a hole in the dust catcher supporting rail (see dashed lines in Fig.1).

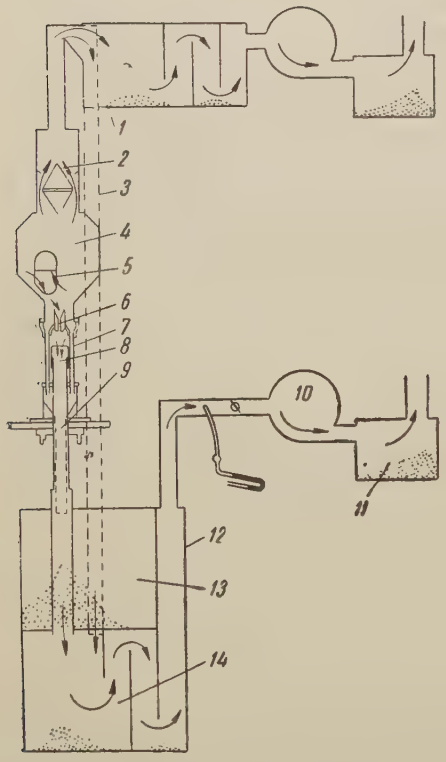

Fig.1. Diagram of blowing system: 1) box with baffles, 2) conical valve, 3) new variant of blow tube, 4) dust catcher, 5) hatch for loading sample, 6) slit-like funnel, 7) wells, 8) blow tube, 9) tube coupling, 10) blower, 11) settling chamber, 12) combined box, 13) chamber for dust collection, 14) chamber with baffles.

It is important to provide suitable thermal insulation for the dust catcher.

As modified the device requires cleaning only once a month.

2. The sample is introduced into the discharge by a specially designed slit-like brass funnel (Fig.2), the plane parallel jaws of which direct the powder in a wide flat stream that intersects the central portion of the arc discharge without contacting the electrodes. This type of funnel makes for efficient utilization of the sample and allows of reducing the exposure time. With an arc current of 20 amp and an exposure time of 15 sec, the sensitivity for determining W, Sb and Hg is 0.001%, the sensitivity for determining Mo is 0.001%.

Slit widths from 1.5 to 3 mm may be used (for the most part we used a 2.5 mm wide slit). The surfaces of the slits that come into contact with the powder should be polished. Generally, the slit is positioned 10-12 mm above the electrode; in analysis of humus substances, however, the slit should be raised to some 20-25 mm above the electrode.

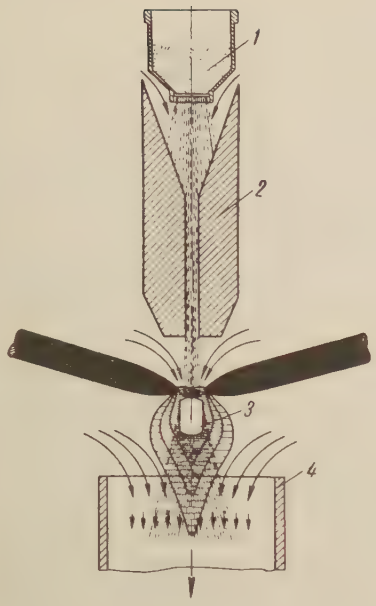

Fig.2. Introduction of sample into arc: 1) powder, 2) slit-like funnel, 3) observed section of arc, 4) receiving tube.

The slit assembly should be massive enough to insure effective heat removal. The draft in the dust catcher is adjusted so that it will not interfere with blowing the powder through the slit.

3. To provide for uniform feed of samples differing as regards structure, density and flowing characteristics, we use an assortment of screens with apertures varying from 1 to 1.8 mm at the bottom of the upper funnel (1 in Fig.2); the most suitable screen for any given sample is found by trial and error. We do not recommend using screens with openings smaller than 1 mm; to restrict the flow it is better to reduce the number of openings.

Enough sample powder should be loaded into the apparatus so that the entire surface of the screen will be covered during the full exposure time.

The productivity of the AVR-2 device modified as described above is such that one can burn up to 900 samples per 6 hour working shift.

Olekminsk Party,
Zabaikal' Geophysical Expedition

LOCAL ANALYSIS OF COMPLEX ALLOYS

- I.L.Mirkin & E.P.Rikman

In investigating alloys there are many occasions when it is necessary to determine the composition in very small volumes. Such occasions arise, for example, when one is studying the distribution of the chemical elements among structural components of the alloys, between the grains of the matrix solid solution, in diffusion layers and in welds, or when one wishes to determine the chemical composition of inclusions, etc.

Some of these problems can be solved by means of local spectroscopic analysis. One such technique is described in Ref.1. High-frequency current supplied by a PS-39 ac arc unit is rectified by a kenotron. The sample is connected as the cathode, the less disintegrated electrode. Kenotrons not only maintain a constant polarity of the electrodes but also limit the current strength in the spark circuit and stabilize its operation.

Special tests showed that the degree of blackening of the lines is determined primarily by the radiation of the vapor from the central "working" zone of the spark pit. The diameter of this zone in our case was ~0.08 mm. The analyzed volume in this case is $\sim 2 \cdot 10^{-5}$ mm^3, and the amount of vaporized material $\leqslant 1\text{-}2 \cdot 10^{-8}$ g. These values can be reduced by coating the electrode with polythene.

To facilitate locating the microsections of interest for analysis and subsequent studying of the area after sparking, we employed a modified PMT-3 microhardness tester; this was installed in place of the regular electrode holder. In conjunction with it we used a metallographic microscope.

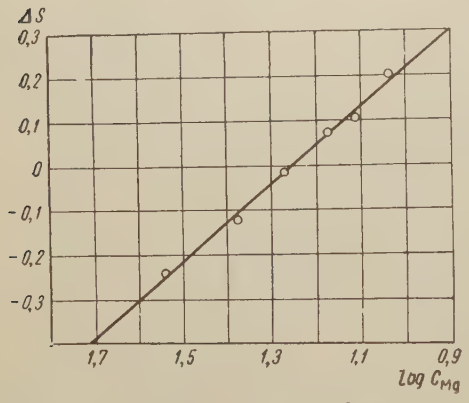

Fig.1. Working curve for determination of the local Mg content in high-strength cast iron by the microspectroscopic analysis.

In the case of highly nonuniform distribution of the elements among the individual phases of complex alloys, it is impossible to obtain conventional uniform standards for plotting the working curves. In such cases we plotted the working curve on the basis of the same samples as used for local analysis. Through repeated chemical analysis we established the average content C of the determined element, while ΔS the blackening difference for the analytic pair was determined as the average for a large number of local measurements. The calibration curve for the determination of Mg in high-strength cast iron is shown in Fig.1. The value of ΔS for each sample was obtained as the average for ~120 measurements.

Of considerable importance where quantitative local analysis is concerned is the influence of the alloy structure on the analytic results. One must distinguish between the effect of 1) heterogeneous distribution of the determined element among the structure components of the alloy and 2) different conditions of vaporization of the determined element from different phases of the alloy. Heterogeneous distribution of chemical elements can be investigated by means of local analysis. Differences in the conditions of vaporization of the individual structural components, as has been shown for a number of alloys, apparently do not play any significant role in the case of excitation by means of a high-frequency discharge.

Local spectroscopic analysis has been successfully employed for investigating the distribution of magnesium in high-strength cast iron[2], the distribution of magnesium in white magnesium pig[3], the distribution of alloying elements

Table 1

Experimental values of ΔS for three alloys

Alloy	Mo		Nb		Ti		Mn		Ni		Cr		Si	
	I	II	I	II	I	II	I	II	I	II	I	II	I	II
FU-2(ФУ-2)	0,04	0,13	0,17	0,38	0,03	0,14	0,06	0,08	—0,31	—0,29	0,45	0,49	—0,41	—0,39
FO-7(ФО-7)	0,00	0,08	0,41	0,71	0,20	0,34	0,00	0,00	—0,26	—0,27	0,36	0,37	—0,26	—0,26
Kh3 (ХЕ)	0,01	0,13	0,43	0,73	0,66	0,83	0,01	0,03	—0,33	—0,30	0,38	0,45	—0,35	—0,34

Table 2

Nb and Ti concentrations in a sample of FU-2 alloy (%)

Element	Average in alloy	In solid solution grains	In excess phases	Data of chemical analysis of precipitate
Nb	0.98	0.79	6.84	7.0
Ti	0.30	0.276	1.19	1.14

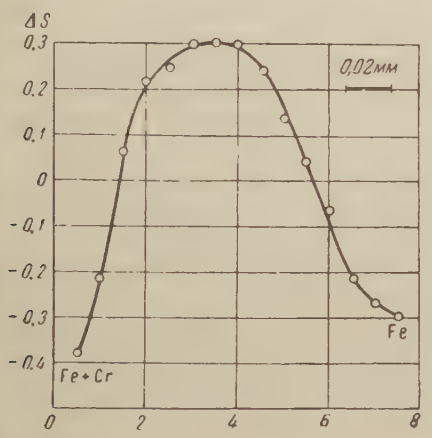

Fig.2. Distribution of molybdenum diffusing into pure iron (right-hand section) and into iron-chromium alloy (left-hand section).

in austenitic heat-resistant alloys and steels with lithoidal fracture, and the distribution of elements in diffusion layers. Below we describe some specific applications of local analysis.

Qualitative analysis of heat-resistant alloys was carried out as follows: for each sample there were photographed two series of spectra: 1) with the spark pits located over the grain cores and 2) with the pits on the boundary layer with a hardening-phase network. Table 1 shows the values of ΔS for three alloys obtained as the average for 15 measurements: I - for grains, and II - for pits including a boundary hardening-phase network.

On the basis of approximate determination of the volume of the hardening-phases and the working curve there was carried out an approximate phase analysis, the results of which for niobium and titanium for one sample are shown in Table 2. For purposes of comparison the results of chemical analysis of the precipitate are listed in the last column.

For investigating diffusion layers we prepared special samples consisting of sandwiches of a source metal and solvent metal plates. Fig.2 shows the diffusion curve for molybdenum obtained by means of a sample consisting of plates of pure iron and iron alloy with chromium between which was welded a molybdenum foil 0.02 mm thick. The sample was annealed at 1200° for 20 hours. The surface of the analyzed section was perpendicular to the metal layers. The first spark pit was located on the solvent metal surface; the centers of the successive pits were shifted in the direction perpendicular to the boundary in 0.01 mm steps and along the boundary of the metals in steps equal to the radius of the "spark spot". The right-hand section of the curve gives the distribution of molybdenum diffused into pure iron; the left-hand section, the diffusion into the iron-chromium alloy. We made an approximate evaluation of the diffusion coefficients on the basis of the experimental curve and obtained

$$D^{Mo}_{Fe} = 9.1\cdot10^{-11}\ cm^2/sec, \text{ and } D^{Mo}_{Fe+Cr} = 2.9\cdot10^{-11}\ cm^2/sec.$$

The first result is close to that obtained by means of radioactive tracers[4]; the second shows to what extent the diffusion of molybdenum is retarded when chromium is present in the iron.

Tula Mechanical Institute

References

1. I.L.Mirkin & E.P.Rikman, Zavodsk.laborat. (Industrial lab.), No.11, (1957).
2. I.L.Mirkin & E.P.Rikman, Liteinoe proizvodstvo (Foundry production), No. 12, (1957).
3. M.A.Krishtal & E.P.Rikman, Ibid., No.7 (1957).
4. I.L.Mirkin & M.A.Krishtal, Diffuziya v metallicheskikh splavakh (Diffusion in Metal Alloys), M., 1959.

* * * * * * * * *

SPECTROGRAPHIC INVESTIGATION OF SURFACE LAYERS FORMING IN THERMOCHEMICAL TREATMENT OF ALLOYS

- A.G.Komarovskii

The purpose of the present work was development of a method of quantitative microspectrographic analysis of the composition of thin surface layers forming in the process of thermodiffusive saturation of austenitic heat-resistant steels and alloys with chromium, aluminum and other elements.

The spectra were recorded on a medium dispersion ISP-22 quartz spectrograph. For excitation of the spectrum we used the high-frequency electric discharge from a TsNIITMASh (Central Scientific-Research Institute of Technology and Machine Building) universal generator[1] by means of which one can restrict the penetration of the surface of the specimen to 5-6 μ during the total time of presparking and exposure, whereas the penetration in working with the standard IG-3 spark generator is of the order of 0.03-0.05 mm. For plotting the working curves we used a special set of standards, the composition of which is shown in Table 1.

Table 1

Composition of standards, %

Melt No.	C	Si	Mn	Cr	Ni	Al	Nb	Mo
1954	0,41	0,58	0,67	0,37	0,54	1,16	—	—
1955	0,48	0,51	0,44	0,35	0,66	2,16	—	—
1956	0,42	0,65	0,70	0,44	0,69	5,60	—	—
1957	0,41	0,65	0,67	0,52	0,68	12,70	—	—
1020	0,14	0,87	0,77	0,40	1,04	29,30	—	—
3231	0,10	0,50	0,75	15,0	10,90	—	0,39	2,0
3249	0,12	0,44	0,69	23,45	8,78	—	1,01	1,82
3246	0,11	0,36	0,86	33,64	9,97	—	1,26	1,30
3248	0,09	0,47	0,86	55,58	7,94	—	1,10	1,30

On the basis of preliminary tests, we chose the following conditions: current in the primary of the transformer - 0.7 amp at 220 v. The unit was operated with two 0.6 mm auxiliary gaps in series; C = 0.0123 μf, L = 0.005 mh; the sidth of the working discharge gap was 1.3 mm. The counterelectrode was a copper rod 6 mm in diameter terminating in a truncated cone with a 1 mm diameter

flat. The width of the spectrograph slit was 0.02 mm; the exposure time 1.5 min.

The spectra were photographed on spectroscopic type II (or spectroscopic type 1-EC) plates.

By way of illustration, the working curves for the determination of Cr and Al in the thin surface layers forming in the process of thermodiffusive saturation of steels and alloys are shown in Figs.1 and 2.

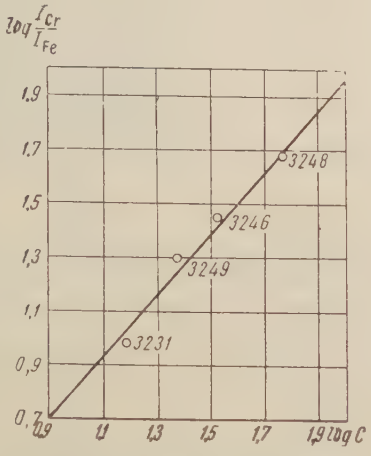

Fig.1

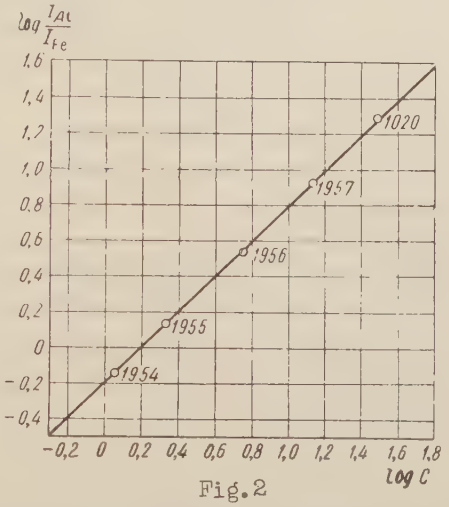

Fig.2

Fig.1. Working curve for determination of Cr in the diffusion layers on heat-resistant steels and alloys. Analytic pair: Cr 2830.16 - Fe 2828.63 Å.

Fig.2. Working curve for determination of aluminum in diffusion layers. Analytic pair: Al 3082.15 - Fe 3083.74 Å.

The depth of the diffusion layers was measured on oblique sections ground with the specimen held at an angle of 45° in a special vise. This angle was chosen in view of the fact that in case of measurement of the depth on an MIM-6 metallographic microscope with a 7 X eyepiece and 21 X objective the measured depth on the eyepiece scale is equal to exactly half the true thickness; thus the measured value had only to be multiplied by a factor of 2.

The method was used for investigating the variation of the layer thickness as a function of the thermodiffusive saturation heating temperature.

Table 2

Sample No.	Heating temp. °C	Layer depth, mm		Cr concentration on surface, %	
		EI405	EI612	EI405	EI612
137	1050	0,030	0,028	58,9	50,2
234	1100	0,040	0,033	64,6	51,3
335	1050	0,032	0,030	46,3	40,8
432	1100	0,043	0,035	58,9	51,3

By way of illustration we give the results for the case of thermodiffusive saturation of steels EI405 and EI612 with chromium. As will be evident from the table, increase of the temperature from 1000° to 1050°C results in an appreciable increase in the thickness of the layer. At the same time the Cr content in the diffusion layer also increases.

Central Scientific-Research Institute of Technology and Machine Building

Reference

1. A.G.Komarovskii, Izv.AN SSSR, Ser.fiz., 19, 152 (1955). (Trans.Bulletin 19, No.2, 141.)

IMPROVED EQUIPMENT FOR LOCAL SPECTROSCOPIC ANALYSIS

- V.V.Bogdanova

Below we describe the equipment used for developing localized spark spectroscopic analysis procedures. Fig.1 shows the electric circuit of the rectified high-frequency current source which supplied a localized spark by means of which one can investigate either a surface layer 2-5 μ in depth or at a "point" to a depth of 0.05-0.15 mm. The sample is connected as the cathode.

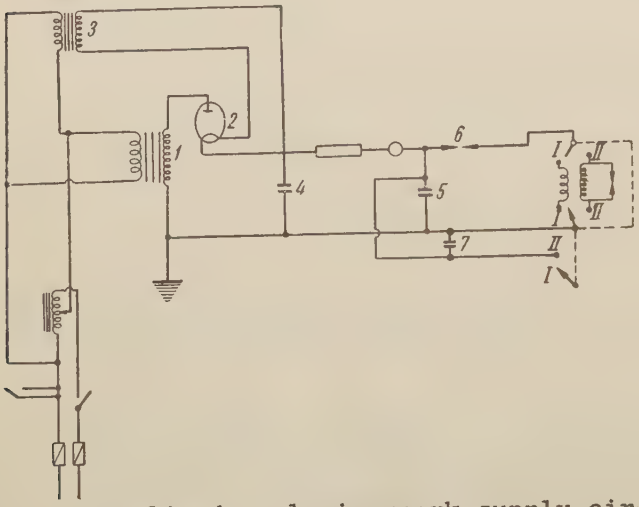

Fig.1. Localized analysis spark supply circuit: 1) step-up transformer, 2) kenotron, 3) filament transformer, 4) C = 0.3 μf, 5) C = 0.1 μf, 6) auxiliary discharge gap, 7) C = 0.05 μf. Setting I-I - for analysis of surface; II-II - for analysis at a "point".

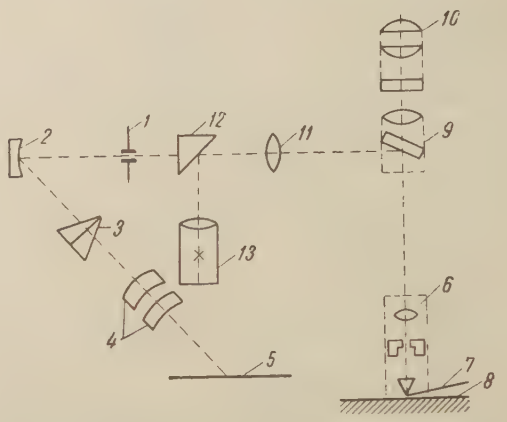

Fig.2. Optical system: 1) spectrograph slit, 2) spherical mirror, 3) quartz Cornu prism, 4) quartz camera lens, 5) photographic plate, 6) microlens, 7) electrode, 8) sample, 9) "opaque illuminator", 10) eyepiece with microscale, 11) quartz collimator lens, 12) glass prism, 13) illuminator with condenser.

An MBI-1 metallurgical microscope modified for the purpose is employed for positioning the spark and examining the surface. The analysis may be carried out either in air or in inert gas (argon). The use of an inert gas serves to enhance the spectrum intensity and allows of reducing the exposure time to 1 min. The gas is fed into the discharge zone at a pressure of ~0.2-0.3 atm.

The optical system of the spectrograph with the auxiliary equipment is shown in Fig.2. The light from the spark is collected by the microlens and directed to the "opaque illuminator"; thence it goes to the f = 130 mm lens mounted at a distance of 165 mm from the slit, and finally illuminates the slit. The retractable glass prism and OI-19 illuminator are used for aligning the sample and upper electrode with the optical axis with reference to a microscale. The sample and electrode setting is observed at a magnification of 400 X. The prism is then retracted, the OI-19 illuminator switched off and the spectrum is photographed in the usual manner.

Using this equipment, we developed a procedure for analysis of medium alloy and Kh18N9T type steels. By way of illustration of one of the practical applications of this procedure, we give the results of investigation of a spot weld of two dissimilar steels. The thickness of the weld is 2.5 mm, the length 8 mm. The analytic results showed that the center of this weld section is enriched in the alloying elements contained in Kh18N9T steel. Fig.3 shows a photograph of

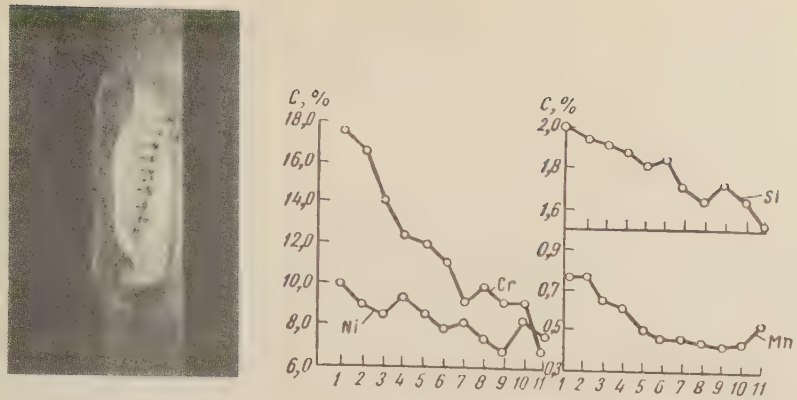

a b

Fig.3. a - Spot weld of 30KhGSN and 18KhN9T steels; b - Cr, Si and Mn concentrations in the weld "spot" (the figures along the horizontal scale correspond to the numbers in the photograph of the weld).

Table

Error in determining different elements (%)

Determined element	Medium alloy steel	Steel Kh18N9T
Manganese	5,0	3,0
Chromium	4,0	4,5
Nickel	3,10	5,0
Silicon	8,0	3,0
Molybdenum	8,0	—
Titanium	—	8,0

the weld and curves characterizing the distribution of Mn, Si, Cr and Ni along a diagonal across the weld (see photograph). To evaluate the accuracy of the procedure, we determined the relative error in determination of a number of elements on the basis of measurements of standard samples (see table).

A 0.3 mm diameter electrolytic copper wire serves as the upper electrode; the tip of the electrode is reduced to the requisite diameter by chemical etching. The electrode is mounted at an angle of 30° to and 0.3 mm above the ground surface of the sample, which may have any desired shape and a weight of up to 100 g.

We used the method of three standards, and plotted the working curves in terms of ΔS vs log C. The analytic line pairs were

Mo 2816.00 - Fe 2828.6
Mn 2939 - Fe 2936.9
Mn 2933.06 - Fe 2936.90
Si 2516.12 - Fe 2518.10
Si 2516.12 - Fe 2517.66
Ni 2416.13 - Fe 2415.06
Cr 2677.17 - Fe 2689.2
Cr 3147.2 - Fe 3154.3
Ti 3349.4 - Fe 3399.33
Ti 3261.1 - Fe 3259.99.

The spectra were photographed on Spectroscopic type II plates (speed 22 GOST units).

Scientific Institute of Aviation Technology

Bulletin of the USSR Academy of Sciences - Physical Series
Vol.23, No.9 - September 1959
Transactions of the Twelfth Conference on Spectroscopy
(Applied spectroscopy)

TABLE OF CONTENTS

	Page Orig.	Trans.
Opening address - S.L.Mandel'shtam	1054	1045
Determination of atomic concentrations in arc discharge plasma from the line widths and correlation between the concentrations in the solid and gaseous phases - I.M.Nagibina	1056	1048
Distinctive characteristics of arc discharges in different gases - V.L.Marzuvanov	1059	1051
Atlas of spectrum lines for high-dispersion grating spectrographs - S.K.Kalinin, V.L.Marzuvanov, E.E.Fain, G.M.Zamyatina, V.N. Perevetun & S.L.Terekhovich	1061	1054
Entry of matter into arc plasma. Case of binary Na + Li mixtures - V.P.Zakharov & A.A.Shishlovskii	1063	1056
Entry of silicon brass into an ac arc - N.K.Rudnevskii, G.I. Golitsyn & V.P.Rybochkin	1065	1058
Entry of lead brass into an ac arc - N.K.Rudnevskii & E.S.Obukhova	1067	1060
Correlation between the compositions of the solid and vapor phases in spectroscopic analysis of iron alloys - O.I.Nikitina, M.G. Sklyar, A.E.Gorevaya & N.K.Ivanova	1069	1062
Influence of discharge time on the rate of evaporation of particles from the surface of metallic arc electrodes - G.E.Zolotukhin & N.M.Zykova	1072	1065
Effect of sample polarity in the excitation of rectified arc spectra - E.A.Silin'sh & L.F.Taure	1074	1067
Influence of the composition of powdered substances on the relative intensity of spectrum lines - A.M.Shavrin & M.A.Zotin	1077	1069
Influence of "third" elements in spark analysis of solutions (A) - A.K.Rusanov & L.I.Sosnovskaya	1079	1071
Influence of "third" elements in using undispersed light as the internal standard - I.S.Abramson, S.N.Murzin & V.A.Slavnyi	1081	1073
Effect of the chemical composition of the sample on the intensity of the matrix spectrum and the analytic results - N.V.Buyanov	1083	1075
Relation between the diluent effect of "third" components and the transport of material in light sources for spectroscopy - A.M. Borbat & A.A.Shishlovskii	1086	1078
Variation of the total intensity of spectrum lines with the atomic concentration in a pulse discharge - E.I.Vorontsov	1088	1080
Investigation of the causes of selective disintegration of alloys by a spark discharge - I.A.Grikit	1091	1083
Influence of "third" elements in spark spectroscopic analysis of molten alloys - L.E.Vvedenskii & V.I.Shekhobalova	1093	1085
Spectroscopic investigation of electroerosion of oxygen-containing titanium - N.S.Sventitskii & K.I.Taganov	1096	1088
Spectroscopic investigations of the effect of polarity in electric erosion of metals - K.I.Taganov	1097	1089
Use of the contact-spark sampling technique in spectroanalytic studies - V.S.Burakov & A.A.Yankovskii	1099	1091
Analysis of an optical system for a mirror spectrograph with large plate length - S.A.Khrshanovskii	1100	1093

Photoelectric equipment for the ISP-22 spectrograph. A new method of automatic spectroscopic analysis of electrolytes - Yu.A.Yakobi & S.I.Maksimov 1103 1095
New photoelectric spectrographic equipment - M.M.Averbukh, N.V. Artsishevskaya, N.V.Belyaev, I.I.Erina, D.I.Pen'kov & I.G. Strel'tsov 1105 1097
Analysis of heat-resistant and light alloys and steels by the photoelectric procedure - K.A.Sukhenko, K.A.Moiseeva, L.D. Metelina, I.G.Tishin, N.V.Penkina & D.G.Bakanov 1107 1099
Photoelectric steelometer with visual monitoring of the position of invisible spectrum lines - M.M.Butslov, A.K.Vinogradova, L.M.Ivantsov, G.N.Kutuzova & S.L.Mandel'shtam 1110 1102
On stabilization of the position of the spectrum by thermostatic equipment for spectroscopic instruments - A.P.Atamanov, V.N. Balandin & L.M.Ivantsov 1112 1104
Photoelectric attachment for ISP-22 type medium spectrographs - L.M.Ivantsov & A.I.Sherudilo 1114 1105
Spectroscopic determination of oxygen in commercial grade titanium - K.A.Sukhenko, V.S.Grigorova, I.S.Lindstrem, N.S.Sventitskii & P.P.Galonov 1116 1107
Concerning spectroscopic determination of oxygen in titanium - N.S.Sventitskii, K.I.Taganov & Z.I.Shlepkova 1118 1110
On the use of the spectro-isotopic procedure for determining hydrogen - T.F.Ivanova, M.É.Trentovius & V.V.Fedorov 1120 1112
Determination of nitrogen in different steels - K.A.Sukhenko, P.P.Galonov & T.V.Barasheva 1123 1114
Influence of the chemical composition and heat treatment of steel samples on the results of spectroscopic determination of nitrogen - N.V.Buyanov, L.M.Fedorova & V.F.Korotkov 1126 1117
Determination of nitrogen in chromium and titanium - S.A.Skotnikov 1128 1119
Analysis of high concentrations allowing for the influence of "third" components - L.I.Topalova 1130 1121
Spectroscopic determination of the major components of noble metal alloys - N.I.Varlamova & N.S.Sventitskii 1133 1124
Spectroscopic determination of high concentration components in steels and other alloys - A.G.Komarovskii 1135 1126
Statistical investigation of analytic results - V.V.Nalimov 1137 1128
Standards for determination of impurities in pulverized complex ferroalloys - A.B.Shaevich 1139 1130
Preparation of standards for spectroscopic analysis of noble metals - A.A.Kuranov 1140 1132
Methods of calibration in analysis of alloys - E.S.Kudelya & A.S.Dem'yanchuk 1143 1135
Use of the "fractional exposure" procedure for analysis of some alloys - E.P.Barankina 1145 1137
Preparation of standards of different alloys and investigation of the influence of "third" elements in them - K.A.Sukhenko, O.I. Mladentseva & A.V.Aksenova 1147 1139
Rapid spectroscopic analysis of metallometric specimens for rare alkali metals, boron, fluorine and other elements - P.A.Stepanov, E.A.Sergeev, M.V.Belobragina & M.S.Leshchinskaya 1149 1141
Quantitative spectroscopic determination of the principal components of intrusive rocks - T.S.Reshetina 1150 1143

Chemico-spectroscopic determination of molybdenum and tungsten in igneous rocks - L.I.Pavlenko	1152	1144
Spectroscopic analysis of luminescence-pure zinc sulfide and sulfate with the aid of chemical enrichment - V.N.Vasil'eva, L.A.Dvorzhetskaya, L.Ya.Markovskii & L.Ya.Khlebnikova	1153	1146
Spectroscopic determination of uranium by the method of isotopic doping - N.P.Ivanov	1154	1148
Spectroscopic determination of the relative Sr and Ca concentrations in biological specimens - G.D.Litovchenko & S.A.Shipitsyn	1156	1150
Spectroscopic determination of microelements in tissue proteins - S.G.Bogomolov, F.D.Drobiz & A.G.Morozov	1158	1152
Development of methods of spectroscopic analysis of blast furnace slag and fluxed sinter - O.I.Nikitina	1159	1154
On minimizing the influence of the mineralogical composition on the results of spectroscopic analysis of fluxed sinter - I.K. Maiboroda	1162	1158
Pneumatic technique for introducing powder specimens into an arc - R.S.Rubinovich & A.S.Pershin	1163	1159
Improved AVR-2 powder-feeding device - I.I.Smolyak	1165	1162
Local analysis of complex alloys - I.L.Mirkin & E.P.Rikman	1167	1164
Spectrographic investigation of surface layers forming in thermo-chemical treatment of alloys - A.G.Komarovskii	1169	1166
Improved equipment for local spectroscopic analysis - V.V.Bogdanova	1171	1168

Translated in 1960 by
Columbia Technical Translations
5 Vermont Ave., White Plains, N.Y.

Translations of the following issues of the Bulletin of the USSR Academy of Sciences - Physical Series - devoted to conferences on spectroscopy and allied topics are still available:

Ninth Conference on Spectroscopy	Vol.18,No.6 and Vol.19, Nos.1 & 2
Eleventh Conference on Spectroscopy (Theoretical spectroscopy)	Vol.22, Nos.6, 9 and 11
Magnetic Radiospectroscopy (1955)	Vol.20, No.11
First Conference on X-Ray Spectroscopy	Vol.20, No.1 (half of issue)
Second Conference on X-Ray Spectroscopy	Vol.21, No.10
Spectroscopy of Light-Scattering Media	Vol.21, No.11
Fourth Conference on Luminescence (Molecular luminescence)	Vol.20, Nos.4 & 5
Sixth Conference on Luminescence (Molecular luminescence)	Vol.22, No.11 and Vol.23, No.1

The uniform price per issue is $20. Tables of contents are available free on request.

Columbia Technical Translations
5 Vermont Ave., White Plains, N.Y.

Transactions

of the

Twelfth All-Union Conference on Spectroscopy

(Moscow, November 19-26, 1958)

In this issue we continue publication of the Transations of the Twelfth All-Union Conference on Spectroscopy (Applied Spectroscopy). A list of the reports presented at the Conference but scheduled for publication in other journals will be found on pages 1262-5.

SOME RESULTS OF SPECTROSCOPIC INVESTIGATION OF THE INDIVIDUAL HYDROCARBON COMPOSITION OF TARTAR PETROLEUMS

- B.Le

We investigated the individual hydrocarbon composition of seven 150°C end point gasolines derived from crudes from the Romashkinsk (Devonian) and Bavlinsk (Devonian & Lower Carboniferous fields in the Tartar ASSR.[1-4] All the gasoline samples were studied by the Raman spectroscopy procedure outlined in Refs.5 & 6.

An attempt was made to establish some regularities as regards the distribution of the hydrocarbon groups in the various gasolines.

Hydrocarbon composition of the gasolines

We studied the hydrocarbon composition of the gasolines from the different horizons of the geologic profile (gaseous hydrocarbons were not considered). The analytical results are given in Table 1 in weight percent.

Table 1

Hydrocarbons	Stalinogorsk horizon of the Lower Carboniferous $C_1^{2\,stal}$	Kynovskaya strata, Franskii level of the Upper Devonian, D_o	Pashiiskaya strata, Franskii level of the Upper Devonian D_I			Zhivetskii strata, Middle Devonian, D_{III}	
	1*	2	3	4	5	6	7
Normal paraffins	29,0	27,9	31,7	27,4	28,2	27,3	32,4
Branched paraffins	35,1	30,9	27,4	29,9	30,2	23,6	26,7
Cyclopentanes	7,9	8,8	7,0	9,7	7,7	7,8	6,4
Cyclohexanes	8,6	10,0	9,9	10,0	11,0	13,5	12,1
Aromatics	2,2	3,7	5,0	4,7	5,4	5,9	5,7
Petroleum density	0,8900	0,8614	0,8490	0,8694	0,8619	0,8400	0,8400
Sulfur content	2,8	1,43	1,23	1,67	1,43	0,9	0,9

*Here and in the other tables the column numbers correspond to the sample numbers.

The following is apparent from the above table.

The lowest isoparaffin content is found in D_{III} petroleum; the highest in the $C_1^{2\,stal}$ petroleum. The amount of isoparaffins is also directly proportional to the sulfur content of the crude. Actually, the sulfur contents in the D_{III}, D_I, D_o and $C_1^{2\,stal}$ horizon petroleums are related as 1:1.3:1.6:3.1, while the amounts of isoparaffins in the same gasolines vary as 1:1.1:1.3:1.4; i.e., these also increase in the same order, although somewhat more slowly. A similar direct relationship obtains between the isoparaffin content and the density of the petroleum.

The content of cyclohexane and aromatic hydrocarbons decreases in going from the lower to higher horizons.

Distribution of hydrocarbons by structure

A number of interesting characteristics may be noted as regards all the gasolines studied (regardless of the origin, formation depth, or horizon). The distribution of the isoparaffins is given in weight percent referred to the gasoline in Table 2.

Hydrocarbons having a single tertiary carbon atom in the chain are predominant among the branched-chain paraffins. Those hydrocarbons which have an odd number of carbon atoms in the main chain usually have a CH_3 group attached at

Table 2

Hydrocarbons	1	2	3	4	5	6	7
2-Methylpentane	4,77	4,78	3,69	5,41	5,18	6,40	6,64
3-Methylpentane	3,21	2,91	1,78	2,59	2,88	1,93	2,06
2-Methylhexane	2,21	1,68	2,43	2,53	1,98	1,78	1,34
3-Methylhexane	4,28	3,57	3,61	3,65	3,46	2,98	2,87
2-Methylheptane	2,79	2,68	2,99	3,54	3,38	2,82	2,58
3-Methylheptane	1,08	1,01	1,30	1,34	0,89	0,92	0,91
2-Methyloctane	0,72	0,60	0,66	0,72	0,86	0,72	0,61
3-Methyloctane	0,96	0,60	0,65	0,81	0,91	0,72	1,02

the second carbon atom; in even-numbered chains the group is linked to the third carbon atom.

The content of monosubstituted naphthenes and benzenes decreases with increase of the alkyl radical chain length (Table 3).

Table 3

Hydrocarbons	1	2	3	4	5	6	7
Cyclopentane	0,28	0,42	0,43	0,28	0,40	0,32	0,31
Methylcyclopentane	1,53	1,18	1,83	1,56	1,39	1,58	1,62
Ethylcyclopentane	0,54	0,64	0,68	0,78	0,59	0,77	0,30
n-Propylcyclopentane	0,15	0,13	0,30	0,31	0,39	0,17	0,11
Cyclohexane	0,75	0,61	1,27	1,04	1,09	1,88	1,49
Methylcyclohexane	2,43	2,14	3,07	2,88	3,34	4,43	3,55
Ethylcyclohexane	0,93	0,91	0,74	0,83	0,83	1,47	1,13
n-Propylcyclohexane	0,07	0,10	0,10	0,10	0,07	0,11	0,10
Benzene	0,20	0,37	0,67	0,44	0,64	0,49	0,63
Methylbenzene	0,68	1,09	1,70	1,62	1,73	1,79	1,74
Ethylbenzene	0,31	0,68	0,62	0,65	0,82	1,26	0,79

Similar regularities are observed in most gasolines from other deposits in the Soviet Union[7-10]. The explanation for this is a problem set for further investigations; these evidently require collection of additional experimental data.

Chemical Institute, Kazan Branch
Academy of Sciences of the USSR

References

1. F.A.Urmancheev, E.A.Robinzon, M.G.Odintsov, S.-Kh.G.Kashaev and B.Le, Izv.AN SSSR, Otd.khim.nauk, No.6, 711 (1957). (Trans.Bulletin Acad.Sci - Div. Chem.Sci.)

2. F.A.Urmancheev, E.A.Robinzon, S.-Kh.G.Kashaev and B.Le, Ibid., No.3, 324 (1958).

3. E.A.Robinzon, O.N.Grishina, L.A.Mukhamedova, F.A.Urmancheev, R.I.Izmailov, B.Le, S.-Kh.G.Kashaev, et al, Izv.Kazansk.fil.AN SSSR, Otd.Khim.nauk, No.4, 93 (1957).

4. F.A.Urmancheev, R.I.Izmailov & B.Le, Izv.AN SSSR, Otd.khim.nauk, (1961). (Trans.Bull.Acad.Sci. - Div.Chem.Sci.)

5. G.S.Landsberg & B.A.Kazanskii, Ibid., No.2, 100 (1951).

6. G.S.Landsberg, P.A.Bazhulin & M.M.Sushchinskii, Osnovnye parametry spektrov kombinatsionnogo rasseyaniya uglevodorodov (Principal Parameters of Hydrocarbon Raman Spectra), Pub.Acad.Sci., AN SSSR, 1956.

7. B.A.Kazanskii et al, Izv.AN SSSR, Otd.khim.nauk, 266, 278,456,865,1053 (19

8. A.V.Topchiev et al, Doklady AN SSSR, 103, 1034 (1955).

9. G.D.Gal'pern, M.V.Shishkina & M.I.Shetsko, Tr.In-ta nefti AN SSSR (Proceedings, Petroleum Inst. of the USSR Acad.Sci., 10, 59 (1957).

10. A.V.Topchiev et al, Khimiya i tekhnologiya topliva (Fuel chemistry and technology, No.2, 9; No.3, 8 (1958).

* * * * *

ANALYSIS OF HYDROCARBON MIXTURES BY RAMAN SPECTROSCOPY

- V.T.Aleksanyan, Kh.E.Sterin & S.A.Ykholin

Raman spectra are extensively used in our laboratory for analysis of natural hydrocarbon mixtures, particularly narrow gasoline fractions. Extension of the procedure to higher boiling fractions, however, involves certain difficulties. This pertains particularly to paraffin-cyclopentane fractions for which clear results can be obtained only in the temperature range up to 150°. Aromatic hydrocarbon mixtures can be studied in greater detail at least to 200°.[1]

Research in the Spectroscopy Commission Laboratory, carried out in collaboration with the Catalytic Synthesis Laboratory of the Institute of Organic Chemistry at the Academy of Sciences of the USSR, is being conducted in two directions, namely, a) study of the spectra of the individual hydrocarbons of different classes, and b) analysis of hydrocarbon mixtures, including the products of various reactions. It should be noted that success in obtaining a correct picture of the reaction frequently depends on the care taken in preparing the samples for spectroscopic study, and on the accuracy of the spectroscopic data (frequencies and the intensities) available.

Catalytic cyclization of n-octane with the formation of homologs of cyclopentane

It was shown previously[2] that paraffin hydrocarbons can be cyclized in the presence of a platinum catalyst to form five-membered rings. Assuming that the reaction takes place without isomerization or cracking of the initial hydrocarbon, one can predict which homologs of cyclopentane should be obtained. For example, 1,1,3-trimethylcyclopentane should be obtained as a result of cyclizing isooctane.

A preliminary study of n-octane showed that it is cyclized with the formation of 1-methyl-2-ethylcyclopentane and n-propyl-cyclopentane. The spectra given in the Landholdt-Börnstein tables, which were not altogether satisfactory, were used for identifying the former hydrocarbon.

A second, verifying study was carried out with higher accuracy. Carefully distilled narrow fractions of the paraffinic-naphthenic portion of the catalyzate (at least 2.2 cm^3 each) were obtained for the optical investigations; we also prepared pure cis- and trans-1-methyl-2-ethylcyclopentane.

Trans-1-methyl-2-ethylcyclopentane was found in the lower boiling fractions (about 1.4% of the catalyzate by weight). n-Propylcyclopentane was found in the last fractions and in the distillation residue (also about 1.4 weight percent of the catalyzate). 4-Methylheptane was also detected with good reliability; this was evidently formed by hydrogenolysis of n-proplycyclopentane.

A narrow bright line at 762 cm^{-1} observed in the spectrum of the distillation residue was tentatively attributed to pentalane (whose spectrum is unknown), which could be formed by a secondary cyclization of n-propyl-cyclopentane or 1-methyl-2-ethylcyclopentane. Some confirmation of this assumption is provided by the fact that the same line was observed in the spectrum of the catalyzate of n-propylcyclopentane.

Homogeneous destructive hydrogenation of tetralin at high hydrogen pressure

According to a previously proposed[3] mechanism for the homogeneous destructive hydrogenation of aromatic hydrocarbons at high hydrogen pressures, one of the reaction products in the case of tetralin should be n-butylbenzene. According to published experimental data, however, tetralin also isomerizes to methylindan. More accurate information was obtained in the present study on the composition of the reaction products, and a general scheme is proposed for the transformation of tetralin under the given hydrogenation conditions (temperature - 440-462°; pressure - to 1200 atm).

The following hydrocarbons were found among the reaction products with boiling points between 136.1 and 183.9°: ethylbenzene 16%, isopropylbenzene 9%, n-propylbenzene 10%, sec-butylbenzene 12%, n-butylbenzene 43%, indan 4%, and α-methylindan 2-4%; in addition, there were found minor quantities (≤ 1%) of: o-oxylene, 1-methyl-2-ethylbenzene, trans-decalin, 1-methyl-2-isopropylbenzene, and 1-methyl-2-n-propylbenzene. The main component of the higher boiling fraction (185-190°) was α-methylindan; n-butylbenzene, β-methylindan (5-10%), and trans-decalin (1-3%) were also found.

It was shown by special tests that the isomerization of tetralin into α-methylindan occurs in parallel with the destructive hydrogenation of tetralin, leading to the formation of n-butylbenzene. On the basis of our spectroscopic studies we propose the following general scheme for the process (a number of details are omitted from the scheme):

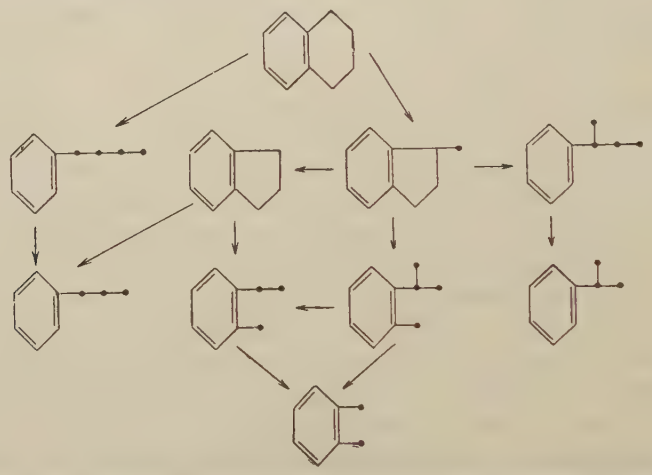

Scheme characterizing the destructive hydrogenation and isomerization of tetralin.

In the present work we also made a special study of the spectra of α- and β-methylindan (the spectrum of the latter compound had not been recorded hitherto)

References

1. B.A.Kazanskii, G.S.Landsberg, and others, Izv.AN SSSR, Ser.fiz., 18, 704 (1954). (Trans.Bulletin, 18, No.6, 386.)

2. B.A.Kazanskii, A.L.Liberman, G.V.Loza, I.M.Kuznetzova, V.T.Aleksanyan & Kh.E.Sterin, Izv.AN SSSR, Otd.khim.nauk, No.6, 1071 (1959). (Trans.Bull.Acad. Sci. - Div.Chem.Sci.)

3. A.E.Gavrilova, M.G.Gonikberg, V.T.Aleksanyan & Kh.E.Sterin, Ibid., No. 8, 981 (1958).

RAMAN SPECTRA OF SOME C_{24} HYDROCARBONS*

- A.N.Kislinskii & A.A.Petrov

We excited and studied the Raman spectra of nine C_{24} hydrocarbons containing phenyl and cyclohexyl rings. The syntheses and properties of these compounds have been described previously[1]. Some of their attributes are listed in Table 1.

Table 1

Physical Properties of the Investigated Hydrocarbons

No.	Hydrocarbons	T_{boil}, °C	n_D^{20}	d_4^{20}
I	1-phenyl-3-hexyl-6-cyclohexyl-hexane	211 (5) *	1,4971	0,8923
II	1-phenyl-1-cyclohexyldodecane	206 (4)	1,4990	0,8960
III	1,1-diphenyldodecane	208 (4)	1,5241	0,9248
IV	1,5-diphenyl-3-heptylpentane	210 (4)	1,5219	0,9233
V	7-phenyloctadecane	191 (1)	1,4800	0,8528
VI	2,11-diphenyldodecane	200 (4)	1,5219	0,9244
VII	1,1-dicyclohexyldodecane	205 (4)	1,4803	0,8758
VIII	7-cyclohexyloctadecane	201 (2)	1,4635	0,8347
IX	2,11-dicyclohexyldodecane	196 (4)	1,4802	0,8759

*The figures in ( ) indicate the pressure in mm Hg.

All of the hydrocarbons were distilled in a 16 theoretical plate column and then purified chromatographically using silica gel. (Their degree of purity is being determined at the present.) In all cases fractions with a constant index of refraction were taken for the spectroscopic studies.

The spectra were obtained on an ISP-51 three-prism spectrograph. The wave numbers of the lines were determined by measurements on an IZA-2 comparator, with reference to a standard dispersion curve. The line intensities were evaluated visually on a ten-point scale.** Since the boiling points of the given hydrocarbons are very high, the samples were not purified by redistillation into the Raman tubes. To reduce background, the spectra were recorded in all cases with the samples heated to 160-170°. For this purpose the horizontal (working) portion of the tube containing the sample was inserted into the spectrograph illuminator in a co-axial glass tube, closed at one end by a glass window and fitted with an internal heating spiral. The data for each spectrum were based on two exposures.

Analysis of the spectra leads to the following conclusions.

1. The presence of phenyl or cyclohexyl rings in the hydrocarbon molecules is clearly evinced in the spectra (Table 2). In the case of phenyl groups, all the lines characteristic of monosubstituted benzene appear: 621, 1002, 1031, 1156, 1182, 1205, and 3065 cm^{-1},[2,3], as well as the lines associated with the antisymmetrical valence vibrations of the benzene ring: ~1580 and ~1603 cm^{-1}. When a cyclohexyl ring is present, there appear its characteristic lines at 1029, 1158, 1267, and 1348 cm^{-1}. [4] The "aromatic" line at 1205 cm^{-1} is absent from the spectrum of 1,1-diphenyldodecane; possibly it merges with the other characteristic aromatic line at 1185 cm^{-1}, the intensity and width of which are much greater in the spectrum of this compound than in the spectra of the other hydrocarbons studied. The lines in the 750 to 900 cm^{-1} region, which are due to the totally symmetrical vibration of the cyclohexyl ring and the radical attached to it[4], are of very low intensity (0-1), except for one case, namely, 2,11-dicyclohexyldodecane,

---

*M.S.Lentovskaya participated in the experimental part of the investigation.

**In the future we plan to employ a photometric procedure.

Table 2

Some Characteristic Spectrum Lines of the Investigated Hydrocarbons

I 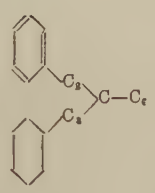	II 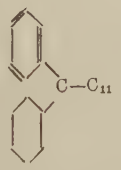	III 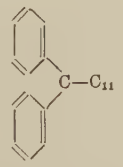	IV 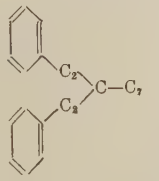	V 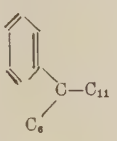	VI 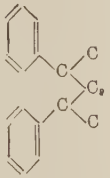	VII 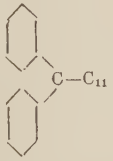	VIII 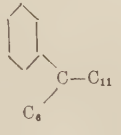	IX 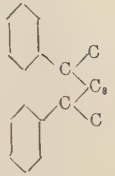
623 (1,5)	620 (1,5)	618 (3)	623 (4)	621 (1)	621 (3)	—	—	—
1000 (10)	1000 (10)	1000 (12)	1002 (15)	1000 (9)	999 (12)	—	—	—
1029 (7)	1032 (7)	1028 (6)	1030 (7)	1027 (4)	1027 (6)	1034 (4)	1029 (2)	1032 (5)
1155 (0,5)	1154 (0,5)	1155 (2)	1157 (1)	1155 (0,5)	1157 (1)	1151 (0)	1148 (0)	1153 (0,5)
1185 (0,5)	1185 (1)	1185 (3w)	1181 (0,5)	1188 (1)	1181 (2)	1179 (0)	1186 (0)	1187 (0,5)
1202 (2)	1194 (2)	—	1201 (6)	1199 (2)	1199 (2)	1197 (0)	—	—
1267 (1,5)	1261 (1,5)	1260 (0)	—	—	1265 (0)	1271 (3)	1267 (1)	1266 (4)
1346 (0)	1344 (0)	1344 (0)?	1347 (0)?	1347 (0)	1341 (0)	1345 (1,5w)	1348 (0,5)	1346 (1d)
1572 (0)	1580 (0)	1579 (0,5)	1581 (0,5)	1581 (0)	1579 (0,5)	—	—	—
1603 (5)	1602 (5)	1598 (6)	1603 (8)	1604 (4)	1602 (6)	—	—	—
3065 (4)	3064 (4)	3064 (10)	3063 (10)	3067 (4)	3063 (10)	—	—	—

w = wide; d = double

in the spectrum of which there is a 771 cm^{-1} line with an intensity of 4.

2. It is possible to judge of the number of phenyl and cyclohexyl rings in a given molecule even on the basis of visual evaluation of the intensity of the brightest lines characteristic of these rings. Table 2 illustrates this point. The line intensities for hydrocarbon I were evaluated in the ten-point scale; then the intensities for the other hydrocarbons were determined by comparison with those of I; all evaluations were made on a DSP-1 double spectroprojector. The table shows a significant increase in the intensity of the 621, 1603, 3065 and 1267 cm^{-1} lines in cases where one phenyl ring (or, one cyclohexyl ring) in the molecule is replaced by two. This effect is evinced more weakly for the 1002 cm^{-1} line because it approaches the maximum blackening in the negative. The effect is masked in some cases where the 1031 cm^{-1} is concerned owing to the fact that this line is characteristic of both phenyl and cyclohexyl rings. However, by comparing the spectra of molecules having one or two identical rings (hydrocarbons III, IV, V and VI, and hydrocarbons VII, VIII and IX, respectively), we can discern considerable differences in intensity even for this line. The 1156, 1182, 1205 and 1348 cm^{-1} lines are too faint for reliable comparison by visual evaluation.

3. The characteristic lines of tertiary C atoms as well as those associated with hycrocarbon chain stretching vibrations, which were noted for paraffins by Sushchinskii[4,5] were very poorly defined; they were either very weak (0-1) or not discernable at all in some cases. These lines, which are generally rather weak as compared to the aromatic and cyclohexyl lines, are evidently masked by the continuum. Thus, the presence of structural elements characteristic of paraffins in the compounds under study cannot be substantiated by examination of their Raman spectra.

Institute for Petrochemical Synthesis,
Academy of Sciences of the USSR

References

1. S.P.Sergienko, L.N.Kvitkovskii, A.L.Tsedilina & A.A.Petrov, Doklady AN SSSR, 120, 541 (1958). (Trans.Doklady - Chemistry.)

2. B.A.Kazanskii, G.S.Landsberg, and others, Izv.AN SSSR, Ser.fiz., 18, 704 (1954). (Trans.Bulletin 18, No.6, 386.)

3. G.S.Landsberg, P.A.Bazhulin and M.M.Sushchinskii, Osnovnye parametry spektrov kombinatsionnogo rasseyaniya uglevodorodov (Basic parameters of hydrocarbon Raman Spectra), M. 1956.

4. M.M.Sushchinskii, Thesis,FIAN (Physical Institute, USSR Acad.Sci.), M., 1957.

5. M.M.Sushchinskii and P.A.Bazhulin, Uspekhi fiz. nauk, 63, 301 (1957).

INVESTIGATION OF AQUEOUS SOLUTIONS OF URANYL NITRATE BY RAMAN SPECTROSCOPY

- S.Mintz & Z.Kentskii

One of the principal fields of research in our laboratory is study of the structure of electrolytes and reactions between ions and solvent molecules. To this end, we employ a number of different methods, including Raman spectroscopy. Using this technique, we studied changes in the structure of nitric acid with variation in the acidity of the medium, etc. Recently, we began to study the concentration dependence of the Raman lines of electrolyte solutions. Some of the preliminary results are reported below.

A solution of uranyl nitrate in water was one of the systems studied. It is known that uranyl ions in solution react strongly with the solvent molecules to form complexes. According to the data in the literature on the vibrational frequencies of the uranyl ion[1-4], the Raman spectrum contains a strong line at 860 cm^{-1} associated with totally symmetrical vibrations, a weak line at 210 cm^{-1} due to deformation vibrations, and a line at 930 cm^{-1} due to asymmetrical vibrations of UO_2^{2+}. We felt it would be of interest to investigate the concentration dependence of the parameters characterizing these lines.

The spectra were investigated by the photographic technique on an ISP-51 spectrograph, the spectra being recorded on Agfa Raman Ortho plates. The spectra were excited by the green mercury line from a one-tube (PRK-2 tube) elliptical illuminator. The plates were scanned on a MF-2 microphotometer. The integral intensities and widths of the lines were determined by the contour method, described in Ref.5. The degree of depolarization was measured by means of two crossed polaroid films, mounted in front of the spectrograph slit. The values were picked off a calibration curve plotted on the basis of tabular data on the degree of depolarization of the lines of carbon tetrachloride and cyclohexane.

The dispersion in the encompassed spectral region was 234 cm^{-1} mm; the apparatus function was 4.7 cm^{-1}; the spectral width of the slit - 6.5 cm^{-1}.

The uranyl ion concentrations were determined gravimetrically by precipitation using o-hydroxyquinoline[6]; the nitrate ion concentrations were determined with a nitrometer[7]; the water concentrations were calculated from changes in solution density. As was shown by special measurements on a "Unicam" spectrophotometer, none of the solutions absorbed light in the excitation region.

The experimental results for the 860 cm^{-1} line associated with totally symmetrical vibrations of the uranyl ion are presented in the Table.

Parameters of the UO_2^{2+} 860 cm^{-1} line in spectra of aqueous $UO_2(NO_3)_2$ solutions

Solution	$UO_2^{+}:NO_3^{-}:H_2O$	Molar integral intensity, I_∞	Line width, cm^{-1}	Depolarization factor
0,41 *M*	1:2:133	98	9	
0,93 *M*	1:2:55	100 *	8	0,18
1,83 *M*	1:2:27	119	11	0,15
2,44 *M*	1:2:19	126	12	
0,94 *M* + + $LiNO_3$ 3*M*	1:5:50	116	10	0,16
0,73 *M* + + $LiNO_3$ 6*M*	1:10:57	130	11	0,16

* Taken as the "standard"

The molar integral intensity was calculated by means of the formula:

$$I_\infty = (S/S_s)(n^2/n^2_s)(C_s/C)\cdot 100$$

where S is the area under the line contour, n is the index of refraction, and C is the uranyl ion concentration in moles per liter; subscript "s" refers to the solution taken as the "standard", while the symbols without a subscript refer to the test solutions. In the present case, all intensities are referred to the intensity of the 860 cm^{-1} line in the spectrum of an 0.93 M uranyl nitrate solution taken as 100.

The results presented are averages for 5 to 8 determinations. The standard devia-

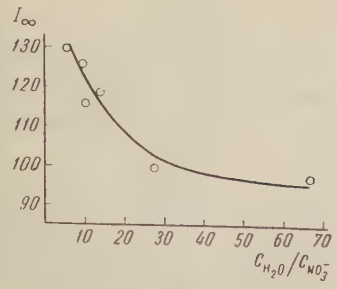

Variation of the molar intensity of the UO_2^{2+} 860 cm^{-1} line with the relative concentration of water and nitrate ions in aqueous $UO_2(NO_3)_2$ solutions.

tions for the intensity measurements did not exceed 10%.

A reduction in the water to nitrate ion concentration ratio is accompanied by an increase in molar intensity of the 860 cm^{-1} line (see figure); this is evidently caused by electron displacements along the O-U-O bonds. It is possible that the nitrate ions in replacing water molecules in the uranyl complexes alter the uranyl electronic shell.

The width of the 860 cm^{-1} line does not change within the limits of the experimental error.

The low degree of depolarization of the 860 cm^{-1} line and its persistence indicate that the uranyl ion retains a linear configuration in the solutions studied.[3,8]

The 210 cm^{-1} line associated with deformation vibrations of the uranyl ion was also observed in the spectra; it was not feasible to measure its parameters owing to its low intensity and the strong background close to the exciting line. It should be noted that we did not observe even a trace of the 930 cm^{-1} line, although the intensity of this asymmetric vibration line in a saturated aqueous uranyl nitrate solution was reported by Sutton[4] to be of the same order of magnitude as the intensity of the 860 cm^{-1} line.

Further study is required for a more consistent interpretation of the results.

Electrochemistry Laboratory,
Institute of Physical Chemistry,
Polish Academy of Science

References

1. G.K.T.Conn & C.K.Wu, Trans.Faraday Soc., 34, 1483 (1938).
2. B.S.Satyanarayana, Proc.Ind.Acad.Sci., 15A, 414 (1942).
3. N.A.Sevchenko & B.I.Stepanov, Zhur.eksp.i teoret.fiz., 19, 1113 (1949).
4. J.Sutton, Nature, 169, 235 (1952).
5. G.S.Landsberg, P.A.Bazhulin & M.M.Sushchinskii, "Osnovnye parametry spektrov kombinatsionnogo rasseyaniya uglevodorodov" (Basic parameters of hydrocarbon Raman spectra). M., 1956.
6. D.I.Rodden, Analytical Chemistry of the Manhattan Project: Uranium and Thorium, N.Y. 1950.
7. G.Lunge & E.Berl, "Chemisch-technische Untersuchungsmethoden. Berlin, 1910.
8. G.H.Dieke & A.B.F.Dunkan, Spectroscopic Properties of Uranium Compounds. N.Y., 1949.

INVESTIGATION OF METHANOL SOLUTIONS OF ZINC CHLORIDE BY RAMAN SPECTROSCOPY

- S.Mintz & S.Osetskii

Investigations of electrolyte-solvent systems[1-3] showed marked changes in the Raman spectra of the solvent and dissolved salt due to reactions between the two components. Primary attention in these studies was given to measurement of the line frequencies.

The observations of Kuchkarev[4], made in the course of electrochemical studies, indicating strong intermolecular interaction in zinc chloride solutions in methanol, prompted us to study these solutions by Raman spectroscopy. The Raman spectra of these solutions were investigated previously by Hibben[2], who noted a shift of the 1033 cm^{-1} methanol line to the side of lower frequencies.

Particular attention was directed in our work to the concentration dependence of the integral intensity, depolarization factor and width of the 1033 cm^{-1} line associated with symmetrical vibrations of the methanol C-O bond. The experimental procedure was similar to that described in Ref.5 (the preceding article). The spectra were excited by the blue mercury line from an elliptical illuminator with a PRK-2 tube.

We employed calibration curves plotted on the basis of the lines of cyclohexane, chloroform and carbon tetrachloride.[6,7] The apparatus function of the spectrograph was 7.5 cm^{-1}. The solutions being studied did not absorb light in the measurement region.

The zinc chloride content was determined by evaporating the methanol and weighing the residue; the methanol content was assumed to be the difference. The main anhydrous solution of zinc chloride in methanol was prepared by displacing the mercury from a methanol solution of mercuric chloride with pure metallic zinc. The solution was filtered through a G-5 filter. The other solutions were obtained by diluting the main solution.

After completion of the measurements, the water content of the solutions was determined using Fisher's reagent and did not exceed 1.1 percent by weight. The root mean square error of the intensity determinations did not exceed 14%. The uncertainty in determining the depolarization factor amounted to ~0.04.

The experimental results are presented in Figs.1 and 2. As will be evident from Fig.1, the molar integral intensity of the 1033 cm^{-1} line increases rapidly with the concentration for $ZnCl_2$ concentrations in the range from 0 to 0.9 moles per liter, while the depolarization factor decreases. This indicates a reduction in the polarity of the methanol C-O bond and increase in the symmetry of the molecule.

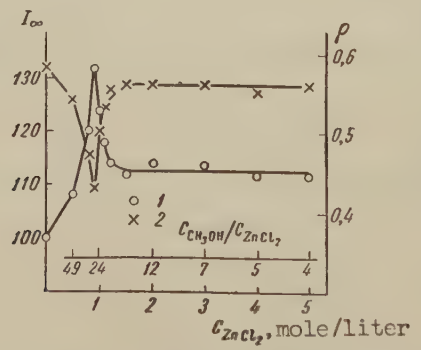

Fig.1

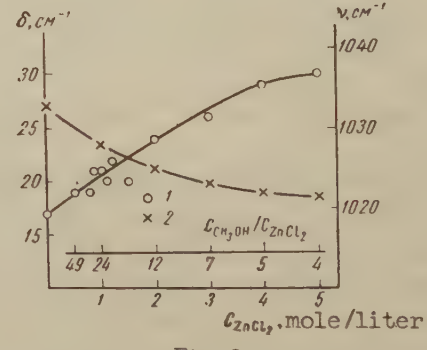

Fig.2

Fig.1. Variation of the molar integral intensity (1) and the depolarization factor ρ (2) of the 1033 cm^{-1} line with the $ZnCl_2$ concentration.

Fig.2. Variation of the width δ (1) and frequency (2) of the 1033 cm^{-1} line with the $ZnCl_2$ concentration.

In the case of solutions with $ZnCl_2$ concentrations greater than 0.9 mole/liter, we observe a decrease in intensity and an increase in the degree of depolarization of the C-O line; this indicates a reduction in the symmetry of the methanol molecule and an increase in the polarity of the C-O bond. We note that the molar integral intensity of the 1033 cm^{-1} line is always higher in solutions as compared with pure methanol, while the depolarization factor is lower.

The nature of the change in the parameters of the 1033 cm^{-1} line gives reason to infer that the causes responsible for the observed effects are coupling of the methanol molecules among themselves through hydrogen bonds and interaction of the methanol molecules with zinc chloride molecules, leading to formation of complexes. Evidently, at $ZnCl_2$ concentrations from 0 to 0.9 mole/liter, the effects observed are due mainly to changes in the coupling of the methanol molecules. The decrease in polarity of the C-O bond and the increase in symmetry of the methanol molecules shows that zinc chloride molecules promote rupture of the hydrogen bonds in this concentration range. At high $ZnCl_2$ concentrations, interaction between the methanol and zinc chloride molecules predominates; this leads to increase in the polarity of the C-O bonds and decrease in the symmetry of the methanol molecules.

The increase in line width can be regarded as a result of statistical superposition of the lines for a large number of dynamic complexes of zinc chloride and methanol having close values of the C-O bond vibration frequency.

The reduction in frequency can be explained by the increase in the effective mass of one of the vibrating groups owing to coupling with zinc chloride molecules.

We were unable to measure the parameters of the other methanol lines because of their low intensity and the strong background. We note that a line at 280 cm^{-1} was clearly discernible in the spectrum; it is presumably associated with vibrations of the methanol-zinc chloride complexes.

The above observations are preliminary in nature; a more complete interpretation is predicated on further study.

Electrochemistry Laboratory,
Institute of Physical Chemistry,
Polish Academy of Sciences

References

1. M.V.Vol'kenshtein, Uspekhi fiz.nauk, 18, 153 (1937).

2. J.H.Hibben, Proc.Nat.Acad.Sci., USA, 18, 532 (1932).

3. J.Coubeau, Z.Phys.Chem., B 36, 45 (1937); A.I.Brodskii & A.M.Sak, Acta physicochimica URSS, 2, 215 (1935); M.S.Ashkinazi & P.V.Kurnosova, Zhur.fiz.khim., Ukrainian SSR, 11, 848 (1938); G.S.Karetnikov, Zhur.fiz.khim., 32, 782 & 603 (1958); and A.Terenin, W.Filimonov & D.Bystrow, Z.Elektrochem., 62, 180 (1958).

4. A.V.Kuchkarev, A.N.Ivashchenko & Ya.I.Tur'in, Doklady AN Uzbek SSR, No.8, 20 (1950), No.6, 27 (1951), No.11, 20 (1951); A.V.Kuchkarev, Zhur.obshch.khim., 22, 1127 (1952); N.I.Shuikin, A.V.Kuchkarev & N.A.Pozdnyak, Izv.AN SSSR, Otdel. khim,nauk, 904 (1954); A.V.Kuchkarev & N.I.Shuikin, Ibid., 470 (1954) and 1469 (1956). (Trans.Bull.Acad.Sci. - Div.Chem.Sci.)

5. S.Mintz & Z.Kentskii, Present issue of the Bulletin, p.1184.

6. G.S.Landsberg, P.A.Bazhulin & M.M.Sushchinskii, "Osnovnye parametry spektrov konbinatsionnogo rasseyaniya uglevodorodov" (Basic parameters of hydrocarbon Raman spectra), 174. M., 1956.

7. K.W.F.Kohlrausch, Ramanspektren, Leipzig.(Cited in Russian translation.)

DETERMINATION OF THE INFRARED ABSORPTION COEFFICIENTS OF CH_2 GROUPS IN DICYCLIC COMPOUNDS

- S.V.Markova & P.A.Bazhulin

Molecular analysis with reference to infrared absorption spectra has acquired increasing practical importance in recent years. The study of high boiling fractions involves the problem of establishing the numbers of CH, CH_2 and CH_3 groups in complex hydrocarbons; to determine the number of groups it is necessary to know the absorption coefficient per group. In the present study we determined the coefficients for the CH_2 groups in the linkage joining two five-membered rings in dicyclic compounds. Since in analogous studies[1-4] the effect of the monochromator slit width on the shape of the recorded bands was not considered, we studied a number of paraffins and naphthenes data on which are already available in the literature, but in doing so we took into account all instrument corrections.

We measured the coefficients of absorption at 730 cm^{-1} of the methylene groups in several five-membered dicyclic hydrocarbons of the type:

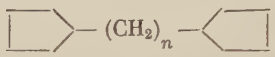

where n varied from 2 to 5, as well as in several normal paraffin hydrocarbons and five-membered naphthenes. All of the work was performed on a double beam instrument consisting of a standard IKS-11 monochromator with an automatic attachment developed in our laboratory[5].

The resolution of the apparatus is characterized by the following parameters: with an instrument time constant of ~1 second and a level of noise, the rms value of which amounted to about 2% of the full scale deflection, the effective slit width equalled about 2 cm^{-1} (0.12 mm) in the 10 μ region. A special grooved cell was used in the work; the thickness of the cell was measured interferometrically to an accuracy of ~5%. To minimize the influence of possible differences in the cell gap thickness due to clamping, we recorded each band 3-4 times with the cell refilled and remounted each time. The absorption band for the substance and a 100% absorption line were recorded on each spectrogram. In processing the results, we determined the intensity I_o as the difference between the "background" of the band and the 100% absorption line.*

An example of a band recording made under close to optimum conditions[6] is reproduced in Fig.1. The slow recording and the large number of individual "throws" make it relatively easy to plot a good average curve by eye. According to Rautian[7], this curve plotting procedure is only slightly inferior as regards accuracy to plotting by the method of least squares, but it is obviously much quicker. A similar record with noise makes it possible to use rather narrow slits. In our case, the slit width amounted to from 0.2 to 0.35 times the band width; hence the corrections for finite slit width were minor. We introduced these corrections graphically using the Raleigh method as improved by Rautian[7]. In addition, we made corrections for the finite size of the region of integration[8]. The measurement results are presented in Table 1.

---

*This procedure involves a systematic error owing to the fact that reflection at the liquid-NaCl interface and scattered light are not fully taken into account. Appropriate corrections for this were introduced.

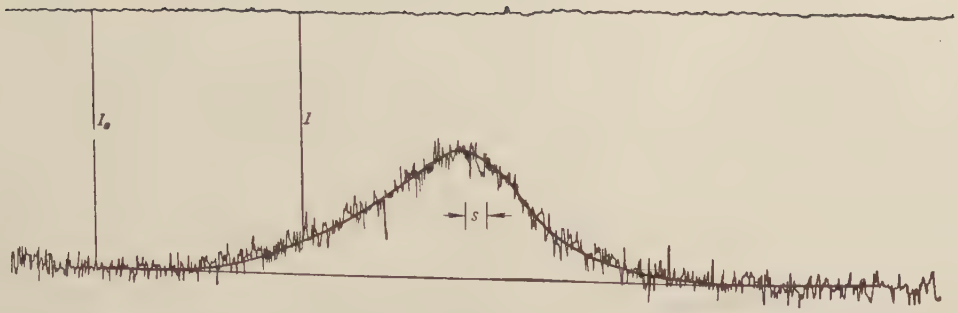

Fig.1. Record of the 729 cm^{-1} band of 1,4-dicyclopentylbutane.

Table 1

Substance	Band peak, cm^{-1}	$K_0 \cdot 10^{-3}$, cm^2/mole	$K_\infty \cdot 10^{-4}$ cm/mole
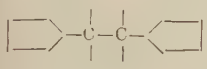	757	8,1	31*
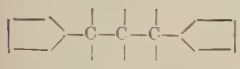	737	15	31
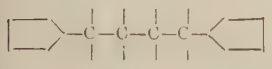	729	20	38
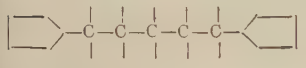	726	28	53

* In this case the measurement error was much greater than usual.

The variation of the integral absorption coefficient with the number of paraffinic CH_2 groups in the molecule is shown in Fig.2 for five-membered dicyclanes, monosubstituted five-membered naphthenes and n-paraffins; it will be seen that the experimental points fit a straight line. Consequently, it may be concluded that the absorption coefficient varies in proportion to the number of absorbing groups. It will also be evident that the numerical values of the absorption coefficients are virtually the same for all three types of compounds. The absorption coefficients at the line peaks also exhibit the same (linear) variation with the number of absorbing groups (Fig.3). A comparison of our results with the data in the literature shows that the frequency of the ~730 cm^{-1} band

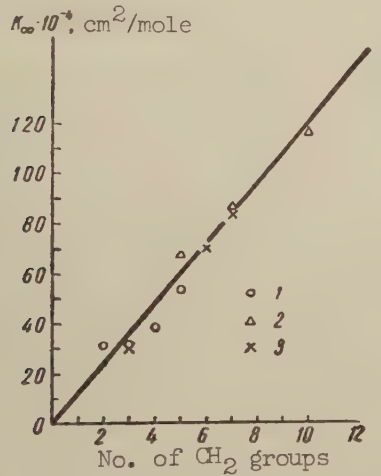

Fig.2

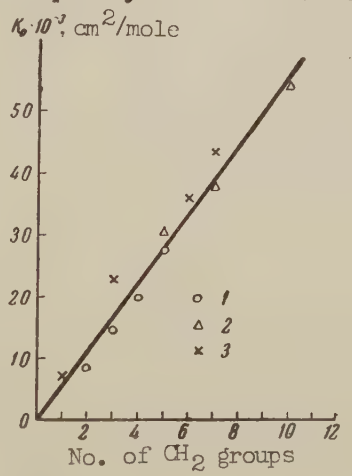

Fig.3

Fig.2. Variation of the integral absorption coefficient with the number of linear CH_2 groups in the molecule: 1) dicyclanes; 2) n-paraffins; 3) monosubstituted naphthenes.

Fig.3. Variation of the absorption coefficient at the line peak with the number of chain CH_2 groups in the molecule: 1) dicyclanes; 2) n-paraffins; 3) monosubstituted naphthenes.

Table 2

No. of CH_2 groups	ν, cm^{-1}	
	Dicyclanes	Naphthenes and paraffins
2	757	750
3	737	728
4	729	726
5	726	723

in the spectra of five-membered dicyclic hydrocarbons varies with the number of intermediate CH_2 groups in the molecule in the same way as in the case of paraffins and naphthenes[1] (Table 2).

The values of the absorption coefficients per CH_2 group, averaged for the three classes of compounds in question, were found to be $K_o = 5.8 \cdot 10^3$ cm^2/mole and $K_\infty = 11.9 \cdot 10^4$ cm/mole (the measurement error is estimated to be ~10%). The validity of this averaging is supported by the data of Hastings et al[1], which show that the absorption coefficients at the ~730 cm^{-1} line are very close for paraffins and naphthenes. Our data are in good agreement with the absorption coefficients obtained for paraffins by Luther & Czerwony[4], namely, $K_o = 6.0 \cdot 10^3$ cm^2/liter and $K_\infty = 12.2 \cdot 10^4$ cm/mole.

In conclusion, it may be noted that it should be possible to obtain comparable results using different types of instruments, provided appropriate corrections are made for apparatus factors. This opens the possibility of utilizing the extensive data on absorption coefficients in the literature for purposes of molecular analysis.

"P.N.Lebedev" Physics Institute,
Academy of Sciences of the USSR

References

1. S.H.Hastings, A.T.Watson, R.B.Willians & J.A.Anderson, Anal.Chem., 24, 612 (1952).
2. S.A.Francis, Ibid., 25, 1466 (1953).
3. H.L.McMurry & V.Thornton, Ibid., 24, 318 (1952).
4. H.Luther & G.Czerwony, Z.Phys.Chem., New Series, 6, 286 (1956).
5. V.I.Malyshev, M.N.Markov & A.A.Shubin, Doklady AN SSSR, 86, 273 (1952).
6. G.G.Petrash & S.G.Rautian, Transactions of the Tenth All-Union Conference on Spectroscopy, Vol. I, p.102 & 107, L'vov, 1957; Inzh.-fiz.zhur (Engin.-Phys. Jour.), 1, No.7, 61 (1958) and 1, No.11, 80 (1958).
7. S.G.Rautian, Thesis, FIAN Physical Institute, USSR Acad. Sci., 1957.
8. M.M.Sushchinskii, Thesis, FIAN, M., 1957.

INTENSITIES OF THE INFRARED ABSORPTION BANDS ASSOCIATED WITH C-H VALENCE VIBRATIONS

- E.I.Pokrovskii

In order to determine the branching in polyethylene and the structure of certain polymers having different numbers of CH_2 and CH_3 groups, we obtained the IR spectra of several of normal paraffins from n-hexane to n-hexadecane in the 3 μ region (Fig.1). We determined the absorption coefficients of their solutions in CCl_4. Overlapping of the absorption bands was taken into consideration in evaluating the coefficients. It was found that the antisymmetrical vibrations of CH_2 and CH_3 groups have a higher intensity than the symmetrical vibrations. This is connected with a larger change of the dipole moment in the case of antisymmetrical vibrations.

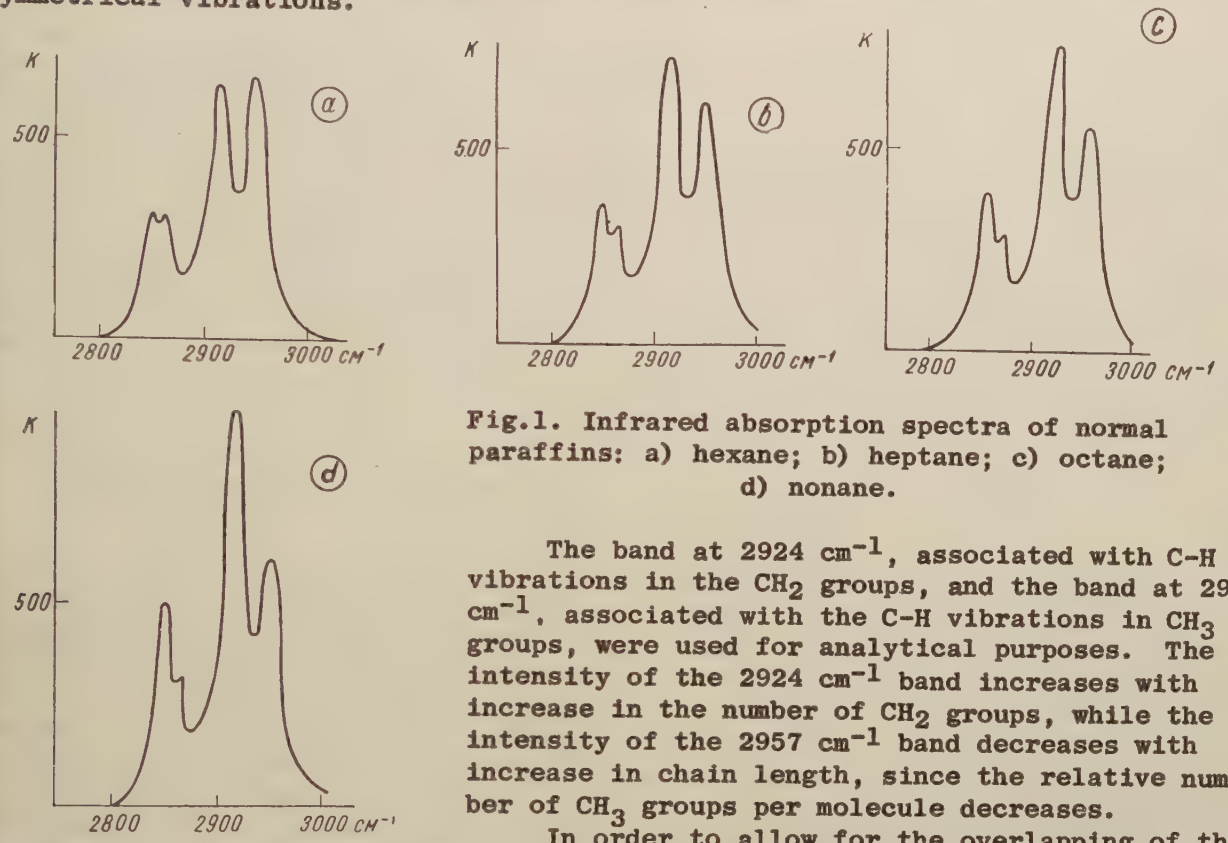

Fig.1. Infrared absorption spectra of normal paraffins: a) hexane; b) heptane; c) octane; d) nonane.

The band at 2924 cm^{-1}, associated with C-H vibrations in the CH_2 groups, and the band at 2957 cm^{-1}, associated with the C-H vibrations in CH_3 groups, were used for analytical purposes. The intensity of the 2924 cm^{-1} band increases with increase in the number of CH_2 groups, while the intensity of the 2957 cm^{-1} band decreases with increase in chain length, since the relative number of CH_3 groups per molecule decreases.

In order to allow for the overlapping of these bands, we determined their half-width and plotted their contours assuming the classical dispersion shape. It was found that the absorption per CH_2 group amounted to 154 liters $mol^{-1}cm^{-1}$ at 2924 cm^{-1}, and to 25.7 liters $mol^{-1}cm^{-1}$ at 2957 cm^{-1}. The absorption per CH_3 group was 232 liters $mol^{-1}cm^{-1}$ at 2957 cm^{-1} and 21.3 liters $mole^{-1}cm^{-1}$ at 2924 cm^{-1}. The ratio of the coefficients K at the absorption peaks of the CH_2 and CH_3 groups equals 0.66 ± 0.01 and does not change in going from the CCl_4 solution to the pure substance or to a film.

In order to analyze the copolymers obtained by polymerization of α-methylstyrene with styrene, the absorption spectra of both monomers as well as for the pure polymers were obtained (Figs.2 & 3). The spectra of the polymers in the 3 μ region differ markedly from those of the monomers. In particular, the weak absorption band due to the valence vibrations of the C-H group, which is adjacent to the $=CH_2$ double bond, disappears, and new bands characteristic of the $-CH_2-$ and $-CH_3$ groups appear. The absorption band at 2850 cm^{-1} for polystyrene and the one at 2986 cm^{-1} for poly-α-methylstyrene were found to be the most suitable for

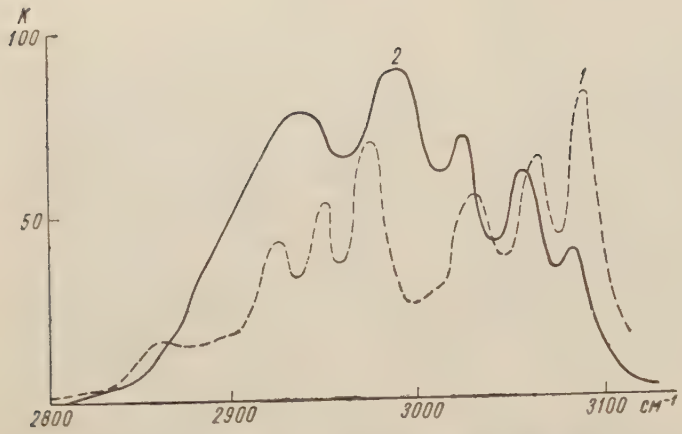

Fig.2. Infrared absorption spectra in CCl_4: 1) α-methylstyrene; 2) poly-α-methylstyrene.

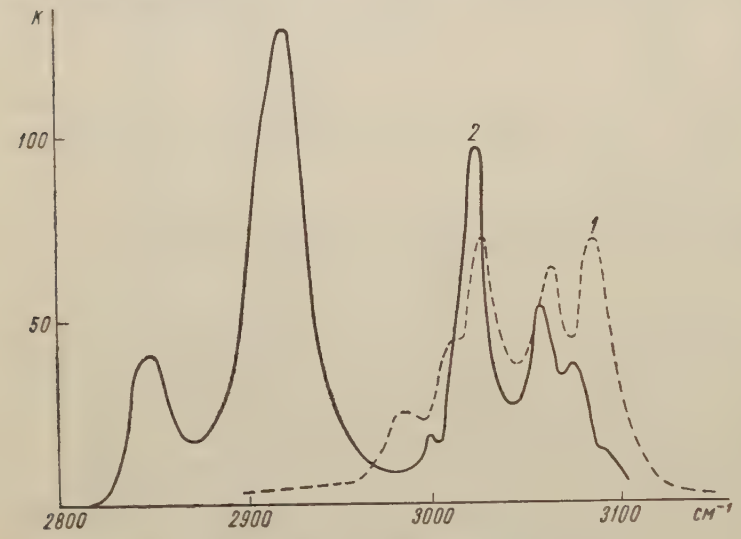

Fig.3. Infrared absorption spectra in CCl_4: 1) styrene, 2) polystyrene.

analytical purposes. The absorption coefficient amounted to 91.2 liters $mol^{-1}cm^{-1}$ for poly-α-methylstyrene in the 2986 cm^{-1} band, and to 9.0 liters $mole^{-1}cm^{-1}$ in the 2850 cm^{-1} band; the corresponding values for polystyrene are 10.0 and 39.1.

The total concentrations determined spectroscopically agreed with the sample weights as taken; individual deviations did not exceed 5% of the total concentration. For five specially prepared mixtures of poly-α-methylstyrene with polystyrene which contained the following polystyrene concentrations: 11.8, 25.0, 53.1, 75.1, and 91.1 mole percent, we obtained 11.2, 24.3, 53.5, 77.9 and 91.6 mole percent, respectively, from the absorption spectra.

References

1. E.I.Pokrovskii, Zhur. fiz.khim., 32, 1410 (1958).

INVESTIGATION OF THE COMPOSITION OF THE HIGH MOLECULAR HYDROCARBON FRACTION OF BITKOVSK PETROLEUM BY INFRARED SPECTROSCOPY

- A.F.Mal'nev, V.T.Sklyar, I.M.Mikhlina, G.A.Puchkovskaya, L.I.Shulyak & E.F.Shevchenko

The present work, which was carried out in cooperation with the Geochemistry of Petroleum Laboratory of the Ukrainian NIGRI (Scientific Research Institute for Geological Prospecting), was concerned with the chemical properties and infrared absorption spectra of petroleum from wells Nos.300, 310 and 350 of the Bitkovsk field in the Western Ukraine.

The hydrocarbon portion of the petroleum, boiling above 300°, was separated into narrow fractions by conventional physical-chemical methods.

A solid fraction, T, was first separated at 0° and at -18° from the petroleum samples. Using the method of Chernozhukov and Kazakova[1], an aromatic portion, AT, was separated from fraction T. The residual solid fraction, OT, was separated by means of complex formation using carbamide into two portions: KT, which formed complexes, and NKT, which did not form complexes. The remaining liquid fraction was separated chromatographically by means of silica gel into a paraffinic-naphthenic fraction PNZh and into fractions containing mono-, di- and polycyclic aromatic hydrocarbons, designated at 1AZh, 2AZh and nAZh, respectively. The paraffinic-naphthenic fraction PNZh was treated successively with carbamide and thiocarbamide. As a result, four (sic) components were obtained, in which the following hydrocarbon groups were predominant: I) normal paraffins, II) isoparaffins and monocyclic naphthenes, and III) isoparaffins and dicyclic naphthenes.

The infrared absorption spectra in the 2 to 15 μ region were recorded on a VIKS-3 vacuum infrared spectrometer; the sample cell thickness was 50-55 μ.

Paraffinic-Naphthenic Fraction

The spectra of the KT solid hydrocarbons are characterized by strong bands in the 3.4-3.5, 6.82, 13.72 and 13.89 μ regions, which correspond to vibrations of the CH_2 groups, and weak bands in the 6.92 and 7.25 μ regions, associated with deformation vibrations of the CH_3 groups. The band at 11.2 μ corresponds to skeletal vibrations of the unbranched paraffin chain[2]. Very weak bands evinced in the 7.6-8.6 μ region may be indicative of the presence of minute amounts of isoparaffins and naphthenes.

An intense band at 13.89 μ appears in the spectra of the fraction I liquid hydrocarbons. The intensities of the bands at 7.25 and 6.92 μ are somewhat higher than in the KT spectra; this is due to the greater weight percent of CH_3 groups in the fraction I molecules.

The spectra of the NKT hydrocarbons are characterized by further strengthening of the 7.25 μ band; this indicates an increase in the weight percent of CH_3 groups. Moreover, the intensity of the 13.89 μ band decreases in the NKT spectra and additional bands appear in the 13.4-13.6 μ region; these are characteristic of short paraffinic chains: $(CH_2)_n$, where n = 1, 2 or 3 (Ref.3).

In the spectra of fractions II, we observed strong bands at 6.92 and 7.25 μ, which are characteristic of isoparaffins, and weaker bands in the 8.3-8.6 μ region, which are presumably characteristic of monocyclic naphthenes. The band at 13.89 μ is weaker than in the I fractions, while the absorption in the 13.6-13.4 μ region is stronger.

In the spectra of fractions III, we observed strong 7.25 and 6.92 μ CH_3 group bands and the band at 13.89 μ, indicating the presence of normal paraffin chains: $(CH_2)_n$, where $n \geqslant 4$. The band in the 10.2-10.3 μ region is characteristic of the given group of hydrocarbons and is evidently associated with skeletal vibrations of dicyclic naphthenes.[4]

It should be noted that no absorption characteristic of the naphthenic or aromatic structures was observed in the KT and NKT solid hydrocarbon fractions.

Aromatic Fractions

In the spectra of the 1AZh fractions, we observed strong bands at 6.2, 12.2, 13.4, 13.8 and 14.3 μ, and weak bands at 9.6, 11.4 and 12.8 μ, characteristic of mono-, di- and polyalkylbenzenes[5]. The bands at 13.8 and 7.25 μ indicate the presence of unbranched and branched alkyl radicals, respectively.

As the index of refraction of the fractions increases, the intensity of the bands at 6.2, 12.2 and 13.4 μ, which characterize the aromatic structure, increases, while the band at 13.89 μ, which corresponds to the unbranched alkyl radical, becomes weaker.

In the case of the 2AZh fractions, with increase of the refractive index the bands at 6.2, 11.4, 12.2, and 13.4 μ become more intense, while the bands at 12.8, 13.8 and 14.3 μ become fainter.

The spectra of the nAZh fractions are characterized by intense bands at 6.2, 11.4 and 13.4 μ; here, particularly bands at 9.6, 11.4 and 13.4 μ become stronger as the index of refraction increases. The band at 9.6 μ is characteristic of a condensed polycyclic aromatic structure consisting of a small number of nuclei[4].

The results of our study showed that the petroleums from different wells in the same area differed from one another. Thus the T fraction from well No.350 contained paraffins with a higher degree of branching than that from well No.310. Petroleum from well No.310 contained a significant quantity of paraffinic hydrocarbons, while that from well No.350 comprised aromatics.

References

1. N.I.Chernozhukov & L.P.Kazakova, Nefyanoe Khoz. (Petroleum Indust.), No.8, 72 (1955).

2. E.Liebnitz and others, J.praktische Chemie, V.R.B.5, H. 1-2, 34 (1957).

3. L.Bellamy, Infrared Spectra of Molecules. (Cited in Russian trans.)

4. F.J.Zinnig and J.E.Stewart, J.Research, National Bureau of Standards, 1, 27 (1957).

5. A.V.Johansen, Infrakrasnye spektry uglevodorodov (Infrared Spectra of Hydrocarbons) in the collection "Fiziko-khimicheskie svoistva individual'nykh uglevodorodov" (Physical Chemical Properties of Individual Hydrocarbons), No.VI, page 481, 1957.

QUANTITATIVE DETERMINATION OF CH_2 GROUPS IN OPEN CHAINS BY INFRARED ABSORPTION SPECTROSCOPY

- E.A.Glebovskaya & E.I.Maksimov

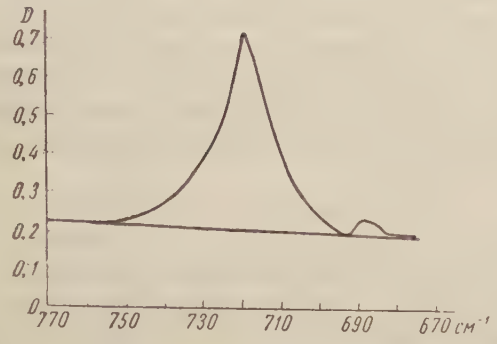

Optical density curve for n-dodecane.

The purpose of the present work was to investigate the 700-800 cm^{-1} frequency range comprising the vibrations of CH-bonds in CH_2 group chains with a view to quantitative determination of CH_2 groups in open chains[1,2]. Such information is needed, in addition to other data, for comparing petroleum fractions and bitumens to solve problems connected with the origin of petroleums.

The work was performed on an IKS-11 spectrometer. We recorded the spectra of the individual pure substances, without a solvent, in 0.06 mm thick layers. As the quantitative measure of absorption we took the integral intensity of the band, measured as the area in square centimeters bounded by the optical density curve and the "base line" (see figure).

For a number of the individual hydrocarbons, we determined the empirical coefficient $K = SV_M/n$ (Ref.3), where S is the measured area of the absorption band, V_M is the molecular volume (equal to M/d, M being the molecular weight and d the density), and n is the number of CH_2 groups per molecule. Values of this coefficient are presented in Table 1; its mean value can be used to characterize the number of chain CH_2 groups per average molecule in a mixture of methane-naphthene hydrocarbons of unknown composition.* In the table Δn is the absolute error in determining the number of CH_2 groups for each case when using the average value.

Results of determining the numbers of CH_2 groups in artificial mixtures are given in Table 2. The mixture compositions are expressed in molar ratios, and the number of CH_2 groups is computed for the average molecule of the mixture, using values of M and d calculated on the assumption of straightforward additivity.

All of the tabular data pertain to substances in the liquid state. Different values of the empirical coefficient were found in investigating the substances in the crystalline state:

Substance	n	K
n-$C_{36}H_{74}$	34	163
n-$C_{20}H_{42}$	18	162
n-$C_{17}H_{35}COOH$	16	164

This is explained by the fact that the density values used in calculating V_M were determined for the melts, while the optical density measurements were made at room temperature at which the substances form fissured crystalline films.

In determining the number of CH_2 groups per molecule, it is very onerous to have to determine V_M, i.e., M and d.

---

*There are indications that the value of the group absorption coefficient differs for short as compared to long chains of CH_2 groups. In view of the small number of examples of hydrocarbons with short chains (1 CH_2 group), only the data given for $n \geq 4$ should be regarded as reliable.

Table 1

Substance	n	K	Δn
n-Heptane	5	219	0.34
n-Octane	6	189	0.34
n-Nonane	7	192	0.41
n-Decane	8	188	0.66
n-Undecane	9	221	0.70
n-Dodecane	10	206	0.05
n-Tridecane	11	205	0
n-Pentadecane	13	197	0.50
n-Hexadecane	14	218	0.90
n-Heptadecane	15	204	0.07
Isopentane	1	233	0.14
Isooctane	1	203	0.01
Ethylcyclohexane	1	195	0.05
Di-N-propyl ketone	4	198	0.10
Average		205	

If we restrict ourselves to determining the weight percent content of CH_2 groups in the given substance, the empirical coefficient becomes $K_1 = S/c_1dx$, where c_1 is the weight concentration of CH_2 groups, d is the specific gravity, x the layer thickness, and S is the measured area of the absorption band. Hence in this case it is not necessary to determine M.

The situation would be even further simplified if the substances could be investigated in solution. One could then determine the CH_2 group content per liter of solution by using the coefficient $K = S/c_2n$ (where c_2 is the molecular concentration of a "standard" substance in the solution, and n is the group concentration). Here, even knowledge of d is not required.

Table 2

Mixture Components	Mixture Composition	Number of CH_2 groups per molecule	
		Calculated	Experimental
Ethylcyclohexane n-Decane	1.69 1	2.97	2.40
n-Hexane n-Dodecane	0.49 1	6.71	6.90
n-Hexane n-Dodecane	3.60 1	2.18	2.18
Methylcyclopentane n-Dodecane	1.92 1	3.42	3.25
Ethylcyclohexane n-Dodecane Methylcyclopentane	1.73 2 0.96	5.06	5.71

At present, however, there are certain difficulties as regards choice of appropriate solvents; these must not absorb in the 700-800 cm^{-1} region and must dissolve natural high molecular weight paraffins. Polyfluoroethylenes, for example, might be suitable solvents.

References

1. S.H.Hastings & J.A.Anderson, Anal.Chem., 24, 4, 612 (1953).
2. S.A.Francis, Ibid., 25, 9, 1466 (1953).
3. E.A.Glebovskaya & A.A.Zakharov, Geokhim sbornik (Collected articles on geochemistry), Vols.2-3, pate 214. Gostoptekhizdat, 1951.

INFRARED SPECTRA OF SOME INTRACOMPLEX COMPOUNDS IN THE REGION OF NH VALENCE VIBRATIONS

- L.A.Kazitsnya, B.V.Lokshin, L.L.Polstyanko & A.P.Terent'ev

Where intracomplex compounds of metals, having a coordination number 4 and a complex core[1] comprising a HN-Me-NH grouping are concerned, we can differentiate between compounds having a planar trans configuration (I, C_{2h} symmetry) and compounds having a planar cis configuration (II, C_{2v} symmetry) or a tetrahedral confuration; this differentiation is based on the number of bands in the infrared absorption spectrum in the 3000-3500 cm^{-1} region:

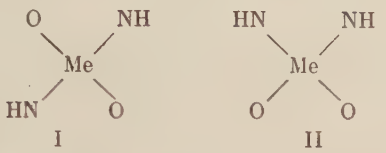

In the case of the trans form, symmetrical vibrations, which occur without change in the dipole moment, are inactive in the infrared spectrum; for the cis and tetrahedral forms, both the symmetrical and antisymmetrical vibrations are active.

Svatos[2] showed that complexes of Cu and Ni with salicylaldimine, as well as sarcosine complexes with Cu and Zn, have a single absorption band in the 3200-3300 cm^{-1} region and attributed planar trans structures to these compounds; this was confirmed for some of them by x-ray diffraction studies[3,4]. Partially repeating the Svatos experiments, we investigated the infrared spectra of a number of intracomplex compounds. Thus, we obtained spectra of Cu, Ni, Pd, Be, and Cd

Fig.1.

Fig.2.

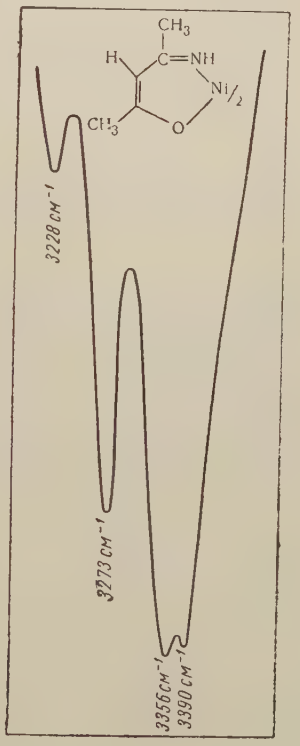

Fig.3.

Infrared absorption spectra of the intracomplex compounds in the NH valence vibration region (ν, cm^{-1})

Addend	Metal				
	Cu	Ni	Pd	Be	Cd
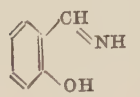	3305 IIIa	3300 IIIb	3303 3243 3175 IIIc	3298 3196 IIId	3351 3260 IIIe
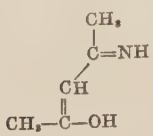	3287 IVa	3390 3356 3273 3228 IVb	3280 IVc		
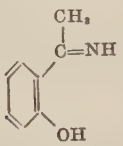	3324 3191 3165 Va	3318 3221 3186 Vb			
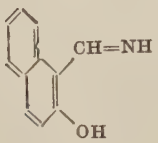	3295 VIa	3318 3303 VIb			
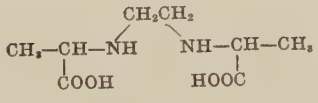	3475 3260 3207 VIIa				
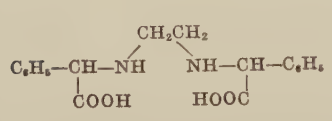	3418 3218 VIIb				

salicylaldimines (III); Cu, Ni and Pd acetylacetoneimines (IV); Cu and Ni o-hydroxyacetophenoneimines (V); Cu and Ni β-hydroxynaphthaldimines (VI); and the copper salts of ethylene-bis-α-iminopropionic and ethylene-bis-α-iminophenylacetic acids (VII).

The spectra of the substances (in the form of pastes in vaseline oil) were recorded on an IKS-11 spectrophotometer. Results are presented in the table; some characteristic spectra are shown in Figs.1-3.

A single intense absorption band, corresponding to antisymmetrical NH vibrations was observed only for compounds III-a, III-b, IV-a, IV-c, VI-a and VI-b (see the table and Fig.1); the presence of this band indicates that these complexes have trans structures (the splitting of the NH valence vibration band for VI is small - 15 cm^{-1} and can hardly be attributed to the existence of some other configuration). Two bands with a separation of 100 cm^{-1} are present in the spectra of compounds III-d and III-e; these correspond to symmetrical and antisymmetrical NH valence vibrations (see the table and Fig.2), which is in agreement with a tetrahedral structure for these complexes. The spectra of VII-a and VII-b also have two absorption bands, but in this case with a separation of 200 cm^{-1}.

It was shown by x-ray diffraction studies[4] that compound III-c has a planar trans structure. A single band is observed in the spectra of solutions of V-a and V-b; the position of this band is virtually identical with the position of the band associated with antisymmetrical vibrations in the solid state[2]; this also indicates that these complexes have a planar trans structure. Consequently, the complicated structure of the spectra of these compounds (see table and Fig. 3) should be attributed to the effect of the crystal lattice.

It is probable that the appearance of several absorption bands in the spectrum of IV-b should also be attributed to the influence of the crystal lattice, since there is no basis for assuming a planar cis or an even more exceptional tetrahedral structure for these complexes.

As a result of our experiments, it may be asserted that the appearance of a single band in the NH valance vibration region of the spectrum intracomplex compounds containing NH groups can be taken as evidence that the given complex has a planar trans structure.

The absence of splitting in the spectra of solutions and the persistence in them of only a single band can be taken as on indication that the complex has a trans structure only when the solvent does not have a substantial effect on the strength and character of the coupling between the metal and the donor atoms.

References

1. L.L.Polstyanko, L.A.Kazitsyna & A.P.Terent'ev, Khim.Nauka i Prom. (Chem. Science & Indust.), 2, 797 (1957).
2. S.Svatos, C.Curran & J.V.Quagliano, J.Am.Chem.Soc., 77, 6159 (1955).
3. M.V.Stackelberg, J.anorg.Chem., 253, 136 (1947).
4. S.M.Simousen & C.E.Peluger, Acta Crystallogr., 10, 471 (1957).

* * * * * * *

CHARACTERISTIC BANDS OF COMPOUNDS IN THE PYRIDINE SERIES

- S.G.Bogomolov, M.G.Bystritskaya & M.M.Kirillova

We studied the infrared and ultraviolet absorption spectra of 16 heterocyclic compounds, several of which were synthesized for the first time. Some of these compounds are biologically active.

The infrared spectra of the substances (emulsified in oil) were recorded on an IKS-6 spectrometer with NaCl and LiF prisms. The ultraviolet spectra were obtained with an SF-4 spectrophotometer; ethyl alcohol was used as the solvent.

Tautomerism of the following type is possible for 2-aminopyridine and a number of its derivatives:

a b

If the compound exists in form "a", absorption bands should appear in the frequency region of the infrared spectrum due to the NH_2 amino group, while a band which corresponds to the deformation vibrations of the NH_2 group should appear in the double bond region at about 1640 cm^{-1}, along with the absorption band

Compound No.	Compound	IR absorption band frequencies, cm^{-1}	Data on UV absorption bands			
			λ_{max} mμ	log ε	λ_{max} mμ	log ε
I	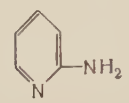	1580; 1650; 3280; 3400			300	3,70
II	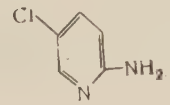	1580; 1640; 3280; 3420	243	4,24	310	3,60
III	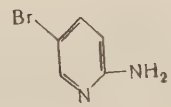	1580; 1640; 3280; 3420	245	3,96	312	3,56
IV	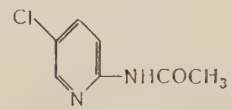	1560; 1690; 3240	245	3,88	285	3,68
V	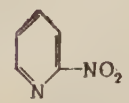	1500; 1580*	235	3,64	267	3,57
VI	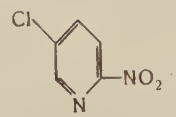	1480*; 1560	250	4,30	278	4,30
VII	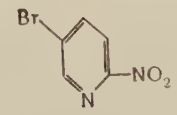	1480*; 1560	260	3,83	281	3,88
VIII	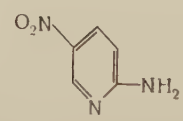	1500; 1520; 1615; 3340; 3450			345	4,13
IX	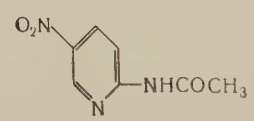	1550; 3240	222	4,2	315	4,3
X	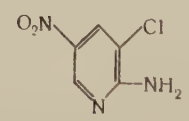	1500; 1560*; 1620; 3300; 3350			342	4,05
XI	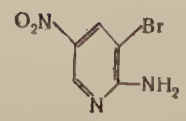	1500; 1620; 3280; 3350			345	4,22

* Wide band.

Continuation

Compound No.	Compound	IR absorption band frequencies, cm^{-1}	Data on UV absorption bands			
			λ_{max} mμ	log ε	λ_{max} mμ	log ε
XII	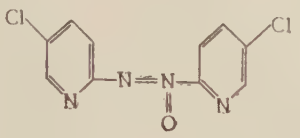	1550; 1580			330	3,7
XIII	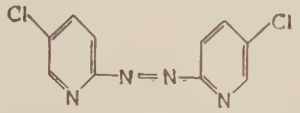	1550; 1580			330	3,45
XIV	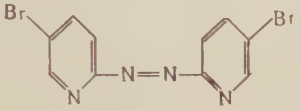	1550; 1580			340	3,28
XV	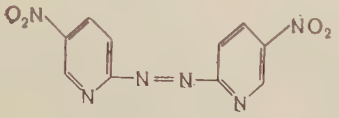	1550; 1580			325	4,5
XVI	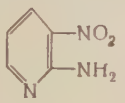	1550; 1630; 3340; 3420			375	3,97

for the pyridine ring at about 1580 cm^{-1}. If the molecule has form "b", only one NH valence vibration band may be expected to appear, while a band associated with C=N vibrations should appear in the double bond region instead of the band characteristic of the pyridine ring. Our experimental data are presented in the table.

Analysis of the spectra of compounds I, II, III, VIII, IX and XVI shows that they exist in the amino form in the crystalline state. In all cases, the amino group is evinced in the form of three bands: two in the 3280 and 3400 cm^{-1} regions, and one in the 1640 cm^{-1} region. In the spectra of nitroderivatives, the NO_2 band is located at about 1500 cm^{-1} in most cases.

It may be concluded from an examination of the infrared spectrum of compound IV, that this acetyl derivative of 2-amino-5-chloropyridine actually has the following structure:

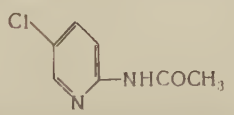

This is confirmed by the presence of a band at about 3240 cm^{-1}, which should be attributed to NH group vibrations. There is a band at 1560 cm^{-1} in the double bond vibration region, which corresponds to vibrations of the pyridine ring, and one at 1700 cm^{-1}, which corresponds to acetyl group vibrations.

Azopyridines are formed as a result of oxidation of 2-aminopyridine. A consideration of the infrared spectra of azopyridines XII, XIII, and XIV fully confirms the structures found by chemical procedures. Thus, there is a band at 1580 cm^{-1} in the spectrum of compound XIII which corresponds to vibrations of the pyridine ring and one at 1550 cm^{-1} corresponding to vibrations of the azo group. As might be expected, there was no absorption band in the frequency region for NH bond vibrations.

The structure of compound XV was determined solely on the basis of its infrared and ultraviolet spectra.

Introducing a halogen atom into the pyridine ring in the derivatives of 2-aminopyridine leads to shift of their absorption spectra some 10-15 mμ to the side of longer wavelengths.

In comparing the ultraviolet spectra of the compounds under study, we note the strong effect of nitro groups on the general form of the spectrum (see the table); this can be explained by the fact that the nitro group essentially forms a new chromophore in combination with the pyridine ring. Thus, compounds VIII and XVI, which are isomers with the nitro group present in the 5 or 3 position of the pyridine ring, respectively, have spectra which differ considerably in the UV region (see the table); this difference could be utilized for analytical purposes.

The spectra of compounds XII, XIII, XIV and XV are very similar. In this case, the chromophoric group evidently is the azo group -N=N- with pyridine rings at its sides, and the introduction of Cl or Br atons, or of the NO_2 radical, as well as replacement of the -N=N- group by a $N{=}\overset{\overset{O}{|}}{N}$ group hardly leads to any changes in the spectrum. It is extremely interesting that the spectra of these compounds are reminiscent of the spectrum of compound VIII. This indicates that the absorption should be the same whether the nitro groups are introduced into 2-aminopyridine (creating additional double bonds) or by creating double bonds involving N atoms that are outside the ring.

Sverdlovsk Medical Institute,
Ural State University

* * * * * * *

USE OF INFRARED SPECTROSCOPY FOR INVESTIGATING THERMAL AGING OF POLYVINYL CHLORIDE

- L.N.Pirozhnaya & G.S.Popova

Polyvinyl chloride (hereinafter - PVC) $(CH_2CHCl)_n$, like other polymers, undergoes changes with time under the influence of external factors, i.e., it "ages". The PVC aging problem has been considered by many investigators during the past decade. The problem has been studied primarily by chemical methods, and these have shown that the PVC molecules split off HCl, under the action of heat and light, to form C=C bonds and that the product thus becomes destroyed and cross-linked.

Ultraviolet and visible absorption spectra have been used for monitoring the rate of PVC aging, and have been interpreted as proof of the presence of polyene systems in aged PVC. The presence of C=O and OH groups in aged PVC has been established by means of infrared absorption spectra. However, although infrared spectra of aged PVC have been obtained by a number of researchers, they have not been analyzed in detail.

Below we present some data obtained during study of thermal aging of PVC by the infrared spectroscopy technique. We paid particular attention to the absorption in the 1500 to 1800 cm^{-1} region. This region is the most suitable for such work since fresh PVC does not absorb here, while two wide complicated bands having absorption peaks at 1610 and 1720 cm^{-1} appear during its aging (Fig.1).

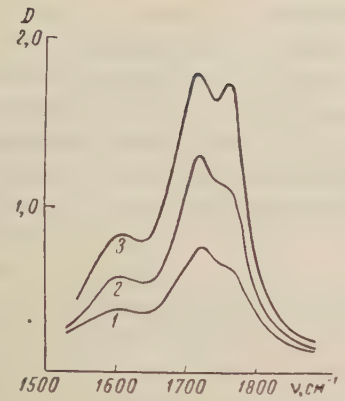

Fig.1. Variation of the infrared spectrum of PVC with aging time at 185°; 1) 17 hours, 2) 30 hours, 3) 50 hours.

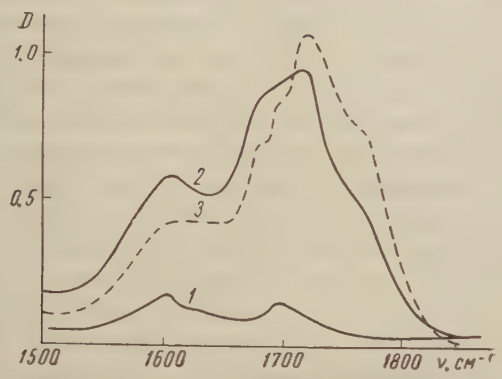

Fig.3. Spectra of PVC samples aged under different conditions: 1) 12.5 hours at 210° in N_2; 2) 12.5 hours at 210° in N_2 and then 40 minutes at 185° in O_2; 3) 17.5 hours at 185° in O_2.

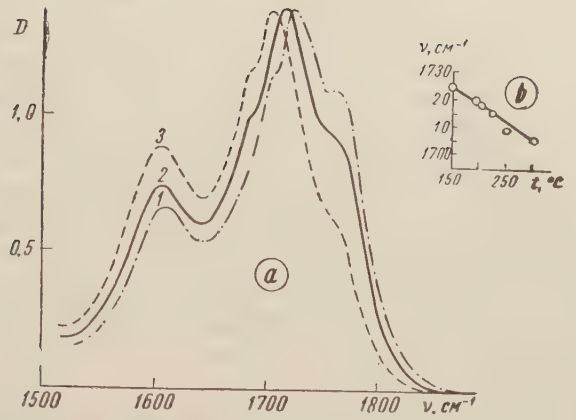

Fig.2. a - Variation of the infrared spectra of PVC with aging temperature: 1) 1000 hours at 150°; 2) 6 hours at 200°; 3) 17 minutes at 300°. b - Variation of the frequency of the C=O group absorption peak with the aging temperature.

The band at 1610 cm^{-1} is usually attributed the absorption of conjugated C=C groups. In the spectra of PVC aged in air at a temperature of 185°, we observed absorption bands in the 700-900 cm^{-1} region which indicate (as do the ultraviolet absorption spectra) the presence in aged PVC of polynuclear aromatic compounds in addition to polyene systems. The presence of polynuclear aromatic compounds in PVC subjected to pyrolysis has been demonstrated by Bersch et al[1].

There are indications in the literature that C=O groups of different types absorb in the 1650-1800 cm^{-1} region. The absorption bands associated with these groups overlap greatly and could not be separated owing to the inadequate resolution of the instrument. However, by comparing a large number of spectra of PVC samples aged under different conditions, and examining the results of special measurements performed with a very narrow slit, one can infer with some degree of certainty that the above mentioned region contains absorption bands with frequencies of 1680, 1700, 1720, 1735 and 1765 cm^{-1}. According to the interpretation used for oxygen-containing derivatives of hydrocarbons, these bands may be attributed to absorption by a C=O group conjugated with C=C or C=O groups of acids, ketones, aldehydes, vinyl esters, and anhydrides, respectively.*

One may, therefore expect the content of such groups, as well as that of C=C groups, to vary in PVC, depending on the temperature and length of aging.

---

*The PVC chlorine atom does not have any effect on the C=O frequency, since the formation of carbonyl groups is accompanied by the loss of a Cl atom in the form of HCl from the corresponding portion of the polymer chain.

A comparison of the absorption spectra of PVC aged at 185° for 17, 30 and 50 hours (Fig.1) shows that the bands at 1775 and 1610 cm^{-1} increase in intensity relative to the 1720 cm^{-1} band, as the aging time increases. A more complicated pattern is observed during aging at different temperatures. The spectra of PVC aged at 150, 200 and 300° are shown in Fig.2. To facilitate comparison, we chose the aging times of these samples so that the optical densities at the absorption peak would coincide. The following changes are observed as the aging temperature is increased: the absorption peak for the C=O group shifts to the side of lower frequencies, and there is a relative strengthening of the band at 1610 cm^{-1} and a weakening of the band at 1765 cm^{-1}.

The 1765 cm^{-1} band pertains to the absorption of secondary oxidation products; this agrees well with the increase in its intensity with increased aging time, but additional information is needed to explain its behavior at different temperatures.

The absorption band peak shifts by 20 cm^{-1} (from 1724 to 1703 cm^{-1}) as the aging temperature is raised from 150 to 300°. In view of this, we can assume that with increase of aging there occurs a reduction in the relative aldehyde content in aged PVC and then a reduction in the relative ketone content, while the quantity of acids and the number of C=O bonds conjugated with C=C increase.

Matters are more complicated as regards absorption in the 1600 cm^{-1} region. The absorption coefficient for C=C bonds both in aromatic and in polyene systems depends greatly on the polarity of neighboring groups[2]. That this fact must be considered in the case of PVC is proved by the following. The spectra of two samples were compared in the 1600 cm^{-1} region; they were aged at the same temperature, but one was aged in an atmosphere of oxygen while the other was aged in nitrogen. The sample aged in nitrogen contained more C=C groups, according to our data, than the sample aged in oxygen; nevertheless, its absorption in the 1600 cm^{-1} region was much weaker (Fig.3). However, the intensity of the bands at 1610 and 1680 cm^{-1} increased sharply within a very few minutes when the sample was placed in an oxygen atmosphere.

It would appear therefore that the increase in the intensity of the 1610 cm^{-1} band with aging time and with increase of aging temperature could be explained either by an increase in the number of absorbing groups or by an increase in the absorption coefficient of the groups already present owing to the appearance of polar C=O bonds in the PVC molecule.

The authors express their thanks to V.M.Chulanovskii for his valuable advice and discussion of the results.

References

1. C.F.Bersch, M.R.Harvey & B.G.Achhammer, J.Res.NBS, 60, 481 (1958).
2. R.R.Stromberg & S.Straus, J.Res.NBS, 60, 147 (1958).
3. M.Josien & N.Fuson, J.Amer.Chem.Soc., 78, 3049 (1956); Bull.Soc.chim. France, Nos.3-4, 389 (1952).

COMPARATIVE INVESTIGATION OF PHOTO AND THERMAL AGING OF ACETALS OF POLYVINYL ALCOHOL BY INFRARED SPECTROSCOPY

- G.S.Popova & E.V.Shuvalova

Spectroscopic methods are being used with increasing frequency for the study of polymer aging. In the present work, photo and thermal aging of several polyvinyl alcohol acetals were investigated by infrared spectroscopy (using an IKS-11 spectrometer with NaCl and LiF prisms). The structural formulas of the substances studied comprise secondary hydroxyl groups in addition to the acetal groups:

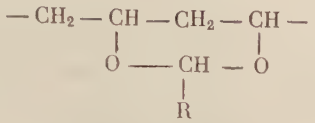

The thermal aging of the first member of this series - polyvinyl formal (R = H) - was studied by Beachell, Fotis and Hucks[1]. The purpose of the present work was to compare the processes of photo aging (illumination by a PRK-2 ultraviolet lamp) and thermal aging (heating at 150°) for two other members of the series, namely, polyvinyl ethylal (R = CH_3) and polyvinyl butyral (R = C_3H_7).

Both photo and thermal aging of the two polymers is accompanied by decrease of the content of OH, CH and C-O- groups together with a build-up of C=O groups; this is shown by a reduction in intensity of the absorption bands in the 3300-3600, 2800-3000, 1300-1500 and 1100-1200 cm^{-1} regions and by an increase in the intensity of the 1730 cm^{-1} band. Moreover, the band at 1240 cm^{-1} in the spectrum polyvinyl ethylal[2] increases in intensity with aging, while the greatest increase in intensity upon aging is observed at 1190 cm^{-1} in the spectrum of polyvinyl butyral (Fig.1). According to the data of Thompson and Torkington[3], the C-O- group in acetates absorbs in the 1240-1250 cm^{-1} region, while in propionates and higher homologs, this group absorbs in the 1180-1200 cm^{-1} region. Consequently, we can infer that acetates are formed during the aging of polyvinyl ethylal, and butyrates during the aging of polyvinyl butyral. Actually, if we assume that one C-O- bond breaks and that this C-O radical becomes stabilized as a carbonyl group, esters of acetic acid (acetates) should then be formed as a result of this

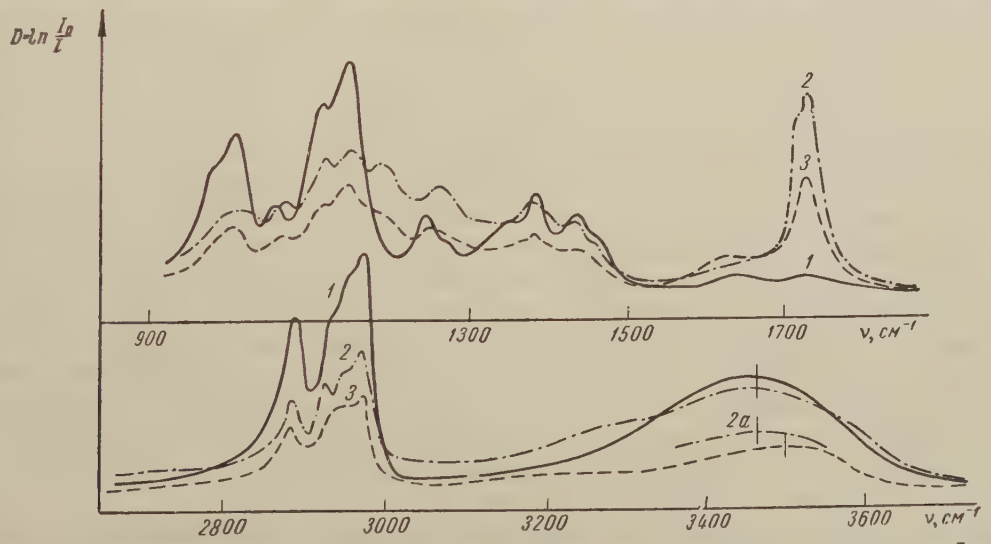

Fig.1. Absorption spectra of polyvinyl butyral in the 900 to 3700 cm^{-1} region: 1) initial sample; d = 4.6 μ; 2) after 15 hr 40 min of photo aging, d = 5.4 μ; 2a) after 50 hours of photo aging; 3) after 300 hours of thermal aging, t = 105° and d = 4.6 μ.

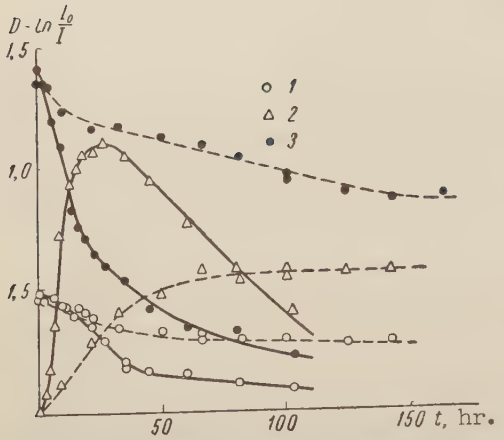

Fig.2. Variation with time of the absorption band intensities in the infrared spectra of polyvinyl butyral during photo aging (solid line) and thermal aging (dashed line); d = 5 μ: 1) OH groups, 2) C=O groups, 3) C-O-groups.

process in the case of polyvinyl ethylal, and esters of butyric acid (butyrates) should be formed in the case of polyvinyl butyral. The carbonyl band of these compounds should appear at 1740 cm^{-1}. The carbonyl band is observed at 1730 cm^{-1} in the spectra of aged samples of polyvinyl ethylal[2] and polyvinyl butyral (see Fig.1). In view of the width and complex shape of this band it may be inferred that the absorption due to the ester groups is masked by more intense absorption due to ketone groups.

All of the above facts are true for either type of aging. Differences between the two kinds of aging become evident in studying the rate of formation and decomposition of the functional groups and in investigating the behavior of the OH absorption bands.

The process of decomposition of polyvinyl butyral (Fig.2) like that of polyvinyl ethylal[2], can be divided into two successive periods. The first period is qualitatively the same for both types of aging. During the second period in thermal aging, there is evinced stabilization of the processes of build-up and decomposition all of the groups; further decomposition takes place during photo aging, where, not only does the content of the initial groups decrease, but so does that of the groups formed during the first period.

It will be evident from Fig.1 that, besides the reduction in the OH group absorption band intensity, which is common to both types of aging of polyvinyl butyral, there is a shift of the band peak to the side of higher frequencies during thermal aging. A similar shift was observed in the spectra of unaged polyvinyl butyral having different OH group contents. Thus, polyvinyl butyrals containing 59.5, 53.1 and 37.7% hydroxyl groups* have the following OH group absorption band frequencies: 3390, 3410 and 3465 cm^{-1}. This may be explained by the fact that the hydrogen of the hydroxyl group in acetals of polyvinyl alcohol may be bound by two different types of hydrogen bonds. In the first type of bond the proton from one hydroxyl group is linked to the oxygen of the other; in the other type of bond, it is linked to the oxygen of the cyclic ether, i.e., to the oxygen of the acetal ring. According to Shigorin[4], the frequency difference between the OH groups coupled by these two types of hydrogen bonds (pure alcohols and solutions of the alcohols in dioxane) amounts to 140-165 cm^{-1}. The absorption bands corresponding to the first and second types of bonding overlap for polyvinyl butyral, and the frequency of the integral band depends on the ratio of the component intensities. The greatest frequency difference between the OH bands of polyvinyl butyral and polyvinyl alcohol (ν_{OH} = 3330 cm^{-1}) equals 135 cm^{-1} i.e., is close to the value given by Shigorin. The shift of the OH band as a result of thermal aging is readily explained by change in the relative intensity of OH bands of the two above-mentioned types.

In conclusion, it should be noted that infrared spectroscopy, in addition to substantiating qualitatively the mechanism proposed for the oxidation of acetals

---

*The hydroxyl group content of the polyvinyl alcohol sample from which the given acetal was obtained was taken as 100%.

by Beachell et al[1], indicates that there is a substantial difference between the processes of photo and thermal aging (see Fig.2and also Ref.2), and that it is necessary to consider different mechanisms for the decomposition of the acetals of polyvinyl alcohol in different types of aging. It is possible that a significant contribution to solution of the problem can be made by investigation of the composition of the volatile products from the decomposition of polyvinyl ethylal and polyvinyl butyral at different stages of photo and thermal aging.

We desire to express our thanks to V.M.Chulanovskii for his constant interest in the work and valuable advice.

Scientific Research Institute
for Polymerized Plastics

References

1. H.C.Beachell, P.Fotis & J.Hucks, J.Polymer Sci., 7, 353 (1951).
2. E.V.Shuvalova, Vysokomolek. soed. (High molecular compounds), 1, 12 (1959).
3. H.W.Thompson & P.Torkington, J.Chem.Soc., 640 (1945).
4. D.N.Shigorin, "Materialy X Vsesoyuznogo soveshchaniya po spektroskopii" (Transactions of the Tenth All-Union Conference on Spectroscopy), p.205. L'vov, 1957.

INVESTIGATION OF ISOTACTIC POLYMERS BY MEANS OF INFRARED SPECTROSCOPY

- E. I. Pokrovskii & M.V. Vol'kenshtein

We recorded the infrared spectra of isotactic polypropene and polystyrene on IKS-2 and IKS-11 spectrometers with LiF, NaCl and KBr prisms. The film thicknesses were ~200 μ for polypropene and ~25 μ for polystyrene. The spectra in the 3000 to 400 cm^{-1} region were recorded at different temperatures ranging from room temperature to temperatures above the melting point of the polymer.

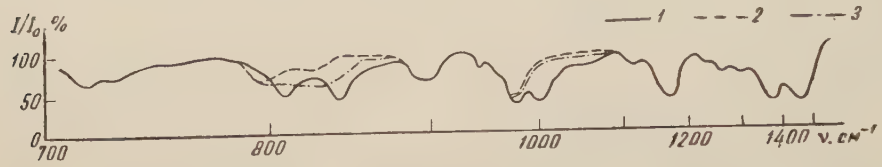

Fig.1. Infrared absorption spectra of polypropene: 1) isotactic at 20°C, 2) isotactic at 170°C and 3) atactic polypropene.

The IR absorption spectra of crystalline and molten isotactic polypropene in the 800-900 cm^{-1} region differ not only from each other but also from the spectrum of atactic polypropene (Fig.1). Moreover, in the absorption spectrum of crystalline polypropene there appears a strong absorption band at 992 cm^{-1}, the intensity of which depends on the degree of crystallinity of the material (Fig.2).

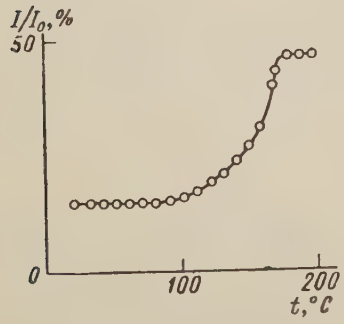

Fig.2. Temperature dependence of the transmission at 992 cm^{-1} in the spectrum of isotactic polypropene.

Inasmuch as the method of determining the "degree of amorphism" on the basis of the "amorphous" band at 790 cm^{-1} does not allow of accurate determination in the case of samples with a high degree of crystallinity[1,2], we chose the absorption band at 992 cm^{-1} for this purpose. In order to avoid measuring the thickness of the samples, we made use of an "internal standard", namely, the absorption band at 969 cm^{-1}, the intensity of which remains constant, i.e., does not depend on the degree of crystallinity of the polymer; this is substantiated by analysis with respect to the absorption band at 790 cm^{-1} and determination of the optical density at 969 cm^{-1} of the same polypropene film in the crystalline state and in the molten state. The degree of crystallinity of polypropene was determined by measuring the optical densities D_1 and D_2 at 969 cm^{-1} and 992 cm^{-1}, respectively, taking into account the overlapping of these bands and the fact that at 100% crystallinity $D_2 = 1.20 D_1$. The degree of crystallinity in the investigated specimens went as high as 96%.

Isotactic polystyrene is characterized by a number of absorption bands in the crystalline state, which vanish or are greatly weakened upon melting of the polymer (Fig.3). The most noticeable crystalline absorption bands are located at ~775, 840, 916, 1315 and 1360 cm^{-1}. The band at ~775 cm^{-1} disappears completely upon melting; in the case of the double band at ~912 cm^{-1}, the high frequency band vanishes, while the low frequency component at 906 cm^{-1} remains. The absorption band at 840 cm^{-1} is shifted somewhat upon melting to the side of lower frequencies. This shift, however, is too small to be used for determining the "degree of amorphism". The degree of crystallinity should preferably be determined with reference to the absorption band at 775 cm^{-1}, with the 700 cm^{-1} or ~760 cm^{-1} band being used as the "internal standard". For such determination one must, of course, have a set of calibration samples with known degrees of crystallinity.

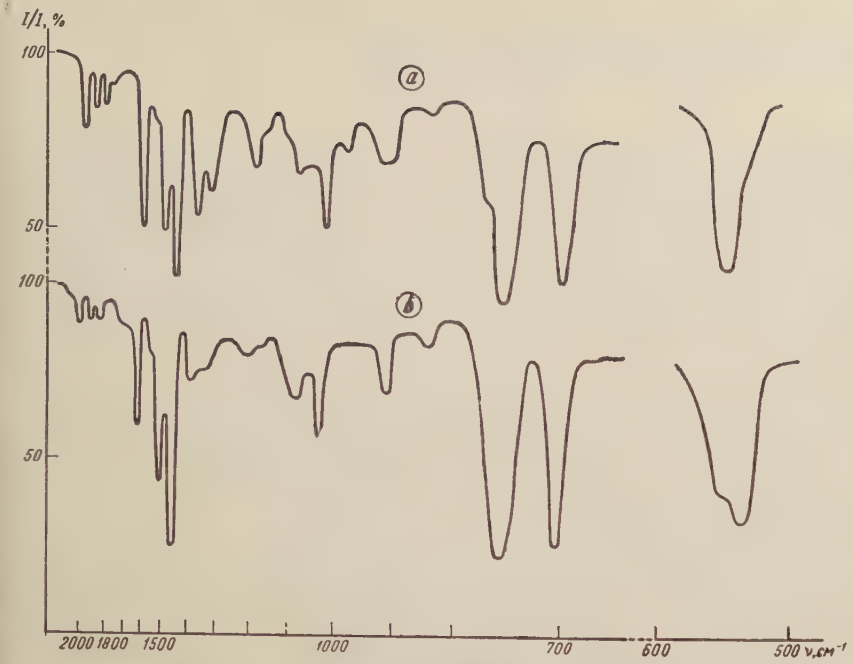

Fig.3. Infrared absorption spectra of polystyrene: a) isotactic crystalline, b) atactic.

In the low frequency region of the spectrum of atactic polystyrene there are observed two absorption bands - at 560 and 540 cm^{-1}; in the spectrum of isotactic polystyrene only one band - at 560 cm^{-1}. The intensity of the absorption band at 540 cm^{-1} decreases with increase of isotacticity. The intensity of the absorption bands does not change when the polystyrene is put into solution. By analogy with polypropene and polymethylmetacrylate it may be inferred that the absorption band at 540 cm^{-1} belongs to syndiotactic polystyrene, the absorption spectrum of which differs from the spectrum of isotactic polystyrene.

References

1. V.N.Nikitin & E.I.Pokrovskii, Doklady AN SSSR, 95, 109 (1954); Izv.AN SSSR, Ser.fiz., 18, 735 (1954). (Trans.Bulletin 18, No.6, 415.)

2. E.I.Pokrovskii & M.V.Vol'kenshtein, Doklady AN SSSR, 115, 3, 552 (1957). (Trans. - Doklady.)

USE OF INFRARED ABSORPTION SPECTRA FOR INVESTIGATING STRUCTURAL CHANGES IN FLUORINE PLASTICS UNDERGOING AGING

- L. I. Tarutina

Polyfluoroethylene $(-CF_2-CFH-)_n$, polytrifluorochloroethylene $(-CF_2-CFCl-)_n$, and the copolymers of tetrafluoroethylene with ethylene $(-CF_2-CF_2-CH_2-CH_2-)_n$ and of vinylidene fluoride with trifluorochloroethylene $(-CF_2-CH_2-CFCl-CF_2)_n$ are new plastics which are very stable with respect to high temperatures and aggressive media. However, they are subject to aging at certain temperatures. The present paper reports a study of this process, using infrared absorption spectra. The measurements were performed on an IKS-11 spectrometer, using films about 100 μ thick.

It follows from our results that the thermal aging of polymers containing both C-Cl- and C-H- bonds or C-F- and C-H- bonds, is mainly determined by the rupture of these bonds with liberation of HCl or HF. During aging in vacuum, this leads to formation of unsaturated bonds or to cross-linking; in the air there is also some oxidation of the material.

Polymerization conditions may affect the thermal aging of the polymer. Thus, the thermal stability of the copolymer of tetrafluoroethylene and ethylene largely depends on the presence of branching. Establishing this fact by spectroscopic studies made it possible to modify the synthesis conditions so as to obtain a polymer having higher thermal stability.*

The copolymer of tetrafluoroethylene and ethylene was subjected to aging in the air and in vacuum at 200, 240 and 290°C. An absorption band was observed in the spectrum of this copolymer at 1390 cm^{-1}; this indicates the existence in the copolymer chain of branched side chains having terminal methyl groups. The thermal aging of the copolymer in the air depends on the amount of branching. New absorption bands appeared in the spectrum of the branched copolymer sample at 1615, 1677, 1755 and 1780 cm^{-1} (Fig.1,b); the same time the sample developed color (see table). Evidently, aging takes place mainly at tertiary carbon atom locations without affecting, however, the number of methyl groups, since the intensity of the CH_3 group band does not change during the aging process. The dependence of the intensity of coloring on the degree of oxidation of the copolymer is an indication that conjugated groupings are formed under the influence of atmospheric oxygen. Increasing the aging temperature to 290°C leads to a significant acceleration of the process of aging in the air (by more than 100-fold) as compared with aging at 240°C (Fig.1,c). This can be explained by the splitting off of HF, which is confirmed by chemical analysis. The spectrum of the copolymer acquires a new feature: an additional band appears at 1720 cm^{-1}; this can be attributed to formation of -CF=CH- groups as a consequence of detachment of F and H atoms. No absorption bands are evident in the 1600-1900 cm^{-1} region of the spectrum of the copolymer aged in vacuum (Fig.1,d). Under these conditions, the splitting off of HF evidently leads to building up of chains.

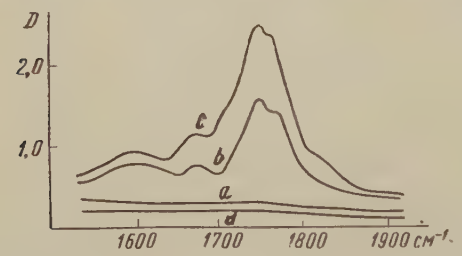

←Fig.1. Absorption spectra for copolymers of tetrafluoroethylene with ethylene: a and b) aged in the air for 260 hours at 240°C (a - weakly branched sample; b - well branched sample); c) 3 hours in the air at 290°C, branched sample; d) 17 hours under vacuum at 290°C, branched sample.

---

*The synthesis of this copolymer was performed by S. G. Malkevich, who participated in the studies of its aging.

Absorption Band Frequencies, cm^{-1} *

Group and vibrations	$(-CF_2-CF_2-CH_2-CH_2-)_n$	$(-CF_2-CH_2-CFCl-CF_2-)_n$	$(-CF-CFH-)_n$	Group and vibrations	$(-CF_2-CF_2-CH_2-CH_2-)_n$	$(-CF_2-CH_2-CFCl-CF_2-)_n$	$(-CF-CFH-)_n$
$-C(=O)H$ (?) **	1615	1614		$-C(=O)O$ (C=O)	1755	1760	1767
C=C (?)	1677	1678		$-C(=O)OH$ (C=O)	1780	1787	
$-CF=CH-$ (C=C)	1720	1721		$-CF=CH-$ (C-H)	3116	3122	

*The frequency values are shifted relative to the frequencies of the same groups in hydrocarbons. The bands were identified by comparing the copolymer spectra with the spectra of model substances and with data in the literature.

**C-O valence vibrations or OH deformation vibrations.

Polytrifluoroethylene. The thermal aging of polytrifluoroethylene was studied at 240°C. An absorption band appeared in the polymer spectrum at 1767 cm^{-1}; this was attributed to C=O vibrations in the $-C(=O)H$ group. At the same time, the intensity of the band at 2987 cm^{-1} (valence vibrations of the C-H polymer bonds) increased and the band contour was distorted. The band at 1767 cm^{-1} was not observed in the spectrum of the polymer aged in vacuum; evidently, cross-linking occurs. These spectrum changes, as was also the case for the copolymer of tetrafluoroethylene and ethylene, were not observed in the spectra of all of the samples, but only in some of them.

The copolymer of trifluorochloroethylene and vinylidene fluoride* undergoes significant changes at 300°C. Aging at lower temperatures (250 and 270°C) proceeds much more slowly, while absolutely no change in the spectrum is observed after heating for even hundreds of hours at 200°C. New absorption bands appear in the spectrum of the copolymer during aging in air (Fig.2); these can be associated with the formation in the copolymer of acid groups (bands at 1614 and 1787 cm^{-1}), aldehyde groups (band at 1760 cm^{-1}), and unsaturated groups (bands at 1721 and 3122 cm^{-1}). Only the last two bands appear in the spectrum of the copolymer aged in vacuum. Together with the appearance of these new absorption bands, there are evinced decreases in the intensities of the main bands at 2983, 3024, 1393 and 1425 cm^{-1} (valence and deformation vibrations of the CH_2 group), 970 cm^{-1} (vibrations of C-Cl bonds) and 1100-1300 cm^{-1} (vibrations of C-F bonds). Thus, on the basis of the spectra we can draw the following inferences with respect to aging-induced structural changes in the copolymer. During the first

---

*E.I.Blyumental' participated in the study of this copolymer.

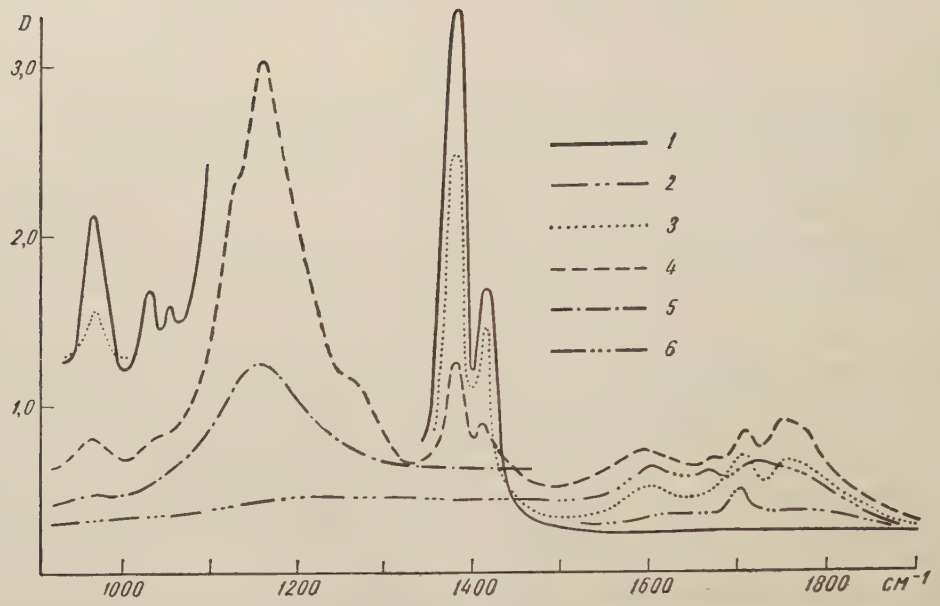

Fig.2. Absorption spectra of the copolymer of trifluorochloroethylene and vinylidene fluoride at 300°C aged in the air: 1) before aging, 2) after 20 hr, 3) 50 hr, 4) 60 hr, 5) 70 hr, and 6) 80 hr.

hours of aging, the C-Cl-, C-H- and C-F0 bonds break up with formation of -CF=CH- groups (Fig.2) and evolution of HCl and HF (mainly HCl). The double bonds formed in the process promote oxidation of the copolymer, leading to formation of oxygen-containing groups. The observed shift of the absorption limit into the visible region of the spectrum indicates formation of conjugated systems.

Polytrifluorochloroethylene. Two absorption bands at 1363 and 1784 cm^{-1}, associated with the formation of $-CF=CF_2$ in groups, are observed in the spectrum of the polymer aged under vacuum at 300°C. The band at 1881 cm^{-1}, which we attributed to $-C(=O)F$ groups, was not observed in the case of aging of the polymer in the air[1]. An insignificant absorption rise appears in the 1810 cm^{-1} region; this can be attributed to oxygen-containing groups of another type (possibly, ketones). The addition of water during aging of the polymer in vacuum causes an increase in the intensity of the bands at 1363 and 1784 cm^{-1}; consequently, water has a catalytic effect on the aging process.

I express my sincere thanks to V.M.Chulanovskii for his interest in the work and useful advice, and to L.V.Chereshkevich, S.G.Malkevich and Ts.S.Dunaevskaya for providing the polymer samples and helpful discussion of the results.

Reference

1. Machio Iwasaki, Machiro Aoki & Rimpel Kojima, Pol.Sci., 25, 377 (1957).

INVESTIGATION OF STRUCTURAL CHANGES IN VULCANIZED RUBBERS EXPOSED TO THE ACTION OF MINERAL ACIDS

- A.F.Postovskaya & A.S.Kuz'minskii

Many rubber articles are required to operate in contact with inorganic acids. The acids cause major changes in the structure of the polymers with deleterious effect on their mechanical properties. The action of acids on vulcanized rubbers has been considered in the literature only from the applied point of view. There have been no investigations in which the functional groups of the conversion products obtained under the influence of mineral acids were analyzed. A knowledge of the character of these products is of considerable practical and theoretical significance, since it would enable establishing just what processes occur in vulcanized rubbers exposed to mineral acids and thus help clarify the mechanism of these processes.

We investigated the structural changes occurring in vulcanized rubbers under the influence of HNO_3 and HCl by infrared spectroscopy. We worked with vulcanized rubbers having different structures, namely, 1) heat vulcanized butadiene sodium rubber (SKB) and heat vulcanized divinyl-styrene rubber (SKS-30). These vulcanized rubbers had the same values of the equilibrium modulus, which is proportional to the number of cross-linkages developed.

The infrared spectra of the vulcanized rubbers were obtained in the 3800 to 600 cm^{-1} range on an IKS-2 double beam spectrometer. Films of the vulcanized rubbers 30 μ thick were exposed to the action of nitric and hydrochloric acids (25 to 50%) at temperatures of 25 and 80°. We used the same samples for the before and after measurements in order to exclude errors associated with sample preparation. The experimental results are presented in Figs.1 and 2.

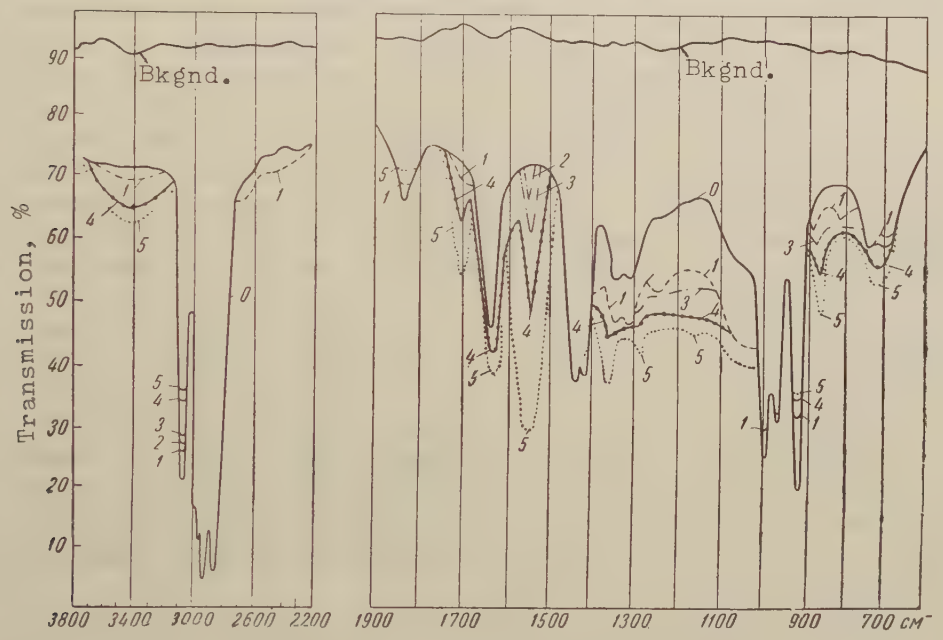

Fig.1. Infrared absorption spectra of heat vulcanized butadiene sodium rubber treated with nitric acid: 0) purified raw SKB rubber; 1-5) heat vulcanized SKB (1 - untreated, 2 - treated with 25% HNO_3 for 12 hr at 25°, 3 - 25% HNO_3 for 24 hr at 25°, 4 - 50% HNO_3 for 24 hr at 25°, 5 - 25% HNO_3 for 1 hr at 80°).

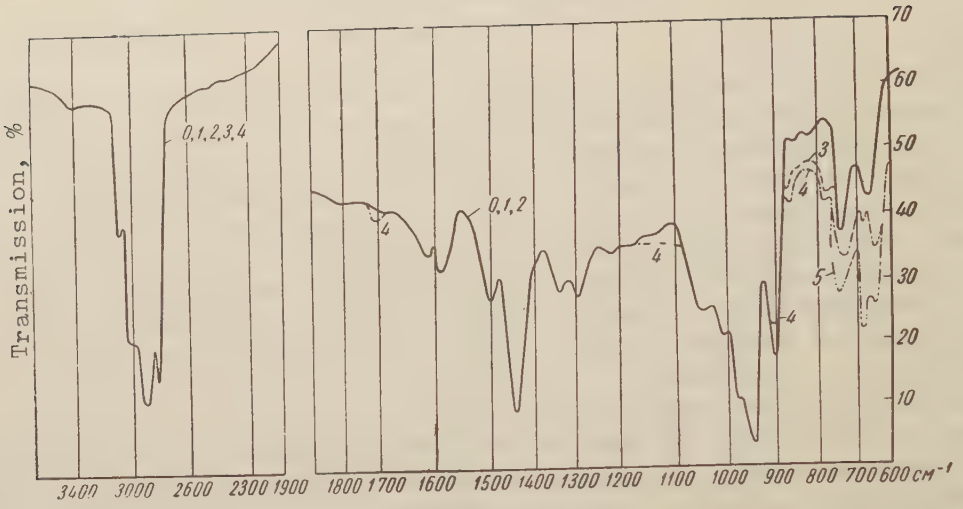

Fig.2. Infrared absorption spectra of heat vulcanized divinyl-styrene rubber (SKS-30) treated with 25% hydrochloric acid at 25°: 0) untreated (control), 1) treated for 1 day, 2) 3 days, 3) 6 days, 4) 14 days, 5) 17 days.

The following absorption bands were observed in the spectrum of purified raw SKB rubber (see Fig.1): 680, 720, 910, 965, 992, 1300, 1360, 1437, 1357, 1640, 1825, 1856, 2926, 2979, 3019 and 3080 cm^{-1}. A detailed interpretation of these bands has been given in our earlier paper[1]. Examination of the spectrum of heat vulcanized SKB shows that the vulcanization process is accompanied by a mild oxidation: new bands appear at 1700-1710, 1240 and 3450 cm^{-1} in the spectrum of the vulcanized product; these indicate the presence of oxygen-containing groups[2-4]. The bands at 1700-1710 cm^{-1} correspond to the carbonyl group $>C=O$, the 1240 cm^{-1} band to the $-\overset{O}{\overset{\|}{C}}-O-R$ group, while the band at 3450 cm^{-1} is characteristic of -OOH and -OH groups. The spectra of films exposed to nitric acid show an increase in the intensity of all bands that correspond to oxygen-containing groups, and exhibit several new absorption bands located at 759, 854, 1360, 1550 and 1672 cm^{-1}; the interpretation of the bands based on the data in the literature[5-9] is the following:

Absorption band	Vibration type
759 cm^{-1}	Deformation, NO_2 group
854	Valence, NO in the R-O-N=group
1360	Symmetrical valence, NO_2 group
1550	Antisymmetrical valence, NO_2 group
1672	Valence, NO in the R-O-N=O group

These data indicate that two processes take place in the heat vulcanized SKB rubber exposed to the action of nitric acid, namely, 1) an oxidation process accompanied by the formation of oxygen-containing groups (hydroperoxide, hydroxyl carbonyl, etc.), and 2) a nitration process leading to the formation of nitro compounds. The nature of the reaction products formed during the action of nitric acid on the polymer depends to a large degree on the concentration of the acid and the temperature. No build-up of oxygen-containing compounds was observed during the action of 25% nitric acid at 25°, although some formation of

nitro compounds did take place. However, during the action of 50% nitric acid at 25°, a build-up of oxygen-containing groups was observed together with the formation of nitro compounds. The nitration and oxidation processes increase greatly in intensity with rising temperature. The same relationships are observed for the action of nitric acid on heat vulcanized divinyl-styrene rubber. Also, it was shown by mechanical and by physical-chemical procedures that this reaction produces major structural changes in the vulcanized rubbers which are evinced in their structuralization (cross-linkage) and destruction. The former predominates during nitration, while destruction is predominant during oxidation.

A study of the spectrum of films of heat vulcanized SKS-30 (Fig.2) treated with 25% hydrochloric acid at 25°, indicates that no significant structural changes occur in the vulcanized rubber for up to 6 days of treatment. No chlorine-containing compounds were detected. These results are in good agreement with data obtained using physical-chemical and mechanical methods of study; the equilibrium modulus, relative elongation, breaking strength, and general unsaturation scarcely change. After 14 days of treatment, however, bands appeared at 600, 650 and 700-750 cm^{-1}; according to literature data[10-11], these can be attributed to chlorine-containing compounds containing one atom of Cl per C atom. Along with the formation of the chlorine-containing compounds, a decrease was observed in the intensity of the absorption band at 910 cm^{-1}, which is associated with vinyl groups. This reduction is evidently connected with the addition of HCl at the double bond in the 1,2 position. Increasing the temperature greatly intensifies the chlorination process.

Data on the change in the mechanical properties (equilibrium modulus and breaking strength) of the vulcanized rubbers indicate that structuralization is the predominant process during hydrochlorination.

We desire to thank V.M.Tatevskii for permission to measure the rubber spectra in his laboratory and M.A.Salimov for assistance in recording the spectra.

Scientific Research Institute of the Rubber Industry,
Chemistry Committee of the Council of Ministers of the USSR

References

1. A.F.Postovskaya, M.A.Salimov, A.S.Kuz'minskii & V.M.Tatevskii, Materialy X vsesoyuznogo soveshchaniya po spektroskopii (Transactions of the Tenth All-Union Conference on Spectroscopy), Vol.1, p.423. L'vov, 1957.

2. G.M.Barrow, J.Chem.Phys., 21, 2008 (1953).

3. R.E.Richards & W.R.Burton, Trans.Faraday Soc., 45, 874 (1949).

4. L.J.Bellamy, The Infrared Spectra of Complex Molecules, 1955.

5. J.C.D.Brand & T.M.Cawthen, J.Amer.Chem.Soc., 77, 319 (1955).

6. Harzberg, The Spectra of Diatomic Molecules. D.Van Nostrand Co, 1950.

7. J.Masson & J.Dunderdale, J.Chem.Soc., 754 (1956).

8. Robert D.Kross & V.A.Fassel, J.Amer.Chem.Soc., 78, 17, 4225 (1956).

9. H.M.Rendall & R.G.Fowler, Infrared determination of organic structures - Torento, N.Y.,L., 1952.

10 H.M.Rendall, R.G.Fowler, Fuson & Dange, Infrared determination of organic structures, N.Y., 1949.

11. Thompson & Torkington, Proc.Roy.Soc.A, 184, 21 (1945).

INFRARED SPECTRA AND THE STRUCTURE OF THE PRODUCTS OF TELOMERIZATION OF DIENE HYDROCARBONS WITH HALOGEN DERIVATIVES

- A. A. Petrov & T. V. Yakovleva

1. It has been shown in a number of studies[1-4] carried out in our laboratory that diene hydrocarbons readily react with halogen derivatives, particularly of the allyl type in the presence of chlorides of Sn, Ti, Zn, Fe and other metals with the formation of mixtures of telomers having the composition $R-(C_nH_{2n-2})_x-Cl$. In this manner there is obtained from isoprene and its hydrochlorides a mixture containing appreciable amounts of geranyl chloride, an important semi-product in the production of citral (geranial), which is used by the vitamin and perfume industries[4]. It is planned to utilize this procedure for large scale production of citral in the USSR.

2. As a result of addition of halogen derivatives to dienes there can be obtained 1,2- and 1,4-products. It is difficult to determine the structure of these products by chemical methods. We have made extensive use of infrared spectroscopy in our laboratory for establishing the structure of telomers. We judged of the telomer structure from 1) the frequency the intensity of the bands associated with the valence vibrations of the multiple bonds (the frequencies corresponding to the $-CH=CH_2$, $-CH=CH-$ and $C=CH_2$ groupings are 1635, 1660 and 1680 cm^{-1}), 2) the presence of corresponding deformation vibration bands in the 800 to 1000 cm^{-1} region ($-CH=CH_2$: 920 and 980 cm^{-1}, $-CH=CH-$: 960 cm^{-1}, etc.) and 3) the presence of a band due to the valence vibrations of $=C-H$ at 3030 cm^{-1} or its overtone at about 6100 cm^{-1}, characteristic of the $C=CH_2$ end grouping. In each case we tried to use all three methods; this, however, was not always feasible.

Telomers obtained from allyl halogen derivatives contain a minimum of two double bonds with the same or different character of substitution. In the latter case, it was not always feasible to resolve the two frequencies in the 1650 cm^{-1} region. It was, however, possible to determine the telomer structure with a high degree of certainty from two other regions of the spectrum.

3. In one of the simplest cases, namely, in telomerization of divinyl with its hydrochlorides there are obtained two products with the composition $C_8H_{13}Cl$.[2] In the spectra of the former, in addition to the bands associated with the $-CH=CH-$ grouping there are also present bands associated with the vinyl group. Hence the inferred structure is

$$CH_3-CH=CH-CH_2-CH_2-CHCl-CH=CH_2;$$

this inference has been substantiated by chemical methods. In the spectrum of the latter product the bands associated with the $-CH=CH-$ grouping stand out clearly, while the bands of the vinyl group are very weak. In view of this we attributed the following structure to the principal part of the latter product:

$$CH_3-CH=CH-CH_2-CH_2-CH=CH-CH_2-Cl.$$

This was also substantiated by chemical methods.

In this case the bands due to the valence vibrations of the multiple bonds (the vinyl group and the $-CH=CH-$ grouping) are well separated. In other cases, for example, in the spectra of the two isomeric addition products of 2-chloropentene-3 and divinyl, these bands are not resolved; the isomers differ, however, as regards their spectra in the 900 to 1000 cm^{-1} region and only the first of them has an overtone at about 6100 cm^{-1}.[3]

4. In some cases, for example, in telomerization of 2-chloropentene-3 with isoprene, piperylene (1,3-pentadiene) and chloroprene, 1,4 addition products are obtained in the amount of 85-90%. In the spectra of these telomers there are clearly evinced only the bands associated with the $-CH=CH-$ grouping, while the

bands of the vinyl group are either weak or absent. After extraction from the mixture of most of the 1,4-isomer by reaction with urotropine, one can detect 1,2 products in the remainder.[3]

5. Through the use of infrared spectroscopy we were able to solve the problem of the virtual identity of the telomers obtained from allyl isomers. In the case of primary-secondary and primary-tertiary allyl isomers there are obtained mainly products involving the primary isomer, regardless of what isomer is taken in the reaction. To some minor extent, however, the second isomer is also involved in the reaction. This was proved by comparison of the spectra of the products of thorough hydrogenization of the telomers with the spectra of the expected saturated hydrocarbons.[2]

6. Of greatest interest from the practical standpoint and at the same time the most complex is analysis of mixtures of telomers obtained in the reaction of isoprene with its hydrochlorides. We inferred from the infrared spectra that there are present in this mixture geranyl, linalyl and terpenyl chlorides, as well as some other chlorides with an undetermined structure.[4]

7. We also used infrared spectroscopy for identifying citral (gerenial) derived from the above mentioned telomer mixture by the Sommelet reaction.[5] Our study showed that synthetic citral is not identical with the usual natural compound, but contains more neral (citral b) and an admixture of undetermined structure. Examination of the Raman and ultraviolet absorption spectra of synthetic citral led to the same inferences.

8. Similar investigations were carried out on some higher telomers; it was shown that their structure approximately corresponds to the structure of the simplest addition products.

References

1. A.A.Petrov & K.V.Leets, Zhur.obshch.khimii, 26, 1113 (1956). (Trans.J. General Chemistry.)

2. A.A.Petrov, Kh.V.Bal'yan, L.I.Bunina-Krivorukova & T.V.Yakovleva, Ibid., 29, 5, 1576 (1959).

3. A.A.Petrov, N.A.Razumova & M.L.Genusova, Ibid., 28, 1128, 2132, 3220 (1958); Hauchn.doklady Vysshei shkoly (University Scientific Reports), 1, 530 (1958); 2, 1 (1959).

4. A.A.Petrov, Kh.V.Bal'yan, Yu.I.Kheruze, E.Yu.Shvarts & L.L.Cherenkova, Zhur.obshch.khimii 28, 1435 (1958). (Trans.J.General Chemistry.)

5. A.A.Petrov, Kh.V.Bal'yan, Yu.I.Kheruze, E.Yu.Shvarts & T.V.Yakovleva, Ibid., 29, 445 (1959).

IDENTIFICATION OF RESIN ACIDS FROM THEIR INFRARED SPECTRA

- N.A.Borisevich, N.I.Makarevich, A.M.Prima, I.I.Bardyshev & E.A.Cherches

Resins from coniferous species (pine, spruce, cedar, etc.) generally contain terpene hydrocarbons and resin acids, which are widely used for the manufacture of turpentine and camphor; these are valuable raw materials employed in the paint & varnish, paper, soap and other industries.

The resin acids are similar in structure and readily undergo isomerization. This explains why the individual resin acids were not separated until recently. In fact, it is only lately that chemists have been able to identify the individual acids contained in natural mixtures of resin acids.

In connection with the substantial difficulties involved in chemical analysis of resin acid mixtures during their manufacture, spectroscopic procedures for analysis of these substances have acquired considerable significance. However, hitherto the infrared spectra of many resin acids had not been studied. The present report covers a thorough investigation of the infrared spectra of abietic (I), laevo-pimaric (II), dextropimaric (III), and dehydroabietic (IV) acids:

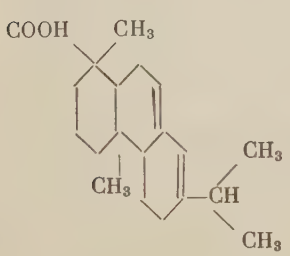

I

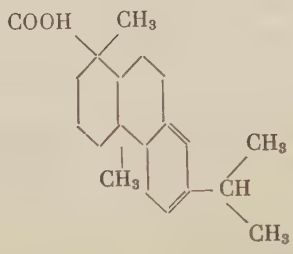

II

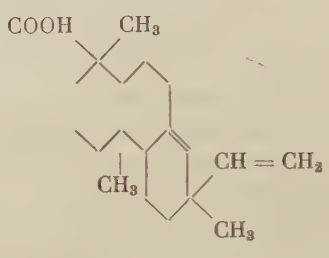

III

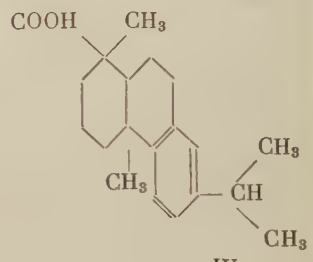

IV

The infrared spectra of solutions of the resin acids in CCl_4 and of plates obtained by compressing the acid with potassium bromide under vacuum at a pressure of 4000 kg/cm^2 were observed on an IKS-11 spectrometer. The spectra of the solutions were virtually identical with those of the compressed samples.

It will be evident from a comparison of the spectra (see figure), that the spectra of acids I, II and IV differ little in the frequency region of the valence vibrations of the CH, CH_2 and CH_3 groups. The significant difference of the spectrum of acid III in this region from the spectra of the three other acids may be attributed to the presence of the vinyl group: $-CH{=}CH_2$.

The frequencies (1685 and 1282 cm^{-1}) of the absorption bands corresponding to C=O and COH groups were found to be relatively insensitive to structural changes in the remainder of the resin acid molecule. The intensity of these bands changed markedly in going from one substance to another.

The following was observed in the frequency region for the C=C double bond. A band of varying intensity at 1544 cm^{-1} was observed in the spectra of I, II and IV. The intense band at 1631 cm^{-1} in spectrum III is related to the presence of the above mentioned vinyl group. We note in passing that another strong band in the spectrum of III, at 1409 cm^{-1}, is also associated with this group. In addition, the spectrum of IV had a band at 1502 cm^{-1}, which is characteristic of the benzene ring. The absence of the other band characteristic of the benzene ring (at ~1600 cm^{-1}) is presumably due to the fact that it is masked by the edge of the strong band at 1685 cm^{-1}.

Finally, we note the presence of a number of intense bands in the 800 to 1100 cm^{-1} region, which are characteristic of the following acids: 893 cm^{-1} (I), 1007 and 1024 cm^{-1} (II), and 821 cm^{-1} (IV); these are evidently associated with vibrations of the molecular skeletons. We also note a sharp band at 905 cm^{-1}

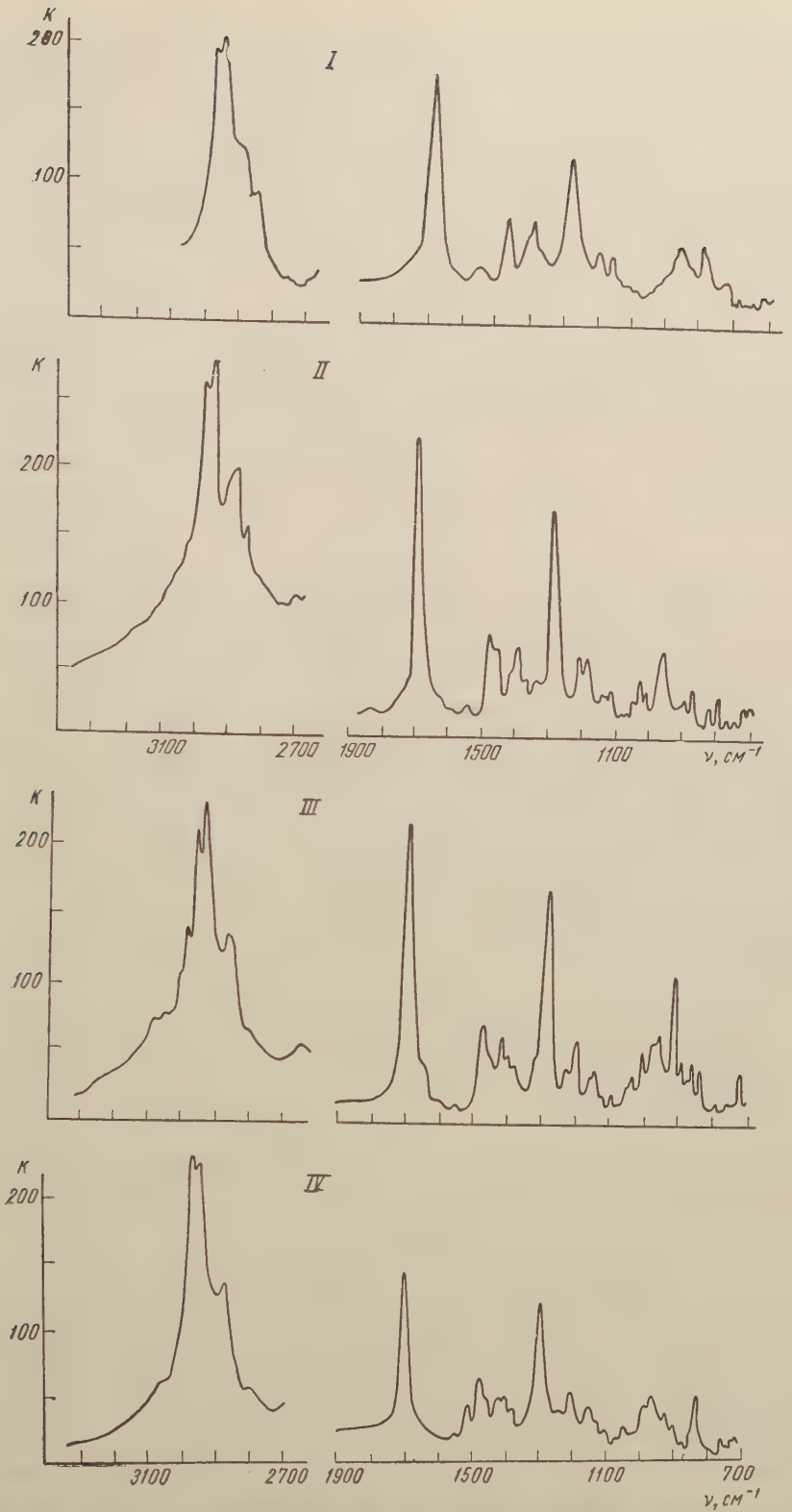

Infrared spectra of compressed plates (KBr) of the resin acids: I) abietic, II) laevo-pimaric, III) dextro-pimaric, IV) dehydroabietic; K is the molar absorption coefficient.

in the spectrum of III, which we attribute to the vinyl group.

The above results regarding the resin acid spectra are not in conflict with data obtained previously by us on the infrared spectra of substances having similar structure: retene, fichtelite, and phenanthrene.[1]

Thus, despite the general similarity in the infrared spectra of the investigated resin acids, there exist characteristic differences by means of which these individual acids can be identified. We plan in the future to develop an infrared spectroscopic procedure for quantitative analysis of resin acid mixtures.

References

1. N. I. Makarevich, A. I. Skrigan & N. I. Borisevich. Collected papers of the First Scientific-Engineering Conference on the Applications of Molecular Spectrum Analysis. Sovnarkhoz of the Belorussian SSR, Minsk, 1958.

* * * * * * *

INFRARED SPECTRA OF CELLULOSE AND ITS DERIVATIVES

- B. I. Stepanov, R. G. Zhbankov & I. N. Ermolenko

Until now infrared spectroscopy has not been utilized to any appreciable extent for the study of cellulose; this is explained by the difficulty of obtaining the spectra of fibrous materials, owing to their strong light scattering.

Most infrared spectra of cellulose were obtained for films of regenerated cellulose or cellophane, i.e., for modified cellulosic substances. Yet, a clear idea of the true spectrum of cellulose can be gained only by investigating fibrous celluloses. Conventional procedures for reducing light scattering (such as dissolving the fibrous celluloses or placing them in an immersion medium) can lead to serious destructive changes and may limit the observable spectral range.

Our procedure is based on compacting of the cellulose fibres passed through a coarse sieve, without addition of any extraneous material. By this procedure we obtained the spectra of different celluloses in the 2.5 to 15 μ range. We give tentative interpretations of all the principal bands in the cellulose spectra on the basis of comparison with the spectra of native cellulose and its derivatives.

Bands were observed in spectra of native celluloses in the following regions: 3330, 2940, 1650, 1428, 1360, 1340, 1325, 1290, 1225, 1190, 1150-910 and 705 cm^{-1}. The band at 3330 cm^{-1} (OH valence vibrations) is sensitive to the nature of the hydroxyl groups and to rupture of hydrogen bonds.

An intense band appears at 1740 cm^{-1} (C=O) in the spectra of oxidized celluloses (except for dialdehyde cellulose). In the spectra of celluloses oxidized by nitrogen dioxide, the intensity of the band at 1740 cm^{-1} is not proportional to the carboxyl group content, but passes through a maximum, as does the total content of carbonyl and carboxyl groups. The intensity of the bands at 1430, 1360, 1340 and 1325 cm^{-1} is sharply reduced as the degree of oxidation of the cellulose by nitrogen dioxide increases, while absorption in the 1280-1160 cm^{-1} region increases. A minor reduction in absorption in the 1400-1300 cm^{-1} region, together with the complete disappearance of the weak band at 1190 cm^{-1} are observed in the case of oxidation with periodates. The spectrum of dicarboxyl cellulose is characterized by greater absorption in the 1280-1190 cm^{-1} region than in the spectrum of monocarboxyl cellulose; it also exhibits considerably less absorption in the 1430-1280 cm^{-1} region (CH_2OH).

An intense band at 1290 and weaker bands at 1390 and 1200 cm^{-1} appear in the spectrum when cellulose is nitrated. The spectrum of unhydrolyzed cellulose residue differs from the spectrum of natural cellulose only in the much greater intensity of the band at 1190 cm^{-1}.

The spectrum of dialdehyde cellulose is characterized by very diffuse absorption in the 900 cm^{-1} region. A weak band appears at 955 cm^{-1} in the spectrum of cellulose having a significant number of carboxyl groups. An intense band at 870 cm^{-1} and a weak one at 770 cm^{-1} appear in the spectrum of cellulose oxidized by nitrogen dioxide. The spectrum of mercerized cellulose is characterized by a sharp increase in absorption in the 910 cm^{-1} region, the appearance of a weak band at 980 cm^{-1}, significant reduction in absorption in the 1430, 1340 and 1325 cm^{-1} regions, and some reduction of the absorption in the 1290 and 1225 cm^{-1} regions. These characteristic features of the spectrum of mercerized cellulose are very noticeable in the spectrum of cellulose treated with 12% NaOH.

From comparison of the spectra of cellulose regenerated after alkaline treatment in a viscose plant using the classical method and in "VA" equipment, it was concluded that the reaction of cellulose with caustic in the "VA" equipment was not uniform. It thus became possible to suggest ways for improving the quality of "VA" process viscose.

The methods of infrared spectroscopy are highly suitable for investigating the ion-exchange properties of oxidized celluloses. An analysis of the spectra of different oxidized celluloses showed that the carboxyl groups were primarily bonded to the cations.

Examination of the spectra of oxidized celluloses treated with basic dyes showed that these dyes were capable of chemically combining with the cellulose carboxyl groups. A comparison of the spectra of mono- and dicarboxyl cellulose showed that a carboxyl group in the second or third position reacts more actively with the dye than do uronic carboxyl groups. By spectroscopic techniques it is possible to determine both the total dye sorption and the sorption of the dye reacting with carboxyl groups. Other procedures are not satisfactory for this purpose.

The methods of infrared spectroscopy also proved to be useful for studying other chemical changes in the structure of cellulose.

Institute of Physics and Mathematics,
Academy of Sciences of the Belorussian SSR.

DETERMINATION OF THE ISOTOPIC COMPOSITION OF DEUTERO-ORGANIC COMPOUNDS BY INFRARED ABSORPTION SPECTROSCOPY

- M.O.Bulanin

1. Organic deuterium compounds find wide application in chemistry for studying problems involving the mutual influence of various atoms in organic molecules, the mobility of hydrogen atoms, the role of the solvent, etc. In the course of synthesizing deutero-organic compounds, there is always need to monitor their isotopic composition. This determination may be realized by combustion followed by isotopic analysis of the water formed, by mass-spectrometry, or, finally, by using infrared absorption spectra. Of the three, the infrared technique has the most advantages: the high sensitivity of this procedure makes it possible to determine the distribution of deuterium among the individual groups, the analysis requires a minimum amount of sample material, and the sample is not decomposed or otherwise harmed.

2. The accuracy of the analysis using infrared spectra depends primarily on which absorption bands of the mixture - those of the main component or those of the impurity - are chosen as the analytic bands. In this connection, we regard as impurities those molecules in the sample which either contain no deuterium or which are insufficiently deuterized. Performing the analysis with reference to the main component bands requires determining their absorption coefficients. For this, it is necessary to have either a pure sample of the deutero-organic compound under study or a sample whose isotopic composition has been established by an independent method, for example, by combustion. The accuracy of the analysis using the main component bands amounts to 7-10% under favorable conditions (absence of superposition).

Much higher accuracy may be attained by using the impurity bands. This is explained by the fact that the impurity concentration in the sample is usually low: the order of a few percent. Thus, if, as in the previous case, the concentration of the impurity is determined with an accuracy of 10%, and the impurity content is, say, 2%, the concentration of the main component would evidently be determined with an accuracy of 0.2%. As a rule, such an accuracy exceeds requirements; this makes it possible to use approximate methods for determining the impurities, for example, to utilize literature data on the intensities of the analytic bands. This is particularly convenient when the impurities are partly deuterized substances.

3. The isotopic composition of deutero-organic compounds is most simply determined in those cases when the analysis involves molecules containing a single X-D group. In this case, those molecules which contain no deuterium represent the impurity, and consequently, the determination of absorption coefficients for their bands presents no difficulty. As examples of such analyses, we may cite the procedures developed in our laboratory for determining the isotopic composition of deuterochloroform $CDCl_3$, monodeuterobenzene C_6H_5D, deuteromethanol CH_3OD, and deuteroacetic acid CH_3COOD.

In analyzing $CDCl_3$ for $CHCl_3$ as the impurity, the main analytical band selected was the CH valence vibration band of $CHCl_3$, located at about 2038 cm^{-1}. As a check, an analysis was also performed with reference to the CH deformation vibration band at 1200 cm^{-1}. The analysis based on the 3028 cm^{-1} band gave a $CDCl_3$ concentration of 99.08 ± 0.07%. The analysis with reference to the 1200 cm^{-1} band gave a $CDCl_3$ concentration of 99.11 ± 0.10%.

The analysis of monodeuterobenzene, C_6H_5D, for light benzene, C_6H_6, as the impurity, was performed with reference to the C_6H_6 composite band at 2211 cm^{-1} as well as with respect to the C_6H_6 fundamental band at 674 cm^{-1} (ν_4 vibrations).

The superimposed absorption of the C_6H_5D limited the sensitivity of the analysis, which showed a C_6H_5D concentration in excess of 97.5%. As a check, a sample of C_6H_5D was analyzed by the proton magnetic resonance procedure; the result in this case was 92 ± 10%.

In analyzing deuteromethanol, CH_3OD, for light methanol, CH_3OH, the band for OH group valence vibrations at 3330 cm^{-1} was taken as the analytic band. This same band served for determining the isotopic composition of the hydroxyl groups in a sample of completely deuterized methanol, CD_3OD. Finally, the band for OH group valence vibrations (3200 cm^{-1} region) was also used for determining the isotopic composition of the carboxyl groups in deuteroacetic acid CH_3COOD. In the last case, check analyses were performed using the CH_3COOH absorption band at 1182 cm^{-1}, and the band at 947 cm^{-1} associated with non-planar OH deformation vibrations. The analytic results based on the different bands showed good agreement.

In the course of determining the isotopic composition of deuteromethane, CD_4, in addition to the bands of the main component, we observed in the spectrum of the sample bands at 2990, 2140, 1035.5 and 1002 cm^{-1}, which we attributed to CHD_3, and a very weak band at 1238 cm^{-1}, which we ascribed to CH_2D_2. In view of the low concentrations of CHD_3 and CH_2D_2, we evaluated their percentages on the basis of the data in the literature on the intensity of the 2140 and 1238 cm^{-1} bands.

The author thanks V.M.Chulanovskii for his continued attention and interest in this work.

Scientific-Research Physical Institute,
"A.A.Zhdanov" Leningrad State University

INFRARED SPECTRA AND STRUCTURES OF THE PRODUCTS OF LINKAGE OF DIFFERENT SUBSTANCES TO VINYL ACETYLENE HYDROCARBONS

- A. A. Petrov & R. V. Yakovleva

In order to establish the fundamental regularities obtaining in single-syster reactions, we investigated the addition reactions of vinyl acetylene hydrocarbons having various structures with a series of electrophilic (bromine, chlorine, iodine, hydrogen halides and alkyl hypohalites), nucleophilic (water, alcohols and amines), and radical (lithium alkyls and diazo-compounds) reagents[1-8]. In all cases, the clearest conclusions as to the structure of the adducts could be drawn from the infrared spectra.

As a result of linkage of the various addends to vinyl acetylenes, one can obtain 1,3-diene, acetylene, or allene compounds by 1,2-, 3,4-, or 1,4-addition, respectively. All of these have highly characteristic IR spectrum bands: the 1,3-dienes in the 1600 cm^{-1} region; acetylenes in the 2100 or 2200 cm^{-1} region, depending on the nature of the substitution, and allenes in the 1960 cm^{-1} region. In addition to these multiple bond frequencies, we also made use of the CH valence and deformation vibration frequencies for determining the structure of the products.

Thus, for example, primarily two substances were obtained as a result of adding bromine to unsubstituted vinyl acetylene: the lower boiling point substance exhibited intense bands at 1558 and 1621 cm^{-1}, characteristic of a Br-substituted 1,3-diene grouping, as well as the usual deformation frequencies of the vinyl group at 928 and 969 cm^{-1}; the higher boiling compound showed the intense band of the allene grouping at 1960 cm^{-1}. Thus, the infrared spectra lead to formulas (I) and (II), which were substantiated by chemical methods[1]:

$$CHBr = CBr - CH = CH_2; \quad \text{(I)}$$

$$CHBr = C = CH - CH_2Br; \quad \text{(II)}$$

$$CH \equiv C - CHBr - CH_2Br. \quad \text{(III)}$$

It was also possible to confirm, using the methods of infrared spectroscopy, the formation of small amounts of a third possible isomer as well. In fact, the spectrum of the dibromides comprised a band at about 3300 cm^{-1}, which could only be attributed to the dibromide with a terminal acetylene grouping.

Dibromides were obtained as a result of adding bromine to vinyl alkylacetylenes; only the triple bond frequencies were evinced in their spectra. In view of this, structure (IV) was assigned to these compounds; this was also confirmed by chemical methods[2]. It was shown in the same way that the alkenylacetylene dibromides mainly had the allene structure (V):[2]

$$R - C \equiv C - CHBr - CH_2Br; \quad \text{(IV)}$$

$$R - CHBr - CH = C = CHBr. \quad \text{(V)}$$

An order of linkage similar to that of bromine was demonstrated spectroscopically for the case of phenylated vinyl acetylenes.[3]

At the same time, it was found that iodine only attaches to triple bonds, regardless of the hydrocarbon structure[4].

As a result of addition of nucleophilic reagents - water and alcohols - to vinyl alkylacetylenes, alkyl propenyl ketones or their enolic ethers were obtained; this was confirmed both chemically and spectroscopically.[6]

Radical reagents, like lithium alkyls, yielded allene compounds exclusively while aromatic diazo-compounds (in the halogenarylization reaction)[8] predominantl

linked up to the double bond to form acetylenic compounds.

Clearest evidence of the structure by infrared spectroscopy was, in general, obtained for the compounds that contain a terminal acetylene grouping, since the CH valence vibration frequency of this grouping is very intense and lies in the 3300 cm^{-1} region, where there are no interfering frequencies. The detection of doubly-substituted acetylenes with reference to the valence frequencies of the acetylene bond is less reliable, because of the low intensity of this frequency in the spectra of some of the addition products.

The detection of allene compounds on the basis of the 1960 cm^{-1} band is hampered by the fact that some 1,3-diene compounds also absorb in this region. We encountered such a case, for example, in studying the bromination of vinyl phenylacetylene.[3]

The detection of 1,3-diene compounds may be hindered by a band characteristic of several acetylene compounds, which appears in the 1640-1720 cm^{-1} region. In this case, particular attention should be directed toward analyzing the spectra in the region of the CH deformation vibrations.

Infrared spectra were also used for establishing the structure of the products obtained by addition of various substances to vinyl-acetylenic alcohols[9] and acid esters[10].

References

1. A.A.Petrov, G.I.Semenov & N.P.Sopov, Zhur.obshch.khim., 27, 928 (1957). (Trans.J.Gen.Chem.)

2. A.A.Petrov & Yu.I.Porfir'eva, Ibid., 23, 1867 (1957); Ibid., 27, 1805 and 2076 (1957); Doklady AN SSSR, 90, 561 (1953).

3. A.A.Petrov & T.V.Yakovleva, Zhur.obshch.khim., 29, 1878 (1959). (Trans. J.Gen.Chem.)

4. A.A.Petrov, Yu.I.Porfir'eva, T.V.Yakovleva & K.S.Mingaleva, Ibid., 28, 2320 (1958).

5. V.M.Al'bitskaya, E.M.Blyakhman, A.A.Petrov & T.V.Yakovleva, Ibid., 29, 2278 (1959).

6. A.A.Petrov & B.S.Kupin, Ibid., 28, 1999(1958).

7. A.A.Petrov & V.A.Kormer, Doklady AN SSSR, 125, 1041 (1959). (Trans. Doklady - Chemistry.)

8. A.A.Petrov, Kh.V.Bal'yan, Yu.I.Kheruze & R.V.Yakovleva, Zhur.obshch.khim., 29, 2101 (1959). (Trans.J.Gen.Chem.)

9. A.A.Petrov & K.B.Rall', Ibid., 27, 2402 (1957).

10. A.A.Petrov, K.B.Rall' & G.I.Semenov, Ibid., 28, 424 (1958).

MOLECULAR SPECTRUM OF HEXAETHYLDILEAD AND DETERMINING ITS CONCENTRATION IN TETRAETHYLLEAD

- N.K.Rudnevskii & N.N.Vyshinskii

Tetraethyllead (TEL) is widely used as an antiknock additive. Hexaethyldilead (HEL) is formed[1] as a by-product during industrial manufacture of TEL and lowers the quality and chemical stability of the latter. There are as yet no reliable procedures for determining HEL in TEL. Accordingly, our work was devoted to exploring the possibility of spectrophotometric determination of HEL in TEL.

The vibrational and electronic spectra of TEL have been studied by a number of investigators.[2-6] Judging from the available literature, the spectrum of HEL has not been investigated hitherto.

We studied the IR spectrum of HEL in the region from 1.5 to 25 μ by means of an IKS-2 spectrometer and a ZMR-2 monochromator. No substantial difference was found in this region between the IR spectra of HEL and TEL; this eliminates the possibility of using the IR spectra for solving the problem. The difference between the electronic spectra of these compounds (Fig.1), obtained with an SF-4 spectrophotometer, however, made it feasible to develop a procedure for quantitative determination of HEL in TEL.

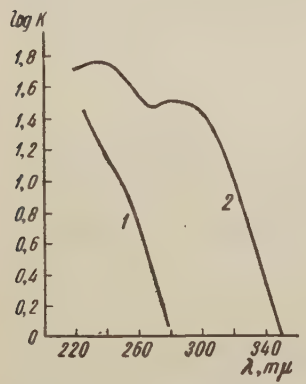

Fig.1. Absorption curves for TEL (1) in HEL (2) in n-heptane. K = g^{-1} liter·cm^{-1}.

If a binary system obeys the Lambert-Beer law and the physical density is constant, the total optical density at a given wavelength is a linear function of the concentration of the determined component. Such a dependence obtains for solutions of HEL in TEL (Fig.2, curve 1). The relative error in determining HEL amounts to ±5% in the 0.5 to 3.5% concentration range.

The optical density increases sharply when the HEL content is greater than 3-4%; consequently, we used n-heptane to dilute the samples. The HEL concentration after dilution was determined using curve 2 of Fig.2, and the initial concentration of HEL in the TEL was then calculated. However, since TEL absorbs in the 320 mμ region, in using curve 2, we obtain an overestimate of the HEL content.

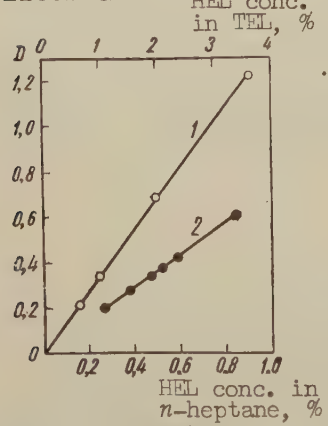

Fig.2. Working curves for determination of HEL (λ = 320 mμ): 1) in TEL (cell thickness 0.100 mm); standard - n-heptane.

It is not hard to show, however, that if the Lambert-Beer law is satisfied, the HEL concentration C' in the sample found from curve 2 is linearly dependent on C, its true value, i.e., that

$$C' = C\left(1 - \frac{1}{a}\right) + \frac{100}{a},$$

where a is the ratio of the absorption coefficients of HEL and TEL in the 320 mμ region. Thus one can easily introduce appropriate correction. The relative error in determining HEL by this method amounts to ±4%. The decrease in the error percentage indicated is due to use of a thicker absorption cell for the diluted solutions.

The described procedure for determining HEL in TEL was for investigating the photo and thermal decomposition reactions of TEL in the absence of atmospheric oxygen. It was shown that the optical density of TEL increased when the compound was irradiated with ultraviolet (Fig.3) or heated. It was assumed that the liquid phase products of

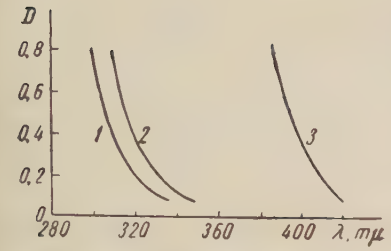

Fig.3. Absorption curves (cell thickness 0.020 mm) of 1) untreated TEL, 2) UV irradiated TEL, 3) HEL.

TEL decomposition comprise HEL. This assumption was confirmed by polarographic[7] and chemical analyses.

A comparison of the results of spectrophotometric and polarographic measurements of the HEL concentration in the thermal decomposition products of TEL showed that the first method gives results which are consistently higher by an amount greater than the error of either procedure. This gives reason to infer that in the process of thermal decomposition of TEL, not only HEL but also other compounds absorbing in the 320 μ region are formed.

References

1. V.V.Korshak & G.S.Kolesnikov, Tetraetilsvinets (Tretaethyllead), 29. Goskhimizdat, M.-L., 1946.
2. C.F.Kettering & W.W.Sleator, Physics, 4, 39 (1933).
3. A.B.Duncan & J.W.Murray, J.Chem.Phys., 2, 636 (1934).
4. Pai N.Gopala, Proc.Royal Soc. (London), A 149, 29 (1935).
5. H.W.Thompson, J.Chem.Phys., 2, 790 (1934).
6. L.Riccoboni, Gazz.chim.ital., 71, 696 (1941).
7. L.N.Vertyulina & I.A.Korshunov, Trudy po khimii (Reports on chemistry), Gor'kii, No.3, 615 (1958).

* * * * * * *

SPECTROPHOTOMETRIC ANALYSIS BY THE "ZERO HETEROCHROMATIC POINT" PROCEDURE

- B. I. Sukhorukov & A. I. Finkel'shtein

In an earlier publication[1] we described a simple technique for compressing plates of the investigated substance with alkali halide salts; this procedure involved preliminary manual forming of the mixture. The applicability of this procedure to determination of the infrared absorption spectra of samples was demonstrated in Refs.2-4.

In the present contribution we examine the theoretical basis for spectrophotometric quantitative analysis by the "zero heterochromatic point" procedure and give an example of use of this procedure for analysis of a mixture of dicyandiamide, $(H_2N)_2—C=N—C\equiv N$, in solid melamine.

Assume that we have chosen in the spectrum of the sample three points with wavelengths λ_i, $\lambda_{ст}$ and λ_0; here λ_i is the wavelength of the chosen analytic point, $\lambda_{ст}$ marks the maximum absorption of the internal standard and λ_0 is a point where the absorption of the analyzed component is low.

As we know, for analysis by the method of internal standards, one must find the quantity

$$R_i = \frac{D_i}{D_{ст}} = \frac{\lg \frac{I_i^0}{I_i}}{\lg \frac{I_{ст}^0}{I_{ст}}}, \qquad (1)$$

where D_i and $D_{ст}$ are the optical densities of the i-th determined component and of the standard substance, I_i^0 and $I_{ст}^0$ are the intensities of the incident light, and I_i and $I_{ст}$ are the intensities of the transmitted light at the wavelengths λ_i and $\lambda_{ст}$.

For determination of I_i^0 and $I_{ст}^0$ by the "zero heterochromatic point" procedure we made use of the equations

$$I_{ст}^0 = aI_0 \quad \text{and} \quad I_i^0 = bI_0, \tag{2}$$

where I_0 is the intensity of the transmitted light at point λ_0, and a and b are constants which depend on the energy distribution in the spectrum of the light source, the absorption and scattering of light by the matrix (principal) substance and the width of the slits; a and b are determined from the spectrum of the sample containing the matrix but neither the analyzed substance nor the standard. If one determines a and b in the absence of the matrix substance the formulas given below become more complicated. It follows from Eq.(1) and Eq.(2) that

$$R_i = \frac{\lg \frac{I_0}{I_i} + \lg b}{\lg \frac{I_0}{I_{ст}} + \lg a} = \frac{\varepsilon_i C_i}{\varepsilon_{ст} C_{ст}} = K_i C_i, \tag{3}$$

where ε_i and $\varepsilon_{ст}$ are constant coefficients, and C_i and $C_{ст}$ are the concentrations of the i-th determined component and the standard.

If the λ_i point is chosen so that it lies in the region of absorption of the standard substance, the equation relating R_i and C_i becomes

$$\frac{1}{R_i} = \frac{\varepsilon_{ст}}{\varepsilon_i} + \frac{\varepsilon_{ст} C_{ст}}{\varepsilon_i C_i} = K_{0i} + K_i \frac{1}{C_i}. \tag{4}$$

In the case of overlapping of the bands of the determined components, we obtain

$$R_i = \frac{1}{D_{ст}} \sum_j D_j = \sum_j K_{ij} C_j, \tag{5}$$

where C_j is the concentration of component j.

When λ_0, $\lambda_{ст}$ and λ_i lie in the region of the spectrum where the transmission changes sharply (owing to overlapping with a strong absorption band of the matrix or the region of anomalous scattering), the constants a and b will vary somewhat, depending on the thickness of the plate, and for accurate analysis this variation must be taken into account. To this end, we determine a and b for one of the plates with $C_i = 0$ and $C_{ст} = 0$, which plate is thereinafter considered the "standard" one, and find the auxiliary constants A and B by means of the following formulas deduced by us earlier:

$$\frac{\lg \frac{I_i^0}{I_{is}}}{\lg \frac{I_0^0}{I_{0s}}} = A \quad \text{and} \quad \frac{\lg \frac{I_{ст}^0}{I_{ст\,s}^0}}{\lg \frac{I_0^0}{I_{0s}^0}} = B, \tag{6}$$

where I_{0s}^0, I_{is}^0 and $I_{ст\,s}^0$ pertain to the standard plate, and I_0^0, I_i^0 and $I_{ст}^0$ to the other plates with $C_i = 0$ and $C_{ст} = 0$, used for determination of A and B.

The correction for plates with the sample is introduced by means of the following equations

$$\lg \frac{I_i}{I_{im}} = A \lg \frac{I_{0s}^0}{I_0} \quad \text{and} \quad \lg \frac{I_{ст}}{I_{стm}} = B \lg \frac{I_{0s}^0}{I_0}, \tag{7}$$

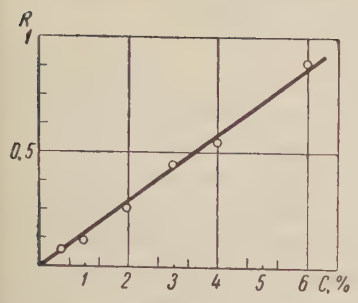

Working curve for determination of dicyandiamide in melamine.

where I^0_{0s} pertains to the standard plate and in practice is replaced by photography of a screen at point λ_0; I_0, $I_{cтm}$ and I_{im} are measured values at the points λ_0, $\lambda_{cт}$ and λ_i, and $I_{cт}$ and I_i are corrected intensity values at the points $\lambda_{cт}$ and λ_i, which are used in the formulas for calculating R_i.

The determination of dicyandiamide in melamine was carried out in the following manner. The concentration of the sample in the compacting material (potassium bromide) was 6%. The sum of the scattered and reflected light exceeded 95%, hence we introduced a correction according to Eqs.(6) and (7). For analysis we used the absorption band of dicyandiamide at 4.6 μ; for λ_0 we chose 4.0 μ. By way of internal standard we used potassium ferrocyanide ($\lambda_{cт}$ = 4.95 μ), which was introduced into the potassium bromide in the amount of 0.15% by joint recrystallization of the salts from water.

The working curve for determination of dicyandiamide is shown in the accompanying figure. The total time required for analysis is 1.5-2 hours, which includes approximately an hour for preparation of the samples (weighing out the materials, hand grinding in a porcelain mortar, etc.).

It should be noted that the "zero heterochromatic point" procedure can be used not only for analysis in the solid phase by means of compacted plates, but also for analysis in the liquid phase (in thin layers if it is necessary to exclude the influence due to differences in layer thickness) and for samples in the form of paste.

In comparing the "zero heterochromatic point" procedure with the "base line" procedure it should be recalled that in case there is no overlapping with the spectrum of the matrix material or the "anomalous scattering" band, both procedures are equally applicable. Where there is such overlapping, however, only the "heterochromatic zero point" method with introduction of corrections according to Eqs.(6) and (7) is applicable.

"Dzerzhinskii" Branch of the
Scientific Research and Planning Institute of the Nitrogen Industry

References

1. A.I.Finkel'shtein, F.L.Molochevskaya, A.M.Fisher & B.G.Rabovskii, Optika i spektroskopiya, 6, 415 (1959). (Trans.Optics & Spectroscopy.)

2. A.M.Fisher, B.G.Rabovskii & A.I.Finkel'shtein, Tr.po khimii i khim. teckhnologii (Research reports on chemistry and chemical engineering), No.1, 102, Gor'kii, 1958.

3. A.I.Finkel'shtein, Optika i spektroskopiya, 5, 832 (1958).

4. B.I.Sukhorukov & A.I.Finkel'shtein, Ibid., 6, 637 (1959). (Trans.Optics & Spectroscopy.)

INVESTIGATION OF AGING OF CASTOR OIL BY OBSERVATION OF ITS ABSORPTION SPECTRA

- M.S.Kozyreva

Castor oil is a complex mixture of triglycerides, i.e., esters of glycerol and higher aliphatic acids. The major component (80-88%) of the acid portion of castor oil is ricinoleic acid. In addition to the triglyceride of ricinoleic acid, glycerides of stearic, oleic and linoleic acids are present in the oil.[1]

Recently, castor oil has found a new use as a liquid dielectric in electric capacitors.[2] In capacitors, the dielectric is simultaneously subjected to the action of an electrical field and to heating. We investigated the effect of an electrical field on the oil in a vessel, similar to one described in Ref.3, in which the volume of air above the oil was significantly greater (by a factor of about 10) than in ordinary capacitors. The treatments to which the various samples were subjected were the following:

Sample No.	Treatment
1	Initial castor oil (i.e., no treatment)
2	~300 hours at 70° (heating in the air)
3	Direct electrical field E = 1 kV/cm ~80 hours. (In this case the field was highly non-uniform: The field strength was appreciably greater at the edges of the electrodes.)
4	Simultaneous action of an electrical field (E = = 125 kV/cm) and heating (50°), ~70 hours.

The treated samples were investigated by infrared spectroscopy. The spectra were obtained on an IKS-11 spectrometer, being recorded by an EPP-09 automatic recorder directly coupled to a FEOU-15 amplifier. Appropriate reference lines were imposed on the spectrograms for determining the frequencies of the absorption bands; this was accomplished by a special device connected in between the FEOU-15 and the EPP-09. Changes observed in the spectra of the samples are described below.

2800-3100 cm^{-1} Region

As can be seen in Fig.1, the intensity of the 3010 cm^{-1} band decreased in the spectra of the treated samples. The weakening of this band is connected with decrease in the number of =CH groups, i.e., with the process of polymerization, and is accompanied by a lowering of the iodine number of the samples.*

1500-1900 cm^{-1} Region

Broadening of the band at 1740 cm^{-1} to the low frequency side was noted in this region for the treated samples (Fig.2); this is due to ester C=O groups and can be explained by the formation of additional carboxyl and carbonyl C=O groups. The increase in the number of carboxyl groups in sample 2 was confirmed by chemical analysis. It will also be evident from Fig.2 that the intensity of the band at 1660 cm^{-1} decreases in the spectra of treated samples, and that a very weak band appears at 1630 cm^{-1}. Similar changes were observed in the spectrum of dehydrated castor oil as it dried with autooxidation, a process in which conjugated bonds develop.[4] According to Bellamy[5], systems containing conjugated C=C bonds have two absorption bands in this region; here the supplementary band (1630 cm^{-1})

---

*The iodine numbers were determined for us by A.G.Melikhova.

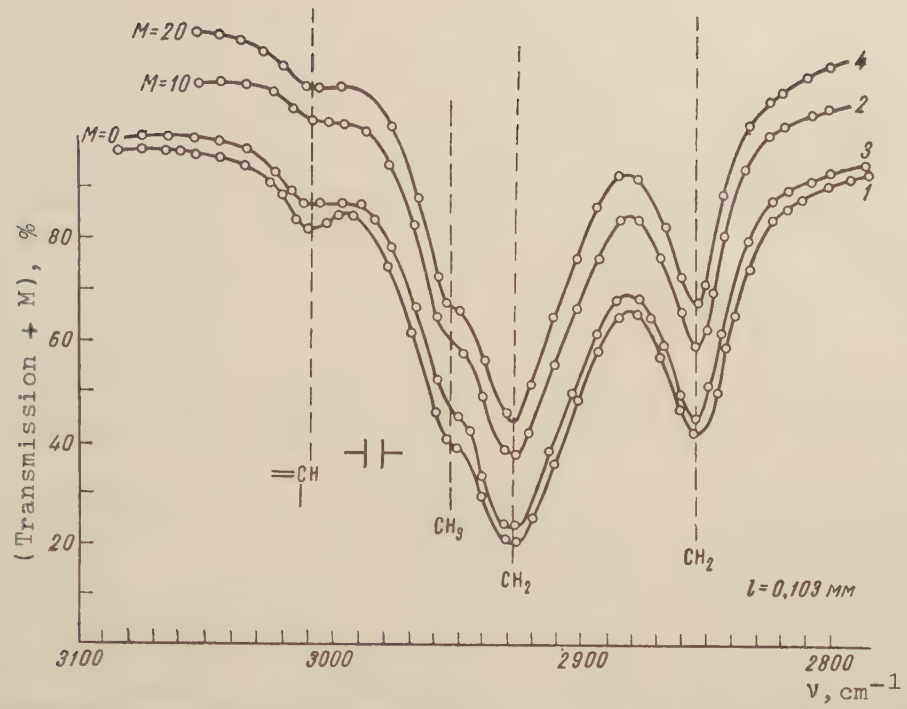

Fig.1. IR absorption spectra of castor oil (solution 2% by weight in CCl_4) in the 2800-3100 cm^{-1} region; 1-4 are the sample numbers.

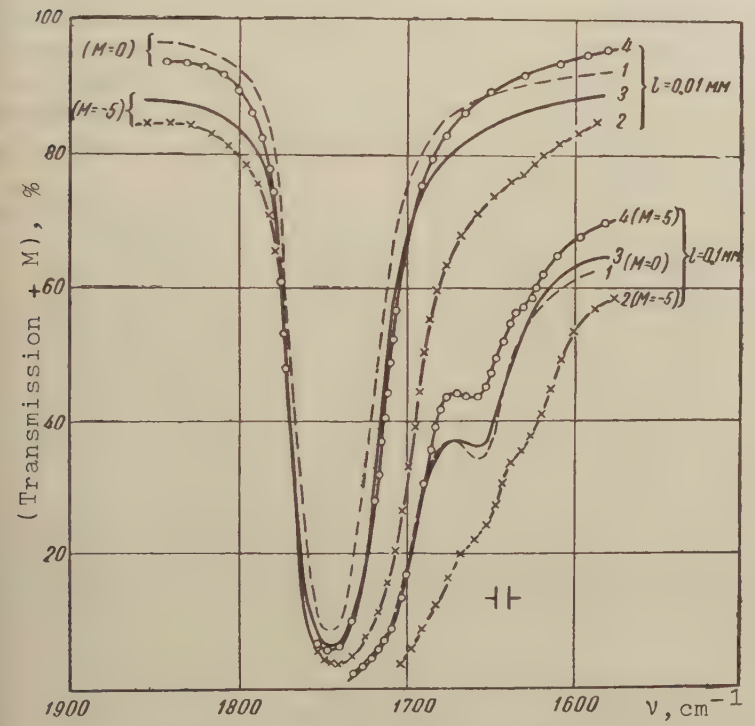

Fig.2. Same as Fig.1 but in the 1500-1900 cm^{-1} region.

should have a frequency some 30 cm^{-1} lower than the frequency of the corresponding unconjugated compound (1660 cm^{-1}). However, the appearance of two conjugated bonds cannot be explained on the basis of the structure of the ricinoleic acid radical (the main portion of castor oil), if one does not consider how it changes during heating. It is known that when ricinoleic acid is heated, dehydration occurs, a molecule of water is split off from each acid molecule and there forms linoleic acid or its isomer with conjugated double bonds[1,6]. The phenomenon of castor oil dehydration was repeatedly observed by us during its heating out of contact with air; this was judged by the reduction in intensity of the band at 3420 cm^{-1}, and has also been noted in the literature[7]. In the present case (samples 3 and 4), the decrease in intensity of

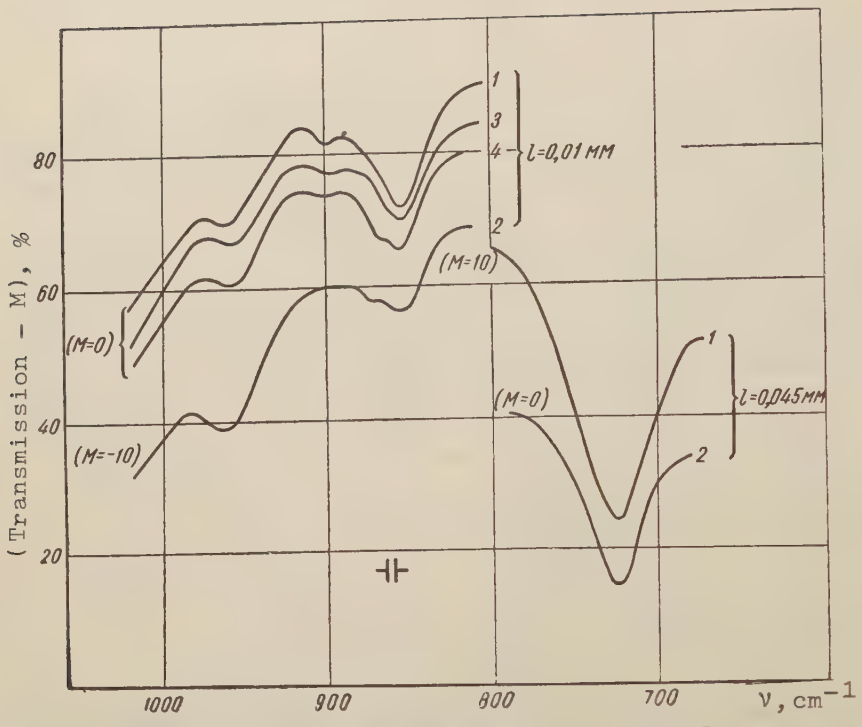

Fig.3. Same as Fig.1 but in the 700-1000 cm^{-1} region.

this band was insignificant; in fact, it was even observed to increase in the case of sample 2. However, it did not appear possible to evaluate the degree of dehydration during oxidation (in the case of heating) from the intensity of this band in view of the simultaneous increase in intensity owing to formation of hydroperoxide and carboxyl OH groups.[4,8]

660-1000 cm^{-1} Region

It can be seen from Fig.3 that an increase takes place in the overall absorption of the samples as a result of aging (treatment). There is an increase evident in the intensity of the band at 960 cm^{-1} and a decrease in the intensity of the band at 725 cm^{-1} (the intensity of this band also decreased in the spectra of samples 3 and 4). Corresponding changes in the 960 and 725 cm^{-1} bands were observed in the process of drying linoleic acid and dehydrated castor oil with autooxidation[4,8]; these were explained[8] by the isomerization of the oil during which the -CH=CH- groups change from a cis to trans configuration with respect to the double bond.

Of the other bands associated with the C=C double bonds, we should remark on the 1660, 900 and 855 cm^{-1} bands, intensities of which decrease as a result of polymerization. It is difficult, however, to evaluate the change in intensity of these bands in the spectrum of sample 2, in view of the strong increase of the integral absorption. It is evident from a comparison of the spectra that the same changes take place under the influence of the electrical field with the oil in contact with air as under the influence of heat. The changes observed in the spectra of castor oil are generally analogous to the changes that occur incident to polymerization (during drying) of linoleic acid and dehydrated castor oil[4,8]; in addition to the data noted in Refs.4 & 8, we observed a minor amount of dehydration. Thus, under the action of an electrical field and heating in contact with air, there occur dehydration and isomerization, leading to polymerization of the castor oil. Moreover, significant oxidation of the castor oil takes place when it is heated in contact with air.

References

1. A.A.Zinov'ev, Khimiya zhirov (Chemistry of Fats), Pishchepromizdat, M.-L., 1952.

2. V.I.Karabanov, Trudy Nauch.Issled.Inst.Radiodetalei, (Proceedings of the Radio-components Research Institute) 3, 6, 70 (1957).

3. V.T.Renne & Tsyui Si-Sin, Zhur.tekh.fiz., 5, 1070 (1956). (Trans.Soviet Phys. - Tech.Physics.)
4. S.B.Cricelius, Ind.Eng.Chem., 47, 8, 1643 (1955).
5. L.Bellamy, Infrared Spectra of Molecules. (Cited in Russian translation.)
6. V.V.Korshak & A.A.Ivanova, Zhur.Priklad.Khim., 28, 5, 523 (1955). (Trans. J.Applied Chemistry.)
7. V.G.Vafiadi, Zhur.Org.Khim. (J.Organic Chem.) 8, 1447 (1938).
8. L.A.O'Neil & C.P.Colle., J.Appl.Chem., 6, 89, 394 (1956).

* * * * * * *

VACUUM DOUBLE-BEAM DIFFRACTION SPECTROPHOTOMETER FOR THE INFRARED

- V.I.Malyshev & S.G.Rautian

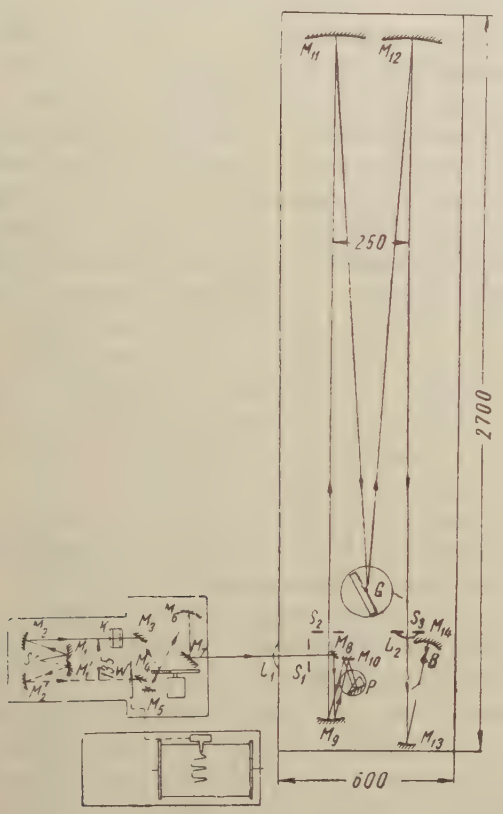

Fig.1. Optical system of the DAIKSF-1 double-beam diffraction spectrophotometer. Double-beam illuminator: spherical mirrors M_1, M'_1 (f = 200 mm, 45 x 85 mm), M_2, M'_2 (f = 180 mm, 75 x 120 mm), M_6 (f = 200 mm, 75 x 85 mm) and plane mirrors M_3, M'_3, M_4, M_5 & M_7. Preliminary monochromator: spherical mirror M_9 (f = = 300 mm, 60 x 95 mm), plane mirrors M_8 & M_{10} and the prism P. Main diffraction monochromator: spherical mirrors M_{11} & M_{12} (f = = 2000 mm, dia. 250 mm), M_{14} (f = 50 mm, 90 x x 90 mm), plane mirrors M_{13} and lenses L_1 (f = 540 mm) and L_2 (f = 700 mm) of KBr.

To facilitate the solution of a number of spectroscopic problems requiring an instrument with high resolution and, in particular, for the purpose of developing procedures for measuring the true widths and intensities of infrared absorption bands, we developed and had constructed in our optical laboratory the double-beam spectrophotometer with interchangeable diffraction gratings described below.* The working range of the instrument extends from 1 to 25 μ.

The instrument comprises three principal parts: a double-beam illuminator with associated photometric detecting and amplifying equipment, a preliminary prism monochromator and the main diffraction monochromator. The optical system of the spectrophotometer is shown in Fig.1. The mirrors M_1, M'_1, M_2, M'_2, M_3, M'_3, M_4, M'_5, M_6 and M_7 form the double-beam illuminator. The spherical mirrors M_1 and M_2 in one beam (and M'_1 and M'_2 in the other) form a 2X magnified image of the source S in the plane of the cell K and the photometric wedge W. The half-disk rotating (9 rps) mirror M_4 alternately directs the two beams on the slit. The mirror M_6 images the photometric wedge with two-fold magnification on the slit S_1 of the prism monochromator. Either a Silit rod or a ribbon filament lamp may be used

---

*A.M.Surov participated in the design of the mechanical assemblies.

as the source. The photometric wedge consists of eight triangular blackened bronze strips 0.1 mm thick and 100 mm long mounted in a frame. The wedge is moved by the servomotor of the tracking system and is mechanically linked with the pen of the recording device.

The preliminary prism monochromator consists of mirrors M_8, M_9 & M_{10} and interchangeable prisms of LiF or KBr with refracting angles of 37.5° and 30°, respectively. The main diffraction monochromator employs the Ebert-Fastie mounting.[1] The collimating spherical mirrors M_{11} and M_{12} have focal lengths of 2 meters and measure 250 x 300 mm. The interchangeable echelette gratings have 300, 200 or 50 lines/mm and were ruled in the State Optical Institute by F.M.Gerasimov. The 50 mm high slits S_2 and S_3 are curved in accordance with the theory of Fastie[1]; the radius of curvature is 125 mm. The radius of curvature of slit S_1 (320 mm) was chosen so that the curvature of its image produced by the optics of the prism monochromator would agree with the curvature of slit S_2 in the middle of the working ranges of the prisms. The exit slit S_3 is imaged by mirrors M_{13} and M_{14} with 12X demagnification on the bolometer B. The collecting lenses L_1 and L_2 serve to eliminate vignetting.

In our spectrophotometer the echelette gratings are used not only with the usual orientation, i.e., in directions close to the peak "throw" from the wide face of the lines, but also in the directions of reflection from the narrower faces (at large angles of diffraction). As we noted earlier[2], this setting of the echelette gratings has a number of advantages as regards resolution, transmission, extension of the working region to the side of longer wavelengths, etc.

The echelette gratings are mounted on a rotating stand with a conical shaft, the full weight of which is carried by an end-thrust bearing. The stand is rotated by means of a feed screw; a nut on the screw contacts a 500 mm lever, the other end of which is linked with the stand shaft. The necessary vacuum tight connection between the shaft and lever is realized by means of a sylphon. The reduction gear driving the feed screw has provision for rotating the gear at 11 different speeds ranging from $5 \cdot 10^{-4}$ to $5 \cdot 10^{-7}$ radians/sec. The angle of rotation of the grating is indicated on a circular dial mounted on the feed screw axis; the range of rotation is 20°.

The radiation detector is a bolometer prepared by Markov[3]. Its principal parameters are the following: sensitivity threshold - $5 \cdot 10^{-11}$ w (with an amplifier time constant of 1 sec), time constant - 0.02 sec, conversion factor - 30 v/w. The bolometer strip is curved in accord with the curvature of slit S_3. The amplifying equipment was developed earlier and is described in Refs.4 & 5. Its time constants are 0.5, 1, 2, 4, 8 and 16 sec. The spectrum is recorded on charts (250 x 550 mm) mounted on a rotating drum. The drum rotation times are 8, 16, 32, 64 or 128 min. The maximum time for full side to side movement of the recording pen is 8 and 16 sec.

The monochromator is assembled on an H-beam (height 600 mm, width of shelf 300 mm). The cover of the instrument is welded of sheet iron and reinforced with ribs; it is provided with a rubber gasket and is attached to the H-beam by bolts. The slit widths are varied and the prism monochromator positioned by means of sylphon manipulators. The instrument chamber is evacuated to 10^{-1}-10^{-2} mm Hg

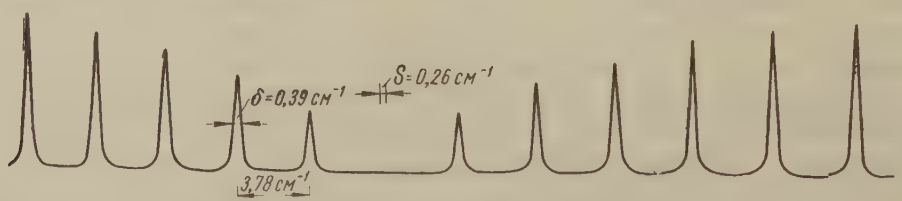

Fig.2. Absorption spectrum of CO in the 4.56 μ region.

by a VN-2 pump. The total weight of the instrument is about 1 ton.

Tests of the instrument showed that the rotation of the grating is realized uniformly and smoothly without jumps or binding. The clear diffraction pattern observed with a narrow slit in the zeroth order is evidence of the high quality of the collimator mirrors of the main monochromator, prepared in the Optical Shop of the Physical Institute of the USSR Academy of Sciences.

The spectra width of the slit in the 1.5 to 5 μ region equals approximately 0.2-0.25 cm^{-1} (with a signal to noise ratio of about 100 and an amplifier time constant of 1 sec). By way of illustration the record of the spectrum of CO in the 4.5 μ region made with a 300 lines/mm grating and a 0.26 cm^{-1} slit is reproduced in Fig.2.

"G.S.Landsberg" Optical Laboratory,
"P.N.Lebedev" Physical Institute,
Academy of Sciences of the USSR

References

1. W.G.Fastie, JOSA, 42, 647 (1952).
2. V.I.Malyshev & S.G.Rautian, Optika i spektroskopiya, 6, 550 (1959). (Trans.Optics & Spectroscopy.)
3. M.N.Markov, Doklady AN SSSR, 108, 428 (1956). Transactions of the Tenth Conference on Spectroscopy, Vol.1, p.403, L'vov, 1957.
4. V.I.Malyshev, M.N.Markov & A.A.Shubin, Doklady AN SSSR, 86, 273 (1952); Izv.AN SSSR, Ser.fiz., 17, 654 (1953).
5. M.N.Markov, Zhur.tekh.fizn., 24, 1867 (1954).

* * * * * * *

THE IKS-12 AND IKS-14 INFRARED SPECTROMETERS

- N.S.Golyandin, I.G.Ptitsyna, I.I.Reshina & I.L.Sakin

These two infrared instruments of domestic manufacture - the IKS-14 spectrophotometer and the IKS-12 spectrometer - are designed for rapid and reasonably accurate recording of absorption spectra.

1. The IKS-14 spectrometer (Fig.1) records the IR absorption spectra of various substances directly in percent transmission. The device may be operated as either a double or a single beam instrument. An operating range from 0.75 to 25 μ is assured by a set of prisms of F-1 glass, LiF, NaCl and KBr.

The spectrum is recorded by a pen on a paper chart, the rate of advance of which can be varied from 0.4 to 100 mm/min. Thus, the spectrum can be recorded

Fig.1. IKS-14 spectrophotometer.

at rates from 0.01 to 1.5 μ.

The instrument operates on the null principle. Radiation from the source (a Silit rod) is divided and directed into two channels. The cell with the test substance is mounted in one channel, while a photometric wedge (weakener) and reference cell are mounted in the other channel. The beams from the two channels alternately (9 cps frequency) enter the monochromator and then fall on the bolometer. The bolometer is connected into a bridge circuit supplied with ~ 2500 cps alternating current; the modulated signal is first amplified at the carrier frequency, and then, after synchronous detection, at a frequency of 9 cps. The synchronous mechanical rectifier is connected at the output of the latter amplifier. The rectified signal is converted into an alternating one with a frequency of 50 cps and controls the output stage of the equipment which is connected to a RD-09 servomotor. This motor moves the pen and actuates the photometric wedge, which serves to nullify the difference between the beam intensities.

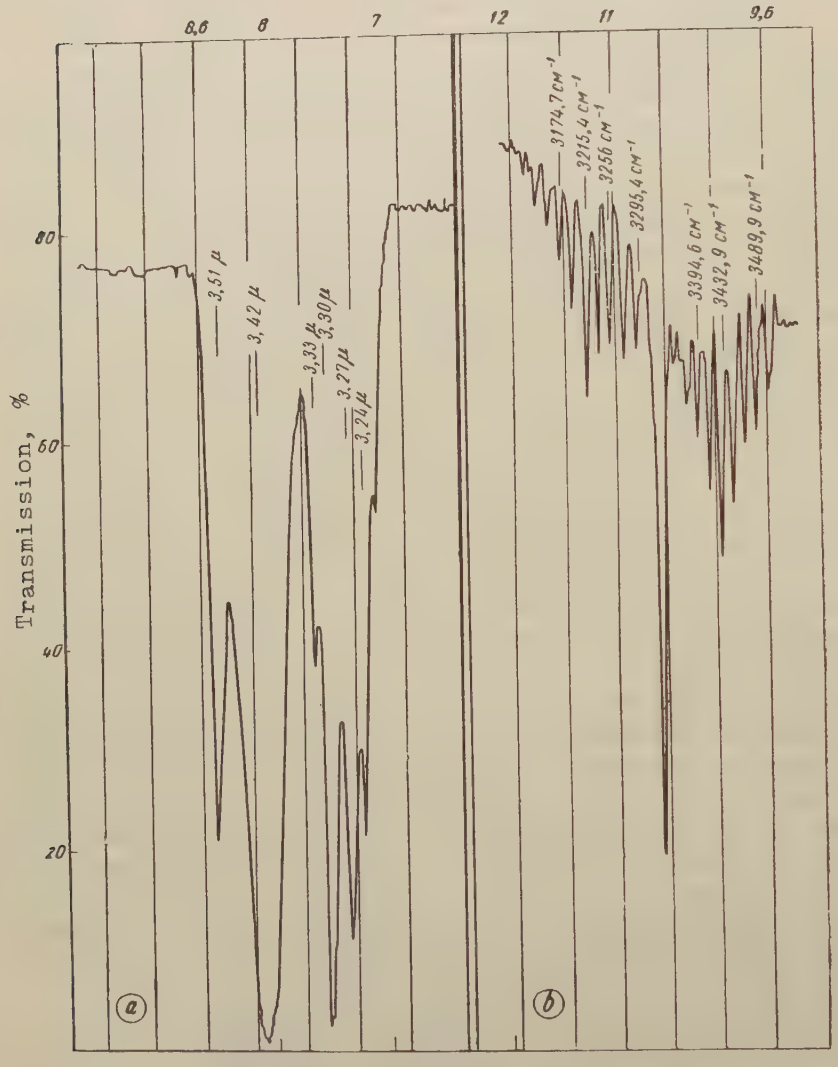

Fig.2. Records made with LiF prism. Each record required 4.7 minutes to cover the range shown: a) polystyrene, 0.05 mm thick, slit width 0.06 mm, trace linear in λ; b) ammonia, p = 200 mm Hg, 0.05 mm slit width, trace linear in λ.

The monochromator of the apparatus employs the autocollimation principle. An off-axis parabolic mirror with f = = 270 mm serves as the collimator. The slit is opened or closed automatically by a cam, assuring a constant radiant energy flux at the monochromator exit. The spectrum can be recorded in either a wavelength or a wave number scale. Appropriate cams are provided for each scale.

The radiation detector is a bismuth vacuum bolometer with a threshold sensitivity of $2\text{-}5\cdot10^{-10}$ w (at Δf = 1 cps).

The instrument is supplied with an assortment of liquid cells with thicknesses ranging from 0.01 to 5 mm and a 125 mm cell for gases.

A test of the apparatus showed that the reproducibility in recording spectra is ± 1%; the calibration reproducibility at a scanning rate of one rotation of the monochromator drum per 4.7 mi is between 0.5 and 1.0 of one of the small division on the drum, which corresponds to 1.0 to 1.5 cm^{-1} with the NaCl prism.

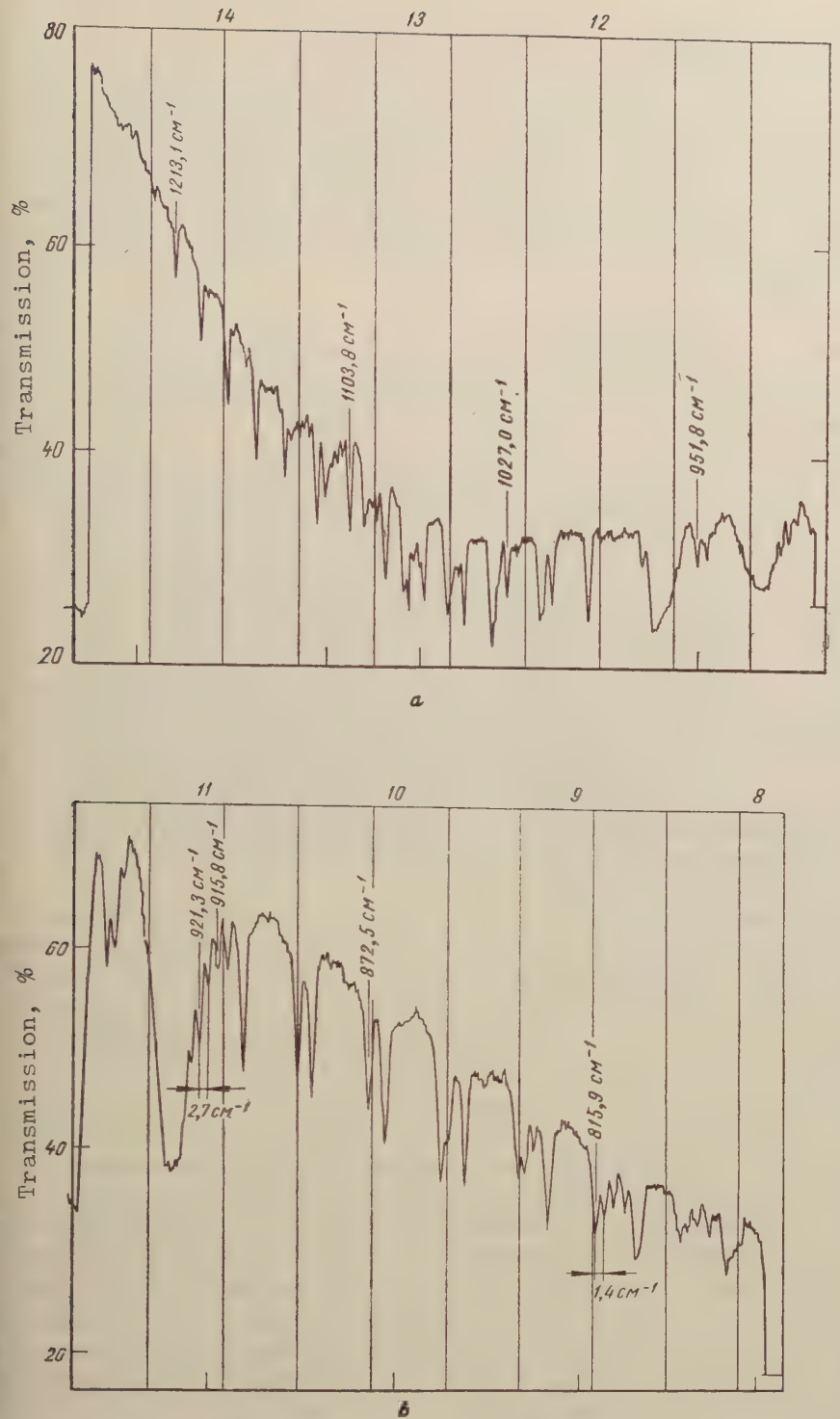

Fig.3. Record made with NaCl prism. Scanning time - 8 minutes per interval. Ammonia, p = 70 mm Hg, l = = 176 mm; slit widths: a) 0.075 mm, and b) 0.012 mm.

The amount of scattered light amounts to about 5% over the entire operating range when working with matte mirrors[1].

The resolution of the spectrophotometer with the NaCl prism is 3-4 cm^{-1} in the 950 cm^{-1} region at a recording rate of 0.16 μ/min.

Records of the absorption spectra of polystyrene and ammonia made with the LiF prism are reproduced in Fig.2.

2. The IKS-12 infrared spectrometer is a modernization of the IKS-11 apparatus[3] and has been in batch production since 1957.

A Silit rod is used as the source; this is superior to the Nernst glower as regards service life and does not require preheating.

Amplification is provided by a two-stage FEOU-18 photoelectro-optical amplifier (sensitivity $0.6\text{-}1.0\cdot10^{-9}$ w/mm; linearity ± 1%). The spectra are recorded by an EPP-09 electronic recording voltmeter. The overall sensitivity of the detecting-amplifying circuit is $4\cdot10^{-10}$ w/mm.

The illuminator, monochromator and cell section are of airtight design, so that the entire apparatus can be purged with dry air or nitrogen to eliminate the absorption bands due to atmospheric moisture and carbon dioxide.

To increase the resolving power of the instrument, additional scanning speeds have been provided in the new model; these correspond to 30 and 15 min per rotation of the monochromator drum. To minimize light scattering, inter-

changeable matte mirrors are used in the illuminator, and an LiF plate is employed as the temperature compensator mirror when using the KBr prism.

A test of the IKS-12 spectrometer showed that the reproducibility of transmission measurements is ± 0.5%. The amount of light scattered when working with matte mirrors does not exceed 4%. The resolution of the spectrometer with the NaCl prism is 1.4 cm^{-1} in the 800 cm^{-1} region (Fig.3). The residual absorption due to atmospheric moisture and carbon dioxide (when the apparatus was dried by the circulation procedure using caustic soda and activated alumina as the absorbers) did not exceed 5-6%.

References

1. I.G.Ptitsyna, I.I.Reshina & L.V.Smirnova, Optikomekhanicheskaya promyshlennost' (Optical-mechanical industry), 4, 16 (1957).

2. I.I.Reshina & N.I.Ivanova, Ibid., 5, 6 (1958).

3. L.V.Smirnova, Ivz.AN SSSR, Ser.fiz., 19, 52 (1955). (Trans.Bulletin 19, No.1, 48.)

* * * * * * *

INFRARED VACUUM SPECTROMETER FOR INDUSTRIAL CONTROL AND DETERMINATION OF OIL IN PETROLEUM PRODUCTS BY ABSORPTION SPECTROMETRY

- A.F.Mal'nev & G.A.Puchkovskaya

We developed a vacuum infrared spectrometer - designated VIKS-4 - for analytic work with reference to absorption spectra. The apparatus consists of a Littrow mounting monochromator and measuring equipment.

The optical system of the spectrometer is illustrated in Fig.1. Infrared radiation from the source is interrupted at a frequency of 20 cps and, after passing through the test substance, falls on the entrance slit of the monochromator. A nickel bolometer[1] is used to detect the radiation. The bolometer output signal is amplified by a transformer and amplifier and then applied to the indicator. Virtually no zero drift was observed despite the fact that the equipment was tested under very unfavorable temperature conditions.

The instrument employs spherical mirrors. The monochromator is located inside a metal cylinder with 10 mm thick walls. The preamplifier is suspended in a shock-absorber mount under the optical bench of the monochromator. The metal cylinder serves simultaneously to maintain a constant pressure inside the monochromator and to protect the preamplifier and transformer against electric interference. The design of the equipment allows of locating the bolometer at a distance of 5-6 cm from the preamplifier which significantly reduced stray induction

The prisms are positioned and the slits are opened or closed by means of cams set on the axis of the graduated circle. There is virtually no backlash or lost motion. A general view of the equipment is shown in Fig.2.

A procedure was developed for determining the oil content of petroleum products by means of the described equipment; this procedure effected a significant reduction in the time required for analysis. The procedure is based on measuring the relative absorption of the test substance in the 7.3 μ region. This band corresponds to symmetrical deformation vibrations of the methyl group, CH_3.

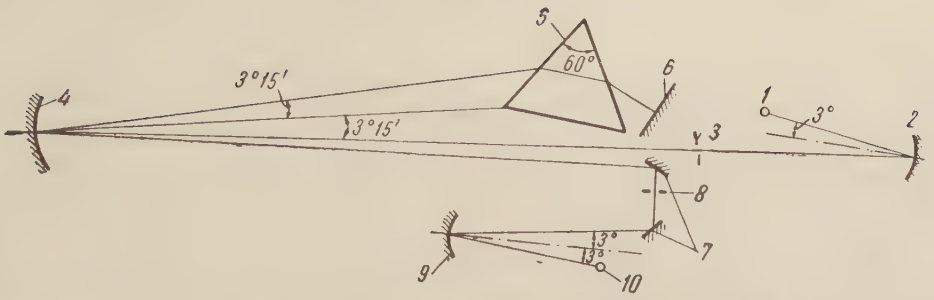

Fig.1. Optical system of the spectrometer: 1) source, 2, 4 & 9) spherical mirrors, 3) entrance slit, 5) prism, 6 & 7) plane mirrors, 8) exit slit, 10) bolometer.

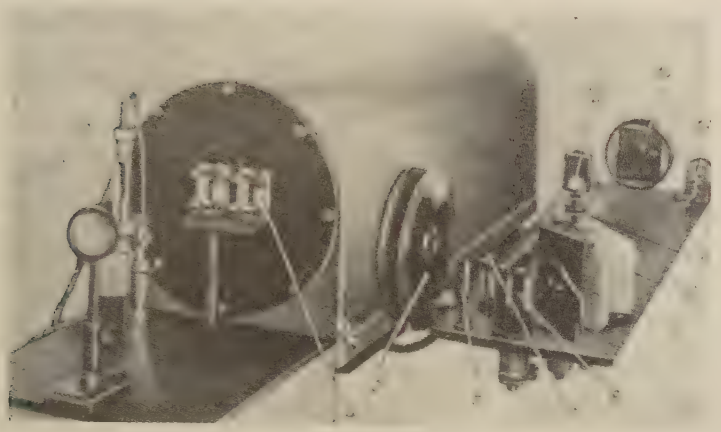

Fig.2. Spectrometer and optical bench: 1) source, 2) modulator, 3, 12 & 14) spherical mirrors, 4) cells, 5) graduated circle, 6 & 9) plane mirrors, 7) exit slit, 8) entrance slit, 10) prism, 11) bolometer, 13) terminal panel.

The percent content of oil in petroleum products was determined from a working curve plotted on the basis of measurements of the relative absorption in the 7.3 μ region of petroleum products containing known oil concentrations. The absorption by the samples was measured with reference to a standard filtrate containing 97% oil. Cells with rock salt windows were used in this work. The ± 0.5% accuracy attained with the procedure is adequate for interdepartmental control of petroleum products. The equipment was constructed in the laboratory of a petroleum plant in the Western Ukraine.

References

1. A.F.Mal'nev, Trudy X Vsesoyuznogo soveshchaniya po spektroskopii (Transactions of the Tenth All-Union Conference on Spectroscopy), Vol. 1, p. 305. L'vov, 1957.

MEASURING ATTACHMENT FOR INFRARED SPECTROMETERS

- A.F.Mal'nev, M.P.Esel'son & L.S.Kremenchugskii

There has been a growing tendency to use infrared spectrometers in chemical and petroleum plants for automating periodic or continuous control of technological processes and also for research work in plant laboratories. Detecting and measuring devices used in conjunction with infrared spectrometers must meet exacting requirements as regards reliability, stability of operation and compactness.

The measuring device developed by us consists of a bolometer bridge, a preamplifier, a main amplifier with a synchronous detector, a generator-modulator with a phase shifter and a power supply unit.

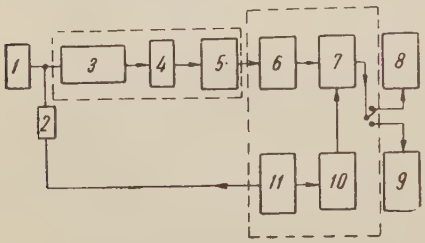

Block diagram of the measuring attachment.

Radiation from the source 1 (see figure), is interrupted at a frequency of 20 cps by the modulator 2 and, after passing through the monochromator 3, falls on the detector 4, which is a nickel bolometer developed in the Physical Institute of the Ukrainian Academy of Sciences.[1] The bolometer forms part of a balanced disparate arm bridge. The bridge arm ratios are such that the transfer constant is 0.75. The primary of a step-up transformer (k_{tr} = 1000) is connected into the bridge diagonal; the transformer is tuned to the 20 cps modulation frequency and has a 2 cps passband. The preamplifier 5 employs a "floating grid" circuit[2] and is enclosed in an inner copper and outer Permalloy housing, which can be located either inside the spectrometer or outside it.

The main amplifier unit consists of a resistor-coupled amplifier 6, a synchronous detector 7, a phase shifter 10 and a generator-modulator 11. The radiation from the source is interrupted by a vibration modulator* 2 assembled about an RP-4 relay which is supplied from the generator-modulator. A reference voltage taken off the same generator is supplied to the synchronous detector through the variable phase shifter 10, which provides the necessary phase relation between the bolometer signal and the reference voltage. By varying the time constant of the filter at the detector output one can provide the necessary passband for the entire measuring device. The output signal can be recorded either by means of the automatic recorder 9 or viewed on the screen of the oscillograph 8.

After a half-hour warm up, the amplification factor of the system does not vary more than 0.5% during the period of a full working day, while the zero drift is virtually nil.

The developed measuring attachment has been used for research work in conjunction with a VIKS-M3 spectrometer and for periodic technological control in conjunction with a VIKS-M4 spectrometer. (Both these spectrometers were developed in the Physical Institute of the Ukrainian SSR Academy of Sciences.)

Use of the VIKS-M4 vacuum infrared spectrometer as the dispersing component made it possible to solve the problem of determining oil in paraffins[3] and that of determining the concentration of ethylene in mixtures of methane, ethane and ethylene.[4]

---

*Developed in collaboration with S.Z.Shul'ga.

References

1. A.F.Mal'nev, Transactions of the Tenth All-Union Conference on Spectroscopy, Vol.1, p.405, L'vov, 1957.

2. V.I.Dianov-Klokov, A.D.Stakhovskii & L.A.Osterman, Izmerit. tekhnika (Measurement techniques), No.2, 37 (1957).

3. A.F.Mal'nev & G.A.Puchkovskaya, Ukr.fiz.zh. (Ukrainian Phys.Journal), 3, 783 (1958).

4. A.F.Mal'nev, L.S.Kremenchugskii, I.P.Dmitrenko, M.P.Esel'son & V.N. Vatulev, Inzh.-fiz.zh., (Engineering-Physics Journal), 1, 104 (1958).

* * * * * * *

NEW EQUIPMENT AND PROCEDURES FOR STUDY OF THE SPECTRA OF REFLECTION FROM THE EARTH'S SURFACE

- K.S.Lyalikov, I.N.Belonogova, K.E.Meleshko, I.V.Semenchenko and A.P.Kharchenko

Development of spectrozonal aerophotography and other advances in this field have made it essential to develop convenient equipment and procedures for investigation of the spectral brightness of ground objects. In addition to the use of procedures of visual and photographic spectrophotometry, there were developed in the Aeromethods Laboratory of the USSR Academy of Sciences two types of photoelectric instruments. For ground investigations, A.P.Kharchenko built a photoelectric spectrophotometer which is intended for use under field conditions. Field tests in 1958 showed that this instrument yields reliable measurements of the spectral brightness in the wavelength range from 400 to 1000 mμ. For investigation of spectral brightness from aircraft Meleshko & Semenchenko built a single-beam photoelectric high-speed spectrophotometer with recording by means of a cathode-ray tube. It allows of recording the spectral brightness curve in the range from 450 to 900 mμ for the reflection of ground objects from an aircraft within an interval of 10^{-2} sec. Flight tests in 1958 showed that the instrument operates reliably both in airplanes and helicopters. The fact that a large number of spectral brightness curves were recorded in a very short period made it necessary to develop a special statistical procedure for processing the results. In 1958 the instrument was used for obtaining the spectral characteristics of a number of ground objects in the southern region of the European part of the USSR.

ON THE FEASIBILITY OF MOLECULAR SPECTROSCOPIC ANALYSIS OF VAPORS IN A WIDE TEMPERATURE RANGE

- A.V. Suvurov, S.A. Shukarev & G.I. Novikov

In order to study the equilibrium of complex systems over a wide temperature range, it is necessary to have an adequately simple and reliable method for determining the fractional composition of the gaseous phase. One feasible method is spectrum analysis in the visible or near ultraviolet regions. The use of infrared spectra for analytical purposes is complicated by the strong influence of temperature. On the other hand, the energy of the quanta in the ultraviolet region is so high that they can produce undesirable photochemical reactions in the system under study.

The spectroscopic technique by itself is insufficient for the study of equilibria in complex systems, since, in addition to determining the partial pressures of the individual components, it is essential to know the total pressure in the system. Any static pressure gage can be used for this purpose, but it is most convenient to employ a diaphragm null-manometer, which can readily be combined with the optical cell into a single unit.

Use of the Lambert-Beer law for absorption analysis in the case of vapors is made difficult by the effect of temperature, on the one hand, and the effect of pressure, on the other. Actually, the influence of pressure becomes significant effect only when studying narrow well-resolved bands; in working with vapors of comparatively complex inorganic compounds of the $FeCl_3$ or WCl_6 type, characterized by continuous absorption spectra, changing the total pressure from 10-15 mm Hg to 1-2 atm has virtually no noticeable effect on the measured absorption.

A change in temperature, on the other hand, has a much greater effect on the absorption. However, the quantitative temperature dependence of the absorption of vapors has not been determined until now.

We made the attempt to evaluate this dependence empirically, making use of an apparatus in which the optical cell was combined with a diaphragm null-manometer; thus we were able to determine both the optical density of the vapor and the total pressure in the system.

It was shown for unsaturated iodine vapor, that the optical density at the long wavelength edge of the absorption band increases linearly with temperature (Figs.1 and 2).[1] Since the concentration remains constant, we have essentially an

Fig.1

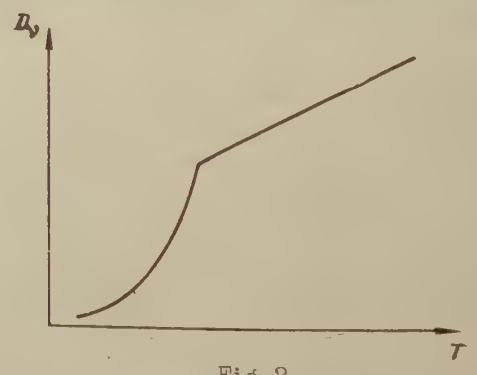

Fig.2

Fig.1. Variation in the absorption of iodine vapor at different temperatures.
Fig.2. Variation in the optical density of iodine vapor with temperature (schematic).

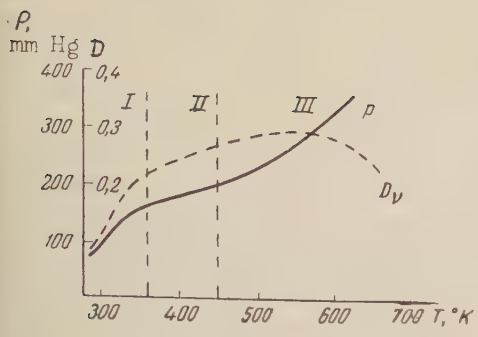

Fig.3. Variation in pressure and optical density in the N_2O_4-NO_2-NO-O_2 system with temperature.

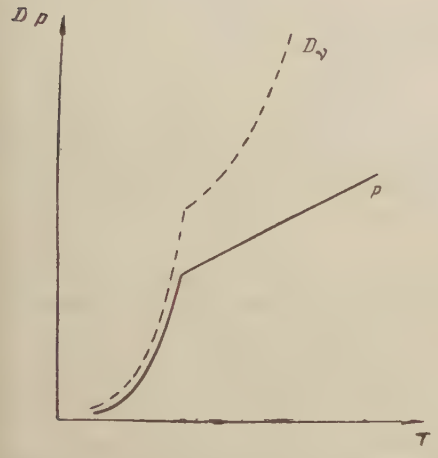

Fig.4. Variation in pressure and optical density in the $WOCl_4$-WCl_6-WO_2Cl_2 system (schematic).

increase of the absorption coefficient; specifically, a very simple dependence is obtained, namely,

$$K_\nu = \varkappa_\nu T,$$

where $\varkappa_\nu$ is a temperature-independent quantity.

The N_2O_4-NO_2-NO-O_2 system, which has been described in detail in the literature[1], was studied to confirm the above dependence. We concurrently measured the optical density at one of the minima between the absorption bands and the total pressure over the 18 to 480°C temperature range.

Three temperature regions can be distinguished in the system under consideration (Fig.3): I) 18 to 100°C, characterized by $N_2O_4 = 2NO_2$ equilibrium, II) 100 to 200°C, the region of existence of pure NO_2; and III) 200 to 480°C, the range of $2NO_2 = 2NO + O_2$ equilibrium.

Since the only colored compound in the nitrogen oxides system is NO_2, knowing the pressure and optical density in the 100-200°C range, it is easy to find the NO_2 absorption coefficient. Moreover, knowing the total pressure at other temperatures, we can compute the amount of NO_2 in equilibrium with N_2O_4 or NO, as the case may be, and, consequently, find the NO_2 absorption coefficient over the entire temperature range from 18 to 480°C.

Since it is easier to use the concept of pressure, rather than concentration, in working with gases and vapors, we can rewrite the Lambert-Beer law for the case of ideal gases in the form:

$$D_\nu = K_\nu p \frac{d}{RT},$$

and, since we assume that $K_\nu = \varkappa_\nu T$, we obtain

$$D_\nu = \varkappa_\nu p \frac{d}{R} \text{ or } \varkappa_\nu = \frac{D_\nu}{p} \frac{R}{d}.$$

Our experiments showed that the magnitude of $\varkappa_\nu$ remains constant, within the limits of the experimental error, over the entire temperature and pressure ranges; specifically, we found $\varkappa_{5575} = 0.0194 \pm 0.0002$.

It is apparent that the $K = \varkappa T$ relationship is not rigorous; actually, the right-hand quantity is the first term in an expansion of some complex function; nevertheless, the relationship can be used for practical purposes.

At the present time, we are studying a number of complex gaseous systems by the optical-tensiometric method. These are WCl_6-WCl_5-Cl_2, $WOCl_4$-WO_2Cl_2-WCl_6-Cl_2, and WO_2Cl_2-WO_3-$WOCl_4$-WCl_6-Cl_2.

The process $2(WOCl_4)_{gas} = (WO_2Cl_2)_{gas} + (WCl_6)_{gas}$ is of particular interest.

Having measured the absorption coefficients of the $WOCl_4$ and WCl_6 vapors (WO_2Cl_2 is colorless), it is easy to find the fractional composition of the system and the thermodynamic characteristics of the process (Fig.4); this cannot be done solely on the basis of pressure data, since this process takes place without volume change.

In conclusion, it should be emphasized that the data we obtained on the temperature dependence of absorption coefficients is completely empirical. Theo-

retical interpretation of these data could be very important for further development of spectrum analysis of vapors.

Chemical Faculty,
"A. A. Zhdanov" Leningrad State University

References

1. S.A. Shchukarev, G.I. Novikov & A.V. Suvorov, Zhur.Neorgan.Khim. (J. Inorganic Chem.), 1, 2433 (1956).

* * * * * * *

ABSORPTION SPECTRA OF INDAN SERIES HYDROCARBONS IN THE NEAR ULTRAVIOLET

- M.M. Kusakov & M.V. Shishkina

Indan and its methylated homologs have recently been found in a number of fractions from different petroleum crudes on the basis of the infrared absorption and Raman spectra.[1-3] Electronic absorption spectra can also be used for identifying indan hydrocarbons in petroleum fractions; however, the electronic spectra are known only for a few methyl- and dimethylindans[4].

In connection with the need to obtain a more complete characterization of indan homologs that might be present in both the gasoline-ligroin and kerosene fractions, a program for synthesizing hydrocarbons of the indan series containing one, two or three substituents of different structure was undertaken at the Laboratory for Petroleum Chemistry of the Institute for Petrochemical Synthesis at the Academy of Sciences of the USSR[5,6].

The absorption spectra of isooctane solutions of indan and fourteen of its derivatives were measured on a photoelectric spectrophotometer.

The spectrum recorded for indan was virtually identical with the indan spectrum given by Friedel & Archin[7]. The spectra of the indan derivatives are not described in the literature.

The absorption spectra of ethyl-, isopropyl-, isobutyl-, tertiary butyl-, isoamyl-, and 2-ethylhexylindan are similar. The absorption band peaks are located at the same wavelengths: 2765, 2710, 2680 and 2630 Å. This indicates that all the enumerated indans have the same type of substitution and that the character of the spectrum, as in the case of alkylbenzenes, hardly depends on the structure of the substituent, provided this is saturated.[8]

It is known from the conditions of synthesis that the substituent group is located in the benzene ring. It was established by comparing the spectra of the monoalkylindans with the corresponding spectra of methylindans[4], that the substituent group occupies the 5 position.

The absorption spectrum of cyclopentylindan is shifted somewhat (10-15 Å) to the longer wavelength side as compared to the spectrum of 5-alkylindans; however, this shift is caused by the naphthenic nature of this substituent[9]. Consequently, there is reason to believe that the cyclopentyl group is also located at the 5 position in this compound.

The spectra of 2-hexylindan and isobutylindan are different in character from the spectra of the preceding compounds, and they almost coincide with the spectrum of 1-methylindan (absorption peaks at 2735, 2665, 2605 and 2545 Å). Thus, the side chain of these alkylindans is located at position 1 in the five-membered ring.

We also obtained the spectra of disubstituted indans containing ethyl, isopropyl and isobutyl groups in the benzene ring. The relative intensities and positions of the absorption peaks are nearly the same in the spectra of these hydrocarbons; this indicates that their structures are similar. Since there are no spectra available for the corresponding dimethylindans, it is not possible to establish the substitution position. It is most probable that the substituents in these compounds are located at the 5,7 or 4,6 atoms in the indan molecule.

Of the trisubstituted indans, we studied the absorption of tri-isopropyl- and tricyclohexylindan. The absorption spectra of these indan derivatives agree completely; the wavelength of the absorption band peak in both spectra is the same (2700 Å); moreover, the spectra are similar in character to the spectra of penta-substituted benzenes. In view of this, we infer that all three of the substituent groups are located in the benzene ring.

Thus, our study of fourteen indan homologs containing one, two, or three substituent groups showed that the distribution of intensity in the absorption bands does not depend on the structure of the substituent groups but is determined only by their number and position in the indan molecule. Hence we can establish the general molecular structure (number and position of substituents) of indan hydrocarbons on the basis of the known spectra of the simpler homologs.

Investigation of the absorption spectra of individual indan hydrocarbons also allows of evaluating the possibility of finding indan hydrocarbons in aromatic petroleum fractions by means of ultraviolet spectroscopy.

Institute for Petrochemical Synthesis,
Academy of Sciences of the USSR

References

1. A.F.Plate, in "Sostav i svoistva neftei i benzino-kerosinovykh fraktsii" (Collected articles on the "Composition and properties of petroleum and of the gasoline-kerosene fraction"), 217, M.1957.

2. A.V.Topchiev, I.A.Musaev, A.N.Kislinskii & G.D.Gal'pern, Ibid., 252.

3. R.B.Williams, S.H.Hastings & G.A.Anderson, Anal.Chem., 24, 1911 (1952).

4. J.Entel, C.H.Rouf & H.S.Howard, Ibid., 25, 1303 (1953).

5. A.V.Topchiev, E.S.Pokrovskaya & T.G.Stepantseva, Doklady AN SSSR, 119, 1164 (1958). (Trans.Doklady.)

6. E.S.Pokrovskaya, Trudy In-ta Nefti AN SSSR, (Proceedings of the Petroleum Institute of the Ac.of Sci. USSR), 16, 29 (1959).

7. R.A.Friedel & M.Orchin, Ultraviolet Spectra of Aromatic Compounds, N.Y., 1951.

8. M.M.Kusakov, S.S.Nivontova, E.S.Pokrovskaya, L.M.Rozenberg, A.V.Topchiev & M.V.Shishkina, "Materialy X Vsesoyuznogo soveschaniya po spektroskopii" (Transactions of the Tenth All-Union Conference on Spectroscopy), Vol.1, 321. L'vov, 1957.

9. G.D.Gal'pern, M.M.Kusakov, E.S.Pokrovskaya, B.A.Smirnov, N.A.Shimanko & M.V.Shishkina, Ibid., 334.

INVESTIGATION OF RADIOLYSIS OF ALKANES BY ULTRAVIOLET AND INFRARED SPECTROSCOPY

- I.Ya.Kachkurova, L.S.Polak, A.V.Topchiev & N.Ya.Chernyak

Radiolysis of alkanes involves rupture of the C-C and C-H bonds; in the case of irradiation in the gaseous phase, there form hydrogen (80-95%) and different hydrocarbon gases (CH_4, C_2H_6, etc.). The splitting off of atomic hydrogen leads to the formation of C_nH_{2n+1} type radicals, which then enter into further reactions; the splitting off of an H_2 molecule leads to formation of olefins, and the splitting off of $2H_2$ leads to formation of dienes and polyenes, which then actively polymerize.

In view of the difficulties of chemical determination of the liquid radiolysis products, the content of which does not exceed 0.1-1.0% in irradiated alkanes, the only practical procedure for investigating them proved to be absorption spectroscopy.

We chose heptane and a number of other normal hydrocarbons for our study. The samples were irradiated with Co^{60} γ-rays in evacuated, outgassed and sealed tubes; after irradiation the tubes were opened and the gaseous and liquid phases analyzed separately. The absorption spectra were measured in the Optical Laboratories of the INÉOS: the ultraviolet spectra on a "spectrovizor" (a spectrophotometer with automatic recording by an SF-4 unit) and the infrared spectra on a VIKS-11 spectrometer with automatic recording. Examination of the absorption spectra of the liquid phase radiolysis products in the 25 000-45 000 cm^{-1} region enabled us to detect the presence of conjugated systems, while the IR spectra (700-2000 cm^{-1} region) served to establish the structure of the compounds obtained as a result of radiolysis.

The UV spectra of the irradiated normal hydrocarbons are presented in Fig. 1. Absorption in this region can be attributed only to diene and polyene systems. It is characteristic that the spectra of irradiated hexane, heptane and octane are similar in the 35-40·10^3 cm^{-1} region, while the absorption increases significantly in the spectra of alkanes having longer chains.

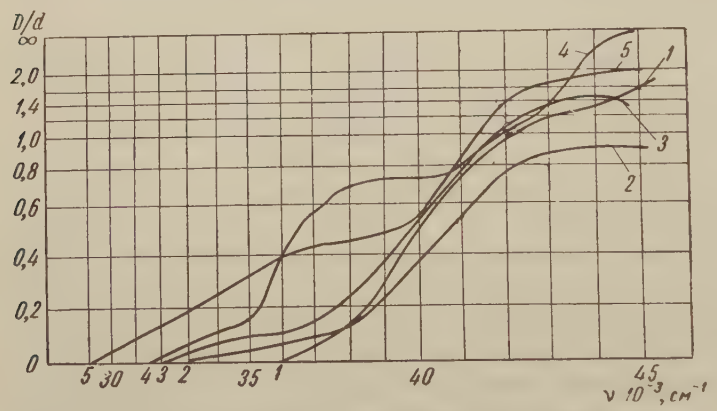

Fig.1. UV absorption spectra of irradiated hydrocarbons: 1) hexane, dose 34·10^6 r, dilution 1:2 (with iso-octane); 2) heptane, 99·10^6 r, 1:10; 3) octane, 40·10^6 r, 1:5; 4) dodecane, 40·10^6 r, 1:10; 5) cetane, 40·10^6 r, 1:15. The thickness d of the absorbing layer was 0.5 cm.

The variation of the absorption in the 38-44·10^3 cm^{-1} region with the hydrocarbon chain length is shown in Fig.2,a. This absorption increases linearly over the range from C_6 to C_{12}, which indicates increasing probability for splitting off of a hydrogen molecule as the number of $-CH_2-$ groups increases.

The UV absorption intensity of the irradiated hydrocarbons increases linearly with the radiation dose (checked for doses up to ~150·10^6 r on heptane, see Fig.2,b); consequently, the number of double bonds formed is directly proportional to the radiation dose. As is to be expected, the plot passes through the origin for zero radiation dose.

The general character of the UV spectra does not change as the temperature at which the alkanes are irradiated is reduced; however, the overall absorption intensity increases with decreasing temperature (Fig.3).

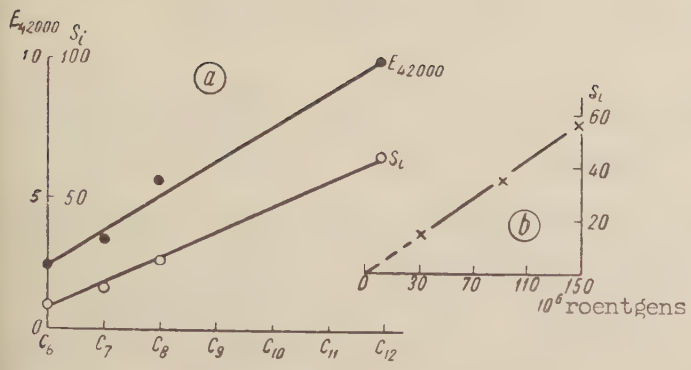

Fig.2. a - Variation of the absorption intensity with the molecular composition of irradiated hydrocarbons (E_{42000} is the absorption intensity at 42000 cm^{-1}; S_i is the area bounded by the absorption curve, the ordinates at 38000 and 44000 cm^{-1}, and the horizontal axis, which was taken as the zero line for the non-irradiated alkane). b - Variation of the absorption of heptane with the radiation dose.

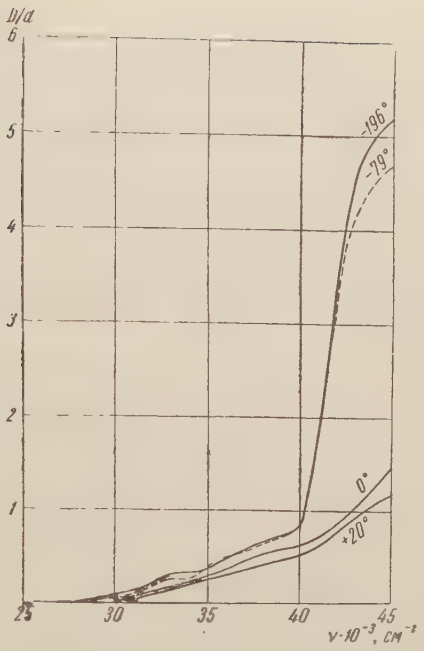

Fig.3. UV absorption spectrum for cetane irradiated at different temperatures (radiation dose = $1 \cdot 10^7$ r).

Although cetane is solid at 0°C (its solidification temperature is 16°), its absorption hardly varies as compared with that of the products of its radiolysis in the liquid phase at 24°C. The absorption in the 40 000-45 000 cm^{-1} region, however, increases fourfold for irradiation temperatures of -80° and -200° as compared with the absorption for room temperature, while the corresponding absorption increase in the $30\text{-}40 \cdot 10^3$ cm^{-1} region is 40%; i.e., absorption by polyenes increases more slowly than does that of dienes. The absorption is practically constant over the irradiation temperature range from -80° to -200°. As was shown by experiments on a number of hydrocarbons, this is due to the fact that a temperature some 60-70° below the solidification point is sufficiently low for the probability for internal rearrangements of the radiation excited molecules to form dienes to be significantly increased as compared to the probability for scattering of the excitation energy (by collisions, etc.). Consequently, further reduction of temperature (i.e., down to -200°) does not noticeably enhance the irradiation effects.

The heptadiene we synthesized absorbed in the same region as irradiated heptane, and its properties agreed with those of the corresponding fraction of the radiolysis products; this fully substantiates our interpretation of the UV spectra of irradiated heptane. Having determined the absorption coefficient of heptadiene (26 000 at 44 000 cm^{-1}), we were able to calculate from the spectra the molar concentration of the dienes formed during γ-irradiation of heptane; this was found to be $3.5 \cdot 10^4$ gram moles per liter (for a radiation dose of $\sim 10^8$ r).

As regards the IR spectra, we note that a band appears at 965-970 cm^{-1} in the spectrum of irradiated heptane; this corresponds to non-planar stretching vibrations of the =CH- group associated with the trans di-substituted double bond.

Institute of Petrochemical Synthesis,
Academy of Sciences of the USSR

INVESTIGATION OF THE AROMATIC PORTION OF THE KEROSENE-GAS OIL FRACTION OF DOLINSK PETROLEUM BY OBSERVATION OF THE ULTRAVIOLET ABSORPTION SPECTRA

- V.T.Sklyar & A.P.Lizogub

The aromatic hydrocarbons extracted from Dolinsk petroleum (Western Ukraine) were distilled into narrow fractions. In most cases, the boiling point range of the fraction did not exceed 2-5°, and the range of the index of refraction was from 0.001 to 0.01 (see Fig.1).

The ultraviolet absorption spectra of the fractions dissolved in isooctane were first photographed by means of an ISP-22 spectrograph. Fractions in whose spectra the positions of the peaks were different, were then photometered on an SF-4 spectrophotometer. As a result, curves were plotted in which the optical density E of a one percent solution in a 1 cm thick layer was taken as the ordinate unit.[1]

The spectrograms of fractions containing benzene homologs were deciphered by the method developed by Topchiev, Kusakov et al[2,3], to which the position of the absorption peaks remains unchanged in the spectra of alkylbenzenes with substitution of a given type[4].

The spectra of 124 fractions containing monocyclic aromatic hydrocarbons were studied. Several spectra are presented in Fig.2 (also see table).

It was found that all the fractions, regardless of their physical-chemical characteristics contain the following hydrocarbon groups: monoalkylbenzenes (evinced by the humps at 256 and 260 mμ), para- and meta-disubstituted benzenes (peaks at 265 and 273 mμ), trialkylbenzenes, especially the 1,2,3- and 1,3,5- types, (shoulders or peaks at 262 and 268 mμ), and tetraalkylbenzenes having all three types of substitution (shoulder or peak at 277.5 mμ).

Examination of the Raman spectra of the two fractions containing monocyclic aromatic hydrocarbons boiling over the 200-225° and 225-250° ranges, showed the presence therein of monoalkylbenzenes, 1,3- and 1,4-dialkylbenzenes, 1,2,4- and 1,3,5-trialkylbenzenes, and 1,2,3,5-tetraalkylbenzenes; this generally agrees with the data based on the ultraviolet absorption spectra.

The fractions containing condensed aromatic hydrocarbons were also subjected to detailed study. More than two hundred narrow fractions containing condensed

Characteristics of fractions separated from Dolinsk crude and subjected to UV spectroanalysis

Fraction No.	Boiling range, °C	n_D^{20}	Fraction No.	Boiling range, °C	n_D^{20}
1	200÷225	1,4703	*14*	194÷195	1,4795
2		1,5052	*15*	200÷201	1,4772
3		1,5107	*16*	203÷204	1,4719
4	225÷250	1,5092	*17*	200÷225	1,5640*
5		1,5203	*18*	225÷250	1,5981
6	250÷275	1,5130	*19*	259÷261	1,5797
7		1,5160	*20*	277÷279	1,5765
8	275÷300	1,5190	*21*	277÷280	1,5980
9	300÷325	1,5081	*22*	303÷309	1,5961
10		1,5103	*23*	321÷328	1,5680
11	325÷350	1,5117	*24*	341÷349	1,6068
12		1,5262	*25*	341÷348	1,6057
13	350÷375	1,5205	*26*	365÷370	1,6276

* At 80°.

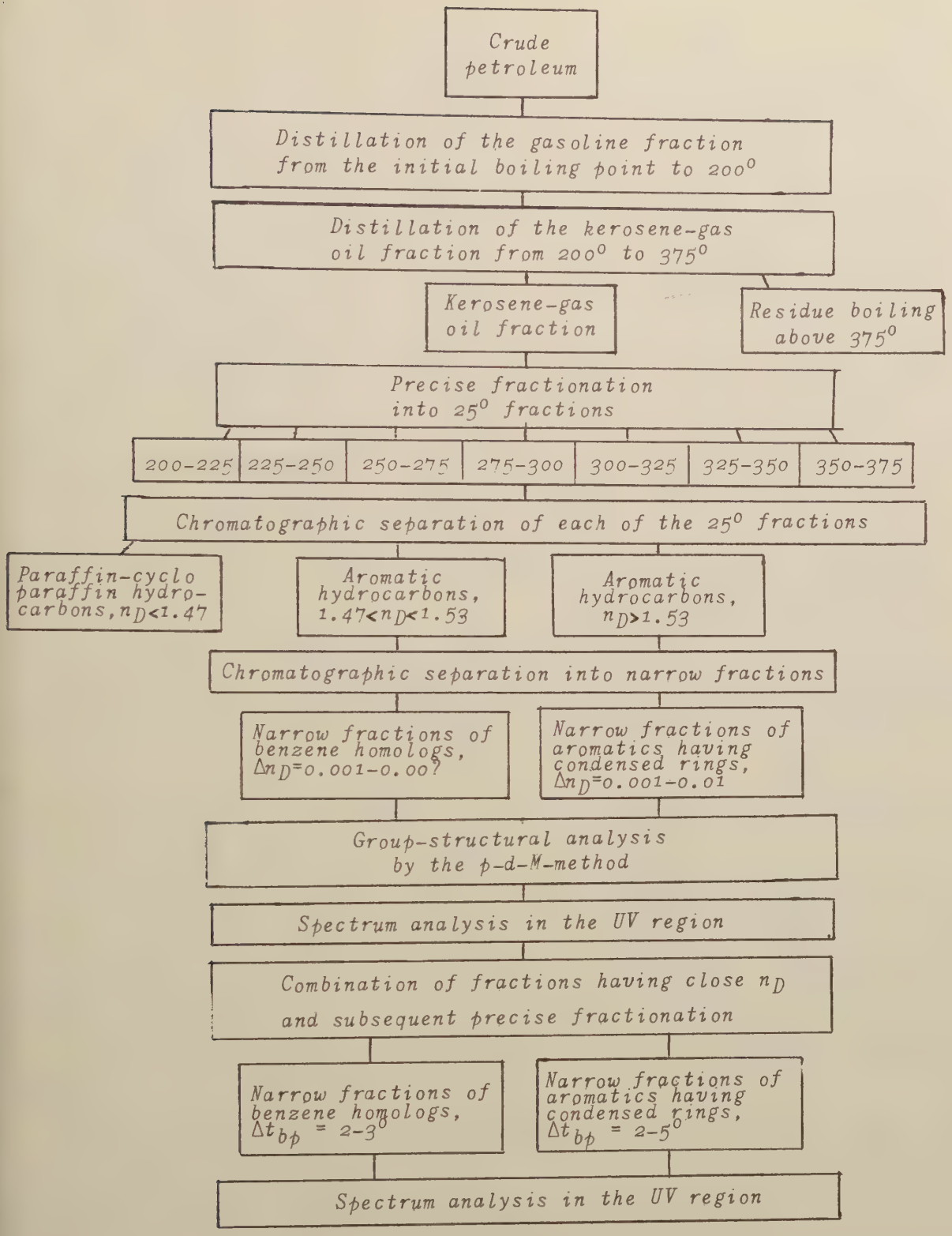
Crude petroleum
Distillation of the gasoline fraction from the initial boiling point to 200°
Distillation of the kerosene-gas oil fraction from 200° to 375°
Kerosene-gas oil fraction
Residue boiling above 375°
Precise fractionation into 25° fractions
200-225
225-250
250-275
275-300
300-325
325-350
350-375
Chromatographic separation of each of the 25° fractions
Paraffin-cyclo paraffin hydro-carbons, $n_D<1.47$
Aromatic hydrocarbons, $1.47<n_D<1.53$
Aromatic hydrocarbons, $n_D>1.53$
Chromatographic separation into narrow fractions
Narrow fractions of benzene homologs, $\Delta n_D=0.001-0.00?$
Narrow fractions of aromatics having condensed rings, $\Delta n_D=0.001-0.01$
Group-structural analysis by the p-d-M-method
Spectrum analysis in the UV region
Combination of fractions having close n_D and subsequent precise fractionation
Narrow fractions of benzene homologs, $\Delta t_{bp} = 2-3^0$
Narrow fractions of aromatics having condensed rings, $\Delta t_{bp} = 2-5^0$
Spectrum analysis in the UV region

Fig.1. Program of investigation of the aromatic hydrocarbons from Dolinsk crude.

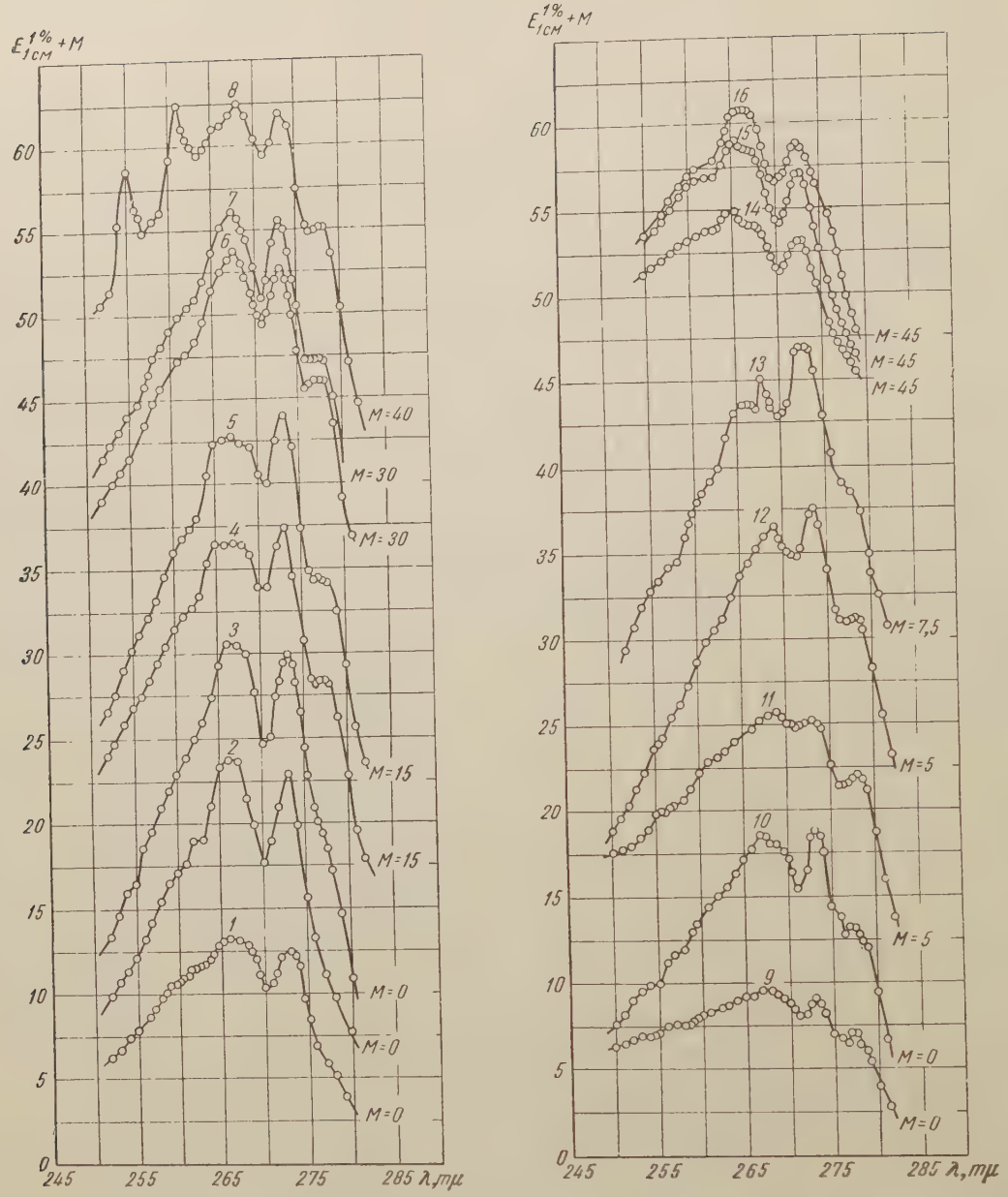

Fig.2. Absorption spectra of petroleum fractions. The numbers at the curves identify the fractions as listed in the table.

aromatic hydrocarbons were obtained from the kerosene-gas oil fraction of the petroleum by means of repeated precise vacuum fractionation and chromatographic separation.

A study of the absorption spectra of these fractions in the near ultraviolet region showed that in most cases there are evident exceptionally well-defined absorption bands characteristic of definite structures of condensed aromatic hydrocarbons or their mixtures.

Fig.3 shows the presence of naphthalene and its homologs (curves 17-23), phenanthrene (curves 24-25), and dimethylphenanthrene (curve 26). Among the homologs of naphthalene we detected: α- and β-alkylnaphthalenes; 1,2-, 1,3-,

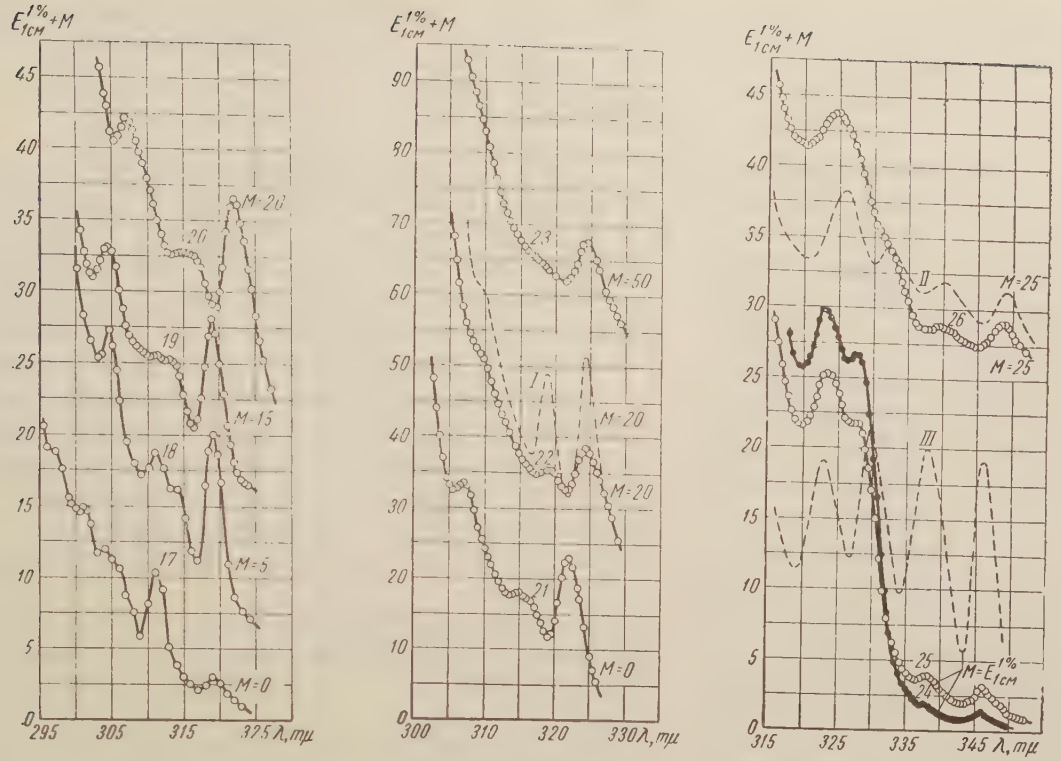

Fig.3. Absorption spectra of petroleum fractions. The arabic figures at the solid curves identify the fractions as listed in the table. The dashed curves represent I) the absorption spectrum of 1,3,5-trimethylnaphthalene, II) spectrum of 2,3-dimethylphenanthrene, and III) spectrum of phenanthrene after Friedel & Orchin[5].

1,5- and 1,7-dialkylnaphthalenes; and 1,3,5-, 1,4,6- and 1,2,5-trialkylnaphthalenes. It is possible that 1,2,3,4-, 1,4,6,7- and 2,3,6,7- tetrasubstituted naphthalenes were also present in some fractions.

An attempt was also made to determine the naphthalene content of the petroleum by means of the absorption spectra of the fractions containing naphthalene (these fractions were commonly separated in the crystalline state). For this purpose, the value of E was found for the absorption peak at 311 mμ, both for pure naphthalene as well as for the fractions under study. The naphthalene contents of the latter were then calculated using the familiar formula[1]. It was found that the naphthalene content of Dolinsk petroleum amounts to 0.04%.

Ukrainian Scientific Research Institute
for Geological Prospecting

References

1. A.E.Gillem & E.S.Stern, Electronic Absorption Spectra of Organic Compounds. (Cited in Russian translation.)

2. A.V.Topchiev, L.M.Rozenberg, M.M.Kusakov & M.V.Shishkina, Izv.AN SSSR, Otdel.khim.nauk, 9, 1109 (1956). (Trans.Bull.Acad.Sci. - Div.Chem.Sci.)

3. M.M.Kusakov, S.S.Nifontova, E.S.Pokrovskaya, L.M.Rozenberg, A.V.Topchiev & M.V.Shishkina, Transactions of the Tenth All-Union Conference on Spectroscopy, Vol.I, p.321. L'vov, 1957.

4. M.S.Norris & N.D.Coggeshell, Anal.Chem., 29, 183 (1953).

5. R.A.Friedel & M.Orchin, Ultraviolet Spectra of Aromatic Compounds, N.Y., 1951.

APPLICATIONS OF MOLECULAR SPECTROSCOPY IN BACTERIOLOGY AND IMMUNOLOGY

- V.M.Vadimov

Ultraviolet absorption spectra of anatoxins

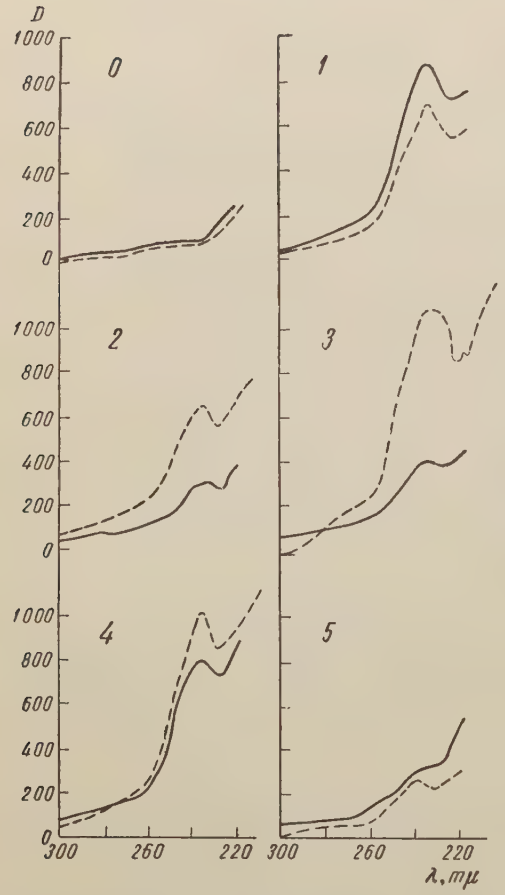

Fig.1. Purified diphtheria anatoxin series 128B 142AE. Absorption curves in the ultraviolet: 0 - unseparated preparation, 1-5 - individual fractions separated according to the luminescence zones after electrophoresis on paper. Dashed lines - nonirradiated anatoxin; solid lines - γ-irradiated anatoxin.

The present work was undertaken in connection with investigation of the possibility of utilizing γ-radiation for "cold" sterilization of bacterial preparations.[1] We were specifically interested in the physical-chemical changes that may occur as a result of irradiation of diphtheria anatoxin with heavy doses of γ-rays.

Even under normal conditions there may be variations in the quality of anatoxin obtained from B. diphtheriae. Biological and biochemical methods of evaluating anatoxins are not satisfactory. The method of electrophoresis on paper with subsequent staining[2] is also inadequate.

Preliminary measurements on an SF-4 spectrophotometer of two samples of diphtheria anatoxin, one of which was γ-irradiated and the other the control, showed that their absorption curves differ little from each other (Fig.1). Hence to bring out the finer physical-chemical changes induced by irradiation, we had recourse to the procedure of preliminary electrophoresis on paper with subsequent analysis of the eluates from the different fractions by investigating their absorption spectra without staining the electrophoregrams, the different luminescing zones in which can readily be distinguished if an acetate buffer is employed.

The diphtheria anatoxin samples were exposed to a 1 500 000 r dose of γ-radiation, fractioned on a strip of filter paper and then dried at 20°. The paper strip after examination in filtered ultraviolet was cut along the boundaries of the luminescence zones. The contents of each zone were washed out with physiologic saline solution and the UV absorption of the eluates was measured on an SF-4 spectrophotometer. It may be noted that the luminescence brightness of the anatoxin is higher after irradiation.

Typical absorption curves of individual fractions (eluates from individual electrophoretic zones) before and after γ-irradiation are shown in Fig.1. It is noteworthy that after fractioning in most cases there appears a peak at about 238 mμ, which is not apparent in the spectrum of the unfractioned material. It will also be evident from Fig.1 that the character of the absorption curves for the individual zones of the irradiated and nonirradiated anatoxin are somewhat different, although the location of the absorption peak at 238 mμ is the same in both. Apparently, these differences are due to some physical-chemical changes occurring as a result of irradiation.

We also found that the absorption curves for different anatoxin series exhibit some differences depending on the specific preparation procedure and the degree of purification of the product; hence absorption spectra may prove to be useful for quality control. Further investigations to this end are under way.

Investigation of the absorption spectra of decolorized stain after staining bacteria in suspension

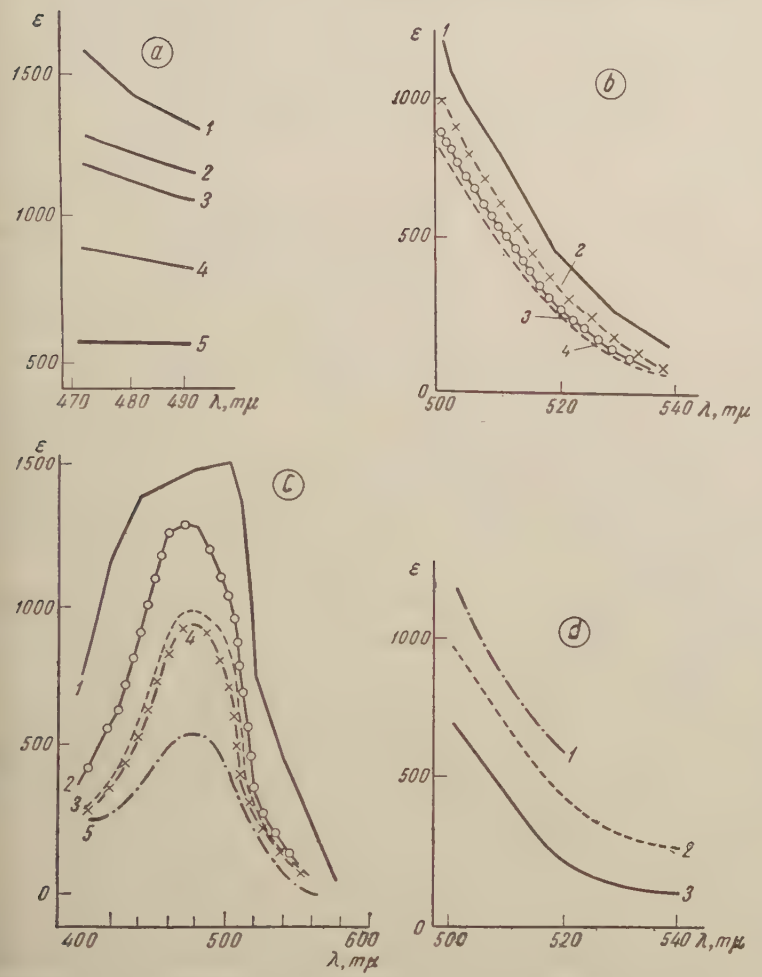

Fig.2. Absorption spectra of dye remainders after staining of bacteria in suspension. a: 1 - pure dye solution, 2 - $166 \cdot 10^6$ bacteria per ml, 3 - $330 \cdot 10^6$ per ml, 4 - $660 \cdot 10^6$ per ml, 5 - 10^9 per ml; b: 1 - dye solution, 2 - live culture of B.coli, 3 - heated vaccine, 4 - boiled vaccine; c: 1 - dye solution, 2 - live bacteria, 3 - 50% live bacteria, 4 - bacteria killed with formalin, 5 - bacteria killed by boiling; d: 1 - dye solution, 2 - live bacteria, 3 - bacteria killed by γ-rays.

The character and intensity of staining of many bacteria changes depending on their state and virulence.[3] Direct spectrometric measurements of the coloring of bacteria in suspension are impossible owing to turbidity. Hence we turned to measuring the color and degree of bleaching of the dyes used for staining the bacteria. Specifically, we investigated the change in the color of acridine orange after staining in suspension of cultures of B.coli in different states. The bacterial suspensions were prepared by washing off cultures from agar with physiologic saline solution; the suspensions were then diluted with an appropriate optical standard and stained by adding a dye solution to the test tube containing the suspension, which was then allowed to settle by standing or centrifuged. We then measured the absorption of the colored, partially bleached liquid above the deposit on an SF-2 or SF-4 spectrophotometer.

Fig.2,a shows how the color of the liquid (decolorization of the stain) varies depending on the number of stained dead coli bacteria. Changes in the intentensity of the stain remainder color in certain other cases are illustrated in Figs.2, b,c & d.

Thus from the spectroscopic characteristics of the stain residue we can distinguish suspensions of live bacteria in physiologic solution from suspensions of dead bacteria. The absorption curves of the decolorized stain remainders may also serve as convenient characteristics of the morphological state of bacteria either partially or entirely killed or otherwise altered by different agents.

"N.F.Gamalei" Institute of Epidemology and Microbiology,
Academy of Medical Sciences of the USSR

References

1. V.L.Troitskii, M.A.Tumanyan, V.M.Vadimov, Z.T.Pershina, D.R.Kaulen, I.M. Goncharenko, A.P.Duplishcheva & V.G.Khrushchev, Tezisy dokladov na Vsesoyuznoi tekhnicheskoi konferentsii po primeneniyu izotopov i izluchenii (Abstracts of reports presented at the All-Union Technical Conference on the Applications of Isotopes and Radiation), p.192, M., 1957.

2. V.M.Vadimov, Meditsinskaya radiologiya (Medical radiology) No.5, 64 (1958).

3. Desbordes, Ann.Inst.Pasteur, 86, 677 (1954).

* * * * * * *

INVESTIGATION OF DIPHENYLCHROMIUM DERIVATIVES BY ELECTRON PARAMAGNETIC RESONANCE

- N.N.Bubnov, Yu.A.Sorokin, S.P.Solodovnikov & V.M.Chibrikin

In earlier contributions[1-3] it was noted that the electron paramagnetic resonance (EPR) spectra of highly diluted solutions of diphenylchromium and its derivatives exhibit a distinct hyperfine structure associated with interaction of the unpaired electron with the protons of the benzene rings directly linked with the metal (chromium) atom. It was found that introduction of a substituent into the benzene ring does not change the g factor (1.986 ± 0.002) or the magnitude of the hyperfine splitting (3.5 ± 0.5 gauss), i.e., does not disturb the spin density distribution of the unpaired electron over the molecule. It was also found that the temperature of the solution and the nature of the solvent or substituent introduced into the benzene ring influence the width of the hyperfine structure components.

Further studies were carried out with a view to elucidating the spin density distribution of the unpaired electron, the nature of the hyperfine splitting mechanism and the factors determining the width of the hyperfine structure components. It was found that in the EPR spectrum of Cr-aromatic compounds, in addition to the earlier described[1-3] splitting due to interaction with the magnetic moments at the benzene ring protons, there occurs additional splitting caused by interaction of the unpaired electron with the magnetic moment of the isotope Cr^{53}. The magnitude of the hyperfine splitting associated with the Cr^{53} atom is 19 gauss[4], a value close to the splitting in chromium salts[5,6]. This gives reason to infer that the unpaired electron spin density is nonzero at the central metal atom and the benzene ring protons.

We turned to the following procedure in order to evaluate the unpaired electron spin density in the π-electron system of the ring. It is known[7,8] that if the π-system of an aromatic compound has a nonzero unpaired electron spin density, the hyperfine splitting of the EPR spectrum due to α-protons in the aliphatic side chain will be approximately of the same order of magnitude as the splitting due to the aromatic ring protons.

Hence we investigated the EPR spectrum of the diphenylchromium cation with cyclohexyl substituents in both rings. It was found that in this compound with

decreasing temperature there occurs additional splitting of each hyperfine component of the spectrum into a triplet. This additional splitting amounts to 1 ± 0.5 gauss and is due to interaction of the unpaired electron with the two cyclohexyl protons in the α-position with respect to the benzene ring.

Thus it may be assumed that for Cr-aromatic compound cations under certain conditions (specifically, in an acetone solution at about -90° and in an alcohol solution at about -30°) the unpaired electron spin density is nonzero in the π-system of the benzene rings.

In investigating the influence of different factors on the width of the hyperfine components in the EPR spectrum, in addition to the previously described[3] influence of the substituent, we found that in highly diluted solutions there is, as a rule, observed monotonic enhancement of the resolution of the EPR spectrum, i.e., decrease in the width of the hyperfine structure components, with decreasing temperature.

In some solvents (for example, in alcohols) the temperature dependence of the spectrum resolution (component narrowing) is anomalous. This effect may be connected with the formation of complexes between the diphenylchromium cations and the solvent molecules, leading to anomalous variation in the width of the hyperfine structure components. To determine the nature of these complexes it would be necessary to carry out a more detailed investigation of the mechanisms responsible for the variation in width of the hyperfine structure components.

Institute of Physical Chemistry of the
USSR Academy of Sciences &
Chemical Institute at Gorki State University

References

1. G.A.Razuvaev, Yu.A.Sorokin, G.A.Domrachev, G.G.Petukhov, Yu.D.Tsvetkov & Yu.N.Molin, Doklady AN SSSR, 113, 1293 (1957). (Trans. - Doklady.)
2. Yu.D.Tsvetkov, V.V.Voevodskii, G.A.Razuvaev, Yu.A.Sorokin & G.A.Domrachev, Ibid., 115, 118 (1957).
3. V.V.Voevodskii, Yu.N.Molin & V.M.Chibrikin, Optika i spektroskopiya (Optics and spectroscopy), 5, 90 (1958).
4. N.N.Bubnov & V.M.Chibrikin, Zhur.fiz.khimii (Journ.Physical Chemistry), 33, 1891 (1959).
5. A.A.Manenkov & A.M.Prokhorov, Zhur.eksp.i teor.fiz., 28, 755 (1955). (Trans.Soviet Physics - JETP.)
6. B.Blaney & K.D.Bowers, Proc.Phys.Soc.A, 64, 1135 (1954).
7. B.Venkataraman & G.Fraenkel, J.Chem.Phys., 23, 588 (1955).
8. D.B.Chesnut, J.Chem.Phys., 29, 43 (1958).

ELECTRON PARAMAGNETIC RESONANCE SPECTRA OF EOSIN SEMIQUINONE AND LIVE LEAF

- N.N.Bubnov, V.F.Tsepalov & V.Ya.Shlyapintokh

The present research was undertaken for the purpose of clarifying the nature of the intermediate products in photochemical reactions of eosin and chlorophyll. The reactions were carried out at room temperature directly in the electron paramagnetic resonance (EPR) spectrometer cavity with high frequency modulation of the magnetic field.[1] The experimental set-up has been described earlier[2].

Photoreduction of eosin

In the case of eosin the photoreduction reaction consists of conversion of the dye to a leuco compound. The mechanism of this reaction was investigated by potentiometric and spectroscopic procedures[3,4], and it was established that the reaction occurs in stages with the formation of an intermediate product. It was hypothesized that the relatively stable intermediate product is a free radical - eosin semiquinone. The lifetime of this intermediate product at room temperature is several seconds.

Upon illumination of the eosin (solvent - pyridine; reducing agent - ascorbic acid) in the EPR spectrometer cavity there immediately appears an EPR signal, which is a triplet with hyperfine splitting $\Delta H = 4.6 \pm 0.2$ gauss. The intensity ratios of the hyperfine structure components are 1:2:1. From analysis of the spectrum it may be inferred that the unpaired electron interacts with two protons located in equivalent positions relative to the free valence. The mechanism of the photochemical reaction is fully explained by Schenck's scheme[5], according to which absorption of a photon is followed by opening of the double bond of the quinoid oxygen. There then forms the biradical II, the structure of which explains its ability to react with the reducing agent and the oxygen[5]. In the photoreduction reaction an H atom is added to the O atom in position 3. The unpaired electron of the C atom in position 9 interacts with the protons in positions 1 and 8 which, as noted above, explains the EPR spectrum of semiquinone. Reaction with the protons of the *d* ring is not evinced in the EPR spectrum inasmuch as the plane of ring *d* is not aligned with the planes of rings *a*, *b* and *c*.

As a result of the transformation of eosin to semiquinone, the absorption band in the optical spectrum is shifted to the side of shorter wavelengths. The shift can be explained by disappearance of the quinoid structure as a result of the photoreduction reaction.

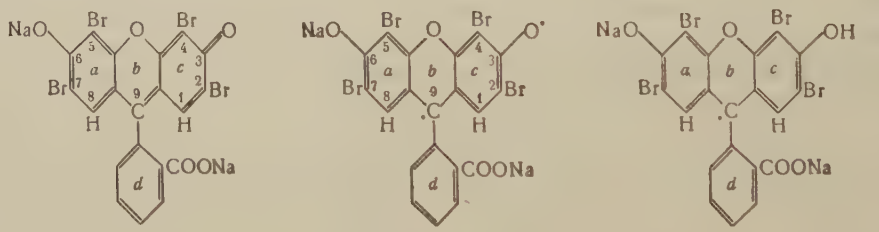

I Eosin II Biradical III Semiquinone

EPR spectrum of live leaf

In our work we obtained the EPR spectrum of live leaf for the first time. For the investigation we chose a leaf of agrophyrum repens. The EPR signal is a doublet with hyperfine splitting $\Delta H = 1.8 \pm 0.2$ gauss. Exactly the same spectrum was obtained in carrying out the reaction of photoreduction of chlorophyll in a model system. By way of solvent we used pyridine; by way of reducing agent,

ascorbic acid. The EPR signal from the leaf and model system disappears within less than 1 sec after turning on the light.

At present we are endeavoring to determine the nature of the detected free radicals.

Institute of Chemical Physics,
Academy of Sciences of the USSR

References

1. A.G.Semenov & N.N.Bubnov, PTE, No.1, 92 (1959). (Trans.Instruments and Experimental Techniques).

2. N.N.Bubnov, L.A.Kobalko, V.F.Tsepalov & V.Ya.Shlyapintokh, Optika i spektroskopiya, 7, 117 (1959). (Trans.Optics and Spectroscopy.)

3. V.F.Tsepalov & V.Ya.Shlyapintokh, Doklady AN SSSR, 116, 641 (1957). (Trans.Doklady.)

4. V.F.Tsepalov & V.Ya.Shlyapintokh, Izv.AN SSSR, Otd.kohm.nauk, 4, 637 (1959). (Trans.Bull.Acad.Sci. - Div.Chem.Sci.)

5. G.Schenck, Elektrochem, 56, 855 (1952).

* * * * * * *

DEVELOPMENT OF A HIGH SENSITIVITY EPR-2 IKhF TYPE MAGNETIC RADIOSPECTROGRAPH

- A.G.Semenov

A commercial model magnetic radiospectrograph designated EPR-2 has been developed in the Institute of Chemical Physics of the USSR Academy of Sciences; the instrument is intended for investigation of chemical samples by electron paramagnetic resonance (EPR). In setting up the technical specifications for the radiospectrograph, in addition to high sensitivity, there were incorporated particularly stringent requirements as regards stability and simplicity of operation.

As a result of extensive experimental work it was established that a radiospectrograph with hf modulation of the magnetic field, a pass-through cavity and automatic control of the klystron generator with reference to the working cavity should be capable of meeting the requirements set up for the instrument.

A block diagram of the EPR-2 radiospectrograph is shown in the accompanying figure. The EPR-2 employs dual modulation of the magnetic field. The low frequency modulation is produced by modulating coils set on the pole pieces of the electromagnet. The high frequency modulation is produced by the method suggested by Buckmaster & Sckovil[1]. To this end the resonator cavity is partially slit so that the slot in its walls will not intersect the shf current lines at the walls. The hf current is brought directly to the resonator. Passing the slot, it produces an hf magnetic field in the cavity. The EPR-2 utilizes a pass-through cylindrical cavity with an H_{011} mode.

The generator producing the hf modulation of the magnetic field has a maximum power of the order of 100 w. The double amplitude of the hf magnetic field in the cavity equals approximately 12 oersted. The EPR signal is discriminated from the detected shf oscillations and amplified by a resonance amplifier tuned to a frequency of 975 kc. The maximum amplification factor is $5 \cdot 10^5$; the width of the passband is 10^4 cps. A synchronous detector employing germanium diodes is connected to the output of the hf amplifier. From the synchronous detector the EPR signal is applied to the vertical plates of an oscilloscope. When it is

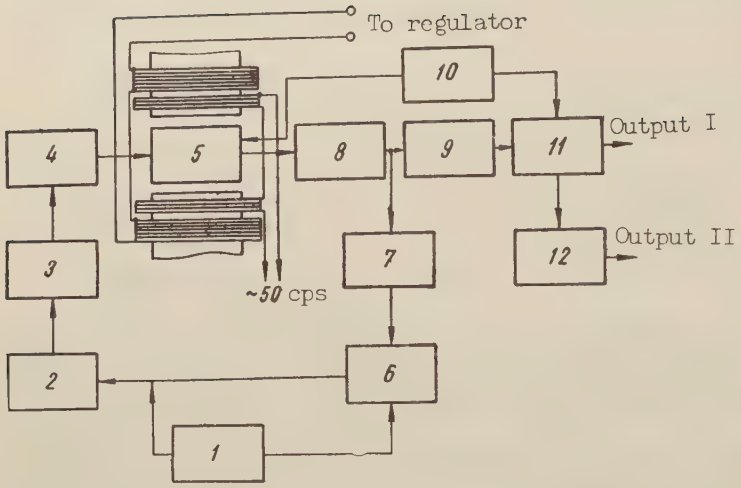

Block diagram of the EPR-2 radiospectrograph. 1) AFC oscillator, f = 630 kc, 2) klystron generator, = 3.2 cm, 3) ferrite decoupler, 4) variable attenuator, 5) cavity with sample, 6) phase-sensitive AFC detector, 7) AFC signal amplifier, f = 630 kc, 8) shf crystal detector, 9) EPR signal amplifier, f = 975 kc, 10) hf generator, f = 975 kc, 11) synchronous detector, f = 975 kc, 12) dc amplifier.

desired to record the EPR signal, a dc amplifier is coupled to the synchronous detector output through an RC network with a large time constant. In this case the low frequency modulation of the magnetic field is cut out and the current in the main windings of the electromagnet is slowly varied by an electronic device which at the same time serves as the current regulator.

The EPR-2 is equipped with an automatic frequency control (AFC) of the klystron generator with reference to the working cavity[2]. The AFC system operates as follows. A voltage of the order of 15 mv is applied to the klystron reflector from the AFC generator (630 kc). This voltage modulates the shf oscillations generated by the klystron. In case of detuning of the klystron frequency relative to that of the resonator cavity, there develops amplitude modulation of the shf oscillations incident on the shf detector, i.e., an AFC signal. The phase of the AFC signal depends on the sign of the detuning and its amplitude is proportional to the magnitude of the detuning. After detection of the shf oscillations the AFC signal is discriminated and amplified by a resonance amplifier (630 kc) with an amplification factor of the order of 10^5 and applied to a phase-sensitive detector. From the phase-sensitive detector the signal is applied to the klystron reflector. Thus the klystron frequency is tuned to the resonance frequency of the working cavity.

Principal Characteristics of the EPR-2 Radiospectrograph

Wavelength	3.2 cm
Maximum sensitivity	$5 \cdot 10^{-12}$ mole diphenylpicryl hydrazyl (standard radical)
Resolution	0.25 oersted
Recording time on automatic recorder	0.5, 3 or 18 min
Sample temperature range	-196 to +200°
Power supply	220 v line (50 cycle)

The EPR-2 is insensitive to mechanical vibrations and variations in ambient temperature.

Institute of Chemical Physics,
Academy of Sciences of the USSR

References

1. H.A.Buckmaster & H.E.D.Sckovil, Canad.J.Phys., 34, 711 (1956).
2. M.D.Krotova, Thesis, Moscow State University, 1957.

CORRELATION BETWEEN THE PROBABILITY OF TRANSITION OF COMPLEX ORGANIC MOLECULES TO THE METASTABLE STATE AND THE SPECTRAL COMPOSITION OF THE LUMINESCENCE*

- V.V.Zelinskii, V.P.Kolobkov & I.I.Reznikova

It was suggested in Ref.1 that there is a correlation between the transition probability P to the metastable state and the frequency of the fluorescence band. This hypothesis can be tested by investigating the variation of the phosphorescence yield q_{ph} or the ratio of the phosphorescence and fluorescence yields q_{ph}/q_{fl} as a function of the fluorescence peak frequency. In the absence of quenching on the metastable level, the variation of q_{ph}/q_{fl} (or q_{ph}) vs ν_{mf}** characterizes the variation of the transition probability P.[2]

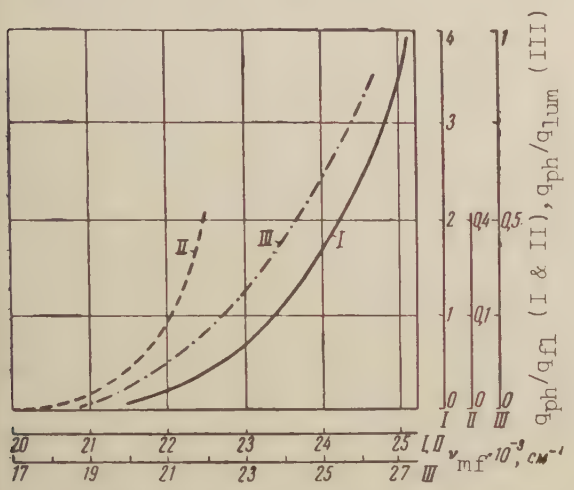

Fig.1. Graphs of variation (at -196°) of q_{ph}/q_{fl} vs ν_{mf} in 3-acetylamino-N-methylphthalimide (I) and 3,6-diacetylamino-N-methylphthalimide (II) and the variation of q_{ph}/q_{lum} vs ν_{mf} in 3-hydroxy-N-methylphthalimide (III).

In Ref.3 we gave the results of measurements of q_{ph}/q_{fl} at -196° for five phthalimide derivatives in 37 different media; the observed regularities are shown schematically in Fig.1. In the case of phthalimide derivatives q_{ph}/q_{fl} in going from medium to medium gradually increases with increase of ν_{mf}. Most of the experimental points for the derivatives fit a common curve. Analysis of the variation of q_{ph}/q_{fl} vs ν_{mf} for the investigated phthalimide derivatives leads to the conclusion that q_{ph}/q_{fl} and, consequently, P do not depend to any significant extent on the chemical nature of the medium or on whether the medium is in the crystalline or glass-like state, but do depend primarily on the position of the fluorescence peak.

So far we have investigated the variation of q_{ph}/q_{fl} with ν_{mf} for only a few phthalimide derivatives. Such variation, however, is not peculiar to these compounds. In Fig.2 we have plotted the values of q_{ph}/q_{fl} vs ν_{mf} for α- and β-naphthols and anthanilic acid. The values for the naphthols were determined in four different media and it will be seen that in this case higher values of the ratio obtain for higher ν_{mf}. The values of q_{ph}/q_{fl} in anthanilic acid were determined in 17 media and for this substance also most of the experimental points fit a single curve. The variation of ν_{mf} in this case is very appreciable - from 21 200 to 25 900 cm^{-1}, while the corresponding variation of q_{ph}/q_{fl} is relatively small - from 0.01 to 0.2 (not including exceptional points departing from the regularity). Qualitative increase of q_{ph}/q_{fl} with ν_{mf} is also observed for β-naphthylamine, phenanthrene and fluorescein. Thus increase of q_{ph}/q_{fl} with increase of ν_{mf} has been observed in the case of an unsubstituted hydrocarbon, in a number of amines, in hydroxy derivatives and in a dye; in other words, it is fairly common regularity. The divergence of individual points from the common curve, which is particularly noticeable in the region of small q_{ph}/q_{fl}, may be attributed either to radiationless deactivation of the metastable state (resulting in decrease of q_{ph}/q_{fl}) or to some specific effect similar to that produced by media whose

---

*The present report was presented at the 11th All-Union Conference on Theoretical Spectroscopy (Moscow, 2-10 December 1957).

**$\nu_{mf} = \nu_{max\ fluor}$ = the frequency of the fluorescence peak.

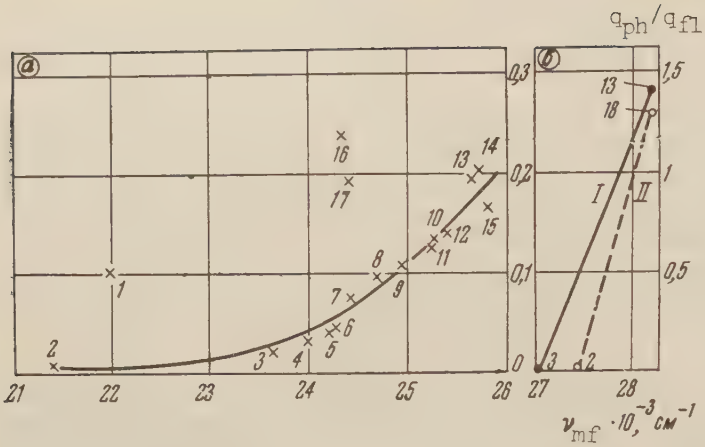

Fig.2. Variation of q_{ph}/q_{fl} with ν_{mf} (at -196°) in anthanilic acid (a), α-naphthol (Ib) and β-naphthol (IIb). Media: 1) crystalline state, 2) benzene, 3) water, 4) carbon tetrachloride, 5) nitromethane, 6) n-octane, 7) pyridine, 8) m-xylene, 9) pseudocumene, 10) toluene (gl), 11) xylene, 12) n-hexane, 13) propylformate (gl), 14) ethylalcohol (gl), 15) ethyl acetate, 16) acetone, 17) anisole, 18) chloroform; (gl) denotes media forming a vitreous mass at -196°.

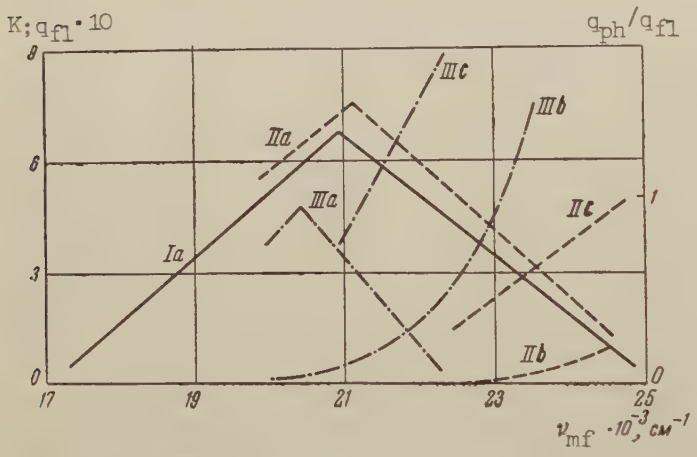

Fig.3. Schematic plots of the variation of q_{fl} at 20° (a), q_{ph}/q_{fl} at -196° (b) and k for quenching by aniline (c) with ν_{mf} in 4-amino-N-methylphthalimide (I), 4-acetylamino-N-methylphthalimide (II) and 3-methylacetylamino-6-acetylamino-N-methylphthalimide (III).

molecules contain bromine atoms[4] (increase of q_{ph}/q_{fl}). The fact that only a few points depart from the common regularity indicates that in most substances in almost all media at -196° there is virtually no radiationless deactivation of the metastable state or exceptional ν_{mf}-independent increase of P.

There is another approach to investigating P. It was shown in Ref. 5 that fluorescence quenching of some compounds by iodine salt is due to increase of P. Hence one can investigate P by determining the influence of extraneous impurities. The results of a quantitative study of the influence of iodine salts and aniline on the lifetime of the excited state of phthalimide derivatives have been given in Ref.6, in which we showed that the effectiveness k of triethylamine iodide and aniline increases as a rule with increase of ν_{mf}. Plots of k vs ν_{mf} show that the points characterizing the values of k for the same fluorescent substance in different solvents fit straight or almost straight lines (Fig.3). Thus the fact that P depends on the frequency of the fluorescence peak has been established in two independent ways. Also confirmed is the hypothesis, advanced in Ref.1, that the decrease of q_{fl} at 20° with increase of ν_{mf} is due to increase of P. Consequently, determination of the variation of q_{fl} with ν_{mf} can also serve as a method of investigating P.*

Let us now compare the data on the transition probability to the metastable state obtained by three different methods. Comparison of the ν_{mf}-dependences of q_{fl} at 20°, q_{ph}/q_{fl} at -196° and k at 20° (Fig.3) shows quantitative agreement. As the fluorescence peaks in different solvents shift to the shortwave side, the rati

---

*Omitted here is a comparison of the relative advantages and disadvantages of the three methods of investigating P, included at this point in the original report presented at the 11th Conference.

q_{ph}/q_{fl} grows, k increases and q_{fl} decreases. Qualitative agreement between the three dependences is retained in going from one substance to another. For example, the curves for 3-methylacetylamino-6-acetylamino-N-methylphthalimide in Fig.3 are shifted relative to the respective curves for 4-acetylamino-N-methylphthalimide, so that at the same position of the fluorescence peak in the first substance the values of q_{ph}/q_{fl} and k are appreciably higher in the second, while the value of q_{fl} is lower.

For the same ν_{mf} the values of q_{ph}/q_{fl} determined directly at -196° are appreciably lower than the values evaluated on the basis of the ν_{mf}-dependence of q_{fl} at 20°. For example, as follows from the ν_{mf}-dependence of q_{fl} for 4-amino-N-methylphthalimide (Fig.3) in the absence of quenching at the metastable level, the value of q_{ph}/q_{fl} corresponding to ν_{mf} = 22 000 cm^{-1} should be at least 0.3. Actually, however, at -196° the substance exhibits no fluorescence at the indicated value of ν_{mf}. The observed divergence might be explained by radiationless deactivation at the metastable level at -196°. In the case of 4-amino-methylphthalimide, however, in view of the fact that the luminescence efficiency at -196° is close to 100% there is evidently little or no radiationless deactivation. Hence this explanation must be rejected. It must also be rejected for the other substances, although possibly not as categorically.

For explaining the difference between the values of q_{ph}/q_{fl} measured directly at -196° and the values evaluated from q_{fl} at 20° one can assume that the fluorescence peak frequency does not determine P directly but rather the transition probability to some intermediate state from which there then occur transitions to the metastable and the ground state with a probability independent of ν_{mf}. Another possible explanation of the divergence is the hypothesis that P increases with increasing temperature (or decreasing rigidity of the medium).

Let us summarize the results of investigation of P. All the three above mentioned procedures yielded results in qualitative agreement. In many cases the quenching action of the solvent, like that of some typical fluorescence quenchers, consists in creating favorable conditions for intramolecular deactivation, amounting to increase of P. However, the character of the effects produced by solvents and fluorescence quenchers are different. Solvents alter the fluorescence spectrum* and thereby change the shape and relative location of the energy surfaces of the ground and excited states. On the other hand, quenchers do not alter the spectrum but only affect the intercombination transition probability.

"S.I.Vavilov" State Optical Institute

References

1. V.V.Zelinskii, V.P.Kolobkov & L.G.Pikulik, Optika i spektroskopiya (Optics and spectroscopy), 1, 161 (1956).

2. B.Ya.Sveshnikov, Thesis, FIAN SSSR, 1951.

3. F.V.Zelinskii & V.P.Kolobkov, Doklady AN SSSR, 119, 922 (1958). (Trans. Soviet Physics - Doklady.)

4. V.V.Zelinskii, N.P.Emets, V.P.Kolobkov & L.G.Pikulik, Izv.AN SSSR, Ser. fiz., 20, 507 (1956). (Trans.Bulletin 20, No.5, 405.)

5. V.V.Zelinskii, V.P.Kolobkov & N.A.Kondaraki, Doklady AN SSSR, 117, 391 (1957). (Trans.Soviet Physics - Doklady.)

---

*In the present work we everywhere compared q_{fl} at 20°, q_{ph}/q_{fl} at -196° and k at 20° with ν_{mf} at the corresponding temperature. At the present, early state of the investigation, we cannot assert that these quantities should be correlated with ν_{mf} rather than with some other characteristic varying in parallel with the fluorescence peak. We can only state that the values of q_{fl}, q_{ph}/q_{fl}, k and, consequently, P depend on the spectroscopic characteristics of the material and the relative positions of the energy surfaces of the ground and excited states.

List of Reports Presented at the Twelfth Conference on Spectroscopy that are Scheduled for Publication in Other Journals

V.V.Voevodskii & L.A.Blyumenfel'd, Radiospectroscopy and problems of modern theoretical chemistry. Uspekhi fiz.nauk, 68, 31 (1959).

L.V.Lipis, Spectrum analysis of pure metals. Uspekhi fiz.nauk, 68, 71 (1959).

V.M.Chulanovskii, Measurements of intensity in infrared spectra. Uspekhi fiz.nauk, 69, 145 (1959).

P.A.Bazhulin & M.M.Sushchinskii, Methods of measuring the intensity of Raman lines. Uspekhi fiz.nauk, 68, 135 (1959).

F.D.Klement, On spectroscopic analysis in crystal and physical chemistry. Transactions of the Inst. Fiz. and Astronomy, Estonian SSR Ac. of Sci., No.7, 3 (1958).

A.N.Zaidel', Spectrum analysis of isotopic composition. Uspekhi fiz.nauk, 68, 123 (1959).

É.V.Shpol'skii, Emission spectrum analysis of organic compounds. Uspekhi fiz.nauk, 68, 51 (1959).

L.A.Tumerman, Use of spectroscopy in biochemistry and biology. Uspekhi fiz.nauk, 68, 93 (1959).

I.M.Belousova, D.B.Gurevich, V.K.Prokof'ev & Yu.A.Snigirev, On the time for attainment of thermodynamic equilibrium in arc discharge plasma. Optika i spektroskopiya, 7, 14 (1959).

A.K.Vinogradova & L.M.Ivantsov, Raster illuminators with cylindrical optics. Optika i spektroskopiya, 6, 829 (1959).

B.V.L'vov, Investigation of atomic absorption spectra by complete evaporation of the substance from a graphite cell. Inzh.-fiz.zh. (Engineering-physics Journal), No.2, 44 (1959).

N.I.Kaliteevskii, G.M.Malyshev & M.P.Chaika, Photoelectric spectrometer with a Fabry-Perot interferometer. Optika i spektroskopiya, 6, 820 (1959).

N.S.Tskhai & S.L.Mandel'shtam, Regarding "influences" on the intensity of the spectrum lines in flame spectra. Optika i spektroskopiya, 7, 141 (1959).

I.V.Podmoshenskii & V.M.Shelemina, Determination of the linear position of analytic arc and spark lines. Optika i spektroskopiya, 6, 813 (1959).

N.K.Sukhodrev & S.L.Mandel'shtam, On the temperature of electrode vapors in a spark discharge. Optika i spektroskopiya, 6, 723 (1959).

F.Z.Pedos, N.S.Sventitskii & Z.I.Shlepkova, Low voltage pulse discharge in vacuum for obtaining spectra. Optika i spektroskopiya, 6, 815 (1959).

O.A.Bochkova, L.P.Razumovskaya, S.É.Frish & N.V.Chernyshova, Simplified method of spectrum analysis of inert gases for impurities. Optika i spektroskopiya, 6, 818 (1959).

Yu.A.Sherstkov, On the applicability of the Cowen-Dieke function to dc arcs. Optika i spektroskopiya, 6, 817 (1959).

V.A.Zubov, G.G.Petrash & M.M.Sushchinskii, Some applications of a high-dispersion spectrometer for molecular analysis on the basis of Raman spectra. Optika i spektroskopiya, 6, 827 (1959).

S.L.Berkovich, M.V.Gofren, M.V.Lobachev, T.K.Fal'k & I.D.Sharonov, The DFS-12 diffraction grating spectrometer. Optika i spektroskopiya, 6, 824 (1959).

G.N.Rassudova & F.M.Gerasimov, Diffraction gratings for separation of spectrum orders. Optika i spektroskopiya, 6, 826 (1959).

I.V.Peisakhson, Optical systems for focusing infrared radiation on small detectors. Optika i spektroskopiya, 6, 831 (1959).

G.G.Slyusarev & N.I.Kulikovskaya, Variation in the distribution of light energy in a diffraction image by variable transparency filters. Optika i spektroskopiya, 4, 486 (1958).

Yu.P.Shchepetkin, On the possibility of correcting vertical astigmatism in Rowland mountings. A vacuum monochromator with a concave grating and a torus mirror. Optika i spektroskopiya, 6, 822 (1959).

M.S.Kiseleva, B.S.Neporent & V.A.Fursenkov, Spectroscopic determination of moisture in the upper layers of the atmosphere. Opt. i spek., 6, 801 (1959).

N.Ya.Buben, V.V.Voevodskii, A.T.Koritskii, Yu.N.Molin, I.I.Chkheidze & V.N.Shamshev, Investigation by electron paramagnetic resonance of free radicals forming in the process of irradiation with fast electrons. Opt.i spek., 6, 806 (1959).

L.A.Ignat'eva, Investigation of α- and β-spodumenes by infrared spectroscopy. Optika i spektroskopiya, 6, 807 (1959).

N.I.Shergina, V.P.Kuznetsova, A.S.Nakhmanovich & I.V.Kalechits, Absorption spectra of phenol in the ultraviolet region. Opt.i spek. 6, 803 (1959).

N.G.Yaroslavskii & A.E.Stanevich, Rotational spectra of H_2O vapor and the absorption of moist air in the 40 to 2500 μ region. Opt. i spek., 6, 799 (1959).

A.N.Sidorov, Infrared spectra of sublimated films of metal hydroxyquinolinates. Opt.i spek., 6, 812 (1959).

L.D.Kislovskii, Reflection spectra and the optical characteristics of terpilene in the 700 to 1300 cm^{-1} region. Opt. i spek., 6, 810 (1959).

Z.V.Zhidkova & T.A.Speranskaya, On measurement of spectra of diffuse reflection in the region of intersection of the dispersion curves of binding media and the substance of particles of scattering media. Opt. i spek., (1960).

A.S.Toporets, Investigation of absorption and scattering of light in pigments. Opt. i spek., 4, 494 (1958).

G.G.Petrash, On choice of the scanning rate, the optimum time constant and the slit widths in spectrometric measurements. Opt. i spek., 6, 792 (1959).

L.S.Agroskii & N.V.Korolev, Microscope-spectrophotometers, Opt.i spek., 6, 832 (1959).

M.V.Lobachev, S.V.Podmoshenskaya, I.I.Trilesnik & A.B.Shadrina, Multiple channel photoelectric DFS-10 equipment for emission spectrum analysis. Zavodsk. laboratoriya, 8, 1013 (1959).

K.S.Garger, G.D.Krivulya, F.S.Ortenberg & V.I.Trofimova, Investigation of the spectrum of converter flames with different methods of blowing. Zavodsk. laboratoriya, No.5, 573 (1959).

O.F.Chesnokov & Yu.A.Kopeikin, Improved procedure for sifting samples through the source for spectrum analysis. Zavodsk. laboratoriya, No.12, 1487 (1958).

M.É.Britske & E.A.Lavrova, Use of the FES-1 photoelectric steelometer for analysis of nonconducting powders. Zavodsk.laboratoriya, 8, 970 (1959).

E.A.Sergeev, L.S.Margolin, P.A.Stepanov, M.V.Belobragina & N.A.Nikitina, Increasing the sensitivity of spectrum analysis of rocks by chemical-thermal concentration of the microelement. Zavodsk. laboratoriya, No.12 (1959).

V.V.Plastinin, Spectrum analysis of micas. Zavodsk. laboratoriya, No.5, 577 (1959).

I.G.Yudelevich, I.R.Shelpakova, T.I.Sosnovskaya & L.S.Bortnik, Spectrographic control of the process of refining rare metals. Zav.lab., 8, 959 (1959).

M.N.Shtutman, V.P.Avdeenko, E.V.Zvereva, V.M.Shteinberg & T.A.Eremeeva, On the possibility of using a pulse source for analysis of slags and agglomerates Zavodsk. laboratoriya, No.12 (1959).

K.I.Ionova, Investigation of the accuracy of spectrographic analysis of open-hearth slags from solutions using spark excitation. Zav.lab., No.12 (1959).

N.V.Korolev, Equipment for emission microspectroscopic analysis, Zav. lab., No.8, 1014 (1959).

A.V.Shaevich, Present state of the problem of preparing standards, Zav.lab., No.12 (1959).

T.K.Aidarov, A.E.Zak & E.S.Safonova, On the influence of certain elements in the determination of alkali metals by flame photometry. Zav.lab., No.3, 263 (1959).

S.I.Berger & L.M.Yablonik, Quantitative spectroscopic analysis of "Alni" type magnetic alloy and B-16 and B-83 babbits by the method of contact spark transfer. Zav.laboratoriya, No.12 (1959).

I.L.Sakharnova, Kh.I.Zil'bershtein, O.N.Nikitina, N.M.Piryutko & T.P.Evtushenko, Spectroscopic analysis of high purity silicon. Zav.lab., No.12 (1959).

N.G.Isaev, Regarding improvement of spectroscopic determination of hydrogen in titanium alloys. Zav.lab., No.12 (1959).

V.N.Vovk & I.G.Savich, Rapid analysis of steels on a mock-up photoelectric installation designed by the GOI. Zav.lab., No.8, 969 (1959).

I.M.Veselovskaya, Rapid analysis of open-hearth slags with the FES-1 instrument. Zavodsk.lab., 8, 981 (1959).

T.V.Kovalenko, Use of the FES-1 steelometer for analysis of gases in metals. Zav.lab., No.12 (1959).

A.V.Iogansen, Determination of open $-(CH_2)_n$ chains of different lengths on the basis of infrared absorption spectra. Zav.lab., No.3, 302 (1959).

A.V.Iogansen & L.G.Zelenskaya, Quantitative determination of the products in the production of caprolactam on the IKS-12 infrared spectrometer. Zav.lab., No.3, 299 (1959).

N.K.Rudnevskii & V.V.Zharkov, Use of quantitative molecular spectrum analysis at certain stages in the production of phenol and acetone. Zav.lab., No.3, 297 (1959).

Ya.I.Gerlovin & P.V.Slobodskaya, Enhancing the sensitivity of the optical-acoustic method of gas analysis by using multiple passage cells. Zav.lab., No.3, 303 (1959).

D.I.Tsekhovol'skaya, T.A.Zavaritskaya, G.S.Denisov & V.M.Chulanovskii, Application of infrared spectroscopy to analysis of titanium tetrachloride. Zav. lab., No.3, 300 (1959).

A.I.Finkel'shtein, Ts.N.Roginskaya, P.N.Balabanova, F.L.Molochevskaya, A.M. Fisher & G.P.Machin, Spectrophotometric methods of analysis of organic compounds in the chemical industry. Zav.lab., No.8, 932 (1959).

M.É.Britske & I.A.Burovoi, An automatic flame spectrophotometer. Tsvetnye metally, (Nonferrous metals), No.9, (1958).

G.I.Kibisov & M.I.Rezvova, Quantitative spectroscopic analysis of substances by the blow-in procedure. Inzh.-fiz.zh. (Engineering-physics Journal), No.6, 47 (1959).

G.V.Ovechkin, Procedure for taking into account the influence of "third" components on the relative intensity of analytic line pairs, Inzh.-fiz.zh., 2, 54 (1959).

V.V.Korolev & É.E.Vainshtein, Use of a pulse excitation source for enhancing the accuracy of spectrum analysis of silicates. Zhur.analit.khimii, 13, 627 (1958). (Trans. - J.Analytical Chem.)

O.P.Semenova, Regarding the influence of "third" elements on the results of quantitative spectrochemical analysis. Nauchnye doklady Vyssh.shkoly (1960).

Ya.D.Raikhbaum, Influence of the chemical composition of the sample on the line intensity in spectrum analysis of ores. Izv.Vyssh.shkoly. Fizika, No.3 (1959).

I.N.Plaksin & V.N.Solnyshkin, Infrared spectra of agents for flotation of coal. Doklady, AN SSSR, 124, 153 (1959).

B.Z.Volchek, Investigation of the swelling of caprone by means of polarized infrared light. Zhur.tekh.fiz., (1960). (Trans.Soviet Physics - Tech.Physics).

N.Ya.Chernyak, N.N.Bubnov, S.S.Polyak, Yu.D.Tsvetnov & V.V.Voevodskii, On certain regularities in the electron paramagnetic resonance spectra of alkyl radicals. Optika i spektroskopiya, 6, 564 (1959).

Yu.N.Molin & Yu.D.Tsvetkov, On variation in the shape of the electron paramagnetic resonance line with temperature in peroxide type radicals. Zhur.fiz. khim., 33, 1668 (1959).

D.S.Gorbenko-Germanovi, R.A.Zenkova & T.L.Bolotina, Procedure for quantitative determination of the water of crystallization in some crystal hydrates from their absorption spectra in the near infrared (0.8-2.5 μ). Zhur.analit.khim., 13, 590 (1958). (Trans.J.Analytical Chemistry.)

D.B.Gurevich, V.K.Prokof'ev & Yu.A.Snigirev, Photoelectric instruments for recording the emission spectra from short term processes. Tr. komissii po pirometrii pri VNIIM, Chapt.I, p.51, Pub. VNIIM, 1958.

I.B.Borovskii, X-ray spectroscopic analysis. Usp.fiz.nauk, 68, 81 (1959).

* * *

Usp.fiz.nauk = Trans.Soviet Physics - Uspekhi
Optika i spektroskopiya = Trans.Optics and Spectroscopy
Zavodskaya laboratoriya = Trans.Industrial Laboratory

Bulletin of the Academy of Sciences of the USSR - Physical Series
Vol.23, No.10 - October 1959
(Continued from Vol.23, No.9)

Transactions of the Twelfth Conference on Spectroscopy (Applied Spectroscopy)

TABLE OF CONTENTS

	Page Orig.	Trans.
Some results of spectroscopic investigation of the individual hydrocarbon composition of Tartar petroleums - B.Le	1174	1177
Analysis of hydrocarbon mixtures by Raman spectroscopy - V.T. Aleksanyan, Kh.E.Sterin & S.A.Ukholin	1177	1179
Raman spectra of some C_{24} hydrocarbons - A.N.Kislinskii & A.A.Petrov	1179	1181
Investigation of aqueous solutions of uranyl nitrate by Raman spectroscopy - S.Mintz & Z.Kéntski	1182	1184
Investigation of methanol solutions of zinc chloride by Raman spectroscopy - S.Mintz & S.Osetski	1184	1186
Determination of the infrared absorption coefficients of CH_2 groups in dicyclic compounds - S.V.Markova & P.A.Bazhulin	1186	1188
Intensities of the infrared absorption bands associated with C-H valence vibrations - E.I.Pokrovskii	1189	1191
Investigation of the composition of high molecular hydrocarbon fraction of Bitkovsk petroleum by infrared spectroscopy - A.F.Mal'nev, V.T.Sklyar, I.M.Mikhlina, G.A.Puchkovskaya, L.I.Shulyak & E.F.Shevchenko	1192	1193
Quantitative determination of CH_2 groups in open chains by infrared absorption spectroscopy - E.A.Glebovskaya & É.I.Maksimov	1194	1195
Infrared spectra of some intracomplex compounds in the region of NH valence vibrations - L.A.Kazitsina, B.V.Lokshin, L.L. Polstyanko & A.P.Terent'ev	1196	1197
Characteristic bands of compounds in the pyridine series - S.G.Bogomolov, M.G.Bystritskaya & M.M.Kirillova	1199	1199
Use of infrared spectroscopy for investigating thermal aging of polyvinyl chloride - L.N.Pirozhnaya & G.S.Popova	1202	1202
Comparative investigation of photo and thermal aging of acetals of polyvinyl alcohol by infrared spectroscopy - G.S.Popova & E.V.Shuvalova	1205	1205
Investigation of isotactic polymers by means of infrared spectroscopy - E.I.Pokrovskii & M.V.Vol'kenshtein	1208	1208
Use of infrared absorption spectra for investigating structural changes in fluorine plastics undergoing aging - L.I.Tarutina	1210	1210
Investigation of structural change in vulcanized rubbers exposed to the action of mineral acids - A.F.Postovskaya & A.S. Kuz'minskii	1213	1213
Infrared spectra and the structure of the products of telomerization of diene hydrocarbons with halogen derivatives - A.A. Petrov & T.V.Yakovleva	1217	1216
Identification of resin acids from their infrared spectra - N.A.Borisevich, N.I.Makarevich, A.M.Prima, I.I.Bardyshev & E.A.Cherches	1219	1218
Infrared spectra of cellulose and its derivatives - B.I.Stepanov, R.G.Zhbankov & I.N.Ermolenko	1222	1220

Determination of the isotopic composition of deutero-organic compounds by infrared absorption spectroscopy - M.O.Bulanin	1224	1222
Infrared spectra and structure of the products of linkage of different substances to vinyl acetylene hydrocarbons - A.A. Petrov & T.V.Yakovleva	1226	1224
Molecular spectrum of hexaethyldilead and determining of its concentration in tetraethyllead - N.K.Rudnevskii & N.N. Vyshinskii	1228	1226
Spectrophotometric analysis by the "zero heterochromatic point" procedure - B.I.Sukhorukov & A.I.Finkel'shtein	1230	1227
Investigation of aging of castor oil by observation of its absorption spectra - M.S.Kozyreva	1233	1230
Vacuum double-beam diffraction spectrophotometer for the infrared - V.I.Malyshev & S.G.Rautian	1237	1233
The IKS-14 and IKS-12 infrared spectrometers - N.S.Golyandin, I.G. Ptitsyna, I.I.Reshina & I.L.Sakin	1240	1235
Infrared vacuum spectrometer for industrial control and determination of oil in petroleum products by absorption spectrometry - A.F.Mal'nev & G.A.Puchkovskaya	1244	1238
Measuring attachment for infrared spectrometers - A.F.Mal'nev, M.P.Esel'son & L.S.Kremenchugskii	1246	1240
New equipment and procedures for study of the spectra of reflection from the earth's surface - K.S.Lyalikov, I.N.Belonogova, K.E.Meleshko, I.V.Semenchenko & A.P.Kharchenko	1247	1241
On the feasibility of molecular spectroscopic analysis of vapors in a wide temperature range - A.V.Suvorov, S.A.Shukarev & G.I.Novikov	1248	1242
Absorption spectra of indan series hydrocarbons in the near ultraviolet - A.M.Kusakov & M.V.Shishkina	1251	1244
Investigation of radiolysis of alkanes by ultraviolet and infrared spectroscopy - I.Ya.Kachkurova, L.S.Polak, A.V.Topchiev & N.Ya.Chernyak	1253	1246
Investigation of the aromatic portion of the kerosene-gas oil fraction of Dolinsk petroleum by observation of the ultraviolet absorption spectra - V.T.Sklyar & A.P.Lizogub	1256	1248
Applications of molecular spectroscopy in bacteriology and immunology - V.M.Vadimov	1260	1252
Investigation of diphenylchromium derivatives by electron paramagnetic resonance - N.N.Bubnov, Yu.A.Sorokin, S.P.Solodovnikov & V.M.Chibrikin	1263	1254
Electron paramagnetic resonance spectra of eosin semiquinone and live leaf - N.N.Bubnov, V.G.Tsepalov & V.Ya.Shlyapintokh	1265	1256
Development of a high sensitivity EPR-2 IKhF type magnetic radiospectrograph - A.G.Semenov	1267	1257
Correlation between the probability of transition of complex organic molecules to the metastable state and the spectral composition of the luminescence - R.V.Zelinskii, V.P.Kolobkov & I.I. Reznikova	1269	1259
List of reports presented at the Twelfth Conference on Spectroscopy that are scheduled for publication in other journals	1273	1262

Translated in 1960 by
Columbia Technical Translations
5 Vermont Ave., White Plains, N.Y.

Transactions

of the

Seventh Conference on Luminescence (Crystal Phosphors)

(Moscow, June 26 - July 3, 1958)

The reports on electro- and cathodoluminescence and most studies of alkali halide phosphors are being published separately under the title "Transactions of the Seventh Conference on Luminescence (Crystal Phosphors)", Tartu, 1959. Some of the reports presented at the Conference have also been published in various issues of Optika i spektroskopiya (Optics and Spectroscopy).

Editorial Board

OPENING ADDRESS

- M.D.Galanin

Our Seventh Conference is devoted specifically to the luminescence of crystal phosphors. This is the second conference devoted to this topic. Only two years have passed since the previous conference held in Tartu. Despite this we could not include in our program all the reports presented to the organizing committee. This is only one indication of the rapid development of this branch of science here in the Soviet Union.

Conferences on luminescence attract the attention of different specialists: physicists, chemists and engineers. It is pleasant to note that at today's conference there are present colleagues from academic and scientific institutes and workers from industrial enterprises located in different cities of our country. I should also like to welcome in the name of the organizing committee and all participants our foreign guests from Hungary, the German Democratic Republic and Poland.

The great diversity of specialists attracted by our conference reflects the complex character and many sidedness of the luminescence of crystal phosphors. This branch of science involves problems of physics and chemistry, spectroscopy and solid state physics. Purely scientific and theoretical research in this field provides the basis for new technical applications of luminescence in diverse realms of engineering and the national ecomony.

The complex nature of the processes involved in the luminescence of crystal phosphors and the intimate relationship between this problem and technical application was frequently emphasized by S.I.Vavilov, the founder of the Soviet school of luminescence. Investigation of the luminescence of crystal phosphors was started in our country on his initiative; 25 years ago Sergei Ivanovich Vavilov published an article on the "Laws of Decay of Phosphorescence", which long determined the orientation of studies in this field, a field that was almost entirely unexplored a quarter century ago. Since then we have learned much. I shall not undertake a survey covering the past 25 years or even attempt to review the major advances during the two years that have elapsed since the preceding conference. I would, however, like to remark on certain tendencies in research that have been becoming evident in recent years and which are obviously reflected in the subjects of the reports included in the conference program.

There has been an increase in the number of investigations on alkali halide phosphors. This, in my opinion, is connected first, with their new field of application in scintillation counters and, second, with the need for elucidating the complex physical processes occurring in the luminescence of phosphors, at least in the case of such classical and, it would appear, comparatively simple materials such as alkali halide single crystals. There has been some increase (although still not enough) in research on the excitation of crystal phosphors by hard radiation - electrons and other particles. Lastly, investigations of electroluminescence, which at the time of the preceding conference were only starting in the Soviet Union, have now yielded very interesting results which utilize the full gamut of experience of the Soviet school of luminescence for exploring the complex relationships characteristic of the luminescence of crystal phosphors.

I shall not undertake, in any case before the start of our conference, to single out for particular mention any particular studies from the great number of high level, valuable and interesting investigations.

Despite the great progress made in recent years, there are many questions that still await solution, for example, the question of the structure of luminescence centers. How very rare still are the cases when we can with certainty

define their structure or at least indicate what atoms enter into the composition of a center. For the most part we have no definite answers to these questions and their solution can be arrived at only as a result of combined application of chemical and new physical methods and procedures as, for example, investigation of paramagnetic resonance or polarization of luminescence.

Continued investigation of the kinetics of phosphorescence has recently led to the conclusion that in studying this effect one must take into account not only electron but also hole and even exciton processes. In many cases we have been able to gain a profound understanding of the mechanism of photosemiconductor processes, determining or involved in phosphorescence, afterglow, quenching and stimulation of luminescence. Yet it must be admitted that even in this field there is much that is still unclear.

For many years we have glibly spoken of luminescence centers ionized as a result of excitation. It would appear now that there is some question regarding the validity of this concept. This question is intimately related with the important problem of transfer of excitation energy from the host lattice to the activator; it is particularly important in the case of excitation by hard radiation and there is much that is still obscure as regards participation in the transfer process of electrons, holes and excitons.

This list of important and difficult problems could easily be extended, but we shall meet with many of these problems in the course of our deliberations. Hence let me terminate at this point.

In the name of the Organizing Committee, I declare the Seventh Conference on Luminescence open and wish all of us success in our collaborative efforts.

TEMPERATURE QUENCHING OF THE LUMINESCENCE OF ZnS:Ag PHOSPHOR WITH EXCITATION BY LIGHT OR α-PARTICLES

- M.D.Galanin & A.V.Raevskii

The luminescence properties of crystal phosphors with excitation by charged particles differ greatly from the luminescence properties with excitation by light. To an appreciable extent this difference can be explained simply by a difference in the excitation density. Where the kinetics of cathodoluminescence are concerned, this matter has been examined by Arkhangel'skaya et al[1] and Belikova[2]. In the case of excitation by high-energy particles, the mean excitation density may be substantially lower than the local density at certain points. The local density depends not only on the specific energy loss of the particles but also on the time lapse after excitation. This process of equalization and overlapping of the excitation channels with excitation by γ-rays has been discussed by Antonov-Romanovskii[3]. In the case of excitation by a low or moderate flux of α-particles, the luminescence consists of individual scintillations. Hence the luminescence properties must be determined by a very high excitation density along individual tracks.

In the present work we investigated from this standpoint temperature quenching of the luminescence of ZnS:10^{-4}Ag(NaCl) heated at 800°.*

Temperature quenching in crystal phosphors of this type is an "external quenching" process, i.e., a process occurring outside the luminescence centers. Hence the quenching depends greatly on the intensity of the exciting light. The simplest hypothesis regarding the mechanism of temperature quenching is that it is due to radiationless recombination of trapped electrons with free holes[4].

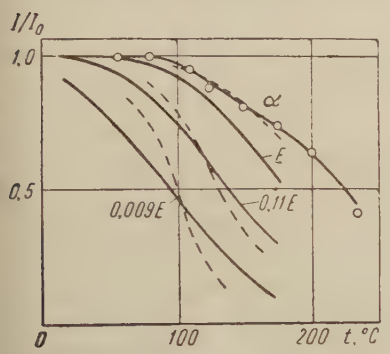

Fig.1. Temperature quenching curves with excitation by α-particles (curve α) and light. The figures at the curves indicated the relative excitation intensities. The dashed curves were derived from curve E by means of formula (1).

Fig.1 shows the experimental temperature quenching curves for excitation by Po^{210} α-particles and 365 mμ light of different intensity. The curves were measured under steady state conditions with slow cooling of the phosphor.**

In order to obtain the maximum possible photoexcitation intensity we used an SVDSh lamp with a large parabolic lens. The absolute intensity of the incident 365 mμ radiation (discriminated by a UFS-3 glass filter and a water solution of $CuSO_4$) was measured by a thermopile calibrated with reference to a Hefner candle. The maximum value of the absolute intensity was approximately 4 w/cm^2. For lower intensity readings the light was weakened by screens and light filters. The intensity I_o in the absence of quenching. The variation of I_o with the intensity of excitation E is nearly linear.

Even for the greatest exciting light intensity attained in the experiments the temperature quenching curve for photoexcitation lies to the left of the curve for α-excitation. In order to have a reasonable basis for extrapolation we had recourse to a simple model of external quenching.

Fig.2 shows the energy diagram for a crystal phosphor with one activator level and one electron trapping

---

*We thank A.A.Cherepnew and M.V.Danilova for preparing the phosphor.

**As control experiments showed, the absorption of the exciting light was great so that variation therein can be neglected. Hence the relative intensity values are close to the relative luminescence yield values.

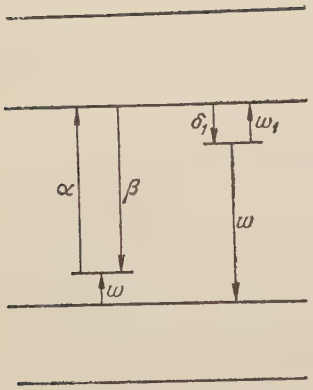

Fig.2. Crystal phosphor energy diagram for calculating first order external quenching.

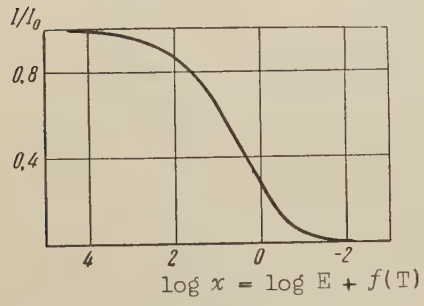

Fig.3. Theoretical variation of I/I_0 with log x.

level. It is assumed that absorption of the exciting light occurs in the activator band and also that the quenching is of the first order (i.e., that the probability for recombination of trapped electrons is higher than the probability for trapping of holes in the activator). Consideration of this model under steady state conditions and on the assumption that the number of free electrons and holes is small leads to the following expression for the relative luminescence yield:

$$\frac{I}{I_0} = 1 - \frac{1}{x}(\sqrt{1+2x} - 1), \qquad (1)$$

where

$$x = \frac{2\beta(w + w_1)}{\delta_1 w^2}\alpha$$

(the designations pertain to the transition probabilities indicated in Fig.2). The value of α is proportional to the excitation intensity E. Hence log x = = log E + log f(T), where f(T) is a function of the temperature.*

Fig.3 shows the variation of I/I_0 with log x following from Eq.(1). Having the temperature quenching curve for one excitation intensity, we can by means of this functional dependence calculate the temperature quenching curve for any other intensity. The curves for intensities of 0.1 E and 0.01 E calculated in this manner from curve E are shown by dashed lines in Fig.1. These curves lie fairly close to the experimental curves. One can scarcely expect complete agreement, not only because of the simplified nature of the assumed model, but also because the experimental curves were recorded for a thick phosphor layer and consequently correspond to different excitation densities.

In attempting to extrapolate and determine the photoexcitation density corresponding to the density of excitation by α-particles, one must also take into account the difference in the absorption mechanism. This difference, however, should not be substantial when the probability for trapping of holes in the activator is great. The high radioluminescence yield of zinc sulfide phosphors is apparently due to the high probability of this process. Hence with the above reservations we can still attempt a comparison between photo- and α-excitation. Extrapolation yields a value of about 12 w/cm^2 for the photoexcitation intensity corresponding to the quenching curve obtained for excitation by α-particles. The absorption coefficient for λ = 365 mμ determined by the method outlined by Antonov-Romanovskii[5] proved to be of the order of 500 cm^{-1}. Accordingly, the mean excitation power density is about $12 \cdot 500$ w/cm$^3 \approx 4 \cdot 10^{16}$ Mev cm^{-3} sec^{-1}. This appears to be appreciably lower than the energy density that might be expected in the initial excitation channel produced by an α-particle. Thus, assuming for

---

*The temperature dependence is here expressed in terms of w and w_1 and in the general case is rather complicated. Mott's formula, $I_0/I = 1 + Ce^{-\varepsilon/kT}$, which is usually valid for temperature quenching in centers, is not applicable to the case of external quenching.

the purposes of rough evaluation that the track length $l \approx 10^{-3}$, the radius $r \approx 10^{-6}$, the scintillation persistence $t \approx 10^{-6}$ sec and the excitation efficiency $\eta \approx 0.25$ (the maximum energy efficiency of radioluminescence), we obtain for a 5 Mev α-particle an excitation power density of $\eta E_\alpha / \pi r^2 l t \approx 4 \cdot 10^{20}$ Mev cm^{-3} sec^{-1}, i.e., a value some four orders of magnitude greater than deduced above.

The relatively low excitation density under the influence of α-particles obtained on the basis of the cited considerations from the temperature quenching curve is in qualitative agreement with the results of Smidt[6]. It is possible, as Smidt suggests, that the decrease in the initial high concentration of electrons and holes is explained by their diffusion from the initial track.

We wish to express our sincere gratitude to M.V.Fog for valuable discussions.

"P.N.Lebedev" Physical Institute,
Academy of Sciences of the USSR

References

1. V.A.Arkhangel'skaya, A.M.Bonch-Bruevich, N.A.Tolstoi & P.P.Feofilov, Zhur.eksp.i teor.fiz., 21, 290, 297 (1951).
2. T.P.Belikova, Ibid., 39, 905 (1955). (Trans.Soviet Physics - JETP).
3. V.V.Antonov-Romanovskii, Ibid., 21, 269 (1951).
4. L.A.Vinokurov & M.V.Fok, Optika i spektroskopiya, 1, 248 (1956).
5. V.V.Antonov-Romanovskii, Zhur.eksp.i teor.fiz., 26, 459 (1954).
6. D.Smidt, Ann.Phys., 15, 325 (1955).

* * * * * * *

NEW DATA ON A SLOW NEUTRON DETECTOR

- T.V.Timofeeva & S.P.Khormushko

Sometime ago we developed a slow neutron detector[1,2] consisting of Ag activated zinc sulfide loaded with boric acid. Boric acid is necessary in order to make the scintillator sensitive to neutrons ($B^{10}(n,\alpha)$ reaction). The α-particles from the reaction produce scintillations in the zinc sulfide which are then detected by the photomultiplier to which the scintillator is coupled. The detectors were prepared in the form of a plane layer (screen) and in the form of a hollow cylinder coated on the inside with the phosphor. The counting efficiency of the plane detector was 5.4 ± 0.4%; the response of the cylindrical detector was some four times higher.

The present communication is devoted to the relation between the counting rate for slow neutrons and the boric acid content and the possibility of increasing the neutron counting rate by using boric acid enriched with B^{10}.

The neutron absorption increases with the B^{10} content. This leads to weakening of the neutron flux reaching the deeper lying scintillator layers. This self-screening effect is substantial for thick detectors such as ours (scintillator thickness 80 mg/cm^2).

In the case of a collimated neutron flux incident normal to the scintillator surface the fraction of neutrons absorbed in the detector is $1 - e^{-\mu d}$, where μ is the absorption coefficient per unit thickness and d is the thickness. For a diffuse neutron flux this fraction α depends on μd in the following more complex manner (Fig.1):

$$\alpha = 1 - e^{-\mu d}(1 - \mu d) + \mu^2 d^2 E_i(-\mu d). \quad (1)$$

This function rises more steeply and attains saturation sooner than $1 - e^{-\mu d}$. Our initial detector had $\alpha = 0.367$; consequently, α and the neutron counting response could be increased by a factor of 2.7. In practice, however, it is not expedient to prepare scintillators with μd greater than unity ($\alpha = 0.78$) inasmuch as a relatively great increase of μd or the B^{10} content results in a relatively small change of α.

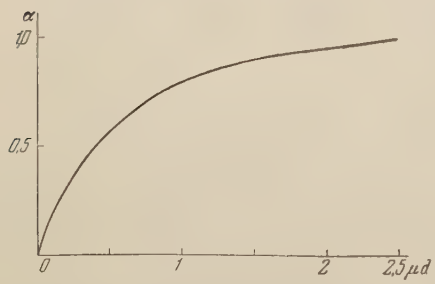

Fig.1. Variation of the fraction of neutrons absorbed in the detector with μd.

Aside from self-screening, insertion of a strongly absorbing neutron detector in the neutron flux may give rise to the so-called "sagging" effect or weakening of the neutron flux in the vicinity of the detector, which leads to diminution of the counting response. Experiments showed that under our conditions of a diffuse neutron flux in a small air space inside the paraffin moderator this effect lies within the limits of the experimental error. Hence the counting rate attainable in practice is determined only by α. The experimentally attainable counting rate I will, however, be appreciably lower as a result of discrimination by the counting equipment. The influence of discrimination will be the greater, the lower the pulse height, which depends on the absorption in the scintillator and the scintillation yield. Thus for a constant discrimination threshold of the associated equipment we will be cutting off a different fraction of pulses.

Let us consider in more detail the question of the relative counting efficiency of the scintillator; this in the given case we define as the ratio of the actual neutron counting rate I, which is dependent on the amplitude of the light pulses, to the fraction α of absorbed neutrons.

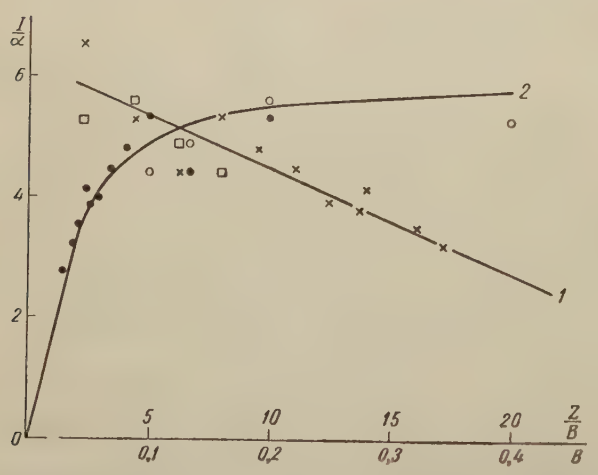

Fig.2. Variation of the counting efficiency with B (1) and Z/B (2).

Loading with boric acid, particularly in large amounts, reduces the counting efficiency. This is explained by the fact that the α-particles always originate in the boric acid and hence lose part of their energy inactively in the acid particles; the luminescence is produced only by the remaining part of the energy absorbed in the zinc sulfide. Moreover, the boric acid affects the optical characteristics of the scintillator. Thus the counting efficiency I/α must be a function of Z/B, where Z is the zinc sulfide and B is the boric acid content of the scintillator. In order to determine this function, we prepared a number of scintillators with different concentrations of boric acid ranging from 4.5 to 40% (in 3-4% steps). The synthesis procedure and the method of determining the response of the scintillators have been

described in Ref.2. Fig.2 shows the experimentally determined dependences of I/α on B (curve 1) and Z/B (curve 2) expressed in weight percent. As the unit counting rate, we took the counting rate of the old plane detector[2]. With the discrimination level of our set-up, the old detector counted 10% of the absorbed neutrons. The layer thickness of all the scintillator was 80 mg/cm^2. It will be evident from Fig.2 that the counting efficiency falls off linearly with increase in boric acid concentration, while the dependence on Z/B is more complex. The counting efficiency begins to fall off rapidly when the proportion of Z to B is 4-5.

Thus the counting efficiency increases with decrease of the boric acid content. From this it could be inferred that replacement of ordinary boric acid with B^{10} enriched acid should, with the same α, yield a scintillator with a higher counting response. Hence through the use of enriched boric acid it should be feasible to obtain a higher counting efficiency inasmuch as in this case a smaller absolute amount of boric acid is necessary to have the same number of reacting B^{10} atoms. To check this we prepared a series of samples containing from 4.5 to 16% boric acid enriched in B^{10} to 77, 87 and 91%. The results obtained are shown in Fig.2 by the square (curve 1) and circle (curve 2) points. Each point pertains to a certain value of B and is the average of the data for all three enrichments. It will be evident that the points lie close to the same curve, i.e., that the counting efficiency varies in accord with the same laws.

With an enrichment of 87% and an acid content of 16% the counting rate is twice that obtained with the old plane detector. With 100% enrichment and loading with 34.5% boric acid we should theoretically obtain the maximum possible increase in the counting rate, i.e., by a factor of 2.5 or by another 20%, but in this case twice as much enriched boric acid would be required, which would substantially increase the cost of the detectors. At a higher boric acid content, the counting efficiency would decrease.

Thus with enriched boric acid there are obtained detectors operating stably with a counting efficiency of 10-14%. By lowering the discrimination threshold, the counting efficiency could be increased to 20-30%.

As was noted earlier, to increase the total response of the detector we prepared it in the form of a hollow cylinder coated on the inside with a layer of the loaded phosphor. The number of counts obtained with such a cylinder is four times greater than for a plane detector. In using the scintillator prepared with enriched boric acid, the ratio of the number of counts obtained with a plane and with a cylindrical detector remained the same. Thus compared with the old plane detector the counting response of the hollow cylinder detector coated on the inside with the B^{10} enriched scintillator material is higher by a factor of seven.

"V.G.Khlopin" Radium Institute,
Academy of Sciences of the USSR

References

1. T.V.Timofeeva, Atomnaya energiya, 3, 156 (1957). (Trans.J.of Atomic Energy).

2. T.V.Timofeeva & S.P.Khormushko, Izv.AN SSSR, Ser.fiz., 22, 14 (1958). (Trans.Bulletin 22, No.1, 13.)

ON PHOTOELECTRIC EFFECTS IN LUMINESCENT ZnS:Cu(Ni,Fe,Co) AND ZnS·CdS:Cu POWDERS

- U.Kh.Nymm

In the present work we investigated photoelectric effects in a number of ZnS·CdS:Cu phosphors containing 45, 35, 25, 18, 8 or 0% CdS and ZnS:Cu(Ni,Fe,Co, ZnO) phosphors mainly by means of the so-called capacitor method. We obtained the spectral and temperature dependences of the photoelectric response (PR). For some of the phosphors we also obtained the luminescence excitation spectra and the glow curves.

Despite the fact that the capacitor method has been fairly widely used for investigating the internal photoeffect in semiconductors and luminescent powders[1-7] certain difficulties are still encountered in interpreting the experimental results. The shortcomings of the method have been discussed by Lashkarev[8] and Kozhevin & Lashkarev[9].

Nevertheless, the method has a number of positive features: it has a fairly high sensitivity, it can be employed with powdered substances and requires relatively small amounts of sample material, and what is sometimes very important, it allows of determining the polarity of the photocurrent carriers from the sign of the PR inasmuch as the polarity of the carriers is uniquely related to the sign of the PR.[6,10]

In the case of the mixed ZnS·CdS:Cu phosphors we studied the long-wave region of the PR spectra (the measurements were carried out on unexcited phosphors). The sign of the effect corresponds to n-type photoconduction, which is in agreement with the polarity of the Hall effect in ZnS and CdS single crystals.[11] With increase of the CdS content the spectra monotonically shift to the short wavelength side. The magnitude of the PR depends to a great extent on the photoconductivity relaxation time; in crystal phosphors the PR effect is the greater, the shorter the afterglow.[3]

We found that the magnitude of the PR is strongly dependent on the temperature. For samples with low CdS concentrations (≤25%) and all ZnS:Cu phosphors the effect was observed only at temperatures above room temperature (with weak monochromatic light beams). Determinations of the sign of the PR at room temperature by means of intense light beams were performed earlier by us[12] and by Bukke[13]. Measurement of the infrared (IR) PR in excited phosphors* is feasible

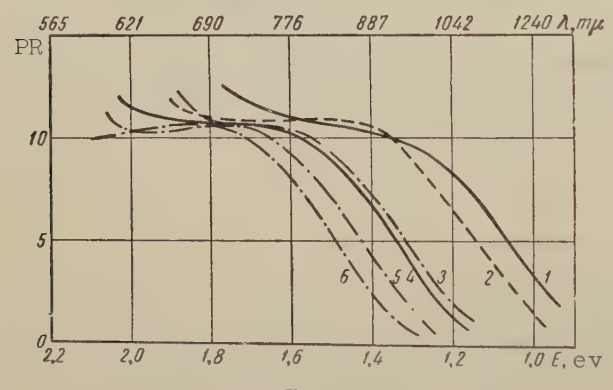

Fig.1

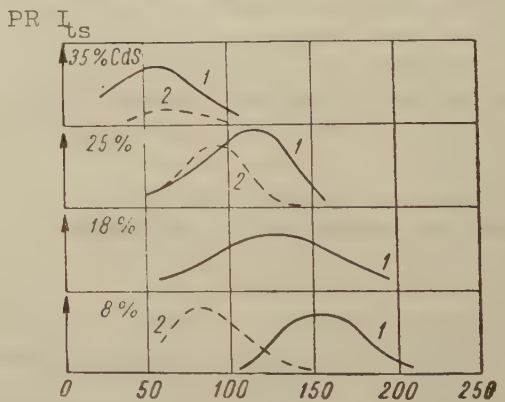

Fig.2

Fig.1. Photoelectric response spectra of excited ZnS·CdS:Cu phosphors: 1) 45%, 2) 35%, 3) 25%, 4) 18%, 5) 8%, 6) 0% CdS.

Fig.2. Temperature characteristics of ZnS·CdS:Cu phosphors: 1) photoelectric response, 2) thermostimulation.

---

*Excitation in the fundamental absorption band.

only at temperatures above room temperature (unexcited phosphors under these conditions exhibited no IR photoelectric sensitivity).

The IR PR spectra consistently shift to the short wavelength side with increase of the CdS content (Fig.1). Of particular interest here is the fact that the IR PR spectrum of ZnS:Cu virtually coincides with the light sum emission spectrum obtained by Reband[14].

Important also is the fact that the IR PR observed by us corresponds to p-type photoconductivity. Control experiments showed that the sign of the IR PR in samples with 45 and 35% CdS does not depend on the direction of illumination* (excitation) and does not change during the afterglow period. The similarity of the optical and photoelectric IR sensitivity spectra and the fact that the PR is of the p-type lead us to infer that the hole mechanism predominates in infrared effects in ZnS·CdS:Cu and ZnS:Cu phosphors.

The temperature dependence of the IR PR is shown in Fig.2. It will be seen that in each case the PR rises to a peak at a certain temperature and falls off to the side of both lower and higher temperatures. Of particular interest is the fact that in the series of ZnS·CdS:Cu phosphors the position of the IR spectrum and the temperature of the PR peak exhibit a parallel variation in going from one sample to another, i.e., with increase or decrease of the CdS content.

Our data are in agreement with the earlier advanced hypothesis that in this series of mixed crystals all the energy levels are proportionally depressed with increase in the content of the heavier component (CdS).[15] Linearity of the effect breaks down at approximately 18-25% CdS content. Above these CdS concentrations nonlinear variation is also observed for such other attributes and effects as the luminescence spectrum, the lattice constant, and quenching by IR light.

In our opinion the observed temperature dependence of the PR can be associated with increase in the rate of liberation of the current carriers from the trapping levels.

The dependence of the PR on the modulation frequency and the intrinsic time of the sample in the case of monopolar photoconductivity was investigated theoretically by Tolpygo[16]. The PR is maximal when the modulation period is equal to the recombination time. For both lower and higher modulation frequencies the PR decreases. From the frequency dependence of the PR one can determine the recombination time T_r, which is connected with the depth of the traps and the temperature. With increasing temperature T_r decreases, while the PR increases to $1/T_r \approx \approx \omega$. The decrease of the PR in the range of high temperatures corresponds to the region where $1/T_r > \omega$. In our opinion in this region in the case of IR PR thermal transitions compete with optical ones. In our experiments we used a modulation frequency of ~200 cps. The high temperature "tails" exhibited by the glow curves substantiate the dependence of the effect under consideration on the trap depth.

In the case of ZnS:Cu(Ni,Fe,Co,ZnO) phosphors, the PT spectrum can be measured both in the infrared and in the visible regions of the spectrum but only at high temperatures and with illumination in the fundamental absorption band. Our experiments showed that the spectral variation of the IR PR does not depend on the nature of the other activator, but the magnitude and temperature variation of the PR do depend on it (Fig.3). The temperature depth of the deep traps can be evalu-

---

*There are two hypotheses explaining the influence of illumination. It is possible that under the influence of illumination there develops excited absorption in the phosphor and that this is responsible for the appearance of new regions of photoelectric sensitivity[5]. It is also possible that illumination produces electric polarization of the sample; in this case the influence of illumination can be reduced to the effect of the electric field on the capacitor response[8,9]. In our opinion, both these mechanisms may be operative.

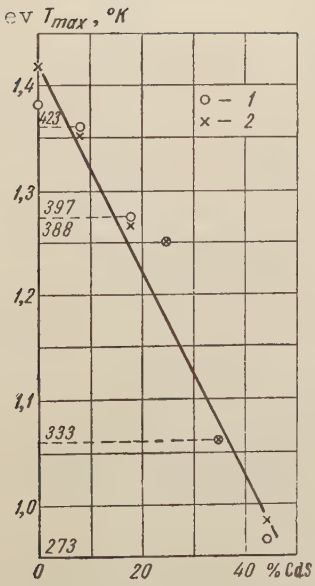

Fig.3. Variation of the temperature and spectral characteristics of the photoelectric response of ZnS·CdS:Cu phosphors on the CdS content: 1) temperature maximum of the PR, 2) position of the IR PR edge.

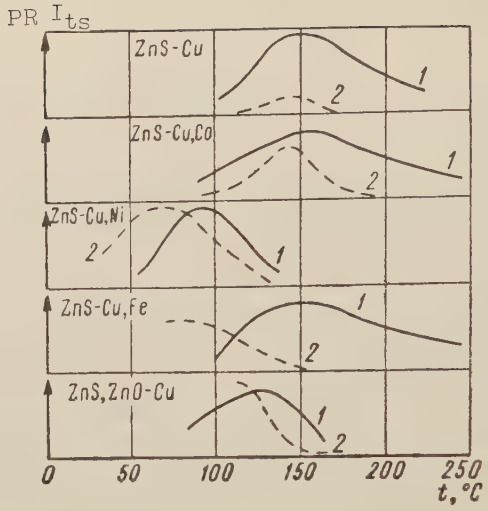

Fig.4. Temperature characteristics of ZnS phosphors: 1) PR, 2) thermostimulation.

ated by means of the glow curves (Fig.4).

In view of the experimental data it may be assumed that in the 140 to 190° temperature interval in all these phosphors there exist deep trapping levels and that the distribution of the levels depends to some extent on the other activator. There is also observed some parallelism between the variation of the PR and "tail" of the glow curves.

As will be evident from the cited data, the capacitor method can be used for investigating trapping centers in zinc sulfide phosphors.

In conclusion I desire to thank my supervisor F.D. Klement for his interest in the work.

Tartu State University

References

1. L.Bergman, Naturwissenschaften, 20, 15 (1932); Physik.Z., 33, 209 (1932).
2. L.Bergman & J.Hänsler, Z.Phys., 100, 50 (1936).
3. L.Bergman & F.Ronge, Physik.Z., 41, 349 (1940).
4. E.K.Putseiko, Doklady AN SSSR, 59, 471 (1948).
5. E.K.Putseiko, Izv.AN SSSR, Ser.fiz., 16, 34 (1952).
6. E.K.Putseiko, Doklady AN SSSR, 67, 1009 (1949).
7. S.M.Ryvkin, Zhur.tekh.fiz., 18, 1521 (1948).
8. V.E.Lashkarev, Trudy (Proceedings), Inst.of Physics of the Ukrainian SSR Ac. of Sci., 3, 3 (1952).
9. V.E.Kozhevin & V.E.Lashkarev, Radiotekhnika i elektronika, 2, 260 (1957). (Trans.Radio Engineering & Electronics.)
10. V.O.Zhuze & S.M.Ryvkin, Doklady AN SSSR, 62, 55 (1948).
11. Lenz, Ann.Phys., 77, 459 (1925).
12. U.Kh.Nymm & L.Ya.Uibo, Trudy (Proceedings), Inst. of Phys. and Astronomy, Estonian SSR Ac. of Sci., No.4, 124 (1956).
13. E.E.Bukke, Optika i spektroskopiya, 3, 334 (1957).
14. K.S.K.Rebane, Present issue of the Bulletin, p.1287.
15. F.D.Klement, Trudy (Proceedings), Inst. of Phys. & Astronomy, Estonian SSR Ac. of Sci., No.1, 3 (1955).
16. K.B.Tolpygo, Trudy (Proceedings), Inst. of Physics, Ukrainian SSR Academy of Science, 2, 25 (1952).

INVESTIGATION OF THE PHOTODIELECTRIC EFFECT IN ZnS:Cu:Fe PHOSPHOR

- P.E.Ramazanov

While there have been many investigations of the photodielectric effect (hereinafter pde) in crystal phosphors there is still no consensus regarding the nature of this effect. Some authors[1] attribute it to a real change in the dielectric properties of the phosphor as a result of excitation, others[2] explain it on the basis of photoconductivity within the phosphor grains, and still others[3] are inclined to attribute it to the simultaneous influence of both factors. Roux[4] investigated the frequency dependences of the pde in a number of phosphors and came to the conclusion that in most cases the experimental facts are not consistent with the model taking into account only photoconductivity, and that the pde at frequencies above 1 kc must be due to polarization of complexes associated with trapped electrons.

There has been proposed a model of a polarizing complex according to which the trap is a double potential well with an internal barrier separating two possible equilibrium positions of the trapped electron. Upon application of an external electric field there are realized through the agency of the thermal energy preferential displacements of the electrons against the field, thereby producing an additional dipole moment. Such polarization must be similar in character to the thermal ionic polarization of the displacements in ionic crystals[5] with the difference that the role of weakly bound ions is played in this case by trapped electrons. In view of this we felt it would be of interest to compare the temperature dependences of the pdc at different frequencies with the theoretical dependences for the case of thermal ionic polarization of displacements. This was the purpose of the present study.

By way of phosphor we chose ZnS:Cu:Fe (Cu - 10^{-4}, Fe - 10^{-5}) in which the pde must be due mainly to trapped electrons[6]. The measurements were carried out by the procedure described earlier[7].

Using a capacitor in which the ZnS:Cu:Fe phosphor was the dielectric, we recorded the temperature dependence of $\Delta \tan\delta$ and $\Delta C/C_d$ where C_d is the dark capacitance) at frequencies of 90.2 kc, 282 kc, 2.94 Mc and 9.69 Mc with the phosphor excited to the equilibrium state and at different stages of decay of the phosphorescence. The experimental results for $\Delta \tan\delta$ and $\Delta C/C_d$ after 15 min excitation of the phosphor are shown in Figs.1 and 2. Characteristic here is the shift of the $\Delta \tan\delta$ and $\Delta C/C_d$ maxima to the side of higher temperatures with increase in the frequency of the applied field. In the case of $\Delta \tan\delta$ this displacement can be qualitatively explained by variation of only the photoconductivity[8], but in this case the height of the maximum should not depend on the frequency whereas, as will be seen from the figures, actually the height of the $\Delta \tan\delta$ peak increases. The fact that there is little or no relation between the pde in ZnS:Cu:Fe and the photoconductivity is also indicated by the shift of the $\Delta C/C_d$ maximum with frequency. If the pde were due only to photoconductivity, $\Delta C/C_d$ should tend to saturation with increasing temperature.

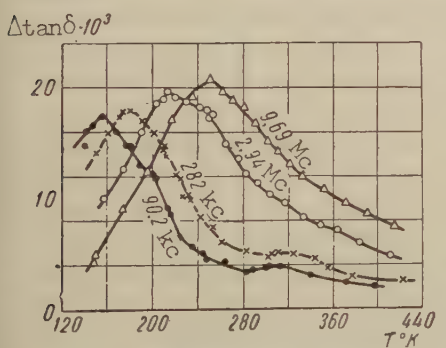

Fig.1. Temperature dependences of $\Delta \tan\delta$ at different frequencies with full excitation of the ZnA:Cu:Fe phosphor (excitation for 15 min).

The decrease of $\Delta C/C_d$ for ZnS:Cu phosphor at high temperatures was attributed by Vergunas & Agashkin[8] to the onset of temperature quenching. This explanation is not applicable to ZnS:Cu:Fe

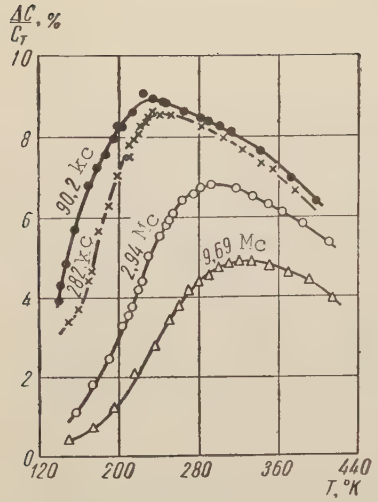

Fig.2. Temperature dependences of $\Delta C/C_d$ at different frequencies with full excitation of the ZnS:Cu: :Fe phosphor (excitation for 15 min).

phosphor, however, inasmuch as the decrease of $\Delta C/C_d$ begins appreciably earlier than temperature quenching; moreover the decrease starts at different temperatures depending on the frequency. These facts, in our opinion, indicate that the pde in ZnS:Cu:Fe is associated with relaxation processes, particularly, since the temperature dependences of $\Delta \tan \delta$ and $\Delta C/C_d$ are very similar to the corresponding dependences observed in dielectrics exhibiting thermal polarization.

If we accept the polarizing complex model proposed by Roux[4] and bear in mind that the number of trapped electrons during excitation of the phosphor to equilibrium varies with the temperature[9] according to the $n \sim e^{\frac{\varepsilon}{2kT}}$ law, where ε is the depth of the traps, then utilizing the theoretical dependence of the dielectric constant on temperature in the case of thermal ionic polarization of the displacements, we can find the conditions for the maximum value of ΔC, namely,

$$b^2\left(\frac{4U-\varepsilon}{2kT_{max}}-1\right)e^{\frac{2U}{kT_{max}}}=1+\frac{\varepsilon}{2kT_{max}}. \qquad (1)$$

Here $b=\omega/2\nu$, where ω is the radial frequency of the applied field, ν is the oscillation frequency of the electron in the equilibrium position, and U is the height of the hypothesized internal barrier. Inasmuch as condition (1) does not depend on the state of excitation of the phosphor, the temperature maximum at a given frequency should not shift in the process of decay of the phosphorescence, which is in fact observed experimentally, except for the first ~2 min of decay. The temperature dependences of $\Delta C/C_d$ for the ZnS:Cu: :Fe phosphor during excitation and at various stages of decay are shown in Fig.3. The reproduced curves were recorded at a frequency of 90.2 kc; similar curves were obtained at other frequencies.

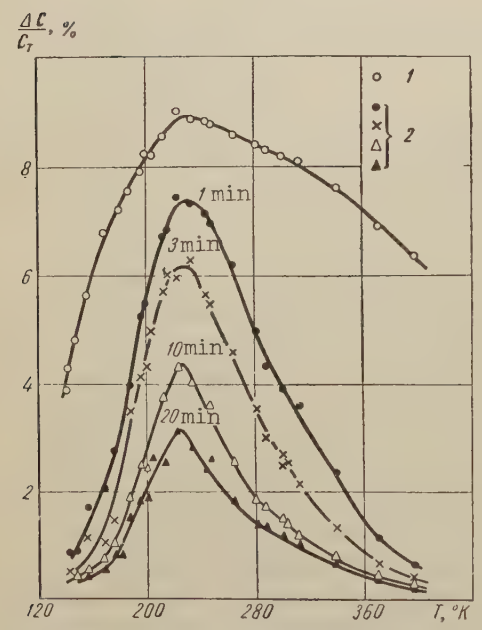

Fig.3. Temperature dependence of $\Delta C/C_d$ for the ZnS:Cu:Fe phosphor: 1) during excitation, 2) at different stages of decay. f = 90.2 kc.

Making use of condition (1) one can evaluate the height of the potential barrier U and the frequency ν. The condition can be written in the following form

$$\lg\omega+\frac{U\lg e}{k}\frac{1}{T_{max}}=\lg 2\nu\sqrt{\frac{\varepsilon+2kT_{max}}{4U-\varepsilon-2kT_{max}}}. \qquad (2)$$

In view of the fact that the right-hand part of the equality is weakly dependent on U and T_{max}, we may expect that plotted in log ω vs 1/T coordinates the experimental points corresponding to T_{max} for different frequencies will fit a straight line, from the slope of which we can evaluate U and

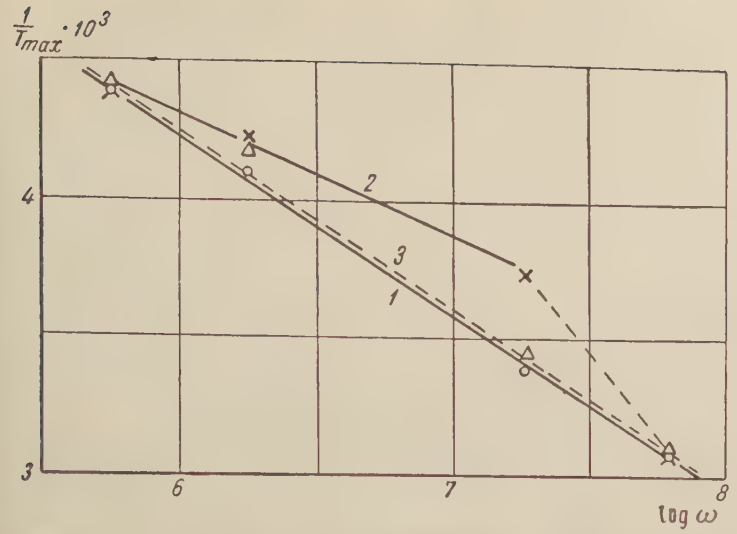

Fig.4. Variation of the position of the $\Delta C/C_d$ maximum with the frequency of the applied field: 1) during excitation of the phosphor, 2) after 1 min decay, 3) after 20 min decay of the phosphorescence.

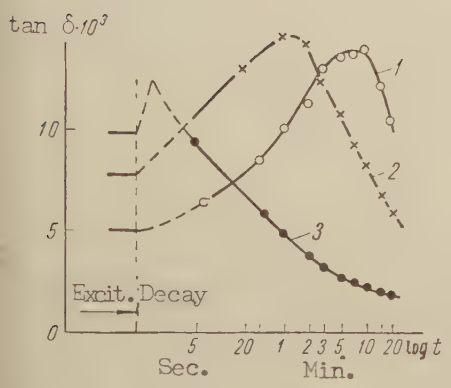

Fig.5. Variation of tan δ with the phosphorescence decay time of ZnS:Cu:Fe phosphor: 1) f = 90.2 kc, T = 193°K, 2) f = 282 kc, T = 189°K, 3) f = 2.94 Mc, T = 193°K.

from the intercept of which on the log ω axis the value of ν. In point of fact, the experimental points for the case of strong excitation and for the later stages of decay do yield a straight line (Fig.4), which gives a value of 0.3 ev for U (which is in agreement with the depth of the most effective traps in ZnS:Cu:Fe found by Nuvar'eva[10]) and a value of about 10^{12} sec^{-1} for ν.

Analyzing the temperature dependences of the pde in ZnS:Cu:Fe at different frequencies, we come to the conclusion that there is more justification for associating this effect with thermal relaxation processes than with photoconductivity. The agreement of the deduced value for U with the depth of the effective traps indicates the possibility of thermal polarization of the displacements connected with retrapping of the electrons. Upon application of an external electric field, the electrons freed from the trapping levels will be imparted a directed displacement and in the case of repeat trapping will be able to yield an additional dipole moment in complete accord with the mechanism of thermal polarization of displacements. Here the potential barrier will be the depth of the traps.

The break in the straight line (Fig.4) for the initial stages of decay may be due to the influence of traps of a different kind. Thus, according to Nuvar'eva[10], in ZnS:Cu:Fe, in addition to the main traps with $\varepsilon = 0.3$ ev, there are traps with a depth of 0.17 and 0.52 ev. Under quasi-steady state conditions (i.e., with excitation of the phosphor to the equilibrium state and at the later stages of decay) these traps may play no significant role, but they should be evinced in the early stages of decay when there can occur redistribution of the electrons between different trapping levels.

The presence of traps of different depths may also serve to explain the fact that in some phosphors[4] the value of U increases substantially in the process of decay. This may occur when in the early stages of decay the effect is produced mainly by electrons freed from shallow traps, while at later decay stages it is produced by electrons from deeper traps.

In this connection it is interesting to note that tan δ goes through a maximum in the process of decay both in the case of ZnS:Cu phosphor[4] and ZnS:Cu:Fe phosphor (Fig.5). The maximum value may be several times greater than the value of tan δ measured during full excitation of the phosphor, while the position of

the maximum may be shifted to the side of longer decay times with decrease in the frequency of the applied field. At a given temperature and frequency the condition for maximum tan δ is attained at a certain value of U which must be the greater, the lower the frequency. Thus at low frequencies the condition for maximum tan δ may be attained later than at high frequencies inasmuch as it will be fulfilled for deeper traps.

Siberian Physical-Technical Institute at
"V.V.Kuibyshev", Tomsk State University

References

1. G.F.J.Garlick & A.F.Gibson, Proc.Roy.Soc.,A, 188, 485 (1947).
2. H.Kallmann, B.Kramer & A.Perlmutter, Phys.Rev., 89, 700 (1953).
3. S.Kronenberg & C.A.Accardo, Phys.Rev., 101, 989 (1956).
4. J.Roux, L'effet photodiélectrique dans le sulfure et dans l'oxyde de zinc. Paris, 1956.
5. G.I.Skanavi, Fizika dielektrikov (Physics of dielectrics), M., 1949.
6. O.V.Agashkin, Optika i spektroskopiya, 3, 87 (1957).
7. P.E.Ramazanov, Izv.Byssh.uch.zav.Fizika (Bulletin of Institutions of Higher Learning, Physics), No.2, 39 (1958).
8. F.I.Vergunas & O.V.Agashkin, Optika i spektroskopiya, 3, 338 (1957).
9. A.V.Yastrebov, Trudy (Proceedings), Physics Inst., USSR Ac.of Sci., 3, 123 (1946).
10. V.V.Nuvar'eva, Thesis, Tomsk, 1956.

RELAXATION OF THE AFTERGLOW, PHOTOCONDUCTIVITY AND LIGHT SUMS OF ZINC SULFIDE PHOSPHORS

- F. I. Vergunas & Yu. L. Lukantsever

Experiments show that in the case of zinc sulfide phosphors not only the afterglow but also the photoconductivity in a certain temperature interval decays according to the hyperbolic law, the decay of the photoconductivity being slower than that of the afterglow. According to the experimental data, the difference α-β, where α and β are the degrees of the hyperbolas describing the decay of the afterglow and of the photoconductivity, respectively, varies from 0.5 to 1.5.

In the present contribution we shall show that the difference between the rates of relaxation of the afterglow and photoconductivity is a consequence of the elementary decay law of Adirovich[1] and that the experimental regularities are in good quantitative agreement with theory. To determine the theoretical relationships between the values of α and β we plotted the variations of log B, log n and log N with log $(1 + pt)$. Here $B = I/p\nu_1$, where I is the afterglow intensity, p is the probability for thermal freeing of trapped electrons, ν_1 is the total number of trapping levels, n is the light sum, and N is the concentration of conduction electrons.

The functional dependence of log B on log $(1 + pt)$ was plotted by the method described by Adirovich[1]. The values of N needed for plotting the variation of log N with log $(1 + pt)$ were determined from the ratio B/n. The theoretical curves were plotted for values of the parameter γ ranging from 100 to 0.4.

The decay curves of the afterglow B, the light sum n and the photoconductivity, proportional to the concentration N of free electrons, at the late stages of decay were approximated by hyperbolas:

$$B = at^{-\alpha},$$
$$N = bt^{-\beta},$$
$$n = ct^{-\xi},$$

for all values of γ there obtained the inequality $\alpha > \beta > \xi$.

We then determined the values of α and β for the theoretical curves corresponding to different values of γ and plotted the variation of $\alpha - \beta$ with α (see figure). For $\alpha = 2$, the difference $\alpha - \beta = 1$. This particular case was considered by Gurevich et al[2] who showed that if the elementary decay law is represented by a second order hyperbola, the afterglow must be described by a quadratic hyperbola and the relaxation of the photoconductivity by a first order hyperbola, i.e., that in this case $\alpha - \beta = 1$.

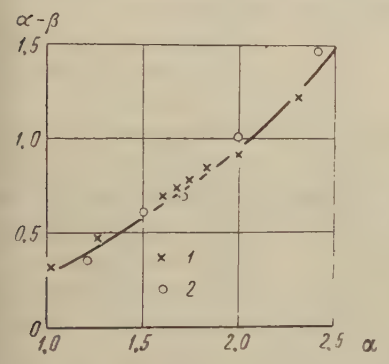

Variation of $\alpha - \beta$ with α: 1) experimental, 2) theoretical points.

Thus the relation between the degrees α and β obtained by Gurevich et al is a particular case of the more general dependence following from the elementary decay law of Adirovich.

For the purpose of comparing theory with experiment we investigated the relaxation behavior of the afterglow, the photoconductivity and the light sums in the case of ZnS:Cu phosphor with 10^{-4} Cu. The experimental dependences were recorded in the temperature region in which the phosphor as regards its properties was close to the "ideal" model, i.e., the model in which the afterglow is associated with trapping levels of one depth and luminescence centers of one kind. For such a phosphor there was obtained an elementary decay law from which there followed the theoretical dependences of $\alpha - \beta$ on α shown in the figure. Consequently, it was essential to compare the theoretical

dependences with experimental dependences obtained for a phosphor close to the "ideal" model. The temperature region in which the phosphor satisfies this condition was found by the procedure described in Ref.3. Moreover, the theoretical curves were calculated for complete population of the trapping levels at the beginning of phosphorescence; consequently, this condition should also have been fulfilled in recording the experimental curves. Actually, however, they are never realized in a real phosphor. To minimize the error connected with incomplete population of the trapping levels our phosphor was excited to equilibrium by light of maximum intensity.

The relaxation curves for n and N were found from the experimental afterglow decay curves. We plotted the variation of I with t. From this we planimetrically determined the light sums n corresponding to different decay times; for the concentration N of conduction electrons we took the ratio of the afterglow intensity I to the corresponding light sum. This followed from the relation $I = AN^{n}$, where A is the probability for recombination of conduction electrons with ionized luminescence centers. The relaxation curves were plotted in terms of log I, log N and log n vs log $(1 - pt)$. The probability p of thermal freeing of electrons was determined by the method described by Vergunas[4]. The experimental curves were recorded for the temperature range close to and in the quenching region. In this temperature range α varied from 1.5 to 2.5. The parameters α, β and ξ were determined from the slopes of the experimental curves at the late stages of decay. It is apparent from the figure that the experimental and theoretical α-dependences of $\alpha - \beta$ are in satisfactory agreement. For small values of α the difference $\alpha - \beta$ is small; it increases with increase of α.

Above we indicated that the concentration N of free electrons and the light sum were found from the afterglow decay curves (I vs t). For one of the temperatures the relaxation curve for N was found by an independent procedure, namely, from the time dependence of $\Delta \tan \delta$, the increment of the dielectric loss tangent due to excitation. The relaxation curve for $\Delta \tan \delta$ at late stages of decay was approximated by a hyperbola, the degree of which agreed with the degree of the hyperbola found by the first method.

Thus it follows from the elementary decay law that even in phosphors the afterglow of which is connected with trapping levels of only one kind, the photoconductivity decays more slowly than the afterglow; the difference $\alpha - \beta$ varies in a wide range, depending on the value of α. This follows from the elementary decay law proposed by Adirovich and has been substantiated by experiment.

References

1. E.I.Adirovich, Nekotorye voprosy teorii lyuminestsentsii kristallov (Some problems in the theory of luminescence of crystals), 1956.

2. D.V.Gurevich, N.A.Tolstoi & P.P.Feofilov, Doklady AN SSSR, 71, 29 (1950).

3. Yu.L.Lukantsever & L.R.Krasovskaya, Izv.AN SSSR, Ser.fiz., 21, 511 (1957). (Trans.Bulletin 21, No.4, 509.)

4. F.I.Vergunas, Optika i spektroskopiya, 1, 416 (1956).

QUENCHING OF THE LUMINESCENCE OF ZnS:Cu PHOSPHOR BY INFRARED LIGHT

- K.-S.K.Rebane

The fact that the luminescence efficiency of ZnS phosphors may depend on the intensity of excitation E was discovered by Riehl[1]. Investigating this dependence, Nail, Pearlman & Urbach[2,3] found that at very low excitation intensities the quantum efficiency q = I/E, where I is the luminescence intensity, does not depend on E. Recently it was shown[4,5] that irradiation of ZnS phosphors with infrared gives rise to a strong E-dependence of q. A number of authors[5-9] proposed and analyzed different models taking into account electron and hole processes for explaining these effects. Additional data on the problem were recently obtained in the investigations of Refs.10 & 11.

Temperature quenching of recombination luminescence is due to thermal freeing of holes from the trapping levels associated with the given luminescence.[12] The mechanism of IR quenching of ZnS phosphors is probably similar[13], i.e., under the influence of the IR light there occurs freeing of holes from the levels normally responsible for the luminescence. If this assumption regarding the electron-hole character of the processes occurring in quenching is true, it may be expected that at a sufficiently high intensity of the IR light there will be freed almost all the holes from the corresponding trapping levels with consequent complete quenching of the luminescence. We measured the variation of q with E during irradiation of a ZnS:Cu(NaCl) phosphor with intense infrared light.[10,11] We measured only the green luminescence of the phosphor. The experimental results are shown in Fig.1,a, from which it will be apparent that q_1, the quantum efficiency of the phosphor not irradiated with IR, is constant in a wide range of E and that only at low excitation intensities does it decrease. If, however, the phosphor is irradiated with IR light, the quantum efficiency is constant for small E: $q = q_2$ but is lower than q_1. At higher values of E the quantum efficiency increases and approaches the value q_1. Increase in the intensity of the IR light does not change the magnitude of q_2; only the region wherein q_2 is constant is shifted to the side of higher excitation intensities. We note that a similar E-dependence of q was obtained by Nail et al[3] in the case of ZnS:Ag:Ni phosphors for different Ni concentrations. Below we give the results of a series of experiments carried out for investigating the state of luminescence with quantum efficiency q_2.

At room temperature ZnS:Cu phosphors have two IR quenching bands located at about 1200 and 800 mμ.[14,15] The quenching in the 1200 mμ band at room temperature is usually appreciably weaker than in the 800 mμ band.*

We felt it would be of interest to determine whether the IR wavelength affects the value of q_2; the curves of Fig.1,b show that the answer to this question is negative.

Some investigators[17] infer that the constant value of q for small E is due to fluorescence of extraneous impurities in the phosphor. We investigated the build-up and decay of luminescence under emission conditions with quantum efficiency q_2 by means of an oscillograph. We found that the decay and build-up of this luminescence occurs without the initial spurt characteristic of fluorescence.

We also obtained the temperature quenching curves for different excitation conditions. We found that the temperature quenching curves for luminescence with quantum efficiencies q_1 and q_2 do not coincide (for more details on this point see Ref.1). We also measured the emission spectra during luminescence with quantum efficiencies q_1 and q_2; these spectra proved to be virtually identical.

---

*At liquid air temperature there is no quenching in the 1200 mμ band.[4,16]

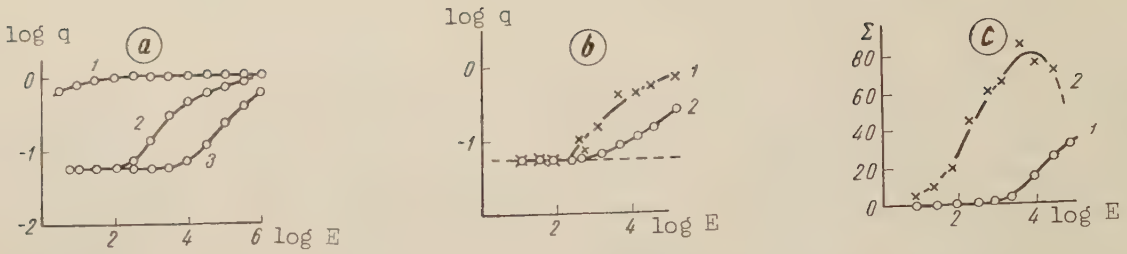

Fig.1. a - Variation of q with E: 1) $I_{IR} = 0$, 2) I_{IR} = 8-10 arbit.units, 3) I_{IR} = = 200-250 arbit.units. b - Same: 1) irradiation with 1000-1300 mμ IR, 2) 700-950 mμ IR. c - Variation of the light sum with E: 1) flare-up of emission upon abrupt increase of I_{IR} from 14-16 to 200-250 arbit.units, 2) build-up light sum.

Earlier we showed that in all ZnS:Cu phosphors there are deep traps which correspond to glow curve maxima at about 40-60° and 110° (or IR sensitivity maxima at about 1200 mμ and 800 mμ, respectively).[18,19] In addition, in ZnS:Cu phosphors there are other trapping levels from which the current carriers are freed at a temperature of about 190° (this corresponds to sensitivity to light in the 550-600 mμ region).[19] That there exist deep trapping levels in zinc sulfide phosphors is also shown by the results obtained by a number of other authors[20-22]. We were interested in the dependence of the light sum stored at deep trapping levels on the intensity of excitation under conditions when $q \approx q_2$. We carried out the following experiment. During steady illumination of the phosphor we illuminated it with IR light in the 800 mμ band; at different intensities of the exciting light we measured the magnitude of the flare-up occurring as a result of abrupt increase in the intensity of the IR light. The results are shown in Fig.1,c (curve 1). The intensity of the IR light was increased from about 15 to 200-250 arbitrary units. If we compare this result with the variation of q (Fig.1,a, curve 2), we find that the accumulation of the light sum at levels corresponding to the 800 mμ band begins in the region of E where $q = q_2$. Curve 2 in Fig.1,c shows the variation of the light sum stored in the phosphor with E (based on measurement of the build-up light sum). It will be seen that whereas q has a wide plateau*, the light sum has only a maximum, the position of which coincides neither with the end nor the beginning of the q plateau.

We also investigated the storage of light sums at levels corresponding to the 800 mμ band in the case when luminescence with quantum efficiency q_2 was attained by irradiation of the phosphor with 1200 mμ IR light. It was found that in this case there is stored in the phosphor a substantial light sum which gives rise to a flash upon irradiation of the phosphor with 800 mμ IR light. The build-up of this light sum with log E = 1.2 occurs over a period of 2-3 hours, i.e., is some three times faster than the build-up in the intensity of luminescence. The initial section of the build-up of the light sum curve has the same break as the curves for the build-up of light sums measured by Eliashberg[22].

The possibility of freeing current carriers from levels corresponding to a longer wavelength band than the de-exciting light is known for many luminescent systems, including ZnS:Cu phosphors.[4,24] The results cited above give reason to infer that the opposite effect also occurs. Direct substantiation of this is given by Fig.2 which shows the spectrum of the de-exciting influence of light for the light sum stored at trapping levels corresponding to the 800 mμ band. It will be apparent that light from the 1200 mμ band is capable of free-

---

*According to the data of Antonov-Romanovskii and his co-workers[23], a decrease of q is observed at high excitation intensities.

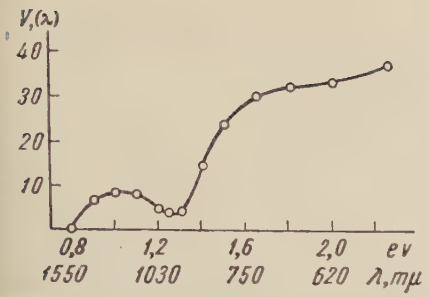

Fig.2. Spectrum of the stimulating effect of light of different wavelengths as regards the light sum stored at trapping levels corresponding to the 800 mμ band.

ing a large fraction of the light sum stored at these trapping levels. The general character of this curve agrees with the curve of the spectrum of the stimulating influence of light for the total light sum stored at all levels of the phosphor (see Ref.19).

The absence of optical quenching under the influence of 1200 mμ IR irradiation at liquid air temperature and the data on the spectrum of the deexciting effect of 800 mμ light indicate the necessity of preliminary thermal activation of the electrons participating in these processes (also see Ref.16).

Comparison of the E-dependence of q with the data on the E-dependence of the light sum gives reason to infer that at low levels of E and with IR irradiation of the phosphor, the dependences of q and the light sum on E are due to different mechanisms or processes in the phosphors. The variation of the light sum with E is satisfactorily described by means of a band model taking into account hole and electron processes. To explain the E-dependence of q in the range of low E, we advance the hypothesis that in addition to electron and hole processes there also exist in ZnS phosphors sensitization processes. According to this hypothesis, holes, freed under the influence of IR light, recombine with electrons at the sensitization centers. The energy liberated incident to this recombination is partially transferred by resonance to unexcited luminescence centers. The quantum efficiency q_2 of sensitized luminescence may in general be either smaller than or greater than the quantum efficiency q_1.

It must be emphasized that our results pertain to only one type of zinc sulfide phosphor. To prove or disprove the proposed hypothesis one must extend the investigations to other ZnS phosphors.

I wish to express my gratitude to Ch.B.Lushchik for his interest in the work and valuable suggestions.

Institute of Physics and Astronomy
Academy of Sciences of the Estonian SSR

References

1. N.Riehl, Z.techn.Phys., 20, 152 (1939).
2. N.R.Nail, D.Pearlman & F.Urbach, Luminesc.Materials, Symposium, N.Y.-L. 1948.
3. N.R.Nail, F.Urbach & D.Pearlman, J.Opt.Soc.America, 39, 690 (1949).
4. K.Rebane, Thesis, Tartu, 1955.
5. L.A.Vinokurov & M.V.Fok, Optika i spektroskopiya, 1, 248 (1956).
6. M.Schön, Z.Naturforsch., a., 69, 251 (1951).
7. S.Roberts & F.E.Williams, J.Opt.Soc.Am., 40, 516 (1950).
8. C.A.Duboc, Brit.J.Appl.Phys., Suppl., 4, 107 (1955).
9. M.V.Fok, Optika i spektroskopiya, 2, 475 (1957); L.A.Vinokurov & M.V.Fok, Ibid., 4, 118 (1958); L.A.Vinokurov & M.V.Fok, Inzh.-fiz.zh.No.2, 58 (1958). (Trans.Engineering-Physics Journal.)
10. K.S.Rebane, Eesti Loodus, 2, 75 (1958).
11. K.S.Rebane, Trudy (Proceedings), Inst.Phys. & Astron., Estonian SSR Ac. of Sci., No.8, 105 (1958).

12. M.Schön, Z.Phys., 119, 463 (1942); H.A.Klasens, Nature 158, 483 (1946); F.A.Kröger, Some Aspects of the Luminescence of Solids -N.Y., 1948.
13. V.V.Antonov-Romanovskii, Trudy (Proceedings), Phys.Inst., USSR Ac.of Sci., 2, No.2-3, 220 (1942); P.Brauer, Z.Naturforsch, a, 2, 238 (1947).
14. N.T.Melamed, J.Electrochem.Soc., 97, 33 (1950).
15. K.K.Rebane, Transactions of the Fifth Conference on Luminescence, Tartu, 1957. (Abstract, Bulletin 21, No.4, 542.)
16. I.Broser & R.Broser-Warminsky, J.phys.et radium, 17, 791 (1956)
17. M.N.Alentsev, Optika i spektroskopiya, 1, 240 (1956).
18. K.-S.K.Rebane, Trudy (Proceedings), Inst. of Phys. & Astron., Estonian SSR, Ac.of Sci., No.4, 81 (1956).
19. K.-S.K.Rebane, Optika i spektroskopiya, 4, 211 (1958).
20. H.Kallmann & G.Spruch, Phys.Rev., 103, 94 (1956).
21. L.A.Vinokurov, Optika i spektroskopiya, 1, 901 (1956).
22. G.M.Eliashberg, Ibid., 4, 66 (1958).
23. M.N.Alentsev, V.V.Antonov-Romanovskii & L.A.Vinokurov, Doklady AN SSSR, 96, 1133 (1954); V.V.Antonov-Romanovskii & L.A.Vinokurov, Optika i Spektr., 1, 66 (1956); Ibid., 2, 71 (1957); V.V.Antonov-Romanovskii, J.phys.et radium 17, 694 (1956).
24. P.A.Khellenurme, Trudy (Proceedings), Inst.of Phys. & Astron., Estonian SSR Ac. of Sci., No.7, 340 (1958); F.N.Zantov, Optika i spektr., 4, 102 (1958).
25. A.Obet, Thesis, Tartu, Riiklik Ülikool, 1958.

* * * * * * *

INFLUENCE OF COMPOSITION ON THE LUMINESCENCE OF ACTIVATORLESS ZnS·CdS PHOSPHORS

- L.Drozd

As is known, the luminescence of ZnS is attributed to a natural activator. This gives reason to assume that there is also present a natural activator in CdS phosphor. In view of this we felt it would be of interest to investigate the possible interaction of natural activators in mixed ZnS·CdS phosphors.

In approaching the problem, the first step was to investigate the influence of the CdS content on the development of luminescence of the activatorless phosphors and the position of the luminescence bands. To this end we prepared 19 mixed phosphors with 0, 0.01, 0.1, 0.3, 1, 5, 10, 15, 20, 50, 80, 90, 95, 99, 99.7, 99.99 and 100 molar percent CdS in the batch. NaCl (2%) was used as the flux. The samples were heated in an oxidizing medium for 15 min at 900°. These synthesis conditions were chosen on the basis of preliminary experiments in which we studied the influence of the atmosphere (H_2S, N_2, O_2), the temperature and heating time and the flux content (0 to 5% NaCl). The brightest luminescence was yielded by samples heated at temperatures from 850 to 900° with flux in an oxidizing medium.

Fig.1 shows the luminescence spectra of the ZnS·CdS phosphors at room temperatures with excitation by 365 mμ light. Introduction of CdS in amounts from 0 to 1% has virtually no effect on the luminescence spectrum of ZnS; also the luminescence spectra of ZnS·CdS phosphors with 0.01, 0.1 and 0.3% ZnS are virtually identical with the spectrum of pure CdS. As will be evident from Fig.1, the introduction of CdS produces a decrease in intensity and gives rise to a consistent displacement of the luminescence peak, located at λ = 469 mμ for pure ZnS, to the side of longer wavelengths (owing to change of the host lattice). For pure

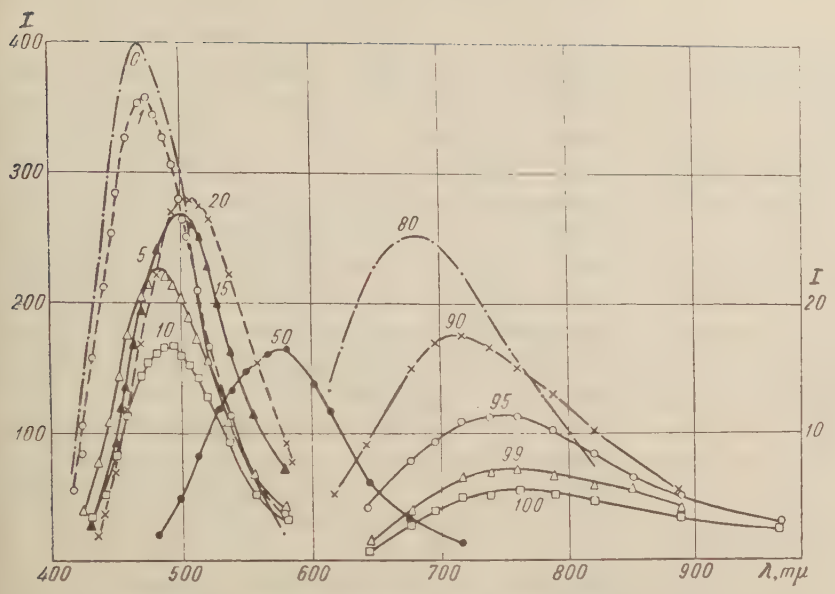

Fig.1. Energy distribution in the spectrum of ZnS·CdS phosphors with different CdS concentrations (indicated in % at the curves). The vertical scale at the left pertains to curves 0-50; that at the right to curves 80-100.

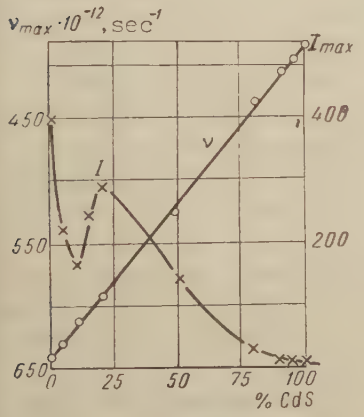

Fig.2. Variation in the position (straight line ν) and intensity of the maximum (curve I) in the spectra of ZnS·CdS phosphors with the CdS concentration.

CdS the luminescence maximum is located at 760 mμ and the color of the luminescence is dark red.

Of particular interest is the distinctive variation in the luminescence intensity with constant excitation, which results in a variation of the relative luminescence output of ZnS·CdS phosphors with increase of the CdS content (Figs.1 & 2). At first there is a rapid decrease of output in the CdS concentration range from 1 to 10%, then in the 15 to 20% range the output increases, and finally it gradually falls off in the range from 20 to 100% CdS. Pure CdS samples yield a comparatively weak luminescence (the height of the luminescence peak is only a fraction of that for pure ZnS). The general shape of the spectra is also the same: as will be evident from Fig.1, the spectral curves consist of a wide band with one maximum at all CdS concentrations.

The indicated variations in luminescence with the CdS concentration are qualitatively characterized in Fig.2 from which it will be evident, in particular, that the frequency shift of the luminescence peak is proportional to the CdS concentration. All these results are consistent with the findings of Levshin & Fridman[1] and the data given by Pringsheim[2] regarding the behavior of the luminescence bands of ZnS·CdS:Cu and ZnS·CdS:Ag phosphors as a function of the CdS concentration. From a comparison of the data given in these references with our data it will be apparent that the influence of CdS on the position of the zinc band is very similar to its influence on the position of the Cu and Ag activator bands.

Despite the fact that the general shape of the luminescence band remains the same we could not be certain that it belongs to the same activator, i.e., could not exclude the possibility that it might pertain to two different natural activators. In order to determine the character of the band in the mixed zinc-cadmium phosphors, we used the method of investigating the influence of the excitation intensity on the shape and position of the band. The excitation intensity was reduced to 50, 20, 8 and 5% of the initial value. Fig.3 shows the results of measurements for the ZnS·CdS phosphor with 5% CdS. One of the curves in Fig.3 represents the luminescence spectrum with the initial

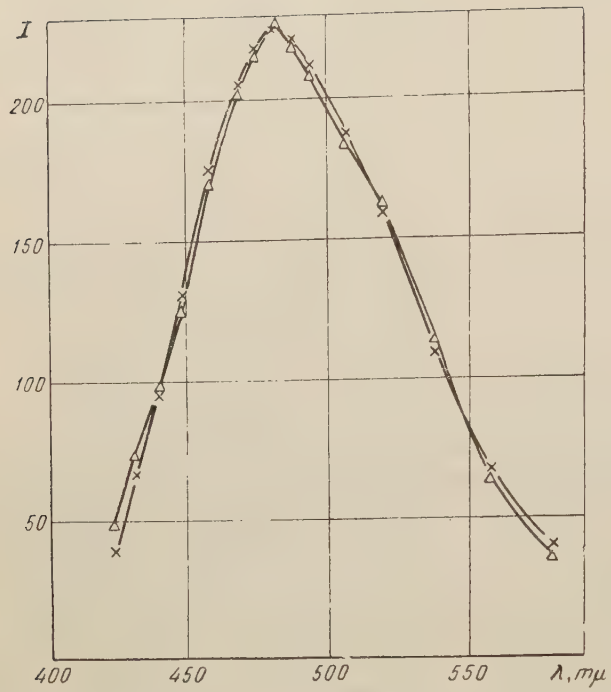

Fig.3. Energy distribution in the ZnS·CdS phosphor spectrum at different excitation intensities.

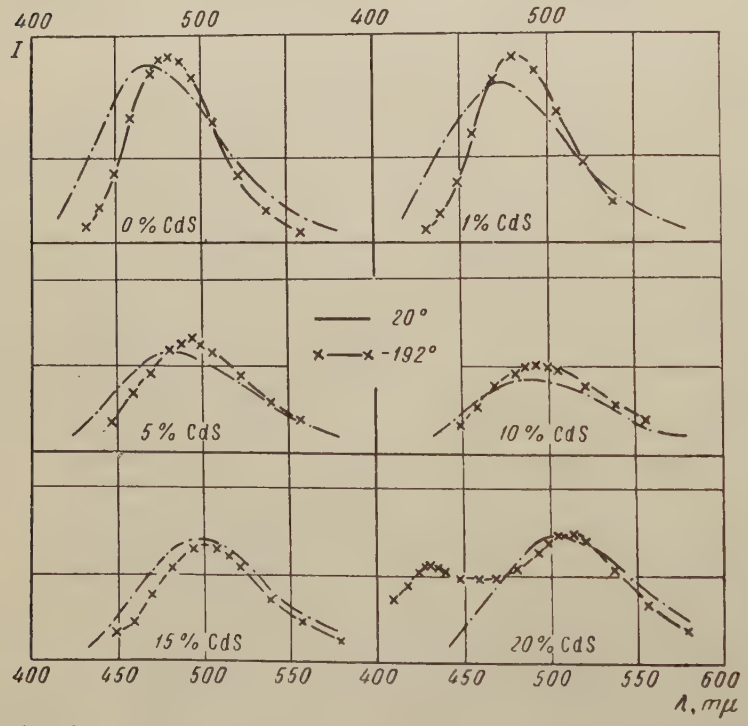

Fig.4. Energy distribution in the luminescence spectrum of ZnS·CdS phosphors at +20° and -192°.

excitation intensity; the other with 5% intensity. The points obtained with excitation at 50, 20 and 8% of the initial light intensity fall within the range of deviation between the two curves, i.e., the deviations do not exceed 3 mμ. Similar results were obtained for phosphor samples containing from 1 to 20% CdS. It is evident that reducing the intensity to 5% the initial does not significantly alter the shape of the spectral curve.

We also obtained the luminescence spectra at liquid air temperature. On the basis of the data, shown in Fig.4, it may be inferred that up to a CdS content of 15% inclusive the spectrum undergoes a temperature displacement but the shape of the curve does not change. At 20% CdS there appears a new short wavelength band peaking at about 430 mμ; it increases in intensity with increase of the CdS concentration to 50% and the luminescence becomes white (it is bright yellow at room temperature). Apparently this band is not associated with the main luminescence band of the material but is a new low temperature band peculiar to mixed phosphors with a high CdS content.

The luminescence of pure CdS at liquid air temperature is characterized by the presence of two bands: a bright green narrow band peaking at 521 mμ and a comparatively weak red band; to the eye the luminescence appears green. As the sample is gradually warmed, the red band increases in intensity, while the green one becomes weaker and disappears at -150°; at the same time there appears a distinct red luminescence, the intensity of which increases only very slightly with further warming to room temperature.

Preliminary temperature experiments showed that the introduction of CdS is accompanied by the appearance of shallow

traps that are evinced in the glow curves in the form of a rather flat peak centered at about -180°.

On the basis of the experimental data it may be asserted that in the investigated activatorless ZnS·CdS phosphors the cadmium does not give rise to its own typical band but acts only to shift the zinc band to the side of longer wavelengths. The influence of the Cd on the Zn band is highly reminiscent of its influence on the Cu and Ag activator bands, as reported in the literature.[1,2]

It is possible that the complexity of the luminescence bands of such mixed phosphors is evinced in the above described complex variation of the luminescence output. There is some divergence between our results and the data reported by Bundel' & Rusanova[3]. A possible reason for this divergence may be differences in the synthesis conditions.

I take this opportunity to express my deep gratitude to V.L.Levshin for valuable advice and interest in the work and to S.A.Fridman for making available the necessary reagents.

Physics Faculty
Moscow State University

References

1. V.L.Levshin & S.A.Fridman, Zhur.fiz.khim. (J.of Phys.Chem.) 6, 1277 (1935).
2. P.Pringsheim, Fluorescence and Phosphorescence, N.Y., 1949. (Cited in Russian trans.)
3. A.A.Bundel' & A.N.Rusanova, Izv.AN SSSR, Ser.fiz., 13, 173 (1949).

CRYSTAL PHOSPHORS WITH A HETERODESMIC STRUCTURE

- M.A.Konstantinova-Shlezinger

In investigating the luminescence of inorganic crystal phosphors in most cases experimenters study luminophors of the alkali halide or zinc sulfide type. Yet crystal phosphors with a heterodesmic structure, with complex ions (phosphates, silicates, tungstates and so on) are more convenient, at least for the first two stages of investigation.

The activator concentration in them is much higher[1], while the influence of harmful and difficult to detect contaminants is lower. There are extensive and as yet unutilized possibilities of partially replacing one type of ions by another and of varying the composition and structure of the luminophors at will. The influence of extraneous, interfering factors, for example, the excitation intensity, is weaker in most cases for these luminophors.

Not infrequently investigators "transfer" to these luminophors the ideas and models derived from investigation of alkali halide and sulfide phosphors; for instance, it is often assumed that the ability of such phosphors to luminesce is also connected with imperfections or defects in the crystal lattice.[2] As substantiation of this, there is cited the fact that the composition of the initial batch in most cases does not correspond to the stoichiometric composition of the synthesized luminophor.

In the present report I shall describe some of the results of experimental research carried out by our group - Gorbacheva, Leonov, Maksimova and Osiko - and on the inferences regarding the nature of crystal phosphors of this class following therefrom.

Gorbacheva[3] investigated the variation of the luminescence properties of cadmium phosphate luminophors with the conditions of precipitation of the initial phosphates and showed that only under certain conditions are they precipitated as individual phosphates with a definite composition and that only in such cases are there obtained bright luminophors. Their composition and structure, or more precisely, interplanar spacing, were established by Gorbacheva by Debye diffraction patterns and by chemical and differential thermal analyses. If the precipitated phosphate is not a single one, but contains admixtures of other phosphates, there appear in its heating (thermographic) curve auxiliary effects, evincing the influence of these impurities. This was demonstrated by Gorbacheva who compared the heating curves of mixtures with different relative contents of two individual phosphors obtained by precipitation (Fig.1).*

Maksimova in synthesizing phosphate cathodoluminophors utilized the procedure of recording the heating curves of the precipitated phosphates for the purpose of evaluating the degree of their individuality (singleness) and consequently their cathodoluminescent quality (Fig.2).

These data are in conflict with the conventional views[2] mentioned above and lead to the model concept of crystal phosphors as integral crystallochemical systems, the imperfection of which consists in the fact that the periodicity of the crystal is disturbed by partial replacement of the host crystal ions (or atoms) by activator atoms. The nonstoichiometric composition of the initial batch is explained by the fact that they are obtained as a result of reactions in the solid phase, which, as was shown years ago by Hedvall[4], usually do not go to completion. Hence the composition of the batch is generally chosen so that after heating there will remain unreacted only such components as do not have an adverse

---

*In her thesis N.A.Gorbacheva shows similar curves but obtained in heating mixtures of other phosphates.

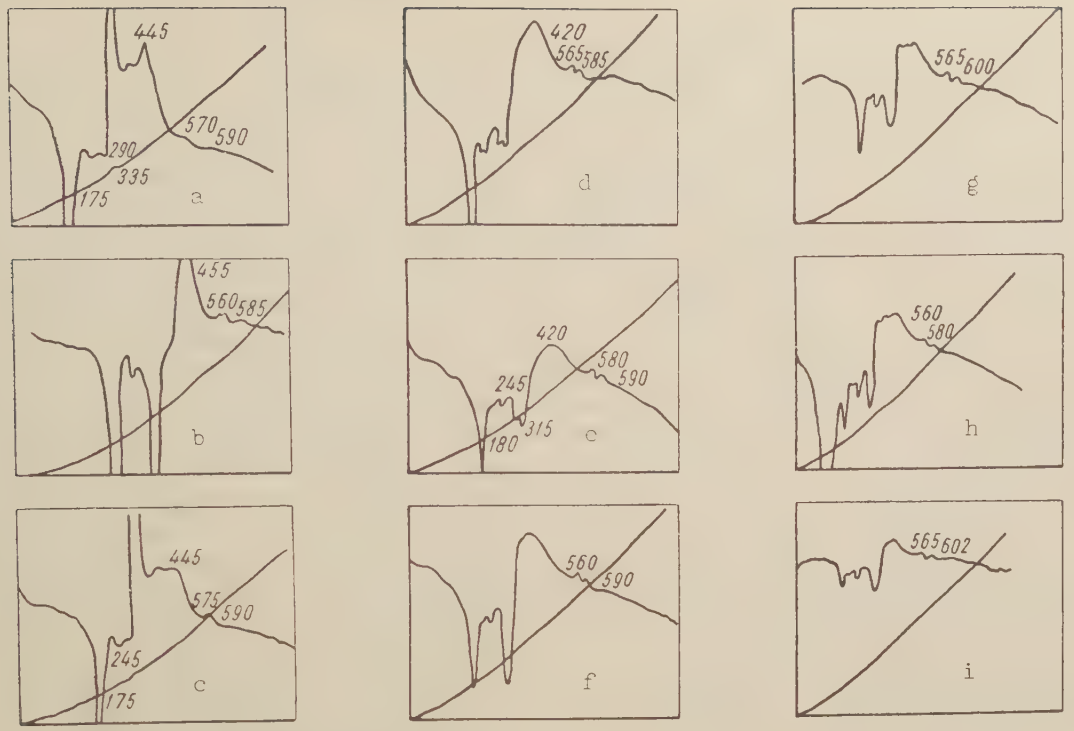

Fig.1. Heating curves for mixtures of cadmium phosphate $Cd_3(PO_4)_2 \cdot 2CdHPO_4 \cdot aq$ (I) and $CdNH_4PO_4 \cdot aq$ (II) taken in different proportions: a) 10% I and 90% II, b) 20% I, c) 30% I, d) 40% I, e) 50% I, f) 60% I, g) 70% I, h) 80% I and i) 90% I.

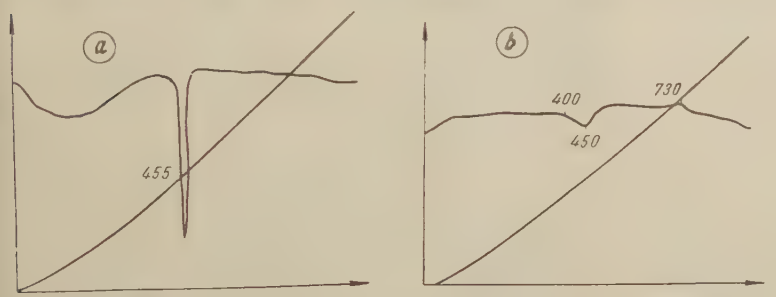

Fig.2. Heating curves for precipitated $SrHPO_4 \cdot aq$: a) "pure" individual phosphate, b) with an admixture of other phosphates.

effect on the luminescent properties of the phosphor. This case has been analyzed in the work of Ouweltjes & Wanmaker[5], who explain the necessity of having an excess amount of magnesium oxide in the initial batch for preparing magnesium tungstate luminophor by the necessity of avoiding the presence of unreacted WO_3 in the final product; with an excess of MgO the luminophor is formed on the surface of the magnesium oxide grains and the remaining unreacted components have no harmful effect.

Leonov[6] investigated in detail mixed tungstate luminophors and showed that to obtain the maximum brightness of $2Li_2O \cdot MgO \cdot WO_3$:Mn phosphor, the batch should contain an excess of tungsten trioxide, and the final product an admixture of the easily fusible phase, lithium tungstate. When the manganese is introduced in the form of sulfate, the excess amount of tungsten trioxide must be greater than when the batch is activated with manganese chloride ($T_{melt} = 650^o$); in the case of activation with uranium, the lack of an excess amount of WO_3 can almost be compensated for by prolonged heating.

According to the data of Osiko[7], a different situation obtains where an excess of silicon dioxide in the initial batch for Zn_2SiO_4:Mn luminophor is con-

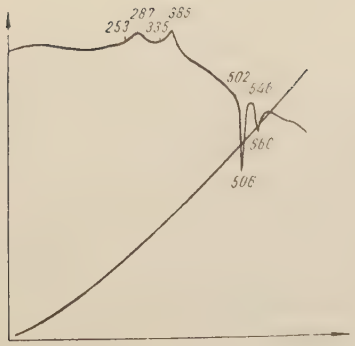

Fig.3. Repeat heating of $CdSO_4$ synthesized by heating at 800°.

cerned. He demonstrated that there forms a phase of varying composition, characterized by the same luminescence properties in a wide range of composition.

Many of the distinctive properties of the luminophors of this class can be understood from the standpoint of the proposed model concept; in particular, one can explain the irreversible changes observed in some luminophors when these are reheated to a temperature below the temperature of synthesis. Thus, for example, $CdSO_4$:Mn phosphor is obtained by heating at about 800°; upon repeat heating of the phosphor, it begins to darken at about 250-300°. Maksimova[8] investigated this phosphor in detail and showed that the temperature of darkening corresponds to a polymorphous transformation evinced by exothermic effects at 247-228° and 335-385° (Fig.3); the high temperature modification, which is not in equilibrium at room temperature, transforms to the low temperature modification. Upon further heating the darkened luminophor again turns white and begins to luminesce; there is again obtained a crystal phosphor but in a different modification.

Relative cathodoluminescence brightness of $Zn_3(PO_4)_2$:Mn phosphor synthesized at 1000° after second heating

Temperature of second heating, °C	Heating time, hrs.	Relative brightness
Initial phosphor	—	23,5
300	3	22,5
450	3	22,0
600	3	23
800		Transition to the green β-modification

At the high temperatures at which luminophors are normally synthesized metastability of the crystal compound forming is probably the rule rather than the exception. However, crystal phosphors differ as regards the height of the energy barrier which must be overcome to transform the metastable modification into a stable one.

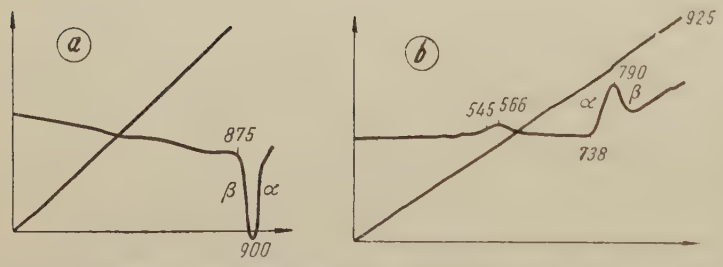

Fig.4. Heating curves for $Zn_3(PO_4)_2$:Mn phosphor: a) primary heating, b) secondary heating.

In the case of zinc phosphate phosphor activated with Mn the transition from the β modification, which luminesces green, to the α modification, which luminesces red, begins at a temperature of about 950°. The high temperature "red" α modification is stable at room temperature and, as Maksimova showed, three hour heating at an elevated temperature has little or no effect on the cathodoluminescence brightness (Table 1). The scatter of brightness values lies within the limits of the experimental error. At a temperature of 100-150° below the temperature of transition from the β to the α modification Maksimova succeeded in detecting in the differential heating curve an exothermic effect at 740-790°, corresponding to the α to β transition (Fig.4). Heating at this temperature changes the color of the cathodoluminescence; it becomes green.

If our concept regarding luminophors of the type in question as consummate defective crystallochemical systems is correct, the possibility of formation of phosphors with a given type of activator is determined by the same conditions as obtain for any inorganic compound. This means that in addition to the ionic radii, the coordination numbers, and so on, a significant role must be played by the energy balance of the reactions involved: the formation of the luminophor must be accompanied by a decrease of the free energy of the system and this decrease must be appreciably greater than in the case of segregation of an activator or other intermediate compounds into a separate phase. From this standpoint we can understand why some activators, regardless of the atmosphere in which the luminophor is synthesized, may be present in different valence states; this may be the case, for example, for manganese and europium. Maksimova used the procedure developed by Kröger[10] for determining the valence of manganese and investigated a large number of luminophors with different colors of luminescence.* The results obtained by her are shown in Tables 2 & 3 (the oxidation equivalent numbers were obtained on the assumption that manganese is tetravalent).

Table 2

Luminophor	Color of luminescence	C_{Mn}, 10^{-3} g/g	Batch, g	Number of oxidation equivalents (x 10^6)	
				theo.	exp.
Zn_2SiO_4 — Mn	Green	5	0,4	~54	0
$Zn_3(PO_4)_2$ — Mn	Green	1,29	0,4	19,2	0
$Zn_3(PO_4)_2$ — Mn	Red	1,29	0,4	19,2	0
$Sr_2P_2O_7$ — Mn	Yellow	5,2	0,4	74	0
$CdSO_4$ — Mn	Rose	5	0,3	54	0,68
$CdSO_4$ — Mn	Green modification	5	0,3	54	0,25
$Mg_2P_2O_7$ — Mn	Red	1,23	0,3	13,4	0,59

Table 3

Luminophor	Character of spectrum***	C_{Mn}, 10^{-4} g/g	Batch, g	Number of oxidation equivalents (x 10^6)	
				theo.	exp.
Mg_4GeO_6 — Mn	Discrete	10,3	0,25	9,4	8,75
Mg_2TiO_4 — Mn*	Discrete bands	1,7	0,4	2,4	2,7
Mg_2TiO_4 — Mn**	Discrete bands	1,7	0,3	1,8	2,08
Li_2TiO_3 — Mn	Discrete bands	8	0,2	5,8	5,12
Mg_2SiO_4 — Mn	spectrum not studied	1,36	0,4	1,48	1,48
$MgSiO_3$ — Mn	spectrum not studied	0,95	0,3	1,04	1,16

*Activator introduced in the form of Mn_2TiO_4.
**Activator introduced in the form of $MnCl_2$.
***The luminescence of all these phosphors is red.

Luminophors activated by both tetra- and divalent manganese exhibit red luminescence; however, a discrete structure of the luminescence spectrum is observed only with valence four. All the luminophors were heated by Maksimova in the same atmosphere in a Silit rod electric furnace; consequently the valence of the manganese was not determined by the thermodynamic conditions of formation of the manganese oxide as is sometimes inferred[10]. The results obtained by Maksimova show that Mn as the activator is tetravalent only in luminophors wherein the cation in the crystal lattice is magnesium or lithium, i.e., where the cation radius

---

*A detailed description of the analyses carried out by her will be given by Maksimova in a separate report.

is very small (Li^+ - 0.68 Å; Mg^{2+} - 0.74 Å; Mn^{4+} - 0.52 Å). A discrete structure of the luminescence spectrum was also found for Al_2O_3:Mn luminophor (Al^{3+} radius = = 0.57 Å); in this case, too, the manganese is tetravalent. We found no indications in the literature of discrete structure of the luminescence spectra of manganese in phosphors comprising cations other than lithium, magnesium and aluminum.

Another conclusion ensuing from our model concepts regarding crystal phosphors is the following. It has been shown experimentally for a large number of organic compounds that the ability to luminesce is evinced only if their molecules have a certain rigidity precluding exchange of excitation energy over vibrational degrees of freedom. In the case of organic molecules this is achieved in some cases by the introduction of addition atoms or groups and in other cases by preparing adsorbates or using viscous solvents. In contrast, in the inorganic crystal phosphors under consideration rigidity is an inherent, natural characteristic, the position of all the ions including the activator ion and the anions surrounding it is fixed by electrostatic and covalent forces, i.e., by coupling with all the neighboring ions. Spatial displacement of the ions from the equilibrium position in the excited state as compared with the unexcited one is little probable, in other words, there is little probability of intersection of the Franck-Condon curves (surfaces) for the excited and unexcited states and little probability of excitation energy exchange over the vibrational degrees of freedom.

Thus the ability to luminesce is an inherent property of most crystallochemical systems with a consummate defect structure; the questions are whether they can be obtained with a given activator, whether they absorb in the requisite region of the spectrum, and how one can eliminate or suppress different extraneous factors tending to quench the luminescence.

It follows from all the above said that of the three principal stages of investigation of crystal phosphors, the first two, namely, determination of the composition and structure and investigation of the luminescence properties in relation to the composition and structure, are more conveniently realized in the case of phosphors with a heterodesmic structure, with complex anions. The complexity of their crystal structure can give rise to difficulties only at the third stage, i.e., in interpreting the luminescence properties from the standpoint of present day physical concepts.

"P.N.Lebedev" Physical Institute,
Academy of Sciences of the USSR

References

1. M.A.Konstantinova-Shlezinger, Izv.AN SSSR, Ser.fiz., 21, 673 (1957).(Abs. Bull.21, No.5, 671); Trans.Fifth Conference on Luminescence, p.43, Tartu, 1957.
2. J.W.Strange, Brit.J.Appl.Phys., Suppl. No.4, 4 (1955).
3. N.A.Gorbacheva, Thesis, IONKh, M., 1957; Transactions of the Fifth Conf. on Luminescence, p.206, Tartu, 1957. (Abstract Bulletin,21,No.5,681.)
4. J.A.Hedvall,Reactionsfähigkeit fester Stoffe, 1938.
5. J.L.Ouweltjes & W.L.Wanmaker, J.Electrochem.Soc., 103, 160 (1956).
6. Yu.S.Leonov, Transactions of the Fifth Conf.on Luminescence, p.197, Tartu, 1957. (Abstract Bulletin, 21, No.5, 686.)
7. V.V.Osiko, Present issue of the Bulletin, p.1302.
8. G.V.Maksimova, Thesis, IONKh, M., 1955;Transac.of Fifth Conf. on Luminescence, p.197, Tartu, 1957. (Abstract Bulletin, 21, No.5, 688.)
9. A.L.Smith, J.Electrochem.Soc., 98, 363 (1951).
10. F.Kröger, Some Aspects of the Luminescence of Solids, N.Y. 1948.

FLUOROPHOSPHATE LUMINOPHORS OF THE WAGNERITE TYPE

- N.A.Gorbacheva

Halophosphate luminophors of the apatite type with the general formula $3R_3(PO_4)_2 \cdot RX_2$, where R = Ca, Ba or Cd and X = F or Cl are well known.

Calcium chlorofluorophosphate, $3Ca_3(PO_4)_2 \cdot Ca(F \cdot Cl)_2$, activated with antimony or manganese has found extensive use as a single component coating for "fluorescent" lamps[1-8]. We investigated the possibility of utilizing the structures of other natural minerals for the synthesis of phosphors.

In examining the properties of different minerals our attention was attracted to wagnerite described by the formula Mg_2PO_4F.[9] Initially we obtained artificial wagnerite by heating a batch consisting of MgO, MgF and $(NH_4)_2HPO_4$ at 1000°. To insure the solid phase reaction going to completion we initially took the ammonium phosphate in a 2% excess above the stoichiometric proportions. It was found, however, that there then remains unreacted MgF_2, which is an inert ingredient. We detected the presence of the MgF_2 phase by luminescence analysis. To this end the base material synthesized by joint heating of MgF_2, MgO and $(NH_4)_2HPO_4$ was reheated at 1000° with 2.5% TiO_2. With excitation of the sample heated with titanium dioxide by ultraviolet (2537 Å) against the dark background of the wagnerite mass there were observed very fine scattered particles with yellow luminescence; this was the second phase (MgF_2) activated by the TiO_2 (Mg_2PO_4F is not activated by titanium dioxide).

In order to obtain a single phase Mg_2PO_4F system we used substances which decompose before reacting; in this case the reaction is described by the equation

$$2MgCO_3 + NH_4F + (NH_4)_2HPO \rightarrow Mg_2PO_4F + 2CO_2 + 2H_2O + 3NH_3.$$

The heating should be carried out in two stages: 1) 1 hour at 500° and 2) for 30 min at 1000°. No particles of yellow luminescing luminophor were detected upon reheating this product with TiO_2. Consequently, in this case the system does not contain MgF_2. Debye powder patterns also showed that in this case MgF_2 is absent; there were also no indications of either $Mg_3(PO_4)_2$ or $Mg_2P_2O_7$ which might form in the reaction. Using similar procedures we synthesized the compounds Ca_2PO_4F, Sr_2PO_4F, Ba_2PO_4F, Zn_2PO_4F and Cd_2PO_4F. The heating temperature was varied depending on the fusion point of the synthesized substances. We tested a number of possible activators in conjunction with the enumerated compounds, but only with a few of them did we obtain effective luminophors. These are listed in Table 1.

It must be noted that manganese activates only Mg_2PO_4F; when doped with Mn the compounds Ca_2PO_4F, Sr_2PO_4F and Ba_2PO_4F yield colored products probably analogous to the mineral sarcopside: $[(Fe^{2+}, Mn, Ca)_2PO_4F]$.[9]

Of greatest interest in our opinion are the cathodoluminophors Mg_2PO_4F:Mn, which luminesces red, and Ca_2PO_4F:Dy, which luminesces yellow and has a persistent afterglow.

So far we have not succeeded in obtaining any promising photoluminophors on the basis of pure wagnerites.

Next we turned to synthesis of luminophors with mixed cations and obtained compounds in which 1/3 of the Mg was replaced by a divalent cation, namely, $(Mg,Ca)_2PO_4F$, $(Mg,Sr)_2PO_4F$, $(Mg,Ba)_2PO_4F$ and $(Mg,Zn)_2PO_4F$. It was found that all these base materials when activated by manganese are excited by ultraviolet (365 mμ) and emit red luminescence.

A different situation obtains in the case of excitation by electrons. We noted (visual observation) that in this case the color of the luminescence changes with change of the substituent cation. At our request, Yu.V.Voronov

Table 1

Photo-(I) and cathodoluminescence (II) colors of the synthesized luminophors

Host	Activator									
	Mn		Sb		Dy		Eu		Sm	
	I	II	I	II	I	II	I	II	I	II
Mg_2PO_4F	Weak red w. 365 mμ excit.	Red					—	Rose	—	Rose
Ca_2PO_4F, Sr_2PO_4F, Ba_2PO_4F	Colored compounds		Blue w. 253mμ excit.	Blue	—	Yellow	Red	Blue		
Cd_2PO_4F	Yellow w. 253 mμ excit.	Orange								
Zn_2PO_4F		Red-orange								

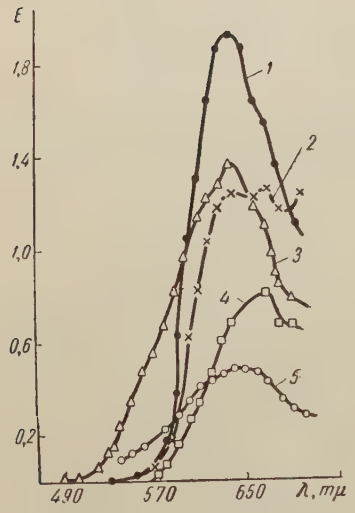

Emission spectra of wagnerite and two cation compounds activated by manganese: 1 - $(Mg,Zn)_2PO_4F$:Mn, 2 - Mg_2PO_4F:Mn, 3 - $(Mg,Ca)_2PO_4F$:Mn, 4 - $(Mg,Ba)_2PO_4F$:Mn, 5 - $(Mg,Sr)_2PO_4F$:Mn.

recorded the emission spectra of these luminophors with cathode-ray excitation. The spectra were recorded from screens with the tube operated at 15 kv and $7 \cdot 10^{-7}$ amp/cm^2. The emission spectra of wagnerite and the two cation compounds activated by manganese are shown in the accompanying figure. It will be seen from the figure that the luminescence of the "progenitor" of this group of luminophors, Mg_2PO_4F, consists of overlapping bands; the peak of the first band is situated at 640 mμ, the peak of the second at 660 mμ. Possibly there are other bands lying beyond 700 mμ.

The complex character of the red band of Mg_2PO_4F:Mn indicates that the manganese is present in the tetravalent state; we infer this by analogy with the case of Mg_2TiO_4:Mn investigated by Kröger[10]. Replacement of part of the magnesium by the enumerated divalent cations with gradual increase of the radius of the substituent cation (Table 2) leads to a change in the appearance of the luminescence spectra, i.e., to a redistribution of the energy among the bands.

Upon replacement of part of the magnesium cations in wagnerite by zinc, calcium or strontium, the luminescence peak at 640 mμ remains distinct, but the peak at 660 mμ becomes increasingly weaker with increase in the radius of the substituent cation. As will be evident from the figure, the change in the luminescence color from red-orange for $(Mg,Zn)_2PO_4F$:Mn to yellow for $(Mg,Ca)_2PO_4F$:Mn and $(Mg,Sr)_2PO_4F$ is due not only to redistribution of the energy between the 640 and 660 mμ peaks but also because the spectra of these luminophors are shifted to the side of shorter wavelengths as compared to Mg_2PO_4F:Mn. In the case of partial replacement of magnesium by barium, which has a larger ionic radius, the color of the luminescence becomes red The emission is more intense in the second band

Table 2

Host cation	Ionic radius, Å	Activator cation	Ionic radius, Å
Mg^{2+}	0,74	Mn^{4+}	0,52
Zn^{2+}	0,83	Sn^{4+}	0,67
Ca^{2+}	1,04	Sn^{2+}	1,02
Sr^{2+}	1,20		
Ba^{2+}	1,39		

and only its maximum is clearly pronounced; this is indicative that there occur more profound changes in the structure of the luminophor than in the case of replacement of the Mg by Zn, Ca or Sr.

In order to compare the structures of the investigated luminophors, we recorded the Debye powder patterns of the non-activated compounds in RKU-86 and RKU-114 diffraction cameras. From a comparison of the interplanar spacings and the intensity of the lines in the powder patterns it may be inferred that in case of replacement of the Mg by Zn or Ca the basic wagnerite lattice is retained, although there does occur some redistribution in the intensity of the diffraction lines; in the case of $(Mg,Ba)_2PO_4F$ there forms a compound with a structure differing from wagnerite. The compound $(Mg,Sr)_2PO_4F$ has a distinctive attribute: in contrast to the other mixed "wagnerites", when irradiated with $\lambda =$ = 1.54 Å it apparently yields x-ray radiation, which we were unable to suppress and which fogs the film. We plan to investigate this effect further, but at present can give no further information on the structure of $(Mg,Sr)_2PO_4F$.

Of special interest are experiments on activation of mixed "wagnerites" by tin. As is known, recently there have been synthesized Sn activated orthophosphate and pyrophosphate luminophors and these are now coming into use for "fluorescent" lamps. Butler[11] found that for obtaining luminescing materials the tin must be present in the divalent state (this may also be inferred from comparison of the ionic radii: only divalent Sn can replace Ca, Sr and Ba - see Table 2). In heating in air, however, the tin oxidizes to the tetravalent state; hence a second heating must be carried out in a rigorously controlled reducing atmosphere (otherwise the tin may be reduced to the metallic state). The need for repeated heating and the necessity of rigorous control of the reducing atmosphere greatly complicate the technology of these luminophors.

Tin exhibits a somewhat different behavior in the mixed "wagnerites" $(Mg,Ca)_2PO_4F$, $(Mg,Sr)_2PO4F$ and $(Mg,Ba)_2PO_4F$. When the tin is introduced into the batch in the form of SnO_2 and the material is heated twice, first at 600° and then at 1000°, there are formed luminophors yielding luminescence ranging from violet to blue. These materials do not have to be heated in a reducing atmosphere; apparently, the tin enters these luminophors in the tetravalent state (the ionic radius of Sn^{4+} is 0.67 Å), readily replacing the magnesium (ionic radius 0.74 Å).

Work on the synthesis of the described luminophors and on investigation of their luminescence centers is continuing.

I desire to express my sincere gratitude to M.A.Konstantinova-Shlezinger for guidance and Yu.V.Voronov for assistance in the work.

"P.N.Lebedev" Physical Institute,
Academy of Sciences of the USSR

References

1. A.A.Bundel', B.I.Vainberg, T.S.Dobrolyubskaya, V.V.Zelinskii, F.M.Pekerman, R.G.Smirnova, A.K.Trofimov & S.I.Frenkel', Izv.AN SSSR,Ser.fiz.,15,815 (1951).
2. B.M.Gugel' & M.M.Shapochnik, Transactions on the Fifth Conference on Luminescence, Tartu, 1957. (Abstract, Bulletin 21, No.5, 704.)
3. H.G.Jenkins, A.H.McKeag & P.W.Ramby, J.Electrochem.Soc.,96,11 (1949).
4. R.Nagy, R.W.Wollentin & C.K.Lui, J.Electrochem.Soc., 95,187 (1949).
5. M.Donerty & W.Harrison, Brit.J.Appl.Phys, 4, 11 (1955).
6. G.R.Fonda, Brit.J.Appl.Phys., 4, 69 (1955).
7. K.H.Butler, M.J.Bergin & V.M.Hannaford, J.Electrochem.Soc.,97,117 (1950).
8. W.L.Wanmaker, A.H.Hockstra & M.G.Tak, Philips Res.Repts, 10, 11 (1955).
9. A.G.Betekhtina, Mineralogiya (Mineralogy), M., 1950.
10. F.A.Kröger, Some Aspects of the Luminescence of Solids, N.Y., 1948.
11. K.H.Butler, J.Electrochem.Soc., 100, 250 (1953).

CHARACTERISTICS OF THE CRYSTAL PHASE OF ZINC SILICATE AND THE LUMINESCENCE PROPERTIES OF Mn ACTIVATED ZINC SILICATE LUMINOPHORS

- V.V.Osiko

The luminescence properties of zinc silicates activated by manganese have been discussed and analyzed repeatedly. It is generally assumed that their characteristic green photo- and cathodoluminescence is associated with a specific chemical compound, namely, zinc orthosilicate, in the crystal lattice of which part of the Zn^{2+} ions are replaced by Mn^{2+} ions. The phase diagram of the binary system zinc oxide-silicon dioxide[1] shows that there forms only one compound in the system: $2ZnO \cdot SiO_2$. In the preparation of this phosphor, however, the initial components of the batch - ZnO and SiO_2 - are generally taken in proportions differing from the stoichiometric to the side of an excess SiO_2. Leverenz[2] showed that the brightness of the cathodoluminescence does not change up to $ZnO:SiO_2 = 1:1$. The two oxides are taken in this proportion in commercial production of this phosphor for "fluorescent" lamps.

The purpose of the present research was to elucidate the variation in the luminescent properties of zinc silicate phosphors activated by manganese as a function of their chemical composition and the conditions of preparation. The luminophors were prepared by heating zinc oxide and silicon dioxide with a certain amount of magnesium nitrate. We varied the composition of the luminophor within the range of the formula

$$(1 - x)ZnO \cdot xSiO_2 \cdot 0.012Mn \quad (x = 0 \text{ to } 1).$$

As will be evident from the formula, the concentration of manganese in all cases was equal to 0.012 gram atom Mn per formula weight of the hose, which is equivalent to ~1% by weight. The time and temperature of heating were varied over a wide range. Curves characterizing the brightness of the photo- and cathodoluminescence of the phosphors as a function of the composition for different heating temperatures are shown in Figs.1 & 2. It will be evident that the character of the curves in both cases depends on the heating conditions. In contrast to the cathodoluminescence curves, the curves obtained for photoexcitation comprise plateaus. Curves 4 (Fig.1 & 2) pertain to mechanical mixtures of previously prepared silicon dioxide and the stoichiometric orthosilicate luminophor. It was established that variation in the shape of the curve occurs only up to a certain limit: no further change in the curves is observed at a result of prolonged heating beyond 12-15 hours at 1350°.

We investigated the phase composition of the luminophors subjected to protract-heating (20 hours at 1350°) by different physical-chemical procedures. We also recorded Debye powder patterns for the zinc silicates of different compositions (these will be published elsewhere).

With increase of the silicon dioxide content above the stoichiometric proportion there occurs a redistribution in the intensity of some of the zinc orthosilicate lines.* No lines characteristic of any modification of silicon dioxide are evinced in the emission; instead there appear several new lines.

Fig.3 shows the results of optical investigation of the zinc silicates by means of the microscopic immersion procedure. By submerging samples of the powders into liquids with different indices of refraction, we determined the upper and lower bounds of the refractive indices of the phosphor crystals. It will be

---

*In our case we are dealing with α-Zn_2SiO_4; under our preparation conditions the other two modifications (β and γ) cannot form.

Fig.1.

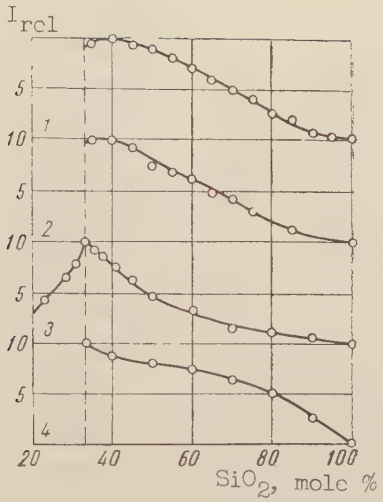

Fig.2.

Fig.1. Variation of the relative photoluminescence brightness with the composition of zinc silicate phosphors: 1) heating for 30 min at 1250°, 2) 4 hours at 1350°, 3) 20 hours at 1350°, 4) Zn_2SiO_4:Mn (20 hours at 1350°) + SiO_2 (20 hours at 1350°). The brightness was measured by means of a universal FM photometer with excitation by the light from a low-pressure mercury vapor tube.

Fig.2. Same as Fig.1 but for cathodoluminescence. The brightness was measured by means of a selenium photocell with excitation by an electron beam with a voltage of 10 kv and a current density of 10^{-7} amp/cm^2.

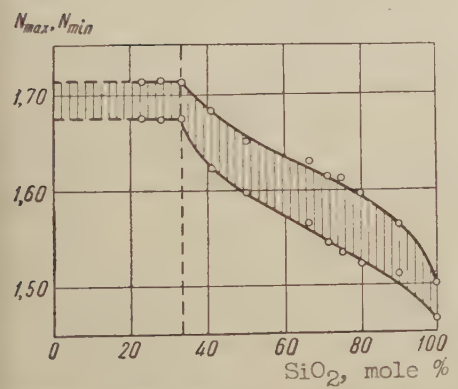

Fig.3. Variation of the upper and lower bounds of the index of refraction of Mn doped zinc silicates (heated 20 hours at 1350°) with their composition.

evident from the figure that these bounds are characterized by smooth curves rather than horizontal straight lines, which would be obtained if the system were a two phase one.

These results show that the phosphor system over its entire range of compositions from zinc orthosilicate to silicon dioxide is a single phase one and is consequently a phase of variable composition. Thermographic analysis led to the same inference.

It must be noted that in the given case there are structural factors favoring the formation of a phase of variable composition, namely, the presence of identical structural units - silicon-oxygen tetrahedra - and the fact that the coordination number of the zinc and silicon atoms with respect to the oxygen is always the same (four). We compared the formula volumes normalized to one gram-atom of oxygen for samples of different composition; the values of the formula volume characterize the packing density of the oxygen ions in the structure. For these calculations we used the experimentally determined values of the specific gravity of the phosphors in powder form. We obtained the same formula volume value for all compositions from the stoichiometric orthosilicate to silicon dioxide, i.e., we found that the packing density of the oxygen ions is constant. This fact again points to the formation of a single phase of variable composition. There are also grounds for assuming the formation of a single phase in view of the characteristics of the process of preparation of the phosphors. These phos-

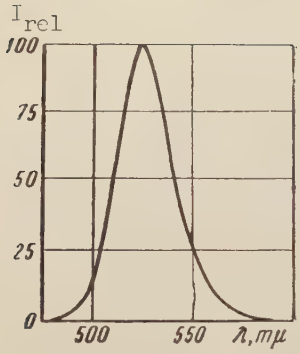

Fig.4. Luminescence spectrum of zinc silicates with manganese in the composition range from 0.66 ZnO·0.34SiO_2:0.12 Mn to 0.25ZnO·0.75SiO_2: :0.012Mn.

phors are formed in the process of a solid phase reaction and subsequent solid phase crystallization. Under these conditions, owing to the low rate of diffusion in solid phases, separation or stratification of the uniform system into two phases - zinc orthosilicate and silicon dioxide - is obviously hampered. In contrast, in the case of crystallization from nonviscous silicon melts, the rate of diffusion of ions is much higher and stoichiometric zinc orthosilicate can crystallize out.

Thus the formation under the synthesis conditions employed of a phase of variable composition does not conflict with the equilibrium phase diagram. The system in this case does not actually attain the equilibrium condition and the fact that with protracted heating (20 hours at 1350°) there is no spontaneous stratification into two phases indicates that the system is metastable as regards the heating temperature.

Only one crystallochemical structure is consistent with all the experimental data, namely, the α-Zn_2SiO_4 structure in which the zinc atoms at the tetrahedral sites are gradually replaced by silicon atoms. It is evident that one silicon atom must replace two zinc atoms with the resultant formation of one tetrahedral vacancy. Thus the zinc orthosilicate structure may gradually go over into the structure of one of the modifications of tridymite.

It is known that the luminescence spectra and other properties of crystal phosphors the matrix of which is a solid solution may vary with the composition. Classical examples are zinc-cadmium sulfide phosphors and sulfide-selenides. In such cases the variation in luminescence properties can be associated with changes in the lattice parameters or with changes in the chemical composition of the luminescence centers. In our case the luminescence centers are Mn^{2+} ions replacing the Zn^{2+} ions in the host lattice. The structure of the luminescence centers does not change with change in the composition of the zinc silicate phase: the centers are still the same divalent manganese ions surrounded by oxygen ions; there also occurs no change in the lattice parameters as is evinced by the absence of any shift in the lines in x-ray diffraction patterns and the invariance of the oxygen packing density. It would follow therefore that the luminescence spectrum of zinc silicate activated by manganese should be independent of the composition in a wide range. We recorded the luminescence spectra of several thoroughly heated samples with compositions ranging from that of the stoichiometric orthosilicate (0.66 ZnO·0.34 SiO_2:0.012 Mn) to 0.25 ZnO·0.75 SiO_2:0.012 Mn. All the points fall precisely on the spectral curve for the stoichiometric luminophor (Fig.4). This result is in conflict with the data of Leverenz[2], Moskvin[3] and other authors, according to whom the luminescence spectrum changes with increase of the SiO_2 content above the stoichiometric: presumably the long wavelength portion of the spectral curve becomes flatter and its peak is shifted to the side of longer wavelengths.

This discrepancy is, however, only apparent. Actually, most authors worked with nonequilibrium zinc silicates forming as a result of relatively brief heating. In this case the changes in the luminescence spectrum observed with variation in the phosphor composition are due to appearance of an orange-red component, which is probably associated with location of part of the Mn^{2+} ions in the octahedral vacancies of the disordered structure.[4,5] With more protracted high temperature heating of the nonstoichiometric zinc silicate phosphors the orange-red component in their luminescence spectrum gradually weakens and finally disappears.

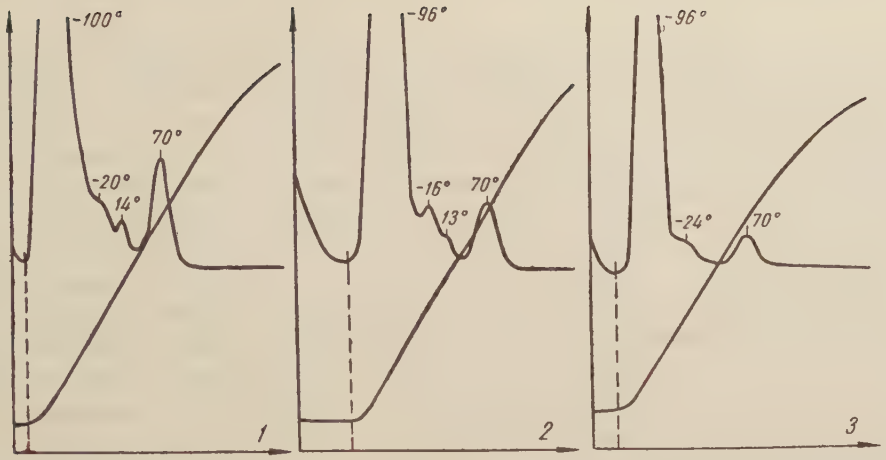

Fig.5. Glow curves: 1) 0.65 ZnO·0.35 SiO_2:Mn, 2) 0.60 ZnO·0.40 SiO_2:Mn, 3) 0.50 ZnO·0.50 SiO_2:Mn. Heating rate 4.5 degree/min.

The glow curves for three luminophors with different composition are shown in Fig.5. It will be evident that the temperatures of the peaks remain virtually the same, whereas if there were changes in structure one might expect evidence of corresponding charges in the system of trapping levels. Thus this behavior of the thermostimulation curves is also consistent with the assumption that there forms a phase of variable composition. One can also explain the difference between the photo- and cathodoluminescence brightness curves (Figs.1 & 2). The fact that the photoluminescence brightness is independent of the composition in a wide range of compositions, on the one hand, and the observed decrease in the cathodoluminescence brightness with increase of the SiO_2 content, on the other hand, can be explained by a difference between the photo- and cathodoluminescence excitation mechanisms in the luminophors subjected to protracted heating.* As is known from the work of Kröger[6] the photoluminescence of Mn activated zinc silicates is due to absorption of exciting radiation in the activator band (λ_{max} = = 250 mμ). This being the case, one can expect a weak structure dependence of the luminescence brightness. In the case of cathode-ray excitation, the electron energy is absorbed by the zinc silicate lattice and in this case the formation of vacancies in the structure can readily lead to decrease in the efficiency of energy transfer from the lattice to the luminescence centers.

I take this opportunity to express my deep gratitude to M.A.Konstantinova-Shlezinger for her guidance in the work.

"P.N.Lebedev" Physical Institute,
Academy of Sciences of the USSR

References

1. E.N.Bunting, J.Res.Natl.Bur.Standards,4,131 (1930);J.Am.Ceram.Soc.,13,5 (1930).
2. H.W.Leverenz, An Introduction to Luminescence of Solids, N.Y., 1950.
3. A.V.Moskvin, Katodolyuminestsentsiya (Cathodoluminescence) Vol.II,p.416, M,1949.
4. J.H.Shulman, J.Appl.Phys., 17, 11, 902 (1946); J.Elec.Soc.,96,57 (1949).
5. V.V.Osiko, Doklady AN SSSR, 121, 507 (1958). (Trans.Doklady).
6. F.A.Kröger, Luminescence of Solids Containing Manganese - Amsterdam,1940.

---

*The idea of different mechanisms was suggested by F.M.Pekerman.

LUMINESCENCE CENTERS IN SAMARIUM ACTIVATED ZINC SULFIDE PHOSPHORS

- Z.A.Trapeznikova

If zinc sulfide is doped with one of the rare earth elements the resultant phosphor has a line luminescence spectrum characteristic of the given rare earth ion. The luminescence spectra of such rare earth activated phosphors, as was shown in earlier studies[1-3], depend on the composition of the gaseous medium in which the phosphor is synthesized and on the presence of extraneous substances as, for example, zinc oxide, halide, etc. or a second activator, for example, copper.

This indicates that there form in the phosphors different luminescence centers depending on the conditions of preparation. By luminescence center here we understand not merely an activator ion per se but an activator ion with its immediate ambiance; hence the formation of different types of luminescence centers is entirely feasible if in addition to an activator, copper, oxygen or chlorine ions are introduced into the zinc sulfide.

It is not impossible, however, that there may also form several different types of luminescence centers in cases when no extraneous atoms are introduced. This may occur, for example, when the incorporation of the activator is accompanied by the formation of anionic or cationic vacancies, which may form in the case of introduction of activators with a valence differing from that of the host atoms. Some of the vacancies may be located close to the activator ions and form new luminescence centers in conjunction with them. New and different luminescence centers may also appear upon increase in the concentration of the activator when the activator ions can link up in pairs.

The present work was undertaken with a view to experimental determination of the possibility of formation of different types of luminescence centers under these conditions. By way of activator we chose samarium inasmuch as the structure of its luminescence spectrum, as earlier studies showed, is very sensitive to changes in the immediate ambiance of the Sm ions.

The samarium activated phosphors were prepared in the following manner. Luminescence pure zinc sulfide was treated with hydrogen sulfide at 900° to remove all oxygen containing impurities. The criterion for purity was absence of the green and blue luminescence of zinc sulfide with excitation by 365 mμ light. Usually after such treatment zinc sulfide has a very weak reddish luminescence. The samarium was introduced in the form of the sulfide in order not to introduce an anion extraneous to the base material. Each batch consisting only of zinc sulfide and samarium sulfide was thoroughly ground and mixed and then placed into an ampoule which was evacuated to $5 \cdot 10^{-6}$ mm Hg while heating at 130°. Upon attainment of the indicated vacuum, the ampoule was sealed and placed in a furnace maintained at 1150°. The phosphors were also prepared by heating in a stream of oxygen-free nitrogen.

For formation of a phosphor the heating temperature must be above 1020°. Heating of the batch at 1000° or lower does not result in formation of a phosphor with a characteristic Sm^{3+} luminescence and absorption spectrum; heating at 1070° or slightly above yields a good phosphor. This indicates that the samarium ions can be incorporated only into the looser structure of hexagonal zinc sulfide.

In the absorption spectrum of ZnS:Sm there were observed 24 lines in the region from 415 to 569 mμ; these are listed in Table 1.

The absorption lines of Sm^{3+} can be observed for phosphors with samarium concentrations equal to $5 \cdot 10^{-4}$ gram-atom/mole ZnS and higher. With increase in the samarium concentration there occurs an increase in the absorption line intensity, but the wavelength and relative intensities of the lines remain the same. The absorption spectrum does not depend on the gaseous medium used in heating; the frequency of the lines also does not change with reduction of the temperature to 77°K.

Table 1

Absorption spectrum of Sm^{3+} in zinc sulfide at 77°K

Line No.	λ, Å	Characteristics	Line No.	λ, Å	Characteristics
1	5692	Narrow, very weak	13	4822	Diffuse, weak
2	5617	Diffuse, very weak	14	4797	Diffuse, medium
3	5353	Narrow, weak	15	4737	" "
4	5088	Extremely weak	16	4722	" "
5	5064	Narrow, very weak	17	4610	Narrow, extremely weak
6	5027	Diffuse, extremely weak	18	4570	" " "
7	4956	Narrow, very weak	19	4451	Extremely weak
8	4948	Narrow, very weak	20	4503	" "
9	4937	Narrow, weak	21	4484	" "
10	4906	Diffuse, very weak	22	4318	Diffuse, weak
11	4883	Wide, strong	23	4296	Wide, very strong
12	4844	Diffuse, very weak	24	4146	Wide, extremely strong

The principal bright luminescence of the rare earth ion is not due to direct absorption of light by it; the luminescence appears as a result of light absorption by the zinc sulfide and also by the centers responsible for the "blue" luminescence of activatorless ZnS. This was demonstrated in earlier studies[1,2] of the excitation spectra of ZnS:Sm and other phosphors. Later it was found that the "blue" and "samarium" centers are distributed independently in the zinc sulfide, i.e., do not represent single formations[4].

Energy transfer from the absorbing "blue" centers to the "samarium" centers is realized through the valence band. The luminescence mechanism may be described as follows. The "blue" centers are ionized upon absorption of 332-334 mμ light; the electrons freed in the process enter the conduction zone from which they go to traps formed by trivalent samarium (an Sm^{3+} ion represents a local excess of positive charge). Upon capturing an electron the samarium goes over into the divalent state. As the result of thermal vibrations the electrons from the valence band are "thrown" into the ionized "blue" centers, while the holes forming in the valence band migrate through this band. When such a hole approaches a divalent samarium ion there occurs recombination of an electron with the hole with simultaneous transition of the trapped electron to an excited level of the trivalent samarium ion; this is followed by radiative transition to the ground state. For this transfer of energy from "blue" centers to "samarium" centers there must be an activation energy for transfer of the electron from the valence zone to a free level of the "blue" center. Investigation of the temperature dependence of the blue and orange-red samarium luminescence of ZnS:Sm phosphor substantiated this, in that it showed that at a sufficiently low temperature there is observed primarily blue luminescence.[4] For intense characteristic samarium luminescence to appear the phosphor temperature must be raised to the point at which transfer of an electron from the valence band to the ground level of a "blue" center becomes highly probable.

Investigation of the luminescence spectrum of ZnS:Sm phosphors prepared, as indicated above without the introduction of extraneous anions and cations showed, however, that there exist at least three different types of samarium luminescence centers to which energy absorbed in the "blue" centers can be transferred.

As is known, the luminescence spectrum of samarium in zinc sulfide consists of three groups of lines: a red, an orange and a green; the most intense is the red group. At room temperature and provided the exposure time is chosen so that

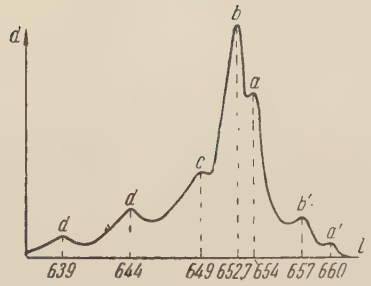

Fig.1. Photometric trace of the luminescence spectrum during excitation of ZnS:Sm phosphor: $C_{Sm} = 10^{-3}$ gram-atom/mole ZnS.

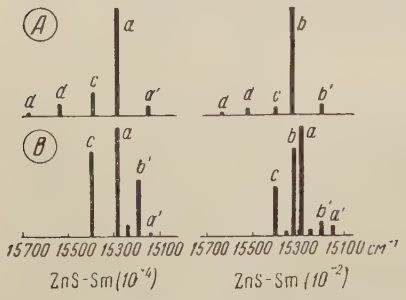

Fig.2. Schematic luminescence spectrum during excitation of ZnS:Sm phosphor by 365 mμ light: A - at 293°K, B - at 77°K

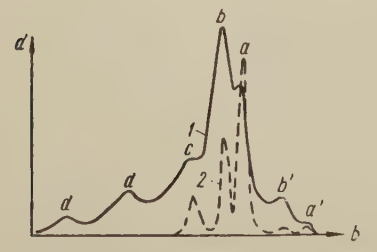

Fig.3. Luminescence spectra of ZnS:Sm (10^{-3}) phosphor during excitation with 365 mμ light: 1 - at 293°K, 2 - at 77°K.

the strongest lines of the red group will not be overexposed, there can usually be distinguished seven lines in this group with the following wavelengths: 639, 644, 649, 652.7, 654, 657 and 660 mμ (Fig.1).

For purposes of further discussion we shall identify these lines by letters as follows: a - 654, b - 652.7, a' - 660, b' - 657, c - 649, and d - 644 and 639 mμ. These lines may be divided into four subgroups with characteristic attributes: the first group comprises the a and a' lines, the second and b and b' lines, the third group the c line and the fourth group the two lines identified by d.

The intensity ratio of the lines of the first and second subgroups varies with the samarium concentration in the phosphor. Reducing the samarium concentration to 10^{-4}, 10^{-5} and 10^{-6} gram-atom/mole ZnS in the case of heating in an evacuated ampoule or to 10^{-5} and 10^{-6} gram-atom/mole ZnS in heating in a stream of nitrogen, one can obtain a phosphor yielding a spectrum from which the b and b' lines are absent. Increasing the samarium concentration to 10^{-2} one can obtain a phosphor the spectrum of which is devoid of the a and a' lines (Fig.2,A). At intermediate Sm concentrations there are obtained phosphors with spectra including all the lines and it is found that the relative intensity of the a & a' and b & b' lines varies consistently with increase or decrease of the Sm concentration.

The intensity ratio of the lines of the first and second subgroups also varies with decrease of the phosphor temperature and also if the phosphor is exposed to the action of infrared during excitation. In the case of auxiliary infrared irradiation during excitation there is observed an increase in the intensity of the b & b' lines and a decrease in the brightness of the a & a' lines. With decrease of the phosphor temperature, on the contrary, the brightness of lines b & b' decreases and the intensity of lines a & a' increases (Fig.3).

These data indicate that the a & a' and b & b' lines pertain to different samarium luminescence centers, "A" and "B" centers, which are characterized by different probabilities for electron and hole trapping. Under the influence of infrared light or heat the ratio of trapping probabilities by these centers changes with the result that the intensity of the lines corresponding to electron transitions in them is altered. Reduction of the phosphor temperature, as was noted above, favors emission by the "A" centers. Even in a phosphor with a high concentration of samarium, in the luminescence spectrum of which at room temperature there are observed only the b & b' lines, upon reduction of the temperature there appears the a line (Fig.2,B).

Table 2

Conditions of preparation of the phosphor or observation of the luminescence spectrum	Line intensity						Remarks
	a 654 mμ 15 290 cm^{-1}	a' 660 mμ 15 150 cm^{-1}	b 652.7 mμ 15 320 cm^{-1}	b' 657 mμ 15 200 cm^{-1}	c 649 mμ 15 400 cm^{-1}	d	
Increase in Sm concentration	Decreases		Increases		No change in intensity or frequency	At low Sm concentrations ν = = 15 540 & 15 680 cm^{-1}, $\Delta\nu$ = 140 cm^{-1}; at high Sm concentrations ν = 15 520 & 15 640 cm^{-1}, $\Delta\nu$ = 120 cm^{-1}	
Reduction of the phosphor temperature	Increases		Decreases		Increases	Decreases & disappears at liquid nitrogen temp.	The variation of $I_{a'}$ & $I_{b'}$ with T and IR is more complex than that of I_a and I_b.
IR irradiation during excitation	Decreases		Increases		Decreases in most cases	Complex dependence: increases in most cases	Varies with variation of the Sm concentration & wavelength of the exciting light.

The c line, which we put in subgroup three, is present in the spectra of all samarium activated phosphors obtained without the introduction of extraneous cations and anions. Its wavelength does not change with variation in the Sm concentration.

The lines of the fourth subgroup, designated d, disappear from the luminescence spectrum if the phosphor is cooled (see Figs.2 & 3). Hence it may be inferred that these two lines are associated with transitions from excited vibrational levels to the ground state. The wavelength of the d lines and the separation between them change abruptly with change in the samarium concentration: at low Sm concentrations the frequency difference is 140 cm^{-1}, while at high Sm concentrations the separation is 120 cm^{-1}.

There is also a frequency difference equal to 140 cm^{-1} between the a and a' lines which pertain to the "A" centers, forming primarily at low Sm concentrations; a frequency difference equal to 120 cm^{-1} is observed between the b and b' lines, corresponding to transitions in the "B" centers which form at high Sm concentrations.

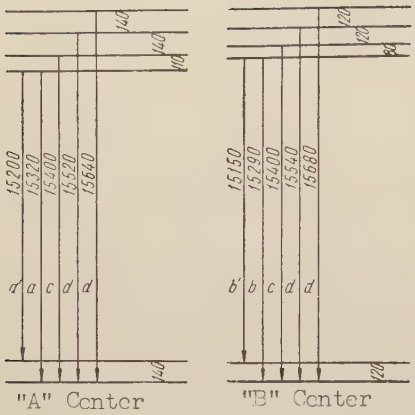

Fig.4. Terms of the "A" and "B" luminescence centers.

The experimental data, which are summarized in Table 2, can be represented in the form of terms of the two centers if we accept that the c line in both centers corresponds to an electron transition from a higher lying excited level to the ground level (Fig.4). The line d must then be attributed to electron transitions from vibrational levels of this excited state.

Thus it may be assumed that samarium in zinc sulfide forms at least two types of centers, the luminescence of which can be observed at room temperature and at liquid nitrogen temperature. The concentration dependence of these centers shows that the "A" centers comprise one Sm ion, while the "B" centers consist of two. This explains the difference between the trapping probabilities of electrons and holes by these centers.

Sometimes one can obtain ZnS:Sm phosphors in the spectra of which the c line becomes very intense and diffuse with excitation by 365 mμ light. This is usually observed in the case of phosphors heated in an atmosphere of hydrogen sulfide and very occasionally in individual samples heated in an evacuated ampoule. The luminescence spectrum of such phosphors during excitation by 365 mμ light differs markedly from the spectra obtained with excitation at wavelengths of 313 and 334 mμ (Fig.5). If, however, during excitation with λ = = 365 mμ the phosphor is irradiated with infrared, its luminescence spectrum becomes similar to the luminescence spectrum with 313 and 334 mμ excitation.

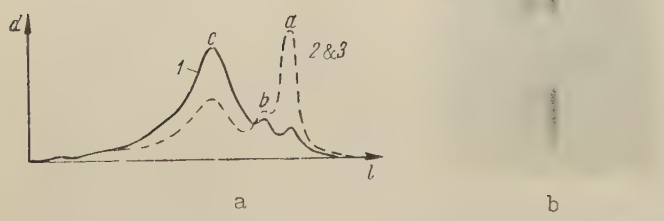

Fig.5. a - Photometric curves of the luminescence spectra during excitation of ZnS:Sm phosphor heated in H_2S: 1) λ = 365 mμ, 2) same but with infrared irradiation, 3) λ = 313 mμ; b - the corresponding spectra.

If one accepts the hypothesis that Sm in zinc sulfide forms two different types of luminescence centers, one can explain the experimental data as follows.

As was noted above, the excitation of the samarium may occur as a result of absorption in the zinc sulfide and in "blue" centers. The absorption maximum of the "blue" centers is located at 332-334 mμ. The absorption of 365 mμ light may be due, on the one hand, to absorption by the "blue" centers located at regular zinc sulfide sites - in this case it will be on the side of the absorption band of the "blue" centers. On the other hand, it is possible that the 365 mμ light may be absorbed by "blue" centers located at defect points in the sulfide lattice. The absorption of such "blue" centers may be shifted to the long wavelength side.

In the case of phosphors prepared by heating in hydrogen sulfide there may form many defects in the form of dislocations, interblock surfaces and large imperfections, for example, as a result of adsorption of excess sulfur. In this case the absorption of 365 mμ light will occur primarily in the "blue" centers lodged in these defects. In this case the energy absorbed by the centers will readily be transferred to the samarium atoms comprised in the luminescence centers also located at these defect points. These luminescence centers, located

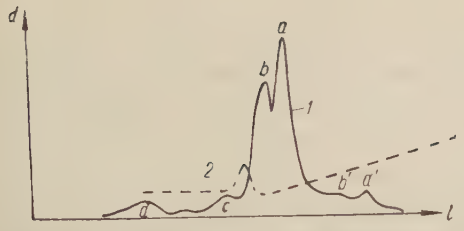

Fig.6. Photometric curves of luminescence spectra during excitation by 313 mμ light. Phosphors: 1) ZnS:Sm(10^{-3}), 2) ZnS:Sm(10^{-3}):Cl(10^{-3}).

not at regular lattice sites, will differ somewhat from each other and the samarium ions comprised in them will be subjected to the action of fields differing somewhat in strength, which should lead to smearing out of the spectrum. If we assume that the a & a' lines upon alteration of the immediate ambiance of the samarium ions located in the regular lattice can shift to the short wavelength side and occupy positions b & b' in the spectrum, we can all the more expect strong smearing out of these lines to the point where they become invisible when there are present many centers differing somewhat from each other, as would obtain for centers lodged at defect points. In fact, a strong background is observed in the luminescence spectrum of ZnS:Sm phosphors with excitation by 365 mμ light. True, in the spectrum of the phosphor with excitation by 365 mμ light there are also present clear but very weak a and b lines, but they may arise as a result of simultaneously occurring ionization of the samarium centers in the volume of the crystal.

The line c, the position of which is very stable in the samarium spectrum, is also smeared out but to a lesser extent and hence we observe it in the form of a broad line. Infrared radiation may remove electrons trapped near the samarium ions at defect points and as a result the intensity of the c line decreases. The electrons freed by the infrared light may be trapped by samarium located in the regular zinc sulfide lattice; this explains why the luminescence spectrum obtained with 365 mμ excitation and simultaneous IR irradiation becomes similar to the luminescence spectrum of the phosphor with excitation by 334 or 313 mμ light.

It should also be noted that at low temperatures there appear in the luminescence of ordinary ZnS:Sm phosphors additional lines at 651 and 656 mμ (see Fig.2). These lines can be attributed to a third type of luminescence center, which is capable of trapping and holding electrons, produced in ionization of "blue" centers, only at low temperatures. The 651 mμ lines in the spectrum of samarium at room temperature can be observed in two cases. First, if the phosphor is prepared from a batch into which there have been introduced chlorine ions in an amount sufficient for the proportion of Sm^{3+} to Cl^- to be equal to unity. In the luminescence spectrum of the resultant phosphor there appears the single λ = 651 mμ line and in addition an intense blue band (curve 2, Fig.6); consequently, in this phosphor there presumably form primarily luminescence centers of the third kind. Second, if in addition to chlorine, copper is introduced as the second activator into the ZnS.Sm phosphor; in the spectrum of ZnS:Sm:Cu (NaCl) there appear lines at 651, 652.7 and 654 mμ. At room temperature the intensity of the 651 mμ line is comparable with the intensity of the 654 mμ line, but its behavior differs from the latter and also from that of the 652.7 mμ line and is virtually identical with the behavior of the copper band[3]. In this phosphor apparently the probability for trapping of electrons and even of holes by the third type of centers at room temperature is comparable with the probability for trapping by "A" type centers.

It will be apparent from the above data that the formation by samarium of different types of luminescence centers and their efficiency as regards trapping of electrons and, apparently, holes, depends on many different factors and requires further investigation.

On the basis of the work done so far one can draw the following conclusions:

1. Samarium in zinc sulfide can simultaneously form three or perhaps more different types of luminescence centers characterized by different electron and

hole trapping probabilities. The number of these centers depends on the samarium concentration and the conditions of synthesis.

2. The relative number of two of these centers depends on the samarium concentration. These two types of centers differ as regards the vibrational structure of the upper excited and lower ground states. Characteristic of these centers is the presence of two excited electron levels, the separation of which for these two types of centers differs (110 and 80 cm^{-1}).

3. The emission brightness of the different centers and, consequently, the luminescence spectrum of the phosphor depend on conditions governing the kinetics of the processes associated with transitions of electrons and holes; they depend, for example, on the temperature of the phosphor and on auxiliary infrared irradiation.

4. When the phosphor is formed with a large number of distortions of the regular lattice, the samarium luminescence spectrum with excitation by 365 mμ light is greatly diffused.

I desire to thank T.I.Voznesenskaya and R.M.Medvedeva for assistance in the work and V.V.Antonov-Romanovskii and M.V.Fok for a number of valuable suggestions and discussion of the results.

"P.N.Lebedev" Physical Institute
Academy of Sciences of the USSR

References

1. Z.A.Trapeznikova & V.V.Shchaenko, Doklady AN SSSR, 106, 230 (1956). (Trans. Doklady.)

2. Z.A.Trapeznikova, Transactions of the Fifth Conference on Luminescence, Tartu, 1957 (Abstract, Bulletin 21, No.5, 677.)

3. V.V.Antonov-Romanovskii & Z.A.Trapeznikova, Optika i spektroskopiya, 1, 204 (1956).

4. Z.A.Trapeznikova, Optika i spektroskopiya, 4, 512 (1959). (Trans. Optics & Spectroscopy.)

SOME DATA ON THE MECHANISM OF FORMATION OF SULFIDE LUMINOPHORS

- A.A.Bundel', A.I.Rusanova & L.G.Taushkanova

The experimentally observed variation of the luminescence properties of sulfide phosphors with the nature of the substances in contact with them during synthesis is usually interpreted as proof of participation of these substances in the formation of the luminescence centers. Generally the influence of such agents on the base material of the luminophor is disregarded. For example, it is still widely held that chlorine atoms from the flux enter into the composition of the luminescence centers, although check experiments failed to substantiate this[1].

Of particular importance from the standpoint of the physical chemistry of zinc sulfide phosphors is the nature of the activating agent in "activatorless" zinc sulfide. Without touching upon the question of the structure of the "blue" luminescence centers, in earlier publications[1-3] we cited a number of facts which indicate that the formation of these centers is connected with deviation from stoichiometry to the side of enrichment of the ZnS with zinc and that the composition of these centers does not comprise any substances extraneous to ZnS. The incorporation of extraneous elements into the zinc sulfide lattice leads to the formation of distinctive luminescence centers, which is evinced by the appearance of the characteristic bands of these elements in the luminescence spectra. Thus, the introduction of oxygen from the gaseous phase into previously prepared activatorless phosphor[4] leads to the appearance of the characteristic oxygen band peaking at about 530 mμ (sphalerite modification).

Recently Riehl & Ortmann[5] reported that in the case of heating of deoxidized ZnS with flux but in the absence of oxygen, the characteristic blue luminescence does not appear. From this they concluded that the oxygen enters into the composition of the blue luminescence centers. They make no mention of the appearance of green luminescence in the presence of oxygen.

Our earlier experiments[2-4] showed that the blue luminescence centers are formed without the participation of oxygen. Hence the explanation for the effect observed by Riehl & Ortmann should be sought in a different type of interaction of ZnS with oxygen than that inferred by these authors. Inasmuch as we earlier studied the introduction of oxygen from the gaseous phase into already formed luminophors with blue luminescence and many aspects of the work of Riehl & Ortmann remain unclear, we felt it expedient to investigate in detail the influence of oxygen on the formation of ZnS:Zn phosphors.

Samples of ZnS luminophors produced by the "Krasnyi khimik" ("Red Chemist") Plant with (Fe + Cu + Ni) $< 1 \cdot 10^{-7}$ g/g and ~1.5% SO_4^{2-} were deoxidized in a stream of H_2S for 3 hours at 900° with a layer thickness not exceeding 8 mm. The resultant product did not luminesce even under intense excitation and no longer contained SO_4^{2-}. Before the experiments the occluded sulfur was eliminated by heating to 300° in a nitrogen vacuum ($O_2 < 1 \cdot 10^{-3}$%, 1 mm Hg). The NaCl flux was introduced in dry form in the amount of 3%.*

The luminophors were heated in quartz boats with a layer thickness of 3-4 mm in a quartz tube connected through a ground joint to the vacuum system and the nitrogen supply which according to analysis contained less than $1 \cdot 10^{-3}$% O_2. After repeated "flushing" of the system with nitrogen and intermediate evacuation, a mixture of Na_2 + O_2 containing from $0.7 \cdot 10^{-7}$ to $6 \cdot 10^{-3}$ g O_2 per gram ZnS was intro-

---

*Deoxidation with H_2S radically alters the properties of the initial ZnS: subsequent heating of the deoxidized ZnS in air yields a product, the luminance of which amounts to only 48-50% of the luminescence brightness of the luminophor obtained from the same initial ZnS.[6]

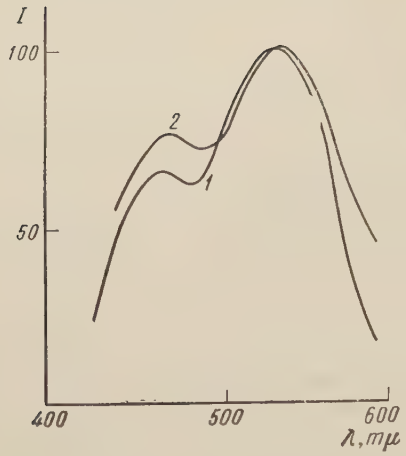

Fig.1

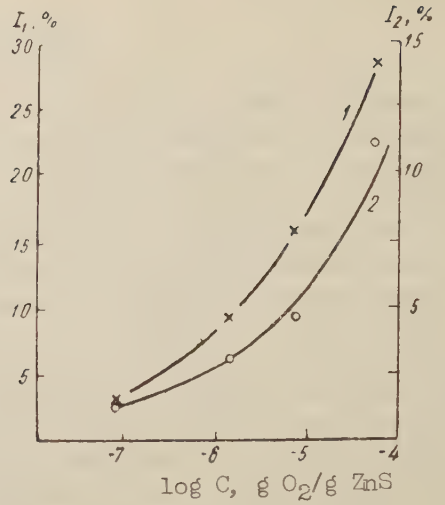

Fig.2

Fig.1. Luminescence spectra of ZnS: 1) formed in the presence of $1.3 \cdot 10^{-5}$ g O_2 per gram ZnS (scale enlarged), 2) produced by the introduction of $3 \cdot 10^{-3}$ g O_2 into previously prepared ZnS:Zn.

Fig.2. Formation of ZnS in the presence of different amounts of oxygen: 1) brightness (referred to ZnS heated in air) of the Zn band, 2) brightness of the O_2 band ($P_{O_2} \leqslant 0.5$ mm Hg).

duced into the tube. The fluxed batches were heated for 20 min at 950°. The resultant product always exhibited both green and blue luminescence. Green luminescence predominated in the upper layers that were in contact with the gaseous medium; the blue band predominated in the deeper layers. Inasmuch as it was impossible to separate the layers the entire mass was thoroughly mixed for luminospectroscopic investigation. The luminescence was excited by the 366 mμ line of mercury.

At room temperature the spectra represent a superposition of two bands: a blue band with λ_{max} = 465 mμ and a green oxygen band with λ_{max} = 530 mμ (Fig.1). At 100° the former is extinguished, and the remaining luminescence consists only of the green band.

The luminescence spectra of phosphors formed in the presence of small amounts of O_2 have the same appearance as those described by us earlier for the case when the oxygen was introduced in the same amounts into the previously prepared luminophor, but the integral brightness of the luminescence is much lower. In the presence of $0.7 \cdot 10^{-7}$ g O_2 per gram ZnS, the brightness of the blue band amounts to only 2.8% of the brightness of the band emitted by the luminophor formed in air, while with $3 \cdot 10^{-3}$ g O_2 per gram ZnS the brightness of the green band does not exceed 15% of its brightness in the case of introduction of the same amount of O_2 into the previously prepared blue luminophor. With increase in the amount of oxygen present the brightness of both bands increases according to the same law (Fig. 2). With increase of the oxygen partial pressure above 0.5 mm Hg the increase in the brightness of the green band ceases and there begins oxidation of the sulfide with the formation of oxysulfide; the presence of this is evinced by the appearance of its characteristic band (λ_{max} = 510 mμ) in the spectrum (see Ref.2).

In order to realize the heating in an atmosphere as free of oxygen as possible, we eliminated all traces of this gas from the reaction volume by means of getters. To this end two separate batches of deoxidized ZnS were introduced into the quartz tube; one of these served as the getter. After "flushing" of the

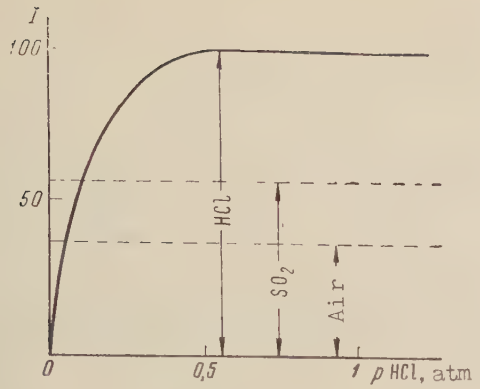

Fig.3

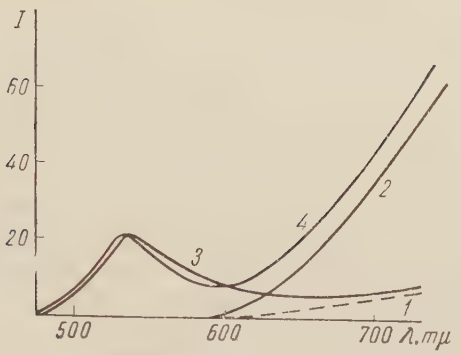

Fig.4

Fig.3. Comparison of the efficiency of HCl, O_2 and SO_2 as agents stimulating the appearance of blue luminescence in heating deoxidized ZnS. The solid curve characterizes the variation of the luminescence brightness with the HCl pressure.

Fig.4. Spectrum of CdS heated: 1) in N_2, 2) in air, 3) with 10% ZnS in N_2, 4) with 10% ZnO in air.

tube and filling it with nitrogen ($O_2 < 10^{-3}$%), the end with the getter batch was heated for an hour at 950° and then the tube was moved further into the furnace so that the second batch of ZnS entered the hot zone. The ZnS serving as the getter exhibited the usual weak luminescence in both bands, whereas the sample heated second showed no luminescence, either blue or green.

Thus, in agreement with the data of Riehl & Ortmann[5], in the case of short term heating of deoxidized ZnS with NaCl in the absence of molecular oxygen no luminescence appears. In the presence of even minimal amounts of O_2 both blue and green luminescence develop. Consequently, we found that in the case of short term heating with NaCl the presence of O_2 is a sufficient condition for the appearance of blue luminescence; we still had to check whether this was a necessary condition.

To this end, using the same equipment, we heated deoxidized ZnS both with and without NaCl in an atmosphere of HCl and of a mixture of HCl with O_2. The HCl was obtained by the action of H_2S on NH_4Cl; the product was condensed and repeatedly fractionated. The work was carried out in an integral-blown glass apparatus with a ground glass joint to the quartz tube. In some experiments after filling the system with HCl, we gettered the reaction volume with ZnS as described above. At HCl pressures above 0.4 atm in all cases we obtained blue luminescing phosphors the brightness of which was 2.8 times greater than the brightness of phosphors obtained by heating deoxidized ZnS in air and some 1.4 times greater than the brightness of phosphors prepared in air from nondeoxidized ZnS.*

The addition of oxygen to the HCl heating atmosphere results in the appearance of green luminescence in the oxygen band peaking at 530 mμ (this is readily and reliably identified from its temperature behavior[7]). At HCl pressures under 0.4 atm the brightness of the blue luminescence rapidly falls off with decreasing HCl pressure (Fig.3).

We also carried out heating of deoxidized ZnS in an atmosphere of SO_2 under the same conditions; in this case there were also obtained blue luminescing phos-

---

*At temperatures above 100° there was evident a very weak blue luminescence the brightness of which did not change with increase of temperature to 200°. This shows that this luminescence is due to copper impurity rather than to oxygen (see Ref.7).

phors the brightness of which was 1.8 times greater than that of deoxidized ZnS heated in air.

These experiments in which we found that completely identical blue luminescence develops as a result of heating in the presence of oxygen as well as of HCl and SO_2 proved that these substances do not enter as structural components into the blue luminescence centers; apparently, they affect the state of the host material and consequently act as mineralizers. Their efficiencies as agents favoring the appearance of blue luminescence are shown in Fig.3. These results are in complete agreement with the data of Smith[8] on ZnS:Ag.

The mineralizing character of the influence of these stimulating agents is also substantiated by microscopic and x-ray diffraction studies; the mean size of the crystals obtained in an atmosphere of air is about 10^{-4} cm, in SO_2 about 10^{-3} cm and in HCl close to 10^{-2} cm.

The role of molecular oxygen as a mineralizer in the formation of sulfide phosphors is clearly evinced in experiments with activatorless CdS (Fig.4). Deoxidized CdS with 3% NaCl heated for 30 min at 900° in nitrogen emits no luminescence under excitation by λ = 365 mμ. When the same material is heated in air under the same conditions there is obtained a bright phosphor with a band beyond 750 mμ. If the oxygen were responsible for the luminescence of the activatorless luminophor as a component of the luminescence centers, the results should not depend on from what compound the oxygen is introduced into the CdS lattice during synthesis. To check this we heated a mixture of 90% CdS + 10% ZnO by weight with 3% NaCl in nitrogen and in air. Only the characteristic luminescence of zinc oxide was observed for the samples heated in nitrogen (the zinc oxide spectrum was shifted somewhat to the side of longer wavelengths owing to formation of mixed CdS-ZnO crystals). No luminescence in the cadmium band appeared although x-ray diffraction studies indicated the formation of mixed ZnO-CdS crystals, i.e., the incorporation of oxygen into the CdS lattice. At the same time heating in an atmosphere of air yielded a phosphor in the spectrum of which, in addition to the ZnO band, there was present the bright band of nonactivated cadmium sulfide.

Thus the agent stimulating the formation of an activatorless luminophor is only molecular oxygen.

The accelerating action of molecular oxygen on the process of formation of luminophors is very effectively evinced in the case of mixed ZnS·CdS:Ag phosphors.*

A batch having the composition

$$55ZnS \cdot 45CdS : 2 \cdot 10^{-4}Ag + 3\%\ NaCl$$

composed of commercial sulfides containing appreciable amounts of oxidized substances when heated in air at 1200° yields a normal luminophor even after only 8 min heating. All the phosphor crystals are identical as regards their emission spectra and the grain-size composition of the powder is characterized by the usual gaussian curve (Fig.5); increase of the heating time results only in some displacement of the granulometric curve to the side of larger particles. In the case of heating of the same batch in nitrogen, the resultant product consists of a mixture of two types of crystals exhibiting different colors of luminescences: greenish-blue and orange-yellow. The granulometric composition curve now exhibits two peaks corresponding to phases with predominance of ZnS and CdS. Upon increase of the heating time there occurs a gradual evening out of both the luminescence properties and the grain-size composition, but the equalization does not terminate even after an hour's heating. Consequently, there was evinced in

---

*The experiments described below were performed by T.G.Bulankova.

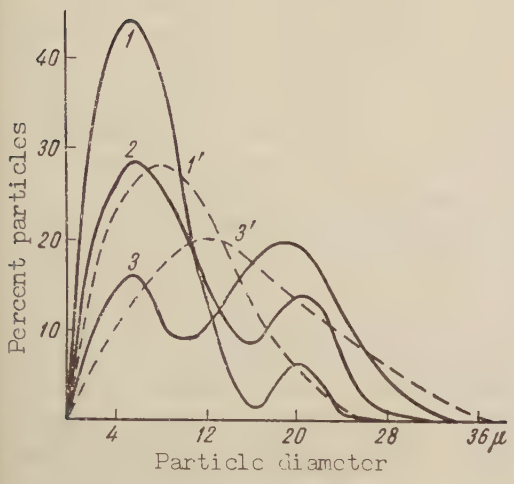

Fig.5. Grain size composition of $55ZnS \cdot 45CdS : 2 \cdot 10^{-4}$ Ag(+3% NaCl) phosphor after heating 1-3) in nitrogen and 1'-3') in air; 1 & 1' - 8 min, 2 - 30 min, 3 & 3' - 1 hour heating.

these experiments the difference between the influences on the formation of luminophors of bound and free (molecular) oxygen. In this respect the described experiments are entirely consistent with the results of earlier work by Klement[9] and Ormont[10].

The rate and character of transformations in the host material may be affected not only by the gaseous phase (heating atmosphere) but also by a condensed phase in contact with the phosphor crystals. Some years ago Riehl[11] noted that in the formation of ZnS:Cu phosphors, the crystallization of ZnS in the presence of copper proceeds appreciably more rapidly than in the nonactivated sulfide; this was subsequently substantiated by our experiments[1,2]. This explains the formation of ZnS:Cu phosphors in the absence of oxygen recorded by Riehl in later experiments[5].

We investigated the influence of inorganic salt fluxes on the kinetics of transformation in the matrix in the specific case of ZnS:Cu phosphors. In 1935 Riehl[12] described the time variation in the character of the luminescence of ZnS:Cu phosphors stored under normal conditions. A detailed investigation of the aging of these luminophors was carried out by Rusanova[13], who showed that the green band in the spectra of all ZnS:Cu phosphors with a Cu content $> 5 \cdot 10^{-6}$ g/g ZnS weakens with time, while the blue band increases in intensity. Rusanova suggested that this may be due not to changes in the structure of the luminescence centers but to phase transformations in the base material; in view of this we decided to study the matter further.

We prepared ZnS:Cu phosphors by heating luminescence grade ZnS with 5% NaCl in air at 950° for 30 min. The samples were then rapidly cooled to room temperature and the luminescence spectrum with excitation by λ = 365 mμ was recorded immediately. Then the samples were subjected to artificial aging by holding at 450°. It was found that the heating time required to attain a steady state increased with decrease of the Cu concentration. With a copper content less than $5 \cdot 10^{-6}$ g/g ZnS the phosphors did not react at all to heating. At all copper concentrations above $5 \cdot 10^{-6}$ g/g ZnS, however, all the samples tended to the same state (curve 2, Fig.6), i.e., a state which apparently corresponds to equilibrium at 450°.

The aging effect is observed most clearly at copper concentrations above 10^{-4} g/g ZnS, i.e., in the region of appearance of the so-called "β-band" of copper; hence we below shall describe mainly our experiments with these luminophors. In the case of sufficiently rapid cooling of phosphors with $C_{Cu} > 2 \cdot 10^{-4}$, the fresh samples are pure white and their spectrum consists of a broad band with one peak; with increase in the copper content the width of the band increases and its peak shifts to the side of shorter wavelengths, in agreement with the observations of Riehl & Ortmann[14]. The blue "β-band" does not appear in the spectrum. Even after a few days at room temperature, however, the samples become grey and the blue band appears in their spectra. At 450° the process terminates within about 3 hours (curve 2, Fig.6) and the samples acquire a dark grey coloration. The aging process is reversible: heating at 950° for 2 hours fully restores the properties of the initial phosphors. At 650° complete restoration of the initial state occurs

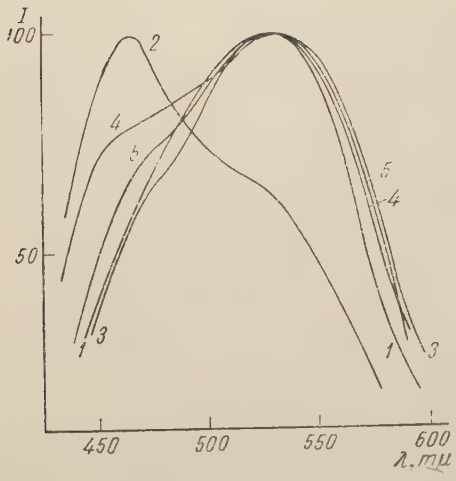

Fig.6. Luminescence of ZnS: $4 \cdot 10^{-4}$ Cu phosphors: 1) initial, 2) aged at 450°, 3) regenerated at 950°, 4) regenerated at 650° for 3 hours, 5) at 650° for 1 hour in vacuum. All values normalized to the maximum.

only for samples containing $C_{Cu} \leqslant 4 \cdot 10^{-4}$ g/g, and even this requires a very appreciable heating time. At higher copper concentrations regeneration at 650° leads to re-establishment of the broad Riehl-Ortmann band, but with its peak shifted somewhat to the side of longer wavelengths; the regenerated samples remain grey although a somewhat lighter shade.

Aging and regeneration of samples occur in the same way both in the presence of flux and with the flux eliminated by washing, both in an atmosphere of oxygen and in argon.

X-ray diffraction studies of freshly prepared samples showed that they consist of 92-95% sphalerite and 8-5% wurzite. After aging the amount of wurzite increases significantly. Regeneration restores the initial structure, but the mean size of the crystals is somewhat increased. Inasmuch as the greying of aged samples is due to the appearance of a new, "dark colored" phase, the absence of new lines in the x-ray diffraction patterns indicates that only a very small quantity of this phase is formed.

The observed changes are due to decomposition of Cu_2S-ZnS solid solution owing to reduced solubility of Cu_2S at lower temperatures. At low temperatures most of the copper in the phosphor is segregated into a new phase so that the blue band of zinc is intensified in the spectrum. Thus the so-called "β-band" of copper is actually the usual band of zinc, as was suggested earlier by Alentsev & Cherepnev[13].

Direct proof of this was furnished by experiments involving heating of aged samples in vacuum. Earlier we showed that as a result of such treatment the bands associated with volatile activators (for instance, zinc) undergo quenching, while the bands associated with less volatile activators (for example, copper) retain their initial brightness[16]. In this case the situation is complicated by the fact that the blue band disappears as a result of repeated heating owing to solution of the phase rich in copper in the zinc sulfide. At 650°, however, the rate of this process is very low compared with the rate of vaporization of zinc, so that heating in vacuum leads to appreciably more rapid quenching of the blue band (curve 5, Fig.6).

The above applies to the case when the luminophor contains flux, inasmuch as even when the phosphor is washed part of the flux remains in the intercrystalline spaces[1]. The behavior of luminophors prepared without flux is entirely different. The broad Riehl-Ortmann band is characterized by appreciable stability and even with a Cu content of 10^{-3} g/g retains its initial appearance both in aging at room temperature and in the case of heating for 3 hours at 450°. Moreover in this case there is no appreciable greying of the samples.

The indications of Riehl & Ortmann that the maximum of the band observed by them in the spectra of luminophors with a high copper concentration shifts to the short wavelength side in switching from 366 mμ excitation to excitation by the 254 mμ line and the deformation of the Riehl-Ortmann band observed by us incident to change in the intensity of excitation led us to the idea that actually this band is the result of addition or superposition of the two usual bands of zinc and copper. Measurements of the spectral composition of the luminescence at 100°

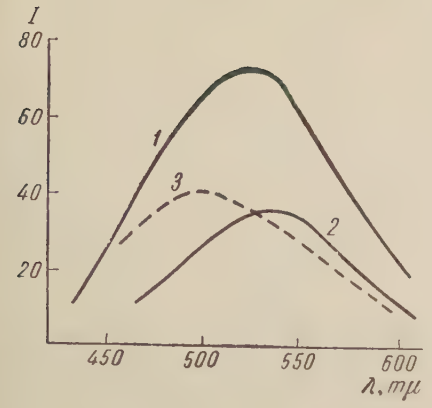

Fig.7. Luminescence of ZnS: :10^{-3}Cu phosphors prepared without flux: 1) Riehl-Ortmann band at 22°, 2) same at 100°, 3) difference between curves 1 & 2.

substantiated this (Fig.7): the luminescence in the green band undergoes temperature quenching and at 100° primarily the green (copper) band remains.

Consequently, at room temperature there is already present in the Riehl-Ortmann band an enhanced zinc band and a weakened copper band, although the luminophor still has a single-phase composition. The explanation for this effect, we feel, should be sought in the mechanism responsible for the appearance of a new phase in supersaturated solutions, which was investigated thermodynamically by Frenkel' and Dehlinger (see Refs.17 and 18).

Local variations in the composition lead to formation of structural elements of the new phase. Owing to deformations of the lattice caused by these fluctuations in the composition, the free energy of the lattice increases. Transition to the state with minimal free energy can be realized either by breakup of the structural element or by its "ejection" in the form of a new phase. At a certain magnitude of the primary structural element, the latter proves to be thermodynamically advantageous. The structural element begins to increase in size and turns into nuclei of the new phase. The size of the nuclei at which the new phase can segregate depends on the surface energy at the phase interfaces; hence the kinetics of development of the new phase depends substantially on the nature of the impurities collecting in the intercrystalline material.

In the case of ZnS:Cu phosphors with a high copper content, in the process of cooling there forms a supersaturated solution with local variation in concentration. These fluctuations lead to the appearance of structural elements of copper sulfide and impoverishment in copper of the neighboring sections of the ZnS lattice; consequently, there are created in them conditions favorable for the emission from zinc centers.

Substantiation of this interpretation of the origin of the Riehl-Ortmann band may be found in the work of Schulman, Ginter & Klick[19] on $NaCl \cdot PbCl_2$ crystals. In this case change in the spectrum and the luminescence output was observed even before separation of the crystals into two phases, which indicates that the process of disproportioning may occur even in a homogeneous medium.

Our experiments indicate that in interpreting the variation of the luminescence properties of sulfide phosphors as a function of the synthesis conditions, it is erroneous to attribute all the effects to changes in the structure of the luminescence centers: no less important, in our opinion, are processes occurring in the base material, regarding which little is as yet known. There can be little doubt, however, that very important here is the nature of the substances - gaseous, liquid or solid - coming into contact with the phosphor and acting as mineralizing agents.

References

1. A.A.Bundel', Zhur.fiz.khim. (J.Phys.Chem.), 30, 2261 (1956).
2. A.A.Bundel', Thesis, Moscow State University, 1956.
3. A.A.Bundel' & A.I.Rusanova, Izv. AN SSSR, Ser.fiz., 13, 173 (1949).
4. A.A.Bundel', Zhur.fiz.khim., 30, 2469 (1956).
5. N.Riehl (Ril') & H.Ortmann, Zhur.obshch.khim., 25, 1289 (1956). (Trans. J.General Chemistry.)

6. L.I.Shekhter, I.A.Myasnikov & S.Ya.Pshezhetskii, Doklady AN SSSR, 109, 1163 (1956). (Trans.Doklady.)
7. M.I.Tombak, A.V.Popova, O.F.Komar & A.A.Bundel', Present issue of the Bulletin, p.1349.
8. A.L.Smith, Trans.Electrochem.Soc., 93, 324 (1948).
9. F.D.Klement, Zhur.fiz.khim (J.Phys.Chem.), 21, 563 (1947).
10. B.F.Ormont, Ibid., 21, 569 (1947).
11. N.Riehl (Ril') & H.Ortmann, Z.Phys.Chem.A, 188, 109 (1941).
12. N.Riehl, Ann.Phys. (5), 24, 536 (1935).
13. A.I.Rusanova, Thesis, Giredmet, M., 1952.
14. N.Riehl (Ril') & H.Ortmann, Doklady AN SSSR, 66, 841 (1949).
15. M.N.Alentsev & A.A.Cherepnev, Zhur.eksp.i teor.fiz., 26, 473 (1954).
16. A.A.Bundel', A.I.Rusanova & R.P.Dobkina, Trudy (Proceedings), Central Scientific Research Institute of Roentgenology and Radiology, 8, 146 (1951).
17. Ya.I.Frenkel', Izv.Sektora fez.-khim.analiza, 16, 50 (1943).
18. M.Dehlinger, Z.Naturforsch.A., 6, 718 (1951).
19. I.H.Schulman, K.G.Ginter & C.Klick, J.Opt.Soc.Am., 40, 854 (1950).

ON THE PHYSICAL-CHEMICAL NATURE OF SILVER ACTIVATOR IN ZINC SULFIDE PHOSPHORS

- A.A.Cherepnev

I. Silver, together with copper, is among the most commonly used activators for zinc sulfide phosphors. Most modern authors assume that the silver in ZnS luminophors is present in the form of singly charged ions (Ag^+).[1-5] It is possible, however, that the silver (like copper and zinc[6]) exists in zinc sulfide phosphors in a dispersed state, in the form of elemental particles. Many authors consider that elemental silver forms in solids and crystals and that it is evinced as such in the absorption and luminescence spectra.[7]

Elemental silver can separate out of silver salts at high temperatures. Silver activator introduced into air-dry ZnS in the form of a solution forms Ag_2S, which noticeably dissociates at 950°; data on the Ag_2S-Ag system can be found in Mellor[8]. When a chloride flux is used, AgCl may form, particularly in the case of heating. AgCl begins to sublime at 260° and is almost completely driven off at red heat. Reaction of silver halides with metal sulfides is characterized by the following equations:[8]

$$M_2S + 4AgCl \rightarrow 2Ag + Ag_2S + 2MCl_2;$$
$$MS + 2AgCl \rightarrow Ag_2S + MCl_2;$$
$$MS_2 + 2AgCl \rightarrow Ag_2S + MS + Cl_2.$$

Upon heating with alkali halide, Ag_2S yields metallic silver. In the presence of oxidizing agents (oxygen from the air or oxygen containing compounds) there may form Ag_2S which then readily decomposes to the metal upon heating. When heated in contact with air Ag_2S oxidizes to Ag_2SO_4. The reaction $Ag_2S + Ag_2SO_4 \rightarrow 4Ag + 2SO_2$ proceeds readily; an SO_2 partial pressure above atmospheric is obtained at about 400°. There may also occur electrolytic deposition of silver on the elemental zinc produced during heating.

The physical and chemical state of silver in the system depends on the present condition and past history of the phosphor; the proportion between components (ZnS, Ag_2S, Ag, Zn, ZnO, flux, atmosphere), the temperature and duration of heating, the crystallochemical behavior of the components, etc. The processes occurring in the formation of ZnS:Ag phosphors are primarily solid-vapor reactions; they are topochemical in character, which explains the specific localized appearance and stability of the different components of the system.[6]

With a view to clarifying the nature of silver activator in zinc sulfide phosphors, we prepared a series of ZnS:Ag samples under different conditions and measured their luminescence with excitation by 365 mμ light at room temperature; we also obtained their absorption spectra. The equipment used was described earlier[9]. The heating except for the use of special atmospheres was carried out under the usual technological conditions.[9-12]

II. Some data on the absorption of ZnS:Ag phosphors will be found in Refs. 13 and 14.

We carried out measurements of the absorption spectra (by the method of diffuse reflection from a thick layer of the powder) of ZnS:Ag samples with different silver concentrations obtained at heating temperatures of 800 to 1100° with NaCl and H_3BO_3 as the fluxes. The results for the 800° phosphors are shown in Fig.1. It will be evident from the figure that there is a sharp decrease in absorption (from the level of intrinsic absorption) at 330-340 mμ. Above an optimum silver concentration (10^{-4} g/g) the absorption increases rapidly, owing primarily to segregation of Ag_2S. The addition of minor amounts of silver to ZnS decreases the absorption compared with pure ZnS (heated under the same conditions but without Ag). This can probably be explained by the fact that at first there

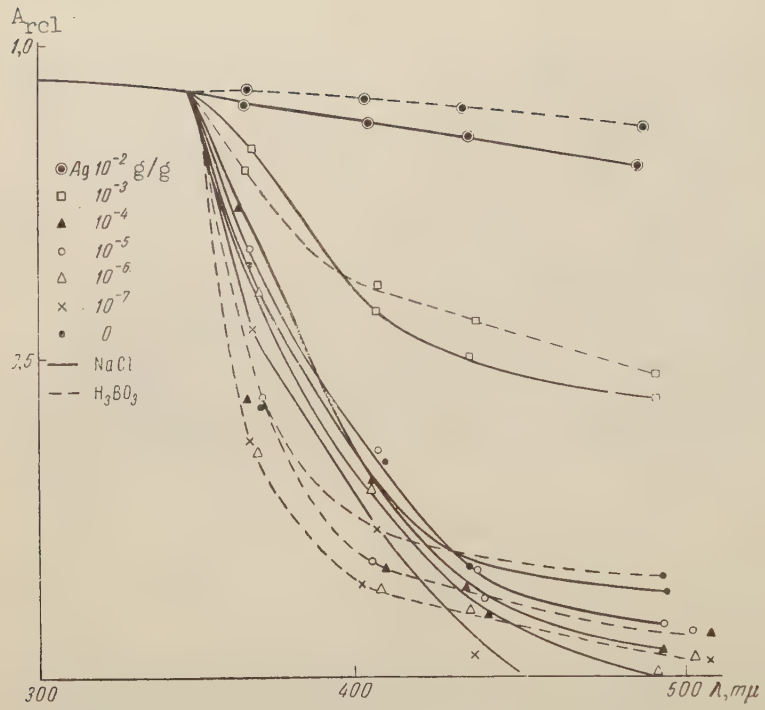

Fig.1. Absorption spectra of ZnS:Ag phosphors heated at 800°.

occurs displacement of the zinc activator by silver. With further increase of the silver concentration there becomes evident absorption due to the silver itself. A similar effect of decrease of the absorption in the presence of small amounts of activator was also observed for copper.[9] The difference in the decreases of absorption for phosphors made with NaCl and H_3BO_3 is probably due to formation of zinc borates in phosphors fluxed with the latter compound.

III. The luminescence spectra of ZnS:Ag phosphors prepared at 800° are shown in Figs.3 & 4. With small amounts of silver (~10^{-7} g/g ZnS) there at first occurs weakening of the luminescence. Probably the silver, replacing the zinc, suppresses the characteristic luminescence of the latter without fully developing its own emission; with further increase in the Ag concentration there is observed an increase in the luminescence brightness to an optimum value (10^{-4} g/g ZnS), after which the brightness falls off rapidly (presumably due to formation of Ag_2S). There is an appreciable difference in brightness depending on the type of flux used; at low temperatures (800°) the most efficient samples are obtained with NaCl; at high temperatures (1100°) - with H_3BO_3. This may be explained by the greater volatility of AgCl and the formation of zinc borates[15] at high temperatures. The shift of the spectral peak for high temperature samples probably occurs due to formation of wurzite structure[16]. In general the peak of the spectrum is displaced to the side of shorter wavelengths with increase of the silver content to an optimum value. This shift can be explained either by weakening of the zinc band owing to replacement of the zinc by silver or by relative weakening of the yellow oxide band in the blue spectrum of ZnS.[10] For phosphors prepared with H_3BO_3, which probably removes some of the zinc through formation of borates[15], the emission maximum is located at shorter wavelengths. Possibly at sufficiently high silver concentrations there may either occur effects analogous to "coagulation" of copper[11] (they are difficult to detect owing to the closeness of the spectral peaks of ZnS:Zn and ZnS:Ag) or nonincorporation of the silver sulfide into the ZnS crystal lattice owing to its limited solubility therein (excess Ag_2S and Ag remain on the surface of the crystals).[1]

IV. A series of special experiments involving variation of the heating temperature of ZnS:Ag with the optimum silver concentration (10^{-4} g/g) yielded samples the spectral characteristics of which are shown in Figs.4 & 5. It will be seen that in each case the brightness goes through a maximum corresponding to a heating temperature of 800-900°.

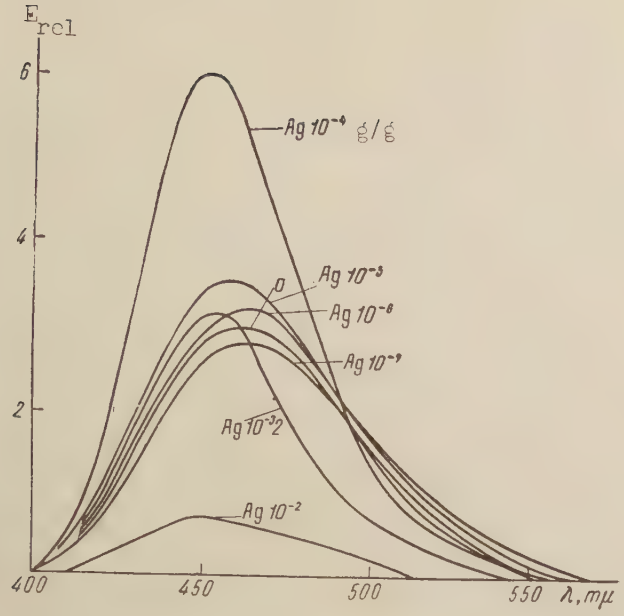

Fig.2. Luminescence spectra of ZnS:Ag phosphors with different silver concentrations heated at 800° with NaCl flux.

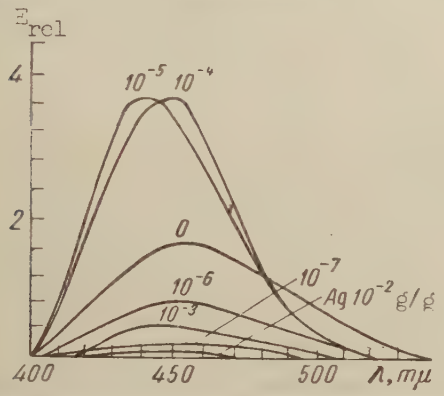

Fig.3. Luminescence spectra of ZnS:Ag phosphors with different silver concentrations heated at 800° with H_3BO_3 flux.

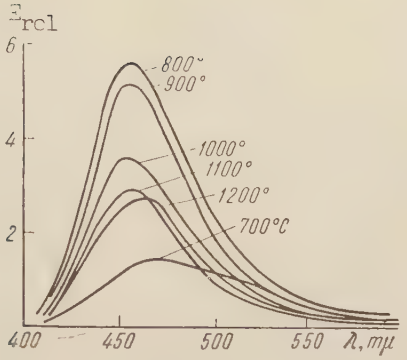

Fig.4. Luminescence spectra of ZnS:10^{-4} Ag phosphors heated at different temperatures with NaCl.

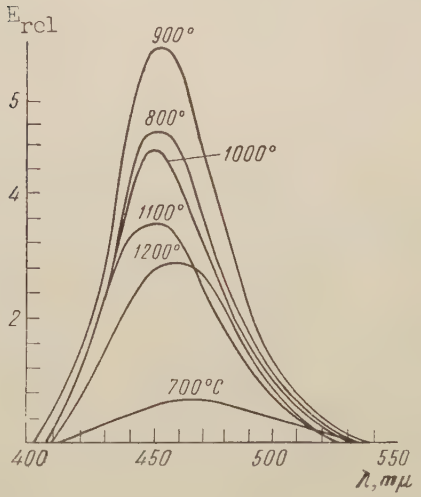

Fig.5. Luminescence spectra of ZnS:10^{-4} Ag phosphors heated at different temperatures with H_3BO_3.

In order to bring out the influence of the heating time, we carried out a series of experiments on mixtures with the optimum Ag concentration and each of the two fluxes. In the case of heating at 1100° with NaCl flux there is observed a slow increase in brightness (to saturation); with H_3BO_3 at the same temperature even brief heating (15 min) yields virtually the maximum brightness, i.e., there is no significant increase in brightness with increased heating time. No shift of the brightness maximum in the wavelength scale was noticed.

V. Von der Forst et al[17] give interesting data on the effect of heating in an atmosphere of hydrogen sulfide in the case of the ZnS-Ag_2S system.

When we heated a mixture of ZnS with 10^{-4} Ag for one hour at 1100° in a stream of hydrogen sulfide, we obtained a nonluminescing product. The addition of small amounts of chloride flux (~1%) had no significant effect inasmuch as the chlorine is displaced by the hydrogen sulfide and lost by evaporation. In the presence of an excess of H_2S, in accord with the law of mass action, one must

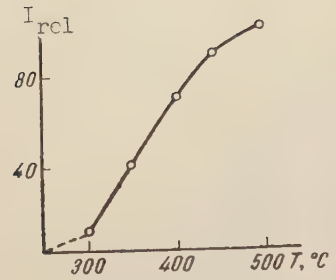

Fig.6. Variation of the brightness with the second heating temperature (30 min) for ZnS:10^{-4}Ag phosphor prepared by heating for 1 hour in 1100° in a stream of H_2S without flux.

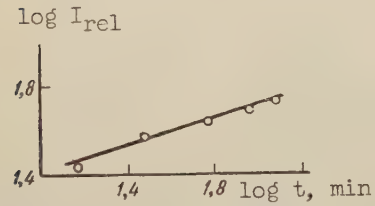

Fig.7. Variation of the brightness of ZnS:10^{-4} Ag phosphor prepared by heating for 1 hour at 1100° in H_2S with the duration of the second heating at 300°.

expect the formation not of free silver but of nonluminescent Ag_2S or even polysulfides. The nonluminescing product upon being heated in the presence of air even at 300° begins to exhibit blue luminescence (spectral peak at 430 mμ) which increases in intensity with further heating. The increase in luminescence brightness with temperature step heating is shown in Fig.6. It will be seen that in the 300 to 500° interval the increase in brightness with temperature is almost linear. Above 500° there occurs increasingly active oxidation inasmuch as the process was carried out without flux; with heating for about 30 min at 700° the blue luminescence changes to yellow.[10] Heating at 600° with NaCl yields the usual fairly bright blue emitting powder (the luminescence is approximately twice as bright as in the case of the above mentioned sample heated at 500°). Isothermal heating of the nonluminescent ZnS:Ag product at 300°, depending on the duration of the operation, yields evidence of bimolecular reaction: the results plotted in logarithmic coordinates (log I vs log t) yield a straight line (Fig.7). It may be assumed that the primary process of formation of an emitting product under the indicated conditions is determined not by decomposition of the nonluminescent sulfide (this reaction is not precluded as a rapidly occurring first stage) but by the result of interaction of silver sulfide with the products of oxidation, leading to the segregation of elemental luminescent silver, since under the influence of oxygen, which is difficult to exclude under the conditions of reheating, there form dioxidized products (Ag_2O and Ag_2SO_4). ZnS:10^{-4}Ag heated at 500° in a stream of H_2S also forms a nonluminescent product. But the same mixture upon being treated with H_2S at 70° (for 1 hour) exhibits blue luminescence. A luminescent product is obtained from the nonluminescent sulfide formed before heating under the usual technological conditions only at heating temperatures above 600°. It must be assumed that in the ZnS-Ag system the formation of emission centers at temperatures of the order of 600° occurs primarily through interaction of Ag_2S with the oxidized product remaining in the batch or introduced into the system together with the H_2S in the form of SO_2, CO_2 or water vapor. The silver segregating in the system at ~600° in an atmosphere of dry H_2S is not subjected to the action of hydrogen sulfide inasmuch as at this temperature the reaction with silver barely begins.[8,18]

In heating ZnS:Ag without flux in a stream of ammonia there is obtained a nonluminescent product (coagulation of silver reduced by hydrogen from dissociation of the NH_3; absence of a dispersing flux); the product obtained with NaCl exhibits luminescence (owing to chlorination).

Heating ZnS:Ag without flux in a stream of nitrogen at low temperature (800°) yields a weakly luminescent product; heating at a higher temperature (1100°) yields a more efficient phosphor (possibly due to traces of oxygen); the brightness increases upon the addition of NaCl to the initial mixture.

VI. Small amounts of zinc oxide (to 1%) are inevitably present in ZnS (either as initial impurities[1] or owing reaction with the atmosphere). The influence of the zinc oxide is evinced in the nature of the physical-chemical processes and

in displacement of the spectrum maximum[13]. In order to elucidate the influence of larger (>1%) amounts of ZnO, we prepared ZnS:Ag samples with additions of different amounts of ZnO obtained by burning ZnS in air at 900° (Ref.10) or taken as the reagent. With additions of 2 to 20% ZnO we observed no noticeable shift of the main spectrum maximum or the auxiliary peaks (in the yellow region). The location of the peak at 450-470 mμ (for products prepared with NaCl and heated at 800 or 1100°) and the asymmetry of the spectral distribution curves demonstrates the influence of ZnO.[10] Zinc oxide, particularly the reagent, has a weakening effect on the integral intensity.

The phosphors obtained with low temperature heating have a high integral intensity. In the case of phosphors prepared by heating at high temperatures (particularly, those with 10^{-4} g/g Ag) the decrease in intensity even with an appreciable ZnO concentration is relatively small. Some decrease in intensity is observed with increase of the heating temperature.

The reactions of the oxidized compounds and sulfides with the formation of elemental luminescent particles occur primarily in solutions of these compounds in ZnS; therein lies their difference from "mechanically admixed" oxides (in Ag_2S).

The glow curves of ZnS:Ag phosphors (obtained with NaCl and H_3BO_3 fluxes by heating at 1100°) exhibit two peaks: the low temperature one (-120°) is apparently associated with silver activator; the other (-60°) with zinc oxide (as in the case of ZnS:Cu - see Refs.19 & 4). The heights of the glow-curve peaks obtained for the phosphors obtained with NaCl and H_3BO_3 reflect the spectral brightnesses. It may be assumed that formation of ZnS:Ag phosphor is a single physical-chemical process of formation of emission centers and the corresponding traps; in the process there are segregated the elemental silver particles and their subsequently eliminated partners (SO_2, ZN, S, etc.), which leave defects (vacancies) in the crystal lattice.[10]

Conclusions

1. The formation of luminescent ZnS:Ag is apparently connected with segregation of elemental silver, which is distributed through the system in dispersed form (as was earlier suggested[6] to be the case for copper in ZnS:Cu phosphors). Inasmuch as the silver in ZnS is initially present in the form of some compound, the process of its precipitation is accompanied by the separation of an anionic component; thus there are simultaneously formed luminescence centers and traps, characterized by blue emission and the low temperature thermostimulation peak.

2. The process of formation of solid ZnS phosphor proceeds primarily in the gaseous phase: the fluxes NaCl and H_3BO_3 are comparatively volatile. This determines the condition of building up of luminescence centers (emission, trapping and quenching centers). Here there occur the effects of precipitation in the solid phase, diffusion of the activators and formation of their active states through "volatile" components as well as other physical-chemical processes. Owing to the presence of the solid system in all the technological stages, the reactions occurring in the formation of ZnS phosphors are topochemical (localized). Owing to the limited time of the heating operation, equilibrium states are not always attained.

3. Although the final states of the activators silver and copper are identical (dispersed elemental particles), the two activators exhibit differences as well as similarities. The similarity is evinced in the rapid falling off of the absorption curve from the maximum value and in weakening of the zinc band in the luminescence spectrum owing to displacement of the zinc by the activator metal. As regards dispersion and coagulation, however, silver behaves differently: silver is segregated more easily than copper and is more stable. The difference between the peaks of the blue luminescence bands of zinc and silver is difficult to distinguish.

4. The specific characteristics of the two fluxes, NaCl and H_3BO_3, used in our experiments result in differences between the processes of formation of the phosphor crystals and between the behavior of activators (Cu, Ag and others) in the ZnS phosphor system. As a flux, NaCl promotes dispersion, chlorination and desulfurization; H_3BO_3 favors vitrification and elimination of ZnO by solution and formation of borates. Intensification of the phosphor formation process in the presence of H_3BO_3 with increasing temperature occurs primarily owing to dissociation of the activator sulfide; in the presence of NaCl, as compared with H_3BO_3, owing to the reactivity of the chloride such processes occur at lower temperatures.

5. The absence of luminescence when ZnS:Ag is heated in an atmosphere of hydrogen sulfide apparently occurs owing to formation of nonluminescent silver sulfide; in the case of preformation active luminescent centers appear at 1100°. The appearance of luminescence is due to the presence of oxidized products. These results are connected with the temperature dependence of the chemical equilibrium in the systems under consideration[8,18].

6. Particularly in view of the work of Kynev[20] on ZnS:Cu phosphors, one cannot exclude the possibility that the luminescent agent in ZnS:Ag is silver sulfide in colloidal form. On the basis of our experimental data and the considerations set forth above, however, we are inclined to believe that the active agent under the conditions of our experiments is dispersed elemental silver.

I desire to thank M.D.Galanin for his interest in the work, M.N.Alentsev for a number of valuable suggestions and M.V.Danilov for assistance in the experiments.

"P.N.Lebedev" Physical Institute,
Academy of Sciences of the USSR

References

1. N.Riehl (Ril') & G.Ortmann, Zhur.obsch.khim. 25,1057 (1956).(Trans.J.General Chemistry); Angew.Chemie,68,513 (1956); Z.phys.Chemie,188,109 (1941); N.Riehl, Lyuminestsentsiya (Luminescence), p.113, M.-L., 1946.

2. F.A.Kröeger & H.J.Vinck, J.Chem.Phys.,22,250 (1954); in Solid State Physics, Edited by E.Seitz & D.Turnbull, Vol.3, N.Y., 1956.

3. H.W.Leverenz, An Introduction to Luminescence of Solids. N.Y., 1950.

4. G.F.Garlick, Luminescent Materials. Oxford, 1949.

5. T.B.Tomlinson, J.Electronics,2,166 (1956); P.F.Browne, Electronics, 2,154 (1956); E.Shrader & S.Larach, Phys.Rev., (2), 133, 1899 (1956).

6. A.A.Cherepnev, Transactions of the Fifth Conference on Luminescence, p.52, Tartu, 1957 (Trans.Bulletin 21, No.5, 672); Izv.AN SSSR, Ser.fiz., 15, 742 (1951).

7. L.M.Shamovskii, L.M.Rodionova, G.A.Sidorenko & Yu.N.Zhvanko, Doklady AN SSSR, 99, 235 (1954); M.V.Savost'yanova, Usp.fiz.nauk, 21, 1 (1939); Ibid., 22, 168 (1939); E.A.Kirillov, Tonkaya struktura v spektre pogloshcheniya fotokhimicheski okrashennykh galoidov serebra (Fine structure in the absorption spectra of photochemically colored silver halides), M.,1954; M.L.Kats, Izv.AN SSSR, Ser.fiz., 21, 550 (1957). (Trans.Abstract Bulletin 21, No.4,546); S.P.Golub, Transactions of the Fifth Conference on Luminescence, p.108, Tartu, 1957.

8. J.W.Mellor, A Treatise on Inorganic Chemistry, vol.III, pp.329,349,394, 402,439,447,453. London, 1936.

9. M.N.Alentsev & A.A.Cherepnev, Zhur.eksp.i teor.fiz., 26, 473 (1954).

10. A.A.Cherepnev, Optika i spektroskopiya, 1, 272 (1956).

11. A.A.Cherepnev & T.S.Dobrolyubskaya, Doklady AN SSSR, 66, 621 (1949).

12. A.A.Cherepnev, Optika i spektroskopiya, 2, 370 (1957).

13. F.A.Kröger, J.Electrochem.Soc., 99, 148 (1952).

14. M.N.Alentsev, Optika i spektroskopiya, 1, 240 (1956); E.M.Brumberg & F.M.Pekerman, Izv.AN SSSR, Ser.fiz., 13, 219 (1949).

15. D.E.Harisson & F.A.Hammel, J.Electrochem.Soc., 103, 491 (1956).
16. F.A.Kroeger, J.E.Hellingman & N.W.Smit, Physica, 15, 1990 (1949).
17. P.Von der Forst, Fr.Ruter & R.Schenck, Z.anorg.Chemie, 262, 100 (1931).
18. K.Jellineck & J.Zakowski, Z.anorg.Chemie, 142, 1 (1952).
19. W.Hoogenstraaten, J.Electrochem.Soc., 100, 356 (1953).
20. K.Kynev, Optika i spektroskopiya, 3, 652 (1957).

* * * * * * *

CHEMICAL ASPECTS OF THE FORMATION OF ZINC SULFIDE-SELENIDE PHOSPHORS

- L.Ya.Markovskii & R.I.Smirnova

In view of the increasing industrial importance of zinc sulfide-selenide and pure selenide luminophors, it is important to understand the condition of their formation since this should be helpful in obtaining phosphors with better luminescence properties.

This question repeatedly came up in our institute in connection with development of selenide phosphors. In particular, until now it remained unclear whether there was a difference as regards properties between selenide luminophors obtained from pure ZnSe and luminophors synthesized by the reaction between ZnS and SeO_2.

To answer the question it was necessary to investigate in detail the chemism of the reaction between zinc sulfide and selenious acid.

Preliminary results were published in 1957.[1] In the present communication we give additional results obtained in continuing studies. As is known, the reaction between zinc sulfide and selenious acid may be realized in two forms:

1) by the "dry" procedure in which a mixture of ZnS and SeO_2 powders is heated at 700-800°, and

2) by the "wet" procedure in which the initial batch is first prepared in an aqueous medium (by mixing ZnS powder with a solution of H_2SeO_3) and is then dried and heated.

It was generally assumed that in both cases the reaction is characterized by the same equation,

$$ZnS + SeO_2 \rightarrow ZnSe + SO_2 , \qquad (1)$$

and yields phosphors of identical quality.[2] It was shown in Ref.1, however, that for the "wet" variant of synthesis this reaction model is not correct.

On the basis of data of chemical, x-ray diffraction and microscopic analyses it was shown that in the interaction of zinc sulfide in suspension with a solution of selenious acid there occur reactions that may be represented by the following summary equation:

$$2ZnS + 3H_2SeO_3 \rightarrow 2ZnSeO_3 + 2S + Se + 3H_2O. \qquad (2)$$

As a result of the exothermic reaction involved, which we shall not describe here in detail and which proceeds in almost the same way regardless of the proportion of initial components, there is obtained a yellowish or orange, rather uniform mixture of zinc selenide powder with elemental sulfur and selenium. The components in the product can be separated either by solution of the $ZnSeO_3$ in a mixture of NH_4Cl + NH_4OH or by extracting the sulfur and selenium by means of appropriate solvents.

We also investigated[3] the phase composition of zinc selenites; it was shown that by the above reaction the zinc selenite is obtained in the form of the monohydrate: $ZnSeO_3 \cdot H_2O$. Thus the batch obtained by the "wet" procedure consists of a mixture of ZnS, $ZnSeO_3 \cdot H_2O$ and elemental S and Se. In particular, in the case of equilmolar proportions of ZnS and H_2SeO_3, for which as is known, there is obtained the best yield of ZnSe, two thirds of the ZnS are converted to $ZnSeO_3$, in accord with reaction (2), while one third remains unreacted. The reactions occurring during heating of this complex mixture must probably differ substantially from the reactions involved in heating a mixture of ZnS + SeO_2 powders.

Reactions occurring in heating batches prepared by the "wet" procedure

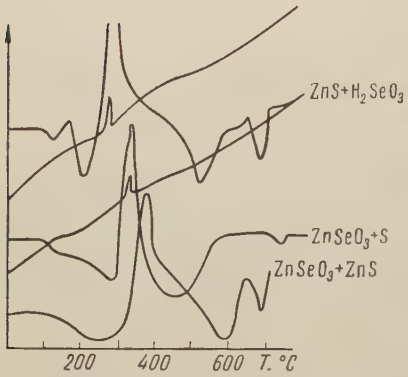

Fig.1. Thermogram

A thermogram (Fig.1) recorded on a Kurnakov (PK-54) pyrometer during heating of a batch prepared of a mixture of ZnS with H_2SeO_3 substantiates the complex character of the reactions occurring, for it discloses, in addition to an exothermic effect, a number of endothermic effects, an interpretation of which will be given below.

The complexity of the processes occurring is also evinced in purely external indications, inasmuch as in heating of the batch in addition to evolution of SO_2, there are sublimated elemental selenium and sulfur (the latter in insignificant amounts) and in the final reaction product there is always (even when the reaction is realized out of contact with air) zinc oxide in the amount of several percent.[1]

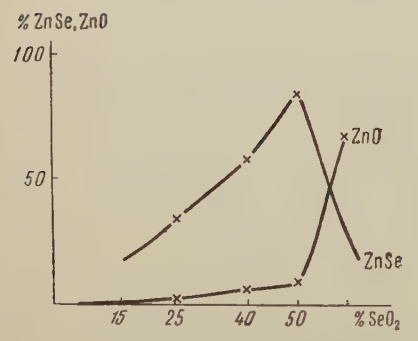

Fig.2. Variation of ZnO and ZnSe in the final product with the H_2SeO_3 content in the initial batch.

Table 1 shows the result of analyses of the products obtained in heating at 800° of batches prepared from ZnS + H_2SeO_3 and also of a mixture of ZnS, $ZnSeO_3$, Se and S. It will be evident from the tabular data that the composition of the final product obtained from the different batches is similar, that there is an appreciable percent of zinc oxide present in the zinc selenide and that in each case there is an appreciable loss of elemental selenium.

Table 2 and Fig.2 show how the composition of the final product heated at 800° depends on the H_2SeO_3 content (expressed in percent SeO_2) in the

Table 1

Analysis of products obtained in heating the batch at 800°

Composition of batch	Composition of product, %				Remarks
	ZnSe	ZnS	ZnO	Se in sublimate	
$(ZnS + H_2SeO_3)$ (1 : 1)	82,1	6,6	11,1	7,0	8 g batch, heated in N_2 under static conditions
	81,7	7,2	10,8	7,2	
	92,4	—	6,7	—	100 g batch, heated in covered quartz crucible
$2ZnSeO_3 + ZnS + 2S + Se$	88,5	—	11,4	—	
	84,2	—	15,7	—	8 g batch, heated in N_2 under static conditions

Table 2

Results of experiments on heating compositions with different amounts of H_2SeO_3 at 800°

SeO_2 in batch, %	Se balance, %				Composition of solid phase, %		
	Introd.	Elem. in sublimate	In solid phase	Total found	ZnSe	ZnS	ZnO
15	10,6	0,4	9,3	9,7	19,0	81,0	—
25	17,3	0,7	17,9	18,6	36,0	64,5	—
40	27,2	3,5	22,3	25,8	57,0	35,8	5,4
50	33,8	4,3	29,6	33,9	85,2	8,8	6,2
60	39,8	32,8	5,8	38,6	28,8	3,0	67,1

initial mixture. With increase in the SeO_2 content the relative percent of elemental Se sublimed increases; this is accompanied by a parallel increase in the ZnO content in the solid phase. The maximum ZnSe content is obtained when the initial ratio of ZnS to H_2SeO_3 is taken close to unity; with further increase in the H_2SeO_3 content there occurs a sharp reduction in ZnSe in the solid phase and increase in the loss of Se.

With ZnS:H_2SeO_3 equal to 2:3 there is obtained pure zinc oxide containing only a few tenths of a percent of selenium. Analysis of the products obtained in heating the batch at different temperatures shows that both with a ZnS:H_2SeO_3 proportion of 1:1 and 2:3 the ZnSe content in the product heated at 500 and 600° is higher than in the products obtained by heating at 800°. It was also found that reduction in the percent ZnSe with increasing heating temperature is connected with its oxidation by zinc selenite or SeO_2 forming as a result of thermal dissociation of $ZnSeO_3$, which begins above 600°.

In further research we investigated in detail by the methods of chemical and x-ray phase analyses of the final products as well as by the thermographic procedure the diverse reactions occurring in heating of a given batch as well as the reactions occurring in heating of "dry" and "wet" batches with different proportions of the components and at different temperatures.

Among the particular reactions we investigated the following: 1) ZnS + SeO_2 (dry batch), 2) $ZnSeO_3$ + S, 3) $ZnSeO_3$ + Se, 4) $ZnSeO_3$ + ZnS, 5) ZnS + Se, 6) ZnSe + + S, 7) ZnO - ZnS, 8) ZnO + ZnS + Se, and 9) thermal dissociation of $ZnSeO_3$.

On the basis of the experimental data, which will be reported on in detail elsewhere, it proved possible to draw certain definite inferences regarding the chemism of the processes occurring in the heating stage. Below we give only the principal deductions arrived at.

Reactions involved in heating a mixture of "dry" ZnS and SeO_2 powders

On the basis of the experimental data and primarily from the proportion between the percentages of SO_2 and ZnSe, it may be inferred that the principal reaction in the case of the "dry" variant of synthesis does proceed in accord with the equation given in the literature:

$$ZnS + SeO_2 \rightarrow ZnSe + SO_2.$$

However, as the data of Table 3 shows, in this case also a significant role is played by the oxidizing influence of SeO_2 at temperatures from 100 to 300°, according to the reactions

$$ZnS + 2SeO_2 \rightarrow ZnSO_4 + 2Se + 76.4 \text{ kcal},$$
$$2ZnS + 3SeO_2 \rightarrow 2ZnO + 2SO_2 + 3Se + 51 \text{ kcal}.$$

As a result of these reactions up to 30% of the ZnS is oxidized to $ZnSO_4$ and ZnO. Hence the zinc selenide product obtained by heating dry batches at 800° contains up to 5-10% ZnO.

Table 3

Results of experiments on heating mixtures of dry ZnS - SeO_2 (1:1) powders

Temperature, °C	Content, %						
	ZnSe	ZnS	$ZnSO_4$	ZnO	Sublimate Se	SO_2 gas	Se in solid phase
500	74,4	15,7	5,8	2,5	7,5	11,7	27,0
800	67,1	17,2	0,1	12,0	7,0	12,1	24,5

It should also be noted that owing to the strong exothermic character of the above mentioned oxidizing reactions, in the case of a rapid rise of temperature of moisture-free mixtures of ZnS and SeO_2 powders, there occurs in the temperature interval from 50 to 150° (depending on the experimental conditions) ignition of the batch. This effect is similar to the flame oxidation reactions occurring between SeO_2 and many organic compounds, described by Emeleus & Riley[4].

Also characteristic of the dry batch procedure is the presence in the final product of an appreciable amount of unreacted zinc sulfide, which is probably due to the fact that in this version of the synthesis procedure the mixture is never as homogeneous as in the case of the "wet" procedure.

Chemism of the reactions occurring in heating batches synthesized by the "wet" procedure

On the basis of the data of reaction balance experiments and taking into account the results obtained in investigating the ZnS + 2ZnO + 3Se reaction, we can write the following scheme for the reaction of ZnS with H_2SeO_3:

$$1)\ ZnS + H_2SeO_3 \rightarrow {}^2/_3\, ZnSeO_3 + {}^2/_3\, S + {}^1/_3\, Se + {}^1/_3\, ZnS + H_2O$$

(at room temperature);

$$2)\ {}^4/_9\, ZnSeO_3 + {}^2/_3\, S \rightarrow {}^4/_9\, ZnSe + {}^2/_3\, SO_2 \quad (< 400°)$$

$$3)\ {}^2/_9\, ZnS + {}^2/_9\, ZnSeO_3 \rightarrow {}^2/_9\, ZnSe + {}^2/_9\, SO_2 + {}^2/_9\, ZnO \quad (400 - 500°)$$

$$4)\ {}^2/_9\, ZnO + {}^1/_9\, ZnS + {}^3/_9\, Se \rightarrow {}^3/_9\, ZnSe + {}^1/_9\, SO_2 \quad (500 - 800°)$$

Or, for the overall equation, we have:

$$ZnS + H_2SeO_3 \rightarrow ZnSe + SO_2 + H_2O. \qquad (3)$$

All the above transformations are evinced in the thermogram (Fig.1), where the exothermic effect should be attributed to the $ZnSeO_3$ + S and $ZnSeO_3$ + ZnS reactions and the endothermic effects to reactions between ZnO, ZnS and Se.

Thus it may be assumed that in the ideal case complete conversion of ZnS to ZnSe occurs according to the above equations. In practice, however, particularly in the case of small batches, one cannot avoid partial vaporization of both elemental selenium and SeO_2; reaction balance experiments show that approximately 5-7% of the Se is lost from the batch by sublimation so that in practice complete transformation of ZnS to ZnSe is unattainable. Actually, even in the best samples of zinc selenide obtained by the described reactions, the zinc oxide content amounts to several percent. More complete conversion is always favored by increasing the size of the batches and by minimizing the flow of gas through the batches with a view to preventing removal of vaporized Se and SeO_2.

Preliminary experiments aimed at investigation of the chemism of the reaction between CdS and H_2SeO_3 showed that in this case the general character of the

interaction is similar to that between ZnS and H_2SeO_3, i.e., that the reaction occurs through formation and reduction of $CdSeO_3$. In the case of cadmium sulfide, however, the reaction with H_2SeO_3 proceeds much more slowly. To insure a more rapid reaction rate, the CdS must be mixed with the H_2SeO_3 solution while heating.

Thus the presence of zinc or cadmium oxide in the products obtained by heating selenium rich batches consisting of ZnS or CdS and H_2SeO_3 is inevitable. Hence it is impossible to obtain high quality pure selenide phosphors without a final step of extracting the zinc oxide impurity.

Influence of the synthesis conditions on the luminescence properties of zinc selenide phosphors

The cathodoluminescence curves for a number of phosphors recorded with V_a = = 9 kv and I_a = 2 μa/cm^2 are shown in Fig.3. The phosphors were heated at 800° in an atmosphere of purified nitrogen (<0.02% O_2) under static conditions, using 2% NaCl as the flux. The zinc selenide used for the syntheses was obtained by precipitation of $ZnSO_4$ with hydrogen selenide and contained some heavy metal impurities (Fe, Cu, Ni, Co and Mn - total amount < $5 \cdot 10^{-5}$%). To drive off the oxygen, the ZnSe was heated at 400° in a stream of hydrogen. The zinc sulfide employed contained $3 \cdot 10^{-5}$% Fe, $5 \cdot 10^{-6}$% Cu, and $1 \cdot 10^{-5}$% Ni and Co.

The selenium dioxide was purified by double sublimation and contained less than $3 \cdot 10^{-5}$% heavy metal impurities. The curves of Fig.3 show the cathodoluminescence spectra of activatorless and copper activated ($5 \cdot 10^{-3}$% Cu) phosphors synthesized of pure ZnSe heated in hydrogen and also phosphors synthesized by the "wet" procedure from ZnS + H_2SeO_3 with component proportions of 1:1 and 2:3. In the latter case (curve 1), as was noted above, there is obtained zinc oxide containing an admixture of a few tenths of a percent of selenium.

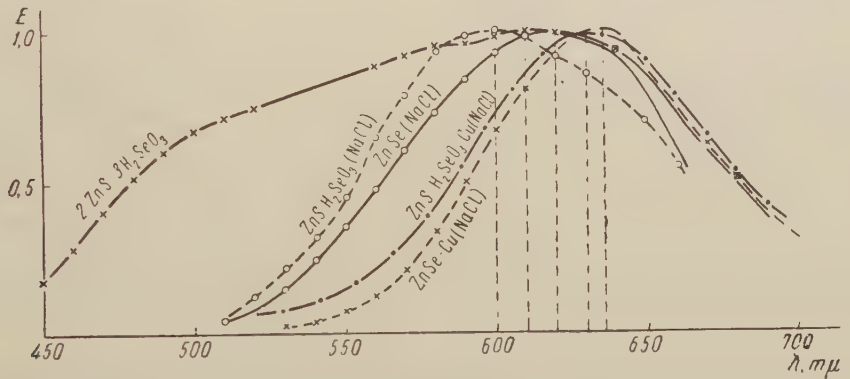

Fig.3. Cathodoluminescence spectra of different zinc selenide and zinc sulfide-selenide phosphors.

According to the data of Bundel' & Ginzburg[5], in this case there is obtained the phosphor ZnO:Se. This luminophor has a broad diffuse maximum in the 590-610 mμ region and also a significant amount of emission in the yellow, green and blue parts of the spectrum. The other curves show that in the case of synthesis by the ZnS + H_2SeO_3 reaction, both in the case of activatorless phosphors and in the case of activation by Cu, the presence in the phosphor of zinc oxide, forming as a result of the above mentioned reactions, leads to an appreciable broadening of the spectral maximum and its displacement some 10-20 mμ to the side of shorter wavelengths.

The luminescence brightness decreases with increase in the amount of zinc oxide present: thus if we take the luminance of ZnS:Cu (NaCl) heated at 800° with excitation by an electron beam of 9 kv and 2 $\mu a/cm^2$ as 100%, we find that the brightness of $ZnS \cdot H_2SeO_3$:Cu (NaCl) is equal to only 75%, that of ZnSe (NaCl) to 45%, $ZnS \cdot H_2SeO_3$ to 4% and ZnO:Se to 6.5%.

Thus in the synthesis of pure selenide phosphors, for example, phosphors intended for color television, the presence of zinc oxide has a deleterious effect. At the same time it may be said that the available data on the luminescence properties of sulfide-selenide phosphors synthesized of ZnS + H_2SeO_3, the ZnSe content in which corresponds to 15, 20, 25 and even 40% SeO_2, exhibit no significant difference as regards brightness and the luminescence spectrum from phosphors synthesized from chemically pure ZnSe. This is due to the fact that with a low content of SeO_2 in the initial batch no significant amount of zinc oxide impurity is formed in the zinc-sulfide-selenide synthesis reaction.

State Institute of Applied Chemistry

References

1. L.Ya.Markovskii & R.I.Smirnova, Zhur.neorgan.khim. (J.Inorg.Chem.) 2, 2752 (1957).

2. L.M.Prokator, Sbornik "Tekhnika televideniya" (Collected articles: "Television engineering") No.10 (16), p.57, M , 1955.

3. L.Ya.Markovskii & Yu.P.Sapozhnikov, Zhur.neorgan.khim. (1960). (Trans. Russian Journal of Inorganic Chemistry.)

4. H.Emeleus & U.Riley, Proc.Roy.Soc., 140, 378 (1933).

5. A.A.Bundel' & A.A.Ginzburg, Sbornik referatov po khimii i tekhnologii lyuminoforov (Collected reports on the chemistry and technology of luminophors), GIPKh, M., 1957.

USE OF THERMOGRAPHY FOR INVESTIGATING ZINC SULFIDE

- E.G.Vasil'eva & S.A.Fridman

The primary purpose of our work was chemical-physical investigation of zinc sulfide phosphors by thermography. In the thermographic procedure different physical and chemical processes are studied on the basis of the exo- and endothermic effects accompanying them.[1] The range of application of thermography is extensive: it allows of detecting changes in state and phase transitions, solution and crystallization, chemical reactions, colloidal processes, etc.

Konstantinova-Shlezinger and her co-workers[2] have used thermography for investigating luminophors based on heterodesmic compounds, the luminescence properties of which are connected with the formation of specific chemical compounds, a process which is clearly evinced in thermograms. To the best of our knowledge the thermographic technique has hitherto not been used for investigating zinc sulfide phosphors. This is explained by the fact that such investigation presents serious difficulties inasmuch as the zinc sulfide base does not undergo any significant chemical reactions incident to heating, except for transition from one crystalline state to another.

Moreover, in working with zinc sulfide there is the added complication that the conventional temperature sensing element, a platinum-platinrhodium thermocouple, cannot be used in view of the fact that the platinum reacts with sulfur.

We decided to check the possibility of using thermography for investigating zinc sulfide particularly with a view to detecting the transformations occurring therein. To prevent the reaction of platinum with sulfur we used special thermocouple jackets of fused quartz. As the raw material we took zinc sulfide produced by the "Krasnyi khimik" (Red chemist) Plant, of the grade now used for the fabrication of most phosphors.

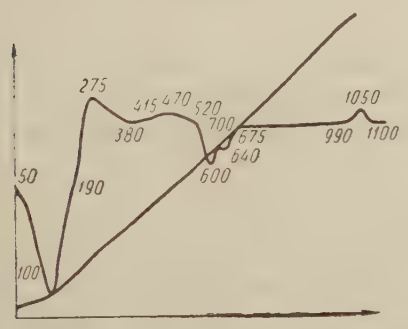

Fig.1. Heating curve for pure ZnS.

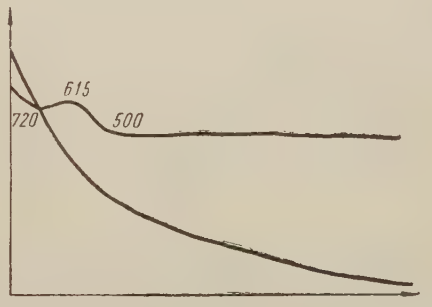

Fig.2. Cooling curve for pure ZnS.

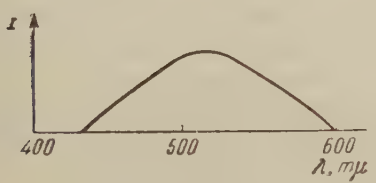

Fig.3. Luminescence spectrum of ZnS heated at 650°.

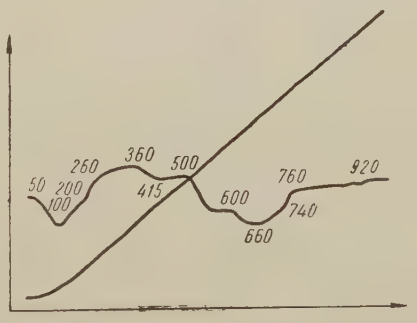

Fig.4. Heating curve for ZnS + 5% NaCl. →→

Fig.1 shows the thermogram obtained for pure zinc sulfide. There are evident in it five thermal effects: 1) a negative effect at 100°, 2 & 3) positive effects at 275 and 475°, 4) a group of negative effects with minima at 600, 645 and 675°,

400°			580°			645°			700°		
d	*I*	*M*	*d*	*I*	*M*	*d*	*I*	*M*	*d*	*I*	*M*
3,14	100	β	3,20	100	$\underline{\beta_x}$*	3,12	100	β	3,20	100	$\underline{\beta_x}$
3,04	15	ZnS_2O_4	3,07	5	ZnS_2O_4	2,67	20	$\underline{\beta_x}$	3,07	15	ZnS_2O_4
2,66	30	ZnS_2O_4	2,45	40	$\underline{\beta_x}$	2,10	2	ZnS_2O_4	2,65	10	$\underline{\beta_x}$
1,64	80	β	1,89	100	β	1,86	100	β	2,09	3	ZnS_2O_4
1,61	3	ZnS_2O_4	1,60	5	ZnS_2O_4	1,79	5	ZnS_2O_4	1,89	100	β
1,34	10		1,47	10	$\underline{\beta_x}$	1,61	80	β	1,64	80	β
1,23	45		1,34	45		1,56	10	$\underline{\beta_x}$	1,55	10	$\underline{\beta_x}$
1,19	50		1,23	50		1,34	30		1,34	20	
1,09	30		1,19	5		1,23	20		1,24	40	
1,03	25	β	1,13	30	β	1,20	10		1,20	10	
0,95	20		0,95	20		1,10	18		1,10	20	
0,91	30		0,91	30		1,03	10	β	1,04	25	β
0,85	20		0,85	15		0,95	8		0,95	18	
0,82	20		0,82	20		0,913	20		0,91	20	
						0,85	5		0,85	10	
						0,82	10		0,82	10	

*The underlined lines differ from those of sphalerite and wurzite.

and 5) a positive effect at 1050°.

In addition to the heating curves, we recorded the cooling curves. The thermographic record for slow cooling is shown in Fig.2 and shows that effect 4 is reversible.

In order to elucidate the origin of these thermal effects we prepared zinc sulfide samples heated at the temperatures corresponding to the noted effects. The samples were studied both by obtaining x-ray diffraction patterns and recording the luminescence spectra.

The luminescence spectra were excited by ultraviolet (λ_{max} = 365 mμ). The zinc sulfide heated at 450° emits a yellowish luminescence (visual observation); that heated at higher temperatures has a yellowish-green luminescence peaking at 510 mμ and with no significant persistence (Fig.3).

The x-ray diffraction data for the different samples are given in the table above.

It will be evident from the table that up to a heating temperature of 580° zinc sulfide has a typical face-centered cubic lattice with the usual interplanar spacing; at 580, 645 and 700° the lattice differs from that of ordinary sphalerite, but the diffraction patterns still contain a number of lines common to sphalerite.

In order to detect the transition and obtain some indications of its character, we recorded the heating curve for zinc sulfide with 5% NaCl (the mineralizing agent or flux commonly employed). The thermogram is shown in Fig.4. It will be evident that the first and second effects are reduced, the third disappears, while the fourth changes somewhat but retains the same general character. We investigated the luminescence spectra of zinc sulfide with 5% NaCl prepared at the temperatures corresponding to the observed effects.

Samples heated at 200, 250, 390 and 420° exhibited no luminescence; that heated at 480° yielded a weak luminescence (visual observation). The samples heated at 560 and 580° show distinct luminescence, the maximum of which lies at 510 mμ; samples heated at 600° exhibit characteristic blue luminescence peaking at 470 mμ. The maximum brightness of the blue luminescence is obtained at t = = 915°; at higher temperatures the brightness decreases (Fig.5). A small shoulder is observed in the thermogram at 600°. X-ray diffraction studies showed that 600-740° there appear new lines; the structure obtained at these temperatures has lines common to sphalerite; no wurzite lines are observed.

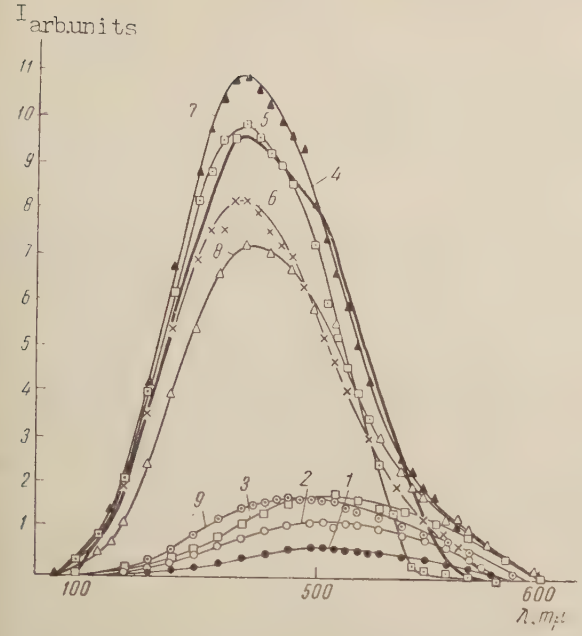

Fig.5. Luminescence spectra of ZnS + + 5% NaCl heated at different temperatures: 1) 560°, 2) 580°, 3) 600°, 4) 620°, 5) 720°, 6) 780°, 7) 915°, 8) 1040° (lower part of sample), 9) 1040° (upper part of sample).

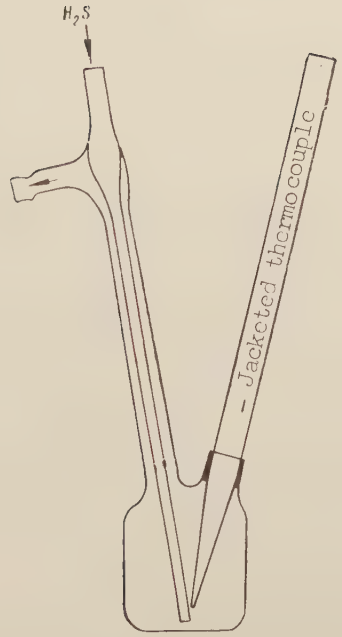

Fig.6. Quartz vessel for heating zinc sulfide in an atmosphere of gas (H_2S).

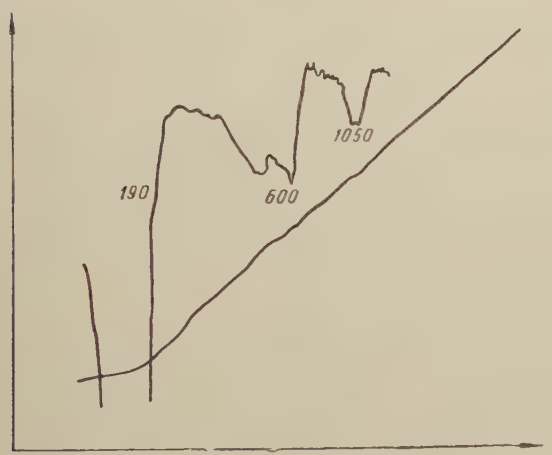

Fig.7. Heating curve for pure ZnS in H_2S.

In addition, we recorded thermograms for ZnS heated in an atmosphere of hydrogen sulfide. For these experiments the powder was enclosed in a special quartz bulb (Fig. 6). The hydrogen sulfide was purified of oxygen and moisture and heated; the outflowing gas was absorbed by caustic soda. The quartz thermocouple jacket was ground to plug the filler opening.

As will be evident from Fig.7, in an atmosphere of hydrogen sulfide, thermal effect 3 disappears, effect 4 acquires "structure", and effect 5 changes sign. On the basis of all the experimental data we propose the following interpretations of the effects.

1. 50-100-190°. The effect is due to elimination of moisture.

2. 190-275-380°. The effect is associated with crystallization following dehydration.

3. 415-475-520°. The effect is due to exothermic oxidation. This is a strong effect which is partially suppressed by the quartz jacket (this was substantiated by thermograms recorded without a jacket). The oxidation reaction is

$$2ZnS + 3O_2 = 2ZnO + 2SO_2 + 121 \text{ kcal};$$

this reaction has been thoroughly studied in connection with the metallurgy of zinc.

4. 600-645-675°. This effect apparently represents a transition to a new crystal form differing from sphalerite and wurzite. It is significant that this effect persists in a reducing medium and in the presence of impurities. Under the usual heating conditions this process proceeds rather slowly and has two minima which are apparently due to the fact that the rearrangement of the lattice occurs in two stages. As noted above, the cooling curve indicates that this effect is reversible.

Buck & Strock[3] investigated zinc sulfide single crystals by means of a high resolution diffraction spectrometer and found that at temperatures from 1020 to 850° there is observed a new crystal lattice of zinc sulfide, which is very similar to sphalerite. In calculating the directionality of the crystal, they found that this lattice is rhombohedral. It is difficult to distinguish in x-ray diffraction patterns inasmuch as its Bragg angles are virtually identical to the Bragg angles of sphalerite. Buck & Strock carried their experiments down to 850°, but infer that the rhombohedal region extends to 600°. We did not have the possibility of checking the crystallographic data, but on the basis of the thermographic curves, we feel safe in asserting that there occurs a polymorphic transformation within these temperature bounds.

It is interesting and significant that blue luminescence begins in this temperature range.

5. 1050°. This effect must be attributed to the formation of wurzite structure. The fact that in heating in air this effect is positive, while in heating in a reducing medium it is negative, indicates that there simultaneously occur two opposed reactions.

The above deductions are of a preliminary nature; further thermographic studies are in progress.

"P.N.Lebedev" Physical Institute
Academy of Sciences of the USSR

References

1. L.G.Berg, A.V.Nikolaev & E.Ya.Rode, Termografiya (Thermography), M., 1944.

2. M.A.Konstantinova-Shlezinger, V.V.Osiko & L.S.Ulanovskaya, Zhur.noergan. khim. (Journal of Inorganic Chemistry), 3, 1286 (1958).

3. C.D.Buck & L.W.Strock, Amer.Mineralogist, 40, 192 (1955).

ON THE FORMATION AND CHARACTERISTICS OF SOME ZINC SULFIDE LUMINOPHORS

- A.V.Lavrov

Experiments with activatorless ZnS

The present work was undertaken with a view to clarifying further the role of oxygen and chlorine in self-activation of ZnS.

One of the first steps in the experimental program was to check the inferences of Riehl & Ortmann[1] regarding the participation of oxygen in the formation of the blue luminescence centers in ZnS.

We heated mixtures of ZnS + 5% NaCl in an atmosphere of purified argon. Oxygen-containing impurities were eliminated from the reagents by a procedure similar to that employed by Riehl & Ortmann. By way of initial material we used zinc sulfide supplied by the "Krasnyi khimik" (Red chemist) Plant, which contained ~0.8% zinc sulfate. The sulfate was completely eliminated by heating the material in H_2S at 500° and the purified zinc sulfide was stored in a vacuum exsiccator. The NaCl (CP grade) was dehydrated by melting under purified argon. Prior to purification the argon contained 0.01% oxygen, which we removed by passing the gas through an alkaline solution of pyragallol, heated copper turnings and a freshly prepared suspension of $Mn(OH)_2$. Water vapor was removed by means of KOH, P_2O_5 and freezing with solid CO_2. The batches for heating were prepared by mixing ZnS(H_2S) + 5% NaCl without further drying. Prior to heating the entire system was purged for several hours with purified argon.

The zinc sulfide batches were heated by two procedures: 1) in a weak flow of argon at 850° for 30 min ("dynamic" conditions) and 2) under static conditions at 980° for 15 min.

In the case of the most complete elimination of oxygen, the characteristic blue luminescence of ZnS was absent. This result was obtained in heating both under the "dynamic" and static conditions. If, however, one uses initial ZnS containing 0.8% sulfate there is obtained a product with bright blue luminescence. Bright luminescence is also obtained in the case of heating a mixture of ZnS(H_2S; 500°) + 2% ZnO + 5% NaCl. The absence of blue luminescence in the oxygen free experiment cannot be attributed to inactivity of the flux as mineralizer. In heating by the static procedure, despite the absence of luminescence of the product there was observed good sintering of the samples. As the results obtained substantiate the inferences of Riehl & Ortmann regarding the role of oxygen in the formation of the ZnS blue luminescence centers. In contrast to the results of Riehl & Ortmann, however, we noted that bound (ionic) oxygen plays an active role in the formation of blue luminescence centers.

To determine whether there is any connection between the presence of residual (not washed out) chlorine and the appearance of the characteristic blue luminescence, we carried out chemical determinations of chlorine in the samples. The chlorine was determined by turbidometric analysis. For purposes of analysis a ~0.2 g sample of ZnS was thoroughly washed to remove chlorine and dissolved in 20 ml chlorine-free 4N H_2SO_4 with gentle heating for 5-8 hours. Portions of the solution were further heated for some time for complete elimination of dissolved H_2S. Then 1 ml 1% $AgNO_3$ solution was added to the test solution and the turbidity of the AgCl suspension was compared with the turbidity of standard solutions with known Cl content.

The results of determination of chlorine in the initial ZnS and also in the luminescent and nonluminescent samples are shown in Table 1.

It will be evident from Table 1 that there is no substantial difference as regards the residual chlorine content in the luminescents and nonluminescent samples. At the same time the absolute chlorine concentration (~$5 \cdot 10^{-5}$ gram-

Table 1

No.	Initial material	$C_{Cl} \cdot 10^{-5}$		Luminescence (λ = 365 mμ)
		g Cl/g ZnS	gram atom Cl / gram mole ZnS	
1	ZnS initial, unheated	1.2	3.3	-
2	ZnS(H_2S;500°) - 5% NaCl; dynamic heating: 30 min at 850°	1.8	5	-
3	ZnS(H_2S;500°) - 5% NaCl; static heating: 15 min at 980°	1.8	5	-
4	ZnS (initial) - 5% NaCl; dynamic heating	1.8	5	Bright blue
5	ZnS (initial) - 5% NaCl; static heating	1.8	5	Bright blue

atom/mole) is very close to the values obtained by Kröger & Hellingman[2]. Noteworthy is the fact that the concentration of not-washed-out chlorine remains constant regardless of the heating conditions (compare samples Nos.2 & 3 and 4 & 5). Our deduction that there is no correlation between the residual chlorine content in the ZnS and the appearance of blue luminescence is consistent with the work of Bundel'[3], but in conflict with the results of Kröger & Hellingman who attribute the appearance of blue luminescence to increase of the Cl concentration in the zinc sulfide.

Role of chlorine in the formation of traps in ZnS:Mn

We felt it would be of interest to determine whether there is any relation between the residual chlorine content and the luminescence properties of other ZnS phosphors. For this purpose it is convenient to use ZnS:Mn, which allows of independent variation of the manganese and chlorine contents.

Table 2

$C_{Mn} \cdot 10^{-3}$, g Mn/g ZnS		$C_{Cl} \cdot 10^{-5}$, g Cl/g ZnS
In batch	After 30 min heating at 850° in N_2	
1	0.56	6.2
3	1.8	8.4
10	6	7.7

Table 2 shows the results of analysis of ZnS:Mn samples, washed before analysis to remove the flux. The chlorine was determined by the procedure described above. The manganese was determined by the following procedure: a weighed amount of sample was dissolved in 4N H_2SO_4, then the manganese was oxidized by potassium periodate to MnO_4 and then determined by calorimetric titration. By way of standard solution we used a titrated solution of $KMnO_4$.

It will be evident from Table 2 that even with an order of magnitude variation in the Mn concentration, the chlorine concentration remains almost the same. On the other hand, it is apparent that there remains in the phosphor only ~60% of the manganese introduced into the initial batch. This decrease in activator concentration is of considerable interest. Hence we carried out analytic determination of Mn in different ZnS:Mn samples that were heated with different fluxes (NaCl and KCl) and without flux (the manganese was added in the form of $MnCl_2$). The results are shown in Fig.1 from which it will be apparent that in going from heating without flux (curve I) to heating with flux (curves II & III) leads to

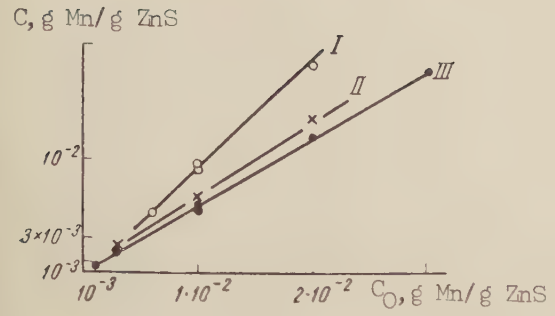

Fig.1. Variation of the manganese concentration C in the phosphor (heated for 30 min at 850°) with the initial Mn concentration C_o in the batch: I - ZnS without flux (heated in N_2), II - ZnS + + 2% KCl (in argon), III - ZnS + 2% NaCl (in N_2).

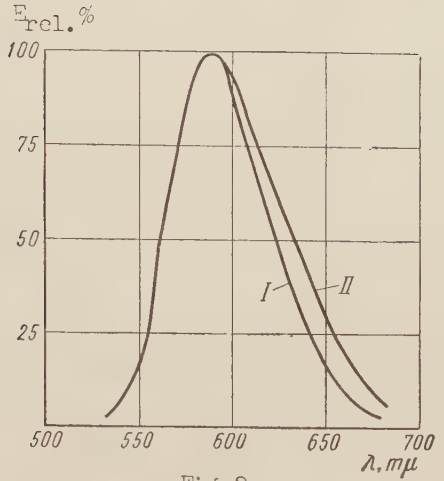

Fig.2

Fig.2. Cathodoluminescence spectra of ZnS: $5.5\cdot10^{-3}$ Mn samples with different chlorine concentrations. Excitation conditions: 10 kv, 10^{-7} amp/cm^2. I - $C_{Cl} = 1.8\cdot10^{-5}$ g/g, II - $5.4\cdot10^{-5}$ g/g.

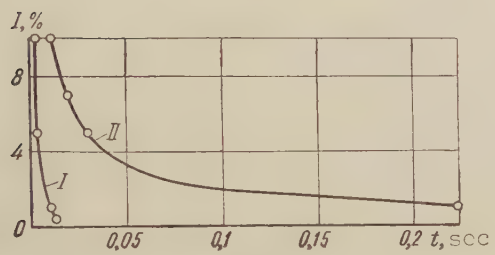

Fig.3

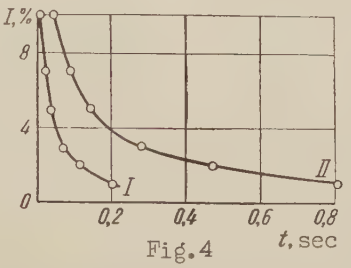

Fig.4

Fig.3. Cathodoluminescence decay curves of ZnS: $5.5\cdot10^{-3}$ Mn samples with different chlorine concentrations: I - $C_{Cl} = 1.8\cdot10^{-5}$ g/g, II - $5.4\cdot10^{-5}$ g/g.

Fig.4. Cathodoluminescence decay curves for ZnS: 10^{-2} Pb (excitation 10 kv, 10^{-8} amp/cm^2). The curves were recorded with a GG-14 filter for discrimination of the Pb band peaking at ~514 mμ. I - ZnS:Pb, II - ZnS:Pb:Cl.

decrease of the percent Mn incorporated into the ZnS from ~95% to ~60%.*

This fact and the linear variation of C with C_o indicate that incomplete incorporation of the Mn into the zinc sulfide in the case of heating with flux is due to distribution of the manganese between the two solvents, namely, the solid ZnS and the molten flux. That such separation between the solvents occurs was proved by direct chemical determination of Mn in the wash water (evaporated to dryness). This analysis showed that approximately 40% of the Mn is carried off with the sodium chloride in the wash water.

To clarify the role of residual (not-washed-out) chlorine in ZnS:Mn phosphors we prepared samples with the same manganese concentration ($5.5\cdot10^{-3}$ g/g by analysis) but with different amounts of chlorine. The samples were heated in purified N_2 for 30 min at 850° without flux; in one case the manganese was intro-

---

*Almost 100% incorporation of Mn can be obtained in heating with a flux provided the manganese is introduced into the batch in the form of its sulfate.

duced in the form of $MnCl_2$, in the other case in the form of $MnSO_4$ (the sulfate was not eliminated from the initial ZnS before heating). The wavelength of the cathodoluminescence peaks and the energy of the peaks for such samples agree (Fig.2). Such samples differ, however, as regards light sum storage. Whereas in the case of the sample with a high chlorine content ($\sim 5.5 \cdot 10^{-5}$ g/g) one obtains a glow curve with many peaks (observations made by V.F.Tunitskaya), in the case of the sample with a low Cl concentration there is no evidence of light sum storage. Consequently, the decay curves for these samples are radically different (Fig.3).

Increase in the chlorine concentration also greatly extends the decay of ZnS:10^{-2}Pb (Fig.4). In view of the experimental results it must be inferred that chlorine in ZnS:Mn and possibly in other sulfide phosphors participates very actively in the formation of traps. Possibly there occurs formation of trapping levels according to Klasens[4].

Conclusions

1. Our experimental data indicate that oxygen in ionic form participates in the formation of the blue luminescence centers in ZnS.

2. The appearance of blue luminescence in the case of activatorless ZnS is not connected with the retention in it of chlorine not washed out with the flux.

3. When ZnS:Mn phosphor is washed to remove the flux (NaCl or KCl) as much as 40% of the Mn present in the batch may be lost.

4. It was found that chlorine impurity in ZnS:Mn plays a decisive role in the formation of the system of trapping levels.

I desire to express my gratitude to V.P.Prokhova for assistance in preparation of the samples, V.K.Verzunov for performing the decay measurements, Yu.V. Voronov for the spectral measurements and V.F.Tunitskaya for observations regarding the storage of light sums.

References

1. N.Riehl (Ril') & G.Ortmann, Zhur.obshch.khim., 6, 1057 (1955). (Trans., J.General Chemistry).

2. F.A.Kroeger & J.E.Hellingman, J.Electrochem.Soc., 95, 2, 68 (1949).

3. A.A.Bundel', Zhur.fiz.khim., (J.Physical Chemistry), 30, 2260 (1956).

4. H.A.Klasens, J.Electrochem.Soc., 100, 72 (1953).

USE OF LUMINESCENCE FOR INVESTIGATING SOLID PHASE REACTIONS IN THE CaO_4-Al_2O_3 SYSTEM

- A.K.Trofimov

The great sensitivity of the luminescence line spectra of rare earth and chromium activated phosphors to changes in the crystal structure of the host material enabled us earlier[1] to follow some simple crystallochemical transformations by observation of these spectra. These observations were limited, however, to establishing the temperature bounds for the existence of individual solid phases of known chemical composition. Yet the use of luminescence line spectra for observation of more complicated solid phase processes with identification of the chemical composition of individual phases should greatly extend the scope of practical utilization of these spectra for physical-chemical analysis. To check this it was obviously expedient to investigate by this procedure some relatively complex crystallostructural process studied earlier by other techniques with a view to comparing the results with the known data. For the purposes of this study we chose the CaO-Al_2O_3 system which, as is known, is important in the technology of different types of cement, particularly so-called alumina cement.

It is known[2] that there occurs complex chemical interaction between CaO and Al_2O_3 in the solid phase at high temperatures and that this interaction leads to the formation of a number of compounds differing as regards composition and crystal lattice. Nagal & Naito[3] established that in the reaction of these oxides, regardless of their proportions, there first forms only calcium monaluminate, $CaO \cdot Al_2O_3$. In the presence of an excess of one of the two oxides, the monaluminate reacts with it to form compounds, the composition of which depends on the quantitative relation between the reacting components. The existence of $3CaO \cdot Al_2O_3$, $5CaO \cdot 3Al_2O_3$ and $CaO \cdot 2Al_2O_3$ has been established with fair reliability, although some authors[4] still question the existence of $3CaO \cdot Al_2O_3$. Toropov[5] recently obtained calcium hexaaluminate, $CaO \cdot 6Al_2O_3$, which belongs in the class of β-alumina. There is only fragmentary information in the literature on the temperature conditions of formation of all the known calcium aluminates. It is reported[2], for example, that $CaO \cdot Al_2O_3$ appears at a temperature of approximately 900-1000°. The other compounds form at 1300° and higher.

In the present report we give the principal results of our investigation by the luminescence line spectra procedure of the chemical interaction between CaO and Al_2O_3. By way of activators we used Eu and Sm. The luminescence of the phosphors obtained by activation of the materials forming in or participating in the solid phase chemical reactions was excited in a GOI (State Optical Institute) spark phosphoroscope[6]. The luminescence spectra were photographed on a diffraction grating spectrograph (dispersion 50 and 25 Å/mm).

The luminescence spectra of CaO and Al_2O_3 activated by Eu and Sm are reproduced in Fig.1. The emission of these phosphors is concentrated in the yellow-red region and consists of a number of lines characteristic of each phosphor. The ability of the initial oxides and, as will be shown below, their reaction products to form bright phosphors with characteristic line spectra is what enabled us to carry out the present investigation.

In order to be able to identify the products of chemical reaction between CaO and Al_2O_3 from their luminescence spectra, we first had to investigate the spectra of all known calcium aluminates. To this end Eu and Sm doped mixtures of the oxides of calcium and aluminum prepared both of oxides roasted beforehand and of mixed water solutions of the nitrates of these elements, taken in molecular proportions of 3:1, 5:3, 1:1, 1:2 and 1:6, were sintered for 1 hour in 1400°. Fig.2 shows the luminescence spectra and Table 1 the wavelengths of the principal lines in the spectra of $3CaO \cdot Al_2O_3$, $CaO \cdot Al_2O_3$, $CaO \cdot 2Al_2O_3$ and $CaO \cdot 6Al_2O_3$

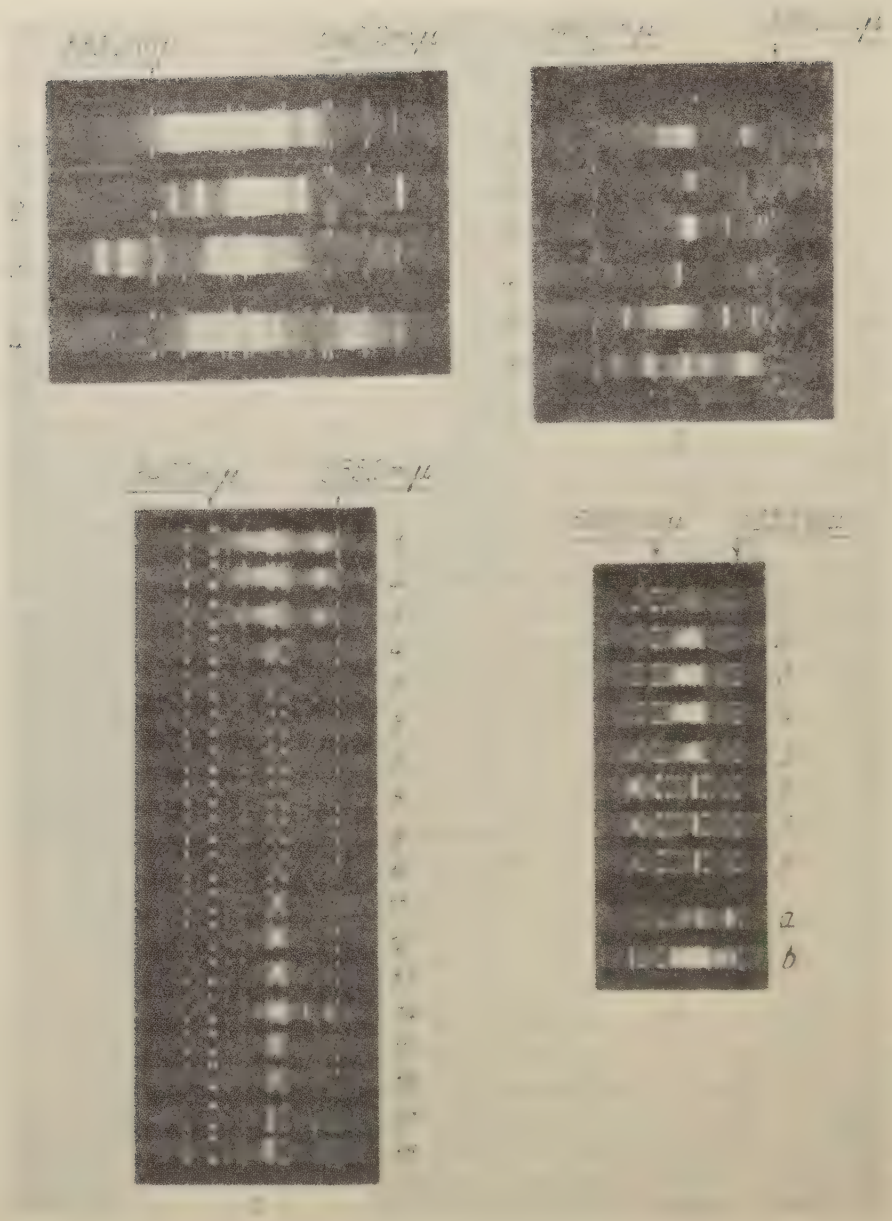

Fig.1. Luminescence spectra of 1) CaO:Eu, 2) Al_2O_3:Eu, 3) CaO:Sm, 4) Al_2O_3:Sm.
Fig.2. Luminescence spectra of 1) $3CaO \cdot Al_2O_3$, 2) $CaO \cdot Al_2O_3$:Eu, 3) $CaO \cdot 2Al_2O_3$:Eu, and 4) $CaO \cdot 6Al_2O_3$:Eu and also of 5) Al_2O_3:Eu and 6) CaO:Eu heated for one hour at 1400°.
Fig.3. Luminescence spectra of mixtures of CaO + Al_2O_3 of different composition (see table 2) heated at 1400°.
Fig.4. Luminescence spectra of $CaO \cdot 6Al_2O_3$ heated for 1 hour at 1) 700°, 2) 800°, 3) 900°, 4) 1000°, 5) 1100°, 6) 1200°, 7) 1300°, 8) 1400°; and luminescence spectra of a) Al_2O_3:Eu and b) CaO:Eu.

activated by europium.*

---

*Inasmuch as all the results obtained for the Eu and Sm activated phosphors agree, hereinafter for the sake of brevity we shall refer only to the luminescence spectra of phosphors containing Eu.

Table 1

Wavelengths of the lines in the luminescence spectra of calcium aluminates of different composition activated by europium

No.	$3CaO.Al_2O_3$		No.	$CaO.Al_2O_3$		No.	$CaO.2Al_2O_3$		No.	$CaO.6Al_2O_3$	
	λ, mμ	Rel. int.		λ, mμ	Rel. int.		λ, mμ	Rel. int.		λ, mμ	Rel. int.
1	579,6	1	1	606,1	1	1	578,9	2	1	590,6	3
2	587,4	2	2	608,4	1	2	588,2	3	2	592,3	4
3	591,8	2	3	610,4	4	3	589,6	4	3	615,0	7
4	593,8	4	4	611,8	4	4	592,2	1	4	617,1	1
5	611,5	10	5	613,1	2	5	599,6	3	5	619,5	1
6	614,7	4	6	615,1	2	6	605,3	2	6	647,5	2
7	616,0	4	7	617,7	1	7	607,4	2	7	655,3	2
8	619,6	3	8	620,3	1	8	611,6	10			
9	623,4	2				9	614,8	5			
10	627,3	3				10	620,0	3			
11	628,9	2				11	626,1	1			
12	649,0	3				12	648,2	2			
13	649,8	1				13	652,6	3			
14	651,9	1				14	655,3	2			
15	654,3	1				15	656,3	2			

It will be evident that these spectra differ noticeably from each other both as regards the number and the wavelengths of the lines. In none of the spectra are the characteristic lines of CaO:Eu or Al_2O_3:Eu evident, which indicates that the above mentioned heat treatment conditions are adequate for the formation of the enumerated compounds. This inference is also substantiated by the results of x-ray diffraction studies. We did not obtain a new, different spectrum for the $5CaO + 3Al_2O_3$ mixture phosphor; this spectrum represents the sum of the spectra of $CaO \cdot Al_2O_3$:Eu and CaO:Eu. The compound $5CaO \cdot 3Al_2O_3$, as Nagal & Naito[3] showed, appears only at temperatures above 1500°.

Thus each compound has its own characteristic spectrum which we utilized in further work as an indicator for detecting the presence of the given compound in the solid phase system.

The difference in the mixture preparation procedure (wet and dry) was evinced only in the brightness of the spectra: the spectra of the products obtained by the wet mixing procedure were brighter. We attribute this result to more perfect crystal formation of the reaction product owing to better intermixing of the particles. In other words, we have here a case of influence of the degree of dispersion (fineness) of the particles on the reaction rate in the solid phase, in accord with the findings of Jander[7].

Having established the character of the luminescence line spectra of most of the known calcium aluminates, we turned to an investigation of the chemical interaction between CaO and Al_2O_3 as a function of the proportion of these oxides in the mixture and the heating temperature. Our purposes were to establish the chemical composition of the primary reaction product and the nature of the secondary products and to determine the temperature bounds of the existence of the various detected calcium aluminates. To this end we prepared Eu and Sm activated phosphors from mixtures consisting of different proportions of the initial components; we gave preference to the wet procedure of forming the mixtures. The molecular compositions of the tested mixtures are listed in Table 2.

In most cases the mixture component proportions corresponded to the calcium aluminates known from the literature, both those the existence of which is reliably known and those that are still in question (the latter are identified by asterisks in Table 2). For the purpose of following the variation of the luminescence spectra of compositions differing little from reliably known calcium alumi-

Table 2

Molecular composition of $CaO + Al_2O_3$ mixtures tested as the phosphor base material

No.	Composition	No.	Composition	No.	Composition
1*	$4\ CaO + Al_2O_3$	7	$5\ CaO + 3\ Al_2O_3$	13*	$3\ CaO + 5\ Al_2O_3$
2	$3\ CaO + Al_2O_3$	8*	$3\ CaO + 2\ Al_2O_3$	14	$CaO + 2\ Al_2O_3$
3*	$5\ CaO + 2Al_2O_3$	9*	$6\ CaO + 5\ Al_2O_3$	15*	$CaO + 3\ Al_2O_3$
4*	$2\ CaO + Al_2O_3$	10*	$11\ CaO + 10\ Al_2O_3$	16	$CaO + 4\ Al_2O_3$
5*	$9\ CaO + 5Al_2O_3$	11	$CaO + Al_2O_3$	17	$CaO + 6\ Al_2O_3$
6*	$12\ CaO + 7Al_2O_3$	12	$4\ CaO + 5\ Al_2O_3$	18	$CaO + 10\ Al_2O_3$

nates we prepared three additional mixtures with slightly different compositions; these are listed as Nos.12, 16 & 18 in Table 2. Carefully weighed out batches of all the mixtures were subjected to 1 hour heating at temperatures ranging from 700 to 1400° in 100° steps. The luminescence spectra showed that the primary reaction product in all mixtures heated at 600° is only $CaO \cdot Al_2O_3$. Increasing the roasting temperature of the mixtures leads to changes in their luminescence spectra.

Fig.3 shows the spectra of different mixtures roasted at 1400°. In the photograph one can distinguish four qualitatively different spectra belonging to $3CaO \cdot Al_2O_3$, $CaO \cdot Al_2O_3$, $CaO \cdot 2Al_2O_3$ and $CaO \cdot 6Al_2O_3$. The lines of the luminescence spectra of the other compositions either belong to the spectrum of one of the enumerated compounds or represent the sum of the spectra of one of the compounds and one of the initial components. From the luminescence spectra of identified composition heated at different temperatures we succeeded in establishing the approximate temperatures of the beginning of formation of each of the above mentioned calcium aluminates. By way of illustration in Fig.4 we reproduce the luminescence spectra of the $CaO + 6Al_2O_3$ mixture heated at different temperatures from 700 to 1400° for 1 hour. As will be evident from the figure, the lines characteristic of $CaO \cdot 6Al_2O_3$:Eu, namely, the 590.6 and 592.3 doublet and the 615.0 mμ line, are already evident in the spectrum for the mixture heated at 1100°, which indicates that this compound begins to form in the solid phase at approximately this temperature.

Similar investigations of the luminescence spectra of other mixtures containing CaO and Al_2O_3 in the proportions 3:1, 1:1 and 1:2 showed that as a result of heating there form in the mixtures the corresponding compounds $3CaO \cdot Al_2O_3$ at 1200°, $CaO \cdot Al_2O_3$ at 900° and $CaO \cdot 2Al_2O_3$ at 1000°. Here it should be noted that the appearance of the line spectra characteristic of a given compound is predicated not simply on the presence of the compound per se, but on formation of its typical crystal lattice. Hence it must be inferred that at the indicated temperatures the forming aluminates already have a crystal structure.

On the basis of observation of the appearance and disappearance of the individual characteristic lines in the luminescence spectra of the mixture samples heated at different temperatures, we arrived at the following conclusions regarding the conditions governing the formation of the various compounds.

1. Tricalcium aluminate, $3CaO \cdot Al_2O_3$, forms from the $3CaO + Al_2O_3$ mixture at 1200°. At lower temperatures we detected the presence of $CaO \cdot Al_2O_3$ in this mixture. Consequently, the $3CaO \cdot Al_2O_3$ formation reaction is presumably

$$CaO \cdot Al_2O_3 + 2CaO \rightarrow 3CaO \cdot Al_2O_3.$$

This inference is substantiated by the fact that with decrease in the amount of calcium oxide in the mixture, the amount of $3CaO \cdot Al_2O_3$ formed decreases and

becomes virtually nil in the case of the mixture having the composition $2CaO + Al_2O_3$.

2. We did not detect the formation of $5CaO \cdot 3Al_2O_3$ at any of the experimental temperatures, i.e., up to 1400°.

3. Calcium monaluminate, $CaO \cdot Al_2O_3$, forms at a rapid rate from the 1:1 oxide mixture in the 900-1000° range. With increase of the heating temperature and the same proportion of oxides, there occurs only ordering of the crystal lattice of this compound inasmuch as the luminescence spectrum does not change in intensity, only the lines become sharper.

4. Calcium dialuminate, $CaO \cdot 2Al_2O_3$, appears, as was noted above, at 1000°. This compound also appears but in smaller amounts in the case of impoverishment of the mixture in alumina (for example, from the $4CaO + 5Al_2O_3$ mixture) or lime (from the $CaO + 4Al_2O_3$ mixture) also at about 1000°. Inasmuch as $CaO \cdot 2Al_2O_3$ is absent below this temperature, while $CaO \cdot Al_2O_3$ is already present in the mixture it may be inferred that the dialuminate forms by the reaction

$$CaO \cdot Al_2O_3 + Al_2O_3 \rightarrow CaO \cdot 2Al_2O_3.$$

5. Calcium hexaaluminate, $CaO \cdot 6Al_2O_3$, which forms from the $CaO + 6Al_2O_3$ mixture at 1100°, also forms together with $CaO \cdot 2Al_2O_3$ in mixtures with smaller amounts of alumina. With increase in the heating temperature the amount of both compounds increases. Inasmuch as the dialuminate appears before the hexaaluminate, it is possible that the latter compound forms by the reaction

$$CaO \cdot 2Al_2O_3 + 4Al_2O_3 \rightarrow CaO \cdot 6Al_2O_3.$$

In view of the considerations set forth above, however, it may be assumed that this compound may also form through the reaction:

$$CaO \cdot Al_2O_3 + 5Al_2O_3 \rightarrow CaO \cdot 6Al_2O_3.$$

Thus utilization of the line luminescence spectra of rare earth phosphors produced by activating the base materials taking part in both the simple and complex reactions in the $CaO-Al_2O_3$ system proved to be a satisfactory means for identifying the chemical composition of the individual solid phases and for determining the reaction temperatures. The lime-alumina compounds detected in this manner are in agreement with those known from the literature. In the course of our investigation we obtained a number of interesting results. Among these is definite proof of the existence of tricalcium aluminate and the fact that this compound and $CaO \cdot 2Al_2O_3$ and $CaO \cdot 6Al_2O_3$ begin to form at temperatures somewhat lower than commonly reported hitherto. Possibly the lower values of the formation temperatures found in our experiments are explained by the fact that the mixtures of the initial oxides employed were practically ideal inasmuch as they were prepared from water solutions of calcium and aluminum salts.

In conclusion I desire to thank P.P.Feofilov for his guidance and friendly assistance in carrying out the present research.

"S.I.Vavilov" State Optical Institute

References

1. A.K.Trofimov & S.S.Tolkachev, Vestnik, Leningrad State University, No.4, 102 (1957).

2. P.P.Budnikov & A.S.Berezhnoi, Reaktsii v tverdykh fazakh (Reactions in solid phases), M., 1949.

3. S.Nagal & R.Naito, J.Soc.Chem.Japan, suppl., 33, 17 (1930).
4. E.Campbell, J.Ind.Eng.Chem., 9, 943 (1917).
5. N.A.Toropov, Khimiya tsementov (Chemistry of cements), M., 1956.
6. E.M.Brumberr, Z.M.Sverdlov & T.V.Timofeeva, Izv.AN SSSR, Ser.fiz., 13, 242 (1949).
7. W.Jander, Z.anorg.Chem., 226, 225 (1936).

* * * * * * *

LUMINESCENCE OF MANGANESE ACTIVATED STRONTIUM METAANTIMONATE

- M.-L.Yu.Allsalu

Manganese activated phosphors described in the literature and used in industry have green, yellow or red luminescence. For example, the following phosphors are known:

Green	Yellow	Red
α-Zn_2SiO_4:Mn (525 mμ)	β-Zn_2SiO_4:Mn (560 mμ)	MgS:Mn (665 mμ)
Zn_2GeO_4:Mn (537 mμ)	$CdSiO_3$:Mn (605 mμ)	Sb_2O_4:Mn (630-640 mμ)
$MgAl_2O_4$:Mn (523 mμ)	CaS:Mn (589-611 mμ)	Mg_2SiO_4:Mn (640-680 mμ)
$CaSb_2O_6$:Mn (510-520 mμ)	ZnS:Mn (586 mμ)	$Ca_2P_2O_7$:Mn (633 mμ)

Among the phosphors that have been more or less thoroughly studied there are almost no cases of shift of the Mn band below the green region. In view of this, investigation of manganese as activator in $SrSb_2O_6$ is of particular interest inasmuch as the peak of the emission band in this case lies in the blue region.

We synthesized the phosphor samples from specially purified Sb_2O_5 and $SrCO_3$ which, according to the data of spectroscopic emission analysis, contained only traces of iron and no other heavy metal impurities. The activator was introduced in the form of repurified $MnSO_4$. In preparing the phosphors, the initial materials, Sb_2O_5 and $SrCO_3$, were thoroughly mixed with a water solution of the activator, dried and then heated. All the operations were carried out under conditions minimizing the possibility of contamination.

To obtain a fully homogeneous fine grain phosphor it is expedient to carry out the heating in two stages with intermediate grinding of the partially reacted batch.

The resultant fine, pure white powder is strongly excited by cathode rays and more weakly by ultraviolet; in the latter case the excitation region extends from 200 to 250 mμ with a peak at 220 mμ. The cathodoluminescence emission band (440-475-530 mμ) is very narrow (half-width ~30 mμ), which results in a high degree of saturation of the emission color.

The host material of the phosphor is apparently strontium metaantimonate, inasmuch as the maximum luminance is observed for phosphors prepared from batches with a composition approximating $SrSb_2O_6$. Shift of the composition to the side of $Sr_2Sb_2O_7$ always results in a decrease in brightness. In the case of phosphors the batch composition of which approaches the pyroantimonate ($Sr_2Sb_2O_7$), prepared at comparatively low heating temperatures corresponding to the region of stability of pyroantimonate, the blue band disappears and is replaced by weak rosy luminescence. A large excess of Sb_2O_5 also has a negative effect on the luminance.

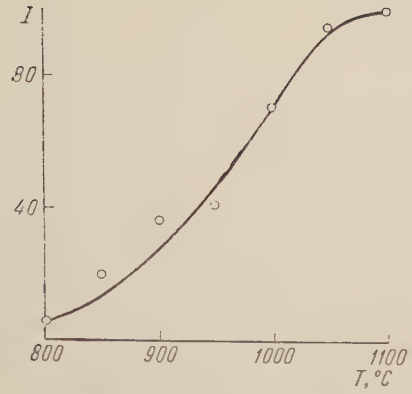

Fig.1. Variation of the cathodoluminescence intensity of $SrSb_2O_6$:Mn with the heating temperature; 1 hr heating; C_{Mn} = = 0.05%.

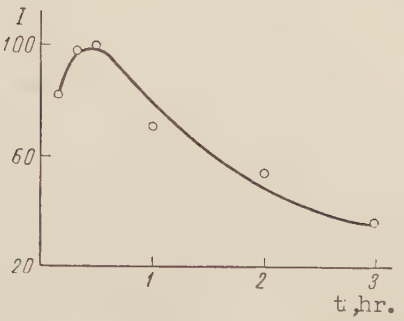

Fig.2. Variation of the cathodoluminescence intensity of $SrSb_2O_6$:Mn with the heating time at 1100°; C_{Mn} = 0.05%.

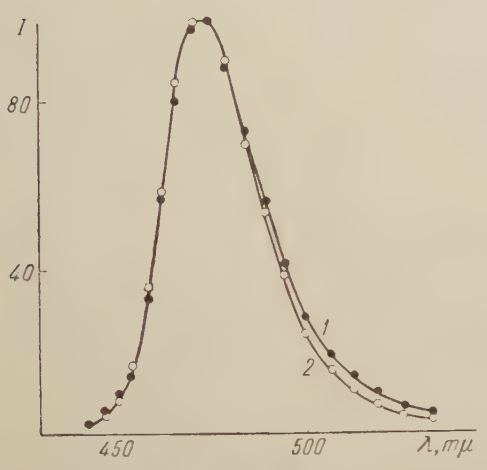

Fig.3. Cathodoluminescence spectra of $SrSb_2O_6$:Mn with different activator concentrations (20 min heating at 1100°): 1) 0.01% Mn, 2) 3% Mn.

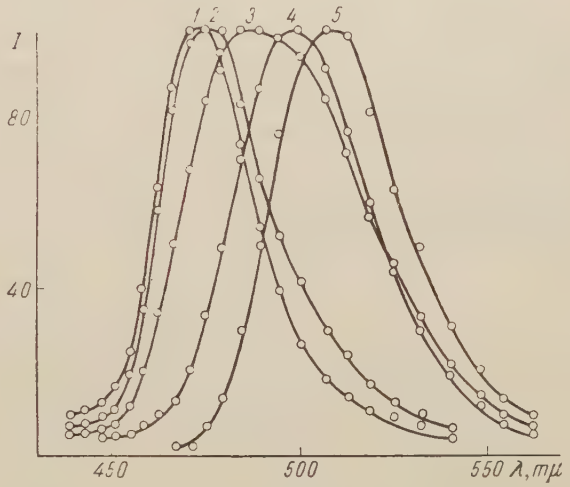

Fig.4. Cathodoluminescence spectra of phosphors in the system (SrO·CaO) Sb_2O_5:Mn (1 hr heating at 950°; C_{Mn} = = 0.03%): 1) SrO·Sb_2O_5:Mn, 2) (3SrO·CaO)Sb_2O_5:Mn, 3) SrO·CaO·Sb_2O_5: :Mn, 4) (SrO·3CaO)·Sb_2O_5:Mn, 5) CaO·Sb_2O_5:Mn.

The character of the activator concentration dependence of the luminescence intensity indicates that in $SrSb_2O_6$ the manganese acts as a typical activator. Nonactivated strontium antimonate does not luminesce. Distinct blue luminescence becomes evident at an Mn concentration of 10^{-3}% by weight. The luminescence brightness and the degree of saturation of its color progressively increase with increase of the Mn concentration, attaining a maximum at about 1% Mn and remaining at a high level up to an Mn content of 3%. With further increase in the activator concentration the cathodoluminescence brightness falls off rapidly.

Formation of an efficient phosphor begins at a heating temperature of 800° and the luminescence intensity progressively increases with increasing temperature to 1100° (Fig.1). The variation of the luminance with the heating time at constant temperature proves to be more complex. The brightest phosphors are obtained with relatively short-term heating: 30 min at 1100° and 1 hour at 1050° (Fig.2). The decrease in brightness with more prolonged heating is probably due

to volatilization of part of the antimony oxide. We measured the relative luminescence intensity by means of an FEU-18 photomultiplier with CR excitation at 4 kv and 0.05 $\mu a/cm^2$. A blue cathodoluminescence band but of different shape is induced in strontium metaantimonate by other activators such as Bi and Ti. One cannot attribute the blue luminescence of $SrSb_2O_6$:Mn to such metal impurities or to a stoichiometric excess of Sb. In addition to the concentration dependence curve, evidence against this is the substantial difference between the photoluminescence excitation regions and also the time lag characteristics of the phosphors.

The cathodoluminescence spectrum of $SrSb_2O_6$:Mn phosphor is characterized by great stability as regards variation in composition and synthesis conditions. The luminescence spectrum also does not depend on the activator concentration (Fig.3), the composition of the mixture up to the point of formation of strontium pyroantimonate and the heating temperature; it changes somewhat but not significantly with variation of the heating time. The cathodoluminescence spectra were recorded with CR excitation of 4 kv and 0.5 $\mu a/cm^2$.

The behavior of the phosphor spectrum in the case of isomorphic replacement of the host cations by calcium is rather interesting (Fig.4). Further studies are necessary to determine whether the observed change is due to shift of one band owing to change of the lattice parameters or to superposition of two independent, close bands.

I desire to express my sincere gratitude to A.V.Moskvin for his guidance in the work.

Tartu State University

SUITABILITY OF THE THIOSULFATE PROCEDURE FOR PREPARATION OF ZINC SULFIDE FOR SYNTHESIS OF PHOSPHORS

- M. I. Tombak, O. V. Popova, A. F. Komar & A. A. Bundel'

At present zinc sulfide for the production of phosphors is prepared by precipitation of the ZnS from a water solution of zinc sulfate with hydrogen sulfide.

Guntz[1,2] proposed a number of other procedures, not involving the use of H_2S, for preparing zinc sulfide, one of these - the thiosulfate procedure - was investigated in detail by Grillot[3,4]. Investigation of the thiosulfate procedure is of considerable interest and value because the phosphors prepared from the product differ as regards properties from phosphors prepared from ZnS produced by the conventional procedure. Grillot[5-7] explains this by the fact that the reaction product in the thiosulfate process is zinc disulfide rather than the usual monosulfide. The disulfide sulfur is uniformly distributed through the bulk of the product and is eliminated only at high temperature, which, in the opinion of Grillot, creates conditions favorable for complete reduction of all the oxygen compounds present in the batch.

Thus the distinctive characteristics of ZnS phosphors obtained by heating amorphous zinc sulfide prepared by the thiosulfate procedure are attributed by Grillot to complete absence of oxygen in the final phosphor, in contrast to phosphors obtained from the ordinary sulfide even after their deoxidation by H_2S.

Inasmuch as some of the points in Grillot's report appeared obscure to us, we undertook an investigation of the reaction of sodium thiosulfate with zinc sulfate and a study of the phosphors prepared of the resultant "zinc disulfide".

Investigation of the mechanism of the reaction of zinc sulfate with sodium thiosulfate

The reaction in question was first described by Allen & Crenshaw[8], who assumed its mechanism to be described by the following equation

$$ZnSO_4 + 4Na_2S_2O_3 = ZnS + 4S + 4Na_2SO_4. \quad (1)$$

Allen & Crenshaw, who worked with dilute solutions, also detected the formation of small amounts of H_2SO_4, SO_2 and H_2S as a result of side reactions.

Grillot investigated this reaction from the standpoint of phosphor chemistry using concentrated solutions. According to Grillot, this is an ionic third order reaction leading to the formation of zinc disulfide and dithionate:

$$Zn^{2+} + 2S_2O_3^{2-} = ZnS_2 + S_2O_6^{2-}. \quad (2)$$

This interpretation of the reaction mechanism is of great interest inasmuch as third order reactions are very rare in general and ionic third order reactions are virtually unknown. Moreover, the reaction products of $Na_2S_2O_3$ with the salts of other heavy metals (Cu, Ag, Hg, Cd, Sr, Co and Pb) are always the corresponding monosulfides.[9]

In our experiments we worked with solutions of the same concentrations at 99 ± 1°C and in general adhered to the conditions described by Grillot.

A detailed description of the chemical aspects of the work will be published elsewhere[10]. Here we only note that on the basis of determinations of variations in the concentration of Zn^{2+}, $S_2O_3^{2-}$, SO_3^{2-} and SO_4^{2-}, of the content of polythionates and dithionate and of the composition of the precipitate at different stages of the process, we definitely established that the reaction of $ZnSO_4$ with $Na_2S_2O_3$ has a mechanism different from that suggested by Grillot.

The reaction mechanism is characterized by the following series of equations:

$$Zn^{2+} + S_2O_3^{2-} + H_2O = ZnS + H_2SO_4, \quad (3)$$

$$Na_2S_2O_3 + H_2SO_4 = H_2S_2O_3 + Na_2SO_4, \quad (4)$$

$$H_2S_2O_3 = H_2O + SO_2 + S, \quad (5)$$

$$6Na_2S_2O_3 + 9SO_2 = 4Na_2S_3O_6 + Na_2S_4O_6 + Na_2S_5O_6. \quad (6)$$

The principal reaction (3) leads to the formation of zinc monosulfide and H_2SO_4. The latter liberates free thiosulfuric acid (4), which by the familiar reaction (5) decomposes into SO_2, H_2O and S; the last settles into the precipitate and contaminates the ZnS. SO_2, interacting with excess $Na_2S_2O_3$, forms a mixture of penta-, tetra- and trithionates (6) which in subsequent stages of the reaction decompose with the formation of S, S^{2-} and H_2SO_4.

Table 1

Composition of precipitate, %	Time from beginning of precipitation, min			
	15	30	60	120
Zinc	58,84	59,42	62,16	42,06
Sulfide S	28,68	29,05	30,34	21,30
Extractable S	—	1,40	2,62	30,70
$ZnSO_4$	4,12	3,80	2,88	2,73
H_2O	8,10	6,20	1,92	2,34
Total	99,74	99,87	99,92	99,13
Zn / Sulfide S, at.%	1:0,998	1:0,998	1:0,998	1:1,025
Zn / Total S, at.%	1:0,998	1:1,04	1:1,08	1:2,52

Despite careful and thorough analysis for sodium dithionate, we failed to detect this compound at any stage of the process.

Inasmuch as the composition of the precipitate forming in the reaction is of definite interest from the standpoint of phosphor chemistry, we list the results of analyses of the precipitate at different stages of the process in Table 1.

Thus the interaction of $ZnSO_4$ with $Na_2S_2O_3$ is a second order reaction, proceeding with the formation of zinc monosulfide, which at later stages of the process is contaminated with elemental sulfur, the amount of which may attain 2.5 atoms S per atom Zn if the process is extended for a considerable period. Up to 97-98% of the surstoichiometric sulfur can be removed from the ZnS by extraction in a Soxhlet apparatus.

Purification of the reagent solutions

The expediency of using the thiosulfate procedure for preparing phosphor zinc sulfide depends primarily on the possibility of adequate purification of the $Na_2S_2O_3$ to eliminate activator cation impurities.

The procedure for purifying zinc sulfate solutions is well known[11-13]. There are no data in the literature, however, on the elimination of metal impurities from hyposulfite solutions; hence we investigated the possibility of purifying $Na_2S_2O_3$ by recrystallization and also of purifying its solutions by coprecipitation and by sorption, chromatographic and extraction techniques.[12] The effectiveness of the different procedures was evaluated on the basis of the impurity content in the sulfide obtained from the reaction of $ZnSO_4$ with $Na_2S_2O_3$ purified by the given procedure.

The results, which are listed in Table 2, show that adequate purification of $Na_2S_2O_3$ can be realized either by sorption or by extraction methods. The choice of procedure to be used in any given case will be determined by technological considerations.

Anionic impurities in ZnS prepared by the thiosulfate procedure

At the instant of precipitation zinc sulfide has a high adsorptive capacity, so that the sulfide precipitate obtained both by the conventional H_2S procedure and by the thiosulfate technique is always contaminated with oxygen containing anionic impurities.

Washing the zinc sulfide, both that obtained by the conventional H_2S procedure and that prepared by the thiosulfate technique, by decanting with water does not fully eliminate the SO_4^{2-}. Usually the sulfate radical is present in the amount of 1-2% in the commercial sulfide. Its content can be reduced somewhat by very thorough washing. According to the data of Polumbo & Levine[14], the SO_4^{2-} can be completely eliminated from ZnS precipitated with H_2S by washing with NaCl solution. In the case of zinc sulfide prepared by the thiosulfate procedure washing with concentrated NaCl solutions does not result in complete removal of SO_4^{2-} but does allow of reducing its content to 0.1%.

In the thiosulfate procedure the precipitate, in addition to SO_4^{2-}, can entrap other oxygen containing anions: $S_2O_3^{2-}$, SO_3^{2-} and $S_nO_6^{2-}$. Determination of these anions in ZnS by conventional analytical methods is impossible owing to the fact that they decompose when the precipitate is being dissolved. We established the presence of oxygen containing anions in the zinc sulfide by investigating the gas evolved in heating the product.

It is known[15] that in the 600 to 700° temperature range zinc sulfide reacts actively with the sulfate according to the equation

(7)

In the case of heating zinc sulfide prepared by the conventional hydrogen sulfide procedure the amount of SO_2 liberated corresponds to that calculated by means of Eq.(7) from the SO_4^{2-} content in the initial sulfide. In the case of heating the product prepared by the thiosulfate method, however, the SO_2 yield is approximately 5 times greater than the amount calculated according to (7).

Hence the zinc sulfide obtained by the thiosulfate procedure is highly contaminated with oxygen containing anions. The presence of a significant excess of elemental sulfur does not assure reduction of the oxygen containing compounds owing to the fact that the sulfur is volatilized at a temperature of the order of 450° and hence cannot participate in the reactions occurring in the solid phase at 600-700°.

Luminescence properties of activatorless ZnS phosphor prepared by the thiosulfate procedure

The spectra of activatorless ZnS phosphors prepared by the thiosulfate technique differ from the spectra of ordinary (H_2S) zinc sulfate phosphors. The characteristic blue band is shifted some 80-100 Å to the side of longer wavelengths. In addition, these luminophors have a persistent green afterglow, the intensity of which depends on how thoroughly the initial sulfide is washed. As regards color and persistence the afterglow is very close to the phosphorescence due to copper. Hence for the purposes of qualitative characterization we compared our samples with a series of ZnS:Cu phosphors with known Cu concentrations.

Zinc sulfide prepared by the thiosulfate procedure and washed with water yields after heating a phosphor with an afterglow persistence close to that of ZnS: $2\cdot10^{-6}$Cu. The same sulfide, but washed with a solution of NaCl and heated under the same conditions, exhibits a phosphorescence identical to that of ZnS: : $2\cdot10^{-7}$Cu. The spectra of these samples are reproduced in Fig.1, from which it

Table 2

Activator metal impurities in zinc sulfide prepared from purified solutions of zinc sulfate and sodium thiosulfate

Purification procedure		Impurities in ZnS, %					
		Fe		Cu		Co	Ni
Zinc sulfide	Sodium thiosulfate	chem.	spectr.	chem.	spectr.	chem.	spectr.
Anionite columns: Fe > $5 \cdot 10^{-6}$%; Cu = $2 \cdot 10^{-6}$%; Co and Ni = 10^{-5}%	Not purified	Very high	$1 \cdot 10^{-4}$	-	$2 \cdot 10^{-4}$	Not analyzed	
	Precipitation with MnO_2 and ZnS	$1 \cdot 10^{-4}$	$1 \cdot 10^{-4}$	$2 \cdot 10^{-4}$	$2 \cdot 10^{-3}$	-	-
Sodium diethyldithiocarbonate and "A" grade charcoal; Fe = $2 \cdot 10^{-5}$%; Cu > $5 \cdot 10^{-5}$%; Co and Ni = 10^{-5}%	Anionite column	-	$5 \cdot 10^{-5}$	-	$1 \cdot 10^{-4}$	$1 \cdot 10^{-5}$	$1 \cdot 10^{-5}$
	Carbon-dimethylglyoxine column	$2 \cdot 10^{-5}$	$5 \cdot 10^{-5}$	$1 \cdot 10^{-4}$	$2 \cdot 10^{-4}$	$1 \cdot 10^{-5}$	$1 \cdot 10^{-5}$
	Recrystallization	-	$5 \cdot 10^{-5}$	-	$5 \cdot 10^{-5}$	Not analyzed	
	Sodium diethyldithiocarbonate with subsequent extraction of heavy metal complexes by isoamyl alcohol	-	$5 \cdot 10^{-5}$	-	$(5-6) \cdot 10^{-6}$	$1 \cdot 10^{-5}$	$1 \cdot 10^{-5}$
	Sorption in columns with PE-9 anionite in OH-form	-	$5 \cdot 10^{-5}$	-	$5 \cdot 10^{-6}$	$1 \cdot 10^{-5}$	$1 \cdot 10^{-5}$
	Coprecipitation with $Mg(OH)_2$ and ZnS	$1 \cdot 10^{-4}$	-	$1 \cdot 10^{-4}$	-	-	-
	Sodium diethyldithiocarbonate with subsequent sorption of heavy metal complexes by activated grade "A" charcoal	$3 \cdot 10^{-5}$	$5 \cdot 10^{-5}$	$(6-8) \cdot 10^{-5}$	$1 \cdot 10^{-4}$	$1 \cdot 10^{-5}$	$1 \cdot 10^{-5}$

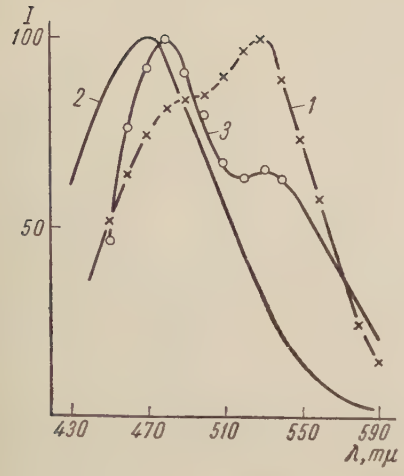

Fig.1. Luminescence spectra of activatorless ZnS phosphors prepared by the thiosulfate procedure and of a sample prepared from a batch doped with 4% $ZnSO_4$: 1) ZnS phosphor prepared from the sulfide washed with water, 2) same but from phosphor with NaCl solution, 3) commercial ZnS phosphor prepared with 4% $ZnSO_4$.

will be apparent that the spectrum of the water washed phosphor contains a green band with λ_{max} = = 530 mμ.

Treatment of the zinc sulfide prepared by the thiosulfate technique with 1 N H_2SO_4 appreciably reduces the intensity of the green phosphorescence. Earlier, one of us (Bundel'[16]) established that activation of ZnS with oxygen leads to the appearance of a green luminescence band close to the characteristic band of copper. Since more thorough washing of the product could not reduce the Cu content in it, it follows that the observed phosphorescence is due to activation of the "thiosulfate" ZnS by oxygen from decomposition of the oxygen containing anionic impurities.

To check this inference we prepared a sample of ZnS obtained by the hydrogen sulfide procedure with the addition of 4% impurity-free $ZnSO_4$. The green band peaking at 530 mμ was also present in the phosphorescence spectrum of this phosphor (Fig. 1, curve 3). This experiment as well as direct analytic determination of Cu, which yielded a value of $C_{Cu} < 5 \cdot 10^{-8}$ g/g, show that this band is due to oxygen activation and should not be confused with the familiar copper band.

Thermal stability of the oxygen band

We found a dependable means for identifying the oxygen band in investigating its thermal stability. Quenching of the oxygen band occurs at a higher temperature then fading of the Zn band: by heating the phosphor to 93° one of us[17] was able to observe it in pure form.

By sublimation in vacuum ($p < 1 \cdot 10^{-3}$ mm Hg) at 1100° we prepared a ZnS:O phosphor the luminescence spectrum of which consisted of the oxygen band with λ_{max} = 530 mμ and a very weak Zn band. Experiments with this phosphor showed that with increase of the temperature from room temperature to 200° the brightness of the oxygen band falls off by a factor of 4 (Fig.2, curve 2). We observed a similar decrease in the brightness of the green band in the emission of activatorless ZnS phosphors obtained by the thiosulfate procedure (Fig.2, curves 3 & 4). The luminance measurements in this case were carried out at temperatures above 100° when the zinc band is suppressed by temperature quenching.

The temperature dependence of the Cu band brightness has an entirely different character: at 200° its brightness is approximately equal to that at room temperature[18]. Thus the difference in thermal stability of the oxygen and copper bands provides a reliable means of distinguishing between them.

Possibility of using the thiosulfate procedure for synthesis of phosphors

With sufficiently careful and thorough washing of the sulfide the intensity of the green phosphorescence due to activation by oxygen can be reduced to the intensity of the green afterglow of phosphors with $2 \cdot 10^{-7}$ g Cu per g ZnS. Such a sulfide obviously cannot be used for the synthesis of blue short-persistence phosphors.

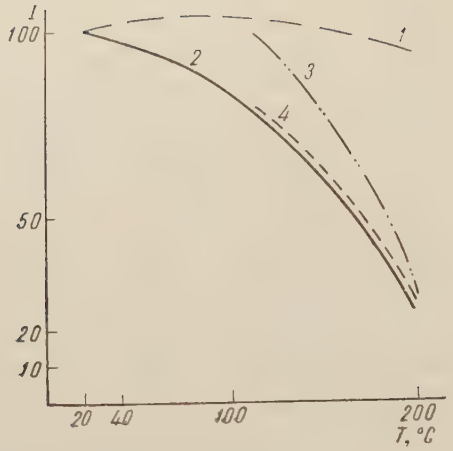

Fig.2

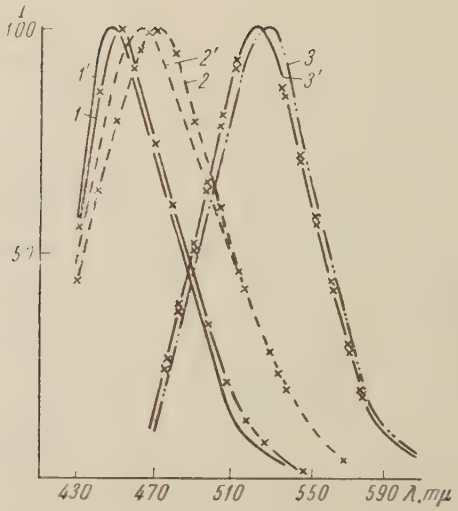

Fig.3

Fig.2. Variation in the brightness of the copper and oxygen bands with the phosphor temperature: 1) Cu, 2) O_2, 3 & 4) brightness of the green band in the luminescence of ZnS phosphors obtained by the thiosulfate procedure.

Fig.3. Luminescence spectra of different phosphors: 1) ZnS:Ag, ZnS obtained by the thiosulfate procedure, 1') ZnS:Ag, prepared from the commercial sulfide, 2) ZnS:Zn, ZnS obtained by the thiosulfate procedure, 2') ZnS:Zn prepared from the commercial sulfide, 3) ZnS:Cu, ZnS obtained by the thiosulfate procedure, 3') ZnS:Cu prepared by the hydrogen sulfide procedure.

Table 3

Phosphor	Luminance compared to commercial samples with excitation by	
	ultra-violet	x-ray
ZnS — Zn	205	200
ZnS — Ag	87	87
ZnS — Cu	110	95
58ZnS·42CdS — 10^{-4} Ag	110	125

The product, can however, be used for the preparation of phosphors with green and yellow luminescence where short persistence is not a requirement. Using zinc sulfide obtained by the thiosulfate procedure we prepared ZnS:Ag (K-5), ZnS:Cu (FK-106) and 58 ZnS·42CdS: :10^{-4}Ag phosphors (the CdS was also obtained by the thiosulfate procedure); the characteristics of these phosphors are shown in Table 3 and Fig.3.

Thus the fact that these phosphors fully meet the current technical specifications for phosphors of the indicated types, the possibility of eliminating the use of H_2S and the simplicity of the technological operations involved make the thiosulfate procedure more promising than the now commonly employed hydrogen sulfide technique.

References

1. A.Guntz, Compt.rend., 226, 80 (1948).
2. A.Guntz, Compt.rend., 226, 1280 (1948).
3. E.Grillot, Compt.rend., 230, 543 (1950).
4. E.Grillot, Bull.Soc.chim.France, 1-2, 39 (1951).
5. E.Grillot & M.Bancie-Grillot, Compt.rend., 231, 966 (950).

6. E.Grillot, J.Chim.phys.et phys.-chim.biol., 50, 515 (1953).
7. E.Grillot, J.Chim.phys.et phys.-chim.biol., 48, 112 (1951).
8. E.T.Allen & J.L.Crenshaw, Amer.J.Sci., 34, 341 (1912).
9. J.W.Mellor, A Comprehensive Treatise on Inor. and Theor.Chem., 10, 489; 4, 588; 4, 945; 3, 321; 8, 783 (1946-1947).
10. M.I.Tombak & A.A.Bundel', Zhur.neorgan.khim., 4, 1568 (1959) (Russian J.of Inorgan.Chem.)
11. A.V.Moskvin, Katodolyuminestsentsiya (Cathodoluminescence) Part.2, p.292 (1949).
12. Transactions of the Fifth Conference on Luminescence, Tartu, 1958.
13. A.M.Gurvich, T.B.Gapon & M.S.Rabinovich, Khim.prom-st' (Chemical industry), No.1, 31 (1956).
14. J.Polumbo & E.Levine, J.Electrochem.Soc., 102, 4 (1955).
15. V.I.Smirnov, Okislitel'nyu obzhig mednykh rud i kontsentratov (Oxidizing roasting of copper ores and concentrates), Sverdlovsk-Moscow, 1938.
16. A.A.Bundel', Zhur.fiz.khim. (J.Physical Chemistry), 30, 2469 (1956).
17. A.A.Bundel', Dissertation, Vol.2, Moscow State University.
18. S.A.Fridman, A.A.Cherepnev & M.S.Dobrolyubskaya, Doklady AN SSSR, 58, 1341 (1947).

ON VARIATION OF THE OPTICAL PROPERTIES OF SULFIDE PHOSPHORS INCIDENT TO ELIMINATION OF THE FLUX

- A.M.Gurvich

Interaction of silver and cadmium sulfides with mineralizing agents during heating

The present research was largely motivated by observation of the following two effects:

1. When 58ZnS·42CdS:Ag phosphor prepared by heating at 1200° with sodium chloride as the flux and containing an appreciable excess of activator (0.2% Ag) is washed with water there is observed a change in the color of the phosphor, i.e., the phosphor acquires a distinct grey hue in reflected light[1,2]. This change in color does not occur if the phosphor is first treated with a 10-20% solution of hyposulfite. Similar effects are also observed in the case of ZnS:0.1Ag(4NaCl) phosphor prepared by 30 min heating at 950°.

2. Treatment of 58ZnS·42CdS:0.02Ag(4NaCl) phosphor heated at 1200° with a 10% solution of sodium sulfide results in a distinct change in its properties: the phosphor acquires a reddish hue in reflected light, its luminescence brightness decreases (see Table 1 below) and the spectral composition of its emission changes: the luminescence band is cut off so that its maximum is shifted to the long wavelength side (Fig.1). At the same time the friability of the phosphor increases (cf.Ref.3). Similar effects occur in the case of treatment of self-activated 58ZnS·42CdS(4NaCl)-1200° phosphor with sodium sulfide solution. On the other hand if the phosphor is first washed with water or hyposulfite solution, the note changes in optical properties do not occur.

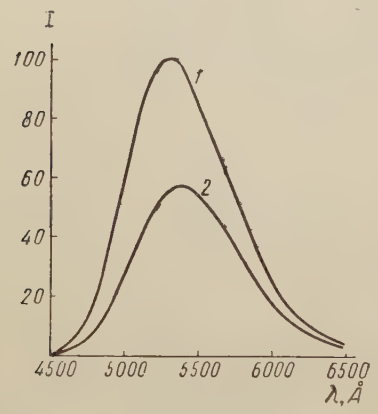

Fig.1. Luminescence spectrum of 58ZnS·42CdS:0.02Ag(4NaCl) phosphor heated for 75 min at 1200° with UV excitation: 1) as prepared and 2) treated with 10% Na_2S solution.

These observations can readily be explained if it is assumed that the surface of the initial (nonwashed) phosphor grains is coated with silver and cadmium chlorides formed during heating. In the process of washing with water the silver not incoporated in the host crystal lattice but present on the surface of the grains in the form of AgCl reacts with the zinc sulfide to form black silver sulfide. Hyposulfite, which forms a stable complex with silver, inhibits this reaction.

When nonwashed ZnS·CdS phosphor is treated with sodium sulfide solution, the latter reacts with the $CdCl_2$ and forms cadmium sulfide on the grain surfaces; this coating selectively absorbs the emission of the phosphor and modifies the color of the powder in reflected light.

That the chlorides of silver and cadmium actually do form in the process of heating is indicated by the following facts. Analysis of the water extract from (Zn,Cd)S phosphor prepared with NaCl as the flux shows the presence of a large number of Cd^{2+} ions. When such a phosphor is heated in a quartz tube partially inserted into a tubular furnace, cadmium chloride condenses on the cold part of the tube walls.

Upon the addition of Na_2S to a hyposulfite extract from previously unwashed ZnS:0.1Ag(4NaCl) phosphor heated for 30 min at 950°, there forms a black silver sulfide precipitate which together with the white color of the phosphor indicates that the silver not incorporated into the host lattice is present primarily in the form of AgCl rather than in the form of Ag_2S or free silver.

Experimental proofs of the formation of zinc chloride in the case of heating ZnS phosphors with chloride fluxes are found in the literature[4-8].

It might be assumed that the AgCl forms by the reaction:

$$Ag_2S + 2NaCl = 2AgCl + Na_2S \qquad (1)$$

However, calculations based on the data in the literature[9-12] showed that at the heating temperatures usually employed, the change in the standard isobaric potential for reaction (1) $\Delta Z_1^o \gg 10\,000$ cal per mole Ag_2S (for example, for reaction at 950°C, $\Delta Z_1^o = 53\,800$) and that consequently this reaction must be regarded as improbable[13].

In order to explain the fact that AgCl nevertheless forms one must take into account the possible participation in the reaction of oxygen from the air, assuming that as a result of the reaction there forms Na_2SO_4 rather than Na_2S, i.e., that the actual reaction is:

$$Ag_2S + 2NaCl + 2O_2 = 2AgCl + Na_2SO_4; \qquad (2)$$

for this process $\Delta Z^o \ll 0$ in a wide temperature range.

Direct experiments show that without oxygen interaction of Ag_2S with NaCl with the formation of AgCl does not occur; whereas in the case of fusion of Ag_2S with NaCl in the proportions of 1:5 by weight in contact with air there forms a large amount of AgCl (readily detectable by conventional chemical analysis), in the case of heating in oxygen free nitrogen the reaction does not occur, i.e., virtually no AgCl is formed.

Thermodynamic calculations also show that the formation of $CdCl_2$ and $ZnCl_2$ in the absence of oxygen is also improbable (cf.Refs.8 & 14); here, however, one must take into account the fact that the appreciably greater volatility of these chlorides as compared with AgCl favors a reaction of type (1).

The fact that under the indicated experimental conditions the silver not incorporated into the host lattice is transformed primarily into AgCl is consistent with the data known from metallurgy regarding the greater susceptibility of Ag_2S as compared with ZnS to chlorination[15]. However, at high heating temperatures and also in the case of prolonged heating at relatively low temperatures the process is shifted to the side of formation of Ag_2S inasmuch as the effect of the reaction

$$2AgCl(liq) + ZnS(sol) = Ag_2S(liq) + ZnCl_2(gas) \qquad (3)$$

(at 950°, $\Delta Z_3^o = -14\,240$) is not compensated by chlorination of the silver sulfide by the sodium chloride.

Zinc and cadmium chlorides, dissolving in molten sodium chloride, enter into reaction with it with the formation of the complexes $2NaCl \cdot ZnCl_2$ and $2NaCl \cdot CdCl_2$.[16] These complexes apparently form only at the time of crystallization from solution; however, their existence, as follows from the general regularities characterizing the behavior of molten salts[17], indicates that reaction of $CdCl_2$ and $ZnCl_2$ with NaCl does occur in the melt, a consequence of which is reduction of the vapor pressure of the volatile chlorides contained therein.

Effects observed as a result of washing phosphors by different procedures

Above we cited examples of particularly marked changes in the properties of phosphors as a result of washing to remove the flux. In the usual practice of flux removal, however, the resultant changes are less pronounced and the causes

producing them less clearly evinced. Nevertheless, the changes in brightness, for example, in the case of washing a phosphor with water or ammonia can be very appreciable.

Table 1 shows the decrease in brightness of 58ZnS·42CdS:0.01Ag(4NaCl)-1200° phosphor following washing by four different procedures. The heated phosphor, after the usual purification under ultraviolet light, was thoroughly mixed and then divided into five equal parts. One part was left untreated, i.e., was not washed to remove flux, each of the other four parts was placed into a tube filled with the indicated washing solution and the mixture was periodically agitated for 30 min, after which the phosphor was filtered off in a Bücher funnel, washed under light suction with distilled water (the total volume of which was 5 times the volume of the main washing solution) and finally dried in air at room temperature. The luminance of the phosphors was measured by comparison with an arbitrarily chosen standard by means of a Pulfrich photometer in a tightly packed, optically "infinitely thick" layer with excitation from the observation side. The excitation sources were an x-ray tube operated at a potential of 70 kv and a current of 4 ma and a PRK-4 mercury vapor tube with a UFS-3 filter. The data presented in Table 1 are averages for six experiments carried out with different phosphor samples.

Table 1

Variation of the luminance of 58ZnS·42CdS:0.01Ag(4NaCl)-1200° phosphor with the washing procedure

Solution used for washing	Brightness in % of the luminance of the unwashed phosphor	
	X-ray excitation	Ultraviolet excitation
20% $Na_2S_2O_3$	90.3	99.0
Distilled water	79.3	85.8
5% NH_4OH	73.9	81.8
10% Na_2S	55.5	69.6

The experimental results show that the luminance of the phosphor with excitation by x-rays and by ultraviolet light changes as a result of washing in the same direction but to different degrees; under the given experimental conditions the brightness with x-ray excitation falls off to a greater extent as a result of washing out the flux (in the case of washing with distilled water, ammonia and sodium sulfide solution the ratio of the reductions in intensity for the two types of excitation amounts to approximately 1.5). This effect was observed earlier by Rusanova[1]. According to our observations, this differential effect always obtains in cases when the decrease in brightness is due to the formation on the surface of the crystal grains of a coating absorbing the emission of the phosphor; in particular, it occurs in the case of washing with water of ZnS:Ag(NaCl) and (Zn,Cd)S:Ag(NaCl) phosphors containing a large excess of activator, in the case of treatment of (Zn,Cd)S:Ag(NaCl) phosphor with sodium sulfide solution, and in the case of formation during heating of a grey coating of Ag_2S on ZnS:Ag(KCl) phosphors containing an excess of silver. In our opinion the difference is due to the fact that with x-ray excitation a greater fraction of the luminescence is emitted from deep lying layers of the powder and hence must pass through more grains with absorbing coatings than in the case of ultraviolet excitation.

In general, the different effects of washing out the flux on the photo- and roentgenoluminescence of phosphors, particularly when it is a question of small changes in brightness, may also be due to differences in the dependence of the absorption and scattering of the exciting radiation on the condition of the grain surfaces, in the possibility of transfer of the energy absorbed by the flux to the phosphor and in the influence on the luminescence brightness of the packing

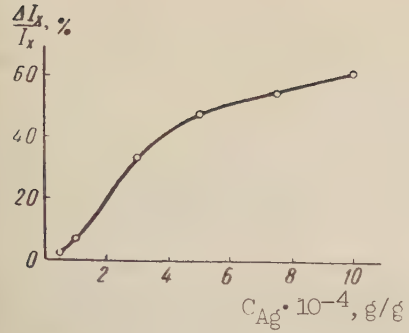

Fig.2. Variation of the reduction in luminance of 55ZnS·45CdS:Ag(5NaCl) phosphor (heated 30 min at 1100°) as a result of washing with water with the activator concentration in the batch. Excitation by 70 kv x-rays.

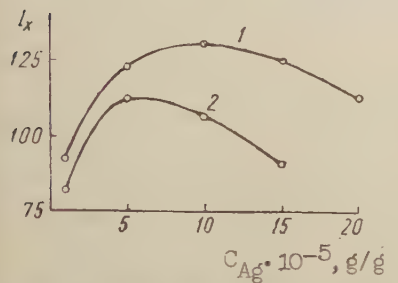

Fig.3. Variation in the luminance of 58ZnS·42CdS:Ag(4NaCl)-1200° phosphor not washed to remove flux (1) and washed with water (2) with the activator concentration in the flux. Excitation by 70 kv x-rays.

of the phosphor grains, the closeness of which depends on the state of their surface and therefore changes incident to washing. The absence of significant absorption and scattering of x-rays by the coatings forming on the grain surfaces during washing and the greater sensitivity of roentgenoluminescence to the formation of layers and films absorbing the luminescence of the phosphor prompted us to use this source of excitation in investigating the role of the products of reaction of sulfides with mineralizing agents in the processes occurring incident to washing of phosphors to remove residual flux.

Fig.2 shows the variation of the decrement in brightness of 55ZnS·45CdS:Ag(5NaCl) phosphor resulting from removal of the flux by washing with water with the activator concentration in the batch. The phosphor was heated for 30 min in quartz tubes inserted into a furnace heated to 1100°. The phosphor samples were washed by five-fold decantation and then dried at 110-120°. The luminance was measured with excitation by x-rays; the standard in each case was the corresponding unwashed phosphor.

With increase of the silver concentration in the batch, simultaneously with increase of the luminance decrement as a result of washing out the flux there occurs a change in the color of the phosphor in reflected light; this is due to formation of silver sulfide. Similar effects occur in the case of ZnS:Ag(NaCl) phosphor; quantitatively they are strongly dependent on the heating conditions (temperature, heating and cooling times, the manner in which the batch is mixed and packed into the tube, etc.) inasmuch as these determine the concentration of AgCl forming on the surface of the phosphor grains.

Since both the luminance of the unwashed phosphor and the decrement in brightness as a result of washing out the flux depend on the activator concentration in the phosphor, the value of the optimum activator concentration in the batch for obtaining the maximum luminance will differ for unwashed phosphors and phosphors washed by different procedures. This is illustrated in Fig.3 which shows the variation in luminance of unwashed and water washed 58ZnS·42CdS:Ag(4NaCl)-1200° phosphors with the silver concentration. For phosphors washed by a procedure precluding the formation of Ag_2S (for example, washed with iodine and hyposulfite[1]), the optimum silver concentration in the batch is the same as for the unwashed phosphor.

The present experimental data indicate that in cases when the silver is introduced into the batch in a low, approximately optimal concentration, part of the activator remains on the surface of the phosphor grains. It would be desirable to check this by using radioactive tracers to determine the silver content in the flux phase.

The action of water, which substantially reduces the roentgenoluminescence brightness of (Zn,Cd)S:Ag(NaCl) phosphors, in contrast to the action of Na_2S, is peculiar to phosphors containing silver activator, and, apparently, like the greying of ZnS:0.1Ag(4NaCl)-950°-30 min phosphor as a result of moistening with water,

is due primarily to the

$$2AgCl + ZnS = Ag_2S + ZnCl_2 \qquad (4)$$

reaction and also to some extent to hydrolysis of the zinc sulfide (the effect of this process is clearly evinced in the case of washing of phosphors prepared with NaI as the flux).

As is known, hyposulfite and ammonia dissolve AgCl. Their effect, however, on (Zn,Cd)S:Ag(NaCl) and ZnS:Ag(NaCl) phosphors is entirely different. Whereas treatment with hyposulfite protects phosphors containing a large excess of silver from the formation of an Ag_2S coating; ammonia, on the contrary, promotes the formation of a silver sulfide coating. This difference in the actions of ammonia and hyposulfite, which is also evinced, as will be apparent from Table 1, in treatment with them of phosphors containing the usual (0.01%) Ag concentration, is explained by the fact that ZnS precipitates Ag_2S from the silver-ammonia complex:

$$2\left[Ag(NH_3)_2\right]^+ + ZnS = Ag_2S + \left[Zn(NH_3)_4\right]^{2+} \quad (k \approx 1\cdot10^{20}), \qquad (4')$$

but does not precipitate it from the hyposulfate complex $\left[Ag(S_2O_3)_2\right]^{3-}$, inasmuch as the reaction

$$2\left[Ag(S_2O_3)_2\right]^{3-} + ZnS \rightarrow Ag_2S + ZnS_2O_3 + 3S_2O_3^{2-} \quad (k \approx 1)$$

is inhibited by an excess of hyposulfite. In addition, it must be borne in mind that ammonia favors hydrolysis of ZnS.

Actually the reactions occurring incident to washing of phosphors with water and water solutions are complicated by the fact that they take place on the surface of a solid phase and that there participate in them substances that are components of a solid solution in which they may be coupled with other components by fairly strong bonds.

There are superposed on the chemical processes discussed above sorption of molecules and ions contained in the wash water, for example, soluble sulfide or H_2S, leading to change in the concentration of free electrons in the phosphor[18-20] and the various effects mentioned above in discussing the differences between the results of washing the phosphor as regards its photo- and roentgenoluminescence brightness, in particular, the changes in the absorption of the exciting radiation incident to elimination of the flux.

All the data discussed above pertain to phosphors prepared with NaCl as the flux. The behavior of phosphors incident to elimination of the flux and their properties at high activator concentrations are strongly dependent on the nature of the halide flux. This is explained by differences in the reaction of sulfides with different fluxes, in the solubilities in the reaction products in water, in their solubilities in melts of the various salts, and in their ability to form complex compounds with fluxes (which determines the vapor pressure of volatile products), in the susceptibility of the fluxes to hydrolysis and oxidation and in the properties of the substances forming as a result of oxidation and hydrolysis.

Thus replacement of NaCl by $MgCl_2$ favors volatilization of the zinc and cadmium chlorides forming in the process of heating. Thus no detectable concentration of Cd^{2-} ions is present in a water extract from $58ZnS\cdot42CdS:0.01Ag(4NaCl_2)$-1200° phosphor. Hence treatment of this phosphor with 10% solution of Na_2S does not have the effect observed by us in the case of $58ZnS\cdot42CdS:0.01Ag(4NaCl)$-1200° phosphor. Also, in the case of the $MgCl_2$ fluxed phosphor there does not occur

so appreciable a decrease in luminance as a result of washing with water as in the case of phosphors fluxed with NaCl.

Finally, it should be noted that not only the composition of the solution used for washing the phosphor but also the washing technique may have a substantial influence on the properties of the final phosphor, particularly if the change in properties incident to washing is caused by slowly proceeding processes such as hydrolysis.

State Scientific Research
Roentgeno-Radiological Institute

References

1. A.I.Rusanova, Thesis, Moscow, 1952.
2. Z.I.Klabukova, Transactions of the Fifth Conference on Luminescence, p.289, Tartu, 1957. (Trans.Abstract, Bulletin 21, No.5, 669.)
3. H.W.Leverenz, U.S.Pantent, No.2421207 (1947).
4. H.Schlegel, Naturwissenschaften, 30, 242 (1942).
5. B.M.Gugel', Izv.AN SSSR, Ser.fiz., 9, 539 (1945).
6. A.L.Smith, J.Electrochem.Soc., 96, 75 (1949).
7. H.W.Leverenz, An Introduction to Luminescence of Solids, p.65, N.Y., 1950.
8. N.Riehl (Ril') & H.Ortmann, Zhur.obshch.khim.25, 1057 (1955). (Trans. J.Gen.Chemistry.)
9. K.K.Kelly, Bull.Bur.Mines (USA), 406 (1937).
10. R.Fichte, Die thermodynamischen Eigenschaften der Metallchloride. - Berlin, 1953.
11. N.A.Landin, Zhur.fiz.khim. (J.Physical Chem) 24, 257 (1950).
12. O.Kubaschewski & E.L.Evans, Metallurgical Thermochemistry (Cited in Russian trans.).
13. B.F.Dodge, Chemical Engineering Thermodynamics, N.Y., 1944. (Cited in Russian trans.)
14. Gmelins Handbuch der Anorganischen Chemie, Sist. - Num.21,S.537, - Berlin, 1928.
15. D.M.Chizhikov, Khlopnyi metod pererabotki polimetallicheskikh rud i kontsentratov (Chlorine method of reprocessing polymetallic ores and concentrates) p.219, ONTI, 1936.
16. E.L.Bakumskaya, Dissertation, Rostov-on-the-Don, 1955.
17. A.I.Belyaev, E.A.Zhemchuzhina & L.A.Firsanova, Fizicheskaya khimiya rasplavlennykh solei (Physical chemistry of molten salts), p.46 & 79, M., 1957.
18. S.Larach, J.Phys.Colloid.Chem., 54, 467 (1950).
19. K.V.Tagantsev & A.N.Terenin, Izv.AN SSSR, Ser.fiz., 21, 525 (1957). (Trans.Bulletin 21, No.4, 523); Optika i spektroskopiya, 2, 355 (1957).
20. F.F.Vol'kenshtein, Transactions of the Fifth Conference on Luminescence, Tartu, 1957.

INVESTIGATION OF THE TECHNOLOGY OF ALKALINE EARTH SULFIDE PHOSPHORS WITH PERSISTENT PHOSPHORESCENCE*

- T.A.Krasnova

It is a familiar fact that the most efficient phosphors with persistent phosphorescence are phosphors with a matrix of either zinc sulfide or the sulfide of one of the alkaline earths.[1,2] Alkaline earth sulfide phosphors have a more persistent afterglow than zinc sulfide phosphors, are less subject to photolysis and are more effectively excited by incandescent light. Our domestic industry, however, has not engaged in the production of these phosphors owing to the fact that these base materials are subject to hydrolysis, which results in a significant loss of brightness.

The purpose of the present research was to investigate and develop the technology of preparation of strontium sulfide phosphor for industrial use and to find reliable means for protecting the phosphor against the influence of moisture with a view of obtaining coatings with a long service life.

1. Synthesis

The phosphor samples were synthesized in two ways:

1) By the familiar procedure of heating a batch consisting of sulfur and strontium carbonate, which react to form a strontium sulfide, and 2) by heating a batch containing strontium sulfide prepared beforehand; the latter procedure has never hitherto been used for the preparation of phosphors of this class.

The strontium sulfide used in the second procedure was obtained by passing hydrogen sulfide over strontium carbonate (we worked with charges of about 200 g) at a temperature of 850-900° for 3-4 hours. The strontium sulfide content in the final product varied from 95-98%.

The initial batches were prepared by the dry technique, i.e., by mixing the components in a porcelain mortar or a ball mill followed by passing through a silk sieve. The activators, Bi and Cu, were introduced in the form of aqueous solutions of the appropriate salts together with the salts used as the flux; the mixture was then dried at ~100°.

2. Characteristics of the phosphor

The luminescence spectrum of the phosphor was excited by ultraviolet light and recorded on an UM-2 monochromator by means of a photomultiplier. The emission maximum was found to lie in the vicinity of 480 mμ. The phosphorescence brightness was determined on a special set-up with a photomultiplier (Table 1). The quantum efficiency of the strontium sulfide phosphor was determined by the GIPKh** procedure and found to be 52%. This is equal to the efficiency of the phosphor designated FKP-03-K [ФКП-03-К].

We also investigated the decay of phosphorescence of the strontium sulfide phosphor at different temperatures (Table 2).

Visual observations of the afterglow of luminous markings and coatings on different manufactured products were carried out in a number of plants and organizations. In general, it was agreed that markings made with our SrS phosphor phosphoresce more brightly than those with FKP-03-K phosphor. It was found, however, that the stability of markings made with the SrS phosphor in tests under

---

*V.M.Shul'man participated in the present research; L.I.Grudkov assisted in the search for protective materials.

**State Institute of Applied Chemistry.

Table 1

Decay time	Phosphorescence brightness, asb			
	Daylight lamp (20 w; 10 min; 20 cm)		Incandescent lamp (20 w; 10 min; 20 cm)	
	SrS	FKP-03-K	SrS	FKP-03-K
1 min	0,6900	0,8400	0,1600	0,1820
5 »	0,2150	0,1580	0,0520	0,0380
10 »	0,1030	0,0585	0,0335	0,0214
15 »	0,0680	0,0361	0,0240	0,0140
30 »	0,0325	0,0135	0,0120	0,0056
1 hr	0,0165	0,0051	0,0053	0,0020
2 »	0,0060	0,0015	0,0025	0,0006
3 »	0,0036	0,0007	0,0016	0,0004
4 »	0,0023	0,0004	0,0010	0,0002
5 »	0,0015	0,0003	0,0007	0,0001 (4)
6 »	0,0012	0,0002	0,0006	0,0001
7 »	0,0009	0,0001 (3)	0,0004	0,0000 (7)
8 »	0,0007	0,0000 (9)	0,0003	0,0000 (5)

Table 2

Variation of the phosphorescence brightness with temperature

Decay time, min	Brightness, asb					
	—49°	—24°	0°	18°	27°	50°
1	0,0125	0,0650	0,2250	0,5700	0,3150	0,2250
5	0,0054	0,0271	0,0790	0,2090	0,1020	0,0705
10	0,0039	—	0,0480	0,1120	0,0590	0,0378
15	0,0030	0,0162	0,0395	0,0770	0,0420	0,0265
30	0,0026	0,0068	0,0187	0,0400	0,0210	0,0141
60	0,0023	0,0058	0,0120	0,0165	0,0083	0,0059
120	0,0018	0,0028	0,0040	0,0065	0,0042	0,0030
180	0,0012	0,0020	0,0026	0,0040	0,0026	0,0010
240	0,0012	0,0015	0,0023	0,0031	0,0023	0,0010

special conditions is inadequate. There was evident need for developing application techniques insuring protection of the phosphor coatings from moisture.

3. Materials for protecting the phosphor from moisture

The principal shortcoming of SrS phosphor is that it undergoes hydrolytic deterioration under the influence of humidity. Hence we paid particular attention to this problem in our work, for it was obvious that the use of phosphors of this type must be severely limited unless suitable means for protection could be developed.

The search for suitable protective materials was carried out in several directions: specifically, we tested 1) synthetic resin varnishes, 2) plastics and 3) enamels. The stability of the different varnish and plastics was determined by measuring the phosphorescence brightness before and after exposure of the samples under different conditions.

Samples were subjected to the combined influence of atmospheric factors by exposure to open air in summer; under laboratory conditions the samples were subjected to the influence of variations in temperature, moist

Table 3

Decrease of phosphorescence brightness of samples with luminous laquers and protected by plastic coatings

Protective material	Decrease in brightness over indicated test period			
	Exposure to atmospheric conditions	Artificial rain	Temperature of -55°	Storage in room
Melamine formaldehyde varnish	1 month 65%	19 days 34%	10 days 75%	4 months 14%
Polybutyl methacrylate varnish	1 month 65%	215 months 56%	10 days 87%	215 months 75%
Polyethylene plastic (covering)	1 month 30%	1 month 20%	10 days 17%	3 months 10%

air and artificial rain. The results of the protective materials tests are given in Table 3.

Attempts to develop luminous enamels with strontium sulfide phosphor failed to yield positive results: in all cases baking greatly reduced the brightness and duration of the afterglow.

Discussion

Tests of strontium sulfide phosphor samples under different conditions indicate that it is feasible to use this luminophor for making identifying markings with persistent afterglow. As regards brightness and duration of afterglow this phosphor is considerably superior to the FKP-03-K phosphor. The results of visual evaluations of identifying markings on different products also favor the SrS phosphor. The character of the temperature dependence of the phosphorescence decay of the SrS phosphor is such that at later stages (to 4 hours) the afterglow brightness at low temperature is somewhat inferior to the brightness at room temperature, but is still probably adequate for most practical purposes. This point is significant as regards extending the scope of industrial applications of this phosphor.

There appear to be only limited possibilities for improvement of the brightness and duration of the afterglow of the synthesized phosphor. The data in the literature[1-5] and our own experiments indicate that the brightness and persistence of phosphorescence change very little with variations in compounding and conditions of synthesis. However, through appropriate modification of the synthesis conditions it should be feasible to improve the grain-size composition of the phosphor with no sacrifice of the afterglow brightness.

At present the problem of protecting the phosphor when used for signs and coatings exposed to weather has not been completely solved. The use of polyethylene for this purpose may lead to positive results provided the stability of the plastic itself can be improved.

References

1. P.Lenard, F.Schmidt & R.Tomaschek, Phosphrescenz und Fluorescenz. Handbuch der Experimentalphysik, XXIII, Leipzig, 1928.

2. N.F.Zhirov, Lyuminofory (Luminophors), M., 1940.

3. L.Verynts, Tr.In-ta prikladnoi khimii (Proceedings, Institute of Applied Chemistry), No.8, 46 (1927).

4. N.F.Zhirov, Zhur.prikladnoi khimii (Journal of Applied Chemistry), 2,3, 5, 7 (1929-1930).

5. U.Beduneau, Rev.prod.chim., 55, 5-6 (1952).

ROENTGENOLUMINESCENCE AND THERMOSTIMULATION SPECTRA OF SIBERIAN DIAMONDS

- E.S.Vilutis

Roentgenoluminescence spectra

There are only scanty data in the literature on the luminescence spectra of diamonds under x-ray excitation. In 1946 Ramachandran[1] described the roentgenoluminescence spectra of two diamonds: one with bright blue fluorescence in the ultraviolet and the other with weak fluorescence. The roentgenoluminescence spectrum of the former had a pronounced dip at 415 mμ and in the long wavelength region was virtually identical with the photoluminescence spectrum, i.e., exhibited four characteristic bands at 427.8, 438.7, 451.3 and 464.3 mμ. In the short wavelength region the spectrum extended from the dip at 415 mμ to 3600 Å and had valleys at 404.1, 395 and 385 mμ. The spectrum of the second diamond was continuous to both sides of the dip at 415 mμ.

In 1951 Bishui[2] investigated the roentgenoluminescence of five diamonds and found that four of them (type 1) exhibited a broad luminescence band extending from 566 to 370 mμ; in the case of two of the samples there were absorption bands at 415 mμ accompanied by a number of bands in the short wavelength region. According to Bishui, the diamond of the second type yielded no luminescence under x-ray excitation. He explained this result by the presence of impurities in the type 1 diamonds and the absence of impurities in type 2 specimens.

In a later publication Sen & Bishui[3] described the results of investigation of seven diamonds of which six were of type 1 and one of type 2. In this case the authors obtained roentgenoluminescence spectra for all seven diamonds including that of the second type. All the spectra were characterized by the presence of a broad luminescence band extending from 390 to 520 mμ, except for the type 2 diamond, in the spectrum of which this band was somewhat narrower. Of all these diamonds only one (type 1) exhibited a narrow absorption band at 415 mμ. In contradistinction with the earlier results of Bishui for the same specimens, the authors found no correlation between the roentgenoluminescence brightness and the data on the absorption edges in the ultraviolet and the intensity of the blue band under ultraviolet excitation; in view of this they infer that different types of impurities are responsible for the appearance of the blue band under x-ray excitation and the effects at 415 mμ under ultraviolet excitation.

For the present work we had available the large collection of diamonds made by the Amakinsk Expedition. In all we studied over 100 specimens. The luminescence spectra were photographed on an ISP-51 spectrograph using "Negative A" film (rating 250 GOST units). The luminescence was excited by x-rays from an AV-25 tube operated at 22 kv and 15 ma. Depending on the fluorescence brightness the exposure time was varied from 10 to 60 hours.

For some of the diamonds the luminescence spectra were also recorded with excitation by bremsstrahlung from a Tl^{204} source with an activity of 20 mC.

Although there were minor differences between the spectra of individual specimens, in general the roentgenoluminescence spectrum of the Siberian diamonds may be described as follows (Fig.1). In the visible region there are two broad bands - a blue and an orange - separated by a diffuse interval of low brightness at 510 mμ. The short wavelength part of the blue band does not have a sharp edge: its intensity monotonically decreases at least to 380 mμ in some cases. (It was found that the detectable extent of the blue band into the short wavelength region depends substantially on the exposure time.) In many cases this part of the blue band has a fairly sharp dip at 415 mμ. Usually there are no indications of structure in the blue region, either as regards the absorption band in the wavelength region under 415 mμ or the emission band in the long wavelength region.

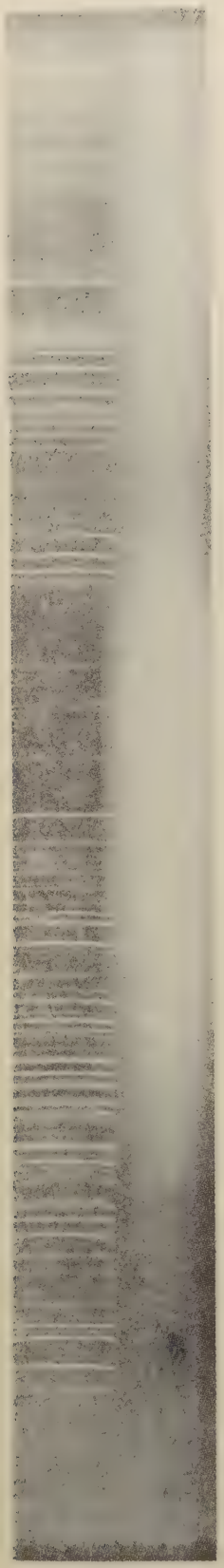

Fig.1. Typical luminescence spectrum of Siberian diamond.

In three cases, however, there were detected signs of structure in the form of emission bands, the peaks of which are located at the same wavelengths as the peaks of the 415 mμ system with ultraviolet excitation. For this reason we question the inference of Sen & Bishui that different impurities are responsible for the blue band under x-ray excitation and the 415 mμ system under ultraviolet excitation.

The orange band, which is bounded on the short wavelength side by the dip at 510 mμ, extends into the long wavelength region to 670 mμ and is apparently in effect limited by the sharp decrease in sensitivity of our photographic film in this spectrum region. In many cases this band exhibits structure, characterized by the presence of three peaks located at 550, 598 and 641 mμ.

We note that to the best of our knowledge there has been no previous mention in the literature of an orange roentgenoluminescence band for diamonds: apparently this band in the roentgenoluminescence spectrum is peculiar to diamonds of Siberian origin.

A noteworthy feature brought out by comparison of the roentgenoluminescence spectra of the numerous Siberian diamonds studied is the lack of any significant correlation between the brightnesses of the blue and orange bands. The variations in brightness are very appreciable and independent. We believe this can only be explained by assuming the presence in Siberian diamonds of two types of luminescence centers, the concentrations of which are also independent.

Thermostimulated emission

The effect of thermostimulated emission of diamonds excited by UV and x-rays was observed visually by Chandracekcharan[4], who found that the de-excitation occurs at 270°. Bull & Garlick[5], investigating the decay and thermostimulation of diamond powders excited by UV, obtained a glow curve containing two peaks at 147 and 247°. Analyzing their data, they came to the conclusion that the luminescence of diamonds is monomolecular in character and that the luminescence centers have two metastable levels.

We investigated the capability of many diamond specimens to store light sums under x-ray excitation. These studies were made by means of an FEU-17 photomultiplier.

Inasmuch as the thermostimulation spectra of the diamond specimens were identical with the fluorescence spectra described above, i.e., contained two bands - a blue and an orange - the glow curve experiments were carried out twice for each specimen with different light filters which allowed of observing the effect separately for each band. It was found that most of the diamonds store up an insignificant light sum; individual specimens distinguished by bright fluorescence proved capable, however, of storing appreciable light sums. Fig.2 shows typical thermostimula-

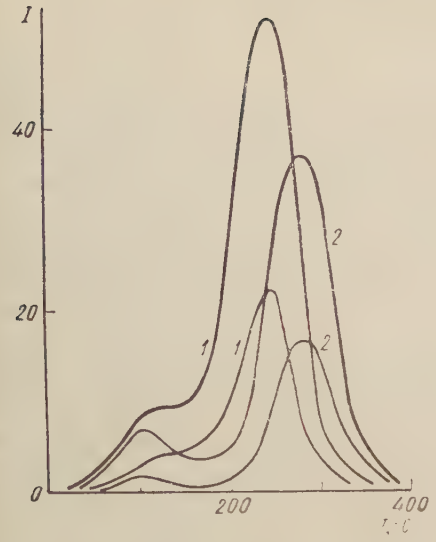

Fig.2. Typical thermostimulation curves for the blue (1) and orange (2) bands of Siberian diamonds.

tion curves for both bands with different excitation doses (90 and 180 min). Owing to the low sensitivity of the FEU-17 photomultiplier in the orange region, for measurements of the orange band we used the maximum sensitivity of the measuring circuit: 16 times greater than that employed in recording the glow curves for the blue band. There is a noticeable disparity between the positions of the temperature peaks: in curves 1 (blue band) the peaks correspond to 90 and 240°, whereas in curves 2 (orange) they lie at approximately 80 and 280°. We note that with good reproducibility of the temperature values for the peaks of each individual specimen, these temperatures for different specimens differ somewhat. The application of special criteria to the investigated specimens showed that the electronic process involved in thermostimulated emission is a first order process. The average values of the thermoactivation energy as determined from the glow curves proved to be 0.42 and 0.64 ev for the blue band and 0.36 and 0.80 ev for the orange band.

Physical Laboratory of the Amakinsk Expedition,
Ministry of Geology and the Conservation of
Natural Resources &
"A.A.Zhdanov" Irkutsk State University

References

1. G.N.Ramachandran, Second symposium of papers on structure and properties of diamond, Proc.Ind.Acad.Sci.A, 24, I (1946).
2. B.M.Bishui, Ind.J.Phys., 25, 575 (1951).
3. S.N.Sen & B.M.Bishui, Ind.J.Phys., 26, 347 (1956).
4. V.Chandracekcharan, Second symposium of papers on structure and properties of diamond, Proc.Ind.Acad.Sci.A, 24, I (1946).
5. C.Bull & F.Garlick, Proc.Phys.Soc.A63 (1950).

LUMINESCENCE OF GLASSES CONTAINING CERIUM*

- G.O.Karapetyan

Introduction

Investigation of glasses activated by cerium is of considerable theoretical and practical interest inasmuch as these glasses exhibit an exceptional resistance to coloring by ionizing radiation.[1-3] At the same time cerium is a luminescence activator and its behavior as such in glasses merits attention. Yet it is not in general feasible to extend to glass with cerium the data on the absorption and luminescence of allied systems, i.e., crystals and solutions containing Ce ions.[4-8]

Investigation of the absorption and luminescence spectra of glasses containing Ce showed that the element may be present in either the trivalent or the tetravalent state.[9] Each valence state is characterized by its own distinctive absorption spectrum. Change in the type of glass (phosphate, silicate or borate) affects the level of oxidation of the cerium and also leads to quantitative changes in the absorption and luminescence spectra.[10]

It is known that only glasses containing cerium in the trivalent state luminescence. Transition of part of the cerium to the tetravalent state results in a substantial decrease in the intensity of luminescence. Some authors, including Ginther[11], report that with increase in the cerium concentration its absorption spectrum in crystals undergoes great modifications connected with the formation of aggregations or clumps of Ce ions.

The present communication is concerned with a number of concentration dependences in glasses activated by cerium. The glasses used in the experiment were characterized by high purity: the iron content did not exceed 0.005%. Carbon or ammonium salts were introduced into the initial batch in order to produce reducing conditions. The glasses were founded in quartz crucibles in an oil fired furnace.

The absorption spectra were measured on a Beckman spectrophotometer using samples 0.1 to 0.5 mm thick and then normalized to a sample thickness of 1 mm. The absorption spectra of cerium were obtained in the form of differential curves: the ordinates of the absorption spectrum of the glass without cerium was subtracted from the corresponding ordinates of the absorption curve for the glass with cerium. The absolute luminescence efficiencies were measured by the sphere procedure on the photoelectric set-up of V.A.Arkhangel'skaya.** The total experimental error did not exceed 10% of the measured values.

Experimental results

We investigated the variation in the intensity of the absorption bands of cerium with its concentration in the glass. In the case of both phosphate and silicate glasses no quantitative changes in the absorption spectrum were observed up to a cerium concentration of 1.5% (Figs.1 & 2). The variation in the intensity of the absorption bands with the cerium concentration obeys Beer's law in the Ce concentration range up to 0.5%; in the region of higher concentrations there is a clear departure from Beer's law (Fig.3). Preparation of glass samples of different composition with high cerium concentrations showed that with increase

---

*The results regarding the photochemical properties of glasses, thermostimulation, thermobleaching and optical stimulation, mentioned in the present report, will be published in "Optika i spektroskopiya" (Optics & Spectroscopy).

**We take this opportunity to thank her for permitting us to use the equipment.

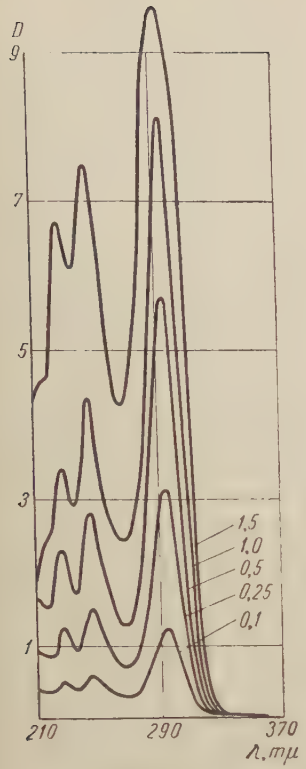

Fig.1.

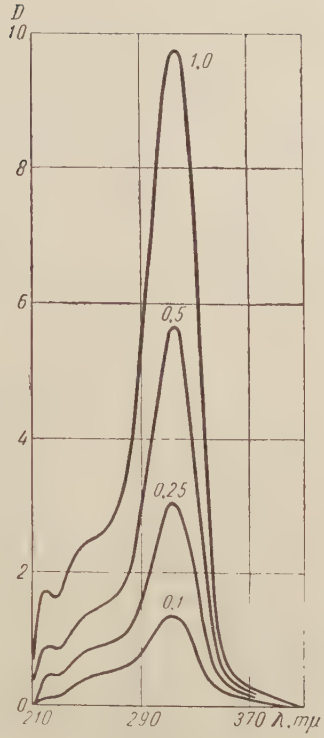

Fig.2.

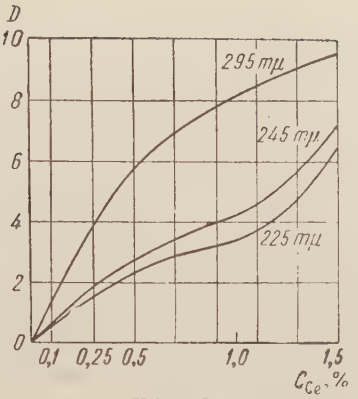

Fig.3.

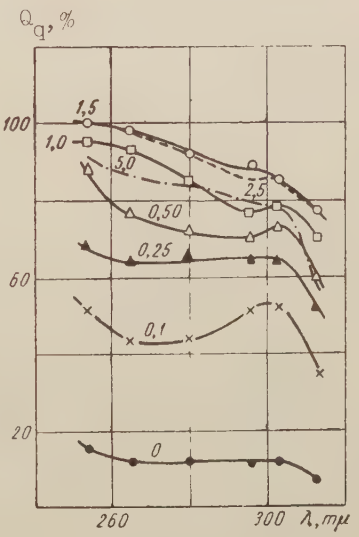

Fig.4.

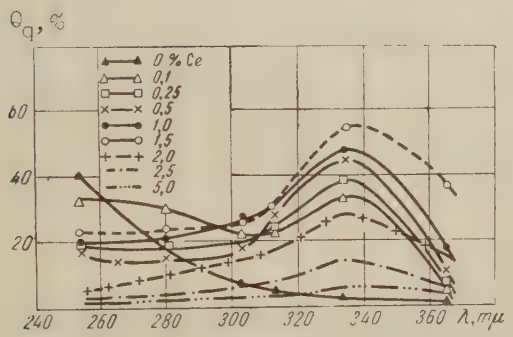

Fig.5.

Fig.1. Absorption spectra of phosphate glasses ($Na_2O \cdot 1.5CaO \cdot 2.5P_2O_5$) with different cerium concentrations (the Ce concentrations are indicated in percent at the curves).

Fig.2. Absorption spectra of silicate glasses ($Na_2O \cdot CaO \cdot 5SiO_2$) with different cerium concentrations (indicated in percent at the curves).

Fig.3. Variation in the intensity of different bands in the absorption spectrum of cerium with its concentration in the glass.

Fig.4. Absolute quantum efficiencies of the luminescence of phosphate glasses as a function of the wavelength of the exciting radiation and the cerium concentration (indicated in percent at the curves).

Fig.5. Absolute quantum efficiencies of luminescence of silicate glasses as a function of the wavelength of the exciting radiation and the cerium concentration.

in the Ce concentration it becomes increasingly difficult to assure the presence of cerium in a single valence state. In glasses founded without a reducing or oxidizing agent, upon increase of the cerium concentration the fraction of it present in the tetravalent state increases rapidly.

The luminescence of trivalent cerium is readily excited by the radiation from a quartz vapor tube: in the case of phosphate glasses in the 250-313 mμ region and in the case of silicate glasses in the 250 to 365 mμ region.

As a result of investigation of the luminescence efficiency of cerium with the wavelength of the exciting light and the Ce concentration in the glass we established the following (Fig.4 & 5):

1. The absolute quantum efficiency depends on the wavelength of the exciting light; in all cases the maximum luminescence efficiency is obtained for radiation with a wavelength greater than that of the maximum of the absorption band of trivalent cerium.

2. The luminescence efficiency is strongly dependent on the cerium concentration; the maximum luminescence output in silicate glasses is observed at a Ce concentration of 1.5%, that in phosphate glasses at a Ce concentration of 2-2.5%.

3. The maximum quantum efficiency of silicate glasses is approximately 55%; the efficiency of phosphate glasses approaches 100%.

Glasses containing trivalent cerium luminesce intensely under the influence of γ- and x-radiation. The roentgenoluminescence intensity increases with increase in the concentration of trivalent cerium. At equal trivalent cerium concentrations the intensity varies greatly with the type of glass. Thus, for example, silicate glasses containing 0.5% cerium completely reduced to the trivalent state have a luminescence intensity approximately 10 times higher than phosphate glasses with an equal concentration of trivalent cerium. Silicate glasses activated by trivalent cerium after γ-irradiation emit an afterglow persisting for several hours. Phosphate glasses, on the contrary, exhibit no detectable phosphorescence after high-energy excitation. We observed a similar afterglow from silicate glasses activated by trivalent cerium with spark excitation. The phosphorescence spectrum of silicate glasses with cerium recorded on a spark phosphoroscope virtually coincides with the luminescence spectrum of cerium excited by the radiation from a mercury vapor tube (wavelength $\leqslant$ 313 mμ). Phosphate glasses exhibit no phosphorescence after spark excitation.

Discussion

The electron configuration of cerium is $4f^2 5s^2\ 5p^6 6s^2$. The absorption and luminescence of cerium in glass should presumably be associated with $4f - 5d$ transitions, which is consistent with the short lifetime of the excited state ($\tau \approx 5 \cdot 10^{-7}$ sec)[12] and the diffuse character of the absorption and luminescence bands. The presence of two peaks in the luminescence band of cerium is connected with electron transitions from the excited state to doublet levels of the ground state.[13] With changes in the character of the medium surrounding the cerium ions there is observed not only a change in the intensity and position of the individual absorption bands, but also a change in the relative intensities of the short and long wavelength peaks; this may be observed, for example, in going from phosphate to silicate glasses. This is apparently connected with reduction of the probability of existence of excited levels corresponding to high energy transitions in the case of enhancement of the interaction of the cerium ions with the surrounding oxygen ions. That the interaction of the trivalent cerium ions with the surrounding medium is stronger in silicate glasses than in phosphate glasses is substantiated by the greater width of the absorption and luminescence bands, the lower values of the quantum efficiency and the earlier onset of con-

centration quenching in silicate glasses.

The absence of qualitative changes in the absorption spectra of glasses with increase of the cerium concentration and the good agreement with Beer's linear law in the region of low concentrations indicate that there exists only one type of absorption centers in each group of glasses (phosphate and silicate). The deviation from Beer's law at higher concentrations of cerium amounts essentially to a relatively faster increase in absorption in the 250 mμ region and a slower increase in absorption in the long wavelength band of trivalent cerium (Fig.3). It is known that the maximum of the absorption band of tetravalent cerium is located in the 250 mμ region.[9] Taking into account the impossibility of retaining the cerium at high concentrations in a single valence state and its tendency in such cases to go over into the tetravalent state, it may be inferred that the observed deviation from Beer's linear law in the range of high cerium concentrations is due to transition of part of the cerium to the tetravalent state.

On the basis of the luminescence efficiency data it may be concluded that the luminescence centers normally present in nonactivated silicate glasses disappear as a result of introduction of cerium. A direct consequence of this is decrease of the luminescence efficiency of such glasses (with excitation in the 254-303 mμ region) upon the introduction of minor amounts of cerium. This behavior is consistent with the hypothesis associating the luminescence of nonactivated glasses with structural defects rather than with impurities.

The results obtained on the excitation of the luminescence of Ce activated glasses with x-rays and γ-radiation indicate that in silicate glasses there is an efficient mechanism of excitation energy transfer from the vitreous network to the cerium ions. In view of the fact that such excitation energy transfer apparently does not occur in phosphate glasses, it may be inferred that an important condition for energy transfer is strong interaction of the cerium atoms with the surrounding medium. The fact that cerium activated silicate glasses have a persistent afterglow when excited by ionizing radiation and the data obtained on thermostimulated luminescence, thermobleaching and optical stimulation give reason to infer that the luminescence of silicate glasses is due primarily to recombination of electrons and holes.

"S.I.Vavilov" State Optical Institute

References

1. N.I.Kreidl & R.I.Hensler, J.Amer.Ceram.Soc., 38, 428 (1955).
2. P.W.Levy, Soc.Glass Techn., 40, 462 (1956).
3. K.H.Sun & N.I.Kreidl, Glass Ind., 33, 511 - 674 (1952).
4. W.Weyl, Coloured Glasses. Sheffield, 1951.
5. I.de Ment, Fluorochemistry. N.Y., 1946.
6. I.H.Lawrence & I.Berestesky, J.Amer.Chem.Soc., 77, 2049 (1955).
7. I.Weiss & D.Porret, Nature, 139, 1019 (1937).
8. V.V.Zelinskii & T.V.Timofeeva, Doklady AN SSSR, 66, 187 (1949).
9. G.O.Karapetyan, Optika i spektroskopiya (Optics & Spectroscopy), 3, 641 (1957).
10. G.O.Karapetyan, Optiko-mekh.prom-st'. (Optical-mechanical ind.), No.4 (1958).
11. R.I.Ginther, J.Electrochem.Soc., 101, 248 (1954).
12. V.L.Levshin, Fotolyuminestsentsiya zhidkikh v tverdykh veshchestv (Photoluminescence of liquids and solids), M., 1951.
13. H.Gobrecht, Ann.Phys., 31, 181 (1938).

ZINC AND STRONTIUM PHOSPHATE BASE PHOSPHORS FOR "FLUORESCENT" LAMPS

- F.M.Pekerman, D.N.Shoikhet & R.A.Shtrikhman

Over the past two years in the State Institute of Applied Chemistry we have been investigating the properties of phosphors for low and high pressure "fluorescent" lamps. Particular attention has been devoted to the properties of phosphates, especially those of the alkaline earth metals. As is known one of these phosphates, namely, calcium halophosphate, is the leading phosphor for low pressure lamps. Research aimed at improving the color characteristics of "fluorescent" lamps led to the development abroad of orthophosphate phosphors activated with tin.[1-3] Recently, Butler and his co-workers[4,5] synthesized Sn activated zinc and strontium orthophosphate which is being used in high pressure lamps.

In his published work Butler gives the excitation and emission spectra of this phosphor and evaluates the possibility of utilizing it in high pressure lamps. He does not, however, give the exact composition or describe the precise synthesis procedure.

In the present work we developed a procedure for the preparation of zinc-strontium orthophosphate phosphor.

For the synthesis of the phosphor we used $SrHPO_4$, $SrCO_3$ and $Zn_3(PO_4)_2$. The activator was added in the form of specially prepared SnO. The maximum brightness was obtained at a $Zn_3(PO_4)_2$ content of 13-15%.

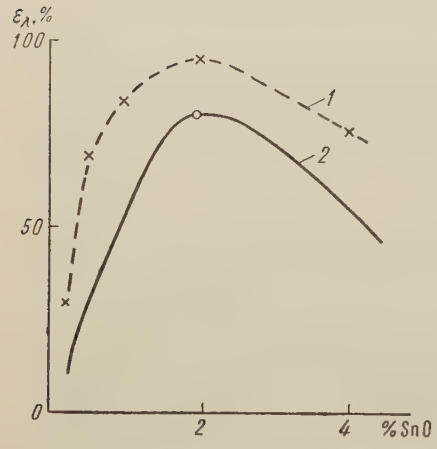

Fig.1. Variation of the phosphor luminance with the activator concentration with excitation at: 1) λ = 254 mμ, 2) λ = 365 mμ.

Fig.1 shows the influence of activator concentration on the luminance of the phosphor with excitation by λ = 254 and 365 mμ. In both cases the optimum brightness corresponds to 2% SnO in the batch.

Serious difficulties were encountered in attempting to provide an appropriate atmosphere that would assure retention of the tin in the divalent state of the process of heating. A strong reducing atmosphere, for example, pure hydrogen or ammonia, results in reduction of the tin to the metallic state, partial reduction of the zinc and even noticeable reduction of the phosphorus. On the other hand, heating in a neutral atmosphere (purified nitrogen) does not yield luminescent samples. The addition of small amounts of hydrogen to purified nitrogen results in samples with the maximum brightness.

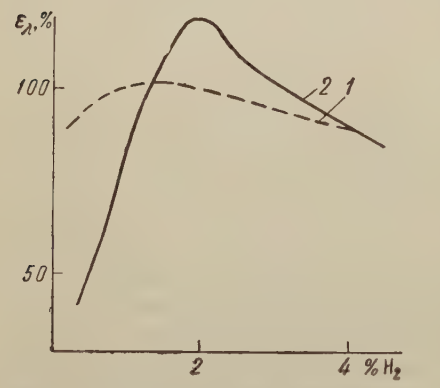

Fig.2. Influence of the hydrogen concentration in the heating atmosphere on the brightness of $(Zn,Sr)_3(PO_4)_2$:Sn with excitation: 1) λ = 254 mμ, 2) λ = 365 mμ.

The effect of the hydrogen concentration in the heating atmosphere on the luminance of the phosphors is shown in Fig.2. The best results as regards brightness were obtained with a hydrogen concentration of 1.0-1.5%.

X-ray diffraction records of the phosphor components and sample powders are shown in Fig.3. The reproduced curves were recorded by Yu.D.Kondrashev by means of a URS-1 ionization camera. The diffraction records show that the best phosphors have

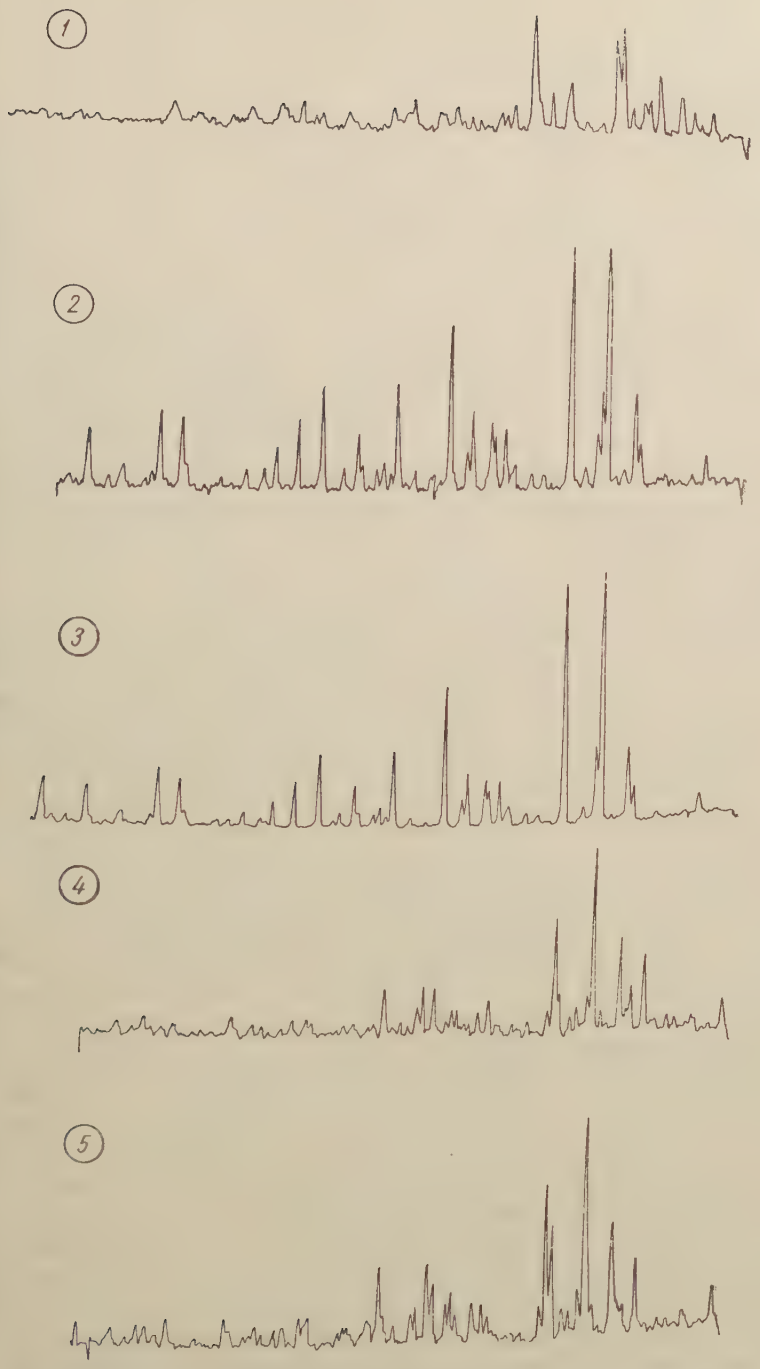

Fig.3. X-ray diffraction records of phosphor samples and initial components: 1 - $Zn_3(PO_4)_2$, 2) $Sr_3(PO_4)_2$, 3) $Sr_3(PO_4)_2$:Sn, 4) CSr, $Zn_3(PO_4)_2$:Sn (standard), 5) $(Sr,Zn)_3(PO_4)_2$:Sn (impurity $Sr_3(PO_4)_2$).

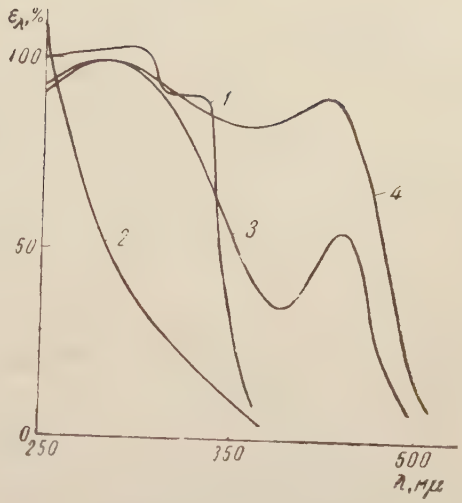

Fig.4. Excitation spectra of different phosphors: 1 - $(Zn,Sr)_3(PO_4)_2$:Sn, 2 - $(Zn,Sr)_3(PO_4)_2$:Sn - $Sr_3(PO_4)_2$:Sn, 3) $Mg_3GeO_5 \cdot MgF_2$:Mn, 4 - $Mg_6As_2O_{11}$:Mn.

an individual lattice differing from the lattices of $Sr_3(PO_4)_2$ and $Zn_3(PO_4)_2$. It should also be noted that change in the synthesis conditions leading to sharp reduction in the phosphor brightness is accompanied by the appearance of the characteristic lines of $Sr_3(PO_4)_2$ in the diffraction patterns.

The excitation spectra of two orthophosphate luminophors are shown in Fig.4 together with the excitation spectra of magnesium germanate and arsenate for purposes of comparison. Curve 1 is for a phosphor excited by long-wave ultraviolet. The x-ray diffraction record for this sample is dominated by the presence of an individual $(Zn,Sr)_3(PO_4)_2$:Sn phase markedly different from pure $Sr_3(PO_4)_2$ and $Zn_3(PO_4)_2$.

Curve 2 in Fig.4 pertains to a sample, the excitation of which lies primarily in the short wavelength part of the spectrum; its quantum efficiency with λ = 254 mμ excitation is ~90%. The x-ray pattern for this sample comprises lines indicating a mixture of two phases, namely, $(Zn,Sr)_3(PO_4)_2$:Sn and

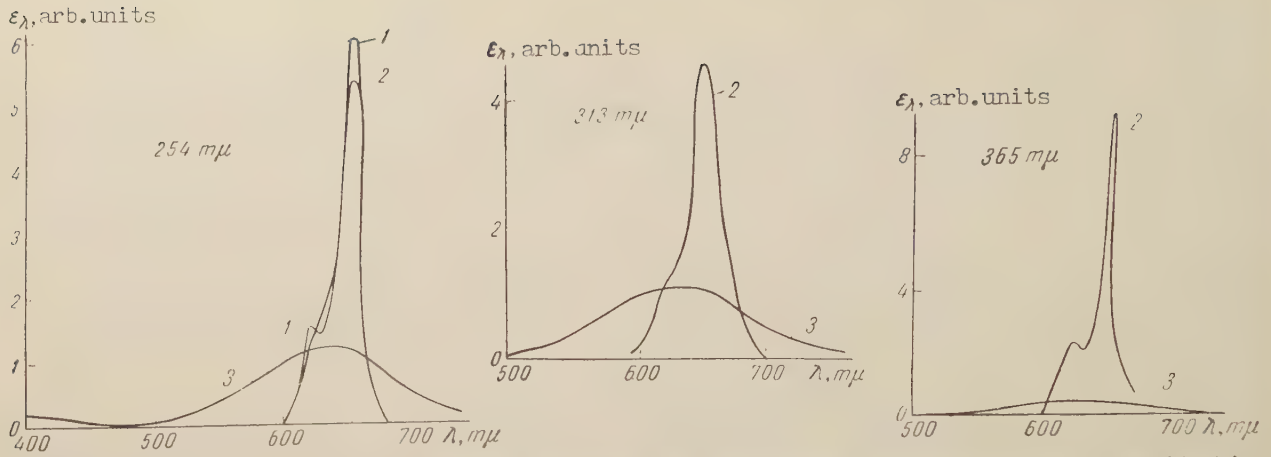

Fig.5. Comparison of the emission spectra of different phosphors with excitation by different wavelengths: 1 - magnesium germanate, 2 - magnesium arsenate, 3 - Zn-Sr phosphate.

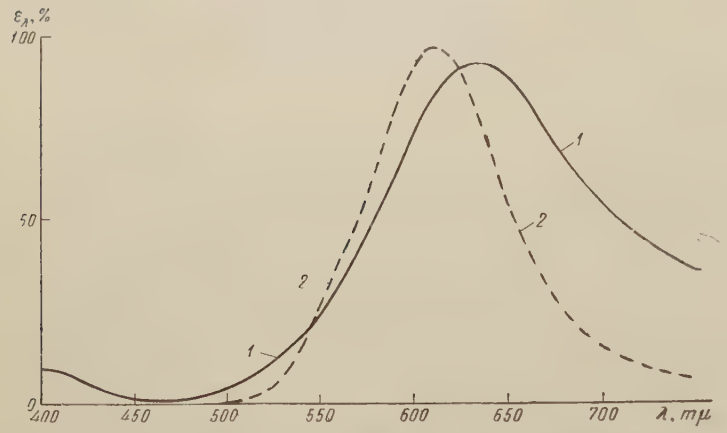

Fig.6. Comparison of the luminescence spectra of $(Zn,Sr)_3(PO_4)_2$:Sn (1) and $CaSiO_3$:Pb:Mn (2) phosphors. Excitation λ = 254 mμ.

$Sr_3(PO_4)_2$:Sn.

As will also be evident from Fig.4, magnesium arsenate is excited by the visible radiation of a mercury vapor lamp down to λ = = 500 mμ, whereas the phosphates are already only weakly excited by the 365 mμ line. According to Butler[5], in a 250 watt low pressure lamp of the 33.6 watts energy emitted in the ultraviolet region 8.9 watts are radiated at λ = 340-400 mμ, i.e., ~26%. This part of the energy is not utilized by Zn-Sr phosphate phosphors; $(Zn,Sr)_3(PO_4)_2$:Sn is also not excited by the blue lines of mercury (405, 436 & 492 mμ). This on the whole is a favorable characteristic inasmuch as the phosphor does not block out these wavelengths from the radiation of the lamp.

The results of our measurements of the luminescence spectra of Zn-Sr phosphate and of magnesium arsenate and germanate with excitation by 254, 313 and 365 mμ light are shown in Fig.5. The distinctive characteristics of the phosphate luminophors are evident from the figure: whereas the emission of magnesium arsenate (and germanate) is characterized by a sharp peak at 640-650 mμ, the Zn-Sr phosphate emits more uniformly over the entire spectrum, which is an added desirable feature.

The radiated energy, characterized by the areas under the spectral curves, is approximately the same for all three phosphors with excitation by 254 mμ photons. With λ = 313 mμ excitation the area corresponding to the Zn-Sr phosphate amounts to only 70% of the area for magnesium arsenate and for λ = 365 mμ excitation to only 17% of the area for Mg arsenate. If one takes into account the visibility factor (luminosity function) for different wavelengths, there result the values listed in Table 1, characterizing the relative light flux emitted by

Table 1

Effective light flux emitted by Zn-Sr phosphate and Mg arsenate phosphors

λ_{rad}, mμ	I x V (intensity x visibility factor)			
	for λ 600 mμ		for all visible radiation	
	Zn-Sr phosphate	Mg arsenate	Zn-Sr phosphate	Mg arsenate
254	135	156	282	156
313	138	147	275	147
365	60	233	245	233

the two phosphors.

The data given in Table 1 are in agreement with those given by Butler[5], who compares two lamps of equal power but with different phosphor coatings: magnesium germanate and Zn-Sr phosphate. The total energy output of both tubes is approximately the same inasmuch as the areas under the curves are equal. If one takes into account the visibility factor, however, the effective energy yield of the phosphate coated tube proves to be several times higher than that of the tube coated with magnesium germanate.

With increase in the temperature of Zn-Sr phosphate to 200° its brightness increase by a factor of almost two; then with further increase in the temperature to 400° there is observed some decrease in brightness, but the phosphor still remains brighter than at room temperature. Thus the maximum luminescence lies in the operating temperature range of mercury lamps.

One serious shortcoming of our phosphor is the decrease in its brightness with reduction in particle size. As a result of heating the phosphor is obtained in coarse grain form and grinding it leads to an appreciable loss in brightness with λ = 365 mμ excitation. Further research is necessary to alleviate this shortcoming.

Tests on samples of our phosphor were carried out at the Moscow Electric Lamp Plant with the help of B.M.Gugel'. The data on the specific light flux are given in Table 2; for comparison we also give the data of Butler[5].

Table 2

Specific light flux of different lamps

Lamp	Power, watts	Coating	lm/w	Data
DRL	500	None	50—54	MELP*
EH-1	400	None	52,5	Butler[5]
DRL	500	Mg arsenate	42	MELP
	500	Zn-Sr phosphate	48,5	
JH-1	400	Mg arsenate	51,2	Butler
S-H1	400	Zn-Sr phosphate	57,5	

*Moscow Electric Lamp Plant

Clearly evident is the appreciable decrease in the light yield of the DRL lamp as a result of coating with the phosphor. Whereas without coating the lamp yields an average of 52 lumens/watt and is comparable in this respect with the American 400 watt lamp, the application of magnesium arsenate reduces the light output by 20%, while the application of Zn-Sr phosphate reduces it by 7%.

In the case of the American lamps application of magnesium germanate results in virtually no decrease in the light output, while coating with Zn-Sr phosphate increases the light output by 10%.

Some decrease in light output in lamps with coatings is natural. However, efficient utilization of the ultraviolet radiation from mercury vapor lamps by

means of phosphors leading to increase of the light yield can compensate losses due to absorption. According to the data of Butler[5], Zn-Sr phosphate more than compensates for these absorption losses, while according to the data of the Moscow Electric Lamp Plant, our Zn-Sr phosphate base phosphor reduces the light yield by 7%, whereas magnesium arsenate reduces the yield by all of 20%.

The relatively low output of the lamp coated with our phosphor may be explained by 1) inadequate brightness of the phosphor, 2) loss in brightness owing to grinding of the phosphor, 3) loss in brightness incident to burning out of the binder (carried out in an uncontrolled atmosphere), and 4) higher than usual absorption by the phosphor.

These factors lowering the output must be reduced or minimized in the course of further research.

As was noted above, the quantum efficiency of Zn-Sr phosphate phosphors with λ = 254 mμ excitation is ~90%. In addition, as will be evident from its luminescence spectrum, most of the energy is emitted in the long wavelength part of the spectrum. In Fig.6 the spectrum of our phosphor is compared with the luminescence spectrum of $CaSiO_3$:Pb:Mn. It will be evident from the figure that the Zn-Sr phosphate can also be used in low pressure lamps for the purpose of improving their color characteristics. Tests to this end were also carried out on the new phosphor at the Moscow Electric Lamp Plant. According to the data obtained, the initial light yield of the lamps coated with this phosphor amounted to 32 lumens/ /watt, i.e., was equal to the best $CaSiO_3$:Pb:Mn coated samples. After some 250 hours, however, the brightness fell off to 87%. Further research aimed at solving this problem is also being undertaken.

State Institute of Applied Chemistry

References

1. Botden, Philips Res.Repts., 7, 197 (1952).
2. J.Butler, Electrochem.Soc., 100, 250 (1953).
3. Koelmans & Cox, J.Electrochem.Soc., 104, 442 (1957).
4. Butler, Illum.Engng., 51, 9, 613 (1956).
5. Butler, Illum.Engng., 52, 5, 279 (1957).

IMPROVEMENT OF THE COLOR RENDITION OF "FLUORESCENT" LAMPS

- R.A.Nilender

Utilization of the potentialities of photoluminescence, which allows of conversion of the wavelength of radiation, made possible the development of present day tubular "fluorescent" lamps. The appearance of these lamps was greeted by light engineers not only because they furnished a more economical light source but also because their technology allowed of varying the spectral composition of the irradiance and consequently its chromaticity. Inasmuch as it is assumed, not without reason, that for optimum utilization of human sight it is essential that artificial illumination conditions be close to natural, i.e., simulate daylight, "fluorescent" lamps approximating the spectral composition of daylight were introduced under the denomination of "daylight" lamps.

Actually, however, the spectral composition of daylight varies over a rather wide range during the course of a normal day. The development of "fluorescent" lamps thus encountered the difficulty of selecting the specific spectral composition to be duplicated.

At the Third All-Union Conference on Luminescence it was formally suggested that there be established four colors of "fluorescent" lamps; this suggestion was subsequently legitimatized by the adoption of a State Standard. There were adopted three colors corresponding to the colors of the standard sources approved for colorimetry by the Internation Commission on Illumination (ICI), namely, sources A, B and C with color temperatures of 2800, 4800 and 6500°K. In addition, there was established a fourth color intermediate between A and B, corresponding to a color temperature of 3500°K.

The corresponding lamps were designated as warm white, cold white and daylight, and the additional one as white. The introduction of the additional color was due to the fact that by means of the then available phosphors for "fluorescent" tubes the highest luminosity (light output) was attained for tubes of this color.

The experience gained over the past two decades shows that most popular in all cases where no special requirements as regards illumination must be met are "KhBS" type tubes, manufactured in the USA and a number of other countries, with a somewhat lower color temperature, namely, 4500°K. Actually during the past few years the color temperature of these lamps has been reduced somewhat and the recommendations of the Internation Electrotechnical Commission fix the color temperature at 4200°K.

Practical experience has shown that more important than the color of the lamps themselves is the question of correct color rendition. It is known that the color of illuminated objects depends not only on their intrinsic optical characteristics but also on the spectral composition of the irradiating light source. Thus a color standard does not uniquely determine the spectral composition of the radiation of a lamp and consequently does not guarantee equivalent color rendition by two lamps with the same "color". Thus to insure correct and consistent color rendition one must provide certain specific standards or norms for the spectral composition of the emission.

The spectral composition of the emission, however, uniquely determines only the color of the illuminated objects. Inasmuch as light engineers are concerned not with color per se but with the color sensation, which also depends on the brightness and the light adaptation of the observer, the question of correct color perception under artificial illumination becomes rather complicated. One must also bear in mind that the question of color rendition has two aspects: on the one hand, there is the matter of attaining the maximum possible distinction between color hues, i.e., there is the question of creating conditions of raising the

threshold sensitivity if only within a certain region of the light field, and, on the other hand, there is the matter of insuring correct perception of relative and absolute colors. This whole complex of problems, however, is of primary concern in physiological optics and not of direct interest to us as light engineers.

Fundamental to light engineering is the dual problem of setting standards for the spectral composition of radiation and finding means of realizing the established standards.

In this connection, the first problem is that of choosing light sources insuring correct color rendition that can be used as "standards" for comparing the actual color rendition quality of real lamps. This problem has not been definitively solved. One thing is clear, however, and that is that the three sources A, B and C, established and approved by the ICI, are not adequate for solution of this problem.

Of the various suggestions that have been put forth for solving this problem the most nearly correct in our opinion is the suggestion that the color rendition of the tested light source be compared with the color rendition provided by a black body with the same color temperature.[1]

A no less important question is that of the method of comparing the test and standard sources. Here again there are numerous suggestions, no single one of which has met with universal acceptance. Most of these proposed means are based on comparison of the relative distribution of the light flux over eight spectral zones. Intrinsically such comparison is rather awkward. The quality of color rendition is evaluated by eight pairs of figures, requiring normalization for the ratio of each pair, which presents appreciable practical difficulties and hampers comparison as regards the quality of color rendition of different light sources. Most of the above mentioned suggestions pertain to the method of obtaining, on the basis of the determined eight pairs of figures, a single figure giving a unique evaluation and thus offering the possibility of comparing different sources with the same color temperature.

Without taking a stand as to which of the various suggested methods is best or most expedient, hereinafter in comparing the quality of color rendition of different "fluorescent" lamps, we shall use the color rendition factor H, proposed by Harrison. Harrison's color factor is calculated by the formula

$$H = 100 - \frac{100}{4}\left[\left(\frac{F_{III}}{F_{VI}}\cdot\frac{E_{VI}}{E_{III}} - \frac{P_{III}}{P_{VI}}\cdot\frac{E_{VI}}{E_{III}}\right) + \left(\frac{F_{IV}}{F_{VI}}\cdot\frac{E_{VI}}{E_{IV}} - \frac{P_{IV}}{P_{VI}}\cdot\frac{E_{VI}}{E_{IV}}\right) + \right.$$

$$\left. + \left(\frac{F_{V}}{F_{VI}}\cdot\frac{E_{VI}}{E_{V}} - \frac{P_{V}}{P_{VI}}\cdot\frac{E_{VI}}{E_{V}}\right) + \left(\frac{F_{VII}+F_{VIII}}{F_{VI}}\cdot\frac{E_{VI}}{E_{VII}+E_{VIII}} - \frac{P_{VII}+P_{VIII}}{P_{VI}}\cdot\frac{E_{VI}}{E_{VII}+E_{VIII}}\right)\right],$$

where F_{III}, $F_{IV} \ldots F_{VIII}$ are the zonal light fluxes of the investigated lamp, P_{III}, $P_{IV} \ldots P_{VIII}$ are the zonal light fluxes of a black body with the same light temperature, and $E_{III}, E_{IV} \ldots E_{VIII}$ are the zonal light fluxes for a source with a uniform spectral intensity of the light flux. Shortcomings of Harrison's factor are that it does not take into account zones I and II, the light flux of which as a rule is determined by the transmission of the mercury vapor lines through the phosphor and also that it merges zones VII and VIII into a single zone.

Before turning to the specific results of our research on the development of "fluorescent" lamps with improved color rendition, we must consider the question of the relation between the luminance (light output) and color rendition quality of "fluorescent" lamps. The spectral characteristics of "fluorescent" lamps, both those prepared with a mixture of magnesium tungstate and zinc & beryllium silicate phosphors and those made with a single halophosphor, if we disregard the transmission of the mercury vapor lines, can be represented by a curve

with two peaks lying in the visible region and falling off to 30-50% of the maximum values towards the boundaries of the region. The same effective lamp color is obtained for narrower bands when the peaks are drawn closer together with a corresponding decrease in the intensity at the boundaries of the visible region. This drawing together of the peaks leads to increase of the radiant energy in the region of the maximum sensitivity of the human eye and consequently, at equal radiant energies, to increase of the luminosity.

Direct comparison of the relative distribution of the radiant flux over the spectral zones with the distribution for a black body and a number of researches carried out in the USSR show that the principal reason for unsatisfactory color rendition by "fluorescent" lamps is inadequate strength of the light flux in the red region. In view of this it is obvious that the above mentioned narrowing of the emission bands, leading to enhancement of the luminosity, leads at the same time to impairment of the color rendition.

Thus, in the case of "fluorescent" lamps employing high efficiency phosphors, enhancement of the light output is in practice possible only through change in the spectral composition of the emission, which inevitably leads to reduction in the quality of color rendition. In other words, enhancement of the color output and the quality of color rendition are contradictory and mutually exclusive requirements.

We can arrive at a satisfactory answer to the question of whether one should strive for a high light output or good color rendition only by concluding that it is essential to produce lamps of two types: 1) standard lamps with the highest possible luminosity meeting at least minimal requirements as regards color rendition and 2) lamps with a color rendition as close to the ideal as possible but with some sacrifice of luminosity (deluxe lamps).

"DC" type lamps with improved color rendition

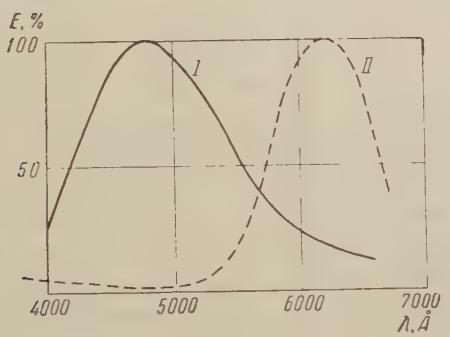

Fig.1

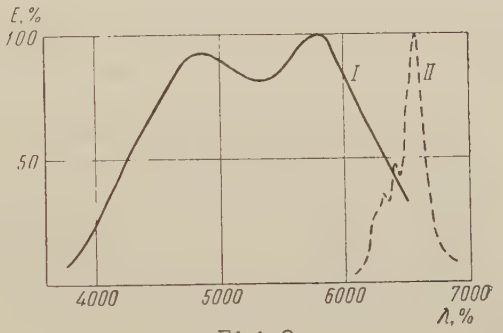

Fig.2

Fig.1. Spectral distribution in the emission of calcium halophosphate activated by Sb (I) and calcium silicate activated by Pb and Mn (II).

Fig.2. Spectral distribution in the emission of calcium halophosphate activated by Sb and Mn in "DC" lamps (I) and magnesium arsenate activated by Mn (II).

Calcium halophosphate, which is distinguished by a high quantum efficiency with excitation by 2537 Å radiation (the role of 1850 Å radiation, as is known, is relatively unimportant where excitation of "fluorescent" lamp phosphors is concerned) and relatively good stability under mercury vapor discharge conditions, can be utilized for preparing lamps with a color temperature of 6500°K, corresponding to that of "DC" type lamps.

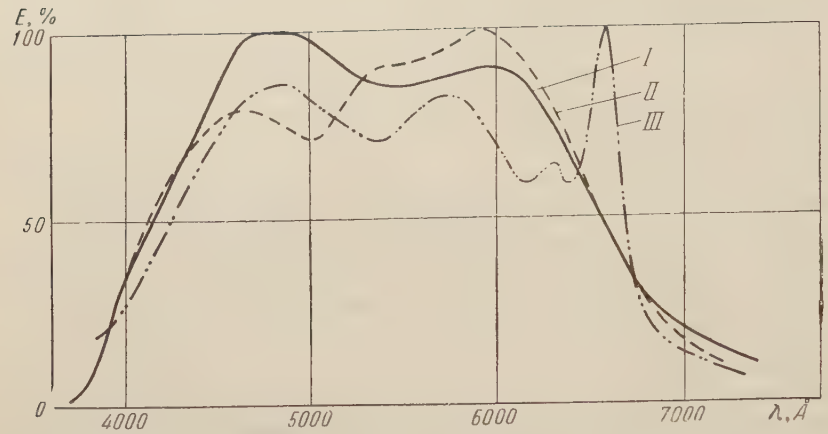

Fig.3. Spectral characteristics of different versions of the "DC" type lamp with improved color rendition: I - $3Ca_3(PO_4)_2 \cdot Ca(F,Cl)_2$:Sb + $CaSiO_3$:Pb:Mn, II - Mg_2WO_5 + (Zn,Be)SiO_3:Mn, III - $3Ca_3(PO_4)_2 \cdot Ca(F,Cl)_2$: :Sb:Mn + $6MgO \cdot As_2O_5$:Mn.

However, as was noted above, the drawing together of the emission band maxima characteristic of calcium halophosphate leads to an appreciable reduction of the emission in the 6500 to 7000 Å region, which lowers the color rendition quality as compared to lamps fabricated with a mixture of magnesium tungstate and zinc & beryllium silicate (the H factor falls off from 74 to 67), which is definitely not permissible for lamps of this type.

The halophosphate can be used in "DC" lamps in mixture with phosphors emitting in the red region. We developed two pairs of phosphors for obtaining "DC" lamps with improved color rendition.

The first pair, the spectral emission of which is characterized in Fig.1, consists of Sb activated calcium halophosphate with blue luminescence (luminescence peak at 4800 Å) and calcium silicate activated by Pb and Mn with orange luminescence (the principal emission peak lies at 6200 Å). The second pair of phosphors (Fig.2) consists of calcium halophosphate activated by Sb and Mn with white luminescence (peak at 5800 Å) and magnesium arsenate activated by Mn with red luminescence (principal peak at 6600 Å).

When the first pair of phosphors is used in the proportion of 60 parts of halophosphate to 40 parts of calcium silicate, there is obtained a luminescent layer with the spectral composition characterized by curve I in Fig.3. Curve II in Fig.3 shows the spectral composition of the emission of a mixture of magnesium tungstate and Mn activated zinc & beryllium silicate. Curve III represents the spectral composition of the emission of the second pair of phosphors taken in the proportion of 85 parts of calcium halophosphate to 15 parts of magnesium arsenate.

The color rendition of lamps made with a coating of the first phosphor pair is substantially superior to the color rendition of the conventional "DC" type "fluorescent" lamps now being produced with phosphor layers of magnesium tungstate and zinc-beryllium silicate with retention of the initial light output. And, since the stability of the new phosphors is appreciably higher, the average light output of the new lamps during their lifetime is increased. (After 3000 hours operation, for example, the light output of the lamps with calcium halophosphate and silicate is higher than the output of the conventional lamps by 20-25%.) The color rendition of lamps coated with calcium halophosphate and magnesium arsenate, although somewhat inferior to that of lamps coated with the calcium halophosphate and silicate phosphors, is still superior to the color rendition of conventional "DC" lamps. At the same time there is obtained an advantage as regards both the initial light output and its stability with operating time.

Thus by going over to calcium halophosphate with the addition of red emitting phosphors one can improve both the color rendition and the light output of "DC" type lamps.

"KhBS" type lamps with improved color rendition

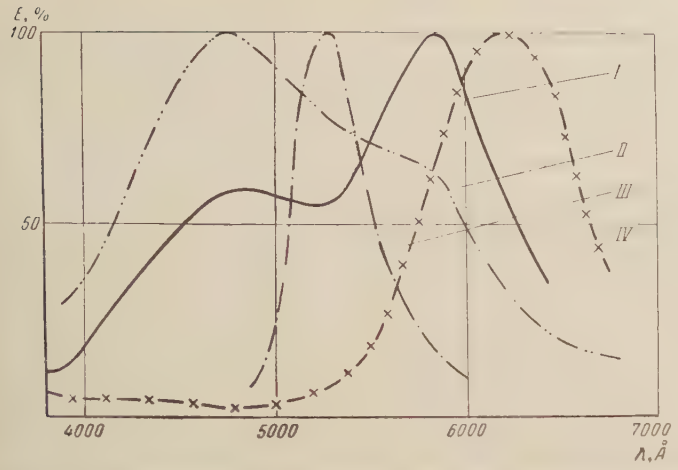

Fig.4. Spectral distribution in the emission of phosphors for standard KhBS lamps (I) and KhBS lamps with improved color rendition: II - $3Ca_3(PO_4)_2 \cdot Ca(F,CL)_2$:Lb,Mn, III - Zn_2SiO_4:Mn, IV - $CaSiO_3$:Pb:Mn.

To obtain "KhBS" type lamps with improved color rendition we employed three phosphors, namely, calcium halophosphate activated by Sb and Mn, the radiation of which predominates in the spectrum of the lamps, willemite which makes up the deficit in the emission spectrum in the green, and calcium silicate activated by Pb and Mn which makes up the emission deficit in the orange-red region. The spectral distribution in the emission of these phosphors and of the phosphor used in the standard "KhBS" type lamp are shown in Fig.4.

Fig.5 shows the spectral characteristic of the "KhBS" lamp with improved color rendition; the color rendition coefficient of this lamp is 96 instead of 77.4 for the standard lamp, the respective light output being 33 and 42 lumens/watt for 15 watt lamps. With the use of phosphors with equal quantum efficiencies there is an improvement in the quality of color rendition with only a slight sacrifice in efficiency.

The three-phosphate mixture consisted of 62% calcium halophosphate, 33% calcium silicate and 5% willemite.

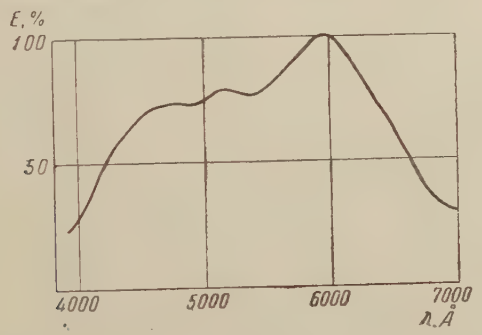

Fig.5

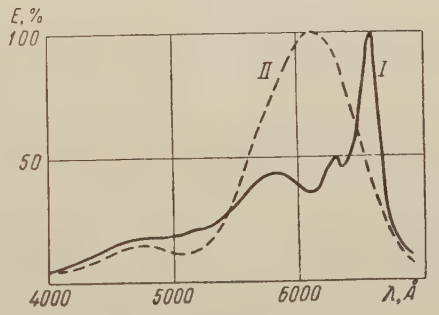

Fig.6

Fig.5. Spectral characteristic of KhBS lamps with improved color rendition.
Fig.6. Spectral characteristics of TBS lamps with improved color rendition (I) and standard TBS lamps (II).

"TBS" type lamps with improved color rendition

For obtaining "TBS" type lamps with improved color rendition, we used a phosphor mixture consisting of calcium halophosphate, willemite and magnesium arsenate. The spectral characteristics of the emission of an improved color rendition "TBS" type lamp are shown in Fig.6 together with the spectral characteristics of a standard "TBS" lamp for purposes of comparison. The color rendition factor of the new lamp is 92 with a light output of 31 lumens/watt for a 15 watt lamp, whereas the efficiency of the standard "TBS" lamp is 46 lumens/watt.

It will be obvious from the cited data that the color rendition of the new "fluorescent" lamps is substantially better than that of the conventional "DC", "KhBS" and "TBS" "fluorescent" lamps now being fabricated for general illumination purposes. Although the correction of the emission spectrum is accompanied by some decrease in efficiency, nevertheless the described lamps with improved color rendition in the 40 watt size have a light output in the range from 40 to 45 lumen/watt and therefore are still greatly superior to incandescent lamps.

References

1. D.Nickerson, Illum.Engineering, 53, 12 (1958).

CLOSING ADDRESS

- F.D.Klement

And so our Conference, having fully completed its proposed program, is coming to a close.

We have reason to believe that the Conference did not do its work too badly. There were presented about one hundred reports, most of them containing interesting and important data. Many reports stimulated extensive and fruitful discussions. The wealth of new results, the conflict of opinions and the lively exchange of views all bear witness to the fact that the scientific collective of Soviet scientists working in the field of luminescence leads a vigorous and creative life.

There are ample indications that since the Fifth Conference on Luminescence (Crystal phosphors)* we have made substantial progress.

The scope of work on luminescence has greatly broadened, as is evinced by the increase in the number of participants and increase in the number of cities represented at the Conference, that is, cities where work is now being done on luminescence. Whereas at the Fifth Conference there were only 270 conferees, at the Seventh Conference there were 350; whereas at the Fifth Conference there were represented only 19 cities of the USSR, at the present conference there were 25 cities. There have appeared new groups working on luminescence in Latvia, Azerbaidzhan, Armenia and the Kirgiz SSR. There has also been set up a new laboratory in Khar'kov.

It is particularly encouraging that in almost all centers where research is now being done on luminescence, there have come forward in recent years capable young scientists, who have often set the tone and tempo in the discussions of individual reports. We must remember that true progress is only possible where there are young scientists capable of going further than their teachers.

We also note with pleasure that our contacts with scientists in other countries have expanded. This is the first conference on luminescence in which foreign scientists participated; we take this opportunity to thank them for their contributions. These contacts must, however, be further broadened and it is essential, in the future, that the Scientific Council on Luminescence take steps to issue invitations to our foreign colleagues well in advance.

If we turn now to the content of our work, to the main directions of research, we conclude that the Conference has fully substantiated the analysis made in his opening address by M.D.Galanin. There has been increased research activity in electroluminescence and radioluminescence. In this respect we have fulfilled the hopes of the Fifth Conference. However, investigations on cathodoluminescence and roentgenoluminescence are still lagging. There is still inadequate contact between workers in the field of luminescence and those in the field of semiconductors. We must encourage their meetings, joint conferences and cooperative work directly in laboratories, utilizing to the full optical, specifically luminescence, methods for investigating semiconductors and the electric methods developed for investigation of semiconductors for work on crystal phosphors.

The reports we have heard and particularly the discussions following them have shown that in addition to experimenters, theoretical physicists are becoming increasingly active in the field of luminescence, which is very important and without which we cannot move forward.

As regards experimental methods and procedures, we have also made significant progress. Photoelectric and other electronic equipment, in particular recording devices, are being increasingly used in our daily work, but here we could and should

---

*The Sixth Conference on Luminescence was devoted to molecular luminescence. (Translation Editor's note.)

move forward more rapidly. We are becoming increasingly familiar and capable of utilizing low temperatures, high pressures, the far regions of the ultraviolet and infrared spectra, as well as new methods such as luminescence-polarization methods and taumetry in the region of very short lifetimes. But here too one could more extensively and more rapidly utilize the great achievements of our industry and technology. V.E.Khartsiev was right in stating that the procedures of paramagnetic resonance are being adopted too slowly. Nevertheless, I would like to call attention to the fact that even now important results can sometimes be obtained by very simple experiments. Examples are the experiments of V.A. Sokolov on candoluminescence, so elegant in their almost classical simplicity, the experiments of N.I.Ivanov on luminescence effects in highly dispersed systems and certain others.

We regret to note that industry and its practical concerns with luminescence were not as well represented at the present Conference as at earlier conferences. We must not neglect the practical aspects of our work and must always maintain close contact between science and technology and allot our attention in proper proportion to theoretical and practical problems.

Apparently, the present conference was overloaded with reports. We have not yet found the most effective form for organization of our collective work at conferences. Possibly at such broad conferences there should be more reviews and survey reports and that in addition to such broad conferences one should more frequently call specialized meetings, discussions on specific problems.

After the Fifth Conference on Crystal Phosphors there was established the Scientific Council on Luminescence. This is an important and encouraging event. It is to be hoped that the Council will utilize to the full its possibilities and capacities as regards

1) coordination of scientific work in the field of luminescence at different centers and in establishing the principal lines of endeavor,

2) examination of questions having to do with assistance to industry and the practical application of the results of scientific investigations,

3) creation of an experimental-technical base for scientific studies of luminescences, i.e., stimulate the construction of scientific equipment, assure an adequate supply of the requisite materials, luminescence pure reagents, etc.,

4) preparation of specialists in the field of luminescence, their training and allocation to various centers and institutions, and

5) publishing activity, namely, creation of a monograph literature on luminescence, publication of bibliographic references, etc.

We trust that the Scientific Council on Luminescence will be active in all these fields.

In conclusion, allow me to thank in the name of all those present the organizers of the Conference who did so much to insure its success: in the first place, Vadim Leonidovich Levshin and Samuil Aronovich Fridman and all the personnel of the FIAN (Physical Institute of the Ac. of Sci.) who participated in the organization work and in serving the conferees.

I should also like to thank the organizations that contributed to setting up the exposition at the Conference and the workers of the FIAN library for the exhibit of the literature prepared by them.

Allow me to wish all participants in the Conference further success in their scientific work. I declare the Seventh Conference on Luminescence closed.

Bulletin of the Academy of Sciences of the USSR - Physical Series
Vol. 23, No. 11 - November 1959
Transactions of the Seventh Conference on Luminescence (Crystal Phosphors)

TABLE OF CONTENTS

	Page Orig.	Trans.
Opening address - M.D.Galanin	1278	1271
Temperature quenching of the luminescence of ZnS:Ag phosphor with excitation by light or α-particles - M.D.Galanin & A.V.Raevskii	1280	1273
New data on a slow neutron detector - T.V.Timofeeva & S.P.Khormushko	1283	1275
On photoelectric effects in luminescent ZnS:Cu(Ni,Fe,Co) and ZnS·CdS:Cu powders - U.Kh.Nymm	1286	1278
Investigation of the photodielectric effect in ZnS:Cu:Fe phosphor - P.E.Ramazanov	1290	1281
Relaxation of the afterglow, photoconductivity and light sums of zinc sulfide phosphors - F.I.Vergunas & Yu.L.Lukantsever	1294	1285
Quenching of the luminescence of ZnS:Cu phosphor by infrared light - K.-S.K.Rebane	1296	1287
Influence of composition on the luminescence of activatorless ZnS·CdS phosphors - L.Drozd	1300	1290
Crystal phosphors with a heterodesmic structure - M.A.Konstantinova-Shlezinger	1304	1294
Fluorophosphate luminophors of the wagnerite type - N.A.Gorbacheva	1310	1299
Characteristics of the crystal phase of zinc silicate and the luminescence properties of Mn activated zinc silicate luminophors - V.V.Osiko	1314	1302
Luminescence centers in samarium activated zinc sulfide phosphors - Z.A.Trapeznikova	1319	1306
Some data on the mechanism of formation of sulfide luminophors - A.A.Bundel', A.I.Rusanova & L.G.Taushkanova	1326	1313
On the physical-chemical nature of silver activator in zinc sulfide phosphors - A.A.Cherepnev	1334	1321
Chemical aspects of the formation of zinc sulfide-selenide phosphors - L.Ya.Markovskii & R.I.Smirnova	1341	1327
Use of thermography for investigating zinc sulfide - E.G.Vasil'eva & S.A.Fridman	1347	1333
On the formation and characteristics of some zinc sulfide luminophors - A.V.Lavrov	1351	1337
Use of luminescence for investigating solid phase reactions in the CaO_4-Al_2O_3 system - A.K.Trofimov	1355	1341
Luminescence of manganese activated strontium metaantimonate - M.-L.Yu.Allsalu	1360	1346
Suitability of the thiosulfate procedure for preparation of zinc sulfide for synthesis of phosphors - M.I.Tombak, A.V.Popova, O.F.Komar & A.A.Bundel'	1363	1349
On variation of the optical properties of sulfide phosphors incident to elimination of the flux - A.M.Gurvich	1370	1356
Investigation of the technology of alkaline earth sulfide phosphors with persistent phosphorescence - T.A.Krasnova	1376	1362

Roentgenoluminescence and thermostimulation spectra of Siberian diamonds - E.S.Vilutis	1379	1365
Luminescence of glasses containing cerium - G.O.Karapetyan	1382	1368
Zinc and strontium phosphate base phosphors for "fluorescent" lamps - F.M.Pekerman, D.N.Shoikhet & R.A.Shtrikhman	1387	1372
Improvement of the color rendition of "fluorescent" lamps - R.A.Nilender	1393	1377
Closing address - F.D.Klement	1399	1383

Translated in 1960 by
Columbia Technical Translations
5 Vermont Ave., White Plains, N.Y.

Transactions

of the

Ninth All-Union Conference on Nuclear Spectroscopy

(Khar'kov, 26 January to 2 February 1959)

Continued from Vol. 23, Nos. 2 and 7

LARGE DOUBLE-FOCUSING ALPHA-SPECTROMETER

- S.A.Baranov, A.G.Zelenkov, G.Ya.Shchepkin, V.V.Beruchko & A.F.Malov

Introduction

The fundamental procedure for direct investigation of the fine structure of α-decay is still deflection of the α-particles in a magnetic field. Most promising in this respect is use of the effect of spatial focusing in a nonhomogeneous axially-symmetric magnetic field.[1-3] At present two operating α-spectrometers of this type are known: one with $\pi\sqrt{2}$ focusing[4] and the other of the semicircular type utilizing the fringe effect.[5] In developing the α-spectrometer described below we chose the first variant. The field distribution in the magnet gap can be represented in the form of a series:

$$\frac{H}{H_0} = 1 + a_1\eta + a_2\eta^2 + a_3\eta^3 + \dots,$$

where H_0 is the field at the central orbit (circle of radius ρ_0) and $\eta = \frac{\rho - \rho_0}{\rho_0}$.

As is well known, spatial focusing of the first order is realized for $a_1 = -1/2$.[1-3] Choosing the constant $a_2 = 1/8$ or $3/8$ assures additional radial focusing of the second order with respect to horizontal φ or vertical ψ angles, respectively. Wild & Huber[6] showed that for a field distribution in the gap characterized by $1/\sqrt{\rho}$ ($a_2 = 3/8$ and $a_3 = -5/16$) there is realized spatial focusing for particles in a wide energy range. In this case there can be attained focusing of higher orders in the vertical plane (angle ψ). This variant is not suitable, however, for spectrometers analyzing heavy charged particles inasmuch as use of a wide gap leads to substantial increase in the power requirements; in addition, the focal plane in such a spectrometer is curved which presents certain inconveniences as regards detection by the photographic procedure. Hence we chose $a_2 = 1/8$. Choice of $a_3 = 1/16$ allows of realizing focusing of the third order with respect to φ for particles with momentum $p_0 = H_0\rho_0$.[7-10] In another contribution by one of us[11] (see next article) it is shown that for $a_3 = 3/16$ there is realized radial focusing of the second order in φ for particles of different energies and there are derived expressions defining the form of the focal surface, the dispersion and the resolution of a spectrograph with the field constants $a_2 = 1/8$ and $a_3 = 3/16$.

A serious shortcoming of extant magnetic α-spectrometers is the relatively low transmission factor (product of the solid angle by the area of the source), which seriously limits the scope of investigation.

The purpose of the present work was to develop an instrument with high resolution and the maximum possible transmission factor, hence we chose a relatively large radius for the central orbit (ρ_0 = 155 cm).

1. Description of the α-Spectrometer

The spectrometer consists of two principal assemblies: the magnet with its winding and a stainless steel vacuum chamber located in the gap. The magnetic circuit is made in the form of a double mushroom and consists of three parts: a cylindrical core and two "caps" (Figs.1-3). The total weight of the installation is about 90 tons.

The width of the pole pieces is ~70 cm; the gap between them 35 cm. The magnet components are machined with relatively high accuracy (tolerance ~0.2 mm). The pole pieces are faced with special liners (nose pieces), the shape of which was designed analytically.

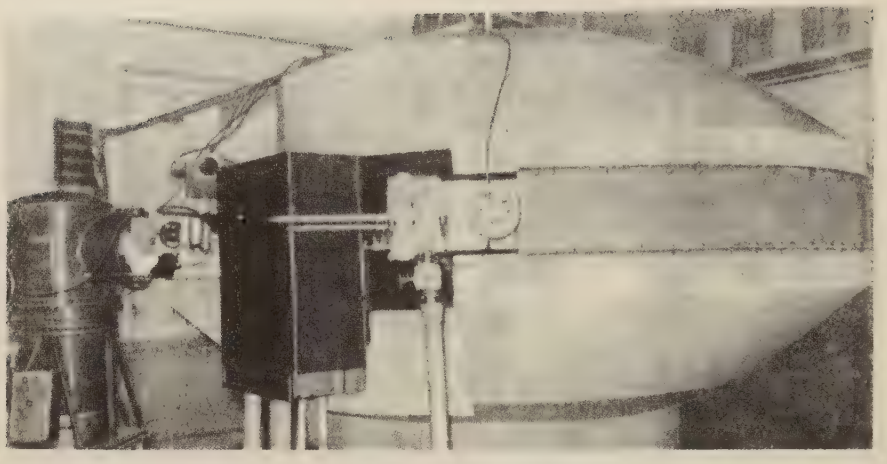

Fig.1. General view of the α-spectrometer.

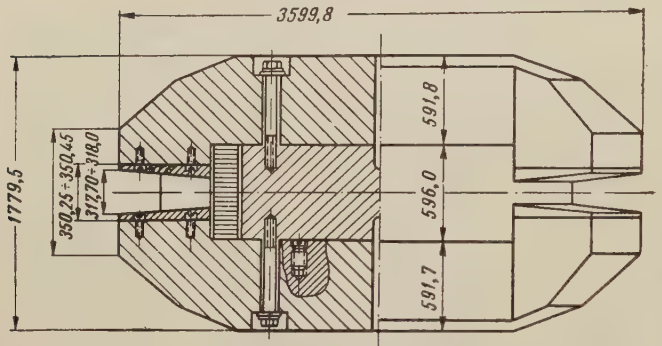

Fig.2. Spectrometer magnet.

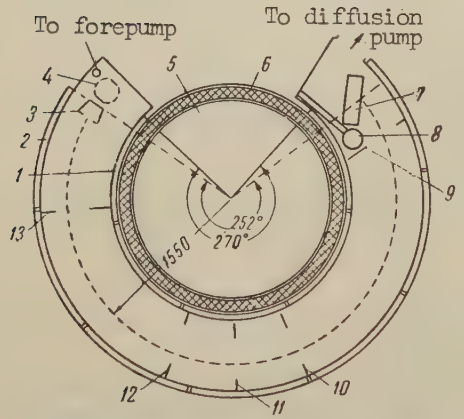

Fig.3. Cross section of spectrometer: 1) inner magnetic shunts, 2) outer magnetic shunts, 3) entrance aperture, 4) device for changing sources, 5) magnet core, 6) magnet winding, 7) photographic cassette, 8) magnetic field probe, 9-13) baffles.

The volume of the vacuum chamber is ~1000 liters. The chamber is evacuated by a VN-2 forepump and a VA-4-5 diffusion pump assembly. The attainable vacuum is of the order of 10^{-6} mm Hg. A 500 liter ballast tank is provided and allows of prolonged operation of the instrument with the forepump shut off.

The sources are mounted in a holder which allows of successive "exposure" of four targets without disturbing the vacuum. The maximum source dimensions are 10 x 100 mm. The section of the vacuum chamber containing the source can be isolated from the main chamber by means of a vacuum lock. This shortens the preparation time and hence facilitates investigation of radioactive substances with a relatively short period. In front of the source is an interchangeable entrance slit which allows of investigating the same target with different resolutions and transmission factors. The α-particle beam is defined by three identical apertures located in the central part of the chamber (at 100, 130 and 160°), where the beam has the maximum cross section. Three additional sets of baffles located along the particle path serve to minimize scattering.

The α-particles are detected by a proportional counter or by thick (nuclear) emulsion photographic plates. Plates having a total area of 480 x 90 mm can be exposed simultaneously. The plates are loaded into a special cassette, which also allows of making four consecutive exposures; the plates are interchanged and the cassettes closed after exposure by remote control without disturbing the vacuum.

2. Magnet Supply

A block diagram of the magnet power supply is shown in Fig.4. The magnet winding consists of 53 turns of 170 x 10 mm bus and is water cooled.

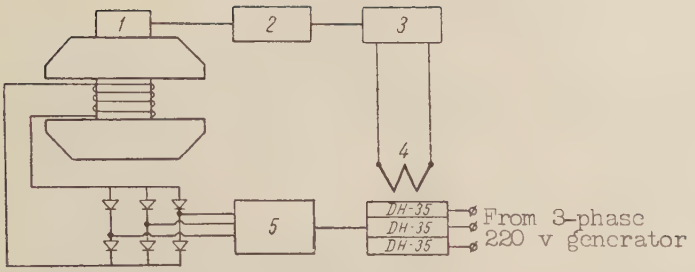

Fig.4

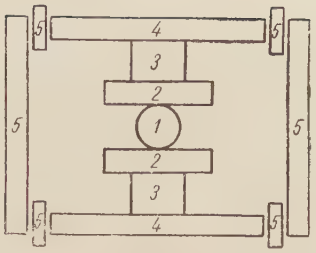

Fig.5

Fig.4. Block diagram of magnet supply: 1) magnetic shunt, 2) two-channel amplifier, 3) unit controlling saturable reactor (DH-35) magnetizing current, 4) DH-35 magnetizing winding, 5) three-phase transformer.

Fig.5. Arrangement for stabilization of the magnetic field: 1) cathode-ray tube, 2) liners, 3) compensating magnets, 4) stationary magnetic shunt plates, 5) moveable plates and "knives" of the magnetic shunt.

The magnet is supplied from a three-phase 220 volt, 35 kwa motor generator. The feed is through a set of DH-35 saturable reactors, which connect to the primary of the step-down transformer. The secondary of the transformer is connected to selenium rectifiers from which the current goes to the magnet winding. The operating current range of the instrument is 700 to 1300 amp, which corresponds to field strengths from 2.0 to 3.5 koe.

The high resolution of the instrument and the necessity of making long exposures impose rigorous requirements as regards stabilization of the magnetic field. For stabilization of the field we chose the system described by Zhukov & Semashko[12]. The field sensing element is a 5L0-38 cathode-ray tube located in the stray field. Two flat electrodes are mounted on the screen; each of these in conjunction with the luminescent layer forms a capacitor. The electron beam is modulated. The signals from the electrodes are fed into a two-channel amplifier; after amplification and detection the difference signal is applied to the input of a phase bridge which controls the magnetizing current in the auxiliary winding of the DH-35 saturable reactors.

The stray magnetic field in the vicinity of the cathode-ray tube is compensated by permanent magnets (see Fig.5). When the compensating-magnet and the stray field are equal, the beam is at the center of the screen, partially covering both electrodes. In this case the two signals nullify each other and no control signal is produced. If for some reason the magnetic field drifts off the set value, the beam is deflected to one side or the other and a signal of appropriate polarity appears at the amplifier output. This changes the DH-35 magnetizing current and leads to a change in the current through the main magnet windings. Thus the magnetic field is maintained at a constant value.

The field setting, i.e., the relation between the stray field and the field in the gap, is varied by adjusting the magnetic shunt. This is realized by displacing the moveable plates or the "knives" of the shunt by means of selsyns controlled from the main control panel.

For purposes of spectrometric scanning the field in the gap can be varied in $<10^{-4}H_o$ steps. In the case of spectrographic measurements the maximum deviation of the magnetic field from the set value H_o depends on the "exposure" time T. Thus, for example, for T_1 = 1 hour and T_2 = 8 hours the deviations are $<10^{-4}H_o$ and $<2\cdot 10^{-4}H_o$, respectively.

3. Measurement of the Magnetic Field

The field strength is gaged by proton paramagnetic resonance. The probe is a half-percent water solution of manganese chloride.

The energy ΔW required for reorientation of the proton spin in a magnetic field H_0 is given by the equation

$$\Delta W = \hbar\omega_0 = \hbar\gamma H_0,$$

where γ is the gyromagnetic ratio $(4.257703 \pm 2.5 \cdot 10^{-5}) \cdot 10^3$ cps gauss^{-1}, and ω_0 is the Larmor precession frequency. Thus measurement of the magnetic field reduces to measurement of the alternating magnetic field at which power is absorbed from the circuit.

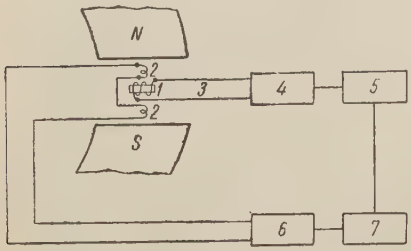

Fig.6. Block diagram of magnetic field measurement apparatus: 1) probe with radiofrequency circuit, 2) modulation coils, 3) coaxial feeder, 4) radiofrequency generator and preamplifier, 5) amplifier, 6) audiofrequency generator, 7) indicator.

The probe is located in a vacuum pocket directly in the magnet gap; special liners are provided to insure a homogeneous magnetic field in the region of the probe.

A block diagram of the proton resonance apparatus is shown in Fig.6. The absorption signal from the rf circuit goes successively to the inputs of the preamplifier, amplifier and indicator unit. To permit observation of magnetic resonance, the fixed magnetic field is modulated by special coils. The radiofrequency generator serves to supply these modulating coils, drive the sweep of the cathode-ray tube in the indicator unit and for supplying the synchronous detector. There is also provision for varying the modulation amplitude, which can be either greater or smaller than the width of the nuclear resonance line.

Initial detection of the nuclear resonance signals is realized with strong modulation of the field and is observed on the screen of a cathode-ray tube. For precise determination of the magnetic field low modulation is employed and the nuclear resonance signal is detected by the synchronous detector. A pointer type null indicator is connected into the plate circuit of the synchronous detector tubes. The generator frequency is varied from the control panel by varying the circuit capacitance by means of a selsyn.

The proton resonance indicator allows of determining the magnetic field to within one part in 10^5 in the operating range.

4. Investigation of the Field Configuration

Particular attention was given to obtaining the requisite field distribution in the magnet gap and investigating its configuration. For the field measurements there were constructed two instruments: in the first, the signal arising as a result of different displacements of the probe coil was measured by means of a ballistic galvanometer; the operation of the second instrument was based on compensation of the signals appearing upon simultaneous 180° flipping of two identical coils connected in opposition. The second instrument allowed of measuring the relative field value to within 1 part in $(2\text{-}4) \cdot 10^4$. Both instruments are characterized by a relatively high sensitivity (~0.05 oersted/mm).

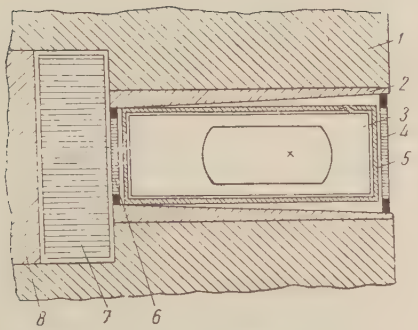

Fig.7. Transverse cross section of magnet pole pieces, magnetic potential dividers and the vacuum chamber: 1) magnetic circuit, 2) pole piece liner, 3) aperture, 4) outer shunt, 5) chamber, 6) inner shunt, 7) winding, 8) core.

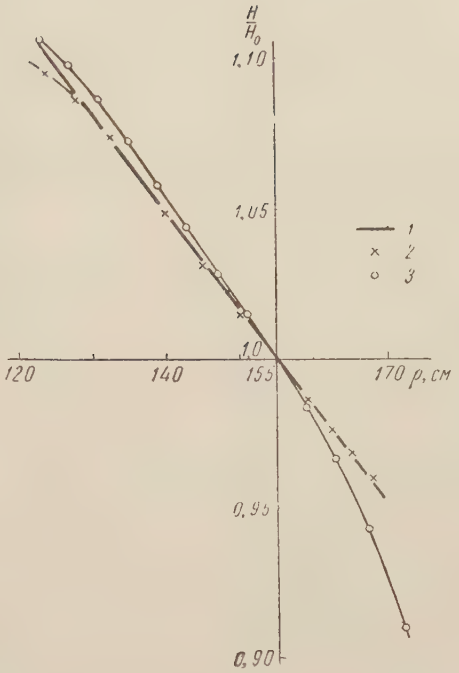

Fig.8. Magnetic field distribution in the spectrometer gap: 1) design curve, 2) with shunt, 3) without shunt.

Fig.8.

To check the quality of machining of the magnet, we carried out measurements of the azimuthal symmetry of the magnetic field distribution and also determined the position of the median surface. It was found that both the aximuthal distortions and the deviations of the median surface from the median plane are within the allowable tolerance. For eliminating the fringe effect we used special magnetic shims, acting like magnetic potential dividers[13]. These shims consist of a set of iron strips interlaid with sheets of cardboard. The location of the strips in the vertical plane was chosen experimentally. Frames with sets of strips were mounted over the full length along the inner and outer boundaries of the gap (Fig.7).

The results of measurements of the field distribution are shown in Fig.8 and the accompanying table.

Results of measurements of the magnetic field distribution $H(\rho)/H(\rho_0)$ in the median plane of the gap (with $\theta = \pi\sqrt{2}/2$)

Δ ρ, mm	Design $\frac{H(\rho)}{H(\rho_0)}$		Experimental $\frac{H(\rho)}{H(\rho_0)}$		
	$a_s = 0$	$a_s = 3/16$	$H_0 = 2$ kOe	$H_0 = 2{,}5$ kOe	$H_0 = 3$ kOe
128,3	0,9595	0,9596	0,9594	0,9589	0,9586
100,4	0,9681	0,9682	0,9684	0,9681	0,9680
75,4	0,9760	0,9760	0,9761	0,9759	0,9757
42,4	0,9864	0,9864	0,9863	0,9861	0,9861
—46,3	1,0150	1,0150	1,0148	1,0149	1,0150
—99,1	1,0325	1,0324	1,0319	1,0320	1,0322
—149,9	1,0496	1,0494	1,0487	1,0490	1,0490
—225,4	1,0755	1,0749	1,0738	1,0740	1,0741
—269,0	1,0906	1,0897	1,0866	1,0868	1,0869

Measurements of the field configuration allowed of choosing the best shape for the apertures defining the α-particle beam and determining the maximum solid angle of the instrument ($\sim 8 \cdot 10^{-4}$ of 4π). A detailed description of the field configuration measurement procedures and the results obtained will be published elsewhere.

5. Investigation of the Ion-Optical Characteristics of the Instrument

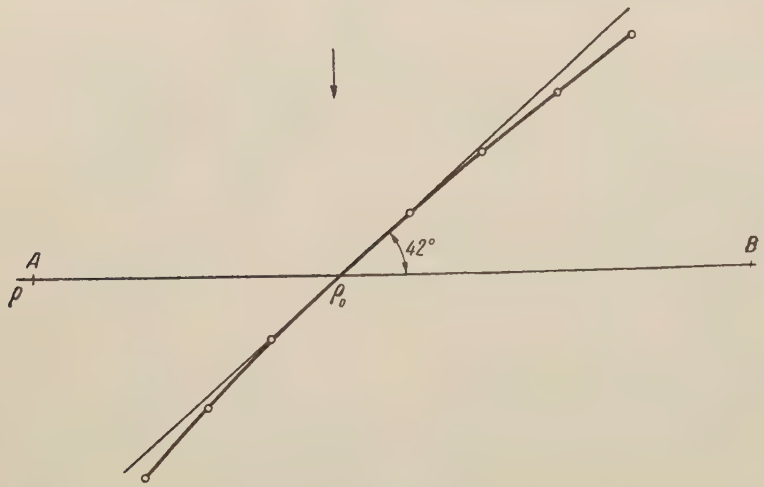

Fig.9. Shape of the focal surface: A & B - vacuum chamber walls. The arrow indicates the direction of α-particle motion.

For the purpose of finding the location of the focal plane and its shape and for energy calibration of the spectrograph, we constructed a special device with proportional counters which could be displaced perpendicular to the radius and rotated about the vertical axis without disturbing the vacuum. By varying the magnetic field the same group of α-particles could be focused in turn on each of the counters.

The location and shape of the focal surface as determined on the basis of these measurements are shown in Fig.9. The energy range $\Delta E/E_0$ of α-particles simultaneously detected by a set of photographic plates is ~10%. The line half-width ($\Delta H\rho/H\rho$) does not exceed 0.07% at any point in the measurement range. The dispersion in the instrument is close to the design value and equals $\sim 2.28 \cdot 10^{-4}$ E_0 per mm. This corresponds to ~1.2 kev/mm for Po^{210} α-particles.

Measurements of the relative variation in the transmission of the instrument along the focal surface were made by means of proportional counters (70 x 8 mm windows) with a 100 mm high source. The measurements were carried out for two values of the solid angle: $8 \cdot 10^{-4}$ and $5 \cdot 10^{-4}$ of 4π. The transmission proved to be maximum for particles moving along the central orbit. Towards the edges of the focal surface the transmission gradually falls off and amounts to ~80% for $l = -240$ mm and 90% for $l = 150$ mm (the distance l is measured from ρ_0 along the surface of the photographic plates).

The resolution of the instrument is illustrated in Fig.10 which shows the results of measurements of the principal α-particle groups from Cm^{242}. The line half-width equals approximately 3.5 kev ($\Delta H\rho/H\rho \approx 0.028\%$).

By virtue of the large size of the instrument ($\rho_0 = 155$ cm) and the relatively large solid angle ($8 \cdot 10^{-4}$ of 4π) the maximum transmission factor of the instrument is several times greater than that of any other spectrometer currently in operation[4,5]. The instrument allows of using samples with up to ~100 μg active material for investigating α-particle groups with a partial period of up to $2 \cdot 10^{10}$ years with relatively high resolution.

We desire to express our sincere gratitude to I.V.Kurchatov and L.A.Artsimovich for their suggestions and assistance in developing the α-spectrometer, V.Z.Bychkov, A.M.Barinov and I.V.Naumov who supervised the construction of the principal components of the spectrometer, S.M.Rubchinskii and M.P.Zel'dovich who

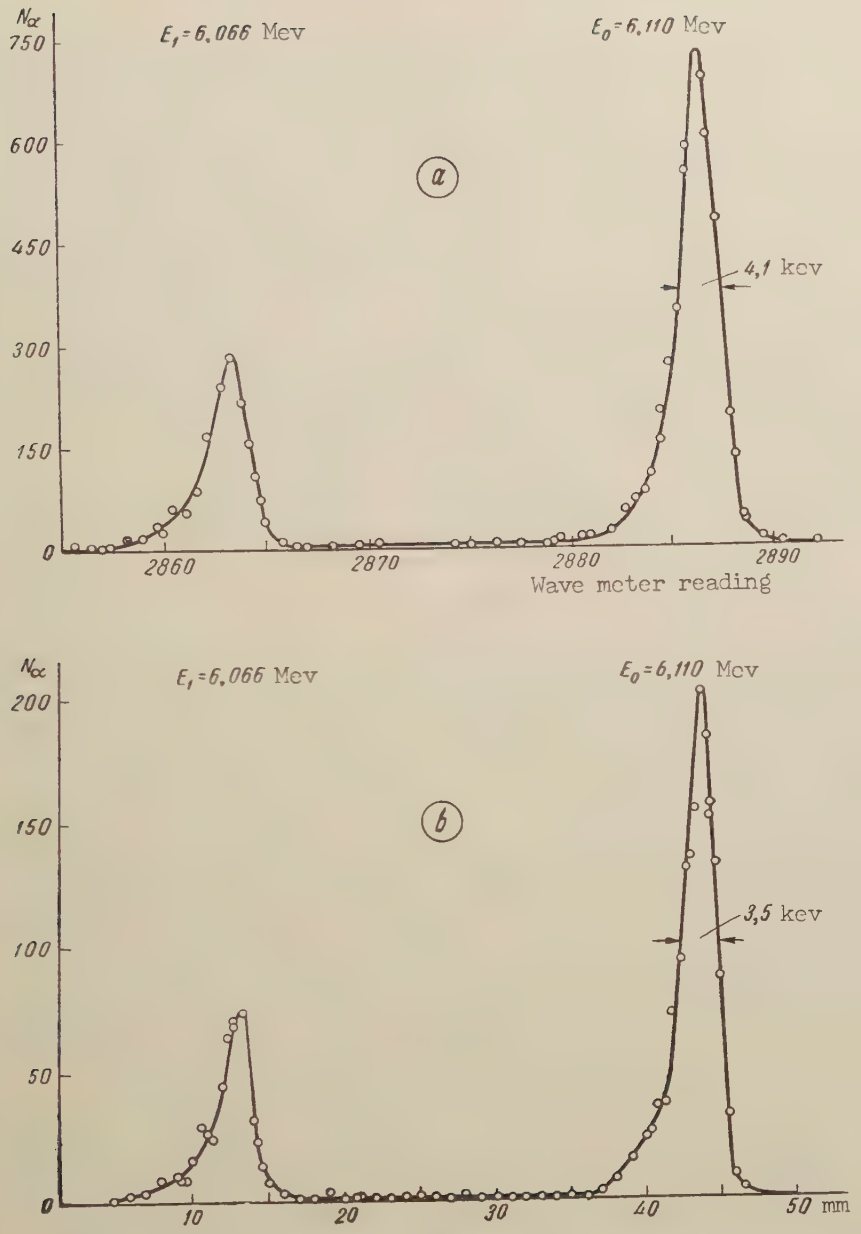

Fig.10. Alpha-spectra of Cm^{242}: a) spectrometric scan, b) spectrographic record.

participated actively in development of the field gaging equipment, V.V.Zhukov, N.N. Semashko, D.V.Pavlov and A.A.Nikulichev for consultation on problems having to do with stabilization and investigation of the field topography, V.M.Kulakov, A.A. Arutyunov, S.N.Belen'ko and A.I.Timoshinov for assistance in developing and adjusting the instrument, and A.D. Runov, I.Ya.Leskov and M.I.Dmitruk for assistance in developing and adjusting the vacuum system.

References

1. N.Svartholm & K. Siegbahn, Arkiv.Mat. Aston.Fysik, 33A, 21 (1946).
2. N.Svartholm, Arkiv. Mat.Astron.Fysik, 33A, 24 (1946).
3. K.Siegbahn & N. Svartholm, Nature, 157, 872 (1946).
4. L.L.Gol'din, G.I. Novikova & E.F.Tret' yakov, Session of the USSR Ac.of Sci. on the Peaceful Uses of Atomic Energy, 1-5 July, 1955, OFMN meeting, p.226, M., 1955.
5. D.L.Judd & S.A.Bludman, Nucl.Instr., 1, 46 (1957).
6. H.Wild & O.Huber, Helv.Phys.Acta, 30, 3 (1957).
7. N.F.Verster, Physica, 16, 815 (1950).
8. P.P.Pavinskii, Izv.AN SSSR, Ser.fiz., 18, 175 (1954).
9. V.R.Saulit, Ibid., 18, 227 (1954).
10. S.A.Baranov, A.F.Malov & K.N.Shlyagin PTE (Instr. & Experimental Techniques), No.1, 3 (1956).
11. A.G.Zelenkov, Present issue of the Bulletin, p.1396.
12. V.V.Zhukov & N.N.Semashko, PTE, No.2, 41 (1958) (Trans.Instruments & Experimental Techniques.)
13. G.Hinman & F.Crane, Rev.Sci.Instr., 23, 438 (1952).

SOME DESIGN CALCULATIONS FOR A DOUBLE-FOCUSING ALPHA-SPECTROMETER*

- A.G. Zelenkov

The basic procedure for investigating the fine structure of α-spectra at present is the method of deflection of the α-particles in a magnetic field.[1-4] The distance between low lying levels in heavy nuclei is usually only some tens of kev, while the intensities of neighboring α-particle groups may differ by a factor of hundreds, so that the apparatus line width must not exceed a few kev. Such narrow lines can be obtained only if the thickness of the source does not exceed ~10 μg/cm^2,[3,5]. Hence the basic requirement set for α-spectrometers is the value of the luminosity L = σT, where σ is the area of the source and T is the fraction of monoenergetic particles detected.

Employment of the principle of double-focusing proposed by Svartholm & Siegbahn[6-8] holds the greatest promise for realizing an instrument with a resolution of the order of 10^{-4} and maximum luminosity. With a $\pi\sqrt{2}$ focusing angle, instruments based on this principle also have double the dispersion compared to instruments with semicircular focusing.

Let us represent the magnetic field distribution in the magnet gap in the form of a series

$$H(\rho) = H_0(1 + a_1\eta + a_2\eta^2 + a_3\eta^3 + \ldots) \qquad (1)$$

Here H_0 is the field along the central orbit (circle of radius ρ_0) and $\eta = \frac{\rho - \rho_0}{\rho_0}$.

It has been shown by Svartholm & Siegbahn[6-8] that to realize spatial focusing the coefficient a_1 must be equal to -1/2. Choice of the coefficient a_2 is more or less arbitrary and depends on the shape of the aperture defining the charged particle beam[9-11].

Lee-Whiting & Taylor[10] and Wild & Huber[11] carried out a detailed comparison of instruments with different values of a_2, assuming a defining aperture of rectangular shape. According to these evaluations, for equal resolution the maximum allowable solid angle will be obtained for $a_2 = {}^1/_8$ and ${}^3/_8$.

As has been shown by a number of investigators[10-16], both these types of spectrometers with appropriate choice of the coefficients in Eq. (1) allow of realizing ideal focusing over radial $(a_2 = {}^1/_8)$ or axial $(a_2 = {}^3/_8)$ angles. Nevertheless, as has been pointed out by Lee-Whiting & Taylor[10] and Wild & Huber[11], choice of the field distribution with $a_2 = {}^3/_8$ for β-spectrometers presents certain advantages as compared with choice of $a_2 = {}^1/_8$. Owing to better axial focusing (the $\varphi_r\varphi_z$ term vanishes) and the smaller value of the factor multiplying z_0^2 in the formula for the abberation, the transmission factor (for the same resolution) is somewhat higher in instruments with $a_2 = {}^3/_8$.[10,11] (Here φ_r is the radial angle, φ_z is the axial angle, and z_0 is the distance of the extreme point of the source from the median plane.) Finally, owing to the fact that with $a_2 = {}^3/_8$ the field distribution is close to $1/\sqrt{\rho}$, it allows of simultaneously realizing spatial focusing of particles in a wide energy range. This is important when the instrument is used as a spectrograph. Wild & Huber[11] analyzed the possibility of realizing a spectrograph with double-focusing $(a_2 = {}^3/_8)$. They showed that the most advantageous value for the third coefficient, a_3, in the series development for $1/\sqrt{\rho}$ is $-{}^5/_{16}$. As compared with a semicircular spectrometer, the double-focusing spectrometer has the following advantages: one can have a much greater solid angle,

---

*This report was presented at the Eighth All-Union Conference on Nuclear Spectroscopy.

the value of which, in contrast to the case of spectrographs with a homogeneous field, remains constant over the entire working range and does not depend on the size of the instrument, and the dispersion is twice as great but differs somewhat for different parts of the photographic plate. This leads to some reduction in the momentum range of simultaneously recorded particles.

Despite the above mentioned advantages of an inhomogeneous field with $a_2 = {}^3/_8$, this type of field is not utilized in spectrographs for investigating heavy particles for the following reasons.[17] The magnet of a double-focusing spectrometer must have a relatively wide gap which in turn involves high power consumption. In addition, with a wide gap there are encountered difficulties in minimizing the fringe effect and obtaining the requisite field distribution in the gap without undue increase in the size of the magnet. Finally, when the instrument is used as a heavy particle spectrograph, it is highly desirable to be able to count individual particle tracks in the photographic emulsion;[3-5] with $a_2 = {}^3/_8$, however, the particles enter the emulsion at almost right angles to the surface of the plate, which obviously presents certain difficulties as regards counting the tracks and identifying the background particles.

Hence there was chosen a field distribution of the type

$$H(\rho) = H_0(1 - {}^1/_2\eta + {}^1/_8\eta^2 + a_3\eta^3 + \ldots). \tag{2}$$

First, let us consider the particular case of motion of the particles in the median plane ($z = 0$). The particle momentum p and the radius R of curvature of the particle orbit are related by the familiar expression

$$pc = RZeH, \tag{3}$$

where c is the velocity of light and Ze is the particle charge. For particles moving along the central orbit, this expression becomes

$$p_0c = \rho_0 ZeH_0. \tag{4}$$

Dividing the first by the second, we obtain after some simple transformations[16]

$$\frac{\rho_0}{R} = \frac{H}{H_0}(1 - \tau), \tag{5}$$

where $\tau = \frac{\Delta p}{p}$.

Inserting Eq. (2) and the expression for R in polar coordinates into Eq. (5), we obtain the following equation (retaining terms through third order):

$$\eta'' + {}^1/_2\eta = -{}^5/_8\eta^2 - \eta\eta'' + {}^1/_2\eta'^2 - {}^3/_4\eta\eta'^2 + ({}^1/_8 - a_3)\eta^3 + \tau(1 + {}^5/_2\eta + {}^{13}/_8\eta^2 + {}^3/_2\eta'^2) + \ldots \tag{6}$$

We shall use the modification of the method of successive approximation developed by Baranov & Malov[16,18] for solving the equation. Let α be the tangent of the angle of emergence of the particle relative to the normal to the radius. Let us write the solution in the form of a series in powers of α and τ:

$$\eta = \alpha f_{10} + \tau f_{01} + \alpha^2 f_{20} + \alpha\tau f_{11} + \tau^2 f_{02} + \alpha^3 f_{30} + \alpha^2\tau f_{21} + \alpha\tau^2 f_{12} + \tau^3 f_{03} + \ldots \tag{7}$$

Here f_{ik} is a function of the azimuthal angle φ. From the boundary conditions $\eta(0) = 0$ and $\eta'(0) = \alpha$, it follows that $f_{ik}(0) = 0$ and $f'_{ik}(0) = 0$, except that $f'_{10}(0) = 1$.

Successive solution of the equations yields the following expressions for f_{ik}:

$$f_{10} = \sqrt{2}\ \sin\ \varphi/\sqrt{2}; \tag{8}$$

$$f_{01} = 2\,(1 - \cos\varphi/\sqrt{2}); \tag{9}$$

$$f_{20} = {}^1/_2 \sin^2 \varphi/\sqrt{2}; \tag{10}$$

$$f_{11} = -\frac{\sqrt{2}}{2}\sin\varphi\sqrt{2} - \varphi\cos\varphi/\sqrt{2} + 2\sqrt{2}\sin\varphi/\sqrt{2}; \tag{11}$$

$$f_{02} = {}^1/_2 \cos\varphi\ \sqrt{2} - \sqrt{2}\,\varphi\sin\varphi/\sqrt{2} - 6\cos\varphi/\sqrt{2} + {}^{11}/_2; \tag{12}$$

$$f_{30} = \frac{9-k}{128}\sqrt{2}\sin\frac{3\varphi}{\sqrt{2}} + \frac{3\,(k-1)}{32}\varphi\cos\varphi/\sqrt{2} - \frac{3\,(5+3k)}{128}\sqrt{2}\sin\varphi/\sqrt{2}; \tag{13}$$

$$f_{21} = \frac{3\,(k-9)}{64}\cos\frac{3\varphi}{\sqrt{2}} - \frac{\sqrt{2}}{4}\varphi\sin\varphi\sqrt{2} + \frac{1-k}{4}\cos\varphi\sqrt{2} + \\ - \frac{3\,(k-1)}{32}\sqrt{2}\,\varphi\sin\varphi/\sqrt{2} + \frac{61k-165}{61}\cos\varphi/\sqrt{2} + \frac{11-3k}{4}; \tag{14}$$

$$f_{12} = \frac{3\,(k-9)}{64}\sqrt{2}\sin\frac{3\varphi}{\sqrt{2}} + \varphi\cos\varphi\sqrt{2} - \frac{k\sqrt{2}}{2}\sin\varphi\sqrt{2} - \\ - \frac{\sqrt{2}}{4}\varphi^2\sin\varphi/\sqrt{2} + \frac{15k-79}{16}\varphi\cos\varphi/\sqrt{2} + \frac{333-5k}{64}\sqrt{2}\sin\varphi/\sqrt{2}; \tag{15}$$

here $k = 16\ a_3$. New here are only the expressions for f_{11}, f_{02}, f_{21} and f_{12}, i.e., Eqs.(11), (12), (14) & (15); the other expressions are familiar from earlier studies[14,16].

Let us now turn to a consideration of the principal characteristics of the spectrograph, namely, the location and shape of the focal surface, the dispersion and the resolution of the instrument. To this end let us rewrite Eq.(7) in somewhat different form:

$$\eta = \alpha\,(f_{10} + \tau f_{11} + \tau^2 f_{12} + \ldots) + \tau\,(f_{01} + \tau f_{02} + \ldots) + \alpha^2\,(f_{20} + \tau f_{21} + \ldots) + \alpha^3 f_{30} + \ldots \tag{7'}$$

Let the focal surface be determined by the condition that there is realized on it first order focusing in α. From this we obtain the equation for the line of focuses:

$$f_{10} + \tau f_{11} + \tau^2 f_{12} = 0. \tag{16}$$

As is known, for $a_2 = {}^1/_8$ and $\tau = 0$ there obtains second order focusing in α. The focusing angle equals $\pi\sqrt{2}$. For particles with $\tau \neq 0$, first order focusing will be realized at a somewhat different value of the angle φ, namely,

$$\varphi = \varphi_r = \pi\sqrt{2}\,(1 + \delta). \tag{17}$$

Expanding the functions (8)-(15) in series in δ about $\varphi = \pi\sqrt{2}$ and substituting the results in Eq.(16), we obtain

$$\delta \approx \tau\left(1 + \frac{63-15k}{16}\tau\right) \approx \varkappa\left(1 + \frac{47-15k}{16}\varkappa\right), \tag{18}$$

where

$$\varkappa = \frac{\Delta p}{p_0}, \quad \tau = \frac{\Delta p}{p} \approx \varkappa\,(1 - \varkappa + \varkappa^2).$$

The dispersion is determined by the second term in Eq.(7'). Proceeding analogously, we obtain

$$\eta(\tau) \approx \tau(f_{01} + \tau f_{02}) \approx 4\tau(1 + 3\tau) \approx 4\varkappa(1 + 2\varkappa); \tag{19}$$

whence the dispersion

$$D = \frac{d\rho}{dp} \approx 4(1 + 4\varkappa)\frac{\rho_0}{p_0}.$$

We see that the dispersion is weakly dependent on the choice of a_3. Equations (18) and (19) are parametric equations of the focal surface. They allow of finding the slope of focal surface relative to the radius[16] and its curvature K:

$$\tan\theta = \pi\sqrt{2}\lim_{\tau\to 0}\frac{\delta}{\eta} = \frac{\pi\sqrt{2}}{4} \approx 1.11;\ \theta = 48^\circ \tag{20}$$

and

$$K = \frac{1.2}{\rho_0}(1 - 0.13k). \tag{21}$$

Lastly, for determining the abberation let us consider the last terms in Eq.(7'):

$$\Delta = \alpha^2 f_{20} + \alpha^3 f_{30} + \alpha^2\tau f_{21} \simeq \frac{3(1-k)}{32}\pi\sqrt{2}\,\alpha^3 + 2(3-k)\alpha^2\varkappa. \tag{22}$$

Thus, whereas with $k = 1$ ($a_3 = {}^1/_{16}$), as is known, there is realized radial focusing of the third order in α, with $k = 3$ ($a_3 = {}^3/_{16}$), there obtains second order focusing for particles with different energies.

We have so far considered the conditions of focusing of a plane beam. It is known that double focusing of particles with different energies obtains only in a field falling off along the radius as $1/\sqrt{\rho}$. For $a_2 = {}^1/_8$ it is disturbed. Let us analyze this effect. To this end let us use the familiar equation relating the angles of radial (ψ_r) and axial (ψ_z) focusing:[19]

$$\frac{1}{\psi_r^2} + \frac{1}{\psi_z^2} = \frac{1}{\pi^2}; \tag{23}$$

substituting Eqs.(17) and (18) therein, we obtain

$$\psi_z = \pi\sqrt{2}(1 - \varkappa). \tag{24}$$

From this we can readily deduce the following expression for the change in the image coordinates:

$$\Delta z = -2\pi\sqrt{2}\,\rho_0\gamma\varkappa,$$

where $\gamma = \tan\varphi_z$. Consequently the height of the image will exceed the height of the source by $4\pi\sqrt{2}\,\rho_0\gamma_{max}\varkappa$.

In conclusion, let us write out the expression for the image coordinates ρ^* and z^* and the basal line width B with the obtained refinements for particles with different momenta ($a_2 = {}^1/_8$). The equations, which are valid only on the focal surface[18,19] are

$$\rho^* = \rho_0 - \Delta\rho + 4\varkappa\rho_0(1 + 2\varkappa) - \frac{4}{3}\rho_0\gamma^2 - \frac{5}{6}z_0^2 + \frac{3\pi\sqrt{2}(1-k)}{32}\alpha^3\rho_0 + 2(3-k)\alpha^2\varkappa\rho_0, \tag{25}$$

$$z^* = -z_0 + \frac{\Delta\rho z_0}{3\rho_0} - \frac{8}{3}\rho_0\alpha\gamma - 2\pi\sqrt{2}\,\rho_0\gamma\varkappa, \tag{26}$$

$$B = \left[\frac{s_1 + s_2}{4\rho_0} + \frac{1}{3}\gamma_{max}^2 + \frac{5}{96}\cdot\frac{h^2}{\rho_0^2} + \frac{3\pi\sqrt{2}\,|1-k|}{64}|\alpha_{max}^3| + \frac{|3-k|}{2}\alpha_{max}^2|\varkappa| \right](1-5\varkappa). \quad (27)$$

Here h is the height of the source, s_1 is its width, and s_2 is the width of the detector slit. The appearance of a common factor in Eq.(27) is connected with variation of the dispersion along the focal surface:

$$\frac{\Delta p}{p} = \frac{\Delta\rho}{pD} \approx \frac{\Delta\rho}{4\rho_0(1+5\varkappa)}.$$

Thus a magnetic field with $a_2 = {}^1/_8$ and $a_3 = {}^3/_{16}$ assures second order radial focusing in the angle φ_r of charged particles of different energy. The basal line broadening owing to third order defocusing amounts to $\frac{3\pi\sqrt{2}}{32}\alpha_{max}^3$. The dispersion varies somewhat along the focal surface. Owing to disturbance of the conditions for axial focusing, the transmission factor of the instrument for particles with $\varkappa \neq 0$ is somewhat lower than for particles with an energy corresponding to $H_0\rho_0$.

I desire to thank S.A.Baranov and A.F.Malov for valuable suggestions in the course of discussing the present work.

References

1. E.Rutherford et al., Proc.Roy.Soc., 139, 617 (1933). Ibid., 142, 347 (1933); Ibid., 145, 235 (1934).
2. E.Cotton, Ann.Phys., 6, 481 (1951).
3. F.L.Reynolds, Rev.Scient.Instrum.22, 749 (1951).
4. L.L.Gol'din, G.I.Novikova & E.F.Tret'yakov, Session of the USSR Ac.of Sci.on Peaceful Uses of Atomic Energy, 1-5 July 1955, PFMN Meeting, p.226, M., 1955, Phys.Rev., 103, 1004 (1956).
5. F.Asaro, F.L.Reynolds & I.Perlman, Phys.Rev., 88, 129 (1952).
6. N.Svartholm, Arkiv Mat.Astron.Fysik., 33A, 21 (1946).
7. K.Siegbahn & N.Svartholm, Nature, 157, 872 (1946).
8. N.Svartholm, Arkiv.Mat.Aston.Fysik., 33A, 24 (1946).
9. E.Huster et al., Z.Naturforsch., 10A, 83 (1955).
10. G.E.Lee-Whiting & E.A.Taylor, Can.J.Phys., 35, 1 (1957).
11. H.Wild & O.Huber, Helv.Phys.acta, 30, 3 (1957).
12. N.F.Verster, Physica, 16, 815 (1950).
13. P.P.Pavinskii, Izv.AN SSSR, Ser.fiz., 18, 175 (1954).
14. V.R.Saulit, Ibid., 18, 227 (1954).
15. P.H.Stoker et al. Physica, 20, 337 (1954).
16. S.A.Baranov, A.F.Malov & K.N.Shlyagin, PTE (Instruments & Experimental Techniques), 1, 3 (1956).
17. R.Rauli, Arkiv fys., 10, 175 (1956).
18. A.F.Malov, Abstracts of Reports presented at the Seventh All-Union Conference on Nuclear Spectroscopy, 1957.
19. K.Siegbahn (editor), Beta- and Gamma-Ray Spectroscopy, Amsterdam, 1955.

NEW DATA ON THE DECAY OF Am^{241}

- P.S. Samoilov

Introduction

The first experimental data on the conversion electrons emitted in the decay of Am^{241} to Np^{237} were obtained in 1951 by O'Kelley[1]. Since then, the activity of this nuclide has been studied by many investigators. The region of the electron spectrum below 10 kev was studied only by Baranov & Shlyagin[2] and Rosenblum & Valadares[3]. However, the resolution and transmission of the spectrometers used in these studies were inadequate for good resolution of the conversion and Auger electron lines and detection of the weakest lines. All investigators who studied the conversion electron spectrum found evidence of six transitions with energies of 26, 33, 43, 55, 60 and 99 kev in Np^{237}. An appreciably greater number of γ-transitions has been observed in investigations[4,5] of β-decay of U^{237} to Np^{237}.

Some levels and γ-transitions known to exist in Np^{237} on the basis of studies[6,7] of Am^{241} α- and γ-radiations were also not detected in observations of the conversion electron spectra. Finally, in 1957, Newton[8] in Coulomb excitation experiments, in addition to the known 33 kev γ-transition, discovered γ-transitions of 42.8 and 76 kev energy in Np^{237}. As regards the multipolarities of these γ-transitions, the data of different authors disagree in many cases. Thus, for example, even for the strongest 60 kev γ-transition the relative L subshell internal conversion coefficients (ICC) reported by different authors differ by as much as 70%. Insofar as has been reported in the literature, the electron spectrum of Am^{241} has been measured only in the energy region from 1 to 100 kev.

With a view to refining and amplifying the data on the levels and γ-transitions occurring in Np^{237} from α-decay of Am^{241} we recorded and analyzed the electron spectrum of Americium in the range from 1 to 400 kev.

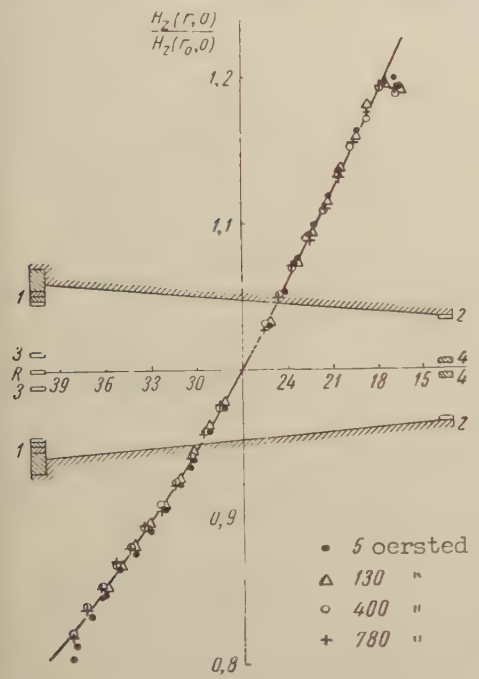

Fig.1. Magnetic field distribution in the magnet gap of the β-spectrometer. The solid line is the theoretical distribution given by Eq.(1) with $\beta = 3/16$. The magnetic shims 1 & 4 give the field distribution for $\beta = 1/8$ and $\beta = 3/16$; the shims 2 & 3 the distribution for $\beta = 3/8$.

1. Procedure

The electron spectrum of Americium was recorded on the $\pi\sqrt{2}$ double-focusing universal β-spectrometer described in Ref.9. This spectrometer employs a magnetic field with axial and mirror symmetry (Pavinskii[10] type) which can be described by the following series:[11]

$$H_z(r,0) = H_z(r_0,0)\left[1-\frac{1}{2}\left(\frac{r}{r_0}-1\right)+\beta\left(\frac{r}{r_0}-1\right)^2+\right.$$
$$\left.+\frac{1}{16}\left(\frac{r}{r_0}-1\right)^3+\frac{31}{256}\left(\frac{r}{r_0}-1\right)^4+\frac{59}{512}\left(\frac{r}{r_0}-1\right)^5-\ldots\right], \quad (1)$$

where $H_z(r, 0)$ is the vertical component of the magnetic field in the median plane of the gap at a distance r from the symmetry axis, and r_0 is the mean radius of the electron trajectories.

It is known that in such a field double-focusing is retained in a certain range of variation of the coefficient β, but the shape of the image changes. In the given spectrometer, without

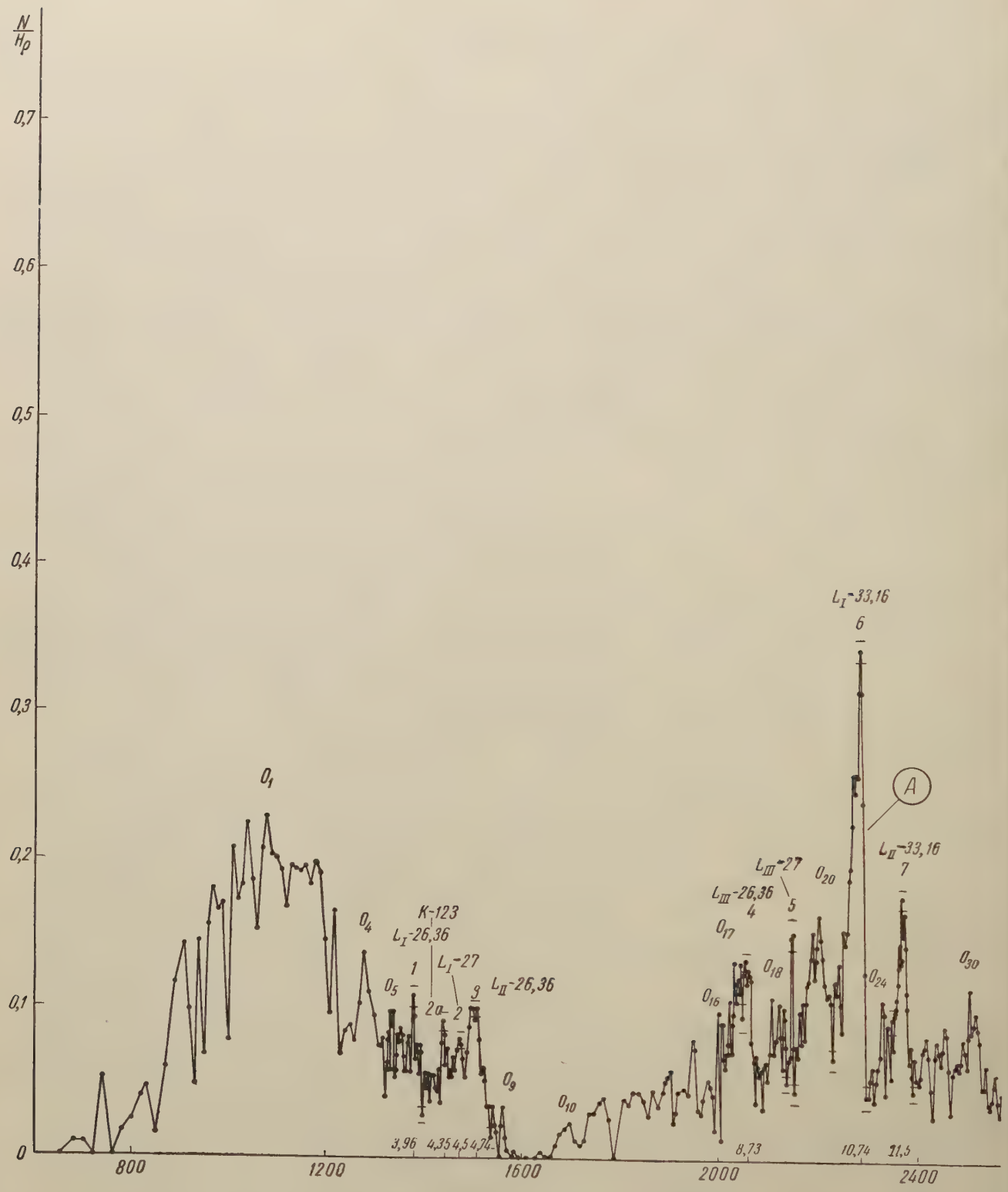

Fig.2. Electron spectrum of Am^{241} in the 1 to 35 kev region: A - section measured

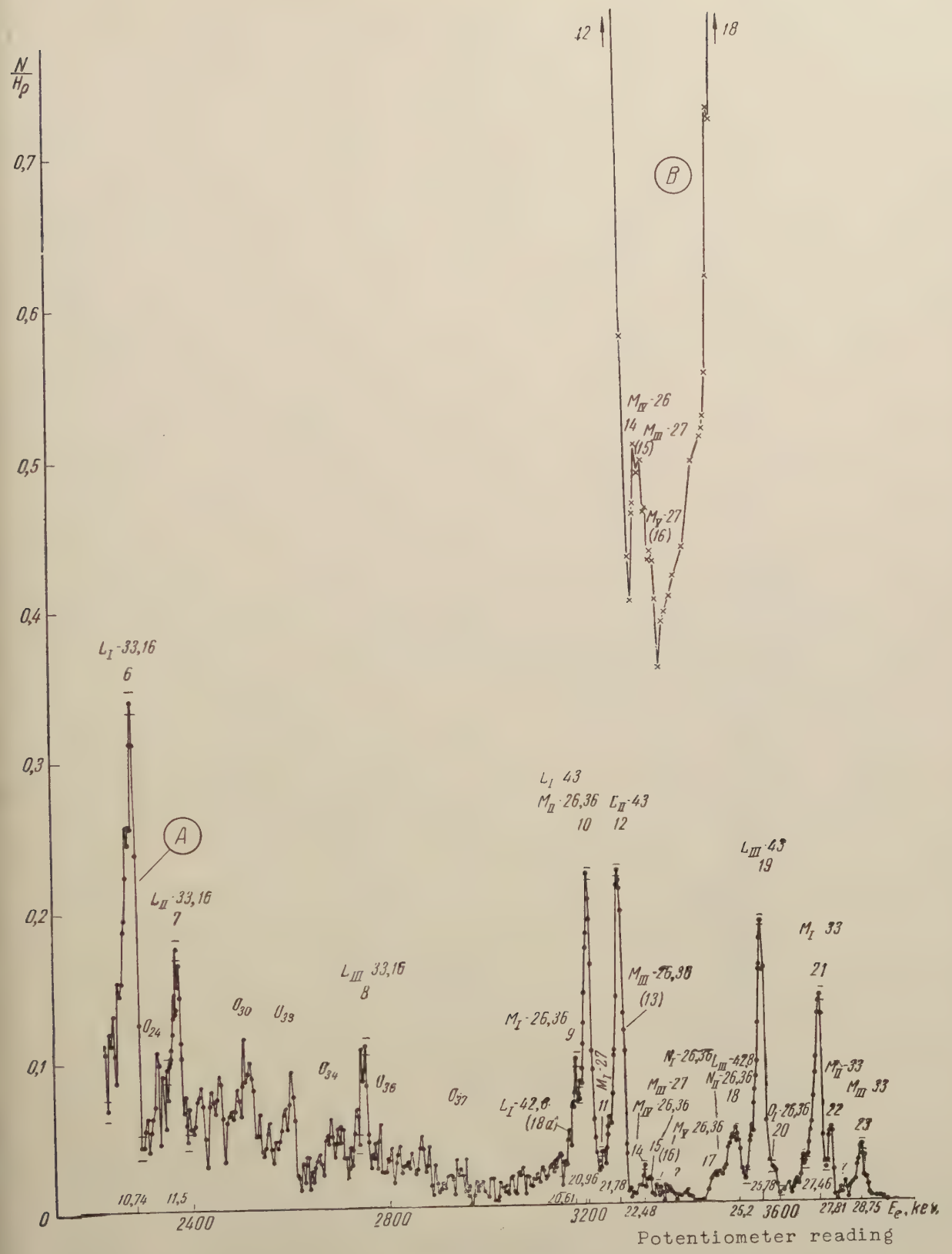

with 4 μg/cm^2 source (size 2 x 20 mm; Ω = 0.4%), B - 30 μg/cm^2 (6 x 26 mm).

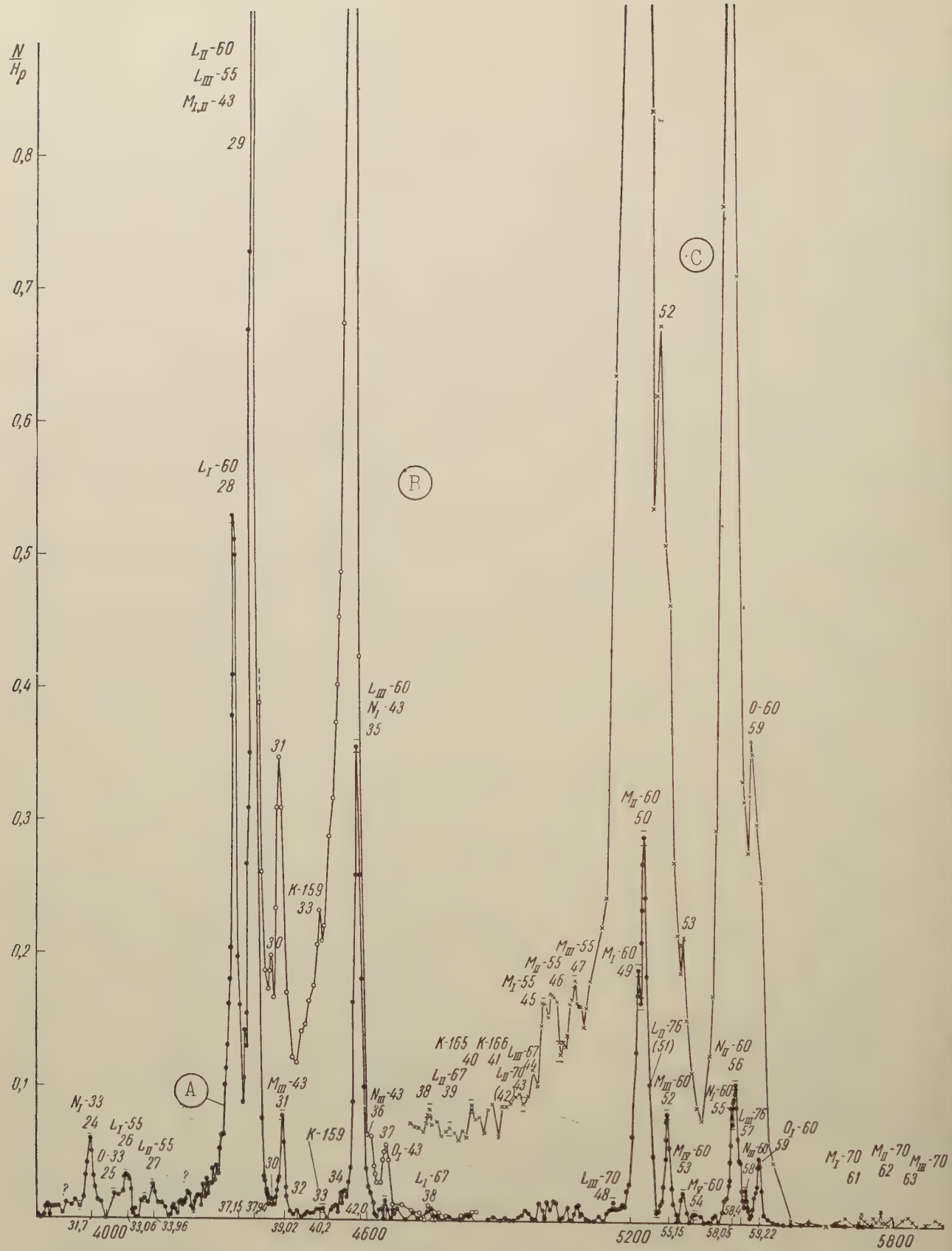

Fig.3. Electron spectrum of Am^{241} in the 35 to 100 kev region. Sources: A - 10 μg/cm² (size 2 x 20 mm; Ω = 0.4%), B - 40 μg/cm² (2 x 20 mm), C - 30 μg/cm² (6 x 25 mm), D - 60 μg/cm² (3 x 26 mm).

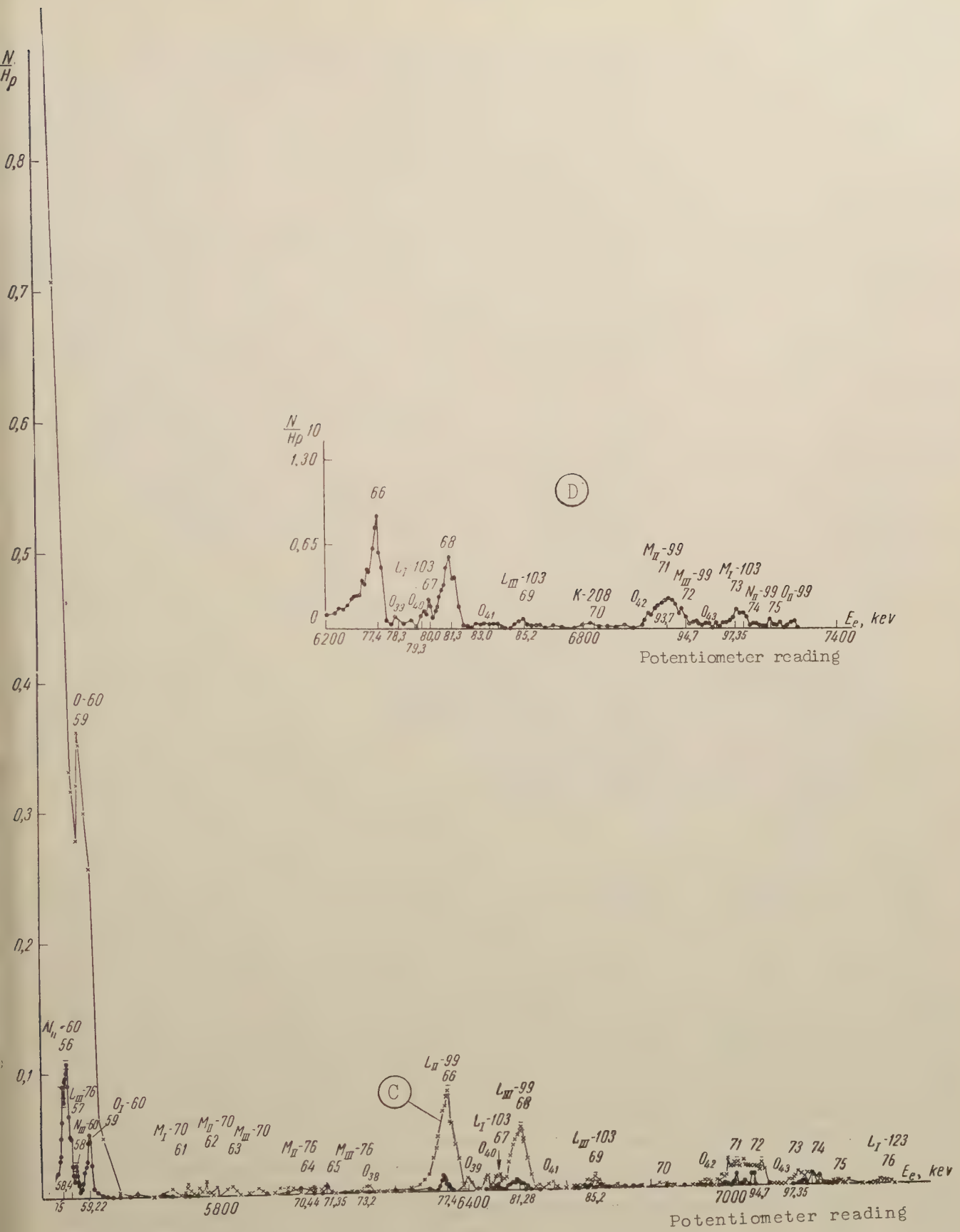

Fig. 3. Continued from opposite page.

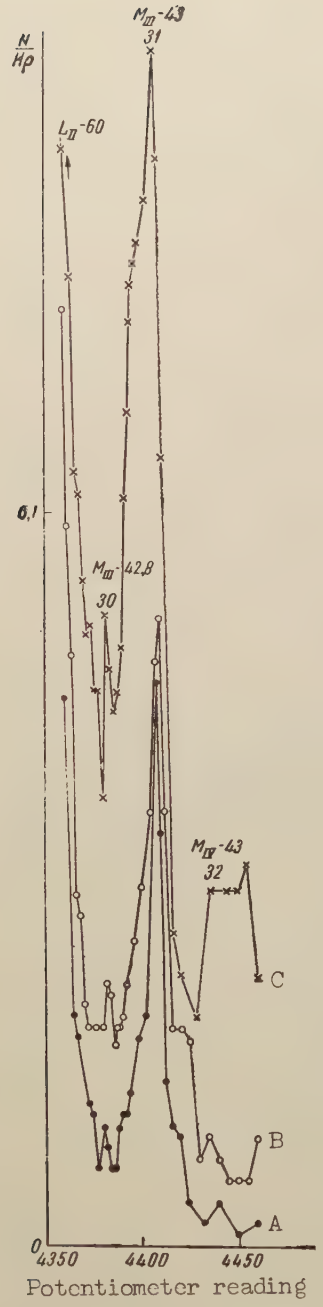

Fig.4. M_{III}-42.8 conversion line measured with sources: A - 4 μg/cm^2, source 2 x 20 mm, counter window 2 x 26 mm; B - 10 μg/cm^2, source 2 x x 20 mm, counter window 1.5 x 20 mm; C - 10 μg/cm^2, source 2 x 26 mm, counter window 2 x 26 mm.

changing the construction of the magnet, one can realize fields described by Eq.(1) with β = 1/8, 1/4, 3/8 or 3/16. This is done by means of "spatial" magnetic shims which are half-rings of Armco iron that are installed directly along the edges of the conical pole pieces and in the air gap between them (Fig.1).

Thus in the case of this spectrometer one can select the optimum conditions for measurement of electron spectra when employing sources of different size and shape. Under our conditions, for sources measuring from 1 x 15 to 15 x 30 mm the optimum field distribution was that given by Eq.(1) with β = 3/16. According to the design calculations, the given magnetic field distribution should persist in the entire range of the field strengths used in the experiment.

In investigating the low energy radiations from Am^{241}, the electron spectrum must be measured from an energy of 2-3 kev. Then, for example, with a mean electron trajectory radius r_0 = 27 cm, a field distribution of the form (1) should obtain from 6 oersted. It was established experimentally that with the given method of correction, i.e., with the shims employed, the desired field configuration obtains from a field strength of 5 oersted. By virtue of this there was obtained good reproducibility as regards the relative half-width and energy position of the electron lines in the region of low energies (see Fig.3).

The magnetic field strength was measured by the compensation method with a saturated Permalloy probe. The accuracy of measurement in the 100 oersted region was evaluated as $2 \cdot 10^{-2}$%. The spectrometer was calibrated with reference to the K conversion line of Cs^{137} (data of Siegbahn & Lindstrem[12]) and the L conversion lines of Am^{241} (data of Day[7]).

In all we carried out 23 series of measurements, using 14 different radioactive samples. Twelve of the sources were prepared on aluminum foils (6 μ thick) or celluloid films (0.05-0.2 μ thick) by evaporation. The dimensions varied from 1 x 15 to 7 x 35 mm; the thickness of the active layer from 3 to 100 μg/cm^2. Prior to applying the water solution of americium nitrate to the organic films, these were coated with a semitransparent layer of aquadag. The other two sources, which had an area of 2 cm^2 each and superficial densities of 0.26 mg/cm^2 and 1.17 mg/cm^2, were prepared by Khlebnikov[13]. By way of detectors we used Geiger-Mueller counters, the windows of which (measuring from 1 x 15 to 20 x 35 mm) were covered with celluloid film passing $\geqslant$ 2 kev electrons. Repeated recordings with an interval of up to several months between runs and measurements with sources of different origin yielded spectra with the same appearance. This gives reason to assume that all the observed electron lines belong to Am^{241}.

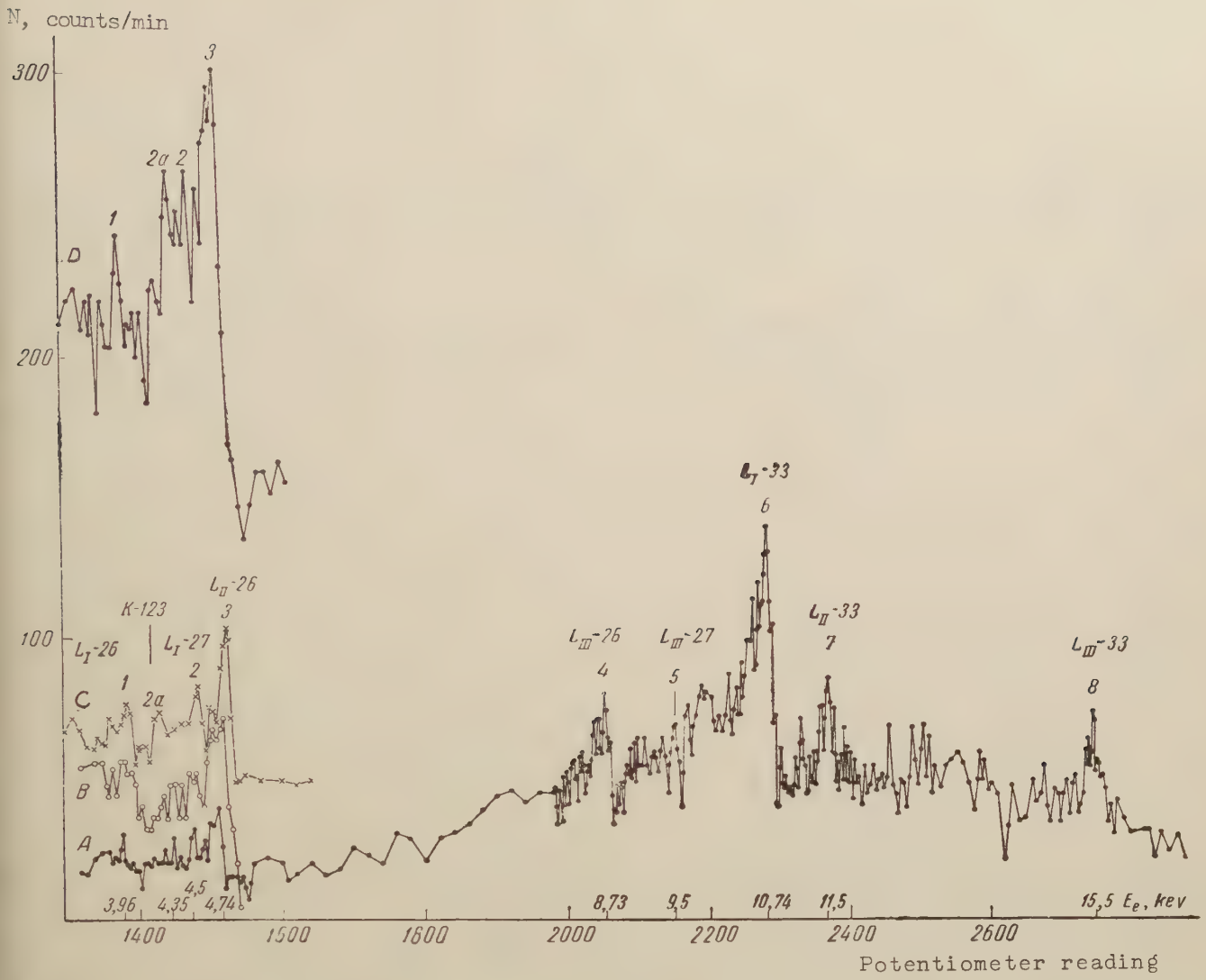

Fig.5. Low energy region of the Am^{241} electron spectrum. Sources: A - 10 μg/cm^2 (1.5 x 20 mm), B - 2 μg/cm^2 (5 x 26 mm), C - 15 μg/cm^2 (2 x 26 mm), D - 30 μg/cm^2 (6 x 26 mm).

2. Experimental Results

The experimental spectra obtained for Am^{241} are shown in Figs.2 through 6. In the 1 to 3.9 kev region the spectrum consists of strong Auger electron peaks: O_1 to O_7 in Fig.2. In the region of higher energies, in addition to the O_8 through O_{45} Auger electron lines, there appear numerous internal conversion lines (numbered from 1 through 100). The experimental results obtained for the conversion electrons from Am^{241} are summarized in Table 1; the results for Auger electrons in Table 2. In addition, for purposes of comparison, we list in Table 1 the data obtained by Baranov & Shlyagin[2], Rosenblum & Valdares[3] and Hollander, Smith & Rasmussen[14].

The electron line intensities were evaluated from their areas in the spectrum. For measuring the areas, the lines were extended to the energy axis in

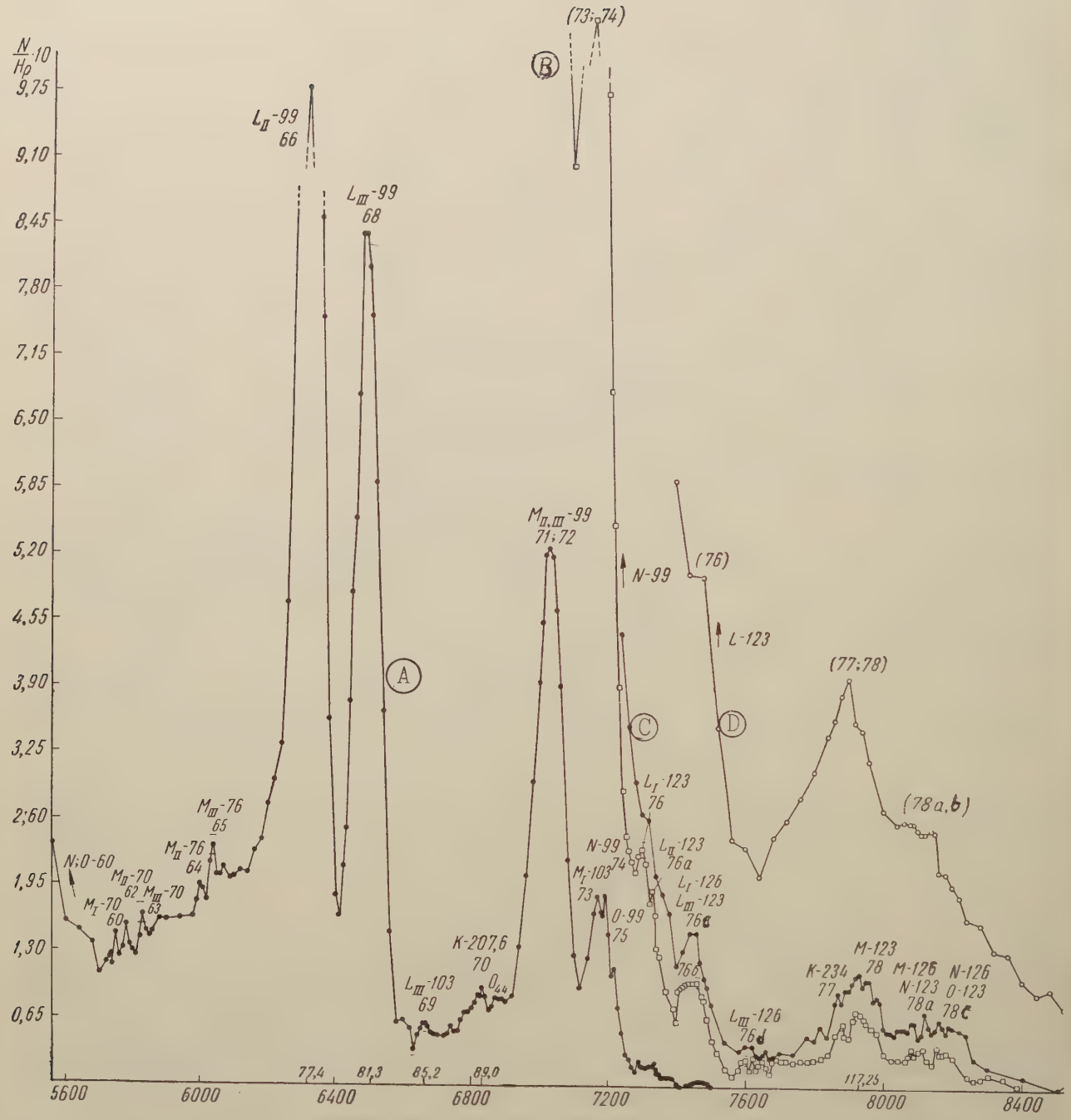

Fig.6. Sections of the electron spectrum of Am^{241} in the 100 to 400 kev region. Sources: A - 260 μg/cm^2 (size 2 cm^2, Ω = 0.4%), B - 1170 μg/cm^2 (2 cm^2, Ω = 0.4%), C - 1170 μg/cm^2 (2 cm^2, Ω = 0.4%), D - 1170 μg/cm^2 (2 cm^2, Ω = 0.6%), E - 720 μg/cm^2 (4 cm^2, Ω = 0.8%).

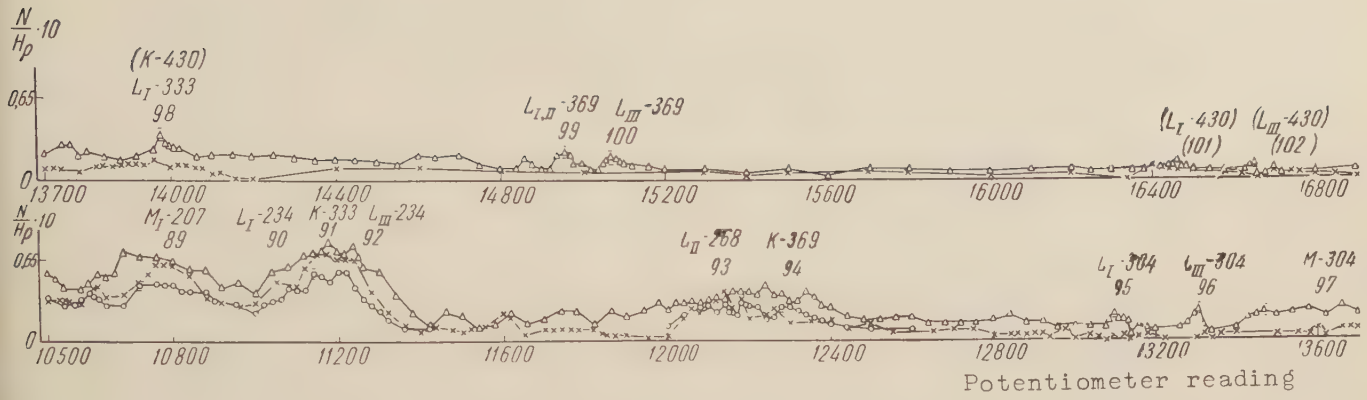

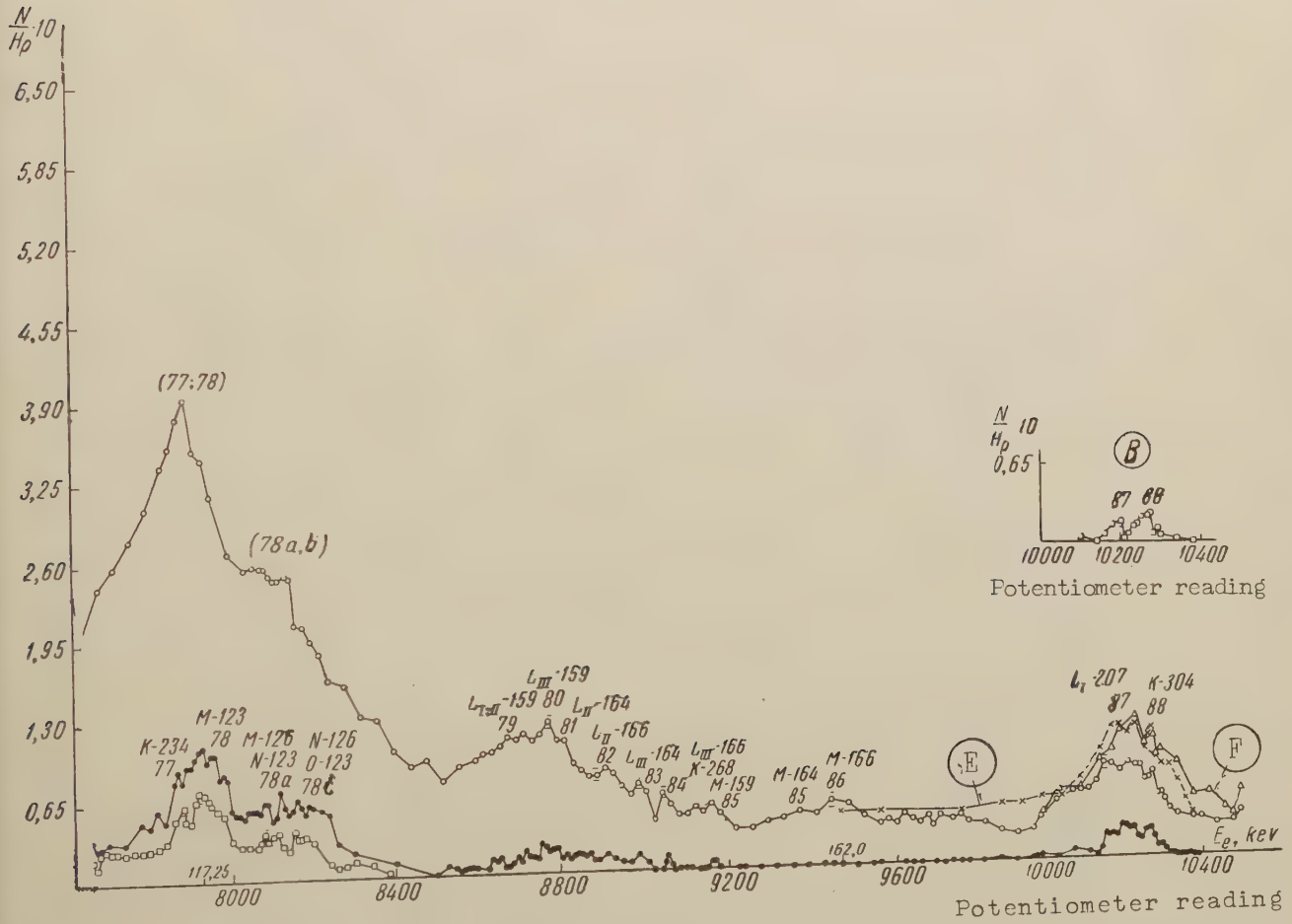

Fig. 6. Continued from opposite page.

Table 1

Experimental results obtained in investigating the conversion electron spectrum of Am^{241}

Our data					Reparted electron energies			Electron line intensity given in Ref. 2
Electron line Nos.	E_c, kev	Shell	Transition energy, kev	Relative electron line intensity	Ref. 2	Ref. 3	Ref. 14	
1	2	3	4	5	6	7	8	9
1	3,96	L_I	26,38	13,95	4,0	—	3,83	9,0
3	4,74	L_{II}	26,34	20,38	4,85	—	4,72	20,0
4	8,73	L_{III}	26,33	25,14	8,75	—	8,64	13,3
9	20,61	M_I	26,35	4,0	20,6	20,61	20,65	—
Coinc. with 10	21,00	M_{II}	26,36	(6,0)	20,98	21,05	—	16,8
Coinc. with 13	21,91	M_{III}	22,34	(7,0)	22,0	21,87	—	—
14	22,48	M_{IV}	26,33	1,6	—	—	—	—
16	22,72	M_V	26,38	1,0	—	—	—	—
17	24,83	N_I	26,33	3,0	24,84	25,00	24,88	26,0
18	25,04	$N_{II,III}$	26,36	(6,0)	—	—	—	—
20	26,03	O_I	26,38	2,0	—	—	—	—
	Average:		26,36 ($E1$)					
2	4,5	L_I	26,92	10,0	—	—	—	—
5	9,5	L_{III}	27,1	4,0	—	—	—	—
11	21,3	M_I	27,04	(3,0)	—	—	—	—
15	22,63	M_{III}	27,06	1,6	—	—	—	—
	Average:		27,03 ($M2$)					
6	10,74	L_I	33,16	55,0	10,75	10,82	10,72	50,8
7	11,55	L_{II}	33,15	17,5	11,6	11,62	11,56	11,6
8	15,5	L_{III}	33,10	11,74	15,64	15,55	15,53	12,0
21	27,46	M_I	33,2	21,57	27,52	27,46	27,4	—
22	27,81	M_{II}	33,17	5,76	27,81	27,84	27,74	34,0
23	28,75	M_{III}	33,18	5,79	28,81	28,8	28,7	—
24	31,7	N_I	33,2	8,75	31,78	31,73	31,64	11,0
25	32,75	O_I	33,11	2,6	—	32,87	32,84	—
	Average:		33,16 $M1$ (96%) + $E2$ (4%)					
18a	20,4	L_I	42,82	(2,0)	—	—	—	—
18	25,2	L_{III}	42,8	8,0	—	—	—	—
30	38,4	M_{III}	42,83	2,0	—	—	—	—
34	41,3	N_I	42,8	(2,0)	—	—	—	—
	Average:		42,81 ($M3$)					
10	20,96	L_I	43,38	33,36	21,06	21,05	20,92	39,7
12	21,78	L_{II}	43,38	31,87	21,78	21,87	21,77	32,7
19	25,78	L_{III}	43,38	31,76	25,79	25,85	25,74	25,6
Coinc. with 29	(37,64)	M_I	—	(9,0)	37,65	37,71	—	11,5
Ditto	(38,0)	M_{II}	—	(8,5)	38,05	37,98	37,95	12,2

(Table 1 continued)

1	2	3	4	5	6	7	8	9
31	38,95	M_{III}	43,38	8,5	38,98	39,05	38,98	—
32	39,52	M_{IV}	43,37	0,4	—	—	—	—
Coinc. with 35	—	$N_{I,II}$	—	(3,0)	—	—	—	—
36	42,3	N_{III}	43,38	1,5	—	42,37	42,26	—
37	43,03	O_I	43,38	1,0	43,12	43,2	43,01	2,8
	Average:		43,38 $M1$ (83%) + $E2$ (17%)					
26	33,06	L_I	55,48	5,5	33,05	33,14	33,1	4
27	33,96	L_{II}	55,56	4,8	33,98	33,99	33,87	2,8
Coinc. with 29	(38,0)	L_{III}	—	(4,8)	—	—	—	—
45	49,77	M_I	55,51	1,4	49,83	49,78	49,76	—
46	50,2	M_{II}	55,56	1,5	—	50,23	50,1	—
47	51,1	M_{III}	55,53	1,5	51,13	51,14	50,96	3,2
	Average:		55,52 $M1$ (83%) + $E2$ (17%)					
28	37,15	L_I	59,57	89,6	37,18	37,16	37,12	72,7
29	37,94	L_{II}	59,54	138,8	38,05	37,98	37,95	154,6
35	42,0	L_{III}	59,6	49,54	41,97	41,96	41,96	33,0
49	53,86	M_I	59,6	20,0	53,85	53,83	53,82	17,8
50	54,18	M_{II}	59,54	45,0	54,24	54,21	54,22	38,8
52	55,15	M_{III}	59,58	9,7	55,2	55,13	55,1	13,7
53	55,72	M_{IV}	59,57	2,3	55,84	55,74	55,68	—
54	56,04	M_V	59,7	2,0	—	—	—	—
55	58,05	N_I	59,55	6,0	58,14	58,07	58,05	14,8
56	58,24	N_{II}	59,56	13,0	—	58,25	58,22	—
58	58,6	N_{III}	59,68	2,0	—	—	—	—
59	59,22	O_I	59,56	6,3	59,26	59,31	59,2	4,2
	Average:		59,59 ($E1 + M2 + E3$)					
38	45,0	L_I	67,4	0,1				
39	45,7	L_{II}	67,3	0,1				
44	49,5	L_{III}	67,1	0,1				
	Average:		67,26 ($M3$)					
(42)	47,8	L_I	70,2	—				
43	48,5	L_{II}	70,1	0,1				
48	52,5	L_{III}	70,1	0,1				
61	64,2	M_I	69,9	0,1				
62	64,6	M_{II}	69,96	0,1				
63	65,9	M_{III}	70,3	0,1				
	Average:		70,1					
(51)	54,4	L_{II}	76,0	—				
57	58,4	L_{III}	76,0	0,1				

(Table 1 continued)

1	2	3	4	5	6	7	8	9
64	70,44	M_{II}	75,8	0,1				
65	71,35	M_{III}	75,78	0,1				
	Average:		75,9 ($E2$)					
66	77,40	L_{II}	99,0	1,26	77,73	77,37	77,26	—
68	81,28	L_{III}	98,88	0,75	81,28	81,4	81,3	—
71	93,7	M_{II}	99,06	0,4	93,36	—	93,44	—
72	94,7	M_{III}	99,13	0,2	94,32	—	94,4	—
74	97,8	N_{II}	99,12	0,1	—	—	97,7	—
75	98,98	O_{II}	99,1	0,05				
	Average:		99,05 ($E2$)					
67	80,0	L_{I}	102,42	0,074				
69	85,2	L_{III}	102,8	0,03				
73	97,35	M_{I}	103,1	0,03				
	Average:		102,8 ($M2$)					
2a	4,35	K	122,97	1				
76	100,8	L_{I}	123,22	0,05				
76a	101,6	L_{II}	123,2	0,02				
76c	105,0	L_{III}	122,6	0,05				
78	117,25	M	123,0	0,03				
78a	121,5	N	123,0	0,01				
	Среднее:		123,0 ($M3$)					
015	8,1	K	126,7	1				
76b	104,2	L_{I}	126,6	(0,02)				
76d	109,0	L_{III}	126,6	0,01				
78a	122,2	M_{III}	126,6	0,01				
78c	125,0	N	126,5	0,01				
	Average:		126,6 ($M2$)					
33	40,2	K	158,8	1,0				
79	137,8	$L_{I, II}$	159,4	0,05				
80	140,8	L_{III}	158,4	0,05				
85	152,7	M_{I}	158,4	0,03				
	Average:		158,8 ($M2$)					
40	46,5	K	165,1	0,1				
81	142,8	L_{II}	164,4	0,05				
83	147,2	L_{III}	164,8	0,05				
	Average:		164,8					

(Table 1 continued)

1	2	3	4	5	6	7	8	9
41	47,6	K	166,2	0,1				
82	145,0	L_{II}	166,6	0,05				
84	149,0	L_{III}	166,6	0,05				
	Average:		166,5					
70	89,2	K	207,8	0,04				
87	184,8	L_{II}	207,2	0,01				
89	201,6	M_I	207,3	0,01				
	Average:		207,4 ($M1$)					
77	115,8	K	234,4	0,01				
90	212,15	L_I	234,6	0,0004				
92	216,8	L_{III}	234,3	0,005				
	Average:		234,4 ($M2$)					
84	149,0	K	267,6	0,002				
93	246,8	L_{II}	268,4	0,01				
	Average:		268,0 ($E3$)					
88	185,8	K	304,4	0,01				
95	281,6	L_I	304	0,001				
96	287,5	L_{III}	305,1	0,001				
97	299	M	304,5					
	Average:		304,5					
91	214,5	K	333,1	0,004				
98	311,4	L_I	333,8	0,001				
	Average:		333,4					
94	251,0	K	369,6	0,01				
99	347,0	$L_{I,II}$	369,4	0,001				
100	351,5	L_{III}	369,1	0,001				
	Average:		369,4					
(98)	311,4	(K)	430	0,0005				
(101)	405,5	(L_I)	427,9	0,0005				
(102)	413,0	(L_{III})	430,6	0,0005				
	Average:		429,5					

accordance with the shape indicated by their upper (resolved) parts. Where a conversion line coincided in energy with an Auger line, we subtracted the intensity of the Auger line from the integral intensity of the overlapping lines. The intensity of the Auger line was assumed to be equal to the intensity of the nearest (in energy) well resolved line associated with an Auger transition of the same multipole order.

In identifying the γ-transitions we were guided by the following considerations.

26.36 kev transition

Conversion electrons associated with this transition were observed only in the work of Refs.2 & 3. In these studies, however, the conversion lines were not resolved from the Auger electron lines. In our measurements (Figs.2 & 5) the L_I, L_{II} and L_{III} conversion lines associated with the 26 kev transition are clearly separated from the Auger electron lines and the conversion lines associated with other transitions. There is virtually no background due to scattered electrons to the right of the L_{II}-26 line, which makes it possible to determine the intensity of this line with good accuracy.

The experimental relative intensity ratios for the L conversion lines (taking into account the contributions of Auger electrons to the experimental lines) are $L_I:L_{II}:L_{III}$ = 55:81:100 (according to Refs.2 & 3 the ratios are 45:100:66). Our data are in agreement with the calculated values $L_I:L_{II}:L_{III}$ = 50:85:100 given by Dranitsyna[16] for an E1 transition.

Among the M conversion lines of this transition, in addition to the M_I-26 line detected by all the above mentioned investigators, we observed the M_{IV} and M_V lines. The intensities of the M_{II} and M_{III}-26 lines, which are masked by the more intense L_I- and L_{II}-43 lines, were determined from the intensity of the M_I-26 line and the theoretical ratios $M_I:M_{II}:M_{III}:M_{IV}:M_V$ = 0.6:0.8:1.0:0.47:0.55, given by Rasmussen, Canaven & Hollander[5] in accord with the theoretical data of Rose for an E1 transition. The experimentally observed relative intensities of the M conversion lines (Table 1) are in qualitative agreement with the cited theoretical data of Rose for an E1 transition.

We attributed the Nos.17 and 18 lines to conversion of the 26 kev γ-rays on the N subshells. Specifically, we interpret line 17 as the N_I-26 line. The intensity of line 18 exceeds the intensity of the M conversion lines; this is explained by the fact that in addition to the N_{II} and N_{III} lines a large contribution to the area of line 18 is made by the L_{III} conversion line of the 42.8 kev γ-transition (see below). The intensity of the $N_I + N_{II}$ line was determined from the intensity of the N_I-26 line and the theoretical $N_I:(N_{II} - N_{III})$ ratio which was assumed to be equal to the $M_I:(M_{II} + M_{III})$ ratio.

27 kev transition

The electron conversion spectrum (Figs.2 & 5) includes lines at 4.5, 9.5, 21.3 and 22.53 kev. There are no strong Auger electron groups from Np^{237} with these energies. Moreover, these lines cannot be attributed to contamination or other spurious causes inasmuch as they were observed in five series of measurements (Fig.5) carried out with different sources and counters. In view of their energy values, we infer that these lines are the L_I, L_{III}, M_I and M_{III} conversion lines of a 27 kev transition. In view of the relative intensity L_I/L_{III} = = 3 and the absence of an L_{II} line it must be assumed that the 27 kev transition is M2.

33.16 kev transition

The relative intensities of the L_I, L_{II} and L_{III} lines were determined taking into account the contribution of corresponding Auger electron groups. The experimental values of the L and M subshell conversion ratios were found to be $L_I:L_{II}:L_{III}$ = 4.6:1.4:1 and $M_I:M_{II}:M_{III}$ = 3.7:1:1; the M/L ratio therefore equals 0.3.

Baranov & Shlyagin[2], Rosenblum & Valadares[3] and Hollander, Smith & Rasmussen[14] report the following L subshell conversion ratios: 4.2:1:1, 4:1:1, and

3:1:1, respectively. It is apparent from the spectrum given by Baranov & Shlyagin that the lower (as compared with ours) values of the L_I and L_{II} line intensities obtained by these investigators may be attributed to the fact that they did not take into account the scattered electron background with adequate accuracy. On the basis of the L subshell conversion ratios all the cited investigators infer that the 33 kev γ-radiation is of mixed multipolarity: M1 + E2. According to our data, if one accepts the theoretical ICC values of Sliv & Band[17], the mixture is 96% M1 and 4% E2. As for the M/L ratio, as was shown by Listengarten[18] on the basis of analysis of experimental data, the M/L ratio is in the neighborhood of 0.3 for M1 and E2 multipoles in a wide energy range.

42.8 and 76 kev transitions

In his Coulomb excitation experiments, Newton[8] detected in Np^{237} an excited level at 76 kev and γ-transitions of 42.8 and 76 kev energy. In our work the 42.8 kev γ-transition was identified from the corresponding L_I, L_{III} and M_{III} lines. The L_{III}-42.8 line coincides in energy with the N_{II}-26.36 line. Hence as was noted above, the intensity of the L_{III}-42.8 line was determined as the difference between the integral intensity of the No.18 line and the $N_{II,III}$-26.36 line. The M_{III}-42.8 line is partially masked by the strong L_{II}-60 and M_{III}-43.4 lines. However, in repeated measurements of this section of the spectrum with different sources the M_{III}-42.8 line was invariably evinced (see, for example, Fig.4 and curve B in Fig.3).

As for the 76 kev γ-transition, in the work of Newton it was less definitely identified than the 42.8 kev transition. In our measurements this γ-transition is evinced only by the weak M_{II}- and M_{III}-76 conversion lines; the L-76 lines are masked by the strong M_{II}-60 and N_{II}-60 lines.

43.48 and 55.52 kev transitions

All the authors that have observed the 43.4 and 55.5 kev γ-transitions have characterized them as M1 + E2. According to our data, the mixture is 83% M1 and 17% E2. It is interesting to note that the M_{III}-43.4 line is some 22 times stronger than the M_{IV}-43.4 line.

59.57 kev transition

In five series of measurements, the L_I, L_{II} and L_{III} conversion lines of the 59.57 kev transition were almost fully resolved with complete absence of a background due to scattered electrons. From these measurements we found $L_I:L_{II}:L_{III}$ = = 1.8:2.9:1.0. In determining the intensity of the L_{II} line we took into account the contribution of the M_I-43, M_{II}-43 and L_{III}-55 lines to the area of line No.29. The intensities of the first two lines were assumed to be equal to the intensity of the M_{III}-43 line which was fully resolved from the L_{II}-60 line, while the intensity of L_{III}-55 line was assumed to be equal to the intensity of the L_{II}-55 line.

The $L_I:L_{II}:L_{III}$ internal conversion ratios reported in Refs.2,3,14 & 18 are 2.2:4.7:1, 1.7:3.3:1, 1.5:3.3:1 and 2.4:4.7:1, respectively. There is the obvious question of why the data of different investigators on these ratios diverge so greatly and which of the values is closest to the true one. To answer this question we deliberately created experimental conditions under which there were obtained results close to some of the cited ratios. It was found that higher than our normal intensity values for the L_I and L_{II} lines, i.e., values approximating those of Baranov & Shlyagin[2] and Canaven[19], are obtained when one uses a

narrow source with a large superficial density, that is, when the L_I and L_{II} lines are poorly resolved and appear against a strong scattered electron background. In the work of Rosenblum & Valadares[3] the L_I and L_{II} conversion lines were well resolved but were also observed against so strong a background of scattered electrons that it was difficult to evaluate the contribution of extraneous lines to the L_{II}-60 line. Obviously, if the background is not properly subtracted the intensity value obtained for this line will be an overestimate. We believe that our evaluations are free of the above shortcoming.

According to the theoretical data of Sliv & Band[17], the relative conversion ratios for an E1 60 kev γ-transition are $L_I:L_{II}:L_{III} = 0.125:0.105:0.10$. It will be apparent that the experimental values of $L_I:L_{II}:L_{III}$ obtained in all the above mentioned investigations do not correspond to the theoretical values for pure E1. Jaffe et al[20] found that the L conversion coefficient for the 60 kev transition equals 0.72 ± 0.07, whereas for a pure E1 transition the coefficient should be 0.32. Thus the experimental data indicate that the 60 kev transition is not a pure electric dipole one.

The relative M-subshell conversion coefficients according to our data are $M_I:M_{II}:M_{III}:M_{IV}:M_V = 2.1:4.5:1:0.25:0.1$. From five series of measurements we found $(M_I + M_{II}):M_{III} = 6.4 \pm 0.2$, which is appreciably greater than the value $(L_I + L_{II}):L_{III} = 4.6$. The M/L ratio according to Listengarten[18] should be equal to approximately 0.3. In this case it is actually equal to 0.35.

According to our data, $N_I:N_{II}:N_{III} = 3:6.5:1$. The ratio $(N_I + N_{II}):N_{III} = 9.5$; it is appreciably greater than the corresponding ratios for the L and M subshells. The N/M ratio equals 0.26 which is in agreement with the data of Listengarten[18].

67 kev transition

Rosenblum & Valadares[3] observed a weak line at 45.3 kev in the electron spectrum of Am^{241}. They advance two interpretations: either this line belongs to Pu^{239}, an admixture of which was present in their source, or it is a conversion line of a 67 kev transition. We observed three conversion lines - 45.0, 45.7 and 49.5 kev - which we attributed to a 67 kev transition. In view of the fact that this γ-transition was not observed in the γ-spectrum and is weakly converted on the L_{II} subshell, it may be assumed that it is M3.

70 kev transition

There are no data in the literature on a 70 kev transition. We observed very weak (Fig.3) conversion lines - Nos.43, 48, 61, 62 and 63 - in several series of measurements. We attributed these lines to a 70 kev transition. The accuracy in determining the energies of these lines, however, is low. Hence the mean value for the transition energy deduced from the conversion lines diverges by 0.45 kev from the energy difference between the levels linked by this transition.

99.1 kev transition

The 99.1 kev radiation is the weakest radiation observed in earlier studies. From several series of measurements (curves B and C in Fig.3 and curve A in Fig. 6) we obtained the ratio $L_{II}:L_{III} = 1.68:1$, which is in agreement with the theoretical data of Sliv & Band[17] for an E2 transition.

102.8 kev transition

There is no information in the literature on conversion electrons associated with this transition. Where γ-ray studies are concerned, its existence is most convincingly demonstrated in the work of Magnusson[21]. We identified this transition from its L_I, L_{III} and M_I lines located at 80.0, 85.2 and 97.35 kev, respectively. The L_{II}-103 conversion line was not detected. The experimental value of $L_I:L_{III} = 2.5:1$ is closest to the theoretical ratio for an M2 transition. We note that the conversion lines of this transition were well resolved from the close K - LL type Auger electron lines.

123 and 126.6 kev transitions

There are no data in the literature on a 123 kev γ-transition. Jaffe et al[20] and Magnusson[21] report the existence of a ~128 kev transition. We attribute the Nos.2a, 76, 76a, 76c, 78 and 78a lines (Fig.6) observed in our experiments to a 123 kev transition. The 76c line has a very wide peak. This is apparently due to the fact that the L_{III} line of the 123 kev transition is not completely resolved from the L_I line of the 126.6 kev transition (line No.76b in Fig.6); both Jaffe et al and Magnusson have definitely established the existence of a transition of this energy. We also attributed lines Nos.76d, 78a and 78c (Fig.6) to the 126.6 kev transition. Judging from the relative intensity of the L conversion lines (Table 1) it may be inferred that the 123 kev transition is M3 and the 126.6 kev transition is M2.

158.8 kev transition

A cross-over transition from the 159 kev level to the ground state of Np^{237} was observed by Day[7] and Magnusson[21]. They did not detect conversion electrons associated with this radiation. We observed electron lines Nos.33, 79, 80 and 85 which we attribute to a 158.8 kev γ-transition. The K conversion line (No.33) was clearly evinced in all the measurement series. The L and M conversion lines are very weak lines and are poorly resolved from the conversion lines of the 164 and 166 kev transitions (Fig.6).

164.7 and 166.5 kev transitions

The weak 47.6 kev electron conversion line observed by Rosenblum & Valadares[3] was attributed by them to a γ-transition of 166 kev energy. Magnusson[21] detected a γ-transition of this energy. We observed two weak electron lines - Nos.40 and 41, Table 1 and curve B in Fig.3 - which we identified as the K conversion lines of 164.7 and 166.5 kev γ-transitions, respectively. The L conversion lines of these transitions are even weaker: we could observe them only in the experiments with the source having an area of 2 cm^2 and a superficial density of 1.17 mg/cm^2 (curve D in Fig.6).

We note that according to our data the intensities of the K conversion lines of the 158.8, 164.7 and 166.5 kev transitions exceed the intensities of the corresponding L lines by a factor of more than 10. In view of the low intensity of the conversion line, however, it is impossible to make a multipole order assignment for these γ-transitions.

207.8, 234.4 and 268 kev transitions

Gamma-radiation of 268 kev energy was observed by Day[7]. There is no data in the literature on 234 kev γ-rays. On the other hand, 208 kev γ-radiation has

been reported by a number of investigators (Refs.7, 21, 22 & others). Wagner et al[22] and later other investigators identified it as M1. According to our data, for it K/L = 4 which is characteristic of magnetic dipole radiation. The L conversion line (No.87) of this γ-transition almost coincides with the K-304.4 kev line. But in Fig.6 (curve B) these lines are fairly clearly resolved.

We identified a 268 kev transition on the basis of very weak lines which were observed in measurements with a 2 cm^2 source (thickness 1.17 mg/cm^2) and a counter with a 20 x 30 mm entrance slit. Because of this, the K and L conversion lines of the 268 kev transition are poorly resolved from the L_{III}-66 and K-369 conversion lines. Inasmuch as for this transition K/L = 1/5 and no L_I and L_{III} conversion lines of noticeable intensity were detected, it may be assumed that it is E3.

We attributed lines Nos.77, 90 and 92 to a transition of 234 kev energy. In spectrum B of Fig.6, the K-234 line is fairly well resolved from the M-123 line. In view of the poor resolution of the L conversion lines, however, we were unable to make a multipole order assignment for the 234 kev transition.

304.4 kev transition

Gol'din et al[6] observed a low intensity (~0.002%) α-particle group in the radiation from Am^{241}, corresponding to a level at 305 kev in Np^{237}. Neither γ-rays nor conversion electrons associated with this group of α-particles were detected. We observed electron lines at 185.8, 281.6, 287.5 and 299 kev, which we attributed to a transition from the 304.4 kev level to the ground level of Np^{237}.

333.4 and 369.4 kev transitions

In the experiments with sources having an area of 4 cm^2 and a superficial density of 0.720 mg/cm^2 (the solid angle of the spectrometer in this case was 0.8% of 4π), we detected the very weak lines designated Nos.91, 94, 98, 99 and 100 (Fig.6), which we interpreted as the conversion lines of 333.4 and 369.4 kev γ-transitions. These weak γ-transitions in Np^{237} were observed only in β-decay of U^{237} (Refs.4 & 5).

Other gamma- and Auger transitions

In addition to the electron lines attributed to the γ-transitions mentioned above, there were observed in the high energy region of the spectrum two extremely weak lines (101) and (102) (Table 1 and Fig.6), and in the region of low energies the strong lines identified as O_1, O_4, O_{20}, O_{30}, O_{33}, etc.

Possibly the (101) and (102) lines are the L conversion lines of a ~430 kev transition. That there exists a level of about this energy in Np^{237} is indicated by Baranov & Shlyagin[4] and Wagner et al[22]. The strong electron lines in the low energy region are apparently the result of surposition of a number of close groups of Auger electrons. At present, in view of the lack of theoretical data on the intensity of Auger transitions, it is not possible to interpret all the Auger electron lines. The interpretation of some of the K - LL and K - LM type transitions is given in Table 2. The energy of the Auger electrons taking into account ionization of the atom is taken from the work of Rasmussen et al[5] and Beling et al[23]. As will be evident from Table 2, among the K - LL Augers there were not detected only electrons of the K - $L_{II}L_{II}$ group although there is no evidence that this group may be masked.

Table 2

Interpretation of some of the Auger electron lines in the spectrum of Am^{241}

Peak No.	E_e, kev	Transition	Electron energy, kev (Ref. 15)	Auger line intensity*
$O_1 - O_9$	1—5,06	$M_i - N_j N_k$		
		$M_i - N_j O_k$		
		$M_i - O_j O_k$		
$O_{10} - O_{36}$	6—15,8	$L_i - M_j M_k$		
		$L_i - M_j N_k$		
O_{37}	16,1—20,8	$L_{II} - M_{IV} N_{II}$		
		$L_{I,II} - N_j N_i$		
		$L_{I,II} - O_j N_i$		
		$L_{I,II} - O_j O_i$		
O_{38}	73,2	$K - L_I L_I$	73,41	
		$K - L_I L_{II}$	74,24	0,034
O_{39}	78,3	$K - L_I L_{III}$	78,26	0,075
O_{40}	79,3	$K - L_{II} L_{III}$	79,04	0,067
O_{41}	83,0	$K - L_{III} L_{III}$	83,06	0,053
O_{42}	90—93	$K - L_{I,II} M_{I,II}$	≈92,0	0,05
O_{43}	94—96	$K - L_{III} M_{III-V}$	≈96,0	0,027
O_{44}	90,5	$K - L_I M_I$	90,5	0,01
O_{45}	107—111,3	$K - M_i M_j$	110	0,01

*Intensities given in the same arbitrary units as for the conversion electron lines.

3. Discussion

Am^{241} decay scheme and Np^{237} level diagram

The decay scheme for Am^{241} including all the experimental data published up to 1958 is given in Seaborg's Table of Isotopes[24]. This scheme shows the following nine γ-transitions: 26, 33, 42.8, 43.4, 55, 60.76, 99 and 103 kev. There are no reports in the literature regarding previous observation of conversion electrons associated with the 42.8, 76 and 103 kev γ-transitions. We substantiated the existence of these transitions in our conversion electron measurements.

We also demonstrated the existence of transitions of 127, 159, 208, 166 and 268 kev energy, which had hitherto only been observed in studies of the γ-radiation accompanying the decay of Am^{241}.

In addition to substantiating the above enumerated transitions, we infer the existence of the following γ-transitions: 27, 67, 70, 123, 164.7, 234, 304.4, 333 and 369 kev. The 27, 76 and 42.8 kev transitions indicate the presence of a level at 76 kev which has hitherto been observed only in Coulomb excitation; this is presumably the second excited level of the ground state rotational band[25]: 0(5/2+), 33(7/2+) and 76(9/2+). The 67, 123 and 166.5 kev transitions substantiate the existence of a level at 226 kev, the existence of which has hitherto been known only from the α-spectrum of Am^{241}. [3,6]

The 304.4 kev transition is further evidence in favor of the 304 kev level, first also established from the α-spectrum of Am^{241} by Gol'din et al[6] and assumed to be the upper excited level of the rotational band: 60(5/2-), 103(7/2-), 159(9/2-), 226(11/2-) amd 304(13/2-).

The presence of the 208, 234 and 268 kev and the 42.8 and 76 kev γ-transitions is evidence of the existence in Am^{241} decay of low intensity (~0.004%) α-particle groups with energies of 5273 and 5464 kev. Further, the 333 and 369 kev levels indicate the existence of α-particle groups with energies of 5208 and 5172 kev and an intensity <0.001%.

The decay scheme for Am^{241} amplified on the basis of our experimental data is shown in Fig.7. The multipole orders that we regard as not firmly established are given in parentheses.

Let us briefly consider the multipolarity of the 26 and 60 kev transitions. Beling, Newton & Rose[23] established that the 26.3 kev γ-radiation is electric dipole (E1). However, the relative L subshell conversion coefficients of the 26 kev transition according to the data of Baranov & Shlyagin[2] and Rosenblum & Valadares[3] are not in agreement with the theoretical values of the conversion coefficients for an E1 transition. Nilson & Rasmussen[26] consider the ICC of this

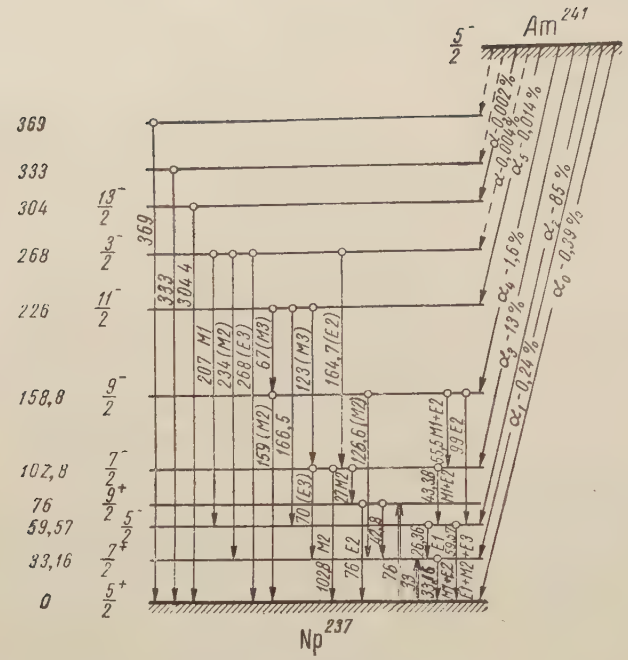

Fig.7. Am^{241} decay scheme and levels of Np^{237}.

transition to be anomalous and explain the anomaly as being due to the effect of finite nuclear size on internal conversion[27]. As follows from our experimental data for the 26 kev γ-transition, the relative L subshell conversion coefficients are in agreement with the values for pure E1. The anomalous values reported by Baranov & Shlyagin and Rosenblum & Valadares may be explained by the fact that owing to inadequate resolution these investigators included in the intensity of the L_{II}-26 conversion line the L_I and K conversion lines of the 27 and 123 kev transitions, the existences of which was not known prior to the present study.

The existence of the 27 and 123 kev γ-transitions cannot be regarded as definitively established. However, as will be apparent from the electron spectrum, lines Nos.2 (L_I-27) and 2a (K-123) are not associated with the 26 kev transition. Hence the internal conversion coefficient of the 26 kev transition is not anomalous and this case cannot be regarded as substantiation of the effect of nuclear structure on internal conversion coefficients.

We note that Grechukhin[28] in his work considered the influence of nuclear structure on the internal conversion coefficients of forbidden M1 transitions and showed that the contribution from finite nuclear size can be substantial only when the conditions of the single-particle model are rigorously fulfilled. An admixture (to the single-particle wave functions) of functions of other configurations with an amplitude of the order of or greater than 2% leads to ICC values independent of the nuclear structure.

In the case of E1 transitions the requirements as regards "purity" of the model are more exacting. In this case, apparently, there is no rigorous conservation of the model "purity".

As regards the 60 kev transition, our experimental values of the relative conversion coefficients of this transition, although they differ from the theoretical values for an E1 transition, are nevertheless appreciably smaller than the values given in Refs.2,3,14 & 19. It must be noted, however, that neither our results nor those of other investigators can be explained, as was suggested by Rosenblum & Valadares[3] by a mixture of E1 + M2 + E3, if one does not take into account interference between multipoles in converted transitions.

Possibly, if interference between the multipoles E1, M2 and E3 is taken into account, one can explain our experimental $L_I:L_{II}:L_{III}$ ratios. It is also not impossible that in this case, when the 90 kev transition is not a pure E1 transition, the reason for the anomalous values of the conversion coefficients, as was suggested by Nilson & Rasmussen[26], is the effect of nuclear structure on internal conversion.

I desire to express my deep gratitude to D.V.Timoshuk and P.E.Spivak for valuable advice, D.P.Grechukhin and M.A.Listengarten for discussion of the results

and M.F.Karmalys and L.E.Morozova for assistance in the work.

References

1. G.D.O'Kelley, Univ. of Calif. Radiation Laboratory Report, UCRL, 1243 (1951).
2. S.A.Baranov & K.N.Shlyagin, Conference of the Acad. of Sciences of the USSR on the Peaceful Uses of Atomic Energy, 1-5 July, 1955, M., 1955. (Trans. Consultants Bureau, N.Y. 1955.)
3. S.Rosenblum & M.Valadares, J.phys.et radium, 18, 609 (1957).
4. S.A.Baranov & K.N.Shlyagin, Zhur.eksp.i teor.fiz., 30, 225 (1956). (Trans. Soviet Physics - JETP.)
5. J.O.Rasmussen, F.L.Canaven & J.M.Hollander, Phys.Rev., 107, 141 (1957).
6. L.L.Gol'din, E.F.Tret'yakov & G.I.Novikova, Conf. of the Acad. of Sci. of the USSR on the Peaceful Uses of Atomic Energy, 1-5 July, 1955, M., 1955. (Trans.Consultants Bureau, N.Y., 1955.)
7. P.P.Day, Phys.Rev., 97, 689 (1955).
8. J.O.Newton, Nuclear Physics, 5, 218 (1958).
9. P.S.Samoilov, PTE, No.6 (1959). (Trans.Instruments & Exper.Techniques.)
10. P.P.Pavinskii, Izv.AN SSSR, Ser.fiz., 18, 175 (1954).
11. V.R.Saulit, Ibid., 18, 227 (1954).
12. K.Siegbahn & Lindstrem, Proc.Phys.Soc., 66, 397 (1956).
13. G.I.Khlebnikov & E.P.Dergunov, Atomnaya energiya, 4, 376 (1958). (Trans. Soviet Journal of Atomic Energy.)
14. J.M.Hollander, W.G.Smith & J.O.Rasmussen, Phys.Rev., 102, 1372 (1956).
15. I.Bergström & R.D.Hill, Arkiv.Fys., 8, 21 (1954).
16. G.F.Dranitsyna, Koeffitsienty vnutrennei konversii na podobolochkakh (Coefficients of internal conversion on subshells), M.-L., 1957.
17. L.A.Sliv & I.M.Band, Tablitsa koeffitsientov vnutrennei konversii γ-izlucheniya (Table of internal conversion coefficients), Part II, L shell, M.-L. 1958.
18. M.A.Listengarten, Izv.AN SSSR, Ser.fiz., 22, 759 (1958). (Trans.Bulletin 22, No.7, 755.)
19. F.L.Canaven, Unpublished results cited in Ref.14.
20. H.Jaffe, T.O.Passell, C.I.Browne & I.Perlman, Phys.Rev., 97, 142 (1955).
21. L.B.Magnusson, Phys.Rev., 13, 161 (1957).
22. J.F.Wagner, J.M.S.Freedman, D.W.Engelkemeir & J.R.Nuizenga, Phys.Rev., 89, 500 (1953).
23. J.K.Beling, J.O.Newton & B.Rose, Phys.Rev., 87, 670 (1952).
24. D.Strominger, J.M.Hollander & G.T.Seaborg, Table of Isotopes, Revs.Mod. Phys., 30, 585 (1958).
25. A.Bohr & B.R.Mottelson, Phys.Rev., 90, 717 (1953).
26. S.Nilson & J.Rasmussen, Nucl.Phys., 5, 617 (1958).
27. E.Church & J.Weneser, Phys.Rev., 104, 1382 (1956).
28. D.P.Grechukhin, Zhur.eksp.i teor.fiz., 33, 183 (1957). (Trans.Soviet Physics - JETP.)

POSITRON SPECTRUM OF THE LUTETIUM FRACTION FROM THE SPALLATION PRODUCTS OF TANTALUM

- B.S.Dzhelepov, O.E.Kraft & E.B.Kreshtofova

The positron spectrum of the lutetium spectrum obtained by chromatographic separation of the lutetium from the other rare earths produced by bombardment of tantalum with 660 Mev protons was investigated on a triple-focusing β-spectrometer[1]. The thin active layer was deposited on a 5 μ aluminum foil.

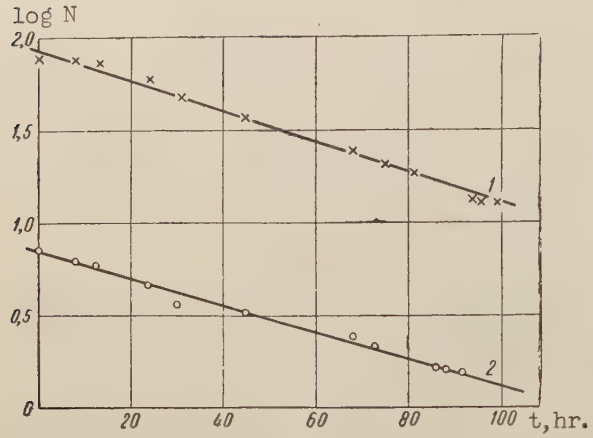

Fig.1. Determination of the decay periods of the lutetium spectra: 1) T = 35 ± 4 hours (low energy spectrum, 2) T = 45 ± 5 hours (high energy spectrum).

We began to study the positron spectrum some 10-12 hours after irradiation of the tantalum. Observations over a period of 200 hours showed that the β^+-spectrum of the fraction actually consisted of two spectra with end-point energies 2440 ± 100 and 1200 ± 70 kev and characterized by different decay periods. For the purpose of more accurate determination of the periods of the responsible activities, intensity measurements at two energies, namely, E_1 = 530 and E_2 = 1650 kev, were continued over a period of 100 hours. The resultant plots are shown in Fig.1. The half-life corresponding to the high energy component proved to be 45 ± 5 hours. No positrons of this energy belonging to long-lived lutetium isotopes (for example, 8-day) were detected. The Kurie plot for the high energy spectrum is shown in Fig.2. This spectrum was extrapolated into the region of low energies assuming a Fermi shape. After this the soft spectrum for each series of measurements was obtained by subtracting the hard component from the total β^+-spectrum: it was found that the low energy spectrum falls off in intensity with a period of 35 ± 4 hours. The Kurie plot for the soft spectrum is shown in Fig.3, from which it will be apparent that this spectrum is complex and consists of two components with energies of 1200 ± 70 and 350 ± 100 kev and relative intensities of 100 and 17. The end-point energy and relative intensity of the 350 kev component could be evaluated only approximately inasmuch as in this energy range the corrections for scattering are appreciable.

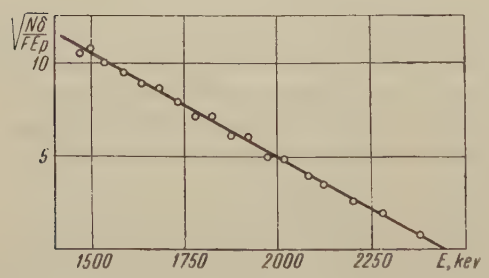

Fig.2. Kurie plot for the high energy component of the β^+-spectrum (T≈ 45 hrs).

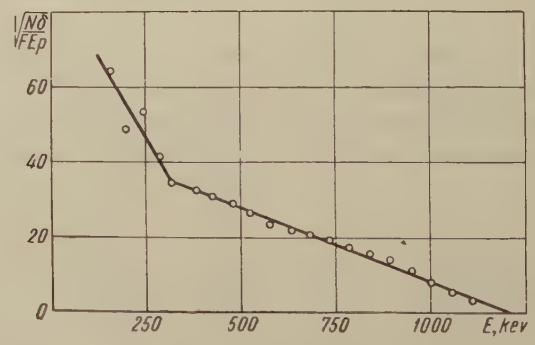

Fig.3. Kurie plot for the low energy component of the β^+-spectrum (T ≈ 35 hrs)

Among the known lutetium isotopes two - Lu^{169} and Lu^{170} - have a period of about 2 days.[2] Despite the appreciable uncertainty in determining the periods, we can safely assert that the observed positrons belong to two different isotopes. We infer that the positron spectrum with end-point energy 1200 kev and a period of 35 hours belongs to Lu^{169} and that the high energy spectrum with end-point energy 2440 and T = 45 hours belongs to Lu^{170}. These deductions are based on the following considerations.

1. According to the mass evaluations given by Levy[3], the Lu^{169} - Yb^{169} mass difference equals 1.9 Mev, while the Lu^{170} - Yb^{170} mass difference equals 2.9 Mev. According to Cameron's semi-empirical formula[4], the corresponding mass differences are 1.9 and 3.5 Mev. If we assume that the β^+-decays of Lu go to the ground levels of the corresponding Yb isotopes, then according to our data the Lu - Yb mass differences are 1.200 + 1.022 = 2.222 Mev $\approx$ 2.2 Mev and 2.440 + 1.022 = = 3.462 $\approx$ 3.5 Mev.

The uncertainty in determining mass differences by means of the semi-empirical formulas is approximately 0.5 Mev. Thus it would appear more probable that the β^+-spectrum with E_{ep} = 2.44 Mev and T $\approx$ 45 hours pertains to Lu^{170}, and the positron spectrum with E_{ep} = 1.2 Mev and T $\approx$ 35 hours pertains to Lu^{169}.

2. In measuring the Lu positron spectrum we observed an appreciable variation of the relative intensities of the hard and soft components depending on the time Δt between bombardment of the Ta and separation of the fraction. For Δt = = 10-12 hours the hard β^+-spectrum amounted to 1/3 the soft one, whereas for Δt = = 1.2-2 hours this fraction was appreciably smaller, namely, 1/6 (the time between bombardment and measurement in both cases was the same: 15-20 hours). This difference becomes understandable if, in accord with the decay schemes of Dzhelepov & Peker[5], we accept that the Lu^{170} appears (if only partially) as a result of decay of Hf^{170}, which has a period of 112 min. In this case the amount of Lu^{170} in the lutetium fraction will depend on the time of separation from the bombarded target. If the separation is carried out 1.5-2 hours after bombardment, it will obviously contain relatively less Lu^{170} inasmuch as by this time only half the Hf^{170} will have disintegrated. On the other hand, if the separation is carried out 12 hours after bombardment virtually all the Hf^{170} will have decayed to Lu^{170}. Hf^{169} is not known; if it exists, it probably has a very short half-life and disintegrates completely to Lu^{169} by the time of separation.

As we noted, the Lu^{170} - Yb^{170} mass difference $\geqslant$ 3.46 Mev. With so appreciable a mass difference one can expect the γ-spectrum of Lu^{170} to be very complex.

It would be of great interest to investigate in detail the high energy region of the conversion electron spectrum of the lutetium fraction; so far this spectrum has been studied only up to 210 kev by Bobrov et al[2]. In the course of exploratory measurements of the high energy section of the conversion electron spectrum of Lu we observed electrons with energies of 860, 1020, 1150 and 1380 kev with a period of about 2 days and relative intensities:

$$\beta^+_{1200} : e^-_{860} : e^-_{1020} : e^-_{1150} : e^-_{1380} = 1 : 0.14 : 0.13 : 0.05 : 0.10.$$

Above these lines and up to 2200 kev there extends a low intensity electron "tail"; the decay period corresponding to this "tail" was not measured. It is quite possible that in this region there are many conversion lines which cannot be detected and resolved with our instrument (relative line half-width 4%).

Scientific Research Physical Institute
"A.A.Zhdanov" Leningrad State University

References

1. B.S.Dzhelepov & O.E.Kraft, Izv.AN SSSR, Ser.fiz., 20, 318 (1956). (Trans. Bulletin 20, No.13, 293.)

2. Yu.G.Bobrov, K.Ya.Gromov, B.S.Dzhelepov & B.K.Preobrazhenskii, Ibid., 21, 940 (1957). (Trans.Bulletin 21, No.7, 942.)

3. Table of Levy's Empirical Atomic Masses. CRP-654, Chalk River, 1956.

4. A Revised Semi-Empirical Atomic Mass Formula. CRP-690, Chalk River, 1957.

5. B.S.Dzhelepov & L.K.Peker, Skhemy raspada radioaktivnykh yader (Decay schemes of radioactive nuclei), M.-L., 1958.

* * * * * * *

DECAY SCHEME FOR 30-HOUR Te^{131}

- A.Bédesku, K.P.Mitrofanov, A.A.Sorokin & V.S.Shpinel'

Introduction

The matter of establishing the empirical regularities in the spectra of the excited state of undeformed nuclei with odd A is fundamental to further development of the nuclear shell model. It is known that the single-particle model does not allow of precise determination of the order of filling of the nuclear levels. The filling sequence can only be determined on the basis of experimental data. From the spins and parities of the ground states of odd A nuclei one can obtain information on the filling of the levels in these nuclei by odd nucleons. It is more difficult, however, to determine the order of filling by even nucleons. This can be done on the basis of the systematics of the energy states of certain groups of nuclei.

It follows from the Mayer single-particle model that in the spectra of the excited states of nuclei with the same number of odd particles outside the closed shell there must be observed "similar" levels, i.e., levels having the same spins and parities and approximately the same location relative to neighboring levels. It has been noted by Zeldes[1,2] and Shpinel'[3] that the appearance of the level shift curve for a group of undeformed nuclei with odd A that have the same number of odd particles, but each of which differs from the preceding one by one pair of even nucleons, can yield valuable information on the order of filling of the levels by even nucleons. It is found that the level shift plot has the appearance of a smooth, slightly cambered curve as long as the added even nucleon pairs fill the same level. When the added nucleon pair starts filling a new level, the shift curve exhibits a break, i.e., a change in direction. A model for explaining the appearance of the level shift plots was proposed in Ref.3.

Of great interest is determination of the order of filling by neutron pairs of the $3s_{1/2}$, $1h_{11/2}$ and $2d_{3/2}$ levels in the iodine isotopes $_{53}I^{125}$, I^{127}, I^{129}, I^{131} and I^{133} by plotting the similar level shift curve for these nuclei. The level diagrams for these isotopes, except I^{127} and I^{129}, have scarcely been studied. Hence in connection with solution of the question of the order of filling of the neutron levels in these nuclei we undertook a comprehensive investigation of the decay scheme for Te^{131}, β-decay of which excites a number of levels in I^{131}.

The decay scheme for $_{52}T^{131}$ is very complex. The few investigations[4,6] devoted to it are in need of verification. The commonly accepted Te^{131} decay scheme was constructed primarily on the basis of the work of Elizabeth Hebb[6] who by means

of magnetic lens spectrometers and scintillation counters investigated the primary and secondary electron spectra and carried out approximate γ-γ-coincidence measurements.

The decay scheme was established mainly on the basis of analysis of the energy balance. De Waard & Gerholm[7] measured the lifetime of the 147 kev level of I^{131}; Alväger & Oelner[8] made an accurate determination of the conversion coefficients of the 180 kev isomeric transition in Te^{131}.

We attempted to refine the Te^{131} decay scheme and to determine the characteristics of some of the low-lying levels in I^{131}.

Source Preparation

For preparation of the source, high chemical purity metallic tellurium was irradiated with thermal neutrons in a pile. By the (n,γ) reaction on Te^{130}, the natural abundance of which is 34.49%, there form simultaneously the 30-hr (activation cross section <8 mb) and the 25-min (activation cross section 0.22 b) Te^{131} isomers. After attainment of equilibrium between the 30-hr and 25-min isotopes and complete disintegration of the 25-min Te^{131} forming directly in the (n,γ) reaction, the irradiated product was dissolved in concentrated nitric acid and the I^{131} forming in the decay of Te^{131} was extracted with carbon tetrachloride. The tellurium dioxide obtained by evaporation of the purified solution served as the source for our measurements. Owing to the small activation cross section for 30-hr Te^{131} the specific activity of the source was only of the order of 1 mC which naturally greatly hampered the measurements.

Gamma-Spectrum

The γ-spectrum of the iodine free activity was measured on a scintillation γ-spectrometer, employing a 30 mm diameter, 20 mm thick NaI(Tl) crystal coupled to an FEU-13 photomultiplier. The resolution of the apparatus is characterized by the fact that the half-width of the Cs^{137} 660 kev line is 10.5%. The γ-spectrum measurements were repeated over a period of several days to elucidate the contribution from long-lived Te isotopes and other impurities. It was found that in the $E_\gamma > 700$ kev region the intensity of all the spectrum lines falls off with the same period, i.e., $\sim$30 hours, in view of which this entire region of the spectrum may be attributed wholly to Te^{131}. The most complicated situation obtains in the 0 to 400 kev region, where there is an appreciable contribution from the long-lived isomers of Te^{123} and Te^{125} and building up I^{131}. The intensity of the lines in the 400 to 700 kev region falls off mainly with a period of $\sim$30 hours, although in this region there is some contribution from I^{131}. The sections of the Te^{131} γ-spectrum in the 500 to 1400 and 700 to 2400 kev intervals are shown in Figs.1 and 2. The spectra were resolved assuming a standard line shape. Data on the relative intensities are listed in Table 1 (the intensity of the 780 kev γ-rays was taken as 100).

As will be evident from Figs.1 & 2, in addition to the γ-transitions observed by Elizabeth Hebb[6], we detected transitions of 2.2 and 1.85 Mev energy; instead of the 1.15 Mev transitions reported by Hebb, we observed two with energies of 1.12 and 1.20 Mev.

We also investigated the high energy (>1.2 Mev) region of the spectrum by means of a spectrometer with a smaller solid angle. These measurements substantiated the fact that the 1.6, 1.85 and 2.2 Mev lines correspond to actual transitions with these energies and are not a result of summing in the crystal of pulses from cascade γ-rays of lower energies. We did not resolve the spectrum in the <700 kev region in view of the above mentioned difficulty in identifying the lines.

Table 1

Energies and intensities of the γ-rays from Te^{131}

No.	E_γ, kev		Relative intensity, %		Method of identification
	scintil. spectr.	photo-electrons	scintil. spectr.	photo-electrons	
1	80±5	—	—	—	Coincidences with 770 kev gammas
2	100±10	—	—	—	
3	147±1	—	strong	—	Decay period of β–γ coincidences
4	200±10	—	—	—	Period scintillation spectrum
5	240±10	—	—	—	Period of β–γ coincidences
6	330±10	—	—	—	
7	440±10	—	—	—	
8	590±15	—	—	—	
9	775±10	780±5	100	100	Period of scint. & photoelectron spectra
10	850±15	850±10	45±10	35±10	
11	920±20*	925±10	~20	15±5	
12	1120±20	1140±15	35±5	30±5	
13	1200±20	1220±15	25±5	25±5	
14	1600±30	—	~5	—	Period of scintillation spectrum
15	1850±40	—	~2	—	
16	2200±50	—	~0,5	—	

*This is not clearly evident in the spectrum of Fig.2, but graphic subtraction shows an excess number of counts in this region.

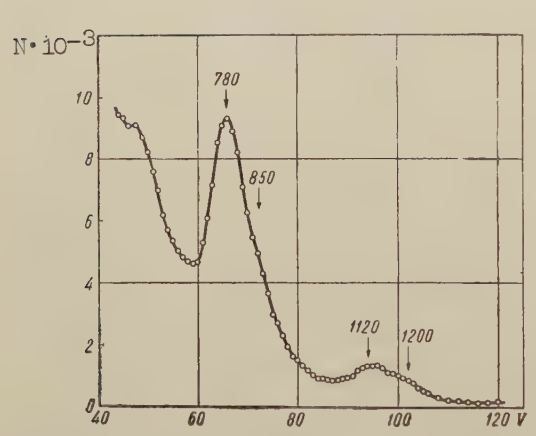

Fig.1. Te^{131} γ-spectrum in the 500 to 1400 kev interval.

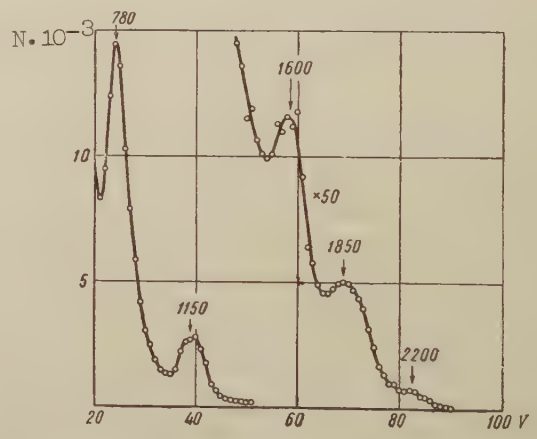

Fig.2. Te^{131} γ-spectrum in the 700 to 2400 kev interval.

For the purpose of verifying the results obtained with the scintillation spectrometer, we also carried out measurements of the photoelectrons by means of the two-lens β-spectrometer described in Ref.9. Specifically we investigated the 600 to 1400 kev interval of the Te^{131} spectrum. With an 8 mm diameter, 11 mg/cm^2 thick lead radiator and a solid angle of 5% of 4π, the relative line half-widths were 3.5-4.0%. For determining the relative intensities of the γ-rays we recorded the spectral sensitivity curve for the spectrometer. For purposes of calibration we used the γ-radiations from I^{131} which builds up in the source as a result of disintegration of Te^{131}. The relative intensities of the γ-rays from I^{131} have been measured repeatedly[10-12] and the results of different investigators are in good agreement.

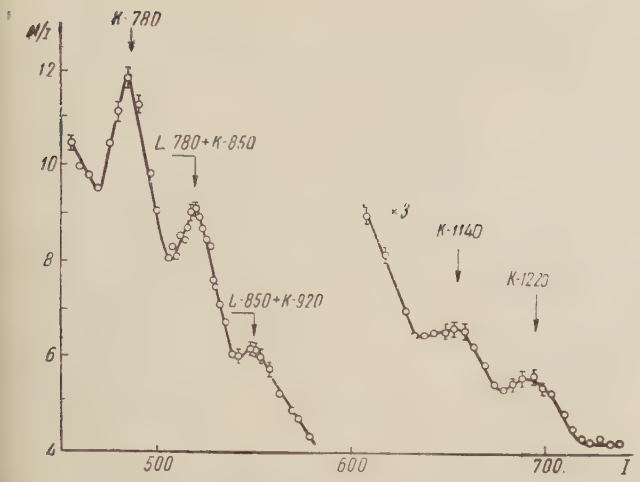

Fig.3. Electron spectrum in the 600 to 1300 kev region.

As a result of comparison of the relative intensities of the 364, 634 and 720 kev γ-transitions and the areas under the corresponding photopeaks, it was established that the spectral sensitivity of the spectrometer coincides with the energy dependence of the total photoelectric effect cross section. In other words, the intensities $I^{(I)}$ and $I^{(II)}$ of two γ-transitions giving rise to photopeaks with areas $S^{(I)}$ and $S^{(II)}$ are related as

$$I^{(I)} : I^{(II)} = \frac{S^{(I)}}{\sigma^{(I)}} : \frac{S^{(II)}}{\sigma^{(II)}},$$

where $\sigma^{(I)}$ and $\sigma^{(II)}$ are the total photoelectric effect cross sections for γ-rays of the given energies.

The experimental curve is reproduced in Fig.3 and shows photopeaks corresponding to γ-transitions of 780, 850, 925, 1140 and 1220 kev energy. The results of these measurements agree with the data obtained by means of the scintillation spectrometer and substantiate the existence of two hitherto unknown γ-transitions having energies of 925 and 1220 kev.

Despite the overlapping of some of the K and L photopeaks, we were able to resolve the photoelectron lines (using the experimentally determined line shapes and K and L photopeak ratio) and determine the relative γ-transition intensities (Table 1).

Coincidence Spectra

The coincidence spectra were measured on a conventional coincidence spectrometer. We used both NaI(Tl) and anthracene crystals. In addition, for the purpose of detecting cascade transitions, we used the summing or the "adding upon coincidence" technique described by Hoogenboom[13]. Although this procedure is particularly advantageous in studying high energy (> 1 Mev) γ-transitions and cases when the cascade transitions depart from the same excited state (as, for example, in (p,γ) reactions), it also proves useful in ordinary spectrometric work for investigating complex decay schemes, inasmuch as there appear in the coincidence spectra only the total energy peaks from the cascade transitions, which greatly simplifies interpretation.

For the summing measurements the equipment was connected as shown in the block diagram of

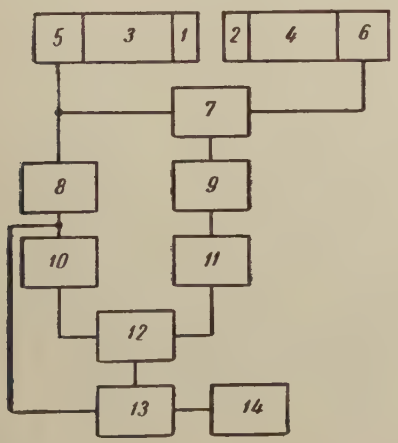

Fig.4. Block diagram of the experimental arrangement for the "addition upon coincidence" measurements: 1 & 2) crystals, 3 & 4) photomultipliers, 5 & 6) cathode followers, 7) summator, 8 & 9) amplifiers, 10) integral discriminator, 11) differential discriminator, 12) coincidence circuit (10^{-7} sec), 13) gate, 14) 20-channel pulse height analyzer.

Fig.4. In order to reduce the resolving time, before being fed into the sum circuit the photomultiplier pulses were clipped to ~0.4 μsec by means of a short-circuited line. Moreover, connection of the coincidence circuit between the sum analyzer and the analyzing channel substantially reduced the background of chance "summed coincidences".

The background of chance coincidences in the measurements by the conventional procedure was calculated in most cases, while in the summing measurements the chance background was found from measurements with two separate sources. All the coincidence measurements were repeated on the following day in order to make sure that the observed transitions fell off uniformly with time.

1. β-γ Coincidences

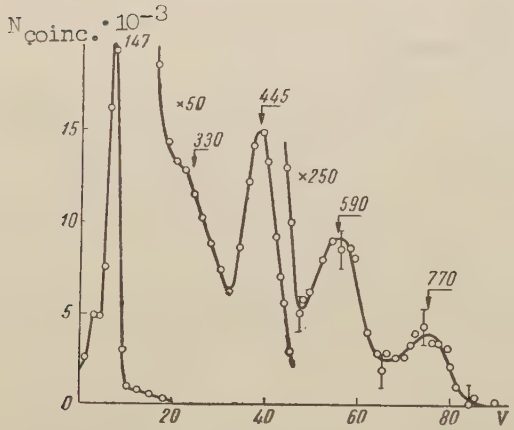

Fig.5. Spectrum of γ-rays coinciding with β-particles (E_β > 1 Mev).

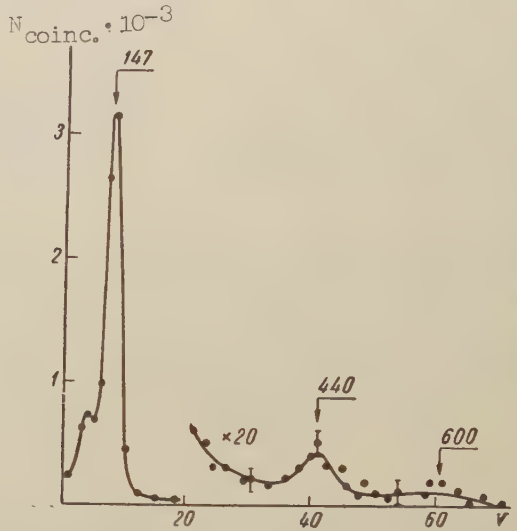

Fig.6. Spectrum of γ-rays coinciding with β-particles (E_β > 1.4 Mev).

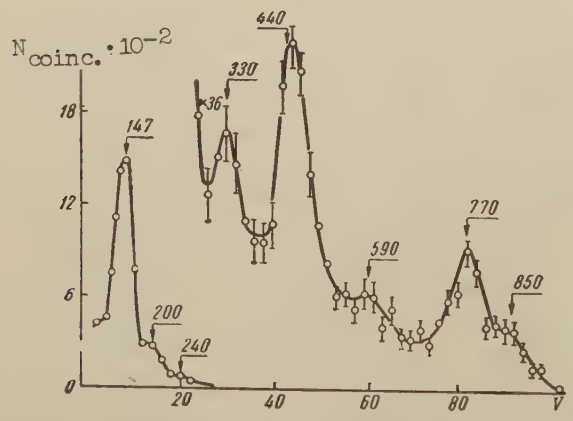

Fig.7. Spectrum of γ-rays coinciding with β-particles (E_β > 550 kev). The peak at 200 kev is due to Compton scattering of > 750 kev γ-rays in the β-counter crystal.

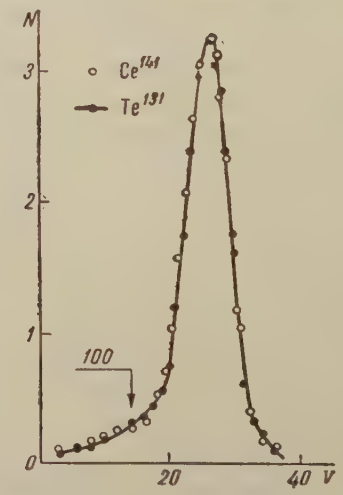

Fig.8. Comparison of the Te^{131} 147 kev and Ce^{141} 145 kev lines. It is evident that there is no ~100 kev γ-transition in the β-γ coincidence spectrum of Te^{131}.

For determining the transitions between the low-lying levels of I^{131} we investigated coincidences of the γ-rays with the high energy Te^{131} β-particles. The measurements of the γ-rays coinciding with β-rays of energies $E_\beta > 1$ Mev, $E_\beta > 1.4$ Mev and $E_\beta > 550$ kev are shown in Figs.5,6 & 7, respectively. As will be evident from these figures, the highest coincidence intensity is associated with the 147 kev transition, particularly for $E_\beta > 1$ and 1.4 Mev. In addition, the 147 kev peak was observed in the coincidence spectrum with the threshold of the β-discriminator shifted to $\sim$2 Mev. This substantiates the fact, inferred from other data, that the 147 kev level is at least one of the lowest lying levels in I^{131} and that it is fed by a β-transition of $\sim$2 Mev energy. Hebb[6] on the basis of the presence in the conversion electron spectrum of a line that was identified as an L line of a 51 kev transition and a line assumed to be the K line of a 99 kev transition, inferred the existence of a level at 51 kev and a 51—99 kev transition parallel to the 147 kev transition.

In order to check this inference, the shape of the 147 kev line in the spectrum of coincidences with $E_\beta > 1$ Mev was compared with the shape of the single Ce^{141} 145 kev line. This comparison is shown in Fig.8 where the two lines are superposed. In these measurements a collimator in the form of a 2 mm thick lead plate with a 5 mm diameter opening was mounted in front of the γ-counter in order to reduce the back scattering peak appearing at $\sim$90 kev and evident in Figs.5,6 & 7. These measurements showed that there is no $\sim$100 kev line in the spectrum and consequently that the cascade transition hypothesized by Hebb does not exist. One can also cite the following arguments against the existence of this cascade. If there really were a 50—100 kev cascade parallel to the 147 kev transition, then, inasmuch as the 780 kev transition is not in cascade with the 147 kev transition, it should not yield coincidences with the 100 kev transition either. Moreover, the conversion line observed by Hebb[6], according to her own statement, may be interpreted either as an L line of a 51 kev transition or the K line of a 79 kev transition. Hebb chose the first interpretation wholly for convenience, for "otherwise no place could be found for it (the 51 kev transition) in the decay scheme."

But in the scintillation γ-spectrum (the single spectrum and in coincidence with the 780 kev line) there is observed a transition of 80 kev energy. From this it may be concluded that the 147 kev level is the first excited level in I^{131}. The energies of the other transitions observed in the present measurements are indicated at the curves in Figs.5, 6 & 7.

2. γ-γ Coincidences

According to the decay scheme proposed by Hebb[6], the 780 kev transition feeds the 147 kev level, and in parallel with it there should be a 440—330 kev cascade. Fig.9 shows the γ-γ coincidence spectrum for the case when the gate of the analyzer in the second channel was set on the 780 kev peak. No peak was observed at 147 kev, but there are peaks evident at 80 and 100 kev. These peaks were also observed in the singles spectrum but their identification was hindered, since it is difficult to determine the period corresponding to this part of the spectrum.

In the "coincidence summing" measurements with the control gate set at 780 kev, no peaks except the total sum peaks were observed in the spectrum (Fig.10). This indicates that there is no cascade parallel to the 780 kev transition and that the 440 and 330 kev transitions are not in cascade.

On the whole, the coincidence measurements yielded evidence of the following γ-γ cascades: 1100—780, 780—330, 850—330 and 780—850 kev.

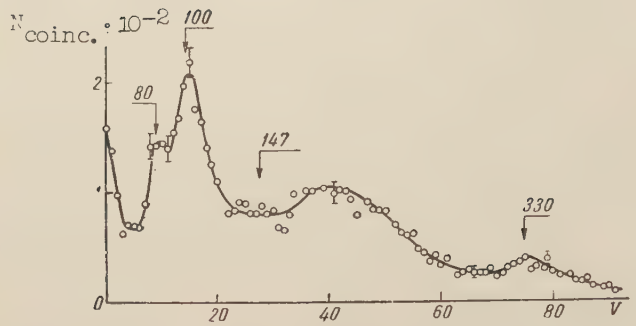

Fig.9

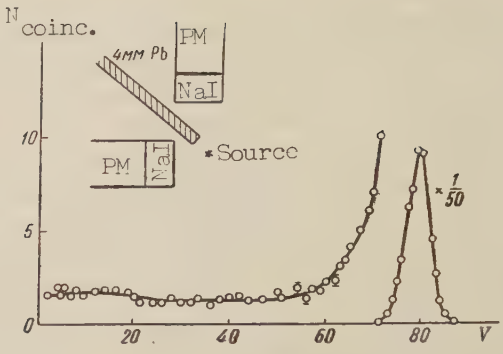

Fig.10

Fig.9. Low energy section of the spectrum of γ-rays coinciding with the 780 kev γ-rays. No 147 kev line appears in this spectrum.

Fig.10. Summed coincidence spectrum (E_{sum} = 770 kev). The insert shows the experimental geometry. The lead plate was clad with cadmium to absorb the Pb x-radiation.

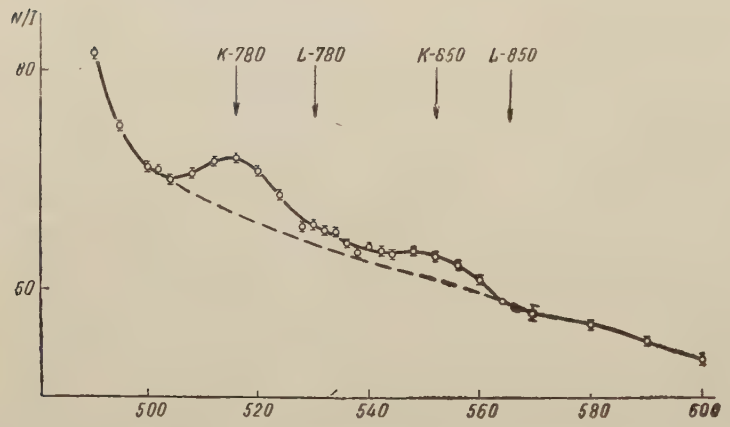

Fig.11. Section of electron spectrum of Te^{131} comprising the 780 and 850 kev transition lines.

Internal Conversion Coefficient of the 780 kev γ-Transition

It follows from the results of the β-γ and γ-γ coincidence measurements that the 780 kev γ-transition goes to the ground state of I^{131}. This being the case, by determining the multipole order of the transition one could make an assignment for the 780 kev level. We undertook to measure the ICC of this γ-transition. We used the method of comparing the ratio of the areas under the conversion lines and photopeaks of the γ-transition with the corresponding areas for a γ-transition for which the ICC is known.

For the conversion line measurements the sources were prepared by the procedure of settling from a suspension of finely ground tellurium oxide powder onto a 1.5 mg/cm^2 thick aluminum foil. We used sources with a diameter of 5 and 8 mm and thicknesses from 0.5 to 4 mg/cm^2. The spectrometer employed had the same operating characteristics as in measuring the photoelectron spectrum. As the transition with a known conversion coefficient we used the 364 kev transition following β-decay of I^{131}; according to Haskins & Kurbatov[11] α_K for this transition is 0.02.

As the result of measurements of the high energy part of the conversion electron spectrum of Te^{131} it was found that in addition to the lines associated with the 780 kev transition one can discriminate in this energy region a line corresponding to the 850 kev γ-transition (Fig.11).

In view of the relatively low resolution of the spectrometer the K and L conversion peaks were not resolved. However, making use of the known value of the K/L ratio, which in this energy region is virtually constant[14] for all low multipole orders, it proved possible to determine the areas of the K conversion peaks

Table 2

Multipole order assignments for the 780 and 850 kev transitions

E_γ, kev	$\alpha K_{exp} \cdot 10^3$	$\alpha K_{theo} \cdot 10^3$			Inferred multiple order
		E1	E2	M1	
780	0,8±0,2	0,84	2,3	3,0	E1
850	1,6±0,6	0,71	1,9	2,5	E2

and thus calculate the K shell conversion coefficients.

The results of our measurements are shown in Table 2 wherein they are compared with the theoretical values of the conversion coefficients taken from the table of Sliv & Band[15].

Decay Scheme for Te^{131}

Fig.12 shows the principal features of the decay scheme proposed for Te^{131}; this includes the lowest 147, 595 and 780 kev levels and the highest lying 2.2 Mev level in I^{131}, which are excited in β-decay of Te^{131}. The results of our β-γ and γ-γ coincidence experiments allow of sketching in some of the intermediate levels, but plotting the complete scheme must await substantiation by measurements of the partial β-spectra based on observation of β-γ coincidences, inasmuch as the tentative diagram is not consistent with the data of Hebb[6] on the end-point energies of the soft β-transitions.

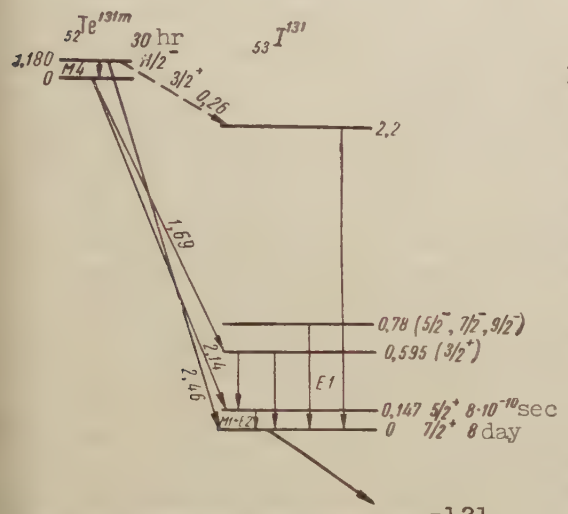

Fig.12. Level diagram for I^{131} plotted on the basis of our experimental results.

The assignment for the ground state of I^{131} is 7/2+ (Refs.16 & 17) which corresponds to the configuration $(1\ g_{7/2})^3$, predicted by the Mayer model[18]. The first excited state is the 147 kev level (see above under β-γ coincidences). Inasmuch as the 147 kev transition is M1 + E2 and the M1 component is l-forbidden[19] one can attribute the configuration $2\,d_{5/2}$ to this level, which is again consistent with the single-particle model. The 595 kev level was introduced on the basis of the fact that in the β-γ coincidence measurements with $E_\beta > 1.4$ Mev there were observed only 147, 440 and 595 kev γ-rays (Fig.6); the 595 kev γ-transition is apparently a cross-over transition from the 595 kev level to the ground state, while the 440 and 147 kev transitions form a parallel cascade. This is substantiated by the measurements of Mallmann et al[5]; according to their data and those of Hebb these two levels are excited mainly by β-decays going to the ground state of Te^{131}.

As was shown above, the 780 kev γ-transition does not feed the 147 kev level. Inasmuch as this transition is one of the most intense transitions in the spectrum and is apparently involved in the de-excitation of most of the high lying states, we introduced a level at 780 kev with the 780 kev transition leading to the I^{131} ground state. Inasmuch as this transition, according to the measured conversion coefficient is E1, the 780 kev level should be attributed odd parity. This fact, however, cannot be explained in the framework of the single-particle model.

The level at 2.2 Mev was introduced in view of the existence of a 2.2 Mev transition, which in view of energy considerations can go only to either the ground state or the 147 kev level. The latter alternative, however, is less probable inasmuch as in this case the corresponding β-transition would have an energy of only ~100 kev.

Conclusions

On the basis of the value of the internal conversion coefficient of the 147 kev transition and the lifetime of the 147 kev level obtained in the work of Sorokin[19], we infer that the first excited level of I^{131} has the spin and parity 5/2+. As was noted above, the assignment for the ground state is 7/2+. According to the shell model, this means that the ground state of I^{131} is $1g_{7/2}$, and the 147 kev state configuration is $2d_{5/2}$. It was inferred in the work of Knight[20], Graves and Mitchell[21], and Pappas[22] that there should also be $1g_{7/2}$ and $2d_{5/2}$ states in the isotopes I^{127}, I^{129} and I^{133}. Actually, however, one can regard the existence of states with these configurations as firmly established only for I^{127} and I^{129}. In both cases the level assignments for the iodine nuclei were determined from the log ft value for the β-transitions going to the given levels.[20,21] The level diagram for I^{133} was proposed solely on the basis of the study by Pappas[22] in which the radiations following β-decay of Te^{133} ($T_{1/2}^{(I)}$ = 53 min and $T_{1/2}^{(II)}$ = 2 min) were measured by the absorption method and according to the author himself involved considerable errors. Hence the existence of a $2d_{5/2}$ state in I^{133} cannot be regarded as definitively established.

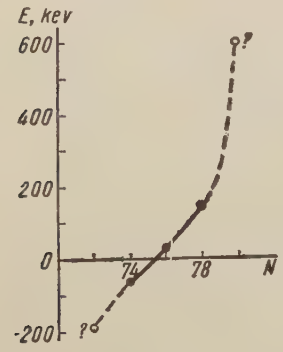

Fig.13. Level shift curve: separation between the $2d_{5/2} - 1g_{7/2}$ proton levels in I^{125}, I^{127} and I^{131} as a function of the even number of neutrons.

On the basis of the data of Sorokin[19] regarding the spin and parity of the I^{131} 147 kev level and the data of Knight[20], Graves & Mitchell[21] and Pappas[22] we can plot the $2d_{5/2} - 1g_{7/2}$ level shift curve for the isotopes I^{127}, I^{129}, I^{131} and I^{133}. The shift curve is shown in Fig.13 where the points corresponding to I^{127}, I^{129} and I^{131} for which the values are accurately known are connected by a solid line. As will be evident from Fig.13, the plot for these three isotopes is a smooth curve. This indicates that in these iodine isotopes the neutron pairs fill the same level with sufficient "capacity" to accomodate at least six particles. In this neutron number region the Mayer model[18] predicts the existence of the following states $3s_{1/2}$ (capacity 2 particles), $1h_{11/2}$ (12 particles) and $2d_{5/2}$ (4 particles). Obviously, in I^{127}, I^{129} and I^{131} the neutron pairs fill the $1h_{11/2}$ level. The great deviation of the point corresponding to I^{133} from the smooth shape of the initial curve may be due, as we noted above, to errors in constructing the decay scheme and making the level assignments for this isotope. It is interesting to note that Mathur & Hyde[23] established the first excited level of I^{127} at precisely 187 kev. As will be seen from Fig.13, the points corresponding to this level lie on a continuation of the 3-point curve plotted for I^{127}, I^{129} and I^{131}. The spin and parity of this level were not determined in either of the investigations[23,24] of the level diagram of I^{125}. In view of the fact that the point for this isotope does fall on the prolongation of the $2d_{5/2} - 1g_{7/2}$ level shift curve for the other iodine isotopes, we infer that the assignment for this level is 7/2+.

Thus on the basis of our results we have been able to plot the $2d_{5/2} - 1g_{7/2}$ level shift curve for the iodine isotope and conclude that the neutron pairs fill the $1h_{11/2}$ level in I^{127}, I^{129}, I^{131} and possibly I^{125}. Further investigation of the shift of similar levels in iodine isotopes must be predicated on more careful investigation of the decay schemes for these isotopes.

We desire to express our deep gratitude to Yu.M.Ukrainskii for making available the purified tellurium source material, N.P.Rudenko and O.M.Kalinkina for

assistance in solving certain radiochemical problems and L.P.Sorokina and V.V. Skvortsov, Moscow State University physics students, for assistance in carrying out the measurements.

Scientific Research Institute of Nuclear Physics
Moscow State University

References

1. N.Zeldes, Nucl.Phys., 2, 1 (1956-1957).
2. N.Zeldes, Nucl.Phys., 7, 27 (1958).
3. V.S.Shpinel', Izv.AN SSSR, Ser.fiz., 22, 995 (1958). (Trans.Bulletin 22, No.8, 984.)
4. K.Geiger, Z.Naturforsch., 7a, 579 (1952).
5. C.A.Mallmann, A.H.Aten, D.R.Bes & C.M.de McMillan, Phys.Rev., 99, 7 (1955).
6. E.Hebb, Phys.Rev., 97, 987 (1955).
7. H.de Waard & T.R.Gerholm, Nucl.Phys., 1, 281 (1956).
8. T.Alväger & G.Oelner, Arkiv Fysik, 12, 319 (1957).
9. K.P.Mitrofanov & V.S.Shpinel', Izv.AN SSSR, Ser.fiz., 21, 1607 (1957). (Trans.Bulletin 21, No.12, 1545.)
10. J.Wolfson, Canad.J.Phys., 30, 715 (1952).
11. J.R.Haskins & J.D.Kurbatov, Phys.Rev., 88, 884 (1952).
12. A.Mijatovic & V.Wintersteiger, Bull.Inst.Nucl.Sci., 3, 57 (1953).
13. A.M.Hoogenboom, Nucl.Instr., 3, 57 (1958).
14. K.Siegbahn, (editor), Beta- and Gamma-Ray spectroscopy, Amsterdam, 1955.
15. L.A.Sliv & I.M.Band, Tablitsy koeffitsientov vnutrennei konversii (Tables of internal conversion coefficients), M., 1956.
16. Y.Livingston, Phys.Rev., 92, 1271 (1953).
17. X.Y.Lipworth, Bull.Amer.Phys.Soc.,Ser.II,2,316 (1957).
18. M.G.Mayer & J.H.Jensen, Elementary Theory of Nuclear Shell Structure. N.Y. – London, 1955.
19. A.A.Sorokin, Present issue of the Bulletin, p.1434.
20. J.D.Knight, Phys.Rev., 102, 1592 (1956).
21. W.E.Graves & A.C.G.Mitchell, Phys.Rev., 101, 701 (1956).
22. A.C.Pappas, Phys.Rev., 87, 162 (1957).
23. H.B.Mathur & E.K.Hyde, Phys.Rev., 95, 708 (1954).
24. J.Bergstrom, Arkiv Fys., 5, 191 (1952).

ON THE l-FORBIDDEN M1 (147 kev) TRANSITION IN I^{131}

- A. A. Sorokin

The lifetime of the 147 kev excited state of I^{131} was measured by de Waard & Gerholm[1] by the method of delayed coincidences; they found $T_{1/2} = (9 \pm 1) \cdot 10^{-10}$ sec.

This value of $T_{1/2}$ on the assumption that the 147 kev transition is pure M1 leads to a value of $1.5 \cdot 10^{-9}$ sec for the radiative lifetime $\tau_{\gamma M1}$, which is approximately half the value given by the empirical relation

$$\log (\tau_\gamma E^3) = -11 \qquad (1)$$

for l-forbidden M1 transitions in odd proton nuclei[1-3]. This deviation may be explained either by a large admixture of E2 for this transition (E2/M1 = 1) or by a large systematic error in the measurements of de Waard & Gerholm.

In the present work the lifetime of this state was also measured by the method of delayed coincidences on a set-up of the conventional type described in Ref. 4. The source was 30-hour Te^{131} obtained by irradiation of a natural mixture of tellurium isotopes with thermal neutrons. Prior to the measurements the activity was purified chemically to remove the built-up I^{131}. We used FEU-33 multipliers operated at ~3 kv and tolan crystals. By way of amplitude equalizer we used 6S3P triodes, which at a current of 10 ma have a cut-off potential of ~1 v. The length of the shaping cable assured a resolving time $2\tau = 3 \cdot 10^{-9}$ sec. The pulses fed into the pulse height analyzer channel were taken off one of the last dynodes of the photomultipliers.

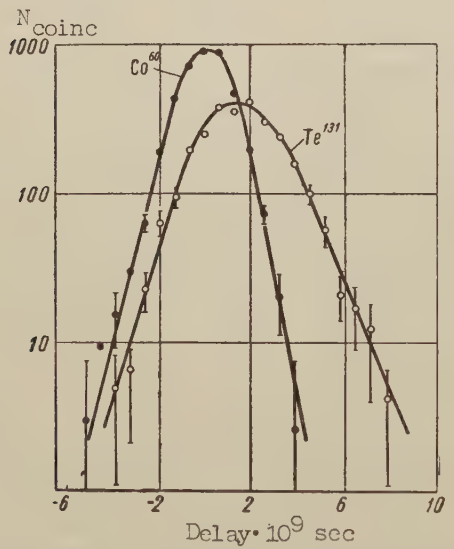

Fig.1. Delay curves for Te^{131} and Co^{60} obtained with the same settings of the analyzer gates and thresholds.

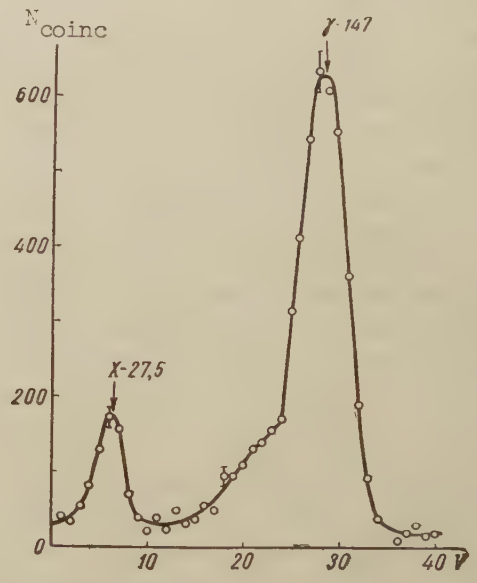

Fig.2. Low energy part of the γ-ray spectrum coinciding with the $E_\beta > 1$ Mev β-rays.

We measured the β-γ coincidences. The analyzer gate in the γ-channel was set on the Compton distribution from the 147 kev γ-rays, while in the β-channel the integral threshold was set at 1 Mev. The method of β-γ coincidences has the advantage over the β-e^- coincidence procedure[1] in that the background due to spurious coincidences is lower. In our case the background was due to coincidences of the β-particles with higher energy (than 147 kev) γ-rays[5] and amounted to

<20% of the useful effect. The averaged results for six series of measurements are shown in Fig.1. The lifetime of the excited state of I^{131} was determined from the slope of the delayed coincidence curve and also from the shift of the centroid of this curve relative to the curve for prompt coincidences in Co^{60} recorded with the analyzer gates and threshold at the same settings. The two procedures yielded results agreeing within the limits of the experimental error; averaging yielded $T_{1/2} = (8 \pm 1)\cdot 10^{-10}$ sec, i.e., a value agreeing within the limits of the experimental error with the result of de Waard & Gerholm[1].

The radiative lifetime for an M1 transition is given by the expression

$$\tau_{\gamma M1} = 1.44\,(1 + \alpha_{\mathrm{tot}_{M1}})\left(1 + \frac{E2}{M1}\right) T_{1/2}, \qquad (2)$$

where $\alpha_{\mathrm{tot}_{M1}}$ is the total internal conversion coefficient for the M1 transition, and E2/M1 is the intensity ratio of the respective components. According to the tables of Sliv & Band[6], $\alpha_{\mathrm{tot}_{M1}} = 0.25$.

In order to determine E2/M1, we measured the K shell conversion coefficient of the 147 kev transition. These measurements were made on the scintillation coincidence spectrometer employed in the work of Ref.5. Fig.2 shows the spectrum of the γ-rays coinciding with $E_\beta > 1$ Mev β-particles. Inasmuch as the contribution from transitions having higher energies than 147 kev is insignificant, the conversion coefficient of the 147 kev transition can be found from the ratio of the photopeaks associated with the 147 kev γ-rays and the 27.5 kev x-rays accompanying the conversion by means of the formula

$$\alpha_K = \frac{S_X}{S_\gamma} \cdot \frac{\varepsilon_\gamma}{\varepsilon_X} W_K\,, \qquad (3)$$

where S is the area under the peak, ε is the detecting efficiency, and W_K is the fluorescence yield of K x-radiation. The K shell conversion coefficient calculated on the basis of the experimental data proved to be

$$\alpha_K = 0.26 \pm 0.05.$$

The indicated uncertainty includes both the statistical uncertainty in determining S_X / S_γ which is estimated to be about 10%, and the possible error in evaluating $\frac{\varepsilon_\gamma}{\varepsilon_X} \cdot W_K$.

$\alpha_{K\,\mathrm{theo}}$[6]		$\alpha_{K\,\mathrm{exp}}$
M1	E2	
0.22	0.33	0.26±0.05

According to the tables of Sliv & Band[6] α_K for a 147 kev M1 type transition should be 0.22; that for an E2 type transition of the same energy 0.33. Thus the value $\alpha_K = 0.26$ leads to the ratio E2/M1 ≈ 0.6. Although with the indicated uncertainty the percent admixture may vary in a wide range, the value obtained may be taken as evidence for a large admixture of E2. Consequently the deviation of $\tau_{\gamma M1}$ from that given by the empirical relation may be explained by this factor.

In general at present the accuracy as regards determination of the ratio E2/M1 in l-forbidden M1 transitions is not high. So far attempts to determine the finer regularities for transitions of this type (for example, the variation of $\tau_{\gamma M1}$ with the number of neutrons in nuclei with the same odd Z) have not been successful (see for example, Alväger, Johansson & Zuk[7]).

I wish to thank graduate student G.K.Ryasnov for assistance in adjusting the apparatus and aid in the measurements.

Scientific Research Institute of Nuclear Physics,
Moscow State University

References

1. H. de Waard & T.R.Gerholm, Nucl.Phys., 1, 281 (1956).
2. R.L.Graham & R.E.Bell, Canad.J.Phys., 31, 377 (1953).
3. H.Vartapetian, Thèses, Faculté des Science de l'Universite de Paris, 1957.
4. R.E.Bell, R.L.Graham & H.E.Petch, Canad.J.Phys., 30, 35 (1952).
5. A.Bedesku, K.P.Mitrofanov, A.A.Sorokin & V.S.Shpinel', Present issue of the Bulletin, p.1424.
6. L.A.Sliv & I.M.Band, Tablitsy koeffitsientov vnutrennei konversii gamma-izlucheniya (Tables of internal conversion coefficients), Parts I & II. M.-L., 1958.
7. T.Alväger, B.Johansson & W.Zuk, Arkiv.Fys., 14, 22, 3733 (1958).

INVESTIGATION OF THE DECAY SCHEME FOR Hf^{181}

- A.V.Borovikov, V.S.Gvozdev, I.A.Kondurov & Yu.L.Khazov

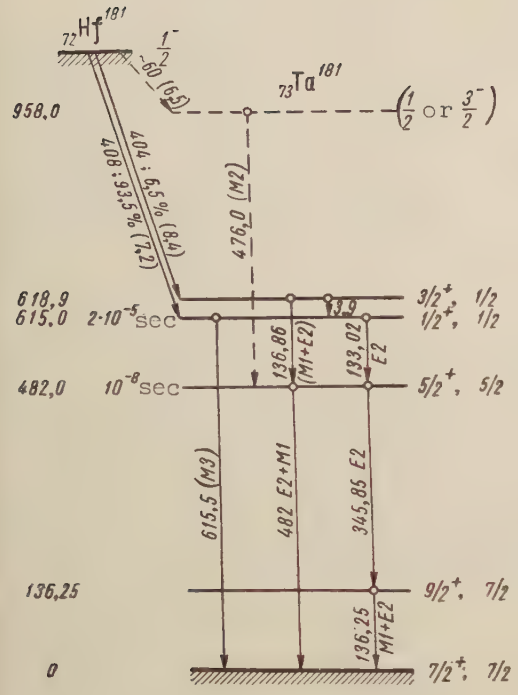

Fig.1. Decay scheme for Hf^{181}.

Beta-decay of 46-day Hf^{181} leads to excited levels of Ta^{181} (Fig.1). The total disintegration energy of Hf^{181} is 1023 kev. Hitherto the excited levels of Ta^{181} have been investigated up to 619 kev energy. Boehm & Marmier[12] report a 476 kev γ-transition in Ta^{181} and infer the existence of an excited level at 958 kev (476——482 kev cascade). Other investigators[2] did not observe coincidences between the 476 and 482 kev γ-rays. Hence the existence of the 958 kev state in Ta^{181} is open to question.

The present work was undertaken for the dual purpose of investigating the excited levels of Ta^{181} primarily in the energy range above 619 kev and for determining the multipolarities of the γ-transitions on the basis of the ratios of the K and L shell and L subshell conversion coefficients.

The β-spectrum and the conversion electron spectrum were investigated on a $\pi\sqrt{2}$ focusing β-spectrometer. For studying the γ-spectrum and elaborating the decay scheme we used a γ-spectrometer with a multiple channel analyzer and the γ-γ and γ-β coincidence technique.

1. Beta-Spectrum and Internal Conversion Electron Spectrum

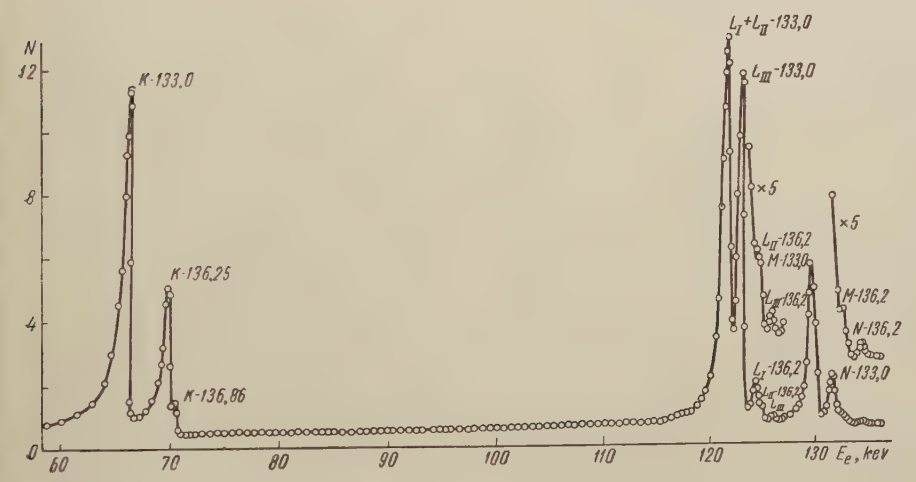

Fig.2. Internal conversion electron spectrum in the 60 to 140 kev range.

We carried out a detailed investigation of the β-spectrum and the internal conversion electron spectrum associated with the decay of Hf^{181} (Figs.2-5). The sources for these measurements were prepared by the settling technique: the activity was deposited on 4 μ aluminum foils from a suspension of hafnium oxide (enriched to 97.3% Hf^{180}) in a solution of shellac in alcohol. The deposits prepared in this manner were irradiated with thermal neutrons in a pile. The measurements were started some 30-40 days after irradiation.

In investigating the internal conversion spectrum we detected three hitherto unreported lines with energies of 280.2 (Fig.3), 551.1 and 531.6 kev (Fig.5). There is also probably a line at 274.9 kev (Fig.s). These lines were identified as the

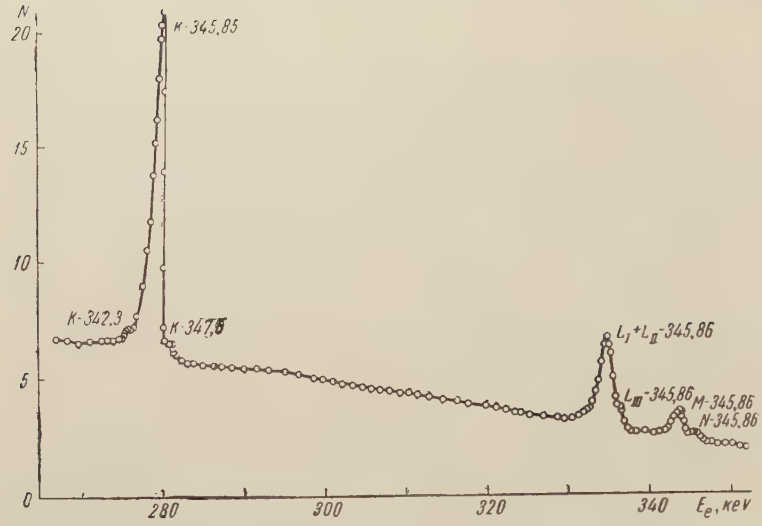

Fig.3. Internal conversion electron spectrum in the 270 to 350 kev range.

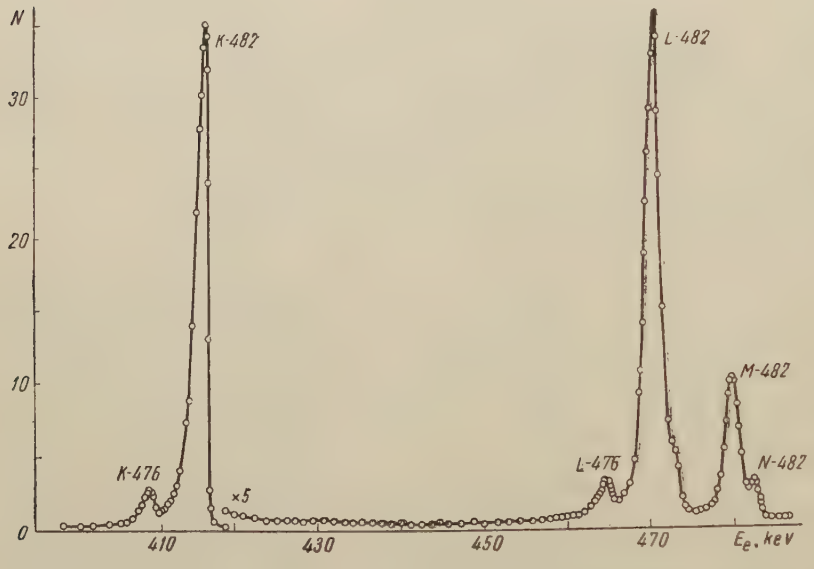

Fig.4. Internal conversion electron spectrum in the 400 to 485 kev range.

K lines of γ-transitions with energies of 347.6, 619, 699 and 342.3 kev, respectively. It will be evident that a 619 kev transition is consistent with the decay scheme for Ta^{181} (Fig.1). No conversion lines were detected in the sections of the electron spectrum not shown in Figs.2-5.

From Kurie plots for the β-spectrum, we inferred the existence of three new β-components of low intensity with end-point energies of ~340, ~550 and ~1050 kev. The ~550 and ~1050 kev end-point energy β-spectra apparently are associated with decay to the excited level at 482 kev and the ground state of Ta^{181}. According to the decay scheme shown in Fig.1, the energies of these β-spectra should be 541 and 1023 kev (Fig.10).

2. γ-γ and γ-β Coincidences

The γ-γ and γ-β coincidence experiments were carried out by means of a fast coincidence circuit with a resolving time $\tau = 3 \cdot 10^{-8}$ sec. For the γ-γ coincidence measurements, we used two FEU-29 photomultipliers viewing NaI(Tl) crystals; for the γ-β coincidence measurements, we used the same photomultipliers but with one NaI(Tl) crystal and one stilbene crystal for detecting electrons. The γ-ray spectrum was investigated by means of a 32-channel pulse height analyzer.

Fig.6 shows the spectrum of the γ-rays coinciding with the 482 kev gammas. In addition to the 135 kev line (133 and 136.86 kev transitions), we observed low intensity lines with energies of 220 ± 10, 270 ± 20 and 480 ± 20 kev. These lines were identified as 217, 259 and 476 kev γ-transitions in the level scheme for Ta^{181} (see Fig.10 below). Evaluation of the relative intensities of the detected γ-transitions is hampered by the difficulty of precise determination of the energy dependence of the detecting efficiency with the given experimental geometry. For close γ-transitions one can give an approximate evaluation of the

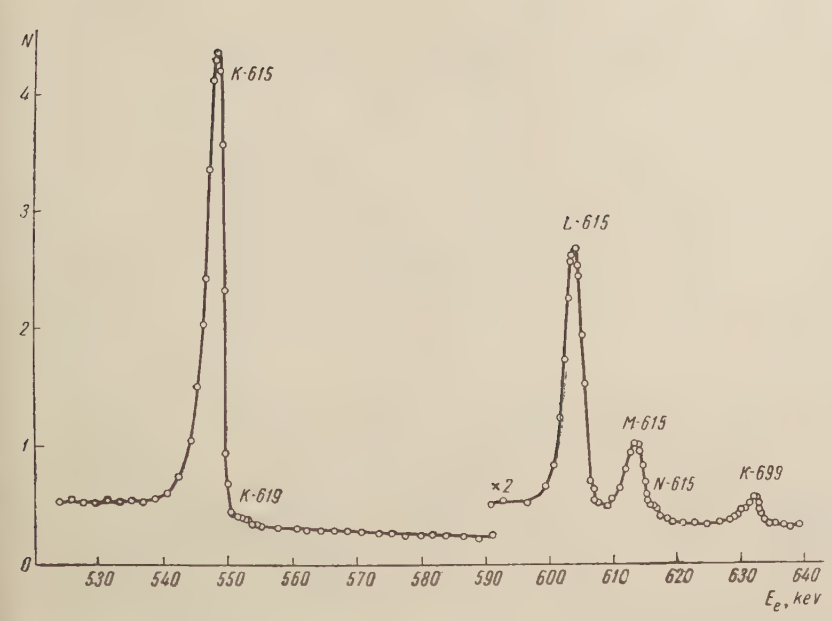

Fig.5. Internal conversion electron spectrum in the 530 to 640 kev range.

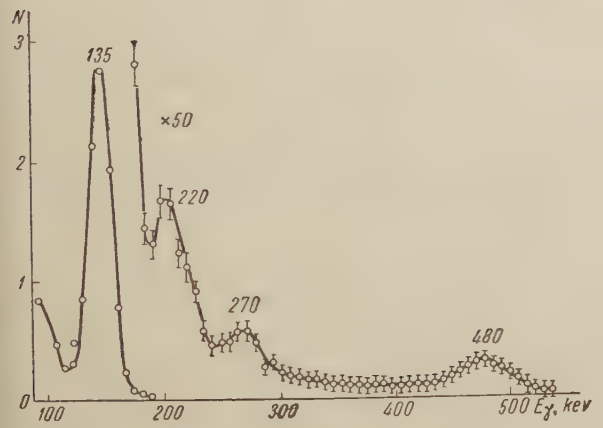

Fig.6. Spectrum of γ-rays coinciding with the 482 kev γ-rays.

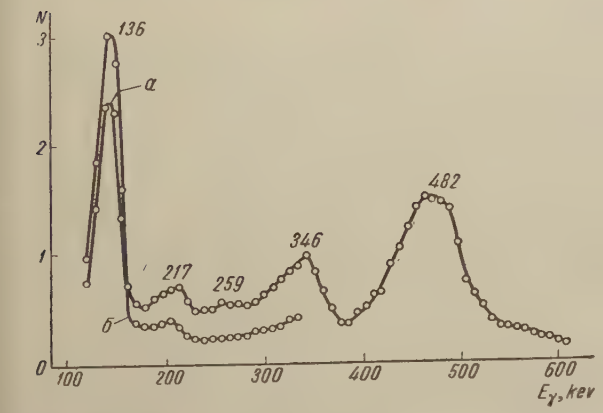

Fig.7. Spectrum of γ-rays coinciding with a) 30 to 60 kev γ-particles and b) >65 kev β-particles.

intensity ratio. Thus the intensity ratios of the 133, 217 and 259 kev γ-rays was evaluated to be 1:0.007:0.003 (uncertainty - 60%).

With a view to determining the location of the 217 and 259 kev γ-transitions in the Ta^{181} level scheme we investigated the spectrum of coincidences with different sections of the β-spectrum. The results of these measurements are shown in Fig.7. The upper curve represents the coincidence spectrum with electrons having energies from 30 to 60 kev; the lower curve the γ-ray coincidence spectrum with electrons having energies above 65 kev. As will be evident from Fig.7, the 217 kev γ-rays yield coincidences with electrons of all energies, while the 259 γ-rays yield coincidences only with low energy electrons.

All the measurements of the low energy part of the γ-ray spectrum were carried out with chemically purified sources free of all extraneous impurities. The effectiveness of the purification may be judged by examining Fig.8. Here curve 1 represents the high energy part of the singles spectrum of γ-rays from the initial Hf^{181} activity. The spectra of the γ-rays associated with impurities remaining after the first and second purification treatment are shown by curves 2 & 3. Curve 4 shows the γ-ray spectrum obtained after two-fold purification of the initial source. All four curves have been normalized to the 482 kev line. As will be apparent from Fig.8, the relative intensities of the 880 and 1100 kev lines from the impurities increase, which gives reason to infer that these lines pertain to another element. The intensities of these two lines are approximately equal. Subsequent measurements led us to conclude that this activity probably belongs to 84-day Sc^{46}.

The high energy part of the γ-ray spectrum was investigated for coincidences with all γ-rays without discrimination as

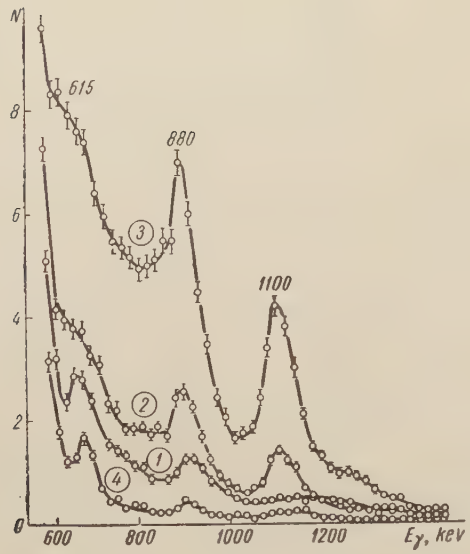

Fig.8

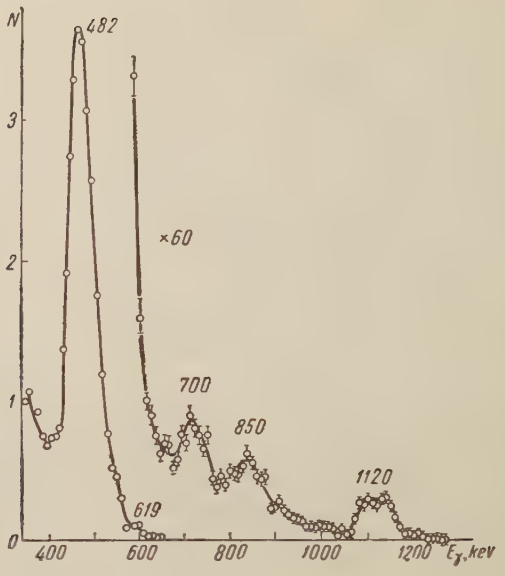

Fig.9

Fig.8. γ-Ray spectra in the high energy region illustrating the effectiveness of chemical purification.

Fig.9. Spectrum of γ-rays coinciding with β-particles (no energy selection).

regards energy. Measurements were carried out with a nonpurified source. There were detected γ-transitions of 700 and 850 kev energy. These lines (700 ± 20 and 850 ± 30 kev) and 619 and 1120 kev γ-rays were detected in the γ-β coincidence spectrum (see Fig.9). In this case the source (also not purified) was mounted inside a stilbene crystal 20 mm thick. In this case there was no energy discrimination of the β-particles.

The 700 kev γ-transition was not detected in either the singles spectrum of the purified source or in the impurity spectrum. This fact together with the data on the relative intensities of the 700, 850 and 1120 kev lines in the γ-β coincidence spectrum gives reason to assert that the 700 kev γ-line belongs to hafnium. The fact that it is not evident in the singles spectrum may be explained by the difficulty of detecting it on the side of the appreciably more intense 615 kev line.

3. Discussion

On the basis of the relative internal conversion electron line intensities we evaluated the K/L, $(L_I + L_{II})/L_{III}$, L/M and M/N ratios for a number of γ-transitions in Ta^{181}. We then made multipole order assignments for these γ-transitions on the basis of the K/L ratio (the $(L_I + L_{II})/L_{III}$ ratio in the case of the 136.25 kev transition). The data on the internal conversion coefficients ratios and the multipole order assignments are given in the accompanying table.

The results of our multipole order determinations agree with the data of Boehm & Marmier[1] except for the 476 kev transition: according to our evaluations this transition is E2 + M1 rather than M2.

We have amplified and supplemented the level scheme for Ta^{181} by inserting the new γ-transitions detected in the present experiments (Fig.10). As will be evident from Fig.6, there are coincidences between the 476 and 482 kev transitions, hence it must be assumed that there actually is a 958 kev level in Ta^{181}. In view of the multipole order of the 476 kev transition and the spin of the 482

Internal conversion coefficient ratios and multipole order assignments

γ-transition energy, kev	Conversion coefficient ratios					Multiple order assignment
	α_K/α_L	$\alpha_{L_I}+\alpha_{L_{II}}/\alpha_{L_{III}}$	α_L/α_M	α_M/α_N	$\alpha_L/\alpha_M+\alpha_N$	
133,02	1,03±0,04	1,38±0,01	4,31	3,7	3,4	$E2$
136,25	5,7	7	4,15	4,27	3,36	12%$E2$+88%$M1$
345,85	3,1±0,1	3,7±0,3	3,93	4,08	3,15	$E2$
476,0	4,91±0,06					79%$E2$+21%$M1$
482,0	4,53±0,08		4,16	3,36	3,2	90%$E2$+10%$M1$
615,5	4,96±0,04				3,02	$M3$

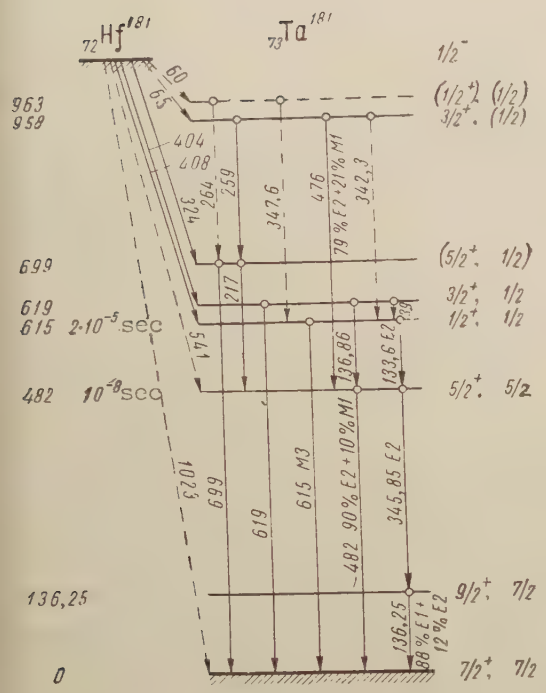

Fig.10. Proposed amplified decay scheme for Hf^{181}.

level it may be inferred that the spin and parity of the 958 kev level are 3/2+. There is probably a 342.3 kev transition departing from the 958 kev level to the 615 kev level (274.9 kev & K-342.3 line in Fig.3).

The 699 kev γ-transition presumably goes to the ground state of Ta^{181} inasmuch as there is a β-component with end-point energy ~340 kev (the more precise value of the end-point energy should be 324 kev - Fig.10).

Inasmuch as the 259 kev γ-rays yield coincidences only with <65 kev electrons (Fig.7), the 259 kev transition must depart from the 958 kev level. The 217 kev γ-transition departs from the 699 kev level and goes to the 482 kev (5/2+) level. The 347.6 kev γ-transition was observed in the internal conversion electron spectrum but not in the spectrum of coincidences with 482 kev γ-rays. If this transition does belong to Ta^{181}, it must feed the level at 615 kev which has a lifetime of $2\cdot10^{-5}$ sec. In view of this it may be inferred that Ta^{181} also has an excited level at 963 kev. The spin of this level should not be large, for with a large spin this level would not form in β-decay of Hf^{181} which has spin 1/2+. If the 963 kev level does exist, the 270 ± 20 kev line in Fig.3 is the sum of two lines: 259 and 264 kev.

According to Nilsson's scheme[3], in addition to the known levels, there should be two close levels in Ta^{181} with spins 1/2+ and 3/2+. The 963 kev level is apparently a single-particle level with spin 1/2+. The level at 958 kev, the assignment for which is 3/2+, may be a single-particle level or it may be the first excited level of a rotational band, lying below the band ground state. A similar situation is observed in some fracium isotopes and obtains when the coefficient a in the formula for the energy of the rotational levels is negative and greater than unity in absolute value.

The excited level at 699 kev is apparently a rotational level with spin 5/2+, the ground state of this band being the 615 kev level (spin 1/2+). The position of the rotational band level with spin 5/2+ may be calculated from the rotational bands of Tm^{169} and Tm^{171}, which in the ground state, has spin 1/2+ with the same

nucleon configuration as the 615 kev state in Ta^{181}. Such calculation shows that the level with spin 5/2+ should have an excitation energy of about 700 kev, which substantiates our inference regarding the rotational character of the 699 kev level. It is not impossible, however, that this level is a single-particle one.

We desire to express our deep gratitude to L.I.Rusinov for his constant interest in the work, D.A.Varshalovich for discussion of the results, A.I.Egorov for chemical purification of the source material and Yu.N.Andreev for assistance in carrying out the measurements.

Physical-Technical Institute,
Academy of Sciences of the USSR

References

1. F.Boehm & P.Marmier, Phys.Rev., 103, 342 (1956).
2. P.Debrunner, E.Heer, W.Kündig & R.Rüetschi, Helv.phys.acta, 29, 463 (1956).
3. S.G.Nilsson, Kgl.Danske Vidensk.Selsk., Mat.-fys.Medd., 29, 16 (1955).

* * * * * * *

DECAY OF Tm^{168}

- V.I.Kochevanov, R.A.Kuznetsov, A.N.Murin, V.N.Pokrovskii & L.A.Smirnov

Among the spallation products of tantalum bombarded with 660 Mev protons there was observed[1,2] a long-lived thulium isotope: Tm^{168} (period 87 days according to Wilkinson & Hicks[3] or 85 days according to Handley & Olson[4]). There were observed γ-rays[1] with energies of 80, 100, 200, 350, 800 and 1100 kev and conversion electrons[2] associated with a 79.7 kev transition. Subsequent investigations (Refs.5-7) of Tm^{168}, in this case formed by bombardment of Er with 22 Mev protons, established the existence of γ-transitions having energies of 79.7, 99.9, 184.6, 199, 247, 448, 720 and 820 kev and of an isomeric level with a half-life of $12 \cdot 10^{-8}$ sec. The level scheme proposed on the basis of γ-γ coincidence experiments is shown in Fig.1. An interesting feature of this scheme is the coincidence in time of the 720 and 820 kev γ-rays; Mihelich & Harmatz[6] noted the prompt ($<10^{-8}$ sec) character of these coincidences.

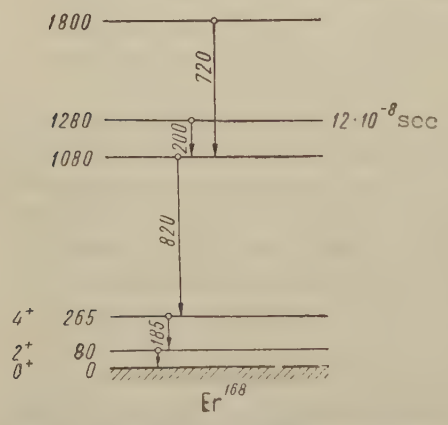

Fig.1. Tentative level scheme for Er^{168}.

In the present study, as in the work of Refs. 1 & 2, there were used Tm^{168} sources obtained by spallation of tantalum. The admixture of other shorter-lived Tm isotopes was negligibly small.

The Tm^{168} activity was studied by means of a scintillation γ-spectrometer and the delayed γ-γ coincidence technique. The γ-spectrometer was calibrated in intensity; the half-widths of the standard Cs^{137} line was ~9% (20 x 30 mm NaI(Tl) crystal coupled to an FEU-S photomultiplier). The coincidence equipment, employing 12 x 30 mm NaI(Tl) crystals, had a resolving time of $2 \cdot 10^{-7}$ sec; the half-width of the standard Cs^{137} line was ~10.5% in each channel. One of the channels incorporated a variable delay line with a delay time range from

Table 1

Energies and relative intensities of Tm^{168} γ-lines
(Results of γ-γ coincidence experiments)

γ-ray energy, kev	Relative γ-ray intensity	Coincid. with other lines*	Is γ-ray delayed	γ-ray energy, kev	Relative γ-ray intensity	Coincid. with other lines*	Is γ-ray delayed
45 (x)	1,6	—	Partial	650	0,20	—	
80	0,11	—	Yes	720	0,45	720 (+), 820 (—)	No
100	0,05	—					
185	0,45	720 (+), 820 (+)	Partial	820	1,0	See above	Yes
				910	0,1	—	
200	0,38	720 (—), 820 (+)	Yes	1090	weak	—	
				1270	0,05	—	No
250	0,09	—		1530	weak	—	No
450	0,30	720 (—), 820 (+)	No	1640	weak	—	No

* (+) means coincidences; (—) no coincidences.

0 to 1 μsec in 0.01 μsec steps. The constant delay in the other line insured observation of prompt coincidences with a delay of 0.3 μsec in the variable line in the first channel.

The experimental results are shown in Table 1.

The lifetime of the metastable level was found from the slope of the resolved delay coincidences curve (for example, x-radiation — 820 kev γ-rays) and proved to be equal to 0.11 ± 0.015 μsec.

The first column of the table we give the energies of the γ-rays detected in our experiments. It must be noted that the 185 and 200 kev γ-lines were not resolved by the spectrometer. Hence we could judge of the presence of these two lines only by the broadening of the curve; the data on the energies of these transitions are taken from Mihelich, Harmatz & Handley[7]. We detected a number of new γ-transitions, primarily in the high energy region of the spectrum. Some of these transitions (640, 940 and 1300 kev) were detected in the work of Groshev et al[8] in the γ-spectrum emitted in the capture of thermal neutrons by Er.

The relative intensities of the γ-transitions listed in the second column of the table were evaluated with an accuracy of ~15% in view of the complexity of the γ-spectrum and the consequent difficulty of resolving it into individual components. It must be noted that a line is clearly evinced at ~1020 kev in the γ-spectrum of Tm^{168}; it was shown, however, that this line is the result of summation of pulses (apparently from the 200 and 820 γ-rays) in the NaI(Tl) crystal. To demonstrate this, the soft (<400 kev) part of the spectrum was attenuated by a lead absorber; as a result the 1020 kev line became unnoticeable and there became evident a weak 1090 kev line.

The third column of the table lists the fully substantiated data on γ-γ coincidences. In observing the coincidences of the 185 and 200 kev γ-rays with the 720 and 820 γ-rays the clearest results were obtained in the case when the stationary narrow channel of the coincidence circuit was set on one of the sides of the peak associated with the 185-200 kev group (in order to discriminate only one line of the group), while the variable channel was adjusted for the 720-820 kev group. A highly interesting result is the absence of 720—820 kev coincidences and the presence of 720 self-coincidences (Fig.2). This is clearly in conflict with the scheme shown in Fig.1. That this tentative scheme is in error is also shown by comparison of the intensities of the 185 and 820 kev transitions: the intensity of the 185 kev transition (multipole order E2) is appreciably lower than the intensity of the 820 kev transition.

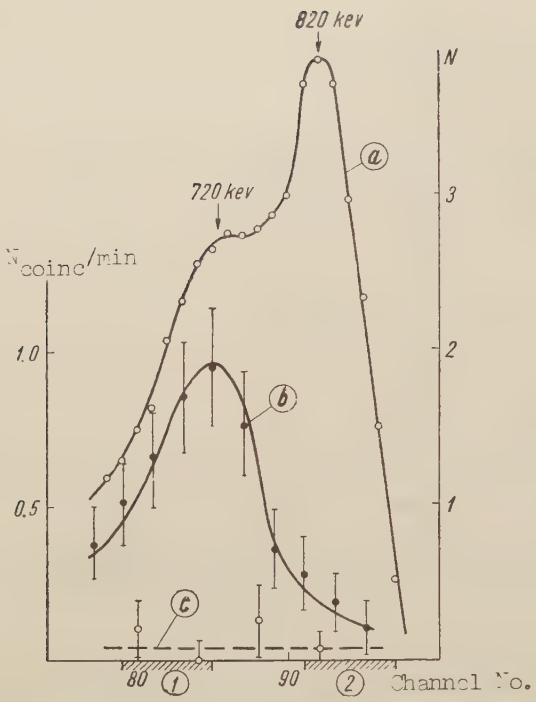

Fig.2. Coincidence spectrum in the 720 to 820 kev region: a) 720-820 kev line group recorded by the variable channel with the stationary channel switched off; b) coincidence spectrum with the stationary channel set on the 720 kev line (in position 1); c) coincidence spectrum with the stationary channel set on the 820 kev line (position 2).

The table does not show the obvious results, i.e., coincidences of the x-radiation with all the γ-rays, the doubtful data such as, for example, coincidences of the 185-200 kev group with the 450 kev gammas, etc. The last column in the table gives information on the degree of delay of the γ-rays. The presence or absence of delay is readily evaluated from the shape of the delayed coincidences resolution curve. The degree of delay is indicated somewhat arbitrarily. For example, the 185 and 200 kev lines yield delayed coincidences with the x-radiation. The intensity of the 200 kev line in the delayed coincidences spectrum is greater than the intensity of the 185 kev line, whereas in the ordinary spectrum (or with nondelayed coincidences), the relative intensities are reversed. It follows from this that the degree of delay of the 185 kev γ-rays is less than of the 200 kev γ-rays. In other words, a relatively larger number of transitions missing the metastable level feeds the departure level of the 185 kev γ-rays. Hence the notation "yes" in the last column does not necessarily mean full delay of the given γ-transitions.

We also recorded the spectrum of delayed coincidences with the x-radiation in the 20 to 250 kev region. In this case the stationary channel was set on the peak of the x-radiation and a delay was introduced into this channel to eliminate nondelayed coincidences; the variable channel was swept through the region from 20 to 250 kev. The intensity ratios obtained for the x-radiation and the 80, 185 and 200 kev γ-rays were approximately:

$$I_x : I_{80} : I_{185} : I_{200} = 40 : 8 ; 40 : 55.$$

The delayed x-radiation arises owing to conversion of the delayed γ-transitions. Hence

$$I_x \approx \omega_K (\alpha_{K\text{-}80} I_{80} + \alpha_{K\text{-}185} I_{185} + \alpha_{K\text{-}200} I_{200}),$$

where ω_K is the fluorescence coefficient, and α_K is the K shell conversion coefficient. Assuming the multipole order of the 80 and 185 kev transitions to be E2, one can find the theoretical value[9] of $\alpha_{K\text{-}80}$ and $\alpha_{K\text{-}185}$ and thus obtain an evaluation of the K shell conversion coefficient of the 200 kev transition. We found $\alpha_{K\text{-}200} = 0.37 \pm 0.1$. In making the evaluation we did not take into account the delayed x-radiation arising as a result of conversion of γ-transitions of higher energy than 200 kev. This does not introduce an appreciable error inasmuch as the conversion coefficient of the 820 kev γ-rays should not be large, and there are not other intense delayed transitions (see Table 1).

Table 2

α_K for the 200 kev transition

$\alpha_{K\,exp}$	$\alpha_{K\,theo}$				
	E1	E2	E3	M1	M2
0.37±0.1	0.043	0.166	0.512	0.34	1.78

The experimental value of α_K for the 200 kev transition is closest to the theoretical value[9] of the K shell conversion coefficient for multipolarity M1 (see Table 2).

After completion of the present experimental work there was published the brief communication of Jacob et al[10] in which there is proposed the following level sequence: 79.9(2+), 264.6(4+), 549.1(6+), 822.0(2+), 896.7(3+), 996(4+), 1095(3 or 4-, T = $12 \cdot 10^{-8}$ sec) and 1543.1 kev (4-). The 822, 897 and 996 kev levels comprise a second rotational band.

Fig.3 shows the decay scheme supplemented by the introduction of levels at 1345 and 1720 kev. The positions of these levels were determined primarily by energy considerations. After their introduction all the observed γ-rays, except the 1530 kev γ-rays, can be fitted into the scheme. Some divergences between the level energy differences and the γ-transition energies may be explained either by inaccuracy in determining the transition energies or by postulating the existence of close transitions not resolved by the spectrometer. These possibilities which are not in conflict with the proposed level assignments are indicated by dashed

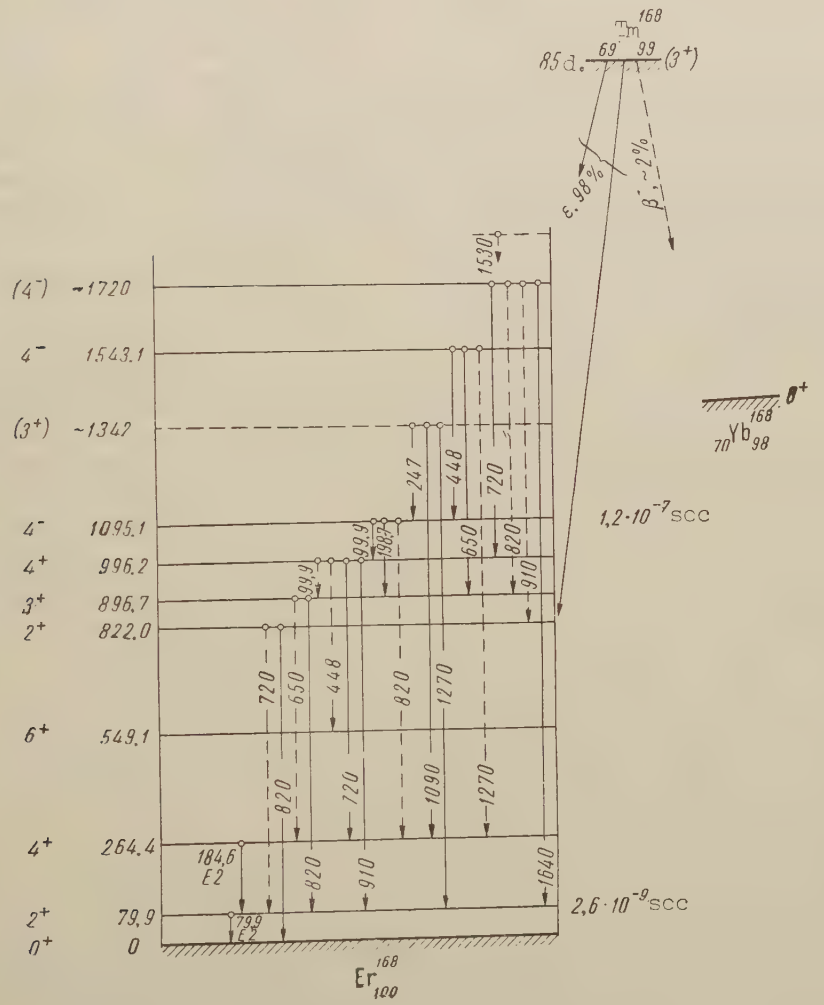

Fig.3. Decay scheme for Tm^{168}.

lines in the figure. The indicated lifetime of the 80 kev state is taken from the work of Berlovich et al[11]. It will be evident from examination of Fig.3 that our data are not in conflict with the proposed scheme except for the multipole order of the 200 kev transition. A more detailed discussion of the decay scheme must await accumulation of additional experimental data.

We desire to express our deep gratitude to I.A.Yutlandov for chemical separation of the irradiated material and L.K.Peker for discussion of the results.

Nuclear Problems Laboratory of the
Joint Institute for Nuclear Research,
"A.A.Zhdanov" Leningrad State University

References

1. G.M.Gorodinskii, A.N.Murin, V.N.Pokrovskii & B.K.Preobrazhenskii, Izv. AN SSSR, Ser.fiz., 21, 1004 (1957). (Trans.Bulletin 21, No.7, 1005.)

2. K.Ya.Gromov, B.S.Dzhelepov & B.K.Preobrazhenskii, Ibid., 21, 918 (1957). (Trans.Bulletin 21, No.7, 920.)

3. G.Wilkinson & H.G.Hicks, Phys.Rev., 75, 1370 (1949).

4. T.H.Handley & E.L.Olson, Phys.Rev., 94, 968 (1954).

5. K.P.Jacob, J.W.Mihelich & B.Harmatz, Bull.Amer.Phys.Soc., Ser.II, 2, 260 (1957).

6. J.W.Mihelich & B.Harmatz, Phys.Rev., 106, 1232 (1957).

7. J.W.Mihelich, B.Harmatz & T.H.Handley, Phys.Rev., 108, 989 (1957).

8. L.V.Groshev, A.M.Demidov, V.N.Lutsenko & V.I.Pelekhov, Atomnaya energiya, 4,5 (1958). (Trans.Soviet Journal of Atomic Energy.)

9. L.A.Sliv & I.M.Band, Tablitsy koeffitsientov vnutrennei konversii (Tables of Internal Conversion Coefficients), Part I, K shell, M.-L., 1956.

10. K.P.Jacob, J.W.Mihelich, B.Harmatz & T.H.Handley, Bull.Amer.Phys.Soc., Ser.II, 3, 358 (1958).

11. É.E.Berlovich, K.Grotovskii, M.Bonits, V.I.Broslav, V.P.Fleisher & B.K. Preobrazhenskii, Materialy soveshchaniya po primeneniyu radiokhimicheskikh metodov izucheniya yadernykh reaktsii i β i γ-spektroskopii neitronodefitsitnykh yader (Transactions of the conference on application of radiochemical methods of investigating nuclear reactions and β- and γ-spectroscopy of neutron-deficient nuclei), Vol.3, Dubna, 1958.

ANGULAR DISTRIBUTION OF PROTONS FROM THE $Be^9(d,p)Be^{10}$, $Si^{28}(d,p)Si^{29}$ AND $Bi^{209}(d,p)Bi^{210}$ REACTIONS

- N. I. Zaika & O. F. Nemets

Investigation of stripping reactions is of interest from the standpoint of both the theory of nuclear reactions and the theory of nuclear models, for it allows of determining the spins and parities of nuclei. Most experimental studies of nuclear stripping reactions were carried out with deuterons of energies not exceeding 3-5 Mev. An exception is the group of studies carried out on the Liverpool cyclotron at a deuteron energy of 9 Mev (Ref.1) and individual studies involving deuterons of up to 15 Mev energy (Ref.2).

Investigation of stripping at high deuteron energies is of great interest inasmuch as, first, at these energies the influence of the Coulomb barrier on the reaction is minimized, which allows of carrying out measurements on medium and high mass number nuclei; second, the contribution from the process involving formation of a compound nucleus, the excited levels of which lie in the region of quasi-continuous states, is reduced, which simplifies comparison of theory with experiment; and, third, investigation of stripping reactions in this energy region is of independent interest from the standpoint of the theory of nuclear reactions.

The fact that there have been few investigations in the high deuteron energy region may be explained by the appreciable difficulties encountered in carrying out such experiments. These difficulties are connected with the requirement for selectivity and good energy resolution (<2-3%) set for the spectrometer. The last requirement precludes the use of spectrometers with absorbers and double crystal selective scintillation spectrometers, the resolution of which is appreciably inferior to 2-3%, and makes it essential to use magnetic spectrometers and ionization chambers. Magnetic spectrometers, while they have a high energy resolution, are characterized by a low transmission factor, yield data the processing of which is highly cumbersome and moreover do not possess universal selectivity.

In view of the above considerations we developed a selective spectrometer designed about an ionization chamber, which is described in detail in Ref.3.

Experimental Procedure

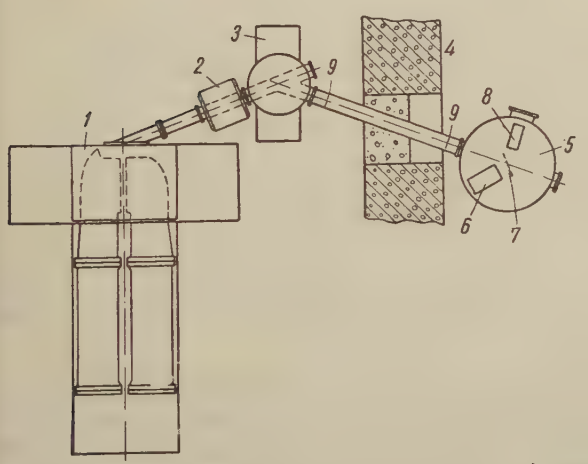

Fig.1. Experimental arrangement: 1) accelerator, 2) focusing magnet, 3) deflecting magnet, 4) shielding, 5) reaction chamber, 6) spectrometer, 7) target, 8) monitor, 9) collimators.

The deuteron source used in the proton angular distribution experiments was the cyclotron of the Physics Institute of the Ukrainian SSR Academy of Sciences. The arrangement of the spectrometer, monitor and collimators is shown in Fig.1. The monitor employed was a threshold scintillation counter.

For the purposes of the present investigation the spectrometer was somewhat simplified, as compared with that described in Ref.3: mainly, the split electrode consisted of only two parts rather than four, as earlier.

The size of the plates was chosen so that at the working pressure in the chamber the deuteron, triton and α-particle ranges terminated within the region of location of the first plate, and only protons could reach the second plate (Fig.2). The selec-

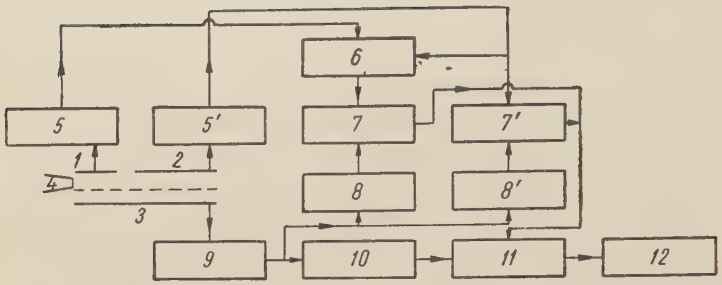

Fig.2. Block diagram of the spectrometer: 1) first spectrometer plate, 2) second plate, 3) main plate, 4) entry foil, 5 & 5') amplifiers, 6) anticoincidence circuit, 7 & 7') coincidence circuits, 8 & 8') discriminators, 9) linear amplifier, 10) delay line, 11) coincidences with retention of amplitude, 12) multiple channel pulse height analyzer.

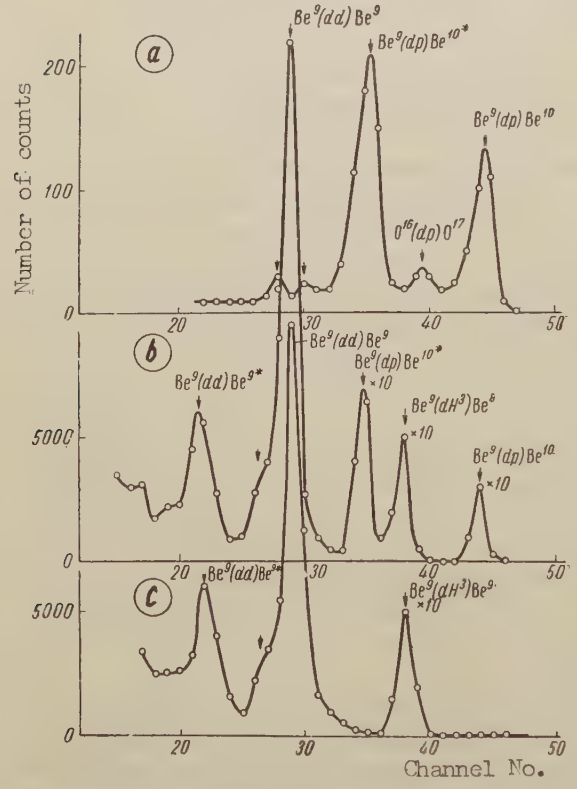

Fig.3. Pulse coincidence spectra for the products of the Be^9 + d reaction: a - from the second and main electrodes, b - from the first and main electrodes, and c - from the first and main electrodes when the circuit is connected for anticoincidence with the pulses from the second electrode.

tivity of the spectrometer for the Be^9 + d reaction is shown in Fig.3. When the circuit is adjusted for coincidence of the pulses from the second and main electrodes only protons are detected (Fig.3,a); when the setting is for coincidence of the pulses from the first and main electrodes, protons, deuterons, tritons and α-particles are detected (Fig.3,b), while when in addition the pulses from the first and second electrodes are fed into the anticoincidence circuit, protons are not detected (Fig. 3,c). After the coincidence-anticoincidence circuit, the pulses are fed into a multiple channel pulse height analyzer with a magnetic memory[4]. The energy resolution of the apparatus was ~3%, but it can be substantially improved.

Experimental Results

The proton angular distributions corresponding to the ground and excited states of Be^{10} and Si^{29} and the ground state of Bi^{210} are shown in Figs.4 through 9. The points indicate the experimental values; the solid lines are the curves calculated according to Butler's formula[5]. In the calculations, the radius for silicon and bismuth was calculated by the familiar formula $R_o = (1.7 + 1.22\ A^{1/3}) \cdot 10^{-13}$ cm. For beryllium the best agreement with the experimental points is obtained with the radius taken equal to $4.8 \cdot 10^{-13}$, a value somewhat greater than that given by the formula.

Discussion of the Results
$Be^9(d,p)Be^{10}$

As will be apparent from Figs.4 & 5, the proton distributions corresponding to the ground and excited state of Be^{10} are in agreement with the theoretical curves for the case when the neutron is captured with orbital angular momentum $l_n = 1$. Assuming the Be^9 ground state spin to be 3/2-, the spins of the ground and first excited

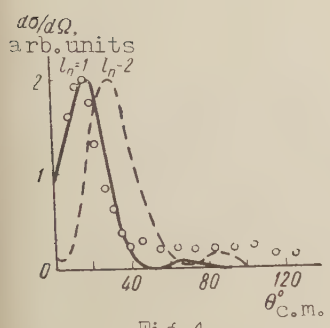

Fig.4

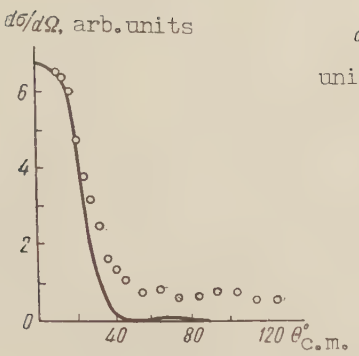

Fig.5

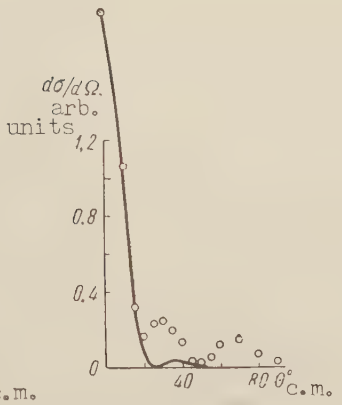

Fig.6

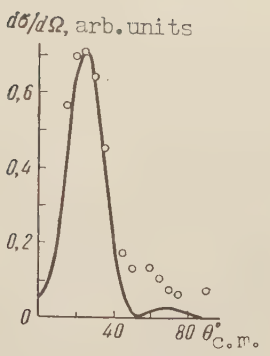

Fig.7

Fig.4. Angular distribution of protons from the $Be^9(d,p)Be^{10}$ reaction. Q = 4.596 Mev; $l_n = 1$; $R_o = 4.8 \cdot 10^{-13}$ cm. Curves calculated according to Butler's formula[5].

Fig.5. Same as Fig.4 but for the $Be^9(d,p)Be^{10*}$ reaction. Q = 1.22 Mev; $l_n = 1$; $R_o = 4.8 \cdot 10^{-13}$ cm.

Fig.6. Same as Fig.4 but for $Si^{28}(d,p)Si^{29}$ reaction. Q = 6.246 Mev; $l_n = 0$; $R_o = 5.4 \cdot 10^{-13}$ cm.

Fig.7. Same as Fig.4 but for $Si^{28}(d,p)Si^{29*}$ reaction. Q = 4.97 Mev; $l_n = 2$; $R_o = 5.4 \cdot 10^{-13}$ cm.

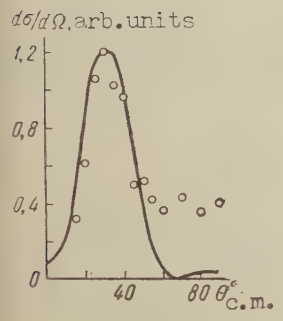

Fig.8

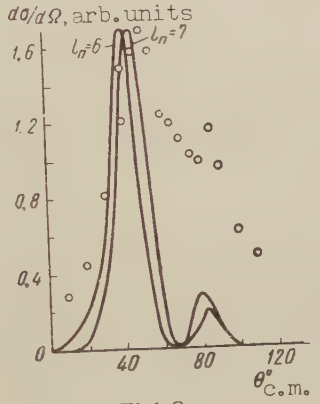

Fig.9

Fig.8. Same as Fig.4 but for $Si^{28}(d,p)Si^{29*}$ reaction. Q = 2.62 Mev; $l_n = 3$; $R_o = 5.4 \cdot 10^{-13}$ cm.

Fig.9. Same as Fig.4 but for $Bi^{209}(d,p)Bi^{210}$ reaction. Q = 1.94 Mev; $l_n = 6$; $R_o = 8.9 \cdot 10^{-13}$ cm.

state of Be^{10} may be 0+, 1+, 2+ or 3+. for the excited state, inasmuch as the 0+ assignment must be excluded in view of the fact that there is a γ-transition from the first excited state.[6]

$Si^{28}(d,p)Si^{29}$

The proton group corresponding to the Si^{29} ground state has an angular distribution consistent with the theoretical one for $l_n = 0$ (Fig.6). This means that the assignment for the ground state of Si^{29} is 1/2+, inasmuch as the nuclear spin of Si^{28} is 0+. In excitation of the first level of Si^{29} a neutron with $l_n = 2$ is captured (Fig.7). The possible assignments for this first excited state are 3/2+ and 5/2+. We were unable to plot the angular distributions for the second, third and fourth levels owing to the low intensity of the corresponding proton groups. For the fifth level $l_n = 3$ (Fig.8) and the possible assignments are 5/2- and 7/2-. The indicated assignments for the ground and first excited states are in agreement with the predictions of the nuclear shell model.[7] For the 3.62 Mev level the shell model allows of only 1/2+. The value obtained by us can be explained if we assume that Si^{29} has an oblate shape[8].

$Bi^{209}(d,p)Bi^{210}$

The $Bi^{209}(d,p)Bi^{210}$ reaction was investigated earlier by a number of authors[2] at deuteron energies of 14-15 Mev. In one set of experiments, however, the proton angular distribution had no pronounced maximum corresponding to the stripping reaction, while in the other set of experiments the spin value deduced for the ground state of Bi^{210} (0-) differs from the value obtained by Smith (cited in Ref.10), but is in agreement with the calculations of Pryce[10] and Brink[9]. Our experimental proton directional distribution has two characteristic peaks at 50° and 85°. The calculated maxima for $l_n = 6$ and $l_n = 7$ lie at 40 & 80° and 45 & 85°; if we take $l_n = 6$, the ground state spin may be 1-. We feel that $l_n = 5$, the orbital momentum value necessary to obtain 0+ for the Bi^{210} ground state, is implausible. For definitive solution of this problem, however, one must take into account both the Coulomb and nuclear interaction.[10]

We desire to thank M.V.Pasechnik for interest in the work and valuable advice, G.A.Kosinov and V.N.Dobrikov for assistance in the experiments, Yu.A.Bin'kovskii for preparing the targets, and the personnel of the cyclotron laboratory for insuring faultless operation of the accelerator.

Physics Institute,
Academy of Sciences of the Ukrainian SSR

References

1. J.R.Holt & T.H.Marsham, Proc.Phys.Soc., A66, 249, 258, 457, 565, 1032 (1953); F.A.ElBedewi, Proc.Phys.Soc., A69, 221 (1956); T.S.Green & R.Middleton, Proc.Phys.Soc., A69, 16 (1956).
2. H.E.Gove, Phys.Rev., 81, 364 (1951); J.Harvey, Canad.J.Phys., 31, 278 (1953); N.S.Wall, Phys.Rev., 96, 664 (1954).
3. O.F.Nemets, Trudy sessii AN USSR po mirnomu ispol'zovaniyu atomnoi energii (Proceedings of the session of the Ukrainian SSR Academy of Sciences on the peaceful uses of atomic energy), p.145, Kiev, 1958.
4. R.G.Ofengenden, L.D.Konenko & V.G.Kotova, Ibid., p.161.
5. S.T.Butler, Proc.Roy.Soc., A208, 559 (1951).
6. W.F.Hornyak, T.Lauritsen & V.K.Rasmussen, Phys.Rev., 76, 581 (1949).
7. P.F.A.Klinkenberg, Revs.Mod.Phys., 24, 63 (1952).
8. D.A.Bromley, H.E.Gove, E.B.Paul, A.E.Litherland & E.Almquist, Canad.J. Phys., 35, 1057 (1957).
9. D.M.Brink, Proc.Phys.Soc., A67, 757 (1954).
10. M.H.L.Pryce, Proc.Phys.Soc., A65, 73 (1952).

NUCLEAR REACTIONS OF MULTIPLY CHARGED IONS WITH CARBON AND OXYGEN AND THEIR INFLUENCE IN INVESTIGATION OF COULOMB EXCITATION

- D.G.Alkhazov, A.P.Grinberg, G.M.Gusinskii & I.Kh.Lemberg

Introduction

Investigation of Coulomb excitation of high-lying levels requires increasing the energy of the bombarding particles. The use of protons or α-particles in such experiments leads to a sharp increase of the γ-background (particularly in the case of bombardment of low mass number nuclei) that arises due to reactions involving the formation of a compound nucleus. In principle, the intensity of the background γ-lines must decrease greatly if heavy ions are employed as the projectiles.[1]

However, even in our first attempt to use 25 Mev nitrogen ions for excitation of high energy nuclear levels in Sn isotopes we encountered a background of γ-lines, the intensity of which was much greater than the expected intensity of γ-rays emitted as a result of Coulomb excitation.

For the purpose of elucidating the origin and character of this background γ-radiation we investigated the γ-spectra of over 40 different elements, their compounds and isotopes, arising as a result of bombardment by C^{12}, N^{14}, O^{16}, Ne^{20} and Ne^{22} ions. The γ-radiation was detected by means of a scintillation spectrometer consisting of a 40 mm diameter, 40 mm thick NaI(Tl) crystal coupled to an FEU-11 photomultiplier and a 50-channel pulse height analyzer. In these experiments we used the same "close geometry" as in our earlier work[2,3] on the γ-rays emitted as a result of Coulomb excitation of nuclear levels. As before, the distance from the target to the face of the crystal was 2.7 mm. The γ-radiations were studied in the region from 0.1 to 2 Mev. The spectrometer was calibrated in energy by means of "standard" radioactive γ-sources.

By way of bombarding particles we used the following ions accelerated in a cyclotron: 13.6 Mev C^{12}, 11 to 40 Mev N^{14}, 18.1 Mev O^{16}, 23.1 to 27.8 Mev Ne^{20} and 25.6 Mev Ne^{22}.

1. Background γ-radiation in the experiments with N^{14} ions

The spectrum of the background γ-radiation was investigated in greatest detail in the case when the projectiles were nitrogen ions, inasmuch as these ions were most frequently used in our studies of Coulomb excitation.

To reduce the number of possible nuclear reactions (modes of disintegration of the compound nucleus), initially we chose a relatively low nitrogen ion energy, namely, 15.9 Mev. It was found that in the case of irradiation of any target containing elements with $Z \geqslant 11$, in addition to the γ-lines associated with Coulomb excitation there were always observed four background γ-lines with energies of 0.35, 0.51, 0.59 and 1.37 Mev; the 0.51 Mev line was always weaker than the 0.59 Mev line. It was also established that the intensity of the enumerated γ-lines (per microcoulomb of the ion beam) increased sharply - in many cases by two orders of magnitude - when the target was of graphite.

It is natural to assume that all the above mentioned background γ-lines are the result of nuclear reactions of nitrogen with carbon. The appearance of exactly the same background lines in bombardment of different targets with nitrogen ions is apparently connected with the presence of carbon either contained in the target as an impurity or deposited on the target surface from the oil vapor and separating from the hydrocarbon compounds owing to dissociation of the compounds under ion bombardment. Below in Section 2 we will adduce further arguments in favor of this assumption.

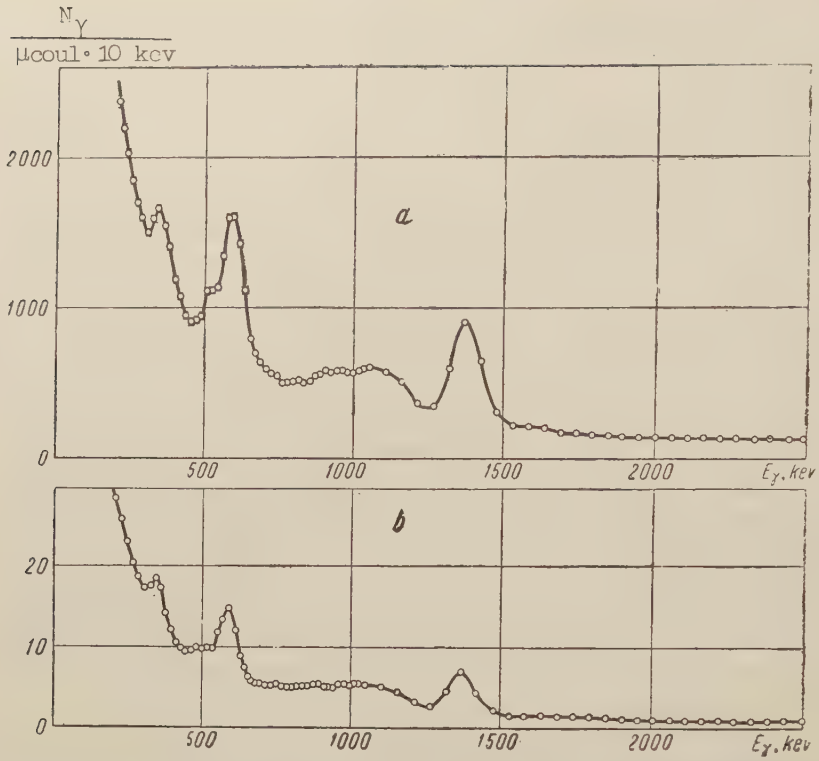

Fig.1. Spectra of γ-radiation emitted in bombardment of graphite (a) and nickel (b) targets with 15.9 Mev nitrogen ions. The vertical scale is laid off in terms of the γ-ray yield normalized to 1 microcoulomb of the ion beam and a 10 kev analyzer channel width.

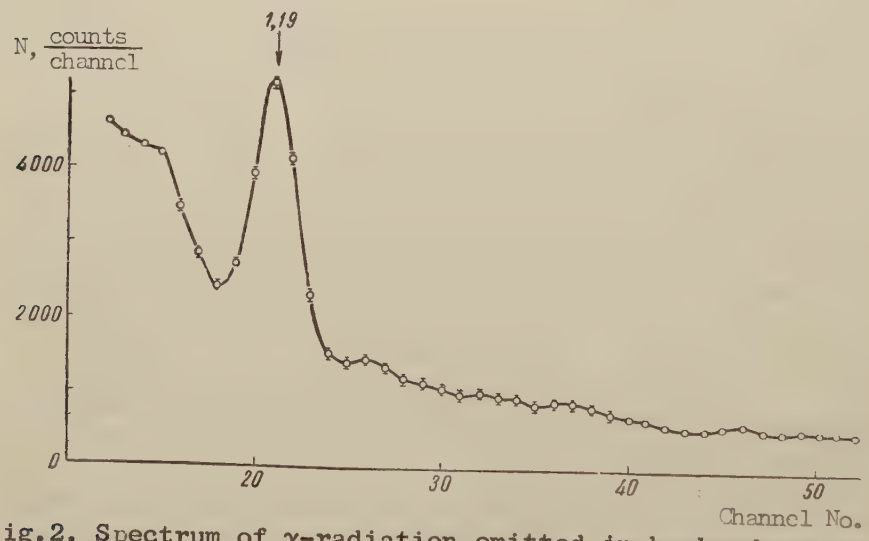

Fig.2. Spectrum of γ-radiation emitted in bombardment of Ni^{62} with quadruply charged 35 Mev nitrogen ions.

Fig.1 shows the γ-ray background spectra emitted in bombardment of carbon and nickel with 15.9 Mev nitrogen ions. It will be apparent that the two spectra are identical.

Upon reduction of the nitrogen ion energy to 11.25 Mev and bombardment of a graphite target the intensity of the continuous γ-background and the background lines at 1.37 and 0.59 Mev decreases, while the 0.51 and 0.35 Mev lines are no longer apparent. Increase of the nitrogen ion energy leads to increase in the intensity of the continuous background and the background lines; concurrently, the relative intensity of the 0.51 Mev line increases as compared with the intensity of the 0.59 Mev line. This is apparently connected with increase in the number of different decay modes of the compound nucleus, leading to formation of β^+-active nuclei.

In the case of bombardment of targets containing light elements, with increase of the nitrogen ion energy there is a marked increase in the continuous γ-background and there appear additional background lines in addition to the four identified above. Thus, for example, in the bombardment of silicon with 25 Mev N^{14} ions there is observed an additional background γ-line at 1.63 Mev; in the bombardment of aluminum - two new lines at 0.69 and 0.81 Mev. With increase of the ion energy there is observed a decrease of the relative yield of the reactions occurring in a thin carbon film; apparently this

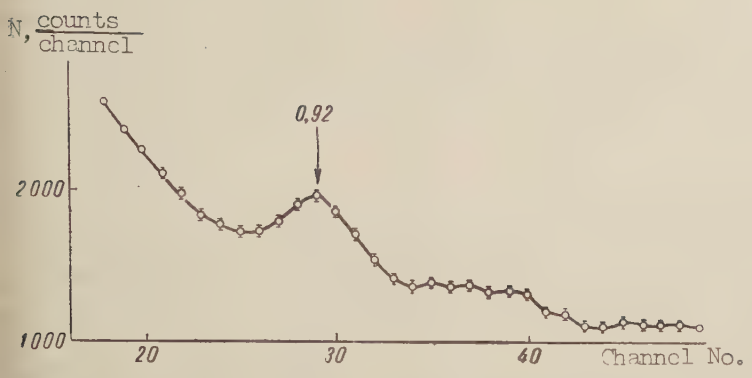

Fig.3. Spectrum of γ-radiation emitted in bombardment of vanadium with quadruply charged 35 Mev nitrogen ions.

is a result of increase of the nitrogen ion range. Owing to this, in a number of cases in bombardment of light elements the 1.37 Mev line is effaced by the continuous background. In contrast, in the case of bombardment of heavy and medium elements the continuous γ-background increases very little and the intensity of the 1.37 Mev line greatly exceeds the background intensity in this spectral region.

The γ-radiation spectra obtained in bombardment of Ni^{62} and vanadium with 35 Mev nitrogen ions are shown in Figs.2 and 3, respectively. The arrows indicate the γ-lines associated with Coulomb excitation of nuclear levels. It will be apparent from the figures that the 1.37 Mev line does not appear in the γ-spectrum in the case of bombardment of nickel and vanadium.

Investigation of Coulomb excitation of the 1.33 Mev level in Ni^{60} proved to be impossible at low values of the nitrogen ion energy E_N owing to the presence of the background line at 1.37 Mev: at E_N = 15.9 Mev the theoretical yield of the Coulomb excitation 1.33 Mev γ-rays from Ni^{60} amounts to 7 counts/μcoul, whereas the experimentally observed "yield" of the 1.37 Mev background line equals 300 counts/μcoul.

On the other hand, it proved feasible to obtain quantitative data on Coulomb excitation of the 1.33 Mev level in Ni^{60} at E_N = 35 Mev in view of the fact that at this nitrogen ion energy the yield of gammas as a result of Coulomb excitation is large compared to the continuous γ-background, while the 1.37 Mev line is so weak compared with the continuum that it cannot be discerned.

In bombardment of carbon with 25 Mev nitrogen ions the 0.51 and 0.59 Mev background γ-lines are also virtually effaced by the continuous background. These lines also disappear in the continuum in the case of bombardment of other elements. However, in the case of light elements (for example, phosphorus) with 25 Mev nitrogen ions the 0.51 Mev peak again appears. Apparently, it must be attributed to the formation of β^+-active nuclei.

With increase of E_N to 35 Mev the 0.51 Mev line reappears in the γ-radiation from a graphite target. Its reappearance is apparently connected with increase in the number of modes of disintegration of the compound nucleus (Al^{26}) leading to the formation of β^+-active nuclei.

In principle, in addition to reactions of nitrogen with carbon, possible sources of the background lines may be reactions of the nitrogen with other light elements present in the target as impurities. We observed γ-lines associated with nuclear reactions in bombarding Li, Be and B with 11.2 Mev nitrogen ions. If E_N is increased to 25 Mev or more, background γ-lines also appear in the bombardment of such elements as P, Al and Si. However, the admixtures of all these light elements in our targets were so small that these background lines were virtually insignificant. Usually a substantial role was played only by oxygen impurity: leaving aside the cases when the target was composed of an oxide, we note that often even targets prepared of a pure metal contain oxygen in the form of a surface oxide film. Moreover, small amounts of various oxides are generally contained in separated isotopes in the metallic state.

In all cases of bombardment of targets containing oxygen with nitrogen ions we observed intense background lines at 0.51 and 1.78 Mev. In addition, we observed an increase in the intensity of the 0.59 and 1.37 Mev lines. With increases of E_N from 15 to 40 Mev in bombarding targets containing oxygen the intensity of the 1.78 Mev line increases appreciably more rapidly than the intensity of the background 1.37 Mev line associated with the reaction of nitrogen with carbon.

2. Background γ-radiation in experiments with C^{12}, O^{16}, Ne^{20} & Ne^{22} ions

Investigation of the background γ-radiation spectra in cases of bombardment of targets consisting of $Z > 11$ elements with C^{12}, O^{16}, Ne^{20} and Ne^{22} ions showed that the character of the background γ-spectrum remains essentially the same in bombardment of different targets with ions of the same type. In all cases the intensity of the background lines increased in the case of bombardment of graphites by a factor of 10 to 100 compared with the intensity of these lines in bombardment of targets of other elements. This fact, together with the experimental results for nitrogen ions noted above, lends support to our hypothesis that the background γ-lines observed in bombardment of different targets are due to nuclear reactions of the bombarding ions with impurity carbon nuclei.

It must be noted, however, that another explanation may be suggested. We have in mind here either pick-off of a neutron or proton by the incident nitrogen nucleus or, on the contrary, transfer of a nucleon from the nitrogen nucleus to a target nucleus. In such cases, regardless of the composition of the target, there must be obtained the same nuclei[4,5], for example, N^{13}. The formation of β-active N^{13} nuclei was established from the decay period and the maximum β-particles energy. It should be noted that in a number of cases (including that of N^{13}) the excited states of the nuclei forming from N^{14} by reactions of the indicated type have not been exhaustively studied so that we do not know precisely what γ-lines are comprised in the de-excitation spectra of these states. Hence the background γ-lines observed by us in bombardment of different targets with nitrogen ions could be explained by de-excitation of N^{13} or other nuclei formed initially in an excited state by pick-off or transfer reactions.

In order to ascertain the origin of the background lines we irradiated a target containing oxygen (a PbO target) with 13.6 Mev carbon ions. In this case there was observed a 1.4 Mev line (due to the C + O reaction) and a 1.63 Mev line; the latter is present in all γ-spectra emitted in bombardment of different elements by C ions. If this line appears as a result of a C + C reaction, i.e., is associated with carbon impurities in the target, it should not be present in the γ-ray spectrum emitted in bombardment of a carbon target with oxygen ions inasmuch as in the O + C reaction there is obtained the 1.37 line but not the 1.63 Mev line. On the other hand, if in bombardment of PbO with carbon ions the 1.63 Mev line is obtained owing to reaction with oxygen nuclei, it should be observed in the γ-radiation emitted in bombardment of carbon by oxygen.

We therefore carried out an experiment in which a graphite target was bombarded with oxygen ions. The ion energy (18.1 Mev) was chosen so that the collision energy in this case would be equal to the collision energy in bombardment of oxygen with 13.6 Mev C^{12} ions. In this case the yield of 1.63 Mev γ-rays referred to 1 microcoulomb of current incident on the target should be the same in the $C^+ + O$ and $O^+ + C$ reactions, but since the oxygen content in PbO is small, the observed 1.63 Mev γ-rays yield in bombardment of C with O^+ must greatly exceed the yield of these γ-rays in bombardment of PbO with C^+. Our experiments showed, however, that the 1.63 Mev line is not observed in bombardment of C with O^+ ions.

Thus for the case of $C^+ + O$ we showed that the background 1.63 Mev line appears as a result of reaction with impurity carbon nuclei and not owing to a

Bombarding particles		E_γ, Mev	
Type	Energy, Mev	Reaction with C	Reaction with O
C^{12}	13,6	0,44 0,51 1,63	0,51 ~1,0 1,37
N^{14}	15,9÷40	0,35 0,51 0,59 1,37	0,51 0,59 ~1 1,37 1,78 (very intense)
O^{16}	18,1	0,51 1,37	—
Ne^{20}*	23,1	—	0,69
Ne^{22}	25,8	**	**

*In bombardment of a graphite target with 27.8 Mev Ne^{20} ions there is observed a large number of background γ-lines; their intensity is low compared with that of the continuous background.

**No background lines of noticeable intensity are observed.

pick-off or nucleon transfer reaction. There is reason to assume that in the other cases, i.e., in the case of reactions induced by nitrogen and oxygen ions, the observed background lines appear as a result of reaction of the bombarding ions with impurity carbon nuclei.

Making use of the experimental data on the yield of 1.37 Mev γ-rays in bombardment of a thick graphite target with 11 to 25 Mev nitrogen ions and the calculated values of dE/dR for stopping of these ions in carbon[6], we evaluated the effective thickness of a carbon film that could account for the yield of gammas observed for different targets. Thus in the E_N range from 11 to 25 Mev the effective average thickness was found to extend from 0.04 to 0.012 μ.

The energies of the γ-rays emitted in bombardment of carbon and oxygen with different ions are listed in the accompanying table.

3. Regarding the origin of the background lines

Most experimental investigations of the reactions of multicharged ions with different elements have been carried out by detecting the particles emitted by the β- or α-active reaction products. There are virtually no data in the literature on the γ-radiations emitted in bombardment of different elements with multicharged ions. Identification of the reaction products on the basis of the γ-rays emitted during bombardment is hampered by the fact that part of the γ-radiation is not associated with the formation of the radioactive reaction products. As a rule, the lifetimes of the excited states are short, and moreover, not known. Hence identification of the reaction products by measuring the lifetime is not feasible. Making A and Z assignments for the reaction products is also hampered by the fact that in reactions with multicharged ions there are generally many modes by which the compound nucleus may disintegrate.

With a view to clarifying the origin of the observed background lines we drew up an energy balance for all imaginable reactions of carbon, nitrogen and oxygen ions with carbon, differing from each other as regards their products. The necessary mass values were taken from Endt & Braams[7].

The following six reactions were found to be possible from the energy standpoint for carbon ions with E_{1ab} = 13.6 Mev:

$$C + C = Mg^{24} + 20.8 \text{ Mev} \quad (1)$$
$$C + C = Mg^{23} + n + 4.2 \text{ Mev} \quad (2)$$
$$C + C = Na^{23} + p + 3.0 \text{ Mev} \quad (3)$$
$$C + C = Ne^{20} + \alpha + 11.4 \text{ Mev} \quad (4)$$
$$C + C = O^{16} + 2\alpha + 6.7 \text{ Mev} \quad (5)$$
$$C + C = C + C' + 6.8 \text{ Mev} \quad (6)$$

The Q-value for reaction (1) is very high and hence disintegration of the compound nucleus by emission of a charged particle is far more probable than by

emission of a γ-ray. The first excited levels of O^{16} forming by reaction (5) have energies of 6.06 and 6.13 Mev; inasmuch as Q for reaction (5) equals 6.7 Mev, this reaction cannot explain the observed background γ-line spectrum. Reaction (6) involving inelastic scattering of the C ions with formation of a compound nucleus is far less probable than the other reactions. Thus it must be assumed that the background γ-lines are formed primarily by reactions (2), (3) and (4). Actually, formation of the β^+-active Mg^{23} nucleus (T = 10.7 sec) by reaction (2) serves to explain the appearance of the 0.51 Mev line, while formation of Na^{23} by reaction (3) can explain the appearance of the 0.44 and 1.63 Mev background lines (it is known that the first excited levels of Na^{23} have energies of 0.44 and 2.07 Mev and that de-excitation of the 2.07 Mev level occurs by emission of cascade 1.65 Mev γ-rays).

The appearance of the 1.63 Mev γ-line can also be explained by reaction (4); the first excited level of Ne^{20} has an energy of 1.63 Mev. As noted above, however, γ-rays of this energy may also be observed as a result of reaction (3) incident to de-excitation of the second excited level of Na^{23}.

Similar analysis shows that in the case of bombardment of carbon with 15.9 Mev nitrogen ions there may occur 14 different reactions. In view of the known data on the decay schemes and excited levels of the product nuclei, in this case the 1.37 Mev γ-line can be explained by occurrence of the $N + C = Mg^{24} + \alpha$ reaction.

Also possible from the energy standpoint is the $N + C = Na^{24} + 2p$ reaction; the compound nucleus Na^{24} may decay by emission of β-rays to the first excited level of Mg^{24} with ΔE = 1.37 Mev. However, measurements of the β-activity (by means of a G-M counter) of a graphite target after bombardment with nitrogen ions showed that there was no significant amount of Na^{24} activity present.

The 0.35 Mev Δ-rays are apparently emitted in de-excitation of the first excited level of Ne^{21} forming by the $N + C = Ne^{21} + \alpha + p$ reaction, while the 0.59 Mev γ-rays are apparently emitted in disintegration of Na^{22} forming by the $N + C = Na^{22} + \alpha$ reaction.

One can list a number of reactions leading to the formation of β^+-active nuclei as a result of bombardment of carbon with nitrogen ions and thereby explain the appearance of the 0.51 Mev γ-lines in the background spectra.

The 1.78 Mev line observed in bombardment of oxygen-containing targets with nitrogen ions can be explained by any one of the following reactions:

$$N + O = Al^{28} + 2p$$
$$N + O = Si^{28} + n + p$$
$$N + O = p^{28} + 2n.$$

The energy of the first excited level of Si^{28} is 1.78 Mev and its de-excitation explains the appearance of the 1.78 Mev line. Al^{28} and p^{28} disintegrate by β^+- and β^--decay to excited levels of Si^{28}.

In our experiments we observed increase in the intensity of the 1.78 Mev γ-line with a period of ~2 min after termination of bombardment of oxygen with nitrogen ions (the lifetime of Al^{28} is 2.3 min). Evaluations indicate, however, that the experimentally observed yield of 1.78 Mev γ-rays cannot be explained solely by the $N + O = Al^{28} + 2p$ reaction.

4. Background γ-lines and investigation of Coulomb excitation

Our detailed experimental data on the energies and intensities of the background γ-lines enabled us to evaluate the possibility of investigating Coulomb excitation of nuclear levels under different experimental conditions.

In experiments[8] with α-particles we noted the absence of the 562 and 590 kev γ-lines which we earlier[1] attributed to Coulomb excitation of levels in In and Mn*.

In view of the present results we can readily see that the misleading observation of these lines in the experiments with N^{14} ions was due to the presence of the 590 kev background γ-line appearing as a result of reaction of the nitrogen ions with carbon.

In view of the fact that in bombardment of a given target with different particles there appear different (rather than the same) background lines, we have the possibility of investigating different sections of the spectra free of background lines by varying the type of bombarding ions.

In some cases the yield of γ-rays associated with Coulomb excitation is much greater than the background γ-yield. Inasmuch as the intensity of interfering background γ-lines can be evaluated approximately from the intensity of other background γ-lines in the same spectrum, the Coulomb excitation yield can be evaluated with fair accuracy by subtracting the interfering background line. Such cases occurred, for example, in our investigations of Coulomb excitation of Mg^{24} (Ref.9) and Sc^{45}(Ref.10).

We take this opportunity to thank A.B.Girshin, Chief of the Operational Group, for assistance in the work.

References

1. D.G.Alkhazov, A.P.Grinberg & I.Kh.Lemberg, Izv.AN SSSR, Ser.fiz., 20, 1365 (1956). (Trans.Bulletin 20, No.12a, 1249.)

2. D.G.Alkhazov, D.S.Andreev, K.I.Erokhina & I.Kh.Lemberg, Zhur.eksp.i teor.fiz., 33, 1347 (1957). (Trans.Soviet Physics - JETP.)

3. D.G.Alkhazov, A.P.Grinberg, G.M.Gusinskii, K.I.Erokhina & I.Kh.Lemberg, Ibid., 35, 1325 (1958). (Trans.Soviet Phys. - JETP.)

4. M.L.Halbert, T.H.Handley, J.J.Pinajian, W.H.Webb & A.Zucker, Phys.Rev., 106, 251 (1957).

5. V.V.Volkov, A.S.Pasyuk & G.N.Flerov, Zhur.eksp.i teor.fiz., 33, 595 (1957). (Trans.Soviet Physics - JETP.)

6. A.P.Grinberg & I.Kh.Lemberg, Izv.AN SSSR, Ser.fiz., 23, 887 (1959). (Trans.Bulletin 23, No.7, 877.)

7. P.M.Endt & C.M.Braams, Revs.Mod.Phys., 29, 683 (1957).

8. D.G.Alkhazov, A.P.Grinberg, K.I.Erokhina & I.Kh.Lemberg, Soobshchenie na VIII ezhegodnom soveshchanii po yadernoi spektroskopii (Reports presented at the Eighth Annual Conference on Nuclear Spectroscopy), Leningrad, 1958.

9. D.G.Alkhazov, A.P.Grinberg, G.M.Gusinskii, K.I.Erokhina & I.Kh.Lemberg, Zhur.eksp.i teor.fiz., 35, 1056 (1958). (Trans.Soviet Physics - JETP.)

10. D.G.Alzhazov, A.P.Grinberg, G.M.Gusinskii, K.I.Erokhina & I.Kh.Lemberg, Ibid., 37, 1530 (1959). (Trans.Ibid.)

---

*The absence of the 590 kev γ-line in Coulomb excitation of Mn was independently shown in a study carried out at Saclay, France (private communication from Dr.Leman).

PARITY NONCONSERVATION IN β-DECAY OF RaE

- B.V.Geshkenbein, S.A.Nemirovskaya & A.P.Rudik

The β-decay of RaE has taken on new interest in connection with parity nonconservation in weak interactions. The shape of the RaE β-spectrum is far from the Fermi type[1]; yet the 1- → 0+ β-transition is a first forbidden Coulomb transition in a heavy nucleus and should, presumably, give a Fermi spectrum. Several authors[2-4] have attempted to explain the unusual shape of this spectrum. The point is that the matrix elements for β-decay in RaE are such that the principal terms cancel, and the remaining terms give the energy dependence of the shape. To obtain the requisite shape, one must take account of the change of the electron wave function inside the nucleus.

Lewis[5] and Fujita et al[6] have pointed out that the principal terms fail to cancel if time-reversal invariance is violated. Thus analysis of the RaE β-spectrum shows that there is no major violation of time-reversal invariance. If one assumes that failure of time-reversal invariance for A and V interaction is due to the complex character of the axial coupling constant, $G_V = g_V$ and $G_A = g_A(1+iF)$ (where g_V, g_A and F are real), agreement between the theoretical and experimental shapes of the spectrum requires that $F^2 \leqslant 6\cdot 10^{-3}$. For S and T interaction time-reversal invariance fails when the scalar coupling constant is complex: $G_S = g_S(1+iF)$, and $G_T = g_T$ (where g_S, g_T and F are real). For the experimental and theoretical spectra to match, it is then necessary that $F^2 \leqslant 10^{-2}$. Let us see why theory and experiment disagree if F^2 is large (of the order of unity). The correction factor C in the case of no time-reversal invariance can be written in the form

$$C(W) = C_0(W) + F^2 C_1(W).$$

We have given expressions for C_0 and ΔC_0 elsewhere[8]; it turns out that ΔC_0 is an increasing function of energy. The experimentally determined correction factor is found to be a strongly decreasing function of energy.

The required experimental energy dependence can be obtained only by means of strong interference in C_0, which then becomes roughly two orders of magnitude smaller than its leading terms. No cancellation can take place in the ΔC term, which is then of the order of the largest terms in C_0. It is therefore necessary that $F^2 \leqslant 10^{-2}$.

A spectrum of the Fermi shape in a first forbidden Coulomb transition implies that the electron polarization is $-v/c$. Since the RaE spectrum is of a significantly different shape, one may expect the emitted electrons to have polarization differing strongly from $-v/c$.

Using the methods of Refs. 4 & 7, we derived expressions for the polarization and angular distribution of the β-electrons from RaE, taking into account violation of space and time-reversal invariance. The nutrino is treated as a two-component particle.

Polarization of the β-electrons from RaE

We write the polarization of the RaE β-electrons in the form

$$\frac{\langle\sigma\rangle}{-v/c} = \frac{D}{C};$$

$$D = D_0 + F^2 D_1 + F D_2; \qquad (1)$$

$$C = C_0 + F^2 C_1;$$

here D_0, D_1 and D_2 are tabulated functions that are dependent on the electron energy and matrix-element ratios

$$x = ig_V \int \mathbf{r} / g_A \int [\vec{\sigma}\mathbf{r}],$$

$$y = g_V \int \alpha / g_A \int [\vec{\sigma}\mathbf{r}]$$

for A and V interaction, and

$$x = ig_S \int \beta\mathbf{r} / g_T [\vec{\sigma}\mathbf{r}],$$

$$y = \int \beta\alpha / \int \beta [\vec{\sigma}\mathbf{r}]$$

for S and T interaction. We have given the expressions for D_0, D_1 and D_2 in our previous work[8]. We note that the polarization depends strongly not only on the absolute value, but also on the sign of F.

In performing the calculations, we took $F^2 = 0$, $3 \cdot 10^{-3}$ and $6 \cdot 10^{-3}$ for A and V interaction and $F^2 = 0$, $3 \cdot 10^{-3}$, $6 \cdot 10^{-3}$ and 10^{-2} for S and T interaction.

Table 1

Values of $-b_1/C$ for A and V interaction with F = 0

x	y	$W = 1,2$	$W = 1,8$	$W = 2,4$	$W = 3,0$
0,2	19,85	0,40	0,58	0,59	0,50
0,5	24,6	0,37	0,59	0,66	0,66
1	32,35	0,31	0,57	0,71	0,79
1,3	37	0,29	0,54	0,72	0,82
1,7	42,95	0,21	0,47	0,67	0,77
2	47,3	0,14	0,38	0,59	0,67

For a given F^2 the values of x and y were chosen to give satisfactory agreement between the experimental and theoretical shapes of the spectrum. Such values of x and y lie along a certain curve. Tables of $\langle\sigma\rangle/(-v/c)$ are given in Ref.8; here we present only the basic results of the calculations.

In the case of time-reversal invariance, for all possible interactions and for all values of x and y on the above-mentioned curve, $\left(\frac{\langle\sigma\rangle}{-v/c}\right)_{\max} \leqslant 0.83$. In the case of V and A interaction, we also have a lower bound: $\left(\frac{\langle\sigma\rangle}{-v/c}\right)_{\min} \geqslant 0.54$.

Table 2

Values of $-b_1/C$ for A and V interaction for different F

F^2	x	y	$W = 1,2$		$W = 1,8$		$W = 2,4$		$W = 3,0$	
			$F < 0$	$F > 0$	$F < 0$	$F > 0$	$F < 0$	$F > 0$	$F < 0$	$F > 0$
$3 \cdot 10^{-3}$	0,2	19,4	0,47	0,27	0,68	0,42	0,78	0,40	0,87	0,34
	1,3	36,55	0,28	0,18	0,49	0,45	0,60	0,68	0,58	0,85
	1,9	45,76	0,22	0,13	0,41	0,41	0,53	0,68	0,50	0,86
$6 \cdot 10^{-3}$	0,2	19	0,44	0,33	0,64	0,48	0,69	0,45	0,70	0,32
	1,3	36,25	0,28	0,22	0,51	0,48	0,64	0,69	0,66	0,84
	1,7	42,4	0,20	0,15	0,41	0,42	0,56	0,68	0,58	0,84

For time-reversal invariance, x can be found from the polarization of the electrons. The measurements of Alikhanov et al[9], namely, $\frac{\langle\sigma\rangle}{-v/c} = 0.733 \pm 0.06$ and 0.725 ± 0.06 (or an average of 0.73 ± 0.04) for β energies $E_{kin} = 125$ and 380 kev)* give $x = 1.5 \pm 0.5$ for A and V interaction, and $x = 0.8 \pm 0.4$ for S

---

*The latest (unpublished) values of $\frac{\langle\sigma\rangle}{-v/c}$ found by these authors for E_{kin} = = 140, 250, 390 and 600 kev are 0.672 ± 0.029, 0.720 ± 0.041, 0.725 ± 0.06 and 0.750 ± 0.051, respectively.

Table 3

Values of $-b_1/C$ for S and T interaction with F = 0

x	y	$W=1,2$	$W=1,8$	$W=2,4$	$W=3,0$
0,2	18,8	0	0,01	0,18	0,30
0,4	22,4	0,21	0,34	0,37	0,30
0,6	25,7	0,26	0,44	0,53	0,53
1,0	32,35	0,32	0,57	0,71	0,79
1,2	35,6	0,33	0,59	0,75	0,85
3,0	64,8	0,37	0,69	0,89	0,99
5,5	104	0,36	0,69	0,89	0,93

and T interaction.

For the case of violation of time-reversal invariance the same experimental data lead to the following results: for V and A interaction when $F^2 = 6\cdot10^{-3}$ and $3\cdot10^{-3}$, the experimentally observed polarization of the electrons in β-decay of RaE eliminates the possibility that $F < 0$. For $F > 0$ theory and experiment agree for $x \approx 0.2$ (with $F^2 = 6\cdot10^{-3}$) or $x \approx 0.7$ (with $F^2 = 3\cdot10^{-3}$).

For S and T interaction, $F^2 = 10^{-2}$ is eliminated on the basis of polarization, though it is permitted when one compares the shapes of the theoretical and experimental spectra. With $F^2 = 6\cdot10^{-3}$ and $3\cdot10^{-3}$, experiment excludes $F < 0$, while for $F > 0$ agreement is obtained for both of the values of F when $x \approx 1.7$.

Angular distribution of β-electrons from polarized RaE nuclei

The angular distribution of β-electrons from polarized RaE nuclei is of the form

$$I(\theta)\,d\theta = \left[C - \frac{1}{3}\left(1 - \frac{3}{2}\bar{\mu}^2\right)b + b_1\bar{\mu}\cos\theta + \left(1 - \frac{3}{2}\bar{\mu}^2\right)b\cos^2\theta\right]\sin\theta\,d\theta, \qquad (2)$$

where θ is the angle between $\mathbf{n}_j$, the polarization vector of the nuclei, and the direction of motion n of the electron, and $\bar{\mu}$ and $\bar{\mu}^2$ are the mean values of the $\mathbf{n}_j$-component of the nuclear spin and its square. In unpolarized nuclei $\bar{\mu} = 0$ and $\bar{\mu}^2 = 2/3$. The expression for C was given in Ref.8. Very cumbersome expressions are obtained for b and b_1 (see Appendix). These quantities depend not only on the absolute value of F but also on its sign. The asymmetry coefficient α is given by

$$\alpha \equiv \frac{2\left[\int_0^{\pi/2} I(\theta)\,d\theta - \int_{-\pi/2}^{\pi} I(\theta)\,d\theta\right]}{\int_0^{\pi} I(\theta)\,d\theta} = \frac{b_1}{C}\bar{\mu}. \qquad (3)$$

The possible values of b_1/C consistent with the shape of the RaE β-spectrum are given in Tables 1-4. The possible values of b/C, for A and V interaction assuming time-reversal invariance, are listed in Table 5.

Table 4

Values of $-b_1/C$ for S and T interaction for different F

F^2	x	y	$W=1,2$		$W=1,8$		$W=2,4$		$W=3,0$	
			$F<0$	$F>0$	$F<0$	$F>0$	$F<0$	$F>0$	$F<0$	$F>0$
$3\cdot10^{-3}$	1,2	35,00	0,32	0,26	0,54	0,54	0,64	0,72	0,62	0,87
	3,0	6.,65	0,32	0,29	0,54	0,62	0,60	0,90	0,46	1,06
$6\cdot10^{-3}$	1,2	34,66	0,32	0,.3	0,51	0,54	0,59	0,72	0,54	0,86
	2,0	47,.0	0,34	0,28	0,55	0,65	0,62	0,87	0,51	1,00
$10\cdot10^{-3}$	0,4	21,94	0,23	0,04	0,32	0,11	0,37	0,12	0,38	0,05
	0,8	27,96	0,28	0,12	0,43	0,33	0,50	0,49	0,48	0,60

Table 5

Values of $-b/C$ for A and V interaction with F = 0

x	y	$W=1.2$	$W=1.8$	$W=2.4$	$W=3.0$
0,2	19,85	0,03	0,14	0,28	0,52
0,5	24,6	0	−0,01	−0,04	−0,10
1	32,35	−0,04	−0,17	−0,36	−0,58
1,3	37	−0,05	−0,23	−0,45	−0,64
1,7	42,95	−0,05	−0,27	−0,47	−0,49
2	47,3	−0,05	−0,25	−0,28	−0,18

In conclusion, we derive the relations between $\bar{\mu}$ and $\bar{\mu^2}$ assuming that equilibrium has been established in the spin states of the RaE nuclei in the magnetic field. Let ω_1, ω_0 and ω_{-1} be the probabilities that the nuclear spin components along the magnetic field are 1, 0 and -1, respectively. Assuming a Boltzmann distribution for these probabilities, we find that they are related according to

$$\omega_1\omega_{-1} = \omega_0^2. \tag{4}$$

The sum of the probabilities must be unity:

$$\omega_1 + \omega_0 + \omega_{-1} = 1. \tag{5}$$

Further,

$$\begin{aligned} \bar{\mu} &= \omega_1 - \omega_{-1}, \\ \bar{\mu^2} &= \omega_1 + \omega_{-1}. \end{aligned} \tag{6}$$

From Eqs.(4), (5) and (6), we find that $\bar{\mu}$ and $\bar{\mu^2}$ are related by

$$3(\bar{\mu^2})^2 - 8\bar{\mu^2} + (\bar{\mu})^2 + 4 = 0. \tag{7}$$

When one can achieve high polarization with $\bar{\mu} \geqslant 0.7$ (for small values of $\bar{\mu}$ we have $1 - {}^3/_2\bar{\mu^2} \approx -\frac{3}{8}(\bar{\mu})^2 \ll 1$), the $\cos^2\theta$ term in the angular distribution becomes significant. Hence, assuming the model to be correct, this term can be used to find $\bar{\mu^2}$, and then the polarization $\bar{\mu}$ can be obtained from (7).

In conclusion the authors express their sincere gratitude to A.I.Alikhanov, who suggested the present work, for many stimulating conversations, and to B.L. Ioffe and V.A.Lyubimov for discussion of the results.

APPENDIX

Formulas for b and b_1

For V and A interaction we have

$$b = b^{(0)} + \Delta b; \tag{A1}$$

$$\begin{aligned} b^{(0)} = \frac{3(2x-1)^2}{4}\bar{L}_2 + 3\left(xy - \frac{1}{2}y - \frac{1}{3}qx^2 + \frac{1}{2}qx - \frac{1}{6}q\right)\times \\ \times[(\bar{L}_1 - \bar{L}_{-1})^{1/2}(\bar{L}_2 + \bar{L}_{-2})^{1/2}\cos(\delta_{-1} - \delta_2) - \\ - (\bar{L}_1 + \bar{L}_{-1})^{1/2}(\bar{L}_2 - \bar{L}_{-2})^{1/2}\cos(\delta_1 - \delta_{-2})] + \\ + 3\left(x^2 + \frac{1}{2}x - \frac{1}{2}\right)\left[(\bar{M}_1 - \bar{M}_{-1})^{1/2}(\bar{L}_2 - \bar{L}_{-2})^{1/2}\cos(\delta_1 - \delta_{-2}) - \right. \\ \left. - (\bar{M}_1 + \bar{M}_{-1})^{1/2}(\bar{L}_2 + \bar{L}_{-2})^{1/2}\cos(\delta_{-1} - \delta_2)\right]; \end{aligned} \tag{A2}$$

$$\Delta b = F^2\left\{\frac{3}{4}\bar{L}_2 - \frac{1}{2}q\left[(\bar{L}_1-\bar{L}_{-1})^{1/2}(\bar{L}_2+\bar{L}_{-2})^{1/2}\cos(\delta_{-1}-\delta_2) - \right.\right. \tag{A3}$$

$$-(\bar{L}_1+\bar{L}_{-1})^{1/2}(\bar{L}_2-\bar{L}_{-2})^{1/2}\cos(\delta_1-\delta_{-2})\Big] -$$

$$-\frac{3}{2}\left[(\bar{M}_1-\bar{M}_{-1})^{1/2}(\bar{L}_2-\bar{L}_{-2})^{1/2}\cos(\delta_1-\delta_{-2}) -\right.$$

$$\left.\left.-(\bar{M}_1+\bar{M}_{-1})^{1/2}(\bar{L}_2+\bar{L}_{-2})^{1/2}\cos(\delta_{-1}-\delta_2)\right]\right\} -$$

$$-\frac{3}{2}F\left\{\left(y+\frac{1}{3}qx\right)\left[(\bar{L}_1-\bar{L}_{-1})^{1/2}(\bar{L}_2+\bar{L}_{-2})^{1/2}\sin(\delta_{-1}-\delta_2) -\right.\right.$$

$$-(\bar{L}_1+\bar{L}_{-1})^{1/2}(\bar{L}_2-\bar{L}_{-2})^{1/2}\sin(\delta_1-\delta_{-2})\Big] + 3x\left[(\bar{M}_1-\bar{M}_{-1})^{1/2}(\bar{L}_2-\bar{L}_{-2})^{1/2}\times\right.$$

$$\left.\left.\times\sin(\delta_{-1}-\delta_{-2}) - (\bar{M}_1+\bar{M}_{-1})^{1/2}(\bar{L}_2+\bar{L}_{-2})^{1/2}\sin(\delta_{-1}-\delta_2)\right]\right\};$$

$$b_1 = b_1^{(0)} + \Delta b_1 \tag{A4}$$

$$b_1^{(0)} = \left\{\left[\frac{1}{3}q^2x - y^2 - \frac{1}{12}q^2 + \frac{2}{3}qy(x-1)\right](\bar{L}_1^2-\bar{L}_{-1}^2)^{1/2} + \right. \tag{A5}$$

$$+(x+1)\left[y-\frac{1}{3}q(x-1)\right]\cdot\left[(\bar{L}_1-\bar{L}_{-1})^{1/2}(\bar{M}_1-\bar{M}_{-1})^{1/2} +\right.$$

$$\left.+(\bar{L}_1+\bar{L}_{-1})^{1/2}(\bar{M}_1+\bar{M}_{-1})^{1/2}\right] -$$

$$\left.-(x+1)^2(\bar{M}_1^2-\bar{M}_{-1}^2)^{1/2}\right\}\sin(\delta_{-1}-\delta_1) - \frac{(2x-1)^2}{4}(\bar{L}_2^2-\bar{L}_{-2}^2)^{1/2}\sin(\delta_{-2}-\delta_2) +$$

$$+\left(-yx+\frac{1}{2}y-\frac{1}{2}qx+\frac{1}{3}qx^2+\frac{1}{6}q\right)\left[(\bar{L}_1-\bar{L}_{-1})^{1/2}(\bar{L}_2-\bar{L}_{-2})^{1/2}\sin(\delta_{-1}-\delta_{-2}) +\right.$$

$$\left.+(\bar{L}_1+\bar{L}_{-1})^{1/2}(\bar{L}_2+\bar{L}_{-2})^{1/2}\sin(\delta_1-\delta_2)\right] +$$

$$+\left(x^2+\frac{1}{2}x-\frac{1}{2}\right)\left[(\bar{L}_2-\bar{L}_{-})^{1/2}(\bar{M}_1+\bar{M}_{-1})^{1/2}\sin(\delta_{-1}-\delta_{-2}) +\right.$$

$$\left.+(\bar{L}_2+\bar{L}_{-2})^{1/2}(\bar{M}_1-\bar{M}_{-1})^{1/2}\sin(\delta_1-\delta_2)\right];$$

$$\Delta b_1 = F^2\left\{\left[-\frac{1}{12}q^2(\bar{L}_1^2-\bar{L}_{-1}^2)^{1/} + \right.\right. \tag{A6}$$

$$+\frac{q}{3}(\bar{L}_1-\bar{L}_{-1})^{1/2}(\bar{M}_1-\bar{M}_{-1})^{1/2} + \frac{q}{3}(\bar{L}_1+\bar{L}_{-1})^{1/2}(\bar{M}_1+\bar{M}_{-1})^{1/2} -$$

$$-(\bar{M}_1^2-\bar{M}_{-1}^2)^{1/2}\Big]\sin(\delta_{-1}-\delta_1) -$$

$$-\frac{1}{4}(\bar{L}_2^2-\bar{L}_{-2}^2)^{1/2}\sin(\delta_{-2}-\delta_2) + \frac{1}{2}\left[\frac{1}{3}q(\bar{L}_1-\bar{L}_{-1})^{1/2}(\bar{L}_2-\bar{L}_{-2})^{1/2} -\right.$$

$$\left.-(\bar{L}_2-\bar{L}_{-2})^{1/2}(\bar{M}_1+\bar{M}_{-1})^{1/2}\right]\sin(\delta_{-1}-\delta_{-2}) +$$

$$\left.+\frac{1}{2}\left[\frac{1}{3}q(\bar{L}_1+\bar{L}_{-1})^{1/2}(\bar{L}_2+\bar{L}_{-2})^{1/2}-(\bar{L}_2+\bar{L}_{-2})^{1/2}(\bar{M}_1-\bar{M}_{-1})^{1/2}\right]\sin(\delta_1-\delta_2)\right\} +$$

$$+F\left\{\left(y-\frac{2}{3}qx\right)\left[(\bar{L}_1+\bar{L}_{-1})^{1/2}(\bar{M}_1+\bar{M}_{-1})^{1/2} -\right.\right.$$

$$-(\bar{L}_1-\bar{L}_{-1})^{1/2}(\bar{M}_1-\bar{M}_{-1})^{1/2}\Big]\cos(\delta_{-1}-\delta_1) -$$

$$-\frac{1}{2}\left[\left(y+\frac{1}{3}qx\right)(\bar{L}_1-\bar{L}_{-1})^{1/2}(\bar{L}_2-\bar{L}_{-2})^{1/2}-3x(\bar{L}_2-\bar{L}_{-2})^{1/2}(\bar{M}_1+\bar{M}_{-1})^{1/2}\right]\times$$

$$\times\cos(\delta_{-1}-\delta_{-2}) - \frac{1}{2}\left[\left(y+\frac{1}{3}qx\right)(\bar{L}_1+\bar{L}_{-1})^{1/2}(\bar{L}_2+\bar{L}_{-2})^{1/2} -\right.$$

$$\left.\left.-3x(\bar{L}_2+\bar{L}_{-2})^{1/2}(\bar{M}_1-\bar{M}_{-1})^{1/2}\right]\cos(\delta_1-\delta_2)\right\}.$$

For S and T interaction the formulas for $b^{(0)}$ and $b_1^{(0)}$ are given by Eqs. (A2) and (A5) with the sign of q changed.

For S and T interaction Δb and Δb_1 are given by

$$\Delta b = F^2x^2\Big\{\overline{L}_2+\frac{1}{3}q\,[(\overline{L}_1-\overline{L}_{-1})^{1/2}(\overline{L}_2+\overline{L}_{-2})\ \cos(\delta_{-1}-\delta_2)- \tag{A7}$$
$$-(\overline{L}_1+\overline{L}_{-1})^{1/2}(\overline{L}_2-\overline{L}_{-2})^{1/2}\cos(\delta_1-\delta_{-2})]+$$
$$+(\overline{M}_1-\overline{M}_{-1})^{1/2}(\overline{L}_2-\overline{L}_{-2})^{1/2}\cos(\delta_1-\delta_{-2})-(\overline{M}_1+\overline{M}_{-1})^{1/2}(\overline{L}_2+\overline{L}_{-2})^{1/2}\times$$
$$\times\cos(\delta_{-1}-\delta_2)\Big\}+Fx\Big\{\Big(y-\frac{1}{6}q\Big)[(\overline{L}_1-\overline{L}_{-1})^{1/2}(\overline{L}_2+\overline{L}_{-2})^{1/2}\times$$
$$\times\sin(\delta_{-1}-\delta_2)-(\overline{L}_1+\overline{L}_{-1})^{1/2}(\overline{L}_2-\overline{L}_{-2})^{1/2}\sin(\delta_1-\delta_{-2})]+$$
$$+\frac{3}{2}[(\overline{M}_1-\overline{M}_{-1})^{1/2}(\overline{L}_2-\overline{L}_{-2})^{1/2}\sin(\delta_1-\delta_{-2})-$$
$$-(\overline{M}_1+\overline{M}_{-1})^{1/2}(\overline{L}_2+\overline{L}_{-2})^{1/2}\sin(\delta_{-1}-\delta_2)]\Big\};$$

$$\Delta b_1 = F^2x^2\Big\{\Big[\frac{1}{3}q\,(\overline{L}_1-\overline{L}_{-1})^{1/2}(\overline{M}_1-\overline{M}_{-1})^{1/2}+ \tag{A8}$$
$$+\frac{1}{3}q\,(\overline{L}_1+\overline{L}_{-1})^{1/2}(\overline{M}_1+\overline{M}_{-1})^{1/2}-$$
$$-(M_1^2-\overline{M}_{-1}^2)^{1/2}\Big]\sin(\delta_{-1}-\delta_1)-(\overline{L}_2^2-\overline{L}_{-2}^2)^{1/2}\sin(\delta_{-2}-\delta_2)+$$
$$+\Big[(\overline{L}_2-\overline{L}_{-2})^{1/2}(\overline{M}_1-\overline{M}_{-1})^{1/2}-$$
$$-\frac{1}{3}q\,(\overline{L}_1-\overline{L}_{-1})^{1/2}(\overline{L}_2-\overline{L}_{-2})^{1/2}\Big]\sin(\delta_{-1}-\delta_{-2})+$$
$$+\Big[(\overline{L}_2+\overline{L}_{-2})^{1/2}(\overline{M}_1-\overline{M}_{-1})^{1/2}-$$
$$-\frac{1}{3}q\,(\overline{L}_1+\overline{L}_{-1})^{1/2}(\overline{L}_2+\overline{L}_{-2})^{1/2}\Big]\sin(\delta_1-\delta_2)\Big\}+$$
$$+Fx\Big\{\Big(y-\frac{2}{3}q\Big)\Big[(\overline{L}_1+\overline{L}_{-1})^{1/2}(\overline{M}_1+\overline{M}_{-1})^{1/2}-$$
$$-(\overline{L}_1-\overline{L}_{-1})^{1/2}(\overline{M}_1-\overline{M}_{-1})^{1/2}\Big]\cos(\delta_{-1}-\delta_1)+\Big[\Big(y-\frac{1}{6}q\Big)(\overline{L}_1-\overline{L}_{-1})^{1/2}(\overline{L}_2-\overline{L}_{-2})^{1/2}-$$
$$-\frac{3}{2}(\overline{L}_2-\overline{L}_{-2})^{1/2}(\overline{M}_1+\overline{M}_{-1})^{1/2}\Big]\cos(\delta_{-1}-\delta_{-2})+$$
$$+\Big[\Big(y-\frac{1}{6}q\Big)(\overline{L}_1+\overline{L}_{-1})^{1/2}(\overline{L}_2+\overline{L}_{-2})^{1/2}-$$
$$-\frac{3}{2}(\overline{L}_2+\overline{L}_{-2})^{1/2}(\overline{M}_1-M_{-1})^{1/2}\Big]\cos(\delta_1-\delta_2)\Big\}.$$

The definition of $\overline{L}_1$, $\overline{L}_{-1}$, $\overline{M}_1$, $\overline{M}_{-1}$, $\overline{L}_2$ and $\overline{L}_{-2}$ will be found in Ref.8.

Institute of Theoretical and Experimental Physics,
Academy of Sciences of the USSR

References

1. E.A.Plassman & L.M.Langer, Phys.Rev., 96, 1593 (1954).
2. M.Yamada, Progr.Theor.Phys., 10, 252 (1953).
3. G.E.Lee-Whiting, Phys.Rev., 97, 463 (1955).
4. H.Takeby, S.Nakamura & M.Taketani, Progr.Theor.Phys., 14, 317 (1955).
5. R.R.Lewis, Phys.Rev., 108, 904 (1957).
6. J.I.Fujita, M.Yamada, L.I.Matumoto & S.Nakamura, Phys.Rev., 108, 1104 (1957).
7. V.B.Berestetsky, B.L.Joffe, A.P.Rudik & K.A.Ter-Martirosjan, Nucl.Phys., 5, 464 (1958).
8. B.V.Geshkenbein, S.A.Nemirovskaya & A.P.Rudik, Zhur.eksp.i teor.fiz., 36, 517 (1959). (Trans.Soviet Physics - JETP, 9, 360.)
9. A.I.Alikhanov, G.P.Eliseev & V.A.Lyubimov, Zhur.eksp. i teor.fiz., 35, 1061 (1959). (Trans.Soviet Physics - JETP, 8, 740.)

POLARIZATION OF INTERNAL CONVERSION ELECTRONS FOLLOWING β-DECAY

- B.V. Geshkenbein

Because parity is not conserved in β-decay, the residual nucleus will be polarized in the direction of the emitted electron. We assume that the parent nucleus is unpolarized and the direction of the nutrino is not recorded. If, then, internal conversion takes place after the β-decay, the conversion electrons should have a definite polarization.

The general expression for the polarization vector $\langle\vec{\sigma}\rangle$ of the conversion electron in the cases of an allowed transition and a first forbidden Coulomb transition should be of the form

$$\langle\vec{\sigma}\rangle = a\,(\mathbf{vn})\,\mathbf{n} + b\,(\mathbf{v} - (\mathbf{vn})\,\mathbf{n}). \tag{1}$$

Here a and b are constants depending on the nuclear spins, which we call I before β-decay, I_1 after β-decay, and I_2 after internal conversion, on the multipole order j, and type of the radiation (magnetic or electric), and on the energy ω of the transition; $\mathbf{v}$ is the electron velocity, and $\mathbf{n}$ is the unit vector in the direction of emission of the conversion electron. We are using the system of units in which $\hbar = c = 1$.

Magnetic transitions

In a pure magnetic transition the polarization of the conversion electrons is characterized by the following expressions:[1]

$$a = \frac{(A_1 - 2A_2)}{vA}; \quad b = \frac{(A_1 + A_2)}{vA}, \tag{2}$$

where

$$A = \frac{2I_1+1}{2j+1}\sum_{j_2 l_2} |a_{\varkappa_2}|^2 (2j_2+1)\,(C^{l_2 0}_{j0;\,l'_1 0})^2\,[W(l_2 j_2 l'_1 j_1;\ {}^1/_2\, j)]^2,$$

$$A_1 = \frac{2I_1+1}{2j+1}\frac{\sqrt{2j+1}}{\sqrt{6}}\,\alpha\,\frac{j(j+1)+I_1(I_1+1)-I_2(I_2+1)}{I_1\sqrt{j(j+1)}}\sum_{j_2,\,l_2 j_3,\,l_3=l_2} (-1)^{j_2-j_3+j_1-l_1-1/2}\times$$

$$\times a_{\varkappa_2} a^*_{\varkappa_3}(2j_2+1)(2j_3+1)\,(C^{l_2 0}_{j0;\,l'_1 0})^2\,W(l_2 j_2 l'_1 j_1;\ {}^1/_2\, j)\times$$

$$\times W(l_2 j_3 l'_1 j_1;\ {}^1/_2 j)\,W(jjj_2 j_3;\ 1 j_1)\,W(j_3 j_2\ {}^1/_2\ {}^1/_2;\ 1 l_2);$$

$$A_2 = \frac{2I_1+1}{2j+1}\frac{\sqrt{2j+1}}{\sqrt{3}}\,\alpha\,\frac{j(j+1)+I_1(I_1+1)-I_2(I_2+1)}{I_1\sqrt{j(j+1)}}\times$$

$$\times \sum_{j_2,\,l_2,\,j_3,\,l_3} (-1)^{j_2-j_3+l_3+j_1-l_1-1/2} a_{\varkappa_2} a^*_{\varkappa_3}\times$$

$$\times\sqrt{(2l_2+1)(2l_3+1)}\,(2j_2+1)(2j_3+1)\,C^{l_2 0}_{j0;\,l'_1 0}\,C^{l_3 0}_{j0;\,l'_1 0}\,C^{20}_{l_2 0;\,l_3 0}\times$$

$$\times W(l_2 j_2 l'_1 j_1;\ {}^1/_2 j)\,W(l_3 j_3 l'_1 j_1;\ {}^1/_2 j)\,W(j_3 j_2\ {}^1/_2\ {}^3/_2;\ 1 l_3)\times$$

$$\times W(l_2 j_2\ 2\ {}^3/_2;\ {}^1/_2\, l_3)\,W(jjj_2 j_3;\ 1 j_1). \tag{3}$$

Here the $C^{c\gamma}_{a\alpha;\,b\beta}$ are Clebsch-Gordan coefficients, $W(abcd;\,ef)$ are Racah coefficients; the electrons in the shell on which conversion takes place have quantum numbers j_1, l_1, $l' = 2j - l$, $\varkappa = (l - l')(j + {}^1/_2)$; α is a coefficient giving the angular distribution of the β-electrons in the decay of a nucleus with spin I_1 to a nucleus with spin I;

$$a_{\varkappa_2} = -i\sqrt{\frac{(2j+1)(2l_1'+1)(2j_1+1)}{j(j+1)}}\, e^{i\delta_{\varkappa_2}}(R_{1\varkappa_2}+R_{2\varkappa_2})(\varkappa_1+\varkappa_2);$$

$\delta_{\varkappa_2}$ is the Coulomb phase shift ($\delta_{\varkappa_2}\to-\frac{\pi}{2}(l_2-1)$ as Z$\to$0), and $R_{1\varkappa_2}$ and $R_{2\varkappa_2}$ are radial integrals, which are defined in Ref.1.

For conversion on the K shell or on any shell for which $l_1=0$, $j_1={}^1/_2$ and $\varkappa_1=-1$, we have

$$\langle\vec{\sigma}\rangle = \varkappa\frac{j(j+1)+I_1(I_1+1)-I_2(I_2+1)}{2j(j+1)I_1(1+|\eta_K^{(0)}|^2)}\left\{(\mathbf{vn})\mathbf{n}+\sqrt{j(j+1)}\,\mathrm{Re}\eta_K^{(0)}(\mathbf{v}-(\mathbf{vn})\mathbf{n})\right\} \tag{4}$$

and

$$\eta_K^{(0)} = \frac{\sqrt{j(j+1)}\{T_{-j}^{(0)}-T_{j+1}^{(0)}\}}{(j+1)T_{-j}^{(0)}+jT_{j+1}^{0}}, \tag{5}$$

where

$$T_{-j}^{(0)} = (R_1+R_2)_{x_2=-j}e^{i\delta_{-j}};\quad T_{j+1}^{(0)} = (R_1+R_2)_{x_2=j+1}e^{i\delta_{j+1}}.$$

Explicit expressions for $\eta_K^{(0)}$ can be obtained in two limiting cases:

1. Z = 0. All the radial integrals are taken in explicit form; we obtain

$$\eta_K^{(0)} = 0, \tag{6}$$

which agrees with the work of Berestetskii and Rudik.[2]

2. Z is large, and the energy of the emitted conversion electron is low, so that $\frac{p}{mZe^2}\ll 1$ (where p is the momentum of the conversion electron). In this case we have $|T_{j+1}^{(0)}|^2\ll|T_{-j}^{(0)}|$ and we obtain

$$\eta_K^{(0)} = \sqrt{\frac{j}{j+1}}. \tag{7}$$

In Table 1 we give values of $\eta_K^{(0)}$ for Z = 80 calculated on the basis of values for the radial integrals kindly provided by L.S.Sliv.

Table 1

Values of $\eta_K^{(0)}$ for Z = 80

ω/m	$\eta_K^{(0)}$		
	$j=1$	$j=2$	$j=3$
0,2	0,74	0,82+0,02 i	0,86+0,01 i
0,25	0,73—0,02 i	0,80+0,04 i	0,84+0,02 i
0,3	0,71—0,02 i	0,79+0,05 i	0,82+0,03 i
0,35	0,71—0,03 i	0,77+0,06 i	0,81+0,04 i
0,5	0,68—0,03 i	0,72+0,07 i	0,76—0,05 i
0,7	0,65—0,04 i	0,68—0,08 i	0,72+0,06 i
1	0,62—0,04 i	0,63+0,09 i	0,67+0,06 i
1,5	0,56—0,02 i	0,58+0,11 i	0,61+0,07 i

We remark that in the two limits dealt with above, the same results are obtained for conversion on the L_I shell and the K shell.

For conversion on the L_{II} shell the electron polarization is given by Eq.(4) with $\eta_K^{(0)}$ replaced by $\eta_{L_{II}}^{(0)}$. A formula for $\eta_{L_{II}}^{(0)}$ was given in Ref. 1.

With the aid of known values for the radial integrals and phase shifts, we calculated $\eta_{L_{II}}^{(0)}$ for Z = = 57, 65, 73 and 81 at transition energies ω/m from 0.1 to 0.7, with $j=1$. It was found that $\eta_{L_{II}}^{(0)}$ depends only weakly on both ω/m and Z in these ranges, and may be considered constant and equal to -0.52. We call attention to the fact that the transverse polarization of the electrons from the L_{II} shell is large in absolute value, and that its sign is opposite from that for the polarization of the K and L_I shell electrons.

Electric transitions

In electric transitions the polarization of the conversion electrons is given by

$$\langle\vec{\sigma}\rangle = a\,(\mathbf{vn})\,\mathbf{n} + b\,(\mathbf{v} - (\mathbf{vn})\,\mathbf{n}),$$
$$a = \frac{1}{vB}(B_1 - 2B_2), \quad b = \frac{1}{vB}(B_1 + B_2), \tag{8}$$

where B, B_1 and B_2 are obtained from A, A_1 and A_2, respectively, by making the substitutions $l_1' \to l_1$ and

$$a_{\varkappa_2} \to b_{\varkappa_2} = \sqrt{\frac{j\,(2j_1+1)\,(2j_1+1)\,(2l_1+1)}{j+1}}\, e^{i\delta_{\varkappa_2}}\left[R_3 + R_4 - \left(1 + \frac{\varkappa_2 - \varkappa_1}{j}\right) R_5 + \left(1 - \frac{\varkappa_2 - \varkappa_1}{j}\right) R_6\right].$$

R_3, R_4, R_5 and R_6 are radial integrals.[1)]

The polarization of K conversion electrons is given by an expression obtained from (4) by replacing $\eta_K^{(0)}$ by $\eta_K^{(1)}$, namely,

$$\eta_K^{(1)} = \sqrt{\frac{1}{j\,(j+1)}}\,\frac{(j+1)\,T_{-j-1}^{(1)} + jT_j^{(1)}}{T_{-j-1}^{(1)} - T_j^{(1)}}. \tag{9}$$

Here
$$T_{-j-1}^{(1)} = (R_3 + R_4 + 2R_6)_{\varkappa_2 = -j-1}\, e^{i\delta_{-j-1}};$$
$$T_j^{(1)} = \left(R_3 + R_4 - \frac{2j+1}{j} R_5 - \frac{1}{j} R_6\right)_{\varkappa_2 = j} e^{i\delta_j}.$$

In the free-electron approximation, the radial integrals can be calculated explicitly; then $\eta_K^{(1)}$ is given by the expression[2]

$$\eta_K^{(1)} = -\sqrt{\frac{1}{j+1}}\,\frac{2\varepsilon_2}{\varepsilon_2 - m}, \tag{10}$$

where ε_2 is the conversion electron energy.

Table 2

Values of $\eta_K^{(1)}$ for Z = 80

ω/m	$\eta_K^{(1)}$		
	$j=1$	$j=2$	$j=3$
0,2	3,98+3,50 i	2,01+0,06 i	1,17 i
0,25	3,64+2,34 i	1,74+0,03 i	1,03−0,01 i
0,3	3,32+1,59 i	1,53	0,92−0,02 i
0,35	3,01+1,16 i	1,37−0,03 i	0,83−0,03 i
0,5	2,34+0,51 i	1,04−0,09 i	0,63−0,05 i
0,7	1,83+0,18 i	0,78−0,13 i	0,46−0,07 i
1	1,41	0,57−0,17 i	0,31−0,09 i
1,5	1,07−0,07 i	0,40−0,19 i	0,17−0,12 i

For large Z the radial integrals cannot be obtained explicitly, and numerical methods are required.

In Table 2 we give values of $\eta_K^{(1)}$ for Z = 80, calculated on the basis of the radial integral values communicated by L.A. Sliv.

As will be evident from a comparison of Table 2 with Eq. (10), the electric field has a significant effect on the polarization of the conversion electrons in the case of electric transitions as well; it will be seen that it even changes the sign of the transverse component of the polarization. Since this transverse component is negative for Z = 0 and positive for Z = 80, there must be some intermediate value of Z for which the polarization goes to zero.

Table 3 gives the values of

$$\frac{\eta_{L_I}^{(1)}}{1 + \left|\eta_{L_I}^{(1)}\right|^2},$$

which determine the transverse polarization of L_I shell electrons. The imaginary part of $\eta_{L_I}^{(1)}$ is small compared with its real part.

Values of $\dfrac{\eta^{(1)}_{L_I}}{1+|\eta^{(1)}_{L_I}|^2}$ Table 3

Z	ω/m						
	0,1	0,15	0,2	0,3	0,4	0,5	0,7
0	−0,05	−0,07	−0,10	−0,13	−0,16	−0,19	−0,23
57	0,06	−0,03	−0,06	−0,12	−0,15	−0,20	−0,26
65	0,47	0,10	0,02	−0,08	−0,11	−0,15	−0,25
73	0,40	0,34	0,16	0,00	−0,04	−0,11	−0,25
81	−0,28	0,43	0,48	0,16	0,01	−0,10	−0,25

It is seen from Table 3 that the electric field has a significant effect on the polarization of L_I conversion electrons, especially at low energies.

The values of $\eta^{(1)}_{L_{II}}$ which give the polarization of electrons ejected from the L_{II} shell, for $j = 2$, are presented in Table 4.

Table 4

Values of $\eta^{(1)}_{L_{II}}$ for $j = 2$

Z	ω/m						
	0,1	0,15	0,2	0,3	0,4	0,5	0,7
57	0,43+0,29 i	0,41+0,26 i	0,38+0,23 i	0,33+0,20 i	0,28+0,19 i	0,25+0,19 i	0,23+0,16 i
65	0,54+0,28 i	0,47+0,25 i	0,43+0,23 i	0,37+0,22 i	0,34+0,20 i	0,30+0,19 i	0,28+0,17 i
73	0,64+0,26 i	0,55+0,26 i	0,47+0,26 i	0,43+0,23 i	0,39+0,21 i	0,36+0,20 i	0,33+0,18 i
81	0,71+0,24 i	0,62+0,25 i	0,56+0,25 i	0,50+0,22 i	0,46+0,21 i	0,41+0,20 i	0,37+0,19 i

Mixed magnetic and electric transitions

Because there is a preferred direction (the direction of emission of the β-electron), there may be interference between electric and magnetic multipoles involved in a conversion transition. Let the multipole order of the magnetic radiation be j and that of the electric be j'. The matrix element for the conversion process is of the form[3]

$$\mathfrak{M} = (I_1 m_1 | Q^{(0)}_{jM} | I_2 m_2)\,(B^{(0)}_{jM})_{21} + (I_1 m_1 | Q^{(1)}_{j'M'} | I_2 m_2)\,(B^{(1)}_{j'M'})_{21}; \quad (11)$$

the nuclear matrix elements can be written in the form

$$(I_1 m_1 | Q^{(\lambda)}_{jM} | I_2 m_2) = Q^{(\lambda)}_j C^{I_1 m_1}_{I_2 m_2; jM}. \quad (12)$$

Inserting (12) into (11) and writing $\delta = Q^{(1)}_{j'}/Q^{(0)}_j$, we obtain

$$\mathfrak{M} = C^{l_1 m_1}_{l_2 m_2; jM}\,(B^{(0)}_{jM})_{21} + \delta C^{I_1 m_1}_{I_2 m_2; j'M}\,(B^{(1)}_{j'M'})_{21} \quad (13)$$

(where we have dropped irrelevant common factors). We remark that δ may be considered positive, and that δ^2 is the E to M branching ratio.

If we know the matrix element (13), we obtain an expression of the form of (1) for the polarization of the conversion electrons when there is interference between magnetic and electric transitions (analogously to the case of pure transitions). In this expression

$$a = \frac{1}{1+\delta^2}\,(a_{\text{mag}} + \bar{\delta}^2 a_{\text{el}} + \bar{\delta}\, a_{\text{int}});$$

$$b = \frac{1}{1+\bar{\delta}^2}(b_{\mathrm{mag}} + \bar{\delta}^2 b_{\mathrm{el}} + \bar{\delta} b_{\mathrm{int}}); \tag{14}$$

here a_{mag}, b_{mag}, a_{el} and b_{el} are given by Eqs. (2) and (8), $\bar{\delta} = \delta(\alpha_{j'}^{(1)}/\alpha_j^{(0)})^{1/2}$ and $\alpha^{(1)}$ and $\alpha_j^{(0)}$ are the conversion coefficients for electric and magnetic radiation. The interference terms a_{int} and b_{int} are given by

$$a_{\mathrm{int}} = \frac{1}{v\sqrt{AB}}(C_1 - 2C_2);$$
$$b_{\mathrm{int}} = \frac{1}{v\sqrt{AB}}(C_1 + C_2); \tag{15}$$

where

$$C_1 = \frac{1}{2\pi\sqrt{6}} v\alpha \sqrt{\frac{I_1+1}{I_1}}(2I_1+1)^{3/2}\cdot(-1)^{I_1-I_2-j_1-1/2} W(j'jI_1I_1;\ 1I_2) \times$$
$$\times \mathrm{Re}\sum_{\substack{l_2=l_3\\ j_2,\ j_3}} (-1)^{j_3-j_2+l_2}(2j_2+1)(2j_3+1)\, a_{\varkappa_2} b^*_{\varkappa_3} C^{l_2 0}_{j0;l'_1 0} C^{l_3 0}_{j'0;l_1 0} \times$$
$$\times W(jj'j_2j_3;\ 1j_1)\, W(l_2j_2l'_1j_1;\ {}^1/_2 j)\, W(l_2j_3l_1j_1;\ {}^1/_2 j')\, W(j_3j_2{}^1/_2\ {}^1/_2;\ 1l_2);$$

$$C_2 = \frac{1}{2\pi\sqrt{3}} v\alpha \sqrt{\frac{I_1+1}{I_1}}(2I_1+1)^{3/2}(-1)^{I_1-I_2+j_1-1/2} W(j'jI_1I_1;\ 1I_2) \times$$
$$\times \mathrm{Re}\sum_{\substack{l_2,\ l_3\\ j_2,\ j_3}} (-1)^{j_2+j_3}(2j_2+1)(2j_3+1)(2l_2+1)^{1/2}(2l_3+1)^{1/2} a_{\varkappa_2} b^*_{\varkappa_3} C^{l_2 0}_{j0;l'_1 0} C^{l_3 0}_{j'0;l_1 0} \times$$
$$\times C^{20}_{l_2 0;l_3 0} W(l_2j_2l'_1j_1;\ {}^1/_2 j)\, W(l_3j_3l_1j_1;\ {}^1/_2 j')\, W(jj'j_2j_3;\ 1j_1) \times$$
$$\times W(j_3j_2{}^1/_2{}^3/_2;\ 1l_3)\, W(l_2j_2\ 2^3/_2;\ {}^1/_2 l_3). \tag{16}$$

Let us turn to the most important case of K shell conversion with $j' = j+1$. For this case we obtain

$$a_{\mathrm{int}} = \alpha \frac{\sqrt{(I_1+I_2+j'+1)(I_2-I_1+j')(I_1-I_2+j')(I_1+I_2-j'+1)}}{I_1(2j'-1)(2j'+1)} \sqrt{\frac{j'-1}{j'}}\,\tilde{a}_{\mathrm{int}}, \tag{17}$$

$$b_{\mathrm{int}} = \alpha \frac{\sqrt{(I_1+I_2+j'+1)(I_2-I_1+j')(I_1-I_2+j')(I_1+I_2-j'+1)}}{2I_1(2j'-1)(2j'+1)} \sqrt{\frac{j'-1}{j'}}\,\tilde{b}_{\mathrm{int}}, \tag{17}$$

where

$$\tilde{a}_{\mathrm{int}} = \frac{\mathrm{Im}[T^{(0)}_{j'}T^{(1)*}_{j'} + (j'+1)(2j'-1)T^{(0)}_{j'}T^{(1)*}_{-j'-1} - j'(2j'+1)T^{(0)}_{-j'+1}T^{(1)*}_{j'}]}{\sqrt{(j'-1)|T^{(0)}_{j'}|^2 + j'|T^{(0)}_{-j'+1}|^2}\cdot\sqrt{j'|T^{(1)}_{j'}|^2 + (j'+1)|T^{(1)}_{-j'-1}|^2}};$$
$$\tilde{b}_{\mathrm{int}} = \frac{\mathrm{Im}[(j'+1)(2j'-1)T^{(0)}_{j'}T^{(1)*}_{-j'-1} + j'(2j'+1)T^{(0)}_{-j'+1}T^{(1)*}_{j'}T^{(1)*}_{j'} - 2j'T^{(0)}_{j'}T^{(1)+}_{j'}]}{\sqrt{(j'-1)|T^{(0)}_{j'}|^2 + j'|T^{(0)}_{-j'+1}|^2}\cdot\sqrt{j'|T^{(1)}_{j'}|^2 + (j'+1)|T^{(1)}_{-j'-1}|^2}}. \tag{18}$$

In Table 5 we give values of $\tilde{a}_{\mathrm{int}}$ and $\tilde{b}_{\mathrm{int}}$ for $j = 1$, $j' = 2$ and Z = 80, calculated using the values of the radial integrals and phase shifts given by L.A. Sliv.

Table 5

The values of $\tilde{a}_{\mathrm{int}}$ and $\tilde{b}_{\mathrm{int}}$ for Z = 80 with $j = 1$ and $j' = 2$

ω/m	0,2	0,25	0,3	0,35	0,5	0,7	1
$\tilde{a}_{\mathrm{int}}$	−0,53	−0,68	−0,47	−0,21	0,45	1,06	1,60
$\tilde{b}_{\mathrm{int}}$	0,56	0,72	0,53	0,30	−0,32	−0,86	−1,33

Polarization of conversion electrons emitted in cascade with one or more γ-rays

Often the conversion process does not occur promptly following β-decay, but only after the emission of one or several γ-rays. Assume that β-decay leaves the nucleus in an excited state with spin I_1. It then undergoes successive transitions to states with spins $I_2, I_3, \ldots, I_{n+1}$, emitting photons of multipole orders $j_1, j_2, \ldots, j_n$, but of unspecified type (magnetic or electric), which are not recorded. This is followed by a conversion process. It is then easily shown that the γ-ray cascade leads to the appearance of the additional factor

$$\frac{1}{2^n}\prod_{i=1}^{n}\frac{I_{i+1}(I_{i+1}+1)+I_i(I_i+1)-j_i(j_i+1)}{\sqrt{I_i(I_i+1)\,I_{i+1}(I_{i+1}+1)}} \qquad (19)$$

in all the expressions for the polarizations.

I desire to express my sincere gratitude to V.B.Berestetskii and A.P.Rudik for suggesting the problem and discussing the results, A.I.Alikhanov and V.A. Lyubimov for interest in the work and for discussions, and L.A.Sliv communicating the values of the radial integrals.

Institute of Theoretical and Experimental Physics,
Academy of Sciences of the USSR

References

1. B.V.Geshkeibein, Zhur.eksp.i teor.fiz., 35, 1235 (1958). (Trans.Soviet Physics - JETP. 8, 865.)

2. V.B.Berestetskii & P.Zh.Rudik, Zhur.eksp.i teor.fiz., 35, 159 (1958). (Trans.Soviet Physics - JETP, 8, 111.)

3. A.I.Akhiezer & V.B.Berestetskii, Kvantovaya elektrodinamika (Quantum electrodynamics). M. 1953.

INELASTIC NEUTRON SCATTERING BY ODD NUCLEI

- A.M.Korolev

Excitation of collective nuclear-surface levels through direct interaction between the nucleus and an inelastically scattered neutron is ordinarily described in terms of the Bohr-Mottelson model.[1,2] It is possible, however, that at resonant energies the neutron may remain for some time close to the nuclear surface, and then a metastable state, which is not a compound nucleus state, may form.[3] We have included this mechanism in treating inelastic neutron scattering by spherical nuclei[4] by Heitler's theory of damping.[5,6]

In the present work we use the methods of our previous analysis[4] to study inelastic neutron scattering by nuclei with half-integral spin. It was found that because of its complexity the problem can be solved only for weakly deformed nuclei and only taking into account excitation of the first two collective levels.

Let us consider the inelastic scattering of neutrons by nuclei with half-integral spin, assuming that primarily only collective levels associated with surface excitations will be excited. Thus, we shall not consider processes having to do with the temporary existence of a compound nucleus. We shall assume that the interaction between the incident neutron and the nuclear surface is small, and, therefore, that the nucleus contains only a few "extra" nucleons in excess of its magic-number core. In treating inelastic scattering we shall use the generalized Bohr model.[1,2]

The Hamiltonian of the system consisting of an odd weakly deformed nucleus and an incident neutron interacting with the nuclear surface is of the form

$$H = H_s^{(0)} + H_p + H', \tag{1}$$

where

$$H_s^{(0)} = H_s + H_p^e + H_e', \tag{1a}$$

is the Hamiltonian characterizing the state of the target nucleus,

$$H_p = -\frac{\hbar^2}{2M}\frac{d^2}{dr^2} + \frac{\hbar^2 l(l+1)}{2Mr^2} + V(r), \tag{1b}$$

is the Hamiltonian of a free neutron moving in a potential well given by $V(r)$, and

$$H' = -kR_0\delta(r - R_0)\sum_\mu \alpha_{2\mu} Y_{2\mu}(\vartheta, \varphi) \tag{1c}$$

is the interaction Hamiltonian for the neutron and the nuclear surface.

The Hamiltonian $H_s^{(0)}$ of the target nucleus describes the interaction between the "extra" odd nucleon and the surface of the even-even core. In (1a) the Hamiltonian H_s for the collective oscillations of the core is

$$H_s = \sum_{\lambda\mu}\left\{\frac{1}{2B_\lambda}|\pi_{\lambda\mu}|^2 + \frac{c_\lambda}{2}|\alpha_{\lambda\mu}|^2\right\}, \tag{1d}$$

and the single-particle "extra" nucleon Hamiltonian H_p^e and the Hamiltonian H_e' giving the interaction of this nucleon with the core surface are of the forms (1b) and (1c), respectively, except that the coordinates of the incident neutron in these expressions must be replaced by those of the "extra" nucleon.

The nuclear wave functions are given by the equation

$$H_s^{(0)}\varphi_{jm}^N = W_{jN}\varphi_{jm}^N, \tag{2}$$

where W_{jN} is the energy eigenvalue, and j and m are the total angular momentum and its z-component, respectively.

Solution of Eq.(2) gives the following wave function for the target nucleus[7]:

$$\varphi_{jm}^N(r_1\Omega_1) = \sum_{N'R'Q'l'} B_{R'Q'l'N'}^{Njm}\psi_{l'}(r_1)\,\Phi_{N'}[R's(Q')\,l'jm], \tag{3}$$

where the amplitudes $B_{R'Q'l'N'}^{Njm}$ and all other notations are specified in the next article[7].

The system we are considering is not stationary during the interaction, so that the Schrödinger equation will be time dependent:

$$i\hbar\frac{d\Psi}{dt} = H\Psi; \tag{4}$$

the Hamiltonian H here is given by Eq.(1).

The orbital angular momentum l and nuclear spin j are not conserved in the interaction between the neutron and the nuclear surface. Hence the total wave function Ψ of the system is characterized by a total angular momentum I and its z-component M.

Let us expand this total wave function for a given I and M in eigenfunctions of the unperturbed system, namely,

$$\Psi_{lM}(r,\,t) = \sum_{N'j'k'l'}\int_0^\infty a_{j'k'l'N'}\psi_{l'}(r,\,p')\,\Phi_{N'}[j's(k')\,l'IM]_{dp'}, \tag{5}$$

where the $a_{j'k'l'N'}$ are the desired amplitudes, the $\psi_{l'}(r,\,p')$ are eigenfunctions of the single-particle Hamiltonian (1b), and $\Phi_{N'}[j's(k')\,l'IM]$ gives the angular part of the total wave function, and is at the same time an eigenfunction of the Hamiltonian (1a). The form of $\Phi_{N'}$ depends on the particular coupling scheme chosen for the angular momenta, and in our case will be determined by the fact that we shall not take into account spin-orbit coupling. The coupling scheme is chosen so that the nuclear spin j' and the neutron spin s couple to give k' which is then coupled with the orbital angular momentum l' of the neutron to give the total angular momentum I of the system. Explicitly,

$$\Phi_N[js(k)\,lIM] = \sum_{m_l m_s}(jsM - m_l - m_s m_s\,|\,jskM - m_l)\,(klM - m_l m_l\,|\,klIM)\times$$
$$\times Y_{lm_l}(\vartheta,\,\varphi)\,\chi_s^{m_s}\varphi_{jM-m_l-m_s}^N, \tag{6}$$

where $\chi_s^{m_s}$ is the spin part of the incident neutron wave function, $Y_{lm_l}(\vartheta,\,\varphi)$ is its angular part, $\varphi_{jm_j}^N$ is the wave function of the odd nucleus, and $(klM - m_l m_l\,|\,klIM)$ is a Clebsch-Gordan coefficient.

For convenience in applying Heitler's damping theory, we go over in the usual way from the x-representation to the p-representation.[4] We then obtain the set of integral equations

$$(E - E_{nN})\,G_{nN}(E,\,p) = \sum_{n'N'}\int_0^\infty (nNp\,|\,H'\,|\,n'N'p')\,G_{n'N'}(E,\,p')\,dp' + \delta_{nn_0}\delta_{N0}, \tag{7}$$

for the amplitudes, where the $G_{nN}(E,\,p)$ are the Fourier transposes of the amplitudes:

$$a_{nN}(t) = -\frac{1}{2\pi i}\int_{-\infty}^{+\infty} G_{nN}(E)\, e^{+\frac{i}{\hbar}(E_n - E)t}\, dE \tag{8}$$

(henceforth we will denote all quantities characterizing a given state by an index n).

According to the general propositions of damping theory, the solution of Eq.(4) should be characterized by the following initial conditions for the amplitudes[6]:

$$\begin{aligned} a_{nN}(t) &= 0 \quad \text{for} \quad t \to 0; \\ a_{n_0 0}(t) &= 1 \quad \text{for} \quad t \to 0_+, \end{aligned} \tag{9}$$

where the index $n_0 0$ denotes the initial state of the system. These boundary values mean that the interaction H' comes into effect at time $t = 0$, when the particle reaches the nuclear surface; they lead to a term of the form $\delta_{nn_0}\delta_{N0}$ on the right side of Eq.(7). The energy $E_{nN} = W_{nN} + E_n(p)$ in (7) is the total energy of the unperturbed system. The Fourier transpose $G_{nN}(E, p)$ is of the form[4,6]

$$G_{nN}(E, p) = [g_{nN}(E, p)\,\xi_+(E - E_N) + \delta_{nn_0}\delta_{N0}]\, G_{n_0 0}(E), \tag{10}$$

where

$$\xi_+(E - E_N) = \left[\frac{1}{E - E_N} + \pi i \delta(E - E_N)\right], \tag{10a}$$

$$G_{n_0 0}(E) = \frac{1}{E - E_0 + \frac{1}{2} i\Gamma(E, p_0)}, \tag{10b}$$

in which

$$\Gamma(E, p_0) = 2i \sum_{n'} (0 n_0 p_0 \,|\, H' \,|\, 1 n' p')\, \xi_+(E - E_{n'1})\, g_{n'1}(E,\ p')\, dp'. \tag{11}$$

Inserting $G_{nN}(E, p)$ from (10) into (7), we obtain the following set of integral equations:

$$g_{nN}(E, p) = (Nnp \,|\, H' \,|\, 0 n_0 p_0) + \sum_{N'n'} \int_0^{\infty} (nNp \,|\, H' \,|\, n'N'p')\, \xi_+(E - E_{nN})\, g_{N'n'}(p', E)\, dp'. \tag{12}$$

To solve (12) in general is by no means simple. According to (1b), however, the interaction H' is δ-like, and the kernel of Eq.(12) is degenerate. Thus (12) is easily reduced to a set of ordinary algebraic equations. Writing

$$g_{nN}(E) = \psi_n(pR_0)\,\psi_{n_0}(p_0 R_0)\, A_{nN}(E), \tag{13}$$

Eqs.(12) take on the simple form

$$A_{nN}(E) = H'_{Nn,\,0n_0} + \sum_{N'n'} H'_{Nn,\,N'n'} L_{n'N'}\, A_{N'n'}(E); \tag{14}$$

$$L_{Nl}(E) = -\frac{M\pi i}{p_N}\,\psi_l^{(+)}(p_N R_0)\,\psi_l(p_N R_0), \tag{15}$$

where $p_N = \sqrt{(E - \hbar\omega_N)\,2M}$ and $\psi_l^{(+)}$ describes an outgoing wave.[4] In calculating the matrix elements $H'_{Nn,\,N'n'}$ one must bear in mind that the deformation parameter $\alpha_{2\mu}$ in (1c) is an operator expressed in terms of destruction and creation operators for surface excitations:

$$\alpha_{2\mu} = \sqrt{\frac{\hbar}{2B\omega}}\,(b_\mu + (-1)^\mu b^*_{-\mu}). \tag{16}$$

In calculating the matrix elements in (12) one must perform some quite complicated sums over magnetic quantum numbers and intermediate angular momentum quantum numbers of products of Clebsch-Gordan coefficients. Eventually one obtains

$$H'_{Nkljλ,\,N'k'l'j'λ'} = -\tilde{g}\,[(2l'+1)(2k+1)(2k'+1)(2j+1)(2j'+1)(2λ'+1)]^{1/2} \times$$
$$\times W(k'2Il;kl')\,W(2jk's;j'k)\,W(2jλ's;j'λ)\,(l'200|l'2l0)\,M(Njλ|N'j'λ'), \qquad (17)$$

where $W(abcd;ef)$ is a Racah coefficient, $M(Njλ|N'j'λ')$ is a partial matrix element involving the state amplitudes of the "extra" nucleon, $λ = j \pm 1/2$ gives the parity of the target nucleus, and

$$\tilde{g} = kR_0\sqrt{\frac{\hbar}{2B\omega}}\sqrt{\frac{5}{4\pi}}.$$

In obtaining (14), we have so far made no approximations. We will now make use of the Tamm-Dancoff method[8], restricting ourselves to the two-phonon amplitudes in (14); from now on we shall assume a very low probability for excitation of the third and higher nuclear levels. Further, we shall assume that all the matrix elements $M(Nλ|N'λ')$ are small except those for which $N' = N \pm 1$ (the harmonic-oscillator approximation).

With these approximations, (14) can be rewritten

$$A_{nN}(E) = H'_{Nn,\,0n_0} + \sum_{n'} H'_{Nn,\,N'n'} L_{n'N'} H_{N'n',\,0n_0} + \sum_{n'n''N'} H'_{Nn,\,N'n'} L_{n'N'} H'_{N'n',\,N''n''} A_{n''N}, \qquad (14a)$$

where $N = 0, 1, 2$.

Assume that the amplitudes which are off diagonal in λ are small, an assumption connected with the condition of adiabaticity of the quadratic matrix element. Then on averaging $M(Nλ|N'λ')\,M(N'λ'|Nλ)$ over λ' (and choosing some mean value $\bar{λ}$ of λ'), we arrive at

$$A_{n_0} = \frac{H'_{0n\,0n_0} + \tilde{g}^2 \tilde{L}_{1l_0} M^2(0λ|1\bar{λ})\,\delta_{nn_0}}{1 - \tilde{g}^2 \tilde{L}_{1l} M^2(0λ|1\bar{λ})}; \qquad (18)$$

$$A_{n'} = \frac{H'_{1n,\,0n_0}}{1 - \tilde{g}^2 \cdot \sum_{N=0,2} \tilde{L}_{Nl} M^2(1λ|N\bar{λ})}; \qquad (18a)$$

$$A_{n2} = \frac{H'_{2n,\,0n_0} + \tilde{g}^2 \tilde{L}_{2l_0} M(2λ|1\bar{λ})\,M(1\bar{λ}|0λ_0)\,\delta_{nn_0}}{1 - \tilde{g}^2 \tilde{L}_{2l} M^2(2λ|1\bar{λ})}, \qquad (18b)$$

where $\tilde{L}_{Nl}(E) = \sum_{l'} (l200|l2l'0)^2 L_{Nl'}(E)$ and $H'_{Nn,\,N'n'}$ is given by (17). When we now insert Eqs.(18)-(18b), (8), (10) and (13) into (5), we obtain the desired wave function of the system for the given value of I.

We are interested in the wave function of (5), a relatively long time t after the interaction. The amplitudes $a_{nN}(t)$ then become the scattering-matrix elements[6]

$$a_{nN}(\infty) = S_{nN,\,n_0 0} = \frac{g_{nN}(E_N)}{(E_N - E_0 - \Delta E_N) + \frac{1}{2} i\,\mathrm{Re}\,\Gamma(E_N)}, \qquad (19)$$

where the real part of $\frac{1}{2}\Gamma(E_N)$ given by (11), is the half-width of the level, and its imaginary part characterizes the shift of the collective levels.

If we take into account all values of I, l and k in the expansion for a plane wave, then, according to Blatt and Biedenharn,[9] we obtain the differential cross section for inelastic neutron scattering by weakly deformed nuclei with collective levels taken into account:

$$d\sigma = \sum_{kk'} \frac{\hbar^2}{2k+1} \sum_{L} B_L(p_0 k;\ pk')\, P_L(\cos\vartheta)\, dp\, d\Omega, \tag{20}$$

where

$$B_L(p_0 k;\ pk') = \frac{(-1)^{K'-K}}{4p_0} \sum_{N} \sum_{l_1 l_1' I_1} \sum_{l_2 l_2' I_2} Z(l_1,\ I_1 l_2 I_2;\ kL)\, Z(l_1' I_1 l_2' I\ ;\ k'L) \times \times \mathrm{Re} S^{*}_{n_1 N,\ n_0 0}\, S_{n_0 0,\ n_2 N}, \tag{20a}$$

and $Z(abcd;\ ef)$ is a Z-coefficient.

Eq.(20) indicates that if inelastic neutron scattering excites collective levels, there should be interference of the outgoing neutron waves corresponding to different l. The scattering-matrix elements of Eq.(19) entering into (20a) correspond to resonance. Hence the energy distribution of the inelastically scattered neutrons is described by a dispersion formula.

None of the approximations involved in the calculation of the A_{nN} violate the usually accepted assumption that the coupling constant $\tilde{g}$ is small. In view of this, the results of the present paper are valid only for weakly deformed nuclei.

Institute of Physics,
Academy of Sciences of the Ukrainian SSR

References

1. A.Bohr, Dan.Mat.-fys.Medd., 26, 14 (1952).
2. A.Bohr & B.R.Mottelson, Dan.Mat.-fys.Medd., 27, 16 (1953).
3. A.M.Korolev, Ukr.fiz.zhur. (Ukrainian phys.jour.), 2, 369 (1957).
4. A.M.Korolev, in Yadrenye reaktsii pri malykh i srednikh energiyakh (Nuclear reactions at low and medium energies), M. 1958.
5. E.Arnous & S.Zienau, Helv.phys.acta, 25, 279 (1951).
6. W.Heitler, The Quantum Theory of Radiation, Oxford (1954).
7. A.M.Korolev, Present issue of the Bulletin, p.1475.
8. I.Tamm, J.Phys., 9, 449 (1945).
9. J.M.Blatt & L.S.Biedenharn, Revs.Mod.Phys., 24, 258 (1952).

ENERGY LEVELS OF WEAKLY DEFORMED NUCLEI

- A.M.Korolev

Introduction

In attempting to explain nuclear level schemes, the interaction between nucleons and the nuclear surface in the last four years has been subjected to theoretical study based on the generalized model of the nucleus.[1,2] Many authors have engaged in this study for both strong and weak coupling between the odd "extra" nucleon and the surface.[1-7] The experimental discovery of rotational levels of highly deformed nuclei gave strong support to the validity of the generalized model. Nevertheless, there remained many unanswered questions such as, for instance, the influence of nonadiabatic terms on the positions of the levels, and of two- and three-phonon states. Although these factors have been studied[7] for intermediate coupling, the explicit analytic dependence of the energy levels on their quantum characteristics have not been given.

The present work uses the generalized model to study stationary states of odd nuclei with intermediate coupling. One- and two-phonon states are included in the treatment, and the wave functions and energy levels of the nuclei are found.

Statement of the problem

Consider the stationary states of a system consisting of an even-even nuclear core in the vicinity of a magic number, and an "extra" odd nucleon interacting with the surface of the core. The solution of this problem involves finding the eigenfunctions and eigenvalues of the bound "extra" nucleon. The surface interaction leads to deformation of the nucleus. We shall assume that this deformation is not strong. In other words, we shall solve the problem by approaching the intermediate coupling case from the weak coupling direction. This treatment imposes a requirement on the single-particle and collective levels which is the opposite of the adiabatic requirement, namely, that the collective levels must lie above the single-particle levels.

We shall treat the collective excitations of the nuclear core by Bohr's generalized model.[1,2] The Hamiltonian of the system consisting of a spherical core and an "extra" nucleon interacting with its surface is of the form[1]

$$H = H_s + H_p + H', \tag{1}$$

where

$$H_s = \sum_{\lambda\mu} \left\{ \frac{1}{2B_\lambda} |\pi_{\lambda\mu}|^2 + \frac{C_\lambda}{2} |\alpha_{\lambda\mu}|^2 \right\} \tag{1'}$$

is the Hamiltonian of the nuclear surface oscillations,

$$H_p = -\frac{\hbar^2}{2M} \cdot \frac{d^2}{dr^2} + \frac{\hbar^2 l(l+1)}{2Mr^2} + V(r) \tag{1''}$$

is the Hamiltonian of a free neutron in a potential well given by $V(r)$ and

$$H' = -kR_0 \delta(r - R_0) \sum_\mu \alpha_{2\mu}(\theta, \varphi) \tag{1'''}$$

is the interaction Hamiltonian. The $\alpha_{\lambda\mu}$ in (1') are the deformation parameters of the nuclear surface. We shall treat $\alpha_{2\mu}$ in (1''') as an operator acting on the nuclear-surface wave function which changes the number of surface quanta (phonons):

$$\alpha_{2\mu} = \sqrt{\frac{\hbar}{2B\omega}} (b_\mu + (-1)^\mu b^*_{-\mu}), \tag{2}$$

where

$$\omega = \sqrt{\frac{C_\lambda}{B_\lambda}}$$

is the phonon frequency, and b_μ and $b^*_{-\mu}$ are phonon destruction and creation operators. These operators satisfy the relations

$$b_\mu b^*_\mu = N_\mu + 1 \quad \text{and} \quad b^*_\mu b_\mu = N_\mu. \tag{3}$$

For a stationary state, the Schrödinger equation is

$$H\Psi = W_I^N \Psi, \tag{4}$$

where we wish to find Ψ, the system wave function, in the form of an expansion over the unperturbed functions

$$\Psi = \sum_{NRkl} a_{NRkl}(p)\,\psi_l(r)\,\Phi_N[Rs(k)\,lIM], \tag{5}$$

where $\psi_l(r)$ and Φ_N are eigenfunctions of the single-particle and collective states, respectively, and are assumed known:

$$\begin{aligned} H_p\psi_l(r) &= E_l\psi_l(r); \\ H_s\Phi_N &= \hbar\omega_N\Phi_N \end{aligned} \tag{6}$$

(E_l and $\hbar\omega_N$ are the single-particle and collective energy levels). The sum in (5) is taken over the number of phonons N, the angular momentum R of the core, the total spin k and the orbital angular momentum l of the odd nucleon; I and M are the total angular momentum of the system and its z-component, respectively.

The wave functions $\Phi_N[Rs(k)\,lIM]$ depend on both the spin and angle variables of the "extra" nucleon. They form a complete ortho-normal set:

$$\begin{aligned} \Phi_N[Rs(k)\,lIM] = \sum_m \sum_{m_s} (RsM - m - m_s m_s \,|\, RskM - m)\times \\ \times (klM - mm \,|\, klIM)\,Y_{lm}(\theta, \varphi)\,\chi_s^{m_s}\,\Phi_{NR}^{M-m-m_s} \end{aligned} \tag{7}$$

We have chosen an angular momentum coupling scheme according to which the nuclear spin R and the nucleon spin s couple to k which then couples with the orbital angular momentum l of the nucleon to give the total angular momentum I of the system. This is possible if we neglect spin-orbit coupling, so that l is a good quantum number.

When including spin-orbit coupling, however, and if the single-particle states have large j, it is more convenient to choose the basis functions according to a different coupling scheme; then l and s give the total angular momentum j of the nucleon, and this couples with nuclear spin R to give the total angular momentum I of the system:

$$\Psi = \sum_{NjlR} b_{Nljr}\psi_l(r)\,\tilde{\Phi}_N[R;\, sl(j)\,IM]. \tag{5'}$$

The relation between the amplitudes a_m and b_n in these two coupling schemes is given by

$$b_{Nljr} = \sum_k (2k+1)^{1/2}(2j+1)^{1/2}\,W(RsIl;\, kj)\,a_{NRkl}, \tag{8}$$

$$a_{NRkl} = \sum_j (2k+1)^{1/2} (2j+1)^{1/2} W(RsIl; kj)\, b_{NRjl}, \tag{8'}$$

where $W(abcd; ef)$ is a Racah coefficient.[8] It is thus easy to go over from one coupling scheme to the other.

Wave functions of odd nuclei

Now from Schrödinger's equation (4), we proceed in the usual way to obtain the following set of coupled equations for the a_{NRkl}:*

$$(W - E_l - \hbar\omega_N)\, a_{mN} = \sum_{m'} \langle mN \,|\, H' \,|\, m'N' \rangle\, a_{m'N'}. \tag{9}$$

We use the Tamm-Dancoff approximation[9] to solve Eq.(9), dropping all states of the core nucleus in which the phonon number N > 2. We make use of the property

$$\langle mN \,|\, H' \,|\, m'N' \rangle = (\delta_{N,\,N'-1} + \delta_{N,\,N'+1})\, \psi_l(\alpha R_0)\, \psi_{l'}(\alpha' R_0)\, H_{mN,\,m'N'}, \tag{10}$$

of the matrix elements and introduce the notation

$$\begin{aligned} a_{mN} &= \psi_m(\alpha_m R_0)\, A_{mN}; \\ E_l + \hbar\omega_N &= E_{lN}, \end{aligned} \tag{11}$$

to obtain the following equations for the amplitudes A_m, B_n and C_r for the no-phonon, one-phonon, and two-phonon states:

$$\begin{aligned} (W - E_{l0})\, A_0 &= \sum_{n'} H_{0n'} \psi^2_{l'} B_{n'}; \\ (W - E_{l1})\, B_n &= H_{n0} \psi^2_{l_0} A_0 + \sqrt{2} \sum_{r'} H_{nr'} \psi^2_{l'} C_{r'}; \\ (W - E_{l2}) C_r &= \sqrt{2} \sum_{n'} H_{rn'} \psi^2_{l'} B_{n'}. \end{aligned} \tag{12}$$

In the general case $\psi_m = \psi_{\beta l}$, where β characterizes the level sequence determined from the condition that the logarithmic derivatives of the internal and external solutions of (6) join smoothly at the boundary. If we recall that levels corresponding to different values of β have large separation[10] and note that only levels in a single shell are of importance, we may drop the sum over β, arriving at

$$\psi_{\beta l} = \psi_l.$$

Further, conservation of total angular momentum I and of parity implies that the sum over the no-phonon states also vanishes, so that

$$A_m = \delta_{ll_0} A_0,$$

where $l_0 = I \pm 1/2$ gives the parity of the state of the system. With this in mind, we arrive at Eqs.(12).

The solution of (12) requires a calculation of the matrix elements $H_{mn'}$ and $H_{nr'}$. This calculation requires summing the products of Clebsch-Gordan coefficients over magnetic quantum numbers. The final results of this summation are

$$H_{0n} = -\tilde{g}\, [(2l+1)(2k+1)]^{1/2} (l\,200 \,|\, l\,2\,l_0\,0)\, W(l_0\, 2Ik; ls); \tag{13}$$

---

*Henceforth we shall denote the complete set of indices Rkl by the single index m.

$$H_{rn'} = -\tilde{g}\,[(2l+1)\,(2R+1)\,(2k+1)\,(2k'+1)]^{1/2} \times (l\,200\,|\,l\,2\,l'\,0)\,W\,(2k'Rs;\,k2)\,W\,(k'\,2\,Il;\,kl'), \quad (13')$$

where

$$\tilde{g} = kR_0\left[\frac{\hbar}{2B\omega}\cdot\frac{5}{4\pi}\right]^{1/2}.$$

Equations (13) and (13') can then be used to solve (12). The amplitudes A_0, B_n and C_r are related by the conditions

$$\psi_{l_0}(R_0)\,A_0 = \frac{1}{\sqrt{N\,(W_I,\,l_0)}}; \quad (14)$$

$$B_{kl} = -\tilde{g}\,[(2l+1)\,(2k+1)]^{1/2}\,(l\,200\,|\,l\,2\,l_0\,0)\,W\,(l_0 2Ik;\,ls)\,\frac{\psi^2_{l_0}A_0}{(W_I - E_{l_1} - 2\tilde{g}^2\alpha_{l_2})}; \quad (14')$$

$$C_{Rkl} = \sqrt{2}\,\tilde{g}^2\,[(2R+1)\,(2k+1)]^{1/2}\,W\,(kRIl_0;\,sl)\sum_{l'}(2l'+1)\,W(2Rl'l_0;\,2l)\times$$

$$\times\,\frac{(l'\,200\,|\,l'\,2\,l\,0)\,(l'\,200\,|\,l'\,2\,l_0)\,\psi^2_{l'}\psi^2_{l_0}A_0}{(W_I - E_{l_2})\,(W_I - E_{l'1} - 2\tilde{g}^2\alpha_{l'2})}, \quad (14'')$$

where

$$N\,(W_I\,l_0) = 1 + \tilde{g}^2\sum_{l}\frac{(l_0\,200\,|\,l_0 2l0)^2\,\psi^2_l\psi^2_{l_0}}{(W_I - E_{l_1} - 2\tilde{g}^2\alpha_{l_2})^2}\left(1 + 2g^2\sum_{l'}\frac{(l\,200\,|\,l2l'0)^2\,\psi^2_l\psi^2_{l_0}}{(W_I - E_{l_2})^2}\right), \quad (15)$$

$$\alpha_{l_0 1} = \sum_{l}\frac{(l_0\,200\,|\,l_0 2l0)^2\,\psi^2_l\psi^2_{l_0}}{W_I E_{l\,1} - 2\tilde{g}^2\alpha_{l_2}(W_I)}; \quad \alpha_{l2} = \sum_{l'}\frac{(l\,200\,|\,l2l'0)^2\,\psi^2_{l'}\psi^2_l}{(W_I - E_{l'2})}. \quad (15')$$

In addition, from the fact that the determinant of the set of equations vanishes, we obtain the following equation for W_I, giving the energy levels of the odd nucleon:

$$W_I = E_{l_0} + \tilde{g}^2\alpha_{l_0 1}(W_I). \quad (16)$$

On inserting (14)-(14'') into (5), we obtain the eigenfunctions of the nucleus as a function of the total angular momentum.

Energy levels of odd nuclei

To solve Eq.(16) for the energy levels of odd nuclei is quite difficult. If, however, we assume that the collective levels lie above the single-particle levels, and this is indeed the case in weakly deformed nuclei, the problem simplifies considerably. Thus, for instance, from Eq.(16) it is very easy to find the ground state of an odd nucleus by the method of successive approximations. Choosing a zeroth approximation $W_I^{(0)} = E_{l_0}$, we obtain

$$W_I^{(1)} = E_{l_0} + \tilde{g}^2\alpha_{l_0 1}(E_{l_0}). \quad (17)$$

For the n-th approximation, we have the simple recursion relation

$$W_I^{(n)} = E_{l_0} + \tilde{g}^2\alpha_{l_0 1}(W_I^{(n-1)}); \quad (17')$$

then the desired ground state energy is given by

$$W_{I0} = \lim_{n\to\infty} W_I^{(n)}. \quad (17'')$$

For coupling which is not too strong, this converges very rapidly, and no great number of successive steps is needed. Let us now assume that the ground

state energy has been found. Then, by simplifying (16) somewhat, we can find the collective energy levels of the system. Neglecting the l-dependence of the denominator in $\alpha_{l_0 1}$ and l_{l_2}, and taking its average value out from under the summation sign, we obtain a cubic equation for the eigenvalues W_{IN}. For the case of coupling which is not too strong, the energy levels of the one-phonon and two-phonon collective states are

$$W_1^I = \overline{E}_{l1} + \Delta W_0 + \frac{2\,[\widetilde{g}^2 \overline{\widetilde{\psi}}_l^2 \overline{\psi}_l^2 + M]}{\overline{E}_{l1} - \overline{E}_{l2} + \Delta W_0}; \tag{18}$$

$$W_2^I = \overline{E}_{l2} - \frac{2\,[\widetilde{g}^2 \overline{\widetilde{\psi}}_l^2 \overline{\psi}_l^2 + M]}{\overline{E}_{l1} - \overline{E}_{l2} + \Delta W_0}, \tag{18'}$$

where

$$\widetilde{\psi}_l^2 = \sum_{l'} (l\,200 \mid l\,2\,l'\,0)^2 \psi_{l'}^2; \quad \Delta W_0 = E_{l_0} - W_{0I};$$

$$M = \overline{E}_{l2}\,\Delta W_0 \left(1 + \frac{\overline{E}_{l1}}{W_{I0}}\right) + \frac{\widetilde{g}^2 \overline{\widetilde{\psi}}_l^2 \overline{\psi}_l^2}{W_{I0}}\,\Delta W_0 + \frac{\widetilde{g}^2 \widetilde{\psi}_{l_0}^2 \psi_{l_0}^2 \overline{E}_{l2}}{W_{I0}}. \tag{18''}$$

M is of second order compared with $\widetilde{g}^2 \overline{\widetilde{\psi}}_l^2 \overline{\psi}_l^2$ (a bar over a symbol means its average value).

Again, for coupling that is not too strong, when $h\omega + E_l - E_{l_0} > \widetilde{g}^2 \alpha_{l_2}$, the second term in (16) is always negative, and the surface interaction always lowers the ground state energy irrespective of the sign of the coupling constant $\widetilde{g}$. As for excited collective levels, for the case of weak coupling to the surface, we may point out the following property. Since in the second term of (18'') the denominator is negative, and the principal contribution to the energy is from $\widetilde{g}^2 \overline{\widetilde{\psi}}_l^2 \overline{\psi}_l^2$, the first collective level is depressed by the surface interaction, while the second one is raised. Thus the separation between the collective levels increases. It should also be pointed out that in an actual nucleus the ground-state spin may not be the same as the total angular momentum of the first or second collective levels; hence the rule which says a level tends to go up or down may be violated for levels with different angular momenta. The indicated tendency should be observed if the first and second levels have a total angular momentum I equal to that of the ground state.

Physics Institute,
Academy of Sciences of the Ukrainian SSR

References

1. A.Bohr, Dan.Mat.-fys.Medd., 26, 14 (1952).
2. A.Bohr & B.R.Mottelson, Dan.Mat.-fys.Medd., 27, 16 (1953).
3. A.S.Davydov & G.F.Filippov, in Yadrenye reaktsii pri malykh i srednikh energiyakh (Nuclear reactions at low and medium energies), M. 1958.
4. D.A.Zaikin, Ibid.
5. K.Ford, Phys.Rev., 90, 29 (1953).
6. A.K.Kerman, Phys.Rev., 92, 1176 (1953).
7. D.C.Choudhury, Dan.Mat.-fys.Medd., 28, 4 (1954).
8. L.S.Biedenharn, J.M.Blatt & M.E.Rose, Revs.Mod.Phys., 24, 242 (1952).
9. I.Tamm, J.Phys., 9, 449 (1945).

MAGNETIC AND QUADRUPOLE MOMENTS OF WEAKLY DEFORMED NUCLEI

- B.D.Konstantinov and A.M.Korolev

Introduction

Bohr's generalized model of the nucleus[1] is now commonly used to explain the experimentally observed magnetic and quadrupole moments of nuclei.

Several authors[2,5] have used this model to treat these moments while taking account of the interaction of an odd nucleon with the nuclear surface. Investigations have published both for strong[2,3] and weak[4,5] coupling. Nevertheless, there remain some questions as to, for instance, the validity of the adiabatic approximation in finding the energy levels and the contribution of two-phonon states to the magnetic and quadrupole moments.[4] Although Choudhury[5] has extended the investigation to three-phonon states with intermediate coupling, the analytic dependence of these quantities on the ground-state quantum numbers of the nucleus has yet to be given.

The method used in the present work is essentially the same as that of Kerman and Choudhury.[4,5] We shall investigate the magnetic and quadrupole moments of nuclei by approaching intermediate coupling from the direction of weak coupling and making use of the results of our preceding work,[6] in which we obtained the wave functions and energy levels of odd nuclei. Nonadiabatic terms and two-phonon states are included in the calculation. Further, the influence of the odd "extra" nucleon on the magnitudes of the nuclear moments will be considered.

Statement of the problem

In order to calculate the magnetic and quadrupole moments of a system consisting of an even-even nuclear core and an "extra" nucleon, one must know the wave function of the system. This wave function is obtained by solving the Schrödinger equation:

$$H\Psi_{IM} = W_I \Psi_{IM}, \tag{1}$$

where the Hamiltonian H is written in the form[1]

$$H = H_s + H_p + H', \tag{2}$$

in which H_s is the Hamiltonian for the surface oscillations of the nucleus, H_p is the Hamiltonian of a free nucleon moving in a potential well given by $V(r)$ and

$$H' = -kR_0\delta(r - R_0)\sum_{\mu}\alpha_{2\mu}Y_{2\mu}(\theta\varphi) \tag{2'}$$

is the nucleon-nuclear surface interaction Hamiltonian.

Eq.(1) with the Hamiltonian (2) may be solved in the second quantization representation by use of the Tamm-Dancoff approximation,[7,8] i.e., on the assumption that only two surface quanta are excited.[6]

We shall attempt to find a solution of (1), for a given value of the total angular momentum I and its z-component M by expanding it in a series of eigenfunctions of the unperturbed system, namely,

$$\psi_{IM}(r) = \sum_{RSKlN} a^{NIM}_{RSKl}\psi_l(r,k)\Phi_N[RS(K)l;IM], \tag{3}$$

where R is the angular momentum of the nuclear surface, S is the nucleon spin, $K = R + S$, l is the orbital angular momentum of the nucleon, I is the total

angular momentum of the nucleus, M is its z-component, and N is the number of phonons present.

The wave functions $\Phi_N[RS(K)l;IM]$ correspond to a fixed scheme for coupling angular momenta and form a complete orthonormal set:[9]

$$\Phi_N[RS(K)l;IM]=\sum_{m,m_s}(KlM-mm\,|\,KlIM)(RSM-m-m_sm_s|\,RSKM-m)\times \times Y_{lm}(\theta,\varphi)\,\chi_s^{m_s}\,\Phi_N^{M-m-m_s}(R). \tag{4}$$

Here $(KlM-mm\,|KlIM)$ are Clebsch-Gordan coefficients, $Y_{lm}(\theta,\varphi)$ are normalized spherical functions depending on the angle variables θ,φ of the nucleon, $\chi_s^{m_s}$ is the spin wave function of the nucleon, $\Phi_N^{M-m-m_s}(R)$ is the wave function of the nucleus with spin R in phonon occuptaion-number space (N-space), and $\psi_l(r,k)$ is the wave function of a free nucleon in the spherical potential $V(r)$. The amplitudes a_{RSKl}^{IMN} in (3) for the no-, one-, and two-phonon states are a_0, $B_{2Kl}^{l_0}$ and $C_{RKl}^{l_0}$, respectively, and are given by[6]

$$a_0=\psi_{l_0}(R_0)\,A_0\delta_{ll_0}=\frac{\delta_{ll_0}}{\sqrt{N(W_I,l_0)}}, \tag{5}$$

where

$$N(W_I,l_0)=1+\tilde{g}^2\sum_l\frac{(l_0200\,|\,l_02l0)^2\psi_l^2(R_0)\psi_{l_0}^2(R_0)}{(W_I-E_{l1}-2\tilde{g}^2\alpha_{l2}(W_I))^2}(1+2\tilde{g}^2\tilde{\alpha}_{l2}), \tag{5'}$$

$$B_{2Kl}^{l_0}=(-\tilde{g})(2K+1)^{1/2}W(l_02IK;lS)(2l+1)^{1/2}\frac{(l200|l2l0)\,\psi_l(R_0)\,\psi_{l_0}(R_0)}{(W_I-E_{l1}-2\tilde{g}^2\alpha_{l2})}a_0, \tag{5''}$$

$$C_{RKl}^{l_0}=2\sum_{l'}(2K+1)^{1/2}(2R+1)^{1/2}W(KRIl_0;Sl)\,W(2Rl'l_0;2l)\times \times\tilde{g}^2(2l'+1)\frac{(l'200\,|\,l'2l0)\,(l'200\,|\,l'2l_00)\psi_{l'}^2(R_0)\psi_l(R_0)\,\psi_{l_0}(R_0)}{(W_I-E_{l2})\,(W_I-E_{l'1}-2\tilde{g}^2\alpha_{l'2})}a_0, \tag{5'''}$$

$$\tilde{g}=kR_0\left(\frac{\hbar}{2B\omega}\right)^{1/2}\left(\frac{5}{4\pi}\right)^{1/2},$$

in which $W(abcd;ef)$ is a Racah coefficient.[10] The inequality $I-\frac{1}{2}\leqslant l_0\leqslant I+\frac{1}{2}$ together with the parity determines l_0 uniquely. Let

$$E_{l1}=E_l+\hbar\omega_2 \quad\text{and}\quad E_{l2}=E_l+2\hbar\omega_2,$$

where E_l is the single-particle level, and $\hbar\omega$ is the collective level. Finally, α_{l2} and $\tilde{\alpha}_{l2}$ are given by

$$\alpha_{l2}(W_I)=\sum_{l'}\frac{(l200\,|\,l2l'0)^2\,\psi_{l'}^2(R_0)\,\psi_l^2(R_0)}{(W_I-E_{l'2})}. \tag{6}$$

$$\tilde{\alpha}_{l2}(W_I)=\sum_{l'}\frac{(l200\,|\,l2l'0)^2\,\psi_{l'}^2(R_0)\,\psi_l^2(R_0)}{(W_I-E_{l'2})^2}. \tag{7}$$

The ground-state energy is given by

$$W_I=E_{l_0}+\tilde{g}^2\sum_l\frac{(l_0200\,|\,l_02l0)^2\,\psi_l^2(R_0)\,\psi_{l_0}^2(R_0)}{W_I-E_l-\hbar\omega_2-2\tilde{g}^2\alpha_{l2}(W_I)}. \tag{8}$$

We can now proceed directly to calculation of the magnetic and quadrupole moments.

Magnetic moments

The partition of the angular momentum between the outer particle and the surface leads to the particle and the surface each contributing separately to the magnetic moment.

For a bound system consisting of an even-even nuclear core and an "extra" nucleon, the magnetic-moment operator may be taken in the form[2]

$$\hat{\mu} = g_j I_z - (g_j - g_R) R_z, \tag{9}$$

where R_z is the z-component of the surface angular momentum, g_R is the g-factor for the surface, and g_j is the g-factor for the single nucleon moving in a spherically symmetrical field.

For a nucleus with a uniform charge distribution, we have[11]

$$g_R = \frac{Z}{A}, \tag{10}$$

while for the single nucleon, we have

$$g_j = g_l \pm \frac{g_s - g_l}{2l+1}, \tag{11}$$

where the sign is chosen in accord with $j = l \pm \frac{1}{2}$, and g_s and g_l are the intrinsic and orbital g-factors in nuclear magnetons.

The magnetic moment μ of the nucleus is obtained by finding the matrix elements of the operator $\hat{\mu}$ of Eq. (9) between the wave functions given by (3) in the state with $I = M$. We must thus calculate a matrix element of the form

$$\mu = \langle g_j I_z - (g_j - g_R) R_z \rangle_{M=I}. \tag{12}$$

To do this, it is convenient to transform from the function of (3) whose coupling scheme is $[RS(K)l;\ IM]$ to a function whose coupling scheme is $[RSl(j);\ IM]$. This transition is made by means of a unitary transformation. The new wave function may be written

$$\psi_{IM}(r) = \sum_{Rj\,lN} b^{IM}_{Rj\,lN}\, \psi_l(r,k)\, \Phi_N[R, Sl(j); IM], \tag{13}$$

where the amplitudes $b^{IM}_{Rj\,lN}$ are related to the amplitudes $a^{IM}_{RK\,lN}$ by

$$b^{IM}_{Rj\,lN} = \sum_K (2K+1)^{1/2} (2j+1)^{1/2} W(RSIl; Kj)\, a^{IM}_{RK\,lN}.$$

To calculate the matrix element of (12), let us break it up into two parts and calculate each separately, writing

$$\mu = \langle g_j I_z \rangle_{M=I} - \langle (g_j - g_R) R_z \rangle_{M=I} = \mu_1 - \mu_2. \tag{14}$$

To calculate μ_1 and μ_2 one must sum products of the Clebsch-Gordan coefficients over magnetic quantum numbers, and of the Racah coefficients over angular momenta. The final result of such summation is

$$\mu_1 = I \left\{ g_I a^2_{l_0 l_0} + \sum_{l,j} g_j (2j+1)\, W^2(2j l_0 S; Il)\, B^2_{l l_0} + \sum_{R,l,j} g_j (2j+1)\, W^2(Rj l_0 S; Il)\, Q_{l_0 l} \right\}; \tag{15}$$

$$\mu_2 = I \left\{ \sum_{l,j} (g_j - g_R)(2j+1) \left[\frac{I(I+1) - j(j+1) + 6}{2I(I_0+1)} \right] W^2(2j l_0 S;\ Il)\, B^2_{l l_0} + \right.$$

$$+\sum_{R,l,j}(g_j-g_R)(2j+1)(2R+1)\times\left[\frac{I(I+1)+R(R+1)-j(j+1)}{2I(I+1)}\right]W^2(Rjl_0S;Il)Q_{ll_0}\},\qquad(16)$$

where Q_{ll_0}, $a_{l_0l_0}$, B_{ll_0} and $C^{l_0}_{ll'}$ are given by

$$Q_{l_0l}=\sum_{l_1,\,l_2}W(2Rl_1,l_0;2l)\,W(2Rl_2l_0;2l)\,C^{l_0}_{ll_1}C^{l_0}_{ll_2},\qquad(17)$$

$$a_{l_0l_0}=\frac{1}{\sqrt{N(W_I,l_0)}}\,^{*},\qquad(17')$$

$$B_{ll_0}=(-\tilde{g})(2l+1)^{1/2}\,\frac{(l200\,|\,l2l_00)\,\psi_l(R_0)\,\psi_{l_0}(R_0)}{W_I-E_{l1}-2\tilde{g}^2\alpha_{l_2}(W_I)}\,a_{l_0l_0},\qquad(17'')$$

$$C^{l_0}_{ll'}=\tilde{g}^2(2l'+1)\,\frac{(l'200\,|\,l'2l0)\,(l'200\,|\,l'\,2l_00)\,\psi^2_{l'}(R_0)\,\psi_l(R_0)\,\psi_{l_0}(R_0)}{(W_I-E_{l2})\,(W_I-E_{l'1}-2\tilde{g}^2\alpha_{l'2})}\,a_{l_0l_0}.\qquad(17''')$$

Thus we have found the total magnetic moment of the nucleus, due both to the surface and the outer nucleon.

Quadrupole moments

In the generalized model of the nucleus, the total quadrupole moment of the system consisting of a nuclear core and an outer nucleon may be written[2]

$$Q=Q_s+Q_p,\qquad(18)$$

where Q_s is the quadrupole moment due to deformation of the nuclear surface, and Q_p is the quadrupole moment of the outer nucleon.

The quadrupole moment operator for the nuclear surface in the liquid-drop model, i.e., when the nucleus is considered to be incompressible and to have a uniform charge distribution, is of the form[4,11]

$$\hat{Q}_s=3Z(5\pi)^{-1/2}R_0^2\alpha_{20}.\qquad(19)$$

On passing to second quantization, this operator becomes

$$\hat{Q}_s=3Z(5\pi)^{-1/2}R_0^2e_2\{b_{20}+b^{*}_{20}\},\qquad(20)$$

where

$$e_2=(\hbar^2/2B_2\hbar\omega_2)^{1/2},\qquad(20')$$

and where b_{20} and b^{*}_{20} are destruction and creation operators for nuclear surface excitations (phonons).

Further, the quadrupole moment operator for the outer nucleon is given by[12]

$$\hat{Q}_p=(16\pi/5)^{1/2}r^2Y_{20}(\theta,\varphi).\qquad(21)$$

This term makes only a small contribution to the total quadrupole moment of highly deformed nuclei, but may be comparatively large when the deformation is small.

In order to find the quadrupole moments Q_s and Q_p we must calculate the matrix elements of $\hat{Q}_s$ and $\hat{Q}_p$ between the wave functions of Eq.(3), i.e., we must calculate the matrix elements

---

*See Eq.(5').

$$Q_s = 3Z(5\pi)^{-1/2} R_0^2 e_2 \langle (b_{20} + b_{20}^*) \rangle_{M=I}; \tag{22}$$

$$Q_p = (16\pi/5)^{1/2} \langle r^2 Y_{20}(\theta, \varphi) \rangle_{M=I}. \tag{23}$$

The operator $(b_{20} + b_{20}^*)$ acts on the nuclear-surface wave function. From the commutation rules for the creation and destruction operators it follows that the matrix elements will fail to vanish only when the phonon number in the two states differs by one, i.e., when $N' = N \pm 1$.

In calculating the matrix elements of (22) and (23) we must sum products of the Clebsch-Gordan coefficients over magnetic quantum numbers. The final result of this summation is

$$Q_s = 6Z(5\pi)^{-1/2} R_0^2 e_2 (2I+1)^{1/2} (2I0I \mid 2III) W(Sl_0I2; Il_0) \times \times \left\{ a_{l_0 l_0} B_{l_0 l_0} + \sqrt{2} \sum_{ll'} W(2l_0 l2; l'l_0) B_{ll_0} C_{ll'}^{l_0} \right\}^*. \tag{24}$$

Similar calculations give

$$Q_p = 2(2I+1)^{1/2} (2I0I \mid 2III) W(Sl_0I2; Il_0) \times \{ (2l_0+1)^{1/2} (2l_0 00 \mid 2l_0 l_0 0) I_{l_0 l_0} a_{l_0 l_0}^2 + + \sum_{l,l'} (2l+1)^{1/2} (2l00 \mid 2ll'0) W(2l_0 l'2; ll_0) I_{l'l} B_{l'l_0} B_{ll_0} + + \sum_{l,l',l_1,l_2} (2l+1)^{1/2} (2l00 \mid 2ll'0) W(2l_1 l_0 2; l_0 l_1) W(2l_1 l'2; ll_1) I_{l'l} C_{l'l_1}^{l_0} C_{ll_2}^{l_0}, \tag{25}$$

where $I_{l'l}$ is an integral of the form

$$I_{l'l} = \int \psi_{l'}^* (r, k) \psi_l (r, k) r^4 dr, \tag{26}$$

in which $\psi_l (r, k)$ is a wave function satisfying the equation whose Hamiltonian is H_p and thus describes the motion of a free nucleon in the potential well given by $V(r)$.

As an example, we have calculated the magnetic and quadrupole moments of neodymium 143, a nucleus which has a single nucleon outside the closed shell. The nuclear radius was assumed to be given by $R_0 = r_0 A^{1/3}$, where $r_0 = 1.45 \cdot 10^{-13}$cm, and the depth of the well was taken as $V_0 = 35$ Mev. The coupling constant in the interaction Hamiltonian was taken to be 25% less than the well depth V_0.[1] The energy of the first excited state of the even-even nucleus was taken as $\hbar\omega_2 = 1.6$ Mev (Ref.13). The mass parameter B_2 was calculated on the basis of the liquid drop model.

The calculations gave

$$Q_{theo} = -1.75 \cdot 10^{-24} \text{ cm}^2 \text{ and } \mu_{theo} = -1.64\ \mu_n.$$

The experimental values[14,15] of the magnetic and quadrupole moments are

$$Q_{exp} = -(1.1 \pm 0.1) \cdot 10^{-24} \text{ cm}^2 \text{ and } \mu_{exp} = -1.0 \pm 0.2\ \mu_n.$$

It will be evident from a comparison of these results that when collective effects are taken into account the theory gives better results, although it still cannot fully explain the magnetic and quadrupole moments. This is probably because the value of B_2 as calculated from the liquid drop model is too low; thus the actual values of the moments should be somewhat larger.

---

*See Eqs.(17')-(17"').

In conclusion, it should be noted that the contribution from the two-photon states to the magnetic and quadrupole moments is probably small for nuclei close to magic numbers, and begins to grow as one goes to higher or lower numbers.

Physics Institute,
Academy of Sciences of the Ukrainian SSR

References

1. A.Bohr, Dan.Mat.-fys.Medd., 26, 14 (1952).
2. A.Bohr & B.Mottelson, Dan.Mat.-fys.Medd., 27, 16 (1953).
3. K.Ford, Phys.Rev., 90, 29 (1953).
4. A.K.Kerman, Phys.Rev., 92, 1176 (1953).
5. D.C.Choudhury, Dan.Mat.-fys.Medd., 28, 4 (1954).
6. A.M.Korolev, Present issue of the Bulletin, p.1475.
7. I.Tamm, J.Phys.(USSR), 9, 449 (1945).
8. S.M.Dancoff, Phys.Rev., 78, 382 (1950).
9. A.M.Korolev, in Yadrenye reaktsii pri malykh i srednikh energiyakh (Nuclear reactions at low and medium energies), M. 1958.
10. L.C.Biedenharn, J.M.Blatt & M.E.Rose, Revs.Mod.Phys., 24, 249 (1952).
11. H.Tolhoek, Physica, 21, 1 (1955).
12. J.M.Blatt & V.F.Weisskopf, Theoretical Nuclear Physics, N.Y., 1952. (Cited in Russian translation.)
13. G.Scharff-Goldhaber, Phys.Rev., 90, 587 (1953).
14. K.Murakawa, Phys.Rev., 96, 1543 (1954).
15. E.F.Kults, V.Kunz & V.G.Hartman, Uspekhi fiz. nauk, 55, 537 (1955).

NUCLEAR POTENTIALS AND NEUTRON STABILITY OF NUCLEI

- P.E.Nemirovskii

In an earlier communication[1] we gave the results of calculation of single-particle states of atomic nuclei with a potential taken from the optical model. It was shown that the level sequence obtained for a well with such a potential is in good agreement with the data on nuclear shells. On the other hand, satisfactory agreement was not obtained for the binding energies.

Further investigations showed that the utilized potential did not take into account all the factors exerting a substantial influence on the stationary states. One of the more important factors in the case of light nuclei is the variation of nuclear forces with isotopic spin. It is known that at low energies the forces between two nuclei in a state with T = 0 are much greater than between two nuclei in a state with T = 1. For light nuclei states with T = 0 or T = 1/2 lie substantially lower than states with T = 1 and T = 3/2, which for ground states is equivalent to dependence of the binding energy on N - Z. This dependence of nuclear forces on the isotopic spin, which is not in conflict with charge invariance, suggests that the effective potential of the self-consistent nuclear field must also depend on N - Z.[2-4]

An analogous dependence is evinced by the familiar isotopic term in the Weizsacker formula. The present study is devoted primarily to this problem. In the last section we shall show how the (N - Z)-dependence of the potential may be utilized for evaluating the maximum number of neutrons in a nucleus with given Z.

I. Determination of the potential

We shall not describe in detail the neutron-nucleus interaction potential assumed in the optical model. We need only recall that the same potential without the imaginary part is utilized for calculating stationary states.

The potential consists of two parts, namely, the principal central interaction and a spin-orbit term. For the central interaction we assume the r-dependence first proposed by Woods & Saxon[5]:

$$V_1 = -\frac{V_0}{1 + e^{\frac{r-R_0}{a}}}. \tag{1}$$

The assumed form for the spin-orbit interaction is

$$V_2 = -\frac{\varkappa}{r}\frac{dV_1}{dr}(\vec{\sigma}\vec{l}), \tag{2}$$

where V_1 is the central potential (the numerical value of $\varkappa$ is given in Section 2).

It is interesting to note that the result of rough evaluation of the spin-orbit interaction energy by means of perturbation theory, which we shall give immediately below, differs little (20-30%) from the result of precise calculation. The splitting of the terms with a given l is equal to the sum of the matrix elements (2) in states with parallel and antiparallel spin and orbit, i.e.,

$$E = (2l+1)\varkappa\int_0^\infty \frac{1}{r}\frac{dV_1}{dr}|\psi|^2 r^2 dr.$$

For purposes of evaluation it may be assumed that $\frac{dV_1}{dr}$ is nonzero in a narrow region close to the nuclear boundary, then $r|\psi|^2$, as a slowly varying function, may be taken out from under the integral for $r = R$ and $E = (2l+1)\times\times(r|\psi|^2)_{r=R}V_1$. If it be assumed that $r^2|\psi|^2$ is virtually constant inside the nucleus, we can write

$$(r\,|\,\psi\,|^2)_{r=R} \approx \frac{1}{R^2}$$

and

$$E \approx \frac{(2l+1)\,\varkappa}{R^2} V_1. \qquad (3)$$

Using the currently accepted parameters, such rough evaluation gives a value of E = 5.5 Mev for the splitting between the $1f_{7/2}$ and $1f_{5/2}$ states of Ca^{41}, which differs from the results of precise calculation by approximately 1 Mev. Formula (3) is particularly convenient for evaluating the role of spin-orbit interaction in states having radial nodes. For states without radial nodes the splitting with increase of R varies appreciably more slowly than according to the $1/R^2$ law, owing to the fact that in such states the nucleons are concentrated at the nuclear surface.

The indicated potential was used in our preceding studies. However, as has already been noted, for stationary states a substantial role must be played by the (N - Z)-dependence of the potential. In order to introduce this dependence we must make certain additional assumptions.

Let us assume that there are formed in the nucleus two independent self-consistent fields - a neutron and a proton field - and that the true interaction potential is the sum of these two potentials taken with statistical weights proportional to the number of protons and neutrons. This point of view is apparently valid for heavy nuclei and in particular it finds substantiation in present day theory of moments of inertia. For light nuclei there are correlation effects between the protons and neutrons which are evinced in the particular stability of nuclei of the $n\alpha$ type; hence our assumption is not valid for such nuclei. As for linear dependence of the potential on N - Z, it must hold for $(N - Z)/A \ll 1$. Investigation of nuclei with a large neutron excess may make it possible to find deviations from this simple dependence.

Hence we take the interaction potential in the form

$$V_n = \frac{N}{A} V_1 + \frac{Z}{A} V_2 = \frac{V_1 + V_2}{2} + \frac{N-Z}{2A}(V_1 - V_2). \qquad (4)$$

where V_1 is the interaction potential of a neutron with purely neutron liquid and V_2 is the interaction with purely proton liquid. It is assumed that the (N - Z)-dependence is the same for both the central potential and the spin-orbital potential. The influence of the second term may be calculated by means of perturbation theory or numerically. The ratio of the constants $V_1(0)$ and $V_2(0)$ and their half-sum should be determined from experiment.

For protons, it is natural to assume the potential in the form

$$V_p = \frac{Z}{A} V_1 + \frac{N}{A} V_2 = \frac{V_1 + V_2}{2} + \frac{N-Z}{2A}(V_2 - V_1). \qquad (5)$$

In view of the considerations set forth above, it may be assumed that $V_2 > V_1$, i.e., that for heavy nuclei $V_p > V_n$. In calculating levels we always use the potential $(V_1 + V_2)/2$. Then for a given N/Z, the parameters $K_0 = \frac{1}{\hbar}\sqrt{2mV_n}$, a and $\varkappa^{1/2}$, which have the dimensionality of length, were varied in the same way in accordance with (4). Incidentally, the changes of $\varkappa$ and a are very small and cannot have a substantial effect on the level energy.

In view of the above, the method of calculating neutron levels should be obvious. The calculation for odd protons is more complicated. In this case one must know the precise value of the Coulomb field acting on the proton. It might seem that this problem could be solved unambiguously. The difficulty, however, stems primarily from the multiplicity of data available. Actually there are the following groups of data:

1. Scattering of electrons by nuclei. The data of electron-nuclei scattering experiments are very precise and give for nuclei with A ⩾ 40 the following expression for the proton density:

$$\rho = \frac{\rho_0}{1 + e^{\frac{r - R_0}{a_0}}}, \qquad (6)$$

where $a_0 = 0.55 \cdot 10^{-13}$ cm and $R_0 = 1.07 \cdot 10^{-13} A^{1/3}$ cm.

For lighter nuclei there is obtained a specific charge distribution; however the difference between the distribution for O^{16} and the distribution given by Eq.(6) is not great.

2. Mu-mesonic atoms yield for uniform charge distribution: $R = 1.18 \cdot 10^{-13} A^{1/3}$ cm.

3. For mirror nuclei Hansen obtained $R = 1.3 \cdot 10^{-13} A^{1/3}$ cm.

4. Lastly, one can attempt to utilize the semi-empirical mass formula. According to the data of Green & Sood[2], who used this method, $R = 1.21 \cdot 10^{-13} A^{1/3}$ cm.

Method 1 is the most precise. However, fast electrons do not affect the nuclear Coulomb field. On the contrary, a proton in attaching itself to a nucleus polarizes the nucleus and hence its interaction with the nucleus must be weaker than is obtained from experiments by method 1. Similar considerations apply to mu-mesonic atoms.

The data of methods 3 and 4 have a more direct bearing on our problem.

For light nuclei the different methods lead to close results. This is due to the low value of the Coulomb interaction. Thus for O^{17} an error of 10% amounts to only 0.3 Mev and hence is insignificant, but for Sb^{121} an error of 10% is already equivalent to 1.3 Mev, while for Bi^{209} the equivalent error is 1.8 Mev; hence correct choice of the nuclear potential is very important for investigation of nuclear potential. We cannot, however, utilize the data of method 4 inasmuch as it comprises a large error. Hence at present calculations of proton levels in heavy nuclei must necessarily be of a tentative, approximate nature.

II. Comparison with experiment

As was already noted, all the parameters, except for the ratio V_1/V_2, were taken from data on scattering of slow neutrons. It was assumed that the real part of the potential is constant in the range from 0 to 8 Mev. Calculations of the effective mass by different authors show that this parameter varies slowly, and hence our assumption is not in conflict with other theoretical considerations. We calculated the curves of Eqs.(1) and (2) using

$$R = 1.24 \; A^{1/3} \cdot 10^{-13} \text{ cm},$$

$$V_0 = 53 \text{ Mev},$$

$$K_0 = \frac{1}{\hbar}\sqrt{2mV_0} = \frac{1}{a},$$

and

$$x = \frac{0.66}{K_0^2}.$$

Then through comparison of the level energy for the given R with the ground state of a number of nuclei with a closed neutron shell plus one neutron we evaluated the parameter V_1/V_2. The best agreement with experiment is given by $V_2/V_1 = 3.44 \pm \pm 0.5$.

The value obtained for the binding energy of the last neutron in nuclei with 21, 29, 51, 83 and 127 neutrons is in excellent agreement with experiment. For 17 nuclei the maximum deviation is 0.46 Mev, the mean deviation is 0.01 Mev and the rms dispersion $\sqrt{\overline{\Delta E^2}} = 0.25$ Mev.

Table 1

Neutron binding energy, spin and parity of the ground states of nuclei with a closed shell plus one nucleon with N > 20

Nucleus	State		State		Nucleus	State		State	
	theo.	exp.	theo.	exp.		theo.	exp.	theo.	exp.
S^{17}	7/2⁻	7/2⁻	4,8	4,48	Zr^{91}	5/2⁺	5/2⁺	6,97	7,16
Ar^{39}	7/2⁻	7/2⁻	6,82	6,6	Mo^{93}	5/2⁺	5/2⁺	7,89	7,85
Ca^{41}	7/2⁻	7/2⁻	8,73	8,37	Xe^{137}	7/2⁻	7/2⁻	4,09	4,40
Ca^{49}	3/2⁻	3/2⁻	5,37	5,15	Ba^{139}	7/2⁻	7/2⁻	4,66	4,72
Ti^{51}	3/2⁻	3/2⁻	6,69	6,35	Ce^{141}	7/2⁻	7/2⁻	5,24	5,40
Cr^{53}	3/2⁻	3/2⁻	7,99	7,93	Nd^{143}	7/2⁻	7/2⁻	5,78	6,06
Fe^{55}	3/2⁻	3/2⁻	9,25	9,30	Pb^{209}	9/2⁺	9/2⁺	4,09	3,94
Kr^{87}	5/2⁺	5/2⁺	5,14	5,53	Po^{211}	9/2⁺	9/2⁺	4,49	4,55
Sr^{89}	5/2⁺	5/2⁺	6,06	6,52	Ge^{73}	9/2⁺	9/2⁺	6,98	6,64

Table 2

Neutron binding energy, spin and parity of the ground states of nuclei with 9, 15 and 17 neutrons

Nucleus	State			
	theo.	exp.	theo.	exp.
O^{17}	$1d_{5/2}$	5/2⁺	5,65	4,14
Mg^{27}	$2s$	1/2⁺	8,70	6,44
Si^{29}	$2s$	1/2⁺	11,13	8,46
Si^{31}	$1d_{3/2}$	3/2⁺	8,80	6,59
S^{33}	$1d_{3/2}$	3/2⁺	11,2	8,65

Table 3

Z-dependence of the neutron binding energy with constant N for nuclei with a closed shell

Z_1	Z_2	N	ΔE theo.	ΔE exp.
20	16	21	3,93	3,89
20	18	21	1,91	1,77
26	20	29	3,88	4,16
26	22	29	2,56	2,96
26	24	29	1,26	1,37
42	36	51	2,75	2,32
40	36	51	1,83	1,63
38	36	51	0,92	0,99
60	54	83	1,69	1,66
60	56	83	1,12	1,34
60	58	83	0,54	0,66
84	82	127	0,40	0,61
14	12	15	2,43	2,02
16	14	17	2,4	2,06

Table 1 lists the neutron binding energies for these 17 nuclei as well as for Ge^{73} in which the $1g_{9/2}$ shell begins to fill. Table 2 lists the binding energies of light nuclei, which with the same computation parameters, differ appreciably from the experimental values. Actually, only O^{17} really has a closed shell plus one neutron; Si^{29} and the other nuclei with 15 and 17 neutrons are obtained from questionable subshells plus one neutron. Inasmuch as the $2s$ and $1d_{3/2}$ states are close to $1d_{5/2}$, here there may not form a rigorously self-consistent field, particularly if the extreme case of j-j coupling does not obtain and the coupling is intermediate.

The O^{16} nucleus apparently has distinctive features which are connected with the pronounced correlation of two neutrons and two protons in light nuclei. Moreover, the charge distribution in O^{16} is apparently better described by a gaussian curve than by exponential decrease. Hence one should not expect good agreement with experiment in the case of O^{17}. Incidentally, agreement of the ground state energy with the experimental value can be attained either by reducing the nuclear radius by 3% or assuming a slightly lower potential at the center.

It should be noted that the potential under consideration not only closely characterizes the neutron binding energy over the entire periodic system, but as a rule correctly reflects the changes in the neutron binding energy incident to the addition of two, four or six protons. This will be apparent from Table 3.

The variation in energy is also correctly rendered for Z = 15 and 17. As compared to the ground state, the agreement as regards binding energy is appreciably poorer for excited states (Table 4).

Table 4

Neutron binding energy for excited single particle levels

Nucleus	State		Binding energy		Nucleus	State		Binding energy	
	theo.	exp.	theo.	exp.		theo.	exp.	theo.	exp.
O^{17}	$1/2^+$	$1/2^+$	3,73	3,27	Zn^{69}	$9/2^+$	$9/2^+$	5,84	6,06
O^{17}	$3/2^+$	$3/2^+$	—0,4	—0,9	Zn^{71}	$9/2^+$	$9/2^+$	5,75	5,47
Ca^{41}	$3/2^-$	$3/2^-$	5,35	6,42	Pd^{109}	$11/2^-$	$11/2^-$	5,55	5,99
Ca^{41}	$1/2^-$	$1/2^-$	3,4	4,42	Cd^{111}	$11/2^-$	$11/2^-$	6,4	6,94
Cr^{53}	$1/2^-$	$1/2^-$	6,21	7,36	Cd^{113}	$11/2^-$	$11/2^-$	6,46	6,06

For O^{17} the calculated energy for the $2s$ excited state is in even better agreement with experiment than for the ground state, which may be connected with the lower sensitivity of the s-state to the form of the potential. In the case of Ca^{41}, we find good agreement of the spin-orbit splitting with experiment: $\Delta E_{exp} = 2.0$; $\Delta E_{theo} = 1.95$.

Of particular interest are nuclei in which the $1g_{9/2}$ and $1h_{11/2}$ states begin to fill. Such nuclei can be of interest only when the neutron is attached to a core producing a self-consistent field. Inasmuch as 38 neutrons correspond to closed $2p_{3/2}$ and $1f_{5/2}$ shells, the Zn^{69} nucleus has a self-consistent core field. The agreement here with theory is excellent. Zn^{71} and Ge^{73} would have a self-consistent core field only if the 39th and 40th neutrons are in the $2p_{1/2}$ state; however, it is not impossible that these two particles are in the $1g_{9/2}$ state and then the field is not self-consistent. The question remains open. Even in this case, the variation in binding energy is correctly rendered.

The filling of the $1h_{11/2}$ state occurs by pairs. Hence it is difficult to say for which nucleus the $1h_{11/2}$ state is still vacant. Incidentally, it is known that spins 5/2 and 7/2 are not encountered in nuclei with $N > 64$. Hence it may be assumed that for 64 neutrons the $1h_{11/2}$ state is still unoccupied and that the $2d_{5/2}$ and $1g_{7/2}$ states are fully occupied. Then comparison for Cd^{113} is legitimate and as may be seen the agreement is satisfactory. Pd^{109} and Cd^{111} undoubtedly do not have a closed shell plus one neutron. However, in view of the great difference between the $1h_{11/2}$, $2d_{5/2}$ and $1g_{7/2}$ states, which are not yet filled in these nuclei, the Cd^{110} and Pd^{108} cores may be regarded as self-consistent fields (only for levels with opposite parity). The agreement obtained is satisfactory particularly for the change in binding energy incident to attachment of two protons. We see therefore that satisfactory agreement with experiment is also obtained with $1g_{9/2}$ and $1h_{11/2}$ states.

It would be of great interest to investigate the $1g_{7/2}$ states in Sr^{89}, Zr^{91} and Mo^{93} and the $1h_{9/2}$ states in Ba^{139}, Ce^{141} and Nd^{143}. Unfortunately, adequate experimental data on the excited states of these nuclei are not available.

A more important question is the applicability of the proposed model to nuclei with an odd proton. In the first place we must check the identity of the neutron and proton potentials in light nuclei where for the core $N = Z$.

For this it is enough to determine whether there is obtained a correct energy difference for mirror nuclei O^{17} & F^{17} and Ca^{41} & Sc^{41} if one adds the Coulomb potential to the nuclear potential. Taking the data of Hofstadter for the charge distribution in O^{16} and Ca^{40}, one can calculate the proton binding energy. It is found that the energy difference varies slowly with change in the level energy, as a result of which poor agreement of the O^{17} energy with the experimental data has almost no effect on the Coulomb energy. The energy difference for the ground states of O^{17} and F^{17} is found to be 3.51 Mev (the experimental value is 3.55 Mev), and for the first excited $2s$ state 3.04 Mev (experimental value - 3.22 Mev).

We see that the lower Coulomb energy for the excited state is explained by the behavior of the wave function of the $2s$ and $1d_{5/2}$ states. Possibly some modification of the form of the potential would make the agreement even closer.

For Ca^{41} and Sc^{41} the calculated energy difference for the ground state is 7.1 Mev (experimental - 6.76 Mev). A deviation of the order of 5% may be attributed to incorrect specification of the Coulomb field. Moreover, small changes in the width of the region of diffusion of the nuclear potential have a stronger effect where the odd proton is concerned as compared with the odd neutron (in view of the more rapid attenuation of the proton function). On the whole it may be said that from the results for mirror nuclei, it follows that with N = Z, the potentials V_n and V_p are equal.

Among the heavier nuclei, so far we have investigated only Sc^{49}, Bi^{209} and Sb^{121} with a potential (5). The results for Sc^{49} are in general not very satisfactory. The calculated value of the proton binding energy is 8.6 Mev and differs from the experimental value by 0.8 Mev. However, substitution of equal potentials for the proton and neutron would lead to a binding energy of 2.5 Mev (instead of 8.6 Mev).

For Bi^{209} calculations given E = 3.3 Mev (the experimental value is 3.78 Mev). This energy, however, is very sensitive to the parameter $1/a$ and its reduction by 6% leads to a decrease of the binding energy by 0.5 Mev with, at the same time, little change in the energy of Pb^{209}. In any case, if one takes for Pb^{209} the same potential as for Bi^{209}, the calculated binding energy differs from experiment by 6 Mev. Thus despite the paucity of the data available it may be asserted that formula (5) gives better agreement with experiment than $V_p = V_n$.

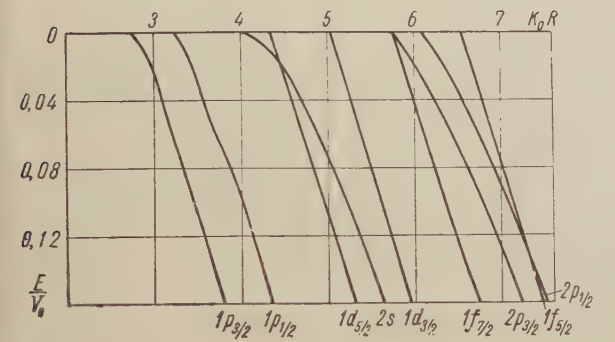

Fig.1. Variation of the binding energy with the nuclear radius for levels with different l and j. Assumed potential well parameters: $V_0 = \frac{\hbar^2}{2ma^2} = 50$ Mev;

$$K_0R = 1.92\,A^{1/3}\quad \varkappa = \frac{0{,}66}{\varkappa_0^2};\ A<60.$$

Finally, a large discrepancy is obtained for Sb^{121}: the theoretical energy value is 3.5 Mev, whereas the experimental one is 5.7 Mev. Although Z = 50 does correspond to a closed shell, the quadrupole moments of Sb^{121} and Sb^{123} are so large that single-particle treatment of the ground states of these nuclei is of questionable validity.

III. Neutron stability

Knowing the variation of the potential with (N - Z), one can readily calculate the neutron binding energy in nuclei with a closed neutron shell plus one neutron as a function of Z. At a certain value of Z the neutron binding energy goes to zero.

It can be shown by analysis of the curves characterizing the variation of the neutron binding energy with the nuclear radius that for low binding energies the boundaries between shells will correspond to different neutron numbers. This follows from the separation between levels. Figs.1 and 2 show the variation of the binding energy with the nuclear radius for N = Z. It will be seen that for E $\approx$ 0, the shells must close for N = 20, 40, 52, 82 and 126.

The maximum values of N as a function of Z found on the assumption that $V_2/V_1 = 3.4$ are listed in Table 5. It will be seen from the table that for all atomic weights minimum Z $\approx$ 0.3 A. Similar calculations for heavy nuclei are precluded by statistical deformation.

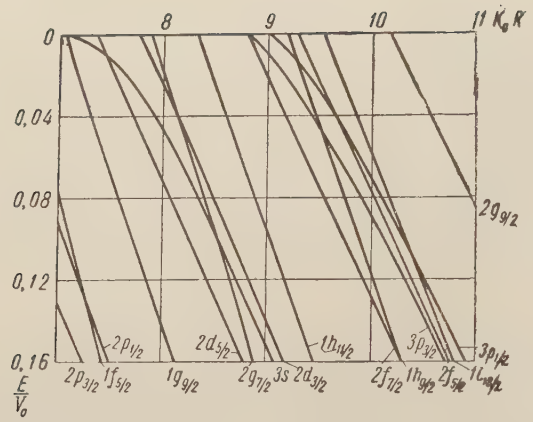

Fig.2. Variation of the binding energy with the nuclear radius for levels with different l and j. Assumed potential well parameters: $V_0=\frac{\hbar^2}{2ma^2}=50$ Mev;

$K_0R=1.92A^{1/3}$; $\varkappa=\frac{0.66}{\varkappa_0^2}$; $A>50$.

Table 5

Variation of N_{max} with Z

Z	N_{max}	A_{max}	Z	N_{max}	A_{max}
8	16	24	26	58	84
10	20	30	28	70	98
12	32	44	30	70	100
14	34	48	32	70	102
18	40	58	34	82	116
20	40	60			
22	52	74			
24	58	82			

Institute of Atomic Energy
Academy of Sciences of the USSR

References

1. P.E.Nemirovskii, Zhur.eksp.i teor.fiz., 33, 746 (1957). (Trans.Soviet Physics - JETP.)

2. A.E.S.Green & P.C.Sood, Phys.Rev., 111, 1147 (1958).

3. L.A.Sliv & B.A.Volchek, Zhur.eksp.i teor.fiz., 36, 539 (1959). (Trans. Soviet Physics - JETP.)

4. P.E.Nemirovskii, Ibid., 36, 889 (1959). (Trans.Ibid.)

5. K.Woods & D.Saxon, Phys.Rev., 95, 577 (1954).

ON "REPULSION" OF NUCLEAR LEVELS WITH THE SAME SPIN AND PARITY

- L.K.Peker

It is known[1] that there occurs in nuclei an interaction between energy levels with the same spin and parity, resulting in mutual "repulsion" of the levels. The character of this interaction depends substantially on the nature of the levels. Up to now the "repulsion" effect has been observed in two different groups of levels.

Kerman[2] directed attention to the fact that in nuclei with odd A, levels with the same spin, belonging to two rotational bands based on single-particle levels with momenta K and K ± 1 interact as a consequence of the coupling between nuclear rotation and the motion of individual nucleons (an effect similar to Coriolis force). This effect has been detected in W^{183} (Ref.2) and possibly in Ta^{181}, Ho^{165} and other nuclei. Gurevich & Pevzner[3] and Hughes[4] have observed the effect of level "repulsion" in reactions of nuclei with slow neutrons in the 8-9 Mev excitation energy region.

In the present note we wish to direct attention to another type of mutual repulsion (levels with the same spin and parity).

Let us consider the properties of two 2+ levels (which are usually interpreted as γ-vibrational) in the even isotopes of $_{74}W$ and $_{76}Os$.

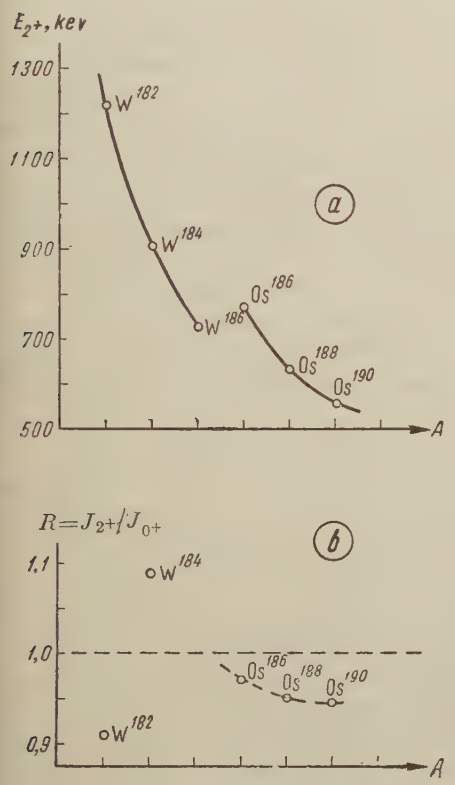

Fig.1. a) Energies of the 2+ γ-vibrational levels in even-even W and Os isotopes. b) Ratios R of the moments of inertia of the 2+ γ-vibrational levels and the ground state.

Data[5] on the energies and moments of inertia of these levels are presented in Fig.1. The point corresponding to W^{184} in Fig.1,a lies on a smooth curve which is similar to the curve for the Os isotopes. In Fig.1,b this point falls out sharply (for W^{184} $R > 1$). This means that in W^{184} the interval between levels with I = 2+ and I = 3+ (in both cases K = 2+) is anomalously small.

The narrowing of this interval can be understood if we assume that there exists another 2+ level located somewhat lower than the 2+ γ-vibrational level (Fig.2), and that there is repulsion between the two levels. In connection with the hypothesis regarding the existence of two 2+ levels with energies of 904 kev (K = 2+) and ~900 kev, let us consider the experimental data[6] on the decay of Re^{184} to W^{184}. Among the several weak γ-transitions which could not be fitted into the scheme proposed by Gallagher et al[6], there is a 788 kev transition. Since according to Gallagher et al, the total disintegration energy of Re^{184} is ~1300 kev, it follows from energy considerations that the 788 kev γ-transition can feed only one of the three levels of the lower rotational band: 0 (0+), 111 (2+) or 364 kev (4+), and, consequently, there must be a 788, 899 or 1152 kev level in W^{184}.

The existence of the 788 and 1152 kev levels is doubtful, for no γ-transitions to other levels of the lower rotational band which might compete with the 788 kev γ-transition were ever observed.

It is more probable that there exists an 899 kev 2+ level. The low intensity of the 788 kev

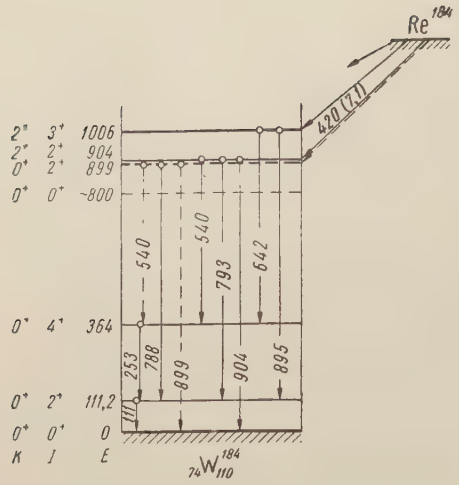

Fig.2. Level scheme for W^{184}. The 2+ level we have introduced is indicated by the heavy dashed line. The proposed β-vibrational level with K = 0+, I = 0+ is indicated by the light dashed line.

γ-rays indicates that the 899 kev level is sparsely populated in Re^{184} decay. In this case the weak 899 kev cross-over γ-transition may be masked by the strong 895 and 904 kev γ-lines. The small fraction of observed 504 kev γ-rays may correspond to a transition from the 899 kev level to the 364 kev (4+) level.

If the proposed interpretation of the 788 kev γ-rays is correct, then the 899 kev 2+ level is the first rotational level of a band based on a ~800 kev β-vibrational level (K = 0+; I = = 0+) in W^{184}. Hitherto β-vibrational levels in the even nuclei $_{74}W$ and $_{76}Os$ have not been observed.

The 899 kev 2+ level is almost contiguous to the 904 kev 2+ γ-vibrational level (the separation between them is ~5 kev).

The "repulsion" effect, which is inversely proportional to the separation between the 2+ levels, may noticeably reduce the interval between the I = 2+ and 3+ (K = 2+) levels, so that R > 1 in W^{184}.

An analogous situation apparently occurs in Pu^{238}, where R > 1 for the 2+ 1030 kev γ-vibrational level, and the 988 kev γ-vibrational (K = 0+; I = 2+) level is located somewhat below it.[7,8] In other nuclei, in which there are known to be β- and γ-vibrational levels, the intervals between these are comparatively large (in $_{62}Sm^{152}$ - 277 kev; in $_{64}Gd^{154}$ - 193 kev; in $_{64}Gd^{156}$ - 344 kev[5]) so that their "repulsion" is significantly weaker, and the inequality R > 1 does not obtain.

Scientific Research Physical Institute,
"A.A.Zhdanov" Leningrad State University

References

1. L.B.Landau & Ya.A.Smorodinskii, Lektsii po teorii atomnogo yadra (Lectures on the theory of the atomic nucleus), M. 1955.

2. A.K.Kerman, Klg.Danske, Mat.-fyz.Medd., 30, 15 (1956).

3. I.I.Gurevich & M.I.Penzner, Nucl.Phys., 2, 575 (1956).

4. D.Hughes, cited in Nucl.Phys., 2, 575 (1956).

5. B.S.Dzhelepov & L.K.Peker, Vozbuzhdennye sostoyaniya deformirovannykz yader (Excited states of deformed nuclei). OIYaI, M. 1959.

6. C.M.Gallagher, D.Strominger & J.P.Unik, Phys.Rev., 110, 725 (1958).

7. B.S.Dzhelepov & L.K.Peker, Skhemy raspada radioaktivnykh yader (Decay schemes of radioactive nuclei). M.-L., 1958.

8. D.Strominer, J.M.Hollander & G.T.Seaborg, Table of Isotopes, Revs.Mod. Phys., 30, 585 (1958).

EQUILIBRIUM SHAPE OF ODD-A NUCLEI IN THE A = 213 TO 221 REGION

- L.K.Peker

In the present paper we discuss the character of the equilibrium shape of off-A nuclei in the A = 213 to 221 region.* In spite of the fact that even-even nuclei in this region are spherical (as indicated by the structure of their excited levels), the question of the equilibrium shape of the odd nuclei is by no means trivial: the presence of an odd nucleon can, in principle, disturb the equilibrium between the forces tending to preserve the spherical equilibrium shape and the forces tending to elongate the nucleus. The possibility of a similar effect in nuclei with A = 103 to 109 was discussed by Alder et al.[1]

It is known that the even-even nuclei $_{44}Ru$, $_{46}Pd$ and $_{48}Cd$ are spherical, while the odd nuclei Rh^{103}, Ag^{107}, Ag^{109} exhibit some properties of nonspherical nuclei.[1] Probably the same effect leads to the fact, noted by Gallagher & Moszkowski[2], that the spins of most odd-odd nuclei are more consistent with the assumption of a slight deformation of the nuclei than with the assumption of their strict sphericity.

The properties of odd nuclei with A = 213 to 221 have scarcely been studied. With a few exceptions, almost nothing is known regarding the spectra of their excited levels, the spin assignments for their excited and ground states, and the β- and γ-transition probabilities and multipole orders.[3,4]

It turns out, however, that some deductions concerning the equilibrium shape of the nuclei under consideration can be drawn on the basis of α-decay probability data.

Earlier it was assumed that increase of the nuclear deformation parameter leads to a significant lowering of the Coulomb barrier and, consequently, to a sharp and considerable (order of ten) increase of its penetrability.[5,6] However, comparison of α-decay probabilities for different even-even nuclei (with $A \geqslant 216$) showed that the probability of penetration of the barrier by α-particles is almost independent of the deformation parameter. More accurate evaluations substantiated this experimental fact. It was found that change of the deformation parameter from $\beta = 0$ to $\beta = 0.2$ is accompanied by an increase in α-decay probability of only about 3 times.[7] Our present α-decay theory is not sufficiently accurate for analysis of such a weak dependence.

Thus, at present it is impossible to conclude anything about the equilibrium shape of the nucleus in the ground state from data on the α-particle penetration probability.

Let us consider the process of α-particle formation. The probability for creation of an α-particle is wholly determined by the quantum characteristics of the states of the nucleons from which the particle is formed. The more similar these characteristics, the more the nucleon wave functions overlap and the stronger their interaction, and consequently, the greater the probability of formation of an α-particle. The latter is maximized when the nucleons differ only as regards the sign of Ω (the projection of the total angular momentum on a symmetry axis). The corresponding α-transition is called allowed, and for it $F = T_{exp}/T_{theo} \approx 1$ (Bohr et al[8]). It is clear that such a transition can take place only between two states characterized by the same quantum numbers.

Odd deformed nuclei are characterized by the quantum numbers N, n_z, Λ, Σ and Ω (Nilsson[9]). Since at any given level (with given Ω) there can be no more than two nucleons, in general there can exist only one odd value of N or Z characterized by the given set of quantum numbers. Inasmuch as the odd N or Z

---

*Odd nuclei with A = 209 to 211 are spherical inasmuch as they have only one to three nucleons outside the closed shells.

changes by two units in α-decay, there should, in principle, not exist allowed transitions to the ground state in deformed nuclei. Actually, however, we occasionally meet situations when in the parent and daughter nuclei the odd nucleons are located on the same single-particle level and, consequently, a direct allowed α-transition is possible. In the A = 223 to 253 region these conditions obtain in only two cases:

$$_{92}U^{233}_{141} \xrightarrow{\alpha} {}_{90}Th^{229}_{139} \text{ and } {}_{99}Es^{253}_{154} \xrightarrow{\alpha} {}_{97}Bk^{249}_{152}.$$

At the same time, in the A = 213 to 221 region there are at least 9 cases of direct allowed transitions with $F \approx 1$ (Table 1).[10]

Table 1

Allowed α-transitions to the ground state

Transition	F	Transition	F
Spherical nuclei			
$_{84}Po^{213}_{129} \rightarrow {}_{82}Pb^{209}_{127}$	2*	$_{85}At^{215}_{130} \rightarrow {}_{83}Bi^{211}_{128}$	3,7*
$_{84}Po^{215}_{131} \rightarrow {}_{82}Pb^{211}_{129}$	1,2	$_{85}At^{217}_{132} \rightarrow {}_{83}Bi^{213}_{130}$	0,60
$_{86}Rn^{217}_{131} \rightarrow {}_{84}Po^{213}_{129}$	4,5*	$_{85}At^{219}_{134} \rightarrow {}_{83}Bi^{215}_{132}$	1,9
$_{86}Rn^{219}_{133} \rightarrow {}_{84}Po^{215}_{131}$	~10**	$_{87}Fr^{219}_{132} \rightarrow {}_{85}At^{215}_{130}$	1,2
		$_{87}Fr^{221}_{134} \rightarrow {}_{85}At^{217}_{132}$	3,3**
Deformed nuclei			
$_{92}U^{233}_{141} \rightarrow {}_{90}Th^{229}_{139}$	1,2**	$_{99}Es^{253}_{154} \rightarrow {}_{97}Bk^{249}_{152}$	1,5**

*The location of the lower levels in the daughter nucleus is known. It is assumed that since the energy of these levels is high, the probability for α-transition to them is low compared to the probability for α-transition to the ground state.

**There are direct experimental data indicating an α-transition to the ground state.

Table 2

α-Transitions accompanied by change in equilibrium shape

Transition	F	Transition	F
$_{88}Ra^{223}_{135} \rightarrow {}_{86}Rn^{219}_{133}$	Large**	$_{89}Ac^{225}_{136} \rightarrow {}_{87}Fr^{221}_{134}$	~7*
$_{89}Ac^{223}_{134} \rightarrow {}_{87}Fr^{219}_{132}$	3,1		

*see Table 1.
** " " "

Such a large number of direct allowed transitions to the ground state clearly indicates that nuclei with A = 213 to 221 have a spherical equilibrium shape. Actually, in spherical nuclei the state of the odd nucleon is characterized solely by the quantum number j (total angular momentum). In any one level there can be $2j + 1$ nucleons and, consequently, there may exist up to $(2j + 1)/2$ different nuclei with odd N or Z and a given j.

Direct α-transitions accompanied by a change in equilibrium shape (Table 2) are of considerable interest. The small values of F for the direct α-transitions in $_{89}Ac^{225}$ and, possibly, $_{89}Ac^{223}$ lead one to conclude that the penetrability of the Coulomb barrier is only weakly dependent on the deformation parameter.

In addition, they indicate that in the deformed nuclei $_{89}Ac^{225}$ and $_{89}Ac^{223}$ the 89th proton is located on the 5/2- level[2,3,5] constituting one of the $h_{9/2}$ sublevels, since the 87th proton in the spherical nuclei $_{87}Fr^{219}$ and $_{87}Fr^{221}$ is located on the $h_{9/2}$ (or $f_{7/2}$) level.

As Table 2 shows, the direct α-transition $Ra^{233} \rightarrow Rn^{219}$ is strongly forbidden (F is large). This high degree of forbiddenness is consistent with the data on the states of the 135th and 133rd neutrons. It follows from analysis of the decay of Th^{227} and Fr^{223} that the ground state of the deformed nucleus Ra^{223} (N = 135) is probably 3/2- (Refs.1, 6 & 7). The 133rd neutron in the spherical product nucleus Rn^{219} must be located in the $g_{9/2}$, $g_{7/2}$ or

$d_{5/2}$ state. Hence the α-transition from the 3/2- to the 9/2+, 7/2+ or 5/2+ states must be greatly inhibited.

The writer is grateful to L.A.Sliv for valuable discussions.

Scientific-Research Physical Institute
"A.A.Zhdanov" Leningrad State University

References

1. K.Alder, A.Bohr, B.Mottelson, T.Huus & A.Winther, Rev.Mod.Phys., 28, 432 (1956).
2. C.J.Gallagher & S.A.Moszkowski, Phys.Rev., 111, 1282 (1958).
3. D.Strőminger, J.Hollander & G.Seaborg, Revs.Mod.Phys., 30, 585 (1958).
4. B.S.Dzhelepov & L.K.Peker, Skhemy raspada radioaktivnykh yader (Decay schemes of radioactive nuclei), M.-L., 1958.
5. D.Hill & J.Wheeler, Phys.Rev., 89, 1102 (1953).
6. L.A.Sliv & L.K.Peker, Doklady AN SSSR, 99, 727 (1954).
7. P.O.Fröman, Mat.Fus.Skr., Dan.Vid.Selsk., 1, 3 (1957).
8. A.Bohr, P.O.Fröman & B.R.Mottelson, Dan.Mat.-fys.Medd., 29, 10 (1955).
9. S.G.Nilsson, Dan.Mat.-fys.Medd., 29, 16 (1955).
10. I.Perlman & J.Rasmussen, Alpha-Radioactivity. - Handbuch der Physik, Springer, Berlin, 1956.

References

1. H. de Waard & T.R.Gerholm, Nucl.Phys., 1, 281 (1956).
2. R.L.Graham & R.E.Bell, Canad.J.Phys., 31, 377 (1953).
3. H.Vartapetian, Thèses, Faculté des Science de l'Universite de Paris, 1957.
4. R.E.Bell, R.L.Graham & H.E.Petch, Canad.J.Phys., 30, 35 (1952).
5. A.Bedesku, K.P.Mitrofanov, A.A.Sorokin & V.S.Shpinel', Present issue of the Bulletin, p.1424.
6. L.A.Sliv & I.M.Band, Tablitsy koeffitsientov vnutrennei konversii gamma-izlucheniya (Tables of internal conversion coefficients), Parts I & II. M.-L., 1958.
7. T.Alväger, B.Johansson & W.Zuk, Arkiv.Fys., 14, 22, 3733 (1958).

SOME CHARACTERISTICS OF NEW PHOTOMULTIPLIER TUBES

- A.G.Berkovskii, I.Ya.Breido, O.S.Korol'kova & L.G.Leiteizen

There have been developed two new photomultipliers for use in scintillation spectrometers.

The FEU-35 photomultiplier has a 25 mm diameter cathode, a maximum diameter of 34 mm and an overall length of 108 mm. The tube has a 10-pin key-type base and no side leads.

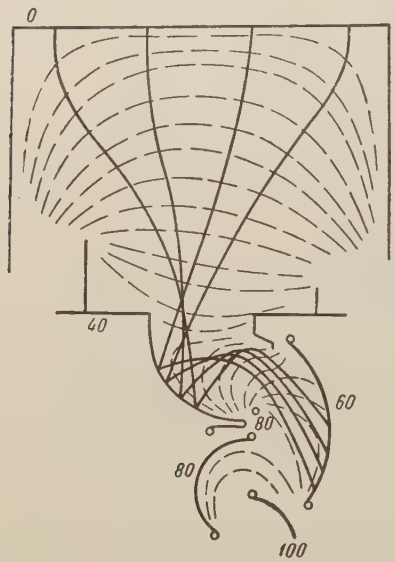

Fig.1. Electron-optical input system of the FEU-35 photomultiplier.

To improve the electron-optical characteristics of the input section the tube design features a focusing cylinder with a skew end face (Fig.1). A cylinder of this type allows of better matching of the axially symmetric input with the inevitably asymmetric first stage of the multiplying system. The new input design insures better energy resolution with a standard voltage divider and uniform voltage distribution between all the stages except for the cathode-first emitter stage to which double the normal stage voltage is applied.

The distribution of a lot of 600 FEU-35 tubes as regards pulse height resolution measured with an NaI(Tl) 20 mm diameter crystal and Cs^{137} is shown in Fig.2. Fig.3 shows the distribution for the same lot of tubes as regards the energy equivalence of intrinsic noise measured at a level of 50 pulses/sec. The average amplification and sensitivity of the photomultipliers and the variation of the dark current as a function of the supply voltage are shown in Fig.4.

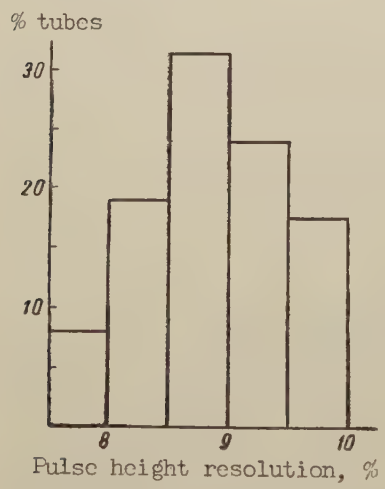

Fig.2. Pulse height distribution in a lot of 600 FEU-35 tubes.

Fig.3. Energy equivalent of intrinsic noise distribution in the same 600 lot of FEU-35 tubes. →→

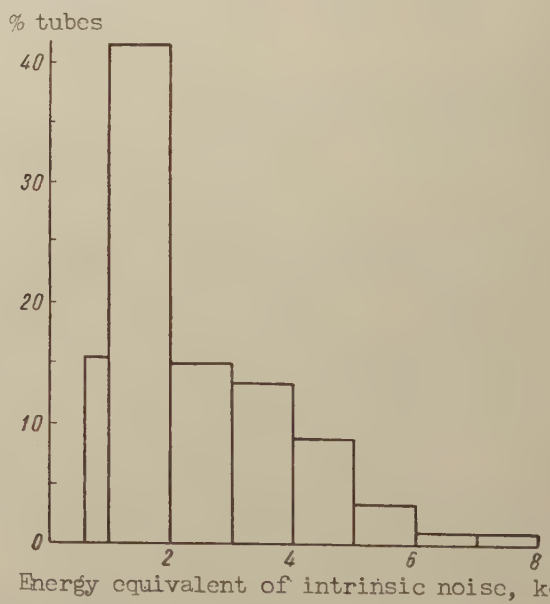

The variation of the output pulse height with the γ-ray energy remains linear up to a pulse height of 10 v with a resistance of 50 kilohm and a capacitance of 10 pf.

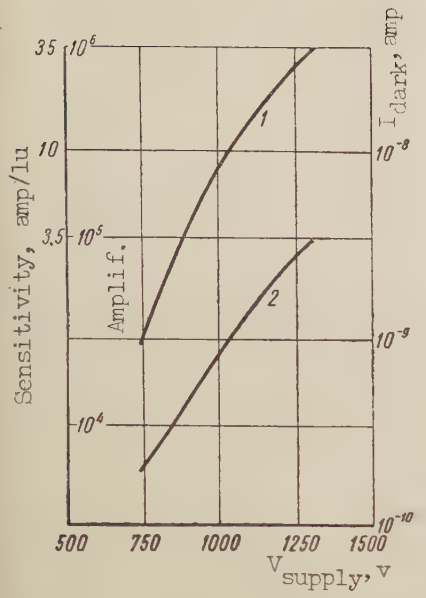

Fig.4. Variation of the anode sensitivity and amplification (1) and dark current (2) with the supply voltage for FEU-35 photomultipliers.

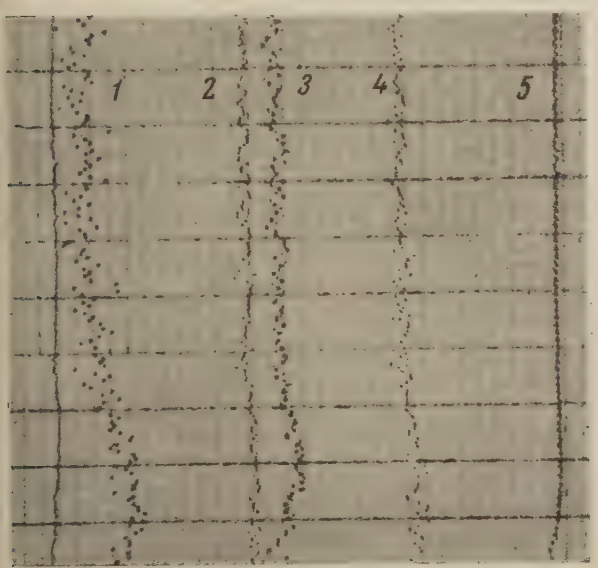

Fig.5. Record of stability of the Cs^{137} photopeak amplitude for four FEU-29 photomultipliers (1-4). Curve 5 - control record.

The FEU-35 is characterized by a high resistance between all the electrodes (10^{11} ohm on the average and not less than 10^9 ohm) which makes this photomultiplier particularly suitable for use in portable equipment.

The sensitivity threshold of the photomultiplier measured at a frequency of 80 cps with the width of the resonance amplifier passband equal to 20 cps is $(6-8)\cdot10^{-12}$ lu on the average.

The other photomultiplier has a cathode diameter of 38 mm, a maximum diameter of 48 mm and an overall length of 190 mm. Like the FEU-35 it has no side leads.

As in the FEU-35 the electron-optical input section insures good amplitude resolution (7.5-10%) with uniform voltage distribution between the electrodes. This photomultiplier is characterized by a low noise level: 1-2 kev at the level of 50 pulses/sec.

For the purpose of testing the stability of the photomultipliers under conditions as close to the usual operating conditions as possible, there was developed a special set-up designed to record the variation with time of the height of the photopeak from Cs^{137} with an NaI(Tl) crystal. The principal component of the set-up is a single-channel analyzer with a "rocking" channel. The analyzer output is coupled to a follow-up system which controls the voltage V_d of the first (principal) discriminator so that V_d follows the signal amplitude. The follow-up system consists of two gates (electronic valves) which open synchronously with rocking of the channel and alternately pass pulse packets to the integrating circuits. The output voltages from the integrating circuits are subtracted from each other and if the rocking of the channel is symmetrical relative to the photopeak the resultant signal is zero. If the peak is shifted, for example, owing to instability of the photomultiplier, there is produced an error signal which goes to the grid of the tube regulating V_d; this readjusts V_d to the level of the photopeak (null error signal regulation). The relative increment $\Delta V_d/V_d$ is separated by a bridge circuit and recorded by the automatic recorder. The recorder strip chart is calibrated in percent of the pulse height ($\Delta V_d/V_d \cdot 100$). For convenience in recording the characteristics of several photomultipliers, the set-up has provision for shifting the chart sidewise to record several characteristics without overlapping.

Fig.5 shows a photograph of the strip chart obtained in recording the position of the photopeak for four FEU-29 photomultipliers tested over a period of five hours (curves 1-4). Each division of the chart on the horizontal scale equals 0.4 of the pulse height; each division along the vertical equals 30 min. With this method of recording one can observe two types of instability: 1) continuous drift in time of the average photopeak amplitude (curve 1) and 2) fluctuations of the peak amplitude about some average value (curves 1-4). The drift of the mean value is apparently due to processes occurring inside the photomultiplier and connected with changes in the structure of the emitting layer.

There is virtually no drift in the case of some tubes (curves 2 & 4); for other tubes there is a drift over a certain period of time (settling time), which differs from tube to tube and appears to increase with the length of time the tube was out of operation prior to the test.

Fluctuations in the pulse amplitude, as characterized by the scatter of the points, are characteristic of all photomultipliers and vary from tube to tube in the range of approximately 0.3% (curve 2) to 1% (curve 1). These fluctuations are apparently due to the presence of a low frequency component in the statistical scatter of the output pulse amplitude.

CALCULATION OF THE ENERGY LEVELS OF Tl^{206} AND Bi^{210}

- Yu. I. Kharitonov

Introduction

The present paper gives the results of an attempt to calculate the energy levels of the odd-odd nuclei Tl^{206} and Bi^{210}. The configurations of these nuclei differ from the configuration of Pb^{208}, which has a doubly closed shell, by the presence of two holes or two nucleons outside the filled shells. For the purposes of the calculation we used the wave functions of neighboring nuclei with one nucleon or one hole outside the closed shells. The radial parts of the wave functions and the energies of the corresponding levels were calculated for the case of a diffuse-boundary potential in the work of Sliv & Volchok.[1]

1. Calculation of the energy levels of Tl^{206}

The $_{81}Tl^{206}$ nucleus has one neutron hole and one proton hole. For calculating the energy levels of this nucleus we used the single-particle wave functions for tne neutron levels of Pb^{207} pertaining to the ground state ($p_{1/2}$) and the first excited 620 kev level ($f_{5/2}$) and the proton levels of Tl^{207} pertaining to the ground state ($s_{1/2}$) and the first 350 kev excited level ($d_{3/2}$). These single-particle states are sufficient for constructing the level scheme for Tl^{206} to 1 Mev. By means of these data one can in the zeroth approximation construct the possible configurations of the energy states of Tl^{207} shown in Table 1.

Table 1

Possible configurations of Tl^{206}

Configuration	Multiplet energy in zeroth approximation, kev	Spins and paritics of levels
$(p_{1/2}s_{1/2})$	0	0⁻, 1⁻
$(p_{1/2}d_{3/2})$	350	1⁻, 2⁻
$(f_{5/2}s_{1/2})$	620	2⁻, 3⁻
$(f_{5/2}d_{3/2})$	970	1⁻, 2⁻, 3⁻, 4⁻

It will be apparent from Table 1 that the first three configurations comprise two levels, i.e., are doublets. The fourth configuration $(f_{5/2}d_{3/2})$ comprises four levels. The further problem consists in finding the forces splitting the levels pertaining to the same configuration. Such forces may be 1) interaction of the nucleons (holes) outside the closed shells with the nuclear surface and 2) weak pair interaction of the neutron and proton holes located in different shells. The purpose of the further calculations was to determine the parameters of these forces and to plot the theoretical level scheme for Tl^{206}.

The nucleon (hole)-nuclear surface interaction operator was taken in the form[2]

$$W_s = \sum_{i=1}^{2} \sum_{\mu} k(r_i)\,\alpha_{2\mu} Y_{2\mu}(\vartheta_i, \varphi_i), \qquad (1)$$

where $k(r_i)$ is the interaction constant, $\alpha_{2\mu}$ is an operator acting on the phonon part of the function, $Y_{2\mu}$ is a spherical function of the second order, and r_i, ϑ_i and φ_i are the coordinates of the i-th particle.

Such forces, regardless of the choice of parameters, do not split the doublet levels but only shift them as a whole. The $f_{5/2}d_{3/2}$ multiplet levels, however, are split, but in view of the fact that the levels of this multiplet lie comparatively high, in further calculations we will restrict our consideration to the doublet levels. The shift $\Delta_s E^0$ of the doublet levels owing to interaction with the nuclear surface depends on the magnitude of E_i^0, $\hbar\omega$, C and K:

$$\Delta_s E_i^0 = \frac{K^2}{C} f(E_i^0, \hbar\omega), \tag{2}$$

where E_i^0 is the energy of the i-th doublet in the zeroth approximation, $\hbar\omega$ is the energy of the first vibrational level, C is the "rigidity" of the nucleus,

$$K = \int R_i(j_1)\, k(r_i)\, R_i(j_2)\, d\tau_i,$$

and the R_i are the radial parts of the wave function of the i-th particle.

According to data on nuclei with one nucleon or hole outside the filled shells, the numerical value of K is approximately 40 Mev. The energy $\hbar\omega$ of the first vibrational level and the rigidity C of the Tl^{206} nucleus are not known. Thus the shift $\Delta_s E^0$ remains a function of two unknown parameters, $\hbar\omega$ and C. This shift was calculated for a number of values of $\hbar\omega$ and C, characteristic of heavy nuclei with configurations close to the configurations of Tl^{206}. Thus, C for Pb^{206} was evaluated from experiments and Coulomb excitation and found to be of the order of 1400 Mev.[3] Calculations showed that the relative separations between doublets do not change substantially with variation of C from 1000 to 1500 Mev and $\hbar\omega$ from 1 to 3 Mev.

Thus in the case of Tl^{206} taking into account the interaction of the holes with the nuclear surface not only does not split the doublet levels but almost does not change their relative separation calculated in the zeroth approximation.

Let us now take into account the pair interaction between the neutron and proton holes. Inasmuch as the specific form of the forces is hardly important where the magnitude of the splitting of the doublet levels is concerned, we arbitrarily assumed a gaussian potential. We took into account the variation of the pair interaction potential with the spin variables. The pair interaction operator W_{pr} was taken in the form

$$W_{pr} = e^{-\frac{(r_n - r_p)^2}{r_0^2}} \{V_s \pi_s + V_t \pi_t\}, \tag{3}$$

where V_s is the singlet interaction constant, V_t is the triplet interaction constant, π_s is the singlet projection operator, and π_t is the triplet projection operator.

In view of the weakness of the pair interaction of the holes located in different shells, the calculations were carried out with the help of perturbation theory. The diagonal matrix elements of the operator W_{pr} after integration were expressed in terms of Slater integrals F_i^k and the constants V_s and V_t (Table 2).

Table 2

Diagonal matrix elements of the operator W_{pr}

Configuration	I	Matrix elements
$(p_{1/2}\, s_{1/2})$	0-	$F_1^0 V_t$
	1-	$^1/_3 F_1^0 V_s + {}^2/_3 F_1^0 V_t$
$(p_{1/2}\, d_{3/2})$	1-	$^1/_3(F_2^0 + {}^1/_5 F_2^2)V_s + {}^1/_3(2F_2^0 - {}^1/_5 F_2^2)V_t$
	2-	$^1/_5(F_2^0 - {}^1/_5 F_2^2)V_s + {}^1/_5(4F_2^0 + {}^1/_5 F_2^2)V_t$
$(f_{5/2}\, s_{1/2})$	2-	$F_3^0 V_t$
	3-	$^3/_7 F_3^0 V_s + {}^4/_7 F_3^0 V_t$

Let us assume that in each doublet, the level with the higher spin lies above the level with the lower spin. Under the above assumption, the following expressions are obtained for the magnitude of the splittings of the doublets under consideration:

$$\Delta_1 = {}^1/_3 F_1^0 (V_s - V_t), \tag{4}$$

$$\Delta_1 = -{}^2/_{15}(F_2^0 + {}^4/_5 F_2^2)(V_s - V_t), \tag{5}$$

$$\Delta_3 = {}^3/_7 F_3^0 (V_s - V_t). \tag{6}$$

The Slater integrals are functions of the parameter r_0, which characterizes the effective range of the pair interaction forces. We took r_0 equal to $1.85 \cdot 10^{-13}$ cm, as is usual in treating nucleon-nucleon scattering. For the given value of r_0, the Slater integrals are positive and equal to $\sim 10^{-2}$. From this, in view of the fact that the ground state spin of Tl^{206} is zero, we can draw the following two important deductions:

1. The difference $(V_s - V_t) > 0$.
2. The split doublet levels have the following spin sequence:

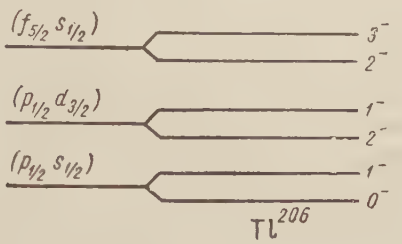

We attempted to determine the constants V_s and V_t from the experimental data on Tl^{206}, with a view to utilizing these values for calculating the energy levels of Bi^{210}.

As was shown in the work of Golenetskii, Rusinov & Filimonov[4], there are actually three doublets in the level scheme for Tl^{206}. The splitting of the second doublet was measured with the highest accuracy and found to be $\Delta_2 = 40 \pm 10$ kev. From this we evaluate the difference $(V_s - V_t)$ to be 12 ± 3 Mev. In this case the splittings of the other two levels are $\Delta_1 = 85 \pm 20$ and $\Delta_3 = 70 \pm 15$ kev. These values are in good agreement with the experimental values for the splittings of these doublets.

It will be evident from Table 2 that the difference between the energies of $(f_{5/2}s_{1/2})_{I=2}$ and $(p_{1/2}s_{1/2})_{I=0}$ levels can be expressed in terms of the zeroth approximation energy and the triplet interaction constant V_t. The value of V_t is very sensitive to small changes in the zeroth approximation energy and one must insure a higher accuracy in determining this constant than was done in the work of Sliv and Volchok.[1]

Thus on the basis of our calculations we propose the following level scheme for Tl^{206}:

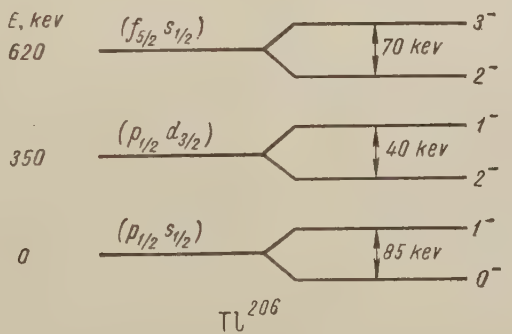

2. Calculation of the energy levels of Bi^{210}

The $_{83}Bi^{210}$ nucleus has one neutron and one proton outside the closed shells. For calculating the energy levels of Bi^{210} we used the single-particle wave functions of the neutron levels of Pb^{209} pertaining to the ground state $(g_{9/2})$ and the

Table 3

Possible configurations of Bi^{210}

Configuration	Multiplet energy in zeroth approximation kev	Spins and parities of levels
$(g_{9/2}h_{9/2})$	0	0⁻, 1⁻, 2⁻, 3⁻, 4⁻, 5⁻, 6⁻, 7⁻, 8⁻, 9⁻
$(i_{11/2}h_{9/2})$	816	1⁻, 2⁻, 3⁻, 4⁻, 5⁻, 6⁻, 7⁻, 8⁻
$(g_{9/2}f_{7/2})$	877	1⁻, 2⁻, 3⁻, 4⁻, 5⁻, 6⁻, 7⁻, 8⁻, 9⁻, 10⁻

first excited 816 kev state ($i_{11/2}$) and the proton levels of Bi^{209} pertaining to the ground state ($h_{9/2}$) and the first 877 kev excited level ($f_{7/2}$). On the basis of these data one can determine in the zeroth approximation the possible configurations of the energy levels of Bi^{210} to 1 Mev shown in Table 3.

The further calculations are similar to those carried out for Tl^{206}, but, as will be apparent from Table 3, the situation is more complicated for Bi^{210}. It was found that taking into account the interaction of the nucleons outside the closed shells with the nuclear surface splits levels belonging to individual multiplets. However, inasmuch as owing to interaction of the nucleons with the nuclear surface the individual levels are shifted downward, while the absolute magnitude of the shift does not exceed 500 kev, we can be sure that the levels of the $i_{11/2}h_{9/2}$ and $g_{9/2}f_{7/2}$ multiplets in shifting relative to each other will not intermix with the levels belonging to the ground state multiplet. Hence in calculating the level scheme for Bi^{210} one can limit the consideration to the $g_{9/2}h_{9/2}$ multiplet. The displacement of the $g_{9/2}h_{9/2}$ multiplet levels owing to interaction of the nucleons with the nuclear surface was calculated for a number of values of $\hbar\omega$ and C. In all the considered cases the spins of the first three levels are arranged in increasing order, 0-, 1- and 2-, but the fourth level has spin 9-. Moreover, the separation between levels for a given C does not at all depend on $\hbar\omega$. Thus, for example, for C = = 1000 Mev, taking into account the interaction of the nucleons with the nuclear surface gives the following sequence for the first four levels:

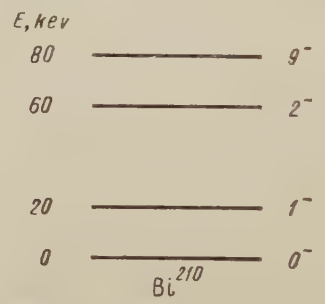

Next we took into account the weak pair interaction between the neutron and proton located in different shells. The matrix elements of the pair interaction were calculated under the same assumptions as for Tl^{206} (Table 4).

The results of further computation depend on the assumption made regarding the Bi^{210} ground state spin. We shall consider two cases:

1. The ground state spin I = 0-. In this case the following level scheme for Bi^{210} is obtained:

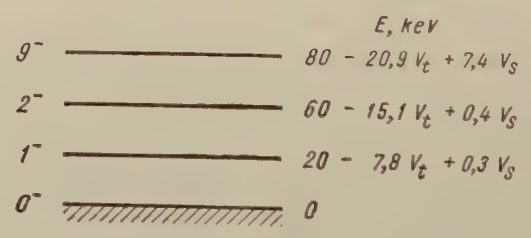

2. The ground state spin I = 1-. In this case we obtained the following level scheme:

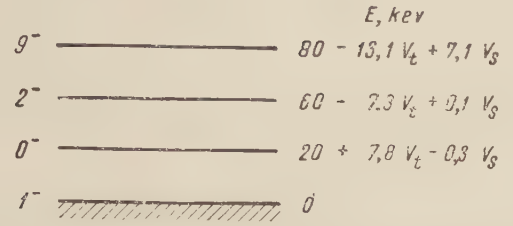

Utilizing the experimental value for the energy of the first excited level in Bi^{210}, namely, ~50 kev, and the value for the difference $(V_s - V_t)$ obtained from calculations of the levels of Tl^{206}, we can construct two variants of the level scheme of Bi^{210}:

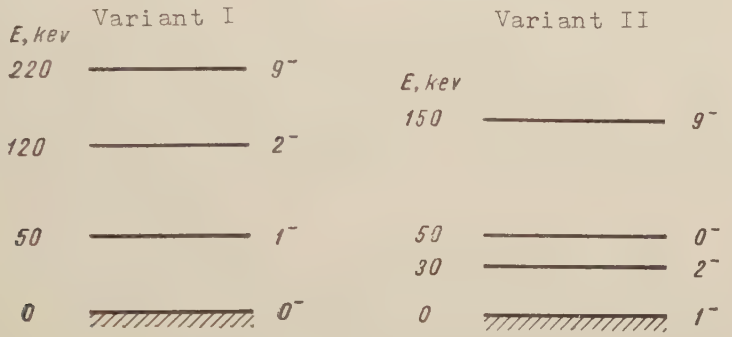

Table 4

Diagonal matrix elements of the operator W_{pr} ($g_{9/2}\ h_{9/2}$ configuration)

I	Matrix elements
0-	$29{,}4\cdot10^{-3}\ V_t$
1-	$21{,}6\cdot10^{-3}\ V_t + 0{,}3\cdot10^{-3}\ V_s$
2-	$14{,}3\cdot10^{-3}\ V_t + 0{,}4\cdot10^{-3}\ V_s$
9-	$8{,}5\cdot10^{-3}\ V_t + 7{,}4\cdot10^{-3}\ V_s$

Conclusions

The Tl^{206} nucleus is a suitable choice for determining the pair interaction constants for unlike nucleons located in different shells. However, the experimental data now available are inadequate for determination of these constants. Hence it would be of interest to carry out the following measurements for Tl^{206}:

1. To measure by observation of conversion or by the correlation procedure the spin of the ground state and of some excited level of Tl^{206} in order to be able to compare the experimental values with the predicted spins of the corresponding levels.

2. To measure the probability for E2 transitions, which will enable us to evaluate the magnitude of K/C, knowledge of which will make it possible to take into account more accurately the interaction of holes with the nuclear surface.

3. To determine more accurately the energy of the levels of Tl^{206} in the zeroth approximation. To this end one must measure the energy of the first excited levels in Pb^{207} and Tl^{207} and also the lifetimes of these levels.

In order to calculate the energy levels of the Bi^{210} one must know the experimental value of the nuclear spin. At present on the basis of the performed calculations one can only assert that the spin of the long-lived level at about 200 kev is 9-.

In conclusion, we would like to note that in our calculations we did not take into account the influence of static deformation. In Tl^{206} the proton spin is 1/2 and hence the quadrupole moment is zero. In Bi^{210} the quadrupole moment may be nonzero, but its influence can hardly be greater than the uncertainty inherent in the calculations.

I desire to express my deep gratitude to L.A.Sliv under whose guidance the present work was carried out and to G.V.Podgaiskaya who participated in the calculations.

Physical-Technical Institute
Academy of Sciences of the USSR

References

1. L.A.Sliv & B.A.Volchok, Zhur.eksp.i teor.fiz., 36, 539 (1959). (Trans. Soviet Physics - JETP, Vol.9, 374.)

2. A.Bohr & B.Mottelson, Dan.Mat.-fys.Medd., 27, No.2 (1953).

3. K.Alder, A.Bohr, T.Huus, B.Mottelson & A.Winther, Revs.Mod.Phys, 28, 432 (1956).

4. S.Golenetskii, O.I.Rusinov & Yu.I.Filimonov, Zhur.eksp.i teor.fiz., 37, 560 (1959). (Trans.Soviet Physics - JETP, Vol.10, 395.)

Fig.5 shows a photograph of the strip chart obtained in recording the position of the photopeak for four FEU-29 photomultipliers tested over a period of five hours (curves 1-4). Each division of the chart on the horizontal scale equals 0.4 of the pulse height; each division along the vertical equals 30 min. With this method of recording one can observe two types of instability: 1) continuous drift in time of the average photopeak amplitude (curve 1) and 2) fluctuations of the peak amplitude about some average value (curves 1-4). The drift of the mean value is apparently due to processes occurring inside the photomultiplier and connected with changes in the structure of the emitting layer.

There is virtually no drift in the case of some tubes (curves 2 & 4); for other tubes there is a drift over a certain period of time (settling time), which differs from tube to tube and appears to increase with the length of time the tube was out of operation prior to the test.

Fluctuations in the pulse amplitude, as characterized by the scatter of the points, are characteristic of all photomultipliers and vary from tube to tube in the range of approximately 0.3% (curve 2) to 1% (curve 1). These fluctuations are apparently due to the presence of a low frequency component in the statistical scatter of the output pulse amplitude.

Bulletin of the Academy of Sciences of the USSR - Physical Series
Vol. 23, No. 12 - December 1959

Transactions of the Ninth All-Union Conference on Nuclear Spectroscopy
(Continued from Vol.23, Nos.2 and 7)

TABLE OF CONTENTS

	Page Orig.	Trans.
Large double-focusing alpha-spectrometer - S.A.Baranov, A.G.Zelenkov, G.Ya.Shchepkin, V.V.Beruchko & A.F.Malov	1402	1389
Some design calculations for a double-focusing alpha-spectrometer - A.G.Zelenkov	1411	1396
New data on the decay of Am^{241} - P.S Samoilov	1416	1401
Positron spectrum of the lutetium fraction from the spallation products of tantalum - B.S.Dzhelepov, O.E.Kraft & E.B.Kreshtofova	1431	1422
Decay scheme for 30-hour Te^{131} - A.Bédesku, K.P.Mitrofanov, A.A. Sorokin & V.S.Shpinel'	1434	1424
On the l-forbidden M1 (147 kev) transition in I^{131} - A.A.Sorokin	1445	1434
Investigation of the decay scheme for Hf^{181} - A.V.Borovikov, V.S. Gvozdev, I.A.Kondurov & Yu.L.Khazov	1448	1437
Decay of Tm^{168} - V.I.Kochevanov, A.R.Kuznetsov, A.N.Murin, V.N. Pokrovskii & L.A.Smirnov	1455	1442
Angular distribution of protons from the $Be^{9}(d,p)Be^{10}$, $Si^{28}(d,p)Si^{29}$ and $Bi^{209}(d,p)Bi^{210}$ reactions - N.I.Zaika & O.F.Nemets	1460	1447
Nuclear reactions of multiply charged ions with carbon and oxygen and their influence in investigation of Coulomb excitation - D.G.Alkhazov, A.P.Grinberg, G.M.Gusinskii & I.Kh.Lemberg	1465	1451
Parity nonconservation in β-decay of RaE - B.V.Geshkenbein, S.A. Nemirovskaya & A.P.Rudik	1473	1458
Polarization of internal conversion electrons following β-decay - B.V.Geshkenbein	1480	1464
Inelastic neutron scattering by odd nuclei - A.M.Korolev	1487	1470
Energy levels of weakly deformed nuclei - A.M.Korolev	1492	1475
Magnetic and quadrupole moments of weakly deformed nuclei - B.D.Konstantinov & A.M.Korolev	1497	1480
Nuclear potentials and neutron stability of nuclei - P.E.Nemirovskii	1503	1486
On "repulsion" of nuclear levels with the same spin and parity - L.K.Peker	1511	1493
Equilibrium shape of odd-A nuclei in the A = 213 to 221 region - L.K.Peker	1514	1495
Some characteristics of new photomultiplier tubes - A.G.Berkovskii, I.Ya.Breido, O.S.Korol'kova & L.G.Leiteizen	1517	1498
Calculation of the energy levels of Tl^{206} and Bi^{210} - Yu.I.Kharitonov	1520	1501
Summary of contents of Volume 23	1526	1513

Translated in 1960 by
Columbia Technical Translations
5 Vermont Ave., White Plains, N.Y.

RESUME OF THE CONFERENCE TRANSACTIONS PUBLISHED IN VOLUME 23

of the

BULLETIN OF THE USSR ACADEMY OF SCIENCES

- Physical Series -

	Issue Nos.
Molecular luminescence (Sixth Conference on Luminescence)	1 (Cont. from Vol.22, No.11)
Nuclear spectroscopy (Ninth All-Union Conference on Nuclear Spectroscopy)	2, 7 & 12
Magnetic materials (All-Union Conference on the Physics of Magnetic Materials)	3 (Cont. from Vol.22, No.10)
Electron microscopy (Second All-Union Conference on Electron Microscopy)	4 & 6
Application of x-rays (Sixth All-Union Conference on the Applications of X-rays to the Investigation of Materials	5
Gaseous electronics (Second All-Union Conference on Gaseous Electronics)	8
Applied spectroscopy (Twelfth Conference on Spectroscopy)	9 & 10
Crystal phosphors (Seventh Conference on Luminescence)	11

Columbia Technical Translations
5 Vermont Avenue, White Plains, N.Y.

SUMMARY OF THE CONTENTS

of

VOLUME XXIII

of the

BULLETIN OF THE ACADEMY OF SCIENCES OF THE USSR

- Physical Series -

SUBJECT SUMMARY - VOLUME 23

TRANSACTIONS OF THE SIXTH CONFERENCE ON LUMINESCENCE
(Molecular Luminescence)
(continued from Vol. 22, No.11)

Number 1

	Page (Trans.)
Luminescence of organic complexes of europium, samarium and terbium - V.V.Kuznetsova & A.N.Sevchenko	3
Distinctive features of the luminescence of ortho-hydroxy substituted aromatic hydrocarbons - Yu.V.Naboikin, B.A. Zadorazhnyi & E.N.Pavlova	9
Formation of luminescence polymers in concentrated acridine orange solutions and investigation of their optical properties - V.L.Levshin & Yu.A.Klyuev	14
Effect of ionization on the luminescence spectrum of 9-aminoacridine and its monochloroderivatives - L.V.Levshin	18
Vibrational analysis of the phosphorescence of coronene - É.V.Shpol'skii & L.A.Klimova	22
Fluorescence spectra of frozen solutions of simple aromatic hydrocarbons - T.N.Bolotnikova	29
Oxygen induced quenching of the fluorescence of heated adsorbates of a number of anthraquinone derivatives - A.V.Karyakin	34
Effect of the position and nature of the substituent on the fluorescence spectra of anthraquinone derivatives in frozen solutions - D.N.Shigorin, N.A.Shcheglova & R.N.Nurmukhametov	39
Effect of excitation energy transfer on the luminescence of molecular crystals - V.M.Agranovich	44
Influence of the thickness of doped anthracene crystals on the luminescence of the host material and the impurity - A.N.Faidysh	53
Wavelength dependence of the polarization of fluorescence of molecular crystals - N.D.Zhevandrov, V.I.Gribkov & V.N.Varfolomeeva	59
Thermal radiation of naphthalene, anthracene and phenanthrene in the infrared region - O.V.Failkovskaya	64
Absorption and luminescence centers in thallium solutions - V.G.Avramenko & M.U.Belyi	67
Determination of the composition of polymers in dye solutions from the absorption and luminescence spectra - M.U.Belyi	71
On "activation" of the fluorescence of chlorophyll and its analogues - V.B.Evstigneev	74
Some features of the luminescence of chlorophyll and pheophytin - L.A.Kravtsov	77
Investigation of the formation of chlorophyll and its state in plant leaves by observation of fluorescence spectra - F.F.Litvin & A.A.Krasnovskii	81
Fluorescence of aromatic amino acids in solutions, crystals and proteins - Yu.A.Vladimirov	85
Fluorescence excitation spectra of proteins - S.V.Konev	88

Location of chlorophyll molecules in chloroplasts - T.N.Godnev & N.K.Akulovich 91
A new fluorometer - A.Yu.Borisov & L.A.Tumerman 94
Luminescence mechanism in plastic scintillators - I.M.Rozman, E.A.Andreeshchev & S.F.Kilin 99
Luminescence spectra of ΩNPO and POPOP in different solvents - E.N.Matveeva, M.N.Medvedev & M.D.Shafranov 105
Quenching of the phosphorescence of organic dyes by electrolyte ions - A.E.Pankeeva 108
Photoluminescence of phthalic and benzoic acid esters - I.B.Dubinskii 111
Variation of the lifetime of the excited state of organic luminophors with the wavelength of the exciting light - G.M.Kislyak 114
Fluorescence spectra of "motorines" (engine fuels) - C.Mikhul, C.Ruscior, V.Pop, F.R.Shvartz & G.A.Redulescu 117
Luminescence spectra of high-molecular-weight petroleum hydrocarbons - Kh.I.Mamedov 121
Variation of the luminescence spectrum of uranine with the pH of the solution - L.T.Kantardzhyan 125
Vibrational structure of the phosphorescence spectra of aromatic acids at liquid oxygen temperature - B.A.Pyatnitskii 129
Phosphorescence decay in magnesia cement and oxide phosphors - V.K.Dvorovenko 132
Phosphorescence spectra of some phenols at liquid oxygen temperature - A.A.Zudin 135
Luminescence spectra of two dicarboxylic acids at different temperatures - E.F.Ryazanova 136
Phosphorescence spectra of some aromatic hydrocarbons at different temperatures - M.S.Fadeeva 139
Luminescence spectra of some dicarboxylic acids - T.S.Navlina 142

TRANSACTIONS OF THE NINTH ALL-UNION CONFERENCE ON NUCLEAR SPECTROSCOPY

Number 2

Internal conversion coefficients of some nuclear transitions in As^{75} - A.A.Bashilov & V.V.Il'in 149
Determination of the relative abundances and conversion coefficients of transitions occurring in the decay of Se^{75} - E.P.Grigor'ev, A.V.Zolotavin, V.Ia.Klement'ev & R.V.Sinitsyn 153
Investigation of the gamma-spectrum of Se^{75} in the 200 to 900 kev region - N.A.Voinova, B.S.Dzhelepov & N.N.Zhukovskii 178
$Yb^{166} \rightarrow Tm^{166} \rightarrow Er^{166}$ decay series - E.P.Grigor'ev, B.S.Dzhelepov & A.V.Zolotavin 180
Radiation from Tb^{160} - E.P.Grigor'ev, A.V.Zolotavin & B.Kratsik 183
Conversion electrons from Eu^{149} - N.A.Anton'eva, A.A.Bashilov, B.S.Dzhelepov, V.V.Il'in & B.K.Preobrazhenskii 196
Gamma-spectrum of I^{131} - B.S.Dzhelepov, V.P.Prikhodtseva & Yu.V.Khol'nov 198
Gamma-radiation from Br^{82} - B.S.Dzhelepov, V.A.Eliseev, V.P.Prikhodtseva & Yu.V.Khol'nov 199
Coincidences between conversion electrons in the decay of Gd^{146} and Gd^{151} - B.S.Dzhelepov & V.A.Sergienko 203
Coincidences between conversion electrons in the decay of Gd^{147} and Gd^{149} - B.S.Dzhelepov, B.K.Preobrazhenskii & V.A.Sergienko 211

Coulomb excitation of nuclear levels in spherical even-even nuclei - D.G.Alkhazov, A.P.Grinberg, K.I.Erokhina & I.Kh.Lemberg 215
Excited states of Ga^{67} and Ga^{68} - A.K.Val'ter, I.I.Zalyubovskii, A.P.Klyucharev, G.E.Krivets & V.A.Lutsik 217
Investigation of gamma-rays emitted in proton bombardment of a target containing Ne^{20} - A.K.Val'ter, V.Yu.Gonchar, A.N.L'vov & S.P.Tsytko 219
Effect of screening on the probability of EO-conversion on the K and L shells at low energies - M.A.Listengarten & I.M.Band 225
Selection rules in conversion transitions - M.E.Voikhanskii & M.A.Listengarten 228
Equipment for measurement and stabilization of the magnetic field in spectrometers - Yu.S.Egorov, D.M.Seliverstov, G.D.Latyshev & A.I.Zhernovoi 234
Frequency meter for nuclear resonance - Yu.S.Egorov, D.M.Seliverstov & G.D.Latyshev 240
Gamma-rays in the decay of As^{78} - Yu.A.Nemilov, A.N.Pisarevskii & L.D.Soshin 244
Concerning linearity in scintillation spectrometry - Yu.A.Nemilov, I.I.Lomonosov, A.N.Pisarevskii, L.D.Soshin & E.D.Teterin 246
Amplification of photomultipliers in pulsed operation - A.N.Pisarevskii & E.D.Teterin 252

Number 7

Magnetic alpha-spectrometer - B.S.Dzhelepov, R.B.Ivanov, V.G. Nedovesov & V.G.Chumin 780
Alpha-spectrum of U^{233} - B.S.Dzhelepov, R.B.Ivanov, V.G.Nedovesov & B.P.Shishin 785
Collective excited states of nuclei - A.S.Davydov 788
Conversion electrons from Yb^{166} and Tm^{166} - V.Brabets, K.Ia.Gromov, B.S.Dzhelepov, A.G.Dmitriev & V.A.Morozov 805
Gamma-spectrum of Tm^{166} and Yb^{166} - V.I.Baranovskii & V.N.Pokrovskii 813
On the decay scheme of Tm^{166} - K.Ia.Gromov, B.S.Dzhelepov & V.N. Pokrovskii 815
Gamma-radiation from Cs^{134} - B.S.Dzhelepov, V.P.Prikhodtseva & Iu.V.Khol'nov 820
Ta^{182} gamma-radiation in the 300 to 1500 kev region - N.A.Voinova, B.S.Dzhelepov & N.N.Zhukovskii 822
Spectra of neutron-deficient Hf isotopes - V.I.Baranovskii & A.V.Kaliamin 825
High-energy part of the gamma-spectrum of radium in equilibrium with its decay products (3100-5600 kev) - B.S.Dzhelepov. B.A.Emel'ianov, Iu. N.Podkopaev, V.N.Podymakhin, I.F.Uchevatkin & S.A.Shestopalova 826
Investigation of the low-lying levels of Cl^{33} by means of the $S^{32}(p,\gamma)Cl^{33}$ reaction - A.K.Val'ter, V.Iu.Gonchar, A.N.L'vov & S.P.Tsytko 829
Elastic scattering and radiative capture of protons by N^{14} - A.K.Val'ter, A.S.Deineko, I.Ia.Malakhov, P.V.Sorokin & A.Ia.Taranov 833
Elastic scattering of protons by A^{40} - A.K.Val'ter, I.Ia.Malakhov, P.V.Sorokin & A.Ia.Taranov 839
Excited states of Ga^{67} and Ga^{68} - A.K.Val'ter, I.I.Zaliubovskii, V.A.Kliucharev & V.A.Lutsik 842

Fine structure of the alpha-spectrum of Th^{229} - G.E.Kocharov, A.P.Komar, G.A.Korolev, I.N.Marov & Iu.A.Surkov 847
Conversion electron coincidences in $Se^{75} \rightarrow As^{75}$ decay - V.E.Bunakov, B.S.Dzhelepov, I.Zvol'skii & V.A.Sergienko 851
Regarding $Er^{160} \rightarrow Ho^{160}$ and $Yb^{166} \rightarrow Tm^{166}$ transitions - E.P.Grigor'ev, B.S.Dzhelepov & A.V.Solotavin 855
Ho^{160} decay and Dy^{160} level diagram - E.P.Grigor'ev, B.S.Dzhelepov, A.V.Zolotavin, B.Kratsik & G.Bitterlikh 859
On calculation of the reduced lifetime of nuclei for unique beta-transitions - L.N.Zyrianova 867
Contribution to the theory of focusing crystal spectrometers (Choice of the reflecting planes) - O.I.Sumbaev 871
Angular correlation of the gamma-rays from Ne^{21} - A.G.Khabakhpashev & E.M.Tsenter 874
Specific stopping losses in heavy nuclei in different substances - A.P.Grinberg & I.Kh.Lemberg 877
Range and specific ionization of multicharged ions - Ia.A.Teplova, V.S.Nikolaev, I.S.Dmitriev & L.N.Fateeva 883
Cascade gamma-transitions in Cl^{36} and S^{33}, accompanying thermal neutron capture - V.R.Burmistrov 886
Cascade gamma-transitions in Nd^{144} - V.R.Burmistrov 890
Contribution to the theory of superfluidity of nucleon gas - Iu.V.Tsekhmistrenko 897
Moments of inertia of nuclei - M.Kazarnovskii 899
Contribution to the theory of superfluidity of nuclear matter - B.B.Dotsenko 901
Statistical theory of the nuclear potential in the "effective mass" approximation - L.Rapoport & S.Kadmenskii 905
On beta-decay of neutrons with oriented spin - B.K.Kerimov 911
Production of electron-positron pairs in the collision of two polarized gamma-rays - F.S.Sadykhov & B.K.Kerimov 915

Number 12

Large double-focusing alpha-spectrometer - S.A.Baranov, A.G. Zelenkov, G.Ya.Shchepkin, V.V.Beruchko & A.F.Malov 1389
Some design calculations for a double-focusing alpha-spectrometer - A.G.Zelenkov 1396
New data on the decay of Am^{241} - P.S.Samoilov 1401
Positron spectrum of the lutetium fraction from the spallation products of tantalum - B.S.Dzhelepov. O.E.Kraft & E.B.Kreshtofova 1422
Decay scheme for 30-hour Te^{131} - A.Bedesku, K.P.Mitrofanov, A.A. Sorokin & V.S.Shpinel' 1424
On the l-forbidden M1 (147 kev) transition in I^{131} 1434
Investigation of the decay scheme for Hf^{181} - A.V.Borovikov, V.S. Gvozdev, I.A.Kondurov & Yu.L.Khazov 1437
Decay of Tm^{168} - V.I.Kochevanov, A.R.Kuznetsov, A.N.Murin, V.N. Pokrovskii & L.A.Smirnov 1442
Angular distribution of protons from the $Be^{9}(d,p)Be^{10}$, $Si^{28}(d,p)Si^{29}$ and $Bi^{209}(d,p)Bi^{210}$ reactions - N.I.Zaika & O.F.Nemets 1447
Nuclear reactions of multiply charged ions with carbon and oxygen and their influence in investigation of Coulomb excitation - D.G.Alkhazov, A.P.Grinberg, G.M.Gusinskii & I.Kh.Lemberg 1451

Parity nonconservation in β-decay of RaE - B.V.Geshkenbein, S.A.Nemirovskaya & A.P.Rudik 1458
Polarization of internal conversion electrons following β-decay - B.V.Geshkenbein 1464
Inelastic neutron scattering by odd nuclei - A.M.Korolev 1470
Energy levels of weakly deformed nuclei - A.M.Korolev 1475
Magnetic and quadrupole moments of weakly deformed nuclei - B.D.Konstantinov & A.M.Korolev 1480
Nuclear potentials and neutron stability of nuclei- P.E.Nemirovskii 1486
On "repulsion" of nuclear levels with the same spin and parity - L.K.Peker 1493
Equilibrium shape of odd-A nuclei in the A = 213 to 221 region - L.K.Peker 1495
Some characteristics of new photomultiplier tubes - A.G.Berkovskii, I.Ya.Breido, O.S.Korlo'kova & L.G.Leiteizen 1498
Calculation of the energy levels of Tl^{206} and Bi^{210} - Yu.I.Kharitonov 1501

TRANSACTIONS OF THE ALL-UNION CONFERENCE ON THE PHYSICS OF MAGNETIC MATERIALS
(Continued from Vol.22, No.10)

Number 3

Investigation of the structure of new deformable magnetic alloys - M.N.Raevskaia 259
Structural changes and antiferromagnetic properties of Ni_3Fe and other alloys in the Fe-Ni system - M.V.Dekhtiar 265
Influence of high-temperature annealing on the magnetic properties of soft magnetic alloys - N.I.Lapkin & V.S.Mes'kin 273
Ferromagnetism of Mn-B alloys - N.Z.Miriasov & A.P.Parsanov 278
Investigation of the $NiO-ZnO-Fe_2O_3$ system - K.A.Piskarev 282
Structure of the family of symmetrical hysteresis loops of ferromagnets (Ni-Zn ferrite) - V.I.Drozhzhina & N.V.Erofeeva 296
Properties of $NiFe_2O_4$-$MgFe_2O_4$ solid solutions - N.A.Smol'kov & Yu.P.Simanov 299
Permeability and losses in magnetodielectrics (molded cores) - K.M.Polivanov, Ya.N.Kolli & L.P.Soboleva 302
High-frequency ferromagnets - L.I.Rabkin 309
Influence of macroscopic heterogeneity on the dynamic characteristics of soft magnetic alloys in weak fields - E.I.Gurvich & E.I.Kondorskii 314
Investigation of dispersion of the permeability and absorption in Mn-Zn ferrites. Part I. Dispersion of the body - L.A.Fomenko 319
Investigation of dispersion of the permeability and absorption in Mn-Zn ferrites. Part II. Dispersion of the material - L.A.Fomenko 326
Influence of magnetic viscosity on the frequency characteristics of ferrites - R.V.Telesnin & A.G.Shishkov 332
Rate of magnetization switching in ferrites - R.V.Telesnin & E.F.Kuritsyna 340
Some attributes of ferrites under pulse conditions - N.A.Smol'kov & V.F.Belov 345
Ferromagnetic semiconductors in super-high frequency fields - A.G.Gurevich 348
Ferrites with a high saturation magnetization and a narrow resonance absorption curve at super-high frequencies - V.A.Fabrikov, V.D. Kudriavtsev & Z.M.Gushchina 359

Some properties of ferrites at super-high frequencies - N.A. Smol'kov & E.I.Fomenko 363
Nonlinear gyromagnetic properties of ferrites at low levels of super-high frequency power - V.A.Fabrikov & E.G.Ritter 366
Electric properties of magnetodielectrics and ferrites - L.I.Rabkin & Z.I.Novikova 373
Investigation of the dielectric properties of ferrites - Z.I.Novikova 380
Investigation of the structure of iron-aluminum alloys with anomalous conductivity - E.N.Vlasova & L.N.Fedotov 386
Magnetization of ferromagnetic powders in strong magnetic fields - G.V.Krasnoperov 389
Atomic magnetic moments, Curie points, exchange energy and paramagnetic susceptibility of ferromagnets - F.M.Gal'perin 391
Investigation of the magnetoelastic effect in ferrites - L.N.Syrkin 397
New high-coercivity alloys in the binary systems Fe-Pt, Fe-Pd and Ni-Pd - Z.I.Alizade 399
Comments on reports 401

TRANSACTIONS OF THE SECOND ALL-UNION CONFERENCE ON ELECTRON MICROSCOPY

Number 4

Dominant trends in modern electron-microscope design - V.N.Vertsner 413
Electron microscope-diffraction camera with a 400 kv accelerating potential - N.M.Popov 421
The UÉMB-100 electron microscope with a two-lens condenser - P.A.Stoyanov, G.A.Mikhailovskii & V.V.Moseev 427
Power supply unit for the UÉMB-100 electron microscope - V.V.Polivanov, V.V.Il'in, A.V.Iz'yurov, N.I.Pyatakov & R.V.Shumova 434
Small electrostatic microscopes - V.I.Milyutin, D.V.Fetisov, K.K. Raspletin, F.U.Spektor & B.I.Pochtarev 438
Electrostatic velocity analyzer for 75 kv electrons - A.N.Kabanov, V.I.Milyutin & D.V.Fetisov 443
Instrument for measuring the resolution and light yield of fluorescent screens (PRS) - B.I.Pochtarev, K.K.Raspletin & D.V.Fetisov 445
Compensation of axial astigmatism in the lenses of a multiple-lens electron microscope - P.A.Stoyanov 449
A simplified ultramicrotome - Ya.Yu.Komissarchik, V.N.Vertsner & L.S.Gol'din 456
Light-electron microscope employing single-crystal high-resolution screens - G.A.Bogdanovskii, V.V.Kuprevich, V.N.Vertsner & I.V.Stepanov 461
X-Ray shadow microscope - G.O.Bagdyk'yants & A.V.Shishatskii 464
The commercial model ÉM-5 electron microscope - V.N.Vertsner, M.G.Ivanov, V.V.Kozelkin, G.A.Bogdanovskii, Yu.V.Vorob'ev, Yu.V.Chentsov, V.E. Klyukin & V.A.Nikiforova 468
Cell for electron microscopic study of objects in a gaseous medium - I.G.Stoyanova 472
High-voltage electron gun - N.M.Popov 477
Concerning the design of electron microscope power supplies - V.V.Polivanov, A.V.Iz'yurov & V.V.Il'in 483
Computer for design calculation of fields in electron-optical systems - G.V.Der-Shvartz & K.A.Netrebenko 488

Shielding electron microscopes against the influence of external magnetic fields - P.A.Stoyanov & V.V.Moseev 492
Some improvements in the design of the ÉM-3 electron microscope - Iu.V.Chentsov, V.N.Vertsner & G.A.Bogdanovskii 499
High-vacuum electron microscope for studying cathodes - A.V.Druzhinin & B.N.Popov 502
New model of an emission microscope for investigation of thermionic and secondary emitters (ÉÉM-50) - A.M.Rozenfel'd & P.V.Zaitsev 507
New universal 100 kv electron diffraction camera with an armored lead-in - Model ÉG-100A - N.P.Levkin & Yu.M.Kushnir 510

Number 6

Investigation of minerals by the microdiffraction technique in a 400 kv electron microscope-diffraction camera - N.M.Popov & B.B.Zvyagin 663
Investigation of the structure of PbS sublimates by electron microscopy and diffraction - V.N.Vertsner 668
Structure and photoelectric properties of lead sulfide layers - R.Ya.Berlaga 672
Electron microscopic investigation of the structure of thin films of antimony sulfide prepared by evaporation in vacuum and in nitrogen at pressures under 4 mm Hg - A.M.Reshetnikov 676
Electron microscopic investigation of finely dispersed carbonyl iron - A.A.Petrova, E.V.Tsvetkova & V.N.Gorshunova 682
Resolution of electrostatic electron microscopes - D.V.Fetisov, F.U.Spektor, V.I.Milyutin & K.K.Raspletin 684
Ultimate resolution of emission electron microscopes - Iu.V.Vorob'ev 688
Resolving power of an immersion objective in the presence of electric and magnetic microfields on the cathode - G.V.Spivak & V.I.Liubchenko 691
Electron-optical properties of quadrupole electrostatic lenses - A.M.Strashkevich 701
A theoretical method of investigating the characteristics of a stigmator - P.P.Kas'yankov 706
On the influence of chromatic aberration due to disadjustment of the aperture on the resolution of a reflection electron microscope - G.V.Der-Shvarts & S.A.Belen'kii 711
Investigation of electron energy loss in thin gas layers - I.G.Stoyanova & A.N.Kabanov 714
Influence of space charge on the image obtained in an emission electron microscope - D.P.Vinogradov 718
Investigation of the compatibility of natural and synthetic rubbers - A.S.Lykin & K.A.Pechkovskaya 720
Observation of ferroelectric and piezoelectric domains by means of an electron mirror - G.V.Spivak, I.A.Priamkova & É.Igras 723
Electron microscopy of temperature induced changes in the magnetic microstructure of ferromagnets - I.S.Sbitnikova, G.V.Spivak & I.M.Saraeva 729
Investigation of ground and polished glass surfaces and of some polishing powders by means of an electron microscope - Yu.I.Smolin & A.I.Korelova 733
Investigation of structural changes in dielectrics under the influence of heat, chemical etching and ion bombardment - A.I.Krokhina & G.V.Spivak 736

Procedure for bringing out the structure of metals and alloys by ion bombardment - V.E.Yurasova, G.V.Spivak & F.F.Kushnir 739
Utilization of an ÉM-3 electron microscope for local x-ray spectrographic analysis - A.M.Solov'ev & V.N.Vertsner 744
Investigation of the heating effect of electrons on the specimen in an electron microscope - I.G.Stoyanova & A.M.Belavtseva 748
Some aspects of investigation of high-molecular compounds by means of electron diffraction - I.G.Stoyanova & A.L.Ziades 752
On obtaining images with pulsed operation of a high-resolution emission microscope - E.M.Dubinina, G.V.Spivak & I.A.Priamkova 756
Accuracy of rendition of potential distribution by the electron-optical shadow technique - L.N.Malakhov & Yu.V.Vorob'ev 759
Application of the electron-optical shadow technique to investigation of germanium p-n junctions - L.N.Malakhov, V.N.Vertsner & A.A.Lebedev 763
Measurement of the scattered electron intensity and elimination of the background in electron diffraction studies - G.O.Bagdyk'yants & A.G.Alekseev 766
Electron microscopic investigation of the influence of the conditions of preparation of lithium grease on its microstructure - A.A.Trapeznikov, G.G.Shchegolev & I.I.Astakhov 769

TRANSACTIONS OF THE SIXTH ALL-UNION CONFERENCE ON THE APPLICATIONS OF X-RAYS TO THE INVESTIGATION OF MATERIALS

Number 5

Characteristics of x-ray shadow microscope images - G.O.Bagdyk'ants & A.V.Shishatskii 521
Absorption coefficient of soft x-rays in beryllium - D.M.Zhukovskaya & Yu.K.Ioffe 524
X-ray shadow microscopy - B.M.Rovinskii, V.G.Lyuttsau & A.I.Avdeenko 528
Electron-optical x-ray image intensifier - M.M.Butslov 535
Influence of minor impurities and roentgenization on the x-ray absorption spectrum of crystalline KCl - K.I.Narbutt & I.S.Smirnova 540
Investigation of the L series of germanium. Influence of impurities - G.P.Borovikova & M.I.Korsunskii 546
X-ray spectroscopic investigation of compounds with the perovskite structure - A.T.Shuvaev 551
Structure of the electron energy spectrum in iron-chromium alloys - N.D.Borisov, V.V.Nemoshkalenko & A.M.Fefer 555
K absorption spectra of chromium in borides, carbides, nitrides and other compounds - S.A.Nemnonov & A.Z.Men'shikov 559
Determination of the radial electron density from the fine structure of x-ray absorption spectra - V.A.Trapeznikov 563
Collective interaction of electrons in crystals and its manifestation in the x-ray absorption spectra of atoms in polar crystals - R.L.Barinskii & E.E.Vainshtein 566
On stresses of the third kind - D.Batsur', V.I.Iveronova & G.P.Revkevich 572
Investigation of the fine structure of Fe-Si alloys under deformation - G.M.Vorob'ev 582
Determination of the static atomic displacements in the slip band of rock salt - P.N.Aronova & V.I.Startsev 587

On eliminating the influence of texture on the intensity of x-ray interferences - V.M.Finkel' 592
Effect of alloying elements on the recrystallization kinetics of nickel alloys - E.E.Zasimchuk, G.V.Kurdyumov & L.N.Larikov 597
Comparison of the principal x-ray procedures for determining the size of mosaic blocks in polycrystalline materials - S.V.Semenovskaya & Ya.S.Umanskii 602
Investigation of the x-ray line width of metals deformed at different temperatures - N.N.Davidenkov & B.I.Smirnov 606
X-ray microbeam investigation of steel deformed at different rates at high temperatures - M.Ya.Fuks & L.Ya.Gol'dshtein 611
On determination of the size of blocks and microdeformations by harmonic analysis - O.V.Bogorodskii 617
Contribution to the theory of diffuse scattering of x-rays and slow neutrons by multiple component alloys - V.V.Geichenko, V.M.Danilenko, M.A.Krivoglaz, Z.A.Matysina & A.A.Smirnov 619
X-ray diffraction investigation of the relation between recovery, recrystallization and ordering in Fe-Co and Ni-Fe alloys - M.M.Borodkina, E.I.Detlaf & Ya.P.Selisskii 622
Investigation of phase transitions in Cu-Sn alloys - M.I.Zakharova & I.B.Mogarycheva 627
Changes in mosaic structure occurring incident to aging of a nichrome base alloy - L.Kh.Pivovarov & Ya.S.Umanskii 633
Structural changes in Ni-Be alloy after aging and high temperature annealing - N.N.Buinov 636
X-ray diffraction studies of alloys of rhenium with molybdenum - N.V.Ageev & V.Sh.Shekhtman 638
Theory of scattering of x-rays and thermal neutrons by fluctuation heterogeneities in solid solutions - M.A.Krivoglaz & E.A.Tikhonova 640
Fine structure of some alloys with anomalous conductivity - E.N.Vlasova 643
On the true temperature of beginning of recrystallization of super-saturated solid solutions - S.S.Gorelik 645
Evaluating the effect of impurities on the x-ray emission spectra of dilute transition metal solid solutions - I.B.Borovskii & K.P.Gurov 648
On the basic techniques of x-ray and γ-ray materiology - V.M.Genkin 655

TRANSACTIONS OF THE SECOND ALL-UNION CONFERENCE ON GASEOUS ELECTRONICS

Number 8

Formation of a high-frequency discharge at low pressures - G.N.Zastenker & G.S.Solntsev 925
Investigation of a self-sustaining super-high frequency pulse discharge in air and its initiation process - P.S.Bulkin, G.S.Solntsev & V.N.Ponomarev 931
Measurement of the charge concentration in plasma by means of super-high frequency probes - S.M.Levitskii & I.P.Shashurin 938
Initiation of super-high frequency pulse discharges in inert gases - V.E.Golant 942
Correlation between the characteristics of super-high frequency and direct currents in gases - V.E.Golant 947

Obtaining high temperatures by means of a spark discharge - M.P.Vaniukov & A.A.Mak 951
Some results of investigation of the excitation functions of the N_2^+ negative system bands - I.P.Zapesochnyi & S.M.Kishko 954
Excitation cross sections for some spectrum lines of potassium and argon - L.M.Volkova 957
Effect of disappearance of negative ions on their concentration in the discharge column - M.V.Koniukov 960
New results of investigations of a long spark - I.S.Stekol'nikov 964
Probe investigations of the field of an ac corona - V.I.Levitov, A.G.Liapin & V.I.Popkov 968
Elementary processes in the ionization zone of corona discharges at atmospheric pressure - G.N.Aleksandrov 976
Charge density oscillation waves in a cylindrical plasma - M.Ia.Vasil'eva, A.A.Zaitsev & E.D.Andriukhina 982
Positive discharge column under diffusion conditions - V.M.Zakharova, Iu.M.Kagan & V.I.Perel' 986
Investigation of the initial stages of a high-frequency discharge from a point in air at atmospheric pressure - A.M.Prokof'ev, O.F.Kabardin & K.F.Kuddu 992
Investigation of resonance charge exchange in monatomic gases and metal vapors - R.M.Kushnir, B.M.Paliukh & L.A.Sena 995
Investigation of anodic oscillations in a low-pressure discharge - A.A.Zaitsev & K.I.Efendiev 1000
Broadening and shift of spectral lines in gas discharge plasma - S.L.Mandel'shtam & M.A.Mazing 1005
Separation of binary mixtures of inert gases in a dc discharge - N.A.Matveeva 1009
Measurement of electric fields in a high-frequency low-pressure discharge by means of an electron beam - G.S.Solntsev, A.G. Porokhin & N.M.Chistyakova 1014
Measurement of the electric field in a super-high frequency plasma - V.E.Mitsuk, M.D.Koz'minykh & I.V.Talalaeva 1019
Influence of the temperature of an auxiliary electrode on the ignition of a high-frequency discharge in helium - Kh.A.Dzherpetov 1024
Conductivity of weakly ionized air at high frequencies - H.Margenau, E.Desloge & D.Stillinger 1027
Low-frequency wave-like effect in glow-discharge plasma - L.Pekarek 1037

TRANSACTIONS OF THE TWELFTH CONFERENCE ON SPECTROSCOPY
(Applied Spectroscopy)

Number 9

Opening address - S.L.Mandel'shtam 1045
Determination of atomic concentrations in arc discharge plasma from the line widths and correlation between the concentrations in the solid and gaseous phases - I.M.Nagibina 1048
Distinctive characteristics of arc discharges in different gases - V.L.Marzuvanov 1051
Atlas of spectrum lines for high-dispersion grating spectrographs - S.K.Kalinin, V.L.Marzuvanov, É.E.Fain, G.M.Zamyatina, V.N. Perevetun & S.L.Terekhovich 1054

Entry of matter into arc plasma. Case of binary Na + Li mixtures - V.P.Zakharov & A.A.Shishlovskii 1056
Entry of silicon brass into an ac arc - N.K.Rudnevskii, G.I. Golitsyn & V.P.Rybochkin 1058
Entry of lead brass into an ac arc - N.K.Rudnevskii & E.S.Obukhova 1060
Correlation between the compositions of the solid and vapor phases in spectroscopic analysis of iron alloys - O.I.Nikitina, M.G. Sklyar, A.E.Gorevaya & N.K.Ivanova 1062
Influence of discharge time on the rate of evaporation of particles from the surface of metallic arc electrodes - G.E.Zolotukhin & N.M.Zykova 1065
Effect of sample polarity in the excitation of rectified arc spectra - É.A.Silin'sh & L.F.Taure 1067
Influence of the composition of powdered substances on the relative intensity of spectrum lines - A.M.Shavrin & M.A.Zotin 1069
Influence of "third" elements in spark analysis of solutions (Abst.) - A.K.Rusanov & L.I.Sosnovskaya 1071
Influence of "third" elements in using undispersed light as the internal standard - I.S.Abramson, S.N.Murzin & V.A.Slavnyi 1073
Effect of the chemical composition of the sample on the intensity of the matrix spectrum and the analytic results - N.V.Buyanov 1075
Relation between the diluent effect of "third" components and the transport of material in light sources for spectroscopy - A.M.Borbat & A.A.Shishlovskii 1078
Variation of the total intensity of spectrum lines with the atomic concentration in a pulse discharge - E.I.Vorontsov 1080
Investigation of the causes of selective disintegration of alloys by a spark discharge - I.A.Grikit 1083
Influence of "third" elements in spark spectroscopic analysis of molten alloys - L.E.Vvedenskii & V.I.Shekhobalova 1085
Spectroscopic investigation of electroerosion of oxygen-containing titanium - N.S.Sventitskii & K.I.Taganov 1088
Spectroscopic investigations of the effect of polarity in electric erosion of metals - K.I.Taganov 1089
Use of contact-spark sampling technique in spectroanalytic studies - V.S.Burakov & A.A.Yankovskii 1091
Analysis of an optical system for a mirror spectrograph with large plate length - S.A.Khrshanovskii 1093
Photoelectric equipment for the ISP-22 spectrograph. A new method of automatic spectroscopic analysis of electrolytes - Yu.A.Yakobi & S.I.Maksimov 1095
New photoelectric spectrographic equipment - M.M.Averbukh, N.V. Artsishevskaya, N.V.Belyaev, I.I.Erina, D.I.Pen'kov & I.G. Strel'tsov 1097
Analysis of heat-resistant and light alloys and steels by the photoelectric procedure - K.A.Sukhenko, K.A.Moiseeva, L.D. Metelina, I.G.Tishin, N.V.Penkina & D.G.Bakanov 1099
Photoelectric steelometer with visual monitoring of the position of invisible spectrum lines - N.M.Butslov, A.K.Vinogradova, L.M.Ivantsov, G.N.Kutuzova & S.L.Mandel'shtam 1102
On stabilization of the position of the spectrum by thermostatic equipment for spectroscopic instruments - A.P.Atamanov, V.N. Balandin & L.M.Ivantsov 1104

Photoelectric attachment for ISP-22 type medium spectrographs - L.M. Ivantsov & A.I.Sherudilo 1105
Spectroscopic determination of oxygen in commercial grade titanium - K.A.Sukhenko, V.S.Grigorova, I.S.Lindstrem, N.S.Sventitskii & P.P.Galonov 1107
Concerning spectroscopic determination of oxygen in titanium - N.S.Sventitskii, K.I.Taganov & Z.I.Shlepkova 1110
On the use of the spectro-isotopic procedure for determining hydrogen - T.F.Ivanova, M.E.Trentovius & V.V.Fedorov 1112
Determination of nitrogen in different steels - K.A.Sukhenko, P.P.Galonov & T.V.Barasheva 1114
Influence of the chemical composition and heat treatment of steel samples on the results of spectroscopic determination of nitrogen - N.V.Buyanov, L.M.Fedorova & V.F.Korotkov 1117
Determination of nitrogen in chromium and titanium - S.A.Skotnikov 1119
Analysis of high concentrations allowing for the influence of "third" components - L.I.Topalova 1121
Spectroscopic determination of the major components of noble metal alloys - N.I.Varlamova & N.S.Sventitskii 1124
Spectroscopic determination of high concentration components in steels and other alloys - A.G.Komarovskii 1126
Statistical investigation of analytic results - V.V.Nalimov 1128
Standards for determination of impurities in pulverized complex ferroalloys - A.B.Shaevich 1130
Preparation of standards for spectroscopic analysis of noble metals - A.A.Kuranov 1132
Methods of calibration in analysis of alloys - E.S.Kydelya & A.S.Dem'yanchuk 1135
Use of the "fractional exposure" procedure for analysis of some alloys - E.P.Barankina 1137
Preparation of standards of different alloys and investigation of the influence of "third" elements in them - K.A.Sukhenko, O.I. Mladentseva & A.V.Aksenova 1139
Rapid spectroscopic analysis of metallometric specimens for rare alkali metals, boron, fluorine and other elements - P.A.Stepanov, E.A.Sergeev, M.V.Belobragina & M.S.Leshchinskaya 1141
Quantitative spectroscopic determination of the principal components of intrusive rocks - T.S.Reshetina 1143
Chemico-spectroscopic determination of molybdenum and tungsten in igneous rocks - L.I.Pavlenko 1144
Spectroscopic analysis of luminescence-pure zinc sulfide and sulfate with the aid of chemical enrichment - V.N.Vasil'eva, L.A.Dvorzhetskaya, L.Ya.Markovskii & L.Ya.Khlebnikova 1146
Spectroscopic determination of uranium by the method of isotopic doping - N.P.Ivanov 1148
Spectroscopic determination of the relative Sr and Ca concentrations in biological specimens - G.D.Litovchenko & S.A.Shipitsyn 1150
Spectroscopic determination of microelements in tissue proteins - S.G.Bogomolov, F.D.Drobiz & A.G.Morozov 1152
Development of methods of spectroscopic analysis of blast furnace slag and fluxed sinter - O.I.Nikitina 1154
On minimizing the influence of the mineralogical composition on the results of spectroscopic analysis of fluxed sinter - I.K. Maiboroda 1158

Pneumatic technique for introducing powder specimens into an arc - R.S.Rubinovich & A.S.Pershin 1159
Improved AVR-2 powder-feeding device - I.I.Smolyak 1162
Local analysis of complex alloys - I.L.Mirkin & É.P.Rikman 1164
Spectrographic investigation of surface layers forming in thermochemical treatment of alloys - A.G.Komarovskii 1166
Improved equipment for local spectroscopic analysis - V.V.Bogdanova 1168

Number 10

Some results of spectroscopic investigation of the individual hydrocarbon composition of Tartar petroleums - B.Le 1177
Analysis of hydrocarbon mixtures by Raman spectroscopy - V.T.Aleksanyan, Kh.E.Sterin & S.A.Ukholin 1179
Raman spectra of some C_{24} hydrocarbons - A.N.Kislinskii & A.A.Petrov 1181
Investigation of aqueous solutions of uranyl nitrate by Raman spectroscopy - S.Mintz & Z.Kentski 1184
Investigation of methanol solutions of zinc chloride by Raman spectroscopy - S.Mintz & S.Osetski 1186
Determination of the infrared absorption coefficients of CH_2 groups in dicyclic compounds - S.V.Markova & P.A.Bazhulin 1188
Intensities of the infrared absorption bands associated with C-H valence vibrations - E.I.Pokrovskii 1191
Investigation of the composition of high molecular hydrocarbon fraction of Bitkovsk petroleum by infrared spectroscopy - A.F.Mal'nev, V.T.Sklyar, I.M.Mikhlina, G.A.Puchkovskaya, L.I.Shulnyak & E.F.Shevchenko 1193
Quantitative determination of CH_2 groups in open chains by infrared absorption spectroscopy - E.A.Glebovskaya & E.I.Maksimov 1195
Infrared spectra of some intracomplex compounds in the region of NH valence vibrations - L.A.Kazitsina, B.V.Lokshin, L.L.Polstyanko, & A.P.Terent'ev 1197
Characteristic bands of compounds in the pyridine series - S.G. Bogomolov, M.G.Bystritskaya & M.M.Kirillova 1199
Use of infrared spectroscopy for investigating thermal aging of polyvinyl chloride - L.N.Pirozhnaya & G.S.Popova 1202
Comparative investigation of photo and thermal aging of acetals of polyvinyl alcohol by infrared spectroscopy - G.S.Popova & E.V.Shuvalova 1205
Investigation of isotactic polymers by means of infrared spectroscopy - E.I.Pokrovskii & M.V.Vol'kenshtein 1208
Use of infrared absorption spectra for investigating structural changes in fluorine plastics undergoing aging - L.I.Tarutina 1210
Investigation of structural changes in vulcanized rubbers exposed to the action of mineral acids - A.F.Postovskaya & A.S.Kuz'minskii 1213
Infrared spectra and the structure of the products of telomerization of diene hydrocarbons with halogen derivatives - A.A.Petrov & T.V.Yakovleva 1216
Identification of resin acids from their infrared spectra - N.A. Borisevich, N.I.Makarevich, A.M.Prima, I.I.Bardyshev & E.A.Cherches 1218
Infrared spectra of cellulose and its derivatives - B.I.Stepanov, R.G.Zhbankov & I.N.Ermolenko 1220

Determination of the isotopic composition of deutero-organic compounds by infrared absorption spectroscopy - M.O.Bulanin 1222
Infrared spectra and structure of the products of linkage of different substances to vinyl acetylene hydrocarbons - A.A.Petrov & T.V. Yakovleva 1224
Molecular spectrum of hexaethyldilead and determining of its concentration in tetraethyllead - N.K.Rudnevskii & N.N.Vyshinskii 1226
Spectrophotometric analysis by the "zero heterochromatic point" procedure - B.I.Sukhorukov & A.I.Finkel'shtein 1227
Investigation of aging of castor oil by observation of its absorption spectra - M.S.Kozyreva 1230
Vacuum double-beam diffraction spectrophotometer for the infrared - V.I.Malyshev & S.G.Rautian 1233
The IKS-14 and IKS-12 infrared spectrometers - N.S.Golyandin, I.G. Ptitsyna, I.I.Reshina & I.L.Sakin 1235
Infrared vacuum spectrometer for industrial control and determination of oil in petroleum products by absorption spectrometry - A.F.Mal'nev & G.A.Puchkovskaya 1238
Measuring attachment for infrared spectrometers - A.F.Mal'nev, M.P.Esel'son & L.S.Kremenchugskii 1240
New equipment and procedures for study of the spectra of reflection from the earth's surface - K.S.Lyalikov, I.N.Belonogova, K.E. Meleshko, I.V.Semenchenko & A.P.Kharchenko 1241
On the feasibility of molecular spectroscopic analysis of vapors in a wide temperature range - A.V.Suvorov, S.A.Shukarev & G.I.Novikov 1242
Absorption spectra of indan series hydrocarbons in the near ultraviolet - A.M.Kusakov & M.V.Shishkina 1244
Investigation of radiolysis of alkanes by ultraviolet and infrared spectroscopy - I.Ya.Kachkurova, L.S.Polak, A.V.Topchiev & N.Ya. Chernyak 1246
Investigation of the aromatic portion of the kerosene-gas oil fraction of Dolinsk petroleum by observation of the ultraviolet absorption spectra - V.T.Sklyar & A.P.Lizogub 1248
Applications of molecular spectroscopy in bacteriology and immunology - V.M.Vadimov 1252
Investigation of diphenylchromium derivatives by electron paramagnetic resonance - N.N.Bubnov, Yu.A.Sorokin, S.P.Solodovnikov & V.M. Chibrikin 1254
Electron paramagnetic resonance spectra of eosin semiquinone and live leaf - N.N.Bubnov, V.G.Tsepalov & V.Ya.Shlyapintokh 1256
Development of a high sensitivity EPR-2 IKhF type magnetic radiospectrograph - A.G.Semenov 1257
Correlation between the probability of transition of complex organic molecules to the metastable state and the spectral composition of the luminescence - R.V.Zelinskii, V.P.Kolobkov & I.I.Reznikova 1259
List of reports presented at the Twelfth Conference on Spectroscopy that are scheduled for publication in other journals 1262

TRANSACTIONS OF THE SEVENTH CONFERENCE ON LUMINESCENCE
(Crystal Phosphors)

Number 11

Opening address - M.D.Galanin 1271
Temperature quenching of the luminescence of ZnS:Ag phosphor with excitation by light or α-particles - M.D.Galanin & A.V.Raevskii 1273
New data on a slow neutron detector - T.V.Timofeeva & S.P.Khormushko 1275
On photoelectric effects in luminescent ZnS:Cu(Ni,Fe,Co) and ZnS·CdS:Cu powders - U.Kh.Nymm 1278
Investigation of the photodielectric effect in ZnS:Cu:Fe phosphor - P.E.Ramazanov 1281
Relaxation of the afterglow, photoconductivity and light sums of zinc sulfide phosphors - F.I.Vergunas & Yu.L.Lukantsever 1285
Quenching of the luminescence of ZnS:Cu phosphor by infrared light - K.-S.K.Rebane 1287
Influence of composition on the luminescence of activatorless ZnS·CdS phosphors - L.Drozd 1290
Crystal phosphors with a heterodesmic structure - M.A.Konstantinova-Shlezinger 1294
Fluorophosphate luminophors of the wagnerite type - N.A.Gorbacheva 1298
Characteristics of the crystal phase of zinc silicate and the luminescence properties of Mn activated zinc silicate luminophors - V.V.Osiko 1302
Luminescence centers in samarium activated zinc sulfide phosphors - Z.A.Trapeznikova 1306
Some data on the mechanism of formation of sulfide luminophors - A.A.Bundel', A.I.Rusanova & L.G.Taushkanova 1313
On the physical-chemical nature of silver activator in zinc sulfide phosphors - A.A.Cherepnev 1321
Chemical aspects of the formation of zinc sulfide-selenide phosphors - L.Ya.Markovskii & R.I.Smirnova 1327
Use of thermography for investigating zinc sulfide - E.G.Vasil'eva & S.A.Fridman 1333
On the formation and characteristics of some zinc sulfide luminophors - A.V.Lavrov 1337
Use of luminescence for investigating solid phase reactions in the CaO_4-Al_2O_3 system - A.K.Trofimov 1341
Luminescence of manganese activated strontium metaantimonate -M.-L.Yu.Allsalu 1346
Suitability of the thiosulfate procedure for preparation of zinc sulfide for synthesis of phosphors - M.I.Tombak, A.V.Popova, O.F.Komar & A.A.Bundel' 1349
On variation of the optical properties of sulfide phosphors incident to elimination of the flux - A.M.Gurvich 1356
Investigation of the technology of alkaline earth sulfide phosphors with persistent phosphorescence - T.A.Krasnova 1362
Roentgenoluminescence and thermostimulation spectra of Siberian diamonds - É.S.Vilutis 1365
Luminescence of glasses containing cerium - G.O.Karapetyan 1368
Zinc and strontium phosphate phosphors for "fluorescent" lamps - F.M.Pekerman, D.N.Shoikhet & R.A.Shtrikhman 1372
Improvement of the color rendition of "fluorescent" lamps - R.A.Nilender 1377
Closing address - F.D.Klement 1383